Close-up of waterjet rust removal action

Proceedings of the 10th American Waterjet Conference

August 14-17, 1999
JW Marriott Hotel
Houston, Texas

The 10th American Waterjet Conference is sponsored by the

WJTA
WaterJet Technology Association

WaterJet Technology Association

The Waterjet Technology Association (WJTA) was created in 1983 at the 2nd U.S. Water Jet Conference, held on the campus of the University of Missouri-Rolla, by members of the waterjet industry acting in concert with university and government officials. The major impetus to the creation of the Association was to provide a means of service and communication within the industry, as epitomized by the biennial waterjet conferences.

Formal objectives of the Association have been adopted as follows:

- To provide a means of cooperation between government, industry, university, and research institutions on all matters of fluid jets, including waterjets and abrasive jets for jet cutting, industrial cleaning, and other uses in the manufacturing, mining, construction, and process industries.
- To foster domestic and international trade in jet cutting and jet cleaning, products and services.
- To promote in general the interests of the jet application industry in all branches, including establishment of recommended practices.
- To promote the mutual improvement of its members, and the study and advancement of the arts and sciences connected with jet cutting and industrial cleaning.

In regard to the third objective, it should be noted that at the 3rd U.S. Water Jet Conference held on the campus of the University of Pittsburgh in May of 1985, the Association adopted the first ***Recommended Practices for the Use of Manually Operated High Pressure Water Jetting Equipment.***

The *Recommended Practices* are revised and updated periodically, the most recent revision being published in April 1999.

1999 WJTA Conference Committee

WJTA Administration

WaterJet Technology Association
917 Locust Street • Suite 1100
St. Louis, MO 63101-1419
Telephone: (314)241-1445 • Fax: (314)241-1449
Email: wjta@primary.net • Website: ww.wjta.org

International Advisors

Foreword

One of the adventures of being human consists of seeking out meaning from the confusion surrounding us. The authors of the papers published in this book have developed new knowledge of waterjets and have agreed to share their knowledge in order to make the understanding of waterjets more widespread. The authors have agreed to fix their new knowledge in place in this book for the benefit of present and future waterjetters. For this the WaterJet Technology Association is grateful.

The authors have also benefitted by writing their papers because the best way to deepen understanding of any human situation is to attempt to describe it.

— George A. Savanick, Ph.D.
President

A primary mission of the WJTA is to provide a means of communication within the industry. These proceedings are a major contribution towards that goal. This tenth volume represents the state-of-the-art in water jet technology and research in 1999. It is also a world-wide view, as evidenced by the number of international contributions presented.

This conference will only be as good as what we put into it. The more practitioners who get involved and share in these meetings the more we will all get out of it. So, as you read these papers think of what knowledge you could contribute, and be ready for the next call for papers in the new millennium.

These papers cover the breadth of our industry: they include abrasive entrained, plain water, pulsating, cryogenic, and cavitating jets. Form theoretical studies and mathematical models to field proven equipment is presented. Applications include: cutting, machining, surface preparation, cleaning and demolishing.

I see a bright future for our industry. New applications are being found every day in a wide variety of industries. We are developing ever more capable equipment and practitioners. Our successes will insure a continually expanding market.

— John Wolgamott
Chairman of the Board,
WaterJet Technology Association

Preface

Modern waterjet technology was sparked in the early 1970s by commercialization and conference interactions. The communication among developers and users, including people from industry, academia, and government, has been the fuel that has kept this technology progressing.

The 1999 American Waterjet Conference is the tenth in this biennial series. The first conference was held in Golden, Colorado, in 1981. Since this time great advances have been made in waterjet technology. Today, the worldwide waterjet business is in the 1.5 to 2 billion dollar range, and the technology is used in over 20 industries.

The biennial conferences organized by the WaterJet Technology Association (WJTA) have become the largest conferences worldwide that focus on this technology. The number of attendees and papers have been steadily growing to over 400 and 75, respectively. Most important and unique to these conferences are the short course offered prior to the conference, the equipment exhibitions, and the technical tours to local industrial sites.

The papers in this conference proceedings are contained in two volumes. As with previous proceedings, the first volume is more related to research, while the second is more related to applications. In addition, a special workshop on contractors' applications is included in Volume 2. For the first time, a CD-ROM is being distributed to provide electronic access to the papers.

A large number of people contributed to the success of this conference. First to be recognized are the authors who submitted their work for publication, presented their work, and responded to questions. The efforts of the conference chairman Pat DeBusk in facilitating the technical tours and the contractors' workshop have been most critical to the success of this conference. The paper review committee members, Prof. Thomas Kim, Bruce Wood, and Forrest Shook, provided timely and scholarly reviews of the papers. They deserve special recognition and thanks for their contributions. Birenbaum and Associates continues to provide excellent administrative support to WJTA. They are especially recognized for organizing the conference and managing the publication of this proceedings. Many thanks to Mark Birenbaum, Ken Carroll, LeAnn Hampton, and Lois Rodewald. Special thanks to Jan Tubbs for keeping up with my editorial demands and changes, logging abstracts and papers, sending review requests, notifying authors, and communicating with numerous national and international authors in a most pleasant and professional way. Kristie Hammond of Hammond Publications has been most helpful in preparing the table of contents and the program schedule and working most efficiently with the WJTA staff. Finally, I would like to thank Nadia, my wife, for her understanding, help, and support and my two sons Ameer and Rami for their continued patience and fascination with waterjets.

I am certain that this proceedings will provide a valuable contribution to the field of waterjet technology and will significantly enhance our knowledge.

— Mohamed Hashish, Ph.D.
Editor

TABLE OF CONTENTS

Proceedings of the 10th American Waterjet Conference

Session R1: Jet Material Interaction

Session R2: Modeling Studies

Session R3: Pressure Effects

Session R8: Abrasives, Recycling and Comminution

Session A1: Rock Cutting

Session A2: Pumps and High Pressure Components

Session A3: Cleaning and Rust Removal

Session A4: Special Environments Demilitarization, Nuclear and Quarries

Session A5: Surface Preparation and Decoating

Session A6: Factory, Field Business and Safety Aspects

Session A7: Cavitating and Pulsating Jet

AUTHOR INDEX

Proceedings of the 10th American Waterjet Conference

C

D

F

G

H

HARKESS, M.

"Hyper Pressure Waterjet and Abrasive Waterjet Cutting"

HASHISH, M.

"Cutting and Drilling at 690-MPa Pressure"
"Demilitarization of Chemical Weapons Using High Pressure Ammonia Fluid Jets"
"Status and Potential of Waterjet Machining of Composites"

HENNING, A.

"Non-Linear Dynamics in Modeling of Cutting Edge Geometry"
"Modelling of Turning Operation for Abrasive Waterjets"

HERBIG, N.

"Calculation of the Efficiency Rate of High Pressure Pumps"

HIBBARD, C.

"Enhancement of Ultrahigh-Pressure Technology with LN_2 Cryogenic Jets"
"Measurements of Water-Droplet and Abrasive Speeds in a Ultrahigh-Pressure Abrasive-Waterjets"

HLAVÁC, L.M.

"Abrasives for High Energy Water Jet: Investigation of Properties"
"Quick Method for Determination of the Velocity Profile of the Axial Symmetrical Supersonic Liquid Jet"
"The Analysis of Magnetohydrodynamic Effects - New Approach to the Pulse Jet"
"Theoretical and Experimental Investigation of a High Energy Waterjet Efficiency on Thermally Treated Rocks"

HLAVÁCOVÁ, I.M.

"Quick Method for Determination of the Velocity Profile of the Axial Symmetrical Supersonic Liquid Jet"
"The Analysis of Magnetohydrodynamic Effects - New Approach to the Pulse Jet"

HOLMQVIST, G.

"Equipment for Discretisized Abrasive Waterjet Milling—Preliminary Tests"
"Influence of Abrasive Waterjet Cutting on the Fatigue Properties of Extra High-Strength Steel"

HOWELLS, W.G.

"SUPER-WATER® Jetting Applications from 1974 to 1999"

HUANG, W.P.

"Application Examples of Waterjet Cutting Processing"
"Extended Technologies for Ultra High Pressure Waterjet Cutting System"

HUANG, Z.

"A Study of Near Well-Bore Formation Processing with High Pressure Rotating Water Jets"

I

ILIAS, N.

"Laboratory Experiments for Cleaning and Polishing the Surface with Hydraulic Jets"
"The Influence of Rocks Parameters During the Cutting Process Using High Pressure Water Jets"

J

K

L

M

N

O

ORTU, G.

"Rock Disintegration Using Waterjet-Assisted Diamond Tools"

OTTERSTATTER, K.

"Hyper Pressure Waterjet and Abrasive Waterjet Cutting"

P

PECMAN, S.

"Removal of Hard Coatings from the Interior of Ships Using Pulsed Waterjets: Results of Field Trials"

PENG, H.J.

"Application Examples of Waterjet Cutting Processing"
"Extended Technologies for Ultra High Pressure Waterjet Cutting System"

PORTER, S.

"The Carving of the Millennium Arch"

PUDE, F.

"Experimental and Theoretical Investigation of the Decoating Process by Pure Waterjet"

R

RADJKO, B.V.

"Analytical Investigations of Hydraulic Breaking Coefficient of Coal Seams"

RADONS, G.

"Non-Linear Dynamics in Modeling of Cutting Edge Geometry"

RADU, S.

"Laboratory Experiments for Cleaning and Polishing the Surface with Hydraulic Jets"
"The Influence of Rocks Parameters During the Cutting Process Using High Pressure Water Jets"

RAMULU, M.

"Modeling and Simulation of Pressure Fluctuations in High Pressure Waterjets"
"Modeling the Waterjet Contact/Impact on Target Material"
"Simulation of Displacement Fields Associated with Abrasive Waterjet Drilled Hole"

RAN, H.

"High Pressure Water Dynamic Fracture of Rock"

RUPPENTHAL, M.

"Purchasing and Running a Profitable Abrasive Waterjet"

S

SACQUITNE, R.

"Hyper Pressure Waterjet and Abrasive Waterjet Cutting"

SANDYS, E.

"The Carving of the Millennium Arch"

T

Y

Z

Proceedings of the
10th American Waterjet Conference

August 14-17, 1999 • JW Marriott Hotel • Houston, Texas

omnipress
omnipro-CD™

Adobe Acrobat®

10th American Waterjet Conference
August 14-17, 1999: Houston, Texas

INFLUENCE OF ABRASIVE WATERJET CUTTING ON THE FATIGUE PROPERTIES OF EXTRA HIGH-STRENGTH STEEL

G. Holmqvist and K.M.C. Öjmertz
Chalmers University of Technology
Göteborg, Sweden

Y. Bergengren and M. Fronzaroli
SSAB Oxelösund AB
Oxelösund, Sweden

ABSTRACT

The erosion based material removal processes active in abrasive waterjet (AWJ) cutting has virtually no thermal impact on the material and produce none or minor residual stresses. The process is therefore an interesting alternative for machining of fatigue exposed structures. The present study presents results from fatigue testing of abrasive waterjet cut specimens in extra high-strength steel. The tested material is a quenched and tempered steel having a yield strength of more than 1100 MPa. The main applications for these extra high strength steels are in heavy construction equipment, cranes, offshore equipment and other highly stressed applications. Many of these applications are fatigue loaded, and thermally cut surfaces are usually the second most common initiation site for fatigue cracks, after weldments. In the study three different AWJ cut qualities were tested. The results show that the cut quality does not significantly affect the fatigue life. Further, the results show a large scatter. Possible reasons for this scatter are discussed. Even though the scatter is large, all test specimens showed a fatigue life longer than what is specified in a widespread design guideline covering thermal processes.

1. INTRODUCTION

1.1 Background

The modern high-strength materials emerging during the last decades have posed an important challenge to the steel industry, and considerable efforts have been made to increase the strength and the general applicability of steel. In the business segment of "heavy plate", with dimensions of 5 mm and thicker, this has led to the development of quenched and tempered martensitic structural steel grades with yield strengths of more than 1100 N/mm^2.

The advantage of using these new steels is the possibility to build extremely light constructions using conventional production methods. Typical applications of the 1100 N/mm^2 yield strength structural steel so far have been in mobile cranes and mobile bridges.

There are two major challenges of using these new structural steels. Firstly, they are not yet covered explicitly by design codes and standards. This leaves many decisions to be made by an experienced design engineer. Secondly, it is a well-known fact that control of the fatigue phenomenon becomes increasingly more important in light-weight structures, due to the higher stresses in the structure.

Preliminary tests performed previously have shown that AWJ cut surfaces can show a relatively good fatigue performance, especially when compared to other cutting methods such as flame cutting. The aim of the present paper has been to study the fatigue performance of AWJ cut surfaces and to try to correlate with existing fatigue design guidelines. Moreover, an effort has been made to evaluate the influence on fatigue performance related to the chosen cutting speed.

Apart from the supposed increased fatigue performance of AWJ cut surfaces, AWJ also presents other advantages in cutting of these steel grades. In comparison with flame cutting, there is no risk of thermally induced hydrogen cracking. Also, the risk of softening of small details cut from plates in these grades is eliminated.

1.2 Alternative Cutting Methods Used for Cutting Extra High-Strength Steels

The most common method for cutting of extra high strength steels today is ordinary flame cutting. However, methods like plasma cutting and laser cutting are increasingly used. All these methods have some disadvantages, since they produce a heat affected zone (HAZ) at the cut surface. This HAZ is typically 4-10 mm for flame cutting, depending on the thickness of the plate. For plasma cut surfaces, the HAZ is less, typically 2-5 mm. Laser cutting gives the least HAZ, 0.4-3 mm. This soft HAZ is disadvantageous in some applications.

Flame cut surfaces are known to give relatively poor fatigue strength, which is attributed to the roughness of the surface, microcracks in the cut surface and the loss of material strength in the HAZ. Moreover tensile residual stresses below the surface also enhance the initiation and further growth of fatigue cracks, even though the residual stress in the superficial surface layer is compressive. The poor fatigue performance of flame cut surfaces is recognized in fatigue design standards and guidelines for steel structures, as for instance in the guidelines of the International Institute of Welding, IIW (Hobbacher, 1996). These standards and guidelines do not distinguish between flame cutting, plasma cutting and laser cutting, the design fatigue strength is the same. These standards and guidelines do not cover abrasive water jet cutting.

For a high strength steel, having a fatigue limit given as stress range of 350 MPa ($\sigma_{min} \approx 0$, $\sigma_{max} = 350$ MPa), the fatigue design strength at long lives may be as low as 60 MPa for a manually flame cut surface.

2. EXPERIMENTAL PLAN AND EQUIPMENT

As the surface integrity has an important influence on fatigue properties, different AWJ cut qualities were tested. Fatigue test specimens in three different surface qualities were tested. Surface measurements were made on test specimens prior to fatigue testing.

2.1 Strategy and Test Set-up for AWJ Cutting

A standard venturi cutting head for abrasive waterjet cutting being traversed by a 2½-axis gantry robot manipulator was used for cutting the test specimens. Abrasives were gravity fed into the cutting head and high-pressure water was supplied from a commercially available intensifier pump unit.

To predict adequate traverse rates for the three qualities to be cut, the empirical cutting model (eq. 1), presented by Zeng and Kim (1993), was used.

$$u = \left(\frac{N_m \cdot P_w^{1,25} \cdot \dot{m}_w^{0,687} \cdot \dot{m}^{0,343}}{C \cdot q \cdot h \cdot D^{0,618}} \right)^{1,15} \qquad (1)$$

where: N_m = machinability number; h = depth of cut [mm]; D = mixing tube diameter [mm]; u = traverse rate [mm/s]; P_w = water pressure [MPa]; $\dot{m}_w$ = water mass flow [l/min.]; $\dot{m}_a$ = abrasive mass flow [g/sec]; q is the quality index, where q=5 is a smooth surface finish and q=1 corresponds to the maximum cutting speed for the present depth of cut (thickness) *h*. For such a model to be reliable, care must be taken to ensure that the model is used under conditions similar to those under which it was established. According to Singh and Munoz (1993) the recommended range of parameter values for validity of the model in eq. 1 is as follows: P_w = 240 to 375 MPa; d_n = 0.18 to 0.45 mm (orifice diameter); D/d_n = 2.5 to 4.5; $\dot{m}_a / \dot{m}_w$ =0.12 to 0.25.

The material's machinability number was determined by milling a slot using a known parameter setting. The depth of the slot, *h*, was probed by a thin 30 mm wide metal sheet, which consequently indicates at what plate thickness full penetration would have occurred along the probed path. The machinability number was determined using eq. 1 setting the quality index to 1. A series of cut qualities, from q=1 to 5 in steps of 0.5, was subsequently produced in the material. By visual inspection, qualities 1, 2 and 3 were chosen as being of greatest industrial relevance, and they were consequently the selected grades for cutting of the fatigue test specimens (figure 1). Table 1 shows the cutting parameters used.

2.2 Mechanical Properties of Steel Used for Specimens

The steel used for the tests throughout this paper had the following chemical composition[1]:

C* max (%)	Si* max (%)	Mn* max (%)	P max (%)	S max (%)	B* max (%)	Nb* max (%)	Cr* max (%)	V* max (%)	Cu* max (%)	Ti* max (%)	Al* total min (%)	Mo* max (%)	Ni* max (%)	N max (%)	CEV typical value (%)
0,21	0,50	1,20	0,10	0,20	0,005	0,04	0,80	0,08	0,30	0,02	0,02	0,70	3,0	0,015	0,70

*) Intentional alloying elements

The material has the following guaranteed mechanical properties:

Yield strength $R_{p\,0,2}$ min [N/mm^2]	Tensile strength R_m [N/mm^2]	Elongation [A)] A5 min [%]	Toughness [B)], transverse Charpy-V test pieces 10*10 mm [C)], min. [J]
1100	1200-1500	10 (12)	27 at -40°C

A. The value is valid for test pieces transverse to the rolling direction. For longitudinal pieces the values are 2 units higher.
B. Average impact energy of three tests. Single value min. 70% of specified average.
C. For plate thickness under 12 mm subsize Charpy-V specimens are used. The specified minimum value is then proportional to specimen cross section.

The specimens used in this paper were taken from a 10 mm WELDOX 1100E plate with the following mechanical properties:

Yield strength $R_{p\,0,2}$ min [N/mm^2]	Tensile strength R_m [N/mm2]	Elongation A5 [%]	Toughness, transverse. Subsize Charpy-V test pieces 7,5*10 mm, [J]
1261	1386	11	37 at -40°C

2.3 Experimental Details

Fatigue testing has been performed in a servo-hydraulic testing machine with a maximum capacity of 500 kN. The stress ratio, $R=\sigma_{min}/\sigma_{max}$, was approximately R=0 and the testing frequency 8-12 Hz, using a sinusoidal loading shape. Failure criterion was a complete separation of the testing specimen. The specimen was simply clamped in the grips of the testing machine followed by dynamic loading. Linearity of the test set-up was checked by strain gauges on both sides of the specimen. Figure 2 shows the fatigue test set-up and figure 3 shows the specimen geometry. The fatigue test specimens were made to specification and cut longitudinal with the rolling direction.

---

[1] Commercial name: WELDOX 1100E manufactured by SSAB Oxelösund AB.

Fatigue testing has been performed at two stress range levels, $\Delta\sigma$=750 MPa and $\Delta\sigma$=550 MPa. In this way, the number of loads can be plotted versus the stress level in a log-log diagram, where the resulting curve is known as the S-N curve (in some literature the Wöhler curve). Thus, the slope of the S-N curve can be determined. Five specimens of each cut surface quality, q=1, q=2 and q=3, were tested at each level.

The original plate surface of the specimens was machine ground prior to testing, to avoid initiation at this position. The edges (corners) of the specimens were not removed, to have realistic testing conditions.

For surface measurements an interference microscope was used. This measuring technique has the advantage of being a quick and non-contacting method. Its main disadvantage is that the possible measuring area is comparatively limited. The interference microscope used was a Wyko RST plus. This is a white light vertical scanning instrument that works with one or several exchangeable magnification objectives. The vertical measurement range is 0.5 mm with a resolution better than 10 nm. Three test specimens of each quality were chosen for the measurements. On each test specimen, measurements were made at 2 different locations, each replicated 3 times, close to the top and bottom edge. Measurement areas as large as possible were chosen. The measured area was 2.6x1.9 mm at the bottom edge of the surfaces and at the top edge 1.2x0.9 mm.

3. RESULTS

The fatigue test results are summarized in figure 4 and table 2. As seen in the figure there is a large scatter in the fatigue test result for all three surface qualities. For instance, the fatigue life at a stress range of 550 MPa ranges from 41000 to 1 million load cycles for surface quality q=2. This is considered as an extraordinarily large scatterband.

The average fatigue life for each surface quality is given in figure 5. The average fatigue life was lowest for the surface quality q=1, having the roughest surface. Somewhat surprising is that the intermediate surface quality q=2 shows the highest average fatigue life of the three. The smoothest surface, q=3, gives higher average fatigue life than q=1 but lower than q=2. However, the large scatter in test results makes conclusions difficult. Obviously, there is a trend towards longer fatigue life with the smoother surface qualities, but individual specimens give rather short fatigue lives.

For design purposes it may therefore be advantageous to put the result of the three surface quality indexes together and compare with so called FAT classes for structural steels (Hobbacher, 1996). The FAT class is defined as the fatigue strength at 2 million load cycles. (Consequently, e. g. FAT 140 means a fatigue strength of 140 MPa at 2 million cycles). Together with the slope, given by the factor *m*, the full design fatigue curve can be established. The fatigue strength corresponding to a certain life, N, can then be calculated using eq. 2, which is valid for the linear part of the S-N curve, that is fatigue lives of less than 5 million load cycles.

$$\Delta\sigma = FAT \cdot \left(\frac{2 \cdot 10^6}{N}\right)^{-\frac{1}{m}} \qquad (2)$$

In figure 6, the present test results (WELDOX 1100) have been plotted with results from previously performed tests on other steel grades and compared with different FAT classes. The previous test results represent a surface quality index of approximately q=2. These test specimens differed from those presently used, in that the original plate surface was not ground, and in that corners were removed. The steel grades tested were structural steels with different yield strengths. Two abrasion resistant steel plates have also been tested with hardness of 400 HB and 600 HB, respectively. The thickness of the plates were 8-15 mm. FAT class 140 together with m=3 has been used as a reference, which corresponds to the highest FAT class for machine flame cut or sheared surfaces. In this class is generally required that corners are removed, no cracks or imperfections are discernible by inspection. Also, FAT 160 with m=3 is shown in the diagram. For comparison, a manually flame cut surface corresponds to a FAT class of approximately 100.

As shown in figure 6 all data are above the FAT 140 design curve with m=3. Therefore using this class may be recommended for design of components cut with abrasive waterjet cutting.

Studies of the fracture surfaces by optical stereo microscopy showed that the fatigue cracks of all specimens tested at a stress range of 750 MPa are initiated not at a corner, but on the AWJ cut surface. For surface index q=1, the fatigue cracks are initiated at the striated part of the cut surface. This behavior is not as apparent for surface indexes q=2 and q=3, but fatigue cracks are initiated on the cut surface.

For specimens tested at a stress range of 550 MPa, the majority of the fatigue cracks are initiated at the corner of the specimen. However it was noted that, on the specimens showing the shortest fatigue lives of surface index q=2 and q=3, the fatigue cracks were instead initiated on the cut surface. This indicates that on some specimens there might be relatively rare irregularities or imperfections that act as initiation sites and thereby reduce the fatigue life.

As the quality index used in the test set-up is process specific, standard surface parameters were assessed, which can be of use for comparisons. As parameters were used Sa, which describes the roughness of the surface, and St (maximum peak to valley distance) which is an estimation of the maximum amplitude of the surface waviness. It was noted that Sa varies only slightly between top and bottom for all qualities, as expected. The Sa value was approximately 4 μm (cut-off length of 0.8 mm). Figure 7 shows the general increase of St towards the bottom of the cut.

4. DISCUSSION

For design purposes, this study shows that abrasive waterjet cut surfaces may show large scatter in fatigue strength, implying that test results on few specimens should be used with care.

The large scatter in the fatigue test result for each surface quality makes it difficult to link the fatigue life to the major surface geometry features that are produced in different cut qualities. It is generally known that abrasive particles from AWJ cutting may be embedded in the surface. Singh and Jain (1995) has indicated that these may cause a wedge effect introducing tensile stresses that in turn initiate fatigue cracks. As this phenomenon applies to all surfaces this effect could be an explanation why no clear correlation between the fatigue strength and the surface quality was found. This is a topic for further investigations on fractured specimens from this study.

Moreover, a scanning electron microscopy (SEM) study may show what kind of surface irregularities that are critical for the fatigue life. This information may be used for more detailed surface studies, focusing on the critical irregularities.

A further study on the impact of AWJ parameters such as abrasive type, grain size and feed rate would yield important information for optimizing cutting parameters for producing elements for fatigue exposed structures.

5. CONCLUSIONS

1. The present results indicate that a class of FAT 140 with a slope of the S-N curve given by m=3 can be used for design of components with abrasive water jet cut surfaces.
2. Fatigue test results show a large scatter. The practical consequence of this is that the surface quality index has little importance for the lower bound fatigue strength. It also implies that test results on few specimens should be used with care.
3. Looking at the average fatigue life, a trend is seen in that the intermediate surfaces quality q=2 shows the longest fatigue life, while the roughest surface quality index q=1 produces the shortest fatigue life.
4. Surface measurements indicate a correlation with the fatigue testing result for surface quality q=1, that is the roughest surface produces the shortest fatigue life. For the two surface qualities with smoother surface, q=2 and q=3, there is no major difference in surface roughness.
5. A large scatter in result indicates either inconsistent surface quality of individual specimens or a low density of sharp irregularities in the cut surfaces that will influence the fatigue life significantly.

6. ACKNOWLEDGMENTS

The authors wish to thank the Swedish National Board for Industrial and Technical Development (NUTEK), ABB I-R Waterjet Systems AB, GANEX AB, Kimblad Technology AB, Projet AB, SAAB AB and Waterjet Service AB for their support. We also thank Mr. Henrik Westberg at the Dept. of Production Engineering at Chalmers University of Technology for performing the surface measurements.

7. REFERENCES

Hobbacher, A.: "IIW Fatigue design of welded joints and components", *Abington publishing*, 1996.

Singh, P.J. and J. Munoz: ”Cost Optimization of Abrasive Waterjet Cutting Systems”, *Proc. 7th American Water Jet Conference*, WJTA, St Louis, MO, USA, pp. 191-204, 1993.

Singh, J. and Jain S. C.: "Mechanical Issues in Laser and Abrasive Water Jet Cutting", JOM, *The Minerals, Metals and Materials Society,* Volume 47, Number 1, January, pp. 28-30, 1995.

Zeng, J. and Kim, T.J.: ”Parameter Prediction and Cost Analysis in Abrasive Waterjet Cutting Operations”, *Proc. 7th American Water Jet Conference,* WJTA, St Louis, MO, USA, pp. 175-190, 1993.

Table 1. AWJ parameter settings.

N_m (machinability number)		75.4
h (depth of cut) [mm]		10.3
D (mixing tube diameter) [mm]		0.8
d_n, (orifice diameter) [mm]		0.25
P_w (water pressure) [MPa]		315
$\dot{m}_w$ (water mass flow) [l/min.]		1.67
$\dot{m}_a$ (abrasive mass flow) [g/s]		5
Abrasives		Garnet, #80 Mined from rock
u (traverse rate) [mm/s]	q=1	3.71
	q=2	1.67
	q=3	1.05

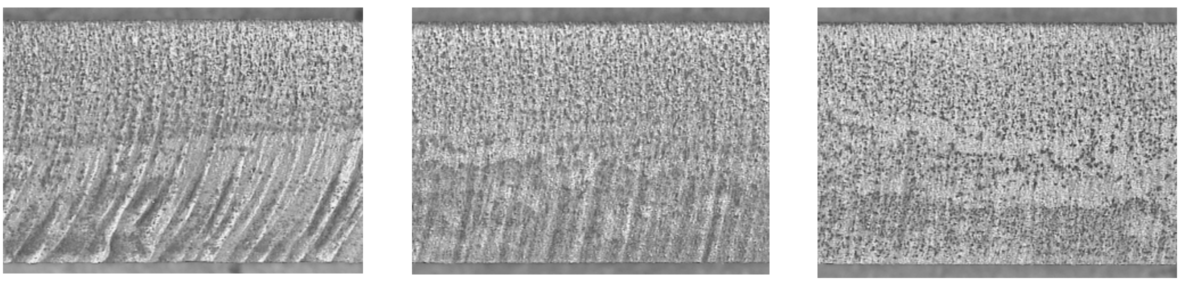

a b c

Figure 1. Selected AWJ surfaces qualities for the study.
Corresponding to a quality index of a) q=1, b) q=2 and c) q=3.

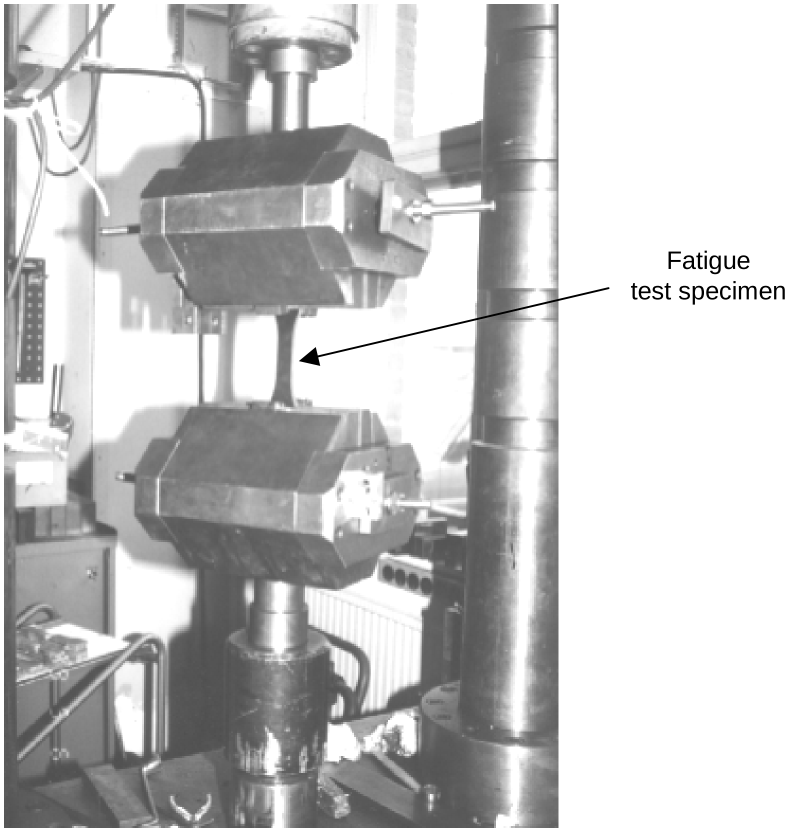

Figure 2. Set-up for fatigue testing.

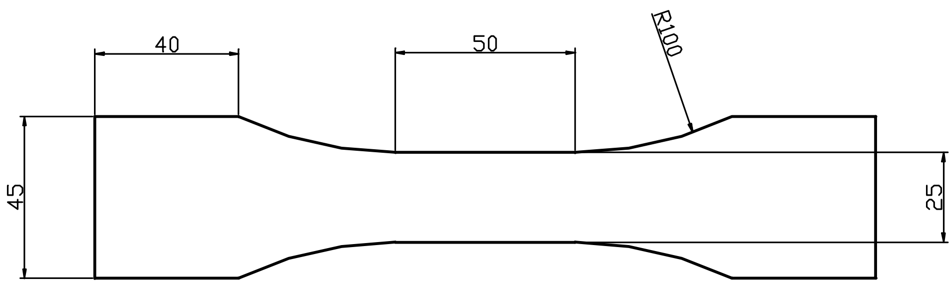

Figure 3. Fatigue test specimen geometry. Plate thickness=10 mm.

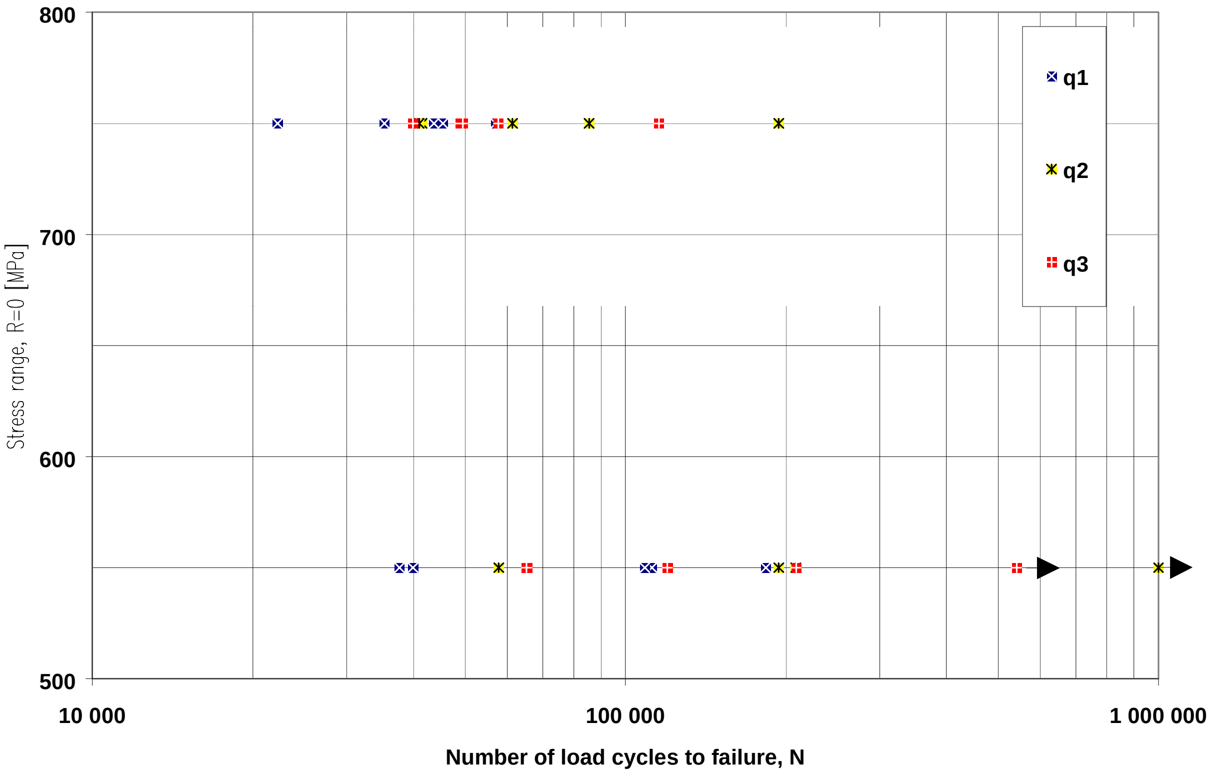

Figure 4. Fatigue test results of the three surface qualities.
Arrows near a point indicate that testing was stopped without failure.

Table 2. Fatigue test results showing the fatigue life (number of cycles).

Stress range [MPa]	q=1	q=2	q=3	Stress range [MPa]	q=1	q=2	q=3
750	22 256	193 973	115 578	550	183 345	193 973	542 000[1]
750	43 711	61 403	49 027	550	112 117	1 000 000[1]	209 061
750	45 440	41 536	49 498	550	108 737	208 634	119 946
750	35 301	41 045	39 946	550	39 932	57 856	65 407
750	57 103	85 434	57 741	550	37 661	41 073	65 236

[1] Testing was stopped without failure of the specimen

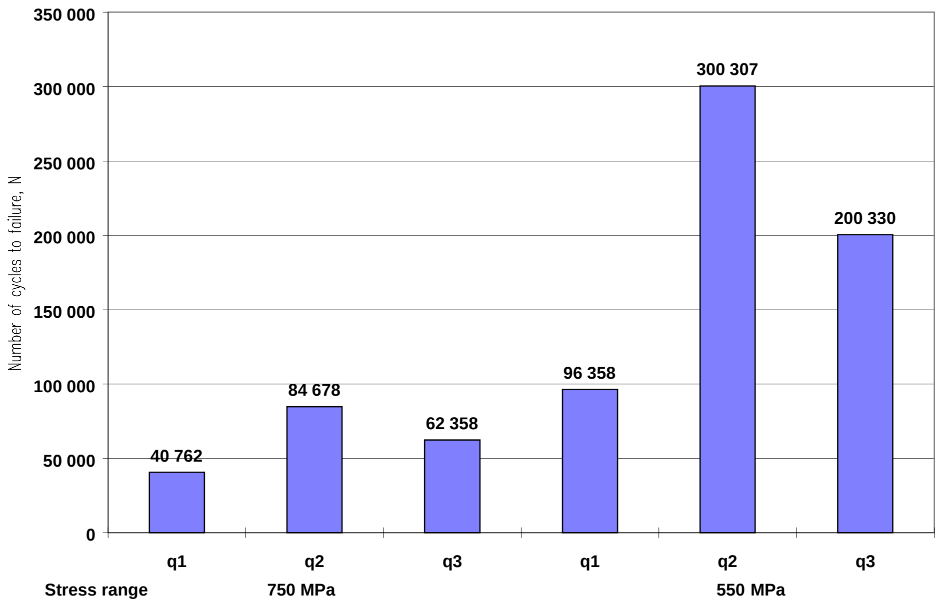

Figure 5. The average fatigue life of each surface quality at a stress range of 750 MPa and 550 MPa respectively.

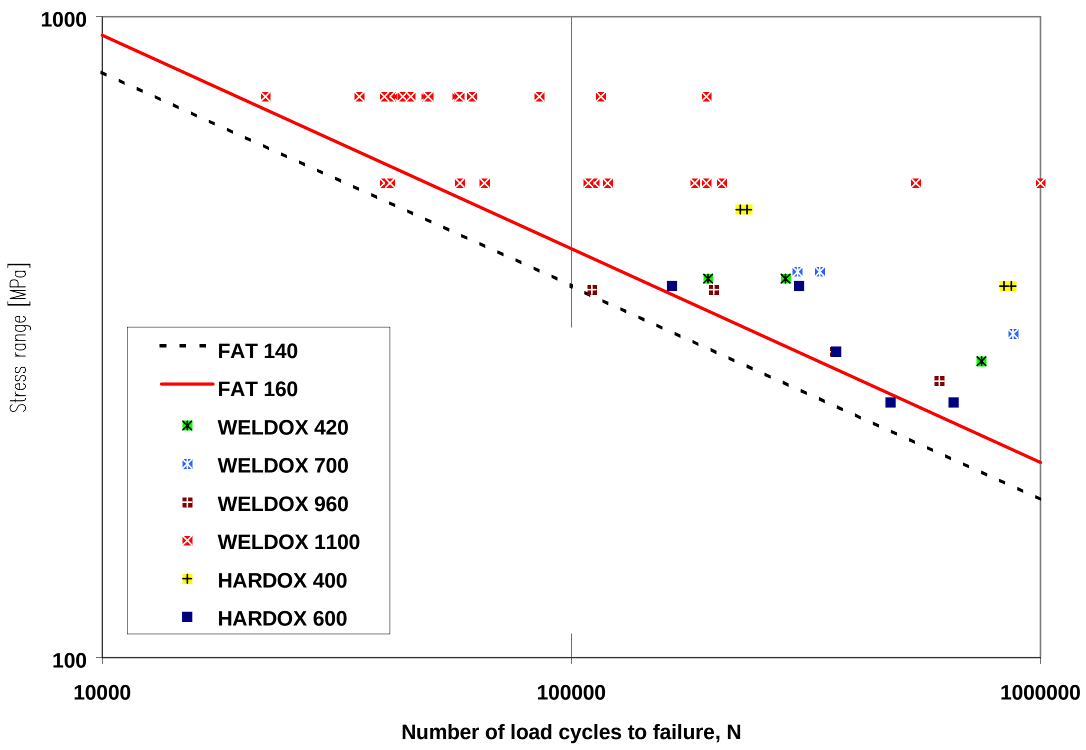

Figure 6. Present and earlier fatigue test results of specimens with abrasive water jet cut surfaces. WELDOX 420 for instance indicates a yield strength of 420 MPa. HARDOX 400 indicates a Brinell Hardness of 400.

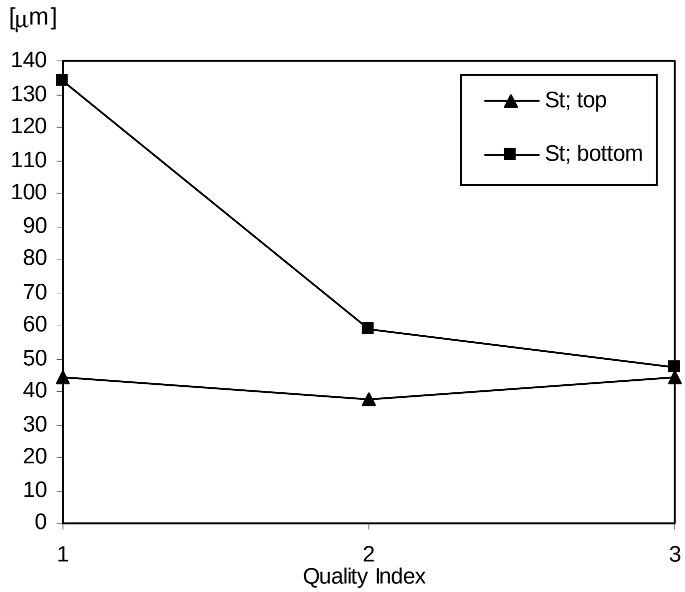

Figure 7. Maximum peak-to-valley distance (St) from interference microscopy surface measurements. Locations: near the top of the cut and near the bottom edge of the cut.

10th American Waterjet Conference
August 14-17, 1999: Houston, Texas

Paper **2**

NON-LINEAR DYNAMICS IN MODELING

OF CUTTING EDGE GEOMETRY

T. Ditzinger, R. Friedrich
Institute for Theoretical Physics III
University of Stuttgart
Stuttgart, Germany

A. Henning, G. Radons
Fraunhofer Institute
Production Engineering and Automation
Stuttgart, Germany

ABSTRACT

Abrasive waterjet cutting has already been established in many fields of industrial production. Yet limited cutting performance and cutting edge quality hinder a wider distribution of abrasive cutting systems. As a major limiting factor process immanent step propagation in the cutting front and thus striation formation can be spotted. In this work we present new nonlinear approaches to the instability problem. In the simplest approximation the front dynamic is described by a first order nonlinear partial differential equation (PDE) of Hamilton-Jacobi type. The relevant solutions typically develop shock structures within finite time. These are understood by considering the evolution of associated Lagrangian manifolds in phase space. On this level only the time-averaged behavior of the cutting front but no instability is found. The inclusion of higher order derivatives in the PDE, however, can explain the observed ripple formation. This is shown by numerical simulations of the resulting PDE, which is related to the Kuramoto-Sivashinsky equation known from other erosion phenomena. Our simulations are compared with edge cutting experiments where multiple reflections of the waterjet are avoided. These approaches provide a better understanding of the involved processes, which ultimately should result in a reduction of striations and a better cutting performance.

1. INTRODUCTION

The water jet technology has already today many industrial applications. Especially when cutting hard-to-machine materials and complex geometry conventional manufacturing processes can be replaced or completed using the high flexibility and universality of this process. For a further spreading of this innovative technology, also in new applications, however both the precision, and the attainable cutting performance must be improved. Therefore profound investigations are necessary for the improvement of the knowledge of the process as well as for its optimization [WES98, HEN98d].

The attainable precision of the cutting process, however, is strongly limited by structure formation at the bottom cutting edge surface. With higher feed-rates unwanted grooves and striations occur at the surface. To avoid these structures sub-optimal cutting velocities are used presently. The small attainable cutting performance thereby leads to high costs of this process. Despite of high costs the procedure finds increasing spreading in the industry already today due to its process specific advantages. By a better control of the process and avoidance or reduction of structure formation at the cutting edge the economic disadvantages could to a large extend be compensated and a spreading of this innovative technique could be supported [WES99].

In this paper the formation of surface structures during the cutting process is analyzed using methods of non-linear dynamic modeling on the basis of the physical behavior of the process. The major object of these modeling approaches is to gain better understanding of the mechanisms of surface formation at the cutting edge. With the identification and intelligent variation of significant factors striation formation may be better controlled and both cutting performance and quality may be improved.

2. CONVENTIONAL PROCESS MODELLING

Modeling of the process behavior plays an important role for the industrial use of the technique. With the gained information jet parameters can be chosen and adapted to the actual cutting task. Also for integration in CAM systems process modeling is necessary [HEN98a]. With the strongly growing distribution of this technique and demands for higher precision and performance the control of the process and the knowledge of geometry which can be expected become more and more important. Because of the very complex and often nonlinear behavior of the cutting contour the modeling of the cutting process is mostly reduced to few significant parameters with limited range. There are three basic approaches to modeling of the cutting contour: functional, analytical, and phenomenological.

Existing approaches of modeling are limited, however, almost exclusively to an experimentally determined correlation between the parameters and processing factors e.g. the maximal cutting depth. Here different factors and materials are considered. The semi-empirical models thereby reduce the process to a functional correlation between the cutting depth and the handling parameters with empirically determined exponents and constants. Thereby their validity is often limited to a small parameter ranges and special boundary conditions (material, abrasives etc.).

Examples of such models are found in the literature among others in Zeng and Kim [ZEN92], Hashish [HAS88] and Blickwedel [BLI90].

Analytic approaches describe the qualitative effect of individual abrasive particle impacts at the workpiece. From hydraulic parameters the energy distribution and thus the erosion effect of particles is calculated (e.g. [RAJ93, NIU97, FUK95]). With this complex system however only few of the relevant parameters are considered. With the help of time discrete simulations the erosion process is represented qualitatively and adapted quantitatively with respect to processing and material constants (e.g. [NIU97, KOV96]). The qualitative description could be improved by the use of a continuous energy model [SAW97]; nonlinear and stochastic effects however were not considered.

First descriptions of the dynamic process were given by phenomenological models [HAS88, BLI90, GUO94]. According to those the quasi-stable and approximately cyclic progress of the cutting process the cutting surface is formed by step propagation. By the use of high-speed cameras first detailed information about the process and the step propagation could be gathered (e.g. [HAS95, OHL95]). Similar process phases could be identified also by evaluation of impact sound signals [MOM95d, MOH95]) and by gravimetric measurements (e.g. [FEK94, OHL94]). Due to the pure two-dimensional photometric analysis, however, no predicates about the full spatio-temporal behavior of the cutting front could be obtained.

The three dimensional structures occurring at the cutting surface could not be explained completely by a considering the process in the cutting plane alone. Especially in the rough cutting zone spatial effects in the form of grooves and striations are found. Also the curvature of the cutting front leads to spatial effects of the kerf when cutting a complex geometry. Existing analytic or semi-empirical modeling approaches focus mainly on the two dimensional behavior of the process and therefore cannot describe these effects. In most modeling approaches only the topology of the surface was measured and described by characteristic values (e.g. [CHA95, KOV91b, TAN86]). Zeng describes in [ZEN92] the surface on base of semi-empirical models by defining surface quality areas. The reduction of the process to only few parameters reduces the complexity of the process significantly. For the end user this makes control of the process much easier but makes no statement about the real spatio-temporal processes and the formation of striation structures.

Guo [GUO94] describes a spatial behavior of the cutting process transverse to the cutting plane. As the abrasive jet leaves the workpiece it shows a complex spatial and temporal behavior indicating a coupled longitudinal and transversal motion and a temporally inhomogeneous advancement of the cutting front. Similar to Guo, also Zeng [ZEN97] and Chao [CHA95] use Fourier analysis for the description of the occurring striation at the surface. So significant wavelengths in different quality areas (i.e. workpiece depths) could be detected. The results of these investigations thereby reach from the identification of an individual significant oscillation [CHA95] up to purely stochastic behavior [ZEN97]. Not only different significant jet parameters but also noise sources like machine vibrations during the process might lead to significant modifications in the development of the surface texture [CHA95]. One conclusion from these investigations is that inference of the process dynamics from a characterization of the static striation patterns is feasible only to a limited extent. First approaches to a more complete dynamical description of the process including coupling of topological and dynamical information is given for example by Ohlsen [OHL95] via photometric and gravimetric signal accommodation. So far these were applied exclusively for the description of the two-dimensional process. Beyond that only linear methods were used in modeling approaches. New fundamental information can be gained using dynamic modeling with nonlinear methods. With this not only the description of structure formation at the cutting edge can be improved but also a better understanding of the underlying process can be expected.

3. NONLINEAR MODELING

In the last years processes of pattern formation were studied in many physical, chemical and biological systems. This was done within the framework of nonlinear dynamics and synergetics [HAK78, BUS89]. Here especially instabilities e.g. of hydrodynamical processes were examined. Starting point is an averaged respectively a coarse-grained description of the system. Depending on the considered system the coarse-graining is over microscopic structures such as atoms, molecules, or grains, and temporal events (e.g. particle collisions or impacts). Mathematically the resulting continuum theories are specified by one or several nonlinear partial differential equations (PDE).

3.1 Experimental Setup

A description of the cutting dynamics by a PDE is based on the assumption of local interactions of the abrasive particles with the workpiece. From waterjet cutting experiments as in [HAS88] or [GUO94], however, we known that the abrasive particles are reflected elastically or inelastically several times as they move along the momentary cutting front. This amounts to a non-local interaction process since e.g. the effect of a secondary impact of abrasive grains at one location depends on the primary impact and the momentary cutting surface at some other location of the cutting front. This leads to the well-known striation patterns as in Figure 1a, where a typical ripple has a diameter (ripple wavelength) of the same order as the waterjet diameter, but has extensions (jet lag) in the feed direction much larger than the diameter of the incoming waterjet. In addition multiple reflections in the transverse direction lead to overhangs at the bottom of the REFcutting zone [GUO94]. Such a situation is mathematically difficult to describe since it needs the inclusion of non-local effects. Presumably this is also the reason why the origin of the structure formation is still not really understood.

In order to reduce the complexity of the experimental situation and to avoid these effects we designed and carried out experiments where multiple impacts of particles are largely avoided. This was done to gain information about effects of the primary erosion process at the first particle impact. The abrasive water jet was placed at the very edge of the material (Figure 1b-d). With this setup the incoming particles are reflected away from the workpiece edge after the first impact and do not erode other parts of the material by secondary impacts. Even with this reduced complexity of the experiment structures and ripple patterns were found. When the jet was placed on the position a=-d/2 (Figure 1d) even small jet lag effects, of course now smaller than the jet diameter, are clearly visible. Our results show that striation formation is already initiated with single impacts of particles. At first sight this may appear as an astonishing effect, we know, however, of related erosion experiments where pattern formation by single impacts was also observed [FIN65], [CAR77]. Possible connections with our jet cutting experiments, however, still have to be explored. The theoretical considerations presented below can be regarded as steps in this direction.

3.2 Basic Model Considerations

The main effect on the work-piece comes from the abrasive particles, which deteriorate the material through its impact by a combination of deformation wear and cutting wear [BIT63]. In this way we get a cutting front moving through the material. This front exhibits a non-trivial spatio-temporal dynamics which is only partially understood and which involves multiple reflections of the jet within the working piece. Our goal in this section is to present results of model considerations for the first impact of the jet on the material and to elucidate its consequences for the full cutting process including multiple reflections.

A simple model for the abrasive process is obtained as follows. We assume that the incident abrasive particles hit a flat work-piece perpendicularly (see Figure 2). They cause removal of material with a rate which is some material dependent function of their velocity and of their impact rate and therefore also of their density. Since in the jet velocity and density are inhomogeneously distributed in space, we model their effect on the work-piece as a function $J(\mathbf{r})$. A typical choice for J are single humped functions like the Gaussian, or polynomial functions, depending only on the radial coordinate $r=|\mathbf{r}|$. It turns out that only qualitative aspects of this function are important for the basic observable phenomena. Under cutting conditions this profile $J(\mathbf{r})$ will move across the work piece with velocity λ (much smaller than the particle velocities) in some direction, which we choose as the x-axis. More generally one could also consider a more complicated time-dependence $J(\mathbf{r},t)$, which arises e.g. for pulsed jets. The second important aspect of the abrasive process lies in its non-trivial dependence on the impact angle of the incoming particles with the momentary cutting front $z=S(\mathbf{r},t)$. This means that the rate of material removal is also a function F of the spatial gradient of $S(\mathbf{r},t)$, or more precisely of its absolute value.

Collecting these ingredients, we obtain for the rate of material removal the following equation

$$\frac{\partial S}{\partial t} = J(\mathbf{r},t) \cdot F(|\nabla S|) \qquad (1)$$

Both J and F are nonlinear functions of their arguments, and therefore equation (1) is a nonlinear partial differential equation (PDE) of Hamilton-Jacobi (HJ) type in two spatial dimensions. In principle one should add to equation (1) a viscosity term $\alpha\Delta S$, possibly higher order terms, and a spatio-temporal noise term describing smoothing effects due to the granularity of the abrasive materials and microscopic inhomogeneities of work piece material and jet respectively. At the moment we neglect these effects, but we will return to it in the next section below. The scalar function F is material dependent. For brittle material such as glass the wear is dominated by deformation wear and therefore the removal rate decreases monotonically from its maximum at $\theta=0$ (perpendicular impact) for increasing impact angles θ (measured with respect to the surface normal). For ductile material such as aluminum the maximum is obtained for some intermediate non-zero angle due to enhanced cutting wear [BIT63]. A sketch of these typical θ-dependencies is plotted in Figure 3.

With the relationship $|\text{grad}\, S(\mathbf{r},t)|=\tan(\theta)$ the θ-dependence of the wear determines the function F. As an example, assuming for the erosion rate the functional form $\sim\cos^2\theta$, which is appropriate for brittle material, one obtains

$$F(|\nabla S|) = \frac{1}{1+(\nabla S)^2} \qquad (2)$$

Assuming that at $t=0$ one starts the process with a flat, horizontally mounted work piece, we have to solve the Cauchy problem for Equation (1) with initial condition $S(\mathbf{r},t=0)=0$.

Due to the connection between HJ equations and Hamiltonian dynamics in phase space [LAN86], [ARN78], one can alternatively consider Hamilton's canonical equations of motion

$$\frac{d\mathbf{r}}{dt} = \frac{\partial}{\partial \mathbf{p}} H(\mathbf{r},\mathbf{p},t) \qquad (3a)$$

$$\frac{d\mathbf{p}}{dt} = -\frac{\partial}{\partial \mathbf{r}} H(\mathbf{r},\mathbf{p},t) \qquad (3b)$$

with Hamiltonian

$$H(\mathbf{r},\mathbf{p},t) = -J(\mathbf{r},t)\cdot F(|\mathbf{p}|) \qquad (4)$$

Hamilton's equations (3) have to be solved for all initial points lying on the surface $\mathbf{p}=0$ in phase space $(\mathbf{r},\mathbf{p})$ according to the correspondence $\mathbf{p}(\mathbf{r},t=0)=\text{grad}\, S(\mathbf{r},t=0)$ yielding the evolution of this Lagrangian surface $\mathbf{p}(\mathbf{r},t)$ in phase space [ARN78]. The function $S(\mathbf{r},t)$, which in a classical mechanics context has the meaning of an action, may either be obtained by integrating $\mathbf{p}(\mathbf{r},t)$ along suitable paths in coordinate space, or by solving in addition to equations (3a,b) the equation

$$\frac{dS}{dt} = \mathbf{p}\cdot\frac{d\mathbf{r}}{dt} - H(\mathbf{r},\mathbf{p},t) \qquad (5)$$

Equations (3) and (5) are the characteristic equations of the first order PDE (1) (see e.g. [LOG94]).

The solutions of the characteristic equations can be very complicated. This is due to the nonlinearities, which may even lead to chaotic trajectories in phase space [LIC83]. Furthermore the functions $\mathbf{p}(\mathbf{r},t)$ or $S(\mathbf{r},t)$ become typically multi-valued after a finite time [ARN78]. This multi-valuedness is resolved by the insertion of shocks by invoking some version of the entropy condition [WHI74], [LEV92], [ARN78], which has its origin in problems of gas dynamics. The importance and generality of these so-called viscosity solutions of HJ equations has been established only recently [CRA83]. They allow for a countable number of discontinuities in its derivatives known as shock waves, which identify them as generalized solution of the PDE. These solutions arise in the limit of vanishing viscosity terms in equations like Equation (1), i.e. in cases where curvature dependencies in the governing PDE are very small. A well-known and particularly simple example is the inviscid Burgers equation treated in many textbook on PDEs and its numerical solutions (see e.g. [WHI74], [LEV92]), which corresponds to the free particle Hamiltonian $H=p^2/2$.

In order to demonstrate some essential features we will in the following concentrate on the simpler two-dimensional case, where one neglects degrees of freedom transversal to the cutting direction x, and discuss its implications for the full three -dimensional problems later. For definiteness we assume for J a spatial variation of the following form $J(x)=(x^2-1)^2$ in the region of the jet $-1< x <+1$, and zero otherwise. Let us consider first the case of water jet drilling, i.e. the case $\lambda=0$. Then Equation (1) with the above-introduced brittle material characteristic (see Equation (2)) reads

$$\frac{\partial S}{\partial t} = \frac{\left(x^2-1\right)^2}{1+p^2} \qquad (6)$$

Constant prefactors on the r.h.s. of this equation are absorbed in the time variable t and determine its scale. The dynamical evolution of the "hole" $S(x,t)$ (starting from a flat surface at time $t=0$) according to equation (3) and (5) and the evolution of the corresponding curve $p(x,t)$ in phase space is found numerically and is shown for several instants in Figure 4 and Figure 5.

The phase portrait of the associated Hamiltonian flow is basically that of a one-dimensional anharmonic oscillator. It consists of an elliptic fixed point at the origin $(x,p)=(0,0)$ and of two lines of parabolic fixed points (for definitions see e.g. [LIC83]) at $p=+1$ and $p=-1$. The inhomogeneous rotation in phase space around the elliptic fixed point explains the evolution of the curve $p(x,t)$ from an initially flat curve $p(x,t=0)=0$. For later times as e.g. in Figure 5 the function $p(x,t)$ becomes multi-valued due to the continuing rotation in phase space. This leads also to a multi-valued $S(x,t)$ (with the typical ‘swallow tail’ singularities [ARN78]) if the initial points in phase space (endowed with initial values $S=0$) are evolved according to the characteristic equations (3) and (5). The correct branches are obtained e.g. by integrating the PDE (1) with an upwind method [LEV92] or other shock capturing schemes, which are known to approximate the correct viscosity solution. The latter is provided by the two lower branches of $S(x,t)$ in Figure 5 (left), i.e. the swallow tail $S>1$ is cut off. For the curve $p(x,t)$ Figure 5 (right) this implies a jump discontinuity from a positive p to $-p$ along the line x=0, i.e. lobes of equal area to the left and right of x=0 are cut off as in a Maxwell construction (equal area rule, entropy condition, see e.g. [ARN78], [LEV92], [WHI74]).

For even later times further tails in $S(x,t)$ and convolutions in $p(x,t)$ develop. These, however, also have to be removed according to the entropy condition implying that the front does no longer exhibit qualitative changes: The edge of $S(x,t)$ at x=0 simply moves to ever increasing values, while at the same time the jump discontinuity of $p(x,t)$ increases.

The given results should provide an intuitive connection between the shape of the cutting or drilling front and the phase space structures of the associated Hamiltonian system. A more comprehensive presentation of this connection, also for cutting conditions and other jet and material characteristics, can be found elsewhere [RAD99]. Here we briefly indicate the main results:

For ductile material and drilling conditions (feed λ=0) the phase portrait of the associated Hamiltonian shows a hyperbolic fixed point at (0,0) and two symmetric elliptic fixed points instead of the only elliptic fixed point for brittle material. As a consequence the drilling front is more complicated at intermediate times where it exhibits two slope discontinuities (shocks), which finally merge into one at large times resulting in a shape similar to the brittle case. An even more complicated behavior is obtained if the unimodal jet profile is replaced by a bimodal characteristic. This may lead to phase space structures e.g. with 4 hyperbolic and 5 elliptic fixed points, resulting in three shocks at intermediate times, again merging into one at large times.

Under cutting conditions, i.e. for a non-zero feed λ, we find a very different behavior. The reason is the moving profile $J=J(\mathbf{r} - \lambda \mathbf{e}_x t)$, where $\mathbf{e}_x$ denotes the unit vector in x-direction, the direction of the feed. In a co-moving frame this gives rise to a Hamiltonian, which is modified by the addition of a convective term, i.e. $H=H_0(\mathbf{r},\mathbf{p})-\lambda p_x$, where $H_0(\mathbf{r},\mathbf{p})$ is the Hamiltonian without feed. One consequence of this is that also the Hamiltonian flow field in phase space gets an additional component $-\lambda \mathbf{e}_x$. This implies that all phase space structures of $H_0(\mathbf{r},\mathbf{p})$ which are localized in coordinate space to the region of the impinging jet, are typically relevant only for times of the order $O(1/\lambda)$. This provides an understanding for the fact that the cutting or kerf depth is also of the order $O(1/\lambda)$. A further important and new finding, most easily understood in one spatial dimension, is the occurrence of a transition from a cutting front with a co-moving shock for low cutting speeds, to one without such a shock at high feed rates. This phenomenon, which is associated with an inverse saddle-node bifurcation in the Hamiltonian flow, may be a possible mechanism for the nucleation of the kink-like structures (step formation) observed experimentally. In any case such shock structures appear to be relevant also for a more complete modeling of the dynamics of the waterjet-cutting front.

A further important conclusion from this section is the fact that the experimentally observed ripples and the associated temporal oscillations cannot be explained on the level of our first order PDE. This can easily be inferred from the evolution of the relevant Lagrangian manifolds that turn out to be asymptotically stationary in the region of the waterjet. This implies that we always get a stationary cutting front for long times as is most easily seen in the 2-d case. The same holds for the full 3-d problem, at least for a cylinder-symmetric waterjet since for the latter the associated Hamiltonian system is also integrable [LIC83] (due to the existence of an additional invariant, an angular momentum). The resulting stationary cutting fronts, with or without shocks, should therefore roughly be interpreted as time-averaged fronts.

3.3 Models for Ripple Formation

The fact that modeling on the basis of a first order PDE cannot explain instabilities and therefore pattern formation has been recognized already by Finnie and Kabil [FIN65] in a similar context. In that work it is also argued that higher order derivatives have to be included. We must note, however, that from the experimental and also from the theoretical side not much is known about e.g. curvature dependent properties of cutting or wear processes. In the following we derive a model for the formation of the striation patterns during the abrasive waterjet cutting process. The resulting equation, which is of Kuramoto-Sivashinsky [SIV77] type, can explain the observed instabilities.

In a co-moving coordinate system the temporal evolution of the surface S(x,y,t) is assumed to obey the equation [FRI99]

$$\frac{\partial S(\mathbf{r},t)}{\partial t} = J(\mathbf{r}) \cdot F(\left|\nabla s(\mathbf{r},t)\right|, \Delta s(\mathbf{r},t), \Delta^2 s(\mathbf{r},t), \ldots) - \lambda \frac{\partial S(\mathbf{r},t)}{\partial x} + g(\mathbf{r},t) \qquad (7)$$

This equation has basically the same structure as the equations of the previous section with the difference that the term *F* of equation (1) is now allowed to depend on higher order spatial derivatives such as the curvature $\Delta S(\mathbf{r},t)$ of the cutting front.EMBED The λ-dependent term is the convective contribution originating from the transformation to the co-moving frame, which led in the previous section to the contribution $-\lambda p_x$ in the Hamiltonian. For completeness a noise term $g(\mathbf{r},t)$ is included in equation (7) describing smoothing effects e.g. due to granularity or microscopic inhomogeneities of the abrasive materials and workpiece, but which is neglected in the following.

One may perform a Taylor expansion to fourth order of the term *F* leading to

$$\frac{\partial S(\mathbf{r},t)}{\partial t} = J(\mathbf{r}) \cdot \left[\frac{1}{1+(\nabla S(\mathbf{r},t))^2} + \alpha(\nabla S)\Delta S(\mathbf{r},t) + \beta(\nabla S)\Delta^2 S(\mathbf{r},t)\right] - \lambda \frac{\partial S(\mathbf{r},t)}{\partial x} \qquad (8)$$

with uneven terms neglected due to symmetry reasons [FRI99]. For λ=0, constant *J*, α, and β, and a quadratic gradient dependence this becomes exactly the Kuramoto-Sivashinsky [SIV77] equation, which has already been investigated also in the context of pattern formation from erosion phenomena (see e.g. [ROS95] and refs. therein). The stationary front solution of equation (8), $S_0(\mathbf{r})$, and its stability can be calculated by means of a stability analysis. Therefore we consider small deviations $w(\mathbf{r},t)$ from the stationary front, $S(\mathbf{r},t)=S_0(\mathbf{r})+w(\mathbf{r},t)$. It can be shown analytically and numerically, that the deviations become unstable in good agreement with the cutting experiments.

The properties of the proposed model can be analyzed by numerical simulations using a semi-implicit hopscotch method. We have neglected the dependency of the parameters α,β on the gradient $S_x(\mathbf{r},t)$ and we have assumed a gaussian profile for the jet characterizing function $J(\mathbf{r})$.

Let us first indicate results for the two-dimensional problem. Figure 6a exhibits the surface S(x,t) as a function of x for a small feed rate at 6 consecutive time instants.

The instability of the cutting front is evident. Like in the real cutting process cusps evolve in time at a certain spatial distance from the leading edge traveling down the cutting front. Since the instability only can grow in the jet region the surface behind the jet is modulated periodically in space.

In order to study the impact of the feed rate λ the results of the cutting simulation for a higher feed rate is shown in Figure 6b for the same six time instants as in Figure 6a. As can be seen a different spatio-temporal behavior arises. The unstable disturbances are convected out of the region under the jet before gaining a reasonable size. This stabilizing influence of higher feed rates to the cutting ground topology can be found in measurements, too ([LAU95], [MOM97]). As can also be seen the feed rate λ influences the cutting depth d_c. Higher feed rates are associated with lower depths as in the simpler model of the previous section and as in the real cutting process [MOM97].

In the following we study the three-dimensional problem, i.e. the case of a surface S(x,y,t). In Figure 7 the results of a numerical simulation of the cutting process are shown. The calculated surface S(x,y,t) of the workpiece is plotted versus spatial coordinates x and y at 4 different times. In the unstable situation the same wavelike structures evolve as in the two-dimensional case. Furthermore, kerfs similar to the ones in the experiment can be seen at the bottom of the cutting line. At the cutting edge inhomogeneities in the surface evolve in close analogy to striation formation observed in the experiment (Figure 1d).

4. CONCLUSION

Abrasive waterjet cutting has found many applications in various industries because of its great process immanent advantages. So far precision and performance are limited by striation structures that occur at the cutting edge. With better control and reduction of ripple formation great advantages could be gained.

In this paper a new approach to understanding the mechanism of structure formation was presented. Based on modeling approaches from nonlinear dynamics we were able to reproduce and understand the development of the spatio-temporal instabilities which cause the ripple patterns at the cutting edge. A deeper analysis of the obtained nonlinear partial differential equations in combination with data driven methods of nonlinear dynamics should enable us to develop new strategies for controlling striation formation resulting in improved cutting performance and quality.

5. ACKNOWLEDGEMENT

We gratefully acknowledge support from the Volkswagen Foundation within the program "Untersuchung nichtlinear-dynamischer Effekte in productions technician Systemen". G.R. thanks R. Grauer and J. Krug for illuminating discussions.

6. REFERENCES

[ARN78] Arnold, V.I.; Mathematical Methods of Classical Mechanics, Springer-Verlag, 1978.

[BIT63] Bitter, J.G.A.; A Study of Erosion Phenomena, Part I \& II, Wear 6, 5-21, 169-190 (1963).

[BUS89] Busse, F.U.; Kramer, L.; Nonlinear Evolution of Spatio-Temporal Structures in Dissipative Contiuous Systems ; Plenum Press ; 1989.

[CAR77] Carter, G. et al., Ion Bombardment Induced Ripple Topography on Amorphous Solids, Radiation Effects 33, 65-73 (1977).

[CHA95] Choa, J.; Zhou, G. ; Leu, M.C. ; Geskin, E.; Characteristics of Abrasive Waterjet Generated Surfaces and Effects of Cutting Parameters and Structure Vibration ; Transaction of the ASME ; Vol. 117 ; November 1995.

[CRA83] Crandall, M.G.; Lions, P.-L.; Viscosity Solutions of Hamilton Jacobi Equations, Trans. Amer. Math. Soc. 277, 1-42 (1983).

[FEK94] Fekaier, A.; Guinot, J.C. ; Schmitt, A. ; Houssaye, G.; Optimization of the abrasive jet cutting surface quality by the workpiece reaction forces analysis ; 12th International Conference on Jet Cutting Technology ; Oct. 25-27 ; 1994 ; Rouen, France.

[FIN65] Finnie, I.; Habil, Y.H.; On the formation of surface ripples during erosion, Wear 8, 60-69 (1965).

[FÖH89] Föhl, J.; Untersuchungen der Werkstoffreaktion bei Einzelstoß mit harten Partikeln zur Vertiefung des Verständnisses von Erosionsverschleiß. Zeitschrift für Metallkunde, Bd 80, H 10, 1989.

[FRI99] Friedrich, R.; Ditzinger, T.; Radons, G.; Henning, A.: A model for the spatio-temporal instability in abrasive waterjet cutting, preprint, 1999.

[FUK95] Fukunishi, Y. et. al.; Numerical simulation of striation formations on waterjet cutting surface in Proceedings of the 8th American Waterjet Conference 1995, Houston Texas.

[GUO94] Guo, N.S., Schneidprozeß und Schnittqualität beim Wasserabrasivstrahlschneiden. VDI-Fortschritt-Berichte, Reihe 2, Nr. 328, Düsseldorf: VDI-Verlag, 1994.

[HAK78] Haken, H.; Synergetics ; An Introduction ; Springer-Verlag ; 1978.

[HAS84] Hashish, M; On the modeling of abrasive waterjet cutting, in Proceedings of 7th International Symposium on Jet Cutting Technology 1984, Ottawa Canada, pp. 249-265.

[HAS88] Hashish, M; Visualization of the abrasive waterjet cutting processes, Experimental mechanics, Jun. 1988, pp. 159-169.

[HAS91] Hashish, M.; Characteristics of surfaces machined with abrasive-waterjets, Transactions of the ASME ; Vol. 113 ; July 1991.

[HEN98a] Henning, A.; Cutting edge quality improvements through geometrical modeling, 14th International Conference on Jetting Technology in 1998, Brugge Belgium.

[HEN98d] Henning, A.; Anders, S; Integration der Wasserstrahltechnik in die Fertigung, VDI-Z 140 (1998), Nr.3/4. S. 54-56.

[KOV96] Kovacevic, R. ; Yong, Z.; Modeling of 3D abrasive waterjet machining; 13th International Conference on Jetting Technology; Oct. 29-31, 1996 ; Sardinia, Italy.

[LAN86] Lanczos, C.; The Variational Principles of Mechanics, 4. ed. (Dover Publ., 1986).

[LAU95] Laurinat, A; Abtragen mit Abrasiv-Druckwasserstrahlen-Hinweise zur Prozessoptimierung. Bautechnik 68 (1995) pp. 242-249.

[LEV92] LeVeque, R.L.; Numerical Methods for Conservation Laws. (Birkhäuser, Basel, 1992).

[LIC83] Lichtenberg, A.J.; Lichtenberg, M.A.; Regular and Stochastic Motion.; Springer, 1983.

[LOG94] Logan, J.D.; An Introduction to Nonlinear Partial Differential Equations. (Wiley,- Interscience, New York, 1994).

[MOH95] Mohan, R.S., Momber, A.W., Kovacevic, R.; Detection of energy absorption durcing abrasive water jet machining using acoustic emission technique; Manufacturing Science and Engineering; 1995, pp. 69 - 84.

[MOM95d] Momber, A.W., Mohan, R.S., Kovacevic, R.; Acoustic Emission Measurements on Brittle Materials During Abrasive Waterjet Cutting; 1st International Machining and Grinding Conference; 1995; pp. 439 - 458.

[MOM97] Momber A, Kovacevic R; Principles of Abrasive Water Jet Machining, Springer, 1997.

[NIU97] Niu, M. ; Fukunishi, Y. ; Kobayashi, R.; Experimental and numerical studies on the mechanism of abrasive jet cutting ; 9th American Waterjet Conference ; August 23-26 ; 1997; Dearborn, Michigan.

[OHL94] Ohlsson, L. ; Powell, J. ; Magnusson, C.; Mechanisms of striation formation in abrasive water jet cutting ; 12th International Conference on Jet Cutting Technology ; Oct. 25-27 ; 1994 ; Rouen, France.

[RAD99] Radons, G.; Hamiltonian Phase Space Dynamics and Shock Structures in Front Propagation Problems, preprint, (1999).

[RAJ93] Rajy, S.P.; Ramulu, M.; A transient model for material removal in the abrasive waterjet machining process, in Proceedings of the 7th American Water Jet Conference 1993, Seattle Washington.

[ROS95] Rost, M., Krug, J.; Anisotropic Kuramoto-Sivashinsky Equation for Surface Growth and Erosion, Phys. Rev. Lett. 75, 3894-3897 (1995).

[SAW97] Sawamura, T.; Fukunishi, Y. ; Konbayashi, R.; Three dimensional model for waterjet cutting simulation ; 9th American Waterjet Conference ; August 23-26 ; 1997 ; Dearborn.

[SIV77] Sivashinsky G; Nonlinear analysis of hydrodynamical instability in laminar flames. Part I. Derivation of basic equations. Acta Astronautica 4: 1177.

[TAN86] Tan, D.K.M.; A model for surface finish in abrasive waterjet cutting. Proc. 8th Int. Symp. on Jet Cutting Technology (Durham, 1986), BHRA, Cranfield, UK, 1986, S. 309-313.

[WES98] Westkämper, E.;Henning, A.; Gottwald, B.; Intelligent means of process control during the high pressure water jet cutting, IEEE98, Aachen, Germany.

[WES99] Westkämper, E; Henning; Radons; Friedrich, R, Ditzinger, T; Nonlinear dynamic modeling of the abrasive waterjet process. In: Investigation of Nonlinear Dynamic Effects in Production Systems, 2nd international Symposium, 25.-26.2.99, Aachen, Germany.

[WHI74] Whitham, G.B.; Linear and Nonlinear Waves. (Wiley, New York, 1974).

[WHT89] Whittaker, E.T.; A Treatise of Analytical Dynamics of Particles and Rigid Bodies, 4.ed., reissued, reprinted (Cambridge Univ. Pr., Cambridge, 1989).

[ZEN92] Zeng, J.; T. Kim; Development of an abrasive waterjet kerf cutting model for brittle materials, in Proceedings of the 11th International Conference on Jet Cutting Technology 1992, pp. 483-501.

[ZEN97] Zeng, J. ; Munoz, J.; Surface finish evaluation for abrasive waterjet cutting ; 9th American Waterjet Conference ; August 23-26 ; 1997 ; Dearborn, Michigan.

7. FIGURES

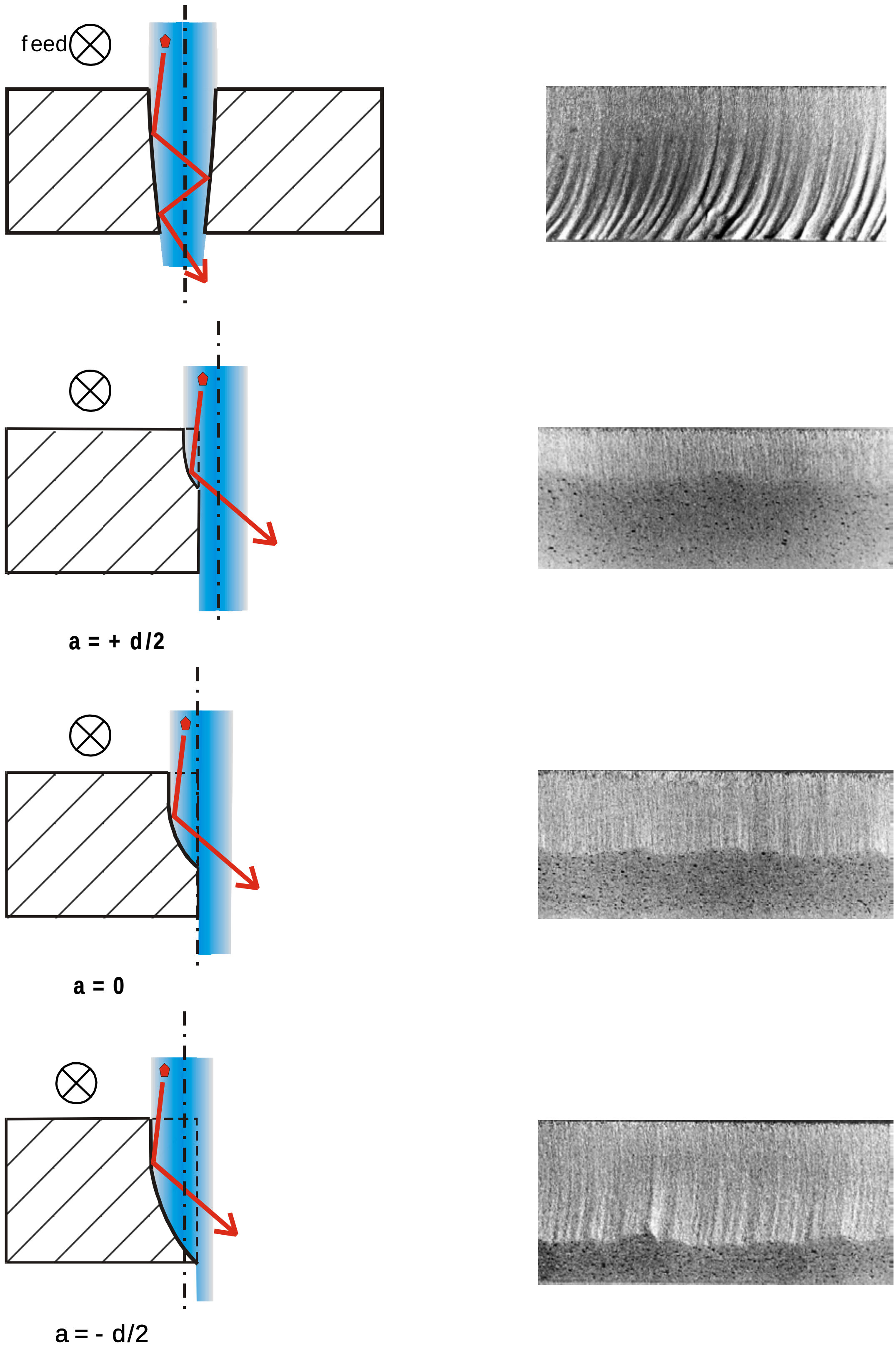

Figure 1: Results of normal (top) and edge cutting. For edge cutting with various distances from the edge (a=+d/2, 0,-d/2) multiple impacts along the kerf are avoided, but one still finds striation patterns.

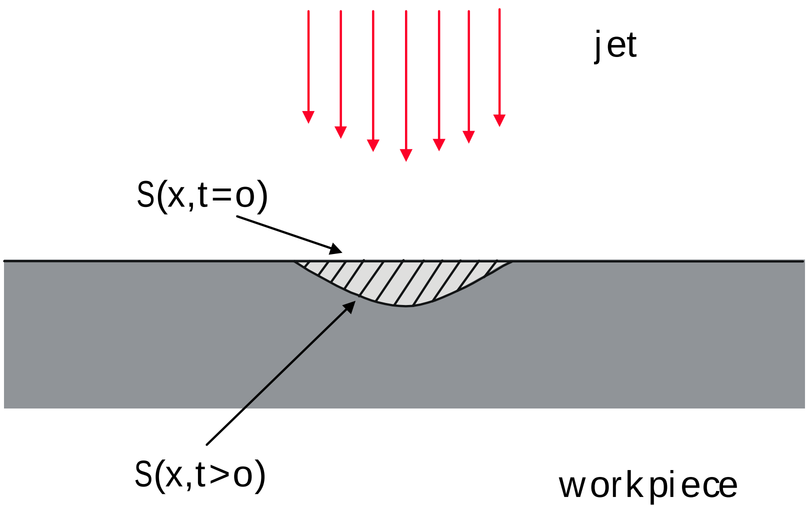

Figure 2: A waterjet containing abrasive particles with a spatially inhomogeneous velocity distribution (arrows) hits the workpiece. From an initially flat surface $S(x,t=0)=0$ an erosion front $S(x,t>0)$ develops (here depicted for drilling conditions, i.e. feed $\lambda=0$). Under cutting conditions (non-zero feed λ) the front moves e.g. to the right.

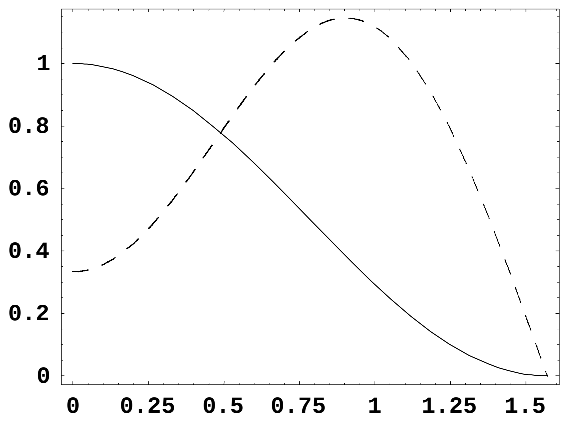

Figure 3: The wear as function of the impact angle (measured to the surface normal). For brittle material the erosion rate is maximal for normal impact ($\theta=0$). A large cutting wear contribution as in ductile materials such as aluminum, leads to a shift of the maximum wear to non-zero angles θ.

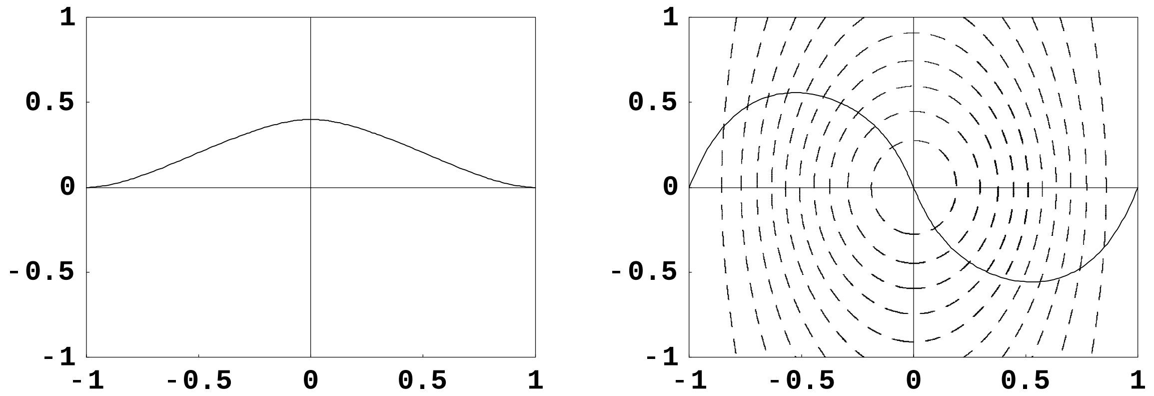

Figure 4: *S*(*x*,*t*) (left) and *p*(*x*,*t*) (right) for *t*=0.4 are depicted. Both functions are single valued for this time instant. The dashed lines in the right figure are the level lines of the associated Hamiltonian, which provide also the phase portrait for the corresponding flow in phase space.

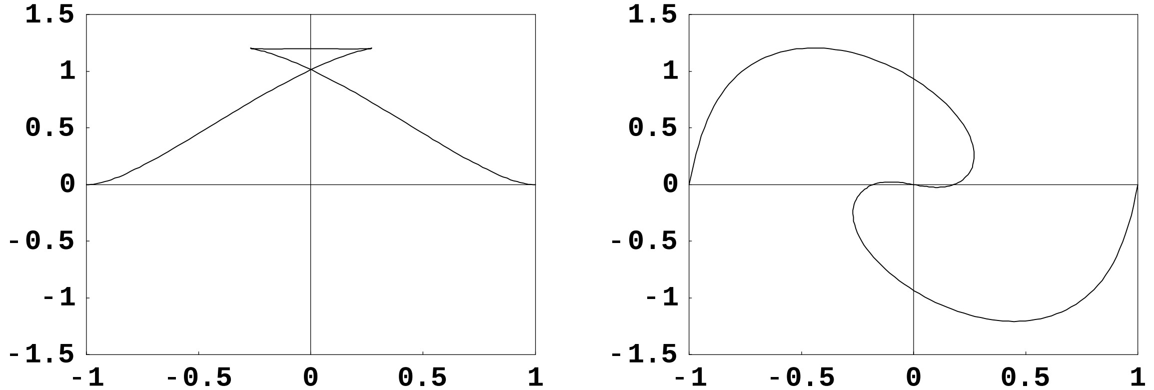

Figure 5: *S*(*x*,*t*) (left) and *p*(*x*,*t*) (right) for t=1.2. The removal of the 'swallow tail' of *S*(*x*,*t*) and of the lobes of *p*(*x*,*t*) (to the left and right of the line *x*=0) provide the correct single-valued functions *S*(*x*,*t*) and *p*(*x*,*t*). The latter are characterized by a slope or a jump discontinuity at *x*=0 respectively.

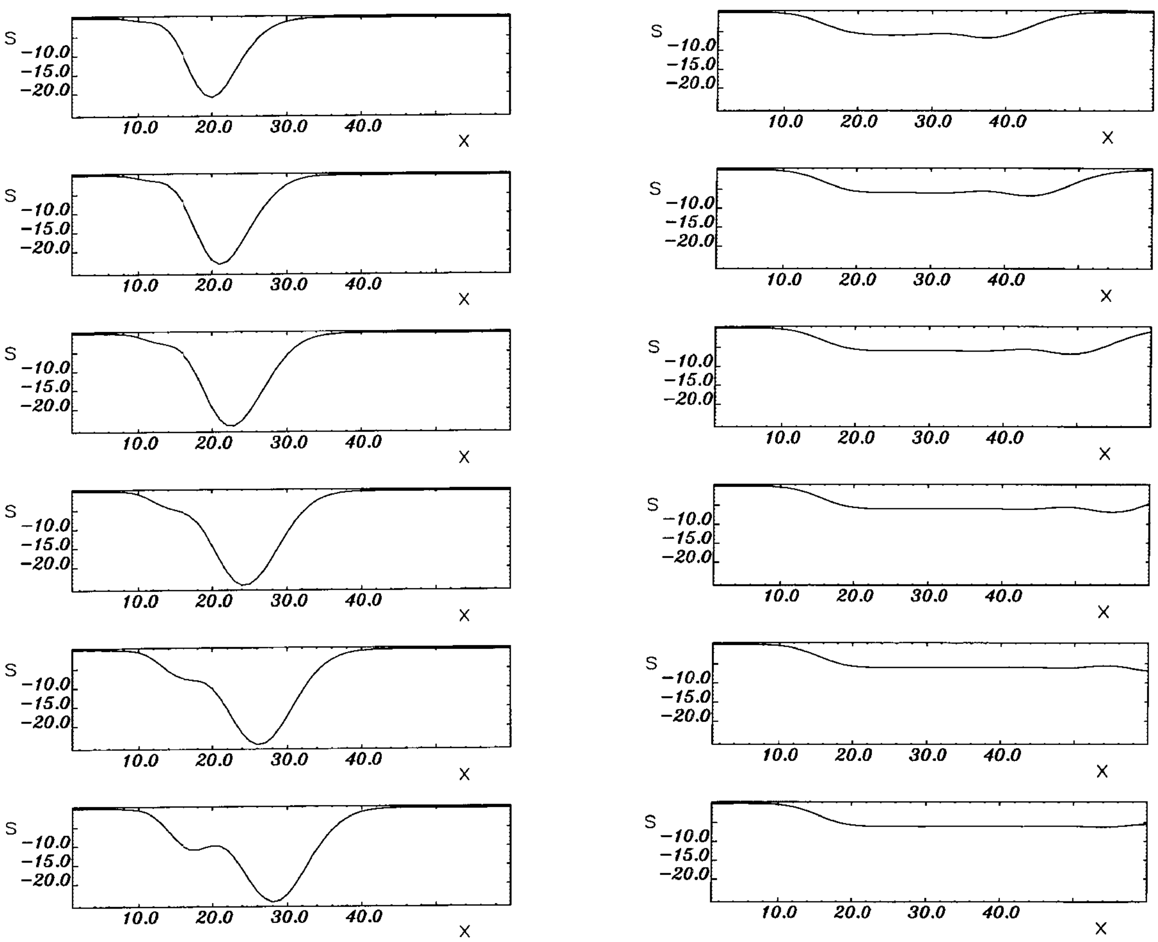

Figure 6: Two-dimensional simulation of the cutting process (jet moving in the direction of increasing x). a (left): The surface of workpiece S(x,t) is plotted versus the coordinate of the feed x for 6 different times t . The evolution of the instability (oscillation) can be observed. b (right): the same for a higher feed rate without formation of kerfs.

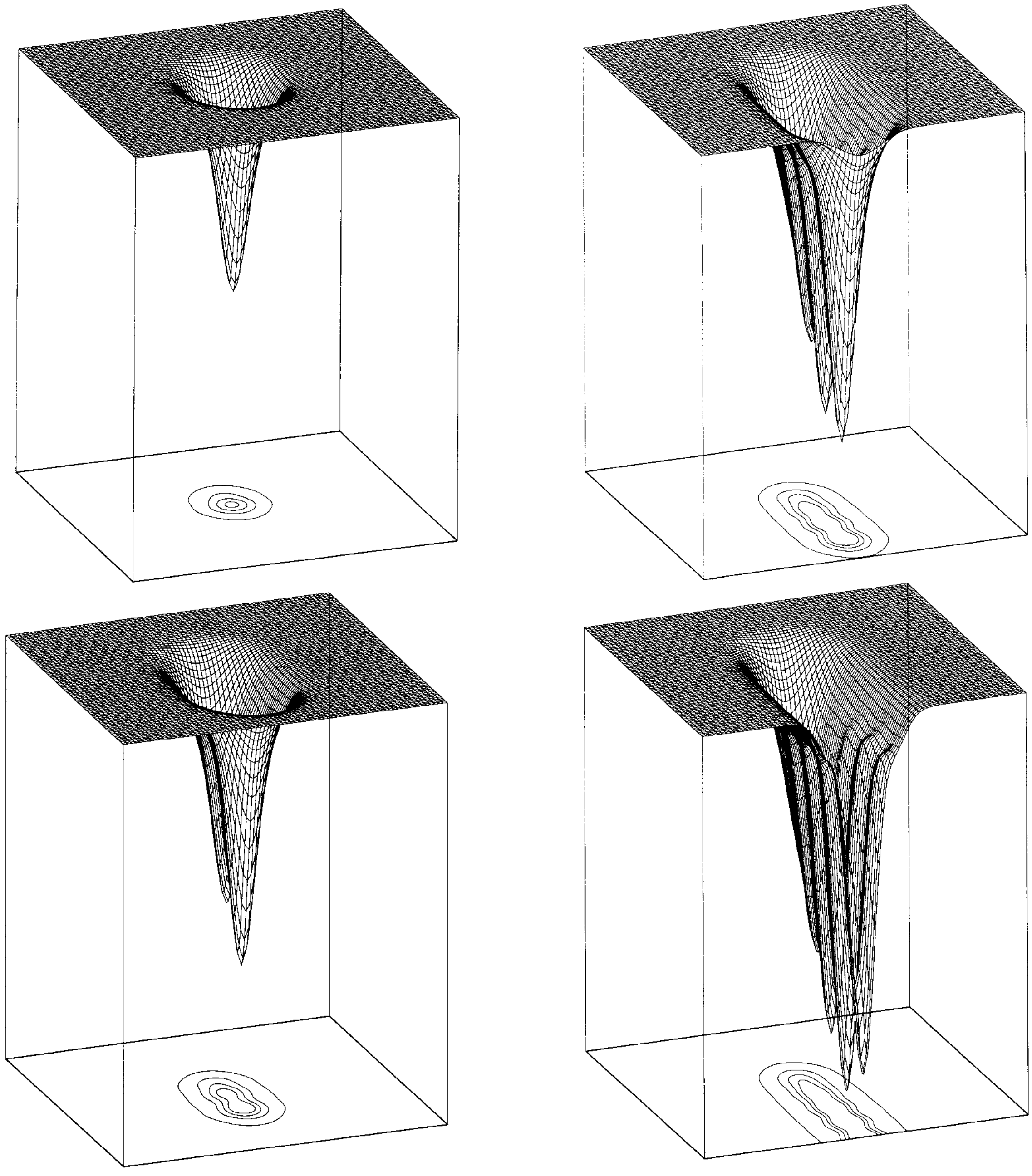

Figure 7: 3-d simulation of the cutting process. For 4 different times (increasing from left to right and from top to bottom) the surface S(x,y,t) is plotted vesus spatial coordinates x and y. The same spatial periodic patterns can be seen at the bottom and at the sides of the cutting surface as in the experiment.

10th American Waterjet Conference
August 14-17, 1999: Houston, Texas

Paper 3

MODELING THE WATERJET CONTACT/IMPACT ON TARGET MATERIAL

Z. Guo* and M. Ramulu** M. G. Jenkins**

*Boston Scientific Corporation
Northwest Technology Center
Redmond, WA

**Department of Mechanical Engineering
University of Washington
Seattle WA

ABSTRACT

Numerical modeling via finite element analyses (FEA) and experimental measurements via moiré interferometry were applied to the investigation of abrasive waterjet (AWJ) drilling. The accuracy of the FEA model is verified by comparing the experimental results with the numerical solution. Polycarbonate and ceramic blocks with dimensions of 25.4 mm x 19.5 mm x 6.25 mm subjected to concentrated static loads were studied experimentally and numerically. A closed form solution confirmed the correlation between the two. Similar comparisons were conducted on ceramic plate material. It was concluded that the FEA model represented actual loading conditions measured under static conditions. This conclusion allowed the application of a hybrid numerical/experimental technique to understand the complex interaction of the target material and the AWJ slurry column during drilling.

Key words:
Moiré interferometry, finite element analysis, static loading

1. INTRODUCTION

Abrasive waterjet (AWJ) machining process has been introduced to industry for almost fifteen years. The ability of the AWJ cutting/drilling, especially in its application to hard-to-cut material is growing. However, the mechanics of abrasive waterjet cutting is complex and our knowledge of the machining process is limited. Understanding the stress field associated with the jet cutting allows one to optimally utilize the equipment and processes, such that cutting energy and material system can be used in more economic ways. One way to address this problem is the use of a hybrid experimental-numerical analysis approach (Kobayashi, 1987) which was used to study the displacement and the stress state of brittle material while pierced by abrasive waterjet (Guo, 1998). Ramulu (1993) studied the mechanics of waterjet and abrasive waterjet machining using dynamic photoelasticity method on transparent materials. An optical experimental technique, moiré interferometry (Post et al., 1994 and 1987; Dally and Riley, 1987), was utilized to investigate the surface displacement in the brittle polycarbonate and ceramic material during AWJ piercing. The state of stresses in the machined specimen was numerically analyzed by using a finite element analysis (FEA) method utilizing the experimental results, where the boundary conditions in the FEA model conformed to those in the experiments. It is essential that the experimental setup and the FEA model are reliable in order to achieve the goal. The purpose of this research is an attempt to apply an optical technique, moiré interferometry, to determine the jet-material interfacial strains at the onset of machining and develop a finite element model to analyze the impacting and piercing process. Both experimental approach and finite element model are verified by analyzing brittle plate materials subjected to concentrated loading.

2. OPTICAL EXPERIMENTS SETUP AND PROCEDURE

The abrasive waterjet system used in the research consists of a high pressure pump, a nozzle assembly, a catcher unit, and an abrasive supply hopper. Inside the abrasive waterjet nozzle there is a waterjet orifice of size 0.30 mm in diameter and a tungsten carbide focusing tube of internal diameter 1.02 mm. Garnet abrasive #80 was chosen. Moiré interferometry was utilized to measure the surface displacement of brittle polycarbonate and ceramic material under static loading. The moiré interferometry experimental system was composed of several pieces of mechanical, optical, and electronic equipment configured together to produce and capture the moiré fringes. The test specimen included polycarbonate and alumina block with dimensions of 25.4 mm x 19.5 mm x 6.25 mm under static loading. The specimen was coated with specimen grating with a density of 1200 lines/mm. Details of the experimental setup can be found in Guo and Ramulu (1995 and 1997).

In addition to the high pressure waterjet piercing experiments, a static load experimental setup was developed to evaluate the displacement field magnitudes and its trends. The optical arrangement of this setup is shown in Figures 1. A static pressure load was applied to the top surface of a specimen by a calibrated weight through an indenter with a diameter of 2 mm. The calibrated weights were placed on a slider bar made of a plastic. The total static load exerted on the specimen was measured with a load cell that was mounted in the middle of slider bar. Since this was a static experiment, only one video camera was used for capturing the moiré fringes. While the *u*-field fringes were being recorded, the *v*-field view had to be blocked, and vice versa. A detailed illustration of the loading frame is in Figure 1(b). An indenter was threaded to the load cell, which is pictured in Figure 1(c). The total load was read off a load cell display, which is illustrated in Figure 1(d). Following the testing procedure for moiré interferometry experiments, both *u* and *v* field moiré fringe patterns indicating the displacement could be captured. The static load was gradually increased from zero by carefully adding more weight blocks on the slider bar. The *u* and *v* fringes were each recorded with a high speed Hi8 video camera after each load increment.

(a) optical experimental setup for a specimen under static loading

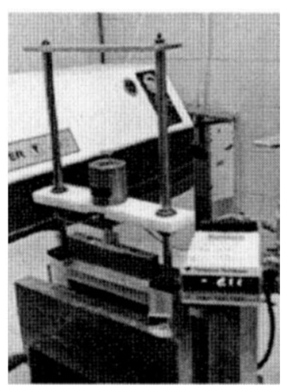

(b) static loading frame

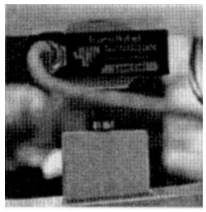

(c) load cell, indenter and specimen

(d) load cell display

Figure 1 Experimental Setup

3 FINITE ELEMENT MODELING

A commercial FEA code was used in this study. In the finite element analysis, the indenter was modeled as a solid cylinder with a diameter of 2 mm. Taking advantage of the symmetry of both load and geometry, a quarter volume for the specimen and the indenter was modeled. During the experimental testing, the bottom surface of the test specimen was adhered using an epoxy to the base bar. Figure 2 is a typical meshed finite element model, which has 2,548 nodes and 1,863 elements. Figure 2(b) shows the enlarged view of the meshed indenter. A three dimensional structural solid element (SOLID45) was used for both the test specimen body and the indenter. The interface between the indenter and the test specimen was modeled with a contact element, (CONTACT49). These displacement fields modeled by the FEA meshes only represent half of the frontal surface of the specimen.

4 RESULTS AND DISCUSSION

Figure 3 shows the moiré fringe patterns in both u and v fields for the polycarbonate specimen for increasing static load from 0 N to 44.5 N. Note that both u and v fields have initial fringes at 0 N load condition. However, moiré fringes in both u and v fields are relatively symmetric with respect to the loading line. The number of moiré fringes increased as the load increased. This was especially the case for the v field, as shown in Figure 3(b). Figure 4 shows the moiré fringes recorded for the alumina specimen in both u and v fields, as the loads were increased from 0 N to 62.3 N. It appears that there were 2 initial fringes in the u field and 3 initial fringes in the v field. As the loads were increased, the moiré fringes in both fields only shifted within the picture frames. There was no increase in moiré fringes for the alumina.

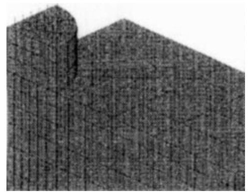

(b) enlarged view

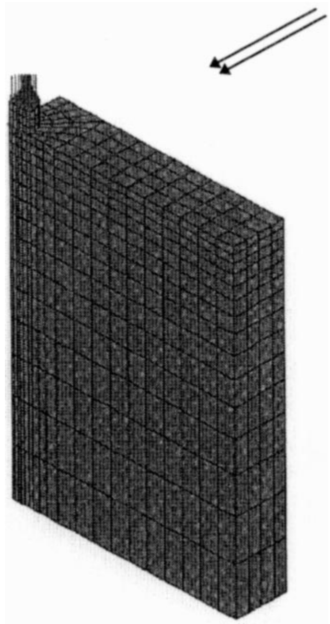

(a) a typical quarter mesh

Figure 2. Typical FEA mesh for the polycarbonate block under static loading

Figures 5(a) and (b) are the FEA generated outer surface displacement contours for polycarbonate at 44.5 N static load. The displacement contours in both *u*- and *v*- fields are symmetric with respect to the centerline of the static load. The outer surface displacement contours in Figure 5 were plotted with each contour line representing the same amount of displacement (417×10^{-6} mm) of one fringe order, the same as represented by a fringe order in the recorded moiré fringe patterns. In Figure 5 (a) and (b), at 44.5 N there are 5 fringes in the *u* field and 13 fringes in the *v* field. Figures 6(a) and (b) are the outer surface displacement contours for the alumina at 44.5 N static load. Each contour line represents a displacement of 1.44×10^{-6} mm in the *u*-field and 4.41×10^{-6} mm in the *v*-field. Even at 44.5 N, the maximum displacement is 7.6×10^{-6} mm in the *u*- field, and 4×10^{-6} mm in the *v*-field, which is20:43 less than the equivalent displacement of one moiré fringe. This also means that the displacement for alumina at load of 44.5 N is too small to be measured with the current moiré technique.

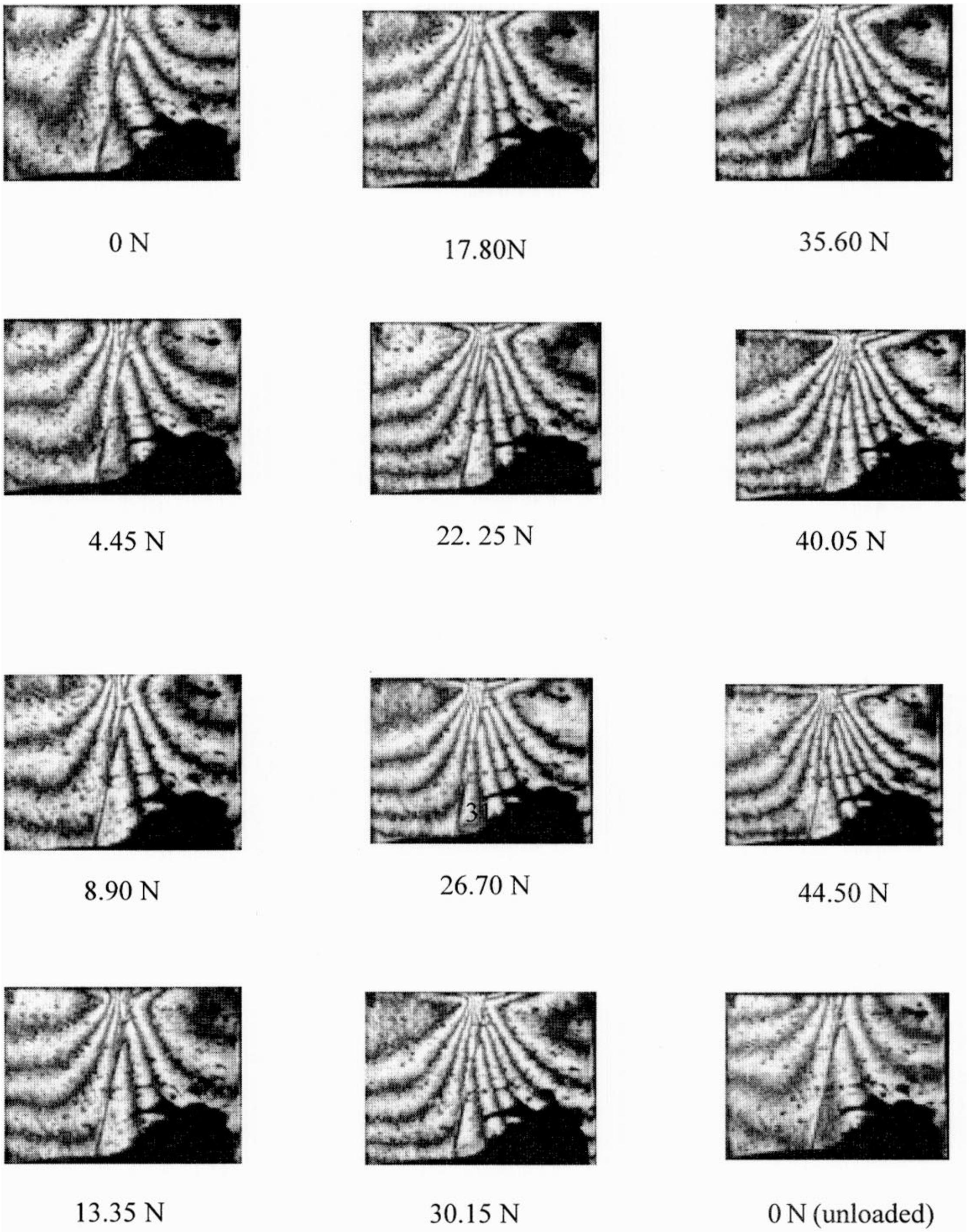

Figure 3(a) *u*-Field Moire Fringes for Polycarbonate Specimen under Static Loading

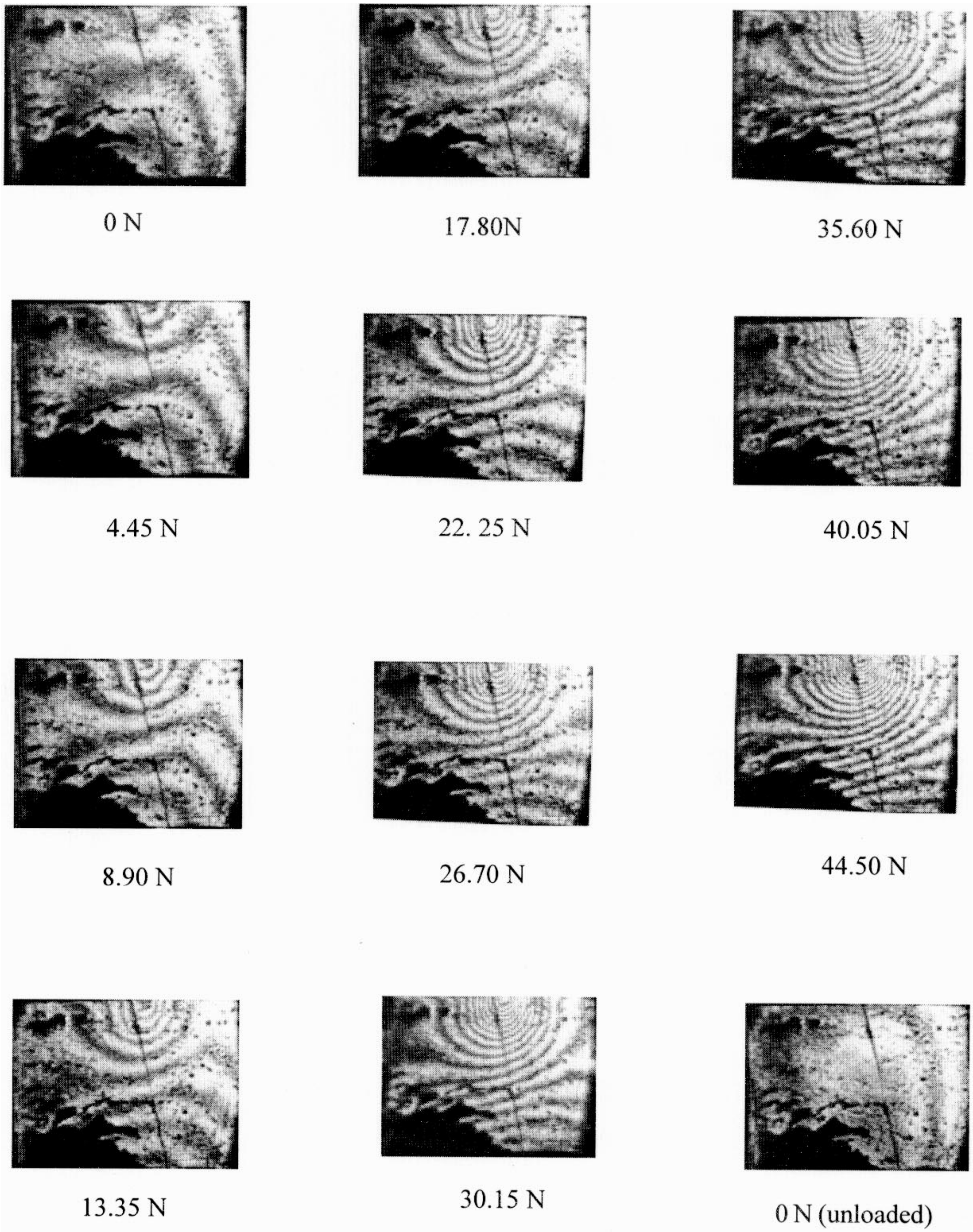

Figure 3(b) v-Field Moire Fringes for Polycarbonate Specimen under Static Loading

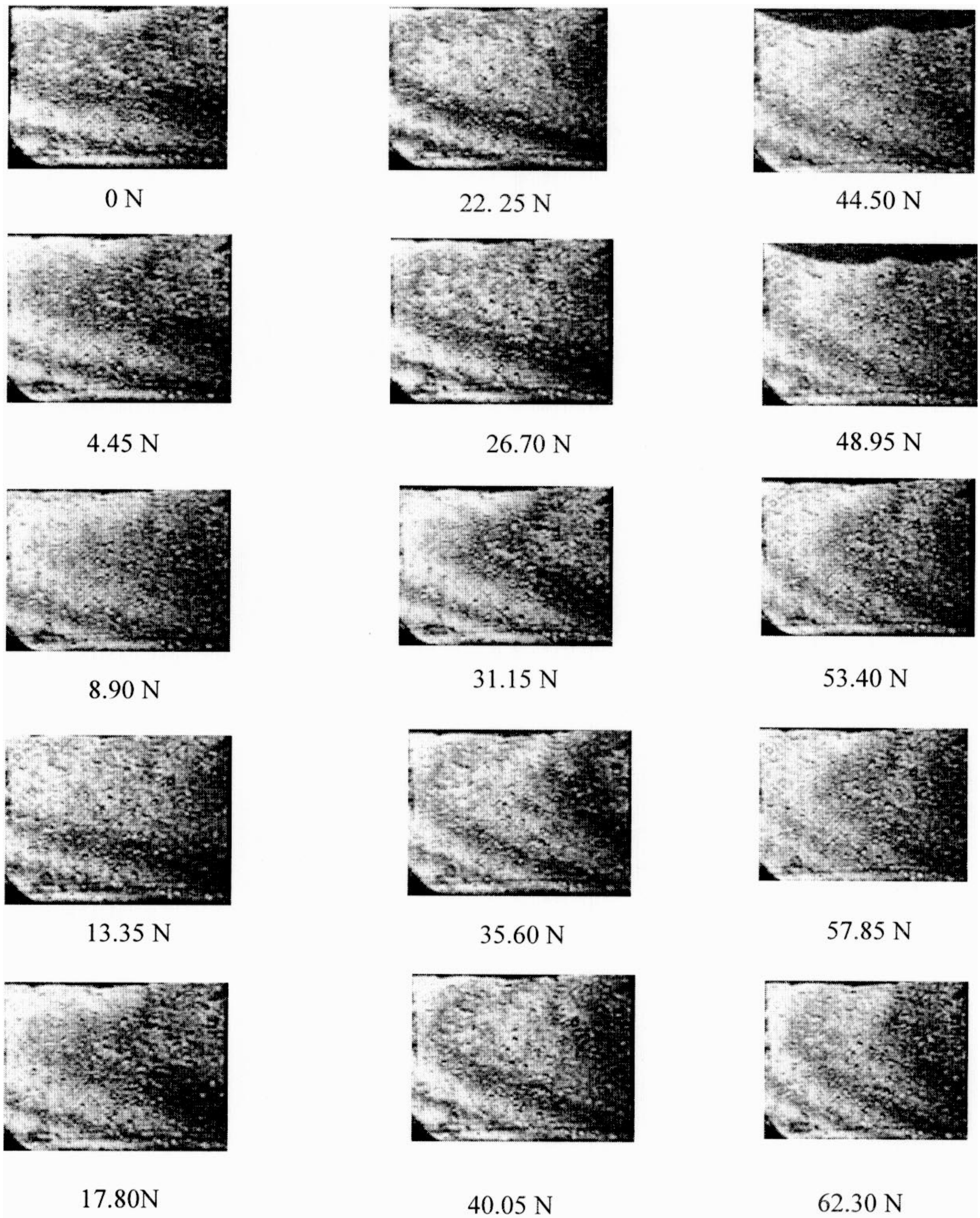

Figure 4(a) u-field Morie Fringes for Ceramic Specimen under Static Loading

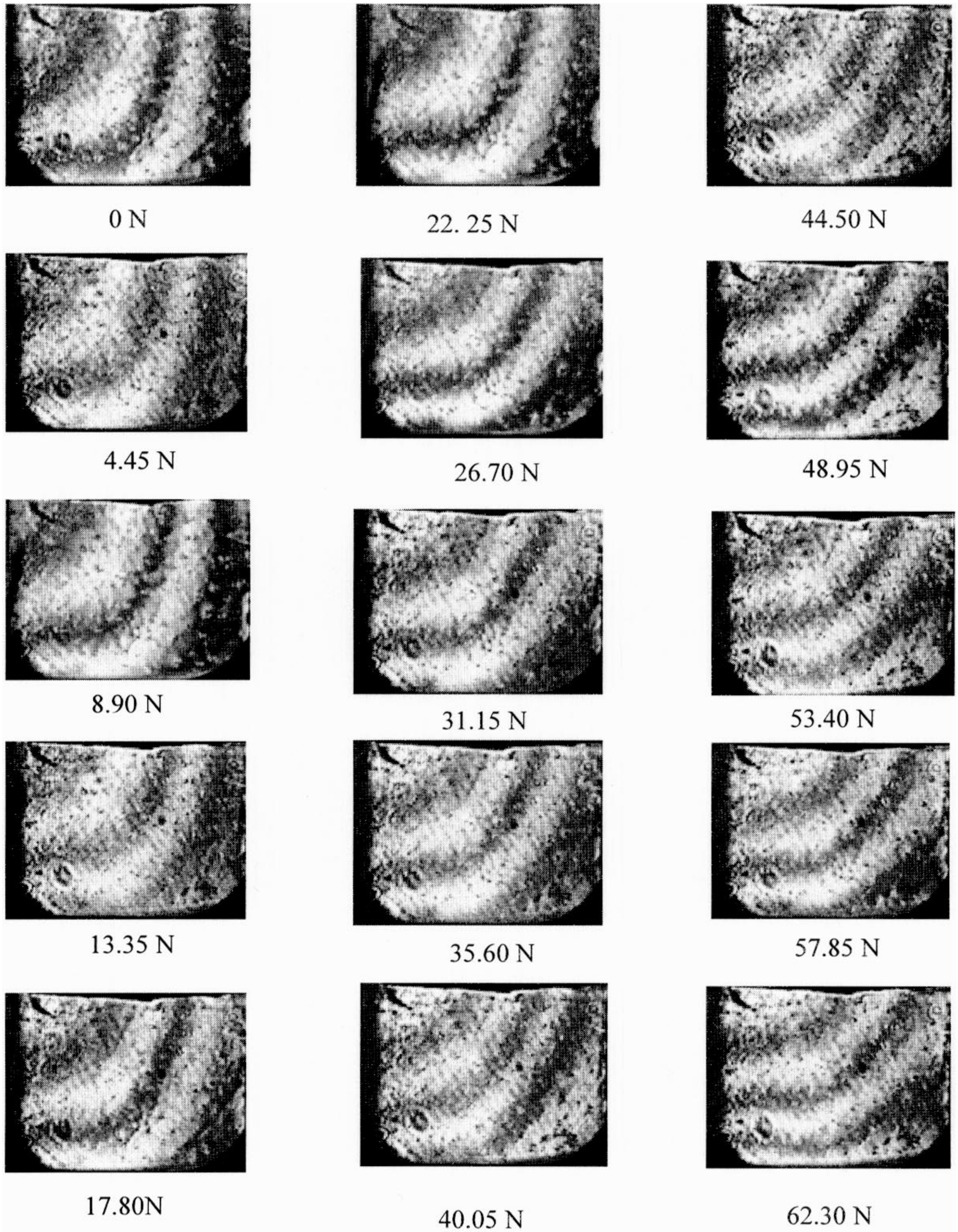

Figure 4 (b) *v*-field Morie Fringes for Ceramic Specimen under Static Loading

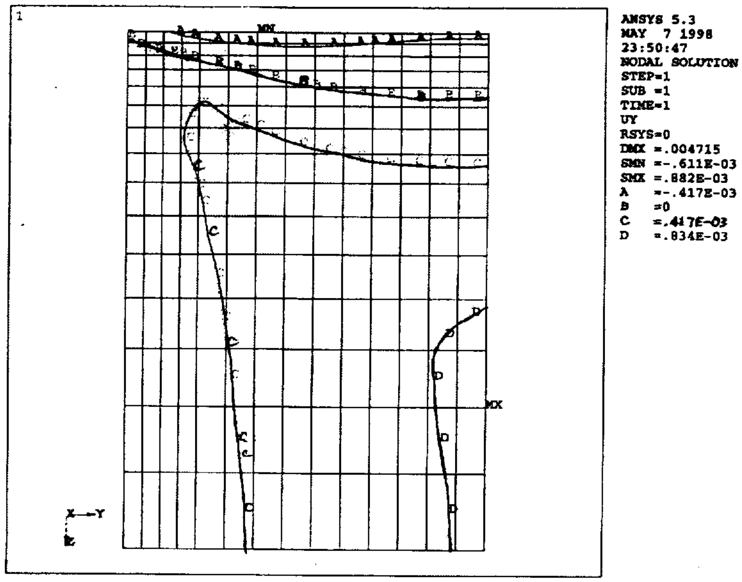

(a)

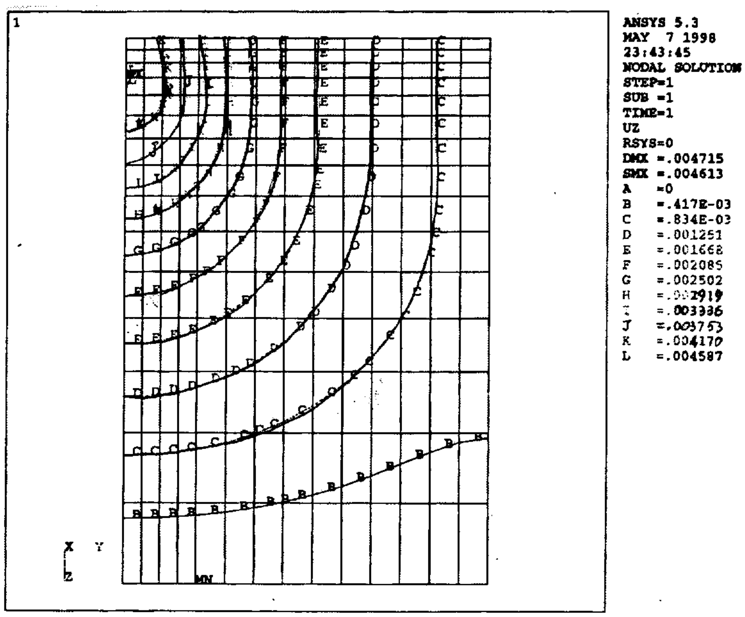

(b)

Figure 5 *u, v*-field displacement contours for polycarbonate block (44.5 N static load)

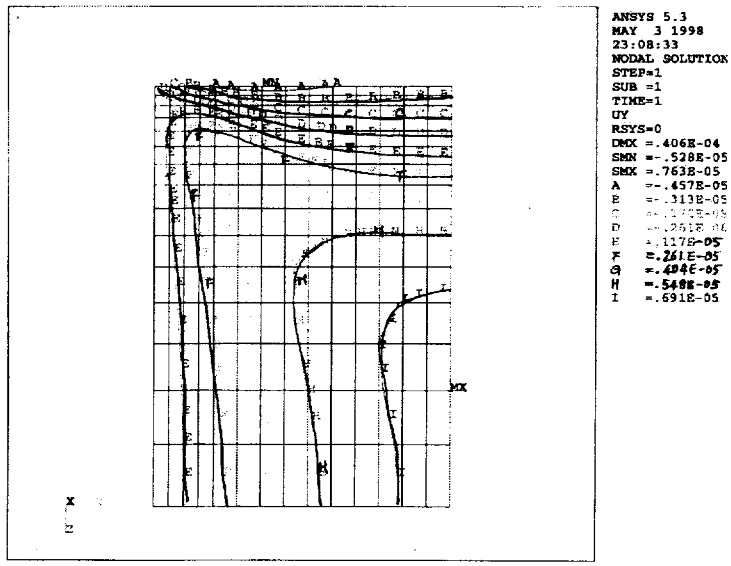

Figure 6 (a) The u-field surface displacement contours for alumina block

(at 44.5 N static load)

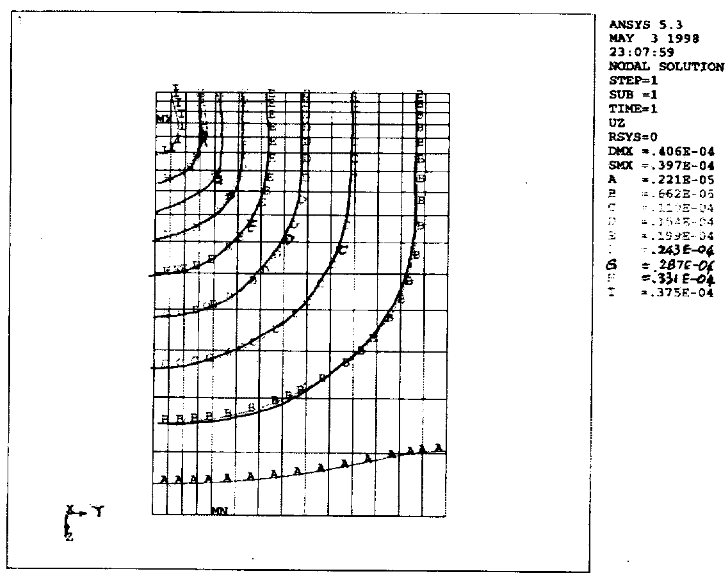

Figure 6 (b) The v-field surface displacement contours for alumina block

(at 44.5 N static load)

Since a closed form solution is not readily available analytically for a static loading on a small specimen block, an idealized model in a semi-infinite body under the pressure of a sharp indenter was used. The point load is illustrated in Figure 7. The concentrated point force *P* was applied at the origin of the cylindrical coordinate system.

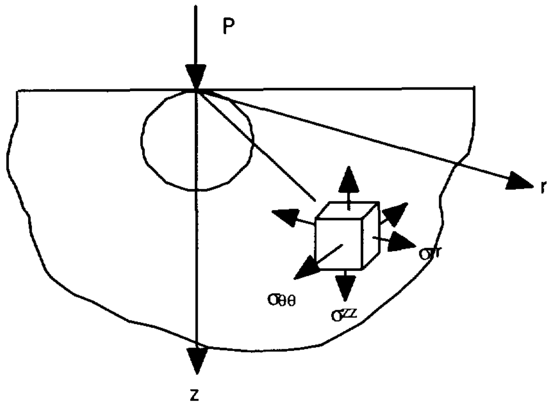

Figure 7 Point force P at the origin of the cylindrical coordinate system

In this cylindrical coordinate system, the displacement components in the r, θ and z axes are denoted by u, v, and w, respectively. The stress components can be expressed as [8]:

$$\sigma_{rr} = \frac{P}{2\pi}[(1-2\nu)\frac{1}{r^2} - \frac{z}{r^2(r^2+z^2)^{1/2}} - \frac{3r^2 z}{(r^2+z^2)^{5/2}}] \tag{1}$$

$$\sigma_{zz} = -\frac{3P}{2\pi}\frac{z^3}{(r^2+z^2)^{5/2}} \tag{2}$$

$$\sigma_{\theta\theta} = \frac{P}{2\pi}[(1-2\nu)[-\frac{1}{r^2} + \frac{z}{r^2(r^2+z^2)^{1/2}} - \frac{z}{(r^2+z^2)^{3/2}}] \tag{3}$$

$$\sigma_{rz} = -\frac{3P}{2\pi}\frac{rz^2}{(r^2+z^2)^{5/2}} \tag{4}$$

The displacement components u (radial direction), v (tangential direction), and w (vertical direction) can be written as [8]

$$u_r = \frac{(1-2\nu)(1+\nu)P}{2\pi Er}\left[\frac{z}{(r^2+z^2)^{1/2}} - 1 + \frac{r^2 z}{(1-2\nu)(r^2+z^2)^{3/2}}\right] \tag{5}$$

$$v_\theta = 0 \tag{6}$$

$$w_z = \frac{P}{2\pi E}\left[\frac{(1+\nu)z^2}{(r^2+z^2)^{3/2}} + \frac{2(1-\nu^2)}{(r^2+z^2)^{1/2}}\right] \tag{7}$$

Within this semi-infinite body, a small volume of the same size of a test specimen centered at the origin of the coordinate system was of the most interest. The displacements in the front surface of the small volume were calculated using the equations 5, 6 and 7. The front surface was divided into a 75 x 100 mesh grid. The coordinates x and y at each grid point was calculated in a Cartesian coordinate system. Therefore, the displacement components in the Cartesian coordinates are as follows:

$$u_x = \frac{(1-2\nu)(1+\nu)P}{2\pi Er}\left[\frac{z}{(r^2+z^2)^{1/2}} - 1 + \frac{r^2 z}{(1-2\nu)(r^2+z^2)^{3/2}}\right]\sin(\arctan(x/y)) \tag{8}$$

$$u_y = \frac{(1-2\nu)(1+\nu)P}{2\pi Er}\left[\frac{z}{(r^2+z^2)^{1/2}} - 1 + \frac{r^2 z}{(1-2\nu)(r^2+z^2)^{3/2}}\right]\cos(\arctan(x/y)) \tag{9}$$

$$w_z = \frac{P}{2\pi E}\left[\frac{(1+\nu)z^2}{(r^2+z^2)^{3/2}} + \frac{2(1-\nu^2)}{(r^2+z^2)^{1/2}}\right] \tag{10}$$

where, $r = \sqrt{x^2 + y^2}$

The analytical solutions for polycarbonate material were calculated using equations 7 to 10. At 44.5 N, the displacement distribution contours in both u- and v- fields for a polycarbonate material are shown in Figures 8(a) and (b). The displacement contours in both u and v fields are symmetric, and the trends are very similar to experimental observations.

A comparison of the experimentally obtained displacement contours with the finite element analysis contours was conducted. The first step for the displacement comparison was to analyze the experimentally recorded moiré fringes. The next step was to place the experimental fringe pictures side by side with the FEA contour plots. It is observed in Figures 3, that the numbers of initial fringes for both u-field and v-field are not zero. The net displacements corresponding to each static load could be obtained by subtracting the initial displacement field from the displacement field of each specific loading. A subtraction was performed numerically for each corresponding point on the outer surface. Figure 9 shows examples of the digitized moiré fringe patterns for polycarbonate specimen under static load of 0 N and 44.5 N. The net displacement contour for 44.5 N load was obtained and is shown in Figure 10(a). The zigzagged curves and other irregularities in Figures 10(a) are due to the numerical noises introduced in the subtraction process. A smooth line would be calculated when the initial fringe pattern matched the loaded fringe patterns exactly. The contour plot algorithm used in the plotting software could be partly responsible for the irregularities in the net displacement contours. The net displacement contour is approximately symmetric with respect to the centerline. The *u*-field displacement contours predicted by the FEA model are illustrated in Figure 10(b) for polycarbonate under static load of 44.5 N. In the net *u*-displacement contour graph in Figure 10(a), there is an approximate symmetry with respect to the centerline of the specimen. There is no *u*-displacement along the symmetry line. On either side of the symmetric line there are three deformation zones. Along the top edge is the upper displacement zone, where the material moves towards the loading point and the centerline. The values of the displacements are negative. In the lower portion of the specimen surface is the lower displacement zone. In the lower displacement zone the material moves away from the centerline. The values of the displacements are positive. The maximum displacement in the lower displacement zone is approximately 834×10^{-6} mm, which can be represented by two moiré fringes. Separating the upper and lower displacement zone is a neutral displacement zone. In the neutral zone there is no displacement. Examining the contour plot obtained from the finite element analysis, as shown in Figure 10(b), there are three displacement zones on either side of the specimen. The magnitudes of the displacements coincide with the experimentally obtained results in Figure 10(a). Therefore, the displacement fields depicted in Figure 10 (a) and 10(b) are very comparable.

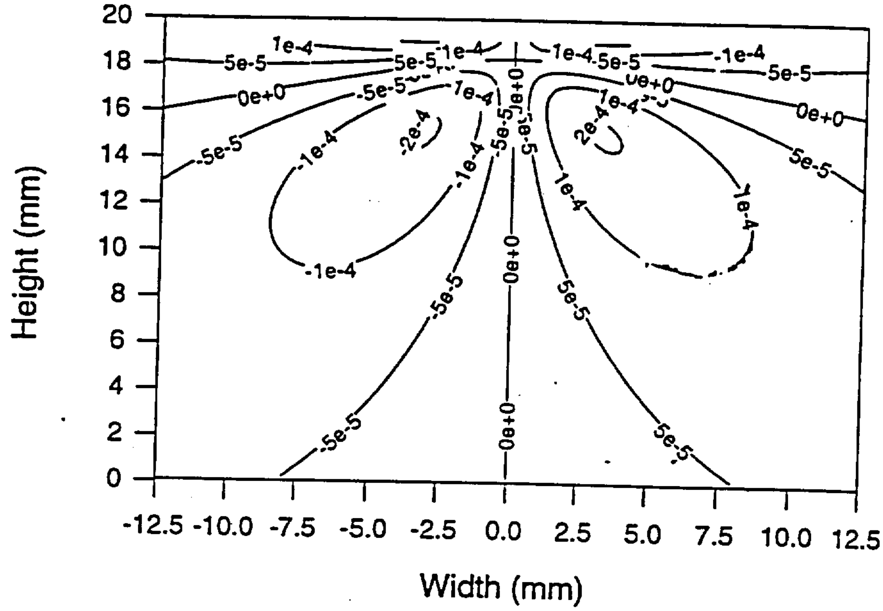

(a) *u*-field displacement contour (mm)

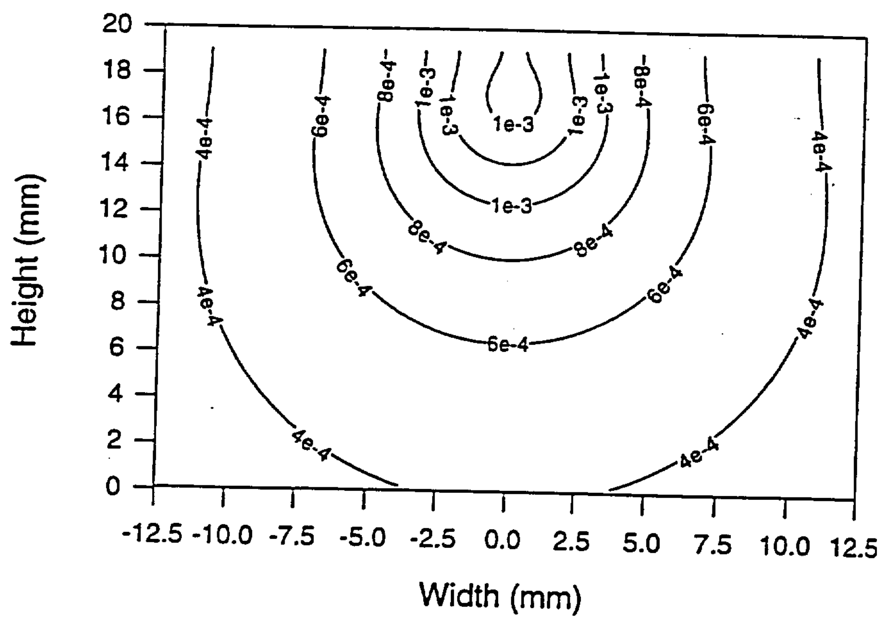

(b) *v*-field displacement contour (mm)

Figure 8 Closed form solutions of displacement contours under a point load

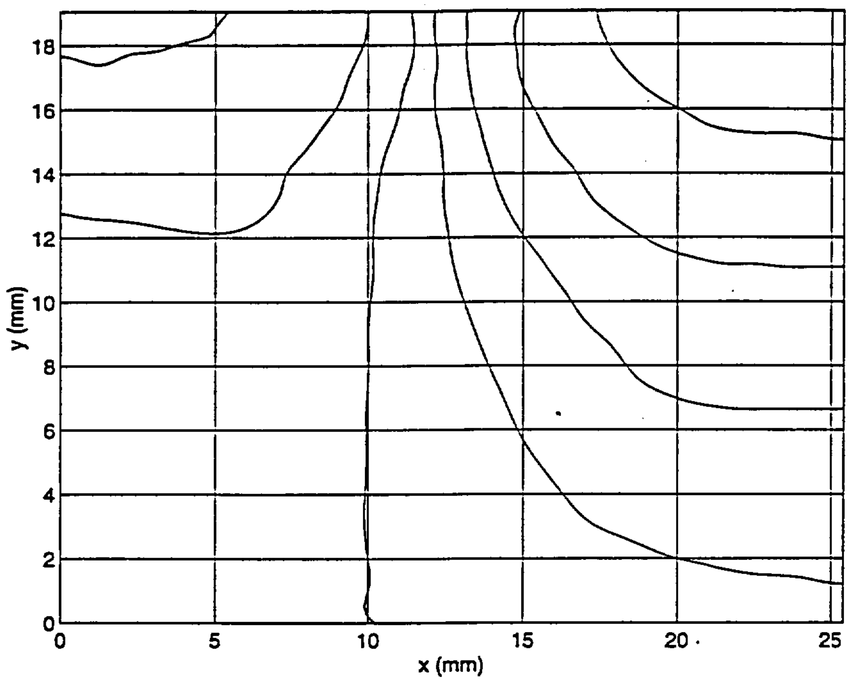

(a) Static Load 0 N)

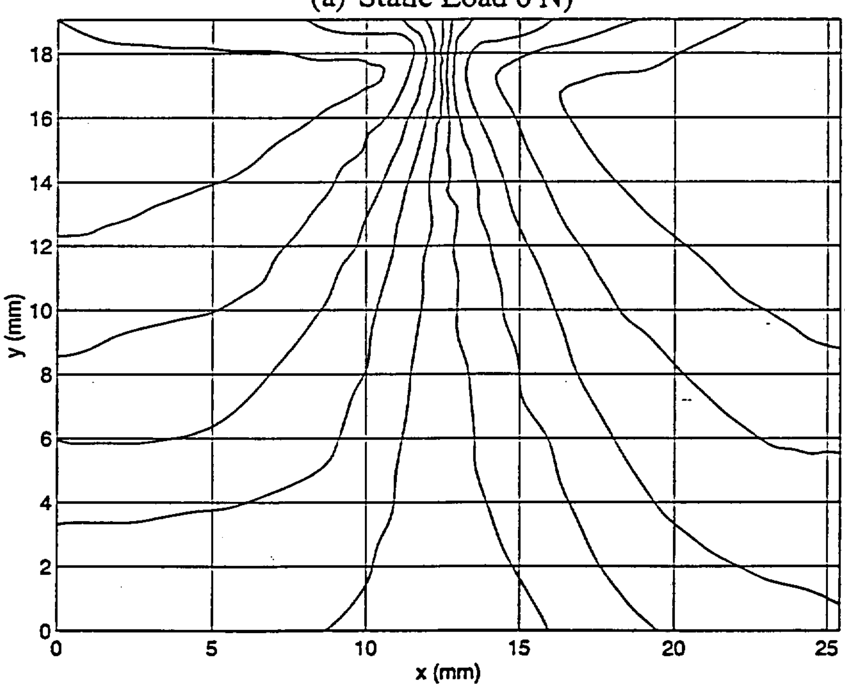

(b)Static Load 44.5 N)

Figure 9 Digitized u-field displacement contours for polycarbonate specimen under static loads

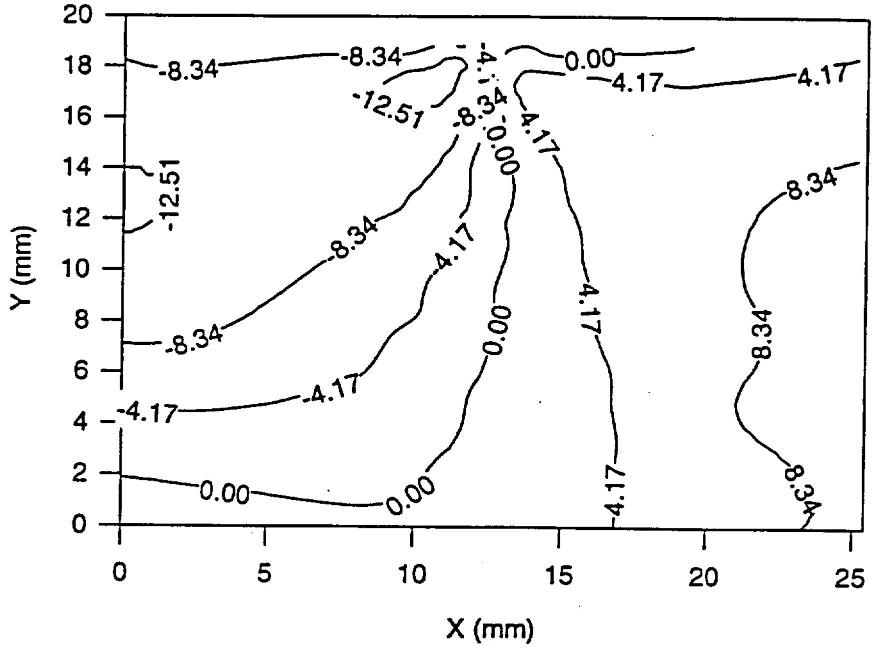

(a) net displacement contour ($x10^{-4}$) mm at static load 44.5 N

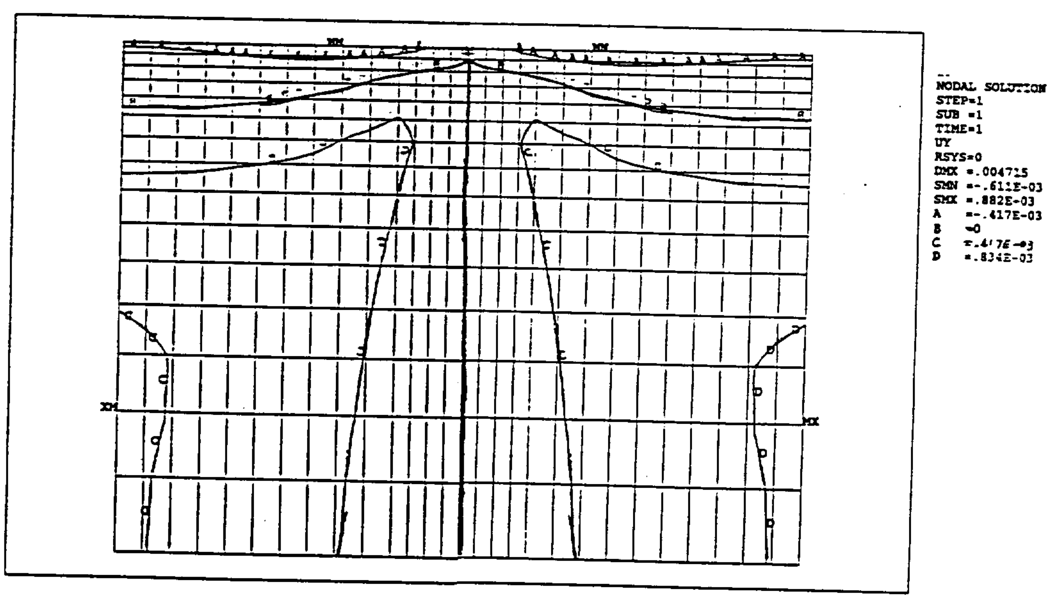

(b) FEA predicted displacement contour (mm) at static load 44.5 N

Figure 10 Comparison of the experimental and FEA results of the *u*-field displacement contours for polycarbonate specimen

A similar comparison was made for the *v*-field displacement contours between the experimental results and the FEA results for the polycarbonate specimen. The net result of the *v*-field displacement contour after subtraction is shown in Figure 11(a), and the FEA predicted contour is shown in Figure 11(b). There is a general symmetry in the *v*-displacement field with respect to the centerline of the specimen, which is the case for the FEA *v*-displacement contour plot in Figure 11(b). Along the lower edge the *v*-displacement is zero. The maximum *v*-displacement is at the loading point, or the center point of the upper edge. The maximum displacements from both experimental and FEA are approximately 5000×10^{-6} mm. There is an apparent close match between the experimental results and the finite element prediction in the *v*-displacement field also. The above comparison in both *u*- and *v*- fields demonstrates that the results from the experiments agree with that of FEA results.

Figures 8 are the contour plots from the analytical solutions described in Equations 1 to 10. The contour plots represent the *u*- and *v*- displacement for a small block of material in a semi-infinite body. Comparing displacement contours in the u and v fields from the analytical solution in Figures 8, with those from FEA and experiments in Figures 6(a) and (b), it is obvious that the displacement contour trends are very similar. However, the magnitude of the displacements of the analytical solution is smaller than the FEA contour indicated, and smaller than the experimentally recorded displacements at their corresponding locations. The analytical *u*-field displacements in Figure 8(a) are about 1/7 of those from the FEA or experiments in Figure 11. The analytical *v*-field displacements in Figure 8(b) are about 1/4 to 1/5 of those from the FEA or experiments in Figure 6(b). The differences in the displacements in both *u*- and *v*-fields are probably due to the different boundary condition between the semi-infinite body and those in the FEA model and experiment. For example, in the experimental setup and FEA model, both sides of the specimen were free of support. In the semi-infinite model, the specimen volume is supported by the adjacent materials, and the adjacent material prevents the material deform freely in the *v*-direction. Thus smaller displacement was observed in the analytical solutions. Another important factor that is attributed to the differences is that the applied load in the analytical model is a concentrated force at the center of the block volume instead of a blunt pressure load, as is the case in experimental and FEA models.

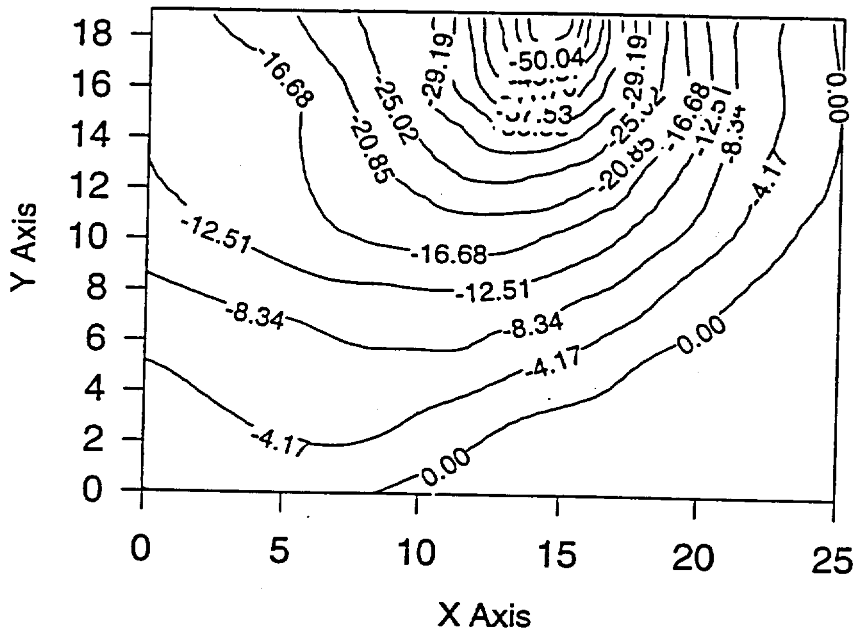

(a) net displacement contour (x10^{-4}) mm at static load 44.5 N

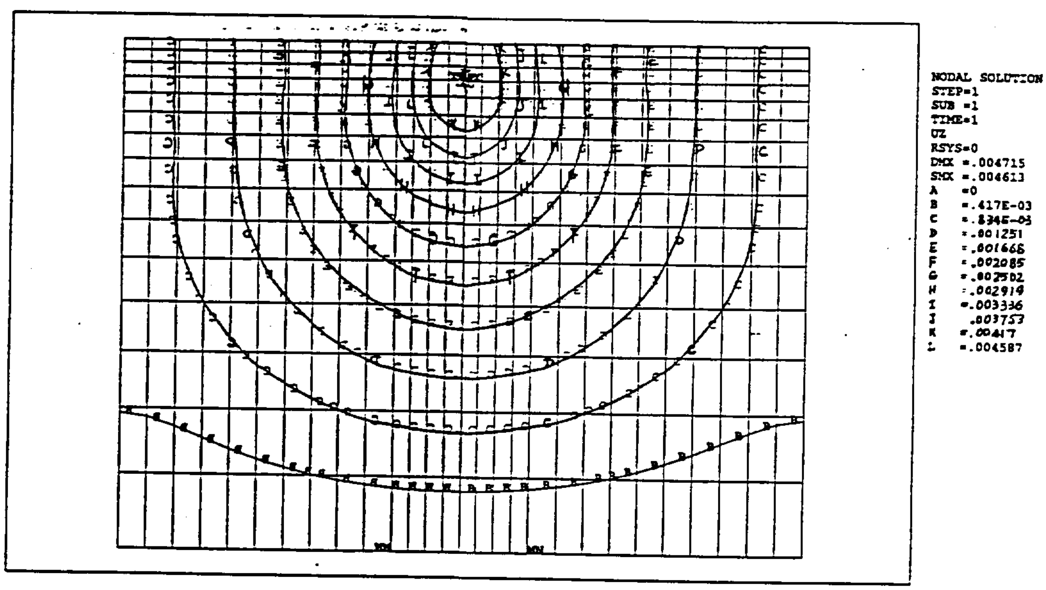

(b) FEA predicted displacement contour(mm) at static load 44.5 N

Figure 11 Comparison of the experimental and FEA results of the v-field displacement contours for polycarbonate specimen

The optical experimental and FEA results for alumina were studied and are also compared here. Figures 4(a) and 4(b) are the moiré fringes pictures from the experiments in *u*- and *v*- displacement fields respectively. Figures 6(a) and 6(b) are the contour plots obtained from finite element analysis for the alumina material. As can be seen in the experimental results shown in Figures 4(a) and Figure 4(b), the number of moiré fringes nearly remained constant in both *u*- and *v*- fields as the static loads were increased from 0 N load to 62 N in both *u*- and *v*-fields. Checking the FEA contours in the *v* fields, as illustrated in Figure 5(b), the maximum displacement at static load of 44.5 N is 3.97×10^{-6} mm, which is still less than that represented by one moiré fringe 417×10^{-6}. In the *v* fields, as illustrated in Figure 5(a), the maximum *u*-displacement at static load of 44.5 N is 7×10^{-6} mm, is also less than the moiré fringe value. The comparison between the FEA results and experimental results in *u*-and *v*- field displacements equally demonstrates that the experimentally obtained displacements agree with those predicted by FEA for the alumina material. From these comparisons, it is obvious that the maximum displacement in both *u*- and *v*- fields at static load of 44.5 N on a polycarbonate is quite different from those of alumina. The displacements for ceramic are much smaller than the polymer because the ceramic is a much stiffer material than that of polycarbonate. Therefore, the displacements for the ceramic under the limited static loads could not be measured by moiré fringes.

6 SUMMARY AND CONCLUSIONS

The surface displacements of polycarbonate and alumina specimens under concentrated static loading were determined by using moiré interferometry experiments and through the finite element analysis models. The boundary conditions for both experimental and numerical studies were the same. The surface displacements were also analyzed using a closed form solution. These results are presented in terms of moiré fringes and contour plots. The experimental findings and the FEA results were compared for the polycarbonate and ceramic specimens under static loading. The patterns of the displacement distribution were similar. In the polycarbonate specimens, the moiré interferometry results were in good agreement with the finite element analysis results. For ceramic specimen the number of moiré fringes did not change as the load was increased from 1 to 62 N. This was due to the high stiffness of the ceramic material. The good correlation between the FEA modeling and the experiments of the static loading on polycarbonate and alumina demonstrates that the FEA modeling is able to predict the displacement distribution for both polycarbonate and alumina under static loading.

References

Dally, J. W. and Riley, W. F., "Experimental Stress Analysis," *3rd Edition, McGraw-Hill*, New York, 1991.

Guo, Z., "Experimental and Numerical Analysis of Abrasive Waterjet Drilling of Brittle Materials," a PhD Dissertation Submitted to University of Washington, 1998.

Z. Guo and M. Ramulu, "Measurement of Strains Associated with Abrasive Waterjet Drilling of Ceramics," *Proceedings of 8th American Waterjet Technology Conference*, Paper 66, Vol.II, August, 1995, pp. 895-905.

Kobayashi, A. S., "Hybrid Experimental-Numerical Stress Analysis," *Handbook on Experimental Mechanics*, ed. A. S. Kobayashi, Prentice-Hall, 1987, pp. 739-767.

Post, D., Han, B., Ifju, P., "High Sensitivity Moiré Experimental Analysis for Mechanics and Materials," *Springer-Verlag*, New York, Inc. 1994.

Post, D., "Moiré Interferometry," *Handbook on Experimental Mechanics*, ed. A. S. Kobayashi, Prentice-Hall, pp. 314-387, 1987

Ramulu, M., "Dynamic Photoelastic Investigation on the Mechanics of Waterjet and Abrasive Waterjet Machining," *Optics and Lasers in Engineering*, 19, 1993, pp. 43-65.

10th American Waterjet Conference
August 14-17, 1999: Houston, Texas

NEURAL NETWORK MODEL OF WATERJET DEPAINTING PROCESS

K. Babets
E.S. Geskin
Waterjet Laboratory, Mechanical Engineering Department
Newark, NJ, USA

B. Chaudhuri
Particle Technology Research Center
Mechanical Engineering Department
Newark, NJ, USA

ABSTRACT

Current study is concerned with numerical modeling of waterjet depainting process. As a modeling tool a simple neural network with backpropagation of error was applied. After the network was "trained" and verified to perform satisfactory it was used for prediction of the output variable- the strip width once the set of input parameters (water pressure, traverse rate, stand-off distance) was specified, for sensitivity analysis and for the process optimization. The average relative error of prediction was 2.4%. Found sensitivity coefficients show how different input parameters influence the output parameter. The water pressure coefficient was found to be always positive, which proved that the increase in water pressure results in increase in a cleaning width. The traverse rate coefficient was always negative. The coefficient for standoff distance starts with positive values, then slowly decreases to zero (as cleaning width reaches its maximum) and takes negative values. The optimization scheme based on the Zoutendijk's method of feasible directions with slight modifications was used to find the set of optimal process parameters.

Organized and Sponsored by the WaterJet Technology Association

1. INTRODUCTION

Phenomena involved in surface cleaning are very complex and often not well understood. Often, physical measurements of the pertinent quantities are very difficult and expensive. These difficulties lead us to explore the use of neural networks systems as a way of processing experimental measurements. Neural networks approach the modeling representation by using precise inputs and outputs to "train" a generic model which has sufficient number of degrees of freedom to formulate a good approximation of the complex relationship between the inputs and the outputs. Neural networks, as a modeling tool, have a number of advantages. They can represent (i.e., model) complex nonlinear relationships, and they effective at classification of phenomena into pre-selected categories used in the training process. They can also deal with the noisy data by separating noise from a real data. On the other hand, the precision of the outputs is sometimes limited because the minimization of least square errors does not mean "zero error." Another drawback is the need for substantial data that are representative and cover the entire range over which the different variables are expected to change.

The detailed explanation of the experimental setup and experimental data used in the construction of Neural Network model are given in paper " Fuzzy Logic Model of Waterjet Depainting: grapho-analytical approach", which will be presented at X Waterjet Technology Conference, Houston, Aug, 1999.

2. INTRODUCTION TO ARTIFICIAL NEURAL NETWORKS

An artificial neural network consists of many interconnected identical elementary processing units or neurons, in architecture inspired by the structure of the cerebral cortex of the brain. A neuron is a simple processing unit (Fig .1), which consists of two parts. First part simply sums up all the weighted inputs (I) from other neurons, while the second part modifies this aggregated input by applying an activation function to it. The input signals X1, X2, X3…, Xn are sent to a processing unit. A connection from an input unit to a processing unit is assigned a so- called weight (w_n), which modifies input signal, making it either positive or negative, which corresponds to acceleration or inhibition of the signal in a biological neuron.

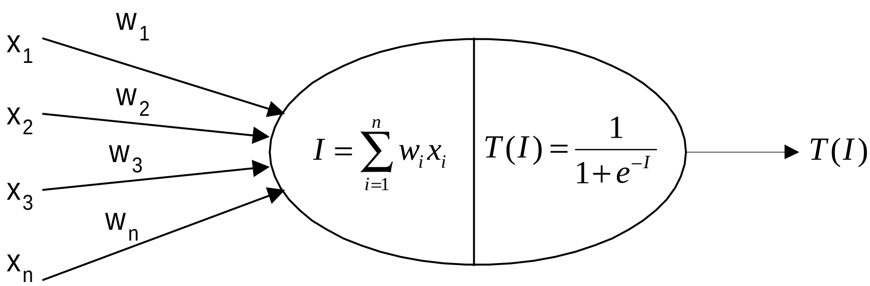

Figure 1. Schematic of an Artificial Neuron.

The working of a neuron is summarized in the following equations. Equation 1 shows that an input to a neuron is composed of the sum of weighted outputs from the neurons in the proceeding layer. Equations 2 and 3 shows that a neuron generates an output by applying a function to its input, found in (Eq.1).

$$\mathrm{I} = \sum_{i=1}^{n} w_i x_i \quad \text{Sum of wighted inputs} \qquad (\text{Eq.1})$$

$$\mathrm{T} = T(\mathrm{I}) \quad \text{Activation function} \qquad (\text{Eq.2})$$

The most widely used activation function is the logistic sigmoid, given by:

$$T(\mathrm{I}) = \frac{1}{1+\mathrm{e}^{-\mathrm{I}}} \qquad (\text{Eq. 3})$$

The activation function limits the values of the output of an artificial neuron to values between two asymptotes (0-1 in this case). This limitation is very useful in keeping the output within a reasonable dynamic range.

The neurons in a network are usually arranged in layers (Fig. A1). A number of layers in the network depend on a problem complexity. Within the network the information from a neuron in the preceding layer goes to all the neurons in the next layer through the network connections. Each connection has its weight associated with the importance of this particular connection. Training or learning is the process of adjusting the internal parameters of a network (its weights) to reach its optimum performance. During training (learning) process these weights are adjusted according to some particular algorithm, thus memorizing a functional relationship between input and output variables. The backpropagation training algorithm is shown in Fig. A2. Prior to training the data base representing the process is divided into training data set and checking data set. The data in each set is represented in form of input – output pairs. In a supervised learning an input pattern, presented to the network, generates some random output. This generated output is compared to the desired target value to define an error. This error is then backpropagated to adjust the weights in order to minimize this error function. These new weights are then assigned to a network and the procedure is repeated for a new input – output pair. This procedure is repeated iteratively until all training data pairs are used. The error after each iteration is stored to accumulate the total error. After all training data pairs are used (one epoch) the total error is compared to some specified error tolerance. If the tolerance is not met the procedure is repeated. If the tolerance is satisfied the procedure is stopped and the weights adjusted after the last iteration constitute the output of the training. These weights are assigned to the network and the network is considered to be trained. To check the network performance the checking data set is used. After the network is checked to perform satisfactory it is used as the model of the process, i.e. for process prediction, sensitivity analysis, optimization, etc.

3. NEURAL NETWORK MODEL OF WATERJET DEPAINTING PROCESS

The network architecture used in modeling of waterjet depainting process is shown in Fig.A1. For this problem the four-layer network is chosen. The input layer consists of three neurons, which corresponds to the number of experimental parameters. That is X_1 represents the water pressure, X_2 represents the traverse rate, and X_3 represents the standoff distance. The output layer consists of one neuron (T), which corresponds to the process output variable, the strip width. Two hidden layers are used in the current network's architecture. Biases (neurons which activation's are always a unity) are also included.

An experimental database representing waterjet depainting was acquired and divided into two data sets- training and checking. The training data set was used to train the network to respond correctly to an input pattern. A simple feed forward algorithm with backpropagation of error was used in the training of the network (Fig (A2)). The detailed discussion of this method is available elsewhere (Tsoukalas et al., 1997), and therefore only a brief summary is presented here.

For a multilayer neural network with two hidden layers, three input neurons, one output neuron and a notation given in Fig. A1 the following set of algebraic equations apply:

$$\text{First hidden layer:} \quad I_{(h)} = U_{0,h} + \sum_{i=1}^{3} U_{i,h} \cdot X_i \qquad \text{(Eq. 4)}$$

$$Z_{(h)} = \frac{1}{1+e^{-I_h}} \quad for\ h = 1,5 \qquad \text{(Eq.5)}$$

$$\text{Second hidden layer:} \quad II_{(j)} = V_{0,j} + \sum_{h=1}^{5} V_{h,j} \cdot Z_{(h)} \qquad \text{(Eq.6)}$$

$$ZZ_{(j)} = \frac{1}{1+e^{-II_j}} \quad for\ j = 1,5 \qquad \text{(Eq.7)}$$

Output layer:

$$I_{(k)} = W_{0,k} + \sum_{j=1}^{5} W_{j,k} \cdot ZZ_{(j)} \qquad \text{(Eq.8)}$$

$$T_k = \frac{1}{1+e^{-I_k}} \quad for\ k = 1 \qquad \text{(Eq.9)}$$

The error is then computed as:

$$\mathrm{E} = 0.5 \cdot \sum_{\mathrm{k}} \left[\mathrm{Y_k} - T_k\right]^2 \quad \text{for k} = 1 \qquad \text{(Eq.10)}$$

where T_k is the network's output and Y_k is the experimental value of the output variable. The equations 4-10 are the standard representation of signal propagation in a feed forward neural network (Tsoukalas et al., 1997). After the error is defined it is propagated backwards to define new weights. A weight updating is then performed according to the following formulae:

$$W_{j,k}^{new} = W_{j,k}^{old} - \eta \cdot \left(\frac{\partial E}{\partial W_{j,k}} \right)^{old} \qquad \text{(Eq.11)}$$

$$V_{h,j}^{new} = V_{h,j}^{old} - \eta \cdot \left(\frac{\partial E}{\partial V_{h,j}} \right)^{old} \qquad \text{(Eq.12)}$$

and

$$U_{i,h}^{new} = U_{i,h}^{old} - \eta \cdot \left(\frac{\partial E}{\partial U_{i,h}} \right)^{old} \qquad \text{Eq.13)}$$

where the expressions in the brackets are the partial derivatives of the error function (Eq. 10) with respect to weights on different connections, and η is a some small constant, called the learning constant. Since error is a function of weights then these partial derivatives are evaluated as follows:

$$\frac{\partial E}{\partial W_{j,k}} = \frac{\partial E}{\partial T_k} \frac{\partial T_k}{\partial I_{(k)}} \frac{\partial I_{(k)}}{\partial W_{j,k}} = -[Y_k - T_k] \cdot T_k \cdot (1 - T_k) \cdot ZZ_{(j)} \text{, for j} = 1{,}5 \text{ and k} = 1. \qquad \text{(Eq.14)}$$

where E is given by Eq.10, T_k is given by Eq.9, and I_k is given by Eq.8. In the similar manner the rest of the desired derivatives is presented:

$$\frac{\partial E}{\partial V_{h,j}} = \frac{\partial E}{\partial T_k} \frac{\partial T_k}{\partial I_k} \frac{\partial I_k}{\partial ZZ_{(j)}} \frac{\partial ZZ_{(j)}}{\partial II_{(j)}} \frac{\partial II_{(j)}}{\partial V_{h,j}} = -[Y_k - T_k] \cdot T_k \cdot (1 - T_k) \cdot W_{j,k} \cdot ZZ_{(j)} \cdot$$
$$(1 - ZZ_{(j)}) \cdot Z_{(h)} \quad \text{for h} = 1{,}5\text{, j} = 1{,}5\text{, k} = 1 \qquad \text{(Eq.15)}$$

$$\frac{\partial E}{\partial U_{i,h}} = \frac{\partial E}{\partial T_k} \frac{\partial T_k}{\partial I_k} \frac{\partial I_k}{\partial ZZ_{(j)}} \frac{\partial ZZ_{(j)}}{\partial II_{(j)}} \frac{\partial II_{(j)}}{\partial Z_{(h)}} \frac{\partial Z_{(h)}}{\partial I_{(h)}} \frac{\partial I_{(h)}}{\partial U_{i,h}} = -[Y_k - T_k] \cdot T_k \cdot (1 - T_k) \cdot W_{j,k} \cdot ZZ_{(j)} \cdot$$
$$(1 - ZZ_{(j)}) \cdot V_{h,j} \cdot Z_{(h)} \cdot (1 - Z_{(h)}) \cdot X_i \qquad \text{(Eq.16)}$$

The new weights are then substituted in to the network and this procedure is repeated iteratively until the network is trained. After the network is trained its performance is verified with a testing data set. At this point only the feed forward part of the algorithm is applied. When the network is verified to perform satisfactory it can be used as the model of the process- for sensitivity analysis, optimization, or for prediction of an output, once an input is specified.

Figure 2 shows the convergence of the training of the neural network for waterjet depainting. The training of this network takes 2,876 cycles; the final error is 0.024. The results of the process prediction using Artificial Neural Network Model are presented in figures A3-A6.

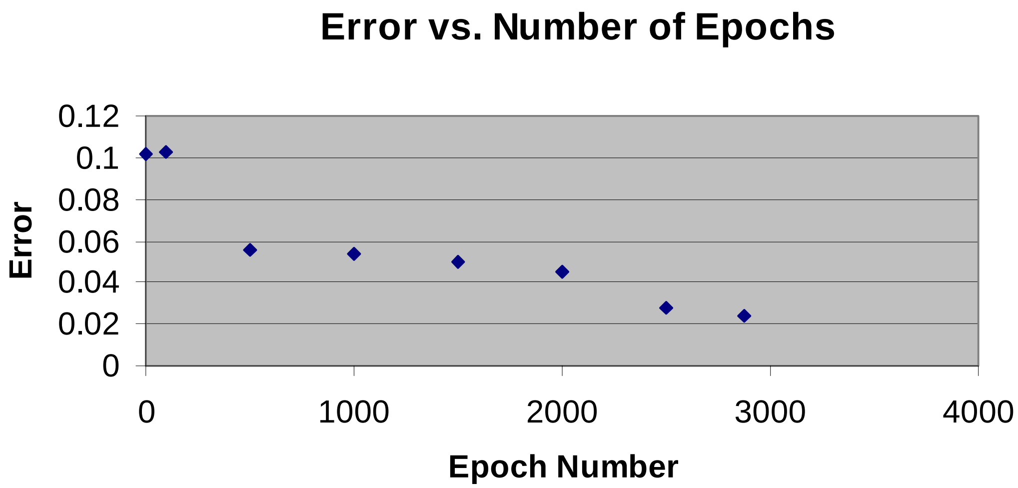

Figure 2. Training of the Neural Network.

4. SENSITIVITY ANALYSIS

In performing sensitivity analysis we are interested in evaluation of the degree of influence of different input variables on the process output. In other words, if we slightly perturb input, how would output react? And what input influences output(s) the most. For the network with two hidden layers, using the notation of Fig. A1 the desired gradients are found in the following manner:

$$\sigma_i = \frac{\partial T_k}{\partial X_i} = \frac{\partial T_k}{\partial I_{(k)}} \frac{\partial I_{(k)}}{\partial ZZ_{(j)}} \frac{\partial ZZ_{(j)}}{\partial II_{(j)}} \frac{\partial II_{(j)}}{\partial Z_{(h)}} \frac{\partial Z_{(h)}}{\partial I_{(h)}} \frac{\partial I_{(h)}}{\partial X_i} = T_k \cdot [1 - T_k] \cdot \sum_{j=1}^{5} W_{j,k} \cdot ZZ_{(j)} \cdot (1 - ZZ_{(j)}) \cdot \sum_{h=1}^{5} V_{h,j} \cdot Z_{(h)} \cdot (1 - Z_{(h)}) \cdot U_{i,h} \quad \text{for i} = 1,3\text{, j} = 1,5\text{, h} = 1,5 \tag{17}$$

where T_k, I_k, ZZ_j, II_j, Z_h, I_h are given by Equations 9,8,7,6,5,4 respectively.

In observing the calculated sensitivity coefficients we could see the following pattern. The coefficient σ1, which corresponds to X1 input variable, is always positive. It suggests that as we increase X1 the magnitude of the output variable Y also increases. As for the coefficient σ2, which correspond to process variable Traverse Rate (X2), we see that it always has a negative value. Which means that positive change in X2 results in a decreasing value of an output variable. Or, in other terms, as we increase traverse rate of the nozzle, a cleaning width will rapidly decrease.

The third sensitivity coefficient, σ3, which shows the influence of the standoff distance on the output variable- the strip width, behaves in the following manner. As we can see from the Fig

A3, strip width increases with increasing standoff distance, until the optimum standoff distance is reached, beyond which the further increase in standoff distance results in decrease in the strip width. The coefficient σ3 starts with positive values, reduce to zero at the point of extremum, and proceeds with negative values.

5. PROCESS OPTIMIZATION

In any cleaning operation we are interested in finding a set of waterjet parameters which produces the highest cleaning rate. The cleaning rate is given by:

Cleaning Rate = Nozzle Traverse Rate * Width of Strip (Eq. 18)

Thus the optimization problem is to determine the set of waterjet parameters which maximize the objective function given as product of Nozzle Traverse Rate (X2) and Width of Strip (T) subject to some process constrains. These constrains limit the waterjet pressure to a chosen range (67 MPa - 276 MPa) and Nozzle Traverse Rate (635 mm/min – 8890 mm/min) since any value of these parameters beyond these ranges will result either in incomplete paint removal or substrata damage. Thus the optimization problem is:

$$\max IP = X2 \cdot T \qquad \text{(Eq.19)}$$

$$\text{subject to :}$$

$$X_{1\min} \le X_1 \le X_{1\max} \;\;,\;\; X_{2\min} \le X_2 \le X_{2\max}$$

where IP is index of perfomance, X_1 is waterjet pressure, X_2 is nozzle traverse rate and T is the process output - the strip width.

The neural network model of the waterjet depainting is a set of algebraic equations. Thus, the problem of determining the set of waterjet parameters for optimal process productivity is a constrained optimization problem for which a number of standard methods can be utilized. In this work the optimization scheme based on the Zoutendijk's method of feasible directions with slight modifications was used. In general all gradient descent methods require calculation of gradient of the objective function with respect to control variables. For the objective function given by equation 19, the desired gradients can be expressed as:

$$\frac{\partial IP}{\partial X_i} = \frac{\partial (X_2 \cdot T)}{\partial X_i} = X_2 \frac{\partial T}{\partial X_i} + T \frac{\partial X_2}{\partial X_i} \quad \text{for i} = 1,2,3 \qquad \text{(Eq.20)}$$

obviously, $\frac{\partial X_2}{\partial X_i}$ is equal to zero if $i \neq 2$, and equal to unity, if $i = 2$.

The evaluation of the gradient d(output)/d(input) is given by Eq.17.

Thus the optimization scheme is given by:

$$X_{i\,new} = X_{i\,old} + \lambda_i \cdot \frac{\partial(X_2 \cdot Y)}{\partial X_i}, \qquad \text{(Eq.21)}$$

Where λ(i) is a step length for simplicity was taken as a small constant, with sign equal to that of the corresponding sensitivity coefficient.

6. RESULTS AND DISCUSSION

In this work we applied the artificial neural network for modeling the waterjet depainting process. The results of the modeling are presented in figures A3- A7. The predicted values of strip widths for different standoff distances at different water pressures correspond to measured ones rather accurately thus the model can be used for practical purposes. The neural network model was also used for sensitivity analysis (Eq. 17), to evaluate the effect of process variables on the process output. As the result of the computation we determine the strong effect of the increase of water pressure and decrease of traverse rate on the strip width. The results are rather obvious and demonstrate the effectiveness of the technique. More interesting is the investigation of the effect of standoff distance on process result. The change of the sign of the coefficient σ3 shows that the relationship between the strip width and the standoff distance has extremal points, which represent the optimal values of this variable. We investigated the effect of the traverse rate and water pressure on the optimal values of the standoff distance. The iterative procedure used for this investigation was similar to that given by Eq. (18-21). In this case the objective function was given by Y (the strip width), and the process variable being optimized was the stand-off distance. Water pressure and traverse rate were fixed. The results of these calculations are shown in Fig. A7. This figure indicates the effectiveness of the increase of the standoff distance as water pressure increases and traverse rate drops. This conclusion constitutes a reasonable recommendation to practitioners. We also investigated the overall process optimization. As a result of the optimization scheme given by Equations 18-21, the following waterjet parameters were obtained: X1 (Waterjet Pressure)= 274.632 MPa, X2 (Nozzle Traverse Rate) =8889.89 mm/min, X3 (standoff distance) = 187.453 mm. These values of the water pressure and traverse rate are the maximum values used in the experimental study. The resulting width of strip is 2.516 mm, productivity of the process was 1.342 m2/hour.

7. CONCLUSION

In the course of this study we applied a neural network procedure for evaluation of waterjet depainting. The process information was rather trivial and can be acquired by routine experiments. The experimental database used for this analysis included 120 data points. No special computational facilities were needed. Thus both experimental and numerical facilities required for this investigation do not exceed capabilities of a small research group. As a result of the performed analysis we generated a trained network, which constitute a reasonable process model. When a new analysis is required a comparatively modest additional training will be needed. Thus a rather practical routine for modeling of waterjet depainting is suggested.

8. REFERENCES

Earl Cox, “The Fuzzy Systems Handbook: a Practitioner’s Guide to Building, Using, and Maintaining Fuzzy Systems,” *AP Professional*, 1994.

Mohammed Hashish, “Prediction Models for AWJ Machining Operations,” *Proceedings of the 7th American Water Jet Conference,* pp. 205-216, Seattle, Washington, 1993.

Spencer T. Johnson, “Advances in Cleaning and Coating Removal Using Ultra-High Pressure Water Jet Technology,” *Proceedings of the 7th American Water Jet Conference*, pp. 607-610, Seattle, Washington, 1993.

H. Louis, W. Schicorr, “Fundamental Aspects in Cleaning with High Speed Water Jets,” *Proceedings of the 6th International Symposium on Jet Cutting Technology*, pp. 217-228, BHRA, Guildford, England, 1982.

P. Meng, “Experimental and Analytical Investigation of Water Jet Cleaning Process,” *Ph.D. Thesis*, New Jersey Institute of Technology, 1996.

P. Meng, E. Geskin, L. Tismenetskiy, “Cleaning with High Pressure Directed Waterjets,” *Proceedings of Japan-USA Symposium on Flexible Automation*, Boston, MA, 1996.

Leftery H. Tsoukalas, Robert E. Uhrig, “Fuzzy and Neural Approaches in Engineering,” *John Wiley & Sons*, 1997.

Jeffrey D. Watson, “Thermal Spray Removal with Ultrahigh-Velocity Waterjets,” *Proceedings of the 7th American Water Jet Conference,* pp. 583-595, Seattle, Washington, 1993.

Samuel S. Wu & Thomas J. Kim, “An Application Study of Plain Waterjet Process for Coating Removal,” *Proceedings of the 8th American Water Jet Conference,* pp.779-792, Houston, Texas, 1995.

9. NOMENCLATURE

X - input signal

Y - target value (experimental)

T(I) - output signal

I - the sum of the weighted inputs to the neurons in the first hidden layer

II - the sum of the weighted inputs to the neurons in the second hidden layer

Z - output of the neurons of the first hidden layer

ZZ - output of the neurons of the second hidden layer

U - the weights on connections to the first hidden layer

V - the weights on connections to the second hidden layer

W - the weights on connections to the output layer

E - error function

σ - sensitivity coefficient

IP – index of performance

η- learning constant

λ - optimization step size

subscripts:

i =1,n – index of the input neurons

h=1,p – index of the first hidden layer neurons

j=1,q – index of the second hidden layer neurons

k= 1 – index of the output layer neurons

10. GRAPHICS

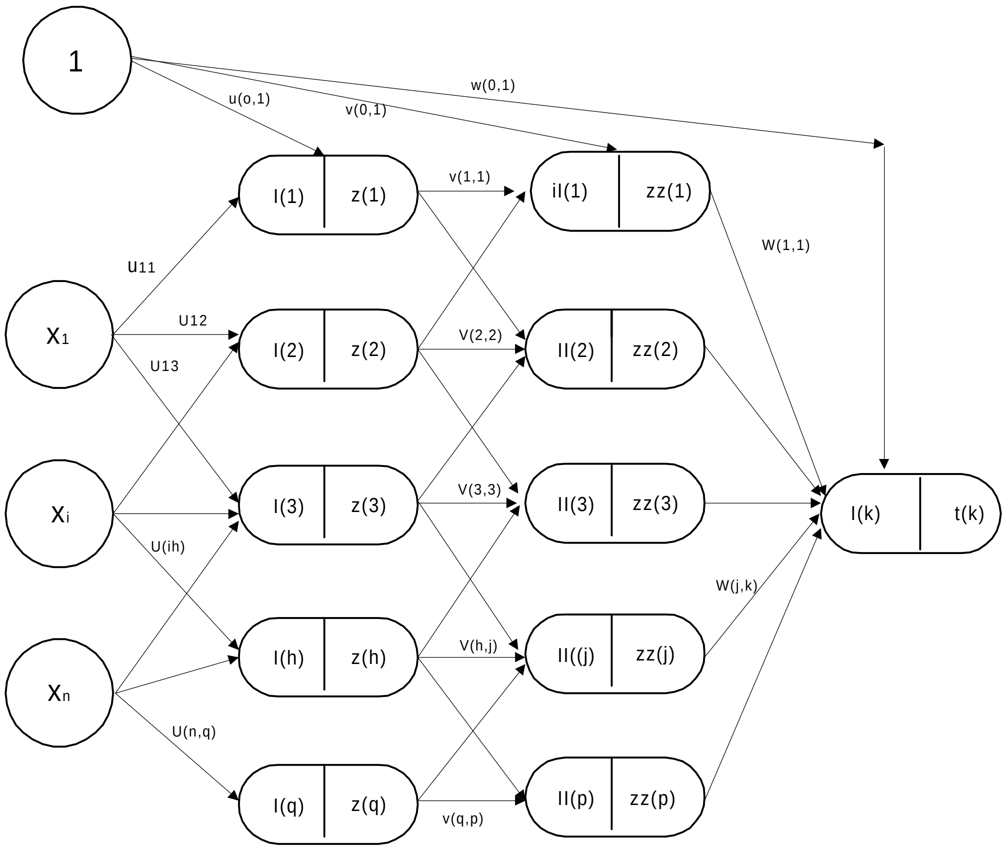

Nodes: x(i), i=1,n z(h), h=1,q zz(j), j=1,p

Weights: u(0,1),…,u(i,h) v(0,1),…,v(h,j) w(0,1),…,w(j,k)

Figure A1. Structure of NN for Waterjet Depainting.

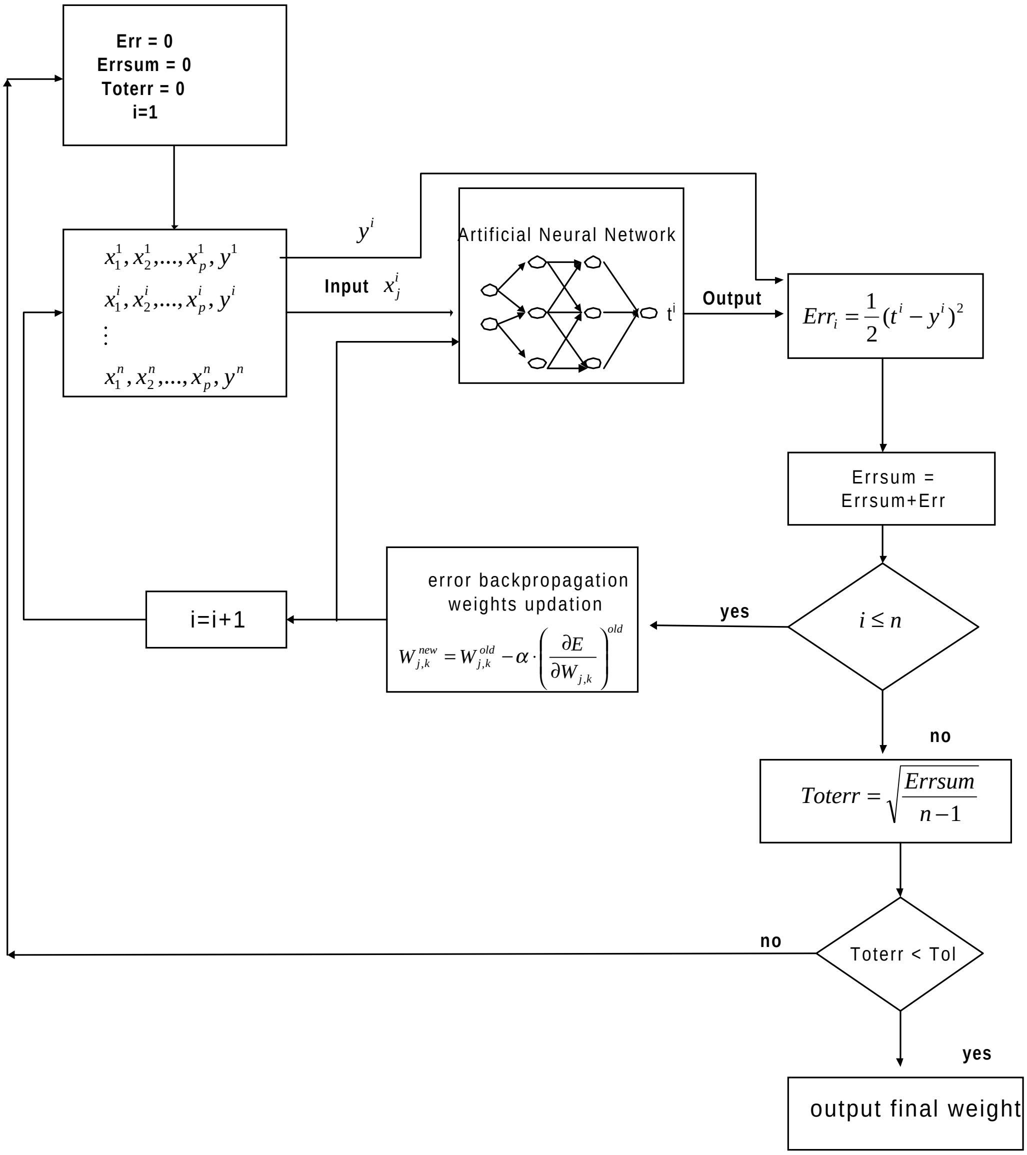

Figure A2. Training of Artificial Neural Network.

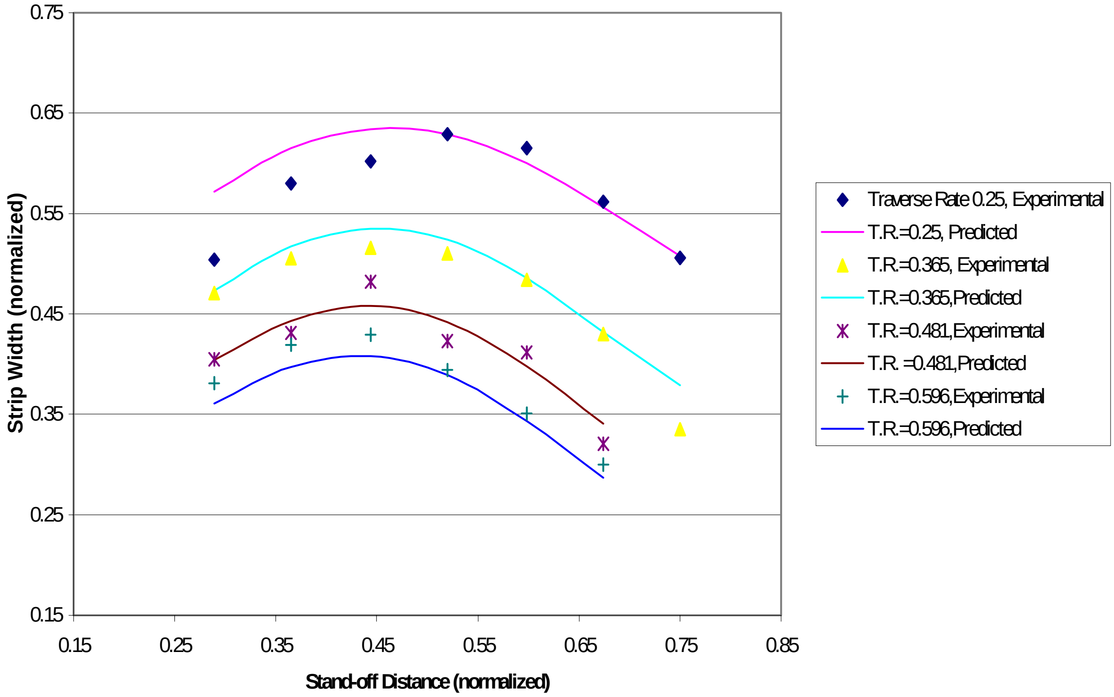

Figure A3. Neural Network Prediction Results. Strip Width vs. Standoff Distance for Water Pressure 138 MPa.

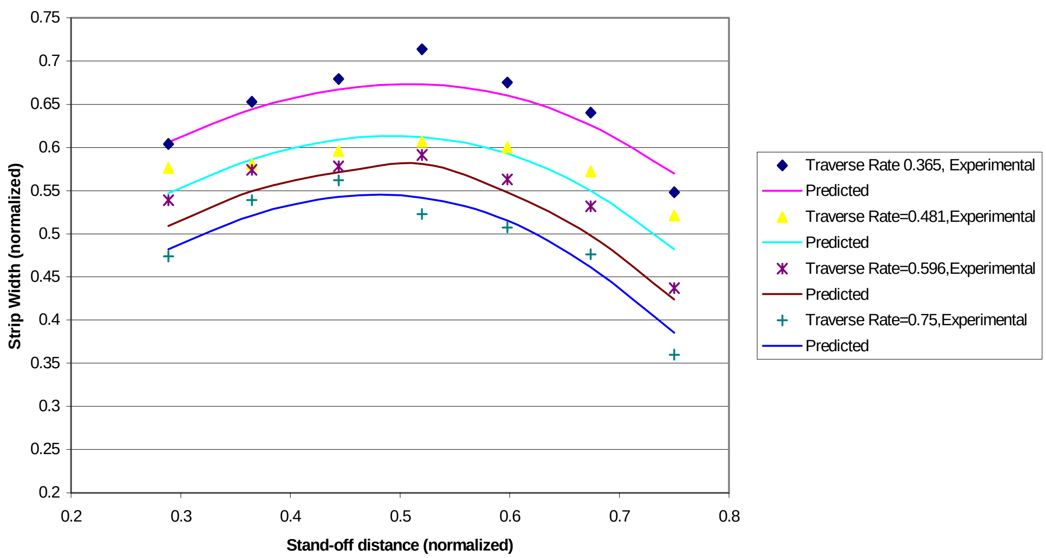

Figure A4. Neural Network Prediction Results. Strip Width vs. Standoff Distance for Water Pressure 276 MPa.

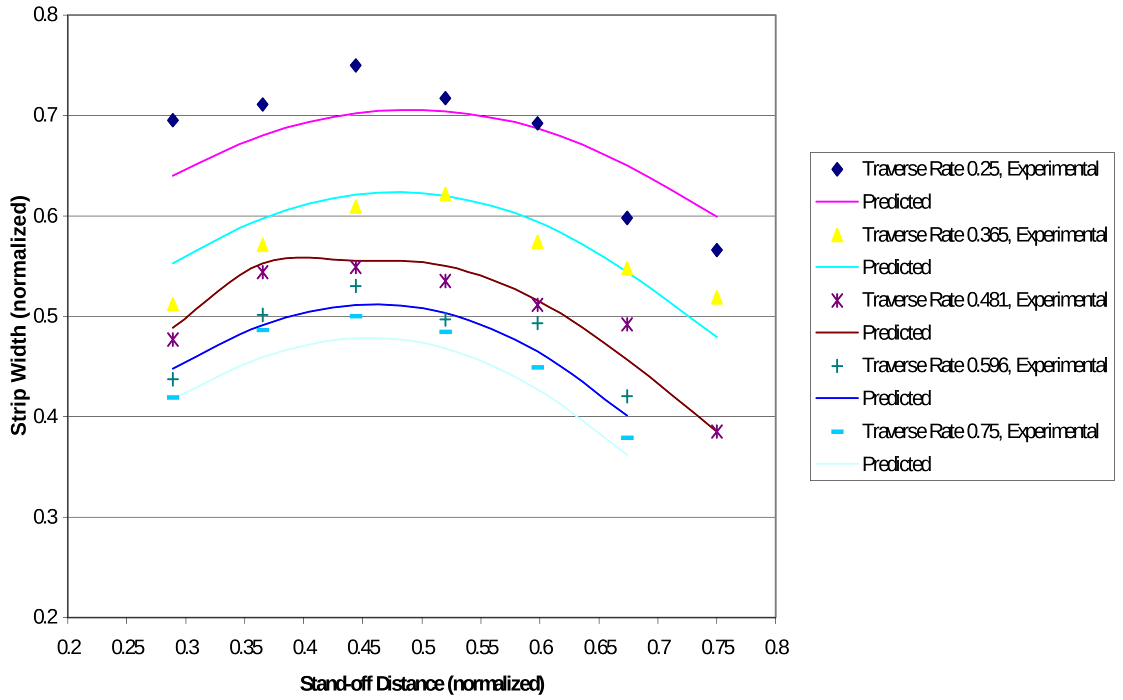

Figure A5. Neural Network Prediction Results. Strip Width vs. Standoff Distance for Water Pressure 207 MPa.

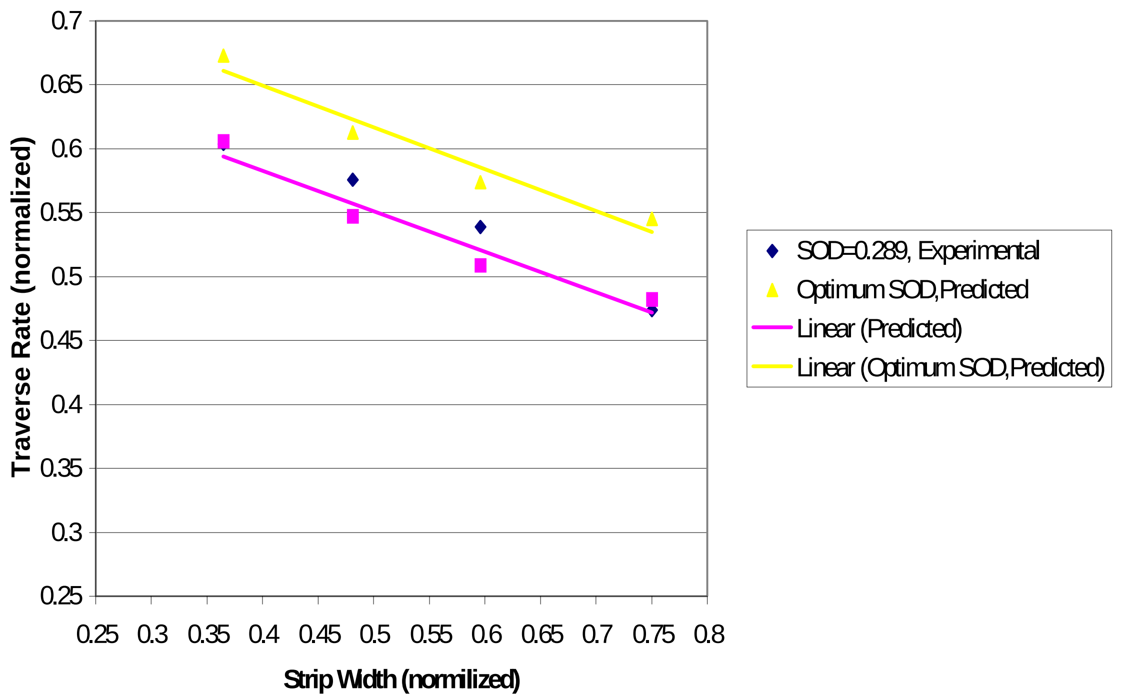

Figure A6. Neural Network Prediction Results. Strip Width vs. Traverse Rate for Water Pressure 276 MPa.

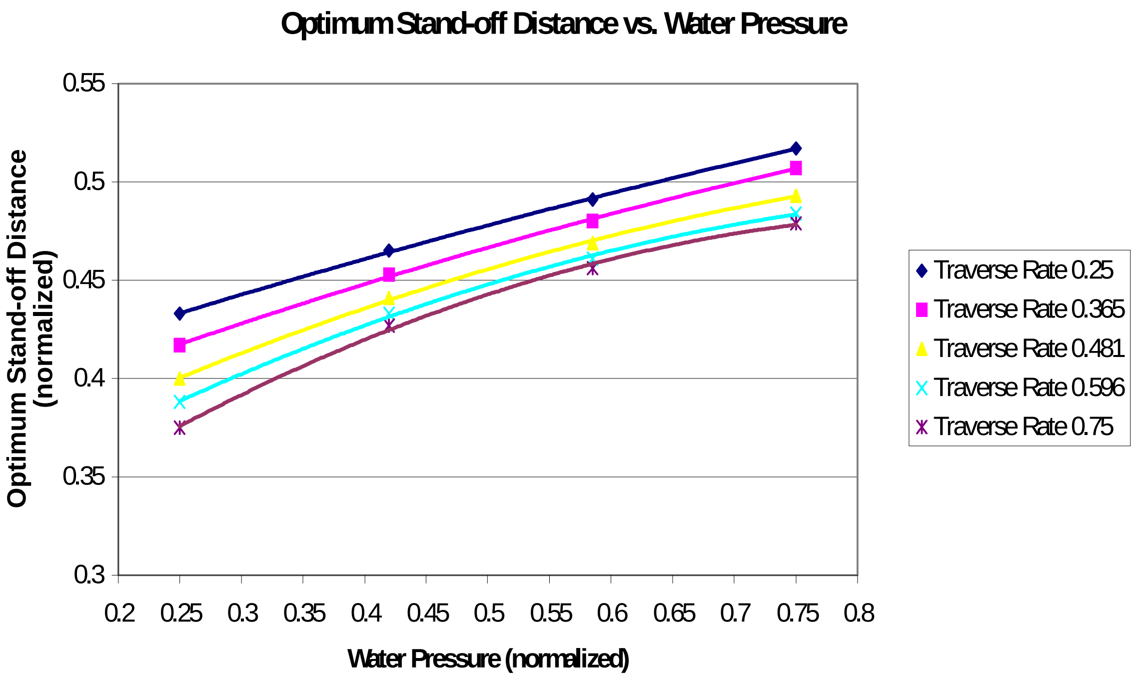

Figure A7. Neural Network Prediction Results.

10th American Waterjet Conference
August 14-17, 1999: Houston, Texas

Paper **5**

FINITE ELEMENT MODELING OF CRACK PROPAGATION IN PCC SLABS SLOTTED WITH ABRASIVE WATER JET

Ram S. Mohan
The University of Tulsa
Tulsa, Oklahoma U.S.A.

Radovan Kovacevic
Southern Methodist University
Dallas, Texas U.S.A.

ABSTRACT

In order to circumvent the disadvantages of the conventional cracking and seating technique a new approach is proposed for rehabilitation of Portland cement concrete (PCC) pavements using abrasive water jet. This approach focuses on controlled and uniform fragmentation of the PCC pavement substrate initiated by previously cut slots using abrasive water jet (AWJ). Initially a parametric study is conducted in order to quantify the influence of the AWJ cutting parameters on the depth of cut on the PCC slabs. Subsequently, detailed investigation of the virtual crack propagation in the PCC slab slotted with abrasive water jet is conducted using finite element modeling technique to evaluate the best geometry of slotting. The stress distribution and nature of crack initiation and crack propagation with varying loads for several depths of slots are evaluated for different slot geometries and compared with that of a concrete slab without any prior slots. The results indicate that diagonal slots not only provide uniform size fragments and crack patterns extending through the entire thickness, eliminating spalling, crack fanning and shattering, but also, preserve the structural strength of the substrate.

Organized and Sponsored by the Waterjet Technology Association

1. INTRODUCTION

National highways and airports of industrialized countries extensively use portland cement concrete as the construction material. Spalling, cracking, joint disintegration and faulted joints cause deterioration of pavement quality considerably, as it ages. Deteriorated PCC pavements pose safety hazards, riding discomfort, and lead to increased maintenance costs, increased vehicle operating costs and other maintenance problems. Rehabilitation of damaged PCC pavements is usually performed by overlaying the pavement with hot mix asphalt (HMA). If proper precautions are not taken before performing the overlay process, the quality of the asphalt overlay could deteriorate considerably due to 'reflective cracking'. 'Reflective cracks' usually propagate through the entire thickness of the asphalt layer. The basic mechanisms responsible for the reflective cracks in the asphalt layer are the horizontal and vertical movements of the underlying PCC pavement (Jayawickrama and Lytton, 1987). The horizontal movement of the PCC substrate is caused by tensile stresses due to expansion and contraction as a result of temperature and/or moisture changes. The vertical movement is produced by high shear stresses in the asphalt layer due to differential deflection and vertical movement caused by wheel loads moving over a crack or joint in the PCC. Several techniques of PCC slab reduction such as cracking and seating, breaking and seating, or rubblizing are resorted to before asphalt overlay to minimize the horizontal and vertical movements of the PCC.

Among the PCC pavement rehabilitation techniques, cracking and seating is found to be very economical especially for those without reinforcements (Schutzbach, 1989). As a result of this technique, the existing slabs, while maintaining some degree of aggregate interlock load transfer are able to undergo the rehabilitation process effectively. Cracking it into small pieces reduces the horizontal movement of the pavement substrate, which causes it to perform as a semi rigid system. Seating the pavement firmly against the sub grade minimizes the vertical movement of the PCC pavement. For heavily reinforced slabs, the steel reinforcement as well as the concrete have to be broken through a technique which is called break and seat technique. Different types of expensive and heavy duty cracking equipment such as hydraulic spring hammer, pile hammer, impact hammer, guillotine hammer, and whip hammer are used nowadays to crack the PCC substrate (Thompson, 1989, Sharpe, et al., 1987, Lukanen, 1987). Disadvantages of the currently used cracking techniques are lack of control on the crack pattern and the size of the slab's fragments, lack of penetration of the crack through the entire thickness of the slab and degradation of the substrate strength due to slab fragments, spalling, crack fanning and shattering (Schutzbach, 1989). The increased difficulty in achieving cracking in PCC pavements with steel reinforcements also contributes to the difficulty of achieving good performance.

In order to circumvent the above disadvantages of the current cracking and seating technique a new approach is proposed in this investigation for rehabilitation of PCC pavements using abrasive water jet. This approach focuses on controlled and uniform fragmentation of the PCC pavement substrate initiated by previously cut slots using abrasive water jet (AWJ). Initially, a brief overview of PCC pavement rehabilitation technique is provided followed by development of an empirical equation relating the AWJ process parameters and the depth of cut. Then, finite element modeling (FEM) is performed to evaluate the crack propagation through the PCC pavement concrete slotted with abrasive water jet. Finally, the results of this investigation of virtual crack propagation in PCC slabs are evaluated to determine the best geometry of AWJ slotting.

2. ROLE OF ABRASIVE WATER JET IN PCC PAVEMENT REHABILITATION

Although cracking and seating has become very popular for PCC pavement rehabilitation, the current techniques used for cracking have several disadvantages as stated above. It is impossible to achieve optimal crack patterns, especially vertical cracks, which are adequate to eliminate thermally related reflective cracking. The size of the fragments has a direct impact on the design considerations as well as long-term performance of the overlay (Crawford, 1989). Also, the crack pattern depends on the impact equipment, energy of impact, slab temperature, inherent stresses in the slab, and sub grade condition. The jackhammers, which are used for the cracking and seating technique are slow, noisy, dusty and labor intensive (Sharpe, et al., 1987). While using them, it is impossible to avoid removing the good concrete along with the bad or damaged reinforcing steel (Sugiyama and Tabata, 1988). Often times, it is also necessary to remove the existing asphalt overlays prior to cracking in order to verify the crack pattern.

Rehabilitation of PCC pavements assisted with abrasive water jets is a viable alternative to prolong the service life of the overlays and decrease the future maintenance costs. The advantages of this technique (Mohan and Kovacevic, 1998) are:

1. The shape and size of the PCC fragments could be controlled. Instead of square or rectangular shaped PCC fragments, any desired shape, which is appropriate for cracking, could be produced.
2. Transverse and longitudinal cracks in the PCC pavements, which have a detrimental effect, could be eliminated.
3. Structural strength of the PCC pavement could be preserved.
4. Spalling, crack fanning and shattering could be eliminated.
5. The crack pattern does not depend upon the impacting force, slab temperature, the residual stresses in the slab, or the sub grade condition.
6. It is relatively easy to cut the reinforcement as well as the asphalt overlay. It is also easy to verify the presence of the crack pattern even when the asphalt overlays are present.

In order to capitalize on the advantages offered by AWJ in PCC pavement rehabilitation, the current investigation is aimed at exploring the feasibility of replacing the existing methods of cracking and seating by notching and seating assisted with AWJ. The efficiency and economy of application of the AWJ in PCC pavement rehabilitation could be improved considerably by an optimum choice of the process parameters and the geometry of slotting. There have been several investigations dealing with concrete cutting with water jet and abrasive water jet (Sugiyama and Tabata, 1988, Fairhurst and Spencer, 1985, Arasawa, et al., 1986, and Schmid, 1989). Investigations of Arasawa et al. (1986) indicated that it is more effective to remove the concrete first and the cut the reinforcements afterwards while cutting reinforced concrete slabs with AWJ. Kokaji et al. (1988) investigated the effect of abrasives on the cutting performance of concrete and concluded that garnet abrasive has the highest cutting performance and that there is no correlation between the grade of garnet and the cutting depth. The present authors conducted a feasibility study (Kovacevic, et al., 1993, Mohan and Kovacevic, 1998) on concrete pavement rehabilitation using abrasive water jet. There have also been few investigations on numerical modeling of crack propagation and fracture in concrete (Gerstle and Xie, 1992, Ingraffea and Saouma, 1984, Swartz and Taha, 1990 and Swenson and Ingraffea, 1988). These investigations highlighted the merits of numerical modeling techniques for predicting the material failure mechanisms in concrete. Current investigation focuses on the usage of finite element modeling techniques for quantifying the effect of different slot geometry on the crack propagation and material failure pattern. A brief description of the experimental set up and procedure is given below.

3. EXPERIMENTAL SET UP AND PROCEDURE

A schematic of the abrasive water jet cutting system used for this investigation is shown in Fig. 1. The system consists of a high-pressure intensifier pump, AWJ cutting head, abrasive metering and delivery system, catcher tank and an X-Y-Z positioning system. The water is pressurized in the intensifier pump and sent to the cutting head where the high-pressure water is converted to high velocity water as it flows through the sapphire orifice assembly. The high velocity water jet is mixed with the abrasive particles in the mixing chamber and the slurry consisting of the abrasive water jet mixture flows through the AWJ nozzle and cuts the work piece. The position of the cutting head could be manipulated by the X-Y-Z positioning system equipped with a CNC controller.

Initially a parametric study is conducted based on 2^4 composite factorial design to quantify the effect of the AWJ cutting parameters namely water pressure, abrasive flow rate, traverse speed and standoff distance, on the depth of penetration. The workpiece material used was Portland cement concrete (PCC) of 15 years age, size 1.8 m X 0.30 m X 0.30 m and an average compressive strength of 34.4 Mpa.

In the second phase of the investigation, crack propagation through concrete slabs previously slotted with abrasive water jet is investigated using finite element modeling technique. Concrete slabs are slotted at different geometries such as longitudinal (case B), transverse (case C) and diagonal (case D). The stress distribution and nature of crack initiation and crack propagation with varying loads for different depths of slots are investigated for each of the above cases and compared with that of a concrete slab without any prior slots (case A). Finite element modeling software, ANSYS was used for the investigation. The element type was defined as STIF65 (DeSalvo and Gorman, 1989) which is primarily a non-linear 3D non-reinforced concrete element with cracking and crushing capability at integration points. STIF65 has also the capability to accommodate temperature sensitive stress distribution. This element type was adopted, as it is capable of treating cracking (in three orthogonal directions) during tension, crushing during compression, plastic deformation and creep. Each element was defined by 8 nodes with 3 degrees of freedom per node and the loading was performed gradually to avoid crushing at integration points. The work piece geometry of 1.8 M X 30 cm X 30 cm was adopted and a symmetry boundary condition about the X-axis and Y-axis was assumed. Analysis type KAN,0 (static) was adopted for the investigation. An overview of the results of this investigation followed by a brief discussion is provided below.

4. RESULTS AND DISCUSSION

4.1 Influence of Process Parameters on the Depth of Cut

In order to quantify the role of each process parameter on the depth of penetration, detailed experiments were conducted based on a 2^4 central composite factorial design of experiments. The parameters investigated were: water pressure (P), abrasive flow rate (Q), jet traverse speed (V) and standoff distance (S). The developed empirical model relating the above process parameters and depth of cut (d) for the above material could be expressed as:

$$d = 1.3545\,P^{0.7903}\,Q^{0.1844}\,V^{-0.5671}\,S^{0.0068} \tag{1}$$

Above equation is valid for the following range of process parameters:

$$103 \le P \le 241\,MPa$$
$$4.54 \le Q \le 9.07\,g/s$$
$$0.85 \le V \le 6.77\,mm/s$$
$$6.35 \le S \le 25.4\ mm$$

The abrasive material used was garnet with mesh size 36. The AWJ nozzle (length = 76.2 mm) inside diameter was 1.2 mm and the sapphire orifice diameter was 0.46 mm. The angle of impingement of the jet was 90^0. An excellent fit to the data was achieved with a multiple correlation coefficient or R^2 value of 0.96.

The above equation indicates that the water pressure, traverse speed and abrasive flow rate are the most influential parameters on the depth of cut. Planes of constant depth of cut of 40/60/90 mm derived from Eq. (1) are shown in Fig. 2. From this figure, it is relatively easy to determine the combination of the AWJ cutting parameters required to achieve the desired depth of cut in the PCC pavement block.

4.2 Finite Element Modeling of Virtual Crack Propagation in the PCC Pavement Slab

The equation (1) provides the relationship between the AWJ process parameters and depth of cut. This equation and Fig. 2 could be used to determine the process parameter settings, which will provide a known depth of slotting in the concrete. However, it is necessary to determine what will be the most optimal depth of cut and the geometry of cut, which will produce a predetermined orientation of crack propagation through the PCC slab during pavement rehabilitation. As noted earlier, prior slotting of PCC pavements with AWJ will also produce uniform size fragments making the rehabilitation process simpler and cheaper. In order to evaluate the geometry of AWJ slotting, a finite element modeling of the stress distribution and crack propagation in the PCC slabs with and without AWJ slotting when subjected to gradual compressive load (till failure) is investigated. Four different depths of slotting were considered namely 25 mm, 50 mm, 75 mm, and 100 mm. Three slotting geometry namely longitudinal, transverse and diagonal are considered (see Fig. 3) for comparison with crack propagation in PCC slabs without slotting. Initial investigations indicated that with increase in depth of slotting the onset of cracks and failure of the PCC slabs were occurring relatively early. However, considering the additional effort needed to slot the PCC with AWJ, savings in the time of crack initiation and propagation through the entire thickness of the PCC slab, and the need to have uniform sized cracks, a slotting depth of 75 mm was found to be optimal. It may be noted that this depth is one fourth of the thickness (300 mm) of the PCC slab. Hence, further investigations to determine the best geometry of slotting were conducted by slotting the PCC slab through a depth of 75 mm. A brief description of the procedure adopted and the results of FEM modeling are given below.

Material characteristics for failure due to cracking/crushing in the ANSYS program are based on an enhanced version of the five parameter William and Warnke (1975) failure model. With the William and Warnke algorithm as incorporated in the ANSYS program, concrete behavior can be modelled with a minimum of two parameters, namely ultimate tensile strength and ultimate compressive strength. Other three parameters that could be input are experimental values for bi-axial crushing stress, bi-axial crushing under ambient hydrostatic stress and uni-axial crushing stress. Temperature-based non-linearity could be taken into account by inputting parameter values at six temperature conditions. Shear friction between the cracked faces is accounted for by user controlled shear transfer coefficients for both opened and closed crack conditions during cracking analyses. The element theory is based upon a formulation, which includes modified extra displacement shapes. A 2x2x2 lattice of integration points were used with the numerical (Gaussian) integration procedure.

As plasticity problems are non-linear, an iteration procedure based on incremental Newton-Raphson method was adopted for analyzing the plasticity effects. For plasticity analysis, plastic incompressibility assumption was adopted where the tensile and compressive yield stresses are related by the consistency equation:

$$\frac{\sigma_{+x} - \sigma_{-x}}{\sigma_{+x}\sigma_{-x}} + \frac{\sigma_{+y} - \sigma_{-y}}{\sigma_{+y}\sigma_{-y}} + \frac{\sigma_{+z} - \sigma_{-z}}{\sigma_{+z}\sigma_{-z}} = 0 \tag{2}$$

where, σ_{+i} is the magnitude of the tensile yield stress in direction *i*, and σ_{-i} is the magnitude of the compressive yield stress. The yield stress must also define a closed yield surface, which is mathematically given as:

$$M_{xx}^2 + M_{yy}^2 + M_{zz}^2 - 2(M_{xx}M_{yy} + M_{yy}M_{zz} + M_{zz}M_{xx}) < 0 \tag{3}$$

which should always be true, where M_{ii} = $(\sigma_{+x}\sigma_{-x})/(\sigma_{-i}\sigma_{+i})$. Creep was also handled by the incremental technique of Newton-Raphson Method. The combined effect of primary creep and secondary creep were used for analysis. Kohnke (1989) may be consulted for further details.

Typical printouts of stress distribution for different types of slotting and various loading conditions are shown in Figs. 4 - 10 for the following cases:

Case A: PCC slab without slotting
Case B: PCC slab with longitudinal slots
Case C: PCC slab with transverse slots
Case D: PCC slab with diagonal slots

The stress distribution and the failure state for each of the above cases are described below.

4.2.1 Case A: PCC Slab Without Slotting

The Fig. 4 shows the PCC slab before crack initiation and Fig. 5 shows the PCC slab after failure. From these figures, it can be seen that failure of the PCC slab is due to localized crushing rather than uniform cracking which is very undesirable for pavement concrete as it will cause excessive loss of structural strength, non uniform and uncontrollable cracking pattern, and will lead to reflective cracking due to the vertical movement of the pavement slab. Fig. 11 shows the applied pressure in the Z-direction at the point of initiation of the cracking and after complete failure. It can be noted that the cracking is initiated at a pressure of about 26 Mpa and the material completely fails (in this case, due to crushing) at a pressure of about 36 Mpa. As can be intuitively expected, relatively larger pressure is required in the case of PCC slab without slotting for crack initiation and failure.

4.2.2 Case B: PCC Slab With Longitudinal Slots

Figure 6 shows the stress distribution in the PCC slab along a plane 75 mm below the Z-axis (where the kerf bottom of the longitudinal slots is present). This figure corresponds to the condition prior to crack initiation. It can be noted that the stress concentrations are along the slotted directions. Analysis of the PCC slab stress distribution after failure indicated that the concrete failure is primarily due to crushing of the slotted top layer rather than induced cracks. From Fig. 11, it can be seen that compared to the PCC slab without slot, lesser load is required to cause crack initiation and material failure for PCC slabs with longitudinal slots.

4.2.3 Case C: PCC Slab With Transverse Slots

In order to clearly visualize the failure mechanisms in the PCC slab with transverse slots, the stress distribution at the plane (Z = -150 mm) before failure for lead step 5 is plotted in Fig. 7. In this case, it can be noted that the stress concentrations are not oriented along the directions of the slots. Failure is due to localized crushing instead of cracking. The transverse slots do not seem to have much influence in reducing the cracking effort or deciding the crack pattern. Even though lesser load is required for causing crack initiation and material failure for PCC with transverse slots as indicated by Fig. 11, the failure mode of crushing is undesirable.

4.2.4 Case D: PCC Slab With Diagonal Slots

Stress concentration, cracks induced and material failure pattern in the PCC slab with diagonal slots at the initial stage of loading is shown in Fig. 8. A bisected view of the PCC slab, which shows the details of the internal cracks and stress concentration before complete material failure, is shown in Fig. 9 to visualize the failure pattern. Fig. 10 shows the crack pattern of the PCC slab after complete material failure. From these figures, it can be seen that the stress concentrations are along the slotted geometry as well as parallel to them. Cracks are clearly seen along the stress concentrations. From Fig. 10, it could be noted that the material failure is primarily due to internal cracking (which is the most desirable) rather than crushing. Fig. 11 indicates that relatively less load needs to be applied on PCC slabs with diagonal slots for causing crack initiation and material failure.

A schematic of the proposed slotting and seating procedure for PCC pavement rehabilitation assisted with abrasive water jet is shown in Fig. 12. Instead of using the currently available cracking equipment, diagonally oriented slots are initially created in the PCC pavement at appropriate depths using AWJ. Subsequently, the notched PCC pavement is subjected to seating process using heavy pneumatic tired rollers. As a result, a diagonal cracking pattern is induced in the PCC pavement, which is ideal for effective pavement rehabilitation. As these cracks propagate through the entire thickness of the pavement slab, all the fragments will be in contact with the supporting base or sub grade, eliminating voids in the PCC structure. Important conclusions from this investigation are briefly given below.

5. CONCLUSIONS

PCC pavement rehabilitation assisted with high-pressure abrasive water jet is a viable alternative to the conventional cracking and seating procedure. This technique could be used for rehabilitation of PCC pavements with and without reinforcements. It offers some unique advantages in terms of uniform fragment size, controlled cracking along predetermined directions, elimination of spalling, crack fanning and shattering, and preserving the structural strength of the pavement.

It is demonstrated that slots of predetermined depth could be cut in the PCC slab using the developed empirical model relating the AWJ process parameters namely water pressure, traverse speed, abrasive flow rate and stand-off distance to the depth of cut. Detailed investigations of the virtual crack propagation in the PCC slab slotted with AWJ using finite element modeling technique indicated that diagonal slots provided uniform-size fragments and crack patterns extending through the entire thickness. Relatively lesser load is sufficient for causing crack initiation and crack propagation in PCC slabs with diagonal slots. Also, diagonal slots ensure material failure due to internal cracking which is the most desirable to preserve the substrate strength.

6. ACKNOWLEDGEMENTS

The authors would like to thank The University of Tulsa, the Center for Robotics and Manufacturing Systems, University of Kentucky and Flow International Inc., Kent, Washington, for providing the necessary financial / experimental support.

7. REFERENCES

Arasawa, H. et al., "Controlled Cutting of Concrete Structure with Abrasive Water jet," *Proceedings of the 8th Int'l Symposium on Jet Cutting Technology,* Cranfield, U.K, 1986.

Crawford, C., "Cracking and Seating of PCC Pavements Prior to Overlaying With Hot Mix Asphalt," *National Asphalt Pavement Association, U.S., Inf. Series,* 98/89, 1989.

DeSalvo, G.J., and Gorman, R.W., "*ANSYS Engineering Analysis System User's Manual (Vol. I)*", Swanson Analysis Systems, Inc., Houston, PA, USA, 1989.

Fairhurst, R.M., and Spencer, S.L., "Abrasive Jet Cutting of High Strength Reinforced Concrete," *BHRA Report, No. RR 2470,* August 1985.

Gerstle, W.H., and Xie, M., "FEM Modeling of Fictitious Crack Propagation in Concrete," *Journal of Engineering Mechanics,* Vol. 118, No. 2, February, pp. 416-434, 1992.

Ingraffea, A.R., and Saouma, V., "Numerical Modeling of Discrete Crack Propagation in Reinforced and Plain Concrete," *Fracture Mechanics of Concrete: Structural Application and Numerical Calculation,* G.Sih, and DiTommaso, eds., Martinus Nijhoff, Hingham, Mass., pp. 171-225, 1984.

Jayawickrama, R. W., and Lytton, R.L., "Methodology for Predicting Asphalt Concrete Overlay Life Against Reflection Cracking," *Sixth International Conference on Structural Design of Asphalt Pavements*, Ann Arbor, MI, 1987.

Kohnke, P., "*ANSYS Engineering Analysis System User's Manual (Vol. IV-Theory),"* Swanson Analysis Systems, Inc., Houston, PA, USA, 1989.

Kokaji, C., Sakashita, F., Oura, S., and Sato, M., "Effects of Abrasives on Concrete Cutting," *Proc. 9th Int'l Symposium on Jet Cutting Technology,* Japan, pp. 571-580. Oct 4-6, 1988.

Kovacevic, R., Mohan, R., and Hirscher, J., "Rehabilitation of Concrete Pavements Assisted with Abrasive Water jets," *Jet Cutting Technology, (ISBN No. 0-7923-1979-6), ed. Lichtarowicz***,** Kluwer Academic/ Dordrecht/ Boston, pp.425-434, 1993.

Lukanen, D.E., "Structural Evaluation of Cracked and Seated PCC Pavements for Overlaying with Hot Mix Asphalt," *National Asphalt Pavement Association, U.S., Inf. Series,* 100/87, 1987.

Mohan, R. and Kovacevic, R., "Pavement Rehabilitation Using High Pressure Abrasive Water Jets," *Water Jet Applications in Construction Engineering, (ISBN No. 90-5410-698-0), ed. A. W. Momber,* A.A. Balkema, Rotterdam, pp.121-148, 1998.

Schmid, R.F., "High Pressure Hydromilling of Concrete Surfaces," *Proceedings of the 5th American Water jet Conference,* pp.157-163, Aug. 29-31, 1989.

Schutzbach, A.M., "The Crack and Seat Method of Pavement Rehabilitation," *Public Works,* pp.52-55, November, 1989.

Sharpe, G.W., Anderson, M., and Deen, R.C., "Breaking and Seating of Rigid Pavement," *Research Report, UKTRP-87-26*, Lexington, KY, 1987.

Sugiyama, H., and Tabata, A., "Abrasive Water jet Method for Effective Cutting of Reinforced Concrete Members (On Vibration Properties when Cutting)," *Proceedings of the 9th Int'l Symposium on Jet Cutting Technology,* Japan, pp. 581-589. Oct 4-6, 1988.

Swartz, S.E. and Taha, N.M., "Mixed Mode Crack Propagation and Fracture in Concrete," *Engineering Fracture Mechanics*, Vol. 35(1/2/3), pp.137-144, 1990.

Swenson, D.V., and Ingraffea, A.R., "Modeling Mixed Mode Dynamic Crack Propagation Using Finite Elements: Theory and Applications, 3.," *Computational Mechanics, 3,* pp.381-397, 1988.

Thompson, R.M., "Breaking/Cracking and Seating Concrete Pavements," *NCHRP Synthesis of Highway Practice,* 144, March 1989.

William, K.J., and Warnke, E.D., "Constitutive Model for the Triaxial Behavior of Concrete," *Proceedings of the International Association for Bridge and Structural Engineering,* Vol. 19, ISMES, Bergamo, Italy, p.174, 1975.

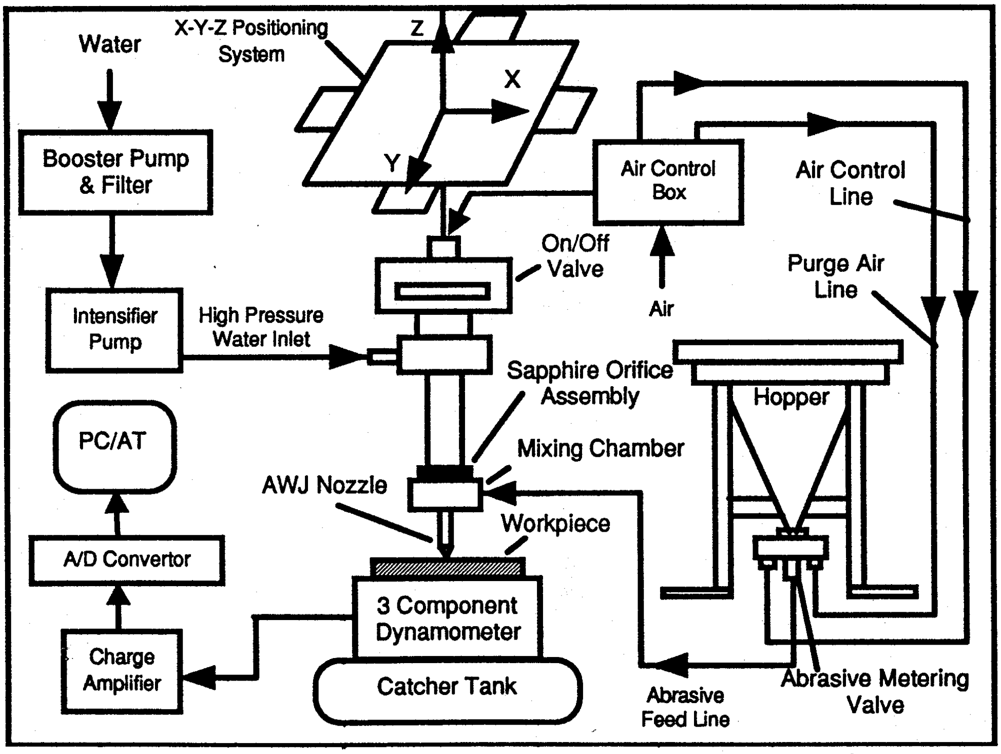

Figure 1. Experimental Set up

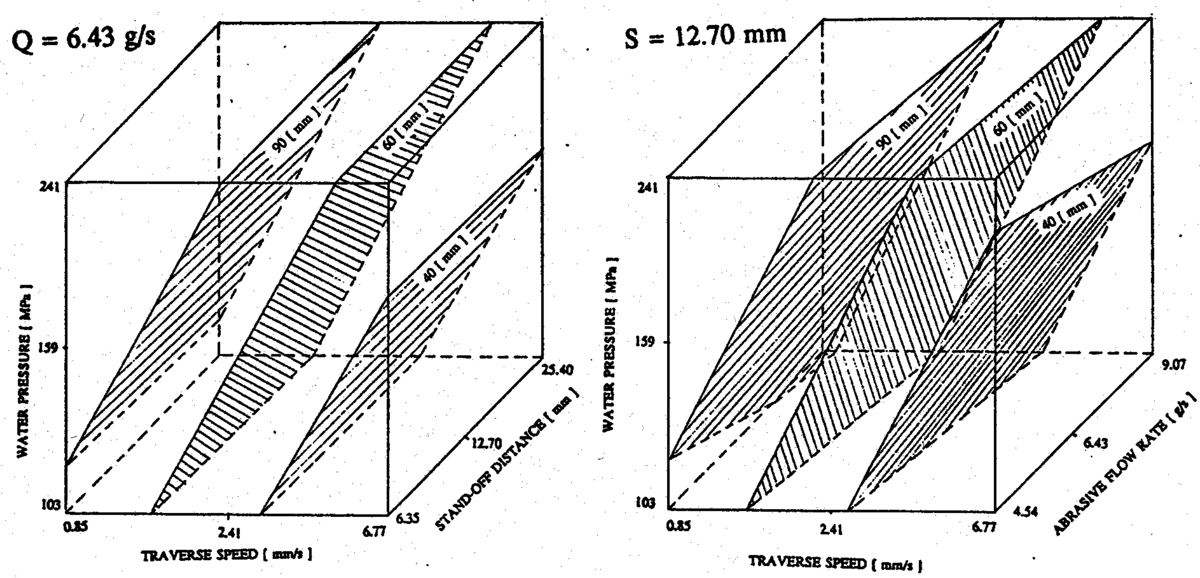

Figure 2. Planes with Constant Depth of Penetration

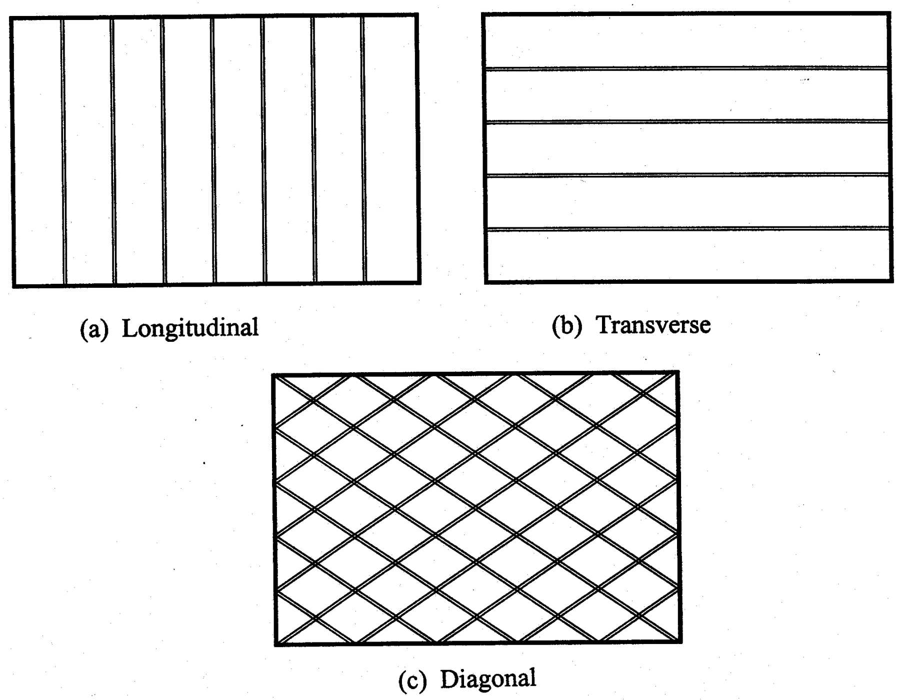

Figure 3. Geometry of AWJ Slotting

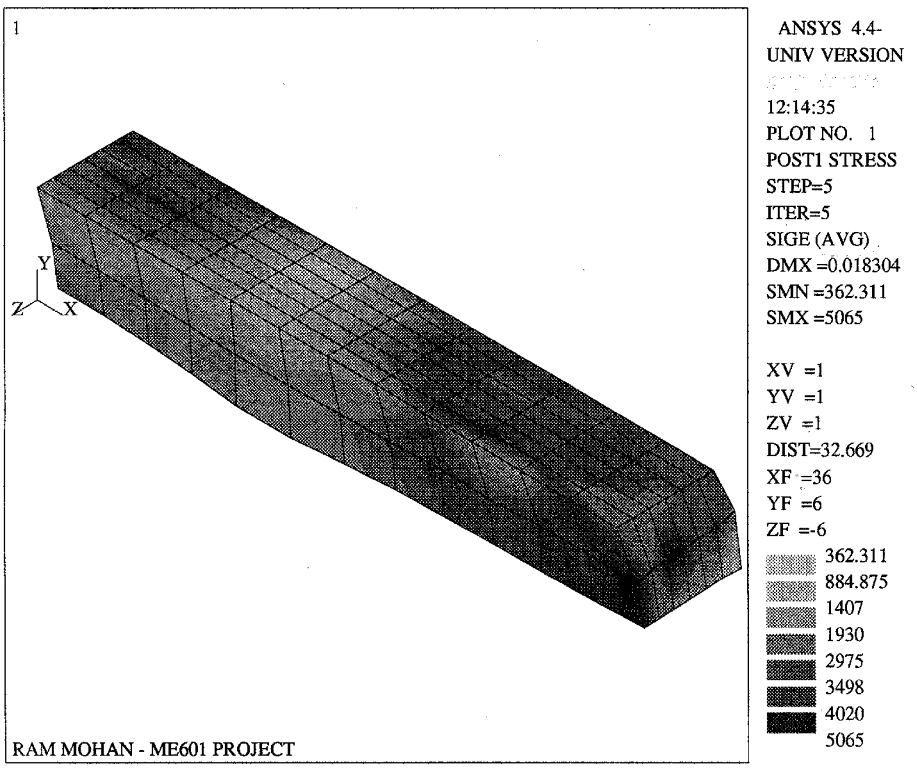

Figure 4. Stress Distribution in PCC Slab without AWJ Slotting (Before Failure)

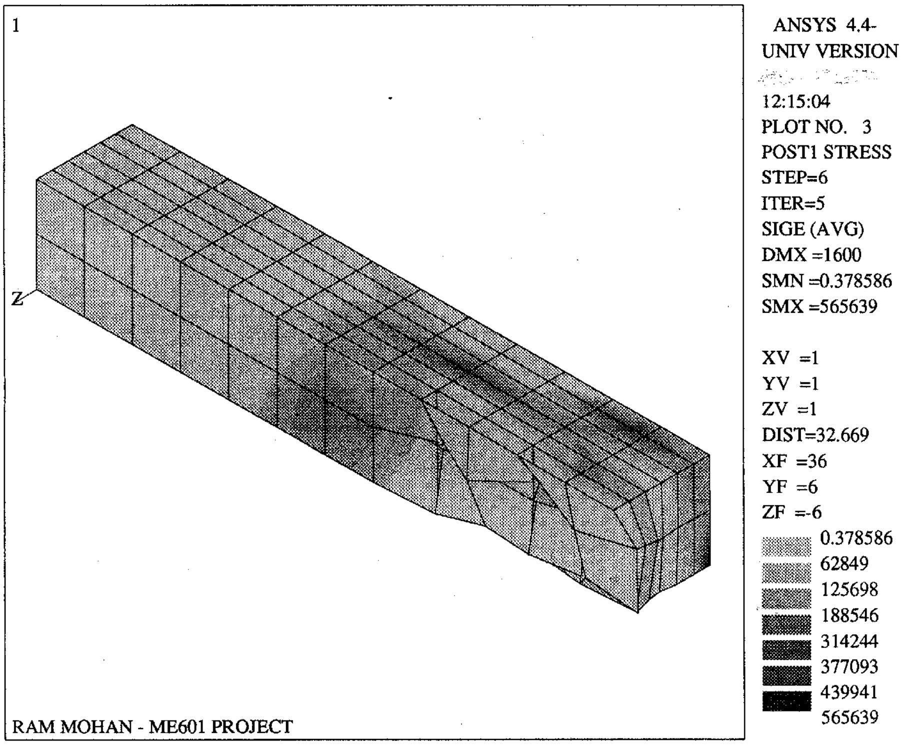

Figure 5. Stress Distribution in PCC Slab without AWJ Slotting (After Failure)

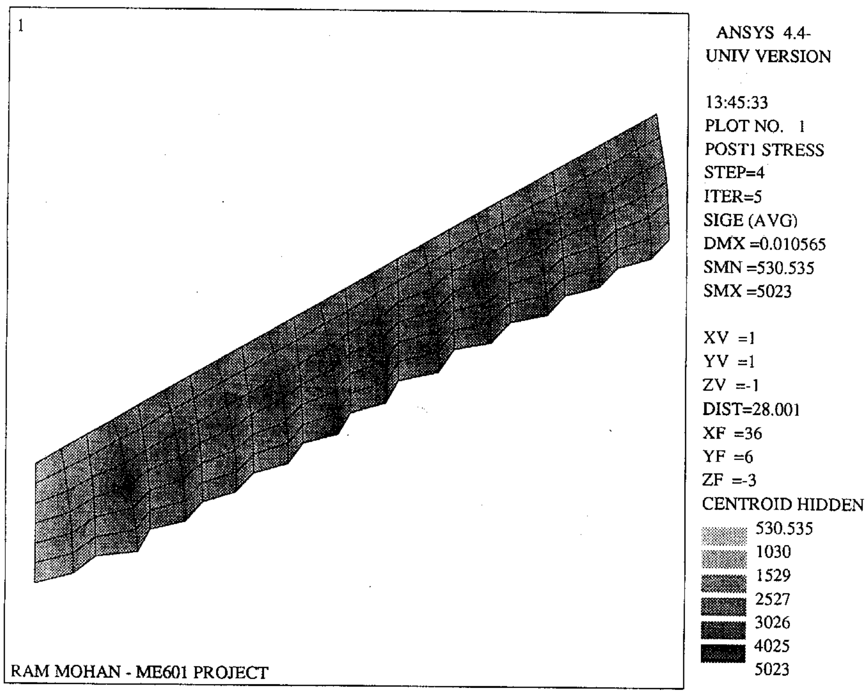

Figure 6. Stress Distribution in PCC Slab at the kerf Bottom of the Longitudinal Slots (Before Failure)

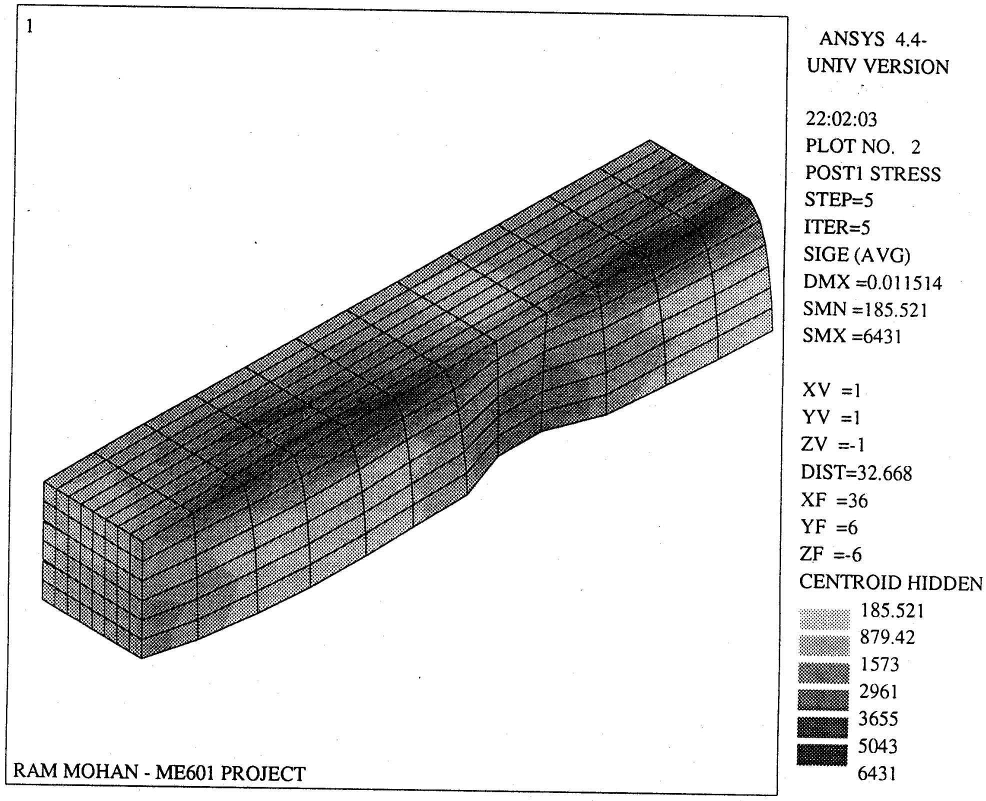

Figure 7. Stress Distribution in PCC Slab with Transverse Slots (Before Failure)

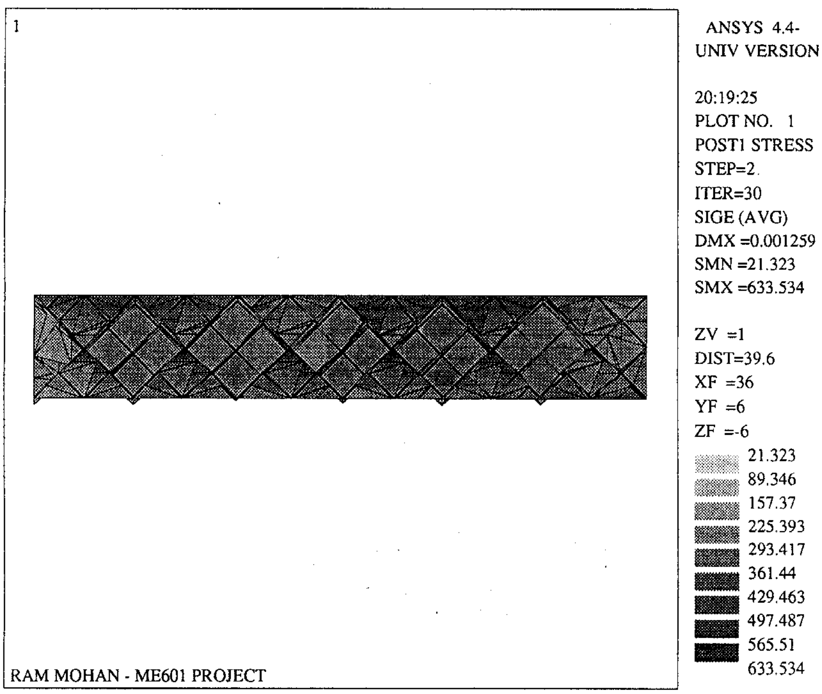

Figure 8. Stress Distribution in PCC Slab with Diagonal Slots (Initial Stage of Loading)

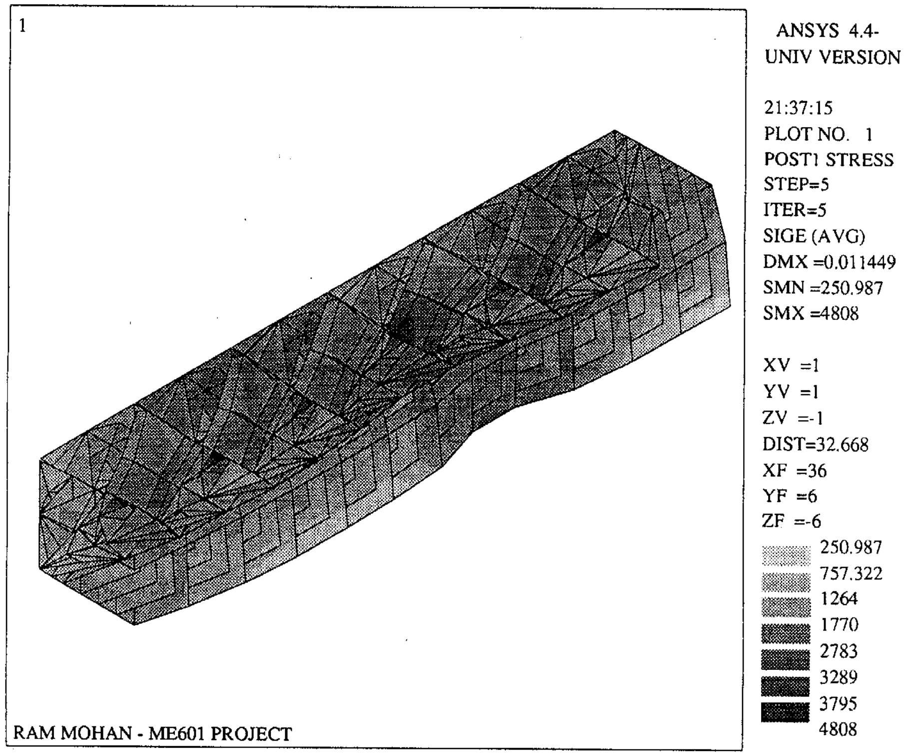

Figure 9. Internal Cracks in PCC Slab with Diagonal Slots (Before Complete Failure)

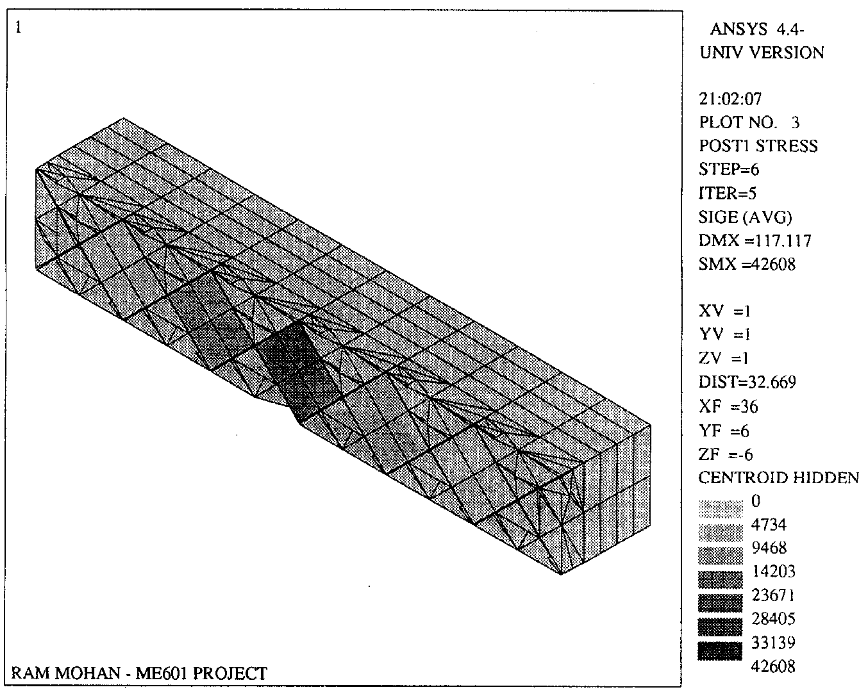

Figure 10. Stress Distribution in PCC Slab with Diagonal Slots (After Failure)

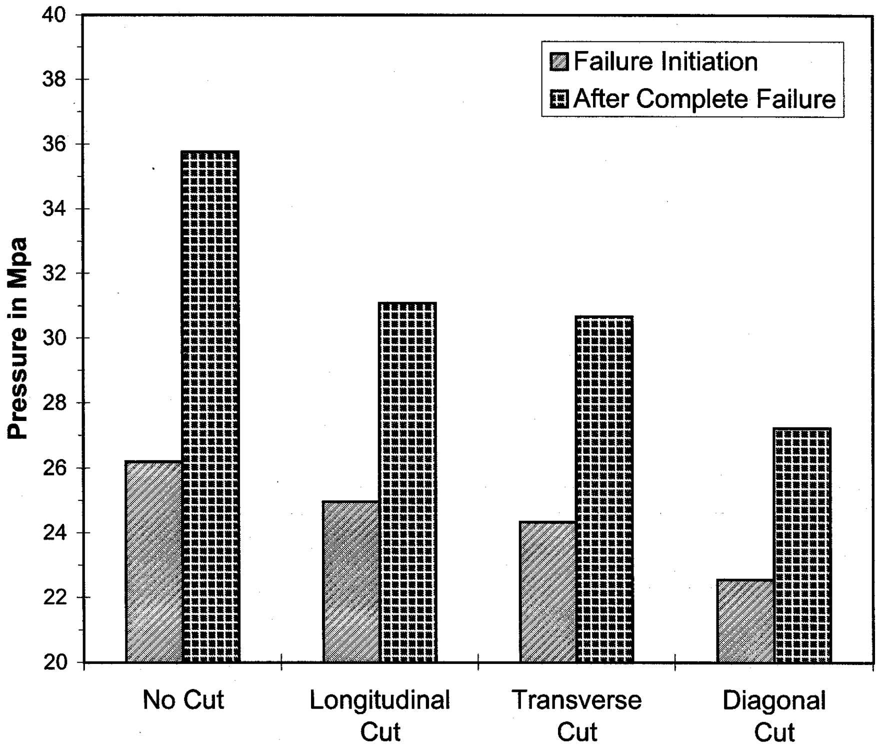

Figure 11. Applied Pressure on the PCC Slabs at the Point of Initiation of Failure and after Complete Failure

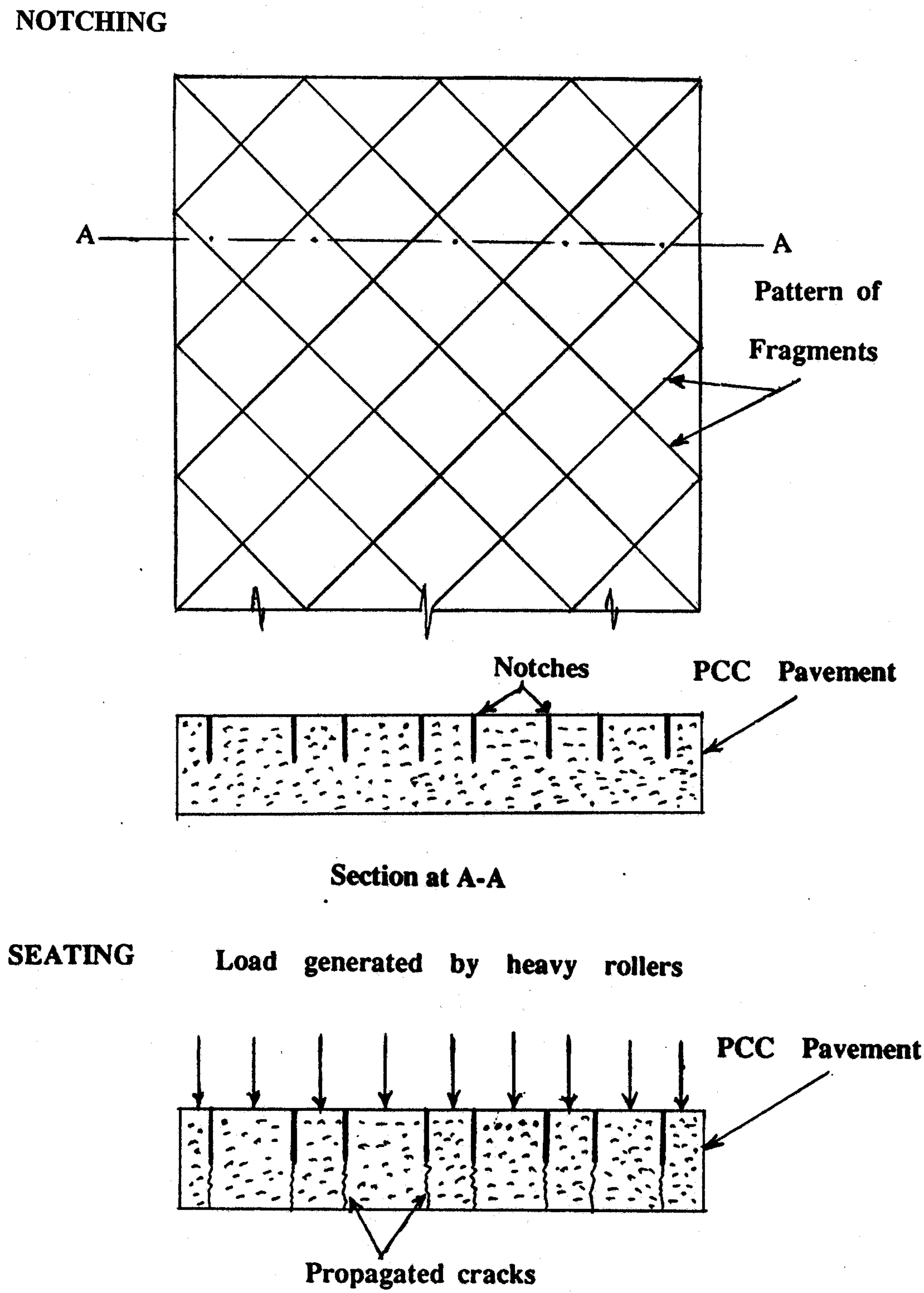

Figure 12. Schematic of PCC Pavement Rehabilitation Assisted with AWJ

10th American Waterjet Conference
August 14-17, 1999: Houston, Texas

Paper **6**

FUZZY LOGIC MODEL OF WATERJET DEPAINTING:

GRAPHO-ANALYTICAL APPROACH

K. Babets
E.S. Geskin
Waterjet Laboratory, Mechanical Engineering Department
Newark, NJ, USA

ABSTRACT

The application of waterjet for paint removal is investigated experimentally. The effect of water pressure, standoff distance and traverse rate on the cleaning width is tested. A new approach for the process modeling, based on the principal of fuzzy logic has been used. In this work the graphical technique is used to construct correlation between input and output parameters. An additional experimental database is acquired to test the model performance. A good agreement between experimental and predicted values is found.

Organized and Sponsored by the WaterJet Technology Association

1. INTRODUCTION

This paper is concerned with numerical modeling of surface decoating. Paint and other coatings are applied to surfaces to enhance corrosion resistance, improve appearance, or both. Often the coatings need to be removed as part of the manufacturing operation. The need for paint removal also occurs later in equipment life as the paint becomes soiled, worn, or damaged with use. In many cases, particularly in the aircraft industry, paint must be removed to allow inspection of the underlying parts. Although decoating can bring about the improvement of the surface in question, at the very least paint removal should cause no damage of the substrate surface. In case of an aircraft and number of other industries this requirement is paramount. The solution to paint removal operations that usually is explored first is not to paint the part and thus avoid the need to strip it. Some airlines have tried polished aluminum skins and report that the appearance is acceptable and the life-cycle cost is lower than painting with periodic removal to allow inspections. However, for most applications, the painting improves appearance or performance or both and must still be used.

The most common way of depainting is the use of solvents. Solvent strippers have been widely used for industrial coating removal for many years. Solvent strippers consist mainly of methylene chloride that typically constitutes 60% to 65% of the formulation. Other ingredients such as activators, corrosion inhibitors, thickeners, and evaporation retarders are used to supplement the methylene chloride to improve coating removal performance. Thirty one percent of methyline chloride produced is consumed for paint stripping, and eleven percents are used for metal degreasing. Use of solvent strippers generates organic vapors, sludge containing solvents and metals. Increasing environmental and health concerns call for the reduced use of solvent strippers.

Cleaner technologies based on physical coating removal are commercially available or are being developed to replace solvent strippers. Physical coating removal technologies take advantage of differences in physical properties between the coating and the substrate to destroy the bonding and/or abrade the coating from the underlying substrate.

Among a number of available paint removing techniques the most attractive ones appear to be blasting technologies. Plastic particles, wheat starch, crushed nut shells, sodium bicarbonate, etc. accelerated by water or air streams, are the basic blasting technologies. The most promising technology, however, is the water blasting. Water droplets accelerated up to the sufficient velocity constitute an effective material removal media, that is an addition of solid particles becomes unnecessary. Water is readily available, comparatively inexpensive, induces no damage to environment. The complete separation of water and debris and thus a material recovery and pollution prevention are feasible. Despite all its advantages, however, waterjet depainting did not find sufficient applications. One of the reasons of the slow advance of waterjet blasting is a possibility of a substrate damage. The possibility of the damage can be completely eliminated by the reduction of the droplet velocity at the impingement zone. This however, reduces process productivity. If the droplet velocity falls below a critical value, depainting becomes impossible. It is necessary to find a range of process variables, which assures both competitive cost and quality of depainting. A practical technique is necessary for identification of this range. The development of such a technique is the objective of this study.

The experimental study was carried out to aggregate a database representing paint removal by water jet at various operational conditions. Fuzzy logic technique was used to process the acquired data and to construct a correlation between process variables (water pressure, standoff distance, and traverse rate) and process results (productivity, water consumption. The prediction results obtained by the use of the proposed technique were validated by the experimental data. The difference between the measured and predicted data ranged between 1 and 7 %.

2. EXPERIMENTAL PROCEDURE

In this experiment the influence of waterjet pressure, standoff distance, and nozzle traverse rate on waterjet depainting was investigated. The experiments were carried out with an Ingersoll-Rand waterjet system. The cleaning head was mounted on a 3-axis gantry robot whose movement was controlled by an Allen Bradley 8200 series CNC controller. The high-pressure water supply system included a water softener, a booster pump, and an intensifier. The water softener was used to remove the iron and calcium, and dissolve solids that would cause damage to the sapphire nozzle. Then softened water was fed to the booster pump which produced the pressure up to 10.4 MPa (1,500 psi), then water was further pressurized by an intensifier using a hydraulically driven plunger pump and carried through a stainless steel pipe to a cleaning head. A sapphire water nozzle with diameter 0.254 mm was used.

Low carbon steel AISI1018, machined to a block with 4x2x1 in3 was chosen as a substrate. An oil-based paint was sprayed on to a slightly ground steel surface, and allowed to dry for 72 hours. The steel samples are shown on Fig.1. The samples were depainted by a moving waterjet normal to the specimen surface. Several strips were generated at each steel block at various operational conditions.

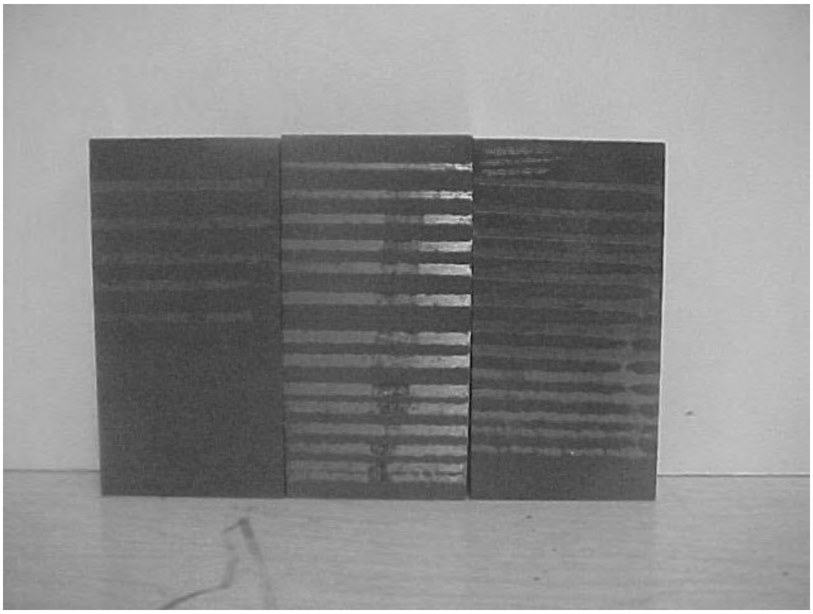

Figure 1. The Experimental Steel Samples.

As a result of the jet impact the paint free strips were generated on the substrate surface. Only successfully depainted strips were further examined. In the course of the further discussion we will term "a strip" the region on the substrate surface, where the paint was considered to be successfully removed. The width of these strips was measured by Mitutoyo Toolmakers Microscope. Since the width of the clean area was not uniform along the strip, five consecutive measurements of the strip width were taken and the average results were used to determine the rate of the paint removal (m2/min) as well as the specific water consumption (m3/m2). The following equations were used for these computations.

$$RMR\left(m^2 \min^{-1}\right) = T_{raverse\,rate} \cdot W_{idth\,of\,strip} \qquad \text{(Eq.1)}$$

$$\mathrm{W_{ater}C_{onsumption}}\left(m^3 / m^2\right) = \frac{C_D \cdot \pi \cdot D^2 \cdot \left(2 \cdot P / \rho_w\right)^{1/2}}{4 \cdot RMR} \qquad \text{(Eq. 2)}$$

where ρ_w is the water density, C_D is the discharge coefficient of the waterjet orifice, whose diameter is $\mathrm{D_n}$. In present work $\mathrm{C_D}$ is taken to be equal 0.7 (Hashish, 1993). The range of the experimental parameters is shown in the Table1. The maximum values of the operational conditions were determined by the equipment capabilities.

Table 1. Ranges of Experimental Parameters.

Process Parameter	Min value	Max Value
Nozzle Traverse Rate	0.635 m/min	8.89 m/min
Stand-off distance	100 mm	330 mm
Water Pressure	69 MPa	276 MPa

In the present study knowledge pertaining to waterjet depainting was obtained from two hundred experimental data points The width of the strips increases monotonously as water pressure increases and the standoff distance drops, because this change of process variables increase the available momentum of the water stream. The extremal character of the relationship between the standoff distance and the strip width (Fig.A2) is due to the increase of the jet diameter and decrease of the water momentum as the standoff distance increases. The rate of material removal (Fig.A3) and water consumption (Fig.A4) per unit of the cleaned area were determined computationally by Equations 1,2.

3. SELECTION OF THE MODELING TECHNIQUE

In our resent study (Meng et al., 1996) an attempt has been made to develop a mathematical model for prediction of water jet depainting based on the Springier theory of material erosion by a liquid impact. The rate of depainting was estimated by the balance of available momentum of impinging droplets and the momentum required for the paint separation. Springier equation determining dimple formation was used to estimate a required momentum while semi empirical equation of the development of a turbulent jet enabled us to estimate the available momentum in the impingement zone. The suggested mathematical model included an empirical variable, which needs to be determined by special experiments. It is expedient however to construct a model of depainting using process characteristics acquired in the course of routine operations. Statistical techniques conventionally used for construction of the empirical correlation are not effective in this case. The form of the correlation needed for the construction of regression equations is not known *a priori*, while the available qualitative (linguistic) information accumulated in the course of technology application cannot be sufficiently utilized by the statistical techniques. It is necessary to select a practical procedure to process the available fuzzy information. Such a technique has been offered by the fuzzy set theory (Cox, 1994, Ross, 1995, Tsoukalas et.al., 1997). In fuzzy systems the input and output variables are encoded in "fuzzy" representations, while their interrelationships take the form of well-defined if/then rules. Fuzzy logic systems address the imprecision of the input and output variables by defining them with fuzzy numbers (and fuzzy sets) that can be expressed in linguistic terms (e.g., low, medium, high). Furthermore, they allow flexibility in formulating system descriptions at the appropriate level of details. This means that complex process behavior can be described in general terms without precisely defining the complex (usually nonlinear) phenomena involved. Also a model constructed for one process can easily be transferred to a similar one. Fuzzy logic technique has the unique capabilities that are useful in information processing. For instance, it can represent mathematical relationships among the numerous variables in complex dynamic process and can be used to control nonlinear systems to a degree not possible with conventional methods.

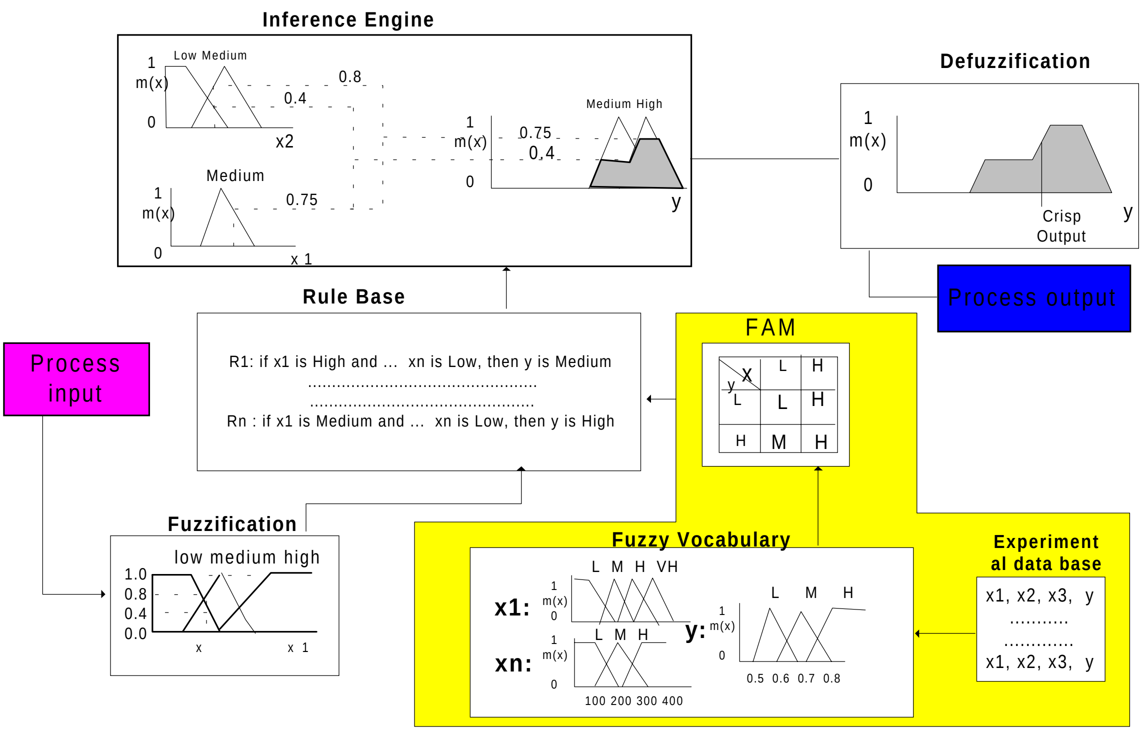

Figure 2. Structure of fuzzy logic based process model.

4. ARCHITECTURE OF FUZZY LOGIC MODELING

In general a fuzzy logic modeling consists of the Fuzzy Preprocessing and Fuzzy Processing modules. Fuzzy preprocessing involves representation of all available information in a form suitable for application of fuzzy logic technique. In fuzzy preprocessing module the knowledge pertaining to the process is obtained from various sources, such as experimental and empirical data, expert knowledge, linguistic formulation, etc. is utilized for process representation. This module consists of three independent modules:

- Knowledge acquisition module
- Fuzzy vocabulary
- Fuzzy associative memory (FAM).

The knowledge acquisition module constitutes a bank of all available pertinent information, crisp or linguistic, which can be stored in a computer memory. There is always a wealth of knowledge that cannot be formalized but nevertheless provides a significant insight about a process. In fact one of the major advantages of the fuzzy logic technique is its ability to utilize this knowledge. The fuzzy vocabulary module enables us to represent all available crisp information in a form acceptable by the fuzzy logic technique. In short, a crisp value of a process variable is replaced by a fuzzy set. The acquired knowledge is translated into a fuzzy language using the following few steps. The first step is identification of the ranges of the change of input and output variables. Then the interval of the change of each variable is divided into a set of subintervals and each of the subintervals is assigned a membership function, and is given an appropriate linguistic name. This combination of a subinterval, its membership function, and its linguistic name constitutes a fuzzy set. Fuzzy sets of one particular variable usually overlap. The degree of overlap reflects fuzziness in the definition of fuzzy sets. The aggregation of all subintervals of one process variable on a single coordinate axis is called the Universe of Discourse of that variable. It is clear, that construction of the fuzzy vocabulary involve in addition to the information acquired in the memory also a knowledge which cannot be stored, for example, an expert opinion.

Finally, the fuzzy logical equations or fuzzy rules relating variables defined by the fuzzy vocabulary are constructed in the FAM module. The fuzzy vocabulary provides just representation of the process variables. The relationships themselves are constructed on the base of all available information, stored in the computer memory or provided by an expert. In the field of fuzzy logic the most common way to express human knowledge is to form it into natural language expressions of the type:

IF premise (antecedent), THEN conclusion (consequent)

This form is commonly referred to as **IF-THEN** rule-based form. It represents the inference such that if we know the antecedent then the consequent can be inferred or derived. The constructed IF-THEN equations relate process variables stored in the fuzzy vocabulary. At the same time these equations express empirical or heuristic knowledge, derived from sources such as experiments or human experience, linguistically in this rule- based format. FAM contains a set of the fuzzy logical equations, which in the final analysis summarize all available knowledge about the process in question and present it in the form available for fuzzy modeling.

Modeling itself is carried out by the Fuzzy Processing Module, which converts the input information about a selected process manifestation into the information about output variables. The prior knowledge accumulated in FAM constitutes the base of these conversions. The Fuzzy Processing Module consists of the following independent modules:

- Process input module
- Fuzzification module
- Inference module
- defuzzification module

Process input module enables us to store the pertinent input information. The fuzzification module converts the stored crisp data into fuzzy logic type information. For each crisp input data this module identifies a corresponding fuzzy set and the degree of the belonging to this set. Due to the overlapping of the fuzzy sets each input can be assigned to several fuzzy sets. The fuzzy information developed in the fuzzification module is fed into the inference module. Here fuzzy rules pertinent to the information in hand are selected (fired) and used to infer fuzzy values of output variables. It is clear that an each equation (fuzzy rule) generates a single fuzzy value of the output variable.

Fuzzy rules give us only linguistic correlation between sets of the input parameters and the output variable, instead we would like to estimate to what degree a rule's consequent (part to the right from the **then** statement) is true. In order to do so we apply the fuzzy inference technique. There are several methods of inference in fuzzy systems: We selected the min-max method, which involves comparatively simple numerical manipulations. In fuzzy min-max implication each rule is evaluated separately. The result of this evaluation is a fuzzy region of the output variable and its degree of belonging to this region. In order to evaluate the degree of the truth (belonging) of the consequent of a rule we examine the degrees of truth of each antecedent and assign to the consequent the minimal one. Then these individual solution regions are aggregated into a final solution region, which determines the fuzzy value of the output variable.

Finally, the defuzzification module converts the fuzzy output of the inference module in a conventional crisp result. The most commonly used defuzzification technique is the centroid method given by the following equation (Cox, 1994):

$$z = \frac{\sum_{i=0}^{n} d_i \mu_y(d_i)}{\sum_{i=0}^{n} \mu_y(d_i)} \qquad \text{(Eq.3)}$$

Here d is the value of the width of strip at some point, and $\mu(d)$ is the truth membership value for that point. The numerical example below elaborates the discussion of the above technique.

5. FUZZY LOGIC MODEL OF WATERJET DEPAINTING

Let us discuss now the modeling of the waterjet depainting. We will use this discussion in order to elaborate the procedure in question.

5.1 Fuzzy Preprocessing Module

5.1.1 Knowledge Acquisition Module

This module involves storing of the experimental database. The data used in the following analysis are obtained experimentally (Fig. A2- A4).

5.1.2 Fuzzification Module

The fuzzification of the water pressure is shown in Fig. 3. As it follows from this figure, the water pressure of 150 MPa has a degree of membership equal to 1 in the fuzzy set Medium (complete representative of this set) and a degree of 0 in the fuzzy sets Low and High (not a member of the sets). The water pressure of 125 MPa has degrees of membership equal to 0.27 in the fuzzy set low, and simultaneously a degree of membership 0.58 in the fuzzy set Medium. Similar charts are constructed for the **traverse rate** (Fig.A6); **standoff distance** (Fig.A7) and the **strip width** (Fig.A5) Membership functions for the water pressure are determined analytically as in 3-6.

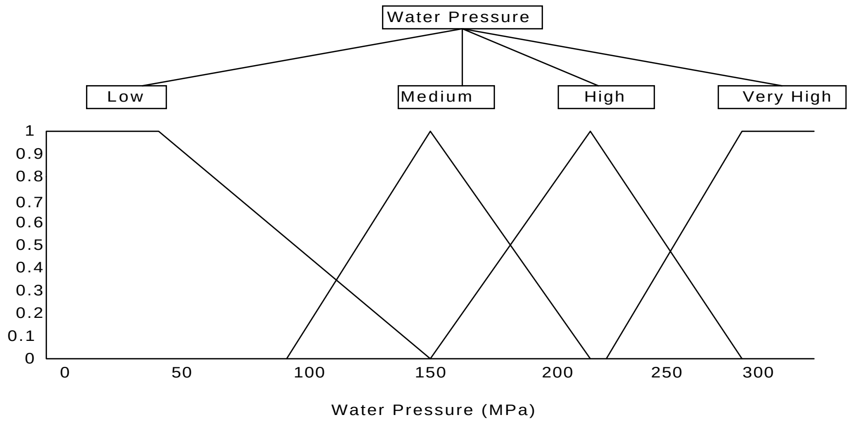

Figure 3. The Universe of Discourse for Process Variable Water Pressure.

$$\mu_{low}(x) = \frac{150 - x}{150 - 60} \quad \text{for } x \in [60,150]$$

Eq. 4

$$\mu_{very\ high}(x) = \frac{x - 210}{280 - 210} \quad \text{for } x \in [210,280]$$

Eq. 5

$$\mu_{high}(x) = \begin{cases} \dfrac{x-150}{210-150} & \text{for x} \in [150{,}210] \\ \dfrac{270-x}{270-210} & \text{for x} \in (210, 270 \end{cases}$$

Eq. 6

$$\mu_{medium}(x) = \begin{cases} \dfrac{x-90}{150-90} & \text{for x} \in [90{,}150] \\ \dfrac{210-x}{210-150} & \text{for x} \in (150, 210 \end{cases}$$

Eq. 7

Similar equations were constructed for other input variables (standoff distance and traverse rate rate) and output variable (strip width).

5.1.3 Fuzzy Associative Memory (Representation of the knowledge of the depainting process)

The experimental knowledge about waterjet depainting was represented in the form of fuzzy rules. The example of a rule follows:

IF **Waterjet Pressure** is *Low* and **Traverse Rate** is *Slow* and **Stand-0ff Distance** is *High* Then **Strip Width** is *Around Medium.*

A collection of all fuzzy rules for one particular system (database) is called - rule base. For a small number of model variables there is a compact form of representing fuzzy rules. This compact form of the rule representation is commonly referred to as Fuzzy Associative Memory (FAM). An example of the FAM for the acquired database is given below (Table 2).

Table 2. Fuzzy Associative Memory, Water pressure "LOW"

Stand-off distance

	EL	VL	L	M	H	VH	VVH	EVVH
VS	****	VL	M	M	AM	AM	L	VL
S	****	VVVL	VL	L	VVL	VVL	VVL	EVVL
M	****	VVVL	VVVL	VVL	EVVL	EVVL	EVVL	EVVL
F	****	****	****	****	****	****	****	****
VF	****	****	****	****	****	****	****	****

Traverse Rate

In the above table the upper row represents fuzzy intervals of process variable "stand-off distance"(Fig. A7), where EL= Extremely Low, VL= Very Low, L= Low, M= Medium, H= High, VH= Very High, VVH= Very Very High, EVVH= Extremely Very Very High, are the linguistic names of these intervals. Similarly the leftmost column represents fuzzy intervals of process variable "Traverse Rate" (Fig. A6), where VS= Very Slow, S= Slow, M= Medium, F=

Fast, VF= Very Fast, are the linguistic names of these intervals. And cells of the table represent fuzzy output intervals of process variable “strip width” (Fig. A5), where L= Low, M= Medium, V= Very, and E= Extremely. Thus according to the Table 2, the combination of “Low” Stand-off distance and “Slow” Traverse Rate results in “Very Low” Width of Strip.

5.2 Fuzzy Processing Module

The use of the Fuzzy Processing Module is demonstrated with the help of the following example.

5.2.1 Process input:

Let us consider the following set of input parameters: Water Pressure 172 MPa, Traverse Rate 5m/min and Standoff Distance 229 mm.

5.22 Fuzzification Module

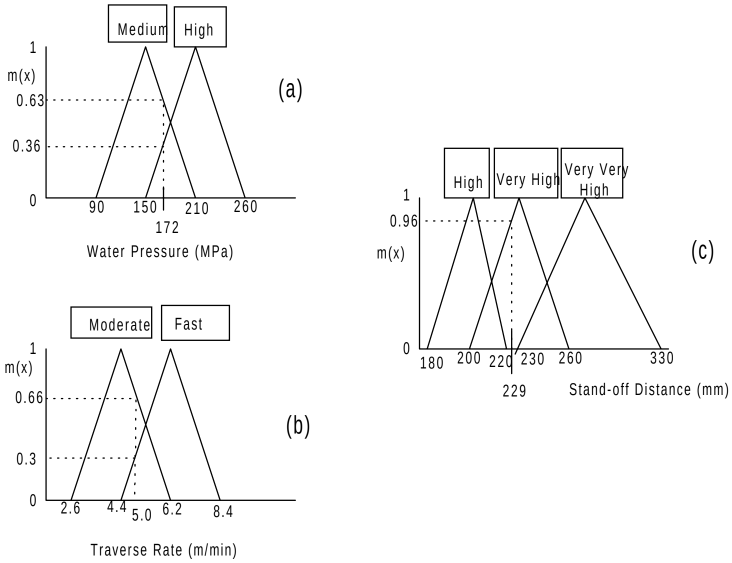

Figure 4. Fuzzification.

From Fig.4 (a) it follows that the pressure of 172 MPa falls into two fuzzy sets- Medium and High with corresponding degrees of membership of 0.63 and 0.36. Similarly, from 4(b) traverse rate of 5m/min falls into two fuzzy sets- Moderate and Fast with corresponding degrees of membership of 0.66 and 0.33 and SOD of 229 mm falls into only one fuzzy set-Very High, with a degree of membership equal to 0.96 (4(c)).

For a given set of the input variables, the following rules were activated:

1. If **Water Pressure** is *Medium* (0.63) AND **Traverse Rate** is *Moderate* (0.66) AND **Standoff Distance** is *Very High* (0.96) then **Strip Width** is *Low*.
2. If **Water Pressure** is *High* (0.36) AND **Traverse Rate** is *Moderate* (0.66) AND **Standoff Distance** is *Very High* (0.96) Then **Strip Width** is *Medium*.

3. If **Water Pressure** is *Medium* (0.63) AND **Traverse Rate** is *Fast* (0.3) AND **Standoff Distance** is *Very High* (0.96) Then **Strip Width** is *Very Low*.
4. If **Water Pressure** is *High* (0.36) AND **Traverse Rate** is *Fast* (0.3) AND **Standoff Distance** is *Very High* (0.96) then **Strip Width** is *Around Medium*.

5.2.3 Inference Module

For the rule 1 the degree of membership of the fuzzy set *medium* of **Water Pressure** is found to be (0.63), the degree of membership of the fuzzy set *moderate* of **Traverse Rate** is found to be (0.66), and the degree of membership of the fuzzy set *Very High* of **Stand-off Distance** is found to be 0.96. We select the minimal out of these three values, which is 0.63. The selected minimal value is assigned to be the degree of the membership of the fuzzy set *Low* of the output variable **Strip Width**. Graphically this procedure can be demonstrated by truncating the triangle of the fuzzy set *Low* of the output variable **Strip Width** at the 0.63 mark. We repeat these steps for other rules (Fig. A1 (a)).

Rule 1: min (0.63, 0.66, 0.96) → 0.63 (μ of fuzzy set LOW of Strip Width).
Rule 2: min (0.36, 0.66, 0.96) → 0.36 (μ of fuzzy set MEDIUM of Strip Width).
Rule 3: min (0.63, 0.3, 0.96) → 0.3 (μ of fuzzy set VERY LOW of Strip Width) .
Rule 4: min (0.36, 0.3, 0.96) → 0.3 (μ of fuzzy set AROUND MEDIUM of Strip Width).

After each rule is evaluated for its truth, we combine these individual truncated regions into a single solution region (Fig. A1 (b)).

5.2.4 Defuzzification Module:

The resultant solution region on Figure 5 provides fuzzy information about the resultant strip width. We can infer from this figure that at the above input parameters the resulting strip width is somewhere between 1 mm to 2.6 mm. But since the truth function of fuzzy set LOW is the biggest one (0.63), it is more likely to expect that the strip width would range from 1.4 to 1.8 mm.

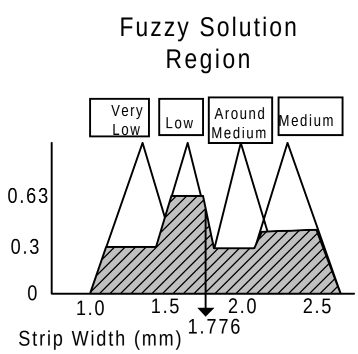

Figure 5. Fuzzy Solution Region and Defuzzified Solution.

Applying the defuzzification technique (Eq. 3) to the solution region under consideration we obtain:

$$Z=1.776 \text{ mm}$$

Comparing this result with the experimental result (1.743-mm) we find that the error is less than 3%, which is regarded acceptable in the current work.

An additional set of experimental data points, different from those used for the model construction has been acquired. This data set enabled us to test the model performance. The results of the testing are tabulated in the Table 3:

Table 3. Comparison of Experimental and Predicted Values of Strip Width

Water Pressure (MPa)	Traverse Rate (m/min)	Stand-off distance (mm)	Strip width (experiment)	Strip width (predicted)
103	3.8	178	1.396	1.370
138	3.3	178	1.869	1.83
172	5	229	1.743	1.776
207	7.6	203	1.832	1.80
241	5.8	216	2.54	2.37

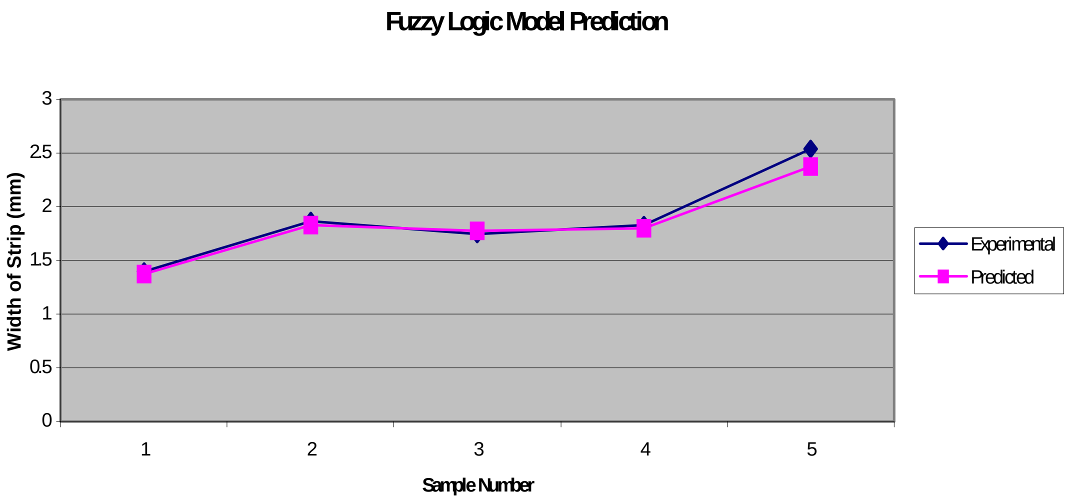

Figure 6. Fuzzy Logic Model Prediction.

6. DISCUSSION OF RESULTS

Presented results show the feasibility of construction of a numerical model of water jet depainting process using fuzzy logic principals. The procedure involved acquisition of the experimental database, fuzzification of the input and output variables, construction of the fuzzy rule representing the acquired database, evaluation of the fuzzy distribution of the output variable for the selected sets of the input variables and evaluation of the crisp value of the output variable. The routines involved in the transformation above are comparatively simple. The error in the predicted results for experimental data different from that used for the construction of the model range between 1-7%. This accuracy is acceptable at the first stage of the process investigation and will be improved, as additional database will be generated. The main advantage of the suggested approach is that it can be easily expanded as new process information is acquired, or new process variables are introduced.

In the presented study the process result is characterized by the strip width, which constitutes the only directly measured output variable. Actual process characteristics (productivity and water consumption) can be readily determined using Equations 1,2. The result of the presented analysis provides guidance to the optimization of the waterjet depainting. Particularly, it is shown that the process effectiveness increases if the water pressure will be taken maximum (276 MPa in this study), along with maximal traverse rate (8.89 m/min). The standoff distance should range between 0.15 and 0.25 m. Analysis was carried out at a constant nozzle diameter of 0.254 mm. The procedure of the model construction can be readily modified to account for this and other process variables.

7. CONCLUDING REMARKS

The approach used in our study is not unique. There several efficient techniques that enable us to reduce database to a compressed process description. Numerical process description can be obtained using well-understood and documented regression analysis. Fuzzy logic technique however has a number of advantages. First of all, there is no limitation on the form of the model. Fuzzy logic can account for any form of process nonlinearity. The inaccuracy (fuzziness) of input information effects the final result much less then that in the case of regression analysis. Model improvement using new acquired information is rather simple. Thus, the use of fuzzy logic will improve the planning and control of the waterjet depainting. Although this study is concerned with prediction of the results of paint stripping, with some modifications it can be applied to other surface processing technologies. In our following work we will show how to expend a model constructed for the existing database for a similar system at a limited initial information.

8. REFERENCES

Earl Cox, “The Fuzzy Systems Handbook: A Practitioner’s Guide to Building, Using, And Maintaining Fuzzy Systems,” *AP Professional*, 1994.

Mohamed Hashish, "Prediction Models for AWJ Machining Operations", *Proceedings of the 7th American Water Jet Conference*, pp. 205-216,Seattle, Washington, 1993.

Spencer T. Johnson, "Advances in Cleaning and Coating Removal Using Ultra-High Pressure Water Jet Technology", *Proceedings of the 7th American Water Jet Conference*, pp.607-610, Seattle, Washington, 1993.

S. Kang, T. Retiree, G., Carlson, "Target Response to the Impact of High-Velocity Non Abrasive Waterjet," *Proceedings of 7th American Water Jet Conference*, Seattle, Washington, 1993.

H. Louis, W. Schicorr, "Fundamental Aspects in Cleaning with High Speed Water Jets", *Proceedings of the 6th International Symposium on Jet Cutting Technology*, pp. 217-228, BHRA, Guildford, England, 1982.

P. Meng, Experimental and Analytical Investigation of Water Jet Cleaning Process, Ph.D. Thesis, New Jersey Institute of Technology, (1996).

P. Meng, E. Geskin, L. Tismenetskiy, "Cleaning with High Pressure Directed Waterjets," *Proceedings of Japan-USA Symposium on Flexible Automation*, Boston, MA, 1996.

Timothy J. Ross, "Fuzzy Logic With Engineering Applications," *McGraw-Hill*, 1995.

P.J. Singh, J. Munoz, W.L. Chen, "Ultra-High Pressure Waterjet Removal of Thermal Spray Coatings," *Proceedings of 11th International Symposium on Jet Cutting Technology*, pp. 461- 480, BHRA, Dordrecht, Netherlands, 1992.

Leftery H. Tsoukalas, Robert E. Uhrig, "Fuzzy and Neural Approaches in Engineering," *John Wiley & Sons*, 1997.

Jeffrey D. Watson, "Thermal Spray Removal with Ultrahigh-Velocity Waterjets," *Proceedings of the 7th American Water Jet Conference*, pp. 583-595, Seattle, Washington, 1993.

Samuel S. Wu & Thomas J. Kim," An Application Study of Plain Waterjet Process for Coating Removal", *Proceedings of the 8th American Water Jet Conference*, pp.779-792, Houston, Texas, 1995.

9. GRAPHICS

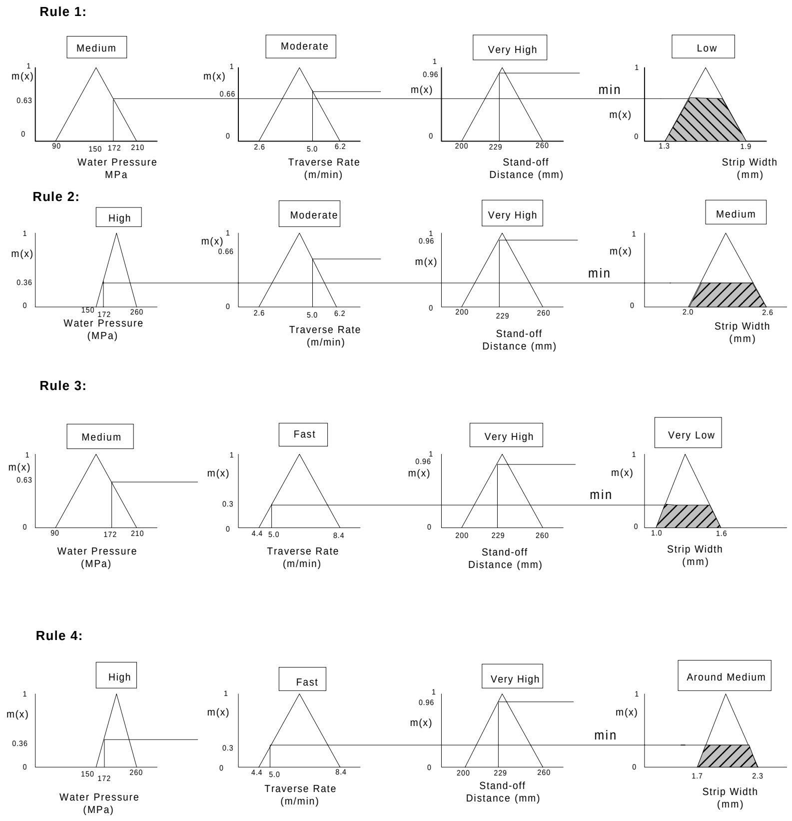

Figure A1 (a). Fuzzy min-max composition.

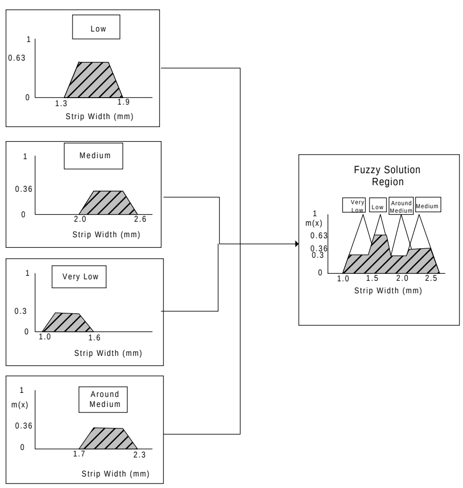

Figure A1 (b). Fuzzy min-max composition.

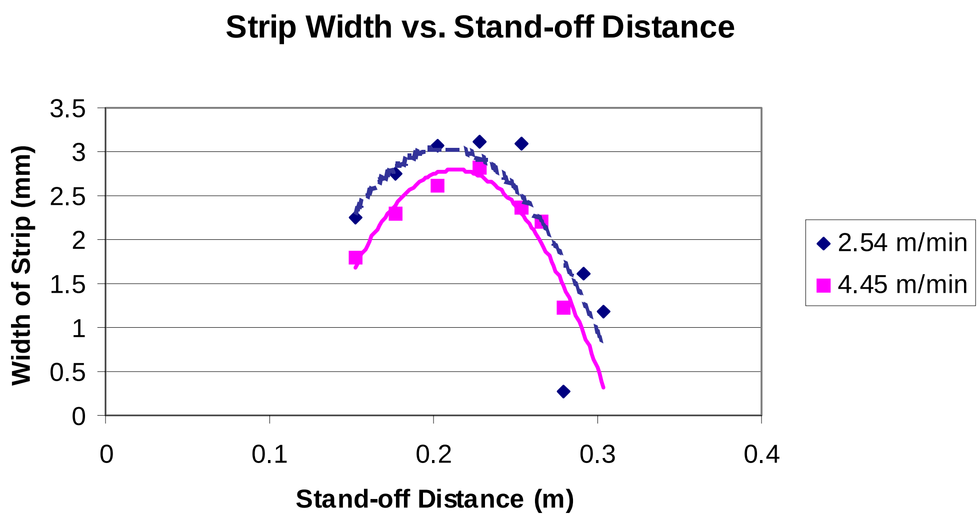

Figure A2. Experimental Results. Width of Strip vs. Standoff Distance for Water Pressure 276 MPa.

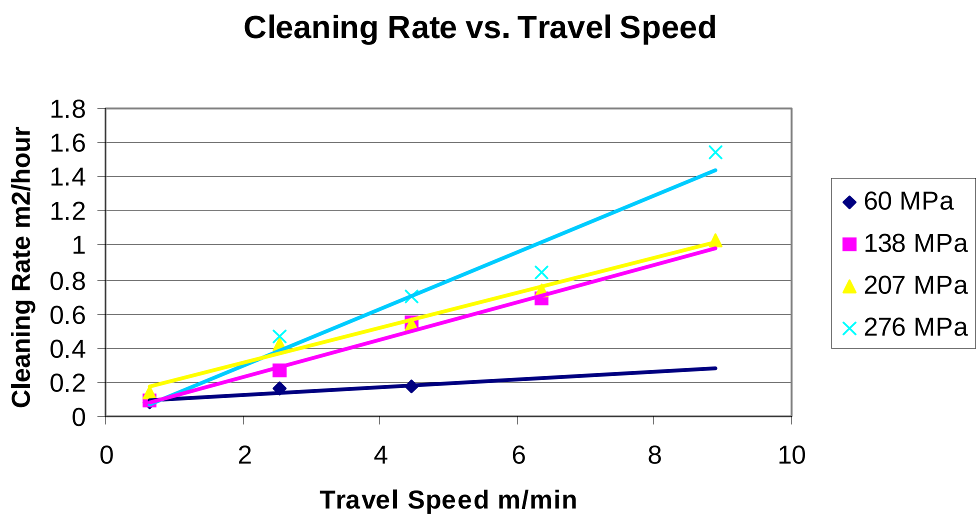

Figure A3. Experimental Results. Cleaning Rate vs. Travel Speed.

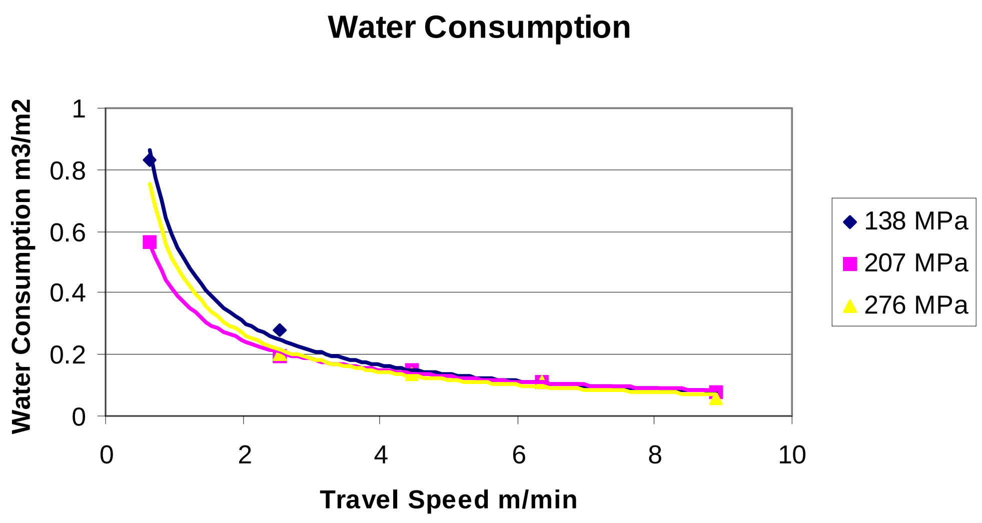

Figure A4. Experimental Results. Water Consumption vs. Travel Speed.

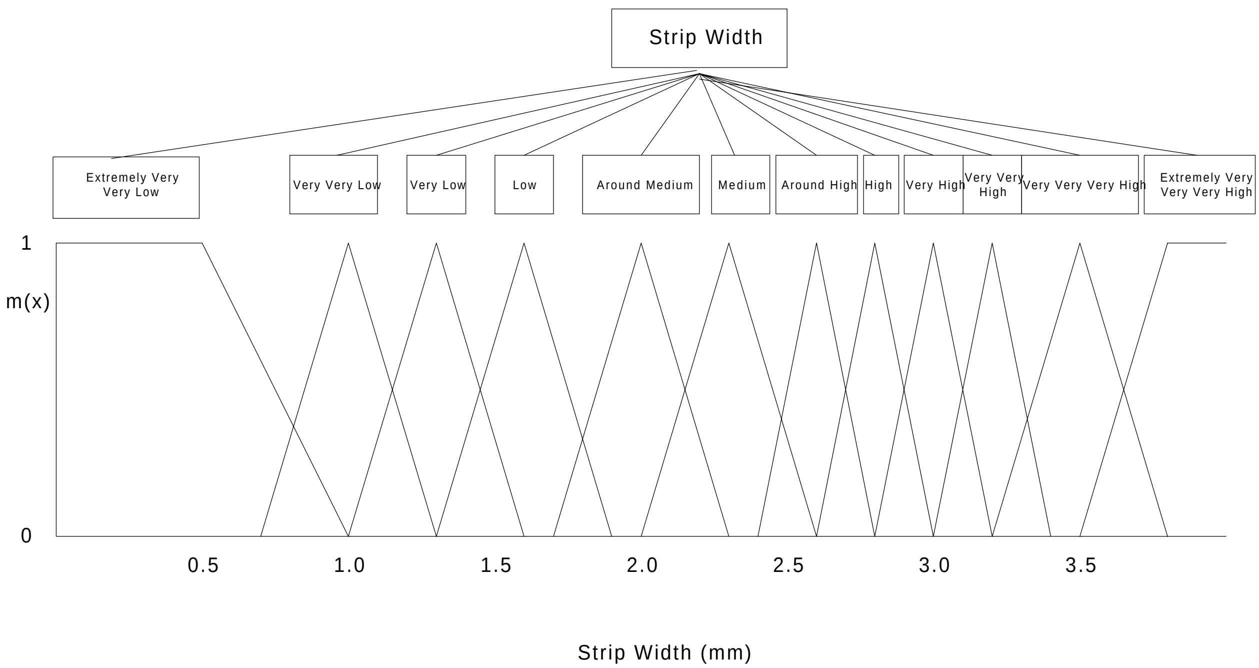

Figure A5. Universe of discourse of the process variable 'Strip Width'.

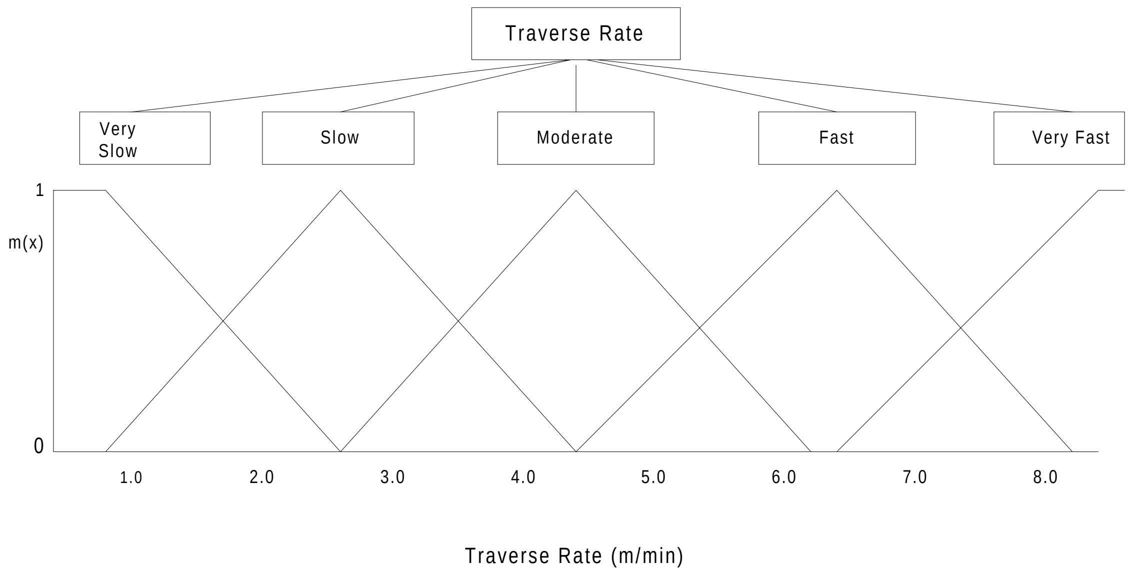

Figure A6.Universe of discourse of the process variable 'Traverse Rate'.

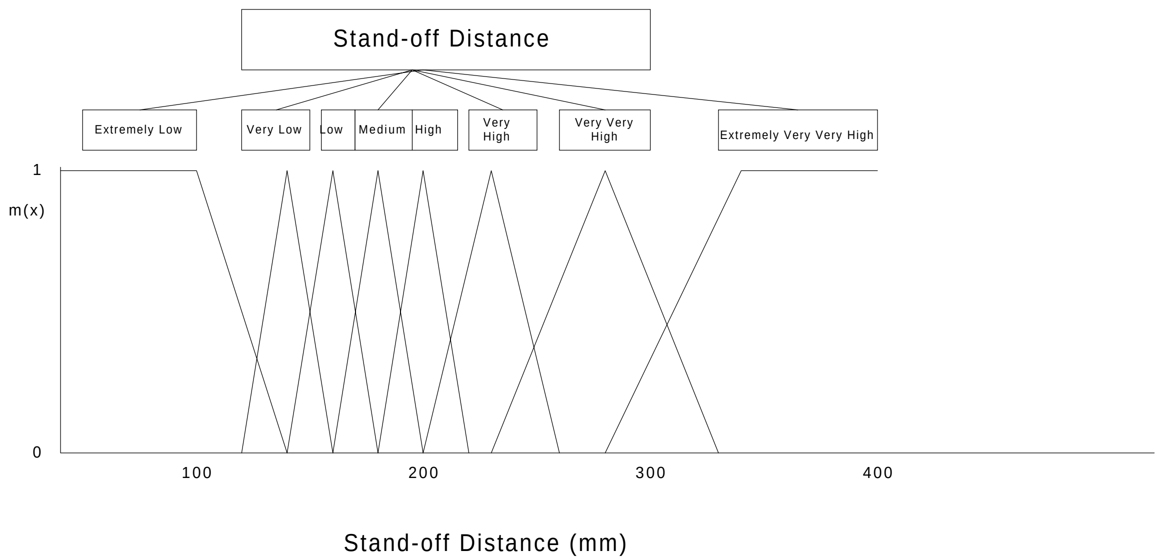

Figure A7. Universe of discourse of the process variable 'Stand-off Distance'.

10th American Waterjet Conference
August 14-17, 1999: Houston, Texas

Paper **7**

MODELING OF FLOW MODULATION FOLLOWING THE ELECTRICAL DISCHARGE IN A NOZZLE

M. M. Vijay, A.H. Makomaski*, W. Yan, A. Tieu and C.Bai
VLN Advanced Technologies, Inc.
Gloucester, ON., Canada
* Consultant to VLN

ABSTRACT

Work is in progress on the design and fabrication of a pre-commercial electro-discharge machine for generating low-frequency (≈0.3 Hz) ultra-high energy pulsed water jets. The machine consists of a 100 kJ capacitor bank, a fairly low pressure (≈34.5 MPa; 5,000 psi) pump, a nozzle-electrode assembly and other accessories. The pulsed waterjet is generated by the rapid discharge of stored electrical energy in the bank between the electrodes in the nozzle. In order to design an efficient, robust and reliable nozzle, it is very important to understand the complex processes that occur after the discharge. This is accomplished by numerical modeling by developing a 2-D axi-symmetric Lagrangian code. The code can employ a variable grid along the axis to elaborate the region of the plasma and the plasma itself.

In the paper, results predicted by the numerical modelling are presented. Details of the shock formation and propagation are discussed. It is shown that modulation of the flow at 34.5 MPa by the rapid electrical discharge generates ultra-high (≈2,000 MPa) impact pressures on the target. The magnitude of such high pressures was observed to depend on the rate of electrical energy release and the standoff distance.

1. INTRODUCTION

The project, currently in progress, is sponsored by the Federal Government Department Natural Resources Canada under the Industrial Energy Research & Development Program (IERD). It is related to the removal of very hard deposits (Fig. 1), mostly undesirable resins, which grow in chemical reactor vessels and other petrochemical process equipment. Ultra-high speed pulsed waterjet generated by the electro-discharge technique was considered suitable for this application for the following reasons:

- The deposits need to be fractured into pieces to facilitate rapid removal;
- The results reported by Vijay & Paquette (1996) and, later by Vijay et al. (1997) appear to confirm that powerful pulsed jets generated by the electro-discharge technique can easily fragment materials;
- Preliminary tests conducted on the 25 cm (9.8 in) sample (Fig. 1) clearly established the superior performance achieved with the high-frequency pulsed waterjet, Vijay et al., 1998. {Test #4: continuous jet; Test #5: pulsed jet; $V_p/V_c \approx 6$ where V_p and V_c are respectively the volumes removed by the pulsed and continuous jets; Pressure = 69 MPa (10,000 psi), Nozzle diameter = 1.37 mm (0.054 in)}.

Extensive details on the electro-discharge technique are reported by Vijay & Paquette (1996) and Vijay et al. (1997 & 1998). As shown schematically in Fig. 2, the electro-discharge pulsed waterjet machine consists basically of electrical energy storage and discharge system (capacitors, switches, etc.), a low pressure pump, and a nozzle-electrode assembly. A schematic view of the proposed portable, light-weight, 100 kJ, 20 kV pre-commercial machine is shown in Fig. 3. The cabinet contains two 50-kJ capacitors, charging and discharging units and control systems. The overall dimensions, excluding the pump, are: 1.22 X 1.04 X 0.76 m (48 X 41 X 30 in). The only component which needs a great attention in the entire system is the nozzle in which the electrical energy is discharged. This is where the modulation of the continuous stream takes place to produce the ultra-high speed pulsed waterjet. The focus in this paper is on: (i) the phenomena that accompany the discharge in the nozzle, (ii) the jet emerging from the nozzle and (iii) interaction of the jet with the target.

2. BASIC CONSIDERATIONS

The numerical code used in the present study is a further development of the approach used for single jets from quiescent water (Vijay & Makomaski, 1998). In this previous study a number of recommendations were made to adapt the code for discharges into continuous steady flows. The steady flow is assumed to be driven by a piston. The numerical method involves a two-dimensional Lagrangian formulation in cylindrical coordinates. Figure 4 shows a typical numerical grid employed in the computations. Initial distribution of pressure, density and velocity in the chamber leading to the nozzle and the nozzle itself are assumed to be one-dimensional. After a number of numerical cycles an approximate two-dimensional steady flow is established, at which moment numerical simulation of the electrical discharge is commenced (30 μs after the start). Water is assumed to be a slightly compressible medium and the plasma resulting from the electrical discharge into water is approximated by water vapour, which is assumed to behave as an ideal gas. The relevant fluid dynamic equations are basically the same as reported earlier (Vijay & Makomaski, 1998) and are reproduced here for the sake of clarity:

Conservation of mass:

$$\rho J = \rho_0 J_0 \tag{1}$$

Equation of motion:

$$\rho \frac{\partial \underline{V}}{\partial t} = -\nabla p + Q_1 \tag{2}$$

Conservation of energy:

$$\frac{\partial e}{\partial t} = -p\frac{\partial \tau}{\partial t} + \frac{\partial E}{\partial t} + Q_2 \tag{3}$$

Equation of state for water:

$$p = \left(p_0 + B\right)\left\{\frac{\rho}{\rho_0}\right\}^{7.15} - B \tag{4}$$

where: B = 3010 atm.

Equation of state of water vapour - assumed as an ideal gas:

$$p = \rho e\,(\gamma - 1) \tag{5}$$

where $\gamma = 1.33$

In the above equations J is a volume Jacobian of transformation, ρ is density, p is pressure, $\underline{V}$ is velocity, τ is specific volume, e is internal energy, E is energy deposited in plasma by electrical discharge and Q_1 and Q_2 are terms connected with an artificial viscosity with directional properties (Vijay & Makomaski, 1998). The subscript 0 indicates initial conditions. It should also be pointed out that an additional equation of state for pressure has been added for pressures < 0.1 MPa (1 atmosphere) to avoid negative pressures at reduced densities. The code has been developed to the point where meaningful information can be obtained on the effect of the various parameters (discharge volume, chamber diameter, time of discharge, standoff distance, etc.) on peak pressure that can be obtained at a target placed at right angles to the issuing jet. For further details, reference should be made to Vijay & Makomaski (1998). Finite difference equations are used to solve these complex differential equations.

3. NUMERICAL RESULTS

Several important results have been obtained from the analysis which will be very useful in the design of the nozzle and to minimize the experimental work.

3.1 X-T Diagram

The sequence of physical events can be followed on distance - time (T) plot for the region near the axis of symmetry. This is shown in Fig. 5 for a chamber and converging nozzle of total length about 8 cm. The target is placed at a standoff distance of 5 cm, pressure at the inlet is about 34.5 MPa (5,000 psi) and the nozzle diameter is 2.16 mm (0.085 in). Steady flow is maintained by a 'piston' in the inlet plane, whose speed is such as to maintain the flow at 49 litre/min.

The electrical discharge is assumed to commence at the time of 30 µs at a distance of about 3 cm from the inlet. It is assumed that 20 kJ of electrical energy is discharged in 20 µs.

It is seen that for t > 30 µs, the plasma (represented here by high temperature water vapour) expands, sending shock waves towards the nozzle (S1) and towards the inlet (S2). Shock S1 leaves the nozzle at approximately 50 µs and forms a high-speed wave (W1) which accelerates the front F1 (of the original steady jet) to F2. The front F2 impacts on the target at 78.2 µs producing a peak pressure of 2388 MPa (346,000 psi) at 81.2 µs (see Fig. 8). This pressure is a result of a particular calculation and the four-figure resolution does not indicate the accuracy with which such peak pressures can be calculated. In general, the accuracy of calculations of peak pressures will improve with the reduction of cell sizes and numerical time increments.

Figure 5 also shows the importance of reflecting shock S2 back towards the nozzle. With the assumed 'piston' in the inlet plane, shock S2 is reflected as shock S3. This shock on passing through the plasma emerges as shock S4 and ultimately causes another high-speed wave W2 in the jet impacting at 104 µs. Shortly afterwards, two pressure peaks, 1704 MPa (246,900 psi) and 1713 MPa (248,300 psi) are created. These results give strong encouragement not to rely exclusively on the primary shock S1, but to seek some arrangement to reflect the shock S2, even if it can be done only partially.

3.2 Contours of Pressure

The contours of constant pressure in the chamber and the nozzle for times 35, 40, 45, 50, 55, 60 and 65 µs from the start of the calculations are shown in Fig. 6. They show clearly the formation of shock wave S1 (the intensity is indicated by the change in colour of the contours; typical values of pressure for each colour are shown in Fig. 8, although the magnitudes vary from one frame to another). As discussed by Vijay & Makomaski (1998), the electro-discharge nozzle, in many ways, is similar to the shock tube except for the varying geometry. Immediately after discharge, the shock waves detach themselves from the surface of the plasma bubble (termed 'black hat' here) and race towards the exit of the nozzle and the inlet plane, the moving 'piston' (Fig. 6A). As expected the pressure increases behind the shock. Subsequently, as the shock wave propagates at high speed, the transient wave phenomena, wave structure and wave interactions become quite complex as shown in Figs. 6(B) to 6(G). For instance, Fig. 6(B) shows the reflection of the incident wave from the nozzle wall. While Fig. 6(C) shows the wave downstream of the plasma racing toward nozzle exit, Fig. 6(D) shows the wave racing towards the inlet. Figures 6(E) to (G) show continued multiple interactions. The incident shock becomes gradually stronger as it moves through the converging part to the nozzle exit and sets up the motion of the high-speed wave (at times 55, 60 and 65 μs) in the jet. This is indicated by the slight bulges at the tips of the jet in Figs. 6(E), (F) and (G). The 'black hat' in Fig. 6 in an outline of the plasma bubble. It is seen in Fig. 5 that its size increases rapidly after 30 μs when the addition of energy commences. The energy deposition ends at 50 μs and at that moment the bubble begins to oscillate. It appears that these oscillations are associated with shock wave reflections at the bubble.

3.3 Jet in the Vicinity of the Target

Figure 7 shows the magnified views of the jet in the vicinity of the target for times 79, 80 and 81 μs. The contours show the approaching front followed by the high-speed wave characterized by a 'bulge'. As already mentioned, the jet impact occurs at 78.2 μs and the jet begins to 'pile' up creating high pressures (white areas). A peak average pressure of 2388 MPa occurs at the target at the time of 81.2 μs. The pressure distribution at that instance is shown in Fig. 8 where, pressure levels (in MPa) are indicated by a color bar.

As discussed before, the average peak pressures are based on pressures in numerical cells adjourning the target and will be lower than the theoretical spikes in negligible volumes adjoining the target. The results are nonetheless useful for determining the relative effects of the various parameters. This approach is adequate for the purpose of optimizing the proposed experimental arrangement.

3.4 Effect of Energy Release on the Impact Pressure

Very useful trends regarding the effects of energy and rate of energy discharge are shown in Fig. 9. These results were obtained for a volume of discharge (volume between the electrodes) of 0.266 cm^3 and at a standoff distance of 5 cm. The figure clearly shows that for a given energy level, the rate of energy release is very important to achieve higher pressures on the target. For instance, for an energy input of 50 kJ, increasing the rate of release from 0.5 kJ/μs to 1.25 kJ/μs increases the pressure of impact from 2,000 to 3,000 MPa (≈289,800 to 434,700 psi). These observations indicate that duration of discharge is quite important, that is, one should reduce it to the minimum achievable in practice.

3.5 Effect of Standoff Distance on the Impact Pressure

Figure 10 shows the effect of standoff distance on the impact pressure on the target. The rate of energy release for this case is 1.0 kJ/μs. The figure shows that for a given energy input, higher impact pressures are achieved at larger standoff distances. This observation seems to confirm the experimental results reported by Vijay et al. (1997) where steel samples placed at several standoff distances up to a maximum of 87 cm were completely ruptured. The standoff distance has to be chosen carefully for high energies (and hence large discharge times), so that all pressure pulse from the discharge have the time to reach the target to maximize the effect.

4. CONCLUSIONS

The purpose of the numerical modeling was to assist in the rapid development of the electro-discharge pulsed water jet machine, in particular the nozzle. The conclusions from the work reported in this paper are:

- The implementation of the code will accelerate the development of the electro-discharge nozzle by minimizing the experimental work;
- Some method must be found to make use of the shock reflected from the inlet plane (Fig. 5);
- Ultra-high pressures, of the order of 2,000 MPa (289,800 psi) can be achieved with the electro-discharge technique;
- The magnitude of energy input and its rate of release are quite important to achieve high pressures on the target;
- Depending on the energy input, the high impact pressures can be obtained at fairly large standoff distances, of the order of 15 cm;
- The numerical results need to be validated by experimental work;
- The electro-discharge technique appears to have a great potential for the removal of hard undesirable deposits (Fig. 1).

5. ACKNOWLEDGMENT

The authors are thankful to Federal Government Department Natural Resources Canada for the partial funding of this project, in particular Mr. J. Guérette, the Program Manager for the project.

6. REFERENCES

Vijay, M.M., and Paquette, N., "Electro-discharge Technique for Producing Powerful Pulsed Water Jets: Potential & Problems," *Proc. 13th International Conference on Jet Cutting Technology*, pp.195-210. BHR Group, Publication No. 21, Cranfield, Bedford, England, 1996.

Vijay, M.M., Bielawski, M and Paquette, N, "Generation of Powerful Pulsed Waterjets with Electric Discharges: Fundamental Study," *Proc. 9th American Water Jet Conference*, pp.415-430, Water Jet Technology Association, St. Louis, Missouri, USA, 1997.

Vijay, M.M., "Design and Development of a Prototype Pulsed Waterjet Machine for the Removal Hard Coatings," *Proceedings of the 14th International Conference on Jetting Technology*, pp. 39-57, BHR Group, Cranfield, Bedford, UK., 1998.

Vijay, M.M., and Makomaski, A.H., "Numerical Analysis of Pulsed Jet Formation by Electric Discharges in a Nozzle," *Proceedings of the 14th International Water Jet Conference,* pp. 73-87, BHR Group, Cranfield, Bedford, England, 1998.

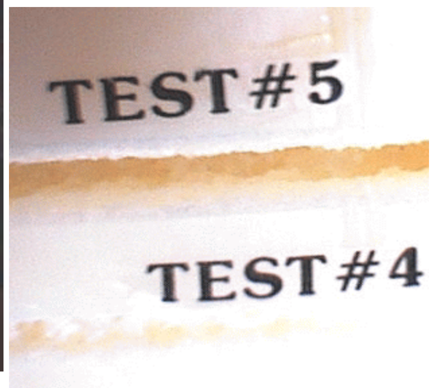

Fig.1. A general view of the kerfs made at 69 MPa (10,000 psi) in the thick (≈ 25 cm; 9.8 in) undesirable deposits (mostly resins). The deposits grow on the walls of the chemical reactor vessels. Test #4: Continuous waterjet. Test #5: Pulsed waterjet. Nozzle diameter = 1.37 mm (0.054 in).

Close-up view of the tests. $V_p/V_c \approx 6.0$. V_p, V_c = Volume removal rates respectively of pulsed & continuous waterjets.

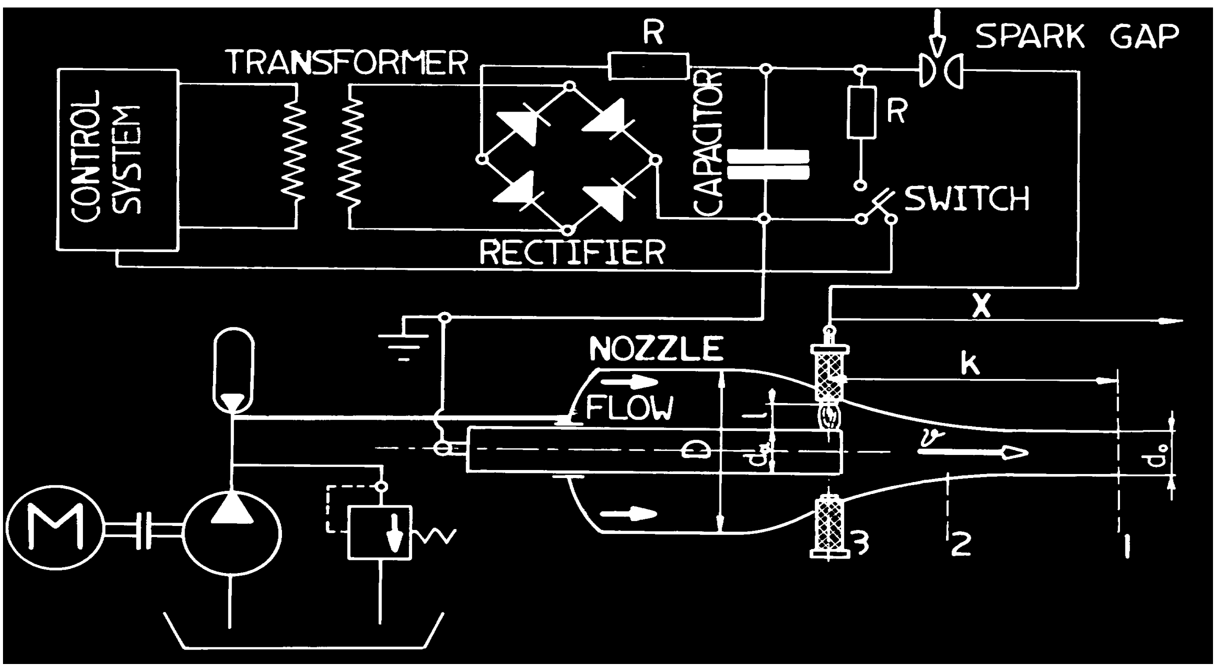

Fig. 2. A schematic diagram of the electro-discharge system for modulating a continuous stream of water for producing powerful pulsed water jets, showing electrical pulsed power system (Max: 20 kV, 100 kJ), pump (< 34.5 MPa) and a typical nozzle configuration with electrodes.

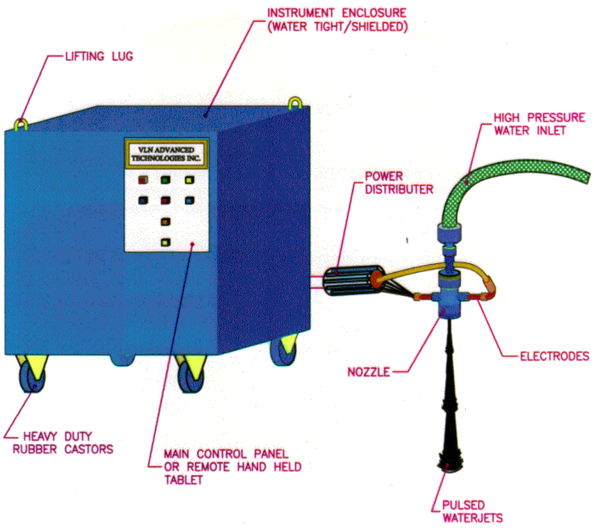

Fig. 3. A schematic diagram of the 100 kJ electro-discharge ultra-high-speed pulsed waterjet machine. The cabinet contains the capacitors and the associated electronics control system.

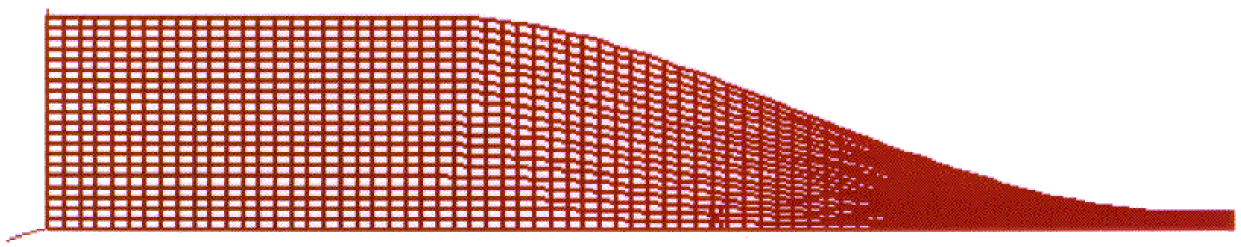

Fig. 4. Schematics of the numerical grid set up in the Lagrangian coordinates in the radial and axial directions.

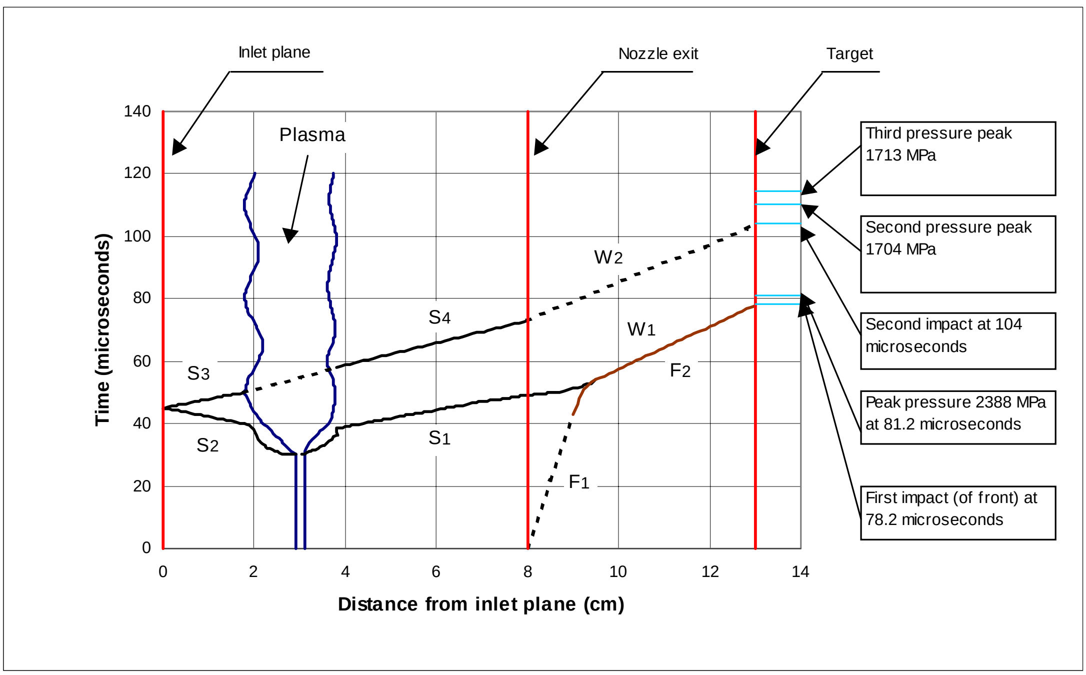

Fig. 5. A plot on the X-T diagram showing the interaction of the shocks with the target material. S1 is the primary shock following the discharge; S4 is the reflected shock from the inlet plane, etc.

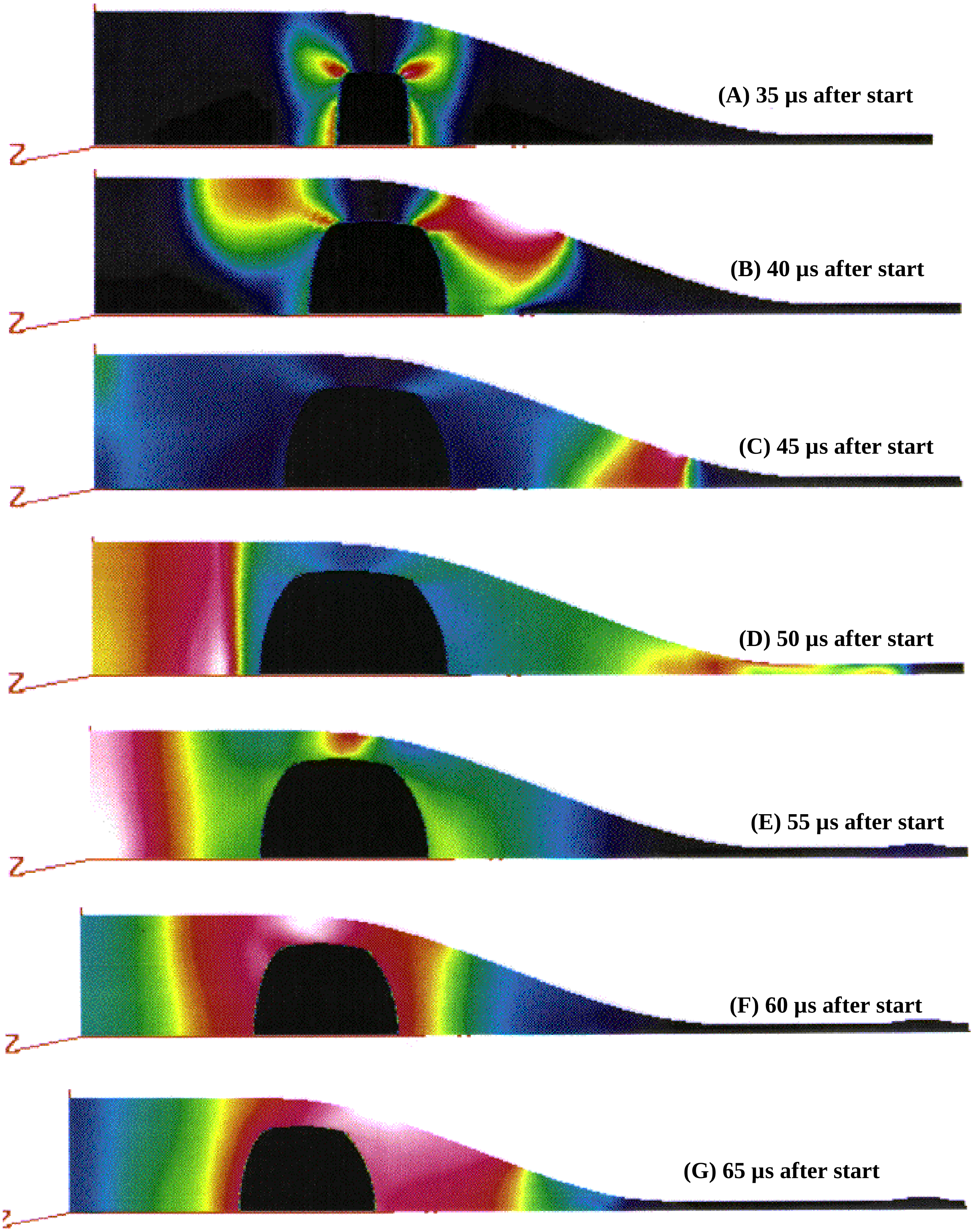

Fig. 6. Formation and propagation of shock waves from the plasma bubble formed between the electrodes after discharge. Discharge energy = 20 kJ. Inlet conditions: Pressure ≈ 34.5 MPa (5,000 psi); Flow = 49 litre/min(13 gpm). Times indicated are after the start of the calculations.

(A) 79 μs after start of calculations

(B) 80 μs after start of calculations

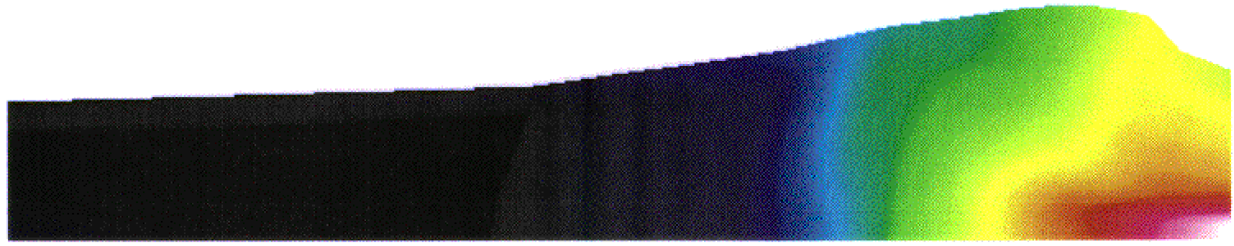

(C) 81 μs after start of calculations

Fig. 7. Influence of the shocks on the development of the jet in the vicinity of the target for the same conditions as in Fig. 6.

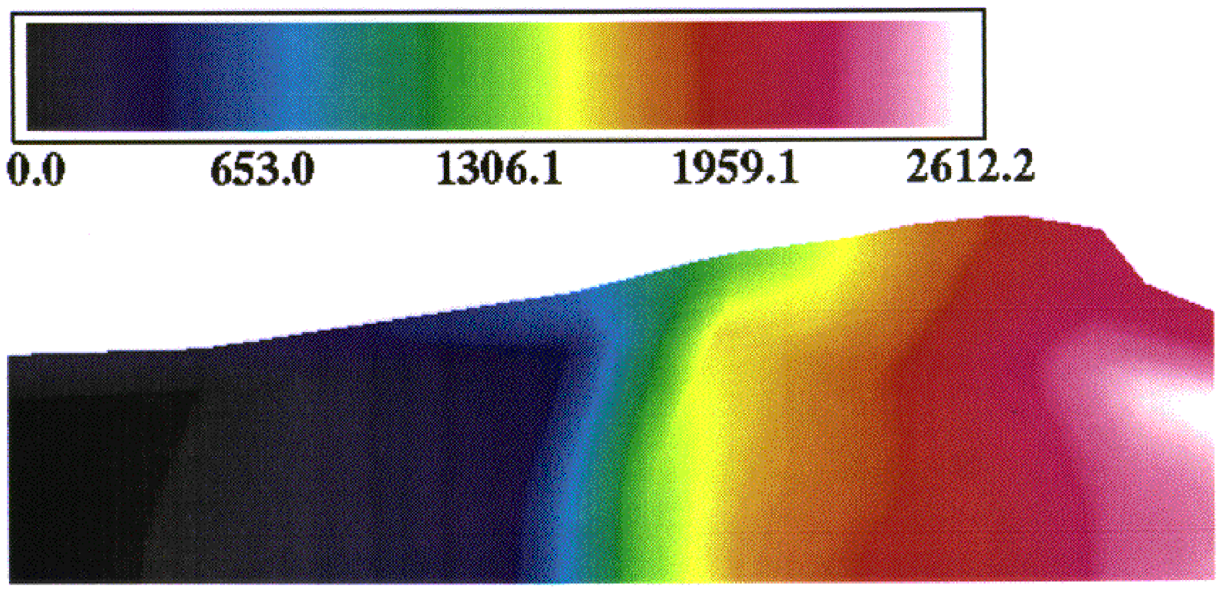

Fig.8. Pressure distribution on the target at 81.2 μs for the conditions listed in Fig. 6. The unit of pressure is MPa.

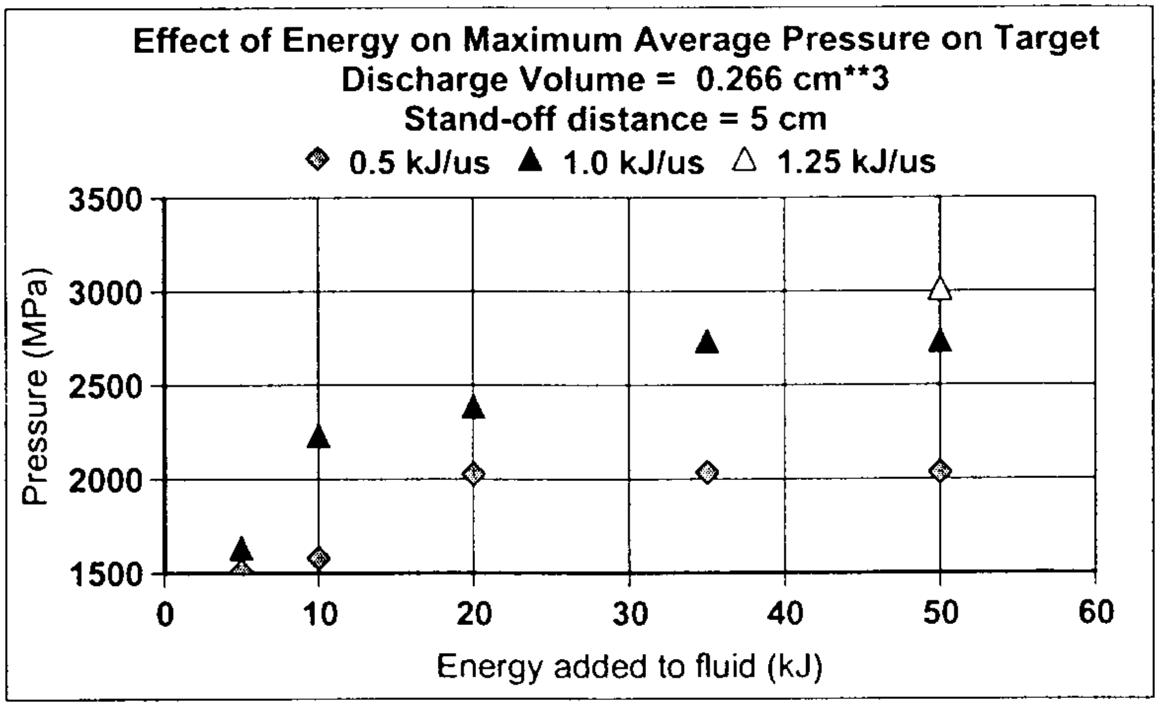

Fig. 9. Distribution of pressure on the target as a function of discharge energy with the rate of release as the parameter. Inlet conditions: Pressure = 34.5 MPa (5,000 psi); Flow = 49 litre/min (13 gpm).

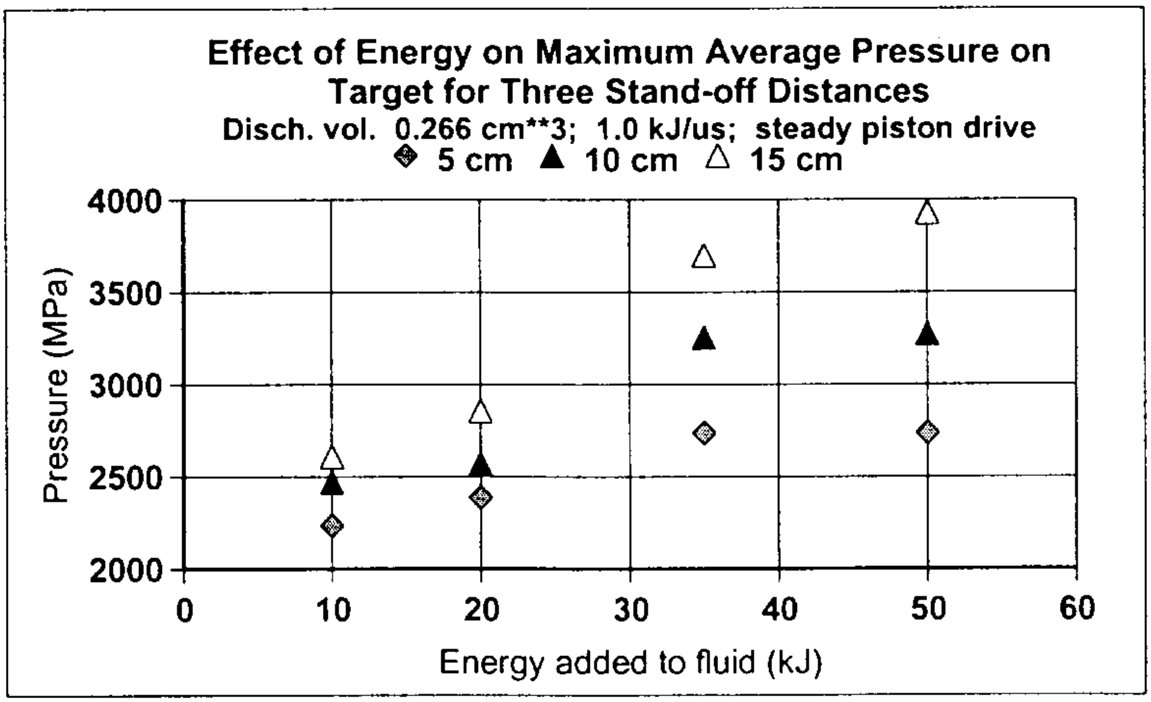

Fig. 10. Distribution of pressure on the target as a function of discharge energy with the standoff distance as the parameter. Inlet conditions: Pressure = 34.5 MPa (5,000 psi); Flow = 49 litre/min (13 gpm).

10th American Waterjet Conference
August 14-17, 1999: Houston, Texas

ANALYTICAL INVESTIGATIONS OF HYDRAULIC BREAKING COEFFICIENT OF COAL SEAMS

B.V.Radjko
LIETS, Eastukrainian State University
Lugansk, Ukraine

ABSTRACT

This paper presents the analytical method to discover the character of influence a number of factors on the hydraulic breaking coefficient of coal seams with plain water jets. It is adduced to the characters of twofold dependencies of the hydraulic breaking coefficient on such factors as dip angle of coal seams, depth of mining, gas concentration and ash share in coal seams, volatile matter of coal and duration of the hydraulic breaking process. The character of these twofold dependencies have been used to construct the empirio-analytical model of the hydraulic breaking coefficient of coal seams with plain water jets to project hydraulic breaking productivity of coal in Donetsk basin hydromines (Ukraine).

It is given the general equation of hydraulic breaking process of solids with plain water jets and analytical model of the hydraulic breaking coefficient of coal seams too.

1. INTRODUCTION

The author worked out the empirio-analytical method of the statistical data investigations. It gives possibility to increase a precision of the project calculations in comparison with the probability method.

The principal statements of the empirio-analytical investigation method were published before (Radjko et al., 1995).

This method was used to construct an empirio-analytical model of coal seams hydraulic breaking with the plain water jets. It consist of the general analytical equation of hydraulic breaking process of solids with plain water jets and multifactorous empirio-analytical model of hydraulic breaking coefficient of coal seams.

The analytical model of the hydraulic breaking coefficient (component of empirio-analytical model) was made the way of discovering twofold dependencies and combining them in multifactorous equation. Numeral parameters of twofold dependencies were calculated using statistical data.

Further it is stated analytical method discovering character of dependent variable (hydraulic breaking coefficient of coal seams) on different factors.

2. MECHANISM OF STATISTICAL DATA FORMING

Investigations show that three reasons take part in forming statistical data characterising hydraulic breaking process of coal seams with plain water jets. They are as follows: determinate influence of factors in force, nature indeterminacy and errors of measurements (observations).

Determinate influence of active factors upon value of statistical data (hydraulic breaking coefficient of coal seams in our case) is realised in different ways: through number of factors taken into account, influence force each of them, peculiarities of interaction between the factors and combinations of their values in the concrete conditions.

A number of factors taken into account play impotent role. It is supposed that the more such factors are the higher is precision of the project calculations. But theoretically precision of calculations is limited by value of nature indeterminacy. Besides, there are errors of measurements, which reduce precision of calculations too. Therefore, it is impossible to get high precision of project calculations only apply to quantity of factors taken into account.

It is so that precision of the project calculations grows with increasing number of factors. But variable curve of calculation precision from number of factors has a form of overturned hyperbola that draws near his limit and never cross it. The more factors taken into account the less is addition of calculation precision. The volume of getting, preparing and processing statistical data grows fast but increasing of calculation precision becomes slow down. Therefore, it is not advisable to take into account a lot of factors.

There is opinion about principal factors. It is supposed that high precision of project calculations obtained by taken into account some principal factors. Striving for simplicity support this mistake. Investigations show that “ principal “ factors no constant and keep their importance only in definite conditions. “ Principal “ factors can become “ secondary “ ones under another conditions and vice versa. Sufficient precision of statistical phenomena forecast can be achieved by taking into account some quantity of active factors. Their number depends on peculiarities of studied phenomenon and demanded precision. The last can not be higher then allows nature indeterminacy and measurement mistakes of course. A list of the factors taken into account is revealed by analysing the ones, which are in force under studied conditions. Necessary number of the factors is determined by introducing them into empirio-analytical model one by one and estimating coefficient of variation.

Above mentioned can be realised if it is known influence force each of the factors in separately, peculiarities of interaction between all of them and their joint affect on the exit characteristic of studied phenomenon, that is on the hydraulic breaking coefficient in our case. Interaction between active factors and their joint influence on the hydraulic breaking coefficient take into account with helping empirio-analytical model of it.

To discover effect force each of separate factors on the hydraulic breaking coefficient it is necessary to fulfil definite investigations. They include revealing character of twofold dependencies and calculating numeral value of their parameters.

Combination of active factors and their values to make project calculations can be find out of geological data.

Precision of forecast in the provinces of nature indeterminacy and random errors of measurements can be risen with taken into account distriction law of random variable.

3. REVEALING CHARACTER OF TWOFOLD DEPENDENCES

Character of determinate effect of the active factors upon hydraulic breaking coefficient is revealed by investigating twofold dependencies for every one of them separately. It is analysed peculiarities of the physical interactions between monitor waterjets and coal massif in existence range of every studied factor. Moreover, it is investigated the border parts and middle fields of twofold dependencies too.

Analysing character of any twofold dependence it is conditioned with using of the principal “other things being equal“. Besides, it is necessary to remember that hydraulic breaking of coal seams with plain water jets realises the way of making and widening of the clefts in a coal massif. Therefore, influence characters of the studied factors are revealed in accordance with their effect on making and widening of the massif clefts.

3.1 Dip angle of coal seams.

It is known from practical experience of hydromines that intensity of hydraulic breaking of coal seams grows with increasing their dip angle. The reason is the one that resists making and widening of the clefts in a coal massif. It can be roof pressure. Normal component of roof pressure decreases with increasing dip angle of coal seams. Therefore resistance for making and widening of the massif clefts decreases with increasing dip angle and intensity of hydraulic breaking of coal seams grows. And vice versa resistance for making and widening of the massif clefts increases with decreasing dip angle and intensity of hydraulic breaking of coal seams gets down.

When dip angle draws near 90 degrees, perpendicular component of roof pressure approaches to nought. But in this case lateral rock pressure takes place and that is why intensity hydraulic breaking is limited. If dip angle draws near nought degree, normal component of roof pressure approaches to maximum value and intensity of hydraulic breaking reduces to a minimum.

Curve of studied dependence has monotonous character as perpendicular component of roof pressure changes regularly.

Thus theoretical character of twofold dependence of hydraulic breaking coefficient on dip angle of coal seams has the view as follows

$$R_0 = a_1 - b_1 \cdot Cos\alpha \qquad (1)$$

It is follows out of equation (1) that hydraulic breaking coefficient decreases with decreasing dip angle of coal seams.

3.2 Depth of mining

It is considered that normal strain of weight of rocks grows with increasing of mining depth. It means that normal component of roof pressure on coal seams changes the same way. But resistance to hydraulic breaking of coal seams grows with increasing of normal component of roof pressure as was grounded before. Therefore it is possible to write equation

$$1/R_0 = a_2 + b_2 \cdot H \qquad (2)$$

and after transformation

$$R_0 = \frac{1}{a_2 + b_2 \cdot H} \qquad (3)$$

It is follows out of equation (3) that hydraulic breaking coefficient reduces with increasing depth of mining according to hyperbola curve.

3.3 Gas concentration in coal seams

Practical experience of hydromines shows that hydraulic breaking of gassy coal seams is produced easier then non-gassy ones. It can be seen well enough while hydraulic extracting gassy coal seams that are dangerous with throwing out a crushed coal and gas.

Probably, absorbed gas weakens internal bonds in a coal massif and assists making and widening clefts in it while hydraulic breaking is realised. The more gas concentration in coal seams is the more intensity of hydraulic breaking takes place. In common case character of twofold dependence of hydraulic breaking coefficient on gas volume in one ton of coal massif has the view

$$R_0 = a_3 + b_3 \cdot (I\char94 x) \qquad (4)$$

But as range of gas concentration in coal seams is limited for practical goals one can assume that dependence has linear character. That is

$$R_0 = a_3 + b_3 \cdot I \qquad (5)$$

3.4 Ash share in coal seams

It is known to break the rock with plain water jets is more difficult then coal seams. Therefore it can be supposed that presence of dirt inclusions in coal seams make resistance to their hydraulic breaking.

Rock inclusions in coal seams exist in a view of fixed ash and barren layers. Presence of fixed ash that is distributed equally in coal seams resists making and widening of the clefts in a massif while hydraulic breaking is realised. The more quantity of fixed ash is the less intensity of hydraulic breaking of coal seams takes place.

Fixed ash changes from a few per cent to a quantity about several tens of the ones in the coal seams and near a hundred per cent in a mine rock. It is obvious that there are high ash seams where coefficient of hydraulic breaking can be equal nought.

From reasoning follows that character of twofold dependence of hydraulic breaking coefficient on fixed ash share has the view

$$R_0 = a_4 - b_4 \cdot A^C \qquad (6)$$

Barren layers in coal seams change their structure and decrease intensity of hydraulic breaking as prevent from selective extraction of coal. Such influence of barren layers on hydraulic breaking of coal seams can be taken into account with corresponding coefficients.

3.5 Volatile matter of coal

It is revealed that resistance of coal massif to be broken with mechanical way depends on composition of organic mass and mineral admixtures. The last ones cement coal massif and make growth its resistance for breaking.

As for organic mass of coals their massifs with high density are broken badly. The less density of organic mass of coal is the more intensity of breaking process takes place.

The most effective criterion to measure density of coal organic mass is volatile matter. The last diminishes gradually from candle and gas coal to lean coal and anthracite. But density of coals changes the other way then volatile matter of them. Minimum density has fat and caking coals, maximum ones have candle coals and anthracites. Therefore, intensity of hydraulic breaking process of coal seams grows at first with increasing of volatile matter reached maximum and decreases then to minimum. Character of twofold dependence of hydraulic breaking coefficient on volatile matter has the view of parabola. Its equation is as follows

$$R_0 = \frac{1}{[a_5 \cdot (V^C - b_5)^2 + c]} \qquad (7)$$

Top of parabola corresponds to caking coal.

3.6 Duration of hydraulic breaking process

It is possible to have two ways of hydraulic extraction of coal. The first one is when waterjet length of hydraulic monitor is constant. It takes place if nozzle of hydraulic monitor follows the coalface. In that case volume of split and duration of hydraulic extraction are constant.

In the second way when the coal face removes from nozzle outlet waterjet length gets longer, volume of split and duration of hydraulic extraction are increasing, but productivity of hydraulic breaking draws down because of diminishing of shocking effect of waterjet on coal massif. With increasing length of waterjet duration of hydraulic extraction grows faster than volume of split. It causes that twofold dependence of split volume on hydraulic breaking duration has a view of overturned hyperbola with a limit corresponding to performing length of waterjets.

That is why equation is as follows

$$V = \frac{1}{(b_6 + a_6\ /T\ )} \qquad (8)$$

And after transformation it has the view

$$V/T = 1/\ (a_6 + b_6 \cdot T) \quad \text{and} \quad V \cdot \rho_c\ /\ T = \rho_c\ /\ (\ a_6 + b_6 \cdot T\ ) = P_{hb} \qquad (9)$$

From equation (9) follows that maximum of productivity takes place at beginning of hydraulic extraction.

To reveal character of dependence of hydraulic breaking coefficient on duration of split extraction one can compare equations (9) and (11). It is clear from comparison that hydraulic breaking coefficient is the only variable which depends on duration of extraction. Therefore its dependence on duration of hydraulic breaking process has the character of hyperbola the same as given with equation (9).

4. ANALYTICAL MODEL OF HYDRAULIC BREAKING COEFFICIENT

Analytical model of hydraulic breaking coefficient of coal seams with plain waterjets is a multifactorous equation, which was constructed by combining some twofold dependencies. It is as follows

$$R_0 = \frac{f \cdot (a_1 - b_1 \cdot Cos\alpha) \cdot (a_3 + b_3 \cdot I) \cdot (a_4 - b_4 \cdot A^C)}{(a_2 + b_2 \cdot H) \cdot \{ a_5 \cdot (V^C - b_5)^2 + c\} \cdot (a_6 + b_6 \cdot T)} \qquad (10)$$

Coefficient “f“ uses to conform the units measure of twofold dependencies in the equation (10) with units measure of the hydraulic breaking coefficient “R_o“ in equation (11). The more active factors are taken into account in equation (10) the more is approximation of unit measure of the coefficient “f ” to its true value and the more is volume of investigations and calculations to reveal it.

Probably coefficient “f” will not have unit measure with being taken into account all of influencing factors. But as for doing it is quite difficult and is not necessary for practical goals one has to use coefficient “f” to conform units measure in model (10).

5. GENERAL EQUATION OF HYDRAULIC BREAKING PROCESS OF SOLIDS

General analytical equation of hydraulic breaking process of solids with plain water jets has the view (Radjko et al., 1998)

$$P_{hb} = \pi \cdot \mu \cdot K \cdot (P_0\text{^}1.5) \cdot (d_0\text{^}2) \cdot R_0 / 2 \cdot \{(2 \cdot \rho_0)\text{^}0.5\} \qquad (11)$$

Equation (11) gives possibility to project productivity of hydraulic breaking of solids with plain water jets.

Interaction of plain water jets with solids while hydraulic breaking process is being realised and physico-mechanical properties of solid bodies are taken into account with hydraulic breaking coefficient “R_o”.

Coefficient “μ“ depends on nozzle geometry and coefficient “K” is necessary to take into account the factors which are unknown yet.

Density of liquid “ρ_0“ applied for hydraulic breaking of solids can be used too to take into account influence of different additions such as polymer, abrasive etc.

Equation (11) is good to decide applied problems, optimise the quantity of specific energy expense of hydraulic breaking or cutting processes, calculate the hydraulic breaking coefficient for different materials etc.

6. CONCLUSION

Hydraulic breaking coefficient of coal seams is a statistical variable and is formed with effecting of three reasons: determinate influence of active factors, nature indeterminacy and errors of measurements. Influence of active factors realises through number of them, effective force each of them, peculiarities of interaction between the factors and combinations of their values in the concrete conditions. All of these influences can be taken into account correctly if it is known character of effect each of the active factors separately.

Analytical investigations of peculiarities of physical interactions between water jet and coal massif fulfilled give possibility to reveal character of twofold dependencies for different factors and construct mathematical model of hydraulic breaking coefficient of coal seams. This coefficient is necessary to use general equation of hydraulic breaking process of solids, which is given.

7. ACKNOWLEDGMENTS

The author is thankful to Prof. G. A. Atanov (Donetsk State University) for the inspiration to write this paper and Docent A. A. Andruschuk (Eastukrainian State University) for assistance when it was preparing.

8. REFERENCES

1. Preparation and Briquetting of Coal. Mining. Encyclopaedic Reference Book. Vol.11, p.10, Gosgortehisdat, Moscow, Russia, 1960, (in Russian).

2. Radjko, B.V.,”Empirico-Analytical Investigations of Coal Seams Breaking Process with Plain Water Jets”. *Proceedings of the 8th American Water Jet Conference*, Vol. II, paper 64, pp. 867-878., Water Jet Technology Association, Houston, USA., 1995.

3. Radjko, B.V.,"General Equation of Hydraulic Breaking Process of Solids with Plain Water Jets, *Proceedings of 5th Pacific Rim International Conference on Water Jet Technology*, paper 60, New Delhi, India, 1998.

9. NOMENCLATURE

$a_1, a_2, ...a_6$; $b_1, b_2, ...b_6$; c — parameters of twofold dependencies
A^c — ash content in coal seams, p.c.
α — dip angle of coal seams, deg.
d_o — nozzle outlet diameter, m
f , K, μ — empirical coefficient
H — depth of mining, m
I — gas concentration in coal seams, $m^3 / (10^3)kg$
P_{hb} — hydraulic breaking productivity of solid, kg / s
P_o — water jet pressure near nozzle outlet, Pa
ρ_c — coal density, kg / m^3
ρ_0 — water density, kg / m^3
R_o — hydraulic breaking coefficient, m / N
T — duration of hydraulic breaking process, H
V — volume of split, m^3
V^c — volatile matter of coal, p. c.

10th American Waterjet Conference
August 14-17, 1999: Houston, Texas

Paper 9

HYPER PRESSURE WATERJET

AND ABRASIVE WATERJET CUTTING

John Xu, Kevin Otterstatter, Mark Harkess, Reynold Sacquitne, Jude Lague
Jet Edge
Minneapolis, Minnesota

ABSTRACT

An intensifier pump was developed by Jet Edge to operate at a pressure of 75,000 psi (520 MPa) for waterjet cutting. Using this intensifier, tests were conducted to examine what influence the higher operating pressure had on cutting speed and edge quality for various materials and thickness'. It was found that a significant improvement was seen in cutting speed when compared to cuts made at 55,000 psi (380 MPa). Tests were conducted using both straight water and abrasive waterjets. The results and analysis found in the testing are presented in this paper.

Organized and Sponsored by the WaterJet Technology Association

1. INTRODUCTION

Waterjet cutting uses a jet of water so powerful that it cuts cleanly and precisely through material in a single pass without shredding or crushing. In the formation of the jet stream, water is pressurized up to 75,000 psi (520 MPa) by a Jet Edge hydraulically driven intensifier pump. The operating pressure currently commercially available is 55,000 psi (380MPa), which is the most common pressure for most waterjet and abrasive waterjet cutting applications. The pressurized water passes through an attenuator, which stabilizes the jet stream. The waterjet cutting action takes place as a result of the ultra-high pressure water being forced through a pre-mounted sapphire orifice as small as .002 in (.051 mm) in diameter. The pressurized water exits the orifice at extremely high velocities as a coherent waterjet stream that produces a clean cut.

Waterjet cutting with water increases production rates on paper products, woven or non-woven textiles and similar materials without shredding or the damage associated with conventional processing methods. The waterjet stream cuts flexible materials quickly and accurately and prevents distortion encountered from compression during conventional die cutting. Waterjet cutting is used in the cutting of materials such as: plastics, corrugated cardboard, insulation, rubber, foods, paper, automotive carpeting and headliners.

Abrasivejet cutting systems use a combination of water and garnet to cut through materials considered "unmachineable" by conventional cutting methods. Using small amounts of water to eliminate the friction caused by tool-to-part contact, abrasivejet cutting avoids thermal damage that can adversely affect metallurgic properties in materials being cut. The ability to pierce through material also eliminates the need and cost of drilling starter holes. Abrasivejet can cut through materials ranging from 1/16 inch (1.6 mm) to 12 inches (305 mm) with an accuracy of ± 0.005 inches (0.13 mm). Abrasivejet is excellent for the cutting of complex shapes and in fragile materials such as glass. The high failure rate due to breakage and chipping of corners during conventional processing is virtually eliminated. Abrasivejet cutting is used in the cutting of materials such as: titanium, brass, aluminum, stone, inconel, any steel, glass, and composites.

Whatever the industrial need, waterjet and abrasivejet are accurate, flexible, and efficient cutting systems. Because waterjet cuts with a narrow kerf, parts can be tightly nested together thus maximizing material usage. The compact, lightweight cutting head is designed for reliability in high cycle, on/off applications. When coupled with a suitable motion control system, waterjet cutting provides extremely accurate cuts with a high degree of repeatability over a wide range of materials and shapes.

Whether or not a customer decides to purchase an ultra-high pressure waterjet system for their cutting application is based upon many factors including performance, capability, operational effectiveness, maintainability, reliability, and cost. In cutting operation cost, abrasive waterjet users have found that the abrasive consumption is the most costly item.

2. DEVELOPMENT OF THE HYPER PRESSURE WATERJET INTENSIFIER

Figure 1 shows the schematic of the intensifier developed for this test program. The intensifier acts as an amplifier as it converts the energy from the low-pressure hydraulic fluid into hyper pressure water. The intensification ratio is 25.4. The maximum pressure is 80,000 psi (553 MPa) with an operating pressure of 75,000 psi (520 MPa). A limit switch, located at each end of the piston travel, signals the PLC to shift the directional control valve and reciprocate the piston movement.

Testing has been completed on the 50 horsepower (37 kWh) and 100 horsepower (74 kWh) intensifier pumps (Figure 2). The pumps were operated to see how running at the hyper pressure would affect the entire structure of the Jet Edge pump and UHP components. These UHP components include the attenuator, high-pressure cylinders, check tubes, backup disks, high-pressure seals, as well as the center piston assembly. These parts have been examined with respect to life expectancy and maintenance considerations. Extensive research was performed on the hyper pressure components as an aspect of the fatigue life, metallurgical, and special processes. The reliability of this hyper pressure intensifier has been improved to a level that can be accepted by users in this industry.

3. CUTTING TEST AND RESULTS

Cutting tests were performed to see what advantages the new hyper pressure intensifier pump can offer. Various materials and thickness' were cut to get a good feel for the capabilities of the higher pressure. From this testing it can be seen that there is a potential for the new line of hyper pressure pumps. During the test, the CNC table manufactured by Jet Edge was used for the motion and speed control.

3.1. Abrasive Cutting System

During test cuts the patented Permalign II cutting head and abrasive delivery system were used (Figure 3 and 4). The design of this cutting head ensures orifice and nozzle alignment. For the solid phase abrasive delivery system, a pressurized hopper is used to force abrasive into a secondary hopper. The secondary hopper has a pneumatically actuated slide gate and dial wheel that provides accurate metering and reliable on/off control of the abrasive through the CNC controller (Figure 5).

3.2. Cutting Data

For the cutting tests, each material was cut at both 55,000 psi (380 MPa) and 75,000 psi (520 MPa). The feed rate was measured to see how much faster the cutting head could operate and still obtain the same quality of separation. For some materials the pressure was kept at 75,000 psi (520 MPa) with the abrasive flow rate reduced to obtain the same cutting speed as that of the 55,000 psi (380 MPa) test. This allowed an examination of how little abrasive could be used when operating at the higher pressure. The results of the cutting tests are shown in Tables 1 to 3. From this data, an average 40-50% increase in feed rate can be obtained by operating at 75,000 psi (520 MPa) vs. 55,000 psi (380 MPa) with an orifice diameter/nozzle diameter 0.010/0.030 inch (0.25/0.76 mm) combination. Cutting through a 14 inch (355 mm) thick forged steel alloy block with a 0.015/0.045 inch (0.38/1.14 mm) combination was also tested.

From these results it looks as though there could be a potential for a pump operating at hyper pressures. If faster cutting speed or less abrasive use were desired, this pump would seem to be a possible solution.

4. COST ANALYSIS

The cost analysis includes pump operation cost and cutting cost (Table 4). During the test at 75,000 psi (520Mpa) operating pressure, there did not appear to be a tremendous increase in pump operating costs. Utilization of cutting water and cooling water as well as power usage showed minor increases compared to the 55,000 psi (380 MPa) test operating at the same horsepower. Cutting costs include abrasive and consumable parts. Since cutting speed increases at 75,000 psi (520 MPa) pressure, costs dramatically decrease. It can be seen that, as an example, the cutting cost decreased 42% when cutting 2.625 inch 4140 Steel.

5. CONCLUSIONS

It has been observed that there is a significant benefit in operating hyper pressure 75,000 psi (520 MPa) waterjet and abrasive waterjet systems over ultra-high pressure 55,000 psi (380 MPa) systems in terms of cutting cost reduction and the capability to cut thicker materials.

6. REFERENCE

Shunk, J.F. "Waterjet Cost Effectiveness: Case Studies in Cutting and Coating Removal" 8th American Waterjet Conference, August 26-29, 1995, Houston, Texas.

Summers, D.A. "Waterjetting Technology" E & F N Spon, 1995.

7. TABLES AND FIGURES

Table 1. 75,000 psi vs. 55,000 psi cutting for 14" thick steel alloy with 0.015 inch diameter orifice and 0.045" diameter nozzle, surface quality at 4.5

Abrasive rate	55K Feed Rates (in/min)	75K Feed Rates (in/min)	% Increase
1.5 lb\min	0.085	0.125	47.1

Table 2. 75,000 psi vs. 55,000 psi abrasive cutting with varying abrasive rate

Quality 1

Abrasive rate (lb/min)	55K Feed Rates (in/min)	75K Feed Rates (in/min)	% Increase
0.2	0.50	0.67	34.0
0.4	0.70	0.90	28.6
0.5	0.78	1.10	41.0
0.6	0.81	1.22	50.6
0.7	0.82	1.28	56.4
0.8	0.82	1.30	58.5
0.9	0.82	1.30	58.5

Quality 2

Abrasive Rate (lb/min)	55K Feed Rates (in/min)	75K Feed Rates (in/min)	% Increase
0.2	0.40	0.58	45.0
0.4	0.56	0.80	42.9
0.5	0.65	0.95	46.2
0.6	0.71	1.05	47.9
0.7	0.75	1.10	46.7
0.8	0.76	1.13	48.7
0.9	0.77	1.15	49.4

Quality 3

Abrasive rate (lb/min)	55K Feed Rates (in/min)	75K Feed Rates (in/min)	% Increase
0.2	0.30	0.40	33.3
0.4	0.40	0.60	50.0
0.5	0.50	0.72	44.0
0.6	0.56	0.82	46.4
0.7	0.60	0.90	50.0
0.8	0.63	0.93	47.6
0.9	0.64	0.94	46.9

Quality 4

Abrasive rate (lb/min)	55K Feed Rates (in/min)	75K Feed Rates (in/min)	% Increase
0.2	0.20	0.25	25.0
0.4	0.30	0.40	33.3
0.5	0.36	0.50	38.9
0.6	0.40	0.58	45.0
0.7	0.42	0.64	54.2
0.8	0.43	0.70	62.8
0.9	0.44	0.72	63.6

Quality 5

Abrasive rate (lb/min)	55K Feed Rates (in/min)	75K Feed Rates (in/min)	% Increase
0.2	0.08	0.12	50.0
0.4	0.15	0.22	46.7
0.5	0.18	0.26	44.4
0.6	0.20	0.29	42.5
0.7	0.21	0.31	47.6
0.8	0.22	0.33	50.0
0.9	0.22	0.35	59.1

Table 3. 75,000 psi straight waterjet cutting

Material	75k Cut Test		.004" HC orifice	
	Feed Rate 75k	Feed Rate 55k	Quality	% Increase
.5" UHMW	18	5	1	260
.5" Neoprene	400	200	1	100
2.125" Rubber	20	4	1	400

Table 4. Cost comparison

Pressure	55,000 psi	75,000 psi	75,000 psi
Water	1 gpm	0.75 gpm	1.3 gpm
Power	50 hp	50 hp	100 hp
Abrasive	0.2-0.9 lb/min	0.2-0.9 lb/min	0.2-0.9 lb/min

With 0.010/0.030 combination
- 2.625" 4140 Steel
- Cutting rate 0.78 in/min at 55,000 psi, 1.02 in/min at 75,000 psi

Pump cost includes:
- Cutting water
- Cooling water
- Power
- Operation consumables

Cutting cost includes:
- Abrasive

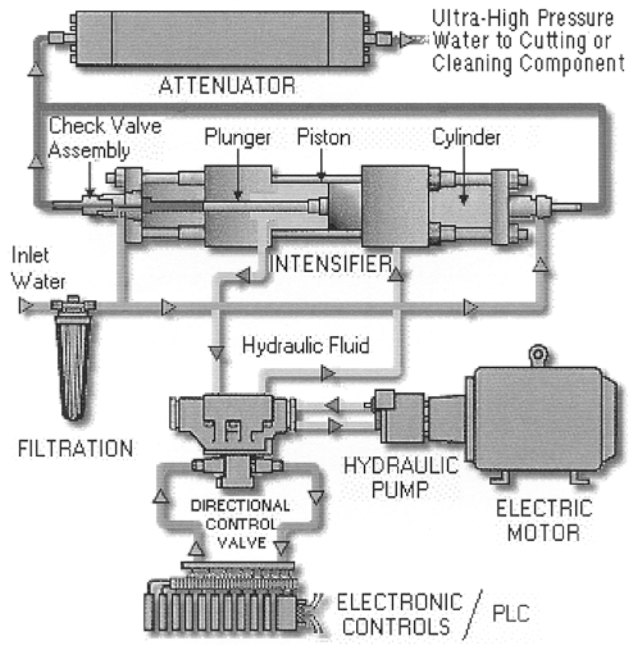

Figure 1. Schematic of the hyper pressure intensifier pump

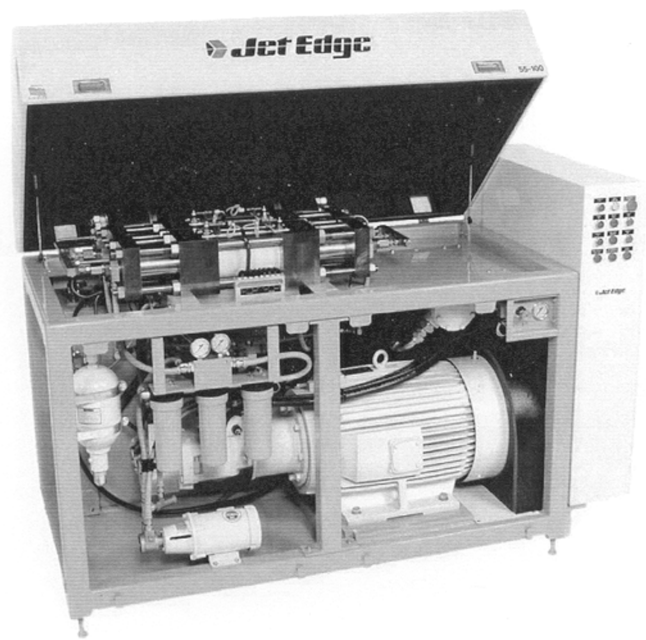

Figure 2. The intensifier pump used for test

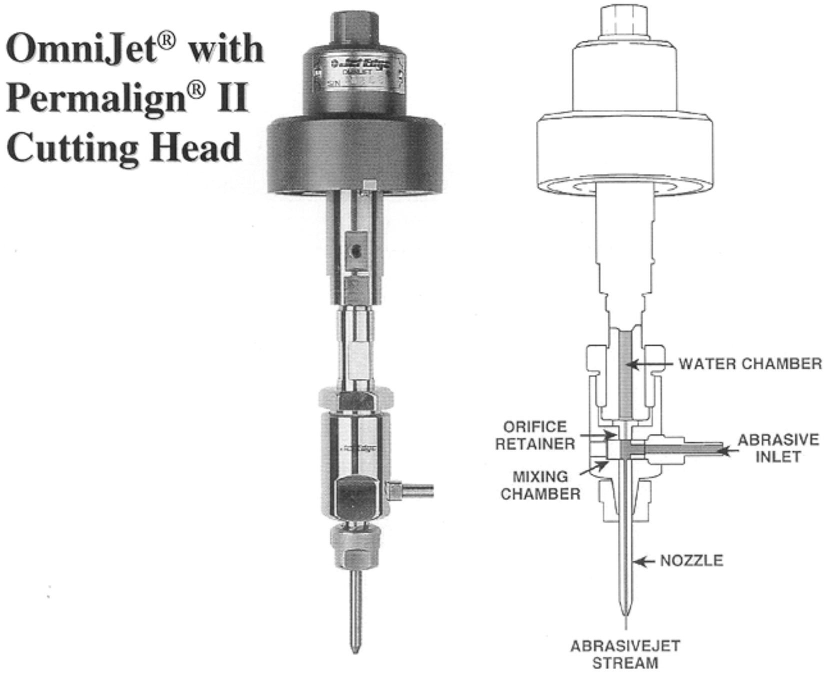

Figure 3. Patented abrasive cutting head with self-alignment

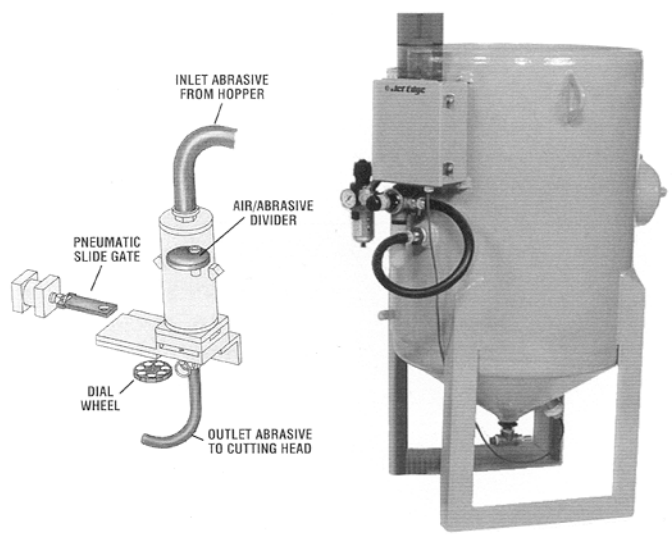

Figure 4. Abrasive delivery vessel and secondary hopper

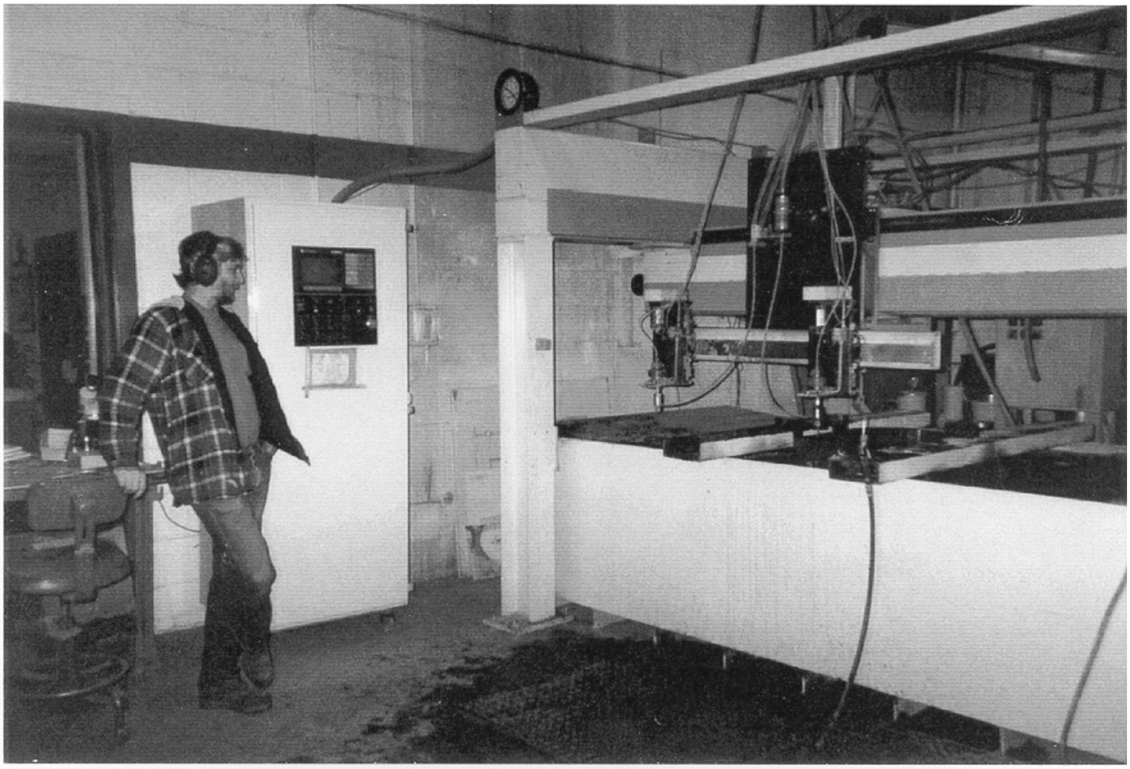

Figure 5. Test cut for 14 inch forged steel alloy on CNC table

10th American Waterjet Conference
August 14-17, 1999: Houston, Texas

Paper **10**

CUTTING AND DRILLING AT 690-MPa PRESSURE

Mohamed Hashish
Flow International Corporation
Kent, Washington

ABSTRACT

The rational for extending the pressure range of waterjet cutting technology is discussed in this paper. The effects of waterjet (WJ) and abrasive-waterjet (AWJ) parameters on cutting of several metals are discussed. From the results of WJ cutting tests, it is observed that the specific power required for cutting is reduced as the pressure increases. Thin sheet metal can be cut effectively with waterjets. However, the cut surfaces are typically rough and deformed. The quality of cut surfaces improves as the pressure increases or small amounts of abrasives are added. Increasing the standoff distance has been observed to increase the cutting speed; this is attributed to the droplet impact effect that becomes dominant at large standoff distances. The cutting test results with 690-MPa AWJs confirmed the linear trend of the effect of pressure on cutting rate. Most importantly, the abrasive consumption was significantly reduced as the pressure was increased. Tests were also conducted to drill small holes in several metals and composites. It was found that pressure ramping yields better drilling results.

Organized and Sponsored by the WaterJet Technology Association

1. INTRODUCTION

Waterjets were commercially introduced for industrial cutting applications in the early 1970s. This was primarily due to the development of 414-MPa (60-ksi) intensifier pumps capable of powering high-velocity waterjets with flow rates of a few liters per minute. This has opened great markets for waterjet technology. Prior to their use at these relatively high pressure levels, waterjets were limited to cleaning surfaces and mining relatively soft formations. High flow rates were mainly used for washing out rather than for material separation. Increasing pressures beyond 414 MPa promises the following advantages:

- More cutting capabilities (composites, thin metals)
- Increased efficiency (specific energy may improve)
- Lower abrasive usage (when using an AWJ)

There has been no change in the peak operating pressure of intensifier pumps (380 MPa) over the last 30 years. Although higher pressures (over 1000 MPa) can easily be generated in the industry today, these units are not intended for continuous operation but for static applications. In this paper, we present data on the potential improvement in cutting and drilling performance when pressures are increased up to 690 MPa.

2. 690-MPa INTENSIFIER PUMPS

The output pressure from any intensifier pump is determined by the inlet hydraulic oil pressure and the pressure intensification ratio. This ratio can be defined as the area of the oil-side piston divided by the area of the pressurized water-side plunger. Increasing the pressure from 380 to 690 MPa can be achieved by altering the oil pressure or the intensification ratio, or by altering both. Typical high-pressure pumps operate with 21-MPa oil and an intensification ratio of 20. Accordingly, producing 690 MPa would require an oil system operating at 35 MPa. This operating pressure would be at the upper limit for typical off-the-shelf oil hydraulic components, and it brings significant increases in wear rates and mechanical loads, with accompanying decreases in design safety factors. For our tests, an intensification ratio of 33 was used. Figure 1 shows a 690-MPa intensifier used to construct pumps for food processing systems.

Another pump concept was identified using multistage intensification featuring two or more intensifiers operating in a series to raise the water pressure in steps. This design capitalizes on the success of the current 690-MPa systems by retaining as much of the current design as possible. With two intensifiers in a series, the first would be a standard production unit that operates in its design mode, using 21-MPa oil to generate 345-MPa outlet water pressure. This would be supplied to the inlet of the second intensifier, which would be a standard unit with the exception of an inlet check valve body built to handle 345 MPa and a modified high-pressure cylinder (to withstand 690 MPa). The second intensifier would use the same 21-MPa oil-side hydraulics to boost the pressure from 345 MPa to 690 MPa. This concept offers the advantage of identical intensification ratios and check valve differential pressures to those presently used in 345-MPa pumps. Also, with a multistage intensifier, lower alternating stresses will be encountered in the 690-MPa stage.

Figure 1. 690-MPa Intensifier

2.1 Flow Characteristics

The flow parameters of a high-velocity jet include pressure (*P*), flow rate (*q*), waterjet diameter (d_n), and power (*E*). Only two of these parameters need to be known to determine the rest. The following formulas relate these parameters:

$$V_{th} = \sqrt{2P/\rho} \tag{1}$$

$$V = c_v V_{th} \tag{2}$$

$$q = K_1 d_n^2 \sqrt{P} c_d \tag{3}$$

$$E = K_2 d_n^2 P^{1.5} c_d \tag{4}$$

where V_{th} is the theoretical waterjet velocity, V is the actual velocity, ρ is the water density, c_v is the coefficient of velocity, c_d is the coefficient of discharge, and K_1 and K_2 are numerical constants.

Figure 2 shows the measured flow rates for different orifice sizes up to 690 MPa. The orifice coefficient of discharge was calculated by dividing the measured flow rate by the theoretical flow rate ignoring water compressibility. This implies that the coefficient of discharge also incorporated the compressibility factor. Figure 3 shows the calculated coefficients of discharge for several orifice sizes. These calculations are very sensitive to the orifice size. Measuring the orifice diameter up to three decimal points may not be accurate enough, especially for small orifices. Figure 4 shows the flow rates from two orifices that are very close in size.

The data in Figure 3 show that the orifice coefficients have about a 10% spread around a mean value of 0.6. A significant improvement in the orifice coefficient is obtained by adding drag-reducing polymers to the water. For example, Figure 3 shows the effect of using a 0.25% SUPER-WATER concentration on the coefficient of discharge.

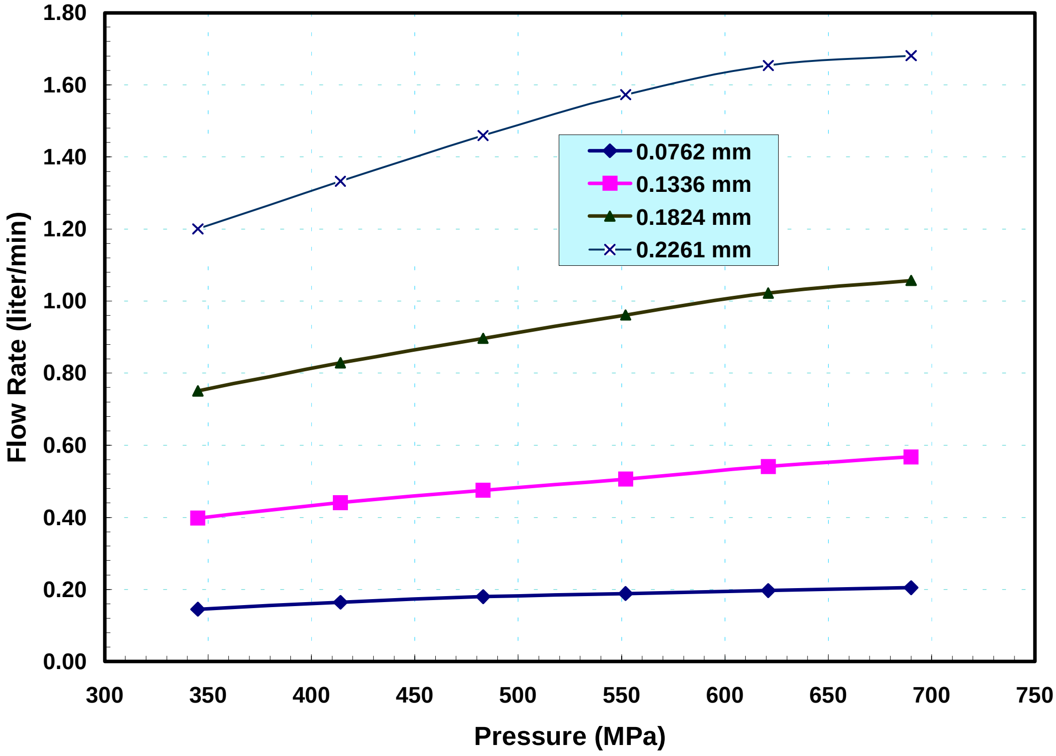

Figure 2. Water Flow Rates for Several Sizes of Sapphire Orifices

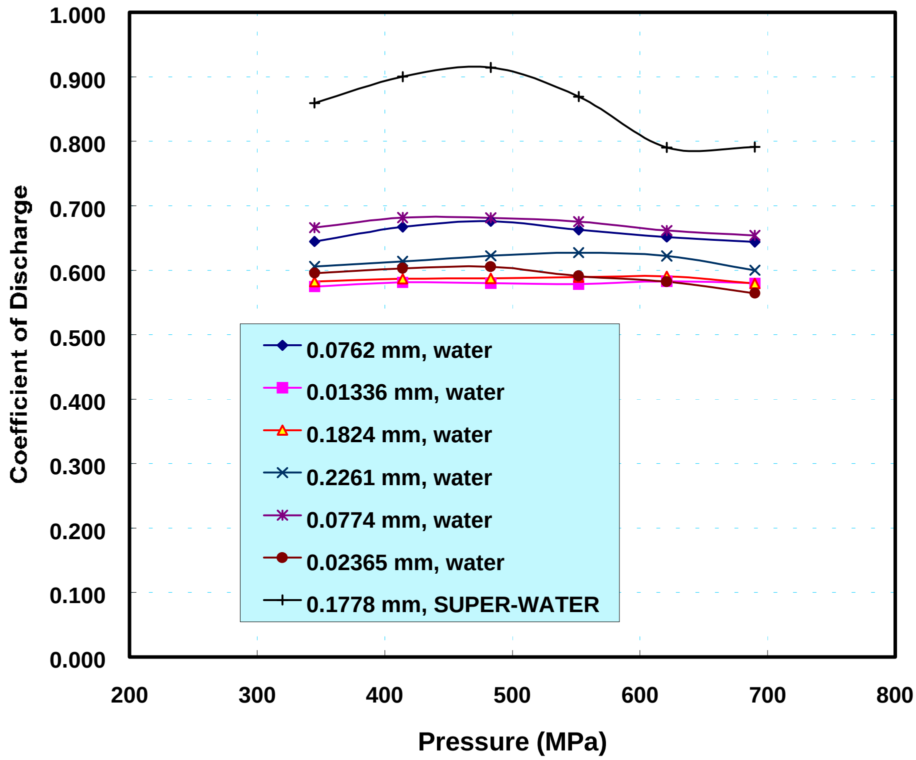

Figure 3. Calculated Coefficients of Discharge

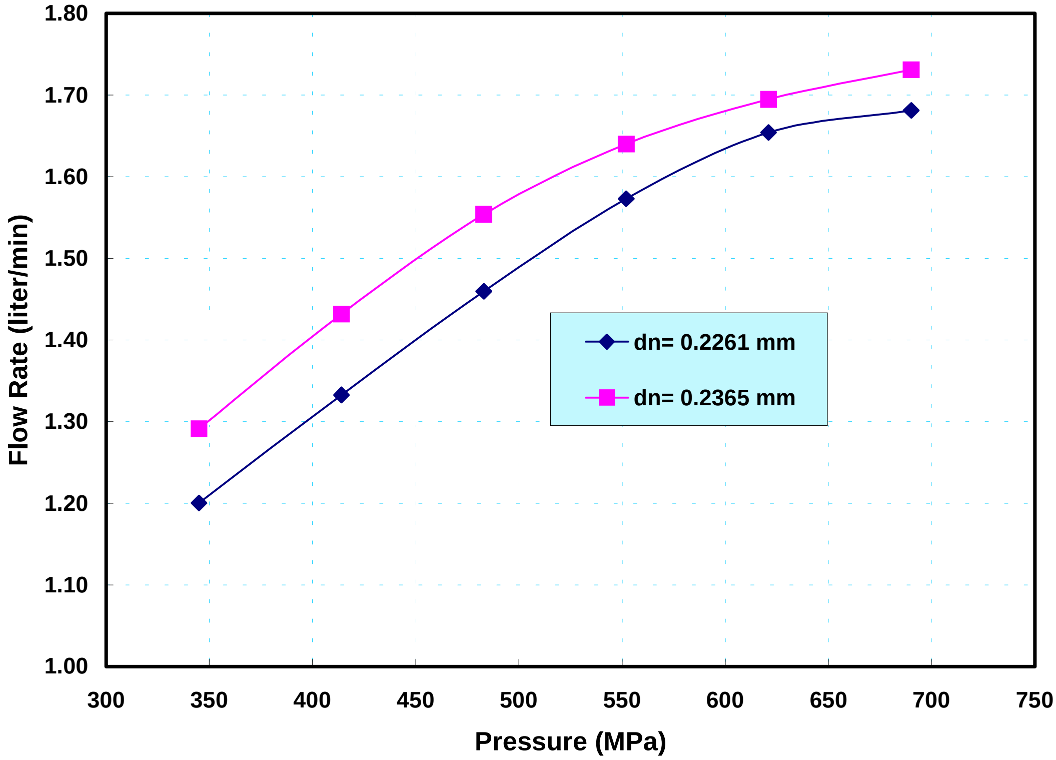

Figure 4. Water Flow Rates for Two Similarly Sized Orifices

2.2 Power Density

From Equations (1) through (4) it can be seen that the power density, defined as the jet hydraulic power per unit area, is a function of pressure:

$$E / A_n = K_3 P^{1.5} c_d \tag{5}$$

where A_n is the orifice cross-sectional area and K_3 is a numerical constant. Figure 5 shows the jet power density for pressures up to 690 MPa. This figure illustrates the power density of typical waterjets and also of both AWJs and abrasive suspension jets. Only the abrasive particle kinetic energy was used in calculating the power density in Figure 5. Observe that doubling the pressure from 345 MPa to 690 MPa results in an increase in power density of 182%, or 2.82 times. The increase in water flow rate is only 41%, i.e., 1.41 times, for a given orifice size. Table 1 shows numerical values of the power density for different jet pressures, flow rates, and orifice sizes for a fixed 29.9-kW waterjet.

Table 1. Power Density for a 29.9-kW Waterjet

Pressure, P (MPa)	Flow Rate, q (l/min)	Orifice Diameter, d_n (mm)	Power Density, kW/mm^2
69.0	30.9	1.239	25
138.0	15.4	0.737	70
207.0	10.3	0.543	129
276.0	7.7	0.438	198
345.0	6.2	0.370	277
414.0	5.1	0.323	364
483.0	4.4	0.288	459
552.0	3.9	0.260	561
621.0	3.4	0.238	669
690.0	3.1	0.220	784

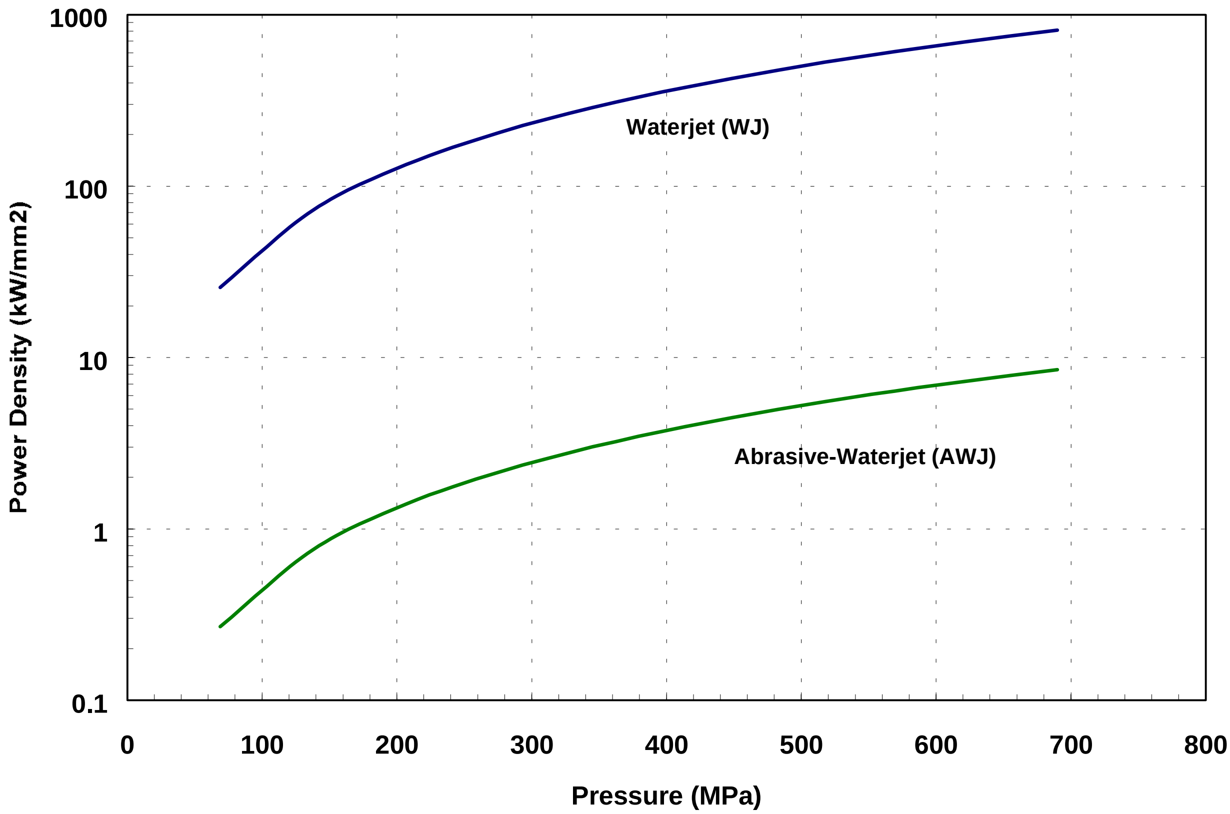

Figure 5. Effect of Pressure Power Density of Waterjets and Abrasive-Waterjets

3. CUTTING OBSERVATIONS

3.1 Waterjets

Figure 6 shows the relationship between the maximum through-cut speed and jet pressure for selected orifice sizes. It is shown that a significant increase in cutting speed occurs as the pressure increases to 690 MPa. The 0.229-mm-diameter orifice improved the cutting rate from about 1.27 mm/s at 345 MPa to 7.2 mm/s at 690 MPa.

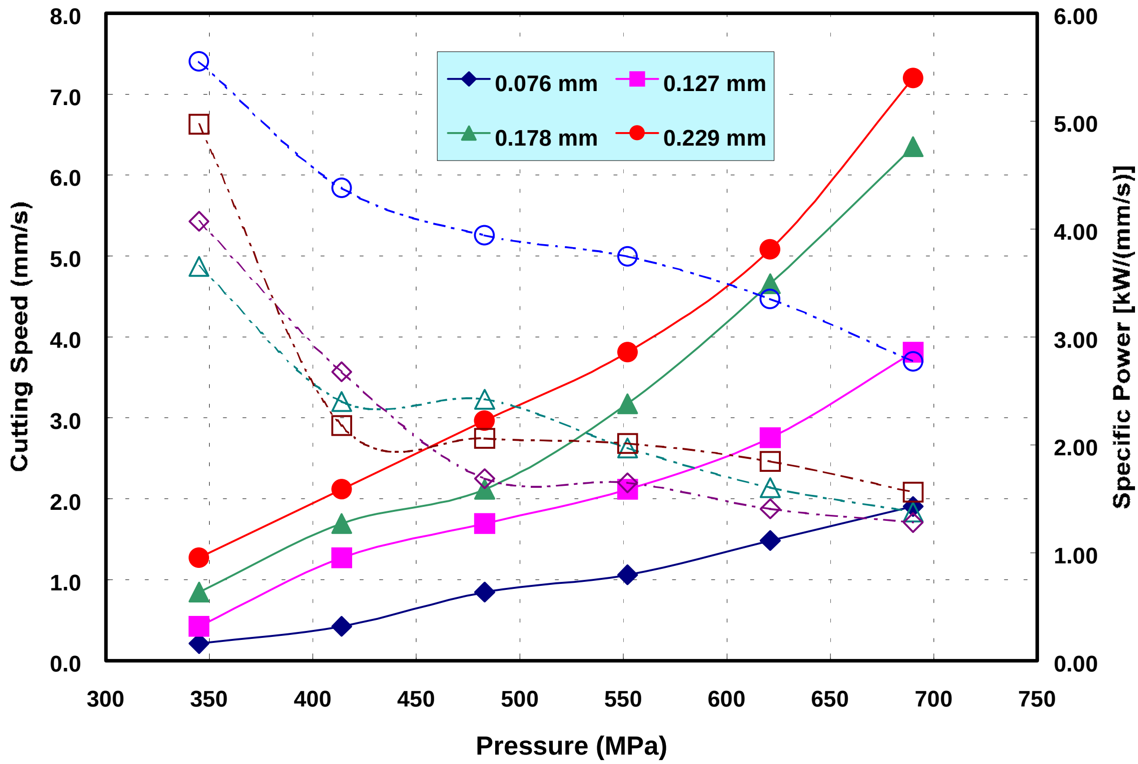

Figure 6. Cutting Speeds and Specific Power for 1.6-mm-thick Aluminum Using Different Orifice Sizes

It should be noted that increasing the pressure also increases the jet power by a factor proportional to $P^{1.5}$. The increases in cutting performance by increasing pressure must result in improved power utilization or reduced cost to justify the use of elevated pressures. Figure 6 shows the specific power expressed as the power required per unit increase in cutting speed for the thickness of material under consideration. In this case, 1.6-mm-thick aluminum is used. Observe that the specific power is reduced as the pressure increases. Figure 7 clarifies this trend for the 0.229-mm jet size.

It is also observed that smaller jets are more efficient than larger ones. Figure 6 shows that the power efficiency of the 0.076-mm-diameter orifice quadrupled from 345 to 690 MPa, while the efficiency of the 0.229-mm jet increased by about 150% in the same pressure range. This trend is sensitive to the material thickness, and it is expected that larger jets become more efficient than smaller ones as the thickness of the material increases.

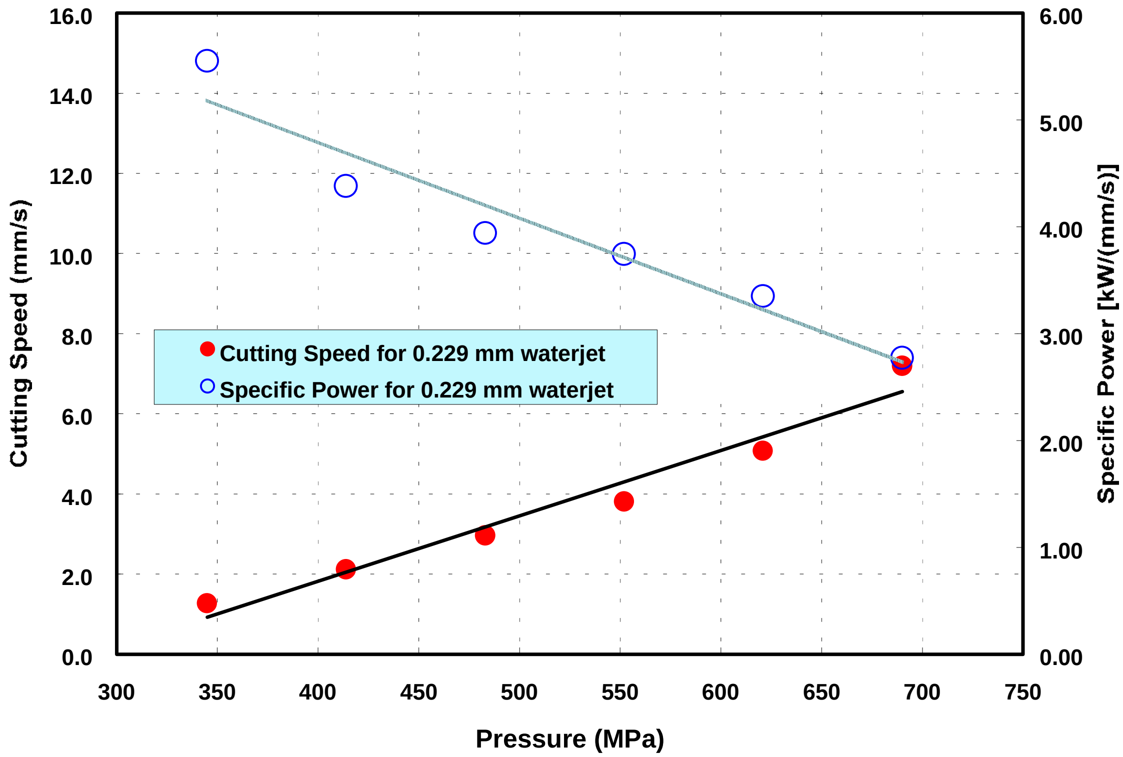

Figure 7. Linearized Trends of Cutting Speed and Specific Power for 1.6-mm-thick Aluminum using 0.229-mm-diameter Waterjet

The existence of a threshold pressure for cutting has long been known in the waterjet literature. Ragahavan and Ting (1991) have reported results for aluminum similar to the data in this paper. It can be shown by simple calculation that the optimal pressure is 3 times the threshold pressure. For cutting metal with waterjets, the threshold pressure is also a function of the traverse rate, and there is no unique number for different metals that can be used to determine the optimum operating pressure.

The water consumption per unit volume of material removed can be computed from the test data in Figure 6. It has been shown (Hashish et al., 1997) that the water usage efficiency increases with both increasing jet pressure and decreasing orifice size (as did power efficiency). For example, the water usage efficiency improved by a factor of 4 with the 0.229-mm-diameter orifice and by a factor of 8 with the 0.076-mm jet for thin aluminum cutting.

Figure 8 shows results of tests in other metals using a 0.229-mm-diameter orifice at 690 MPa to determine the maximum possible cutting traverse rates. Additional results are shown in Table 2. Of particular interest is the ability of plain waterjets (at 690 MPa) to cut composites such as graphite epoxy and fiberglass without surface layer delamination. The cutting rates shown in Table 2 were not associated with any delamination.

Figure 9 shows the relationship between cutting speed and standoff distance for several metals. The trend of increased cutting speeds with increasing standoff distances is attributed to the fact that these materials are more sensitive to droplet impact.

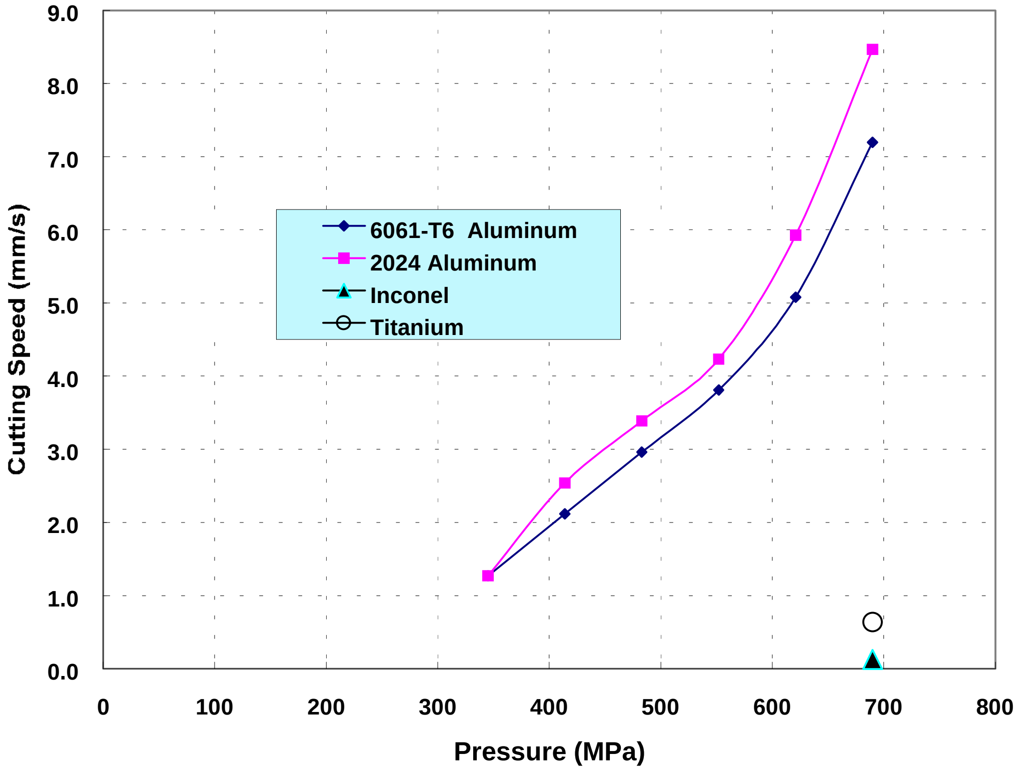

Figure 8. Effect of Pressure on Cutting of Several Materials Using a 0.229-mm-diameter Waterjet

Table 2. Maximum Cutting Traverse Rate (Material Thickness is 1.6 mm)

Material	Cutting Speed (mm/s)
1018 Steel	2.33
4130 Steel	1.06
15-7 PH Stainless Steel	0.85
321 Stainless Steel	0.74
Titanium 6Al/4V	0.42
301 Stainless Steel	0.42
Hastelloy	0.36
301 Stainless Steel	0.32
Inconel	0.21
Printed Circuit Board	74
Graphite Epoxy (6.3 mm thick)	74
Copper-Clad Fiberglass	74

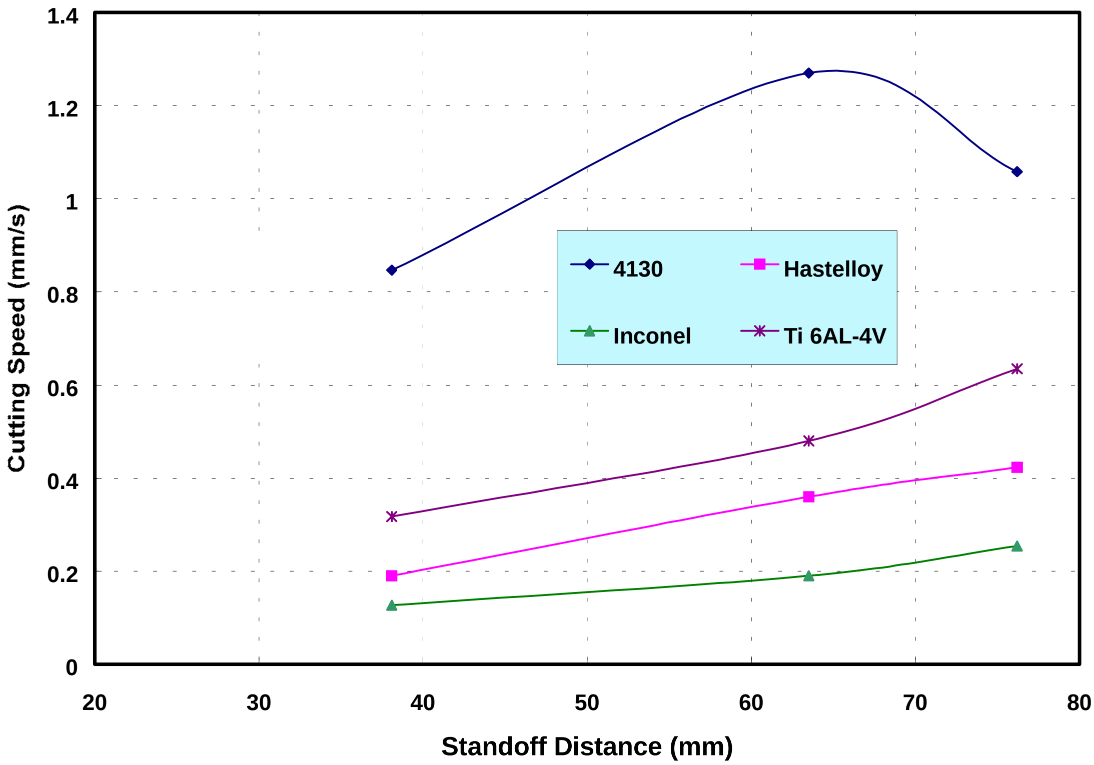

Figure 9. Effect of Standoff Distance on Cutting Speed for 1.6-mm-thick Materials at 690 MPa

3.2 Polymer Waterjets

SUPER-WATER additive in 0.25% concentration was used in some limited cutting tests focusing on the effect of standoff distance at elevated pressures. Information on SUPER-WATER and its advantages can be found in Howells (1990).

Figure 10 shows the linear trends of the effect of pressure on depth of cut for a waterjet in aluminum at three different standoff distances using a traverse rate of 1.69 mm/s and a 0.178-mm-diameter waterjet. Observe how the standoff distance affects the slope of the line. It is surprising to see that, as the pressure increases, a shorter standoff distance is more effective. Figure 11 shows the linear trends for a SUPER-WATER jet, which indicates that an optimal standoff distance exists. This has been observed previously by Franz (1974).

Comparing the data in these two graphs suggests that cutting with SUPER-WATER will result in improved cutting rates when the standoff distance increases, but not at small standoff distances. This is also a surprising result, because SUPER-WATER will at lease deliver more hydraulic power (more flow rate) at the same pressure. More accurate and systematic tests are needed to fully characterize the effects and expected benefits of SUPER-WATER.

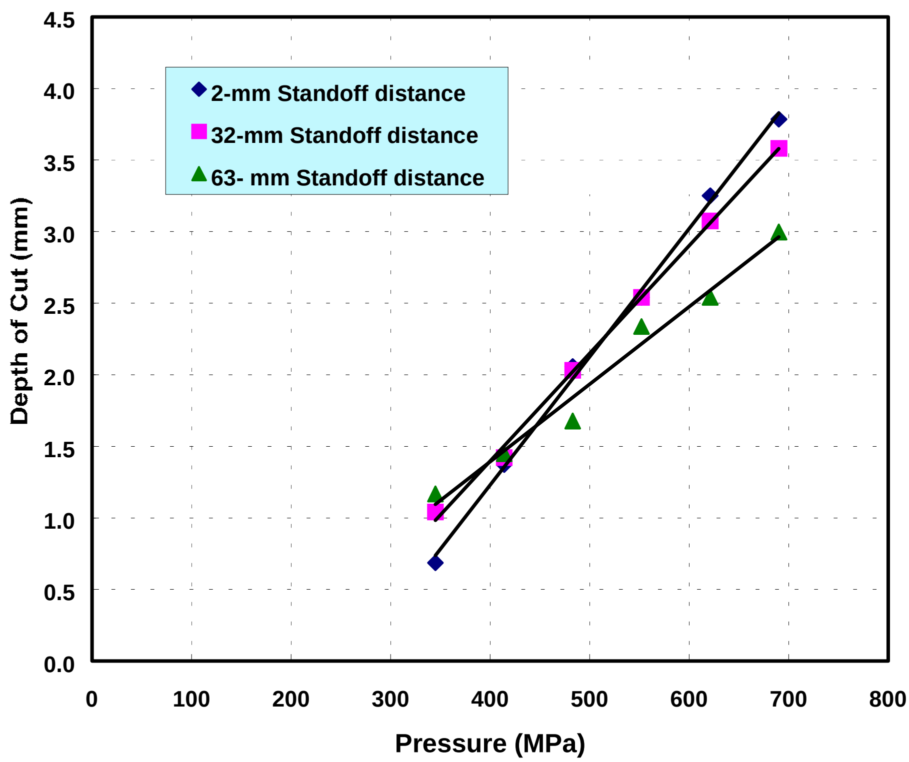

Figure 10. Effect of Pressure and Standoff Distance on Waterjet Cutting of Thin (1.6-mm) Aluminum and Steel

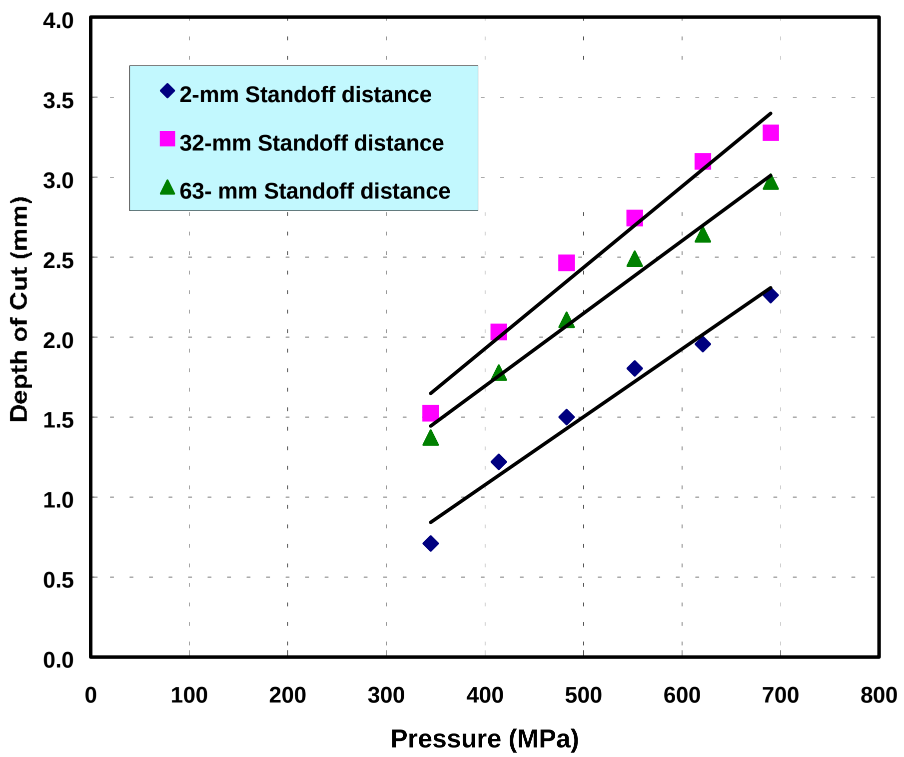

Figure 11. Effect of Pressure and Standoff Distance on SUPER-WATER Jet Cutting of Thin (1.6-mm) Aluminum and Steel

3.3 Abrasive-Waterjets

A typical AWJ nozzle with 690-MPa pressure capability was used to perform the AWJ cutting tests. The following parameters were used:

- Nozzle diameter, d_n = 0.229 mm
- Mixing tube diameter, d_m = 0.787 mm
- Mixing tube length, l_m = 50 mm
- Garnet mesh 100 abrasive
- Abrasive flow rate, m_a = 3.75 g/s

The cutting results for both thin and thick aluminum and steel are shown in Figures 12 and 13. In Figure 12, linear trends are shown for the effect of pressure on cutting speed. The cost index shown in Figure 13 is used to express the total cost in cents per square centimeter of cut surface. The cost includes the cost of equipment, pump maintenance, nozzle wear, abrasives, water, power, and disposal. The effect of pressure on these cost items was incorporated.

Observe that the cost of operation is reduced as the pressure increases and becomes flat for over 400 MPa. These are just preliminary data with assumptions on the performance of elevated pressure equipment. It is of interest to note that the power efficiency does not improve with increasing pressure with AWJs as it does with plain waterjets. This can be deduced from the data shown in Figures 12 and 13. To improve the power efficiency of AWJs at elevated pressures, nozzle designs must be developed and optimized for working at these high pressures.

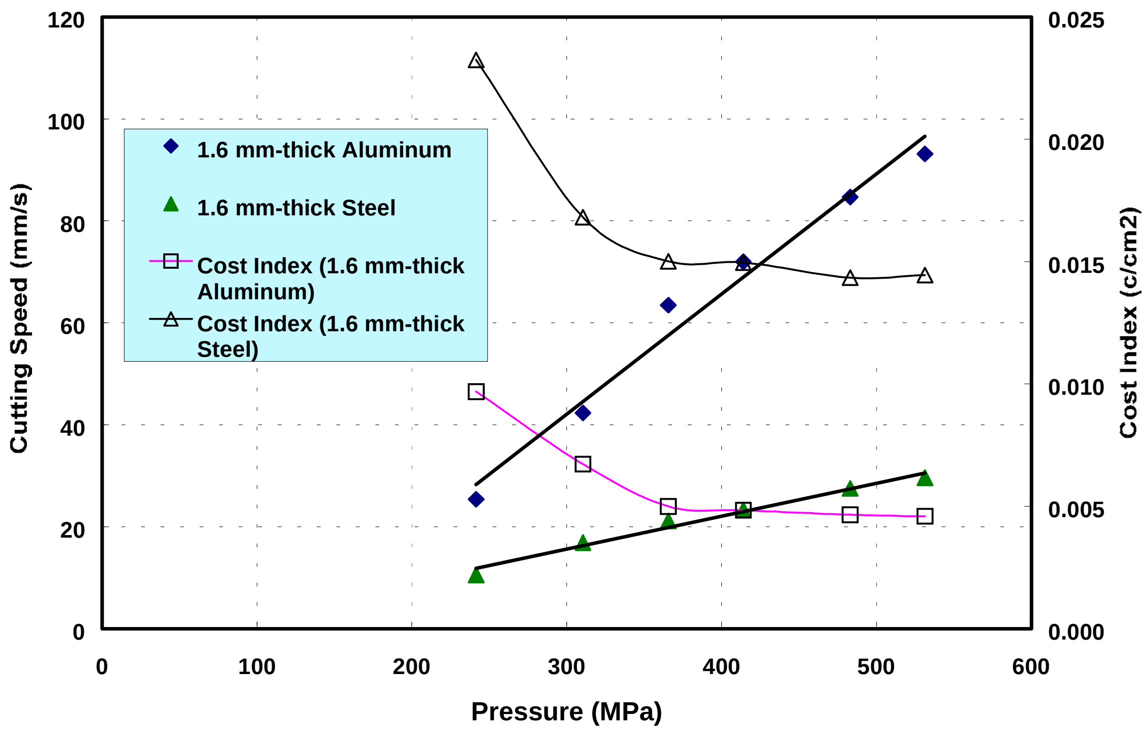

Figure 12. Effect of Pressure on Cutting Speed and Cost Index for AWJ Cutting of Aluminum and Steel

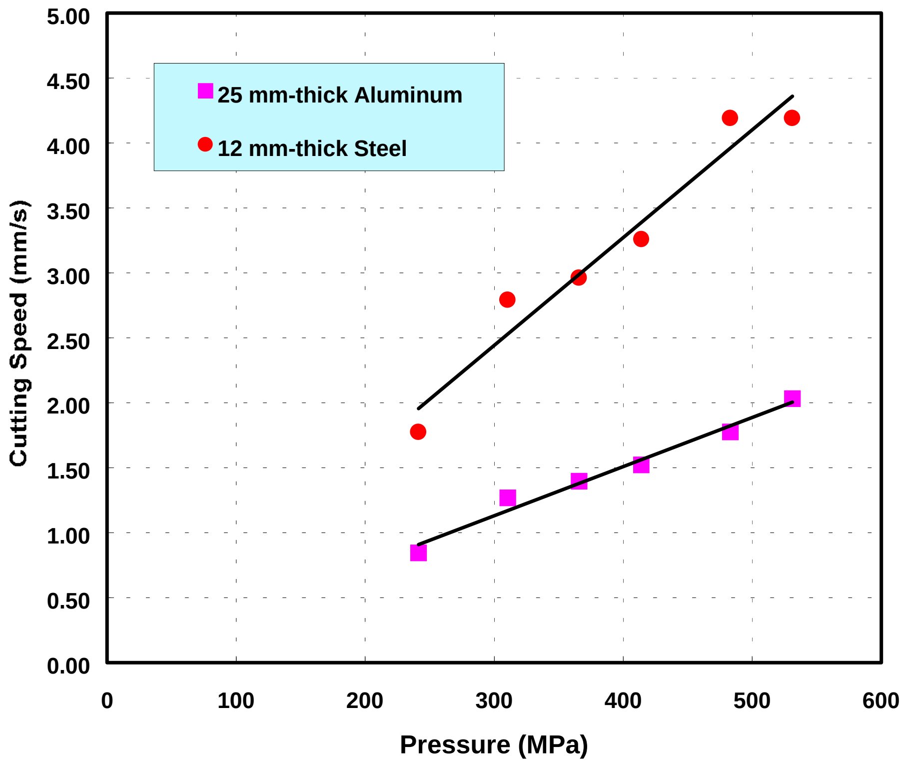

Figure 13. Effect of Pressure on Cutting Speed for AWJ Cutting of Aluminum and Steel

In previous work (Hashish et al., 1997) very small jets were used and were shown to achieve a great enhancement in power efficiency. The cutting of thin (1.6-mm) aluminum using a 0.025-mm-diameter orifice resulted in significant improvements in cutting speed by increasing the pressure from 345 to 690 MPa. This is because the threshold pressure for cutting was very close to the 345-MPa starting pressure. Over the same range, the power efficiency of the 0.025-mm AWJ improved by 370%.

It should be emphasized that a significant performance enhancement can be made with AWJs at pressures up to 690 MPa. This is primarily related to reducing the abrasive flow rates (compared to current typical values), which represent the most significant cost factor for AWJ operations.

4. DRILLING

Hole drilling tests were conducted with 690-MPa waterjets and abrasive-waterjets. It was observed that holes drilled with plain waterjets are irregular in shape. This is due to the effect of the return flow, which causes asymmetry of the jet action while drilling. The upper edge of the hole is slightly rounded due to erosion by the spread jet and by the reflected jet before complete piercing. It was also observed that the bottom edge of the hole is sharp, even, and mainly free of burrs. However, the hole size is significantly larger than the jet diameter. In some cases, the hole diameter is more than 5 times the diameter of the jet. Again, this is attributed to the return flow of the incompressible water. Sectional photos of waterjet-drilled holes show a slight taper from the top to the bottom. This is typical and can be changed by controlling the dwell time.

Drilling with AWJs was found to be much more controllable, especially with the use of computer-controlled pressure ramping. With pressure ramping, the pressure never reaches 690 MPa before the material is penetrated. Drilling with 690 MPa jets will likely be limited to very hard materials where hole geometry is not critical.

5. CONCLUSIONS

- Cutting with plain waterjets at elevated pressures is highly promising for composites and thin sheet metal.
- The specific power, expressed as the power per unit increase in cutting speed, with plain waterjets improves significantly with increasing pressure for relatively thin materials.
- Polymer additives may greatly enhance the performance of 690-MPa waterjets, especially for large standoff distances.
- Elevated-pressure AWJs promise cost reduction, but power efficiency needs to be improved. Cutting with AWJs up to 690 MPa will minimize abrasive usage and reduce kerf width.
- It has been confirmed that there is an optimal standoff distance for metal cutting with plain waterjets.
- Hole drilling is best accomplished by pressure ramping if the quality of the hole geometry is important. Drilling with 690-MPa waterjets does not result in a rounded hole; further work is needed to improve the process.

6. ACKNOWLEDGMENTS

Some of the work presented in this paper was performed under funding from the National Center for Manufacturing Sciences (contract number NCMS-89-MPM-2) at Waterjet Technology, Inc. (previously Flow Research, then QUEST Integrated). Work on the 690-MPa pump and some AWJ cutting tests were conducted at Flow International. The author is grateful for this support. Thanks also to Hammond Publications for editing this paper.

7. REFERENCES

Franz, N. C., "The Influence of Standoff Distance on Cutting with High Velocity Fluid Jets," *Proceedings of the Second International Symposium on Jet Cutting Technology*, pp. B3-37 – B3-46, BHRA Fluid Engineering, Cambridge, England, 1974.

Hashish, M., Steele, D. E., and Bothell, D. H., "Machining with Super-Pressure (690 MPa) Waterjets," *Int. J. Mach. Tools Manufact.*, Vol. 37, No. 4, pp. 465-479, 1997.

Howells, W. G., "Polymerblasting with SUPER-WATER® from 1974 to 1989: A Review," *International Journal of Waterjet Technology*, Vol. 1, No. 1, pp. 1-15, 1990.

Raghaven, C., and Ting, E., "Hyper Pressure Waterjet Cutting of Thin Sheet Metal," *Proceedings of the 6th American Water Jet Conference*, pp. 493-504, Houston, Texas, Water Jet Technology Association, 1991.

8. NOMENCLATURE

A_n	orifice cross-sectional area
c_d	coefficient of discharge
c_v	coefficient of velocity
d_m	mixing tube diameter
d_n	waterjet diameter
E	power
K_1, K_2, K_3	numerical constants
l_m	mixing tube length
m_a	abrasive flow rate
P	pressure
q	flow rate
V	actual velocity
V_{th}	theoretical waterjet velocity
ρ	water density

10th American Waterjet Conference
August 14-17, 1999: Houston, Texas

Paper **11**

CHARACTERIZATION OF LOW PRESSURE AWJ CUTTING

David G. Taggart, Madhusarathi Nanduri and Thomas J. Kim
University of Rhode Island
Kingston, RI U.S.A.

ABSTRACT

In recent years, advances in entrainment based abrasive waterjet (AWJ) technology have led to commercial systems which operate at increasingly high water pressures. The motivation for these improved systems is higher cutting speeds for manufacturing applications. For certain applications, parameters such as overall system size, weight, cost and consumption parameters such as water and abrasive consumption take precedent over cutting speed. For example, for materials which are relatively easy to machine, adequate cutting speeds may be achieved using low pressure, and hence low cost, AWJ cutting systems. Similarly, portable AWJ systems require minimum system size and weight. For applications where abrasive and water contamination is an issue, minimization of the abrasive and water consumption rates is critical. In this study, the performance of entrainment based AWJ cutting at low pressures in the range of 35-140 MPa is evaluated. Conditions which provide abrasive entrainment are identified. A series of trials are performed to determine the depth of cut in mild steel as a function of various AWJ parameters. An empirical cutting model is developed. Finally, the effect of standoff distance, multiple passes and abrasive type on cutting performance is evaluated.

1. INTRODUCTION

In typical industrial applications of entrainment based AWJ machining, maximized cutting speed is desired. For these applications, commercial AWJ systems which operate at water pressures of 200-420 MPa are commonly used. For certain specialized applications, however, cutting speed may be less important than other factors. Examples of such applications include portable cutting systems requiring lightweight pumps and low volume applications where the capital cost associated with high pressure pumps can be prohibitive. For portable systems, abrasive and water consumption rates can be critical if the consumables need to be transported. Similarly, abrasive and water consumption is critical in applications where abrasive and water disposal is required for environmental reasons.

In this study, the cutting performance and abrasive and water consumption rates for low pressure (35-140 MPa) AWJ cutting are characterized. An empirical parametric model is developed to provide predictive data for use in configuring an AWJ system for particular applications. This parametric model development parallels similar work by Zeng (1992) and Zeng and Kim (1993). In Zeng's model, developed for pressures in the range 140-280 MPa, the depth of cut is given by

$$h = \frac{N_m \; P^{1.25} \; m_w^{0.687} \; m_a^{0.343}}{C_s \; u^{0.866} \; d_n^{0.618}} \tag{1}$$

where h is the depth of cut in mm, N_m is the material machinability number (N_m=87.6 for mild steel), P is the water pressure in MPa, m_w is the water flow rate in liter/min, m_a is the abrasive flow rate in g/s, C_s is a constant (=8800), u is the jet traverse speed in mm/s and d_n is the nozzle diameter in mm. This parametric model provides a tool for determining the relation between water pressure, abrasive consumption, water consumption and cutting performance. Note that the water consumption, Q, can be computed from the orifice cross-sectional area, A, and the water pressure, P, using the relation (Hashish, 1989)

$$Q = C_{da} A \sqrt{2P / \rho_o} \tag{2}$$

where C_{da} is the orifice coefficient of discharge and ρ_o is the ambient density of water. Appropriate orifice coefficients of discharge have been determined experimentally (Hashish, 1989) to be in the range of 0.65-0.75. Unfortunately, since Zeng's model (Eq. 1) was developed at water pressures in the range 140-280 MPa, its application to pressures in the range 35-140 MPa is expected to give unreliable predictions. Therefore, development of a low pressure parametric model is required and provides the motivation for the study described in this paper.

2. EXPERIMENTAL PROCEDURES

In the first phase of this study, a Taguchi based experimental design was implemented to quickly assess the cutting performance of a wide range of experimental parameters. These results were then fit to a preliminary empirical cutting model which was used to screen future experimental trials. During the first phase of the study, it was observed that several combinations of parameters did not induce sufficient vacuum for effective abrasive entrainment. For this reason, the second phase of the study consisted of a series of experiments to determine the combinations of parameters which do provide sufficient entrainment. Using the preliminary cutting model and the results of the entrainment study as a guide, a more extensive set of cutting trials was performed and a revised parametric cutting model was developed. Finally, the effect of standoff distance, multiple passes and abrasive type on cutting speed and consumption rates was investigated.

3. TAGUCHI BASED EXPERIMENTAL DESIGN

Abrasive waterjet cutting performance is dependent on a number of system parameters. To effectively optimize the parameters for a given application requires that a large number of trials be performed. To quickly assess a range of parameters which are promising, a Taguchi based experimental design (Roy, 1990) was performed. In these experiments (see Table 1), nine combinations of parameters were evaluated. For each combination, the cutting speed required to penetrate 38 mm thick mild steel was determined.

For five of the nine combinations, it was determined that the conditions did not provide sufficient suction to entrain the abrasive into the waterjet stream and therefore, cutting was not achieved. For the four combinations for which entrainment was achieved, a series of cutting trials were performed (see Figure 1). Preliminary empirical cutting models for depth of cut or, alternatively, cutting speed, were developed. These models are given by

$$\begin{aligned} h &= 6.28 P^{-0.071} d_o^{-0.44} d_n^{-1.61} m_a^{-0.00474} u^{-0.697} \\ u &= 0.42 P^{0.0146} d_o^{-1.34} d_n^{-3.12} m_a^{-0.254} h^{-1.07} \end{aligned} \tag{3}$$

where h is the depth of cut in mm, P is the water pressure in MPa, d_o is the orifice diameter in mm, d_n is the nozzle diameter in mm, m_a is the abrasive flow rate in g/s, and u is the jet traverse speed in mm/s. The accuracy of these models was assessed by comparing the predicted depth of cut to the actual depth of cut and the predicted cutting speed to the actual cutting speed (see Figure 2). These results indicate that the cutting models reasonably predict the observed cutting performance and can be used to screen future trial combinations.

For the four combinations which provided effective cutting, the abrasive and water consumption rates were determined. The consumption rate per unit length of cut was then computed. As shown in Table 2, there is a trade-off between consumable weight and pump pressure. Since the required pump pressure directly influences the system weight, the optimum system design for a given application will require an appropriate balance between pump size and required consumables.

4. CHARACTERIZATION OF ABRASIVE ENTRAINMENT

Since the Taguchi trials gave several combinations of parameters which did not provide sufficient entrainment, a series of trials to assess the effect of pressure, orifice size and nozzle size on abrasive entrainment was performed. In the first experiment, the abrasive delivery tube was closed so that zero air flow was allowed. The orifice diameter and pressure were varied and the vacuum induced in the abrasive tube was monitored. The results of these trials are shown in Figure 3. It is observed for pressures above 103 MPa, a nearly full vacuum is obtained. Below 103 MPa, the induced vacuum is significantly reduced.

To better evaluate the effect of pressure, orifice diameter and nozzle size on abrasive entrainment, the maximum abrasive flow rate for several combinations of these parameters was determined. These results are given in Figures 4 and 5. Figure 4 shows the abrasive flow rates which can be achieved using a 1.09 mm diameter nozzle. Figure 5 shows similar results for a 0.74 mm diameter nozzle. For the larger nozzle (Figure 4), it is observed that for orifice diameters above 0.25 mm, abrasive flow rates in excess of 360 g/min can be achieved, even at low pressures. For the smaller nozzle (Figure 5), entrainment at pressures lower than 105 MPa was difficult to achieve, especially for the smaller orifices.

5. DEVELOPMENT OF PARAMETRIC MODEL

Using results of the abrasive entrainment trials, the cutting performance of the following orifice / nozzle combinations was evaluated: d_o/d_n= 0.36 mm/1.0 mm, 0.25 mm/1.0 mm, 0.36 mm/0.74 mm, 0.25 mm/.74 mm. For most of these trials, a water pressure of 103 MPa was used and the abrasive flow rate was varied from 170 – 395 g/min. For each case, a series of depth of cut vs. traverse speed trials were performed and the speed required to penetrate a 38 mm thick mild steel plate was determined. For other combinations of orifice and nozzle diameter, the speed required to penetrate the steel was determined. These results are shown in Table 4.

From these results, the weight of consumables required a unit length of 38 mm thick mild steel was determined and tabulated in Table 4. It can be seen that the combination requiring the least consumable weight was the 0.30 mm/1.04 mm orifice/nozzle combination with an abrasive flow rate of 240 g/min. To assess the effect of reducing the pressure, the cutting performance of this same orifice / nozzle combination and an abrasive flow rate of 170 g/min was measured. As shown in Table 3, there is a dramatic increase in weight of consumables as the pressure is reduced from 103 MPa to 34 MPa.

The results of all of these trials were combined in an empirical cutting model given by

$$h = 0.477\, P^{1.68} d_o^{1.91} d_n^{0.77} m_a^{0.1} u^{-0.77} \tag{4}$$

where h is the depth of cut in mm, P is the water pressure in MPa, d_o is the orifice diameter in mm, d_n is the nozzle diameter in mm, m_a is the abrasive flow rate in g/min, and u is the jet traverse speed in mm per minute. Figure 6 shows the predicted depth of cut vs. the actual depth of cut, again demonstrating reasonable correlation of predicted and observed cutting depth.

6. EFFECT OF STANDOFF DISTANCE, MULTIPLE PASSES AND ABRASIVE TYPE

The final series of trials were designed to provide an assessment of the effect of standoff distance, multiple passes, abrasive size and abrasive type on cutting performance. For these trials, the 0.30 mm/1.04 mm orifice/nozzle combination was used. The water pressure was 103 MPa . For the standoff distance trials, garnet #80 abrasive at a flow rate of 240 g/min was used. As seen in Figure 7, there is little variation in cutting depth for standoff distances less than about 4 mm. There is a slight reduction in cutting performance if the standoff distance is increased to 13 mm.

The effect of multiple passes on cutting performance is shown in Figure 8. In this plot, the total time required to penetrate 38 mm mild steel was determined for the 0.30 mm/1.04 mm orifice/nozzle combination, a water pressure of 103 MPa, a standoff distance of 1.0 mm and a garnet #80 abrasive at a flow rate of 240 g/min. It is seen that the most effective cutting mode is a single pass. This is believed to be due to the reduction in cutting performance with standoff distance, particularly for the final passes where the standoff distance is large.

The effects of abrasive type and size on cutting performance are shown in Fig. 10. Two abrasive materials, garnet and aluminum oxide (Al_2O_3) and two sizes #80 and #120 were evaluated. As shown in Figure 9, there is little effect on cutting performance, with garnet #120 providing a slightly higher cutting depth.

7. CONCLUSIONS

In this study, AWJ cutting of mild steel at low pressures was investigated. A Taguchi based experimental design was implemented to identify combinations of parameters which provide effective cutting. Another series of trials was performed to identify parameters which provide adequate abrasive entrainment. It was found that for a given orifice/nozzle combination, a critical pressure exists, below which abrasive entrainment is difficult to achieve. A parametric cutting model was developed and applied to identify cutting conditions which minimize abrasive and water consumption. A study of standoff distance demonstrated that cutting performance is independent of standoff distance for standoff distances less than about 4 mm. It was also shown that multiple passes at higher speeds did not improve performance as compared to slower single pass cutting. Finally, it was shown that abrasive materials garnet and aluminum oxide and abrasive mesh sizes #80 and #120 gave comparable cutting performance.

8. ACKNOWLEDGEMENTS

Financial support from the Office of Special Technology is gratefully acknowledged. The authors would also like to thank Russell C. Ide and Jose Almeida for their assistance in preparing the figures.

9. REFERENCES

Hashish, M., 1989, "Pressure Effects on Abrasive-Waterjet (AWJ) Machining," *Journal of Engineering Materials and Technology*, Vol. 111, pp. 221-228.

Roy, R. R., 1990, *A Primer on the Taguchi Method*, Competitive Manufacturing Series, Van Nostrand Reinhold, New York, 1990.

Zeng, J., 1992, *Mechanisms of Brittle Material Erosion Associated with High Pressure Abrasive Waterjet Processing - A Modeling and Application Study*, Ph.D. Dissertation, University of Rhode Island, Department of Mechanical Engineering and Applied Mechanics.

Zeng, J. and Kim, T. J., 1993, "Parameter Prediction and Cost Analysis in Abrasive Waterjet Cutting Operations," *7th American Water Jet Conference*, Seattle, WA, pp. 175-189.

10. NOMENCLATURE

Cs	constant
d_n	nozzle diameter
d_o	orifice diameter
h	depth of cut
m_a	abrasive flow rate
m_w	water flow rate
N_m	material machinability number
P	water pressure in MPa
u	traverse speed

TABLE 1. Test conditions and penetration speeds (Taguchi tests).

Condition	ma (g/min)	do (mm)	dn (mm)	P (MPa)	u (mm/min)
1	110	0.23	0.51	83	N.A.E.*
2	230	0.28	0.76	83	N.A.E.
3	340	0.33	1.02	83	6.3
4	340	0.23	0.76	110	N.A.E.
5	110	0.28	1.02	110	6.2
6	230	0.33	0.51	110	N.A.E.
7	230	0.23	1.02	138	10.0
8	340	0.28	0.51	138	N.A.E.
9	110	0.33	0.76	138	12.6

- N.A.E. = No abrasive entrainment achieved

TABLE 2. Water and abrasive consumption (Taguchi tests).

Condition	m_a (g/min)	d_o (mm)	d_n (mm)	P (Mpa)	u (mm/min)	$m_a + m_w$ (g/min)	Water + Abr. consumption (g/mm)
3	341	0.33	1.02	83	6.3	1820	289
5	114	0.28	1.02	110	6.2	1343	216
7	227	0.23	1.02	138	10.0	1154	115
9	114	0.33	0.76	138	12.6	1999	158

TABLE 3. Parametric trial results.

d_o (mm)	d_n (mm)	m_a (g/min)	P (MPa)	u (mm/min)	Water + Abr. consumption (g/mm)
0.15	1.04	170	103	1.27	422
0.15	1.04	320	103	0.76	901
0.15	1.04	395	103	0.51	1499
0.20	1.04	170	103	2.54	320
0.25	1.04	170	103	5.08	229
0.25	1.04	320	103	6.35	207
0.25	1.04	395	103	5.84	237
0.30	1.04	*170*	34	1.27	785
0.30	1.04	*170*	69	3.81	349
0.30	1.04	*170*	103	8.89	178
0.30	***1.04***	***240***	***103***	***11.43***	***144***
0.30	1.04	*320*	103	11.43	151
0.33	1.04	170	103	10.16	179
0.33	1.04	320	103	11.43	172
0.33	1.04	395	103	11.43	179
0.36	1.04	170	103	10.16	203
0.36	1.04	320	103	12.70	175
0.36	1.04	395	103	12.70	180
0.41	1.04	170	103	11.43	229
0.41	1.04	320	103	13.97	198
0.41	1.04	395	103	13.97	203
0.23	0.74	170	103	2.54	385
0.23	0.74	320	103	2.54	444
0.25	0.74	170	103	5.08	229
0.25	0.74	320	103	5.08	258
0.36	0.74	170	103	7.62	271
0.36	0.74	320	103	10.16	218
0.36	0.74	395	103	10.16	226

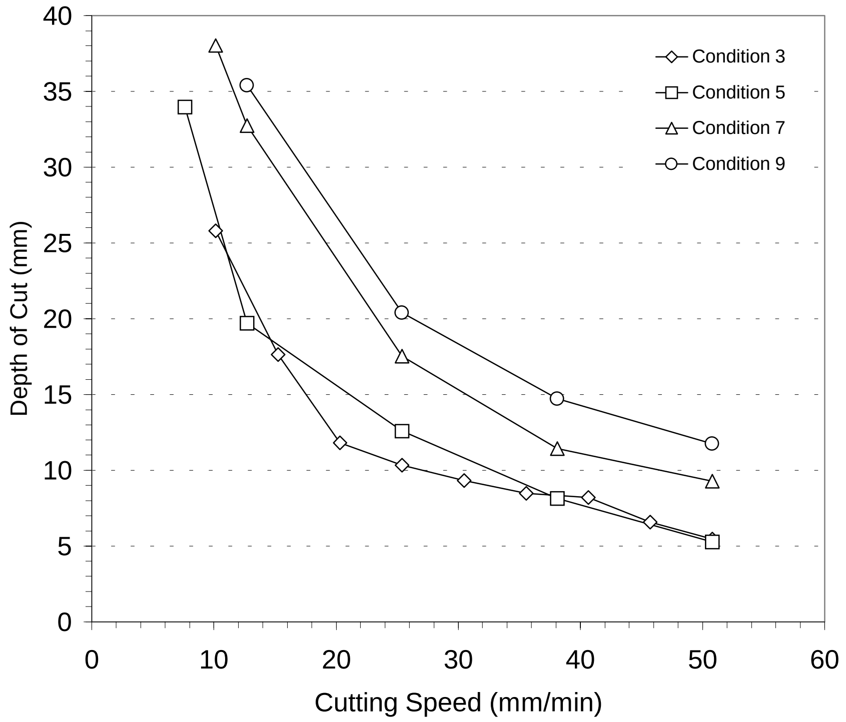

Figure 1. Preliminary cutting trial results (Taguchi tests).

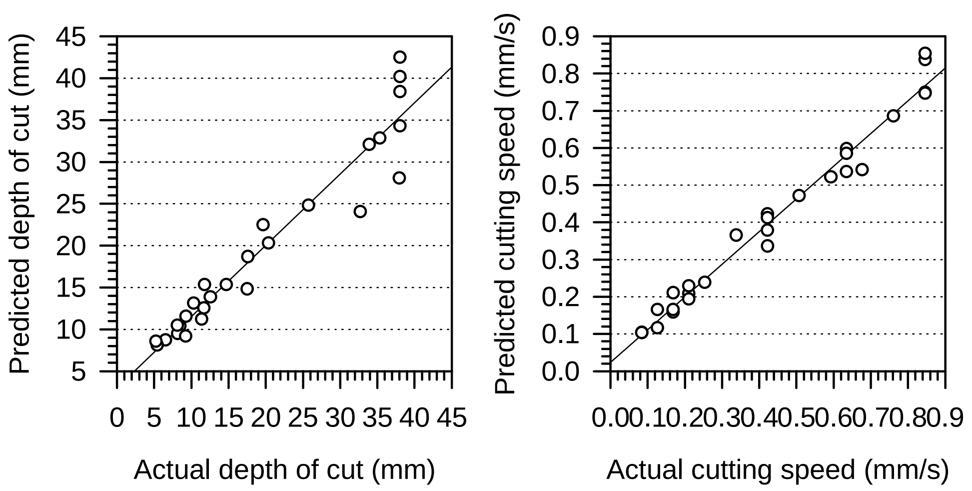

Figure 2. Correlation between predicted and actual data. (Taguchi tests).

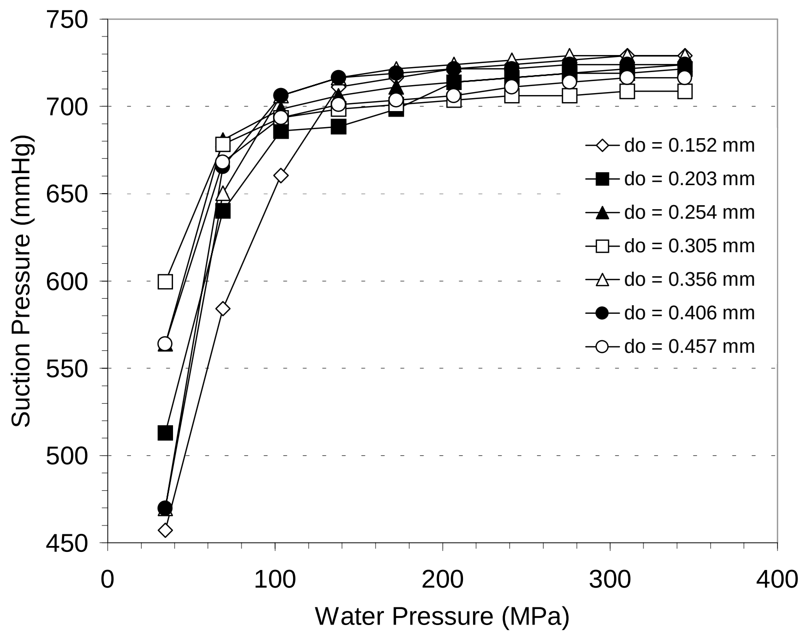

Figure 3. Suction pressure as a function of water pressure for various orifice sizes (zero air flow, d_n=1.09 mm).

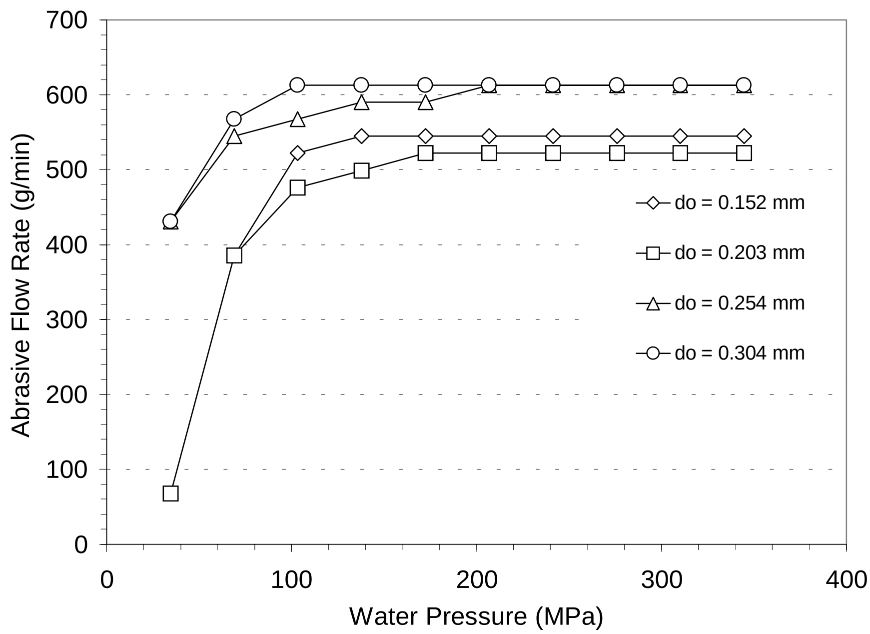

Figure 4(a). Abrasive flow rate as a function of water pressure (d_n=1.09 mm).

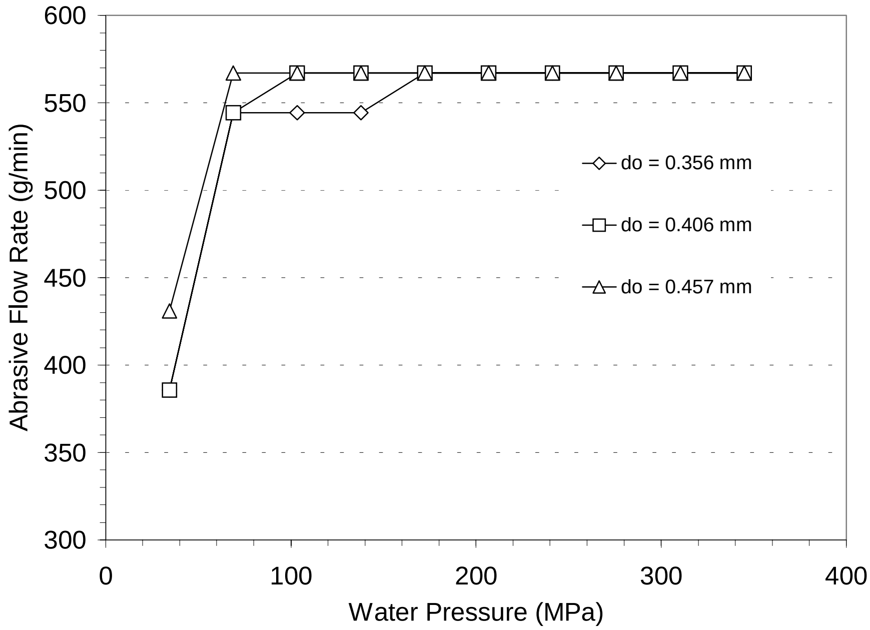

Figure 4(b). Abrasive flow rate as a function of water pressure (d_n=1.09 mm).

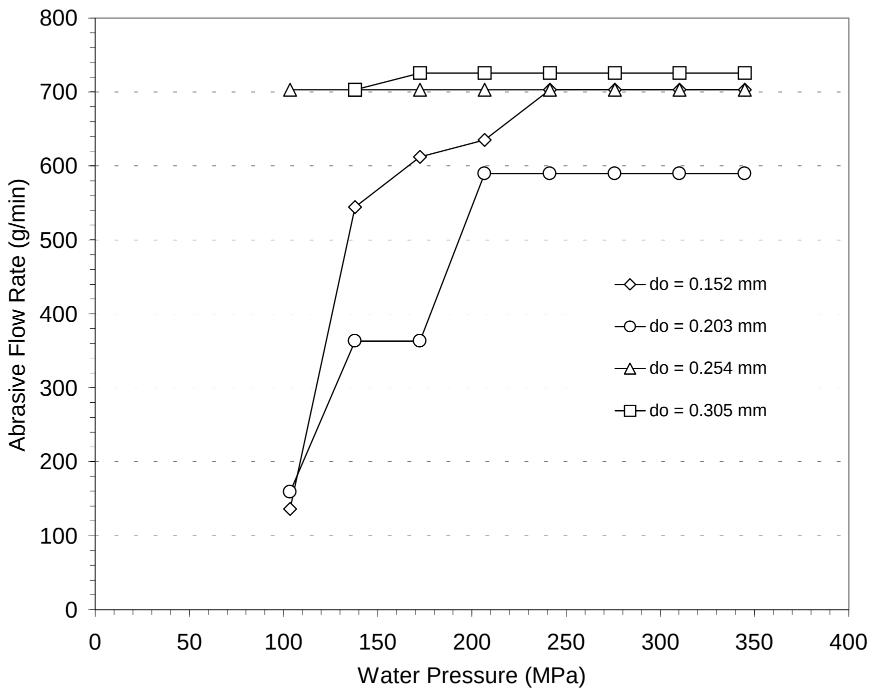

Figure 5. Abrasive flow rate as a function of water pressure (d_n=0.74 mm).

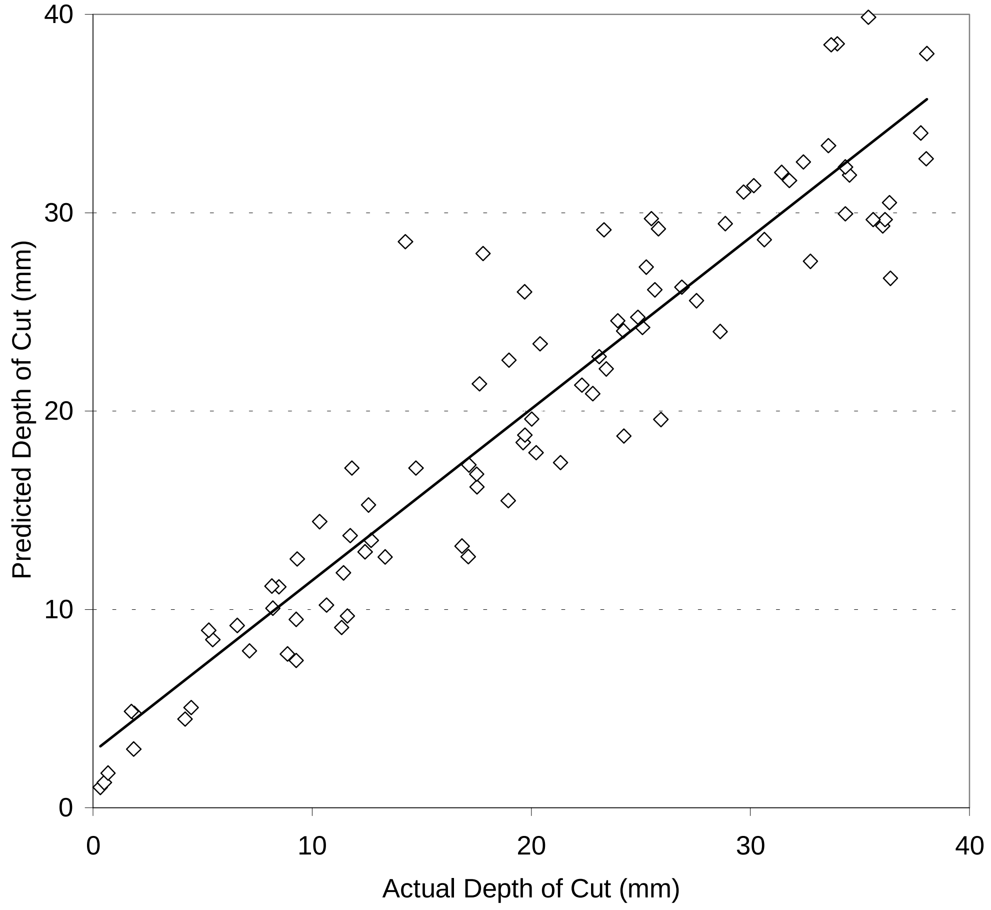

Figure 6. Correlation between predicted and actual depth of cut.

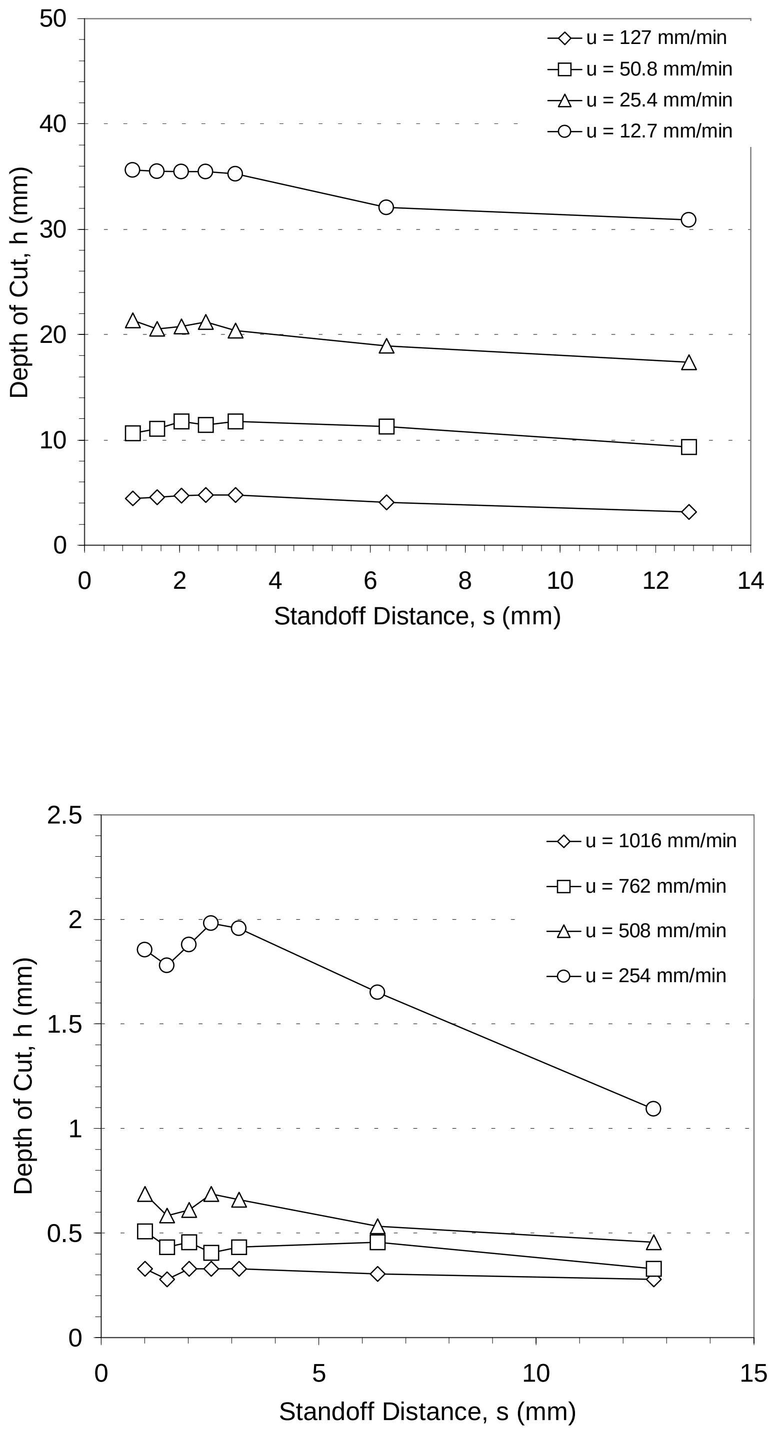

Figure 7. Effect of standoff distance. Orifice: 0.30 mm; Nozzle: 1.04 mm; Pressure: 103 MPa; Abrasive: Garnet #80 @ 240 g/min.

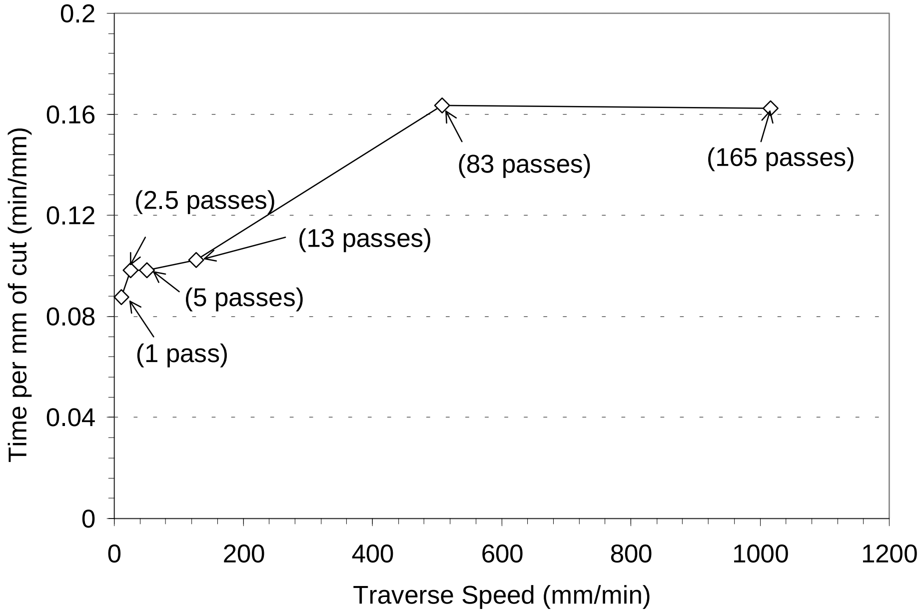

Figure 8. Effect of multiple passes. Orifice: 0.30 mm; Nozzle: 1.04 mm; Pressure: 103 MPa; Abrasive: Garnet #80 @ 240 g/min.

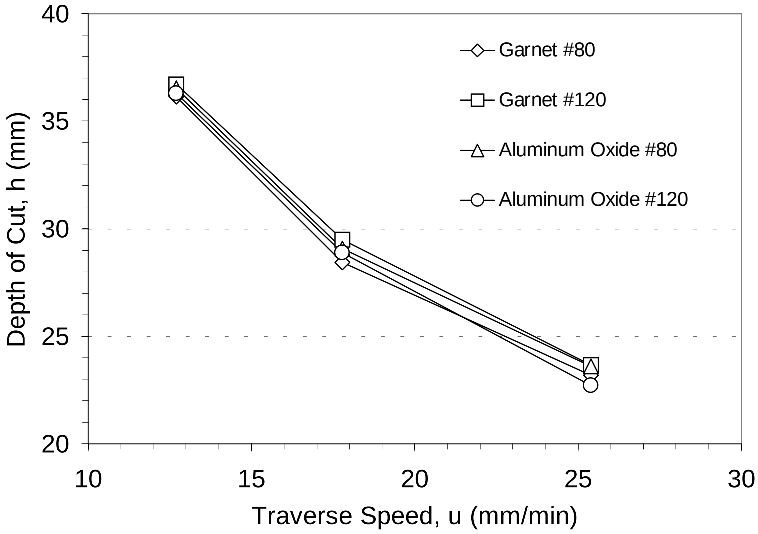

Figure 9. Effect of abrasive type. Orifice: 0.30 mm; Nozzle: 1.04 mm; Pressure: 103 MPa; Abrasive: Garnet #80 @ 240 g/min.

10th American Waterjet Conference
August 14-17, 1999: Houston, Texas

Paper 12

MODELING AND SIMULATION OF PRESSURE FLUCTUATIONS IN HIGH PRESSURE WATERJETS

M. Tremblay and M. Ramulu
Department of Mechanical Engineering,
University of Washington, Seattle

ABSTRACT

The pressure fluctuations within a waterjet machine were investigated through a computer simulation and experimental analysis. A mathematical model accounting for the compressibility of water at high pressures was derived. The variation of the water properties at high pressures and the acceleration and stagnation motion of the piston were also incorporated in the model in order to determine which system parameters influenced the pressure fluctuations the most. Simulation and experimental results were compared and observations were made regarding the time history of the discharge pressure. It was found that the motion of the piston and the operating pressure condition greatly influenced the magnitude of the pressure fluctuations. Furthermore, it was noted that increasing the bulk modulus and/or decreasing the density of the water resulted in a pressure fluctuation increase.

Organized and Sponsored by the WaterJet Technology Association

1. INTRODUCTION

Over the past few years, waterjetting technology has drawn a lot of attention in industry as well as in academia. Waterjets are a versatile, non-traditional machining tool that are currently used in many different industrial operations. Waterjet machines have found there way into a variety of applications [1]. Considerable waterjet research has focused on understanding the mechanics of material removal due to the impingement of a high pressure water jet. Work has also been done in equipment development to reduce pressure fluctuations within the waterjet and optimize the cutting process. Research has shown that pressure and flow variations are highly undesirable, especially in high precision cutting applications. For these applications, any variations in jet quality can lead to unacceptable surface finish. These undesirable fluctuations have also been found to cause a reduction in the life of many waterjet system components. For instance, the nozzle life can be as low as a few hundred hours. Frequent replacement of the nozzle makes this cutting technique expensive and leads to costly downtime. The pressure pulsations in reciprocating pumps can also result in valve failures (due to cavitation) and fluid pulsations in the pipes. Furthermore, the pressure fluctuations are often a constraining factor that limits the applications where the waterjet machine can be used.

Better understanding of the important system parameters that cause these fluctuations is needed in order to design a machine that could eliminate the pressure pulsations occurring throughout the waterjet system. This would allow the waterjet machine to perform more accurately in high precision applications and increase the achievable cutting tolerance.

Recently, several investigators [4,5] have used computer models to simulate intensifier pump dynamics. Most of the research in this field was driven by the modeling of the pressure fluctuations in order to better understand their origin and effects on the pump efficiency and quality of cut. This lead to various alternative intensifier designs that attempted to alleviate the pressure fluctuation problem [2,3]. Although these designs effectively reduce the amount of fluctuation, there is still room for improvement and analysis of the system. The work done in determining the pressure fluctuations falls under three categories: mathematical modeling [7,8], computer simulation [4,5] and experimental analysis [6]. It should be mentioned that the authors who focused on theoretically solving the problem at hand through modeling also included experimental data to corroborate their findings. However, not much emphasis was put on the experimental analysis and the methods used to arrive at the experimental data were not well conveyed. Only two papers [2,6] presented on-line experimental data of the system pressure variations. Ideally, the three types of analysis could be combined to obtain a clear picture of the system dynamics that cause the pressure fluctuations. The purpose of this research is to obtain a better understanding of the system characteristics that lead to these unwanted pulsations. Therefore, an attempt is made to develop a computer simulation that accounts for the reciprocating pump dynamics in order to predict the pressure fluctuations observed through experimentation.

2. COMPUTER SIMULATION AND EXPERIMENTAL ANALYSIS

2.1 Computer Simulation

2.1.1 Mathematical Foundations

The waterjet system aims to deliver flow continuously. However, the pump does not deliver pressurized water to the discharge at all times. During a certain period of time, there is no flow between the pump and the discharge. It is during this time that the pressurized water is delivered from the attenuator. Consequently, the pressure drops in the attenuator, in the nozzle assembly and throughout the piping system. A control volume analysis was performed to determine the amount of time that the no-flow condition lasted (t_o) and how much the pressure dropped during this time. Recall that the valve will be closed for as long as the cylinder pressure (p_c) is smaller than the attenuator pressure (p_d).

Two control volumes were established. One for the high pressure cylinder which contains the low pressure water about to be pressurized and one of the attenuator and piping volume containing high pressure water about to be depressurized. Figure 1 describes both control volumes for the specific case where the piston just starts accelerating towards the right. Note how all check valves connecting the pump to the discharge are closed at this time.

The mathematical analysis can be separated into two sections. First, the pressurizing of

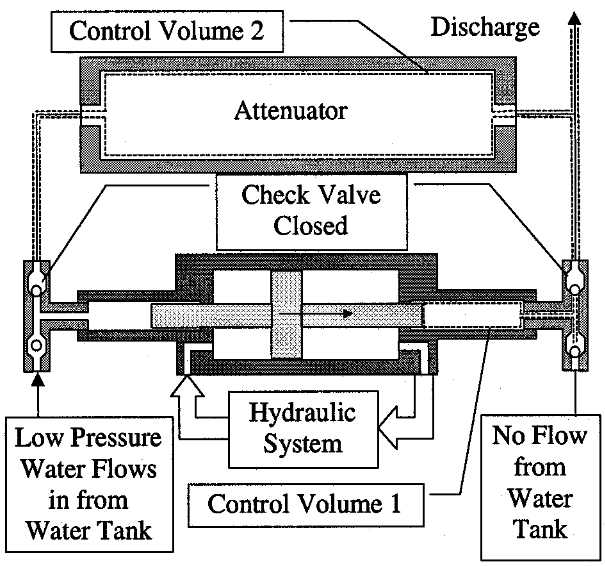

Figure 1: Control Volumes used in Mathematical Analysis

the water in control volume 1 will be looked at. Following this, the depressurizing of the attenuator will be analyzed using the above defined control volume 2.

2.2 Pressurizing of water in cylinder

Assumptions:

- Valve does not leak
- Valve closes instantaneously and is massless
- Motion of piston is not affected by the expansion of the high pressure water contained in the clearance volume in the suction cylinder

Recall the continuity equation :

$$\frac{dV_{cv}}{dt} + \frac{V_{cv}}{\beta}\frac{dp}{dt} = \frac{m_{in} - m_{out}}{\rho(p)}$$

Where:

β = Bulk Modulus

m = Mass flow rate

ρ = Density

$p = p_c$ = pressure of water in cylinder

$$V_{cv} = V_{cyl}(t) = (s - y(t))A_{cyl} = \text{cylinder volume} \tag{1}$$

And where *y(t)* is the displacement of the piston and *s* is the stroke length.

Differentiating equation 1 with respect to time yields:

$$\frac{dV_{cv}}{dt} = -v_{piston}(t)A_{cyl}, \quad \text{where } v_{piston} \text{ is the velocity of the piston}$$

Since there is no mass flow coming in or out of control volume 1:

$m_{in} = 0$

$m_{out} = 0$

The continuity equation can therefore be written as:

$$\frac{dp_c}{dt} = \frac{\beta(p_c)}{V_{cyl}(t)}\left(v_{piston}(t)A_{cyl}\right) = \frac{\beta(p_c)}{(s - y(t))}\left(v_{piston}(t)\right) \tag{2}$$

2.3 Depressurizing of water in attenuator

Assumptions:

- Valve is perfectly closed and does not leak

- Valve closes instantaneously

Once again starting from the continuity equation:

$$\frac{dV_{cv}}{dt}+\frac{V_{cv}}{\beta}\frac{dp}{dt}=\frac{m_{in}-m_{out}}{\rho(p)}$$

Now, for control volume 2:

$\rho = p_d =$ discharge pressure
$V_{cv} = V_{att} + V_{pipe} =$ attenuator volume + pipe volume

And since the volume is constant:

$$\frac{dV_{cv}}{dt}=0$$

There is no flow coming into control volume 2, but the waterjet system continues to deliver a high pressure flow through the orifice.

$$m_{in}=0$$

$$m_{out}=\rho_{out}Q_{out}=\rho_o C_d A_o y_c(p_d)\sqrt{\frac{2p_d}{\rho_o}}$$

Where $y_c(p_d)$ is the ratio between the jet velocity for a compressible flow and the jet velocity for an incompressible flow. The continuity equation becomes:

$$\frac{dp_d}{dt}=-\frac{\beta(p_d)}{V_{att}+V_{pipe}}\frac{\rho_o}{\rho(p_d)}C_d A_o y_c(p_d)\sqrt{\frac{2p_d}{\rho_o}}$$

2.1.2 Simulating the pressure fluctuations

Some further assumptions were made in order to determine the pressure drop of the waterjet system at different operating conditions. The velocity profile of the piston motion was assumed to vary in time along the piston's stroke length. Five distinct areas were assumed in this variation. These are shown in Figure 2.

In region I, the velocity of the piston is zero. The piston does not move for this small fraction of time due to the time tag resulting from the activation of the solenoid valve which switches the direction of flow in the hydraulic. The piston then proceeds to accelerate quite rapidly towards it's maximum speed *(sp1).* It accelerates rapidly since the hydraulic force exerted on the piston is much higher than the resistive force exerted by the pressurized water since at the beginning of the stroke motion, the water pressure is relatively low. After the acceleration phase, the piston reaches a steady velocity during which the valve eventually opens once the cylinder pressure overcomes the attenuator pressure. During region III, the piston is assumed to move at a constant speed since the driving hydraulic force and the discharge pressure become relatively equal. In region IV, the piston gradually slows down as the resistance due to the pressurized water increases. Finally, in region V, as the piston approaches the end of it's stroke length, the

Figure 2: Velocity Profile of Piston/Plunger Assembly Motion

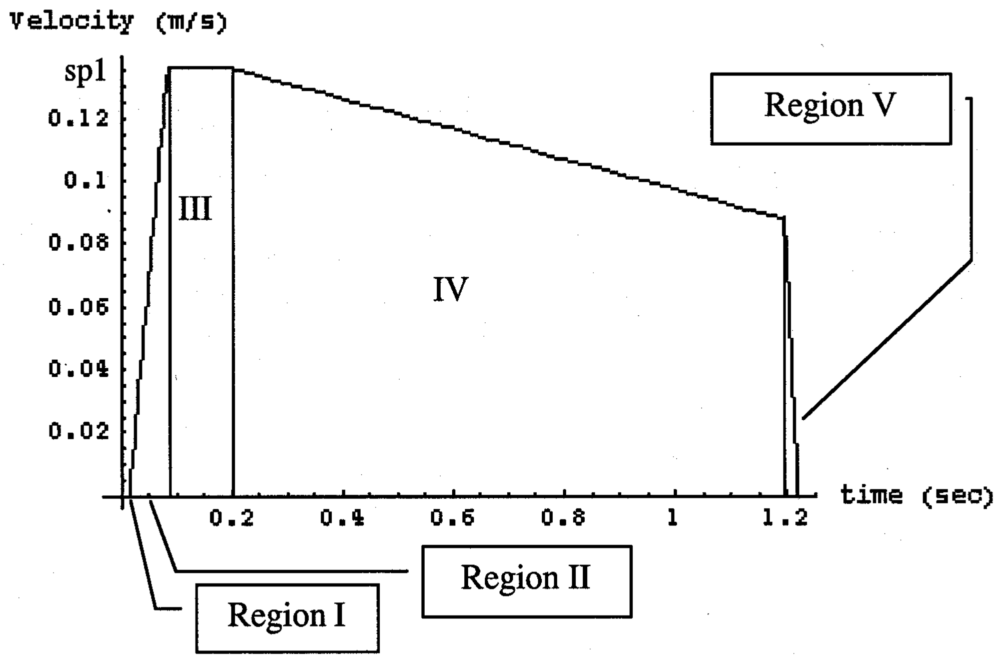

solenoid valve is actuated by a sensing mechanism and reverses the hydraulic flow so as to stop the motion of the piston.

The simulation only looks at the case where the valve is closed and therefore the piston will only go through regions I, II and a fraction of III. The velocity profile was modified from the profile assumed by Singh in his simulation [4]. He had assumed that during 16% of the stroke period, the piston traveled 20% of its stroke length at a constant speed *sp1*. During the last 84% of the stroke period, the piston traveled the remaining 80% of it's stroke length at another constant speed *(sp2)* smaller than *sp1*. Singh's model is shown in Figure 3. Conversely, the model proposed here accounts for the switching time and the acceleration phase, which occurs before the piston reaches the first constant speed rate *(sp1)*.

As will be seen later, the simulation results varied depending on the length of the acceleration phase relative to the total time period. Furthermore, it was assumed that the maximum pressure delivered the waterjet system occurred right before the valve opened. This assumption was also made by Hu and Robertson [5] also by Tikhomirov et at. [8]. The length of the stagnation was assumed to be a constant 0.015 sec. This assumption was also made by Tikhomirov [8] in his simulation.

The system parameters were determined through existing drawings of the watejet machine available in our laboratory [9]. The following data was used in the simulation:

Table 1: System Parameters

Total piping length	11.16 meters
Attenuator Volume	0.5 liters
Pipe Diameter	0.1524 cm
Stroke Length	13.284 cm
Orifice Diameter	0.02794 cm
Cylinder Diameter	1.66 cm
Overall Discharge Coefficient	0.695

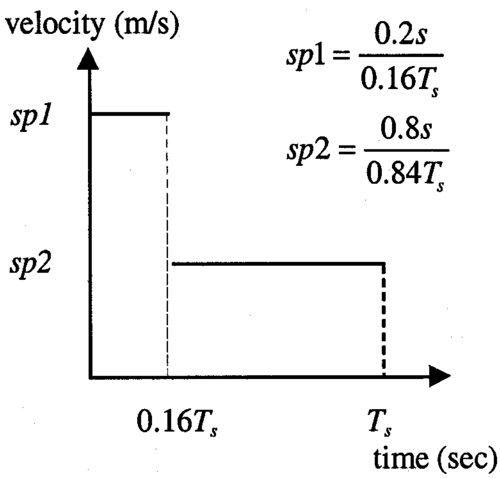

Figure 3. Velocity Profile Assumed by Singh [4]

The overall discharge coefficient was obtained from the work performed by Hashish [10]. Although his results showed that the overall discharge coefficient decreased as the operating pressure increased. It was assumed to be constant in the simulation since the decrease was considered to be negligible. For instance, for a 0.0254 cm orifice diameter, at 100 MPa the discharge coefficient is 0.7 while at 160 MPa it drops to 0.69. The significance of this assumption was examined through a sensitivity study.

Mathematica was used to solve this problem. The required inputs to the simulation are the stroke period and the maximum operating pressure. For the model validation, both of these inputs were determined experimentally. The iteration process begins with a guess for t_o (the no-flow time) and the value of t_o is incremented in steps of 0.001 sec until the cylinder pressure at time t_o is greater or equal to the attenuator pressure. The pressure fluctuation is therefore calculated as the maximum operating pressure minus the pressure of the attenuator at time t_o.

2.2 Experimental Analysis

2.2.1 Experimental Set-up

The objective of the experiment was to measure the pressure fluctuations of the pressurized water at the entry of the waterjet nozzle. It is very difficult to capture the pressure fluctuations within the nozzle itself due to its geometry and design. To adequately measure the variation of static pressure, the pipe carrying the high pressure water needed to be tapped into without disrupting the water flow. The pressure waveform that was obtained corresponded to that of the flow right before the nozzle orifice.

The existing pipe connecting the waterjet's on/off valve to the orifice was removed and replaced by a new pipe that had a connecting tee in it. The tee was located approximately at 17 cm from the orifice assembly. Swagelok's Sno-Trik connectors were used for this purpose. The branching tube was connected to an adapter on which a pressure transducer was mounted. The adapter was specifically machined for this application. To obtain an accurate depiction of the pressure variations, the system needed to be leak proof and precautions were taken in this regard. Figure 4 shows the experimental set-up used to determine the pressure fluctuations.

A PCB Piezotronics pressure transducer (Model 119A11) was used to capture the pressure fluctuations. The charge output signal of the transducer was then conditioned by a charge amplifier (PCB Model 462A). The resulting voltage signal was sent to a Tektronix digital oscilloscope (TDS 420A). This allowed visualization of the time history of the pressure waveform, which was then downloaded to a computer. The piezoelectric transducer did not yield the absolute value of pressure since it is a dynamic sensor and the steady-state component gradually bleeds off to zero. So when the operating pressure reaches an operating pressure of 200MPa, the new output voltage will bleed out the static component and the 200MPa will correspond zero. All measurements are therefore taken about this new zero. The transducer was well suited for the intended application since it captured the high frequency components of the pressure waveform. These high frequency components needed to be considered since they are indicative of the sharp pressure surges and drops seen in the pressure time history results. To obtain an absolute pressure reading, another transducer that only reads the static component

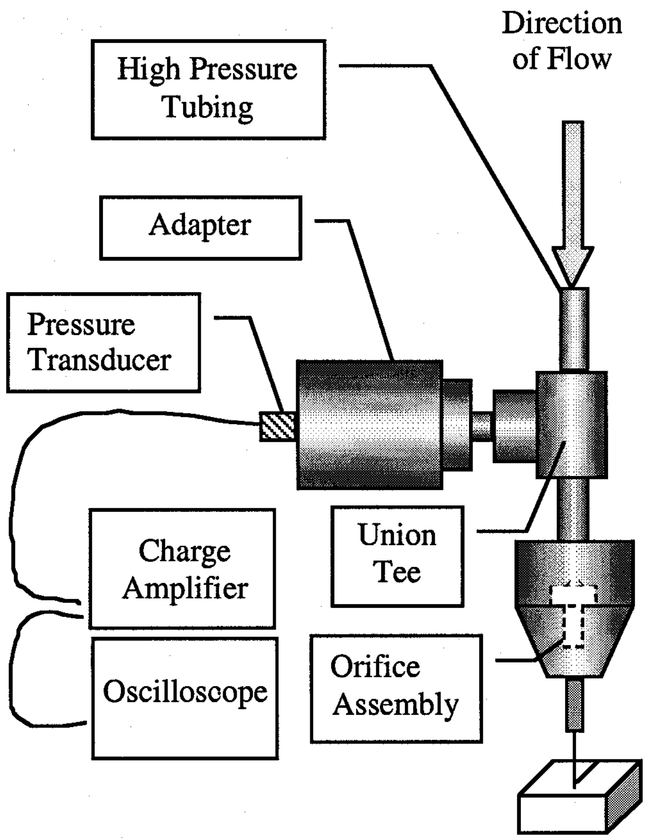

Figure 4: Experimental Set-up

could have been used in conjunction with the dynamic piezoelectric transducer. Alternatively, one strain gage type transducer could have been used to capture both components. It should be mentioned though that the latter option would not yield such good results for this investigation, which sought to capture higher frequencies of the pressure waveform to accurately determine the pressure drop and depict the pressure fluctuations.

The cable connecting the pressure transducer to the charge amplifier is a low capacitance, high impedance cable as to not shunt down the charge output of the transducer. The charge amplifier needed to be set to the correct input pC/psi (pico-coulombs per psi). A calibration chart was provided with the transducer. The transducer was calibrated to 0.307 pC/psi. Furthermore, the gain (psi/V) of the amplifier was set to give a readable output on the oscilloscope.

To obtain the pressure drop, the voltage drop was first obtained and then multiplied by the gain:

$\triangle p = \triangle V \times \text{Gain}$ [Vxpsi/V]

2.2.2 Experimental Procedure

Data was collected for three pressure settings (153.4, 181.0 and 215.5 MPa). For each setting, at least 2 test runs were done. The pressure waveform was captured and the maximum pressure was read from the pressure dial gage. Furthermore, the period of oscillation was obtained from the oscilloscope for each of the test runs.

3. RESULTS

3.1 Experimental Results

Results were obtained for three different operating conditions. The waterjet machine was first set at to operate at a maximum operating pressure of approximately 22250 psi (153.4 MPa). The pressure was then increased to 26250 psi (181.0 MPa) and to 31250 psi (215.5 MPa).

For each pressure setting, the pressure fluctuations were determined. The time that the valve was closed was also found from the oscilloscope output. Figure 5 shows an example of the pressure waveforms obtained during experimentation. Note how the pressure fluctuates between two different peaks: a high peak and a low peak. It clearly shows the pressure drop that occurs after the discharge pressure reaches one of the peaks. The duration of the no-flow condition (t_o) can be determined by reading the time lapse between the start of the pressure drop and the sharp pressure increase that takes place when the check valve opens as shown in Figure 5. Similar results to that shown in Figure 5 were obtained for the two other pressure settings and are shown in Figures 6 and 7.

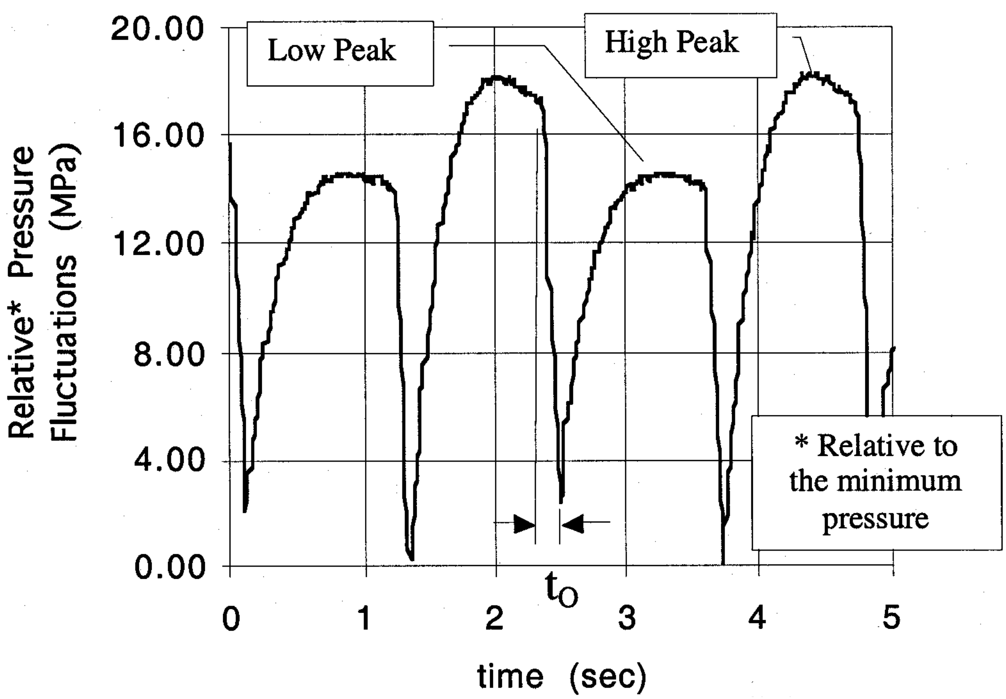

Figure 5: Relative* Pressure Fluctuations at 153.4 MP*a*

It can be noted that the experimental results show a certain degree of repeatability, especially the results obtained at 153.4 MPa and 181.0 MPa. At 215.5 MPa, the results seem to vary a little more than at the two lower pressure settings.

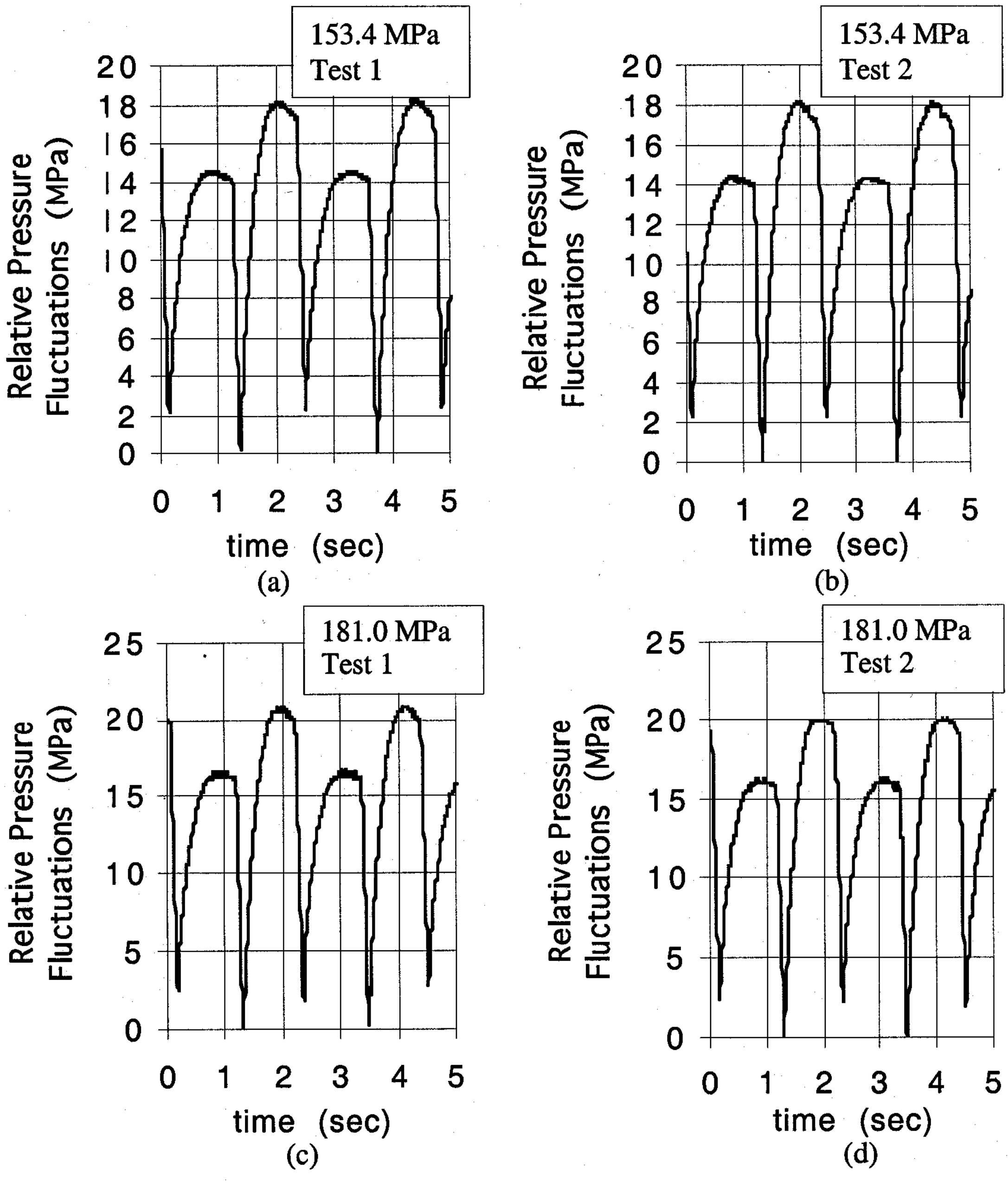

Figure 6: Experimental Results at 153.4 MPa and 181.0 MPa - tests 1 & 2

Note: All pressures shown are relative to the minimum pressure of the operating condition

The pressure fluctuations were found for the high peak and low peak cases. This data is plotted in Figure 8a along with the data obtained from the computer simulation. Note how the low peak drop is generally smaller than the high peak drop. Furthermore, note that as the operating pressure is increased, the magnitude of the pressure drop also increases. The percentage pressure drop however tends to decrease for increasing operating pressure as shown in Figure 8b. The

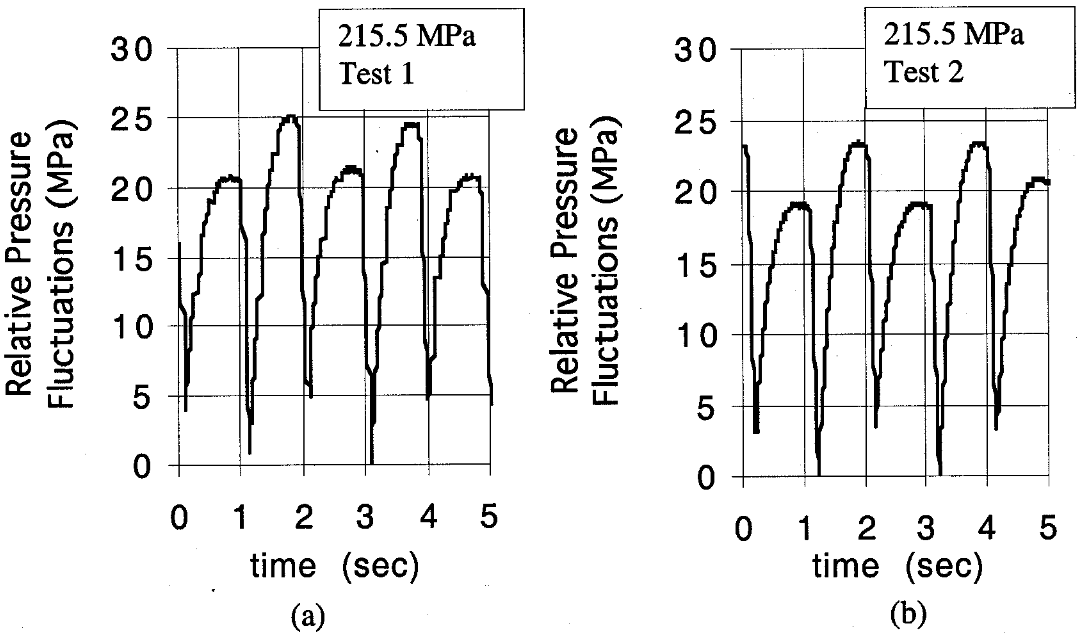

Figure 7: Experimental Results at 215.5 MPa - tests 1 & 2

Note: All pressures shown are relative to the Minimum pressure of the operating condition

period of oscillation was also determined experimentally. This period of oscillation corresponds to the stroke period (i.e. the amount of time it takes the piston to travel the stroke length). Figure 9a shows the variation in stroke period at the different operating pressures. As the operating pressure increases, the stroke period decreases. A smaller stroke period indicates that the piston is moving more quickly (since it covers the same length in a smaller time). As it will be seen later, the velocity of the piston is an important factor that greatly affects the size of the pressure pulsations. The magnitude of the pressure pulsations increase as the velocity of the piston increases. The faster moving piston does not mean that the check valve will be open for less time. This can be seen in Figure 9b where as the stroke period is decreased (and the piston velocity is increased), the time of no-flow increases.

So, although the piston does move faster when the stroke period is increased, it takes longer for the piston to compress the water and for the check valve to open. It takes more time to open the check valve since the compressed water in the attenuator that is being depressurized is at higher pressures (i.e. the low pressure water needs to be pressurized even more at higher pressures). This is corroborated by Figure 10. Note how at higher pressures (and for higher pressure drops), the time of no-flow increases.

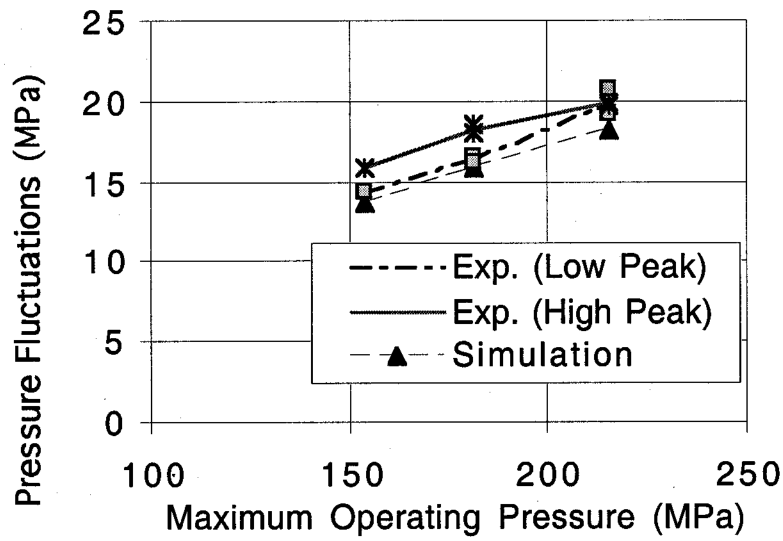

Figure 8a: Pressure Pulsations at Various Operating Pressures

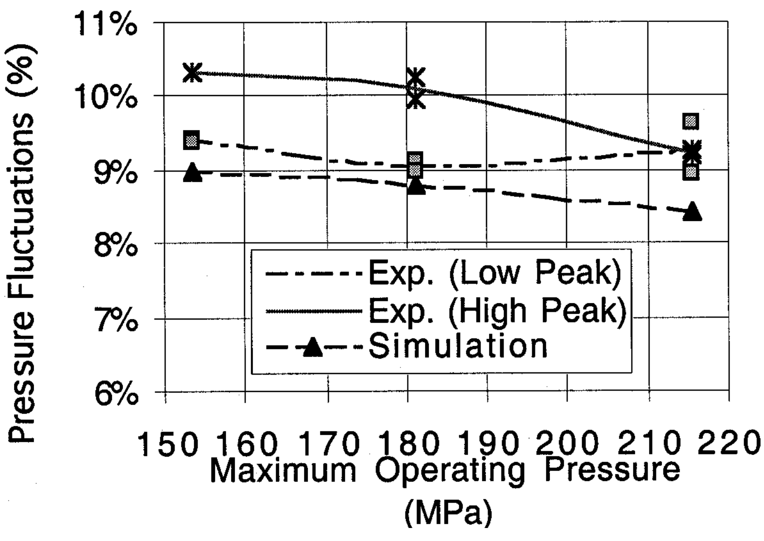

Figure 8b: Percentage Pressure Drop at Different Operating Conditions

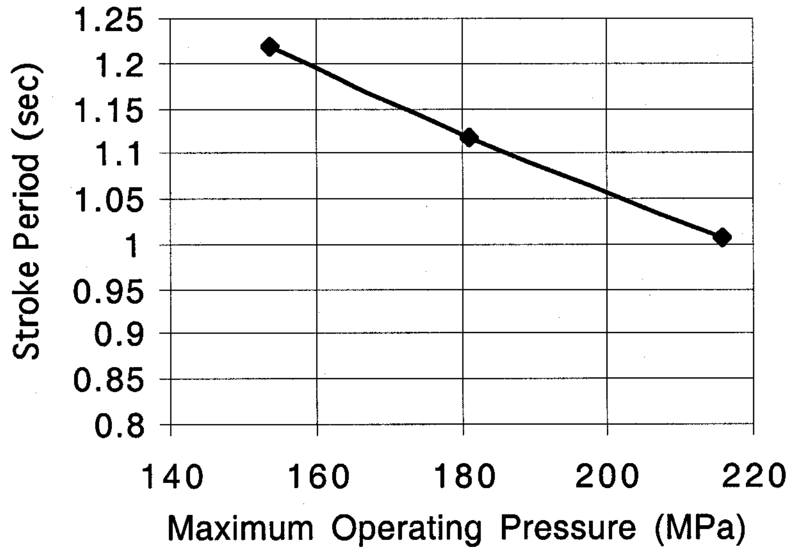

Figure 9a: Stroke Period versus Maximum Operating Pressure

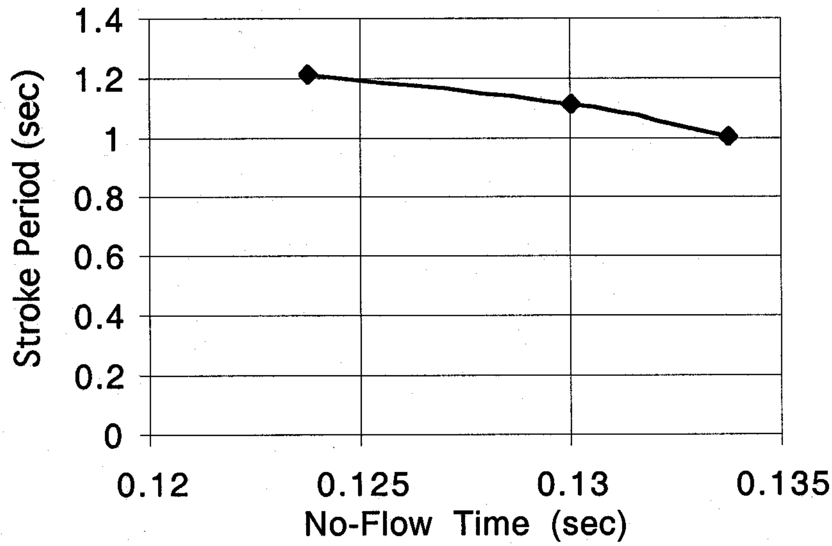

Figure 9b: Relation Between Stroke Period and No-Flow Time

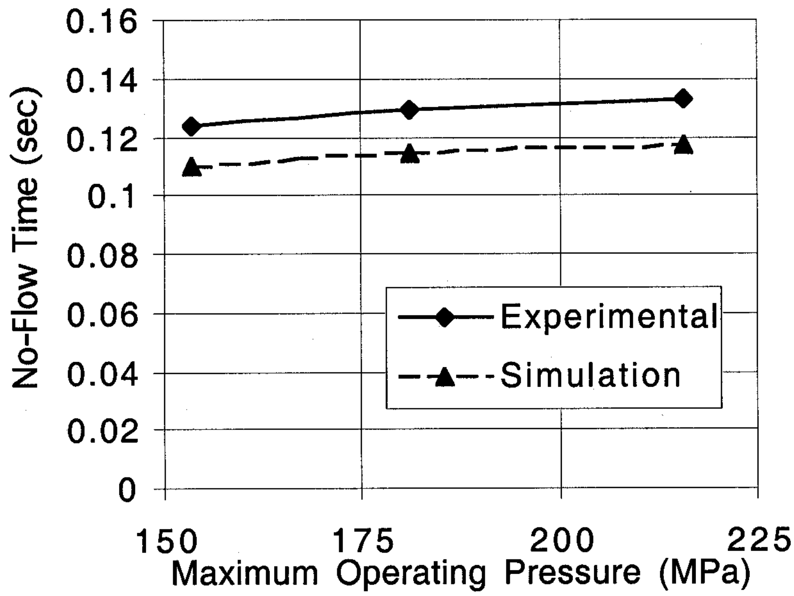

Figure 10: No-Flow Time for Various Operating Conditions

The above mentioned results can also be observed by looking at the pressure waveforms obtained at the different pressure settings. Figure 11 shows the waveforms for the three different operating pressure conditions. Note how as the operating pressure increases, the pressure drop tends to increase and the stroke period decreases.

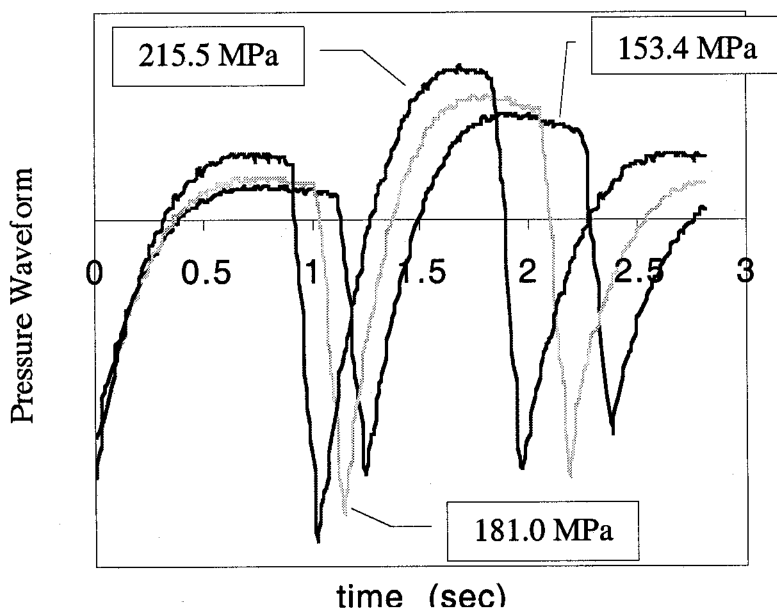

Figure 11: Pressure Waveforms Obtained Experimentally

2.2.3 Simulation Results

Once the experiments were conducted, the simulation results were obtained by using the known period as an input parameter. Other assumptions were made regarding the velocity profile of the piston. It was assumed that the acceleration phase lasted 8/100 of a stroke period for the 1st test at 153.4 MPa. Knowing the stroke period for the first test at 153.4 MPa, the time of no-flow was determined. In an effort to maintain the time of compression constant (or slightly larger), the acceleration phase was modeled to last 9/100 of a stroke period for the test at 181.0 MPa and 10/100 for the final set-up at 215.5 MPa.

As the acceleration phase is increased, the pressure fluctuations increase. This is shown in Figure 12. Note that if the velocity profile assumed by Singh [4] was used in this simulation, the acceleration phase would be zero (since the piston is assumed to speed up instantaneously to a constant speed) and the pressure pulsation would be smaller than it should be. However, the lag of the system in switching direction of travel and accelerating to a steady speed both need to be accounted to carefully depict the system's pressure fluctuations.

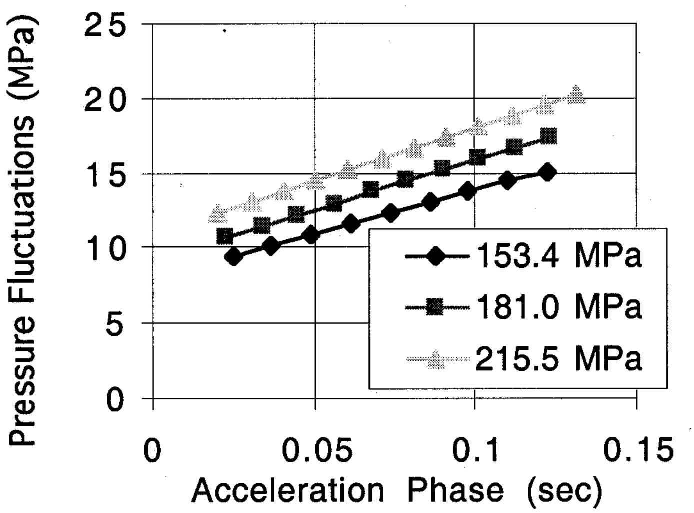

Figure 12: Effect of the Length of the Acceleration Phase on the Pressure Drop

The pressure fluctuation results obtained from the simulation with the corrected acceleration phases were previously shown in Figures 8 and 10.

Other parameters of the computer simulation were varied to examine if the trends observed in literature could be reproduced. The discharge coefficient and attenuator were varied as shown in Figures 13 (a) and (b). Figure 13 (a) shows how increasing the overall discharge coefficient also increases the pressure losses. It is interesting to note that an increase in system losses (i.e. a decrease of the overall discharge coefficient) actually decreases the fluctuations. This is due to the fact that increasing the discharge coefficient increases the volumetric flow at the discharge. This is analogous to an increase in piston speed (or increasing the orifice diameter) which we already know causes an increase in fluctuations. The results for Figure 13 (a) are for a pressure of 215.5 Mpa, a stroke period of 1.008 see and an acceleration phase of 7/100 of a stroke period. The constant discharge assumption used in the simulation might account for some of the discrepancy between the simulation and experimental results. Note how increases the discharge coefficient from 0.65 to 0.8 results in an increase in pressure fluctuation of 3.5 MPa.

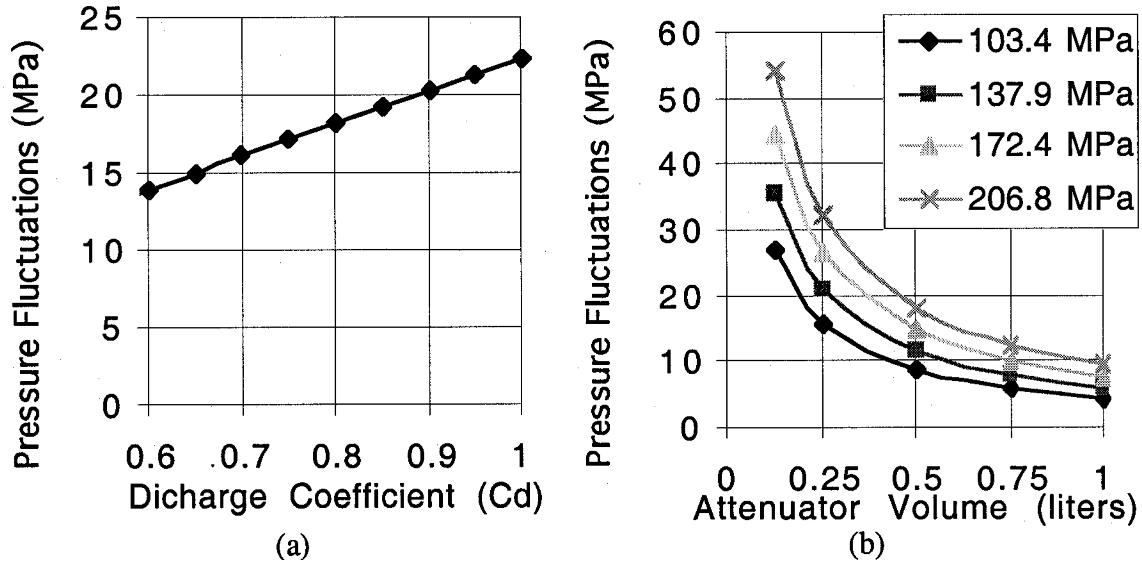

Figure 13: Sensitivity Analysis of Various Simulation Parameters

The results for the simulation are shown in Figure 13 (b) and correspond to a constant stroke period of 1.22 sec and an acceleration phase of 7/100 of a stroke period. The increase in attenuator volume gave similar results to those seen in literature [4,6,7,8]. Figure 14 shows how the results obtained with the simulation follow the same trend observed in literature.

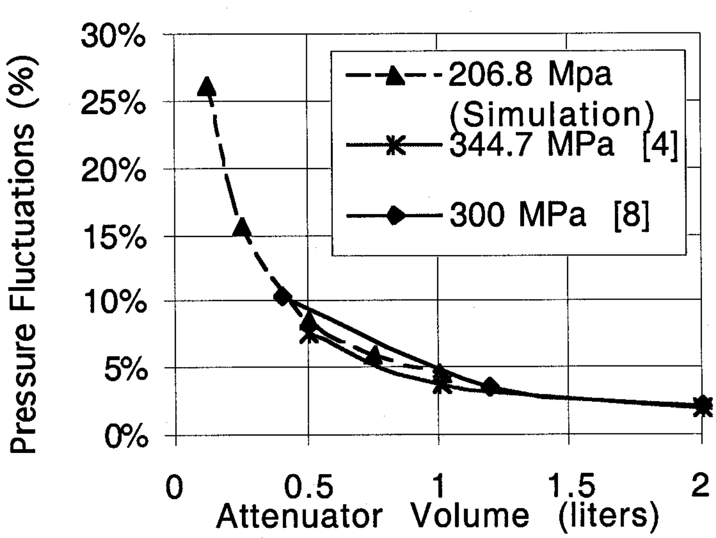

Figure 14: Simulation Results versus Results Found in Literature

The effect of the modeling of the physical properties of water is shown in Figure 14. Note that as the operating pressure increase, the effect of the fluid properties on the pressure fluctuations increases. The "norm" plotted in Figure 15 corresponds to the case where the stroke period is 1.22 sec and the acceleration phase lasts 7/100 of a stroke period. As shown below, keeping the density constant increases the pressure fluctuations while keeping the bulk modulus constant decreases the fluctuations. Keeping all water properties constant yields smaller pressure fluctuations than the norm. This implies that an increase in density decreases the pressure fluctuations while an increase in bulk modulus increases the fluctuations.

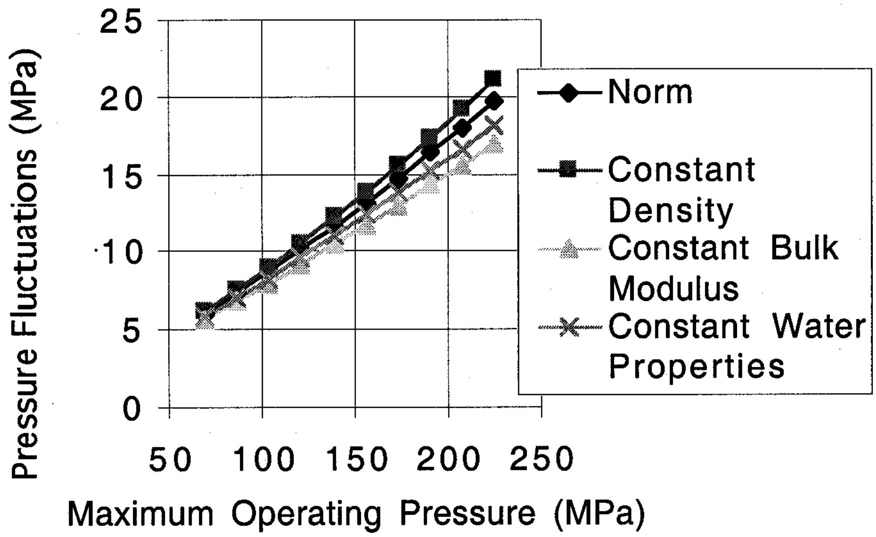

Figure 15: Effect of the Modeling of the Water Properties on the Pressure Fluctuations

4. DISCUSSION

4.1 Modeling the displacement of the piston

The velocity profile proposed by Singh [4] was modified to account for the switching time and the acceleration phase of the piston. The length of the stagnation period due to the switching time was assumed to be a constant of 0.015 sec as seen in literature [8]. The simulation also assumed that the acceleration phase duration was to remain as close to constant as possible as the operating pressure increased.

The experimental and simulation results showed that the motion of the piston greatly affected the pressure fluctuations obtained through experimentation and computer simulation. It was shown in Figure 9a that the plungers stroke period decreased as the operating pressure was increased. The shorter stroke period indicates that the piston moves quicker since it covers the same distance in a shorter amount of time. The faster piston motion resulted in greater pressure fluctuations as the operating pressure increased (Figure 8a).

It was also experimentally determined that at larger operating pressures, the time of no- flow was increased (Figure 10). Although the piston moved faster to compress the low pressure water, it needed more time to complete the pressurizing process since the system was operating at a higher pressure. Obviously, as the operating pressure increases, the water needs to be compressed to a higher level and this takes a significant amount of time. So a larger and larger fraction of the stroke length is spent compressing the water. Therefore, it can be stated that the acceleration phase also increases in length since it takes longer and longer for the piston to reach its maximum speed. *The length of the acceleration phase is very important and can significantly affect the resulting pressure fluctuation result* (Figure 12).

A better model would therefore incorporate the hydraulic system dynamics in conjunction with the waterjet dynamics analysis. These two systems are coupled by the motion of the piston, and as indicated by the results, it would be preferable to model the waterjet system this way. Obtaining the accurate velocity profile of the piston would also allow the modeling of the discharge pressure throughout the entire piston stroke period. This would allow the correct calculation of the time at which the maximum pressure occurs. Recall that the simulation assumed that the maximum pressure occurred when the piston reached the end of the its stroke length. However, experimental results (Figure 6 and 7) showed that the actual maximum pressure occurred as the piston approached the middle of its stroke length. Therefore, the assumption made by the simulation did not characterize the pressure time history as well as it could have.

The velocity profile affects the discharge pressure throughout the entire stroke length. The experimental results show that as the piston reaches the end of its stroke length, it decelerates before stopping. This can be seen in Figure 5. Note that before the sharp pressure drop occurs (i.e. before the no-flow condition is initiated), the pressure decreases at a slower rate. The slight rounding off of the "steady-state" maximum pressure condition observed could be due to the rapid deceleration that the piston undergoes at the end of its stroke period.

4.2 Modeling the water properties

The equation of density was in accordance with Tait's Equation. The secant bulk modulus definition was used to depict the variation of bulk modulus at high pressures. The water properties at high pressures were shown to affect the pressure fluctuations significantly (Figure 15). Note how increasing the bulk modulus results in an increase in pressure fluctuations and that an increase in pressure fluctuations can also be achieved by decreasing the water density.

By assuming constant density (i.e. at atmospheric conditions), the mass of the water flowing through the system is reduced at high pressures since the density was modeled to increase with pressure. Note that in the pressurizing process governed by Equation 2, there is no density term. Therefore, the pressurizing process is not affected by assuming constant density. Since there is less mass to discharge from the system, the depressurizing process occurs more rapidly and the consequent pressure drop rate is increased. Assuming constant bulk modulus affects the elastic properties of the fluid. Once again, the bulk modulus was modeled to increase with pressure. Physically, this means that it gets harder and harder to compress the water as the pressure increases. If the bulk modulus is smaller, the water is more compressible, the depressurizing and the pressurizing process are decelerated. Recall that the attenuator uses the fact that water tends to decompress and expand during the no-flow condition and this alleviates the pressure fluctuations. So a lower bulk modulus will allow it to work better since the water will tend to expand more. Mathematically, a constant bulk modulus assumption reduces the numerator of both Equation 2 and Equation 3, which consequently also reduces the pressure drop.

The simulation results obtained were consistently lower than the experimental results (Figures 8 and 10). The difference between the simulated and experimental results ranged from 1.9 to 2.7 MPa. This could be due to an underestimation of the actual value of the bulk modulus. Therefore, the assumption of the secant bulk modulus definition accurately depicted the variation of water properties at high pressure is questioned. It is believed that the tangent bulk modulus would overestimate the actual value of the fluctuations and that the true value of a lies between the value found for the tangent bulk modulus and the value determined for the secant bulk modulus. The bulk modulus of the water in the system is believed to be lower than the bulk modulus of pure water (the tangent bulk modulus) since the presence of bubbles in the system would diminish the value of the waters bulk modulus considerably.

4.3 Computer Simulations

The simulation presented in this paper attempted to incorporate the following system parameters so as to properly predict the pressure fluctuations of a waterjet system observed through experimentation:

- The change in fluid properties of water at high pressures
- The stagnation and acceleration phases of the piston
- The switching time of the solenoid valve
- The fluid jet compressibility

The model assumed:

- A constant overall discharge coefficient
- A modified bilinear velocity profile of the piston
- The time required to compress the water remained constant as the operating pressure increased
- The bulk modulus varied according to the secant bulk modulus definition at high operating pressures
- The maximum discharge pressure occurred at the end of the stroke length

Experimental results were found to be generally slightly larger than the simulation results. It is believed that this discrepancy is partly due to the approximate velocity profile used in the simulation and the bulk modulus variation at high pressures.

Through the computer simulation results, it was seen how the water properties at high pressures affected the pressure fluctuations in the system. The computer model also calculated the time of no-flow. These results were compared with experimental results. As the operating pressure increased, it was found that the duration of the time of no-flow increase d while the stroke period decreased.

5. SUMMARY AND CONCLUSIONS

The pressure fluctuations in a waterjet system were investigated through modeling, simulation and experimental efforts. The modeling and simulation attempted to solve for the time of no-flow and the pressure fluctuation for a given stroke period and maximum pressure. The fluid jet compressibility, overall discharge coefficient of the system were accounted for as well as the variation of the water properties at high pressures. The motion of the piston was based on the bilinear profile assumed by Singh [4], however it was modified to also incorporate the stagnation and acceleration phases of the piston motion. To validate the model, the simulation results were compared to experimental results for the same operating conditions. The stroke period and the maximum pressure were determined experimentally and used in the simulation to determine the theoretical pressure fluctuations.

It was found that the pressure fluctuations increased as:

- The stroke period decreased
- The acceleration phase increased
- The time of no-flow increased
- The attenuator volume decreased
- The bulk modulus of the water increased
- The density of the water decreased
- The discharge coefficient increased

The following observations were made from the experimental results:

- The non-symmetric design results in high and low pressure peaks
- The maximum pressure occurs as the piston reaches the middle of its stroke length
- The magnitude of the pressure drop increases as the operating pressure condition increases since the time of no-flow also increases

5. REFERENCES

1. Summers, D., Waterjetting Technology. E&FN Spon, 1995.

2. Singh, P. and Benson, D., "Development of Phased Intensifier for Waterjet Cutting", Proceedings of the I Ith International Conference on Jet Cutting Technology, St-Andrews, Scotland, September, 1992, pp 305-318.

3. Yie, G.G., "A pulsation-free fluid pressure intensifier", Proceedings of the 9th American Waterjet Conference, Dearborn, Michigan, August 23-26, 1997, pp 365- 369.

4. Singh, P., "Computer Simulation of Intensifiers and intensifier systems", Proceedings of the 9th American Waterjet Conference, Dearborn, Michigan, August 23-26, 1997, pp 397-413.

5. Hu, F. and Robertson, J., "Simulation and control of discharge pressure fluctuation of ultra high-pressure waterjet pump", Proceedings of the 7th American Waterjet Conference, Seattle, Washington, August 28-31, 1993, pp 337-349.

6. Chalmers, E., "Pressure Fluctuation and Operating Efficiency of Intensifier Pumps", Proceedings of the 7th American Waterjet Conference, Seattle, Washington, August 28-31, 1993, pp 327-336.

7. Susan-Resiga, R., "Attenuator's Volume Influence on High Pressure's Pulsations in a Jet cutting unit", Proceedings of the Ilth International Conference on Jet Cutting Technology, St-Andrews, Scotland, September, 1992, pp 37-45.

8. Tikhomirov, R.A. and al., High-Pressure Jetcutting. ASME Press, 1992, pp l2l-129.

9. Maintenance Manual Powerjet Model 20-55, Powerjet Inc.

10. Hashish, M., "Pressure Effects in Abrasive-Waterjet (AWJ) Machining", Journal of Engineering Materials and Technology, 11 1, 1989, pp 221-228.

11. Singh, P., and Madavan, N., "Complete Analysis and Simulation of Reciprocating Pumps Including System Piping", Proceedings of the 4th International pump Symposium, 1987, pp 55-73.

10th American Waterjet Conference
August 14-17, 1999: Houston, Texas

Paper 13

QUICK METHOD FOR DETERMINATION OF THE VELOCITY PROFILE OF THE AXIAL SYMMETRICAL SUPERSONIC LIQUID JET

L.M. Hlaváč, I.M. Hlaváčová, V. Mádr
VŠB - Technical University
Ostrava, Czech Republic

ABSTRACT

To be able to apply the theoretical model of abrasive jet for calculations essential in real-time control, it is necessary to find out very quick and precise method for description of the liquid stream structure. The simplified model was derived to determine the liquid jet attenuation in the medium outside the nozzle. The relationships for description of the equivalent jet structure evolution provided the presumption of the jet axial symmetry were derived. Taking into account, the well-known principles of hydrodynamics and some unorthodox views of the liquid jet formation inside the nozzle, the set of equations for the calculation of the cross-sectional velocity field inside jet was derived. The set of equations is useful for determination of both the attenuation and the jet structure development in the medium surrounding the nozzle. The derivation of analytical relationships is completed by experimental results obtained in the Institute of Geonics. The experimental data were measured using a special sensor developed for the jet structure investigation. The theory was also compared with summarised results of foreign authors dealing with the jet structure problems both theoretically and experimentally. All presented results (both theoretical and experimental) were obtained in air, but the theoretical relationships are appropriately valid in other media, e.g. in liquids.

1. INTRODUCTION

During investigation of the liquid jet effect on material the velocity profile of jet flow after leaving the nozzle appears to be a very important parameter. Its structure can be determined by means of various theories describing the jet flow development by the system of partial differential equations with boundary conditions. These methods are, however, rather time consuming even if the efficient computers are used. If only approximate knowledge of the velocity flow development is necessary, moreover with minimum time requirements, as far as it represents a small part of calculation in a complex control program for automated technology process, these ways of velocity profile determination appear to be unreasonable. Therefore it was necessary to derive the model presented here which enables to determine the cross-sectional velocity profile of high energy jet and development of this profile as a function of the distance from the nozzle outlet with minimum requirements on the computer equipment efficiency. The model enables very effective and sufficiently exact determination of a velocity profile and therefore it is appropriate for incorporation into the software for control of automated technology units with high energy liquid jets.

2. THE BASIC CONDITIONS FOR THEORETICAL DESCRIPTION OF THE HIGH ENERGY JET OUTLET FROM THE NOZZLE

The specific energy is an important quantity in evaluation of the efficiency of technology using the high energy liquid jet (HELJ). As far as the specific energy must not depend on the pump efficiency, its determination is based on the jet kinetic energy find out from the Bernoulli equation as presented Noskievič (1987). Some terms can be neglected in this equation, as far as the analysed processes are characterised by the following physical conditions: the pressure in the high pressure unit is many times higher than the possible hydrostatic pressure; the pressure of the medium into which the liquid flow penetrates is substantially lower than the pressure of liquid in the pumping unit; the rest pressure in the liquid flow is negligible in comparison with the pressure in the pumping unit. As far as the liquids cannot be considered as ideal ones in the operating conditions, two correction parameters were introduced into the Bernoulli equation: the pressure depending parameter precising liquid density and parameter specifying energy dissipation by friction and contraction of liquid inside the nozzle. The Bernoulli equation modified according to the presented assumptions and conditions has the following form

$$\frac{1}{2}\rho_o v^2 = \mu p_o (1 - \gamma p_o) \tag{1}$$

The equation (1) enables to determine the maximum velocity of the liquid flowing out from the nozzle outlet. However, this value of velocity can be expected only in the vicinage of the flow axis. In order to use the relationship (1) for calculation of the out flowing liquid velocity, it is necessary to determine the compressibility γ of the liquid compressed by pressure p_o and the nozzle discharge coefficient μ, which in fact defines the nozzle quality. The dependence of water compressibility on the compressive state is given by a regression formula based on the experimental data presented in physical tables prepared by Brož et al. (1980). The relationships describing the flow inside a nozzle were used for derivation of the relationship for the nozzle discharge coefficient.

3. ANALYTIC DESCRIPTION OF THE JET OUTLET FROM THE NOZZLE

The theoretical maximum velocity of the compressible liquid in the nozzle can be also determined from the Bernoulli equation provided the term characterizing liquid compressibility is considered. Apart from the compressibility another factor starts to play role during the liquid outlet, namely the friction (intrinsic friction of the liquid and the friction with the nozzle walls). Considering the friction, the velocity is not unique throughout the cross-section of the flow. It starts from zero by the nozzle walls and grows up in the direction of the flow middle. The liquid moves with the maximum velocity near round the flow axis. In the case of small friction and contraction losses the maximum value of velocity approaches to the ideal velocity of the compressible liquid without friction that is determined by the following relationship

$$v_{id} = \sqrt{2 p_o \rho_o^{-1} (1 - \gamma p_o)} \qquad \textbf{(2)}$$

The liquid velocity in the nozzle varies from the original input value, which approaches zero, to the maximum value at the outlet from the nozzle into the free space. Therefore instead of the classical value of the Reynolds' number defined for the flow with small velocity fluctuation the "effective value" of the Reynolds' number in the nozzle is determined.

$$Re = \frac{\sqrt{2}}{2} d_o \rho_o v_{id} \eta^{-1} \qquad \textbf{(3)}$$

The velocity profile at the nozzle outlet can be determined using the formula derived to satisfy the experimental results in the broadest possible range of Reynolds' numbers (from very low values up to very high ones). This semiempirical relationship was prepared during analyses of the high energy liquid outflow from the nozzle performed by Hlaváč (1995).

$$v_{oc} = v_{oa} \left[1 - \left(\frac{2r}{d_o} \right)^{log(Re + 1)} \right] \qquad \textbf{(4)}$$

The formula (4) makes possible to determine the velocity profile of the symmetrical liquid flow within the stable borders and therefore it is possible to use it for the determination of the velocity profile at the nozzle outlet. The original anticipation was not verified, however, that this relationship should be used for description of the high velocity jet after its outflow into surrounding environment even though the borders of the liquid flow are not stable. Comparison with the experimental data obtained for high energy water jet was performed especially by Hlaváč (1995) and Sitek & Vala

(1995). It was found out that the character of the velocity profile far from the nozzle outlet approaches to the Gaussian distribution which corresponds with theoretical and experimental results of Yanaida (1974), Yanaida & Ohashi (1978, 1980), Wang & duPlessis (1973) and Przyklenk & Schlatter (1986).

The discharge coefficient μ is a product of the nozzle contraction and velocity coefficients. The contraction coefficient seems to be sufficiently defined by nozzle geometry and for a certain shape it is practically a constant. Contrary to it the velocity coefficient depends on many factors - the input-output pressure difference, nozzle wall roughness, length of the cylindrical part of the nozzle outlet, nozzle diameter, dynamic viscosity and density of the used liquid. Majority of them project into the friction coefficient which can be calculated from the relationships derived by Blasius as presented by Noskievič (1987). As far as the Reynolds' number in the case of practical applications of liquid jet technology typically varies within the range 4×10^4 and 1.6×10^5, the following formula for discharge coefficient was determined

$$\mu = \alpha_c \left(1 - 0.184\, Re^{-0.2}\, l_o\right) \qquad \textbf{(5)}$$

During derivation of this relationship the formula for friction of the turbulent flow in pipes with smooth walls derived by Blasius was used, namely in the form which is valid very exactly for Reynolds' numbers exceeding 8×10^4. For the interval of Reynolds' number between 4×10^4 and 8×10^4, however, it is possible to use more precise relationship also derived by Blasius. Nevertheless, the difference between values determined by the more precise relationship and the ones determined using relationship that is valid more exactly for Reynolds' numbers between 8×10^4 and 1.6×10^5, is no more than 1% at worst case. But that case lies in fact outside the area determined by the common usage of the technology; the Reynolds' number approaches the value 4×10^4. There is no reason to introduce more precise relationship even for a less important part of the interval of Reynolds' numbers determined for limit cases used in practice (4×10^4 and 1.6×10^5) because the relationships for jet structure calculation should be to no purpose more complicated and respective calculations more time consuming.

In order to describe the jet development outside the nozzle, it was necessary to deal with the expansion of the compressed liquid at the nozzle outlet as well. The minimum jet dispersion length can be calculated using the relationship

$$L_{disp} = \sqrt{2\mu p_o \rho_o^{-1} (1 - \gamma p_o)}\; \frac{d_o}{2 v_e} \qquad \textbf{(6)}$$

in which v_e is the jet expansion velocity after the flow loses the borders

$$v_e = \sqrt{2(p_o - \frac{1}{2}\rho_o v_{oo}^2 - p_{at})\rho_o^{-1}} \tag{7}$$

In thorough analytic description of the high-speed liquid flow from the nozzle one must take into account that a compact convergent jet core is forming. This jet core contains the prevalent part of the flow energy in the initial stadium of the jet propagation outside the nozzle. If the relationship (4) is used for description of the velocity profile, the part of the profile which is not included in the core is defined by the decrease of liquid velocity (kinetic energy) at the boundary layer of the flow under a certain limit value. It is supposed that all the liquid as far as 95% downfall of velocity regarding the maximum value determined at the flow axis belongs to the core. Using relationship (4) it is possible to specify the radius of validity for this condition and this radius is assumed to be the jet core radius.

$$r_c = \frac{1}{2} d_o (1 - 0.05)^{log^{-1}(Re+1)} \tag{8}$$

The initial jet core radius and the nozzle outlet length hence define the core convergence angle and divergency of the core as a whole. All other relationships, describing an actual jet velocity profile at certain distance *L* from the nozzle outlet, were derived based on this presumption. The tangent of a divergence angle after the jet outlet from the nozzle is given by the jet core radius at the nozzle outlet and the cylindric nozzle outlet length. The corresponding formula has this form

$$tg\,\delta = \frac{(d_o - 2r_c)}{2l} \tag{9}$$

The jet core radius in the distance *L* is then given by the relationship

$$r_{cL} = r_c - tg\,\delta\, L \tag{10}$$

From the formula (10) it is possible to define a critical length within which the core disappears

$$L_{cr} = \frac{r_c}{tg\,\delta} \tag{11}$$

The presented relationships make possible to define both the jet diameter in the distance L from the nozzle outlet and jet velocity profile. The profile shape depends on the fact whether the core has disappeared or not in distance L. The dependance of the jet diameter on the distance from the nozzle outlet is expressed by this equation

$$d_L = 2r_c \quad e^{\frac{1}{2}\xi L} + \frac{L}{l}(d_o - 2r_c) \tag{12}$$

To be able to describe jet structure in a simple way the flow axis velocity was determined at the distance L from the nozzle outlet supposing exponential attenuation.

$$v_L = \sqrt{2\mu p_o \rho_o^{-1}(1 - \gamma p_o)} \quad e^{-\xi L} \tag{13}$$

The attenuation coefficient ξ was derived from the relationships describing the cumulative charge (Lavrentjev, 1957), to which the jet moving through the liquid continuum surrounding the nozzle resembles from a physical point of view.

$$\xi = \frac{C_x}{\mu} \frac{\rho_{env}}{\rho_o p_o} \tag{14}$$

The above presented relationships are completed by conditions defining the liquid velocity in the distance y from the jet axis depending on the distance L from the nozzle outlet (i.e. depending on the core disappearance).

$$v_L(y) = v_L \qquad \text{is valid for} \quad (r_{cL} - |y|) > 0 \tag{15}$$

$$v_L(y) = v_L e^{-\left[\frac{2(|y| - r_{cL})}{d_L}\right]^2} \qquad \text{is valid for} \quad (r_{cL} - |y|) \le 0 \tag{16}$$

The conditions (15) and (16) accomplish derivation of theoretical relationships describing high energy liquid jet movement and its structure after leaving the nozzle. These theoretical relationships enable to study physical processes during jet interaction with medium through which it propagates as well as the effects which take place during jet interaction with solid phase material in distance L from the nozzle outlet.

4. COMPARISON OF THEORY AND EXPERIMENTAL DATA

The comparison of presented theory with results of experimental studies was performed in two phases. The first one was a comparison of jet velocity profile development determined according to the above presented theory with the shape determined from experimental results and theories prepared by Yanaida (1974), Yanaida & Ohashi (1978, 1980), Wang & duPlessis (1973) and Przyklenk & Schlatter (1986). Based on these publications a scheme of the jet development after leaving the nozzle was prepared in the Institute of Geonics in Ostrava. The scheme was published in studies aimed at the jet structure investigation made by Hlaváč (1995) and Sitek & Vala (1995). It is presented in the Fig. 1. It represents demonstration of velocity field development of symmetrical flow obtained by compilation of published results into one complex. The graph in the Fig. 2 represents velocity profile development determined according to the presented theory. Comparison of the profiles in the Fig. 2 and Fig. 1 leads to the conclusion that they correlate very well.

The second comparison is based on the experiments made in the Institute of Geonics in Ostrava. The measuring method and the experimental device described by Sitek & Vala (1994) enable to obtain information not only about forces caused by the jet impact on the solid plate but also about the flow structure. The measuring procedure was described in detail particularly by Vala & Sitek (1995). The experimental results, however, need an additional treatment as far as the direct output of the experiment represents only force records on the sensor and holes shot through the metal plate serving as a separator of the active and non-active part of the jet. The active part makes a hole of the respective diameter and causes the force registered by sensor while the non-active part is shaded by the unbroken part of the plate. Extending the jet impact time, it is possible to increase the jet part passing through the shield. Dividing the measured force by area of the orifice made in the separation plate the medium pressure caused by flowing liquid can be determined in certain concentric circles round the jet axis. The corresponding average velocity was determined then from this pressure according to the simplified Bernoulli equation. The experimental results gained by this way were compared with velocity profiles determined from the presented theory in Fig. 3. The figure shows that correlation between the theoretical curves and the experimental data is very good.

5. CONCLUSIONS

Theoretical description of a liquid stream outlet from the nozzle and conformable velocity profile development during the jet expansion through the environment between the nozzle and the material is in very good correlation with results obtained by other theories. The correlation of the theoretical high-velocity water jet profile and results calculated from measurement of the dynamic forces made in the Institute of Geonics also shows that presented simplified theory of jet structure development is sufficiently accurate. Therefore, the theoretical model is considered to be suitable for quick and acceptable exact determination of the liquid jet structure in the software for on-line control of the waterjet technology. The theoretical description of the liquid jet presented here was used for modelling of disintegration of abrasive particles in the mixing chamber during analysis of the injection abrasive liquid jet origin.

6. ACKNOWLEDGEMENTS

The authors are grateful to the Grant Agency of the Czech Republic for support of the presented work by grant No. 106/98/1354.

7. REFERENCES

Brož, J., Roskovec, V., and Valouch, M.: “Physical and Mathematical Tables,” *SNTL*, Praha, 1980.

Hlaváč, L.M.: “Diagnostics of the High-Velocity Liquid Jet Structure,” *Proceedings of the International Scientific Conference VŠB-TU*, pp.37-42, Ostrava, Czech Republic, 1995.

Lavrentjev, M.A.: “Cumulative Charge and Principles of Its Work,” *Achievements in Mathematics*, Volume 12, Number 4, pp.41-56, 1957. (in Russian)

Przyklenk, K., and Schlatter, M.: “Simulation of the Cutting Process in Water Jetting with the Finite Element Method,” *Proceedings of the 8th International Symposium on Jet Cutting Technology*, pp.125-135, BHRA, Durham, England, 1986.

Noskievič, J., and team: “Fluid Mechanics,” *SNTL*, Praha, 1987. (in Czech)

Sitek, L., and Vala, M.: “Contribution to Continuous High-Velocity Non-Flooded Water Jet Velocity Profile Determination,” *Proceedings of the National Scientific Conference with International Participation Engineering Mechanics '95*, pp.457-462, Svratka, Czech Republic, 1995. (in Czech)

Vala, M., and Sitek, L.: “The Method and Equipment for Measurement of Small Dynamic Pressure Forces from High-Velocity Fluid Flow Stopping,” *Proceedings of the 33rd Conference EAN '95*, pp.219-224, Třešť, Czech Republic, 1995. (in Czech)

Wang, R.L., and duPlessis, M.P.: “An Explicit Numerical Method for the Solution of Jet Flows,” *Transactions of the ASME - Journal of Fluids Engineering*, March, pp.38-52, 1973.

Yanaida, K.: ”Flow Characteristics of Water Jets,” *Proceedings of the 2nd International Symposium on Jet Cutting Technology*, paper A2: pp.19-32, BHRA, Cambridge, England, 1974.

Yanaida, K., and Ohashi, A.: “Flow Characteristics of Water Jets in Air,” *Proceedings of the 4th International Symposium on Jet Cutting Technology*, paper A3: pp.39-54, BHRA, Canterbury, England, 1978.

Yanaida, K., and Ohashi, A.: “Flow Characteristics of Water Jets in Air,” *Proceedings of the 5th International Symposium on Jet Cutting Technology*, pp.33-44, BHRA, England, 1980.

8. NOMENCLATURE

α_c	nozzle contraction coefficient
γ	compressibility of the liquid under the pressure p_o [MPa]
C_x	coefficient of resistance of the environmental continuum to the jet
δ	angle of flow divergence [rad]
d_o	water nozzle diameter [m]
d_L	diameter of the liquid jet in distance L from the nozzle outlet [m]
η	dynamic liquid viscosity [$N.s.m^{-2}$]
l	length of the cylindrical part of the nozzle outlet [m]
l_o	length of the cylindrical part of the nozzle outlet in multiples of d_o
L	distance from the nozzle outlet [m]
$_{Lc}$	distance from the nozzle outlet where the jet core disappears [m]
L_{disp}	minimum distance from the nozzle outlet where the expansion of the pressurized liquid comes to an effect [m]
ξ	coefficient of attenuation of jet caused by resistance of the medium between nozzle and material [m^{-1}]
p_o	liquid pressure before the nozzle inlet [Pa]
p_{at}	atmospheric pressure [Pa]
ρ_o	liquid density in noncompressed state [$kg.m^{-3}$]
ρ_{env}	density of the medium outside the nozzle outlet [$kg.m^{-3}$]
r	radius of the elemental annulus of the jet cross-section [m]
Re	Reynolds' number
v	velocity [$m.s^{-1}$]
v_{oa}	jet velocity on the axis at the nozzle outlet [$m.s^{-1}$]
v_{oc}	jet core profile velocity at the nozzle outlet [$m.s^{-1}$]
v_e	velocity of the compressed liquid expansion [$m.s^{-1}$]
v_{id}	ideal jet velocity at the nozzle outlet [$m.s^{-1}$]
v_L	jet velocity at the distance L from the nozzle outlet [$m.s^{-1}$]
y	coordinate in the radial direction perpendicular to the jet axis [m]

9. FIGURES

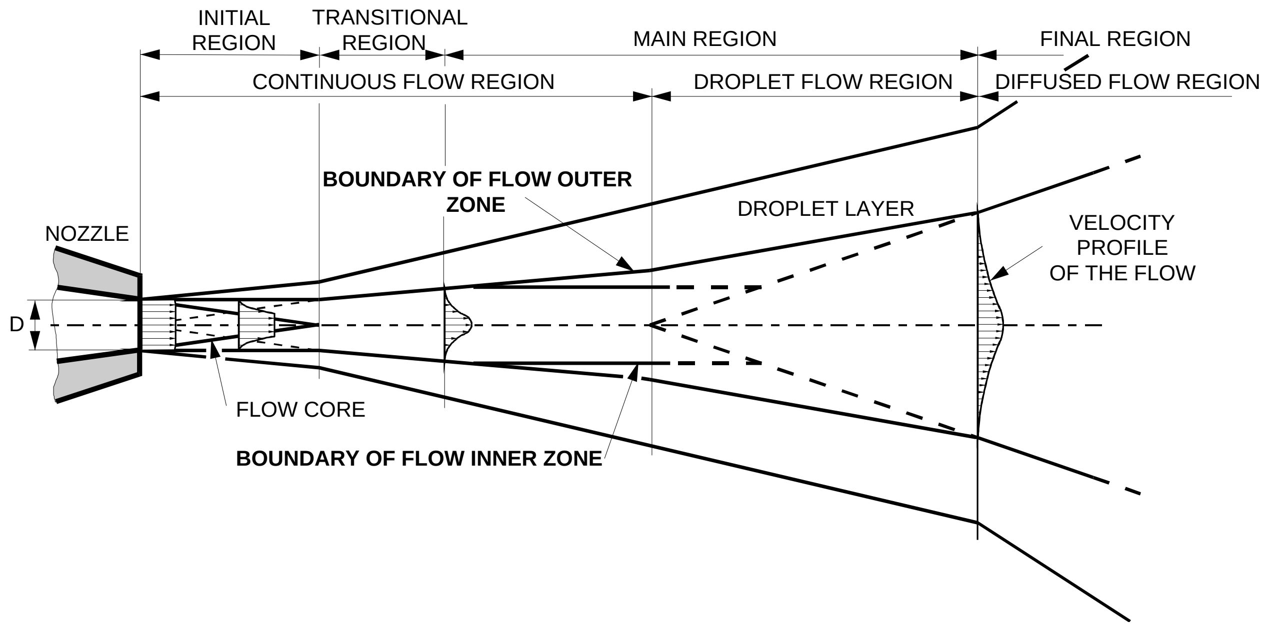

Figure 1. Jet structure determined according to the theories and experiments of Yanaida, Ohashi, Wang, duPlessis, Przyklenk and Schlatter by Sitek and Hlaváč

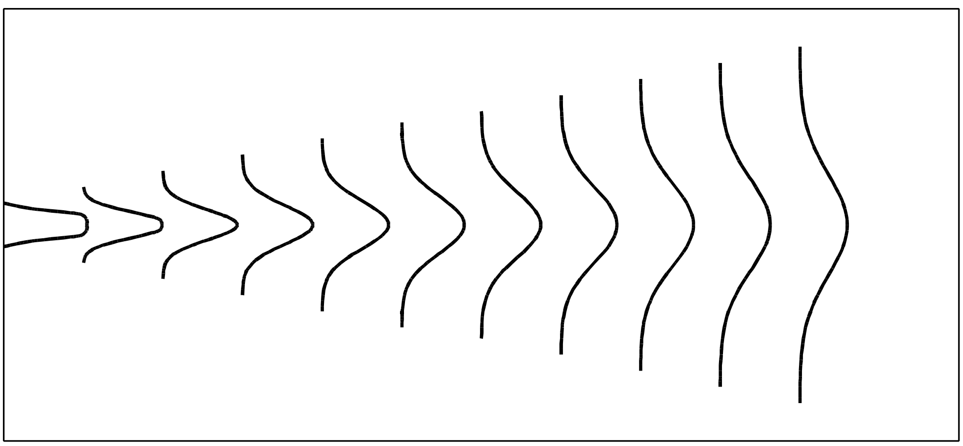

Figure 2. Velocity profile development determined by the presented theory for the nozzle with diameter 0.325 mm and water pressure before nozzle 250 MPa. Velocity field development is plotted with step 50 mm from the nozle outlet up to distance 500 mm.

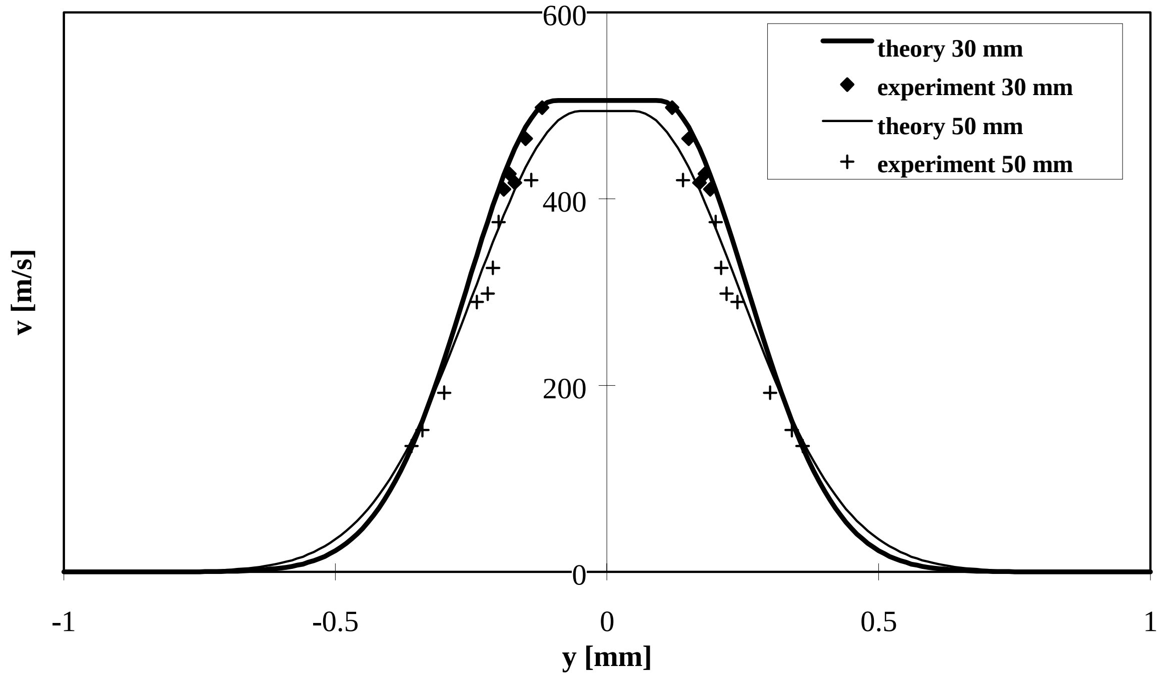

Figure 3. Comparison between the velocity profile curves calculated for the symetrical water jet using presented theoretical relationships and conformable experimental results. Two distances from nozzle outlet are selected: 30mm and 50mm. In this figure y means distance from the jet axis (radius) in which velocity of liquid flow is equal to v.

10th American Waterjet Conference
August 14-17, 1999: Houston, Texas

Paper 14

MEASUREMENTS OF WATER-DROPLET AND ABRASIVE SPEEDS IN A ULTRAHIGH-PRESSURE ABRASIVE-WATERJETS

H.-T. Liu, P. J. Miles, N. Cooksey, and C. Hibbard
Waterjet Technology, Inc.
Kent, Washington

ABSTRACT

A dual-disc apparatus, based on the time of flight principle, was upgraded for measuring the speed of water droplets and abrasive particles exiting an abrasive-waterjet (AWJ) nozzle. The apparatus consists of two coaxially rotating discs with a fixed separation. A set of narrow slots 180° or 90° apart was machined on the upper disc. A third disc made of different materials pinned to the lower disc was used as the "write-once" data recorder. Speed measurements were conducted by shooting an AWJ perpendicularly toward the discs, with the AWJ traversing radially inward. Water droplets and/or abrasives passed through the slots and produced erosion marks on the data disc. The displacement angles between the radially oriented erosion marks and the leading edges of the slots were used to derive the speeds of the water droplets and/or the abrasives. With the use of data discs made of Lexan, aluminum, and stainless steel, threshold speeds below which no erosion mark was produced by the waterjet (WJ) and/or the AWJ were determined. Test results show that the threshold speeds of the WJ for Lexan and for metals (aluminum and stainless steel) are about 600 m/s and greater than 820 m/s, respectively; the former is about 3 times that of the abrasives – Barton 220 mesh. The erosion marks produced by the WJ were very narrow, indicating the WJ was well collimated and that only the speeds exceeding the threshold speed were recorded. In other words, the droplet speed is biased to the high values. On the other hand, the erosion marks produced by the abrasives were considerably wide spread, indicating a broad distribution in the abrasive speed. The measured water-droplet speed of the WJ with the feed port closed agreed well with the Bernoulli speed; the speed was 3 to 7 % lower when the feed port was open. For the AWJ, both the water droplets and the abrasives produced their own erosion marks for abrasive mass concentration, C_a, below 40%. From the widely spreading erosion marks, the maximum and minimum abrasive speeds and their average values were derived. The abrasive speeds decreased hyperbolically with increasing C_a.

Organized and Sponsored by the WaterJet Technology Association

1. INTRODUCTION

For machining metals, glasses, and ceramics with AWJs, the material is primarily removed by the abrasives, which acquire high speeds through momentum transfer from the ultrahigh-speed waterjet. Several methods such as laser Doppler anemometers or LDVs (Neusen et al., 1992), laser transit anemometers or LTAs (Chen and Geskin, 1990), dual rotating discs (Stevenson and Hutchings, 1995), and others (Swanson et al., 1987; Isobe et al., 1988) were used to measure the speeds of the waterjet and/or the abrasive particles to understand the mechanism of momentum transfer in the mixing tube in which the abrasives accelerate. There is a large spread in the experimental results mainly due to the difficulty in distinguishing the speeds of water droplets, V_{wa}, and of the abrasive particles, V_a, by using optical methods. For the WJ, experimental results have shown that the speed of the WJ downstream of the sapphire nozzle (referred to as the sapphire WJ) ranges from 85% to nearly 100% that of the values derived from the Bernoulli equation (Chen and Geskin, 1990; Neusen et al., 1992); the latter is referred to as the Bernoulli speed. The speed of the WJ decreases as the high-speed water flows through the carbide mixing tube (the WJ through carbide nozzle is referred to as the carbide WJ). For long mixing tubes, the speed ratio of the carbide and sapphire WJs decreases with the increase in the diameter ratio of the sapphire nozzle and the carbide nozzle. For a typical AWJ nozzle with a diameter ratio of 1/3, the speed ratio was measured to be about 0.9 (Chen and Geskin, 1990). For the AWJ, experimental results show that the abrasive speed is about 40% of that of the carbide WJ (Chen and Geskin, 1990).

It is important to note that previous measurements of the speed of the carbide WJ were mostly conducted in the absence of abrasives in the mixing tube. As such, the water-droplet speed of the AWJ downstream of the carbide nozzle or V_{wa} should be lower than that of the carbide WJ or V_w in the absence of abrasives, as a part of the kinetic energy is transferred to the abrasives. Therefore, the abrasive speed is expected to be higher than 40% the actual water-droplet speed in the AWJ. It is essential to determine the distribution of the kinetic energy in order to understand the mechanism of kinetic energy transfer from the carbide WJ to the abrasives, which can only be achieved by measuring both the abrasive and water-droplet speeds. Such an understanding would serve as the basis for modeling the machining and drilling processes using the AWJ (Liu et al., 1998).

2. EXPERIMENTAL METHOD

An extensive review of existing methods for measuring water-droplet and/or abrasive speeds led to the conclusion that the relatively simple dual-disc method offered the best chance for both measurements. The method was originally developed for studying the processes of solid-particle erosion and dry-grit blasting (Levy, 1995; Ruff and Ives, 1975). An upgraded test apparatus was designed and assembled. Figure 1 shows a conceptual drawing of the experimental setup consisting of an AWJ shooting perpendicularly onto two rotating discs, with a separation S, mounted on a common rotating shaft. An electric motor drives the two discs at high rotation speeds, ω. Up to four radial slots on the upper disc provide four data sets per run. Attached to the lower disc is a target or "write-once” data disc made of a relatively soft material like a compact disc (CD). During the test, the AWJ traverses radially inward. The AWJ is blocked by the upper disc except at the openings of the slots. Four sets of erosion marks are generated on the data disc by the AWJ through the slots of the upper disc.

Let's consider one such set of erosion marks. Ideally, there are two sets of distinctive marks as illustrated in Figure 1. With $V_{wa} > V_a$, the erosion marks generated by the abrasives (heavy shaded) displace farther than those generated by the water droplets (light shaded) away from the reference line (dashed) projected from the leading edge of the slot on the upper disc. By moving the AWJ in the radial direction, composite erosion marks as shown in Figure 1 are formed. The mean positions of the erosion marks may be represented by two lines drawn through the leading edge of those marks. Let's define α_{wa} and α_a as the angles between the reference line and the lines through the centers of the erosion marks generated by the water droplets and the abrasives, respectively. The angles are functions of ω, S, and the average maximum water-droplet and abrasives speeds, V_{wa} and V_a, according to the following relationships:

$$\alpha_{wa} = (\omega / 60)360S / V_{wa}, \tag{1}$$

and

$$\alpha_a = (\omega / 60)360S / V_a. \tag{2}$$

The average maximum speeds that correspond to the centerline speed of an axisymmetric jet can therefore be derived from these two equations, which serve as the basis for data analysis using the dual-disc apparatus described below.

3. EXPERIMENTAL APPARATUS AND SETUP

Figure 2 is an engineering drawing of the dual-disc apparatus, with the rotating discs installed in a protective steel housing. The discs were driven by a 2HP electric router (DeWalt, Model 621) with a maximum rotational speed of about 21,000 rpm at 110 volts AC. Both the upper and lower discs were made of 3.2-mm-thick aluminum plates with a diameter of 14 cm. Four slots with widths of 1.6 mm were machined on the upper disc. CDs were found to be most suitable as the data disc to record the erosion marks generated by the AWJ. They are lightweight, precisely fabricated, and inexpensive; the coating on them can easily be removed to facilitate accurate measurement of the angles of the marks using an optical comparator or profile projector (Mitutoyo, Type PH-350). The three discs were pinned together to maintain a fixed orientation when assembled. Several spacers equipped with two pins were machined to separate the discs apart at the distance S.

To facilitate accurate measurement of the angles, an exact duplicate of the upper disc was machined (except the slots were widened for use with the optical comparator). The CD was pinned to the reference disc in exactly the same orientation as when it was assembled together with the dual-disc apparatus during the tests. The erosion marks and the corresponding leading edges were projected simultaneously on the screen of the comparator. The angles of the four data sets recorded on each disc were measured, and the average angle was derived.

The AWJ consisted of a WTI Intelligent Nozzle with a 0.18-mm-diameter sapphire orifice and a 0.51-mm-diameter mixing tube 6.4 cm long. The UHP pumps consisted of a bank of six intensifier pumps operating in parallel with a maximum flow rate of 22.7 liters/min at 380 MPa. Barton 220-mesh garnet abrasives were used for the tests. The abrasives were fed from a hopper equipped with a precision metering gauge.

The AWJ was mounted on an ASI manipulator with a 5-axis capability and a FANUC controller. The ASI manipulator has a computer-controlled high-pressure pumping system and a working envelope of $3 \times 2.4 \times 0.9$ m ($10 \times 8 \times 3$ ft) and is mounted on an isolated concrete foundation for precision machining applications of large and small structures. During the tests, the manipulator traversed the AWJ radially inward across the CD.

Before each test, the AWJ nozzle was moved to its starting position just outside the outer edge of the discs. The bottom of the steel housing below the AWJ nozzle was protected by a carbide plate. Experiments were conducted following the procedure described below.

1. Turn on the power and adjust the pressure to the predetermined value.
2. Open the valve upstream of the AWJ nozzle to stabilize the jet pressure.
3. Turn on the motor of the dual-disc apparatus and measure the rotational speed of the discs with an optical tachometer (Cole-Parmer, Model E-08203-20).
4. Open the abrasive feed valve for the AWJ runs.
5. Traverse the AWJ nozzle across the discs radially inward at predetermined speeds, which increase with the jet pressure to ensure that distinct erosion marks are generated on the data discs to facilitate accurate measurements of the displacement angles.
6. Turn off both the AWJ and the traverse as soon as the AWJ passes the ends of the slots.
7. Remove the CD from the assembly and replace with a new one for the next run.

The erosion marks were visualized using a PC-based imaging system. The video camera (Cohu Model 8400) was equipped with a zoom objective (Titan tool) to magnify the views of interest. The imaging system also consisted of a PCI bus mastering image acquisition plug-in board (National Instruments Model PCI-1408) and several imaging processing packages (e.g., Image Pro Plus by Media Cybernetics and IMAQ Vision by National Instruments). Both the top and cross-sectional views were captured with the imaging system. For the cross-sectional view, the CD was cut perpendicular to its surface and to the erosion mark. The marks were illuminated with a white light source equipped with a fiber-optic guide.

4. EXPERIMENTAL RESULTS

Preliminary tests were conducted to optimize the performance of the dual-disc apparatus, the experimental procedure, and the method of data analysis. During the test period, several revisions were implemented:

- Increased the rotation speed of the discs from 21,000 rpm to 23,800 rpm by using a Variac transformer that increased the AC voltage from 110 to 140 volts.
- Reduced the experimental error by increasing the separation between the top surfaces of the upper discs and the CDs to 6.39 cm.
- Develop and implement the method for accurate measurements of the displaced angles of the erosion marks on the CD.
- Develop the technique for visualizing and quantifying the profiles of the erosion marks.

A series of experiments was subsequently conducted to measure the maximum water-droplet speed of UHP WJs without using abrasives, with the abrasive feed port closed and open, respectively. Finally, the same experiments were repeated using the AWJ. For a free WJ, the maximum water-droplet speed always takes place along the jet centerline (Yanaida, 1974). In the absence of abrasives and with the abrasive feed port closed, the presence of the 0.51-mm ID and 6.4-cm-long mixing tube has little effect on the WJ exiting the 0.18-mm-diameter sapphire nozzle, provided the WJ is aligned properly with the centerline of the tube. In other words, the WJ is essentially a sapphire WJ that does not touch the sidewall of the mixing tube as it passes through the tube. For the same WJ with the abrasive feed port open, on the other hand, the entrained garnet abrasives through the port tend to break up the WJ into fine droplets. The WJ expands rapidly and is confined by the sidewall of the mixing tube. As a result, the WJ assumes the properties of a carbide WJ. For the above scenarios, the measured maximum water-droplet speeds, V_w and V_{wa}, and the maximum abrasive speed, V_a, at large x/D correspond to the centerline speed of these axisymmetric jets.

4.1 Erosion Patterns

Figure 3 illustrates the overall erosion marks generated on the CD by the WJ at p = 345 MPa. There are four sets of erosion marks corresponding to the four sets of slots machined on the top disc. Also shown, just counterclockwise to the marks, are the leading edges of the slots on the reference disc pinned to the CD. As shown in Figure 1, the angles α_w of the four erosion marks were measured with respect to these leading edges. Note that the lines drawn through the average leading edges of the opposite erosion marks go through the center of the disc.

Figures 4a and 4b show the top views of the erosion marks generated by the 345-MPa WJ, with the abrasive feed port closed and open, respectively. The bright and dark regions correspond to the eroded and original surfaces of the CD; the left edges coincide with the leading edges of the marks. From the scale (1 mm/division) shown on the bottom of the figures, the maximum widths of the marks generated by the WJs with the port closed and open were measured to be approximately 1.3 and 1.0 mm, respectively. It is evident that the WJ is more powerful with its port closed than open, as expected. The evidence is even more convincing when the cross-sectional views of the two cases are compared in Figures 5a and 5b. In the figures, the camera is oriented to look toward the center of the CD. The images are flipped horizontally so that the left edges are coincident with the leading edges of the marks, consistent with those in Figure 4. The images in Figure 5 were processed using the Image Pro Plus software to measure the cross-sectional profiles of the erosion marks. The results are plotted in Figure 6. There is a significant difference in the maximum depth of the two marks. The maximum depths of the corresponding two cases are measured to be about 1/2 and 1/7 of the thickness of the 1.2-mm-thick disc. Based on the maximum width and depth of the marks, the volumes removed per unit length along the radial distance are estimated to be 0.5 and 0.1 mm^2, using the trapezoidal rule.

The erosion marks produced by the WJ are much different from those of the AWJ. First of all, the WJ is considerably more coherent than the AWJ. In addition, depending on the material of the workpiece, the threshold velocity of the water droplets for material removal is also much higher than that of the abrasive particles, as expected. From the results obtained from tests using data discs made of several materials, the threshold speeds for these materials were estimated and plotted in Figure 7. Figure 8 shows photographs of typical erosion marks created by the WJ and AWJ with different abrasive concentrations, C_a, defined as the percentage ratio of the abrasive master flow rate in pounds per minute to that of the water flow rate in gallons per minute. As a result, the erosion mark of the WJ is very narrow and sharp (Figures 3 and 8b) whereas that of the AWJ is distributed over a relatively large area (Figures 8c through 8f). The broad distribution of the erosion on the CD surface indicates that there is a large spread in the velocity of the abrasives exiting the AWJ nozzle. Because the threshold velocity of the abrasives is considerably lower than that of the water droplets, the erosion marks produced by the AWJ on the rotating discs are much wider than those produced by the WJ.

As the abrasive concentration increases, more abrasive particles are being accelerated by the high-speed water droplets. Meanwhile, the water droplets decelerate as the result of the momentum exchange. For example, for C_a = 10%, most of the abrasives accelerate to very high speeds through multiple collisions with the water droplets. As shown in Figure 8c, both the high-speed water droplets and the abrasives produce distinctive erosion marks on the CD; the marks produced by the water droplets preserve the same characteristics of the pure WJ. On the other hand, the marks produced by the abrasives are distributed over a relatively large area. There are deep pockets eroded by the abrasives that achieve very high speeds. As C_a was increased to 40% and beyond, the water droplets could no longer produce erosion marks on the CD because the probability of collision was so high that the velocity of the water droplets had dropped below the threshold value.

4.2 Speed Measurements

The fact that only speeds higher than the threshold speed for the target material induce erosion marks on the data disc indicates that the speeds measured with the dual-disc apparatus are biased to the high value. Such characteristics should be kept in mind when the results are being examined and interpreted.

4.2.1 Waterjet

Figure 9 illustrates the water-droplet speed versus several operating pressures from 207 MPa to 345 MPa, with the abrasive feed port closed and open. With the port closed, the results show that the measured water-droplet speed (solid circles) agrees very well with the Bernoulli speed (solid curve) given by

$$V_B = \sqrt{2p/\rho}\,, \tag{3}$$

where p is pressure and ρ is the density of the water. Evidently, the WJ passes through the mixing tube with little contact with the tube wall, and the WJ behaves just like a sapphire waterjet as if the mixing tube is absent. The good agreement is in part due to the fact that the Bernoulli speed is a measure of the maximum speed of a top-hat velocity profile, while the speed measured with the dual-disc apparatus is biased to the high value.

As soon as the abrasive feed port is open, the entrained air tends to destabilize the waterjet and causes the jet to spread out. As the boundary layer develops along the tube wall, the jet is affected by a certain amount of friction loss. This results in reducing the water-droplet speed between 3 and 7%. Results of a regression analysis show that there is a linear relationship between the carbide speed, V_{wa}, and the Bernoulli speed, V_B. The best-fit curve (dashed) is given by

$$V_{wa} = 6.036e^{1} + 8.71e^{-1}V_B = 6.036e^{1} + 8.71e^{-1}(2p/\rho)^{1/2} \tag{4}$$

As shown in Figure 3, the erosion mark for the WJ with the feed port closed is very narrow, indicating that the distribution of the water-droplet speed (i.e., V_B) is tight. Similar narrow erosion marks were also observed for the runs (e.g., Figure 8b) with the port open, although the erosion mark is shallower for the runs with the port open than for those with the port closed. In other words, less material was removed by the WJ with the port open than by that with the port closed due to the lower water-droplet speed of the former. Note that the material removal rate is proportional to the square of the droplet speed. The maximum and minimum speeds were shown in Figure 9 as the ends of the error bars. Note that the minimum speed is considerably higher than the threshold speed of about 600 m/s (Figure 7).

4.2.2 Abrasive-Waterjet

Figure 10 presents the abrasive speeds of an AWJ, operating at 345 MPa and having a 0.18/0.51 nozzle combination, as a function of the abrasive concentration C_a. Barton 220-mesh garnet was used as the abrasives. The abrasives were fed from a hopper equipped with a metering valve. The squares, diamonds, triangles, and circles in Figure 10 represent the Bernoulli speed of the WJ at 345 MPa, and the maximum, average, and minimum abrasive speeds, respectively. The maximum and minimum speeds were derived from the angles of two lines that were drawn radially along the envelope of the erosion marks. The average speed is defined as the mean value of the maximum and minimum speeds.

For C_a = 0%, the speed corresponds to V_{wa} of a WJ with the feed port open. The three abrasive speeds should approach asymptotically to V_{wa} for C_a = 0% as C_a decreases. This trend is illustrated in Figure 10 by the fitted curves that decrease hyperbolically with increasing C_a, as given by

$$(V_a)_{\max},\ \ (V_a)_{ave},\ \ (V_a)_{\min} = V_o + \frac{ab}{b + C_a} \tag{5}$$

where the best-fit coefficients, V_o, a, and b, are given in the equations shown by the individual curves in the figure. For C_a < 40%, as shown in Figure 8, a part of the erosion marks on the CDs was contributed by the water droplets, and the maximum speeds are expected to be slightly biased to the high side because of the high threshold speed of water droplets.

It is evident that the maximum and minimum speeds of the abrasive particles decrease with increasing C_a. The difference between the two speeds also increases with increasing C_a. Figure 11 shows a comparison of the abrasive to Bernoulli speed ratios as a function of C_a. In the figure, the Bernoulli speed is the reference line with a speed ratio of unity. For C_a = 100%, the ratio between the average abrasive speed and the Bernoulli speed is about 0.5. Again, the solid curves are the best-fit curves, represented by Equation (5), that show the trend of hyperbolic decrease with increasing C_a.

6. SUMMARY

The concept of measuring the time delay of particles moving past two planes with a fixed separation was successfully applied to measure the speeds of water droplets and abrasives in UHP WJs and AWJs. A dual-disc apparatus originally used for measuring the speed of abrasives for sand blasting was upgraded for the intended measurements. The apparatus consisted of two coaxial discs rotating at the same speed. A set of two to four radial slots was machined on the upper disc. Compact discs were pinned to the lower disc to record the erosion patterns produced by the water droplets or abrasives. The displacement angles between the leading edges of the slots and the lines drawn through the centers of the erosion patterns were measured to determine the speeds of the water droplets and/or the abrasives [see Equations (1) and (2)]. Depending on the relative positions of the lines, the maximum, minimum, and average speeds of the abrasives can be determined. Using data discs made of different materials, the threshold speeds of the WJs and AWJs for those materials can be determined. The threshold speeds are defined as the speeds below which no erosion takes place on the surface of the data disc. From the geometry of the erosion patterns, the removal rates for different materials can also be measured.

Several series of laboratory experiments using a WTI Intelligent AWJ nozzle operating at several pressures with and without abrasives were conducted. The nozzle was mounted on a 5-axis ASI robotic manipulator. The most important findings are summarized below:

- The threshold speed of the WJ for Lexan is measured to be about 600 m/s, which is about 3 times that of the AWJ using Barton 220-mesh garnet; the threshold speeds of the abrasives change only marginally for materials from Lexan, and aluminum, to stainless steel. For the

WJs, only water droplets that have acquired speeds exceeding the threshold speed for the target material would remove the material from the data disc. In other words, for a CD made of Lexan, a portion of the kinetic energy of the water droplets in a UHP WJ is being wasted simply because of the high threshold speed. When Barton 220-mesh garnet is fed into the WJ, those particles acquiring speeds higher than 180 m/s will begin to remove material effectively from the disc. This is one of the main reasons that the AWJ is more powerful than the WJ.

- The material removal rate of the WJ drops noticeably when the abrasive feed port of the AWJ nozzle is open. Air drawn through the feed port tends to destabilize the WJ, causing the WJ to spread and interact with the sidewall of the mixing tube.
- The speed of water droplets exiting an AWJ nozzle with the abrasive feed port closed, V_w, agrees well with the Bernoulli speed, V_B, derived from the Bernoulli equation [Equation (3)]. Note that the speeds measured by the dual-disc apparatus are generally biased to the high value because only speeds higher than the threshold speed for the target material induce erosion marks that facilitate the speed measurement. On the other hand, the Bernoulli speed is a measure of the maximum speed of a top-hat velocity profile of the WJ. This explains in part the excellent agreement between V_w and V_B.
- Opening the feed port reduces the speed of the water droplets, V_{wa}, by 3 to 7%. A linear relationship between V_{wa} and V_w or V_B has been established [Equation (4)]. The material removal rate drops even further as it is proportional to the kinetic energy of the WJ or the square of the droplet speed (Figures 4 through 6).
- The dimensional and dimensionless abrasive speeds decrease hyperbolically with increasing C_a [Equation (5)]. On the other hand, the difference between the maximum and minimum abrasive speeds increases with increasing C_a. For C_a = 100% and p = 345 MPa, the average abrasive speed reduces to about 400 m/s, which is about one half of the Bernoulli speed but is still considerably higher than the threshold speed for stainless steel (≈ 230 m/s). The reduction in the material removal rate due to the drop in V_a is compensated for by the increase in the number of abrasive particles. For each application and experimental setup; there is an optimum value of C_a at which the material removal rate peaks. This optimum value is yet to be determined.

6. ACKNOWLEDGMENTS

This work is sponsored by a U.S. Army SBIR Contract No. DAAJ02-97-C-0025 and by internal funding for Waterjet Technology, Inc. The authors wish to thank Mr. Bob Legaspi for carrying out the measurements.

7. REFERENCES

Chen, W.-L., and Geskin, E. S., "Measurements of the Velocity of Abrasive Waterjet by the Use of Laser Transit Anemometer," *Proceedings 10th International Symposium on Jet Cutting Technology*, BHRG Fluid Engineering, Amsterdam, Netherlands, October 3-November 2, pp. 23-36, 1990.

Hashish, M., "Cutting with High-Pressure Abrasive Suspension Jets," *NSF Conference Proceedings*, SME, October, 1992.

Isobe, T., Yoshida, H., and Nishi, K., "Distribution of Abrasive Particles in Abrasive Waterjet and Acceleration Mechanism," *Proceedings of 9th International Symposium on Jet Cutting Technology*, Sendai, Japan, October 4-6, pp. 217-238, 1988.

Levy, A., *Solid Particle Erosion and Erosion Corrosion of Materials*, AMS International, Ohio, p. 4, 1995.

Liu, H.-T., Miles, P., and Veenhuizen, S. D., "CFD and Physical Modeling of UHP AWJ Drilling" *Proceedings of the 14th International Conference on Jetting Technology*, Brugge, Belgium, September 21-23, pp. 15-24, 1998.

Neusen, K. F., Gores, T. J., and Labus, T. J., "Measurement of Particle and Drop Velocities in a Mixed Abrasive Water Jet Using a Forward-Scatter LDV System," *Jet Cutting Technology*, Lichtarowicz, A. (Editor), Kluwer Academic Publishers, pp. 63-73, 1992.

Ruff, A. W., and Ives, L. K., "Measurement of Solid Particle Velocity in Erosive Wear," *Wear*, 35, pp. 195-199, 1975.

Stevenson, A. N. J., and Hutchings, I. M., "Scaling Laws for Particle Velocity in the Gas-Blast Erosion Test," *Wear* 181-183, pp. 56-62, 1995.

Swanson, R. K., Kilman, M., Cerwin, S., and Tarver, W., "Study of Particle Velocities in Water Driven Abrasive Jet Cutting," *Proceedings 4th U.S. Water Jet Conference*, ASME, Berkeley, CA, August 26-28, pp. 103-107, 1987.

Yanaida, Y., "Flow Characteristics of Waterjets," *Proceedings of the 2nd International Symposium on Jet Cutting Technology*, BHRA, England, April, 1974.

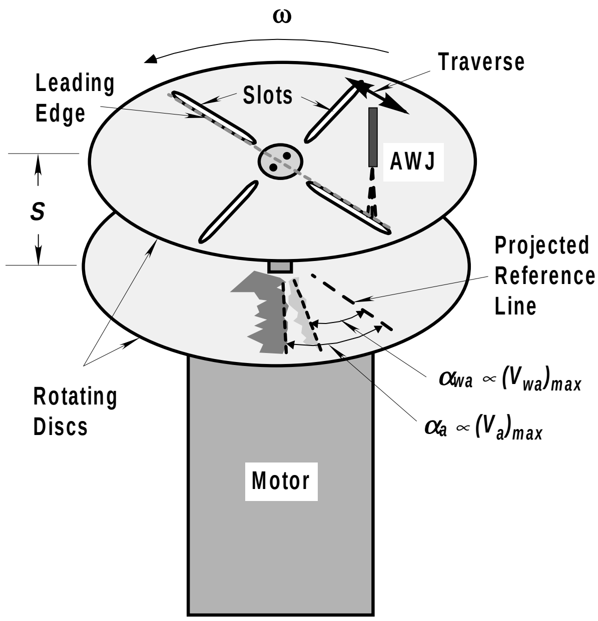

Figure 1. Conceptual Sketch of the Dual-Disc Method for Simultaneously Measuring Water-Droplet and Abrasive Speeds in an AWJ

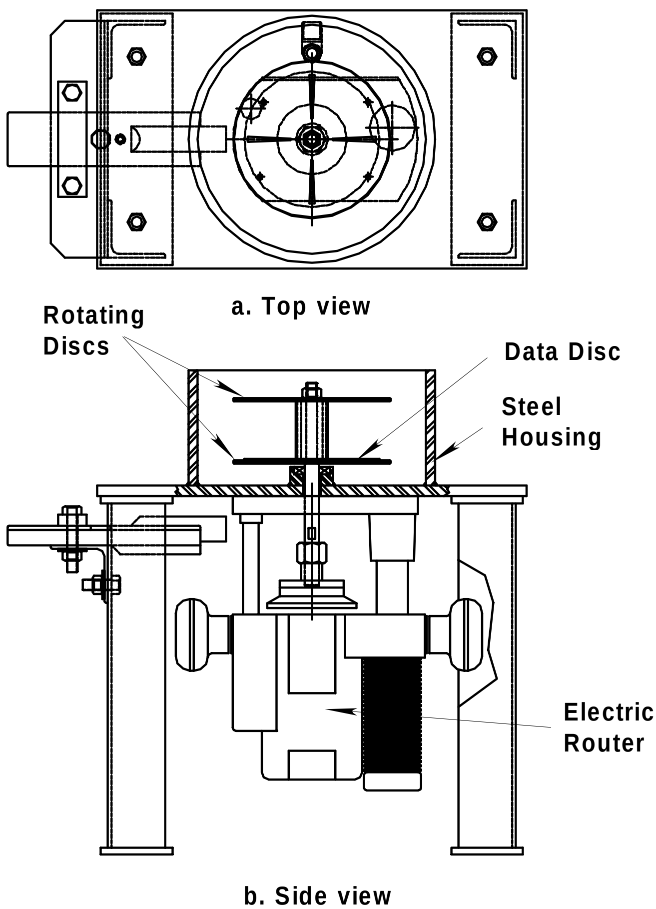

Figure 2. Engineering Drawing of the Dual-Disc Apparatus

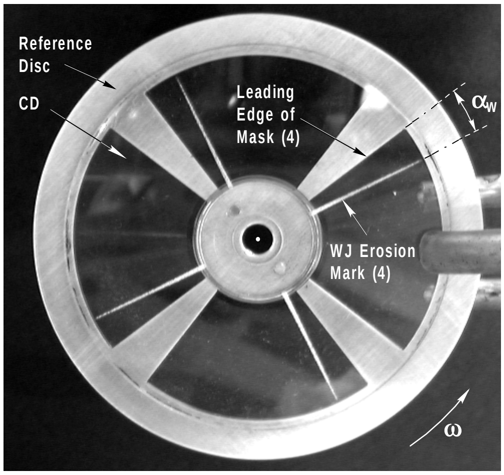

Figure 3. Erosion Patterns Created by a WJ on a CD Pinned to the Reference Disc.
Abrasive Port Closed, p = 345 MPa, WJ Traverse Speed = 1.27 m/s,
Rotational Speed = 23,800 rpm**.**

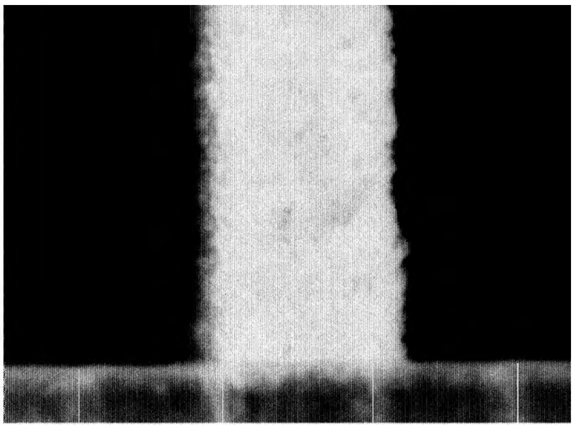

a. Port closed

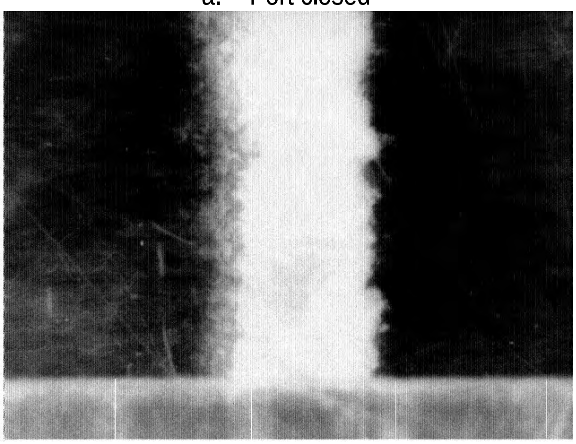

b. Port open

Figure 4. Comparison of Erosion Patterns Generated on the CD by a UHP WJ at 345 MPa (Top View). Scale: 1 mm/div.

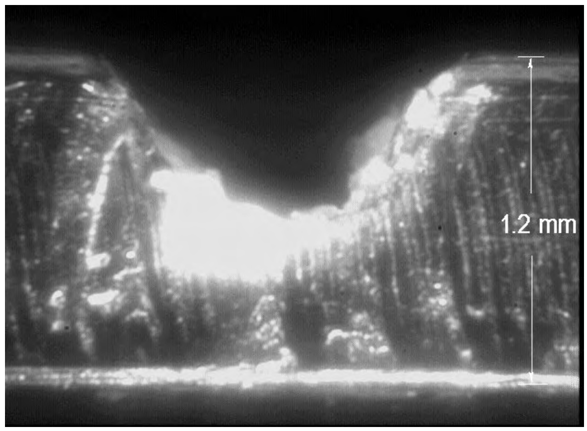

a. Port closed

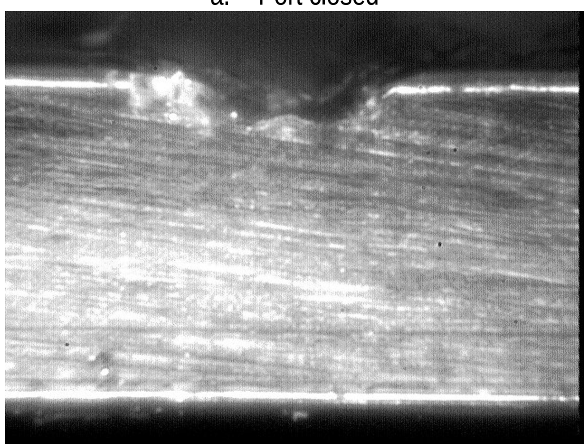

b. Port open

Figure 5. Comparison of Erosion Patterns Generated on the CD by a UHP WJ at 276 MPa (End View).

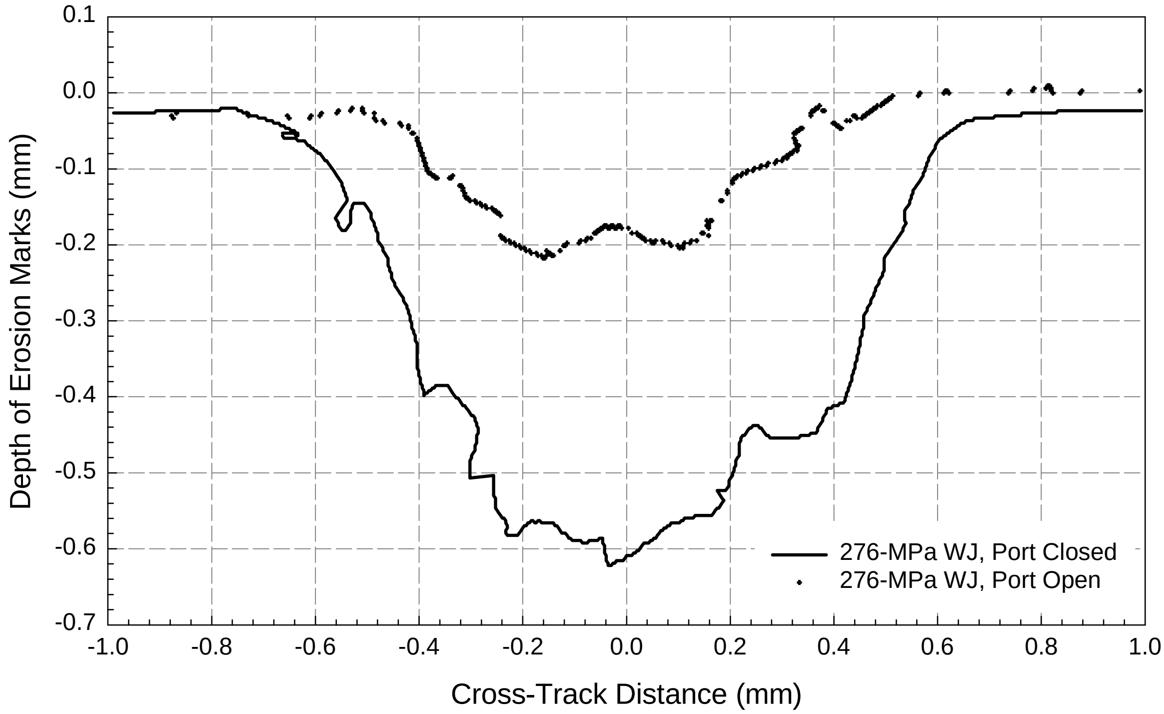

Figure 6. Effect of Abrasive Port Closure on the Erosion Depth Produced by a WJ

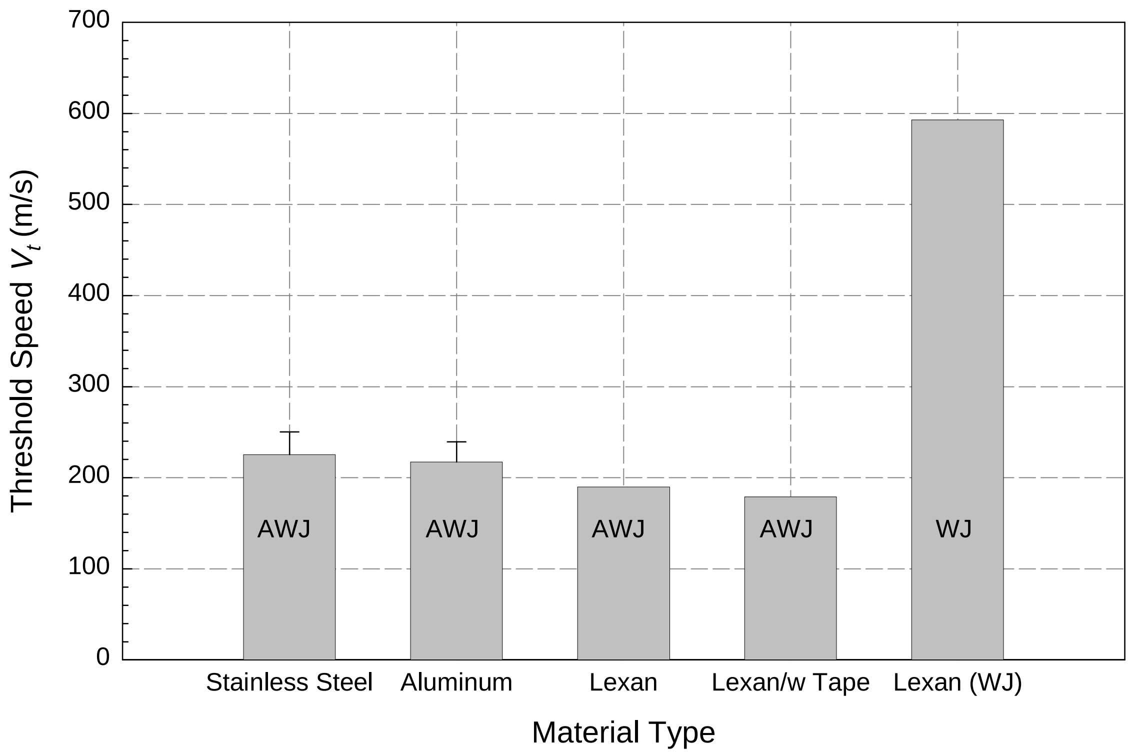

Figure 7. Threshold Velocities of WJ and AWJ for Several Materials. Note that V_t of the water droplets for metals are greater than 820 m/s, the Bernoulli speed at 345 MPa.

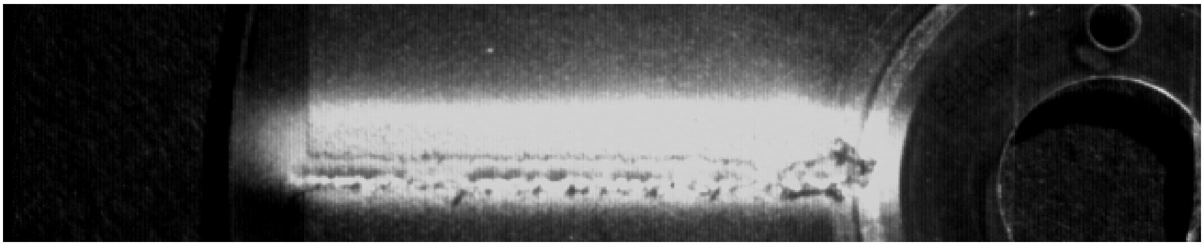

a. $\omega = 0$, $C_a = 10\%$

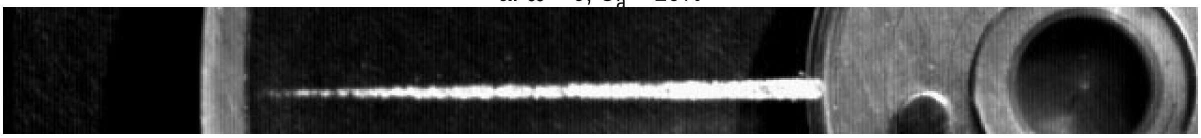

b. ω= 23,800 rpm, C_a = 0% (WJ with feed port open)

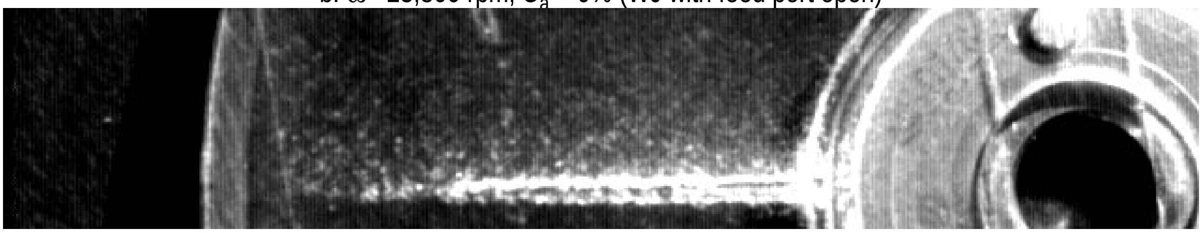

c. ω= 23,830 rpm, C_a = 10%

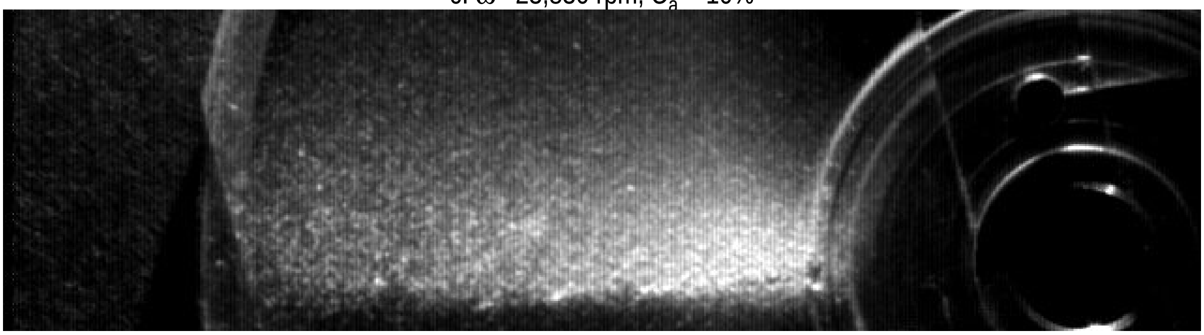

d. ω= 23,800 rpm, C_a = 40%

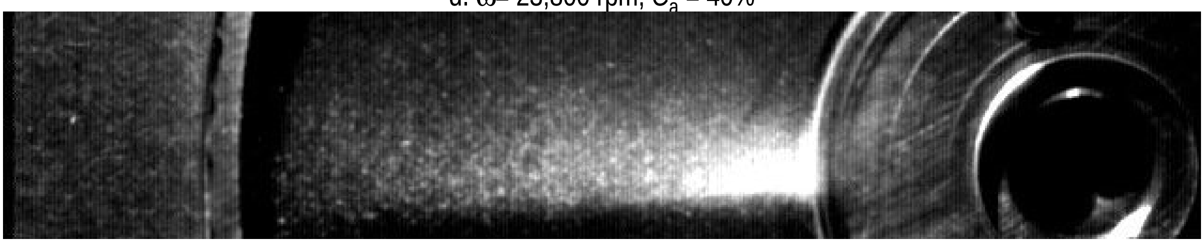

e. ω= 23,850 rpm, C_a = 50%

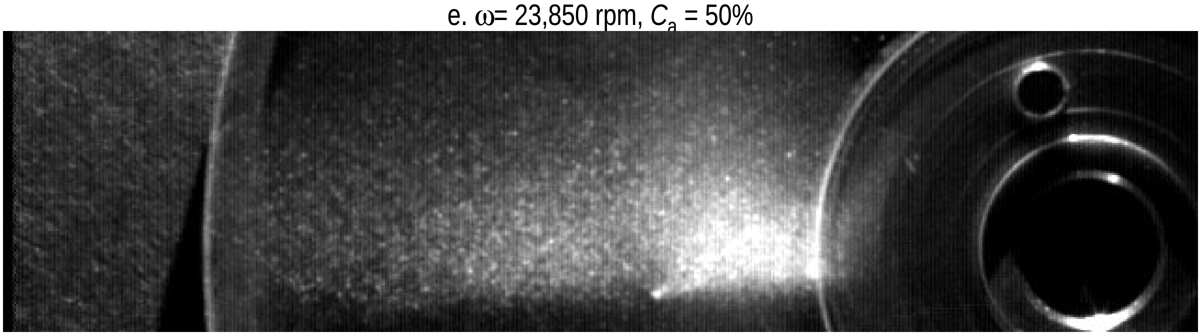

f. ω= 23,840 rpm, C_a = 100%

Figure 8. Erosion Patterns on CDs Generated by UHP WJs and AWJs at $p \approx$345 MPa

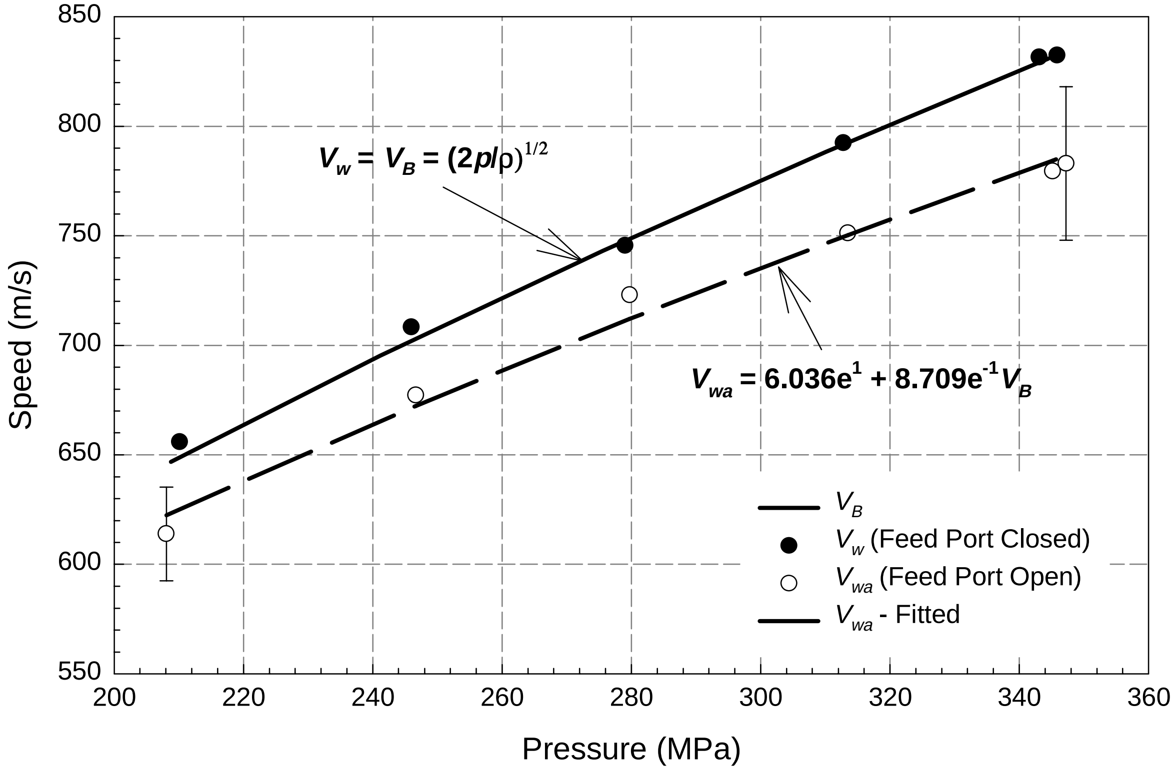

Figure 9. Average Water-Droplet Speed Measured with the Dual Disc Apparatus

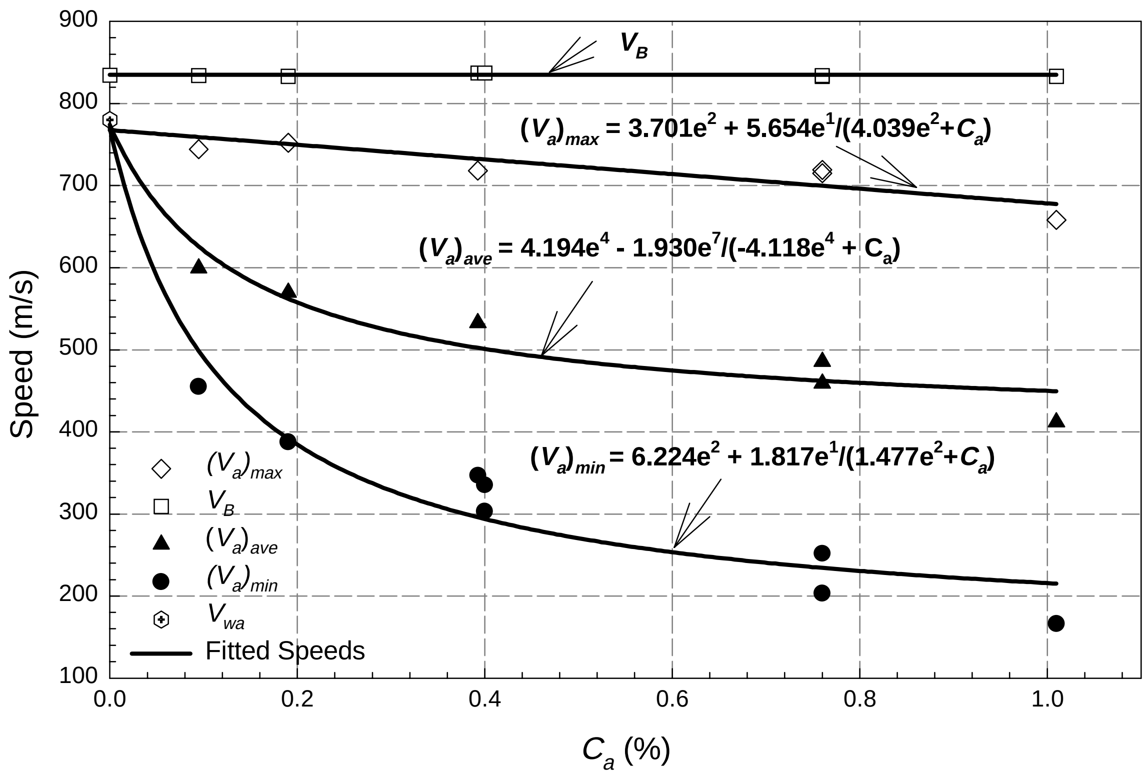

Figure 10. Abrasive Speeds as a Function of the Abrasive Mass Concentration. p = 345 MPa, 0.18/0.51 nozzle combination.

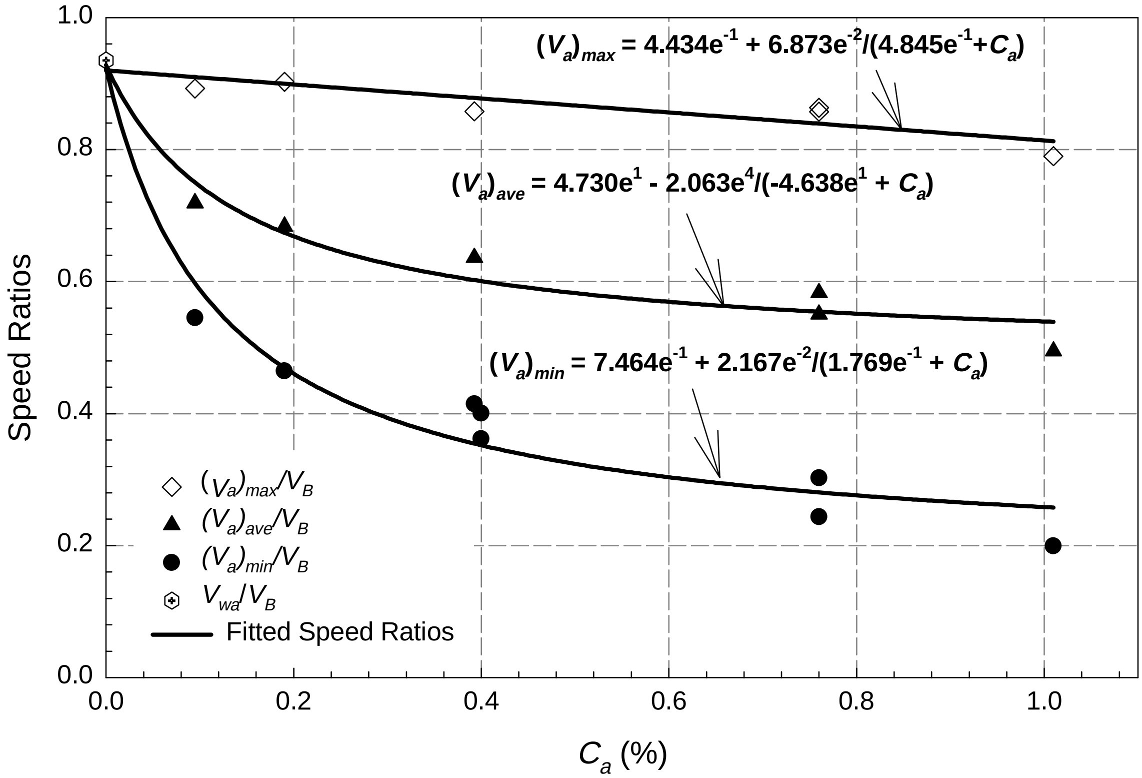

Figure 11. Abrasive and Bernoulli Speed Ratios as a Function of Abrasive Mass Flow Rate

10th American Waterjet Conference
August 14-17, 1999: Houston, Texas

Paper 15

CUTTING EFFICIENCY OF ABRASIVE WATERJET NOZZLES

Madhusarathi Nanduri, David G. Taggart, Thomas J. Kim
University of Rhode Island
Kingston, RI U.S.A.

ABSTRACT

The cutting efficiency of abrasive waterjet nozzles was investigated in conjunction with nozzle wear. It was observed that the cutting efficiency of the nozzle deteriorates as it wears. There is a correlation between wear and cutting efficiency. The operating conditions that produce the most efficient jets also cause the most wear in the nozzle.

Organized and Sponsored by the WaterJet Technology Association

1. INTRODUCTION

An abrasive water jet (AWJ) system typically consists of a high pressure pump, abrasive cutting head, abrasive delivery system, nozzle, motion system, control unit, spent abrasive catcher unit and settling tank. High pressure water flows through a sapphire or diamond orifice into the mixing chamber of the cutting head and creates a partial vacuum that draws in a metered flow of abrasive. The abrasive combines with the water jet to create the AWJ cutting stream that exits through the nozzle. Typical operating conditions are 200-350 MPa water pressure, mesh #50 - #120 abrasive, 0.24-0.40 mm orifice diameter, 0.76 - 1.70 mm nozzle diameter and 3.8 – 15.0 g/s abrasive flow rate. Robotic manipulation of the cutting head and careful control of cutting parameters result in excellent surface quality and precision in machining of complex geometries in practically any material.

The nozzle is the shortest lived component in the entire system. Until recently, nozzles were made from conventional tungsten carbide, which gave an effective life of about 4 hours when used with garnet abrasive. A new composite tungsten carbide nozzle material called ROCTEC® has recently been developed to extend the nozzle life up to 100 hours (Doty et al., 1989). Nevertheless, this material exhibits a relatively short life with hard abrasives such as Al_2O_3 and SiC (Ness et al., 1994), thereby limiting the cost effectiveness of AWJ machining with such abrasives.

Nozzle wear is a complex phenomenon influenced by the AWJ system parameters, and nozzle geometric and material parameters. It has been receiving significant attention (Nanduri et al., 1997, Taggart et al., 1997, Hashish 1997). Wear and cutting efficiency of the nozzle under varying geometric and AWJ system conditions are reported in this paper.

2. WEAR CHARACTERIZATION

Details of nozzle wear testing and measures are given in Nanduri et al., 1996. Nozzle wear is monitored through exit diameter, nozzle weight loss and internal bore profile measurements at periodic intervals. Weight loss rate is almost perfectly linear throughout the useful life of the nozzle in contrast to the exit diameter growth, which is highly non-linear. Therefore, weight loss rate is used in comparative nozzle performance evaluation. Methods to monitor the wear profile include casting the bore using a silicon resin, depth measurements using progressively larger gage pins inserted into the nozzle, and measurement of wear profile after sectioning the nozzle.

Figure 1 shows bore profiles of a WC/Co nozzle that was subjected to 3 hours of garnet abrasive wear at a water pressure of 310 MPa and an abrasive flow rate of 3.8 g/s. The wear profile is characterized by a wave-like wear pattern as revealed by the profile obtained from the sectioned nozzle. This actual profile correlates very well with the profile obtained by the pinning procedure. Pinning reveals the profile as a series of steps, which represent the trailing portions of the “waves”. Profiles in figure 2 (taken at 1, 2 and 3 hour intervals) clearly illustrate that pinning is a non-

® ROCTEC is a trademark of Greenfield Industries, Inc., or its affiliates destructive measuring technique that provides an excellent description of nozzle wear. These profiles reveal that as wear progresses, the wave-like structure grows in magnitude and propagates down the nozzle bore.

Accelerated wear test procedures were used to conduct parametric studies on nozzle wear and cutting efficiency quickly and cost effectively. The procedures use standard AWJ operating parameters and a hard abrasive (aluminum oxide) to accelerate the wear process. The validity of this procedure was demonstrated by conducting a series of long term wear tests using garnet abrasive and comparing the results with accelerated test results (Taggart et al., 1997). The trends observed in volume loss and exit bore growth in both short and long term data were similar.

3. CUTTING EFFICIENCY CHARACTERIZATION

Cutting efficiency tests conducted included depth of cut measurement on wedge shaped and uniformly thick samples (at constant speed), traverse speed to fully separate a specific thickness of material, and specific material removal rate. These tests revealed an excellent correlation between the different methods. In AWJ kerf cutting, minor changes in operating parameters affect the traverse speed to fully cut through a specified thickness, which limits the accuracy of measurement. This leads to the determination of a small range in cutting speed instead of a specific value. The depth of cut obtained on wedge shaped samples is also very sensitive to operating conditions. However, the target specific volume loss, defined as the volume of material removed per unit volume of abrasive, is a fairly repeatable value and easy to measure. The jet is traversed at a high speed to avoid complete penetration of the specimen. This ensures complete usage of jet energy for material removal. Specific volume loss is computed using specimen weight loss, specimen density, jet traverse time and abrasive flow rate, which are known quantities.

4. EXPERIMENTATION

Cutting efficiency and nozzle wear tests were conducted at the University of Rhode Island Waterjet Laboratory. In a typical wear test, the nozzle is installed in the cutting head and the jet stream is aligned. The abrasive flow rate and water pressure are adjusted. During the test, the jet is allowed to impinge on the steel balls in the catcher tank to dissipate its energy. The test is stopped at predetermined intervals for exit diameter, weight loss and bore profile measurements. A standard cutting efficiency test protocol was developed that has excellent reproducibility and accuracy. Cutting efficiency tests were conducted during the wear test measurement intervals. The duration of a cutting efficiency test was about 15 seconds, which was accounted for in the time segments of the wear test. Thus, during the tests, wear and cutting efficiency as a function of time as well as nozzle exit diameter, are simultaneously monitored. The cutting efficiency tests were repeated to average out any noise. Average depths of the randomly selected samples were used to confirm the trends observed.

The parameters investigated were nozzle length, inlet angle, nozzle diameter, orifice diameter, water pressure and abrasive flow rate. Accelerated wear tests (using aluminum oxide mesh #80 abrasive) were performed varying each parameter independently to understand its effect on nozzle wear. Tests were conducted using WC/Co nozzles with 60° inlet angles. Test and typical values of the parameters are given in table 1. The inlet angle tests were conducted using ROCTEC 100 nozzles with 1.0 mm bore diameter, 0.33 mm diameter orifice, 310 MPa water pressure, and an abrasive flow rate of 7.6 g/s.

To determine the cutting efficiency, grooving tests were conducted by traversing the abrasive waterjet across 50 mm long stainless steel samples (type SS 304) 6.4 mm thick at a constant rate of 17 mm/s. The standoff distance was kept constant at 1.2 mm. In reporting the results, exit diameter increase rate is expressed in %/min and weight loss rate in g/min. Cutting efficiency is expressed as the weight loss of the sample per gram of abrasive. The cutting efficiency of the nozzles tested remained essentially constant with less than 10% variation as long as the exit diameter growth was limited to within 10% of the initial diameter. Therefore, the cutting efficiency reported in most plots is an average value of cutting efficiencies obtained from nozzles whose exit diameter increased up to 10% of the initial diameter.

5. RESULTS AND DISCUSSION

5.1 Inlet Angle

A general trend of reduced exit bore growth with increasing inlet angle was observed in short (15 min) duration tests as shown in figure 3. However, longer duration tests on different inlet angle nozzles revealed identical nozzle lives (Nanduri 1997). A significant difference in the bore profiles of different inlet angle nozzles is the proportion of wear along the length of the nozzle. As the inlet angle increases, the profile becomes more “wavy”. Uniform bore profiles lead to uniform exit diameter growth. Therefore, smaller inlet angle nozzles exhibit superior linearity in exit diameter growth compared to larger inlet angle nozzles. Cutting efficiencies of the 10° and 30° nozzles are shown in figure 4. The cutting efficiency of the 10° nozzle at equivalent exit bore size is always superior to that of the 30° nozzle. The figure also shows there is a direct correlation between percent exit diameter increase and percent reduction in cutting efficiency. The lower inlet angle results in a much more focused stream and increases the momentum transfer efficiency. The jet stream emanating from the 10° nozzle was much more coherent from visual observations during the wear tests. The kerf edge and surface quality of the cut was always superior with the 10° nozzle. The depth of cut was also more uniform. Figures 5 and 6 show the bore profiles of the 10° and 30° nozzles. The profiles show that undulations occur much earlier in time and are more pronounced in the 30° nozzle when compared to the 10° nozzle, which causes non-linear exit bore growth. The increased non-linearity of the bore profiles also results in reduced cutting efficiency. The more uniform internal profile of the 10° nozzle clearly increases its cutting efficiency.

5.2 Nozzle Length

Exit bore growth decreases with an increase in nozzle length as shown in figure 7. Nozzle weight loss rate increases with increasing nozzle length as expected. If nozzle weight loss rate is normalized and plotted as grams per minute per unit length, it shows the same decreasing trend as the exit diameter wear rate curve. Bore profiles of nozzles with different lengths show that although the internal profiles develop identically, nozzle length has a direct influence on the exit bore growth by delaying the developing wear profile from reaching the exit. The flow pattern upstream within the nozzle is unaffected by an increase in nozzle length. The effect of nozzle length on cutting efficiency is shown in figure 8. As the length increases the transverse velocity of the abrasive particles decreases and the particles are better aligned with the flow resulting in increased cutting efficiency. It is clear from figure 8 that beyond a certain length the cutting efficiency does not increase any further and the added manufacturing and material costs may not be justified.

5.3 Nozzle Diameter

Figure 9 shows the exit bore growth (%/min) and weight loss rate (g/min) as a function of nozzle diameter. The exit wear curve suggests that for a particular orifice/nozzle combination, nozzle wear would reach a maximum. It is known that keeping the ratio, R_o, of orifice diameter to nozzle diameter around 0.3-0.4 (all other process parameters remaining constant) will result in optimum mixing conditions. Cutting efficiency results (figure 10) indicate that mixing conditions resulting in most efficient momentum transfer to the abrasive particles not only enhance the cutting performance but also increase nozzle wear.

The bore profiles of the 0.79 mm nozzle reveal a flow that is choked excessively resulting in inefficient transfer of momentum from the water to the abrasive. There is excessive localization of wear in the upper portion of the nozzle that leads to increased weight loss of the nozzle. On the contrary, the 1.63 mm diameter nozzle is too large to provide efficient momentum transfer. Both cases result in reduced exit wear. A 1.14 mm diameter nozzle ($R_o = 0.33$) results in typical mixing conditions and exhibits nominal exit wear.

5.4 Orifice Diameter

Figures 11 and 12 summarize the effect of orifice diameter on nozzle wear and cutting efficiency. The correlation between cutting efficiency and nozzle wear is again evident. The cutting efficiency increases with increase in orifice size. Figure 11(b) indicates a drop in nozzle weight loss rate at high water flow rates (larger orifices). As the water flow rate increases, the abrasive-to-water mass ratio (R) decreases and there is improved transfer of momentum to the abrasive particles. However, velocity measurements (Chen and Geskin 1991) indicate that the acceleration of abrasive particles is dependent on the rebound effect, which is a function of distance between the jet's core and the surrounding nozzle wall. The distance between the jet and the nozzle wall decreases with increasing R_o, therefore, an optimum condition (a maximum) is expected. This suggests that the cutting efficiency may not improve beyond a limit.

5.5 Abrasive Flow Rate

The effect of abrasive flow rate on nozzle wear and cutting efficiency is summarized in figures 13 and 14. Particle velocity tends to decrease with an increase in abrasive flow rate (Chen and Geskin 1991). Conversely as the mass flow decreases, velocity increases, and as the flow rate tends to zero, the velocity tends to equal the waterjet velocity. In the range of flow rates tested, it was observed that the weight loss rate of the nozzle increased almost linearly with an increase in flow rate, as expected. The cutting efficiency results show that the maximum efficiency is attained at a flow rate of 7.6 g/s. Beyond a certain limit, increase in abrasive flow rate increases the loading ratio, R, to a level where energy transfer starts to deteriorate.

5.6 Water Pressure

As the water pressure increases, nozzle weight loss and cutting efficiency increase due to higher water flow rate and velocity. This is clear from figure 15, which shows the exit bore growth and weight loss rate as a function of abrasive flow rate. Cutting efficiency results shown in figure 16 correlate well with the wear results.

6. CONCLUSIONS

- Cutting efficiency of abrasive waterjet nozzles was investigated in conjunction with nozzle wear.
- The effects of nozzle length, diameter, inlet angle, orifice diameter, abrasive flow rate and water pressure were systematically investigated.
- Cutting efficiency of the nozzle deteriorates as it wears. There is a direct correlation between nozzle wear and cutting efficiency. It was observed that the operating conditions that produce the most efficient jets for cutting purposes also cause the most wear in the nozzle.

7. REFERENCES

Chen, W.L. and Geskin, E.S., 1991, "Measurement of the Velocity of Abrasive Waterjet by the Use of Laser Transit Anemometer," *10th International Symposium on Jet Cutting Technology*, Amsterdam, 31 Oct. - 2 Nov. 1990, Elsevier Science Publishers Ltd., pp. 23-36.

Doty, P.A., Groves, K.O. and Mort, G., 1989, "Composite Carbides - A New Class of Wear Materials from the ROC Process," *First International Ceramic Science and Technology Congress*, Anaheim, CA.

Hashish, M., 1997, "Mixing Tube Material Effects and Wear Patterns," In *Proceedings of the 9th American Water Jet Conference*, Dearborn, MI, pp. 211-222.

Nanduri, M., Taggart, D.G., Kim, T.J., Ness, E., Haney, C. and Bartkowiak, C., 1996, "Wear Patterns in Abrasive Waterjet Nozzles," In *Proceedings of the 13th International Conference on Jetting Technology - Applications and Opportunities,* BHR Group, Mechanical Engineering Publications Limited, London, pp. 27-43.

Nanduri, M., Taggart, D.G., Kim, T.J., Haney, C. and Skeele, F.P., 1997, "Effect of the Inlet Taper Angle on AWJ Nozzle Wear," In *Proceedings of the 9th American Water Jet Conference,* Dearborn, MI, pp. 223-238.

Ness, E.A., Dubensky, E., Haney, C., Mort, G. and Singh, P.J., 1994, “New Developments in ROCTEC Composite Carbides for Use in Abrasive Waterjet Applications,” *Proceedings of the 12th International Conference on Jet Cutting Technology*, Rouen, France, pp.195-211.

Taggart, D.G., Nanduri, M., Kim, T.J., and Skeele, F.P., 1997, “Evaluation of an accelerated wear test for AWJ nozzles,” In *Proceedings of the 9th American Water Jet Conference*, Dearborn, MI, pp.239-250.

8. ACKNOWLEDGEMENTS

The authors would like to acknowledge Boride Products for providing the nozzles used in this study.

Table 1. Test parameters and values

Parameter	Values Tested	Typical Value
Nozzle length	32.5, 50.8, 76.2 and 101.6 mm	50.8 mm
Nozzle inlet angle	10°, 20°, 30°, 40°, 50° and 180°	60°
Nozzle diameter	0.79, 1.14 and 1.63 mm	1.14 mm
Orifice diameter	0.28, 0.33, 0.38 and 0.43 mm	0.38 mm
Water Pressure	172, 241, 310 and 359 MPa	310 MPa
Abrasive Flow Rate	1.9, 3.8, 5.7, 7.6, 9.5 and 11.4 g/s	3.8 g/s

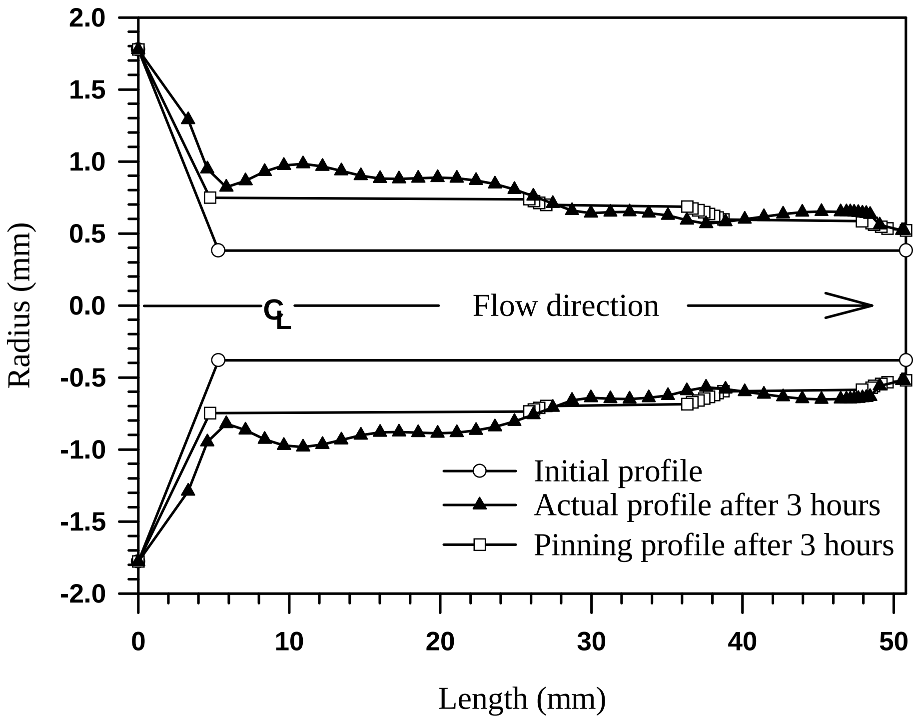

Figure 1. Comparison of pinned and actual profiles of WC/Co nozzle after 3 hours testing.

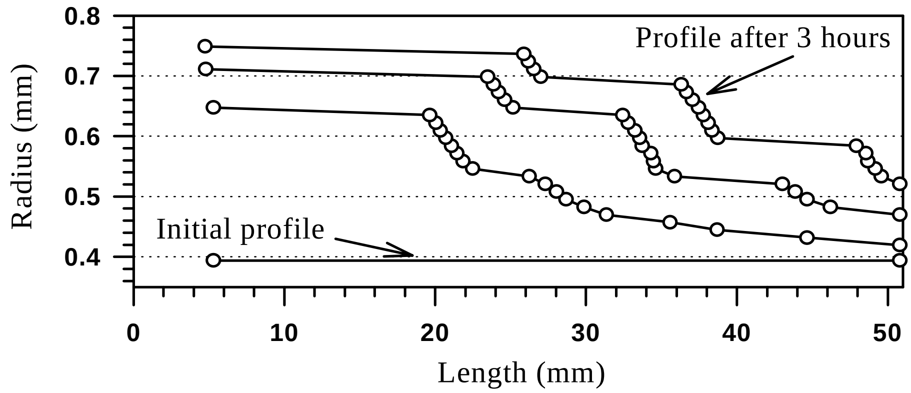

Figure 2. Bore profiles of WC/Co nozzle (nozzle center at Y zero).

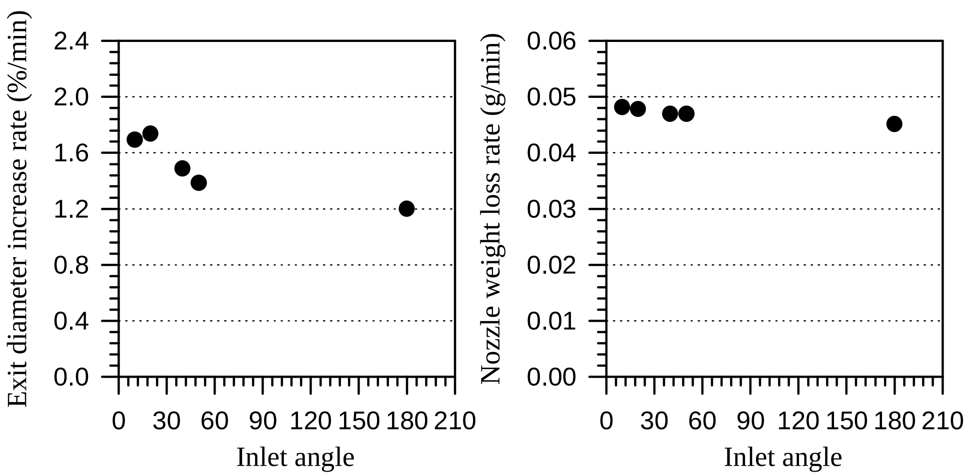

Figure 3. Effect of inlet angle on nozzle wear. (a) Exit diameter increase rate and (b) Nozzle weight loss rate.

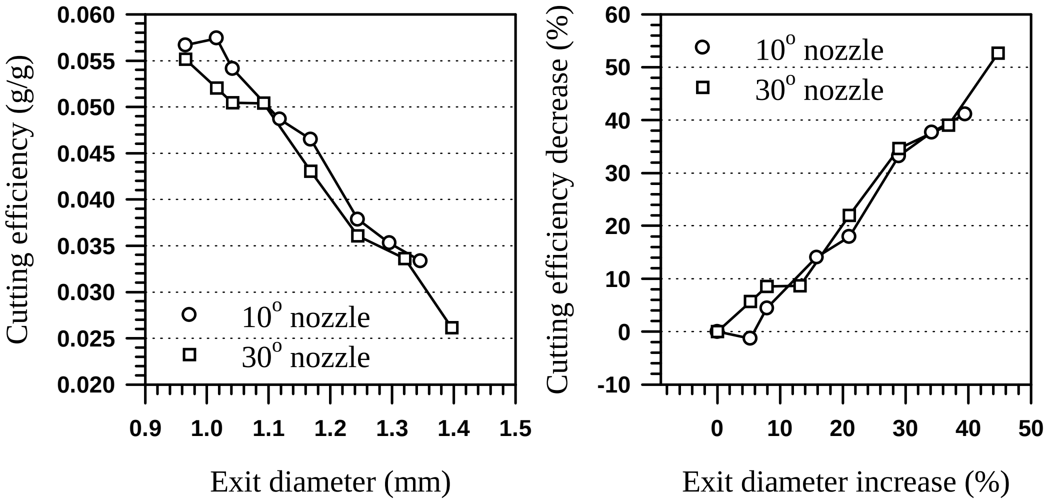

Figure 4. Cutting efficiency of 10° and 30° inlet angle nozzles.

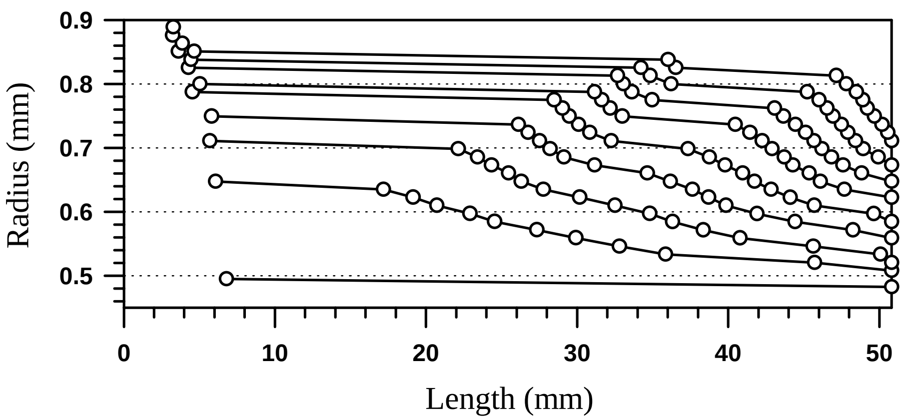

Figure 5. Bore profiles of 10° inlet angle nozzle at 0 - 40 minutes in 5 minute intervals.

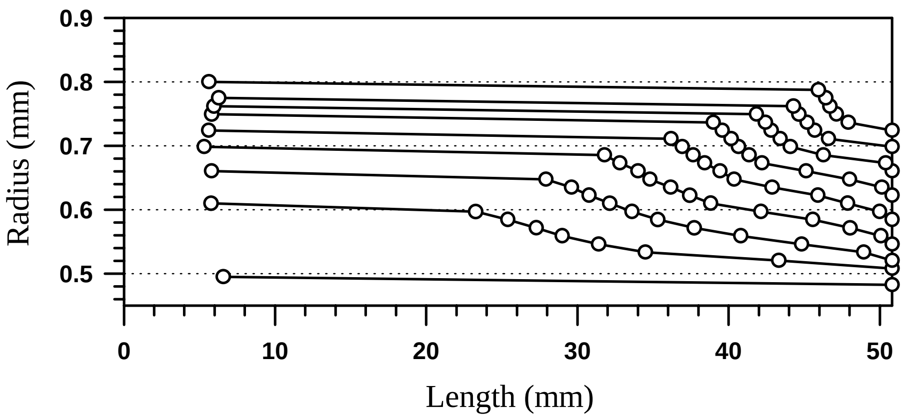

Figure 6. Bore profiles of 30° inlet angle nozzle at 0 - 40 minutes in 5 minute intervals.

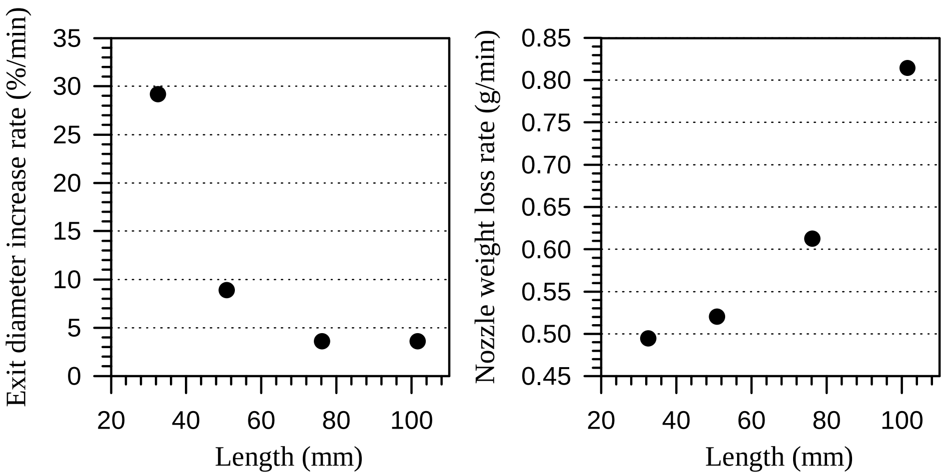

Figure 7. Effect of nozzle length on nozzle wear. (a) Exit diameter increase rate and (b) Nozzle weight loss rate.

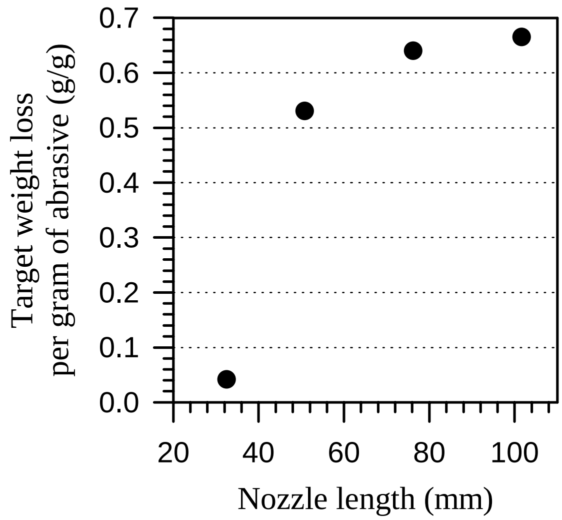

Figure 8. Effect of nozzle length on cutting efficiency.

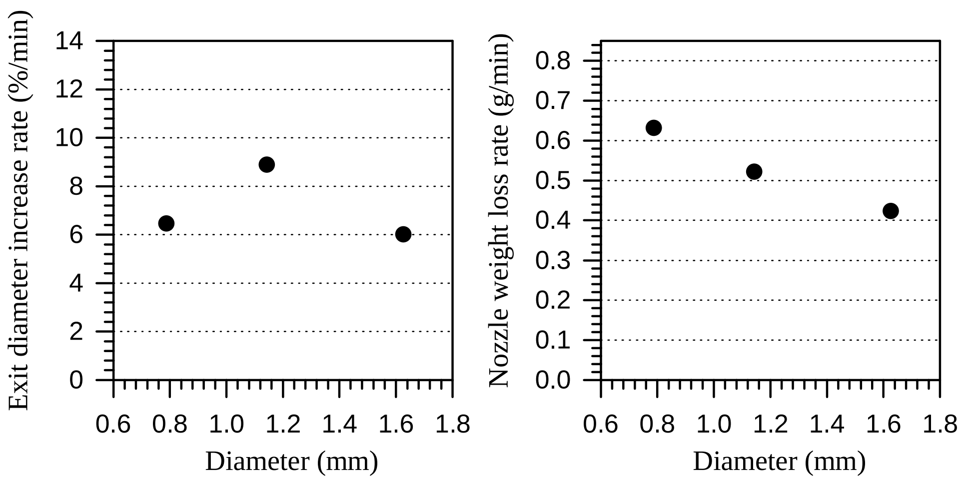

Figure 9. Effect of bore diameter on nozzle wear. (a) Exit diameter increase rate and (b) Weight loss rate.

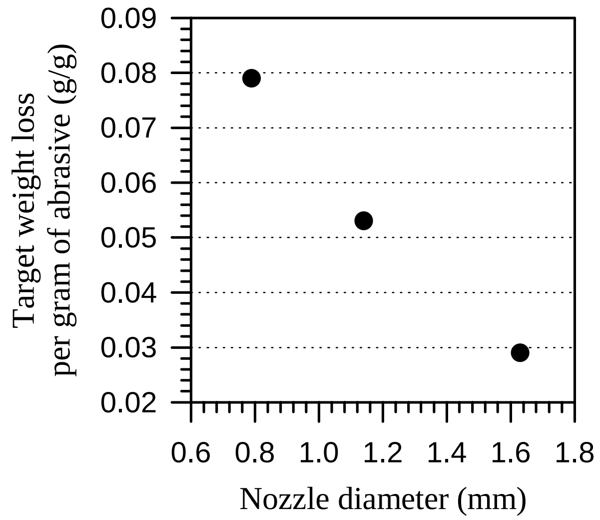

Figure 10. Effect of nozzle diameter on cutting efficiency.

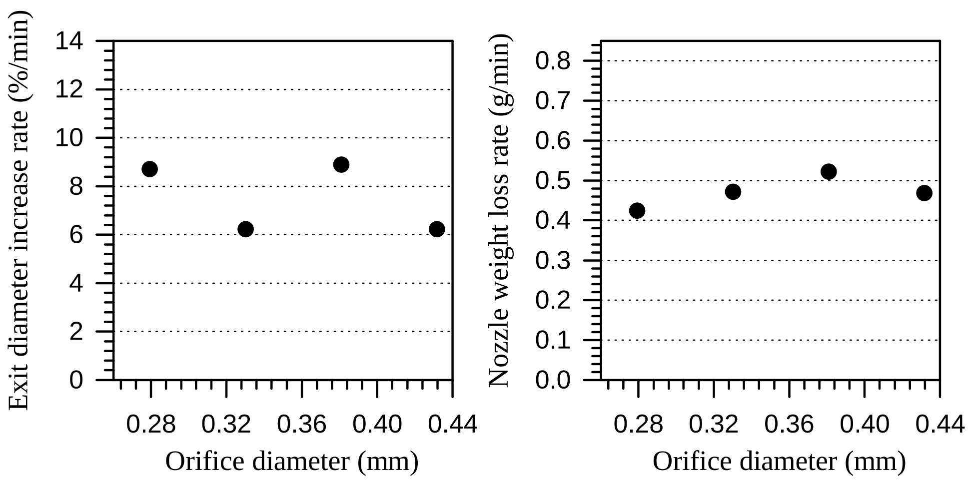

Figure 11. Effect of orifice diameter on nozzle wear. (a) Exit diameter increase rate and (b) Nozzle weight loss rate.

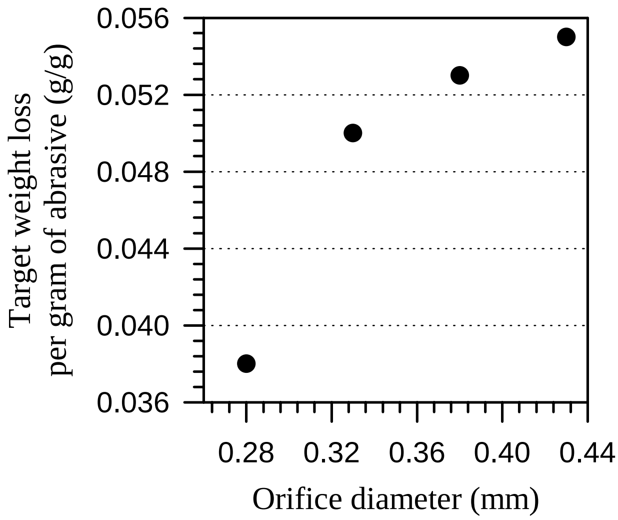

Figure 12. Effect of orifice diameter on cutting efficiency.

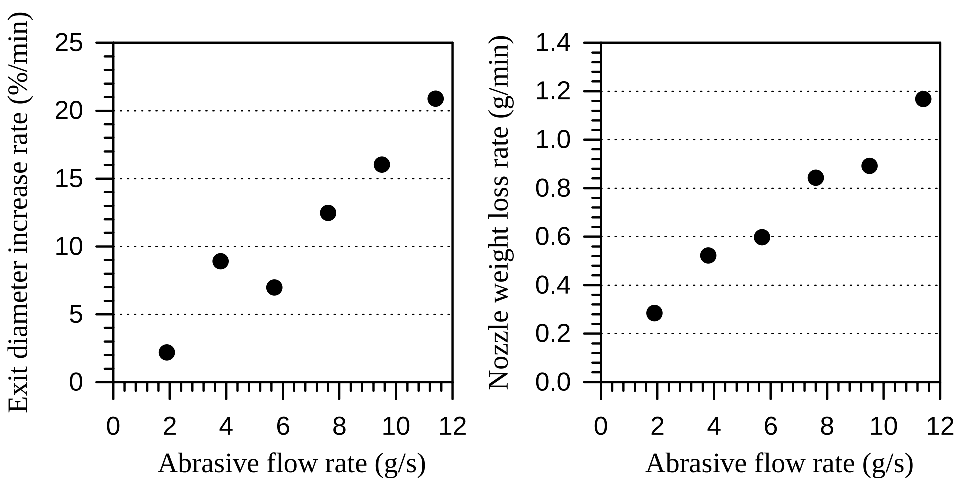

Figure 13. Effect of abrasive flow rate on nozzle wear. (a) Exit diameter increase rate and (b) Nozzle weight loss rate.

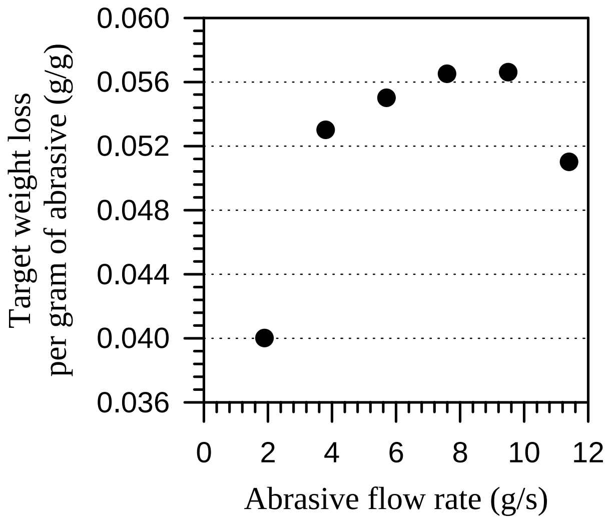

Figure 14. Effect of abrasive flow rate on cutting efficiency.

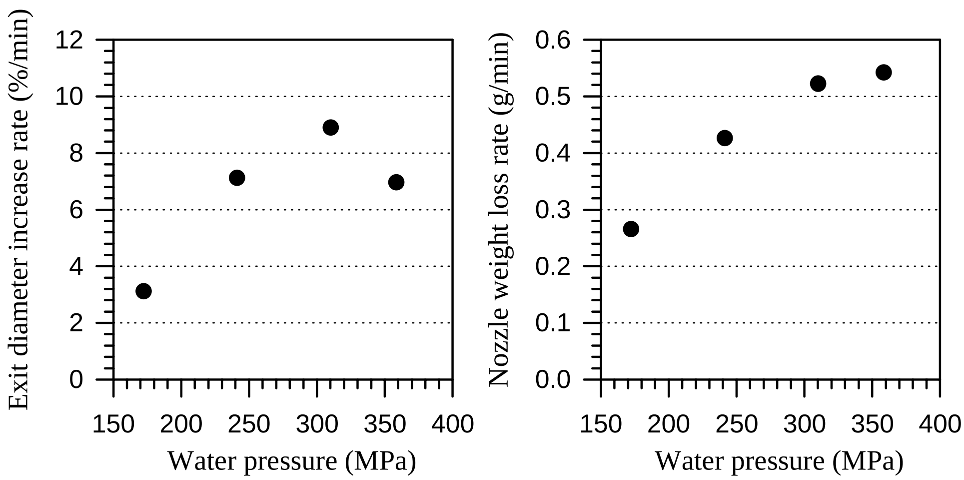

Figure 15. Effect of water pressure on nozzle wear. (a) Exit diameter increase rate and (b) Nozzle weight loss rate.

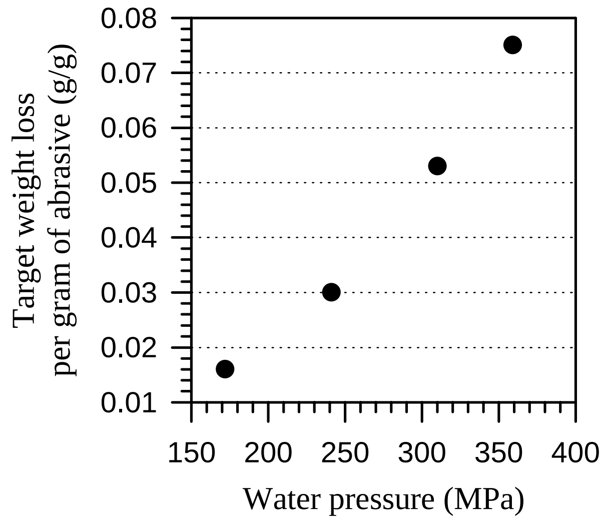

Figure 16. Effect of water pressure on cutting efficiency.

10th American Waterjet Conference
August 14-17, 1999: Houston, Texas

Paper 16

STUDY ON DYNAMIC CHARACTERISTIC OF AIR NUCLEI IN AERATED WATER JET

Jinmu Zhu, Jingzhi Liu, Hongqi Lu
Wuhan University of Hydraulic and Electric Engineering
Wuhan, Hubei, P. R. China

ABSTRACT

In this paper, by analysis of the motion process of aerated water jet in the air and consideration of pulsation characteristics of turbulence, the jet velocity of the flow fluid can be expressed by means of Fourier integral equation. Provided that the air quantity aerated is very small and there is no interference between nuclei, the pressure gradient along the direction of jet axis is zero and thus the volume of the air nucleus is no variation through the motion process. Since the cavitation flow immediately jets into the air, the air nucleus can be considered as a small rigid spherical particle after the jets enter the air. The computational expression of the air nucleus size in the aerated water jet is derived by means of BBO equation. Based on the particle size of the air nucleus solved as before, Lamb's research work and the hypothesis that liquid is inviscid, incompressible and in infinite region while gas is in adiabatic state, bubble-wall velocity is derived. The formulae to calculate the velocity and pressure fields of liquid are also presented.

Organized and Sponsored by the WaterJet Technology Association

1. INTRODUCTION

Cavitation has a powerful destructive action on material. The attention is paid to taking advantage of this destructive action to clean or cut by more and more researchers. If proper quantity of the air is aerated in waterjet, cavitation occurrence will be speeded up, which is conducive to cleaning or cutting. Liu Jingzhi et al. (1993) has developed a type of cavitating waterjet spray head as seen in Figure 1. It is mainly composed of waterjet nozzle, suction chamber and throat pipe. The high-pressure water jets out of water nozzle and entrains the air in the suction chamber, then enters the throat pipe together. In the throat pipe, the air entrained is broken up into micro-bubble by waterjet. Since advisable quantity of the air is entrained, the quantity of foreign matter in water increases and reduces tensile strength of water. Cavitation occurrence is accelerated (Knapp et al., 1970). The micro-bubble and cavitating bubbles (both are called air nuclei) evenly mix with waterjet, which forms cavitating waterjet in the air that jets out of the exit of the throat pipe.

After the jets enter the air, the bigger air nuclei will escape from waterjet or collapse and perish before they reach material surface; the smaller will dissolve in water directly. These two types of air nuclei have not destructive action on material and thus do not achieve the goal of cutting. Only have the air nuclei which do not escape from waterjet and not dissolve in water and are able to follow waterjet destructive action on material. When these air nuclei reach the surface of material, because of the action of bumping pressure, they abruptly collapse and perish, and meanwhile powerful pressure produces so as to cut or clean

Obviously, the action of the cavitation waterjet on the material is related to the flow field around the air nucleus after and before it collapses and perishes. The size of the air nucleus before the burst of it has a significantly influence on the flow field structure after the burst of the air nucleus. In this paper, by analysis of the motion process of aerated water jet in the air and consideration of pulsation characteristics of turbulence, the jet velocity of the flow fluid can be expressed by means of Fourier integral equation. The computational expression of the air nucleus size in the aerated water jet is derived by means of BBO equation. The flow fields when the air nucleus collapses is also analyzed.

2. DETERMINATION OF THE SIZE OF THE AIR NUCLEI

2.1 Unsteady Phenomenon of Jet

The consideration of water spraying into the air is taken into. When the flow rate is large enough, the surface of jet will take on wave because of disturbance, which is unsteady phenomenon of jet. It is reasonable to express the turbulent velocity of jet by means of Fourier integral equation, i.e.,

$$u = \int_{-\infty}^{\infty} E(\omega) e^{-i\omega t} d\omega \tag{1}$$

$$u_g = \int_{-\infty}^{\infty} S(\omega)E(\omega)e^{-(i\omega t+\varphi)}d\omega \qquad (2)$$

where u is the velocity of liquid in aerated waterjet; ω is angular velocity, $\omega = 2\pi f$; f is the turbulent frequency of jet; $E(\omega)$ is the amplitude dependent of ω; $S(\omega) = u_g / u$ is the slip ratio; φ is the difference of phase angle between the velocities of the air and liquid.

Generally speaking, fully developed turbulent flow includes various turbulent frequencies from low to high. The higher the frequency is, the less the action on heat, momentum, mass transfer is. The momentum, mass, heat transfer is mainly dependent on lower frequency large eddy and higher frequency small eddy dissipates energy, so it is mainly dependent upon lower frequency large eddy for the air nucleus to be able to gain momentum and to follow liquid to move. The turbulent frequency f can be less value. On the other hand, when $S(\omega)$ value is less, bigger air nuclei may escape from waterjet and smaller may dissolve in water, so $S(\omega)$ value cannot be too less. When $S(\omega)$ is close to $S = 1$, the air nuclei can better follow liquid to move. Once the following condition is known, the size of air nucleus may be determined. $S(\omega)$ can be determined in next section.

2.2 BBO Equation

Provided that (1) the air quantity aerated is very less; (2) there is no interference between nuclei; (3) the gradient of the pressure along the direction of axis of jet is zero and thus the volume of the air nucleus is no variation through the motion process since the cavitation flow immediately jets into the air, the air nucleus can be considered as a small rigid spherical particle after the jets enter the air.

Consideration of a flow field constructed by viscous flow fluid is taken into, to place a small sphere of a in radius in the field, not to vary boundary condition of flow and initial condition for far enough away from the core of small sphere. Since the flow fluid has of viscous, the velocity of the fluid mass on the surface of the sphere is equal to the velocity of the mass on the spherical surface. The relative velocity of fluid mass in the field to the core of small sphere is very low. According to superposition theorem and Newton's Law II, the kinetic equation of a small rigid spherical particle in absolute coordinate system (Maxey et al., 1983) can be obtained as following

$$\begin{aligned} m_g \frac{dV_i(t)}{dt} &= (m_g - m_F)g_i + m_F \frac{Du_i^F}{Dt}\Big|_{Y(t)} - \frac{1}{2} m_F \frac{d}{dt}\left\{V_i(t) - u_i^F{}_{[Y(t),t]}\right\} \\ &- 6\pi a\mu\left\{V_i(t) - u_i^F{}_{[Y(t),t]}\right\} - 6\pi a^2 \mu \int_{-\infty}^{t} \frac{\frac{d}{dt}\left\{V_i(t) - u_i^F{}_{[Y(t),t]}\right\}}{\sqrt{\pi\nu(t-\tau)}} d\tau \\ &+ \pi a^3 \mu \nabla^2 u_i^F\Big|_{Y(t)} \end{aligned} \qquad (3)$$

where m_g is the mass of particle; m_F is the mass of liquid of being same volume as that of the particle; g_i is the component of acceleration of gravity; $V_i(t)$ is the component of the velocity of the core of particle in the absolute coordinate system; u_i^F is the absolute velocity of undisturbed flow field; $Y(t)$ is the position vector of small rigid sphere in absolute coordinate system; a is the radius of particle; μ is dynamic viscosity; ν is kinematic viscosity.

We suppose once more that: (1) velocity gradient of undisturbed flow field is very less; (2) the component of acceleration of gravity is neglected; (3) the flow is incompressible and potential; (4) only is one dimension flow considered, so $V_i(t)$ becomes u_g and u_i^F becomes u, and thus simplified BBO equation changes into

$$m_g \frac{du_g}{dt} = m_F \frac{du}{dt} - \frac{1}{2} m_F \frac{d(u_g - u)}{dt} - 6\pi a\mu(u_g - u) - 6\pi a^2 \mu \int_{-\infty}^{t} \frac{\frac{d}{d\tau}(u_g - u)}{\sqrt{\pi\nu(t-\tau)}} d\tau \tag{4}$$

2.3 Determination of the Size of the Air Nuclei in Aerated Waterjet

Consideration of aerated waterjet entering the air is taken into. The gradient of the pressure along the direction of axis of jet is zero and thus the density of the air nucleus in jet is no variation before it reaches the surface of material and collapses. It means that the air nucleus can be considered as a small rigid spherical particle and solved by means of BBO equation.

The diameter of the air nucleus is D_0, radius R_0, density ρ_g, velocity u_g, and the density of water is ρ, velocity u. Substuting into equation (4), we have

$$\begin{aligned} &\frac{\pi}{6} D_0^3 \rho_g \frac{du_g}{dt} = \frac{\pi}{6} D_0^3 \rho \frac{du}{dt} + 3\pi\mu D_0 (u - u_g) + \frac{\pi}{12} D_0^3 \rho \left(\frac{du}{dt} - \frac{du_g}{dt}\right) \\ &+ \frac{3}{2} D_0^2 \sqrt{\mu\pi\rho} \int_{-\infty}^{t} \left\{ \left[\frac{d}{dt}(u - u_g) \right] / \sqrt{t-\tau} \right\} d\tau \end{aligned} \tag{5}$$

The above equation can be rewritten

$$\frac{du_g}{dt} + Au_g = Au + B\frac{du}{dt} + C\int_{-\infty}^{t} \frac{\frac{d}{\tau}(u - u_g)}{\sqrt{t-\tau}} d\tau \tag{6}$$

where $A = \dfrac{36\mu}{(2\rho_g + \rho)D_0^2}$, $B = \dfrac{3\rho}{2\rho_g + \rho}$, $C = \dfrac{18\mu}{(2\rho_g + \rho)}\sqrt{\dfrac{\rho\mu}{\pi}}$.

Considering equation (1) and (2), we obtain

$$\frac{du_g}{dt} = -i\int_{-\infty}^{\infty} \omega S E e^{-i(\omega t+\varphi)} d\omega \tag{7}$$

$$\frac{du}{dt} = -i\int_{-\infty}^{\infty} \omega E e^{-i\omega t} d\omega \tag{8}$$

$$\int_{-\infty}^{t} \frac{du_g / dt}{\sqrt{t-\tau}} d\tau = \int_{-\infty}^{t} \frac{-i\int_{-\infty}^{\infty} S\omega E e^{-i(\omega t+\varphi)} d\omega}{\sqrt{t-\tau}} d\tau \tag{9}$$

Equation (9) can be rewritten

$$\int_{-\infty}^{t} \frac{du_g / dt}{\sqrt{t-\tau}} d\tau = -i(i+1)\int_{-\infty}^{\infty} \sqrt{\frac{\pi\omega}{2}} S E e^{-i(\omega t+\varphi)} d\omega \tag{10}$$

In the same method, we can obtain

$$\int_{-\infty}^{t} \frac{du / dt}{\sqrt{t-\tau}} d\tau = -i(i+1)\int_{-\infty}^{\infty} \sqrt{\frac{\pi\omega}{2}} E e^{-i\omega t} d\omega \tag{11}$$

Substituting equation (7), (8), (10), and (11) into equation (6) and deriving, we obtain

$$S = \sqrt{\frac{(A + C\sqrt{\pi\omega / 2})^2 + (B\omega + C\sqrt{\pi\omega / 2})^2}{(A + C\sqrt{\pi\omega / 2})^2 + (B + C\sqrt{\pi\omega / 2})^2}} \tag{12}$$

Given f , ρ_g / ρ , S , the diameter D_0 of the air nucleus can be calculated out

3. FLOW FIELD AROUND AIR NUCLEUS IN THE PROCESS OF BURST

3.1 Foundational Theory

The kinetic and continuity equations for incompressible, non-steady, potential, ideal fluid can be expressed in tensor as

$$\frac{\partial u_i}{\partial t} + u_j \frac{\partial u_i}{\partial x_j} = F_i - \frac{1}{\rho}\frac{\partial p}{\partial x_i} \tag{13}$$

$$\frac{\partial u_i}{\partial x_i} = 0 \tag{14}$$

When ϕ stands for the potential function of velocity, integrating equation (13) and paying attention to equation (14), we have

$$\frac{p}{\rho}+\frac{u^2}{2}-\frac{\partial\phi}{\partial t}-F=C(t) \tag{15}$$

For incompressible and regardless of gravity, we have

$$\frac{p_\infty}{\rho}=\frac{p}{\rho}+\frac{u^2}{2}-\frac{\partial\phi}{\partial t} \tag{16}$$

For ideal gas and isoentropic process,

$$pv^\gamma = const \tag{17}$$

where p_∞ is the pressure at infinitely distance place; R is the radius of the bubble; γ is adiabatic index; v is the specific volume of the gas.

3.2 Velocity of Bubble Wall in the Process of Burst of Air Nucleus

Put a spherical bubble into boundless and motionless water, when its size is changed, the potential function of velocity of liquid around it can be expressed as following by Lamb (Knapp et al., 1970)

$$\phi=\frac{R^2}{r}\frac{dR}{dt} \tag{18}$$

Radial velocity u of any mass of water against the core of air nucleus can be derived from equation (18)

$$u=\frac{\partial\phi}{\partial r}=\frac{R^2}{r^2}\frac{dR}{dt} \tag{19}$$

When $r=R$, the kinetic equation of bubble-wall can be derived from equation (16)

$$-R\frac{dU}{dt}-\frac{3}{2}U^2=\frac{p_\infty-p_{(R)}}{\rho} \tag{20}$$

where r is the radial distance from the center of the air nucleus; t is the time; U is the bubble-wall radial velocity, $U = \frac{dR}{dt}$; $p_{(R)}$ is the outside pressure of bubble-wall.

Since the burst of the air nucleus is extremely rapid, the process can be considered to be adiabatic. Regardless of the effect of viscosity, we have

$$p_{(R)} = p_1 (\frac{R_0}{R})^{3\gamma} + p_v - \frac{2\sigma}{R} \tag{21}$$

Substituting equation (21) into (20), we obtain

$$R\frac{dU}{dt} + \frac{3}{2}U^2 = \frac{p_1}{\rho}(\frac{R_0}{R})^{3\gamma} - \frac{2\sigma}{\rho R} - \frac{1}{\rho}(p_\infty - p_v) \tag{22}$$

where R_0 is the radius before air nucleus collapses; p_1 is the atmospheric pressure inside the air nucleus, when $t = 0$, then $R = R_0$, $U = 0$; p_v is the vapor pressure inside the bubble, $p_v = p_v(t)$; σ is the surface tension of water, $\sigma = \sigma(T)$; T is the absolute temperature.

Integrating equation (22), bubble-wall velocity can be derived

$$U = \left\{ \frac{2}{3\rho}(p_\infty - p_v)\left[(\frac{R_0}{R})^3 - 1 \right] - \frac{2p_1}{3(1-\gamma)\rho}\left[(\frac{R_0}{R})^3 - (\frac{R_0}{R})^{3\gamma} \right] + \frac{2\sigma}{\rho R}\left[(\frac{R_0}{R})^2 - 1 \right] \right\}^{1/2} \tag{23}$$

3.3 Velocity and Pressure Fields of Liquid in the Process of Burst of Air Nucleus

Radial velocity u of any mass of water relative to the core of air nucleus can be determined from equation (19)

$$u = \frac{R^2 U}{r} \tag{24}$$

For pressure field, consider unit mass of fluid being r from the core of bubble (as seen in Figure 2.), the pressure p, the velocity u, so the acceleration a_r can be given by the equation

$$a_r = -\frac{du}{dt} = -\frac{\partial u}{\partial t} - u\frac{\partial u}{\partial r}$$

On the other hand, according to Newton's law, we have

$$\rho dxdydr \bullet a_r = (p + \frac{\partial p}{\partial r}dr)dxdy - pdxdy$$

$$\therefore a_r = -\frac{\partial u}{\partial t} - u\frac{\partial u}{\partial r} = \frac{1}{\rho}\frac{\partial p}{\partial r} \tag{25}$$

Substituting equation (19) into (25) and integrating it, we obtain

$$p = (\frac{2R}{r} - \frac{R^4}{2r^4})U^2\rho - \frac{p_\infty R_0}{rR^2} + p_\infty \qquad (26)$$

Substituting equation (23) into the above equation, we can calculate the pressure value of any point at any instant.

4. CONCLUDED REMARKS

Liu et al. (1993) has studied on the flow field around the air nucleus before burst of it for aerated waterjet in the air, but the size of the air nucleus and the flow fields around it in the process of burst have not been studied. In this paper, the author probes into these problems. From the air nucleus producing to perishing, the change of its size is quite complicated. Since the pressure gradient along the direction of jet axis is equal to zero, and thus the volume of the air nucleus is no variation through the motion process. The air nucleus can be considered as a small rigid sphere after the jets enter the air and its size can be calculated out by means of BBO equation, which is a prerequisite to figuring out flow fields at the air nucleus surroundings.

5. REFERENCES

Liu, J. Z. and Zhu, J. M., "Theoretical Study on Flow Characteristic of Cavitating Waterjet," *Journal of Water Resources (in Chinese),* Vol. 201, No.10, pp. 33-38, 1993.

Knapp, R. T., Daily, J. W. and Hammitt, "Cavitation," McGraw-Hill, New York, 1970.

Maxey, M. R. and Riley, J. J., "Equation of Motion for a Small Rigid Sphere in a Non-uniform Flow," *Phys. Fluids*, Vol. 28, No. 4, pp. 883-889, 1983.

Xie, X. C., "Theory and Calculation of Turbulent Jet," *Publishing House of Science (in Chinese)*, 1975.

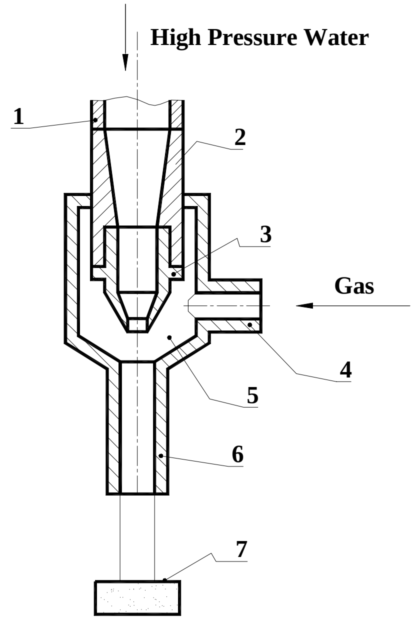

Figure 1. Cavitating Waterjet Spray Head

1. High Pressure Water Pipe; 2. Nozzle Holder; 3. Waterjet Nozzle; 4. Air Pipeline; 5. Suction Chamber; 6. Throat Pipe; 7. Test Sample.

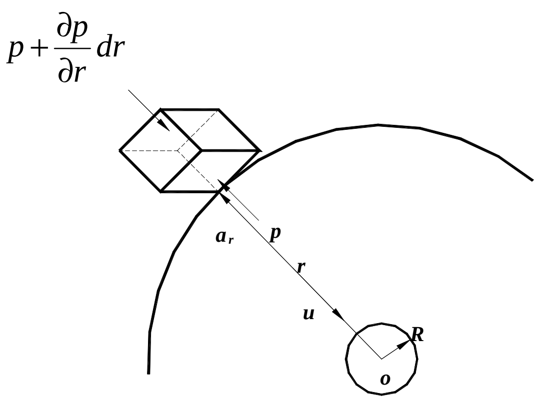

Figure 2. Computational Sketch of Pressure Field

10th American Waterjet Conference
August 14-17, 1999: Houston, Texas

EQUIPMENT FOR DISCRETISIZED ABRASIVE WATERJET MILLING – PRELIMINARY TESTS

G. Holmqvist and K.M.C. Öjmertz
Chalmers University of Technology
Göteborg, Sweden

ABSTRACT

This study addresses the development of a viable abrasive waterjet milling process. It constitutes a continuation of previous studies in which a discrete approach has been suggested and developed. The creation of the high pressure required for machining is accomplished by a high-voltage electrical discharge in a small water-filled chamber. Tests of the experimental equipment indicate a successful water jet/slug formation. It is shown that the jet is powerful enough to create indentation marks on metal sheets and penetration of softer materials. No effort to optimize the energy transfer has been made so far. Experiences of a practical nature are presented and discussed. Problems associated with the present design are discussed, and improvements are suggested. This includes a strategy for assuring that the electrical discharge takes place between the electrodes in the water filled discharge chamber. Furthermore, discharge voltage and power characteristics are analyzed. An important characteristic of the process for the application, the expelled volume, is quantified and analyzed.

Organized and Sponsored by the WaterJet Technology Association

1. INTRODUCTION

1.1 Abrasive Waterjet Milling

The scope of using the abrasive waterjet as a method for three-dimensional material removal (AWJ milling) is of great industrial relevance, and several studies on the subject have been reported. However, increasing the demands on the AWJ machining operation to incorporate precise jet penetration depths brings about process control problems that are inherent to the sensitive and stochastic nature of the AWJ process. The characteristic process variations yield a cutting capability that varies over time, resulting in a poor depth tolerance.

It was first shown by Hashish (1987) that a drastically increased traverse rate over the work surface produced a more narrow depth tolerance. Laurinat et al. (1993) stated that the cyclic AWJ cutting process stabilized upon exceeding a certain critical traverse rate, or rather a critical energy transfer rate. By the fast traverse method, pockets could be milled with good depth tolerance by traversing the AWJ in multiple adjacent and partially overlapping passes over the surface. However, this method brings about a problem in that the traverse rate needs to be kept constant throughout the machining operation. Generally, a prefabricated mask has been necessary to cover up the areas where the manipulator does not maintain constant traverse rate when changing traverse direction.

1.2 Discretisized AWJ Milling

Öjmertz and Amini (1994) introduced a discrete approach to the AWJ. The method utilized a conventional venturi type cutting with a continuously running water jet. By injecting precise portions of abrasive into the mixing chamber, small ”unit” cavities could be eroded on the target material. These unit cavities could readily be replicated in practice, and a geometrical model was suggested and evaluated. The concept of discretisized AWJ milling (DAWM) introduced a different approach to AWJ milling, which has benefits in eliminating the problems in manipulator dynamics as well as offering lower sensitivity to process variations. Although the machining action established material removal in discrete volumes, the concept of using a continuous water jet as the energy source has limitations. When machining softer materials, the drop erosion inflicted damage to the work piece in the period between the machining cycles. To eliminate this problem a fully discretisized process is needed, which uses a momentary energy pulse to accelerate the abrasives.

An electro-hydraulic approach was chosen, and an apparatus using electrical discharges for pressure build-up in a closed volume of water was suggested and built by Holmqvist and Öjmertz (1997). The apparatus uses the energy released by the discharge for creating a high water pressure that expels a short water slug through an orifice. This slug can either carry suspended abrasives along from the chamber or be used for accelerating abrasives in a mixing chamber, similar to the conventional AWJ. Figure 1 shows the apparatus with the electro-magnetic field shielding removed. This paper describes observations and experiences made from preliminary tests performed on the experimental electro-hydraulic pulsing apparatus.

2. ELECTRO-HYDRAULIC PULSING

The concept of creating a pulsed water jet through the use of high voltage discharges is often referred to as electro-hydraulic pulsing. The main parts of an equipment for the purpose consist of a capacitor bank for energy storage and a pair of electrodes mounted in a water filled pressure chamber. The capacitors are charged by a high voltage supply, after which the circuit is closed with a fast switch, releasing the energy in the water filled electrode gap. The discharge creates a quickly developing and expanding plasma. As the inertia of the water resists the expansion, high pressures are created.

Several studies on the phenomenon described above can been found. Naydan and Aker (1972) patented a design incorporating a spark chamber, electrodes and a nozzle. Sandia laboratories (1976) investigated the electrical requirements of an electro-hydraulic equipment for use in drilling in limestone and sandstone. Huff and McFall (1977) tested the technique experimentally. In a study by Hawrylewicz et al. (1986), later on continued by Vijay and Paquette (1996), the electrical discharge was used to interrupt a continuous flow of water, and momentarily intensify the pressure by the pressure pulse created. This equipment proved to be capable of breaking large blocks of granite. In another study, Vijay et al. showed that jet speeds of up to 500 m/s could be achieved at an overall energy efficiency of 20% (1997). Vijay and Makomaski performed a numerical analysis of the jet formation (1998), showing the importance of electrode location, and indicated the occurrence of jet precursors. In a study by Ilias et al. (1994), the mechanical design incorporated a small encapsulated water volume, a check valve through which water was fed at a low pressure (450 kPa), and a nozzle body. In the paper, pressure levels up to 650 MPa are reported, using a discharge voltage of 30 kV.

High-voltage electrical discharges and the consequent formation of plasma are often explained as follows (Khalifa, 1990): Affected by an electric field, electrons are emitted from the negative electrode (the cathode). The electrons will travel along the electric field lines, which generally start perpendicular to a surface. On their way to the anode, the electrons collide with molecules knocking off electrons, which creates an avalanche effect as the number of free traveling particles rapidly increases, which causes an accelerated ionization in the electrode gap. Depending on the geometry, the electric field is normally non-uniform. With a shorter distance from cathode to anode and at small radii, the field becomes stronger, causing more electrons to travel and generate. Thus, in this direction the flow of particles will establish first, and then a so-called plasma streamer is developed. The instant when this occurs is referred to as breakdown. This streamer will expand if the available energy is sufficiently high or if the current is high enough. The process is mainly thermodynamic. A result of the expansion is also that the resistance in the electrode gap will diminish. The expansion of the plasma channel is so fast that an impulse pressure, a shock wave, is developed, followed by a relief portion of declining pressure (Murr, 1988). The expanding plasma causes a displacement effect, which could also produce a hydrostatic pressure if the plasma volume is not too small in relation to the water volume. The pressure created can be used to expel a slug of water through a nozzle.

3. EXPERIMENTAL EQUIPMENT

3.1 Concept and System Components

The design of the experimental equipment has been guided by previous research. Several solutions are unique, partly due to the specific application. The maximum energy level in each pulse is approximately 0.5 kJ, which is relatively low compared to most of the studies mentioned previously. The choice of energy level was based on the effectiveness of the electro-hydraulic pulsing process, known from previous work, as well as on rough calculations based on known levels of material removal rates and specific energy for the AWJ milling process.

The equipment has been designed for a maximum voltage of 30 kV, which governs the physical distances between components of different voltages within the circuit as well as the choice of electric components. Special energy storage *capacitors*, which can withstand the high voltages and the fast discharges, were chosen. A particular kind of *switch*, a triggered spark gap switch, was chosen for the application. In this, a breakdown over a spark gap can be triggered electrically resulting in switching times in the region of tens of nanoseconds, which is sufficient for the present application. *The high voltage power supply* should have a power level to match a desired charging time. *Electrode isolators* were fabricated in aluminum oxide and designed for minimizing tensile stresses, which can be detrimental to ceramic materials. This was accomplished by a design where fastening is made by clamping between two conic surfaces, pre-stressing the material. Figure 1b shows the electrodes assembled in the discharge chamber.

3.2 Electric Circuit and Equipment Operation

The circuit diagram is shown schematically in figure 2. The bold lines indicate the main circuit (high currents). The operation of the equipment is as follows: The manual switch being in position 1, the capacitor bank is charged by the power supply. Next, the manual switch is put in position 2, and the spark gap switch is triggered, which closes the main circuit and causes a breakdown in the water between the electrodes in the discharge chamber. Any remaining energy in the circuit can be taken care of by grounding the circuit via position 3 on the manual switch. When the manual switch is put in position 4, the circuit is short-circuited. A grounded cage prevents hazardous flash-over and protects from electro-magnetic radiation (see figure 3).

4. EXPERIMENTS

4.1 Set up and Procedure

The aim of this first phase of the experimental activities, using the new equipment presented here, was threefold. First, to learn how to operate the equipment in a safe and effective manner. Second, to identify the most obvious deficiencies of the equipment. Third, to start analyzing the process by studying how basic process parameters influence the result. Important process parameters, which can be identified, are; voltage level, capacitance, electrode distance and fluid chemistry. Parameters analyzed so far are the voltage level and the capacitance. The electrode distance has been 4 mm in all tests. For evaluating the energy transfer, the possibility to machine or deform different materials has been tested. For analyzing the circuit performance, the voltage between the electrodes as a function of the time, $U_d(t)$, and the volume of water expelled from the discharge chamber were used as parameters.

4.2 Practical Considerations and Problems

A problem identified was that flash-over occurred, not as supposed between the electrodes, but instead from the high voltage electrode to the discharge chamber wall. This was discovered by small spark erosion marks on the chamber internal walls. The reason is believed to be the sharp edge of the rear end of the electrode tip, where the electric field could concentrate. Changing the geometry of the electrode tip was not easily accomplished. Instead the problem was solved by electrically connecting the discharge chamber at an electrical potential in between the high voltage and the ground level, resulting in a larger voltage difference between the electrodes than between the electrodes and the chamber wall. The present circuit can be seen in figure 4.

When raising the voltage level over 20 kV, mechanical failure of the electrode isolators occurred. The fracture had in both cases appeared at the same location, at the base of the ”neck” of the isolator. This part is not pre-stressed, which can be observed in figure 1b. However, the discharge produces a shock wave, which will propagate further into the neck of the isolator, where other stress conditions prevail, whereby a critical tensile stress can be exceeded. This is believed to have caused the failure.

4.3 Experimental Results

4.3.1 Evidence of Jet Formation

Experiments so far have been made with a pure waterjet only. The very first experiment was carried out at the minimum energy level for which the equipment was designed. Parameter settings were: Voltage 12 kV (which is the minimum voltage at which the spark gap switch can be operated), and capacitance of 0.3 μF, resulting in an input energy level of 22 J. The water was allowed to escape through the end opening of a 3.2 mm pipe. The result was encouraging, since the expelled slug of water penetrated the cardboard paper placed in front of the tube opening.

In the following experiments, when standard waterjet nozzles were used, clear indentation marks on metal sheets were observed. Figure 5 shows some resulting marks from slugs produced with a 0.5 mm diameter waterjet-nozzle striking copper sheet surface. In addition to the indentation marks, a bending edge on the surface can be seen. The latter being due to a supporting edge.

4.3.2 Expelled Volume

The water volume expelled is an important feature of the apparatus to be effective for use in discretisized abrasive waterjet milling. As a first step, the influence of capacitance and voltage on the expelled volume was investigated. The expelled volume was determined by measuring the water level in the outlet pipe. (The discharge chamber assembly was turned upside down during the experiments.) First, water was let out through the opening of the pipe, not using any nozzle. It was found that the expelled volume was substantial, and that it generally increased with both increasing capacitance and voltage. Figure 6a shows the expelled volume as a function of the capacitance, at a voltage of 15 kV. In figure 6b can be seen the expelled volume for different voltages at a capacitance of 1.2 μF. The maximum expelled volume so far is approximately 580 mm^3.

When using waterjet nozzles to confine a jet, the expelled volume was slightly diminished. When using a 0.5 mm nozzle, a capacitance of 1.2 μF and a voltage of 20 kV, the expelled volume was approximately 500 mm^3. This should be compared to an average of 550 mm^3 without using a nozzle. For a nozzle with a diameter of 0.3 mm, the expelled volume was measured to be approximately 300 mm^3.

4.3.3 Discharge Characteristics

Figure 7 shows schematically the typical behavior of the discharge voltage U_d (the voltage measured over the electrodes) as a function of the time, t. At t=0, the spark gap switch is triggered, almost instantly increasing the voltage over the electrodes to the input voltage U_0. Then follows a lag time before breakdown occurs. During the time lag (which has been different from time to time) the voltage decreases, indicating the presence of a current in the circuit. The reason for the time lag has not yet been clarified. Just after the breakdown occurs, the plasma channel develops, and the voltage drops rapidly, followed by a damped oscillation of the voltage. The oscillation is due to the presence of inductance in the circuit, and the oscillation (dissipation of the energy) is due to the presence of electrical resistance.

From a diagram of discharge voltage as a function of time, also a discharge time can be determined. This corresponds to a half period in the voltage oscillation curve. The discharge time could hereby be measured to be in the range of 2-4 μs. From this, a rough measure of the peak current and the peak power of the circuit could be calculated. An alternative is to calculate the current in an explicit form using the formula; $I_d=-C(dU_d/dt)$. From the oscilloscope, a maximum differential dU_d / dt can be determined. Thus, for a 20 kV and 1.2 μF discharge, a typical current could be calculated to be approximately 10 kA. This leads to a development of peak power in excess of 100 MW.

5. DISCUSSION

An experimental apparatus for discretisized abrasive waterjet milling (DAWM) has been developed. The basic concept for the apparatus has proved to be functional and the results are promising. Underwater electric discharges of high power can be obtained. A considerable amount of water is expelled, which is expected to be a necessity for the use in DAWM. Even at comparatively low power levels, the water slug is powerful enough for penetration of softer material and for creating indentation marks in sheet metal. An important parameter for future work is the obtainable velocity of the expelled water slug. Next, a test of the use of either a pre-mixed slurry, or accelerating abrasives by the venturi method is needed. The complex process of pressure build-up needs to be addressed in this context. A low overall efficiency of energy transfer can be anticipated to be an obstacle to overcome. This can be achieved by a development of the geometrical features of the chamber and outlet.

An important problem observed, namely flash-over occurring from one electrode to the chamber wall, was eliminated. The development work is far from being completed for an industrial use of the technique. New phenomena are continuously found during the course of experimentation. An important matter to continuously keep in mind is the safety of operating the equipment.

The total cost of the experimental components has so far not exceeded 25 % of that of an ordinary intensifier pump unit. As the pressurizing unit may be incorporated with the cutting head, the technique will significantly reduce the need for expensive high-pressure components. Components that today restrain a high machining rate are to be found in the high voltage power supply system. The filling of water may also be a problem for a high frequency pulsing. If the filling is not made in a controlled manner, there is a risk of entrapped air in the discharge chamber.

Allowing oneself to take a visionary view, several advantages of the discretisized AWJ technique may be envisioned. At the same time, this discussion points out directions in which further development is needed. If developed into a *high frequency machining* unit, such an apparatus may become a viable as well as an economical tool. The unit cavities may be made smaller, thus enhancing the ”milling resolution” in favor of better machining tolerances, combined with acceptable material removal rates.

6. ACKNOWLEDGEMENTS

The authors wish to thank Mr. Sture Johansson at the Dept. of Production Engineering at Chalmers University of Technology for vital support regarding the design of the electrical circuits presented in this paper. Also, we thank Mr. Dick Olofsson at the Dept. of Production Engineering at Chalmers University of Technology for support in fabrication of mechanical parts for the new apparatus.

7. REFERENCES

1. Hashish, M.: ”Milling with Abrasive-Waterjets - A Preliminary Investigation”, *Proc. 4th U.S. Water Jet Conference*, WJTA, St. Louis, MO, USA, pp. 1-10, 1987.

2. Laurinat, A., Louis, H., Meier-Wiechert, G.: ”A Model for Milling with Abrasive Water Jets”, *Proc. 7th American Water Jet Conference*, WJTA, St. Louis, MO, USA, pp. 119-139, 1993.

3. Öjmertz, K.M.C. and Amini, N.: ”A Discrete Approach to the Abrasive Waterjet Milling Process”, *Proc. 12th Int’l Conference on Jet Cutting Technology*, BHRG, Cranfield, UK, pp. 425-434, 1994.

4. Holmqvist, G. and Öjmertz K.M.C.: ”Process Development and Apparatus for Discretisized Abrasive Waterjet Milling”, *Proc. 9th American Waterjet Conference*, WJTA, St. Louis, MO, USA, pp. 77-91, 1997.

5. Naydan, T. and Aker, W.W.: ”Process and Apparatus for the Production of Hydroelectric Pulsed Liquid Jets”, U.S. Patent No. 3700169, 1972.

6. Sandia Laboratories: ”Drilling Research on the Electrical Detonation and Subsequent Cavitation in a Liquid Technique (Spark Drilling)”, *Sandia Report No. SAND 76-0086*, 50 p., 1976.

7. Huff, C.F. and McFall, A.L.: ”Investigation into the Effects of an Arc Discharge on a High Velocity Liquid Jet”, *Sandia Laboratory Report No. SAND-77-1135C*, 27 p., 1977.

8. Hawrylewicz, H.M., Puchala R.J., Vijay M.M.: ”Generation of Pulsed or Cavitating Jets by Electric Discharges in High Speed Continuous Water Jets”, *Proc. 8th Int’l Symposium on Jet Cutting Technology*, BHRA, Cranfield, UK, pp. 345-352, 1986.

9. Vijay, M. and Paquette, N.: ”Electro-discharge Technique for Producing Powerful Pulsed Water Jets: Potential and Problems”, *Proc. 13th Int’l Conference on Jetting Technology*, BHRG, Cranfield, UK, pp. 195-209, 1996.

10. Vijay, M.M., Bielawski, M., Paquette, V.: ”Generating Powerful Pulsed Water Jets with Electric Discharges: Fundamental Study”, *Proc. 9th American Waterjet Conference*, WJTA, St. Louis, MO, USA, pp. 415-430, 1997.

11. Vijay, M.M., Makomaski, A.H.: “Numerical Analysis of Pulsed Jet Formation by Electric Discharge in a Nozzle”, *Proc. 14th Int’l Conference on Jetting Technology*, BHRG, Cranfield, UK, pp. 73-87, 1998.

12. Ilias, N., Magyari, A., Radu, S., Achim, M.: ”Research Concerning Water Jets Rock Cutting and Water Jets Assisted Rock Cutting”, *Proc. 12th Int’l Conference on Jet Cutting Technology*, BHRG, Cranfield, UK, pp. 265-280, 1994.

13. Khalifa M.: ”High Voltage Engineering, Theory and Practice”, Marcel Dekker Inc., New York, USA, 524 p., 1990.

14. Murr, L.E.: ”Shock Waves for Industrial Applications”, Noyes Publications, Park Ridge, New Jersey, USA, 533 p., 1988.

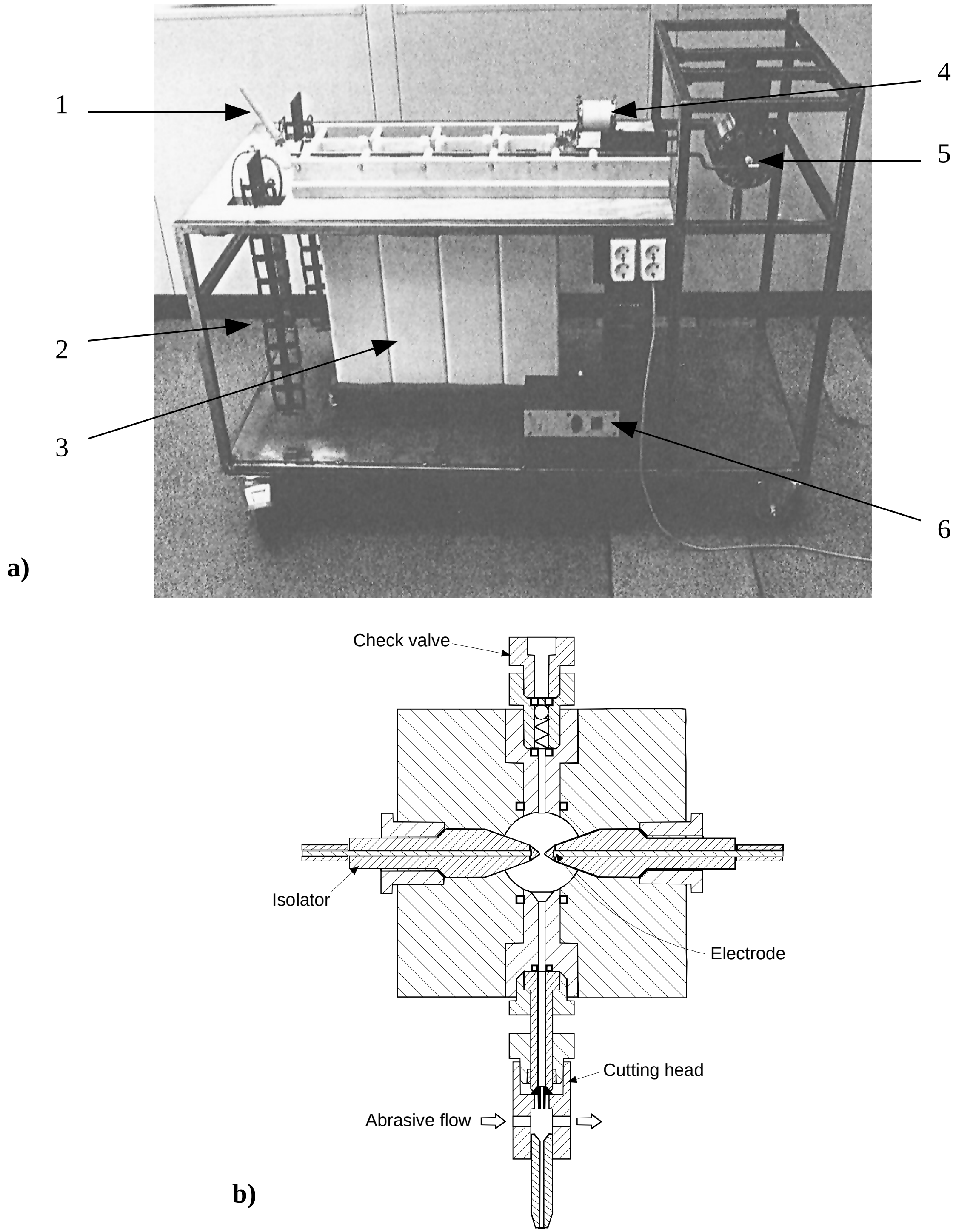

Figure 1. a) Apparatus for discretisized abrasive waterjet milling, shown without the electro-magnetic shielding: 1) Manual switch, 2) Resistors, 3) Capacitors, 4) Spark gap switch, 5) Discharge chamber, 6) Trigger generator.
b) Discharge chamber, shown with an attached AWJ cutting head.

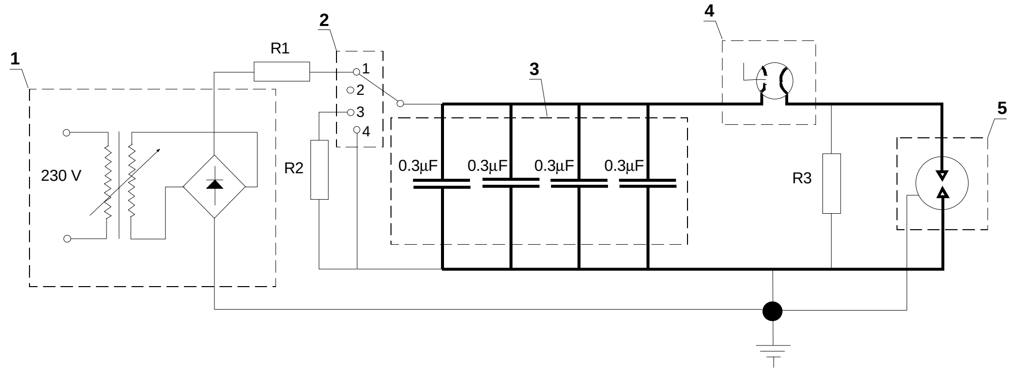

Figure 2. Electric circuit, main circuit in bold lines. Components: 1) Power supply, 2) Manual switch, 3) Capacitor bank, 4) Spark gap switch and 5) Discharge chamber incorporating the electrodes.

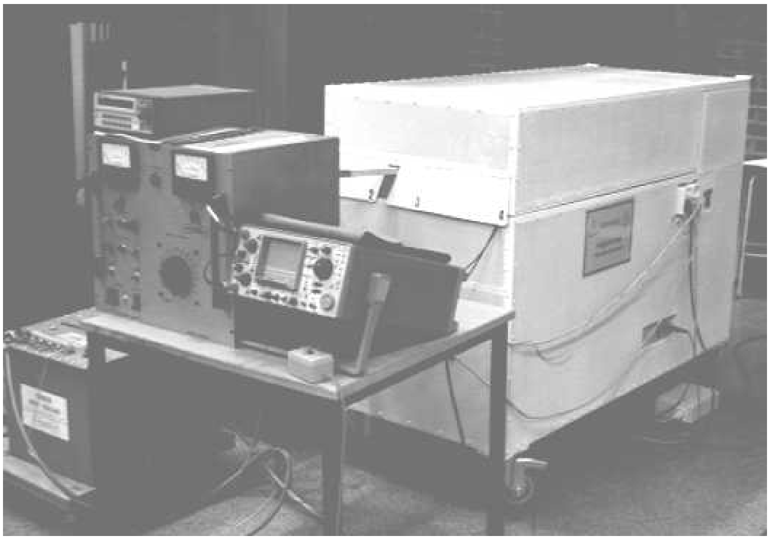

Figure 3. The experimental set-up with the grounded shielding cage for electro-magnetic radiation protection.

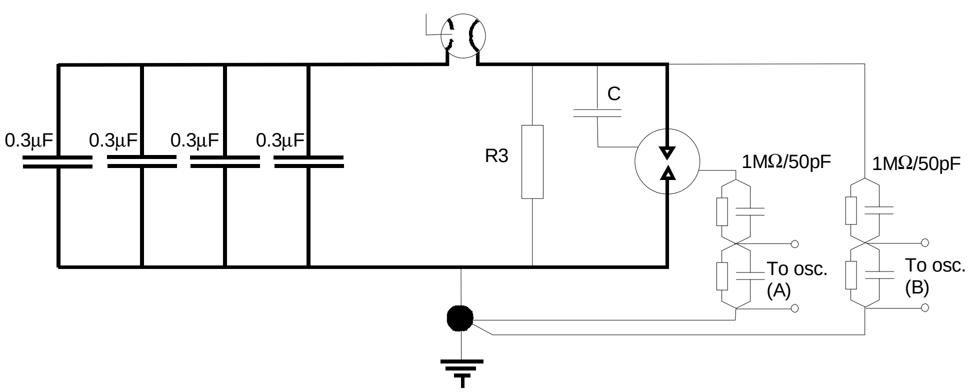

Figure 4. Present electric circuit, including a capacitor connecting the discharge chamber to the high voltage level, and the two high voltage probes.

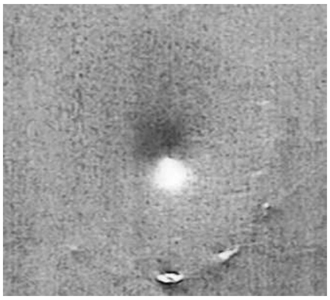

a

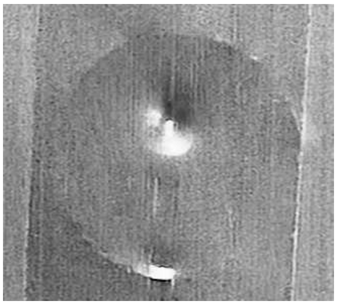

b

Figure 5. Evidence of water jet/slug formation from indentation marks in thin (0.05 mm) metal sheet. Diameter of supporting edge: 9 mm. Voltage level: a) 15 kV, b) 20 kV.

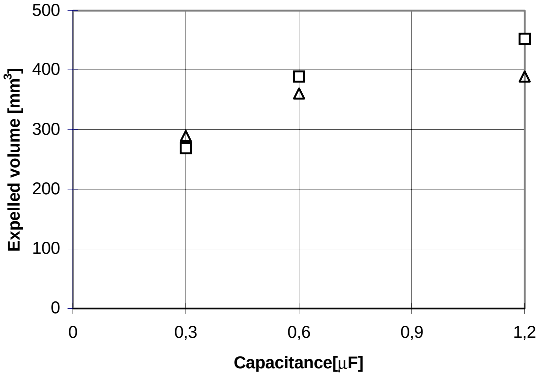

a

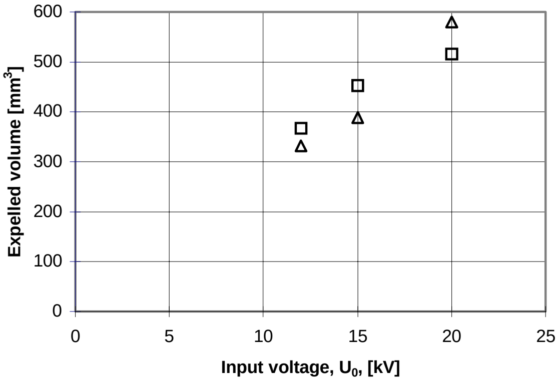

b

Figure 6. a) Expelled volume of water as a function of capacitance at a voltage of 15 kV and b) as a function of voltage at a capacitance of 1.2 μF. Results from two replicates are shown.

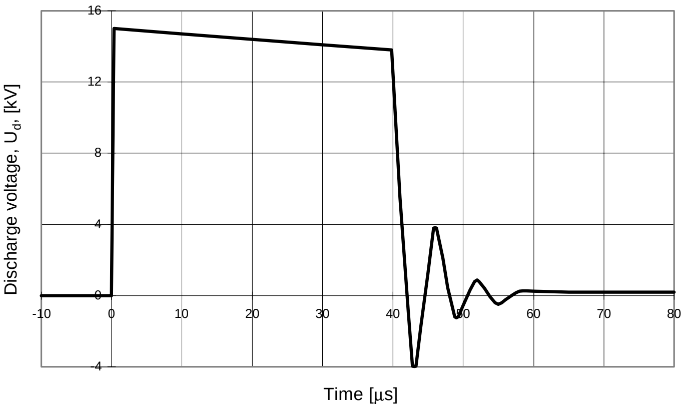

Figure 7. Discharge voltage $U_d(t)$ at an input voltage U_0 of 15 kV and capacitance of 0.6 μF. The data was collected from the oscilloscope screen.

10th American Waterjet Conference
August 14-17, 1999: Houston, Texas

Paper **18**

ASPECTS ON HIGH PRESSURE JET ASSISTED TURNING

P. Dahlman, J. Kaminski
Chalmers University of Technology
Göteborg Sweden

ABSTRACT

The high requirements on production efficiency in turning operations demand faster and more reliable cutting processes in order to achieve a better utilization of machine tools.

This paper summarizes advantages and difficulties encountered in water jet assisted turning. Clear results of the effect of high-pressure jet assisted turning has been achieved as well as knowledge of what precautions that has to be considered before using the technique. The presented results show that the high-pressure jet assisted turning has a high potential for improvement of production efficiency.

Pressures in the range of 40 – 300 MPa has been used in the experiments. Three major topics have been investigated: chip control, temperature reduction and tool wear mechanisms.

1. INTRODUCTION

One of the most important pre-requisitions in metal cutting is a total chip control with respect to chip form, flow and breaking. It is well known that a good chip control has a great influence on the tool life, machined surface quality, cutting forces, reliability of the machining process etc. Also the productivity is heavily influenced since in cutting operations with poor chip control the machine must be frequently stopped and chips must be removed manually from the working area. This is especially important when turning smaller inner diameters of products since the limited space fast can be filled with chips and damage the machined surfaces.

Commonly, a “partial” chip control is achieved using indexable inserts equipped with various chip former configurations. Up to now, research concerning chip control mainly was concentrated on development of new, more effective chip formers. Hundreds of different chip former shapes are available on the market. They are specially developed to meet requirements in specific operations. Depending on the profile geometry on the tool rake face it is possible to attain chips with different shapes. The familiar limitation for the various moulded insert shapes is the limited cutting data region for chip breaking. Commonly, the tool manufacturers recommend a region in cutting depth – feed rate diagram, in which a good chip breaking/control is possible. If one or both of the two parameters is out of range, there is an obvious risk that the chip control may be totally lost. This can be clearly observed in profile turning with varying cutting depth.

The problem concerning chip braking and chip control is so important that an extensive summary of the research on chip control was made by I. S. Jawahir and C.A. van Luttervelt in CIRP Keynote paper “Recent developments in Chip Control Research and Applications”, 1993, [2]. Many other interesting papers have also been published [3,4,5,6].

The general trend in manufacturing is dry machining. However, many modern materials can not be machined dry even with the latest coated tools, due to the high temperatures in the cutting zone. Materials like austenitic stainless steel, high-temperature alloys, titanium, and hardened steel demand cutting fluids. It has been shown in our research [2], and by others [3,4] that High Pressure Cooling (HPC) of cutting tools is a very effective method, which can drastically increase the production economy in workshops. By applying a high pressure fluid jet, it is possible to achieve advantages, such as significantly decreased temperature in the cutting zone, increased tool life in certain cases up to several hundred percent, lower forces due to better frictional conditions between the tool face and the chip, and lower levels of vibrations. This results in improved surface integrity and better dimensional accuracy of the produced parts. Nevertheless water jet assisted machining also induces some new precautions to be made before using the technique. Today insert geometries and grades are not developed for this application and the choice of a regular recommended insert can actually cause lower productivity with water jet assisted machining than with conventional cooling.

The above mentioned effects do not only depend on the effective heat dissipation, but also on reduction of the contact length between the chip and the rake face. Since the high-pressure jet partially penetrates the tool/chip interface a hydro-wedge is created which provides a hydrodynamic lubrication of the friction zone. The shorter contact length and lower friction force cause a larger shear plane angle, and thus lower chip compression factor.

2. CHIP CONTROL

2.1 Experimental Set-ups

Two different experimental sets were used for testing the chip formation. Work material was SS2258; SAE 52100. Commonly this material produces long and continuos chips. The inserts used in both chip formation set-ups were flat-faced Al_2O_3 coated carbide tools SPUN 190412 K15 (P10). The cutting speed was 300 m/min, feed rate 0,2-0,3 mm/rev and cutting dept i.e. pipe wall thickness was 3 mm.

2.1.1 Up-curl

To single out the up-curl radius of produced chips, oblique cutting conditions with single straight cutting edge were used, in turning of tube end. In order to obtain tubular helical chips of different diameters depending on the jet data, the insert was mounted above the work piece centre line, which corresponds to turning with –6 degrees tilt angle of the cutting edge, figure 1. The used insert had a flat rake surface without chip breaker. The rake angle was 6 degrees. This arrangement gives us a fairly good possibility to produce chips with defined helix angle, which is necessary to make a correct evaluation. Since the chip flow is directed away form the work piece, the risk for disturbances is nearly eliminated.

The water jet was applied in, for both up-curl and side-curl experiments, in axial direction, perpendicularly to the cutting edge. The angle between the jet and the rake surface was 6 degrees. As viewed in figure 2a it is assumed that the water jet fills a constant volume between the chip and the tool rake, and thus a water wedge is established.

This wedge is working as an adjustable/“soft” chip former that bends the chip upwards giving it a desirable up curling. Since the jet is directed exactly onto the middle point of the contact width between the chip and the tool rake, the pressure distribution is assumed to be symmetrical, figure 2b. By controlling the jet parameters, i.e. pressures and flow, it is possible to control the up-curl radius of the produced chips.

2.1.2 Side-flow Angle

When investigating the side-curl of the chips the experiments were under orthogonal cutting conditions. In order to achieve short chips and facilitate measurement of the produced chips two grooves were done by sawing in each work-piece, which means that during one revolution two separate chips were produced.

To investigate the side-curl it was necessary to direct the created chip sideways. In order to achieve the jet was applied just 0.5 mm from the work-piece outer diameter as described in figure 3 This arrangement makes it possible to create a water wedge that gives an unsymmetrical pressure distribution on the chip. A difference in pressure distribution along the cutting edge gives a bending moment that forces the chip sideways. Depending on the jet data, that is, jet diameter, pressure and direction, the chip flow is controlled.

2.2 Evaluation Methods

2.2.1 Up-curl

After each experiment the chips were collected and analysed with respect to form and diameter. To calculate the mean chip diameter, nine chips from each test were measured with a slide calliper rule. Different kinds of chip shapes were achieved depending on the feed rate and the jet data. Nevertheless, with the used cutting feeds the evaluation and measurements of the chips was easily done. The general chip shape produced is exemplified in figure 4.

2.2.2 Side-flow Angle

The chips produced in the experiments commonly had a spiral-conical form, figure 5. However, in the cases when the jet momentum was to low or in dry machining the chips had a spiral-flat form. This means that only up curl was observed. In evaluation of the side flow angle two assumptions was made. The first one was that a part of each chip had a form that is similar to Archimedes spiral. It can be seen in figure 5 that the pitch of the helix is fairly constant. The second assumption was that the side displacement or side flow angle during one revolution is constant. By measuring in a microscope the two radii R_1 and R_2 and the distance Z it was possible to estimate the side flow angle, β, of the chips produced. The calculation was made in the following way:

The length of the spiral, L, during one revolution is:

$$L = \pi \cdot (R_1 + R_2) \tag{1}$$

Assuming that the chip side displacement during this revolution is Z, the side flow angle is:

$$\beta = \arctan\left(\frac{Z}{L}\right) \tag{2}$$

2.3 Results and Discussion

2.3.1 Up-curl

The experiments show that the water wedge created between the chip and the tool rake, successfully controls the up-curl radius of the produced chips, table 1. It is clearly observed that the chip radius does not only depend on the actual jet power, but also on the correlation between water pressure and flow. This means that for a constant power, for example 2 kW, a lower chip radius will be achieved if a high flow, 4,75 l/min, and low pressure, 25,1 MPa, are used. Flow has greater influence on the chip radius than the jet pressure. This implies that there is another parameter that better discriminate the relation between the up-curl radius and the water jet beam. It has been shown by Crafoord et al (1999) [1] that a more suited parameter is the water jet's momentum. The water jet momentum is described as follows:

$$F = v \cdot q \cdot \rho \tag{3}$$

Where v is the jet velocity and q is the density. This expression integrates both the jet flow and the jet pressure. The equation above expresses the force acting on the orifice. As mentioned earlier, the actual force acting on the chip is more difficult to calculate. This since the geometry where the control volume is acting is not completely known and it yields only the resultant force not the point where it is acting. But still, this relationship gives the "potential" force and it is a comprehensive parameter to use. It was shown that the up-curl relationship with jet momentum could be calculated as described in figure 6.

As presented above the chip up-curl radius can be controlled. However to achieve good chip control this is not enough. In order to obtain chip breakage, in materials that produce long continuos chips, it is important to bend the chip into an obstacle e.g. unmachined material or onto the tool.

2.3.2 Side-flow Angle

The experimental results show that it is fully possible to control the chip flow direction, and that it is not only the jet momentum but also the jet diameter, which together influence the chip side flow angle. An important factor to be considered is the shape of the pressure distribution surface. Depending on the jet diameter (nozzle diameter), pressure and impact position the pressure distribution is controlled. Using equation 3 the force caused by the water wedge created between the chip and rake surface can be described as the integral over the pressure distribution as described in equation 4. To make the pressure non-dimensional the p_{chip} is divided with the stagnation pressure p_o.

$$F_{chip} = p_0 \cdot \int_A \frac{p_{chip}}{p_0}(x, y)dA \tag{4}$$

It is clearly observed, see figure 7, that the jet momentum influences the side-flow angle significantly. It is also observed that the smallest nozzle (0,6 mm in diameter) gives the highest side-flow angle while nozzle 0,8 mm the lowest angle. However, the angle is relatively small that is between 0,5 and 2,5 degrees, the discharge of chips from the cutting area is changed dramatically. Depending on the jet impact position along the cutting depth, the discharge of chips is controlled outwards or inwards the pipe. This is of great importance in longitudinal turning.

The chips can be controlled in a direction that they will not damage the already machined workpiece surface.

It should be noted that to obtain the same level of force on the chip by using a smaller nozzle it is necessary to use a higher pressure. This means that the pressure distribution surface will be different than when using a large nozzle diameter, see figure 8. In the first case (figure 8a), the appearance of a high pressure peak makes the centre of gravity for the pressure distribution to move to the left, that is to the outer diameter of the workpiece. This induces a strong torque which forces the chip sideways, giving the chip a desired side flow angle. When using nozzles with a larger diameter the pressure distribution will be wider and have a lower pressure peak (figure 8b). The centre of gravity will then move towards the centre of the cutting depth, thus making the torque smaller, than when using a small nozzle and a high pressure.

When combining the knowledge from up-curl and side-curl radius control a big step has been taken to enable modeling chip control in water jet assisted turning. Ongoing research in this area is using the knowledge from flat faced tools tests together with inserts with moulded chip forming geometries. The goal is the develop knowledge for modeling of chip flow direction in order to predict and control optimal chip breaking.

3. TEMPERATURE

3.1 Experimental Set-up

Two high-pressure pumps were used in the experiments. The first one was an intensifier of the type used in water jet cutting systems. This intensifier gives water pressures in the range of 70 and 360 MPa and volumes up to 1.9 l/min. The second one was a piston pump with pressure ranging from 5 to 74 MPa and significantly higher fluid volumes, that is up to 24 l/min.

The tests were carried out with Al_2O_3 coated Sandvik Coromant carbide inserts SPUN 19 04 12, 3015 K15 (P10) and on alloyed steel SS2541-03 as workpiece material. The inserts have a flat rake surface without chip breaker. The corner radius was 1.2 mm. The selected cutting data were cutting speed= 150, 225 and 300 m/min, cutting depth= 3 mm, and feed rate= 0.3 mm/rev.

Temperature in the cutting zone has been measured using a new method where thermocouples, placed on the clearance surface, are integrated with the insert. The thermocouples are manufactured using a thick-film technique and are placed directly on the insert coating (Al_2O_3), which constitutes an electrical insulating layer, [4, 5, 6]. A more thoroughly description is presented in Kaminski, Alvelid (1997) [7].

By applying two thermocouples on the clearance surface, it is possible to measure temperatures in two points very close to the cutting edge. The first thermo-element was located just 0,5 mm below the cutting edge and the second one 1 mm. This gives information about the temperature distribution in the vicinity of the cutting zone. An example showing two registered signals corresponding to temperatures at two thermo-elements is shown in figure 9. We can observe that the temperature measuring method have a very short response time. Later this information will be used for modelling of the isotherms in the zone using a FEM-software. Since the response time for the thermocouples is very short and accuracy is high, the thermocouples can be successfully used for the registering of rapid temperature changes during a cutting process. In all experiments concerning measurement of temperature pure water was used as coolant.

3.2 Results and Discussion

The results achieved in this experiment show that a very effective cooling of the cutting zone is possible using a medium pressure coolant jet. It is evident, see figure 10, that a significant decrease of temperature occurs already at pressures ranging between 20-70 MPa. An additional increase of the fluid pressure does not significantly influence the tool temperature. In the case of conventional cooling, the water was applied with the pressure of 0.6 MPa using a pipe, 10 mm in diameter. The water was applied on the top of the cutting zone.

Decrease of the temperature using conventional cooling, in comparison with temperature, which occur in dry machining, is only about 15 %. The water steam, which is generated around the hot surfaces of the insert and the chip, effectively prevents the water from cooling the cutting zone and dissipate the generated heat. In spite of this fact the overhead cooling is frequently used in the industry. To achieve a 40-45% reduction of the temperature it is necessary to break the thin skin of steam with a concentrated water jet. The preliminary results show that this is possible already at relatively low pressures, from 20 MPa and above, depending on the cutting parameters. When the jet partially penetrates the tool/chip interface, a high-pressure wedge of water is created, which effectively dissipates the heat. Moreover, a relation between the stability in chip breaking and the stability in the registered temperatures has been observed.

When translating the mV unit into the corresponding temperatures, according to Kaminski, Alvelid (1997) [7], the change in tool temperature in mV can easily be recalculated into degrees Celsius. The temperature reduction as a function of applied water pressure is clear but not linear as viewed in figure 10.

Regarding the importance of the applied flow considering cooling effect, it is observed that the water flow (l/min) does not significantly affect the temperature. The temperatures shown in diagrams in figure 11 do not show a significant trend. It should be noted that water flow for the different nozzle diameters and water pressures strongly differs, see table 2. Instead the water flow and the jet momentum have a great effect on the chip breaking and the shape of produced chips.

4. TOOL LIFE

4.1 Experimental Set-up

The goal of this tool life test was to simulate real production cutting conditions in order to compare conventional cooling with water jet assisted cooling, therefore higher feed rates and different cutting speeds than in the other tests were used. In manufacturing large series and many machines raise the cost for using high-pressure pumps. Therefore pressure of 40 MPa was used, together with a nozzle diameter of 0,9 mm. The used cutting data differs from the above used. The used cutting speed was 250-350 m/min, feed was 0,55 mm/min and cutting depth was 1,5 mm. Work material was SS SS2258, SAE 52100 and the used inserts were CNMG 120412-PR 4015 from Sandvik Coromant and CNMM 120412 KC 850 from Kennametal. The cutting operations were carried out as longitudinal turning. A standard synthetical cutting fluid with concentration of 5% was used. The jet was applied at a distance of 20 mm.

4.2 Results and Discussion

4.2.1 Abrasive Wear

The most common way to measure tool life in turning operation is the value of flank wear. A limit is commonly set be 0,3 mm of flank wear before the tool is discarded. The results from the tests show that the flank wear is significantly reduced when using water jet assisted turning. As a comparison between conventional cooling and high pressure cooling an increase of about 50 percent was observed, figure 12. It is also possibly to increase the cutting speed from 250m/min to 350 m/min with a preserved tool life if the jet fluid is used.

4.2.2 Erosion Wear

The purpose for this test was to investigate the tool life in short repetitive engagement times to monitor the effects of so called thermo-shocks. During the tests a new erosion wear was observed, which could not be found when cutting with conventional cooling. It is believed that the efficient cooling of the cutting zone caused this wear. When the insert is engaged in cutting the jet fluid can not penetrate into the cutting zone but after disengagement the tool is rapidly cooled. Several near transient changes in temperature, thermo-shocks, probably cause the coating layer to crack and fragment, see figure 13. After when the coating is removed the softer base material is exposed erosion wear. Significant is that the wear occurs on the boundary of the contact zone and the water wedge i.e. in the area where the temperature gradient is highest. It is probably the different temperature dilatation in the coating and substrate that causes the coating fragmentation.

By aiming the jet fluid to either the main edge side or the secondary edge side it is clearly observed that the tool life of the insert with the jet fluid on the secondary edge is significantly higher, than when directing the jet towards the main edge. The improvement in tool life could be recorded to 40% depending on the impact position, figure 14. Why the improvement occurs is not yet fully investigated. However, it is believed that the temperature distribution on the rake side of the tool is one of the reasons. It can also be noticed that the form of the tool life curve, when direction the jet towards the secondary edge, bear more likeness towards tool life curves from cutting with conventional cooling.

It is very important to use suitable inserts in combination with the high-pressure jet cooling. The commercially available inserts are not intended for this technique, due to their sensitivity to high temperature gradient.

5. CONCLUSIONS

From the experiments it is clearly observed that the most important controlling parameters of chip control and breaking are the fluid jet direction and it's momentum. The chip flow direction i.e. up-curl and side-flow angle can be successfully controlled be the jet. Different type of chips could be manufactured, with jet assisted turning, using the same cutting parameters and flat-faced tools, without chip breaking geometry. The possibility to control the chip shape is partially reduced in turning with low cutting depth and high feed rate.

- Ability to control chip with certain limits.
- Different impact positions produce different chip shapes.
- Problems with chip control in internal turning can be reduced when using the jet.
- Temperature reduction gives longer tool life when regarding abrasive wear.
- Temperature shocks can lead to coating fragmentation, erosion wear and micro-cracks.
- Environmental and economical improvements can be achieved due smaller amounts of cutting fluid, longer tool life and increased production rate.

6. ACKNOWLEDGEMENTS

The authors wish to thank Stig Lagerberg at Sandvik Coromant, for support and valuable discussions, and The Swedish National Board for Industrial and Technical Development for financial support.

7. REFERENCES

1 Crafoord, R,, Kaminski, J., Lagerberg, S., Ljungkrona, O., Wetland, A., “Chip Control in Tube Turning Using a High Pressure Water Jet” Accepted for publication in Journal of Engineering Manufacture. Will be published during 1999.

2 Jawahir, I. S. and van Luttervelt, C. A., “Recent Development in Chip Control Research and Applications”, *Annals of the CIRP*,42(2) (Keynote Paper 1993

3 Jawahir, I. S., ”On the Controllability of Chip Breaking Cycles and Models of Chip Breaking in Metal Machining”, *Annals of the CIRP*, 39(1), pp. 47-51 (1990)

4 Jawahir, I. S., “The tool Restricted Contact Effects as a Major Influencing Factor in Chip Breaking: An Experimental Analysis”, *Annals of the CIRP*, 37(1), pp. 121-126 (1988)

5 Nakayama, K., Arai, M., “Comprehensive Chip Form Classification Based on the Cutting Mechanism”, *Annals of the CIRP, 41(1),* pp. 71-74, (1992*)*

6 Mazurkiewicz M., et al, Metal Machining with High-Pressure Water-Jet Cooling Assistance - A New Possibility, *Journal of Engineering for Industry,* February 1989, Vol. 111/7.

7 Kaminski, J., Alvelid, B., “High Pressure Cooling of Cutting Area for Machining of Modern Materials”, Proceedings of the International Conference Challenges To Civil and Mechanical Engineering in 2000 and Beyond, Wroclaw, Poland, June, 1997.

8. NOMENCLATURE

β Side flow angle.
F_{chip} Resulting force acting on the chip.

9. TABLES

Table 1. Resulted chip diameter is dependent on jet momentum and not on jet power.

Jet Power [kW]	Nozzle Dia. [mm]	Pressure [MPa]	Jet Momentum [N]	Chip Dia. [mm]
2	0,5	47,3	13,1	6,1
2	0,6	37	14,6	5,9
2	0,7	30,2	16,3	5,8
2	0,8	25,3	17,8	5,6

Table 2. Water flow in [l/min] for the used nozzle diameters and water pressure.

Water pressure [MPa]	Dia 0.25 mm	Dia 0.5 mm	Dia 0.7 mm
50	0.65	2.60	5.11
80	0.82	3.30	6.46

10. GRAPHICS

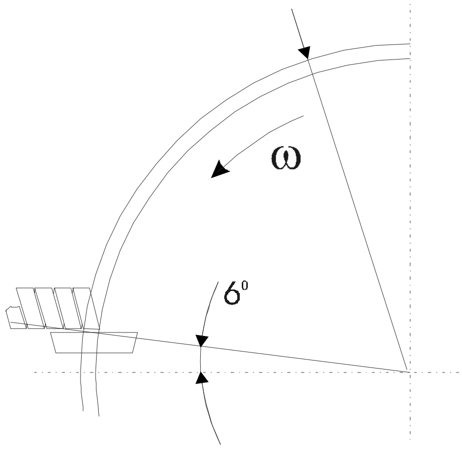

Figure 1. Tool set-up, in axial view, when investigating up-curl.

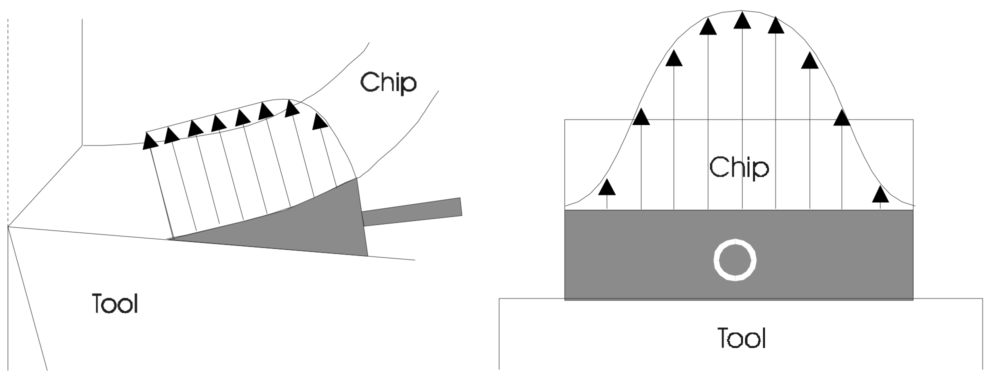

Figure 2. Pressure distribution of the fluid wedge, a) radial view, b) axial view.

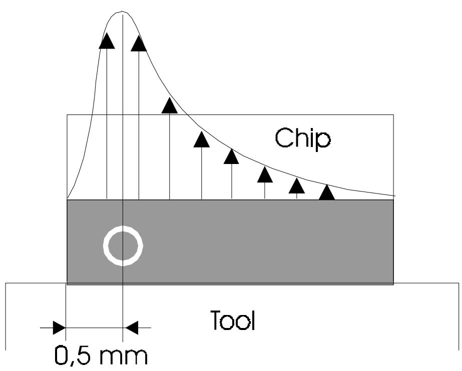

Figure 3. Approximate pressure distribution with jet impact position at the side of the chip.

Figure 4. Chips produced with a feed rate of 0.2 are mm/rev were easy to evaluate.

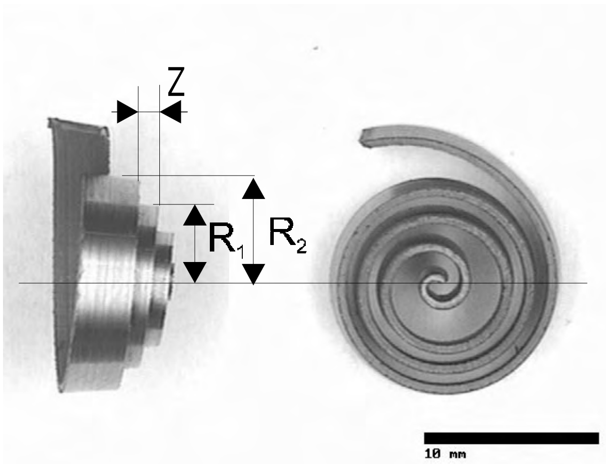

Figure 5. Example on conical and spiral form when produced with jet fluid directed at the side.

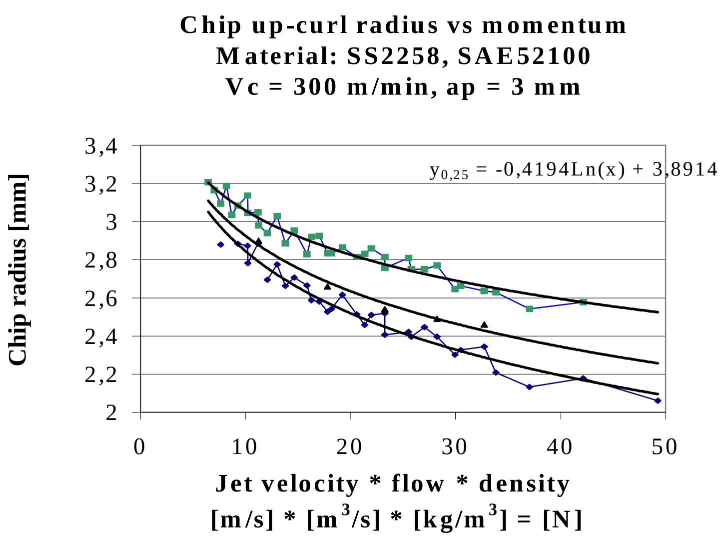

Figure 6. The diagram shows correlation between the up-curl radius and the jet momentum.

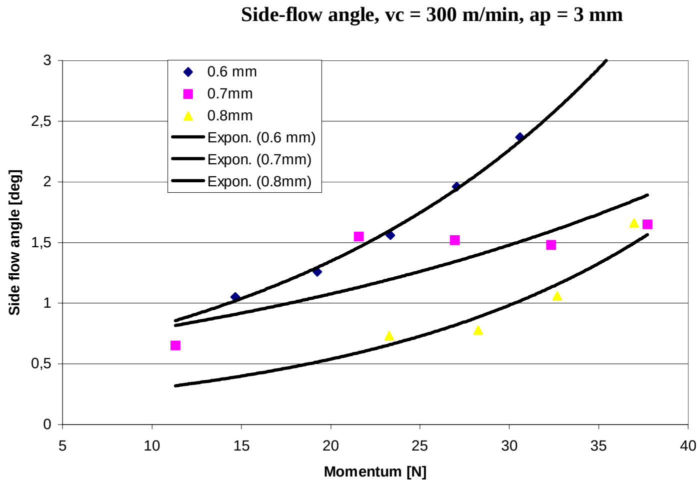

Figure 7. The side-flow angle for different nozzle diameters.

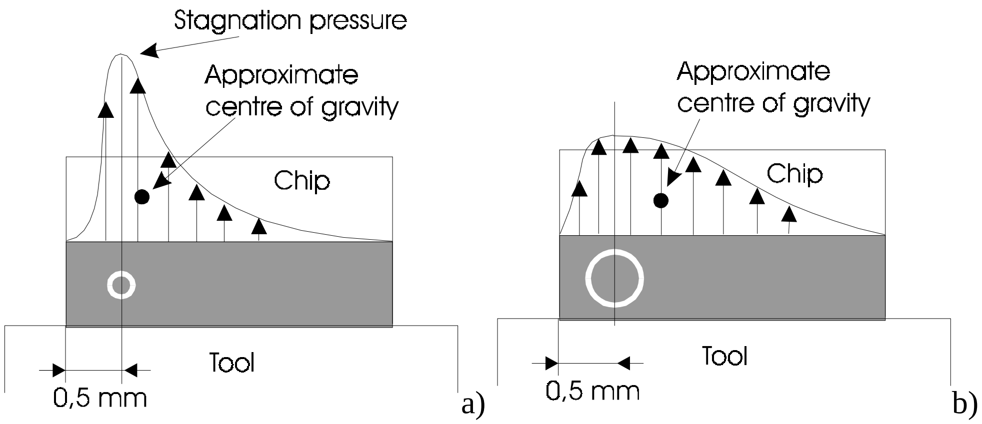

Figure 8. Difference of pressure distribution when using a) a small nozzle diameter and b) a large nozzle.

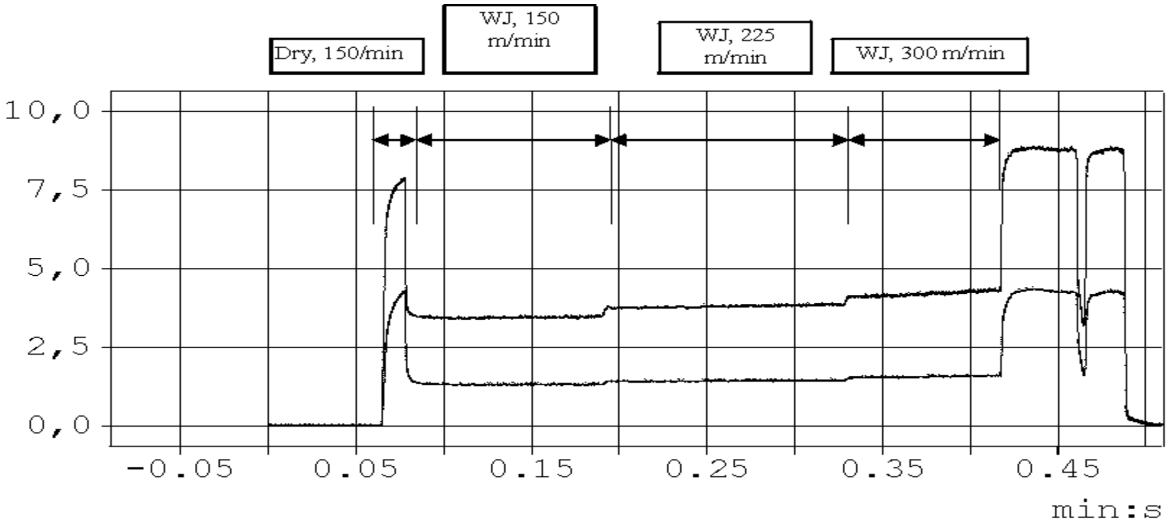

Figure 9. Temperatures registered for three different cutting speeds and for fry and jet assisted machining. The pressure was 50 MPa.

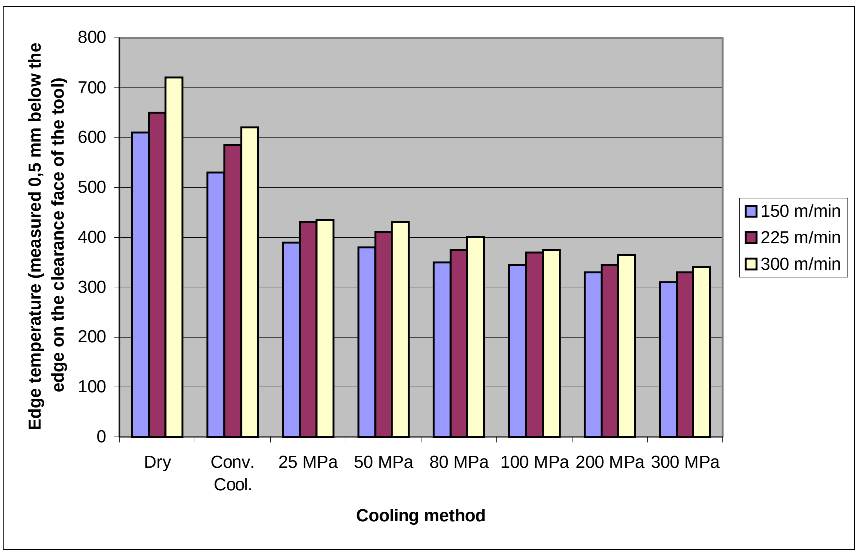

Figure 10. Temperatures in C° for the upper and the lower thermocouples for various water jet pressures. The nozzle diameter is ϕ = 0,25 mm, cutting depth = 3 mm and feed rate 0.3 mm/rev.

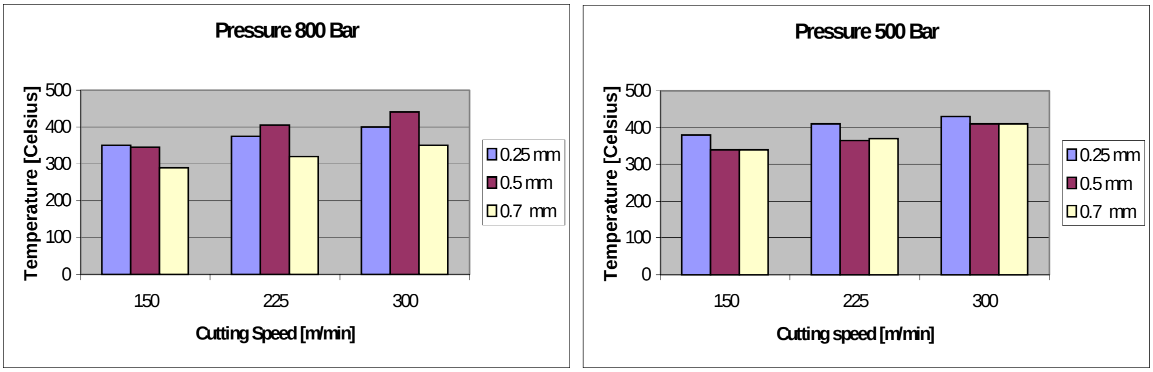

Figure 11. Temperatures in C° registered by the upper thermocouple for different nozzle diameters and different water pressures a) 80 MPa, b) 50 MPa.

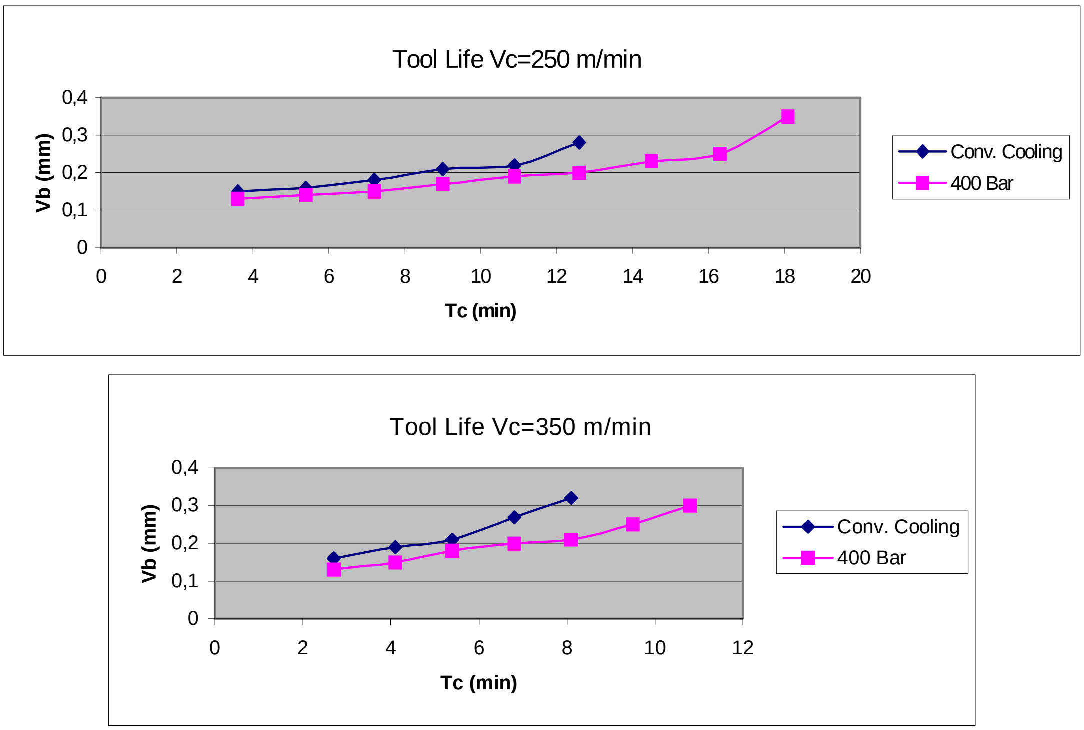

Figure 12. Increase in tool life when applying high pressure cooling compared with conventional cooling.

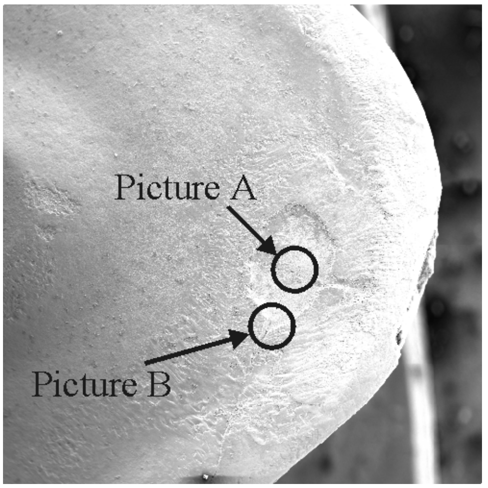

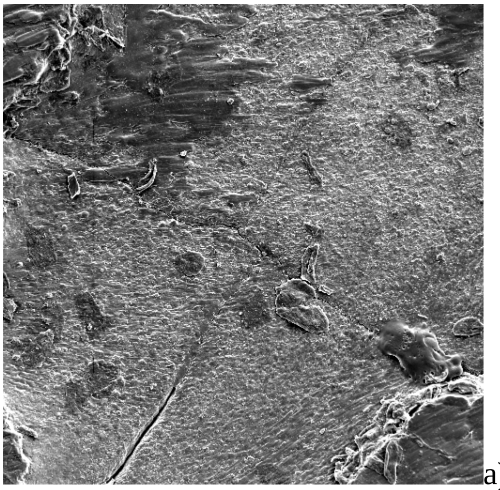
a)

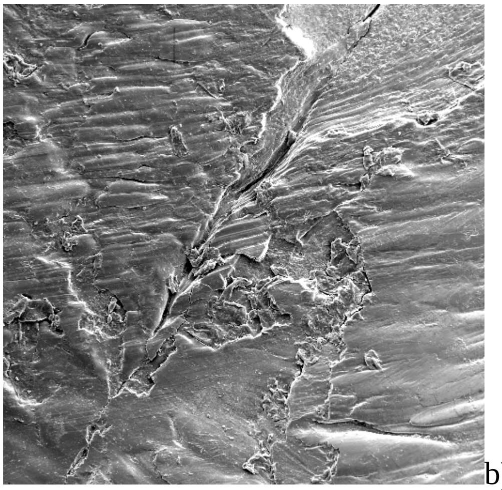
b)

Figure 13. SEM pictures at magnification of 200 times, a),b), showing examples of cracks and flaking of the coating and base material which believed is a result from the jet fluid.

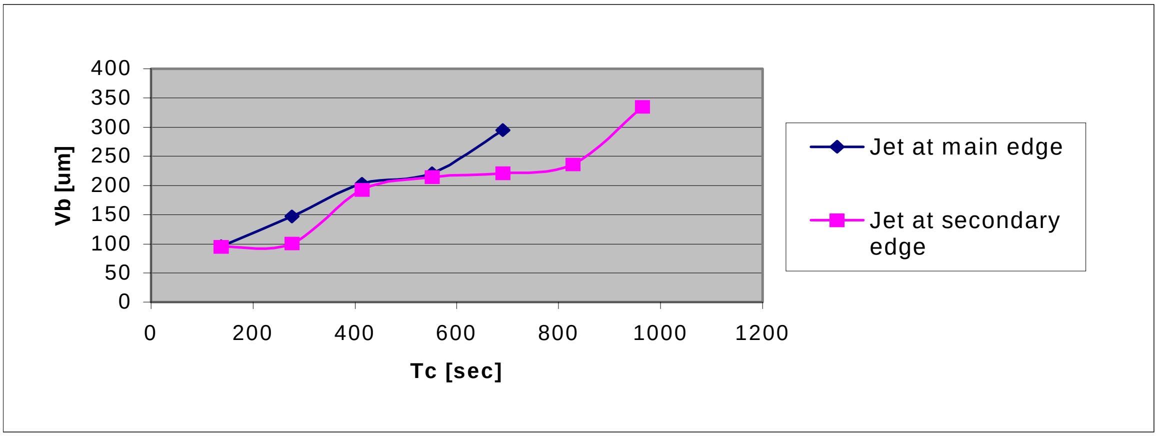

Figure 14. Difference in tool life depending on jet impact position.

10th American Waterjet Conference
August 14-17, 1999: Houston, Texas

Paper **19**

SIMULATION OF DISPLACEMENT FIELDS ASSOCIATED WITH ABRASIVE WATERJET DRILLED HOLE

Z. Guo* and M. Ramulu**

*Boston Scientific Corporation
Northwest Technology Center
Redmond WA

**Department of Mechanical Engineering
University of Washington
Seattle WA

ABSTRACT

In this paper, the displacement fields associated with abrasive waterjet drilling process is simulated by finite element method. It was assumed that the pressure load in the abrasive waterjet can be resolved into three pressure load components, such as *impact jet pressure, shear* and *normal pressure.* The effect of these three pressure loads and their magnitudes on the surface displacement were investigated as a function of the depth of hole. It was found that the shear contributes the most in shaping the displacement contours patterns and the jet pressure does not play a dominant role in determining the *u*-field displacement. A uniform shear along the kerf proves to render distribution contour that is closest to the experimental observations. The assumed pressure components and their magnitude found from this study can be used for numerical modeling of the AWJ drilling more accurately.

Key words:
Moiré interferometry, finite element analysis, numerical simulation

1 INTRODUCTION

High Pressure abrasive waterjet (AWJ) has been widely used in the industries for machining hard-to-cut materials. As an alternative tool, it is also applied in the field of milling, turning, drilling and polishing. In abrasive waterjet machining, high-velocity water is used to entrain and accelerate abrasive particles, such as garnet or silica sand, to achieve the performance needed for machining of metals, ceramics and composites. AWJ machining is cost effective and produces reasonable quality surfaces. However, the abrasive waterjet machining mechanism has not been entirely known to date.

Many investigators have attempted to study the interaction between the abrasive waterjet and the workpiece with various techniques. Using a photoelasticity experimentation, Ramulu investigated the material removal process during abrasive waterjet machining process (Ramulu, 1993 and Guo, 1998). It was concluded that the process is very complex and consists of microcrack initiation, micromachining and erosion (Ramulu, 1993). Photoelasticity experimental technique was used to measure the stresses in an AWJ drilled specimen and to study the AWJ machining mechanisms (Ramulu and Wong, 1991). In an experimental work conducted by the authors (Guo and Ramulu, 1991), moiré interferometry technique was utilized to measure the surface displacement during AWJ drilling process. Numerical modeling is a new tool that people have utilized in studying the AWJ machining process. The process was modeled with finite element method under certain assumed loading conditions in order to obtain the associated stress and strain distributions in the machining zone. However, the jet impact load distribution within the cavity created by the abrasive waterjet drilling is unknown to formulate the material removal model.

The purpose of this paper is to seek the most reasonable loading conditions in the abrasive waterjet impingement zone for finite element simulation, as well as to better understand the relationship among the jet induced pressure loads and the material responses. The numerical experiments were executed to study the effects of these loads on the displacement distribution as a function of the depth of AWJ drilled hole. The feasibility of using finite element model is also verified by comparing moiré interferometry experimental results with the numerical results.

2 NUMERICAL MODELING

Three dominant types of jet actions are involved during the jet impacting and penetrating process as per Tikhomirov et al (1992). They include the impact jet, slipping jet, and slanting jet. These pressure loads were assumed during the AWJ drilling process as shown in Figure 1. The impact *jet pressure, p_j*, is exerted in a small impingement area in the bottom of the hole generated by the AWJ in the case of progressing hole (Figure 1(a)). The *shear*, τ_n, is caused by the reverse flow of the abrasive waterjet (Figure 1(b)); and 3) the *normal pressure, p_n*, acts on the kerf of the hole (Figure 1(c)). The combined pressure loading associated with AWJ impacting/piercing is depicted in Figure 2. The three loads are assumed to vary in both magnitude and direction at different locations along the kerf of the hole, and depend on the jet conditions. The penetrating jet-material interactions were evaluated in terms of material displacements with pressure conditions. The *jet pressure, p_j*, represents the direct impact of the waterjet at the stagnation area. The direction of the jet pressure is the same as the jet direction. The normal pressure simulates the quasi-hydrostatic loading in the machined hole due to the high pressure of the waterjet. The *normal pressure, p_n*, is applied in the direction normal to the kerf surface. The *shear*, τ_n, is caused by the return flow of the abrasive waterjet on the kerf surface, which is applied to the kerf surface in the direction tangent to the kerf. The whole kerf surface is affected by the shear. The effect of the three pressure loads on the surface displacement distribution was studied by varying the three assumed pressure load conditions. In each of the FEA loading simulations, two parameters were fixed while the third one was varied.

Figure 3 shows the typical holes drilled by an abrasive waterjet and the associated displacement fields as captured by the optical method, moiré interferometry. A typical finite element mesh model that was used to model the cavity is shown in Figure 4. The interaction between the AWJ and the solid model with a hole of four selected depths was modeled numerically to mimic the continuous machining process. Modifications on the depth of a hole were made to the finite element model accordingly. The assumed hole depths in the numerical modeling were 2mm, 4 mm, 6mm, and 8mm respectively.

Since the analysis only addresses the elastic deformation, basic load values or unit loads for the pressure of interest were used for the analysis. In the numerical experiments, the normal pressures varied from 0, 1psi, 2 psi, 3 psi, to 5 psi and the applied jet pressure varied from 0 to 1.25 psi. The applied shear included 0, 0.025 psi, 0.15 psi, 0.25 psi, and 0.5 psi. The displacement distribution on the frontal surface under each loading condition at each depth was examined. The modeled surface distributions were compared with the experimentally obtained displacement contours, or the moiré fringe patterns. Both *u*-field and *v*-field displacements were compared.

3 RESULTS AND DISCUSSION

Figures 5(a) and (b) are typical surface displacement distribution contours calculated using ANSYS finite element analysis (FEA) program, in the *u*-field and *v*-field for a hole depth of 8 mm, with a normal pressure of 5 psi, a shear of 0.2 psi and a jet pressure of 0 psi. The normal pressure was applied to the kerf surface, starting from the mid-height to the top of the hole. Note that the *u*-field displacements (*du*) are symmetric with respect to the x=0 plane (Figure 5(a)). The displacements in the area of x>0 are normally positive in sign. They are negative in the area of x<0. Physically it means that the material is moving away from the middle of the specimen under the AWJ action. Near the top edge, there are two "eye" patterns. The maximum and minimum *u*-field displacements are normally located in the two centers of the eyes. In the middle of the frontal surface, there is a horizontal narrow strip. This narrow strip has the minimum *u*-field displacement. Along with the vertical symmetric line x=0, it forms a zero displacement region (ZDR). The height of the zero displacement region varies as the loading conditions are changed. In the vertical displacement or *v*-field (Figure 5(b)), the displacement contour has two important regions, or patterns. On the top of the model is the maximum compressive region. In the lower portion of the model is the island pattern region. The maximum compressive region normally lies in the upper middle area, where it has the maximum *v*- displacement (*dv*) with a negative sign assigned to it. The island like source pattern in the bottom half of the surface represents an area of positive displacement. Along the bottom edge of the model (z=0), the *v*- displacement is zero, or *dv*=0.

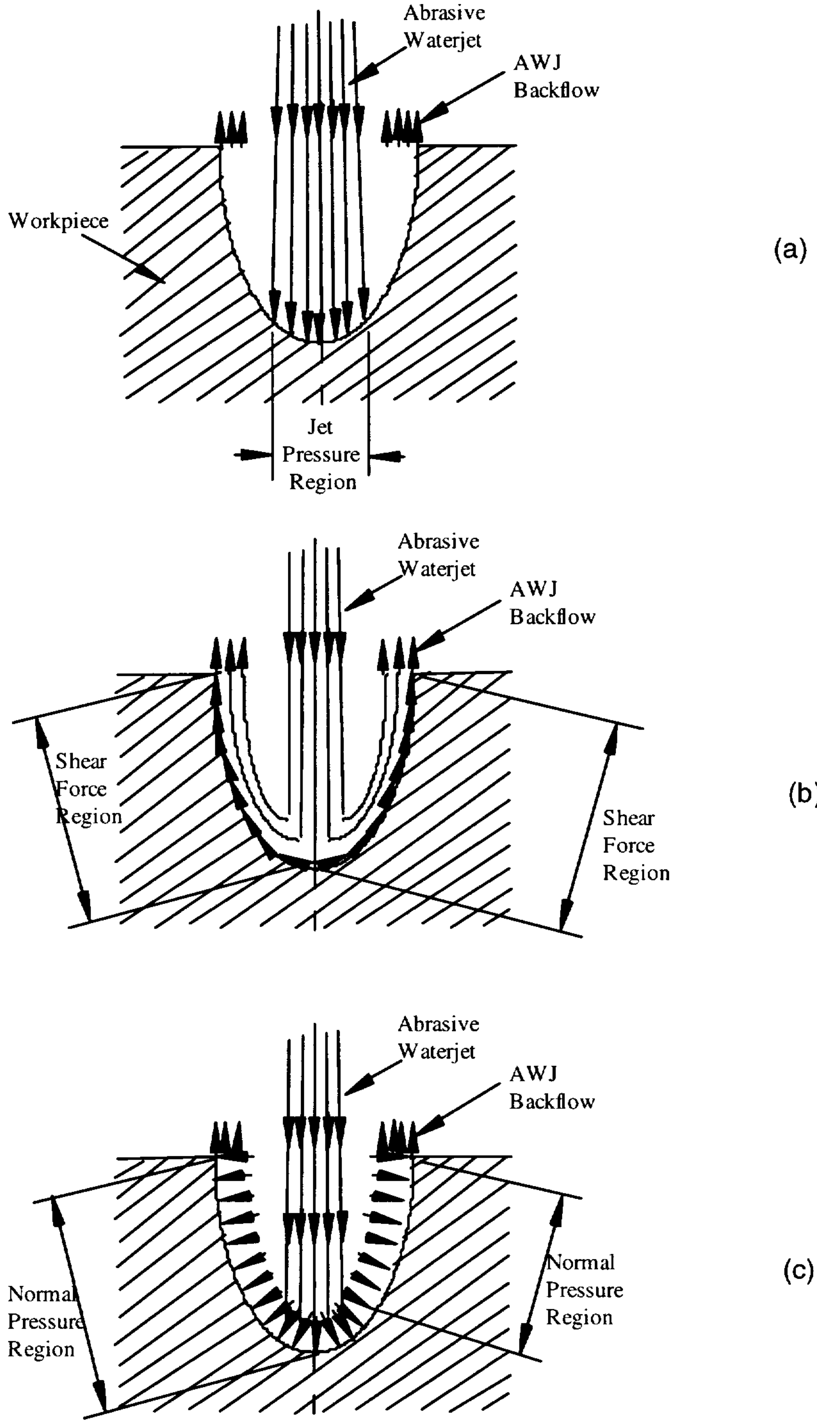

Figure 1 Schematic of the AWJ Pressure Loading Components

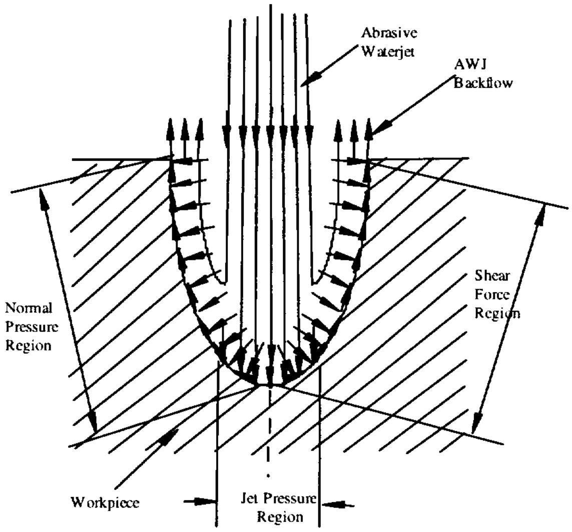

Figure 2   Schematic of the combined AWJ Pressure Loading

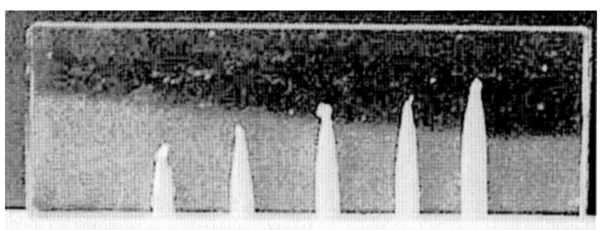

(a) AWJ drilled hole in polycarbonate specimen

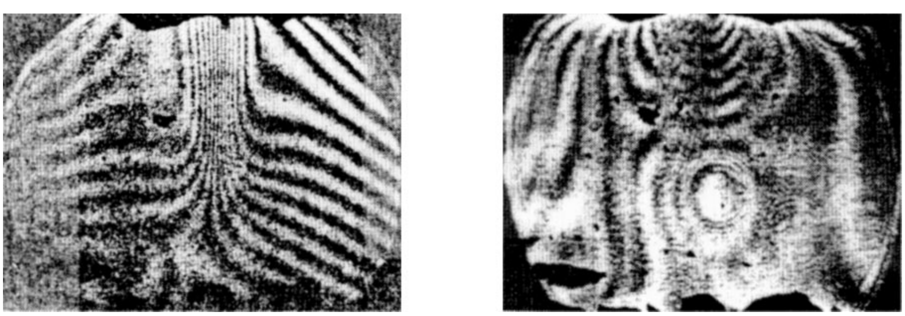

(b) u field   (c) v field

(supply pressure 207 MPa; SOD 1mm; garnet mesh #50; jet exposure time 2.4 seconds)

Figure 3 Typical AWJ Drilled Hole and Moiré Fringe Patterns

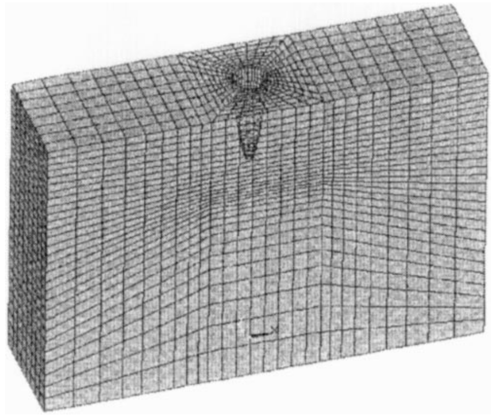

Figure 4 A FEA mesh for a full model of a specimen with a AWJ drilled hole

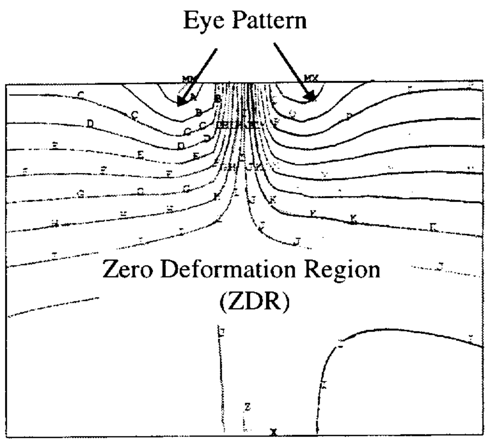

Figure 5(a) Typical u-field surface displacement distribution contours (FEA)

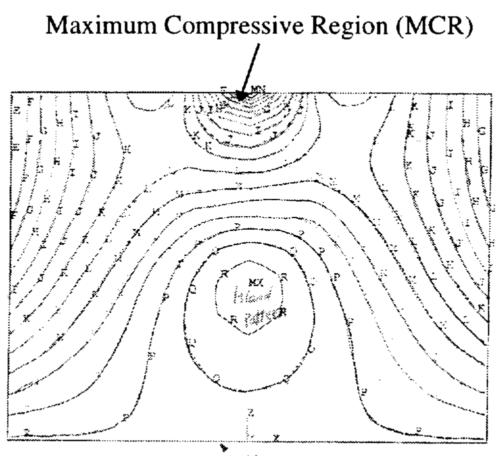

Figure 5(b) Typical v-field surface displacement distribution contours (FEA)

3.1 Effect of the Loading Variables

All the simulation results are presented in the following sections for varying depths. The three loading pressures, i.e. impact jet pressure, normal pressure, and shear were varied to study the effect of each pressure load on the displacement field in the front surface of the model. Since the loads applied to the FEA model were in English units, in this paper the English units were kept unchanged. The pressure loads used are unit pressure for simplicity reasons. In this section, the plots are processed for a typical depth of 6mm.

- **Jet Pressure**

The displacement distributions were generated by varying the jet pressure for a constant penetration depth, normal pressure and shear. The jet pressure (p_j) used in the FEA analysis included 0 psi, 0.25 psi, 0.75 psi, and 1.25 psi. The shear (τ_n) and the normal pressure (p_n) were fixed at 0.2 psi and 5 psi, respectively. Figure 6 shows the displacement pattern. In the *u*-field, increasing the impact waterjet pressure lowered the zero displacement region, and the two eyes as well. It can be observed that the zero displacement region was raised upward as the depth of hole is increased for all four loading cases. In the *v*-field, when the jet pressure is increased, the area of the minimum displacement region got larger, and the absolute value of the minimum displacement correspondingly larger. However, as the jet pressure increased, the area of the *v* -displacement island contour was reduced.

The variations in maximum and minimum displacement fields are plotted as a function of jet penetration depth for constant τ_n =0.2 psi and p_n = 5 psi for varying jet pressure conditions in Figures 7. Note that by increasing the impact pressure from 0 psi to 1.25 psi, the variations in the magnitudes of maximum and minimum displacements *(du)* on the surface are minimal as seen in Figure 7. However, Figure 7b shows that as the depth of hole was increased, the absolute value of the minimum displacement *dv* became larger, and the maximum displacement *dv* became smaller. When the depth of hole was 2 mm, a positive displacement island region was not formed, even when the jet pressure was increased to 1.25 psi. This implies that the jet pressure effect is prominent on the v-displacement and has minimum influence on u-displacement distributions on the surface.

- **Normal Pressure**

Figure 8 shows the typical surface displacement distribution for constant shear (τ_n = 0.0025) and jet pressure (p_j = 0.25), but varying normal pressure (p_n) of 1 psi, 2 psi, and 5 psi respectively. In the u-field, it appears that the normal pressure exerted on the kerf surface has less dramatic changes to the displacement distribution on the front surface of the model. Increasing the normal pressure lowers the position of the eye pattern slightly. In the v-field, increasing the normal pressure does not change the shape of the displacement contour patterns much. However, the magnitude of the v-displacement represented by each contour line increases. Increasing the normal pressure will not significantly change the location of the contour patterns on the surface.

Figure 9 shows the variations in maximum and minimum displacement fields as a function of jet penetration depth for constant τ_n =0.025 and p_j = 1 for varying normal pressure conditions. The absolute values of the maximum and minimum u-field displacements *du* increase, and appear to be proportional to the normal load (Figure 9a). In contrast, the maximum v-fields, *dv*, did not change significantly, but has an effect in the magnitudes of minimum v-displacements as the depth of jet penetration was increased. These observations are not surprising since the normal pressure on the kerf does not contribute significantly to the material removal but it does influence on the surface displacement distributions.

- **Shear**

The effects of shear loading on the surface displacement field contours as the jet penetration increased were simulated and presented in Figure 10. The normal pressure (p_n=5), and jet pressure (p_j = 1) was kept constant and the shear (τ_n) loading was varied from 0.15 psi, 0.2 psi, 0.25 psi, and 0.5 psi. Figures 11 (a) and (b) show the variations in maximum and minimum displacement fields as a function of jet penetration depth for a constant jet pressure of 0.25 psi, a constant normal pressure of p_n = 5, and varying shear. It appears that the shear has the most profound effect on the displacement contour patterns. In the u-field, as the shear increases, the zero displacement zone is raised upward, and the "eye" pattern is reduced in size. The absolute value of the maximum and minimum displacement also increases. When all three loads were kept the same and depth of hole was varied, the zero displacement region also moved upward. At shear of 0.5 psi, the "eyes" almost disappear.

The compressive displacement contours dominate the full field of the front surface. When shear remains at 0.2 psi, the compressive area becomes smaller and smaller as the depth of hole increases. An island of positive v-displacement is formed. The position of this positive island is lowered as the depth of hole increase. In the v-field, the area of the negative displacement region is reduced if the shear is increased. Eventually the negative displacement region will disappear when the shear load is increased to a certain level. The island contour pattern, representing the positive displacement region, is formed and raised. The deeper the hole, the higher the zero displacement region in the u-field, and vise versa. The depth of hole does not have a significant effect on the displacement distribution in the v-field with the shear at 0.025 psi, normal pressure at 5 psi, and jet pressure at 1 psi.

3.2 Loading Non-uniformity along the Depth of Hole

In the above parametric numerical analysis, the impact jet pressure, normal pressure, and shear were applied to the kerf surface with the same magnitude. In this section, the effect of the non-uniformity of these loading variables was investigated. Figure 12 is an illustration of the loading non-uniformity applied in finite element analysis. The normal pressure is divided into two sections along the kerf surface. The magnitudes of the normal pressure in the upper portion and the lower portion are different. Similarly, the magnitudes of the shear in the upper portion and the lower portion are also different, as illustrated in Figure 12 by the length of the arrows. In all the cases studied, the jet pressure was kept constant at 0.25 psi. Figure 13 is the typical parametric FEA results, and their corresponding loads are printed in the bottom of each graph.. It appears that greater normal pressure in the lower portion of the kerf than in the upper portion reduces the size of island pattern in the v-displacement field. Increasing the shear in the top portion of the kerf moves the island pattern upward. The results of this parametric study demonstrate that a uniform shear along the kerf surface of the hole produces the best displacement distribution contours matching the experimental moiré fringe pattern.

4 DISCUSSIONS

For numerical modeling, the displacement distribution contours in both u- and v- fields under various assumed loading conditions were shown in Figures 6, 8 and 10. In the above parametric numerical analysis, the displacement contour patterns changed as the loading conditions were changed. The maximum and minimum displacements under each loading condition are analyzed to help better understand the loading effect. The maximum and minimum displacements as a function of hole depth are depicted in Figures 7, 9 and 11 for different, jet pressures, normal pressure and shear respectively. As can be seen from Figures 7a, 9a and 11a, the maximum and minimum displacements are symmetric with respect to the vertical axial. Their corresponding u-displacements are equal in value and opposite in signs. This means that all u-displacement contours are symmetric with respect to the x=0 plane.

Figures 7b, 9b and 11b show the v-field displacements and these curves demonstrate that the v-displacement is not linearly related to the magnitude of the shear applied to the kerf surface. At jet pressure of 0.25 psi and normal pressure of 5 psi, if the shear is very small (for example, at 0.025 psi), the maximum v-field displacement is almost zero, while the minimum displacement possesses the largest absolute value. When the shear forces are larger, (for example, 0.5 psi), the maximum value is the largest, and the minimum value is the smallest among all cases studied. For shear of 0.2 psi, normal pressure of 5 psi, the differences in u-field displacements for the impact jet pressure from 0 psi to 1.25 psi are very small. This means that the jet pressure does not significantly affect the u-field displacements.

Figure 3 is a typical moiré fringe pattern recorded during an abrasive waterjet drilling process using moiré interferometry experimentation. The moiré fringes illustrated the displacement distribution in the frontal surface of a specimen during AWJ drilling. A comparison of the experimental displacement distributions with the numerically modeled displacement distributions indicated that the results in Figures 3 and 6 are very similar to those recorded from the experiments. Especially when the normal pressure is at 5 psi, the jet impact pressure at 0.25 psi and the shear at 0.2, the displacement contours from the FEA are the closest to the experimentally recorded. In Figure 6 the shear was 0.025 psi and is a relatively small value. The displacement contours do not like realistic even wen the normal pressure was varied at 1 psi to 5 psi. Then three pressure loads were applied to the kerf surfaces, the displacement distributions shown in Figure 13 looks very odd. This is an indication that the pressures exerted on the kerf surfaces by AWJ is somewhat uniform. From the analyses for the maximum and minimum displacement as a function of the hole depth, it is obvious that the surface displacements are symmetric with respect to the jet if the specimen is also symmetric to the jet.

5. SUMMARY AND CONCLUSIONS

It is concluded that finite element analysis can be used to simulated the AWJ drilling. The assumption of three pressure loads, such as normal pressure, jet pressure, and shear, are reasonable. The three loading parameters are very important in determining the displacement distributions of a specimen under AWJ drilling. It was found that the shear contributes the most in shaping the displacement contours patterns and the jet pressure does not play a dominant role in determining the *u*-field displacement. A uniform shear along the kerf proves to render distribution contours that are closest to the experimental observations.

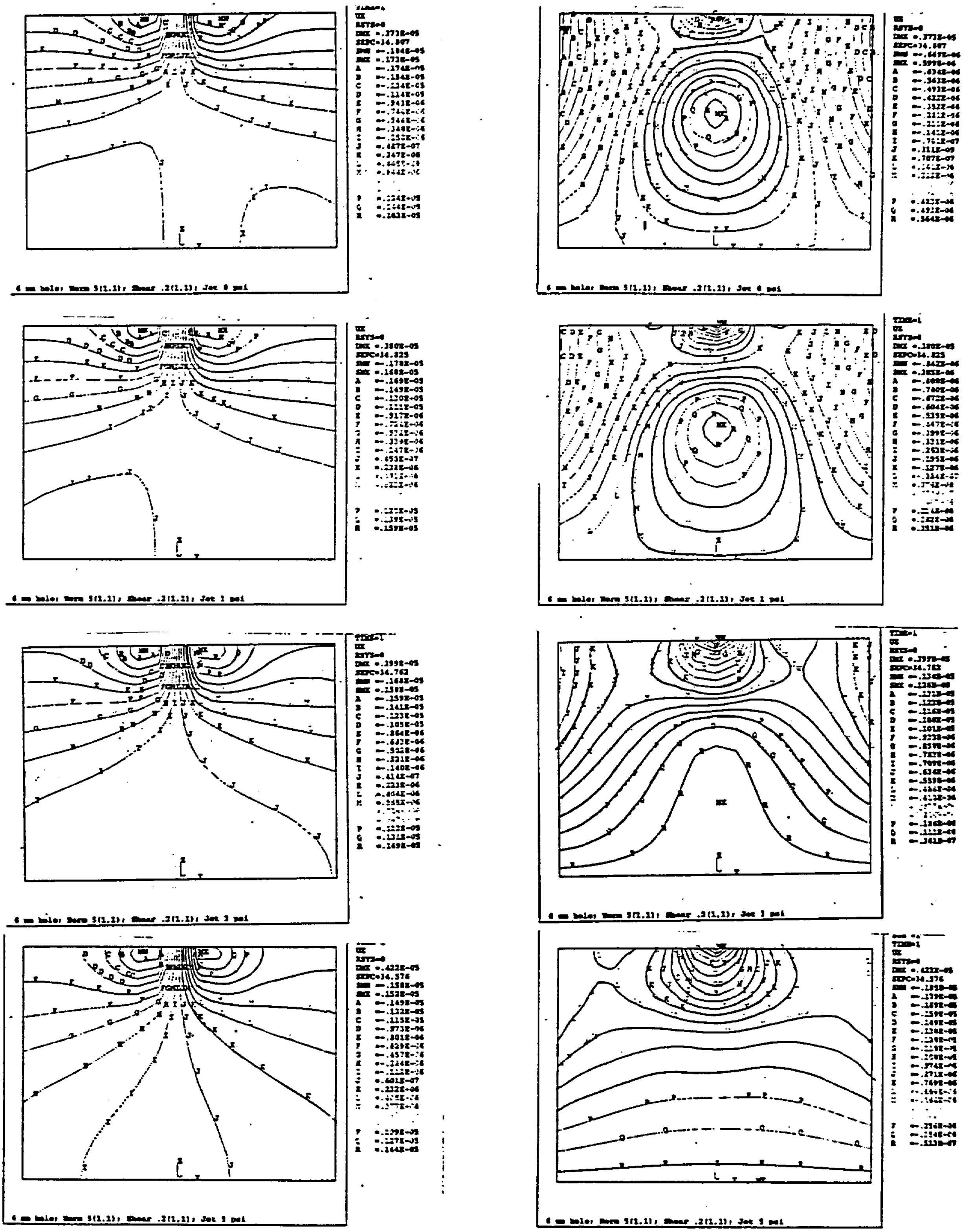

Figure 6 Effect on displacement with varying jet pressures

(p_n=5 psi; τ_n=0.2 psi)

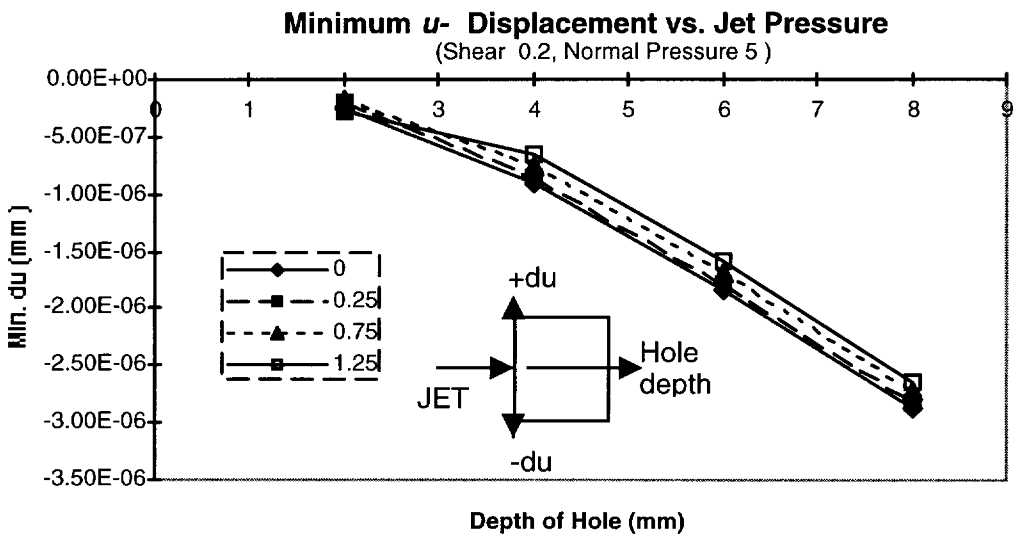

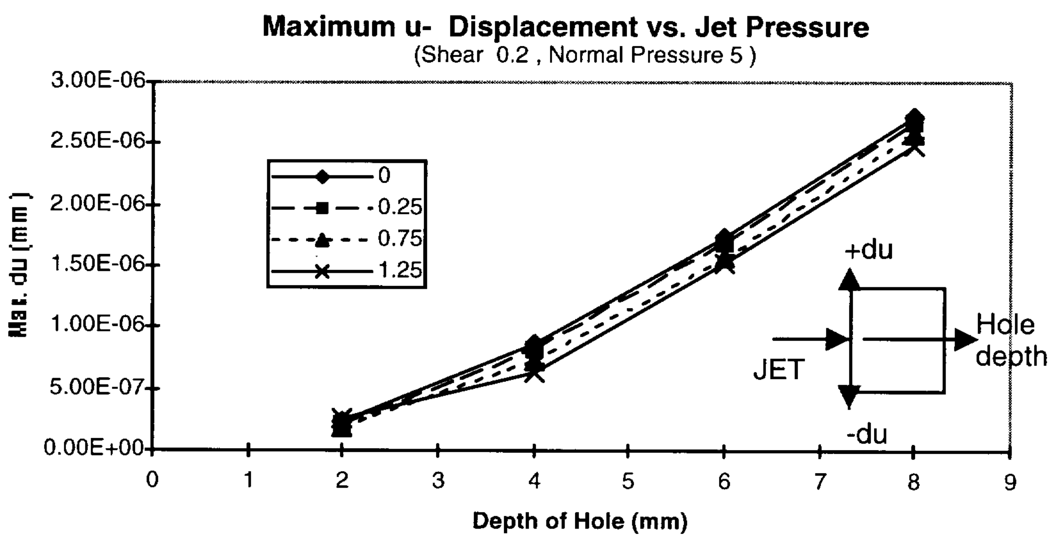

Figure 7 (a) *u*--displacement vs. jet pressure

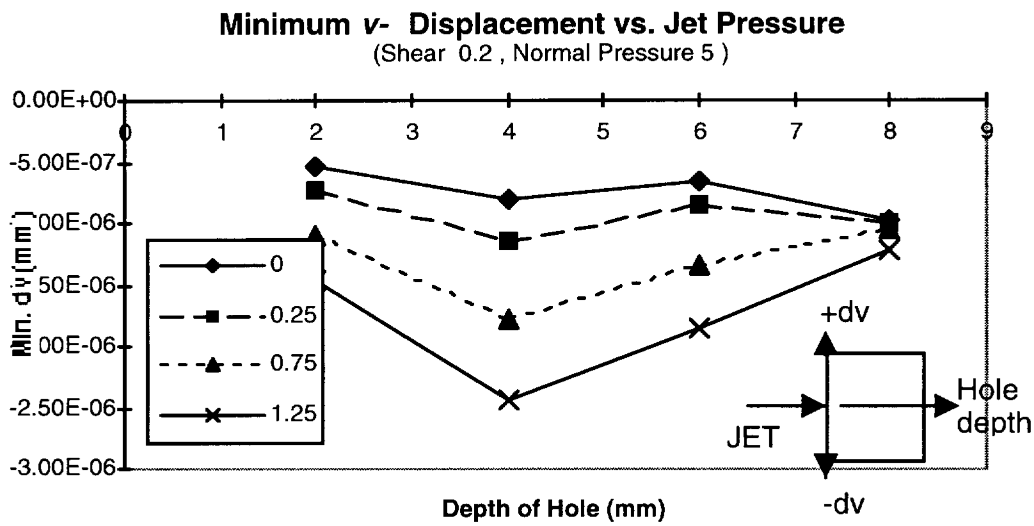

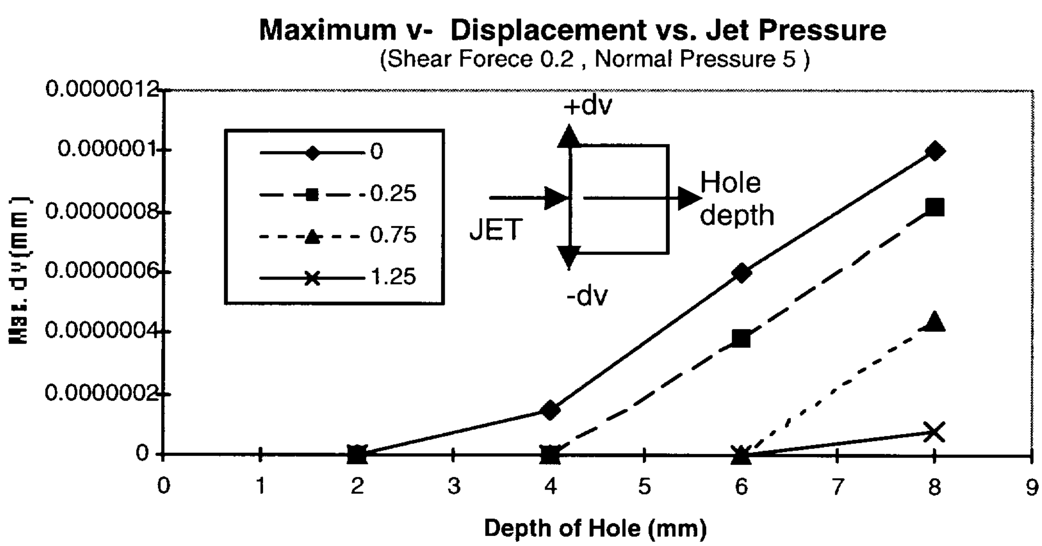

Figure 7(b) v--displacement vs. jet pressure

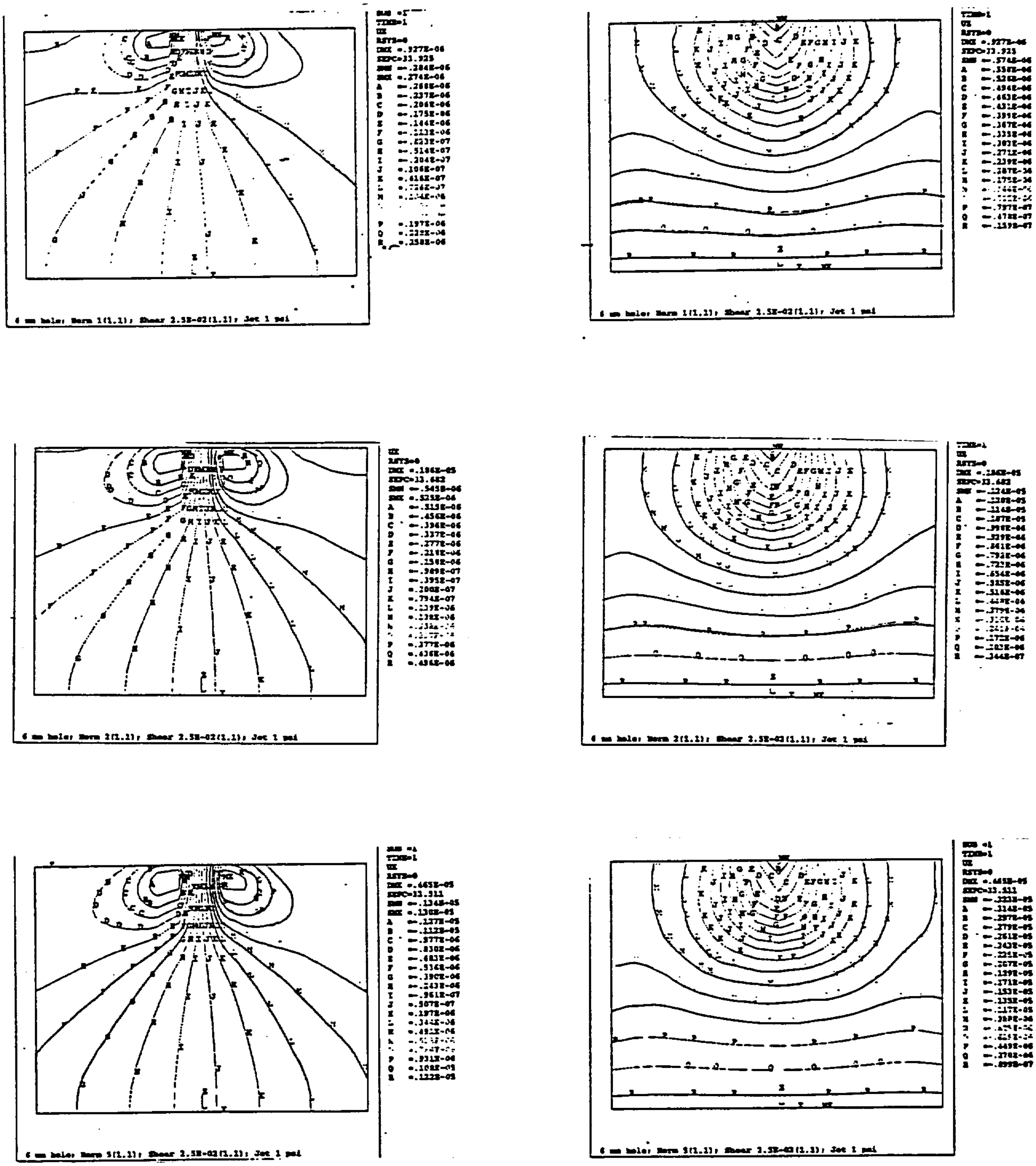

Figure 8 Effect on displacement with varying normal pressures

(p_j =0.25 psi; τ_n=0.025 psi)

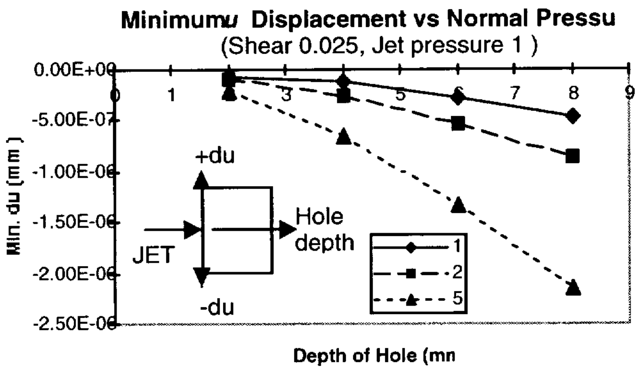

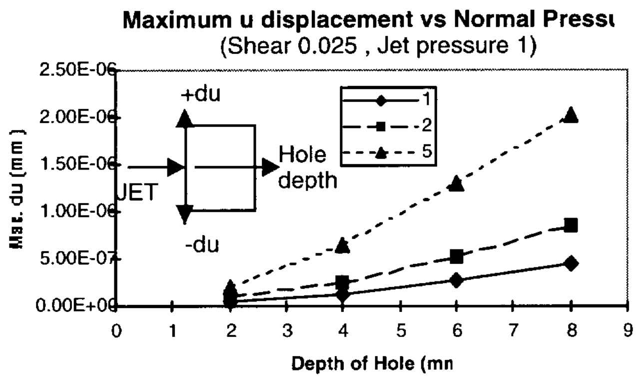

Figure 9(a) *u*--displacement vs. normal pressure

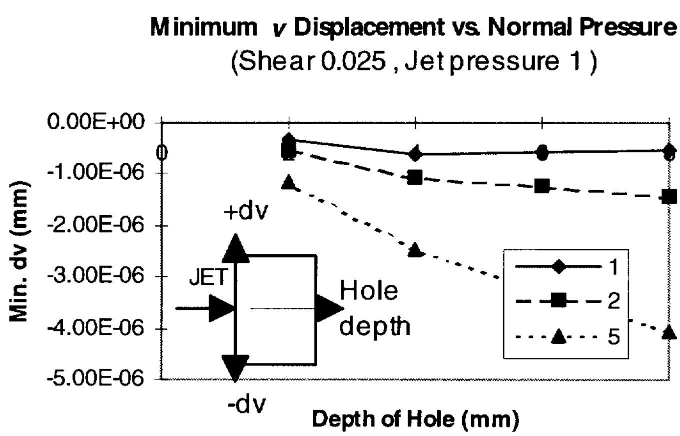

Figure 9(b) *v*--displacement vs. normal pressure

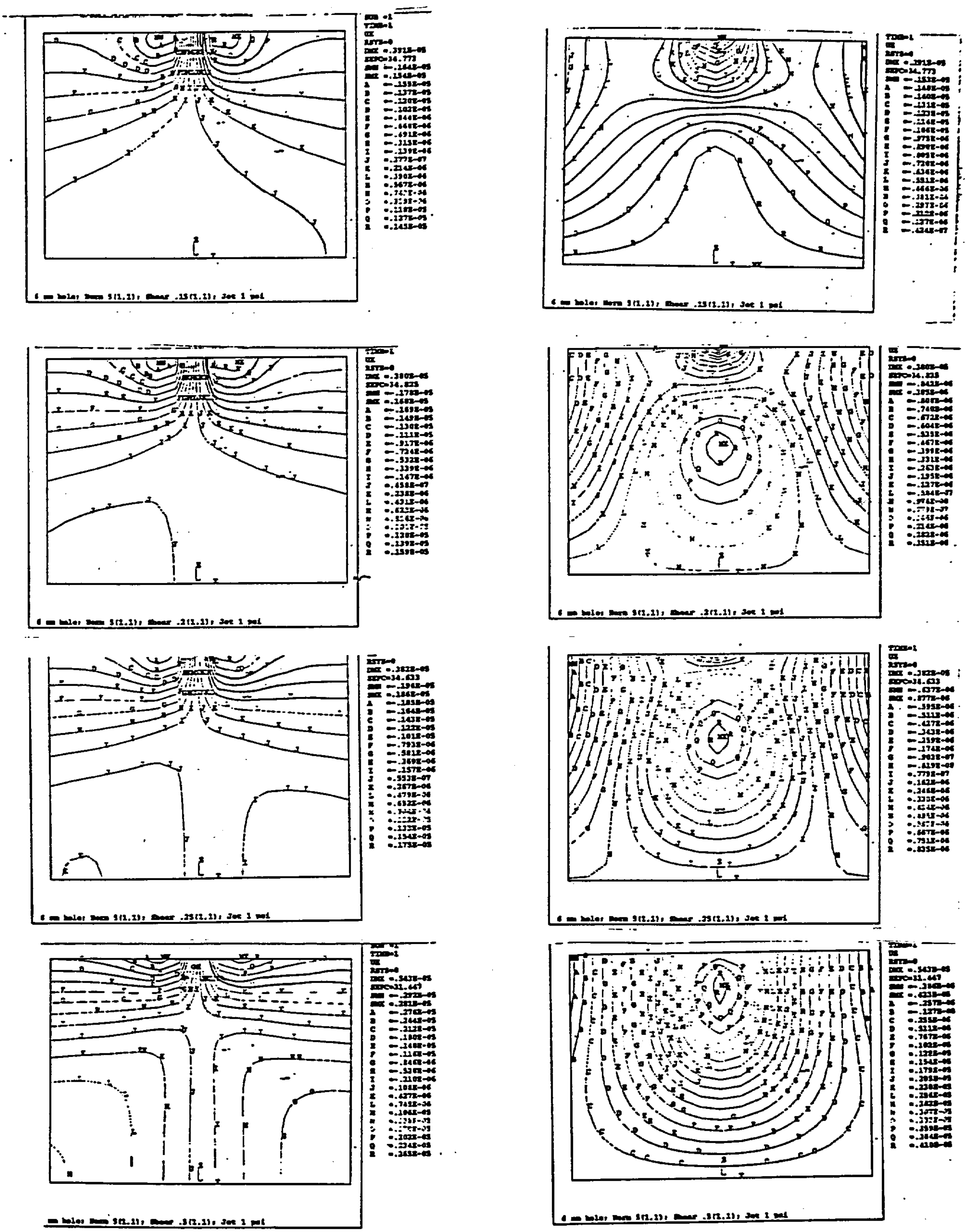

Figure 10 Effect on displacement with varying shear

(p_n=5.0 psi; p_j =1.0 psi)

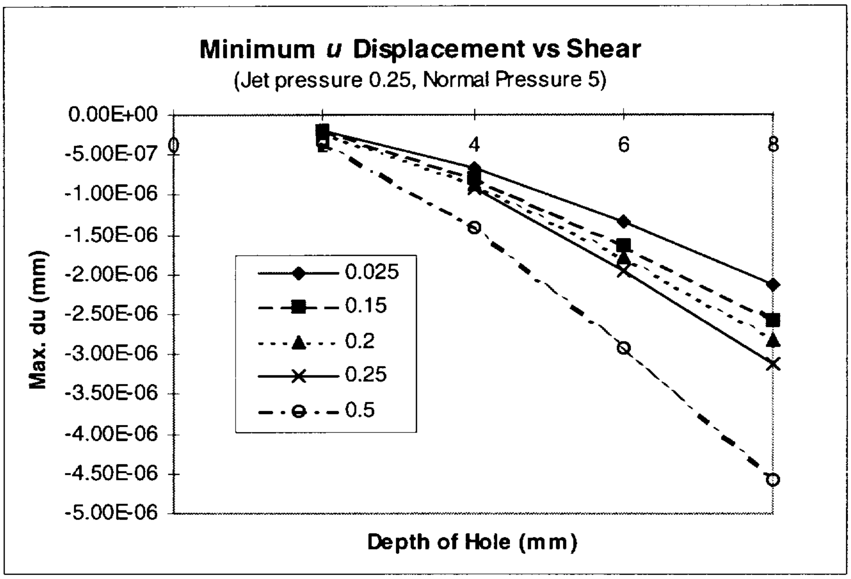

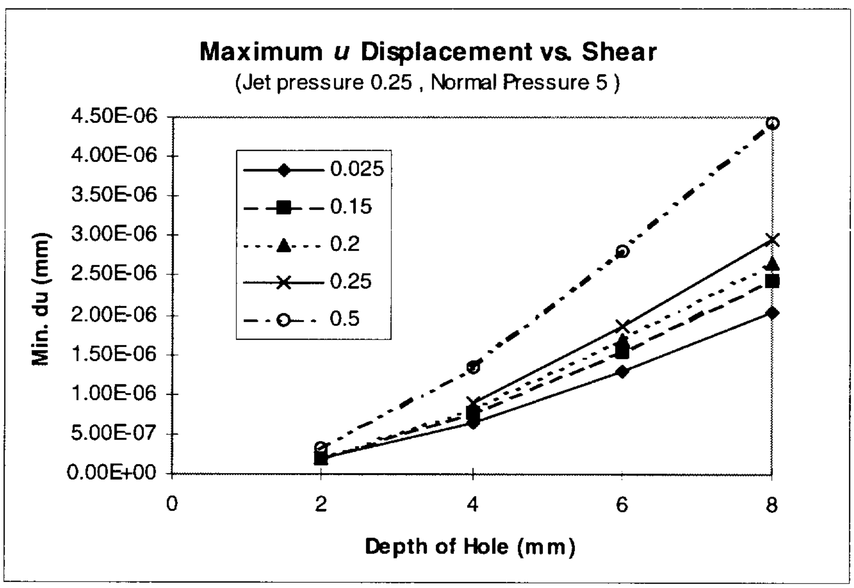

Figure 11(a) u--displacement vs. shear

(p_n=5.0 psi; p_j =0.25 psi)

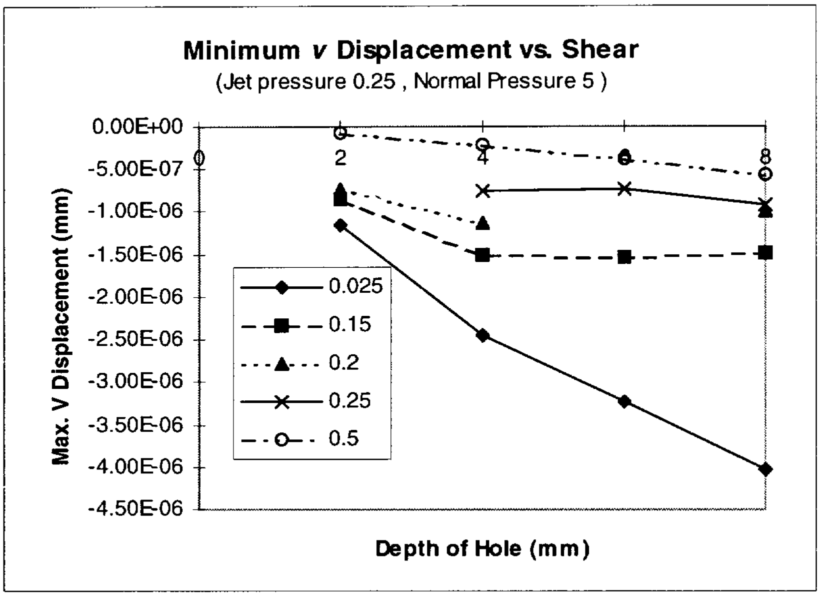

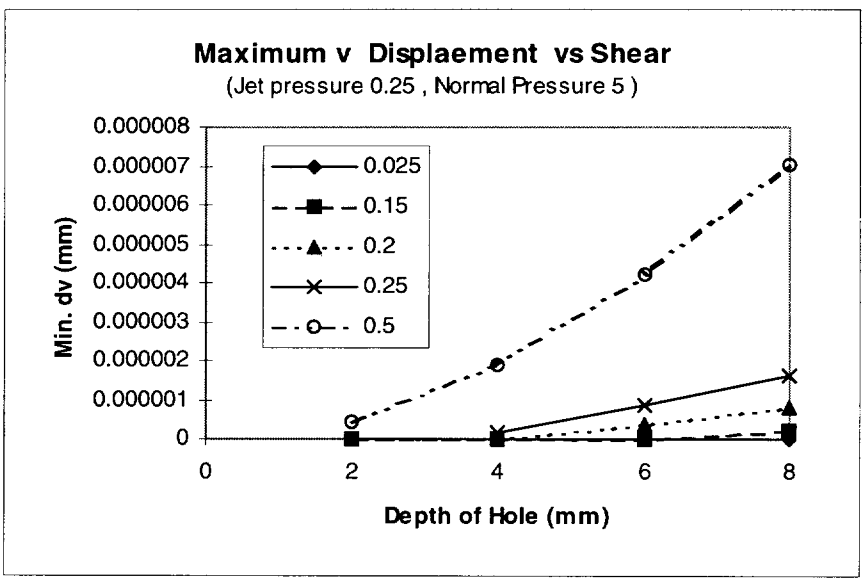

Figure 11(b) v--displacement vs. shear

(p_n=5.0 psi; p_j =0.25 psi)

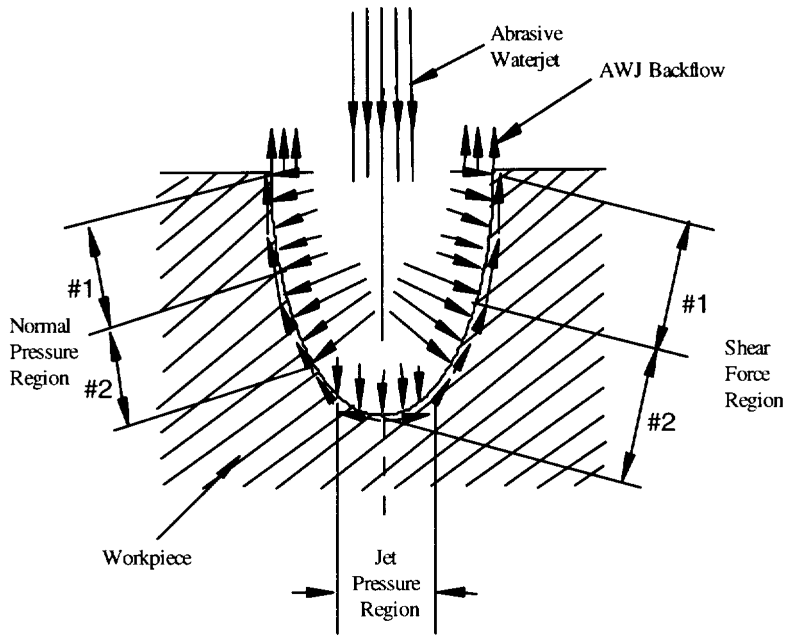

Figure 12 Schematic of the Un-uniform AWJ Pressure Loads

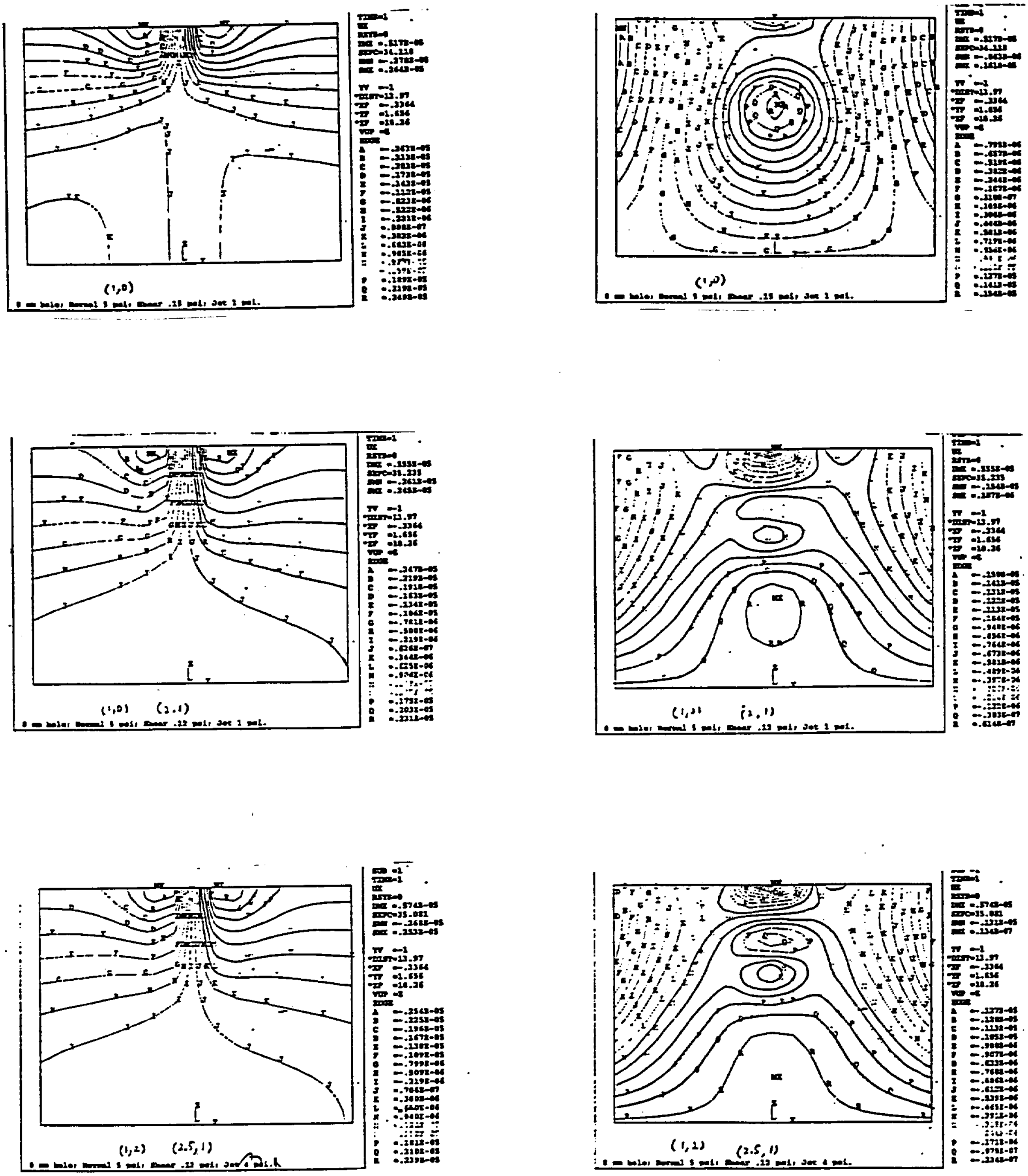

Figure 13 Effect on displacement with non-uniform normal pressure

REFERENCES

Guo, Z., "Experimental and Numerical Analysis of Abrasive Waterjet Drilling of Brittle Materials," *Ph. D Dissertation, University of Washington*, 1998.

Guo, Z., and Ramulu, M., "Surface Displacement Measurement with Moiré Interferometry Technique," *8th American Waterjet Confe, Aug., 1996; Houston, TX*

Ramulu, M., and Wong, K., P., "Preliminary Investigations of Abrasive Waterjet Piercing 1987 Process by Dynamic Photoelasticity," *International Journal of Water Jet Technology*, vol. 1, no. 2, Sept. 1991, pp. 53-63.

Ramulu, M., "Dynamic Photoelastic Investigation on the Mechanics of Waterjet and Abrasive Waterjet Machining," *Optics and Lasers in Engineering,* 1993, pp. 43-65

Tikhomirov, et al., "High-Pressure Jetting," *ASME Press Translations*, 1992.

10th American Waterjet Conference
August 14-17, 1999: Houston, Texas
Paper 20

FINITE ELEMENT MODELING OF COOLANT FLOW AT THE CUTTING ZONE IN HIGH PRESSURE WATER JET ASSISTED MILLING

Ram S. Mohan, Ph.D.
The University of Tulsa
Tulsa, OK

Radovan Kovacevic, Ph.D.
Southern Methodist University
Dallas, TX

V. Chiratanagandia, M.S.
Case Corporation
East Moline, IL

ABSTRACT

In metal machining, material removal in the form of chips takes place due to shearing action caused by the relative motion between the tool and the workpiece. The resulting friction and plastic deformation at the cutting zone lead to higher energy consumption and heat generation. This causes an increase in the frictional forces, workburn, tool wear, chip burn and poor surface quality. These detrimental effects can be reduced if the thermal/frictional conditions at the cutting zone are controlled. Cutting fluids have been traditionally used as an external means for heat removal and lubrication.

A coolant/lubricant system is developed here for face milling operations based on high pressure waterjet (up to 380 MPa) in order to improve the process performance. The coolant is injected through the rake face of the tool so that it can reduce the secondary shear, lower the interface temperatures and the temperature of the insert itself. The design consists of a high-pressure intensifier pump, a rotary swivel, main flow channel, radially extending feed channels, sapphire orifice and an insert with EDM driller hole. In this investigation, the fluid flow in the cutting zone is numerically simulated in order to visualize the effect of jet orientation, location of the EDM drilled hole, and change in volume flow rate for optimum performance of the coolant/lubricant system. Properly oriented jet not only dissipate the heat generated and provide good lubrication at the cutting zone but also create fluid pressure at the tool-chip interface improving the wettability. The high-pressure water jet was simulated at micro-level to better understand the pressure distribution and quantitatively estimate the interface fluid velocity.

Detailed experiments of the developed system indicate that due to the improved effectiveness of the jet lateral flow in reducing the tool-chip contact area, the cutting forces are reduced by 30% to 50% with increase in coolant flow rate. The decrease in tool wear caused by the high pressure coolant leads to about 50% improvement in R_a. Also the chips produced by high pressure water jet cooling were small, without any burrs, folded over and were having bright surfaces indicating improved thermal/frictional conditions existing at the tool-chip interface.

10^{th} American Waterjet Conference
August 14-17, 1999: Houston, Texas

Paper **21**

ENHANCEMENT OF ULTRAHIGH-PRESSURE TECHNOLOGY WITH LN_2 CRYOGENIC JETS

H.-T. Liu, S. Fang, C. Hibbard, and J. Maloney
Waterjet Technology, Inc.
Kent, Washington, U.S.A.

ABSTRACT

Laboratory tests have demonstrated that an ultrahigh-pressure (UHP) abrasive cryogenic jet (ACJ) using liquid nitrogen (LN_2) as the working fluid has about the same material removal capability as a UHP abrasive-waterjet (AWJ) under similar operating conditions. Further studies have demonstrated that the performances of the two jets differ considerably because of the fundamental differences in the physical and thermodynamic properties of the two working fluids. Understanding the differences between the waterjet (WJ) and the cryogenic jet (CJ) would help optimum selection of one jet versus the other for various applications. This paper examines important differences in the two jets and discusses their advantages and disadvantages for selected applications. Preliminary test results are presented to demonstrate performance superiority of the CJ/ACJ to the WJ/AWJ for a number of applications in which the latter has shown marginal to unsatisfactory performance. The CJ/ACJ and WJ/AWJ complement each other, greatly enhancing the versatility and performance of UHP technology as a whole. Maturity of the CJ/ACJ technology would further promote UHP technology for a wide range of machining services and surface preparation, completing favorably with other technologies.

1. INTRODUCTION

The UHP WJ and AWJ have gone through significant technological advancement since they were pioneered at Waterjet Technology, Inc., or WTI (then Flow Industries, Inc.) during the 1970s and 1980s. The advancement is multi-faceted, including but not limited to improvements in hardware reliability, material removal rate, user friendliness, operational safety, surface and kerf quality, and process efficiency and precision. For example, the AWJ has been applied successfully for milling light weighting aerospace components and large optic structures (Miles, 1998) and for drilling small-diameter and large-aspect-ratio holes on high-performance aircraft engine components (Liu et al., 1998). An abrasive suspension or slurry jet (ASJ) has recently been developed and applied for near-net shaping of three-dimensional optical components (Liu, 1998). For surface preparation, WJ/AWJ has been established as an effective alternate for conventional dry-grit blasting, which is being phased out due to environmental concerns and inadequate performance. In particular, a Newjet™ nozzle (patent pending) was successfully introduced by Surface Protection, Inc. (SPI) to replace dry-grit blasting. Field results have shown that the Newjet is faster (2 to 3 times), cheaper (30%), better (white-metal surface finish), and safer (no airborne dust) compared to dry-grit blasting.

Nowadays, UHP WJ/AWJ has been widely accepted as one of the mainstream machining and surface preparation tools. The WJ/AWJ has been competing on an equal basis with conventional tools and modern technologies such as the laser, EDM, diamond turning, and chemical stripping, etc. One of the advantages of the WJ/AWJ over the laser and EDM is that the WJ/AWJ is material independent with only few exceptions. Being a cold process that induces the minimum thermal (high-temperature) and mechanical stresses to the workpiece, the WJ/AWJ is superior to the laser and EDM for processing materials that are susceptible to thermal damage. Under certain circumstances, the laser and EDM may induce recast on the materials; recast is one of the sources for initiating surface and subsurface cracks that significantly weaken the strength of the materials. For precision machining, the laser is incapable of drilling straight holes because of the "hour-glass" waist at the focal point. On the other hand, EDM is not suitable for machining that requires removing large amount of materials. In particular, the AWJ is superior to the laser and EDM for drilling small-diameter and large-aspect-ratio holes.

The WJ/AWJ is however not suitable for applications that are incompatible with the use of water or wet abrasives. Such applications include processing hygroscopic and chemically reactive materials and, in some cases, jobs performed in close proximity to high-voltage, toxic, and radioactive sources. For processing toxic and radioactive materials, spent water and abrasives become contaminated and are difficult and expensive to be treated and disposed of. As a continued effort in advancing UHP technology and broadening its application base, WTI has successfully developed a UHP cryogenic technology to complement its water-based counterpart.

This paper examines and discusses the differences between the CJ/ACJ and WJ/AWJ. Applications that take advantage of their differences are investigated, with emphasis on those in which the WJ/AWJ cannot produce satisfactory results. Sample test results are presented to demonstrate the superiority of the CJ/ACJ to its water-based counterpart for those applications.

2. UHP JETTING TECHNOLOGIES

The UHP cryogenic technology is an extension of its water-based counterpart. There are several common key components of the two technologies, including the UHP pump, the orifice, the abrasive nozzle, and the mixing tube. A brief description of the two technologies is given below. For detailed information, refer to Hashish (1989) and Liu and Butler (1998).

2.1 Waterjets and Abrasive-Waterjets

The UHP WJ is formed by pumping water through a small-diameter orifice at pressures up to 380 MPa. Abrasives are fed into an AWJ nozzle consisting of a feed port and a carbide mixing tube. The feed port is placed immediately downstream of the orifice to take advantage of the suction created at the exit of the WJ -- the "jet pump" effect.

In general, the WJ can cut a variety of soft and thin materials such as fabrics, paper, rubber, plastic, and wood. With the incorporation of a swivel, the WJ has been used as a surface preparation tool to remove corroded paint layers and rust and to scarify concrete surfaces. To increase the material removal rate, pulsed WJs of different configurations have been successfully developed (e.g., Vijay, 1998). For cutting hard and thick materials such as metals, glass, ceramics, and some composites, AWJs using abrasives with hardness tailored to that of the target workpiece must be used. To improve the material removal efficiency, abrasive suspension or slurry jets or ASJs, have been developed. The material removal rates of the ASJ has shown to be about 3 to 5 times faster than those of the AWJ. (Hashish, 1990). To date, the AWJ is mainly limited to cutting and machining applications. Efforts to develop a swivel that would increase the size of the footprint while resisting the wear of abrasives has shown little progress. The innovative Newjet™ nozzle that has no moving part is specifically designed for surface preparation.

Recent advancements in nozzle design, process control, and computer-controlled manipulators have facilitated the WJ/AWJ and ASJ for precision machining and surface preparation tasks that cannot be accomplished technologically or economically with other tools. Several such fielded and factory applications are listed below and illustrated in Figures 1 and 2.

- WJ/AWJ surface decontamination and size reduction for nuclear facility D&D (Figure 1)
- Pulsed WJ or water cannon for breaking rocks (Figure 1)
- AWJ breaking up toxic waste for removal and disposal (Randolph et al., 1997)
- WJ/AWJ on-site underwater cleaning of jet pumps for nuclear power plants (Figure 1)
- Newjet™ removing paint, rust, and marine growth on ship hulls and platforms (Figure 1)
- AWJ drilling of small holes on engines of high-performance aircraft components (Figure 2)
- Pocket milling of aerospace materials for light weighting (Miles, 1998) and (Figure 2)
- Near-net shaping of optical components with ASJs (Liu, 1998) (Figure 2).

New applications for the WJ/AWJ and ASJ continue to surface as UHP technology matures and gains acceptance from the industry and military. Our extensive experience in testing the

WJ/AWJ and ASJ for various applications has revealed certain weaknesses of the water-based UHP technology for some applications, as mentioned in Section 1:

- For processing hygroscopic, chemically active, and explosive materials
- At sites very close to high-voltage and explosive sources
- At sites where generation of secondary wastes must be minimized
- For processes that have low or no tolerance to substrate damage (depainting of composite aircraft components) and delamination (drilling holes in laminated parts)
- For processes that require high-quality surface finish and kerf quality

2.2 Cryogenic Jets and Abrasive Cryogenic Jets

UHP cryogenic technology was initiated at the Idaho National Environmental and Engineering Laboratories (INEEL). Preliminary results have shown great promise for developing a cryogenic cutting and cleaning tool. In late 1993, WTI began developing a liquefied-gas jetting technology in an attempt to mitigate the weaknesses of the water-based UHP technology. Success in such an development would further increase the market potential of the UHP technology.

Initial efforts were focused on developing techniques for forming liquefied carbon dioxide (LCO_2) jets at relatively high temperatures (218 to 248K). High-speed LCO_2 jets at pressures up to 340 MPa were successfully formed and exhibited significant cutting, drilling, and material surface-removal capabilities (Dunsky and Hashish, 1994). However, because the liquid phase of CO_2 is thermodynamically unstable at ambient pressures, attention has since focused on LN_2 jets for the development of useful cutting and surface-preparation tools. LN_2 jets produced in early work had poor coherence and very limited cutting power. Insufficient cooling of the pressurized LN_2 was identified as the primary reason for this low performance.

Supported by DoC and DoE SBIR projects, with substantial in-kind contributions of liquid nitrogen and cryogenic handling equipment and of cryogenic know-how from Praxair, Inc., a modern cryogenic facility was established at WTI in 1995. The facility included an LN_2 supply and delivery system equipped with an 11,360-liter LN_2 storage tank, a cryogenic pump, subcoolers, and an in-line cooler. Figure 3 shows the LN_2 storage tank and accessories; a sketch of the jet cutting station constructed to study cryogenic processes is shown in Figure 4. Standard WJ/AWJ nozzles, as illustrated in Figure 5, were used to form the CJ/ACJ driven by a 117-MPa cryogenic crankshaft pump. Tests were conducted to determine the performance of the cryogenic jets. For example, it was discovered that the coherency and therefore the strength of the CJ increases with decreasing temperature, an essential feature for developing a CJ capable of cleaning and cutting. The CJ/ACJ was found to have material removal capability similar to that of the WJ/AWJ under the same operating conditions (Dunsky and Hashish, 1996; Hashish and Dunsky, 1998). To be compatible with the performance of commercial WJ/AWJ systems, it was therefore necessary to drive the CJ/ACJ at 240 MPa or higher.

Subsequently, a 240-MPa crankshaft cryogenic pump was developed at WTI. The decision to develop the crankshaft pump rather than the intensifier pump was based on the ability for meeting the requirements of mobility, compactness, and simplicity, mechanical and thermal efficiency, and user friendliness. Experiments were conducted to explore the feasibility of developing a versatile tool for depainting aircraft, for nuclear facility D&D, and for demilitarization. For aircraft depainting, a vanishing abrasive cryogenic jet or VACJET was developed by using CO_2 solid particles as the abrasives. Test results are encouraging for mitigating damage on thin-clad aluminum and composite substrates. However, the footprint of the CJ and VACJET must increase considerably for them to become viable depainting tools. The adaptation of the Newjet™ nozzle to form the CJ and VACJET has shown great promise toward achieving the required performance enhancements.

For nuclear facility D&D and for demilitarization, an enclosed ACJ cutting and scarifying workstation was constructed to collect and dispose of the spent N_2 and abrasives (Figure 6). The spent abrasives are airborne as soon as the LN_2 evaporates upon impinging the target workpiece. Tests were conducted to cut and scarify various building materials. The test results compared favorably with those using existing and emerging tools for nuclear facility D&D. The ACJ was also successfully applied to cut access holes in composite coupons, simulating typical environments and conditions for carrying out demilitarization tasks.

2.3 WJ/AWJ Versus CJ/ACJ

Although the WJ/AWJ and CJ/ACJ operating at the same pressure display similar cutting and cleaning power, their performances differ in many ways. Basically, the distinction in the thermodynamic properties of the working fluids is responsible for their differences:

- LN_2 in the CJ/ACJ changes phase and evaporates upon impacting the workpiece, whereas water in the WJ/AWJ remains liquid throughout the process.
- The CJ/ACJ and WJ/AWJ are operating, respectively, at cryogenic temperatures and at slightly above ambient temperature

As a result, the two types of UHP jets behave quite distinctly in their formation and interactions with the media being processed. Important behavioral and performance differences in terms of environmental impact, process control, operational safety, surface finish, substrate integrity, and others include but are not limited to:

- Abrasives in the ACJ become airborne after the LN_2 evaporates, whereas the AWJ generates a minimal amount of airborne dust.
- CJs generates no secondary waste and is considered to be environmentally “green”, whereas WJ generates considerable secondary waste.
- The CJ/ACJ and the WJ/AWJ are cryogenic and cold processes, respectively. At cryogenic temperatures and in an N_2-rich environment (depletion of oxygen), the CJ/ACJ has proven to be non-explosive, chemically inactive or inert, and biologically sterile and is most suitable for food processing (without abrasive), demilitarization, and nuclear facility D&D.
- The CJ/ACJ is strictly a non-wetting process, whereas WJ/AWJ tends to wet the workpiece; the former is most suitable for processing hygroscopic materials that could trigger chemical reactions when wetted (e.g., rusting, heat generation, explosion, etc.)
- The ACJ has an extensive range of aggressiveness, from that of dry-grit blasting to that of UHP AWJ cutting; it can be tailored to the mechanical strengths of the target workpiece.

    - For surface preparation, corroded surface coatings can be effectively removed without damaging the underlying substrate (e.g., for depainting airframes made of thin-clad aluminum or composite).
    - For machining, the quality of kerf edges can be improved by fine tuning the aggressiveness of the ACJ.
- The effective standoff distance (SOD) of the CJ/ACJ is considerably shorter than that of the WJ/AWJ. The CJ/ACJ loses its cutting power rapidly with increasing SOD, an important property that can be utilized to better control the machining and cleaning processes.
- The ACJ tends to have weaker residual cutting power than does the AWJ, as the (airborne) abrasives in the ACJ disperse in all directions after the LN_2 changes phase. In the absence of phase change, the AWJ is more or less unidirectional.
- The CJ/ACJ is less penetrative than the WJ/AWJ. The spent LN_2 evaporates in N_2 rapidly and the phase change reduces the kinetic energy per unit by about 2 orders of magnitudes. On the other hand, the spent water droplets maintain a high kinetic energy per unit area; the former is less potent than the latter in causing substrate damage, particularly in composites.

3. RESULTS AND DISCUSSION

To demonstrate the performance difference between the CJ/ACJ and WJ/AWJ discussed in Section 2.3, selected results of tests described in Section 2.2 are presented in this section.

3.1 Aircraft Depainting

The CJ and the VACJET using CO_2 particles as the abrasives have been found to be most suitable for airframe depainting (Liu and Butler, 1998). The potential of cryogenic technology as a next-generation airframe-depainting technology has been demonstrated by its environmentally green nature and by the ability to fine tune its aggressiveness, to mitigate substrate damage and to preserve the mechanical integrity of the delicate substrates. The CJ and VACJET create zero added waste. After depainting a commercial aircraft, the spent N_2 can readily be released back into the atmosphere after passing through a HEPA filter. The only waste to be disposed of is the few hundred kilograms of paint chips. When the starch medium blasting (SMB) method is used, for example, many tons of contaminated starch must be treated as hazardous material and disposed of. For a comparison of the performance of several aircraft depainting technologies, refer to Liu and Butler (1998) and Wolbach et al. (1997).

In the same context, the highly penetrative power of the UHP WJ was demonstrated when it was used to remove paint without a primer on an aluminum substrate. As illustrated in Figure 7a, the return water flow got under the paint coating at the interface, and it broke up and lifted the paint layer in an irregular pattern on the edges of both sides of the cleaned path. When the CJ was used, as can be seen in Figure 7b, no irregular breakup of the paint edges resulted. Evidently, the phase change of the LN_2 significantly reduces the penetrative power of the CJ as it transforms from a liquid jet to a gaseous jet. Such a liquid-to-gas transformation can be taken advantage of for controlling the aggressiveness of the CJ.

The weaker penetrative power of the spent N_2 gas than that of the water thus demonstrated would have important impact on scarifying contaminated layers from porous materials such as concrete. Such impact will be discussed later in this section.

3.2 Access Holes Cutting

The ACJ was also applied to cut 6.4-mm-diameter access holes on the bottom metal skin of four-layer composite coupons. The coupons consisted of a 9.5-mm-thick aluminum top skin, a 3.2-mm-thick stainless steel second layer, a 10.2-cm-thick hygroscopic filler made of plaster of Paris, and a 3.2-mm-thick stainless steel bottom skin. Cutting was conducted by mounting the coupons on a turntable with the nozzle mounted on a two-axis linear traverse inside the enclosed ACJ cutting and scarifying workstation (Figure 6). Figure 8 displays four snapshots of a coupon taken during one of the cutting sequences. To gain access to the bottom skin, 7.6-cm-diameter holes were first cut in the top three layers (Figures 8a through 8c). The filler core was either pulled out manually or scarified away by moving the nozzle toward the rotational center. Finally, the nozzle was lowered close to the bottom stainless steel skin to cut out the 6.4-mm-diameter hole (Figure 8d).

Four coupons were processed with the ACJ operating at pressures between 138 and 241 MPa. As illustrated in Figure 9, the ACJ successfully cut out the access holes in the top three layers without disturbing the remainder of the hygroscopic filler. During cutting, the filler layer chilled by the LN_2 and by the latent heat absorption was frozen solid, greatly enhancing its structural stability. The ACJ and AWJ are dry and wet processes, respectively. If an AWJ is used, the spent water trapped in the cavity of the coupon will be absorbed by the filler material, potentially leading to considerable swelling of the filler material. Soaking of the filler material by the spent water could cause the side wall to collapse or trigger a strong chemical reaction provided the filler material is strongly acidic or alkaline. The most difficult step when an AWJ is used is to keep the spent water from leaking through the bottom access hole after it is drilled through. For certain demilitarization applications, even a small amount of water leakage below the skin layers could be disastrous. The ACJ process creates an N_2-rich cavity at cryogenic temperatures, greatly minimizing hazards when operating in an explosive environment.

Table 1 shows the results of the coupon cutting tests. When the ACJ pressure was increased from 138 to 241 MPa, the speed of cutting individual layers was increased by more than 4 times. The overall process time was 2 times faster, decreasing from 16 min at 138 MPa to 6.8 min at 241 MPa. The total processing time can be further minimized through hardware and process optimization.

3.3 Nuclear Facility D&D

For nuclear facility D&D, the CJ/ACJ is currently being tested for cutting and/or scarifying a variety of building and specialty materials in order to demonstrate the advantages of the CJ/ACJ over the WJ/AWJ. For D&D processes that are incompatible with water, the CJ/ACJ has a clear advantage, especially for processing materials that are hygroscopic or reactive to wetting.

As discussed in Section 2.3, the CJ/ACJ is expected to minimize secondary-waste generation and mitigate disastrous wetting of radioactive components. Depending on the mechanical properties of the materials, either a CJ or ACJ can be used. Because the CJ generates the least amount of secondary waste that can be effectively removed using HEPA filters, it is the preferred tool for nuclear facility D&D whenever applicable. Table 2 lists the results of selected construction materials cut with a CJ at 207 MPa. Figure 10 illustrates several such samples processed with the CJ. Tests conducted so far have indicated that the CJ has about the same material removal power as the WJ/AWJ for cutting relatively soft and thin materials or removing thin coatings. The depth of cut is generally shallower for the CJ than for the WJ because the effective standoff distance is considerably shorter for the former. For some applications, the short standoff distance of the CJ could be advantageous over the WJ when fine control of the amount of material removal is called for.

A large number of nuclear facility D&D applications involve dismantlement and size reduction of contaminated equipment made of materials that must be processed with an ACJ rather than a CJ. As discussed in Section 3.2, the capability of cutting metal plates has been demonstrated. Therefore, the ACJ can be readily applied to process most contaminated equipment because the ACJ or AWJ process is material independent, as stated in Section 1. Both the spent abrasives and N_2 are contaminated and must be treated and disposed of. The secondary wastes generated by the ACJ are, however, considerably less than those generated by the AWJ. The spent abrasives (common to both ACJ and AWJ) after treatment must be disposed of as low-level radioactive waste. Because the spent abrasives generated by the ACJ are dry, it may be less costly and/or more efficient to treat these spent abrasives than it would be to treat the wet ones generated by the AWJ. The spent N_2 generated by the ACJ can be readily released back into the atmosphere after passing through highly efficient HEPA filters (> 99.9%), whereas, the contaminated water generated by the AWJ is difficult and expensive to be treated and disposed of because mechanical filters for water are less efficient than HEPA filters are for gas. Time-consuming and expensive evaporative methods are often used to decontaminate the spent water in order to meet the requirements for disposal of the treated water as uncontaminated waste.

For decontamination of concrete slabs or other porous materials by scarifying the contaminated surface layers exposed to long-term radiation, it is speculated that the high-speed water droplets in the AWJ could drive surface contaminants farther into the otherwise uncontaminated interior. As a result, more materials must be removed and therefore disposed of to reach a certain level of decontamination. On the other hand, the use of the ACJ would minimize the penetration of contaminants into the interior because the LN_2 changes phase upon impinging the target surface and loses most of its penetrative power. In other words, the high-speed abrasives alone in the ACJ are responsible for scarifying the contaminated layers. The absence of a strong liquid coflow with the abrasives in the ACJ makes it unlikely that surface contaminants would be driven into the interior of porous structures. To achieve the same level of decontamination, therefore, less material removal would be required when the ACJ rather than the AWJ is used.

Another advantage of the ACJ over the AWJ pertains to secondary waste treatment and disposal, as mentioned above. In the long run, the higher costs of using LN_2 as the working fluid in the ACJ are expected to be compensated for by the added time, effort, and costs required for treatment and disposal of the contaminated water in the AWJ.

Experiments to scarify concrete slabs are planned using both the WJ/AWJ and CJ/ACJ to investigate this particular issue of interest. A Newjet™ nozzle (patent pending) will be adopted for the ACJ to increase the footprint and the material removal rate for the scarifying tests. The results will provide the necessary information to compare the overall performance of the ACJ and AWJ as a scarifying tool for nuclear facility D&D.

4. SUMMARY

Supported by DoE and DoC and with substantial in-kind contributions from Praxair, WTI successfully launched in late 1993 a research program on developing UHP cryogenic technology to complement and broaden the applications of UHP technology as a whole. Although the water-based UHP technology pioneered at WTI two decades ago has matured and gained acceptance by the industry as one of the main machining and surface preparation tools, there are several applications in which the WJ/AWJ has shown marginal to unsatisfactory performance. Such applications include but are not limited to the following situations:

- Materials incompatible with water or wet abrasives
  - Hygroscopic (some light-weight honeycomb cores)
  - Chemically active when wet (strongly acidic, basic, and explosive materials)
- Environment incompatible with water or wet abrasives
  - Close proximity to high-voltage and explosive sources
- Generation of harmful byproducts
  - Difficult treatment and costly disposal of spent water contaminated with toxic and radioactive wastes (depletion of disposal sites for secondary wastes)
- Excessive aggressiveness of the WJ/AWJ
  - Surface/subsurface damage to laminated and/or composite parts
  - Forcing surface contaminants to penetrate farther into interior of porous structures

Using the non-wetting, chemically inert, and cryogenic LN_2 as the working fluid, the CJ/ACJ is expected to work well for applications in which its water-based counterpart fails. In particular, the potential of a strong chemical reaction or explosion is minimized as the ambient air is replaced by the spent N_2 at cryogenic temperatures. Test results of cutting various building materials and cutting access holes on composite coupons have largely confirmed the superiority of the CJ/ACJ to the WJ/AWJ for these applications. For surface preparation, the footprint of the CJ/ACJ generated by standard WJ/AWJ nozzles is too small to be useful as effective scarifying tools. The cryogenic conditions have made the use mechanical swivels impractical. Currently, a rotating nozzle without the use of a swivel is under development. Furthermore, the Newjet™ nozzle which has no moving part is currently being adopted for the ACJ nozzle to increase both the footprint and the materials' removal rate. For aircraft depainting, a VACJET using solid CO_2 particles as the abrasives has shown promise for enhancing the depainting rate of the CJ without inflicting damage to underlying thin-clad aluminum and composite airframe skins.

Experiments are being prepared to compare the performance of the ACJ and AWJ for scarifying concrete slabs. Emphasis will be made to determine whether the considerable difference in the penetrative power of the two working fluids would indeed lead to differences in the penetration of surface contaminants into the interior of the concrete slabs.

5. ACKNOWLEDGMENT

This work is supported by contracts from Lawrence Livermore National Laboratory (B501537), DoE (DE-FG03-98ER82711), DoC (50-DKNB-6-90162), and from a WTI internal fund.

6. REFERENCES

Dunsky, C. M., and Hashish, M., “Feasibility Study of Machining with High-Pressure Liquefied CO_2 Jets,” *Proceedings of Symposium on Nontraditional Manufacturing Processes in the 1990s*, Chicago, ASME, 1994.

Dunsky, C. M., and Hashish, M., “Observations of Cutting with Abrasive-Cryogenic Jets,” *Proceedings of the 13th International Conference on Jetting Technology*, Sardinia, Italy, October,. 1996.

Hashish, M., “Advanced Machining with Abrasive-Waterjets - Theory and Applications,” *Proceedings of the Nontraditional Machining Conference*, SME Conference Reading, Orlando, Florida, October 30-November 2, 1989.

Hashish, M., “Entrainment Versus Direct Pumping Abrasive-Fluid Machining Systems,” *Proceedings of the 10th International Symposium on Jet Cutting Technology*, BHRA, Amsterdam, Netherlands, October 31-November 2, 1990.

Hashish, M., and Dunsky, C. M., “The Formation of Cryogenic and Abrasive-Cryogenic Jets” In *Proceedings of the 14th International Conference on Jetting Technology,* Brugge, Belgium, September 21-23, 1998.

Liu, H.-T. and Butler, T., “A Vanishing Abrasive Cryogenic Jet for Airframe Depainting,” In *Proceedings Of the 14th International Conference on Jetting Technology*, Brugge, Belgium, pp. 519-533, pp. 329-343, September 21–23, 1998.

Liu, H.-T., “Near-Net Shaping of Optical Surfaces with Abrasive Suspension Jets,” *Proceedings Of the 14th International Conference on Jetting Technology*, Brugge, Belgium, September 21 – 23, pp. 285-294, 1998.

Liu, H.-T., Miles, P., and Veenhuizen, S. D., “CFD and Physical Modeling of UHP AWJ Drilling" *Proceedings Of the 14th International Conference on Jetting Technology*, Brugge, Belgium, September 21–23, pp. 15-24, 1998.

Miles, P. J., “Light weighting Large Optics with Abrasive Waterjets,” Proceedings of the SPIE, Vol. 3430, pp. 304-312, July 20-21, 1998.

Randolph, J. D., Burks, B. L., Rinker, M., Summers, D., Blank, J., Lloyd, P. D., Johnson, M. A., Mullen, D., and Alberts, D., "Development of a Waste Dislodging and Retrieval System for Use in the Oak Ridge National Laboratory Gunite Tanks," *Proceedings of the American Nuclear Society 7th Topical Meeting on Robotics and Remote Systems*, April, 1997.

Vijay, M. M., "Design and Development of a Prototype Pulsed Waterjet Machine for the Removal of Hard Coatings," *Proceedings Of the 14th International Conference on Jetting Technology*, Brugge, Belgium, pp. 39-57, September 21–23, 1998.

Wolbach, C. D., Venkatesh, S., and Wander, J., "Current Status of Large Aircraft Frame Paint Stripping Technologies," *Proceedings of the DOD/Industry Aerospace Coatings Conference*, Las Vegas, Nevada, May 13-15, 1997.

Table 1. Comparison of ACJ Performance for Cutting of Composite Coupons

Test Coupon ID	p (MPa)	T (K)	ω (rpm)	SOD for Metal Layers (mm)	SOD for Filler (mm)	t_o (min)	V_o (cm/min)	V_{al} (cm/min)	V_{SS} (cm/min)
CC#1	138	105	25	3.2-5.1	15-100	16	≈37	≈ 61	≈109
CC#2	138	105	50	<3.2	15-100	15	≈ 80	≈ 127	≈239
CC#3	241	105	50	3.2-5.1	15-100	6.8	175	300	478
CC#4	207	105	50	3.2	15-100	7.8	152	267	399

Note: p = pressure, T = temperature, ω = rotating speed of turntable, t_o = overall cutting time of the coupon as a whole, V_o = overall cutting speed of the coupon, V_{al} = cutting speed of 9.5-mm-thick aluminum plate, V_{SS} = cutting speed of 3.2-mm-thick stainless steel plate.
Cutting speed = hole perimeter*ω/cutting time

Table 2. Cutting of Soft Construction Materials with CJ at 207 MPa

Description of Material	SOD (cm)	V_j (cm/s)	T (K)	Through Cut
Floor tile (Figure 10a)	0.32	1.27[a]	111	Yes
Pipe foam insulation 7.6-cm O.D. (Figure 10b)	0.32	1.27	107	Yes
Oak, 1.9-cm thick	0.32	0.064[b]	115	No
Oak, 1.9-cm thick	0.32	1.27	116	No
Plywood, 1.9-cm thick	0.32	0.064	115	No
Solid UHMW, 3.8-cm diameter (Figure 10c)	0.32	0.064	116	Nearly
Fabric-reinforced rubber hose, 5.1-cm O.D. (Figure 10d)	0.32	0.64	117	No
Fabric-reinforced rubber hose, 5.1-cm O.D.	1.27	0.25	115	One Side
Fabric-reinforced rubber hose, 5.1-cm O.D. (Figure 10d)	0.32	0.25	115	One Side
Plastic tubing, white, 1.27-cm O.D.	0.32	1.27	116	One Side
Plastic tubing, white, 1.27-cm O.D.	0.32	0.25	115	One Side
Plastic tubing, white, 1.27-cm O.D.	0.32	0.13	113	One Side
Rubber hose, 3-cm O.D, 0.48-cm I.D. (Figure 10e)	0.32	0.064	116	No
Fabric-reinforced rubber hose, 10-cm O.D. (Figure 10f)	0.32	0.064	116	One Side
Fabric-reinforced rubber hose, 10-cm O.D. (Figure 10f)	0.32	0.05	117	One Side
Hard rubber tube, 5.1-cm O.D., 0.8-cm wall (Figure 10g)	0.32	1.27	115	No
Hard rubber tube, 5.1-cm O.D., 0.8-cm wall (Figure 10g)	0.32	0.064	118	One Side
Hard rubber tube, 5.1-cm O.D., 0.8-cm wall (Figure 10g)	0.32	0.64	117	One Side
Pipe foam insulation 7.6-cm O.D., 2.5-cm wall (Figure 10h)	0.32	1.27	115	Yes

[a] Highest available speed
[b] Lowest available speed

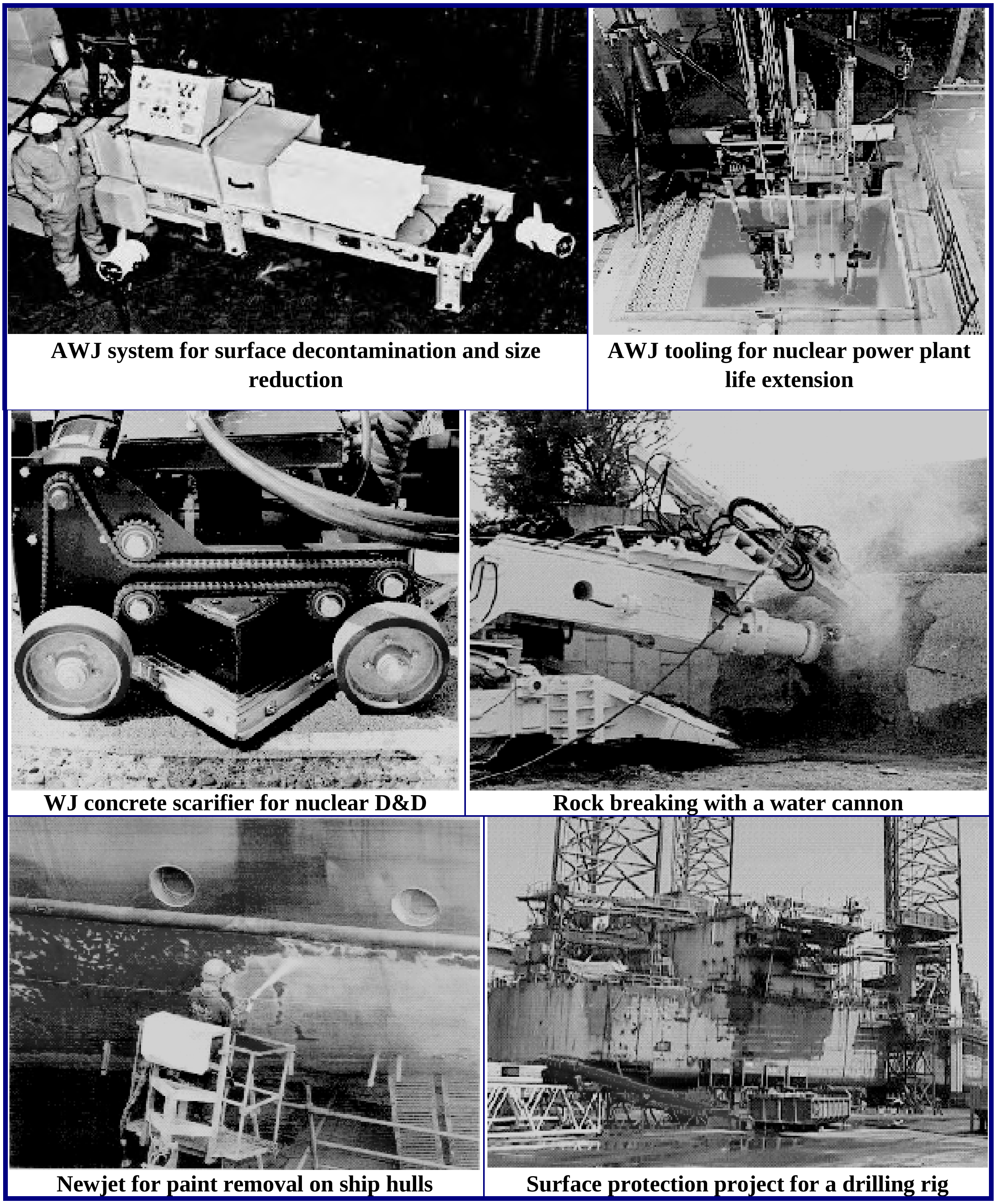

AWJ system for surface decontamination and size reduction

AWJ tooling for nuclear power plant life extension

WJ concrete scarifier for nuclear D&D

Rock breaking with a water cannon

Newjet for paint removal on ship hulls

Surface protection project for a drilling rig

Figure 1. Field Application Examples of Water-Based UHP Technology

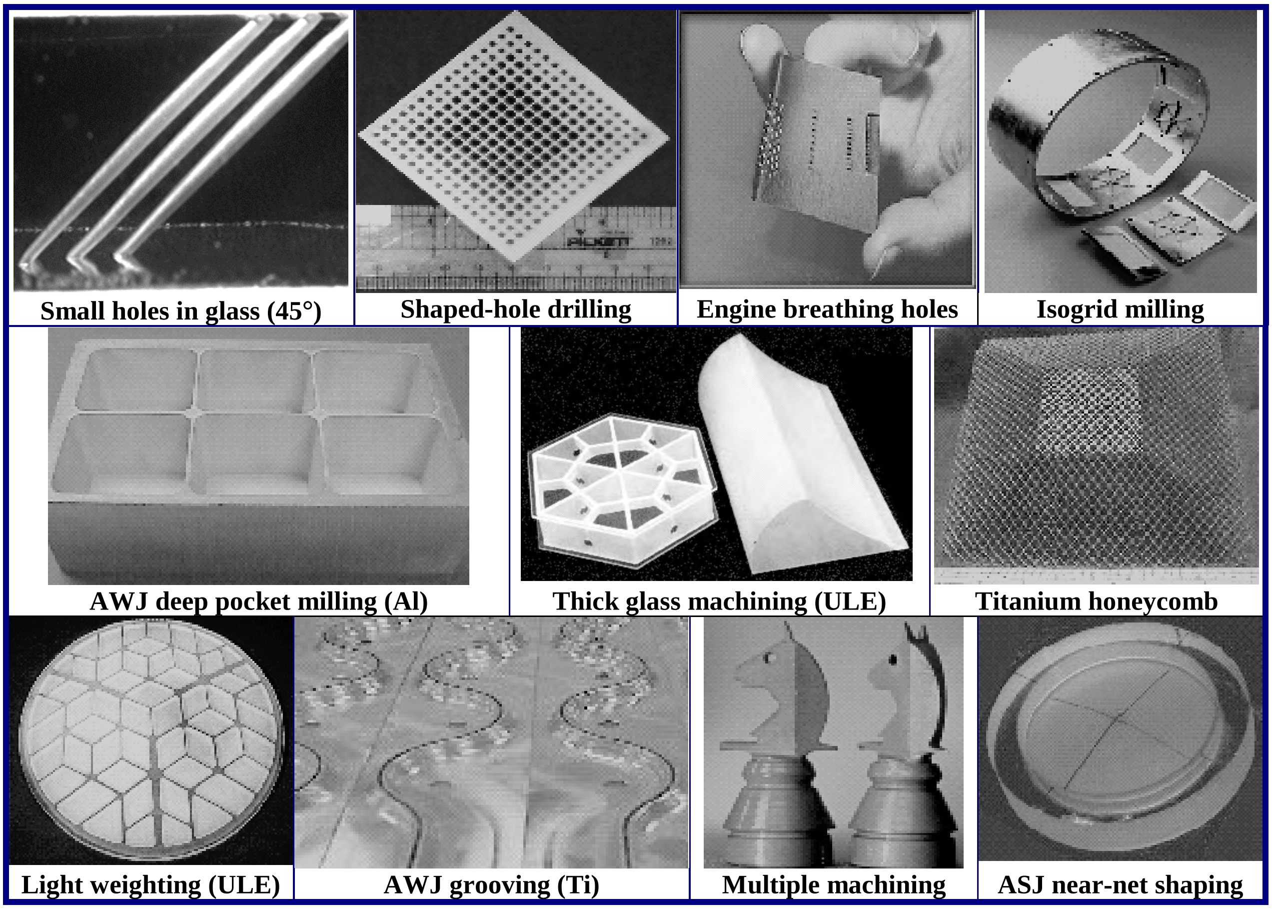

Figure 2. Factory Application Examples of Water-Based UHP Technology

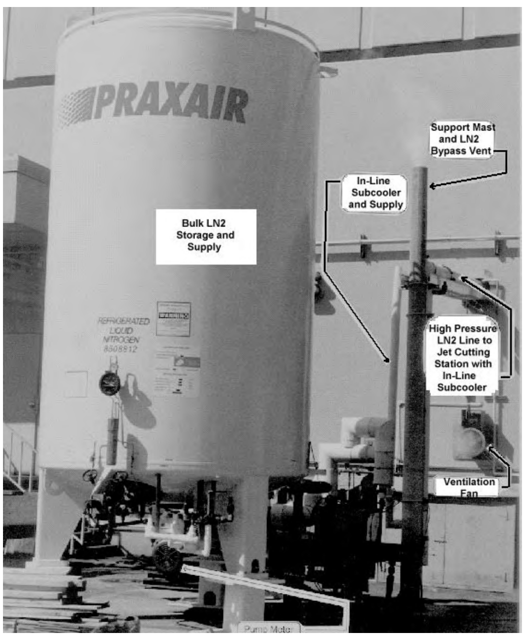

Figure 3. LN_2 Delivery System

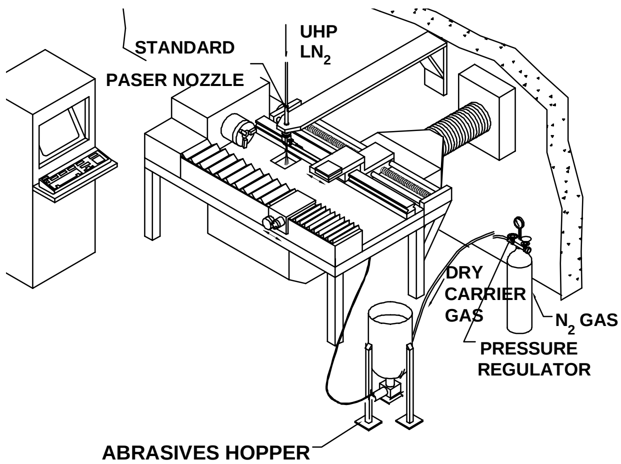

Figure 4. Sketch of Open High-Pressure Cryogenic Jet Workstation

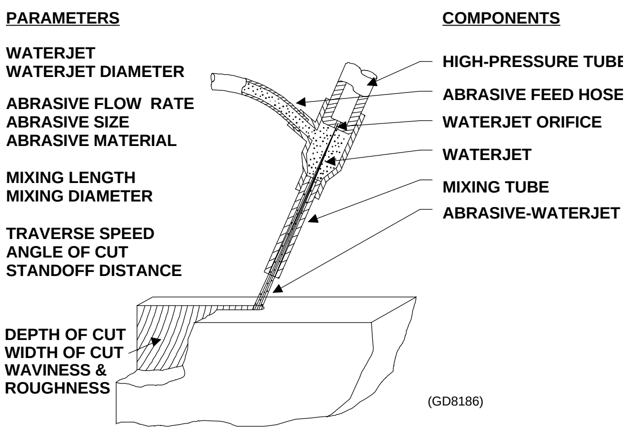

Figure 5. Abrasive-waterjet nozzle

Figure 6. Enclosed ACJ Cutting and Scarifying Workstation (Hood Open)

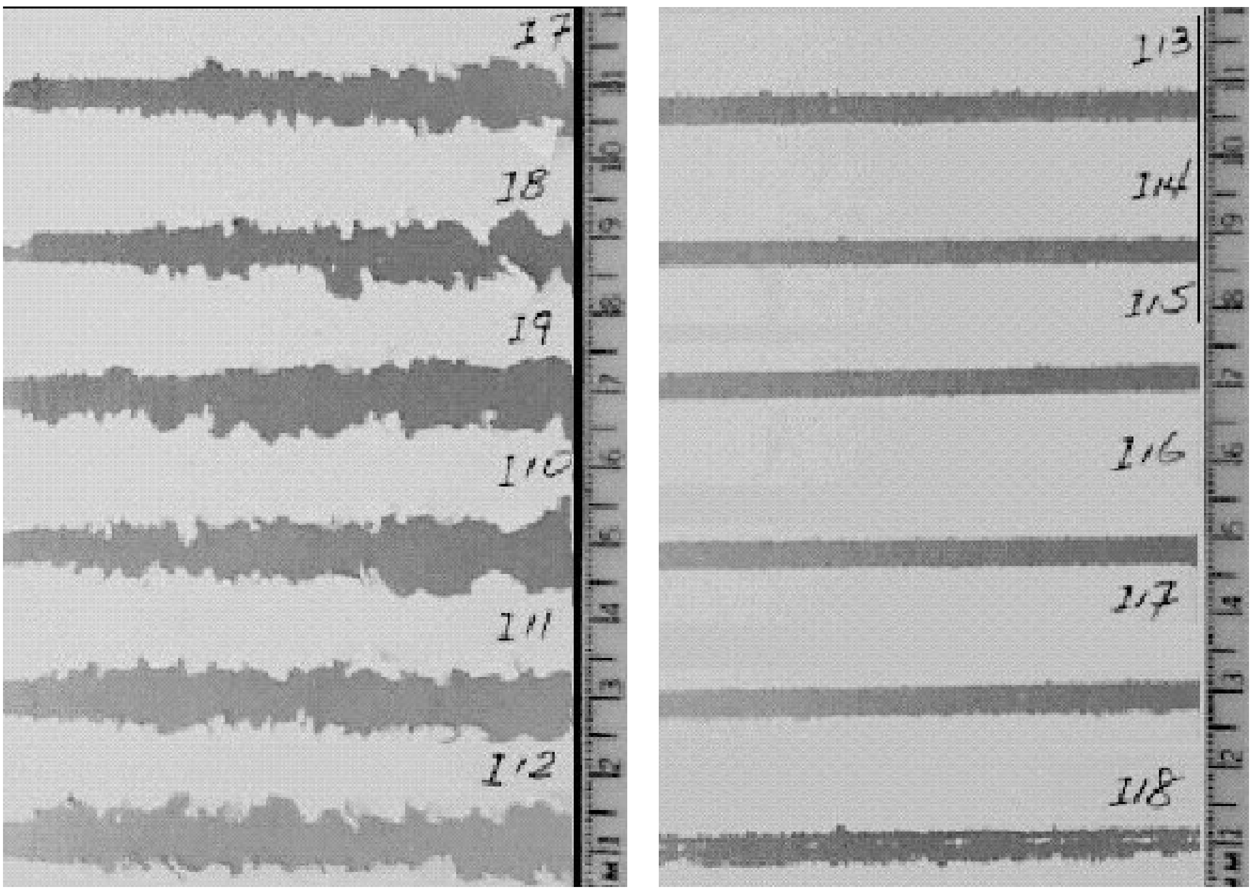

a. Waterjet

b. LN_2 cryogenic jet

Figure 7. Removal of Paint on Aircraft Aluminum Substrate (no Primer) with a 138-MPa Rectangular Water Jet and Cryogenic Jet

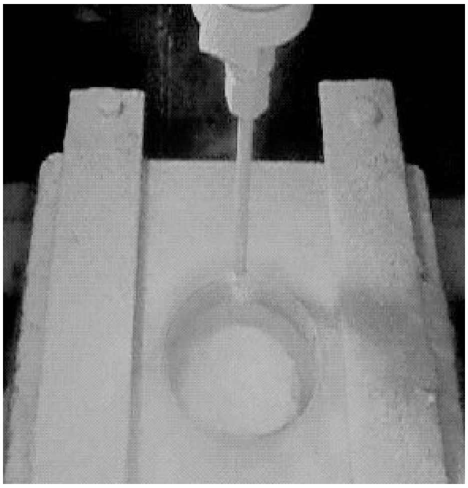

a. After through-cutting top two layers (14 Min)

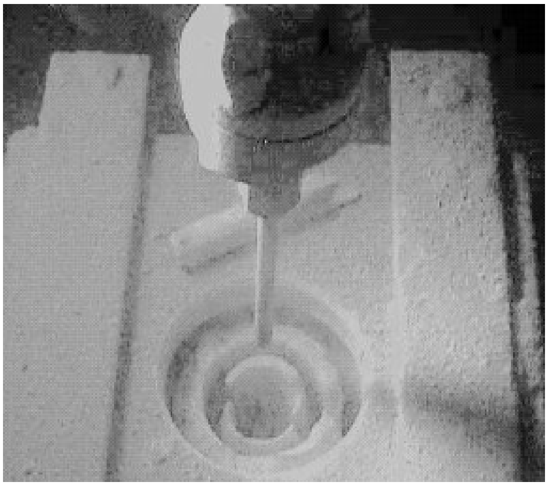

b. After rimming the plaster core twice (45 sec)

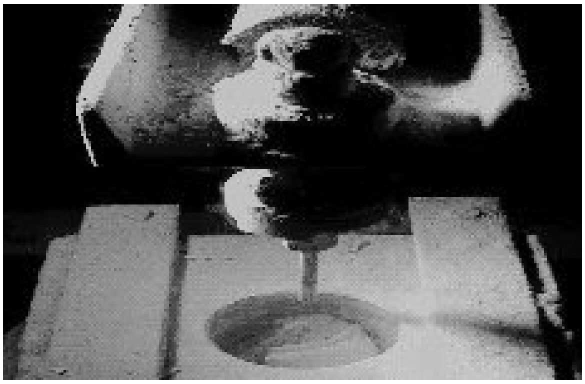

c. After rimming the core three times (60 sec)

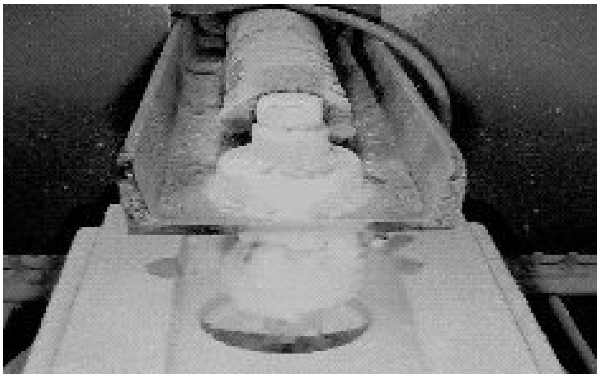

c. After through-cutting the bottom layer (45 sec)

Figure 8. Photographs of Composite Coupon #1 at Different Stages of Cutting

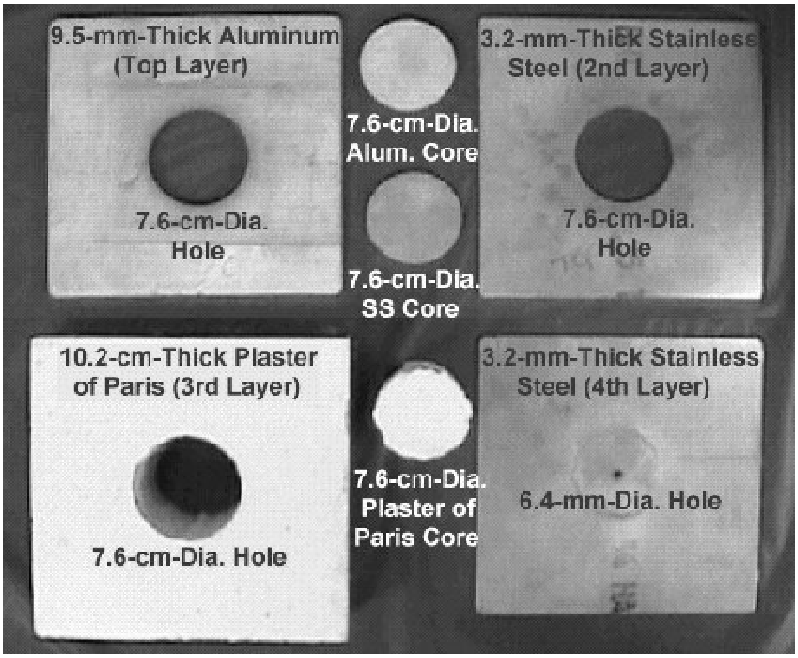

Figure 9. Access Holes Drilled with a 207-MPa ACJ in Composite Coupon

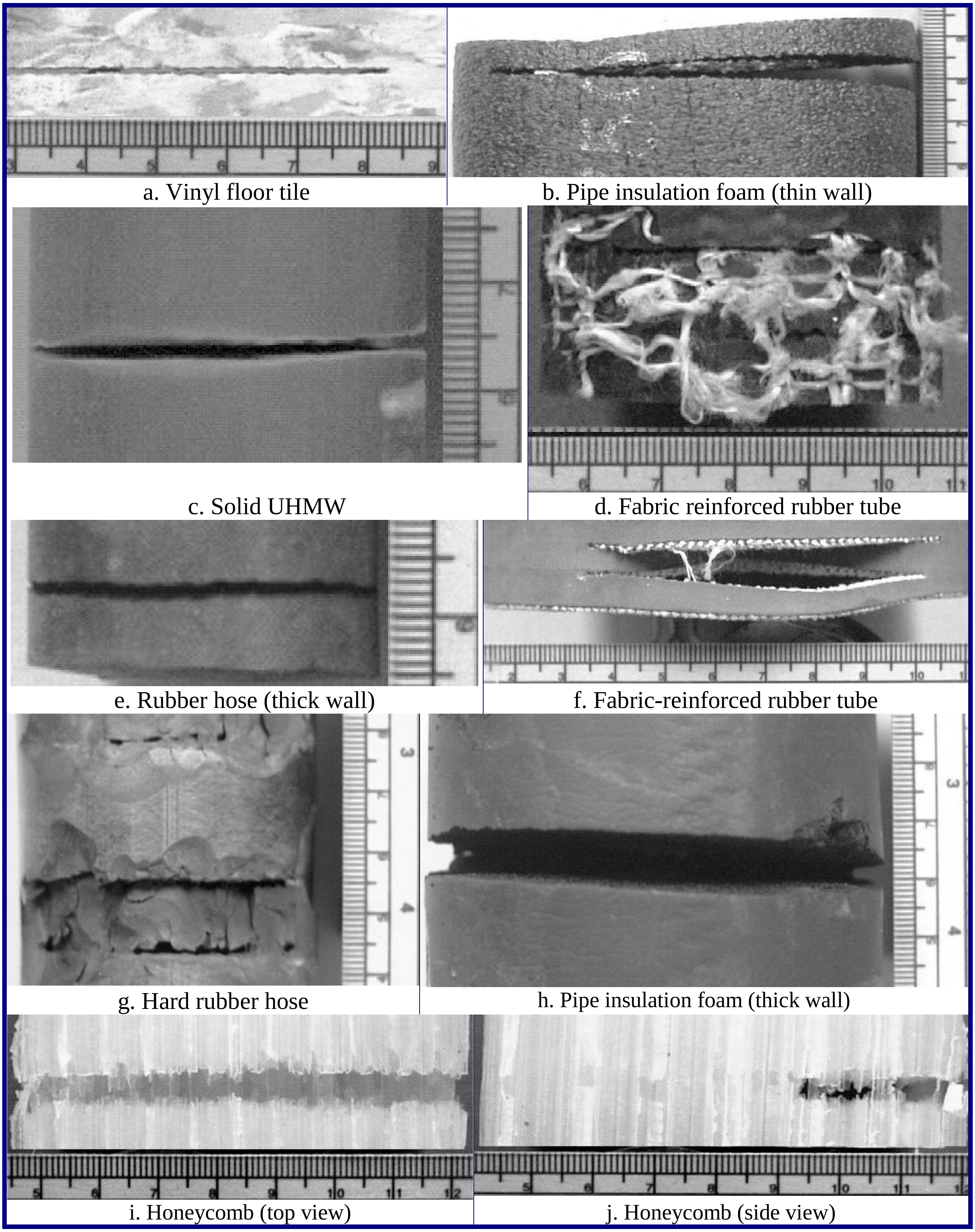

Figure 10. Samples of Building Materials Cut with CJ Operating at 207 MPa

10th American Waterjet Conference
August 14-17, 1999: Houston, Texas

Paper **22**

APPLICATION OF ICE PARTICLES FOR PRECISION CLEANING OF SENSITIVE SURFACES

E. S. Geskin, D. Shishkin, K. Babets
Laboratory of Waterjet Technology, ME Department
New Jersey Institute of Technology
Newark, NJ

ABSTRACT

Entrainment of the ice particles by the waterjet and particles formation within the water stream was investigated. FIDAP package was used to determine probability of particles surviving in the course of the jet formation. Another part of the study was concerned with the use of the ice-air jet. It was demonstrated that at the optimal range of process conditions this jet constitutes a precision tool for selective material removal operations. Number of experiments was carried out in order to demonstrate this technology. Various electronic devices (computers, calculators, electronic games and watches) were disassembled and electronic boards were contaminated by grease and metal powder. Then the boards were cleaned and reassembled. The computer, calculators and watches worked normally. Other experiments involved degreasing, depainting and deicing of liquid crystals, polished metals, optical glass, fabric, removal emulsion from a film, etc. The feasibility of the damage free and pollution free decontamination of highly sensitive, highly countered surfaces was demonstrated. A low cost of ice-air cleaning will enable us to use it for processing large surfaces at a high rate. On-line degreasing of metal in the course of rolling or prior to machining illustrates this application. A generic environmentally friendly surface processing technology is emerging as the result of the presented study.

1. INTRODUCTION — DEVELOPMENT OF ICE AIRJET TECHNOLOGY

In our previous works the formation and application of ice-water jet (IWJ) was investigated (Geskin et al. 1995, 1995(a), 1996, 1997, 1997(a), 1999). Several systems for ice jet formation were tested and comparatively stable process was designed. The experimental study of the ice assisted cutting and cleaning was carried out. We demonstrated that the addition of ice particles into water stream enhances machining ability of the stream. The properties of IWJ were similar to those of the abrasive waterjet and feasibility of removal of hard-to-machine materials was demonstrated. However the rate of material removal by IWJ was much lower than theoretically expected. In order to investigate the reason of the insufficient process productivity we numerically examined entrainment of ice particles by the waterjet. We found that the main reason of the low process productivity was melting of ice particles in the mixing chamber. Thus prevention of particles destruction is the necessary conditions of the of the process development.

The use of the ice particles is simplified if the particles are entrained in the air stream. There is a number of suggested air-ice based technologies. One of the first of such suggestions is a car washing machine, utilizing ice particles (US Patent 1955). The stream of the charged frozen particles precisely controlled by a set of coils was directed at treated surfaces (Kanno et al, 1991). Szijcs (1991) proposed cleaning of the sensitive surfaces by the impact of the fine grade blast material and air. The blast material is formed by the atomization of the liquid in the air stream and subsequent freezing of the generated fine droplets. The freezing occurs by the addition of the refrigerant (N2, CO2, Freon) into the stream, in the mixing chamber or by the addition of refrigerant into the jet after the mixing chamber. The use of ice particles which have the uniform grain size of ultra fine water for cleaning the surface and grooves of the ferrite block (Tomoji,1992). Ice blasting devise using stored particles was suggested by Harima (1992). S. Vissisouk (1994) suggested to use ice particles near melting temperature in order to effectively remove coating. A nozzle for enhancement of the surface cleaning by ice blasting was suggested by Mesher (1997). Shinichi (1997) suggested cleaning inexpensively various surfaces by mixing ice particles, cold water and air. Niechial (1998, 1998a) proposed an ice blasting cleaning system containing an ice crusher, a separator and a blasting gun. Settles (1998) suggested producing ice particles of a size range below 100 micrometers within the apparatus just prior to the nozzle.

Although the use of ice blasting is suggested by a number of inventors, the practical application is much more limited. Herb and Vissaisouk (1996) report the use of ice pellets for precision cleaning of zirconium alloys in the course of production of bimetallic tubing. It is reported that ice blasting improved the quality of bimetals. The use of air-ice blasting for steel derusting is reported by Liu et al (1998). The following operational conditions were maintained during blasting: air pressure: 02-0.76 MPa, grain diameter: below 2.5 mm, ice temperature: - 50C, traverse rate: 90 mm/min, standoff distance; 50 mm. At these conditions the rate of derusting ranged from 290 mm2/min at the air pressure of 0.2 MPa to 1110 mm2/min at the air pressure of 0.76 MPa. The quality of the treated surface complied with ISO 8501-1 Sa 2. The presented work demonstrates the feasibility of metal derusting by air-ice mixture if adequate process conditions are selected.

We investigated the application of ice-air jet for surface cleaning. It was demonstrated that at the optimal range of process conditions this jet constitutes a precision tool for selective material removal operations. Number of experiments was carried out in order to demonstrate this ability of the air-ice jet. Various electronic devises (computers, calculators, electronic games and watches) were disassembled and their electronic boards were contaminated by grease and metal powder. Then the boards were cleaned and reassembled. The computer, calculators and watches worked normally. Other experiments involved degreasing, depainting and deicing of liquid crystals, polished metals, optical glass, fabric, removal emulsion from a film, etc. (Fig.4, 5) The feasibility of the damage free and pollution free decontamination of highly sensitive surfaces was demonstrated. Because our system was designed to produce fine particles, it was not applicable for removal of heavy deposit, for example rust. Modification of the operational conditions, including the increase of the parts size, will address this problem. A generic environmentally friendly surface processing technology is emerging as the result of the above experiments.

2. COMPUTER MODELING OF ICE-WATERJET FORMATION

Abrasive nozzle head assures entrainment of abrasive particles by water stream and formation of the homogeneous or almost homogeneous slurry. However, as it was shown earlier (Raissi et al., 1996, Osman et. al, 1996) the mixing chamber constitutes an "intermediate storage" of particles, fed from the inlet port and feeding the focusing tube. Because conventional abrasive particles constitute a thermodynamically stable system, the dwell time in the mixing chamber has no effect on the system performance. At the same time the ice particles can survive at a temperature above 0°C only very short time. We used finite element method to investigate the behavior of the water jet and behavior of ice particles in the mixing chamber of a nozzle. The commercial package Fidap was employed for this purpose. The Boundary conditions were defined and the appropriate mesh was constructed. At this stage the objective of our investigation is the identification of the conditions of particles entrainment. The previous study of material removal by ice show the extreme instability of this process. We address this phenomenon to the particles melting. In order to evaluate this hypotheses we studied the conditions of particles entrainment in the mixing chamber. The estimated particle trajectories are shown in the following figures. These figures demonstrate that the residence time in the mixing chamber change in the extremely wide range. And for the most particles it was extremely high. It has no practical effect on the use of the stable abrasives as garnet, while it has the decisive effect on the ice particle. The study shows the importance of the changing the mixing chamber design and undertaking certain steps, such as cooling of the water prior to the nozzle, to assure ice particles survival.

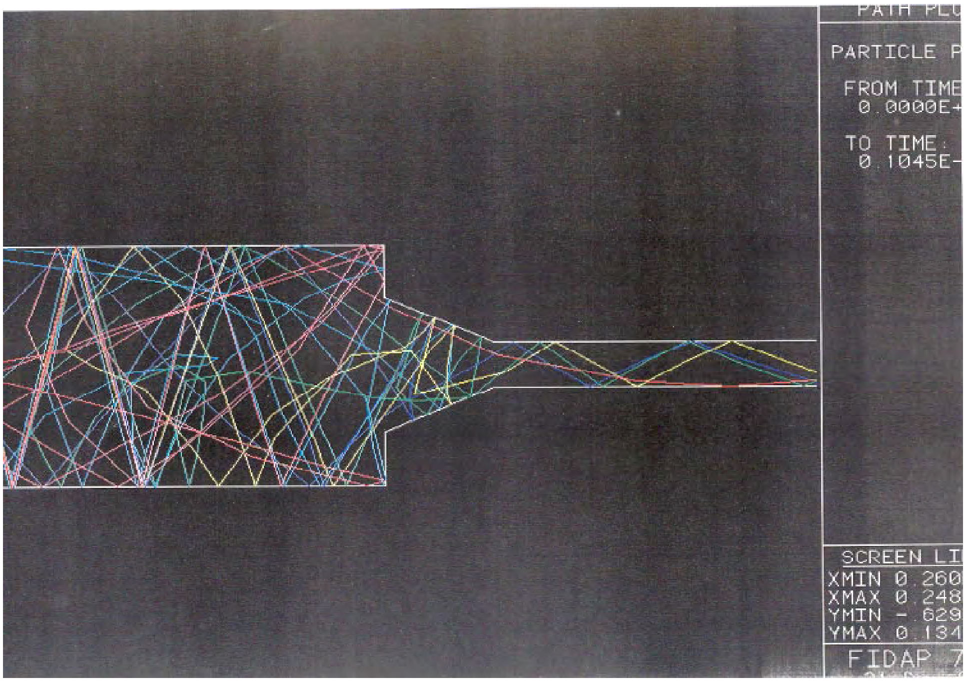

Figure 1. Fidap modeling of particles motion in the mixing chamber. Notice extended dwell time of particles in the mixing chamber.

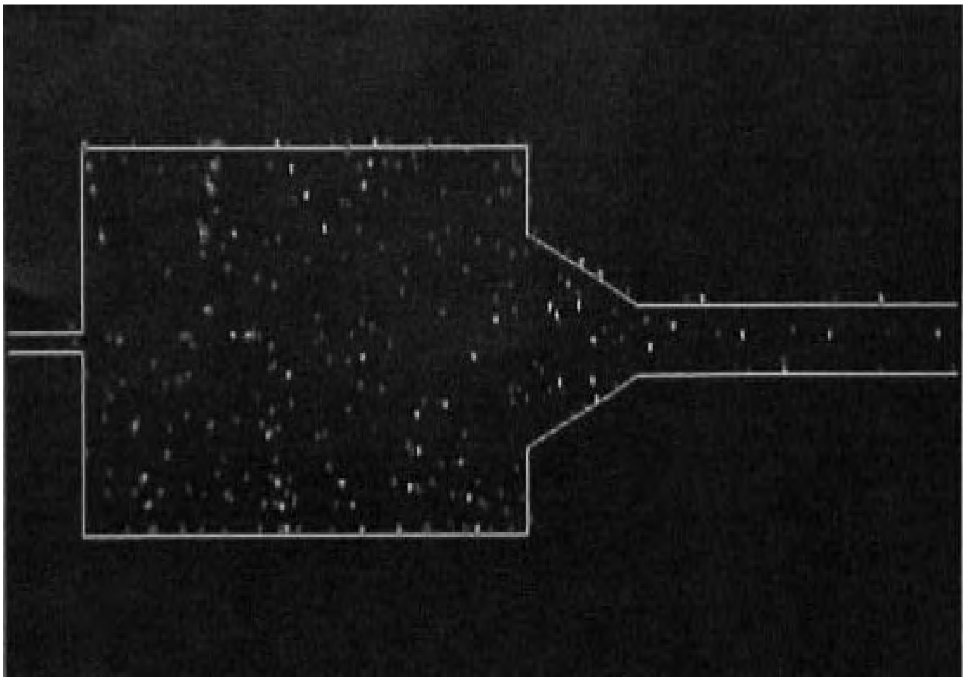

Figure 2. Particles distribution in the mixing chamber and focusing tube. Excessive residence time in the mixing chamber brings about disappearance of ice particles.

3. EXPERIMENTAL SETUP

The reliable system for Ice-Airjet formation is constructed (Figures 3,4). The system operates as following:

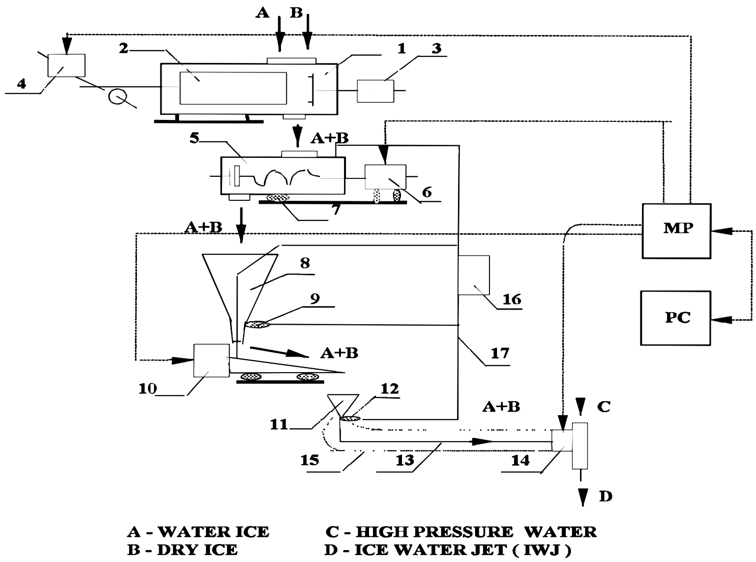

Figure 3. Schematic of the System for Ice Formation.

1-the first stage of crushing, 2- the piston, 3- the knives motor of the first stage of crushing, 4- the piston motor, 5- the second (precise) stage of crushing, 6- the knives motor of the second stage of crushing, 7- the amortizator of the second stage of crushing, 8- the intermediate supply bunker #1, 9- the amortizator of the intermediate supply bunker #1, 10- the electromagnetic vibrator, 11- the intermediate supply bunker #2, 12- the amortizator of the intermediate supply bunker #2, 13- the intermediate supply line, 14- the electrical heater, 15- the insulation enclosure of the intermediate supply line, 16- the adjustable speed and force vibrator, 17- the vibration transfer stainless steel rods.

Ice cubics are cooled by the cold air down to the temperature of –50 C and are supplied into the first stage of the crushing. Here the piston 1 moves ice to the rotating knives 2. The obtained coarse particles are supplied to the screw conveyer of the second stage. This conveyer delivers particles to the rotating knives, which generate fine particles. These particles are supplied into bunker 8 and then to the vibrator 10. The vibrating rod 9 assures continuity of the flow through the bunker 9. The vibrator 10 supplies particles to the bunker 12 and then to the tube 13. The suction created by the water nozzle assures delivery of the particles to the nozzle head. The heater 14 prevents clogging of the of the entrance port. Vibration of the crushers, bunkers and intermediate lines assures continuity of the powder flow. The rate of the vibration as well as operations of both stages of the crushing is controlled by PC via the microprocessor MP. The crusher bunkers and vibrator 10 are located within the insulated enclosure. The supply line 13 is also located in the enclosure. The air at the temperature of -70 C is supplied into the enclosures. The tests showed the stability of the operation of this system.

Figure 4. The System for Ice Formation (General View)

The ice powder generated by the system above was entrained into the air stream. Mixing of the ice particles and air occurs in a mixing chamber. The powder was driven into this chamber by the suction force developed by the air stream. The mixture exited via a cylindrical nozzle where the ice-air jet was formed. The jet was directed to the substrate surface and at this stage was guided manually.

4. EXPERIMENTAL PROCEDURE

In the course of this study air pressure was maintained at 80 psi, the nozzle diameter was 5 mm, ice flow rate was 40-60 g/min, the size of the ice particles ranged from 2 to 5 mm. In the course of experimental study the IJ was used for cleaning of various electrical and electronic components, contaminated by a mixture of a lithium grease and copper powder. Then these components were assembled and normal operation of the devise demonstrated the quality of cleaning. Another experiment involved depainting of various substrates, including mirror like surfaces and the surfaces of the soft substrates. The results of the cleaning were evaluated by the completeness of the depainting and the absence of the surface damage. The generated surfaces were inspected visually.

5. EXPERIMENTAL RESULTS AND DISCUSSION

A series of experiments were carried out in order to evaluate the potential of the application of IJ for the surface processing. The description of these experiments is given below.

5.1 Cleaning of Electronic Boards

A TV set was disassembled (Fig.A1 (a)) and electronic boards covered by heavy dust. Then the boards were decontaminated by IJ and reassembled. The TV set performed normally (Fig.A1 (b)). The architecture of the boards in question was extremely complex and contained a number of very sensitive sites, like electrical contacts. Any damage to the board components, for example weakening the contacts or removal of breaking wire will result in the distortion of the set operation. It is obvious that the ice-air stream induced no damage. More difficult task however, was the complete grease removal. Even small portion of the grease remaining at hidden pockets will distort the set performance. It is clear that the jet was able to remove soil from all difficult to reach pockets.

Another experiment involved decontamination of the computer boards. Various devises (PC, electronic watches, computer games, etc) were disassembled. The boards were covered by the mixture of the lithium grease and then decontaminated by the IJ. Clean boards were reassembled and tested. All devises with no exception worked perfectly. Some of the devises above were used for several tests. No deviation in the computer operation was noticed. The boards above were populated by a large amount of rather fragile components such as chips, connectors, etc. Any damage to any of these components, as well as any presence of grease on the board will disable the devise. In all performed experiments the deposit was removed completely and no damage was induced to the board components. The examples of the boards decontaminated in the course of these experiments are shown in Figs. A2 (a) and A2 (b).

5.2. Decoating of Sensitive Surfaces

The experiments involved depainting of a compact disc (CD). The disk was painted. Then this paint as well as two layers of the coating originally deposited on the disk were removed (Figs. A3 (a) and A3 (b)). The layers were removed separately with no damage to the underlining surface. Another experiment involved painting and subsequent depainting of the mirror like surface of the stainless steel (Fig. A4 (a)). No change in the surface topography was noticed. Further experiments involved depainting of china (Fig. A4 (b)), egg (Fig. A5 (a)), and glass lining of pharmaceutical reactors (Fig.A5 (b)). The most representative experiments, however, involved depainting of LC display (Fig.A6 (a)) and degreasing of the optical glass A6 (b).

5.3. Decoating of Soft Substrate

These experiments involved depainting of a soft plastic (Fig.A7 (a)) and fabric (Fig. A7 (b)). Decoating of a substrate having mechanical strength inferior to that of the coat constitutes a challenging task. IJ is able to perform this task.

5.4. Restoration of Electromechanical Devises

A solenoid valve (Fig.A8 (a)) and DC motor (Fig.A8 (b)) were completely disabled by painting of all contacts. After IJ cleaning the devises performed normally.

5.5. Removal of Highly Adhesive Surface Layer

An aluminum plate was covered by a heavy layer of the tar. Then the tar was removed mechanically from the part of the plate. However, a highly adhesive thin layer remained on the surface. It was not possible to remove it using mechanical means. The layer was removed completely by the ice-airjet (Fig. A9 (a)).

5.6. Etching applications.

An emulsion of a photo film was removed with no damage to the substrate (Fig. A9 (b)). This demonstrates the feasibility of the use of IJ as an etching agent.

6. CONCLUSION

Although the ice waterjet constitutes an effective material removal tool, it is necessary to improve conditions of the jet formation in order to assure its adoption by the practice. However, the ice-airjet is suitable for immediate application. It can be used for decontamination of very demanding and complex surfaces as well for such manufacturing applications as etching. Simplicity and complete absence of environmental damage constitute the main advantages of this process. The further development of ice-air surface processing will involve improvement of the control of particles properties and enhancement of material removal by ice particles accelerated by the air. This enhancement will enable us to modify material polishing, surface modification, and, perhaps, grinding.

7. ACKNOWLEDGEMENT

This study was supported by NSF Grants DDM931758 and DDM931280.

8. REFERENCES

E. S. Geskin, L. Tismenetskiy, E. Bakhromi, F. Li, "Investigation of Ice Jet Machining," *Proceedings of International Symposium on Electric Machining*, pp. 833-890, Lausanne, Switzerland, 1995.

E. Geskin, Tismenetskiy, E. Bakhromi, F. Li, "Investigation of Icejet Machining", *Proceedings of 1995 NSF Design and Manufacturing Grantees Conference*, San Diego, CA,1995.

E. Geskin, Tismenetskiy, E. F. Li, "Investigation of Icejet Machining", *Proceedings of 1996 NSF Design and Manufacturing Grantees Conference,* Albuquerque, NM,1996.

E. Geskin, Tismenetskiy, E. F. Li, D. Shishkin, "Investigation of Icejet Machining," *Proceedings of 1997 NSF Design and Manufacturing Grantees Conference,* Seattle, WA, 1997.

E.S. Geskin, L. Tismenetskiy, F. Li, P. Meng and D. Shishkin, "Investigation of Icejet Machining," *Proceedings of 9th American Waterjet Conference,* pp. 281-290, Houston, TX, 1997.

E. Geskin, D. Shishkin, K. Babets, "Investigation of Icejet Machining," *Proceedings of 1999 NSF Design and Manufacturing Grantees Conference*, Long Beach, 1999.

Harima, "Ice Blasting Device and Manufacture of Ice Blasting Ice Grain," *Japanece Patent 04360766 A,* 1992

B. Herb and S. Visaisouk, "Ice Blast Technology for Precision Cleaning," *Precision Cleaning,* pp. 172-179,Witter Publishing Company, Anaheim CA, 1996.

Kanno et al, "Cleaning Device Using Fine Frozen Particles, " *US Patent 5,074,083,* 1991.

O.D. Liao, X.D. Zhao and T.Y. Long, "Prediction of Turbulent Flow Field for Dilute Polymer Solution Jets," *Proceedings of 5th American Waterjet Conference*, pp. 367-377,Toronto, 1989.

R. Lombardi, "Ultra-High Pressure Non-Abrasive Polymer Jetting, A Production Environment Implementation," *Proceedings of 9th American Waterjet Conference*, Dirborn, August, 1997.

F. Li, E. S Geskin, and L. Tismenetskiy, "Development of Icejet Machining Technology," *Proceedings of 8th American Water Jet Conference*, pp.671-680, Houston, 1995.

F. Li, E.S. Geskin, L. Tismenetskiy, "Development of Icejet Machining Technology", *Proceeding of XIII International Symposium on Waterjet Technology,* pp. 725-734, BHRA, Sardinia, 1996.

W.S. Melvin, and J. Graham, "Method to Demilitarize, Extract and Recover Ammonium Perchlorate, Composite Propellant Using Liquid Ammonia", US *Patent 4854982*,1993.

W.S. Melvin, "Method to extract and Recover Nitramine Oxidizers from Solid Propellants Using Liquid Ammonia," *US Patent 5284995,* 1994.

T. Mesher, "Fluidized Stream Acceleration And Pressurizer Apparatus," *US Patent 5,607,478,* 1997.

R. Niechcial, "Ice Blasting Cleaning System and Method of Blasting," *Inernarnational Patent, Publication, WO 98/36230*,1998.

R. Niechcial, "Ice Blasting Cleaning System," *US Patent 5,820,447*, 1998.

G. Settles, "Supersonic Abrasive Ice Blasting Apparatus," *US Patent 5,785,581*,1998.

H. Shinichi, "Surface Cleaning Method and Device," *Japanese Patent 09225830 A*, 1997.

J. Szijcs, "A Method for Cleaning Surfaces," *European Patent 0 509 132 B1*, 1991.

M. Tomoji, "A Precision Cleaning Method," *Japanese Patent 04078477*, 1990.

S. Vissisouk and S Vixaysouk, "Particles Blasting Using Crystalline Ice," *US Patent 5,367,838*, 1994.

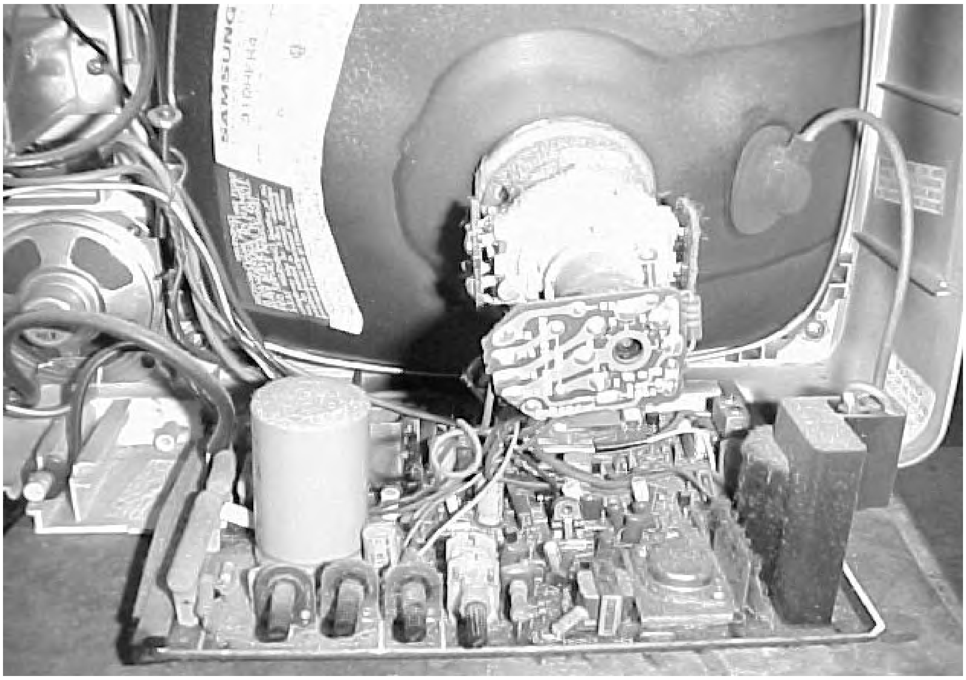

(a)

(b)

Figure A.1 (a) and (b) photographs of electronics board of TV set. Notice the heavy layers of dust and dirt on the electric and electronic components of board.

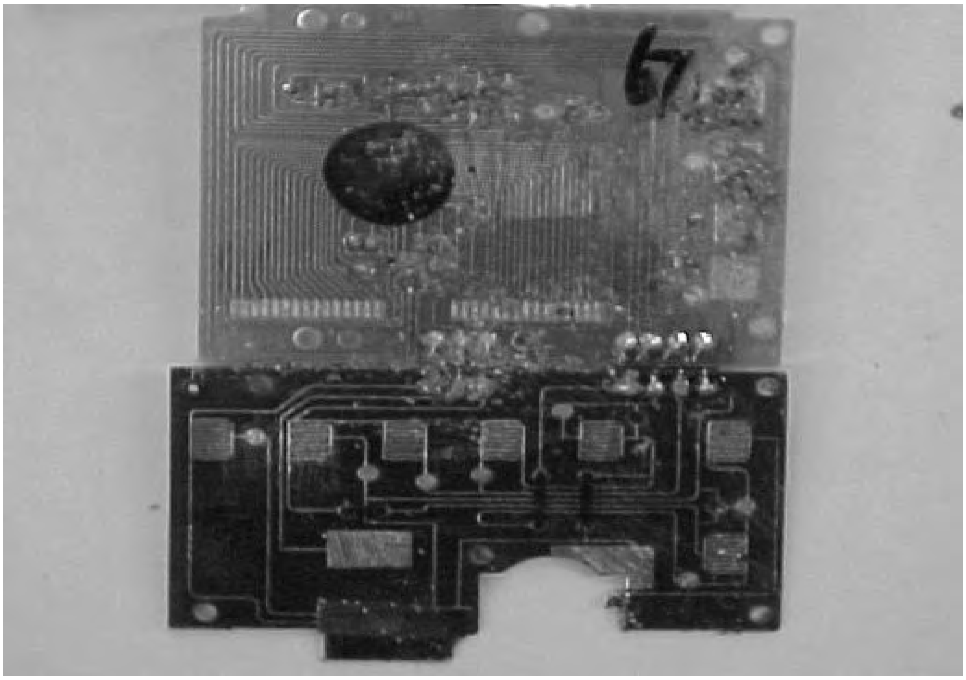

(a)

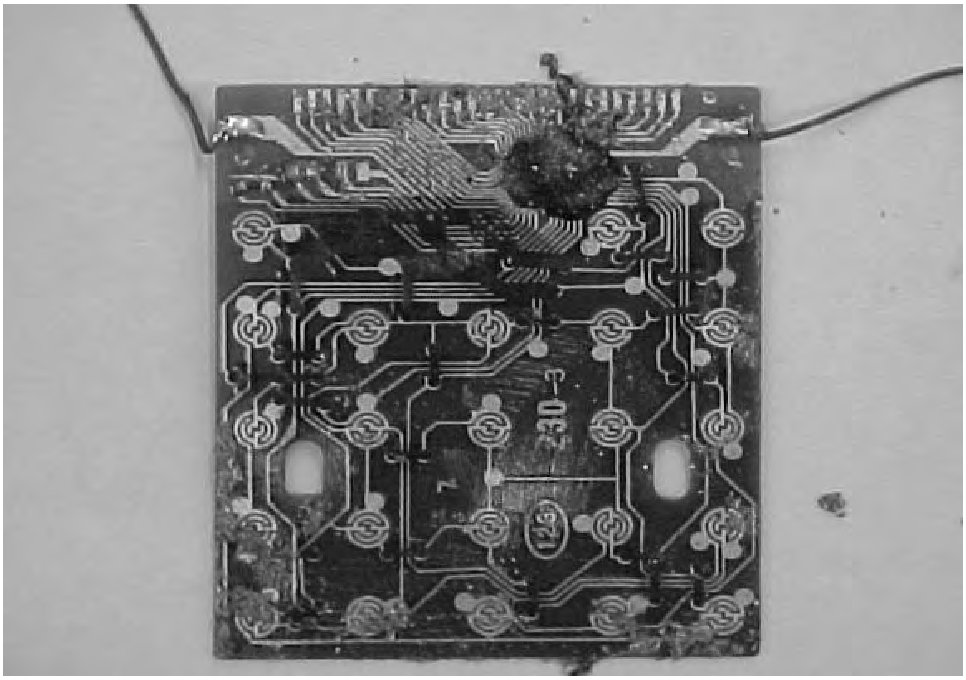

(b)

Figure A.2 (a) and (b) photographs of the board of the electronic games containing electric conduits, microchip and electronic matrix. The board was covered by the mixture of the lithium grease and copper powder and disabled. Notice the cross contamination of electric conduits of the board. After cleaning the game performed normally.

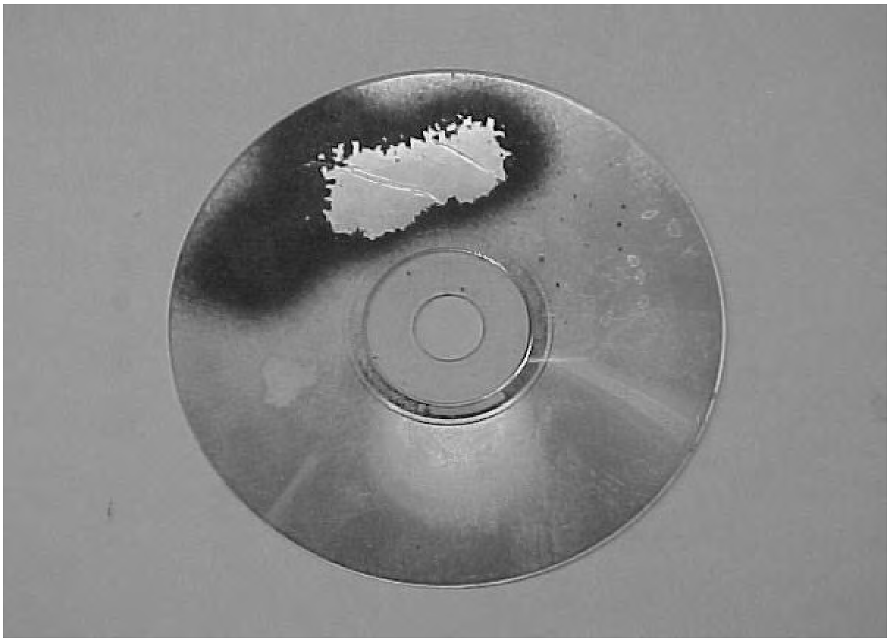

(a)

(b)

Figure A.3 (a) photograph of the CD-ROM covered by Rust-Oleum gloss protective enamel. The paint was partially removed from the CD ROM surface. No surface damage was observed in the course of IJ cleaning, and (b) photograph of the CD-ROM partially cleaned by using of IJ technique. Notice that both layers of paint and emulsion were removed. No surface damage was observed in the course of IJ processing.

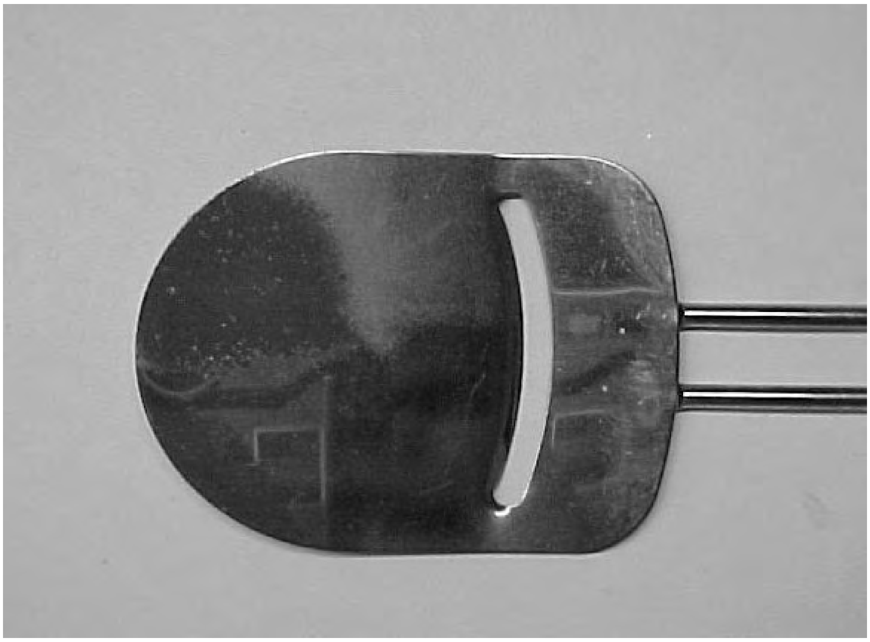

(a)

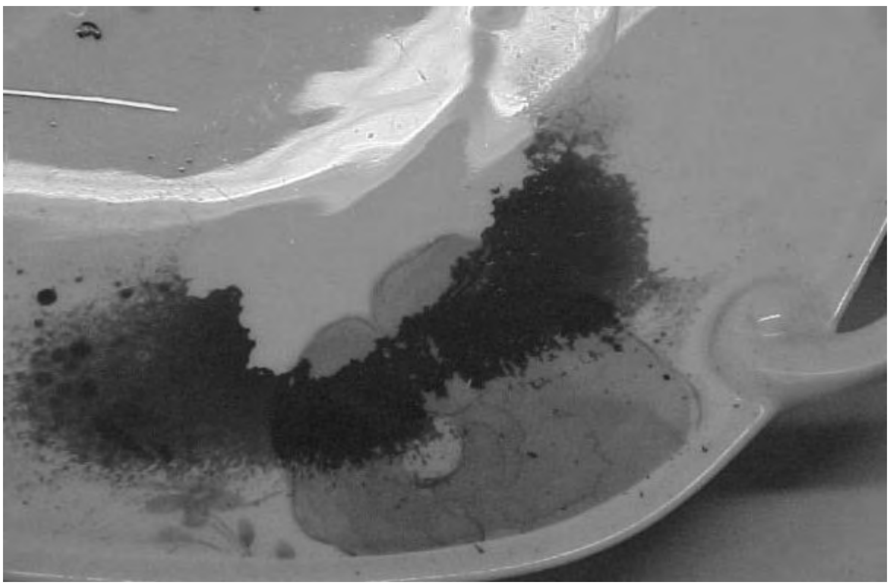

(b)

Figure A.4 (a) Photograph of the polished steel surface. The polished steel surface was contaminated by the Rust-Oleum gloss protective enamel. The paint was partially removed from the polished surface. No surface damage was observed in the course of IJ cleaning. The feasibility of the precision cleaning of polished surfaces was demonstrated, and (b) photograph of the strip of soft plastic covered by Rust-Oleum gloss protective enamel. The paint was partially removed from the plastic surface. No surface damage was observed. The feasibility of restoration and fabrication of plastic parts was demonstrated.

(a)

(b)

Figure A.5 (a) Photograph of the egg. The egg surface was painted by Rust-Oleum gloss protective enamel. After this the egg was partially decontaminated by IJ. No damage of the egg surface or penetration of the ice particles through the egg shell was noticed. The feasibility of decontamination of highly unstable and brittle surfaces was demonstrated, and (b) photograph of the cover of a pharmaceutical reactor contaminated by the lithium grease. Then the grease was partially removed from the surface of the cover by IJ. No damage of the Phaulder glass in the course of IJ cleaning was noticed.

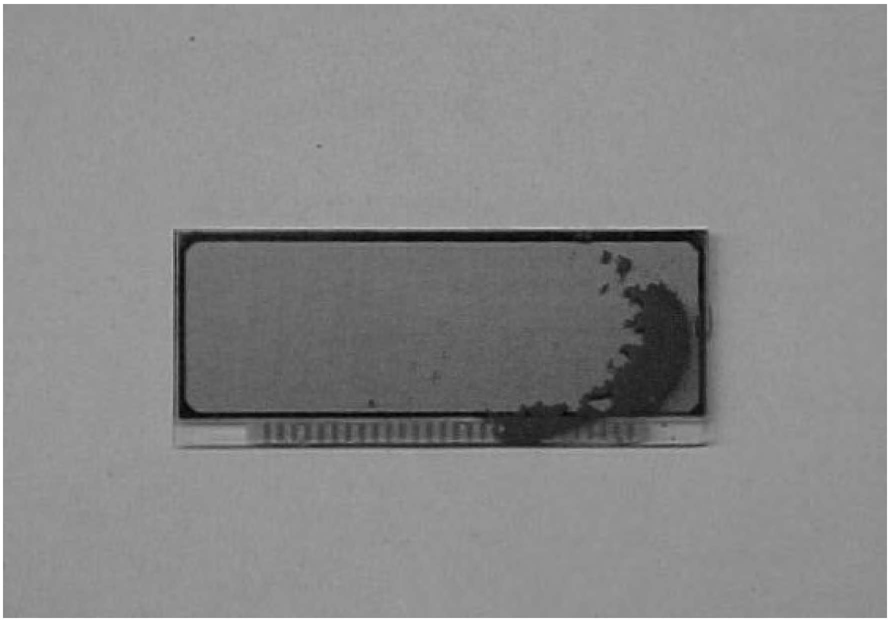

(a)

(b)

Figure A.6 (a) photograph of the LC display of the calculator containing electronic matrix and LCD conduits. The display was contaminated by Rust-Oleum gloss protective enamel. Then all elements of LC display were decontaminated by IJ. In assembly of the calculator the LC display performed normally, and (b) photograph of the magnification lens. The lens was contaminated by the lithium grease. The grease was partially removed from the lens surface. Notice that no damage of the lens surface was observed.

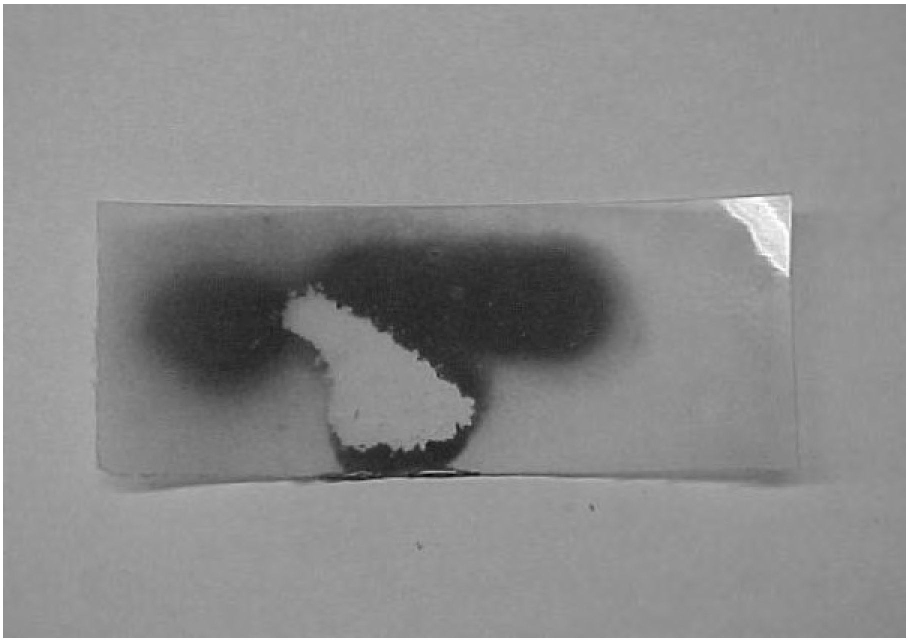

(a)

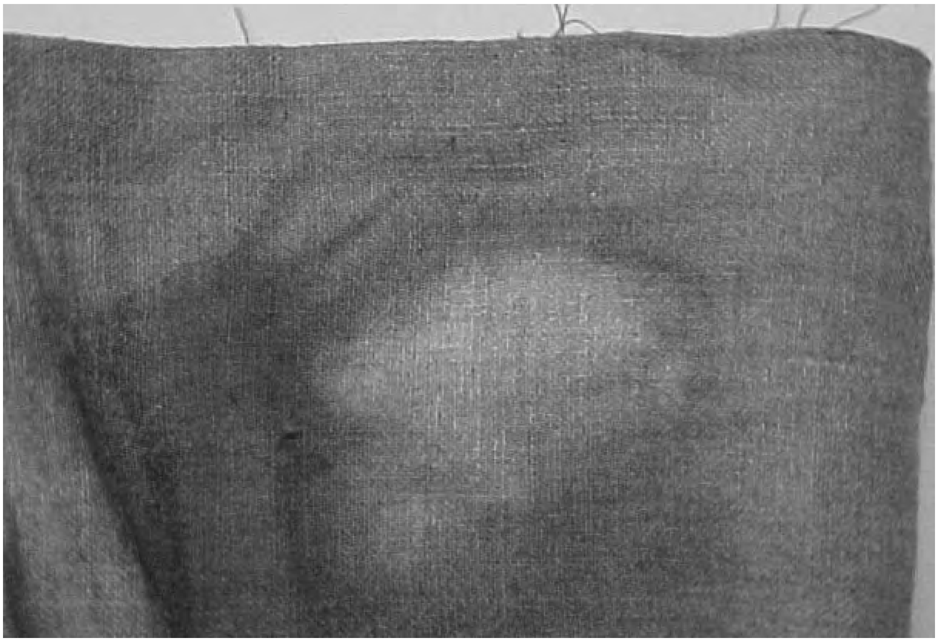

(b)

Figure A.7 (a) photograph of the strip of soft plastic covered by Rust-Oleum gloss protective enamel. The paint was partially removed from the plastic surface. No surface damage was observed. The feasibility of restoration and fabrication of plastic parts was demonstrated, and (b) photograph of the of a cotton fabric. The fabric was contaminated by the Rust-Oleum gloss protective enamel. Then the paint was partially removed from fabric surface. The feasibility of the use of ice particles for decontamination of different fabrics was demonstrated.

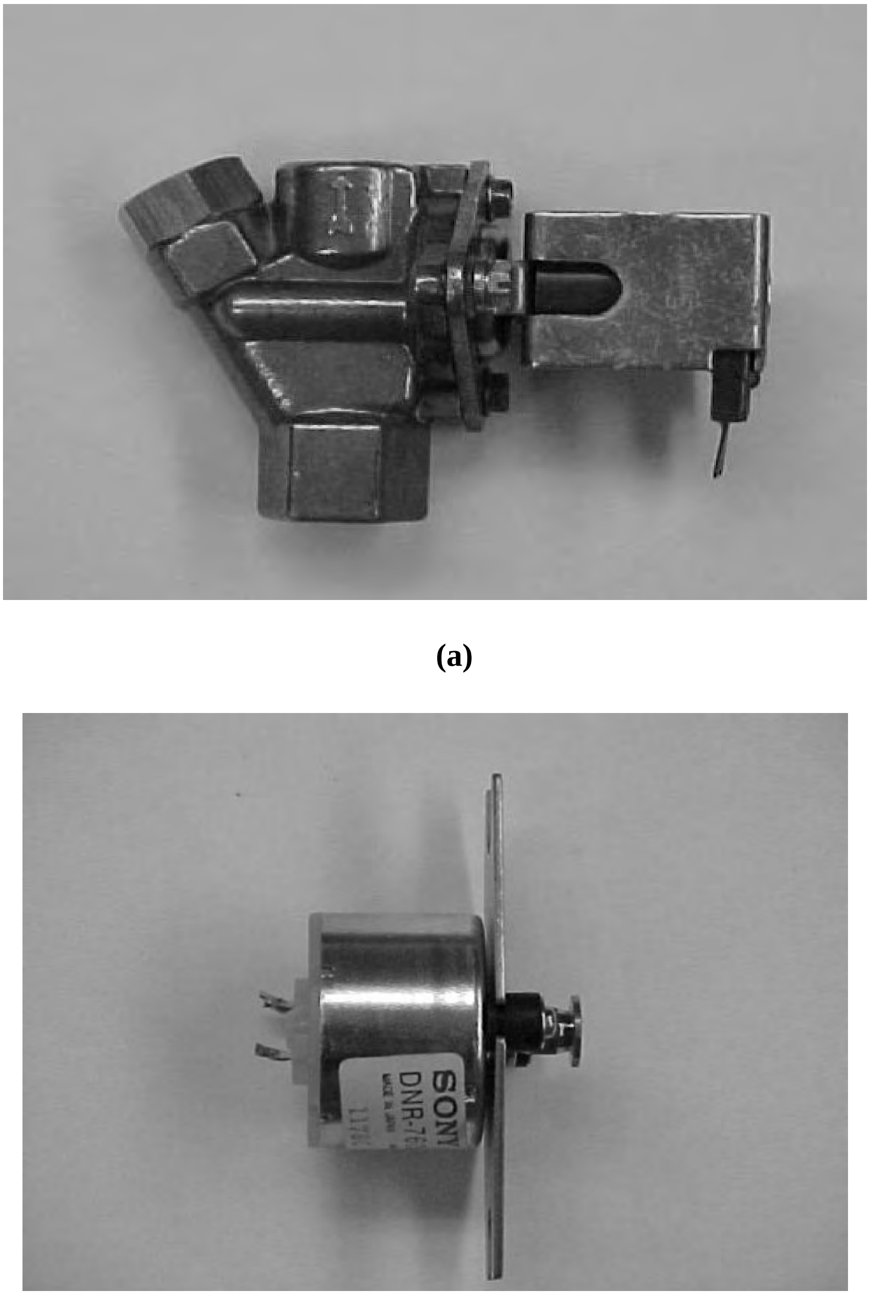

(a)

(b)

FigureA.8 (a) photograph of the electrical solenoid valve with connectors contaminated by Rust-Oleum gloss protective enamel. The contacts of solenoid valve were cleaned by IJ. After cleaning the solenoid valve was connected to the electrical supply source and performed normally. This experiment demonstrated the feasibility of using IJ technique for decontamination and restoration of contacts of different electronic devices, and (b) photograph of the DC motor. DC motor was disassembled and all elements were covered by the mixture of lithium grease and copper powder. DC motor was cleaned by IJ. In assembly DC motor performed normally.

(a)

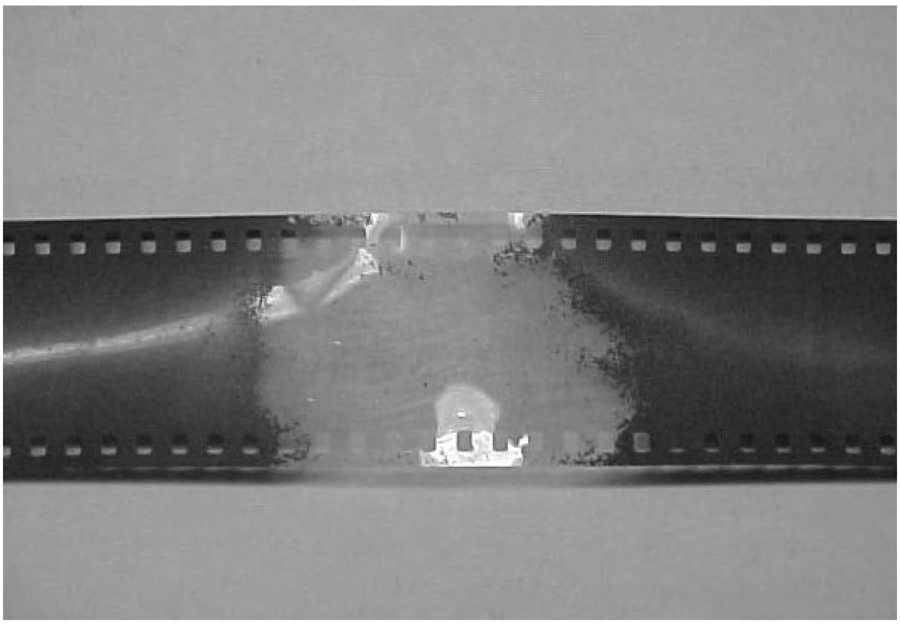

(b)

Figure A.9 (a) photograph of the grinded aluminum surface contaminated by the thick layer of tar. The bulk of the tar was removed by WJ and knife scrubbing. The highly adhesive thin layer was removed by ice etching. No damage of the metal surface was noticed, and (b) photograph of the strip of the photo film. The photo emulsion was partially removed from the film surface. No surface damage was observed in the course of IJ. The feasibility of complete and selective emulsion removal from thin film was demonstrated.

10th American Waterjet Conference
August 14-17, 1999: Houston, Texas

Paper **23**

THE ANALYSIS OF MAGNETOHYDRODYNAMIC EFFECTS - NEW APPROACH TO THE PULSE JET

I.M. Hlaváčová, L.M. Hlaváč
VŠB - Technical University
Ostrava, Czech Republic

ABSTRACT

The improvement of water jet efficiency is required in civil engineering, mining and quarrying. Pulsing jets can contribute to solving of the problems as it was proved many times. However, there is still a lot to improve in the range of designing of devices producing pulsing jets. It is necessary to reduce strong dependence of pulse jet efficiency on stand-off distance. To make pulse jets work effectively within a large domain round the optimum stand-off distance the new approaches to the pulse jet generation need to be studied. The magnetohydrodynamics is one of them because it can be utilised even for control or automation. The theoretical investigation of the liquid stream behaviour provided influenced by hydrodynamic effects is the topic of the paper. The main effort was aimed at a theoretical derivation of proper parameters triggering such modulation in a liquid stream that amplitude of velocity oscillation downstream is at least five percent of the corresponding unmodulated stream. Results of physical analysis are discussed and they are also used for designing of a device located upstream the resonator generating pulsing jet.

1. INTRODUCTION

Intensification of liquid jet energy utilization for rock material disintegration has been studied for few years. The continuous jets have been studied first. Their interaction with rock material has been described by theoretical relationships based on the physics of the inherent processes. Nevertheless, from the point of view of industries like mining, quarrying or civil engineering the efficiency of continuous jets is quite low even when liquid pressure in a pump exceeds 300 MPa. It is supposed that no further resounding success can be expected regarding the increase of efficiency obtained by special treatment of water or use of better nozzles. Studies of abrasive water jets, both injection ones and the ones with direct pumping of slurry, proved that they are not convenient for purposes needed by potential customers from the range of mining, quarrying and civil engineering. It is caused specially by the fact that maximum traverse rates resulting from the physical substance of the inherent processes are still very low compared with required ones. Pulsing water jets, on the contrary, seem to have some possibilities to eliminate mentioned disadvantages of continuous water jets and abrasive water jets.

This assumption is based on the analysis of effects of the jet impact on material. The theoretical and experimental studies proved that the jet effect is not steady in time. Analyses of the impact time evolution show that the initial part of the jet impingement is the most effective period of the disintegration process on the material surface. This period can be characterized by very rapid growth of the pressure on the contact area. It was proved by Rochester & Brunton (1972), Huang et al. (1972), Daniel et al. (1974), Reinecke (1974), Lesser & Field(1974), and others that the pressure peak appears several times exceeding the pressure of the liquid jet acting constantly with unalterable parameters if the physical behaviour of the liquid and solid round the contact zone is studied. Therefore, the idea appeared to replace a continuous jet by a pulsing one in which the initial impact should form much greater part of the interaction time Sami & Ansari (1981), Chahine & Conn (1983), Puchala & Vijay (1984), etc. Thus the effectiveness of the liquid jet should significantly increase and it is supposed that it may extend the range of commercial use in above mentioned industrial spheres. However, the problem is to prepare such a device producing pulsing jets that will be sufficiently small and simple, easy to manufacture, shockproof and stable in function. The Helmholtz type resonator is an element that should comply with such conditions provided it produces sufficient modulation of water jet.

Our effort is aimed at generation of fluctuations in flow. It is related to the up to date studies of the problems concerning modulated and subsequent pulsing jets because the two basic approaches to their generation can be mentioned as the most significant ones. One of them is to create interruptions or changes in liquid flow speed by mechanical tool (e.g. a vibrating tip near the nozzle inlet). The second one is to amplify liquid velocity fluctuations by some type of acoustic resonator (Helmholtz resonator). The second way seems to have some advantages. The question may be, however, to gain adequate initial velocity fluctuations. In this paper an idea is adumbrated and discussed to use an electromagnetic field for generation of definite perturbances of velocity as preliminary fluctuations for the reason that Helmholtz resonator can produce pulsing water jet of required parameters even for liquid pressures higher than 300 MPa and nozzle diameters between 0.1 and 0.5 mm.

2. THEORY OF PULSING JETS

Generation of pulsing jet means that liquid jet should break due to inherent fluctuations into separate drops in a certain distance l_o from a nozzle outlet. This distance ought to be quite short and it can be determined from relationships derived by Sami & Ansari (1981) or Chahine & Conn (1983) provided jet fluctuations can be described within the range of their presumptions. They presumed that jet velocity fluctuates round an average value v_m with frequency f_m and amplitude Δv. Resulting relationships of their analyses slightly differ from each other. Equation derived by Sami & Ansari (1981) has the following shape.

$$l_o = \frac{v_m}{\pi m f_m} \tag{1}$$

Chahine & Conn (1983) derived the equation with different constant.

$$l_o = \frac{v_m}{4 m f_m} \tag{2}$$

Evidently there is no explicit relationship between distance necessary for pulsing jet formation and the nozzle diameter. Nevertheless, both modulation ratio m and frequency f_m depend on it. Theoretical analysis of relationship (1) has been made regarding influence of water pressure, modulation ratio and frequency and results are presented in Fig. 1 through 3. Limiting the distance of jet breakage l_o by demands of practice, it is considered to be an independent variable in the derivation of resonator parameters. The average jet velocity is determined by water pressure. The average jet velocity is calculated from equation (3).

$$v_m = v_o = \sqrt{\frac{2\mu_n \gamma_o p_o}{\rho}} \tag{3}$$

v_o is the medium outlet velocity of a liquid stream core. Parameter μ_n depends on the nozzle outlet diameter. Using equations (1) and (3) the range of parameters m and f_m can be determined for pressures p_o and distances l_o resulting from practical demands. Typical breakage length l_o, necessary for practice, lies between 20 and 100 mm. The respective modulation ratio decreases from approximately 0.65 to 0.13 within the mentioned scope of l_o for frequency 15 kHz and pressure 350 MPa (see Fig. 2). Calculations of necessary modulation frequency for pressure 350 MPa, provided the modulation ratio is close to 0.15 (Fig. 3), yield values decreasing from approximately 100 to 13 kHz for appropriate breakage length. Such high frequencies can be quite sufficiently generated by electric field. Thus the idea originated to premodulate the liquid stream by influence of magnetohydrodynamic effects in flowing liquid.

3. BRIEF THEORY OF RESONATORS

Basic common condition for length of a resonator similar to organ-pipe (the resonator with an open end) is determined by equation

$$L = p_{qw} \frac{\lambda_w}{4} \tag{4}$$

Knowing the wave speed in medium inside the resonator, the equation (4) can be transformed for calculation of preferable frequency into the equation (5) provided the parameter *p* is number of quarter-wavelengths

$$f_p = \frac{p_{qw} c_w}{4L} \tag{5}$$

The physical relationships described by equations (4) and (5) are valid for all types of resonators. However, Shen Zhong Hou & Wang Zhi Ming (1988) derived another equation. Their equation is to describe further conditions for frequency of Helmholtz resonators.

$$f_r = \frac{c_s}{2\pi d_r} \left(\frac{d_i}{L_r} \right)^{1/2} \tag{6}$$

The parameters c_s, f_r, L_r can be determined from liquid properties and demands on resonator size. Nevertheless, it is necessary to consider the conclusions obtained during analyses of equation (1). Studying graphs shown in Fig. 1 through 3 we can realise that frequency for generation of pulsing jet ranges between 20 and 100 kHz according to equations presented in section 2, assuming the modulation ratio could be approximately 0.1, water pressure is 350 MPa and jet breakage length lies between 20 and 100 mm. Demand of practice is to minimize geometrical size of device producing pulsing jets. Therefore the presumption can be made that length of the resonator L_r is close to 10 mm. Using equation (5) the frequency for assumed resonator length, medium pressure inside the resonator and number of quarter-wavelength *p* can be determined provided the relationship between liquid compressibility γ_{po} and sound speed c_s is known.

The relationship between liquid compressibility and equivalent sound speed is expressed by equation

$$c_s = \frac{1}{\sqrt{\gamma_{po} \rho_o}} \tag{7}$$

Supposing the liquid is pure water the equation (7) can be completed by equation derived for relationship between liquid pressure and compressibility by regression of experimental data tabled by Brož et al. (1980).

$$\gamma_{po} = \gamma - \sqrt{p_o}\,.10^{-14} \qquad \textbf{(8)}$$

Changes of compressibility regarding water pressure are graphically expressed in Fig. 4. Changes of sound speed in compressed water are shown in Fig. 5. Using equations (5), (7) and (8) the frequency approximately 48 kHz is determined for longitudinal waves in the resonator with the length 10 mm provided only one quarter-wavelength is present in a resonator. Calculation was made for water pressurized to 350 MPa. Nevertheless, the modulation ratio for this pressure and breakage length between 20 mm and 100 mm need to range within 0.2 and 0.04 respectively. Supposing the modulation ratio about 0.1 has to be achieved by common resonator with gain near 10 we need to introduce fluctuations about 0.01 of the average velocity into flow upstream the resonator. Fluctuations of velocity with such a high frequency are supposed to be excited using variable electric and magnetic fields.

4. THEORETICAL DESCRIPTION OF THE PROBLEM

The derivation is based on the physical phenomenon that moving charges change their directions under the influence of the magnetic field having non-zero component perpendicular to the velocity vector. This phenomenon is usually described subsequently. A conducting fluid moving through a magnetic field may induce an electric field and consequently a current that interacts in turn with the magnetic field to produce a body force on the fluid. This behaviour is caused by free charges inside conducting fluid moving inside magnetic field thus subjected to an influence of the Lorentz force.

The complete electromagnetic body force in a conducting fluid may be derived, microscopically, from the Coulomb law, or by a virtual work and energy method. The body force density in the rest frame is given by

$$\boldsymbol{f}_e = \rho_e \boldsymbol{E} + \boldsymbol{j}\times\boldsymbol{B} - \frac{1}{2}\varepsilon_o E^2 \nabla\varepsilon_r - \frac{1}{2}\mu_o H^2 \nabla\mu_r + \frac{1}{2}\varepsilon_o \nabla\left(E^2 \frac{\partial \varepsilon_r}{\partial \rho}\rho \right) + \frac{1}{2}\mu_o \nabla\left(H^2 \frac{\partial \mu_r}{\partial \rho}\rho \right) \qquad \textbf{(9)}$$

In magnetohydrodynamics only the first two terms are important. These two terms are covariant, i.e. the expressions hold in any frame of reference, so that

$$\boldsymbol{f}_e = \rho_e \boldsymbol{E} + \boldsymbol{j}\times\boldsymbol{B} \qquad \textbf{(10)}$$

Alternative description is given by the electromagnetic stress tensor. The body force density is given by relationship expressed by equation

$$f_i = \frac{\partial T_{ij}}{\partial x_i} - \frac{\partial g_i}{\partial t} \tag{11}$$

where g_i is the electromagnetic momentum flux vector. The electromagnetic stress tensor T_{ij} (if the striction effects are neglected) is expressed by

$$T_{ij} = -\frac{1}{2}(\boldsymbol{D}\cdot\boldsymbol{E} + \boldsymbol{B}\cdot\boldsymbol{D})\delta_{ij} + D_i E_j + b_i H_j \tag{12}$$

For all practical purposes the term $\partial g_i/\partial t$ is negligible and it is of no concern in problems related to magnetohydrodynamics. We can diagonalize the stress tensor thus determining the principal stresses. To simplify the equations (9) through (12) some basic assumptions which are valid in magnetohydrodynamic problems were introduced:

- the electric terms in the stress tensor are negligible (as the electric field is of order $\boldsymbol{v} \times \boldsymbol{B}$ and $\boldsymbol{E}$ fields involved are induced or of the order of the induced field);
- $\boldsymbol{B}$ and $\boldsymbol{H}$ are collinear (we are dealing with nonrelativistic speeds, all velocities are small compared to that of light, so that the term $v^2/c^2 \ll 1$.).

The result for the three principal stresses λ_i obtained using presented approach is

$$\lambda_1 = \frac{1}{2}\boldsymbol{H}\cdot\boldsymbol{B}, \quad \lambda_2 = \lambda_3 = -\frac{1}{2}\boldsymbol{H}\cdot\boldsymbol{B} \tag{13}$$

and the three principal axes are oriented so that λ_1 is a tension along the magnetic field lines and λ_2 and λ_3 represent a compression normal to the field lines. We can say that there is a hydrostatic compression of $\boldsymbol{H}\cdot\boldsymbol{B}/2$ with a tension of $\boldsymbol{H}\cdot\boldsymbol{B}$ (along the field lines) superposed on the hydrostatic compression. This body force, however, is not a physical tension or pressure in the fluid, but it enters into a momentum equation as a body force and consequently may generate mechanical stresses. In static equilibrium, the pressure gradient must be balanced out by the tensor divergence of the electromagnetic stress tensor, which physically is a body force.

The basic equations of magnetohydrodynamics can then be written as the Maxwell equations, Ohm's law, the equation of continuity, the equation of motion with the $\boldsymbol{j} \times \boldsymbol{B}$ body force (the Maxwell equation $\nabla \times \boldsymbol{B} = \boldsymbol{j} + \boldsymbol{D}'$ was used together with the fact that $\boldsymbol{D}'$ is negligible) and the energy equation with Joule heating. In all magnetohydrodynamic problems, even in unsteady ones, it is supposed that space charge transport is negligible compared to $\boldsymbol{j}$. We must also use nonrelativistic Lorentz transformations.

The complete solution of a real problem would be rather complicated but the analysis of a simplified problem (known as the Hartmann's problem) may be sufficient for the rough estimation whether it would be possible to use magnetohydrodynamic effects for high energy liquid jet modulation.

Let us discuss a steady flow of an electrically conducting, viscous, incompressible fluid between parallel plates with an applied transverse magnetic field. We assume the flow to be fully developed so that only pressure varies in the x direction. Velocity of the fluid can be written as $\boldsymbol{v} = (u,v,w)$ and from the equation of continuity $v = w = 0$.

The channel extent in the z direction is much greater than in the y direction so that no variations occur with z. The electrodes are assumed to be perfect conductors, and the fluid has conductivity σ. The applied magnetic field $\boldsymbol{B}_o$ is steady and uniform. We can list all the equations for this problem:

Maxwell equations:

$$\begin{aligned} \nabla\times\boldsymbol{H} &= \boldsymbol{j} \\ \nabla\cdot\boldsymbol{B} &= 0 \\ \nabla\times\boldsymbol{E} &= -\frac{\partial\boldsymbol{B}}{\partial t} = 0 \\ \nabla\cdot\boldsymbol{j} &= 0 \end{aligned} \quad \textbf{(14)}$$

From $\nabla\cdot\boldsymbol{j} = 0$ we conclude that j_z must only depend on y and so the

Ohm's law

$$\boldsymbol{j} = \sigma(\boldsymbol{E} + \boldsymbol{v}\times\boldsymbol{B}) \quad \textbf{(15)}$$

would take form

$$j_z = \sigma(E_z + uB_o) \quad \textbf{(16)}$$

Equation of motion

$$\rho\left[\frac{\partial\boldsymbol{v}}{\partial t} + (\boldsymbol{v}\cdot\nabla)\boldsymbol{v}\right] = -\nabla p + \nabla\cdot\tau + \boldsymbol{j}\times\boldsymbol{B} - \rho\nabla\psi \quad \textbf{(17)}$$

where ψ is the gravitational potential (which can be neglected) and τ is the mechanical stress tensor. For a Newtonian fluid it is assumed that the stress tensor is linearly related to the strain rate tensor e_{ij} defined by the following equations

$$
\begin{aligned}
e_{xx} &= \frac{\partial u}{\partial x} & e_{xy} &= e_{yx} = \frac{1}{2}\left(\frac{\partial u}{\partial y} + \frac{\partial v}{\partial x}\right) \\
e_{yy} &= \frac{\partial v}{\partial y} & e_{yz} &= e_{zy} = \frac{1}{2}\left(\frac{\partial v}{\partial z} + \frac{\partial w}{\partial y}\right) \\
e_{zz} &= \frac{\partial w}{\partial z} & e_{zx} &= e_{xz} = \frac{1}{2}\left(\frac{\partial w}{\partial x} + \frac{\partial u}{\partial z}\right)
\end{aligned}
\tag{18}
$$

If we use the fact that the flow is steady in the x direction and constant in the z direction, we can rewrite the equations (18) into

$$
\begin{aligned}
e_{xx} &= 0 & e_{xy} &= \frac{1}{2}\frac{\partial u}{\partial y} \\
e_{yy} &= 0 & e_{yz} &= 0 \\
e_{zz} &= 0 & e_{zx} &= 0
\end{aligned}
\tag{19}
$$

The most general relationship for the mechanical stress tensor has the following form

$$\tau_{ij} = -p\delta_{ij} + 2\eta e_{ij} + \delta_{ij}\eta_s\phi \tag{20}$$

where ϕ is the fluid dilatation which is zero for an incompressible fluid, δ_{ij} is the Kronecker delta and η_s is a second coefficient of viscosity. For the modelled case

$$(\nabla\tau)_x = \eta\left(\frac{\partial}{\partial x}\cdot\frac{\partial u}{\partial x} + \frac{\partial}{\partial y}\cdot\frac{\partial u}{\partial y} + \frac{\partial}{\partial z}\cdot\frac{\partial u}{\partial z}\right) = \eta\frac{d^2u}{dy^2} \tag{21}$$

and so the equation of motion in the x direction can be written in this way:

$$0 = -\frac{\partial p}{\partial x} + \eta\frac{d^2u}{dy^2} - \sigma(E_z + uB_o)B_o \tag{22}$$

From $\nabla \times \boldsymbol{E} = 0$ we conclude that E_x is a constant; since there is no field applied in the x direction, we can arbitrarily take it zero. The electrodes have high conductivity, therefore $E_y = 0$ in the electrodes and hence everywhere. It follows that E_z is a function only of y.

The boundary conditions $u = 0$ and $y = \pm y_0$ give solution in the form

$$u = \left(\frac{1}{\sigma B_o^2} \cdot \frac{\partial p}{\partial x} + \frac{E_z}{B_o} \right) \left[\frac{\cosh\left(B_o \sqrt{\frac{\sigma}{\eta}}\, y \right)}{\cosh\left(B_o \sqrt{\frac{\sigma}{\eta}}\, y_o \right)} - 1 \right] \tag{23}$$

Introducing the Hartmann's number M

$$M = \sqrt{B_o^2 y_o^2 \frac{\sigma}{\eta}} \tag{24}$$

and putting the solution into the Ohm's law, we can find j_z as

$$j_z = \sigma E_z \frac{\cosh\left(M \frac{y}{y_o} \right)}{\cosh M} + \frac{y_o}{M} \sqrt{\frac{\sigma}{\eta}} \frac{\partial p}{\partial x} \left[\frac{\cosh\left(M \frac{y}{y_o} \right)}{\cosh M} - 1 \right] \tag{25}$$

It is possible to determine the induced magnetic field H_x now, using the Maxwell equation $\nabla \times \boldsymbol{H} = \boldsymbol{j}$

$$\frac{dH_x}{dy} = -j_z = -\sigma E_z \frac{\cosh\left(M \frac{y}{y_o} \right)}{\cosh M} - \frac{y_o}{M} \sqrt{\frac{\sigma}{\eta}} \frac{\partial p}{\partial x} \left[\frac{\cosh\left(M \frac{y}{y_o} \right)}{\cosh M} - 1 \right] \tag{26}$$

which after integration gives

$$H_x = \frac{y_o^2}{M} \sqrt{\frac{\sigma}{\eta}} \frac{\partial p}{\partial x} \frac{y}{y_o} - \left(\frac{y^2}{M} \sqrt{\frac{\sigma}{\eta}} \frac{\partial p}{\partial x} + \frac{I}{2L} \right) \frac{\sinh\left(M \frac{y}{y_o} \right)}{\sinh M} \tag{27}$$

5. DISCUSSION

Let us discuss the problem of velocity fluctuations now, namely the limits in which the velocity fluctuations may range. The resistivity of pure water is $2.27*10^5$ Ω.m, therefore the conductivity of the fluid may range probably between nearly 4.4×10^{-6} S and almost 0.03 S for common water from water-supply. Using some ingredients, the conductivity should be even improved. The viscosity of liquids is usually of the order 10^{-3} Pa.s, which gives these limits for the term based on the liquid constants

$$0.0664 < \sqrt{\frac{\sigma}{\eta}} < 5.48 \tag{28}$$

The channel width is supposed to be of the order of centimeters and its appropriate height oughts to be of the order of milimeters. The electric field can be applied up to approximately 1000 $V.cm^{-1}$ (for one half of the dielectric strength of water). The magnetic induction can fluctuate between 0 T and approximately 0.25 T. The velocity at the axis may then fluctuate round the average value u_o with the amplitude Δu_o that is expected to be at least 0.01 u_o for some configuration. These fluctuations of velocity in the direction of flow were estimated analysing the equation (23) for $y = 0$, i.e. study behaviour of u on the axis of the channel.

$$u = \left(\frac{1}{\sigma B_o^2} \frac{\partial p}{\partial x} + \frac{E_z}{B_o} \right) \left[\frac{1}{\cosh M} - 1 \right] \tag{29}$$

The Hartmann's number M (equation 24) is in fact a measure of the ratio of the magnetic body force to the viscous force, an increasing Hartmann's number should mean increasing interaction.

If the (grad $p)_x$ is a constant, it is obvious that with constant B_o the change in E_z would influence the value of u_o (and u as a whole). If we apply external field $\boldsymbol{E}$ varying in time, the u_o will also vary, the sign of the changes, however, will be opposite to the sign of E_z.

The condition for magnetohydrodynamic influence of the liquid flow follows directly from the equation (29).

$$\frac{\partial p}{\partial x} \lesssim \sigma E_z B_o \tag{30}$$

The gradient of pressure namely determines the value of liquid stream velocity and it can be evaluated from magnetohydrodynamic channel cross-section and flow rate demands regarding the velocity of the flow through the channel is constant without fields. Taking into account the typical parameters of waterjets (generated by 350 MPa) the graph presented in Fig. 6 was determined for the relationship between a magnetic field induction and potential modulation ratio of the velocity provided the electric field of specified parameters is applied. The channel dimensions are 10×10×2 mm and the voltage is 1000 V. It is evident that such a configuration of parameters exists that the fluctuations exceeding 0.01 of the maximum velocity value are induced. These fluctuations are supposed to be sufficiently intensified by Helmholtz resonator.

Theoretical studies of the physical relationships in Helmholtz resonators indicate, however, that designing of this type of resonator for very high pressures is a great problem. It is caused especially by the fact that the diameter of the resonant cavity has to be very small (as it follows up directly from equation 6). It is even questionable if the resonant cavity can be considered a resonator of Helmholtz type because resulting cavities are very similar to a shallow cavity. Nevertheless, this knowledge corresponds with Rockwell & Naudascher (1978) who classed the Helmholtz resonator with shallow cavities. However, a very precious accuracy of all dimensions is needed because small differences yield large changes in output behaviour of produced jet. Therefore, it is necessary to determine the initial parameters and demands exactly. Anyway many configurations need to be theoretically analysed before choosing the most suitable one. Nevertheless, designing the Helmholtz resonator for producing of pulsing jets, it is necessary to keep in mind that the breakage length should be suitable for practice. This demand helps to limit the range for product of modulation ratio and frequency. The practical demands help to prescribe also some cavity dimensions, e.g. cavity length and diameter of the outlet nozzle. The criterion of manufacturing ability is the decisive one and gives the limits to this type of pulse jet generation from highly pressurized water ($p_o \gtrsim 300$ MPa).

6. CONCLUSIONS

The most important results of the presented theoretical analysis aimed at magnetohydrodynamic influence of a liquid stream as an element creating primary fluctuations with determined frequency for Helmholtz resonators can be summarized in the following few remarks:

- the frequency of modulation must be higher than 20 kHz for water pressures exceeding 300 MPa;
- the modulation ratio of the outlet velocity of the jet, for breakage length closed to practice, lies between 0.04 and 0.4, depending on frequency of modulation for water pressures higher than 300 MPa;
- the magnetohydrodynamic phenomenon can be utilized for generation of the primary fluctuations of determined frequency and amplitude;
- the dimensions of elements, resulting from presented theoretical analyses, seem to be workable in practice.

7. ACKNOWLEDGEMENTS

The authors are grateful to the Grant Agency of the Czech Republic for supporting the work presented in this paper by project 106/98/1354.

8. REFERENCES

Brož, J., Roskovec, V., Valouch, M., "Physical and mathematical tables," SNTL, Prague, 1980.

Chahine, G.L., and Conn, A.F., "Passively-Interrupted Impulsive Water Jets," *Proceedings of the 6th International Conference on Erosion by Liquid and Solid Impact*, pp. 34:1-9, Cambridge, England, 1983.

Daniel, I.M., Rowlands, R.E., and Labus, T.J.: "Photoelastic Study of Water Jet Impact," *Proceedings of the 2nd International Symposium on Jet Cutting Technology*, Paper A1, BHRA, Cranfield, Bedford, England, 1974.

Huang, Y.C., Hammitt, F.C., and Yang, W.J.: "Mathematical Modelling of Normal Impact Between a Finite Cylindrical Liquid Jet and Non-Slip, Flat Rigid Surface," *Proceedings of the 1st International Symposium on Jet Cutting Technology*, Paper A4: pp. 57-68, BHRA, Cranfield, Bedford, England, 1972.

Lesser, M.B., and Field, J.E.: "The Fluid Mechanics of Compressible Liquid Impact," *Proceedings of the 4th International Conference on Rain Erosion and Associated Phenomena*, pp. 235-269, RAE, Farnborough, United Kingdom, 1974.

Puchala, R.J., and Vijay, M.M.: "Study of an Ultrasonically Generated Cavitating or Interrupted Jet: Aspects of Design," *Proceedings of the 7th International Symposium on Jet Cutting Technology*, Paper B2: pp. 69-82, BHRA, Cranfield, Bedford, England, 1984.

Reinecke, W.G.: "Rain Erosion at High Speeds," *Proceedings of the 4th International Conference on Rain Erosion and Associated Phenomena*, pp. 209-234, RAE, Farnborough, United Kingdom, 1974.

Rochester, M.C., Brunton, J.H.: "High Speed Impact of Liquid Jets on Solids," *Proceedings of the 1st International Symposium on Jet Cutting Technology*, Paper A1: pp. 1-24, BHRA, Cranfield, Bedford, England, 1972.

Rockwell, D., Naudascher, E., "Review - Self-Sustaining Oscillations of Flow Past Cavities," *Transactions of the ASME - Journal of Fluids Engineering*, Vol. 100, pp. 152-165, 1978.

Sami, S., and Ansari, H., "Governing Equations in a Modulated Liquid Jet," *Proceedings of the 1st U.S. Water Jet Symposium*, pp. I-2.1-9, Water Jet Technology Association, St. Louis, Missouri, 1981.

Shen Zhong Hou, and Wang Zhi Ming, "Theoretical analysis of a jet-driven Helmholtz resonator and effect of its configuration on the water jet cutting property," *Proceedings of the 9th International Symposium on Jet Cutting Technology*, pp. 189-201, BHRA, Cranfield, Bedford, England, 1988.

9. NOMENCLATURE

$\boldsymbol{B}$	magnetic induction field [T]
$\boldsymbol{B_0}$	applied magnetic field [T]
c	velocity of light [$m.s^{-1}$]
c_w	wave speed [$m.s^{-1}$]
c_s	sound speed [$m.s^{-1}$]
d_i	diameter of the resonator inlet nozzle [m]
d_r	diameter of the resonator cavity [m]
$\boldsymbol{D}$	displacement field [$C.m^{-2}$]
$\boldsymbol{D}$	time derivation of displacement field [$A.m^{-2}$]
ε	permittivity [$F.m^{-1}$]
ε_o	permittivity of free space [$F.m^{-1}$]
ε_r	relative permittivity
e_{ij}	strain rate tensor [s^{-2}]
$\boldsymbol{E}$	electric field [$V.m^{-1}$]
$\boldsymbol{f}$, $\boldsymbol{f_e}$	body force density [$N.m^{-3}$]
f_m	frequency [s^{-1}]
f_p	preferable frequency [s^{-1}]
f_r	resonant frequency [s^{-1}]
γ	compressibility of water under normal conditions [$N.s.m^{-2}$]
γ_o	compressibility factor of pressurized water
γ_{po}	compressibility of water under the pressure p_o [$N.s.m^{-2}$]
$\boldsymbol{g}$	electromagnetic momentum flux vector [$N.s.m^{-3}$]
η	fluid viscosity [Pa.s]
η_s	second coefficient of viscosity
$\boldsymbol{H}$	magnetic field [$A.m^{-1}$]
$\boldsymbol{j}$	current flux [$A.m^{-2}$]
λ_i	principal stresses [Pa]
λ_w	wavelength [m]
l_o	length of disintegration of the outflow [m]
L	length of the resonator [m]
L_r	length of the resonant cavity for the frequency f_r [m]
μ	magnetic permeability [$H.m^{-1}$]
μ_o	magnetic permeability of free space [$H.m^{-1}$]
μ_n	nozzle discharge coefficient
μ_r	relative magnetic permeability
m	modulation ratio ($\Delta v/v_m$)
M	Hartmann's number
p	pressure [Pa]
p_o	pressure before the nozzle [MPa]
p_{qw}	number of quarter-wavelength
ρ	liquid density in noncompressed state [$kg.m^{-3}$]
ρ_e	charge density [$C.m^{-3}$]
σ	electrical conductivity [S]

t	time [s]
T_{ij}	electromagnetic stress tensor [Pa]
τ_{ij}	mechanical stress tensor [Pa]
u	x component of velocity [$m.s^{-1}$]
v	y component of velocity [$m.s^{-1}$]
$\boldsymbol{v}$	velocity vector [$m.s^{-1}$]
v_m	medium velocity of modulated jet [$m.s^{-1}$]
v_o	outlet velocity of the resonator [$m.s^{-1}$]
w	z component of velocity [$m.s^{-1}$]
ψ	gravitational potential [$m.s^{-2}$]

10. FIGURES

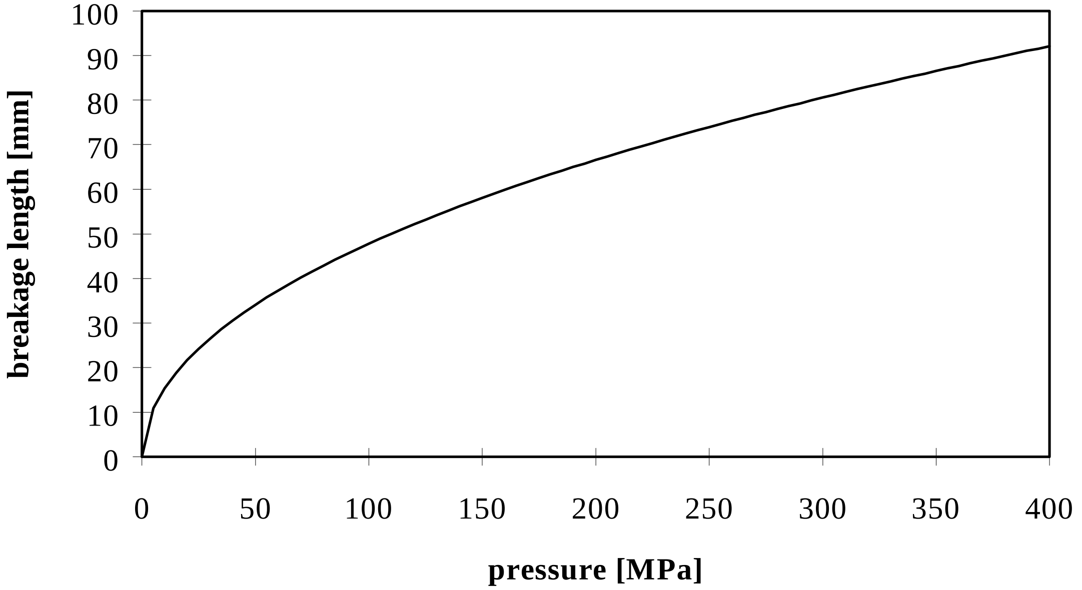

Figure 1. Theoretical relationship of the breakage length of pulsing jet on water pressure. Modulation ratio 0.15, frequency 15 kHz.

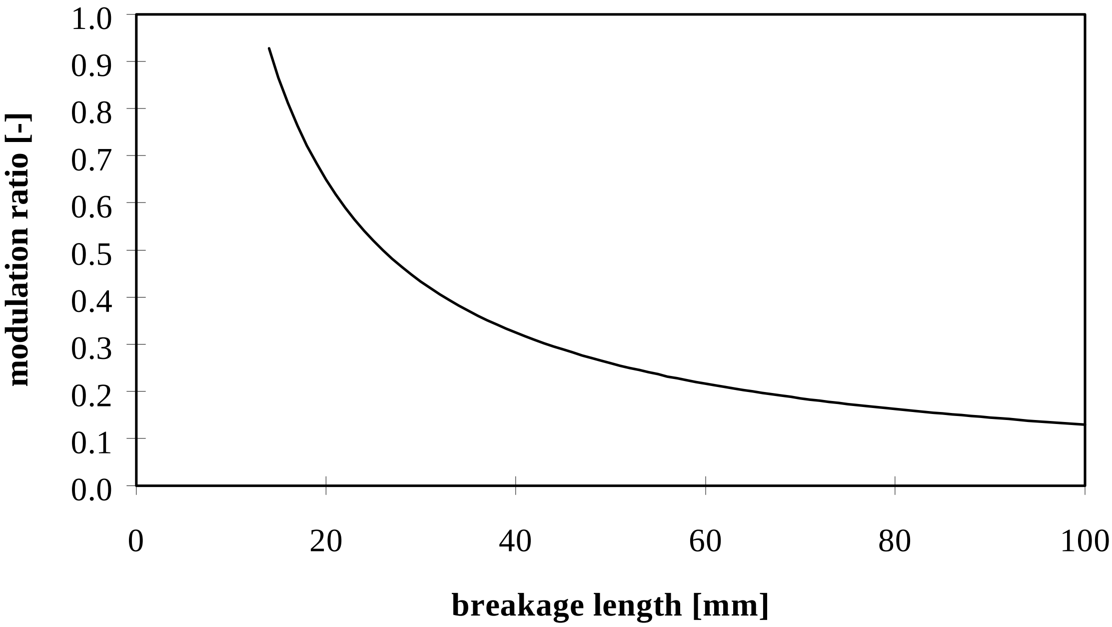

Figure 2. Theoretical relationship of the modulation ratio on the breakage length of pulsing jet. Frequency 15 kHz, water pressure 350 MPa.

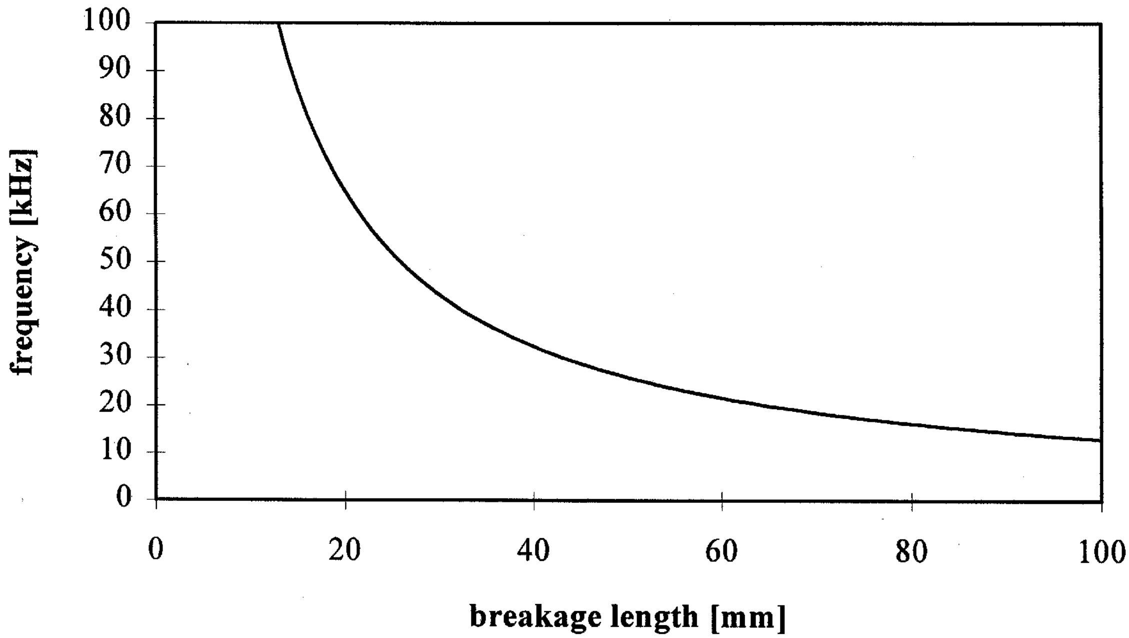

Figure 3. Theoretical relationship of the modulation frequency on the breakage length of pulsing jet. Modulation ratio 0.15, pressure 350 MPa.

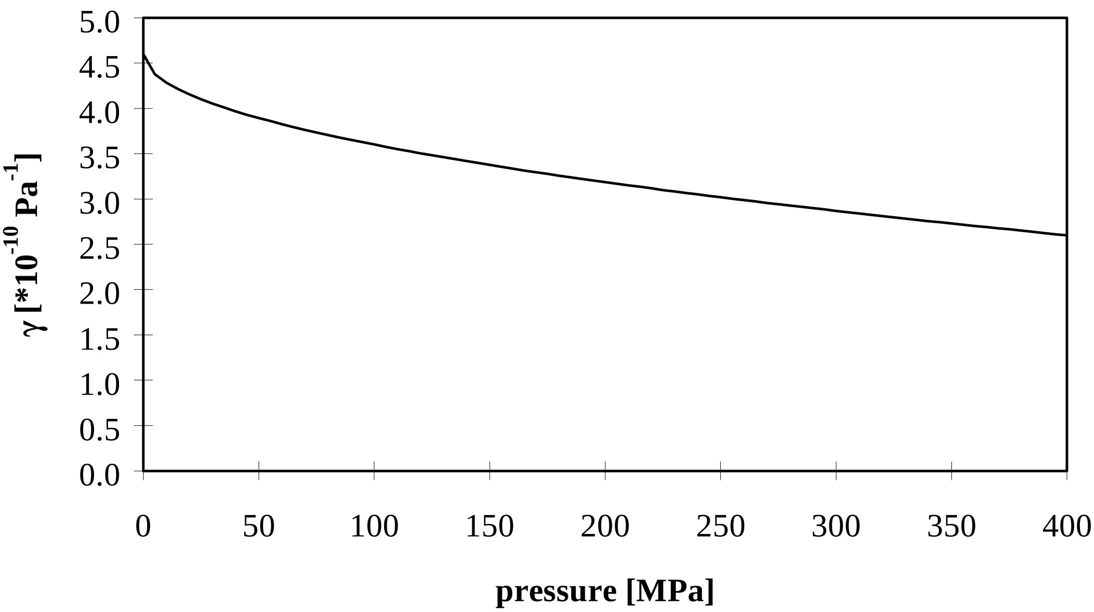

Figure 4. Regression relationship of water compressibility on the internal water pressure.

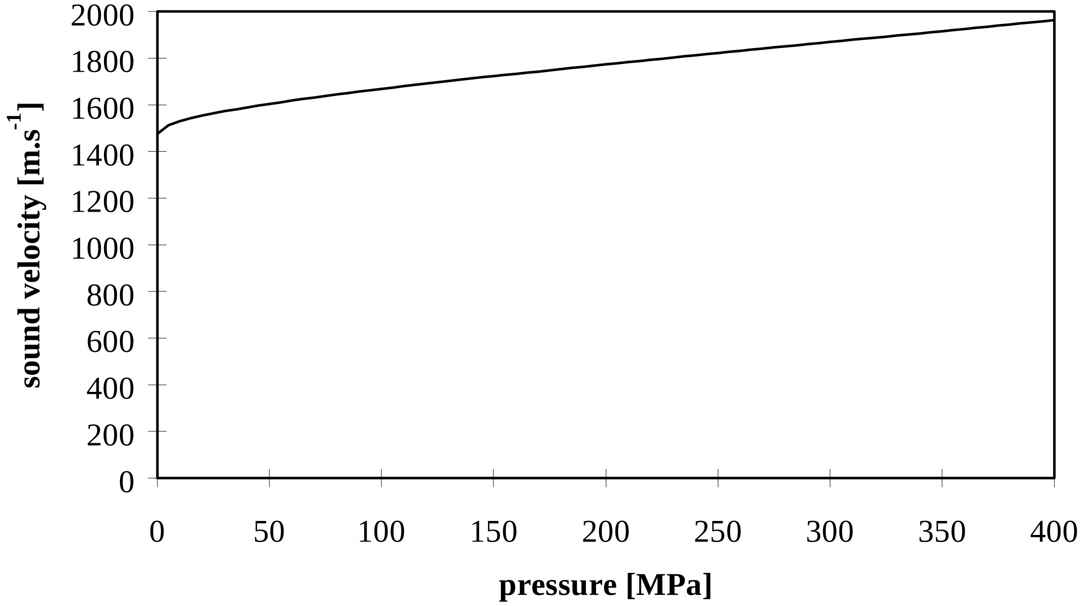

Figure 5. Relationship of sound speed in water on the internal pressure.

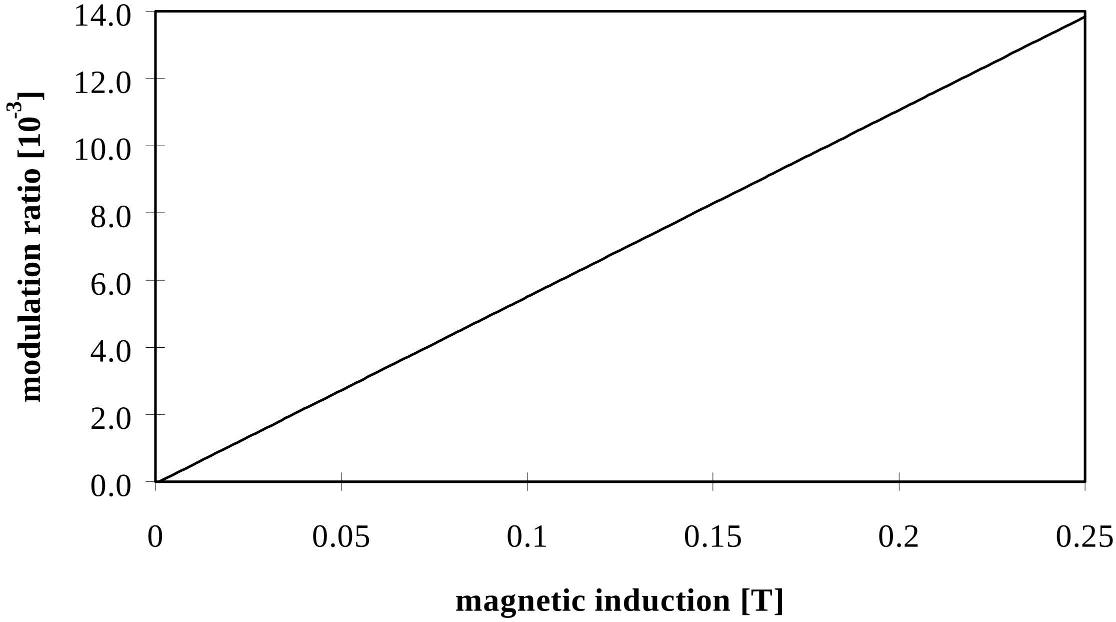

Figure 6. Relationship between magnetic induction and modulation ratio of velocity inside magnetohydrodynamic channel. Water pressure 350 MPa, voltage 1000 V, conductivity 0.01 S, channel width 10 mm, channel length 10 mm, channel heigth 2 mm.

10^{th} American Waterjet Conference
August 14-17, 1999: Houston, Texas

Paper 24

A HIGH EFFICIENCY JET NOZZLE WITH FLOW DEFLECTOR

Chen Yufan
Beijing JieJing Pipeline-Cleaning Institute
Beijing, P.R. China

Gong Weili, Fang Mei, Xu Xiaodong
School of Resources Engineering,
University of Science & Technology Beijing
Beijing, P.R. China

ABSTRACT

The high-pressure water jet cleaning technique has been grown in application. The jet nozzle is a key component in the complete sets of high-pressure water jet cleaning equipment. In order to enhance the jetting efficiency of the jet nozzle, a new type of jet nozzle with flow deflector is proposed in this paper. In the presence of the flow deflector, the generating of the vortices and the separating of the shear layer are avoided thereby the energy loss of the jet nozzle is reduced considerably. The theoretical analyses and experimental study are carried out. The obtained results indicate that the jet nozzle with flow deflector is highly efficient in cleaning operation. Both lab tests and on-site application demonstrate that the jetting efficiency of the jet nozzle with flow deflector is much higher than that of the nozzle without flow deflector. And the information acquired in this study is expected to be useful in the design of the jet nozzle for developing high-pressure water jet cleaning equipment.

Organized and Sponsored by the WaterJet Technology Association

1 INTRODUCTION

Up to now, the high pressure water jet (hpwj) have been widely used as a tool for cleaning municipal water-supply and sewer pipe lines, industrial pipe lines such as sewage pipe lines, oil pipe lines, and gas pipe lines etc, both at home and abroad.

The improvement of jetting efficiency of jet nozzles is attaching more and more attention of scientists in this field, as the jet nozzles are the key technique of the complete sets of hpwj cleaning equipment. The design of the nozzle and its machining quality are the factors that influence the impact effect and cleaning efficiency substantially.

In order to reduce energy loss and enhance jetting performance, a new type of high efficiency jet nozzle was developed. The new type of jet nozzle has a specially designed flow deflector inside, which allows smaller pressure drop due to the reduction of the turbulence level, vortex flow loss and secondary circulating flow loss within the flow passage of the nozzle. Thus enhances the jetting performance of the nozzle.

The theoretical analysis has been made and the experiments were carried out in order to confirm the validity of the design and determine its structural parameters. The obtained results in this study are expected to give some useful information with regard to the jet nozzle design for hpwj cleaning technology.

2 NOZZLE DESIGN

When the pressured water is passing though a jet nozzle, the vortex flow and the secondary circulating flow occur for the influence of the variations of the direction, shape and dimension of the flow passage within the nozzle. These disturbances would generate energy loss and lower jetting efficiency.

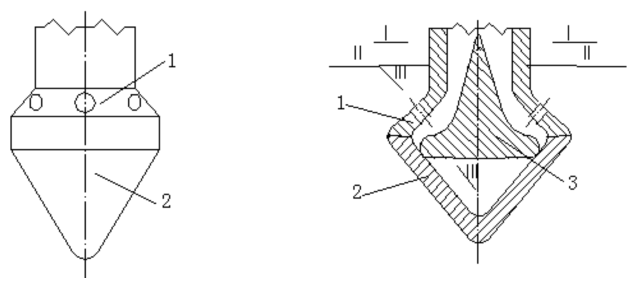

Figure1 Schematic drawing of the deflector type nozzle
1-Nozzle body; 2-Flow deflector; 3-Bullet-shaped head.

In Figure1 the deflector type nozzle has been shown. The nozzle is composed of nozzle body (1), bullet-shaped head (2) and the flow deflector (3). Between the inner wall of the nozzle body and deflector surface, a smooth flow passage is formed while the variations of its flow area being kept to minimum. Thereby the energy loss of the nozzle is reduced considerably. When the other nozzle parameters are fixed, the deflecting effect mainly depends on the three parameters of the deflector, that is, flow area of the flow passage, quality of the surface finish and flow-deflecting angle of the flow deflector.

The variation of the flow area for the flow passage should be as little as possible. When flow area keeps unchanged, the fluid, while flowing though the passage, will cling tightly to the inner wall of the passage, without any vortices being produced. In this case, the energy loss caused by the variation of the flow passage equals zero.

The space encircled by the nozzle body and the flow deflector is known as deflecting space. The quality of surface finished (surface roughness) of the inner wall of the deflecting space also influences the jetting quality and impact effect immensely. Generally, the higher the surface finish quality, the lower the energy loss. But high quality of surface finish would result in machining difficulties and high manufacture costs. Therefore, the rational range of surface finish should be adopted so that the energy loss is reduced to the minimum level at relatively lower manufacture costs.

The top angle of the flow deflector is known as flow deflecting angle θ, which is the crucial parameter determining the shape of the surface curve of the deflector, or, the shape of the flow passage within the jet nozzle. The sudden turn would result in the separation of the flow with the inner wall of the flow passage and produce vortices, thereby increases energy loss of the fluid. The smaller deflecting angle leads to sudden turn of the flow passage, thereby causing higher energy loss, and so does the larger deflecting angle. While other structural parameters for the jet nozzle are given, there would be an optimum flow- deflecting angle, at which the energy loss can be reduced to the minimum.

3 THEORETICAL ANALISIS

In a deflector type jet nozzle there are mainly three kinds of resistance leading to the energy loss of the fluid within the nozzle, neglecting the frictional resistance caused by the length of the flow passage. The three kinds of resistance are the flow area related resistance (denoted with h_A), the deflecting angle related resistance (denoted with h_θ), and the surface finish related resistance (denoted with h_ε).

The flow area related resistance is created by the variation of the flow area of the flow passage. Between section 1-1 and section 3-3 the Bernoulli’s formula is,

$$\frac{p_1}{\rho}+\frac{u_1^2}{2}=\frac{p_3}{\rho}+\frac{u_3^2}{2}+gh_A \tag{1}$$

Between section 1-1 and section 3-3 the momentum equation is,

$$(p_1-p_3)A_3=\rho A_3 u_3(u_3-u_1) \tag{2}$$

Eq. (2) can be rewritten as,

$$\frac{p_1 - p_3}{\rho} = u_3(u_3 - u_1) \tag{3}$$

Substituting Eq. (3) into Eq. (1) and simplifying it we can obtain,

$$h_A = \left(\frac{u_1}{u_3} - 1\right)^2 \frac{u_3^2}{2} = \zeta_A \frac{u_3^2}{2} \tag{4}$$

Where, ζ_A is defined as the drag coefficient associated with h_A. Since the fluid velocity is inversely proportional to the flow area of the flow passage, ζ_A can be written as,

$$\zeta_A = \left(\frac{u_1}{u_3} - 1\right)^2 = \left(\frac{A_3}{A_1} - 1\right)^2 \tag{5}$$

While $A_3/A_1 = 1$ or $u_1/u_3 = 1$, namely, $A_3 = A_1$ or $u_1 = u_3$, the drag codfficient ζ_A would be equal to zero. According to the above theoretical analysis we can conclude here that in the structural design of the jet nozzle, the flow area variation of the flow passage should be avoided in order to eliminate the caused resistance.

The method of dimensionless analysis is adopted to examine the resistance h_θ with deflecting angle θ, and resistance h_ε with surface roughness of the deflector ε. Assuming that the flow area of section 1-1 equals to the flow area of section 3-3, that is, the velocity of the fluid u can be described as,

$$u = u_1 = u_3 \tag{6}$$

The flow field between section 1-1 and section 3-3 can be described as,

$$f(u, \rho, d, \Delta p, \mu, \varepsilon, r) = 0 \tag{7}$$

Among all the seven parameters in Eq. (7), choosing u, ρ, d as a basic dimension group, the number of dimensionless parameters should be $7 - 3 = 4$, that are,

$$\pi_1 = \frac{\Delta p}{\rho u^2} = \frac{p_1 - p_3}{\rho u^2} \tag{8}$$

$$\pi_2 = \frac{\mu}{u d \rho} = \frac{1}{\mathrm{Re}} \tag{9}$$

$$\pi_3 = \frac{\varepsilon}{d} \tag{10}$$

$$\pi_4 = \frac{r}{d} \tag{11}$$

In the course of derivation of the above dimensionless variables $\pi_1 \sim \pi_4$, the principle of Dimensional Homogeneity was applied.

Curvature radius (r) is related to the flow-deflecting angle (θ) and the length of the sectional curve of the flow deflector (l), or, $r \sim l/\theta$, thus the equation (11) can be further expressed as,

$$\pi_4 = \eta \frac{l}{d\theta} \tag{12}$$

where, η is an amending coefficient.
According to the π theorem (Zhou Hengda, 1991), Eq. (7) can be rewritten as:

$$f_1(\pi_1, \pi_2, \pi_3, \pi_4) = 0 \tag{13}$$

or,

$$\pi_1 = f_2(\pi_2, \pi_3, \pi_4) \tag{14}$$

Substituting Eq. (8)~(13) into Eq. (14) gives,

$$\frac{\Delta p}{\rho u^2} = f_2\left(\mathrm{Re}, \frac{\varepsilon}{d}, \frac{l}{d\theta}\right) \tag{15}$$

With a fixed pump pressure and flow rate, Reynolds number is an invariable. Hence Eq. (15) can be rewritten as:

$$\Delta p = f_3\left(\frac{\varepsilon}{d}, \frac{l}{d\theta}\right)\frac{\rho u^2}{2} \tag{16}$$

Eq. (16) then is the overall pressure drop within the flow field between section 1-1 and section 3-3. From the principle of superposition, the overall pressure drop Δp can be divided into two parts, the pressure drop (Δp_1) generated by the roughness of flow deflector, and the pressure drop (Δp_2) generated by the flow deflecting angle. That is,

$$\Delta p = \Delta p_1 + \Delta p_2 \tag{17}$$

Δp_1 given by,

$$\Delta p_1 = \phi_1\left(\frac{\varepsilon}{d}\right)\frac{\rho u^2}{2} = \zeta_1\frac{\rho u^2}{2} \tag{18}$$

where, ζ_1 is the drag coefficient related to the roughness of the deflector surface.

Δp_2 can be expressed as:

$$\Delta p_2 = \phi_2\left(k\frac{180}{\theta^\circ}\right)\frac{\rho u^2}{2} = \zeta_2\frac{\rho u^2}{2} \tag{19}$$

where, ζ_2 is the drag coefficient related to the flow deflecting angle, k is an amending coefficient in connection with l/d.

4 EXPERIMENTAL RESULTS

The plot of dimensionless pressure drop $\Delta p_1/p$ against flow deflecting angle θ based on the surface finish quality of the flow deflector is equal to $1.6\mu m$ shown in Figure 2. From Figure 2, we can see that the minimum pressure drop is achieved at the flow deflecting angle equals to 25 degrees. In the case of smaller and larger deflecting angle high pressure drop would exist for the sudden changes of the direction of the flow within the flow passage. The optimum range of flow-deflecting angle should be in the vicinity of 25 degrees.

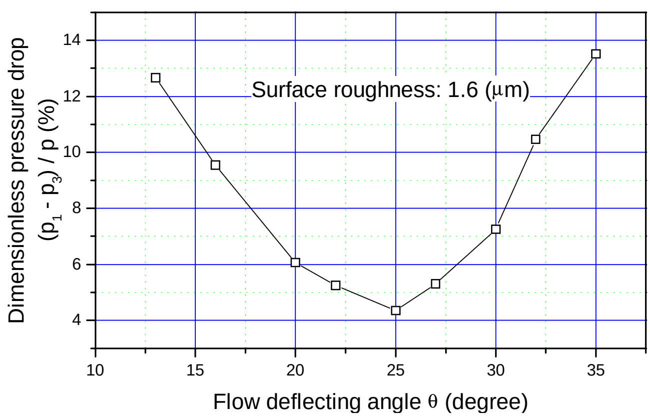

Figure 2 Dimensionless pressure drop vs. flow deflecting angle

Figure 3 reveals the dimensionless pressure drop versus the roughness of the surface of the flow deflector while flow deflecting angle $\theta = 25^\circ$. The pressure drops steeply at a surface roughness more than $1.6\,\mu m$, after that drops slightly in succession, and remains unchanged at a surface roughness under $0.8\,\mu m$.

Decreasing the surface finish quality leads to increase the relative surface roughness (ε/d) of the flow deflector. Thereby, the flow passage is in the state of the so-called hydraulic coarse tube (as discussed by Sheng Jingchao 1980). In this case, the pressure loss is directly proportional to the 2nd power of fluid velocity u. Increasing the surface finish quality, as opposed to the former, the flow passage is in the state of hydraulic smooth tube, and the pressure loss is directly proportional to u to the power of 1.75. That is the reason why the pressure drop with high surface finish quality is much lower than that with low surface finish quality. It is apparent that the above discussion is based on the turbulent flow occurs within the jet nozzle.

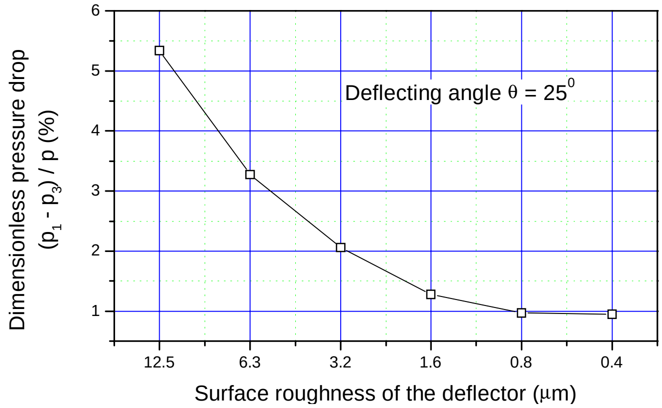

Figure 3 Dimensionless pressure drop vs. surface roughness of the deflector

A cleaning test was made for comparing the performance between the jet nozzle with flow deflector and the jet nozzle without flow deflector. The test facility is a fouled pipe heat exchanger. The rate of fouling removal against pump pressure is shown in Figure 4. The plot reveals the fact that the rate of fouling removal for jet nozzle with flow deflector is much higher than that for jet nozzle without flow deflector. From Figure 4 we can see that the rate of fouling removal for flow deflector type nozzle reaches 100% under the pump pressure 40 MPa. However, the same task achieved by the jet nozzle without flow deflector needs the pump pressure up to 500 MPa. That is to say, the jetting efficiency for the jet nozzle with flow deflector is much higher than that for the jet nozzle without flow deflector.

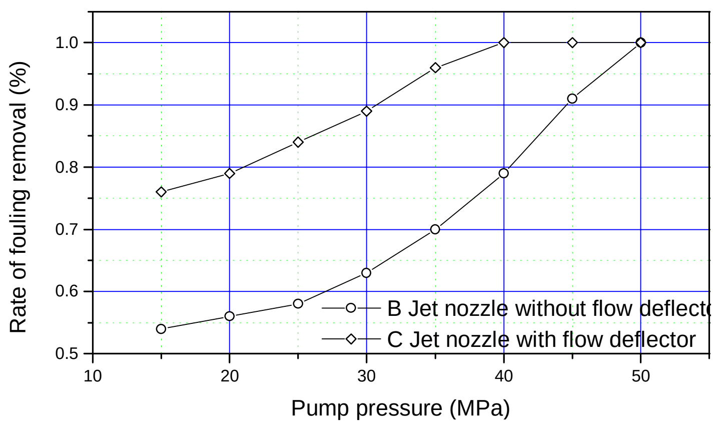

Figure 4 Rate of fouling removal vs. pump pressure

5 CONCLUSION

The theoretical analysis and the experimental study as well as the subsequent practical application in cleaning projects demonstrate that the jet nozzle with flow deflector has higher jetting efficiency than the jet nozzle without flow deflector. The information can be summarized as:

- The variations of the flow area should be avoided.
- The optimum flow-deflecting angle is in the vicinity of 25 degrees.
- The surface roughness might be under/equal to 1.6 μm.

6 REFERENCES

Sheng Jingchao, "Hydraulic Fluid Mechanics," pp.125-132, Mechanical Industry Publishing House, Beijing, 1980.

Zhou Hengda, "Engineering hydromechanics," pp. 196-197, Metallurgical Industry Publishing House, Beijing, 1991.

7 NOMENCLATURE

Abbreviations

hpwj	high pressure water jet

Symbols

θ	flow deflecting angle of the flow deflector
u	velocity of the fluid within the flow field of the jet nozzle
u_1	velocity of the fluid at the section 1-1
u_3	velocity of the fluid at the section 3-3
A_1	flow area at section 1-1
A_3	flow area at section 3-3
ρ	density of the fluid
d	inlet diameter of the flow deflector type jet nozzle
Δp	overall pressure drop, $\Delta p = p_1 - p_3$
μ	dynamic viscosity
ε	roughness, or surface finish degree of the flow deflector
r	curvature radius of the sectional curve of the flow deflector surface,
Re	Reynolds number
l	length of the sectional curve of the flow deflector
η	amending coefficient concerning r, l and θ
h_A	resistance created by the variation of the flow area for the flow passage

ζ_A	drag coefficient associated with h_A
h_θ	resistance related to the variation of the flow-deflecting angle
ζ_2	drag coefficient related to the flow-deflecting angle
k	amendment coefficient for ζ_2 in connection with l/d
h_ε	resistance produced by the roughness of the surface of the flow deflector
ζ_1	drag coefficient related to the roughness of the deflector surface.
Δp_1	pressure drop concerned with ζ_1, $\Delta p_1 = \zeta_1 \dfrac{\rho u^2}{2}$
Δp_2	pressure drop concerned with ζ_2, $\Delta p_2 = \zeta_2 \dfrac{\rho u^2}{2}$
$\pi_1 \sim \pi_4$	dimensionless parameters

10th American Waterjet Conference
August 14-17, 1999: Houston, Texas

Paper 25

SUPER-WATER® JETTING APPLICATIONS FROM 1974 TO 1999

W. Glenn Howells

ABSTRACT

SUPER-WATER® concentrated industrial water blasting additive (abbreviated to S-W®, developed in 1974, was first used to clean hard intractable deposits from ISOMAX Hydroprocessing reactor exchangers in 24-hours instead of the 3-months taken by previous methods. The mechanism and general applicability of S-W® to clean hard deposits at nominal pressures and flow rates of 10,000 psi and 10 gpm will be described.

Later it was determined that S-W® was equally effective at lower pressures and for use in pressure washers (i.e. less than 6,000 psi) and could be equally well applied to "soft" materials. The successful removal of epoxy-bound rubber from space shuttle booster motors ultimately lead to ultra-high pressure jet cutting of shoe soles at 50,000 psi and then of use for an entire range of rubber and related products from semi-liquid Vistanex to 90 Durometer material.

S-W® has been used for slotting and drilling granite and concrete and more recently in the abrasive suspension jet (ASJ technique for precision cutting of "soft" metals, e.g. lead (Mohs' hardness 1.5) to hard ceramics (Mohs' hardness >9). It increases the effectiveness of the standard abrasive water jet (AWJ) by producing narrower kerf widths and reducing abrasive consumption by 50%.

Future methods of using S-W® with abrasives will be discussed as well as submerged applications with or without abrasives. New, more efficient and far less costly techniques of injecting S-W® into intensifier cutting and hydroblasting cleaners are now available and in use worldwide.

Finally the availability of companies providing contract cutting evaluations of S-W® with and without abrasives are listed together with safety and environmental considerations.

1. OBJECTIVE

A description will be given of the many advantages that are obtained across the full range of waterjet applications by using SUPER-WATER®, a water-soluble polymer.

A previous review (1) has detailed the applications achieved from 1974 to 1989.

2. BACKGROUND

SUPER-WATER® concentrated industrial water blasting additive (abbreviated here to S-W® was first used in 1974 to clean Chevron USA ISOMAX Hydroprocessing reactor exchangers in approximately 24-hours in contrast to previous methods which took 3-months **(2).**

The polymer, a linear macromolecular partially hydrolyzed polyacrylamide (with a molecular weight of 16 to 18 million), was found to increase cleaning efficiency from 2 to 50 times depending on the material being removed **(2).** This technique has since been used for cleaning in a very wide range of industries **(1, 3).**

The 1500 U-shaped tubes of the Chevron ISOMAX unit were clogged with extremely hard deposits of fused coke but these were readily removed with S-W [RI. Consequently initial applications of S-W® tended to concentrate on removal of hard materials. in large measure this derived from Chevron USA's knowledge that Russian workers had reported **(4)** they could cause "destruction of metallic obstacles (sic) by a jet of dilute polymer solution".

The Russians used:

(i) submerged jets
(ii) centrifugal pumping and
(iii) recirculated the dilute polymer solution.

Each of these conditions has relevance in using S-W® and will be further discussed below.

3. MECHANISM OF S-W® APPLICATIONS

As detailed previously **(1, 3)** there are three steps which result in S-W® being more effective than plain waterblasting. They are:

(a) Drag reduction

For liquids flowing through a hose or pipe this results in nozzle pressures more closely matching the pump pressures.

(b) Jet focusing

This provides increased power density on the target.

(c) Macromolecular bombardment

As indicated above S-W® molecules have a molecular weight ranging from 16 to 18 million and at supersonic velocities they behave as though they are rigid. This greatly enhances the effect of bombardment on a substrate **(1, 3).**

"All molecules undergo varying degrees of intramolecular vibration. It is possible to envisage intramolecular stretching, bending, and twisting and to appreciate that the larger the molecule, the greater will be the time frames of these motions. During high-pressure polymerblasting with jets often impacting at supersonic speeds, the S-W® macromolecules and their associated aggregates of water do not have sufficient time for complete stretching, bending or twisting. As a result, the jet's effectiveness on the target is enhanced by bombardment with molecules that are "rigid" **(1, 3).** The Deborah number, D, is related to this effect. D is defined as the ratio between a polymer aggregate's relaxation time and the characteristic time scale during which the fluid stream undergoes deceleration. It is predicted that when D is greater than unity, "solid-like" behavior is exhibited because the polymer aggregate has an inadequate opportunity to adjust (relax) to its changing environment **(5)."**

The S-W® polymer functions by imparting more structure to water and it does so by hydrogen bonding large aggregates of water molecules to itself.

It is well known that the hydrogen bond plays a critical role in a wide array of chemical functions and activities.

In the liquid phase water molecules do not exist as individual entities. For example, two adjacent molecules of water are hydrogen bonded to one another. The partial positive charge of a hydrogen atom on one molecule is electrostatically attracted to the partial negative charge on the oxygen atom of the other molecule. There is substantial evidence that water molecules spontaneously form multi-molecular aggregates and this tendency has been found to be especially prevalent in situations where water molecules exist adjacent to water-wet surfaces.

Because the individual monomeric acrylamide and acrylic acid groups of S-W® are themselves each capable of hydrogen bonding 13 to 14 water molecules **(6)**, extended aggregates are formed.

(These have been likened to a series of spinal columns, or polymer backbones within the bulk of a volume of water, as well as to the reinforcement bars used in concrete structures to develop overall strength).

Such longitudenal structures result in cylindrically oriented water sheaths around the linear S-W® macromolecules **(3)**. The presence of such extended or macrostructures would be expected to promote or stabilize laminar-flow **(7)** and decrease turbulence or the formation of vortices in boundary layers: this could be the basis for drag reduction.

Furthermore the hydrogen bonding of water molecules to S-W® and, on a molecular level, an extended macrostructure, is retained after emergence from the nozzle. This is manifested as a well collimated or focused jet **(8)** as seen in **FIGURE 1.**

Under conditions where S-W® jets are traveling at supersonic speeds, it is tempting to regard the S-W® molecules and their associated aggregates of water as being linearly aligned in the direction of flow **(3)**. Such an assumption, however, is not altogether necessary because on a molecular level, cordoned **(9),** helical **(10)**, or any ordered or extended macrostructure could bring about the observed jet focusing. The important feature is that structure is imparted to the water **(3).**

4. APPLICATIONS AT 10,000 PSI AND 10 GPM

Early successes in cleaning or removing hard deposits with S-W® in the mid 1970's mostly used nominal pressures and flow rates of 10,000 psi and 10 gpm respectively. For reasons - usually of confidentiality - most of these applications were not reported in the open literature until much later **(2, 11).**

At Chevron USA's Richmond, California refinery, a 20-inch natural gas line that develops very hard sulfur deposits and is cleaned once per year during the annual shutdown was first handled in 1974 in a considerable shorter time with S-W® **(2).**

Fiberboard Company's vertical evaporators in Antioch, California were cleaned in 4-days during 3 x 8-hour shifts with S-W®. Plain waterblasting was totally ineffective and the evaporators (each with 700 x 1 1/4-inch OD x 40-feet stainless steel tubes) were previously replaced (and buried on-site!) on a regular basis **(11)**.

Coke was removed from 40-foot pipes of 12-inch ID (Chevron USA**,** El Segundo, California) with plain water at 5-feet in 12-hours. S-W® effected removal at 30-feet in 4-hours - 18 times as fast **(11).**

Other hard deposits removed more effectively with S-W® than with plain water included **(2):** hard coke following a refinery fire, plugged second stage urea decomposer tubes, coke from cokers and gas effluent overhead, coke - from discharge headers of coke gas compressors, - from coke heater barrels and - from vapor lines, calcium carbonate and slurry deposits from boiler slagging slurry lines, calcium carbonate and dense magnesium salts from boiler tubes, hard scale from Benson sulfur recovery systems, calcium and iron fluorides from hydrofluoric acid alkylation plants and plastic, at large standoff distances, from batch reactors.

This last-listed application was followed, at a plastics plant, by the cleaning of a 100-foot section of 10-inch drain line plugged with phenolic resin. Goldsmith **(12)** used a self-propelled sewer lance (with multiple jets: 2 forward, 10 back at 10,000 psi) with plain water but only succeeded in making a 2-inch to 3-inch diameter hole in the bottom of the pipe. The first time the pipe was cleaned with S-W®, 5 x 55-gallon drums of crumbled resin (like stones) were removed. The S-W® totally cleaned the 10-inch pipe all the way to the skin.

Other successes achieved by Goldsmith included **(12)**:

(a) removal of polyester resin from a reactor,

(b) removal of refractory slag from a coal-fired power plant,

(c) installation of vents and pipes in 10-inch concrete walls,

(d) paint removal from a block building and

(e) the cleaning of pulverized coal slag and ice from a 12-inch pipe about 1200-feet in length.

5. APPLICATIONS AT LESS THAN 10,000 PSI

Somewhat later a decision was made to use S-W® at lower pressures as exemplified by the following applications.

(a) Sewer cleaning at 3,900 psi

In 1980 at a Redwood City, California construction site of the South Bay Systems Authority, concrete had been inadvertently poured into a combination sewer line resulting in **total** plugging. The sewer line consisted of an 11-foot down pipe with a 90° bend leading into a 20-foot horizontal section. Jetting with plain water proved to be ineffective.

However using a 0.3% aqueous solution of S-W® the concrete from the two sewer lines, which had internal diameters of 5-inches and 10-inches was removed. One pun unit delivered the S-W® on the target material while another was used for back flushing out the removed concrete with a 6-jet nozzle **(13).**

(b) Nuclear power plant cleaning at 5,600 psi

In 1990, S-W® was used to remove "sludge" (consisting of magnetite, metallic copper and oxides of copper) with a compressive strength of 15,000 psi from the tube sheets of nuclear power steam generators at the Ontario (Canada) Hydro Bruce Power Plant **(14).** In this instance, where once again plain water was ineffective, the pump pressure used was 5,600 psi.

Ontario Hydro had no limitations on the pressure capabilities of the pumps used. But it was determined that "no tube damage could be detected when lancing at pressures up to 15,.000 psi. However, when using S-W® at 8,500 psi the jet cut through a tube in about 5 minutes."

The Ontario Hydro report **(14)** at one and the same time indicates the "potency" of S-W® and vividly confirmed the findings of the Russian workers referred to previously **(4).**

Somewhat later Goldsmith **(15)**, who has used S-W® in waterblasting (i.e. 10,000 psi and 10 gpm), started to apply the product under "pressure washer conditions", arbitrarily assigned here as being at or less than 6,000 psi.

One example from Goldsmith's work involves cleaning badly weathered cedar siding from a commercial building. The siding was marred by dead oxidized wood and algae and was stripped down to give a new-looking wood finish. In this case, compared to plain water, the production rate was easily doubled using 0.3% S-W® at 3,000 psi and 5 gpm **(15).**

Similar results were obtained by Goldsmith **(15)** in:

(a) stripping failing paint from windows and facia trim of homes,

(b) cleaning the exterior of buildings and concrete floors and walls with accumulated grease and dirt,

(c) cleaning out plugged sewer lines in homes,

(d) cleaning aluminum/metal sidings to remove oxidized paint that was faded and stained with mildew,

(e) cleaning dirt from large earth moving-, trenching- and farming-equipment,

(f) cleaning concrete walls and concrete floors,

and lastly and perhaps of widest applicability because, in the absence of satisfactory coatings, it needs to be done annually

(g) cleaning wooden decks (that have weathered and are coated with dead oxidized wood) and restoring them to new-looking wood.

6. APPLICATIONS OF S-W® TO "SOFT" MATERIALS

In 1978 **(16),** a trivial assessment of polymerblasting "to clean" at 9,,000 psi and 12 gpm was obtained by "cutting" the following materials under controlled conditions: block salt, red brick, fire brick, oolitic Indiana limestone, block ice, rubber sheeting, concrete slab, plywood, volcanic rock and asphalt.

In each case S-W® improved the cutting, as determined by the depth and incisiveness of the cuts.

One significant conclusion, already discussed, was that S-W® was effective with respect to hard materials, e.g. oolitic Indiana limestone, concrete and volcanic rock. With the volcanic rock, for example, a plain waterjet merely discolored the surface. In contrast S-W® cut a 1-inch deep slot.

The second conclusion was that it was similarly effective on "soft" material such as rubber.

During this study in 1978 **(16),** S-W® completely cut a canvas-backed rubber mud flap under controlled conditions (i.e. 9,000 psi, 12 gpm, 9-inch standoff distance, traversal rate of 1-foot/second). By contrast plain water merely "reshaped" the rubber and wetted the canvas. This result showed rubber materials were amenable to cutting by S-W®.

7. S-W® FOR REMOVING RUBBER COATINGS

S-W® is used in many industries **(1,3,16)** but of especial significance was that in the space shuttle program, S-W® removed residual carbonized epoxy-bound rubber-based propellant **(17)** from the booster motors of the Titan and Challenger rockets. These motors were located at United Technology, Coyote Hills, California and Morton Thiokol, Brigham City, Utah, respectively and nominal conditions of 10,000 psi and 10 gpm were used. This application prompted much of the following work although they are achieved at ultra-high pressures, i.e. >40,000 psi.

8. CUTTING RUBBER MATERIALS WITH S-W®

1. Cutting shoe soles

In 1988 **(1)**, Imlay used S-W® to cut clay rubber composite material in the manufacture of shoe soles at the U.S Shoe Company (Crothersville, Indiana).

Cuts were far more precise with S-W® than with plain water (**1**) and resulted in the absence of striations which is a frequent feature of plain water jet cutting. The production rate was 15% higher and lower pressure was required (50,000 psi versus 55,000 psi with plain water).

The drag reduction of S-W® results in lubricity and as a result the Ingersoll-Rand intensifiers and nozzles experienced less wear. For intensifiers this translates to a 38% reduction in operating and maintenance costs **(18)** and for diamond nozzles a lifetime extension of 2.8-6.0 (U.S. Shoe Company data). These advantages cost 58¢/hour for the S-W®.

2. Additional rubber cutting applications

S-W® is effective in precision cutting a wide range of rubber type products from those that are "very soft", such as Vistanex LM-MH, to those that are "hard" such as 1-inch thick 4-ply 90 Durometer rubber **(17).**

Plain water jets by contrast, as described below, in most cases are slower and yield less well defined cuts. Before describing the specific applications given in (a) through (h) below, general comments on the use of S-W® for cutting rubber products are appropriate.

Because S-W® cuts are smooth and without striations, good surfaces are provided for subsequent adhesion processes.

Another distinct advantage of this technique includes the absence of a heat affected zone (HAZ) and related mechanical distortion as occurs with many mechanical cutting methods. The presence of a HAZ can also bring about chemical degradation or in some instances depolymerization of a substrate. To be able to carry out processes and procedures without producing an HAZ could offer important advantages for a tire manufacturer **(17).**

Also, while it is obvious that ultra-high pressure equipment inevitably has operating and maintenance costs, use of a S-W® jet, as noted above, reduces these costs by 38% **(18)** and extends nozzle lifetime by 2.8-6.0 times.

a) Vistanex LM-MH (a product of Exxon Chemical derived from iso-butylene) is a soft, very viscous (Brookfield Viscosity @ 350°F : 47,500-68,500 cps), permanently tacky, clear yellow to water-white semi-liquid. It is used in a wide range of applications such as asphalt blends, chewing gum base, grease and oil additives, emulsions, and solvent release caulks.

   Plain water cuts only half-way through 15-cm thick Vistanex LM-MH. The partially cut material must then be broken by hand **(19)** which is inconvenient and labor intensive.

   However S-W® completely cuts 15-cm thick Vistanex LM-MH without any striations. This result suggests that S-W® cutting of low durometer rubber materials in general would prove extremely useful.

(b) Foam rubber cutting with S-W [R] has been more completely studied **(20)** than most other rubber substrates. Summers **(20)** used a factorial design experimental series in which, for foam rubber (as well as polystyrene foam and soft Polyurethane foam), five parameters were varied including: traverse speed, pump pressure, the diameter of the waterjet nozzle, the concentration of S-W® and the foam density. Equations were developed interrelating these five parameters.

The important conclusions were that for foam rubber (density 66 Kg/cubic meter) the depth of cut increased with increasing S-W® concentration and the quality of cut was much superior over the entire depth of up to 15-inches.

Both of these factors are important because the studies were targeted at determining the ideal way of cutting foam rubber used in packaging U.S. Navy stores to be shipped around the world: consequently tight tolerances were essential to ensure a close fit.

(c) Silicone rubber (1 1/4-inch thick) is cut with a 0.1% solution of S-W® at 48,000 psi, with identical cut quality, but 60% faster (80-inches/minute) than with plain water (50-inches/ minute). This costs 36¢/hour for S-W® **(21).**

(d) Similarly, increased cutting speeds are obtained for rubber gaskets and 1/2-inch thick silicone rubber as well as 10-inch thick polyurethane foam **(22).**

(e) Nylatron (Nylon with added molybdenum sulfide) has been cut more precisely with S-W® than with plain water using an intensifier at 40,000 psi, a flow of 0.33 gpm, a nozzle diameter of 0.15-mm and a standoff distance of 4-mm **(16).**

(f) Nitrile rubber, natural rubber, styrene-butadiene rubber and neoprene are being cut with intensifiers operating at 48,000 - 49,000 psi using a 0.1% solution of S-W® with a diamond nozzle (diameter 0.007-Inch) at a standoff distance of 1/2 to 3/4-inch **(17).**

The author observed that S-W® reduces the wetting of substrates (**1**), as would be expected from a jet in air, characterized as shown in **Figure 1,** by distinct coherence and an essential absence of spray. The diameters and lengths of the jets and nozzle housing shown in **Figure 1** are 34% less than actual size. Thus the orifice container is 1.125-inches in diameter, the inset diamond nozzle has an internal diameter of 0.01-inch and the photographed length of both jets is actually 6.9-inches.

Because of the absence of spray there is a diminished tendency for a S-W® jet to wet substrates. In the case of multi-levels of substrate, this lack of wetting precludes fluid entering the space between adjacent layers. Consequently there is no fluid between the layers that, on evaporation, would give rise to water spotting.

The following example can be used to appreciate this decrease in wetting by a S-W® jet:

With its incisive cutting ability, S-W® successfully removed 20,000 sq. ft. of adhesive-attached cork from a concrete ceiling. By contrast plain waterjet fluid, with its inevitable associated spray, was completely absorbed by the 8-inch thick layer of cork which was virtually unaffected and remained in place **(1, 12).**

Similarly the extent of coherence of a S-W® jet, as shown in **Figure 1,** may be gained from the following examples:

Tree bark is removed at 10,000 psi and 10 gpm at a standoff distance of 40-feet with a 0.06-inch nozzle **(1**).

A 1-inch hole is drilled in 5/8-inch thick plywood in 5-8 seconds at a standoff distance of 10-feet using 9,000 psi, 12 gpm and a 0.067-inch nozzle. A plain water jet merely wets the plywood.

(g) Rubber (90 Durometer) (4-ply and 1-inch thick) can be cut at 39-inches/minute with a plain waterjet (0.22 gpm at 48,500 psi) and a 0.007-inch nozzle at a standoff distance of 1/16-inch. The cuts produced however have very marked striations **(17).**

When the same conditions are used with a solution of 0.3% S-W® cutting can be conducted at an increased speed of 49-inches/minute with a virtual absence of striations **(17).**

(h) The descriptions given of cutting of gaskets and various other thin sheets of rubber materials is achieved with accuracy and speed. These two factors could be crucial in cutting all rubber products especially where current methods have a tendency to bring about deformation.

3. Detailed Study Of S-W®'s Cost Effectiveness In Cutting

Cost effectiveness in precision cutting at 40,000-45,000 psi has been very accurately determined over a period of 3-years by Lombari **(23)** using typical intensifiers. His results parallel those for precision cutting of the materials listed above.

Lombari found that relative to plain water, S-W®:

(a) Improves the quality of cut: i.e. no subsequent sanding is required saving $15,000 annually in labor costs **(24, 25).**

(b) Increases cutting speed by 30%-200% giving an estimated annual production increase of $420,000 in receivables **(24, 25).**

(c) Reduces intensifier operating and maintenance costs by 38%. (From $11.12/hr in 1993 to $6.86/hr in 1996 is a reduction of $4.26/hr). The annual operating savings are $1,025 **(24, 25).**

Lombari **(25)** reports that for an annual expenditure of $200.00 for S-W®, Decoustics, Toronto, Canada achieves a return on investment (ROI) of >2,000 to 1. This application, which is for cutting fiberglass acoustic panels ranging from 1/8-inch (3.2-millimeters) to 4-inches (101.6-millimeters) thick, gives an unambiguous demonstration of the economic advantages of using S-W® in ultra-high pressure waterjet cutting.

9. SLOTTING AND DRILLING WITH S-W®

(a) Spinning waterjets can cut slots in massive structures

The half-scale model of Stonehenge at the University of Missouri - Rolla **(1)** (named by the National Society of Professional Engineers as one of the "Ten Outstanding Engineering

Achievements in the United States in the 19th Annual Competition in 1984") was made from granite by Professor David A. Summers and his co-workers using waterjets. Conditions used were; pump pressure 15,000 psi, water flow 10 gallons/minute, dual nozzles (0.032- inch ID) spaced 1.5-inches apart with an included angle of 30°, rotating at 100 rpm at a standoff distance of 1-2 inches and a traversal rate of 10 feet/minute.

S-W® was used for cutting-along the granite grain.

(b) Spinning waterjets can drill precise holes.

Following the California Loma Prieta earthquake on October 17, 1989, the Oakland-San Francisco Bridge partially collapsed as did many other concrete structures. It was realized that extensive retrofitting was needed to increase the stability of bridges and overpasses to withstand future seismic activity. One possible way of stabilizing structures involved installing additional steel reinforcement bars. Such installation required precision drilling of holes in the various concrete structures. In a model study using S-W®, Raether **(13)** was able to precisely drill 3-inch diameter holes through a concrete block (3-ft x 3-ft x 3-ft) with a compressive strength of 5,000-6,000 psi,. at angles normal to the block and at oblique angles, at a rate of 10 inches/minute. Conditions used were: S-W® at 3,000 ppm, pressure 35,000 psi, flow rate 3 gallons/minute, "zero" standoff distance using two proprietary spinning nozzles. Very significantly the cost of drilling with S-W® was $6/foot compared to the more conventional diamond bit drilling which costs between $50/foot and $100/foot **(13).**

10. S-W®/ABRASIVE CUTTING (ABRASIVE SUSPENSION JET - ASJ)

In 1983, at the Second American Water Jet Conference (Rolla, Missouri) the topic possibly discussed more than most others was the use of abrasives in waterjetting.

When noting that this combination had first been used in the 1960's, Griffiths **(26)** explained:
"........ because of the pressure limitation of existing pumps and ancillaries, particularly hose (maximum pressure usually 5 - 8,000 psi), a method of enhancing the cleaning power of the water jet was sought, and the answer appeared to be the addition of abrasives into the water jet stream".

It was obvious that S-W® would be used with abrasives and this combination was studied in 1984 by Yie and Howells **(1)**.

In 1989 Hollinger et al. **(27)** described "Precision Cutting with a Low Pressure, Coherent Abrasive Suspension Jet" using S-W® at 1.5% concentration in which garnet abrasive (diameter: 75-106 micrometer) was suspended. Hollinger gave examples of the abrasive suspension jet (ASJ) for cutting aluminum, mild steel, plate glass, yellow brass and lead at moderate pressures (5,000-7,500 psi). Using this technique at 7,500 psi furnished superior cuts (with smaller kerf widths i.e. < 0.79 mm versus 1.6 mm), and consumed 86% less power and 62% less abrasive than an abrasive waterjet (AWJ) operating at 30,000 psi.

Hollinger gave an example of cutting composite material in which parallel microcuts (width 0.08-0.10 mm) were made only 0.3-mm apart in gold-coated quartz wafers (thickness 0.15-mm).

It was pointed out that "closer cuts can be made depending upon the precision of the positioning mechanism".

Hollinger's paper, followed by another paper on the same topic **(28) -** which received the best paper award of the 8th American Water Jet Technology Conference (Houston, Texas, 1991) - ushered in a new era of precision cutting. In his 1991 publication Hollinger **(28)** pointed out that for success of the ASJ technique the viscoelastic component of S-W® solutions was a controlling parameter for jet penetration and cut width.

Enormous potential exists for application of the high power density of the ASJ. For example, Hashish **(29)** reports that the ASJ achieves fast thin-kerf cutting of metals (steel, aluminum, lead, titanium, stainless steel, tungsten and Inconel), cuts hard materials such as carbides (silicon carbide, alumina-reinforced silicon carbide) and a wide range of other commercially available carbides e.g. ROCTEC 100.

Hashish's studies **(29)** were very detailed and included examination of the following abrasive suspension parameters: S-W® concentration, abrasive type, abrasive size, abrasive concentration, nozzle length, nozzle diameter, pressure, standoff distance, traverse rate and angle of cutting.

Hashish concluded **(29)** that S-W® can yield a viable suspension for automated suspension preparation based on stability and ease of preparation, can cut a wide variety of metals from lead (Mohs' hardness of 1.5) to tungsten, as well as carbides (Mohs' value of >9.0) and ceramics.

Liu **(30)** reports that the ASJ gives "Up to fivefold improvements in cutting rates over AWJ's observed with this approach under identical hydraulic and abrasive conditions. Current and future development efforts for the ASJ system are addressing specific hardware components such as check valves, pressure vessels, and nozzles". Because ROCTEC 100 is the most resistant to cutting it suggests it may be the best candidate for ASJ carbide nozzle material **(29).**

11. S-W®/VENTURI-INDUCTED ABRASIVES (AWJ)

The ASJ technique has lived up to the expectations expressed by many participants at the 6th American Water Jet Conference held in Houston in 1991 - namely that it would be the most significant advance in waterjetting of the 1990's.

However the 1990's are about to end and so in the interim, while awaiting ASJ commercial development, other methods of combining S-W® and abrasives are being used.

Venturi-inducted/aspirated/educted/suctioned abrasive waterjetting (AWJ) is the current "standard" in the industry. Three separate phases exist in the AWJ process - one solid, one liquid and one gaseous. As pointed out previously **(22)** this "standard" method suffers from having to bring about effective momentum exchange between a liquid and an abrasive in the presence of a gas phase.

However distinct improvements result **(22)** when S-W® is used instead of plain water in the standard AWJ method.

(a) For example S-W®, used with 100 grit copper slag as an abrasive, cuts laminated glass (13/16-inch thick), aluminum (1/4-inch thick) and stainless steel (up to 1-inch in thickness) 20% faster than with copper slag/plain water. This higher production costs 90¢/hour for the S-W® **(22).**

Weber **(31)** has determined that S-W® used in the "standard" Venturi abrasive technique provides a better quality of cut and a narrower kerf. It also substantially reduces abrasive consumption when cutting either 304 L stainless steel or aluminum.

(b) 304 L stainless steel (10-millimeters thickness) can be cut at 143-mm/per minute with 80 mesh (Australian) Barton abrasive. (Pressure: 43,000 psi, fluid flow rate: 1.85 L/minute, nozzle diameter: 0.25-mm, standoff: 4-mm). 16 Kg/hour of abrasive was used with 0.3% S-W® but plain water required 30 Kg/hour of abrasive. This 47% decrease in abrasive consumption was accompanied by a smaller kerf and better cut quality **(31).**

(c) An aluminum (thickness 25-mm) is cut at 67.5-mm/minute with 80 mesh Quality GANEX. (Pressure: 50,400 psi, fluid flow rate: 1.80 L/minute, sapphire nozzle: 0.25-mm, focusing tube diameter: 1.05-mm, standoff distance: 3 mm). 200/250 grams/minute of abrasive was used with 0.3% S-W® but plain water required 400/500 grams per minute. This 50% decrease in abrasive consumption was accompanied by a better cut quality **(31).**

(d) More recently Weber has reported that Baccarat crystal is drilled more precisely with 120 mesh abrasive and S-W® than with abrasive and plain water at 43,000 psi and at a standoff distance of 5-mm using a nozzle of 0.8-mm diameter **(16).**

12. FUTURE METHOD FOR USING S-W® WITH ABRASIVES

As noted Howells **(22)** and others have pointed out the less than satisfactory situation of having to bring about effective momentum exchange between a solid and a liquid in the presence of a gaseous phase. It was suggested **(22)** that, if the abrasive were to be introduced into the "standard" Venturi system as a suspension in S-W®, it might prove possible to increase the efficiency of the momentum exchange. Additionally this approach could yield results more closely matching the ASJ results **(22).**

This modified Venturi approach (termed the Lombari technique **(16))** for which a patent is now pending, is under development.

13. SUBMERGED APPLICATIONS-OF S-W®

As noted above, the Russian publication **(4)** presented data from experiments conducted under submerged conditions, employing centrifugal pumping and recirculation of the polymer solution.

The inappropriateness of centrifugal pumping and recirculation of S-W® have both been discussed previously **(1)**. These procedures bring about elongational shearing of the macromolecules, which results in a reduction in molecular weight and a parallel reduction in effectiveness.

The flow characteristics of submerged polymer solutions (containing dye) were first described by Gadd **(32).** In 1977, prompted in part by Gadd's results, it was determined in conjunction with Chevron USA at Taft, California, that S-W® under submerged conditions increased the effective standoff distance of waterjetting by 15 to 30 times over that achieved by plain water **(1,3).**

This led to further studies by Zublin **(1,33)** and Cobb and Zublin **(34).** They confirmed the increase in effective standoff distance using S-W® under submerged conditions and showed the marked improvements obtained in cleaning oil-well liners.

They also presented a graph of power (percentage of power at the target) versus standoff distance comparing plain water to S-W®. This graph was eventually reproduced (without error) in Chemical Processing **(11)** and vividly shows the advantage of using S-W® under submerged conditions.

14. APPLICATIONS OF THE ASJ UNDER SUBMERGED CONDITIONS

The combination of the Russian paper **(4)**, Gadd's work **(32),** Zublin and Cobb's findings
Zublin and Cobb's findings **(33, 34),** and Hollinger's ASJ technique provides a critical background for the later work of Alberts and Hashish **(35).**

These workers, using hyperbaric chambers to simulate deep ocean conditions, cut stainless steel with an ASJ S-W® jet at pressures equivalent to depths of 6,000 meters **(35).**

This depth is very significant because, apart from the deep trenches (e.g. the Mariana - maximum depth of 11,033 meters at Challenge Deep, the Peru Chile trench - maximum depth of 8,064 meters), the dominant portions of the worlds oceans have depths of 6,000 meters or less. Consequently a method (for cutting rock and metal, and for coring) by deployment from remotely operated vehicles is now available for worldwide oceanic applications.

15. CRITICAL IMPORTANCE OF S-W® INJECTION SYSTEMS

S-W®, as sold, is in the form of a water-in-oil emulsion. The internal water phase contains the polyacrylamide. In order to use the product, the emulsion has to be broken or - more exactly - inverted to an oil-in-water emulsion. This absolutely necessitates use of specific types of injection systems which, placed **after the filter,** accurately meter the requisite amount of S-W® , into the water stream.

(Filters also cause elongational shearing of macromolecules leading to a reduction in molecular weight and a parallel reduction in effectiveness **(1)**.

A brief description of the meaning of "elongational shearing" might be useful. In solution the macromolecular molecules of S-W® and their associated aggregates of water are coiled although they might adopt some measure of linearity under conditions of flow. During centrifugal pumping or in passage through filters the hydrogen-bonded aggregates of water would be "stripped away" exposing the carbon-carbon backbone. The backbone whilst being elongated would be readily accessible and shearing by carbon-carbon bond scission will occur **(1)**.

The diluted S-W® then flows through a static mixer - in which complete and uniform emulsion inversion is ensured - to the main stream of the waterjetting fluid. Prior to use, S-W® requires 5 to 6 minutes to become fully hydrated. The active ingredients in S-W® are, as mentioned previously, macromolecular with a molecular weight ranging from 16 to 18 million, so the bonding of water molecules (or hydration) takes a finite time. This is because each monomeric unit of polyacrylic acids and of polyacrylamides bonds 13 to 14 molecules of water **(6).** Obviously this aggregation of polymer and water can not take place instantaneously because it must proceed by formation of sequential layers of the 13 to 14 water molecules.

The hydration can be achieved in either a holding tank or a length of low pressure tubing.

16. SAFETY AND ENVIRONMENTAL CONSIDERATIONS

The usual safety precautions employed during hydroblasting (often called waterblasting and in countries, other than the U.S.A., hydrablasting) **(36)** are appropriate for ultra-high pressure precision cutting with S-W®.

Because of its incisive cutting ability, S-W® must be handled with very great care both from the standpoint of the equipment being used and operator exposure.

The OSHA Material Safety Data Sheet for S-W® describes general precautions but it should be noted that upon appropriate dilution (i.e. 0.1-0.3%) the properties, apart from flow characteristics, closely approach those of water.

Neither polyacrylamide nor polyacrylic acid, or **combinations,** are listed in the EPA Consent Decree **(37),** and neither are they in the list of chemicals described as being carcinogenic **(38).**

(a) S-W® is biodegradeable and does not foul oxidation ponds **(3).**

(b) The chemical oxygen demand of S-W® is 706 g/L (at a use concentration of 0.1% it is 0.7 g/L) and the biological oxygen demand is 87 g/L (at 0.1% it is 0.09 g/L).

(c) The LC 50/96 hr is 53 ppm (Rainbow Trout) and 84 ppm (Blue Gill Sunfish). The acute oral toxicity (rat) is >10 ml/Kg and the dermal toxicity LC 50 (rabbit) is also >10 ml/Kg.

(d) Code of Federal Register Conformations. S-W® conforms to the Federal Food, Drug and Cosmetic Act as amended in 1958 and 1960, specifically Chapter 21 CFR, Section 176.110 as a component of paper and paperboard in contact with food and Section 175.105 as a component of adhesives in contact with food. Other S-W® components conform to CFR 21, Sections 178.3400 and 178.3650 **(39).**

(e) Because S-W® is a "non-regulated material, liquid, cleaning compound, NMFC 48580 class 55", it is shipped by truck, ship, and air - including UPS.

17. ACKNOWLEDGEMENTS

The author appreciates and gratefully acknowledges the contributions to this paper provided by Messrs. Vincent L. and Adam H. Imlay of Water Jet, Inc., Seymour, Indiana, Mr. Renato Lombari, Soheil Mosun Ltd., Toronto, Canada, Mr. Jim Price, Biltrite Corporation, Ripley, Mississippi, Dr. David A. Summers, Curator's Professor of Mining Engineering and Director of the High Pressure Waterjet Laboratory at the University of Missouri-Rolla, Missouri and M. Daniel Weber, Weber Lubrifiants Rixheim, Cedex France.

18. REFERENCES

1. W. G. Howells, "Polymerblasting with SUPER-WATER® from 1974-1989: a Review" International Journal of Water Jet Technology, Volume 1, Number 1, (March 1990), pp. 1-16.

2. D. Alexander and **J.** T. Regan, "Polymer blasting eliminates hard deposits in refinery heat exchangers", Chemical Processing, May 1984.

3. W. G. Howells, "Polymerblasting - a Chemist's Point of view", Proceedings of the Second US Water Jet Conference, (Rolla, Missouri, USA: May 24-26, 1983), pp. 443-447.

4. A. M. Kudin, G. I. Barenblatt, V. N. Kalashnikov, S. A. Vlasov and V. S. Belokon, Nature, Vol. 245, 95, 1973.

5. Private communication between Berkeley Chemical Research, Inc. and Professor M. C. Williams, University of California at Berkeley, California, June 1978.

6. S. Majumdar, S. H. Holay and R. P. Singh, European Pblymer journal, 16, p. 1201.

7. A. White and J.A.G. Hemmings, "Drag Reduction by Additives" Review and Bibliography, BHRA Fluid Engineering, Cranfield, Bedfordshire, U.K. 1976.

8. Brochures on "SUPER-WATER® concentrated industrial water blasting additive", published by Berkeley Chemical Research, Inc., P. 0. Box 9264, Berkeley, California 94709. Also references 1, 2, 3 and website:http://www.berkchem.qpg.com

9. Chemical Week, May 24, 1 969.

10. B. Maijgren, Paper presented at EUROMECH 82, Royal Institute of Technology, Sweden, August 27-30, 1974.

11. A. E. Hodel, "New ideas, tried-and-true methods boost cleaning efficiency", Chemical Processing, March 1993.

12. R. Goldsmith, Letters to the Editor, Jet News*, June 1990.

13. W. G. Howells, "Enhancing waterjetting by use of water soluble additives", in Water Jet Applications in Construction Engineering, Editor A. W. Momber, published by A. A. Balkema, Rotterdam, Netherlands, 1998, (ISBN 90 5410 698 0).

14. J. Malaugh, S. Ryder and D. St. Louis, "Bruce NGS-A Support Plate Inspection and Waterlancing", Proceedings of the 10th International Symposium on Jet Cutting Technology (Amsterdam, Holland: August 31 - September 2, 1990), pp. 449-471.

15. W. G. Howells, "Increasing Waterjet Efficiency by Use of Water Soluble Additives", published in "Cleaner", November 1998, pp. 70-71, by Cole Publishing Inc., 1720 Maple Lake Dam Road, P.O. Box 220, Three Lakes, Wisconsin 54561.

16. W. G. Howells, Vincent L. Imlay, Renato Lombari and Daniel Weber, "Ultra-high pressure precision jet cutting using SUPER-WATER®", Proceedings of the International Composites EXPO 99, Cincinnati, Ohio, May 10, 1999.

17. W. G. Howells, " SUPER-WATER® provides precision cutting of rubber", Rubber & Plastics News, May 31, 1999.

18. R. Lombari, letter to the Editor, ..."the longevity of our consumable jet components due to the lubricity of SUPER-WATER ®", Jet News*, November 1996, pp. 2 and 11.

19. D. Weber, letter to the.Editor, Jet News*, December 1997, pp. 7 and 8.

20. S. Yazici and D. A. Summers, "The Use of High Pressure Waterjets in Cutting Foam", "Proceedings of the 4th American Conference, (Berkeley, California, August 26-28, 1987), pp. 11-18.

21. W. G. Howells. Unpublished data obtained during demonstration at the 7th American Water Jet Conference (Seattle, Washington, August 28-31, 1993).

22. W. G. Howells, "Additive Improves Abrasive Jet Cutting" Jet News*, December 1995, pp. 5 and 10.

23. R. Lombari, "Ultra-High Pressure Non-Abrasive Polymer Jetting: a Production Implementation," Proceedings of the 9th American Waterjet Conference, (Dearborn, Michigan, August 23-26, 1997), Paper 17, pp. 251-266.

24. R. Lombari, "Cutting Fiberglass Accoustical Panels", Jet News*, December 1997, p. 7.

25. R. Lombari, letter to the Editor, . . .”Dear Jet News”, Jet News*, December 1997, pp. 8 and 10.

26. N. J. Griffiths, Proceedings of the Second US Water Jet Conference, (Rolla, Missouri, USA: May 24-26, 1983), pp. 423-432.

27. R. H. Hollinger, W. D. Perry and R. K. Swanson, Proceedings of the Fifth American Water Jet Conference, (Toronto, Canada, August 1989), pp. 245-252.

28. R. H. Hollinger and R. J. Mannheimer, Proceedings of the Sixth American Water Jet Conference, (Houston, Texas, August, 1991), pp. 515-528.

29. M. Hashish, Proceedings of the Ninth American Water Jet Conference, (Detroit, Michigan, August, 1997), pp. 267- 280.

30. H-T. Liu, "Near-net shaping of optical surfaces with UHP abrasive suspension jets", Proceedings of the 14th International Conference on Jetting Technology, Brugge, Belgium, 21-23 September 1998.

31. D. Weber, letter to the Editor, Jet News*, February 1997, p. 12.

32. G. E. Gadd, Nature, 1966, Vol. 212 (No. 5065), 874-877, November 1966.

33. C. W. Zublin, Proceedings of the Second US Water Jet Conference, (Rolla, Missouri, USA: May 24-26, 1983), pp. 159-166.

34. C.C. Cobb and C.W. Zublin, Petroleum Engineers International, pp. 56-66, October 1985.

35. A. Alberts and M. Hashish, "Observations of Submerged Abrasive-Suspension Jet Cutting for Deep Ocean Applications" Proceedings of the 8th American Water Jet Conference, Houston, Texas, August 1995, pp. 735-749.

36. See, for example, "Recommended Practices for the Use of Manually operated High-Pressure Water jet Equipment" issued by the Water Jet Technology Association, St. Louis, Missouri.

37. Q. B. Stork et al., Journal of Chromatographic Science, Vol. 18, November 1980.

38. Second Annual,Report on Carcinogens, December 1981, U.S. Department of Health & Human Services, Public Health Services (National Toxicology Program).

39. A complete description of the relevant Chapter 21 CFR conformations is available from Berkeley Chemical Research, Inc.

* Jet News is a bimonthly publication of the Water Jet Technology Association, St. Louis, Missouri, U.S.A.

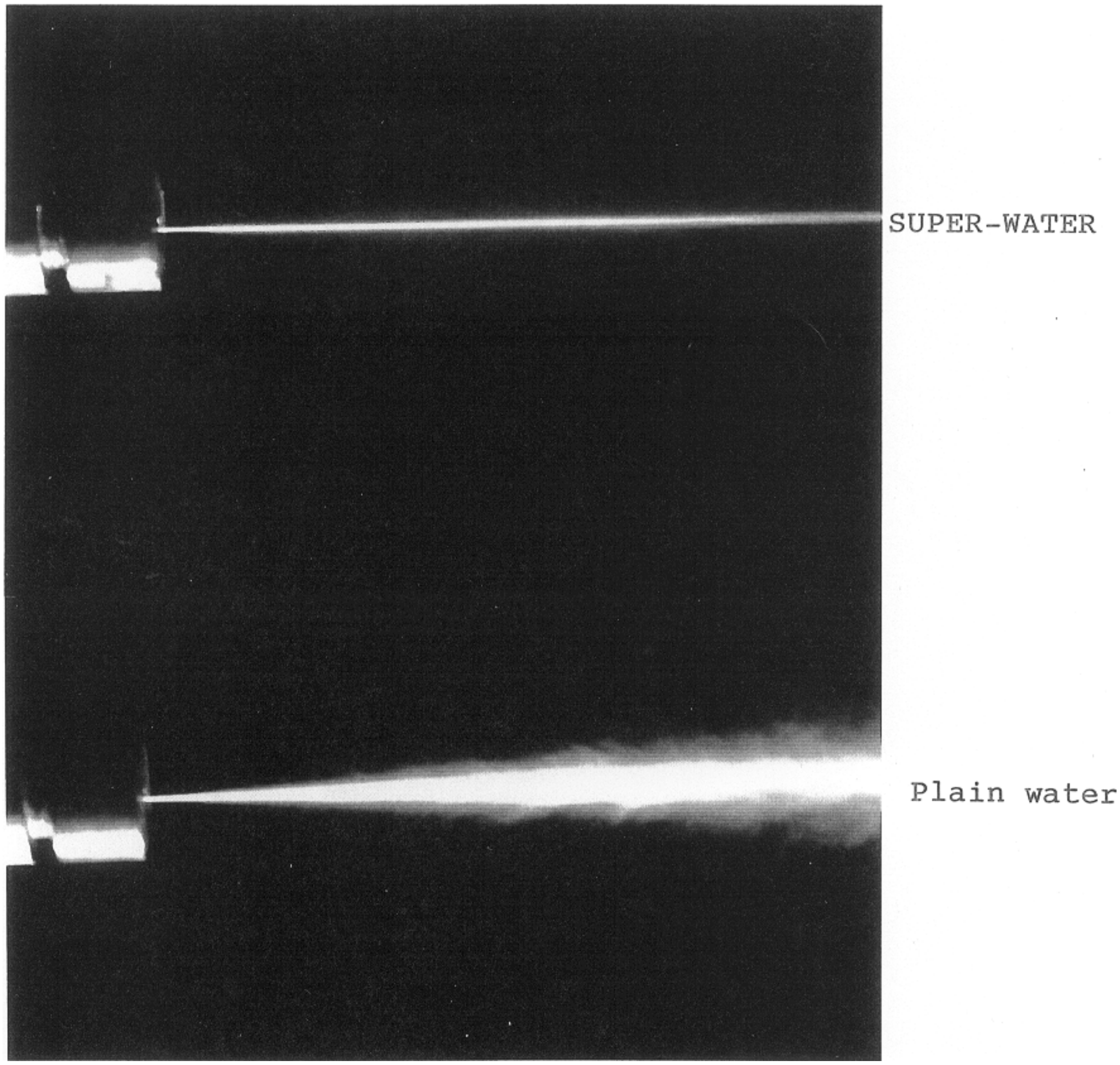

Comparison of Super-Water and Plain Waterjets (28)

Figure 1

10th American Waterjet Conference
August 14-17, 1999: Houston, Texas

Paper **26**

PROFILING WITH 400 MPA FINE-BEAM ABRASIVE WATER JET

St. Brandt, H. Louis
Institute of Material Science,
Hannover, Germany

ABSTRACT

Suspension jets are established in decommissioning, on- and offshore technology but not in manufacturing industry. The development of a 400 MPa suspension jet system to generate Fine-Beam Abrasive Water Jets for manufacturing industry is part of a BriteEuram-Project funded by the European Commission. Goal of the project is to decrease the kerf width to 0.3 mm or smaller by exploitation of the potential of the suspension jet technology.

Organized and Sponsored by the WaterJet Technology Association

1. INTRODUCTION

The development of Abrasive Water Suspensions Jets started in the early 60's with direct pumping systems for off-shore application with a system pressure of 69 MPa as mentioned by Lancaster, J. C. 1994. Since this time the development of AWSJs preceded. Today AWSJs are inserted in cleaning, decommissioning, demilitarisation etc. with pressures up to 200 MPa as state of the art.

The industrial insert of AWSJ as a manufacturing tool is not very high. As commercial applications are mentioned the cutting of armored metal sheets and ceramics. Research investigations have been started to use the AWSJ as a tool for polishing diamonds (Hashish et al. 1993) and near-net shaping of optical glasses (Liu et al. 1998).

The most important goal of a AWSJ-system as a manufacturing tool should be the reduction of the generated width of kerf smaller than 0.3 mm. The state of the art of todays AWSJ-systems and the development of a 400 MPa-Fine Beam Abrasive Water Jet System will be described in the next chapters.

2. STATE OF THE ART

Abrasive Water Suspension Jets are generated in three principles, see figure 1. First principle is to pump the premixed suspension directly through a nozzle, this method is called "direct pumping". This principle has only been realised for assistance of exploration in oil and gas industry. From today's state of art, such a system can be build up with pressures up to 100 MPa by using membrane pumps and "soft" abrasives.

The second principle is called "indirect pumping". Main part of this system is an abrasive storage vessel with an isolator inside. The high pressure water from the pump is used to move the isolator downwards, so that the premixed suspension is pumped towards the suspension nozzle. Due to the particle sedimentation the using of polymers is required. In addition the change of abrasive concentration during the cutting process is not possible with this system.

The third principle, which is called "bypass-principle", is one of today's commercial systems and has also been used for the presented cutting experiments. It follows basically the DIAJET-principle developed by BHR Group, U.K. in 1984, Bloomfield et al. 1984. The water stream, delivered by the pump, is divided into a main water stream and the so called bypass stream. The bypass stream is used to feed the abrasive particles out of the vessel into the plain water stream in a special mixing unit. The resulting suspension is pumped through a flexible hose towards the nozzle. A restriction valve is used to control the water flow rate in the bypass line and hereby to regulate the abrasive loading ratio of the jet.

The first Bypass-AWSJ system has been operated at a maximum pressure of 15 MPa. In 1986 a 34.5 MPa system was developed. In 1988 the first two vessel system also with 34.5 MPa was designed to allow a continuous cutting operation. In 1990 a two vessel 69 MPa system was presented. Since than the development work focused on the reliability of the system and the adaptation to different applications (Brandt, C. et al. 1996). Today pressures up to 200 MPa are state of the art and have been successfully applied for dismantling nuclear power plants (Brandt, C. et al. 1998).

Investigations have been started on system pressures higher than 200 MP. Hashish (1991) presented the capacity of suspension jets generated by an indirect pumping system, with a pressure of 345 MPa.

The development of this technology for manufacturing application will be described in the next chapter.

3. REQUIREMENTS FOR 400 MPA-SYSTEM

Main goals of development of a Fine-Beam Abrasive Water Jet System are:

- Reduction of width of kerf < 0.3 mm
- Increase of traverse speed
- Control of mass flow rate

To reduce the width of kerf below 0.3 mm, the outlet diameter of the nozzle has to be decreased below 0.25 mm. By using constant pressure the reduction of the diameter leads to a reduction of flow rate and to a reduction of hydraulic power. To allow the increase of traverse speed the pressure has to be raised up.

The small nozzle diameter requires small abrasive particles below 100 µm. Flow behaviour and settling velocity of particles changes by decreasing the diameter. In a low pressure perspex test unit the flow behaviour of small abrasive particles has been investigated. To investigate the discharge behaviour of small abrasive particles a flat storage vessel model has been used. It could be shown that in the centre of the mass a dynamic channel is built by abrasive particles in motion. The diameter of the channel increases in direction of the suspension surface. On top of the suspension surface a cone with an angle of 60° is formed during the discharge process. This cone consists until the suspension surface reaches the bottom of the storage vessel. As a result of these investigations the bottom of the storage vessel was designed with a cone of 60° to support the flow out of suspension. At the perspex unit the ratio between bypass flow rate and mass flow rate has been investigated, too. By weighing the discharged suspension every 10 seconds during constant bypass flow rate it could be shown that there is a linear ratio, figure 2.

When stopping the cutting process by closing the bypass valve, the depressurisation and by this the transportation of highly concentrated suspension out of the storage vessel as well as by gravitation has to be avoided. The typical design of AWSJ-bypass-systems shows a valve under the storage vessel to avoid settling of particles after finishing the cutting process, see figure 3, left. Until yet, suspension-valves to switch the suspension during cutting process are not developed for pressures higher than 70 MPa. At the low pressure test rig a new design was tested by installing the mixture unit above of the top of the storage vessel. This design allows to reduce the number of valves and it allows to switch off the bypass flow rate and with this the mass flow rate, see figure 3, right.

4. DESIGN

To run a 400 MPa-AWSJ-system, a high-pressure intensifier was adapted. At the Waterjet Laboratory Hannover (WLH) a Böhler Hochdrucktechnik-intensifier is installed. This intensifier delivers a pressure up to 400 MPa and a maximum flow rate of 4 l/min. This leads to a limitation of maximum nozzle diameter to 0.3 mm. The aim of a AWSJ-system as a manufacturing tool should be the decreasing of the generated kerf width to become competitive against other cutting technologies like laser.

Former research work at the Institute of Material Science on nozzle design (Brandt, C. et al., 1998) has lead to a special nozzle shape for 70 MPa-systems. An optimal nozzle, resulting from the experiences, with a long inlet curve and a long cylindrical part to get a coherent jet, was designed for the 400 MPa-system with a diameter of 0.25 mm, figure 4. The nozzle is fixed by a special nozzle holder.

Figure 5 - 6 shows the 400 MPa-system in the Waterjet Laboratory Hannover. Figure 5 shows the storage vessel and the control valves in the main stream and in the bypass stream. The flow rates are measured by turbine flow meters. The 2.5 l-storage vessel from Böhler Hochdrucktechnik will be filled, under environmental pressure, through two pipes, fixed at the top of the vessel. A membrane pump delivers the high concentrated suspension into the vessel and presses the same volume of water out of the vessel. The bypass flow is lead through a third tube into the vessel.

After the mixing process of the main flow stream and bypass flow stream carrying a high concentrated suspension the mixture of this suspension flows through a flexible hose to the nozzle, which is connected to a XY-table. The construction of the XY-table allows to cut on air and under water. The advantages of cutting under water are the reduction of noise and reducing the forces acting at the work pieces and the work piece holder.

The next chapter will describe the first trials to generate a fine-beam.

5. TRIALS

The first cut was carried out at 150 MPa with a 0.25 mm-nozzle. The result has shown the big potential of such a system. The test lead to a width of kerf of 0.3 mm and a surface roughness (R_a) of 1.8 µm, figure 7.

Following cutting tests have shown periodical striation marks on the cutting edge. By variation of the traverse speed it could be shown that there is a relationship between the frequency of the intensifier and the generated marks on the cutting edge. Further investigations by varying the mass flow rate have shown the possibility to decrease the influence of the pressure pulsation by increasing the mass flow rate. Another way to eliminate the marks could be the installation of an accumulator. Figure 8 shows two work pieces which were cut with a pressure of 300 MPa and with a mass flow rate of 0.5 g/s (left) respectively with 1.6 g/s (right). The effect on the cutting edge is visible.

Figure 9 shows a cut in aluminium (thickness 20 mm) with a pressure of 400 MPa and a traverse speed of 200 mm/min.

6. CONCLUSION

A 400 MPa-Abrasive Water Suspension Jet System has been built up successfully.

First tests have shown the high potential of high-pressure Abrasive Water Suspension Jets.

Future activities will be focused on cutting and kerf tests to show the potential of a 400-MPa-suspension jet system regarding the traverse speed, the material thickness, the very small width of kerf and the high quality of the surface.

The process-safety has to be investigated regarding a control of the cut quality by monitoring volume flow rate, mass flow rate etc..

The possibility to profile almost all materials with Fine-Beam Abrasive Water Jets will open new possibilities for manufacturing applications.

7. ACKNOWLEDGEMENT

Main parts of this paper are based on a research program with the project number BE96-3622 sponsored by the European Union. The authors are member of the Arbeitskreis Wasserstrahltechnologie (AWT), Germany.

8. REFERENCES

Lancester, J. C.: “Underwater jetting: exploring new frontiers.” *Cleaner Times 6 (1994)*, No. 3, pp. 18/20.

Hashish, M., Bothell, D., “Diamond Polishing with Abrasive Suspension Jets,” *Proceedings of the 7th American Water Jet Conference*, Volume 2 pp 793/800, Water Jet Technology Association, St. Louis, Missouri, 1993.

Liu, H-T: “Near-net shaping of optical surfaces with UHP abrasive suspension jets,” *14th International Conference on Jetting Technology*, pp. 285-294, Bury St Edmunds, London: Professional Engineering Publishing Limited, 1998.

Bloomfield, E. J. and M. J. Yeomans "DIAJET - a review of progress", *Proc. 1st Asian Conference on Recent Advances in Jetting Technology*, CI-Premier PTE. Ltd, Singapore, (1991) S. 21-30.

Brandt, C., Louis, H., Tebbing, G.: Abrasive water suspension jets – State of art and future developments. Geomechanics 96, Balkema, Rotterdam.

Brandt, C., Brandt, St., Louis, H., Milchers, W., Rad v. Chr., "Application of Abrasive Water Suspension Jets for Nuclear Dismantling", *14th International Conference on Jetting Technology* (1998). London: Professional Engineering Publishing Limited, pp. 119/129.

Hashish, M., "Cutting with high-pressure abrasive suspension jets", *Proceedings of the 6th American Water Jet Conference* pp. 439/455, Water Jet Technology Association, St. Louis, Missouri, 1991.

Brandt, C., Louis, H., Ohlsen, J., Tebbing, G., "Influence of nozzle geometry on Abrasive Water suspension Jets," *5th Pacific Rim Conference*, pp. 330/344, 1998.

9. GRAPHICS

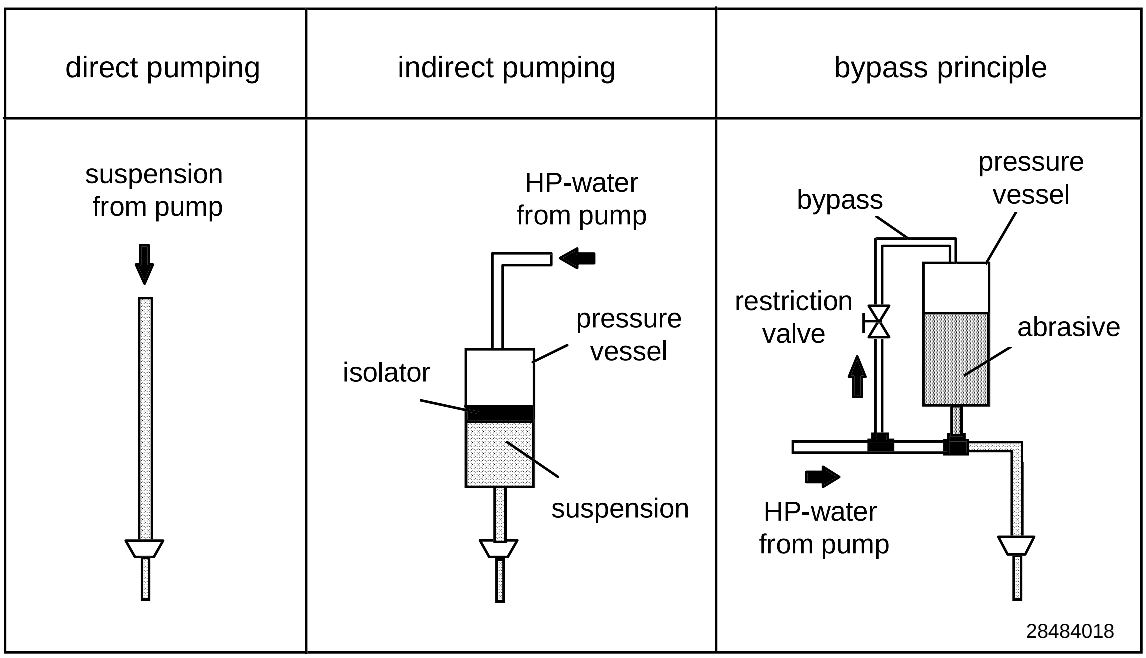

Figure 1. Principles of AWSJ generating

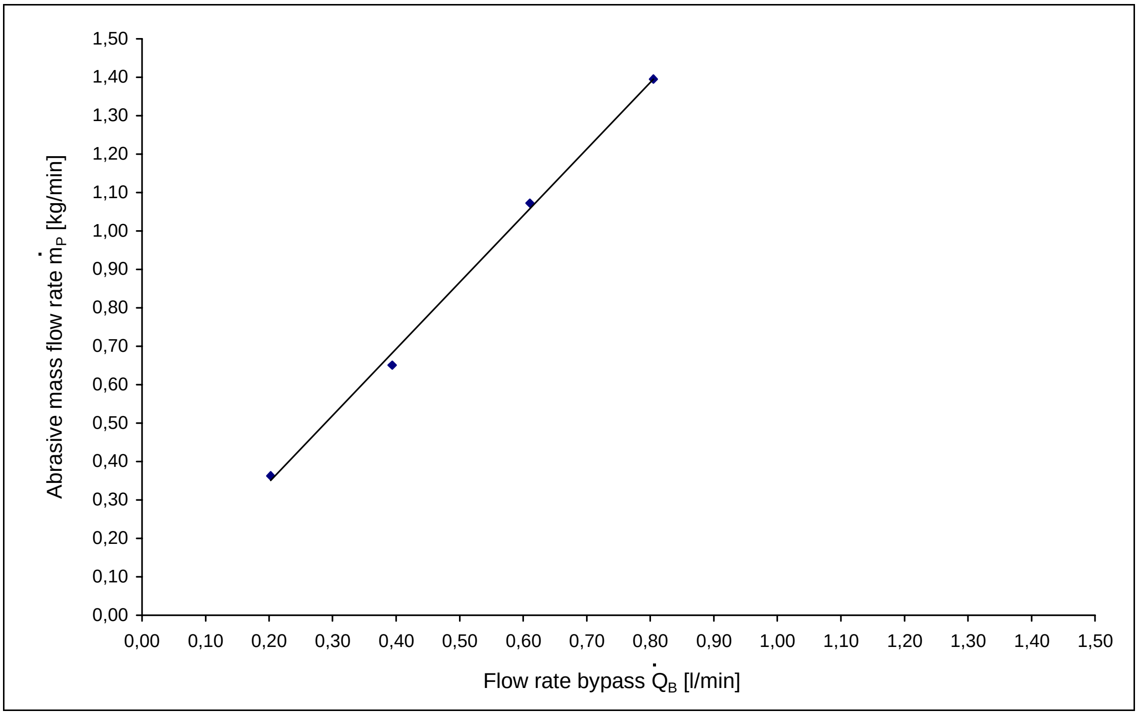

Figure 2. Bypass volume flow rate – Abrasive mass flow rate

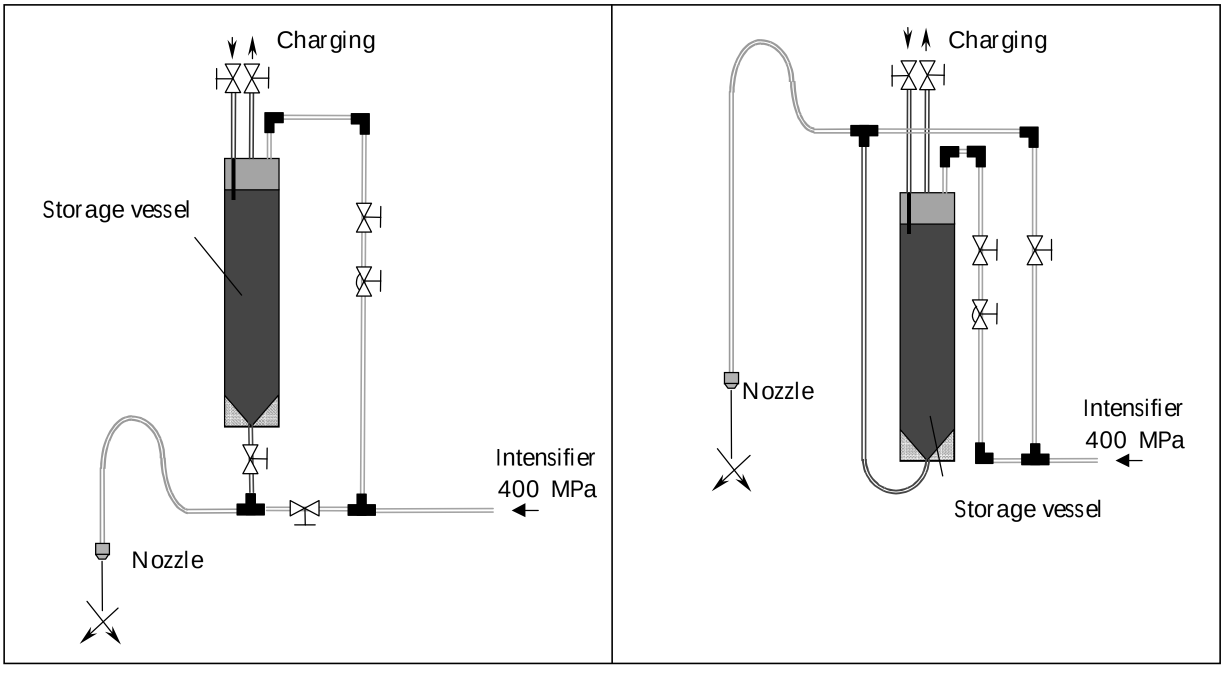

Figure 3. Different methods to build up a bypass system

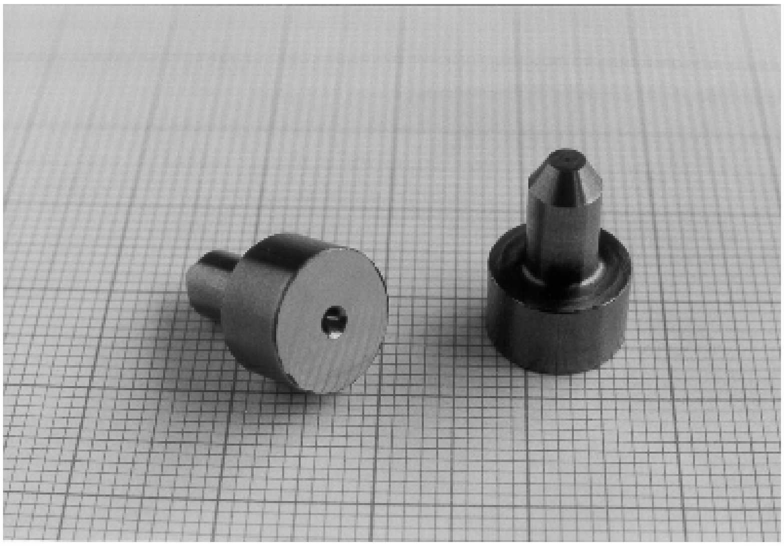

Figure 4. Suspension nozzles

Figure 5. 400 MPa-System

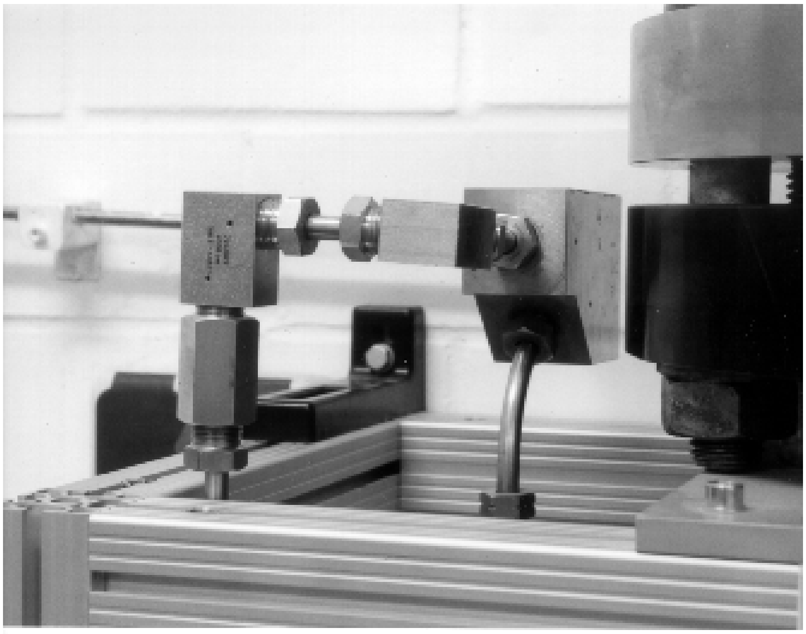

Figure 6. Mixture unit

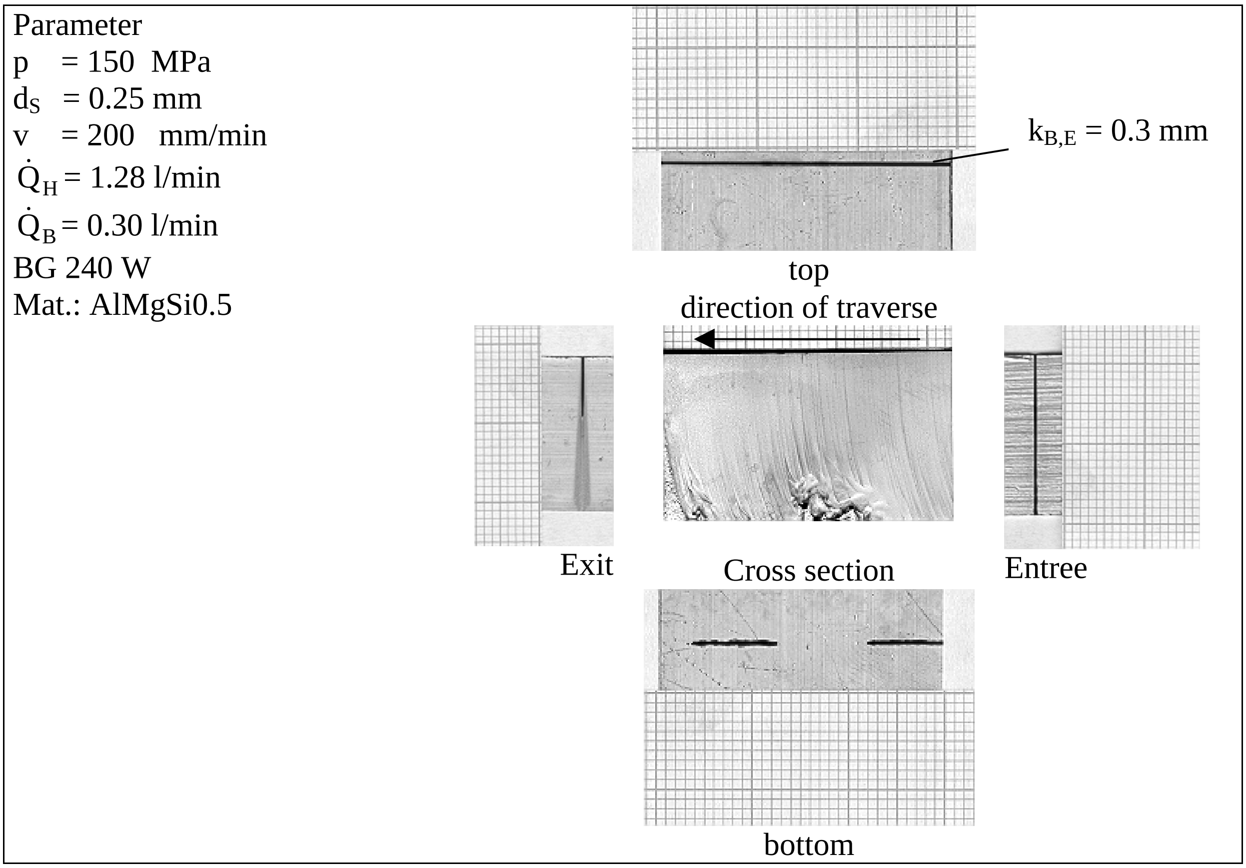

Figure 7. First cut

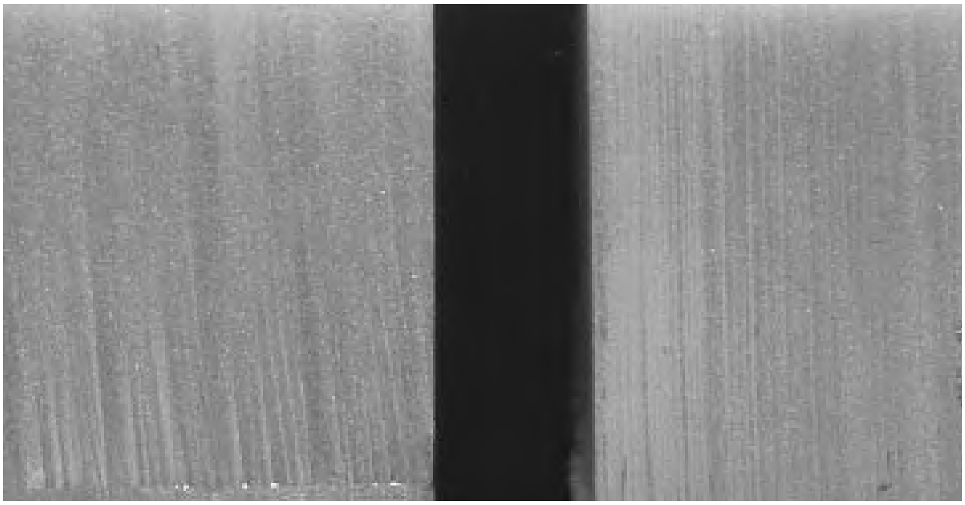

Figure 8. Striation marks caused by the intensifier in relation to the mass flow rate

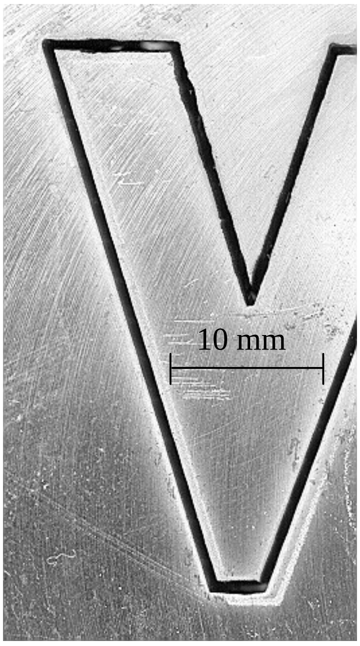

Figure 9. Profiling with 400 MPa

10th American Waterjet Conference
August 14-17, 1999: Houston, Texas

Paper 27

MICRO ABRASIVE WATERJETS (MAWs)

D. Miller
Miller Innovations
Harrold, Bedford, UK.

ABSTRACT

As a result of the world wide drive to miniaturize products, the market for micro machining is predicted to grow to over 10 billion US dollars per year by 2010 from about 1 billion dollars in 1995. The micro machining market needs new machining techniques that reduce manufacturing costs, enable advanced materials to be exploited and allow designers to take advantage of better design and manufacturing methods. Micro abrasive waterjets (MAWs) will be one of these new micro-machining techniques.

Operating with jet diameters less than 100 µm, micro abrasive waterjets match the intricate machining capabilities of other micro machining technologies. As with conventional abrasive waterjets, they can cut, profile and drill a wider range of metals, ceramics, polymers and composite materials than any other technology. The equipment to produce micro abrasive waterjets uses existing technologies, is modest in size and cost, and can readily be integrated with robotic manipulation systems.

The paper introduces micro abrasive waterjets and the markets for the technology. The development of micro abrasive waterjet equipment for 50 µm (micron) diameter jets is described.

Organized and Sponsored by the WaterJet Technology Association

1. INTRODUCTION

The remarkable success of the abrasive waterjet (AWJ) industry reflects its commercial drive and the unique machining capabilities of AWJs. This paper outlines the potential for the AWJ industry to use its commercial drive to break into the micro machining market, a market that needs the unique machining capabilities of AWJs. To enable the industry to do this, micro abrasive waterjet (MAW) technology and equipment is being developed for exploitation.

It is useful to start with a few details about micro abrasive waterjet equipment to power a 50-μm nozzle at 700 bar water pressure. Water consumption is 2 liters per hour and abrasive consumption 200 grams per hour. The pumping unit consists of two 6 mm diameter plunger pumps installed within 80 mm diameter pneumatic cylinders. A compressor powered by a single phase, 2 kW electric motor is sufficient to drive the pumps.

MAW equipment is small compared to conventional AWJ equipment, with water and abrasive flow rates that can be less than 1 percent of conventional AWJ equipment. However, cutting energy densities of the jets are the same as conventional AWJs, which means jets will cut the same materials as conventional AWJs, albeit through thinner sections.

Micro machining markets and their requirements from new machining technologies, are outlined in Section 2. Methods of generating MAWs are considered in Section 3. After discussing in Section 4 the factors that limit the minimum diameters of abrasive waterjets, the strategy for development of MAW equipment is presented in Section 5. Details of the flow circuit and components for MAW equipment is given in Section 6, and information on initial trials with 50 μm diameter jets in Section 7. Future developments are considered in Section 8, followed by conclusions in Section 9.

2. THE MICRO MACHINING MARKET

A key characteristic of the current industrial revolution is the miniaturization of products and processes. Device and component manufacturers require smaller and smaller features to be machined, with increasingly tighter tolerances, on a growing range of high technology, often difficult to machine materials. Japan’s Micro Machine Centre estimated that the world wide micro machining market will reach over $10 billion dollars by 2010 (Weiss, 1995).

To support their industries, governments in the major industrialized countries are funding research into new micro machining methods. Most of this research is directed at photonic techniques, such as lasers. Little research currently appears to be directed to micro machining with abrasive waterjets. This is unfortunate as AWJs could become the preferred micro machining technique in a wide range of applications.

Technologies for micro machining include: high performance lasers; electron beams; wire EDM; chemical etching; high speed routers; fine pressing; diamond tooling. Each of these techniques has advantages and limitations compared to each other and to micro abrasive waterjets. The established advantages and disadvantages of conventional AWJs, relative to other machining techniques, extend down to MAWs. For instance, compared to lasers, the cutting speeds of AWJs are much lower for materials that are suitable for laser cutting but AWJs can machine a much wider range of materials and provide better cut edge qualities, free of heat affected zones.

Three examples will illustrate the kind of application where micro abrasive waterjets could become the machining method of first choice.

2.1 Manufacturing

A company produces a wide range of flat springs, small enclosures and other fine pressings from a wide variety of metals in strip form. The company needs to be able to rapidly produce prototypes and small batches of components, without the cost of tooling. Currently prototypes are produced by hand using fly presses. This can take several hours, depending on component complexity. The process is error prone. Laser profiling is not acceptable because of cracking from heat affected zones and problems with cutting copper based alloys such as beryllium copper. This is a good application for a MAW mounted on a small X-Y table.

2.2 Job Shop

A job shop with a number of conventional AWJ cutting systems receives a steady stream of requests from customers to profile small intricate components but the components cannot be profiled on its existing machines. A MAW profiling system, using the same software and control systems that the company currently uses, would provide the required intricate machining capability with minimum investment.

2.3 Electronics

One of the products of an advanced materials manufacturer is a light weight, high conductivity, metal matrix composite for heat sinks in aerospace electronic applications. The composite consists of ceramic particles in an aluminum matrix and is produced in the form of small plates. The material cannot be profiled with conventional tooling or lasers because of the ceramic particles. The machining detail required is beyond the capability of conventional AWJs. The current method of profiling is to diamond drill starter holes and sub contract the rest of the machining to a wire EDM job shop. This is an expensive process with time penalties. AWJs cut and drill the material as if it were aluminum. A small MAW profiling system would be a cost effective solution.

3. METHODS OF GENERATING AWJs

There are 3 methods for generating abrasive waterjets:

3.1 Entrainment Method

AWJs for precision machining use a high velocity water jet to entrain air laden with abrasive particles into a ceramic focusing tube. In the focusing tube energy is transferred from the water to the abrasive particles to produce a cutting beam. As focusing tube bore diameters are decreased below 0.5 mm the entrainment process begins to break down and the transport of abrasive particles to the focusing tube becomes problematic. Modifications to the entrainment process, due to Hashish et al. (1990), allows entrainment cutting heads to function with focusing tube diameters down to 0.25 mm. The entrainment method cannot be used for micro machining.

3.2 Suspension Method

The suspension method involves using an additive to suspend abrasive particles in water. High pressure water is used to displace the abrasive suspension out of a vessel and through a cutting nozzle. Extensive research work has been carried out on the suspension method, particularly by the Southwest Research Institute, (Hollinger et al., 1990) and Quest Integrated (Kovacevic et al., 1997). Commercial systems based on the suspension method have not been developed because of formidable technical problems posed by the complexity of the flow circuits and with valves. The suspension method is at present ruled out for MAWs because of these technical problems.

3.3 Carrier Method

In the carrier method a percentage of the high pressure water flow to a cutting nozzle is diverted through an abrasive storage vessel. On leaving the storage vessel the diverted water carries abrasive particles out of the vessel and into the main water flow before it reaches the cutting nozzle. The originators and main developers of carrier fluid technology are BHR Group in the UK under the name DIAJET. BHR Group has produced equipment with cutting jet diameters ranging from 0.5 mm to 2.8 mm. This equipment has been extensively used for on site demolition and the cutting up of munitions to recycle or to destroy explosives and propellants. BHR Group have also produced precision machining systems.

For the same cutting performance, carrier fluid systems can operate at about 25 percent of the pressure required by entrainment systems but the equipment to produce carrier jets is more complicated. For the same power input and operating pressure a carrier system would produce over four times the cut surface area per minute as an entrainment system. Development of the carrier method for precision machining started 10 years after the commercialization of the entrainment method. The carrier method faces a long uphill struggle to become established in the precision machining market in the face of the proven and highly successful entrainment method. It is likely to be some time before the market situation is such that the higher cutting speeds offered by the carrier method will become sufficiently attractive for main stream AWJ companies to exploit the technology. Carrier fluid technology is well suited to the generation of MAWs.

4. LIMITATIONS ON THE MINIMUM SIZE OF MAWs

Micron and sub micron abrasive particles are used in many machining operations. For instance, drilling the bore of ceramic nozzles for MAWs may be carried out using micron sized diamond particles applied in a fluid to rotating tooling. It is known that about 80 percent of abrasive particles break up in the focusing tubes of entrainment AWJs. This breakup results in the formation of millions of micron and sub micron particle per second. These particles are responsible for a significant part of the cutting action of entrainment abrasive waterjets. Based on the above observations, it can be reasoned that abrasive waterjets with diameters under 10 µm would cut if it were possible to generate such jets.

Practical limits on how small abrasive waterjets can be made are due to:

a) As nozzle diameters are decreased water flows in fluid circuits becomes laminar, rather than turbulent, and inter particle forces on fine abrasive particles causes the particles to become more cohesive. As yet it is not known what limitations these physical phenomena will place on minimum jet diameters. For 50 µm diameter jets, the Reynolds Number (ratio of inertia to viscous forces) is sufficiently high to maintain turbulent flow in critical components and inter particle forces do not appear to be a serious problem.

b) The ability to drill and shape nozzle bores in very hard materials. Proven methods are available for drilling nozzles with bore diameters down to 50 µm. Nozzle bore diameters down to 10 µm are possible with existing technologies but research is needed to establish whether hole quality and manufacturing costs are acceptable.

c) A fall off in the cut surface area generated per minute as jet diameter is decreased. Setting aside effects due to viscosity, surface tension, particle size and other physical phenomena, then for a given water pressure and abrasive concentration, the cut surface generated per minute varies linearly with jet diameter, as does the thickness of material that can be cut. This linear relationship is known to apply for jet diameters from 2 mm down to 200 µm but there are indications of departures from a linear relationship by 50 µm jet diameter.

It can be concluded that there are no serious restrictions on producing MAWs with diameters down to 50 µm but research and development is needed to be able to operate substantially smaller diameter jets.

5. STRATEGY FOR EQUIPMENT DEVELOPMENT

Micro abrasive waterjets are defined as abrasive waterjets with diameters between 100 µm and 1 µm. A 50 µm jet diameter has been selected for initial equipment development, with the capability to scale the equipment to operate with smaller and larger diameter jets. The carrier fluid method, discussed in Section 3, is used to generate the abrasive in water flow at the cutting nozzle.

The success of conventional AWJ equipment owes a lot to the simplicity of its high pressure water circuit and the small number of mechanical components in the circuit. Companies have been able to concentrate developments on these components to achieve high equipment reliability. Conventional equipment is easy to understand, to trouble shoot and to service and it has a good safety record. The word dependable is appropriate to describe AWJ equipment provided by the leading suppliers. The same level of dependability must be achieved by MAW equipment.

The following strategy has been adopted to maximize the opportunities of MAW equipment achieving good dependability early on in the product development cycle:

a) A simple water flow circuit has been devised.

b) The water flow circuit is made up of a small number of mechanically simple components.

c) Abrasive is loaded into the equipment in sealed cartridges to prevent contamination of the abrasive. This simplifies the equipment as there is no need for an abrasive replenishment system.

d) Pumping units are based on standard pneumatic components and control systems, with plunger pumps driven by pneumatic cylinders.

e) The cutting nozzles are made from the same ceramics used for entrainment focusing tubes. Because nozzle wear is linked to the cutting energy density of an abrasive jet, the energy density in MAW nozzles needs to be limited to those of entrainment jets in order to have similar nozzle wear rates. A MAW operating at 700 bar water pressure has roughly the same cutting energy density as that of an entrainment AWJ operating at 3000 bar. An operating pressure of 700 bar has been selected for initial MAW equipment developments.

f) The normal mode of operation for the equipment is with the water flow permanently on. This allows rapid on/off cutting action to be achieved by starting and stopping the abrasive flow, rather than the alternative of starting and stopping both the abrasive and the water flow. With an operating water pressure of 700 bar most engineering materials are not marked by the water jet and the water flow is only 2 liters per hour, for a 50 µm diameter jet.

6. FLOW CIRCUIT AND COMPONENTS

The basic flow circuit, which is the subject of a patent application (Miller. 1999), is shown in Figure 1. Referring to Figure 1, pressurised water from the pump is fed to a flow controller. The flow controller has two main modes of operation:

1. It directs all of water flow from the pump towards the cutting nozzle. In this mode of operation the controller also applies suction to the top of the abrasive storage vessel shown in figure 1. The suction stops the flow of abrasive particles from the bottom of the vessel.

Or

2. It directs a percentage of the water flow from the pump to the top of the abrasive storage vessel. Water flowing into the top of the vessel displaces abrasive particles and water out of the bottom of the vessel, into the main water flow on its way to the nozzle.

Figure 2 shows the twin, synchronized pumps, used for development trials. The pumps, which are the subject of a patent application, are incorporated in proprietary compact pneumatic cylinders. Control of the pumps is by a small programmable logic controller (PLC).

The abrasive storage vessel shown in Figure 1 can either contain abrasive in a cartridge or abrasive can be transferred to the vessel from a cartridge. Figures 3 and 4 show the abrasive storage vessel with and without the vessel barrel in place. Without the barrel the removable cartridge containing abrasive can seen. Cartridges contain enough abrasive for one hours cutting with a 50 µm diameter jet.

A 50 µm bore nozzle design in silicon carbide has been developed. The nozzles are proving to be effective with the prospect of similar operating lives to those achieved by entrainment AWJ focusing tubes.

7. CUTTING WITH 50 MICRON DIAMETER JETS

It is likely that most MAW machining systems will have a working area under 500 X 500 mm and have a motion system made up of a combination of linear ball screw actuators that have a repeatability better than 10 µm. There is great flexibility in how actuators are configured to form an X-Y table. A 300 X 300 mm table, Figure 5, is being used for profiling trials and to investigate table configurations.

Referring to Figure 5, the abrasive storage vessel along with the cutting nozzle assembly can be mounted directly on the X axis, or the storage vessel can be located remotely and abrasive and water fed to the nozzle through tubing. Provision has also been made for mounting the pumping unit, flow controller and other flow circuit components on the X axis. Work pieces are carried on the Y axis, with a linear jet catcher tank under the X axis. Alternatively the jet catcher tank can be built into the Y axis.

At the time of writing, commissioning of the equipment is underway with the first trials confirming that MAWs will cut the same range of materials as conventional AWJs. 50 µm diameter jets have successfully cut plastic, aluminum, mild steel, high alloy steel and glass using Barton Mines garnet abrasive.

8. FUTURE DEVELOPMENTS

In order to provide a firm base for the exploitation of MAWs, effort is currently directed at providing dependable systems for cutting operations with 50 µm diameter jets. In the development processes it has become clear that MAWs have additional capabilities to conventional AWJs. These capabilities are associated with:

1. The coherent nature of MAWs.

2. The speed with which the cutting action can be turned on and off. In the longer term, it should be possible to start and stop the cutting action several hundred times per second.

Coherent abrasive waterjets that can be rapidly turned on and off can be used to mark surfaces, mill features into surfaces and remove material by percussion drilling. The research needed to develop these capabilities is well suited to academic research in universities and other institutions.

Developments for conventional AWJ systems will also be of value to MAW systems. In particular, improved nozzle materials will make it economic to operate at higher pressures with benefits in increased cutting speeds. As discussed in Section 5, research is needed to be able to operate with jet diameters substantially less than 50 µm.

9. CONCLUSIONS

There is a large market for AWJ machine tools in micro machining. Micro abrasive waterjet equipment is under development that will allow AWJ machine tool manufacturers to enter the micro machining market.

The operating mode of micro abrasive waterjets allows them to carry out machining operations that are not practical with conventional abrasive waterjets. Research in academic institutions is needed to develop the technologies to exploit micro abrasive waterjets for percussion drilling, etching, and marking, milling and other applications. Research is also needed in using micro abrasive waterjets in the fabrication of miniature components in difficult to machine materials.

10. ACKNOWLEDGMENTS

Research into the feasibility of micro abrasive water jets was part funded by a Smart Award from the UK Department of Trade and Industry. This funding is gratefully acknowledged.

11. REFERENCES

Hashish, M. A., Craigen, S.J., " Abrasive Nozzle Assembly for Small Hole Drilling and Thin Kerf Cutting," European Patent Application Number: 90200835.8, Publication Number 0 391 500 A2, 1990.

Hollinger, R.H., " Process for Cutting with Coherent Abrasive Suspension Jets," United States Patent Number: 5,184,434, 1990.

Kovacevic, R., Hashish, M., Moham, R., Ramulu, M., Kim, T.J., Geskin, E.S., " State of the Art of Research and Development in Abrasive Waterjet Machining," Transactions of the ASME, Vol. 119, pp. 776-785, 1997.

Miller, D. S., "Fluid Abrasive Jets for Machining," International Patent Application Number PTC/GB98/02627, 1999.

Weiss, S.A. " Think Small: Lasers Compete in Micromachining," Photonics Spectra pp. 108-114, October, 1995

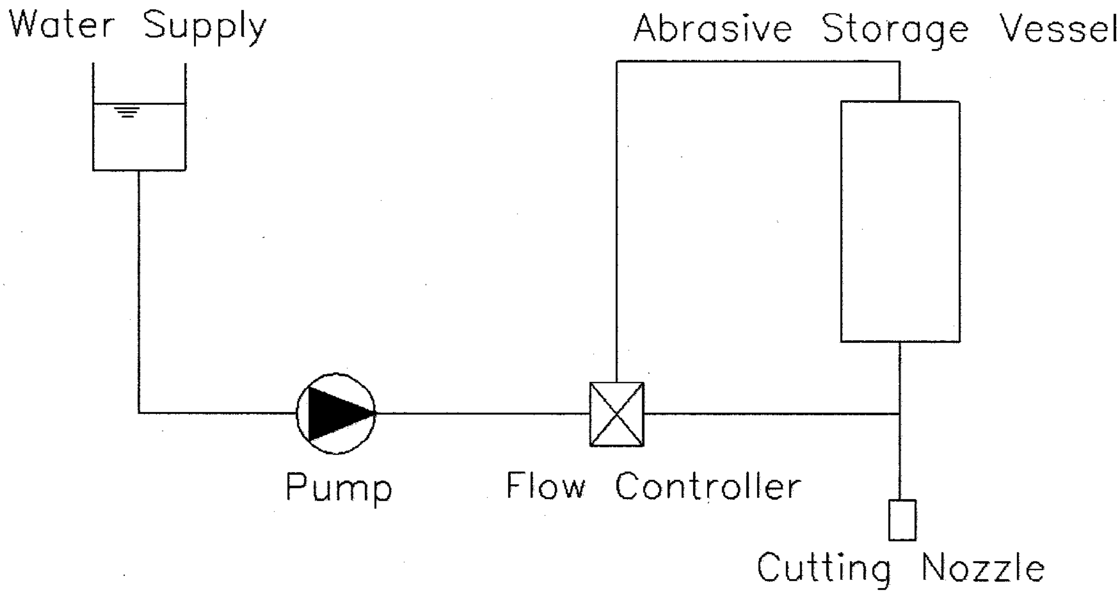

Figure 1 Flow Circuit for Micro Abrasive Waterjets

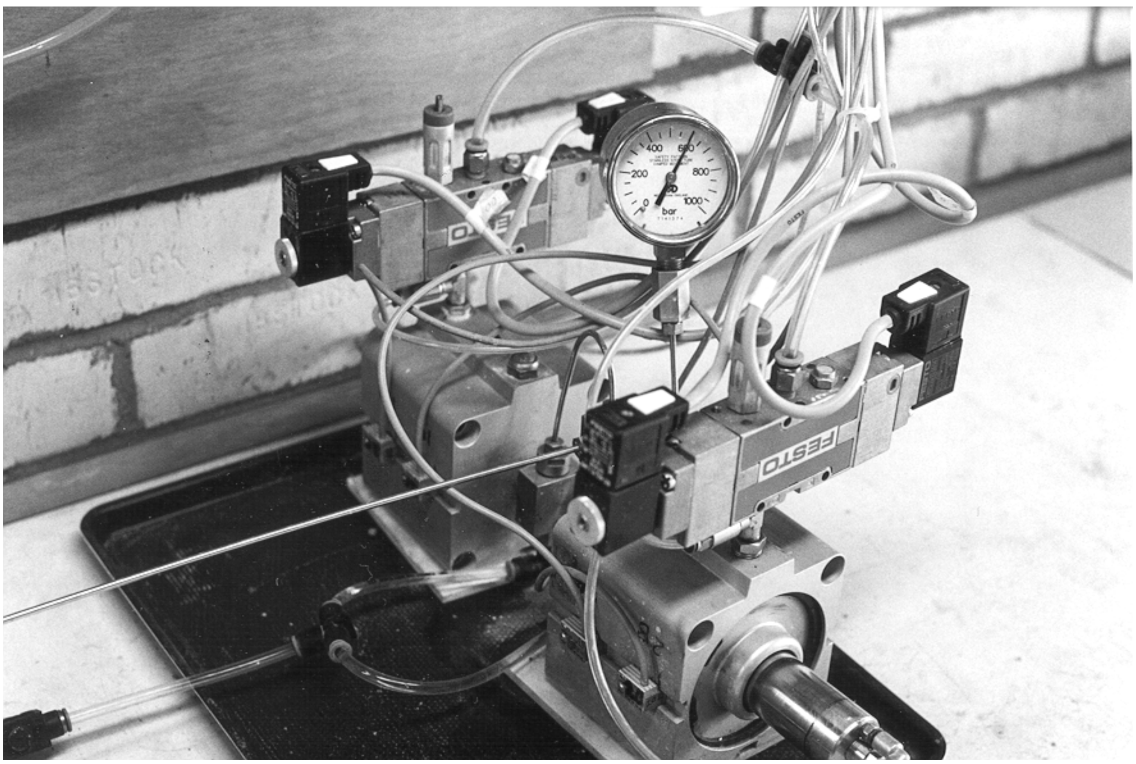

Figure 2 Pumping Unit for Trials

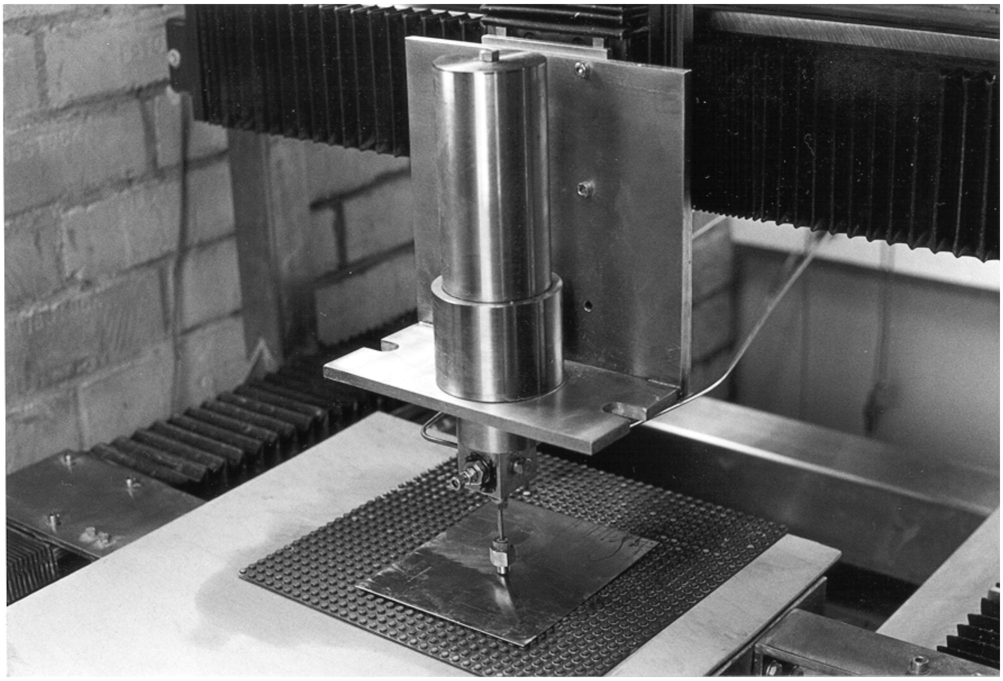

Figure 3 Abrasive Storage Vessel and Cutting Nozzle

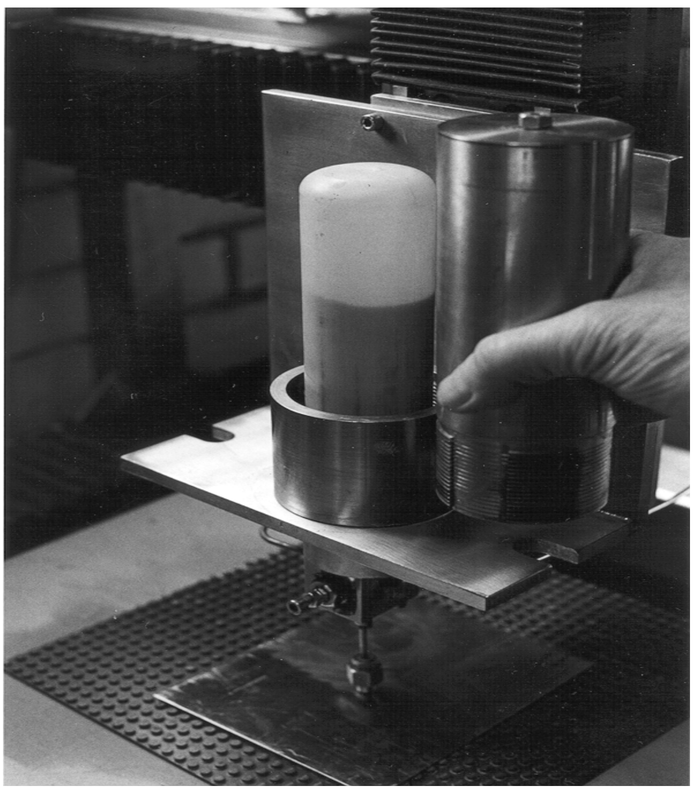

Figure 4 Abrasive Cartridge Installed in Storage Vessel

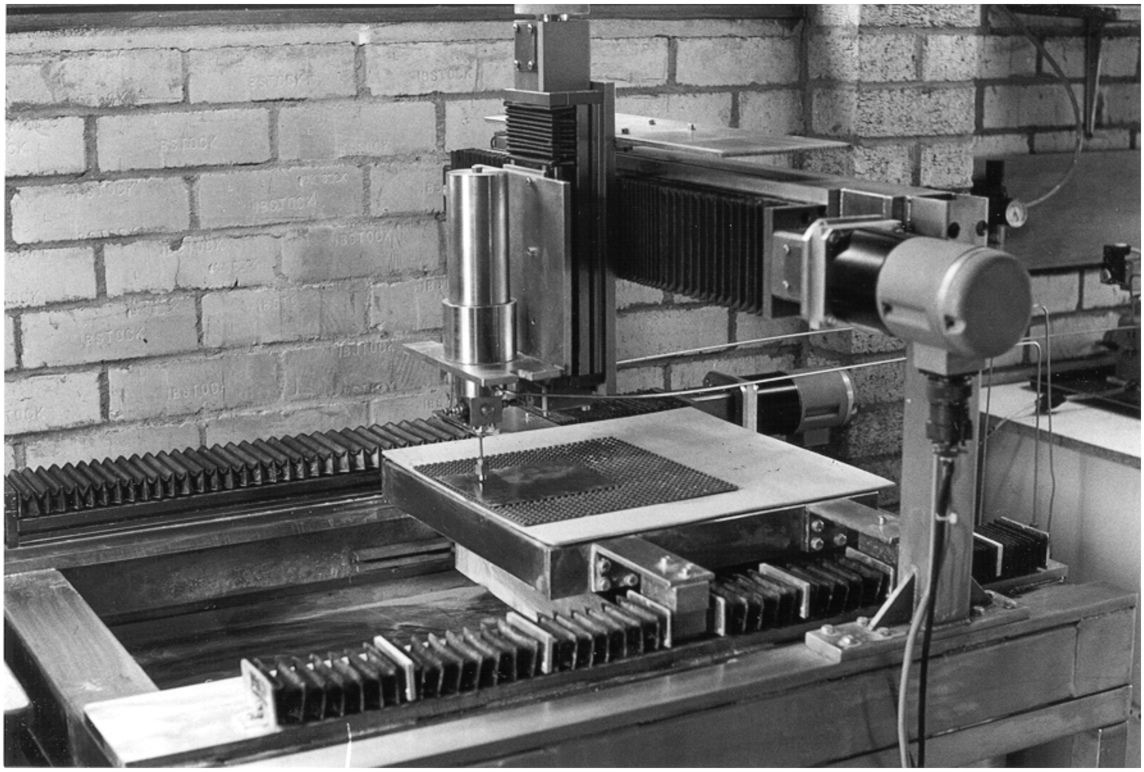

Figure 5 X-Y Table for Profiling Trials

10th American Waterjet Conference
August 14-17, 1999: Houston, Texas

Paper **28**

A STUDY ON TECHNOLOGY AND EQUIPMENT FOR CANNON BORE CLEANING BY ABRASIVE SUSPENDING WATERJET

Gao Zidong
Changsha Institute of Mining Research
Changsha 410012, Hunan Province, The People's Republic of China

ABSTRACT

In order to clean all adhesives, produced by shooting, in various cannon bores, some feasibility tests for both high pressure waterjet and abrasive waterjet cleaning were made, and a kind of technology and equipment for cannon bore cleaning with the abrasive suspending waterjet was developed successfully. This paper describes the preparation and recycle use of the abrasive suspending liquid, and presents the general structure, working principle and main performance parameters of this cleaning equipment.

Organized and Sponsored by the WaterJet Technology Association

1. INTRODUCTION

The cannon which uses the gunpowder as power to shoot a bullet is generally called as artillery such as field -shipboard -, tank - and antiaircraft - artillery etc. Most of artillery are called as rifle artillery also, because there are many spiral lines, which are called as rifling, being correspondingly laid out on the faces evenly in the cannon bore. The cross section of this gun barrel is similar to an internal gear shown in Fig.1-b. At the moment of shooting a bullet, the bullet is momentarily put out the cannon bore by high temperature and pressure generated by gunpowder burning. While in a high speed friction of bullet, especially the bearing band of bullet, with the cannon bore, there remain some such adhesives as copper, aluminum and nylon etc on all faces in the cannon bore (Fig.1-a). Meanwhile, the cannon bore is polluted by gunpowder burning also, that is to say, the carbon deposit is generated in it. These polluted adhesives are more difficult to be cleaned out, because they adhere firmly to the cannon bore. The more the bullets are shot, the thicker the adhesives are deposited, which has a direct effect on the precision of cannon bore and the accuracy of shooting, so it is necessary to often clean these adhesives in time.

2. FEASIBILITY TESTS

The aim is to make an approach to the feasibility which the high pressure waterjet or the abrasive waterjet is used to clean the adhesives in the cannon bore, from which whether or not a kind of equipment for cannon bore cleaning can be developed.

2.1 Pure Waterjet Tests

This test was one for which the waterjet cutting machine was used. Under the condition of constant flow rate, the pressure was divided into several rating from high to low, then the tests were made rating by rating. When the pressure was increased to > 140MPa, the adhesives in the cannon bore were cleaned out but slowly. If the cleaning time is shortened, the flow rate should be increased to > 100l/min. At that time, this pump with high flow rate and pressure was difficult to be available commercially, so it was not suitable to use the pure waterjet for cleaning.

2.2 Abrasive Waterjet Tests

In order to find a suitable abrasive material and its matching size, many tests for such abrasive materials as saw dust, walnut shell, talcum powder, garnet and pearl stone etc were made early or late, under the condition of same/different water pressure and flow rate. Obviously, the cleaning effects of the light and soft abrasive materials was not best, while the heavy and hard abrasive materials cleaned out the adhesives quickly but did the damage to cannon bore matrix. Based on all aspects of requirements, the comparison and choose were made. It was considered that pearl stone used as an abrasive material was more ideal. Used as the abrasive waterjet, such an abrasive material as pearl stone can clean out the adhesives in the cannon bore at 25MPa. The density and Moh's hardness of pearl stone were $2.35 \pm 0.1\%$ (lighter) and $5.5 \pm 0.5\%$ (softer) respectively. Pearl stone contained SiO_2 (70~73%), Al_2O_3 (11~13%), Na_2O (2.6~4.1%), K_2O(2.5~4.5%) and CaO (1~1.5%) in main and a little amount of MgO and Fe_2O_3, with stable chemical property. And it can be available at any time.

However, the abrasive waterjet has some such disadvantages as higher consumption of abrasive material, uneasy control of abrasive-water ratio, more difficult and complicated recycle use of abrasive material and so on.

2.3 Abrasive Suspending Waterjet Tests

In order to find suitable pressure and flow rate, pearl stone abrasive was mixed with water in the certain proportion, then stirred in the stirring tank into an abrasive suspending liquid and directly pumped to the nozzle where the abrasive suspending waterjet was formed to make a cleaning test for the cannon bore. Meanwhile, the dynamic characteristics of this solid-liquid two phase flow, the critical velocity of homogeneous suspending of abrasive material and the effects of abrasive concentration and size etc were determined. Also, the effects of this abrasive suspending liquid on the pump and its important parts were checked. In addition, some approaches to the structural model of nozzle were made. Based on these tests and inspections, it was considered that using the pearl stone abrasive suspending waterjet to clean the cannon bore was feasible, and the recycle use of abrasive suspending liquid was easy made.

3. DEVELOPMENT OF ABRASIVE SUSPENDING WATERJET CLEANING MACHINE FOR CANNON BORE

3.1 Requirements for Technical Performances

The main requirements for technical performances put forward by users in the contract were as follows:

(1) All artillery with 25~155mm in bore size can be cleaned.

(2) The longest cleaning time for the artillery which is the most difficult to be cleaned is not more than 2hrs.

(3) After cleaning, any remnant adhesives can not exist in the cannon bore; meanwhile, the damage to the cannon bore is not allowed.

(4) The recycle use of abrasive suspending liquid can be made, and this liquid can be complemented or renewed periodically.

(5) This cleaning machine is safe and reliable, and can be operated by one cleaning worker.

3.2 Components and Working Principles

A complete set of equipment is consisted of abrasive suspending liquid feeding system, pressurized delivery system, cleaning system, electric control system and abrasive suspending liquid recycling system etc.

As shown in Fig.2, according to the specified weight ratio, pearl stone abrasive and water in stirring tank (19) are stirred into an abrasive suspending liquid, then this liquid is pressurized by pump (23) and delivered to ejecting head (14) by feeding rod (5) along high-pressure hose (1); in this time, the abrasive suspending waterjet ejects. Driven by rotary mechanism (2), the ejecting head and the feeding rod can make a forward or reversal rotation. Hauled by chain (3), the rotary mechanism goes forward or backward along guide rail (4) together with the feeding rod and the ejecting head, and its distance of travel is controlled by over travel limit switch (10), by cleaning request. The chain is driven by drive chain wheel (7). The waterjet from the ejecting head impacts on the cannon bore (12), then along the bore flows into covered hopper (11) to storage (17). Recovery pump (16) is controlled automatically by liquid-level controller (15) installed on the storage, its flow rate is more than that of pump (23), and pumped the abrasive suspending liquid in the storage into the stirring tank to make a recycle use. Filter (18) is installed on the stirring tank. In the process of cleaning, pearl stone abrasive and water in the stirring tank are stirred continuously, while the ejecting head ejects, rotates and goes forward or backward at the same time in the cannon bore repeatedly till cleaning out. Afterwards, close valve (20) valve—(21) is closed also, open intermediate valve (22), start pump (23) and use the pure water to clean the pump, pipeline, ejecting head and cannon bore to avoid the abrasive material depositing in the equipment. In this time, water is not allowed to enter the stirring tank to avoid the abrasive material reducing its concentration.

According to amount of adhesives in the cannon bore and the extent of cleaning difficulty or simplicity, the reciprocal cleaning times is preset. The rotation, going forward or backward, travel length and reciprocal times of ejecting head are controlled automatically. As for the artillery with various bore sizes, the sizes of ejecting head and guide device are different. Tens of nozzles are laid out evenly on the ejecting head, whose distribution is like as radiation. As for the rifle artillery, in order to clean out the two sides of rifle simultaneously, the nozzle should meet at the certain intersection angle to radial to increase an impacting force of waterjet on the rifle sides.

In order to ensure the smooth operating of feeding rod and avoid it bending, floating support (8) is added on the guide rail, and guide device (13) is installed on the feeding rod near the location of ejecting head to make the feeding rod and ejecting head situate always on the intermediate axle line of cannon bore. According to diameter and length, the feeding rods are divided into three types and used for the cannon bores in three-kind bore sizes respectively.

The biggest and longest feeding rod is connected with several short rods. However, this extended rod must meet the following requirements:

(1) The rod is hollow, with an adequate rigidity.

(2) The seal at the location of connection is reliable, without leakage.

(3) After connecting, the rod is a firm one and can propagate a positive or reversal torque.

(4) After connecting, the outside diameter of this rod must be kept same so that it can smoothly go forward or backward in the support.

In the process of cleaning, it is not allowed that the abrasive suspending liquid drains out of the tail of cannon bore, so the tail must be blocked. The front part of cannon bore should be inclined downward so that the abrasive suspending liquid after ejecting flows into the storage along the cannon bore.

Fastening support (6) is articulated with the guide rail. In this way, the guide rail can make a transversal motion up and down and is allowed to make a pitch motion or side-to-side swing to the certain angle. Adjustable support (9) is articulated on the front part of guide rail. In this way, the guide rail can make a pitch motion or side-to-side swing to the certain angle so that the adjustment can be done to make the feeding rod coaxial to the cannon bore prior to cleaning.

4. CONCLUSIONS

Through a preliminary test and check before acceptance, the abrasive suspending waterjet cleaning machine for cannon bore met all requirements for the technical performances specified by the user in the contract, and was committed to operation in December 1997.

As for this cannon bore cleaning machine, the abrasive-to-water ratio was 15~18% (by weight), the pressure was 3.5~5MPa, and the flow rate was 110~240l/min.

5. ACKNOWLEGEMENT

The author extends his hearty thanks to a troop in the Chinese People’s Liberation Army for providing the funds support and the specimen of cleaning test, to Wei Ying (Professor), Liao Xingbin (Senior Engineer) and Cao Haoxiang (Senior Engineer) etc. for taking part in his study, and to the High Pressure Waterjet Research Institute, Changsha Institute of Mining Research, for its great support in the process of his study.

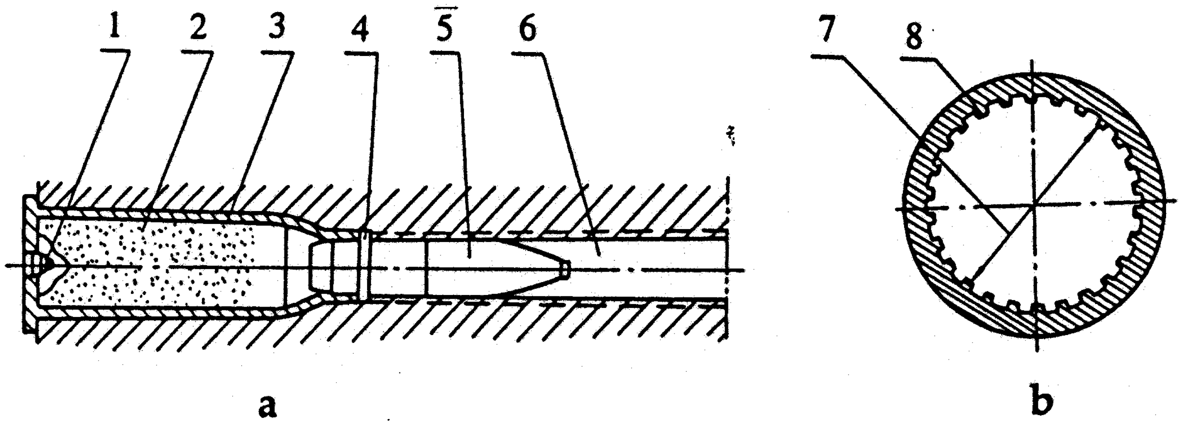

Fig.1

a-bullet in cannon bore; b-cross section of gun barrel; 1-primer; 2-gunpowder; 3-cartridge case; 4-bearing band; 5-bullet; 6-cannon bore; 7-artillery bore size; 8-rifling

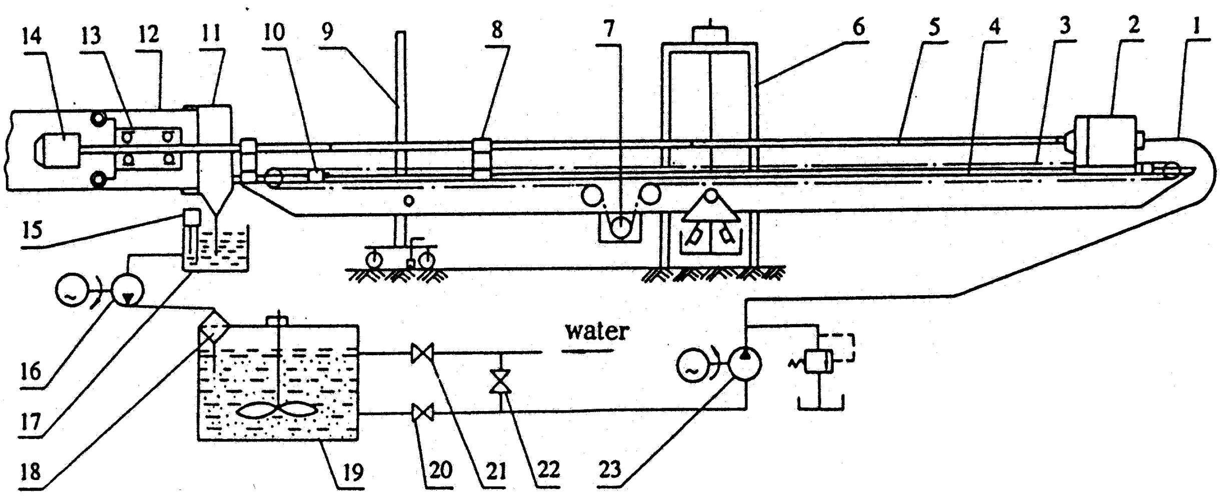

Fig.2 Diagram of the Working Principle

1-high-pressure hose; 2-rotary mechanism; 3-chain; 4-guide rail; 5-feeding rod; 6-fastening support; 7-drive chain wheel; 8-floating support; 9-adjustable support; 10-travel switch; 11-covered hopper; 12-cannon bore; 13-guide bracket; 14-ejecting head; 15-liquid-level controller; 16-recovery pump; 17-storage; 18-filter; 19-stirring tank; 20-slurry valve; 21-pure water valve; 22-intermediate valve; 23-high-pressuse pump

10th American Waterjet Conference
August 14-17, 1999: Houston, Texas

ABRASIVES FOR HIGH ENERGY WATER JET:

INVESTIGATION OF PROPERTIES

L.M. Hlaváč, L. Sosnovec
VŠB - Technical University
Ostrava, Czech Republic

P. Martinec
Institute of Geonics, Academy of Sciences
Ostrava, Czech Republic

ABSTRACT

The analyses of physical properties of several abrasive materials are the topic of the paper. The great effort was devoted to the studies of processes leading to the abrasive grain damage during injection abrasive jet formation. Few important parameters substantially influencing the amount of abrasive material damage were determined and studied in correlation between theory and experiment. Resulting values of specific energy for surface enlargement are compared with the ones obtained by calculations based on energy of the atomic bonds and the lattice parameters. All characteristics are utilised for completing of the prediction program JETCUT. Knowledge of relationships among parameters makes possible to recalculate a material parameter determined from the testing cut made on material using specific type of abrasive to any type of abrasive with different parameters, characteristics and level of damage. The results are discussed and compared with experiments.

1. INTRODUCTION

The specific energy necessary for enlargement of the new free surface (rising during process of breaking of material) is a basic parameter to be determined for abrasives provided the theoretical modelling of interaction processes should be studied. In past several papers were devoted to the problem of abrasive particles breaking during mixing process namely Hlaváč et al. (1995), Hlaváč (1996), Hlaváč & Sochor (1997) and Hlaváč & Martinec (1998). Nevertheless, all experimental attempts to determine the specific energy for generation of a new free surface fell flat yet. Using theoretical formulae presented, e.g. by Hlaváč & Martinec (1998), however, the specific energy for surface enlargement can be determined provided the parameters characterizing the amount of internal damage, disorders and failures in material are determined with appropriate accuracy. Determination of the specific surface energy from lattice parameters and from experimental results aimed at disintegration of the abrasive material during mixing processes typical for injection abrasive jet generation is the topic of the work partly presented in this paper.

2. THEORETICAL BACKGROUND

The theoretical studies started when we tried to find out the appropriate values of specific surface energy for garnets in various publications. The estimations made according to Davidge (1979) yield values of the specific surface energy for rocks from about 20 up to roughly 60 $J.m^{-2}$. Moreover, his conclusions indicate decreasing trend for relationship of the specific energy on the rock material grain size. We tried to approximate the value of the specific surface energy using the molar energy of almandine published by Keller (1954). The area of disintegration can be expressed using atomic radii and the number of particles in 1 mol of matter. The consistent equation for the specific surface energy can be expressed using a respective average atomic bond length calculated from atomic radii of elements in material:

$$E_{SS} = \frac{8E_M}{\sqrt{3}N_A l_B^2} \tag{1}$$

This expression also yields specific surface energy values of the order of the tenths of Joules per square meter. Nevertheless, such value did not correlate with specific surface energies equivalent to the amount of disintegration caused by high energy water jet during mixing process provided the energy transmissions from water jet to the abrasive particle was determined only by drag force coefficient as it was presented by Hlaváč (1995).

$$E_{TR} = \frac{1}{2} C_D P_{kL} a_o c^{-1} \tag{2}$$

The transmitted energy and respective specific surface energy determined from experimental data by relationships derived by Hlaváč et al. (1995) and filled in by new definition of norm setting constant by Hlaváč & Martinec (1998) yield values from about ten times higher up to approximately thirty times higher than the ones determined by above presented approaches of Davidge and Keller. Therefore, we tried to determine the specific surface energy using results of quantic mechanics. We based our calculation on the following presumptions. Each atom inside the crystal lattice has several neighbours. We can determine the average number of neighbours on the opposite side of the plane of dislocation and also the average length of the respective bonds. The appropriate energies of the bonds can be found in literature or they can be calculated by approximate methods from wave functions for atomic orbits. We can also use simple expression by Coulomb forces. The number of atoms situated on one side of the plane of dislocation can be determined considering the number of atoms on the elementary planes designated by lattice parameter, crystal type and atomic structure. The analysis of the process of crystal lattice dislocation results then in the following equation for a specific surface energy provided that only Coulomb forces are considered:

$$E_{SS} = k n_o \frac{e_o^2}{4 \pi \varepsilon_o r_a a^2} \qquad \textbf{(3)}$$

Another method checked up for determination of the specific surface energy is based on experiments marked out for designation of the microhardness of garnets. This method, however, is just in the stage of searching for appropriate model describing the stress and strain field formation inside the tested sample. The model is essential for separating the influence of less hard and less brittle but much more plastic basic matter and the behaviour of the particular garnet material. The samples for microhardness tests are plates made from special cement into which the garnet grains were mixed.

The last method presented here is based on the experimental results evaluating disintegration of garnet grains during mixing process. Nevertheless, the energy losses during interaction process between jet and target (an abrasive particle in this case) are very important. The methods based on atomic bonds and molar energies yield values of the specific surface energies of one order lower than they seem to be using equation (2). This difference provoked further and more detail physical studies of the interaction process between a liquid jet and abrasive particle. It was realized that in regard of the high density of the energy transfer from the liquid jet into the abrasive grain within the first impingement the grain does not behave as exactly rigid. Inversely to it the liquid due to very high velocity and from it resulting short interaction time is not absolutely fluent and behaves like plastic solid. Therefore the energy utilizable for grain damage is substantially lower than should be valid for the drag coefficient because great amount of it is absorbed in elastic-plastic deformations. Hence the problem of interaction is studied as a stroke of two solid bodies. The impingement is considered to be rather elastic with coefficient of energy transfer determined by equation

$$k_{ET} = \frac{3(1 - 2\mu_P) K_W}{E_G} \qquad \textbf{(4)}$$

This equation accrues from the presumption that coefficient of energy transfer can be expressed as a ratio of the respective moduli of bulk elasticity of liquid and abrasive material.

3. THEORETICAL AND EXPERIMENTAL RESULTS

Using the approach presented by Keller (1954) to the calculation of the bond energy we can obtain the value 133,44 kJ.mol^{-1} for garnet almandine ($Fe_3Al_2Si_3O_{12}$). The average distance between atoms is the weighted average of the bond length determined from the atomic radii of the atoms in the lattice structure: Fe^{2+}, Al^{3+}, Si^{4+} and O^{2-}. The resulting value is 0.192 nm. The atomic radii were taken from tables compiled by Brož et al. (1980). Dividing one mole of almandine into two layers of tetrahedrons with an edge equal to the average bond length the total free surface originated is determined by equation

$$P_N = \frac{1}{4} N_A \left(l_B \frac{\sqrt{3}}{2} l_B \right) \tag{5}$$

The specific surface energy 27.76 J.m^{-2} is calculated from molar energy of almandine mentioned above and the originated total free surface of one mole of almandine provided the bond length is a weighted average of bond lengths for all possible combinations of atoms.

The equation (3) enables to calculate the specific surface energy directly from the parameters of the crystal lattice. It was determined for garnet almandine that average number of broken off atomic bonds is four. The number of atoms with broken bonds per elementary plane determined by lattice parameter is eight. The average energy of one atomic bond was determined from the electrostatic Coulomb force acting between two elementary inverse charges outlying distance determined from the lattice parameters an average atomic radius. Using the lattice parameter of almandine 1.154 nm, presented by Martinec (1994), the value of the average atomic radius is 0.204 nm. The equation (3) then yields the value of the specific surface energy 27.17 J.m^{-2}.

The last presented method of determination of the specific surface energy is based on utilization of the theory presented by Hlaváč et al. (1995) and filled in by Hlaváč and Martinec (1998). The energy transferred from the liquid jet into an abrasive particle is determined by equation (6) involving the coefficient of energy transfer expressed by equation (4)

$$E_{TR} = \frac{3(1 - 2\mu_P)K_W}{E_G} C_D \frac{\pi a_o^2}{4} \mu p_o \gamma_R v \frac{a_o}{c} \tag{6}$$

The calculation of the average surface of grains before mixing and after it from experimentally determined average grain sizes and jet parameters was made both for spherical grains and for cubic ones. The appropriate specific surface energies were determined for 10 individual garnet samples each tested by 10 different liquid pressures (i.e. from 100 values). They were determined provided that the grain shape is either spherical or cubic. Another value of the specific surface energy was determined from graphic correlation between theory and experiment. The respective values of the specific surface energies determined by equation (6) from the experimental data and parameters were

39.74 J.m^{-2}, 20.81 J.m^{-2} and 20.38 J.m^{-2}. The average of the three values of the specific surface energy taken out processing experimental data is then 26.98 J.m^{-2}.

4. DISCUSSION

All presented methods of calculation used for specific surface energy of garnet almandine lead to the average value round about 27 J.m^{-2}. The values obtained from experimental data were compared with the ones evaluated by theory from either molar energy or energy of atomic bonds. It is necessary to point out that the value of specific surface energy determined from experimental data for spherical shape of grains is higher than theoretical one. Contrary to it the value determined for cubic grains is lower than theoretical one. If the value of the specific surface energy is calculated for percentage statements of spherical shape, the value corresponding to the 70% of a spherical pattern is very close to the value determined by theories. The specific surface energy corresponding to this grain shape is 27.82 J.m^{-2}. The cube shows similarity to the spherical pattern only 52.36%. The result implies that the shape of grain corresponding to the specific surface energy determined from theories is close to the polyhedron. This is in a good agreement with experimental results published by Martinec (1994).

Contrary to values determined from theories and suitable for polyhedron approaching to sphere from 70% the value 20.38 J.m^{-2} was determined by optimizing process correlating the theoretical curves for the average grain size after mixing process and respective experimental data. This energy is almost the same as the one acquired for cubic shape of grains, 20.81 J.m^{-2}. Considering these results, we could conclude that in the injection mixing process both the input grains and the output ones are cubic. Nevertheless, this conclusion should ignore the establishment of previous experimental works showing that usually a great amount of internal damage is present inside each grain just before mixing process.

Comparing the specific surface energy determined from mentioned optimizing process correlating theory and experiment and the average one calculated from various theories we can establish that internal damage reduces the specific surface energy to the 75% of its average theoretical value. It means that abrasive grains contain such amounts of damage reducing their strength as if 25% of grains are destroyed or 25% of each grain is destroyed. This discovery is in a very good agreement with experimental results got by Martinec (1994).

The results of the theoretical research were used for calculation of the garnet damage inside mixing chamber and mixing tube. The coefficient of energy transfer was expressed by equation (3). Theoretical results and experimental data are compared through graphic presentation in Fig. 1 through 3. Specific surface energies determined by explicit methods are summarized in Table 1.

5. CONCLUSIONS

Comparing the results acquired by presented methods of calculation for the specific surface energy of rock materials it is possible to make the following conclusions:

- specific surface energies determined by all presented methods are almost equal;
- comparison of the value of the specific surface energy calculated from experimental results of abrasive material damage in mixing chamber and mixing tube and the one determined from molar energy of the rock or energy of atomic bonds and appropriate average atomic bond lengths can yield information about initial grain damage or shape provided the complementary parameter of them is known;
- specific surface energy determined from molar energy of matter or energy of atomic bonds and appropriate average atomic bond lengths can be used for evaluation of the abrasive grain disintegration provided the amount of initial damage of grains and their shape is known.

6. ACKNOWLEDGEMENTS

The authors are grateful to the Grant Agency of the Czech Republic for support of the work presented in this paper by grants No. 205/96/0931 and 106/98/1354.

7. REFERENCES

Brož, J., Roskovec, V., and Valouch, M.: “Physical and Mathematical Tables,” *SNTL*, Praha, 1980.

Davidge, R.W.: “Mechanical Behaviour of Ceramics,” *Cambridge University Press*, Cambridge, England, 1979.

Hlaváč, L., Sochor, T., Sitek, L., Martinec, P., and Vala, M.: “Physical Study of a High Energy Liquid Jet as a Milling Tool,” *Proceedings of the 4th Pacific Rim International Conference on Water Jet Technology*, pp. 449-456, Kajima Institute Publishing Co.,Ltd., 1995.

Hlaváč, L.M.: “Physical Analysis of the Energy Balance of the High Energy Liquid Jet Collision with Brittle Non-Homogeneous Material,” *Proceedings of the 8th American Water Jet Conference*, pp. 681-697, Water Jet Technology Association, St. Louis, Missouri, 1995.

Hlaváč, L.M.: “Interaction of Grains with Water Jet - the Base of the Physical Derivation of Complex Equation for Jet Cutting of Rock Materials,” *Proceedings of the 13th International Conference on Jetting Technology*, pp. 471-485, BHR Group, Prof. Eng. Pub. Ltd., Bury StEdmunds and London, 1996.

Hlaváč, L.M. and Sochor, T.: ”Mineral Grain Destruction During the Process of Material Disintegration by Abrasive Water Jet,“ *Geomechanics 96*, pp. 351-354, Rotterdam, Balkema, 1997.

Hlaváč, L.M. and Martinec, P.: “Almandine Garnets as Abrasive Material in High-Energy Waterjet - Physical Modelling of Interaction, Experiment, and Prediction,” *Proceedings of the 14th*

International Conference on Jetting Technology, pp. 211-223, BHR Group, Prof. Eng. Pub. Ltd., Bury StEdmunds/London, 1998.

Keller, W.D.: "The Bonding Energies of Some Silicate Minerals," *American Mineralogist*, Vol. 39, pp. 783-793, 1954.

8. NOMENCLATURE

a	lattice parameter [m]
a_o	size of a material element - grain [m]
γ_R	compressibility factor
c	sound velocity [$m.s^{-1}$]
C_D	drag coefficient
ε_o	absolute dielectric constant (dielectric constant for vacuum)
e_o	unite charge (charge of proton)
E_G	Young's modulus of elasticity for garnet [Pa]
E_M	total energy of atomic bonds for 1 mol of matter [$J.mol^{-1}$]
E_{SS}	specific surface energy [$J.m^{-2}$]
E_{TR}	energy transferred to the target object [J]
k	average number of broken bonds per atom
k_{ET}	coefficient of energy transfer
l_B	length of the atomic bond in material [m]
μ	nozzle discharge coefficient
μ_P	Poisson's ratio
n_o	number of atoms on the basic area cell of material lattice
N_A	Avogadro's number (number of particles in 1 mol of matter)
p_o	liquid pressure before the nozzle inlet [Pa]
P_{kL}	power of the jet at the distance L from nozzle outlet [W]
r_a	radius of the atom [m]
v	jet velocity [$m.s^{-1}$]

9. TABLES

Table 1. Comparison of the specific surface energies determined by presented methods.

	molar energy [$J.m^{-2}$]	atomic bonds [$J.m^{-2}$]	TJMPI, spherical gr. [$J.m^{-2}$]	TJMPI, cubic gr. [$J.m^{-2}$]	TJMPI, correlation [$J.m^{-2}$]	TJMPI, average [$J.m^{-2}$]	TJMPI, 70% of spherical gr. [$J.m^{-2}$]
E_{SS}	27.76	27.17	39.74	20.81	20.38	26.98	27.82

Legend: TJMPI - theory of jet - material particle interaction (equation 6)

10. FIGURES

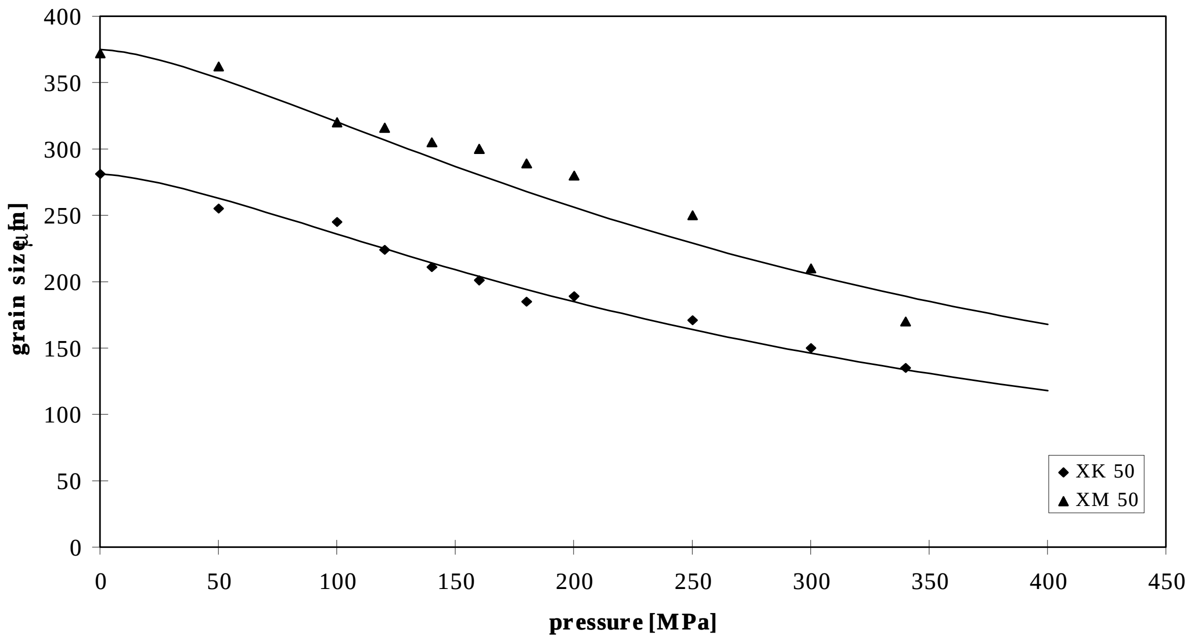

Figure 1. Disintegration of almandine grains from two deposits with increasing water pressure. Mesh No. 50. Lines calculated from theory, points determined by experiment.

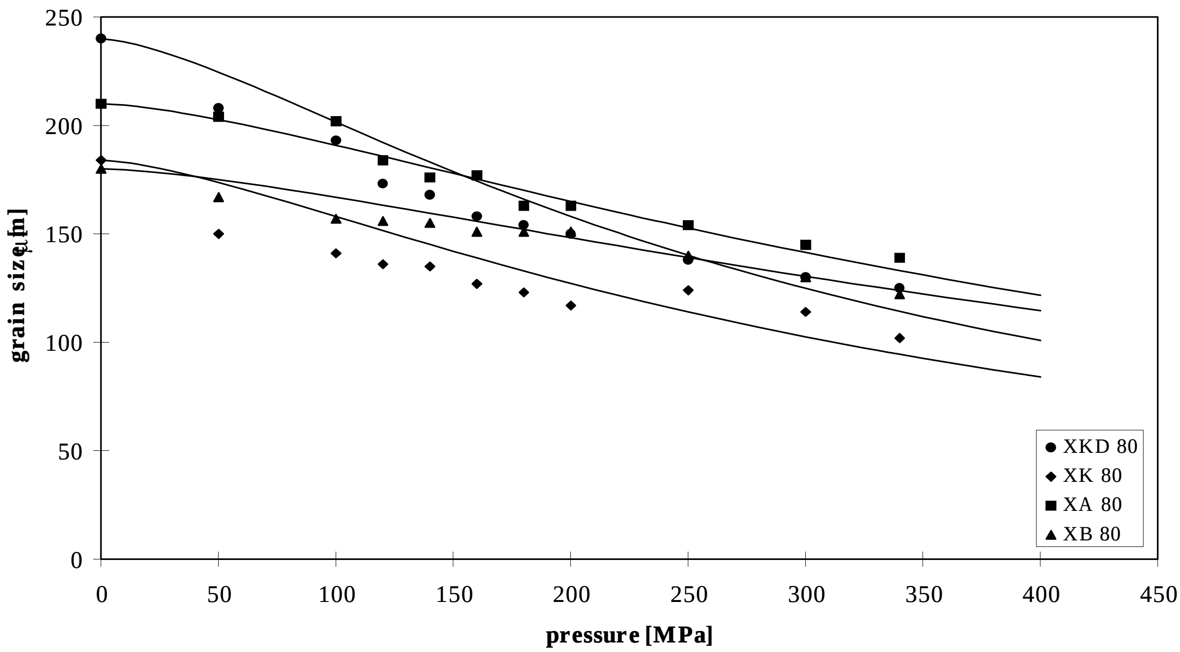

Figure 2. Disintegration of almandine grains of various deposits with increasing water pressure. Mesh No. 80. Lines calculated from theory, points determined by experiment.

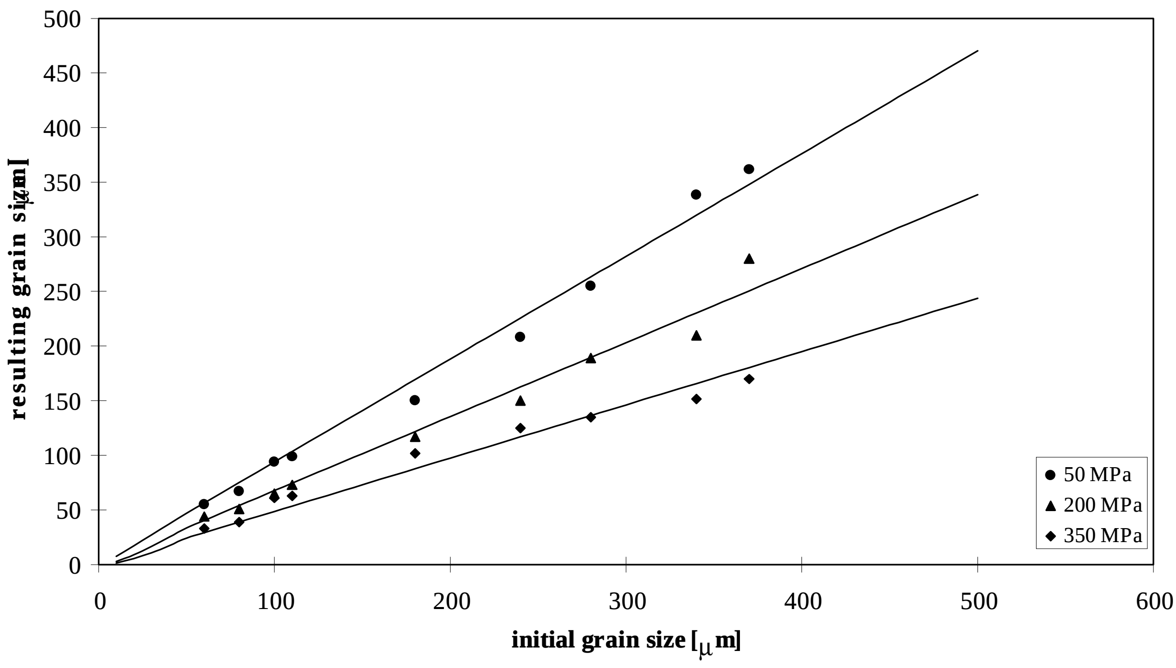

Figure 3. Pressure depending relationship between initial and resulting grain sizes for almandines from various deposits. Mesh number varies from 50 to 240.

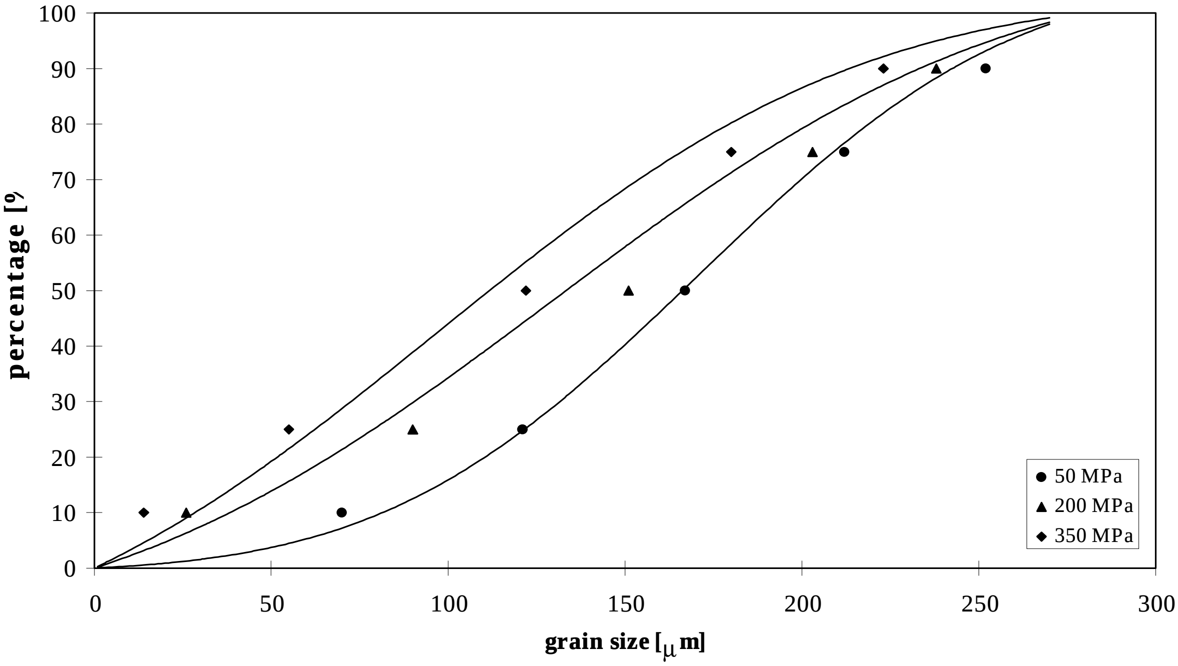

Figure 4. Pressure depending cumulative distribution of the grain size of one type of almandine, Mesh No. 80. Lines calculated from theory, points determined by experiment.

10th American Waterjet Conference
August 14-17, 1999: Houston, Texas

Paper 30

SOME INVESTIGATIONS ON ABRASIVES IN ABRASIVE WATERJET MACHINING

O.V.Krishnaiah Chetty and N.Ramesh Babu
Indian Institute of Technology Madras,
Chennai, 600 036, INDIA

ABSTRACT

Abrasive particles in Abrasive Waterjet Machining play a dominant role in controlling the quality of the final product and economy in production. This paper deals with the results of preliminary investigations conducted on locally available garnet abrasives and validation of an empirical model. The influence of the particle distribution, combined with process parameters, on the taper of cut and the finish of the cut surface of black granite using garnet abrasives are also reported. Studies on recycling of this locally available garnet on the recovery and cutting efficiency are presented.

Organized and Sponsored by the WaterJet Technology Association

1. INTRODUCTION

Waterjet cutting technology has found a variety of applications world over as it offers wide ranging benefits. The utilization of this technology in India is at the low ebb. The recent exposures of manufacturers, academicians, researchers and managers in India to a series of seminars and conferences highlighting this technology has given fillip to the activities (this has also provided a momentum, specially for research). The research group at this institute has done considerable work in granite cutting using Abrasive Waterjet Machining (AWJM). Indigenously available garnet abrasives have been tested for their suitability. Elaborate experimentation proved their efficiency of cutting on par with imported abrasives. The findings related to cutting of a variety of granites are reported in Chakravarthy et al. (1998). Further studies on local abrasives are being continued.

Economical production must focus on cost reduction. One of the factors contributing to the production cost in AWJM is the cost of abrasives. The type of abrasive used in AWJM can have a large impact on the performance of cutting. The more difficult the cut, the more important the abrasive selection becomes.

The natural characteristics like hardness, shape, specific gravity of abrasives will affect their effectiveness in cutting. Also man-made characteristics resulting out of production of abrasives namely; purity, and particle size will influence cutting (Ohman, 1993). Desired rate of cutting, and surface quality of cut surface, influence the selection of abrasives. Cost of operation of AWJM will be influenced by abrasives. High quality abrasives cost more but must be weighed against the performance. In his analysis, Ohman (1993) found that a very low cost abrasive may successfully cut a metal but at higher total costs; while higher performance abrasives saves considerable amount of money by its superior performance. The depth of cut achieved varies widely and seem to be independent of mineral type; however, damaged grains may be a key factor (Vasek et al., 1993). Different sized particles cut at different speeds. A consistent particle size distribution is essential for even cutting performance. A good waterjet abrasive should have consistency, both in its distribution and its range (Ohman, 1993). Their detailed investigations are limited in literature. Momber et al. (1996) found that depth distribution and surface roughness are very sensitive to the abrasive grain size distribution, where as average depth of kerf is not influenced significantly.

One of the restrictions to the AWJM in the field of industrial production seem to emanate from the high costs of abrasives, handling and disposal of used abrasives (Guo et al., 1994). Recycling of abrasives seems to be a good plan to minimize use of abrasives (Guo et al., 1992; Knapp and Ohlsen, 1994). A model of disintegration of abrasives to study the particle size distribution has been proposed by Guo et al. (1994). Such a model is expected to reduce extensive experimentation. An analysis of disintegration by Guo et al. (1994) infers that mixing and accelerating process in the focusing tube leads to tremendous disintegration. Quality cut causes less disintegration than rough-cuts and the size of the particle has an influence on the degree of disintegration. While increase in pressure or cutting rate leads to increased disintegration, increase in abrasive flow rate is found to have no significant influence. Under the experimental conditions reported by Martinee (1994), garnet abrasives under 100 μm have exhibited a stable chip like shape regardless of the nature of process of disintegration. General experience has shown that through recycling of abrasives, tool and running costs may be reduced by about 25 percent (Knapp and Ohlsen, 1994).

1.1 Scope of Present Work

The present paper discusses the preliminary studies on the influence of locally available garnet abrasives in cutting black granite. The validity of an empirical model developed using multi-regression analysis to predict depth of cut is presented. The influence of distribution of local garnet abrasive along with the AWJM parameters in cutting black granite. Studies are confined to kerf width, taper of cut and finish of cut surface. Considering the importance of recycling of abrasives, cutting efficiency and finish of cut surface with recycled abrasives are reported.

2. EXPERIMENTAL

The details of equipment used for experimentation are shown below.

2.1 Equipment

- Abrasive Waterjet Machining System: M/S WOMA, Austria
  High pressure intensifier pump type : IP236-22
  Discharge pressure : 360 MPa
  Vibratory abrasive feeding system
  CNC work cell with two axis control : Zinser CNC type 500/35/92
  Primary Nozzle Diameter : 0.25 mm
  Secondary Nozzle : 0.8 mm
- Surface Finish Measuring Equipment : Perthometer S5P
- British Standard Sieves Scanning Electron Microscope : JEOL JSM-5300
- Local Abrasive - Garnet [$Fe_3Al_2(SiO_4)_3$]
  Sp. gravity : 3.8
- Work Material: Black Granite (Kfeldspar and quartz)
  Sp. gravity : 3.6
- Angle of jet : 90^0
- Stand off distance : 3 mm
- Special Screening Cloth

2.2 Experimental Procedure

The procedure used for investigations are presented in three parts; preliminary investigations, effect of distribution of abrasives and AWJM parameters, and studies on recycling of abrasives.

2.2.1 Preliminary Investigations

Preliminary experimentation is done to study the influences of Waterjet Pressure, Jet Traverse Rate and Abrasive Flow Rate on the depth of cut in cutting black granite with local abrasive. An empirical model to determine the depth of cut has been developed based on multi-regression analysis, the details of which are available in Gowrisankar (1998). This model is tested with the experimental results shown in Figure 1.

2.2.1.1 Observations/Discussions

The capabilities of the local abrasive in cutting black granite are available in Figure 1 and can be used to select the process parameters in cutting operations. It can be seen from this figure that the depth of cut with the local abrasives behaves in the expected fashion. Increase in waterjet pressure leads to increased depth of cut while increase in the jet traverse rate has the opposite effect. Increase in abrasive flow rate beyond 50 gms/min has not significantly influenced the depth of cut. The multi-regression model of Gowrisankar (1998) predicts the depth of cut within an error of 10 to 18%.

2.2.2 Effect of Distribution of Abrasives and AWJM Parameters

In order to study the effect of distribution of abrasive particles, samples of abrasives are formulated to have close fineness numbers. Standard sieve analysis is used to provide information on the fineness number of the local garnet abrasives. By definition, fineness number is the average grain size, and corresponds to the sieve number whose opening would just pass all the particles if all were of the same size. This number is convenient means of describing the relative fineness of abrasives. A standard set of sieves are used to sieve a dried 500 gm. sample. The particles retained on each sieve and the bottom pan are weighed and their percentages to total sample are determined. The percentage retained on each sieve is multiplied by a factor, which is the mesh number of the sieve, which allowed these particles to pass through. Average grain fineness number is equal to the sum of these products to the total percentage retained on all the sieves and the bottom pan.

In the present case, three sample types have been prepared by selectively adding particle sizes. These samples have almost same fineness numbers in the range of 52 to 54.56 as detailed in Table 1. Sample type 1 has abrasives retained on one mesh while sample 2 has those retained on three meshes and sample three has those of four meshes. In sample types 1 and 2 the quantity retained on a single mesh number dominates. Sample type 3 has particles retained on two meshes dominating. These sample types are chosen to have distribution varied. Orthogonal Array Design L_9 shown in Table 2 has been employed to study the influence of the AWJM process parameters namely, waterjet pressure, and traverse rate, on the behavior of these samples. The top kerf width, bottom kerf width and finish of cut surface are measured. Taper of cut is calculated which is usually defined as a non-dimensional ratio between the top cut-width and bottom cut-width (10).

2.2.2.1 Experimental Conditions

The details of the parameters, fixed and variable, are as follows.

Angle of jet: 90^0
Stand off distance: 3 mm
Work Material thickness: 20 mm
Length of cut: 25 mm
Variables: Waterjet Pressure,
Traverse rate, and
Sample of abrasive.

The results obtained are shown in Table 3. The response graphs are shown in Figure 2.

2.2.2.2 Observations/Discussions

The influence of distribution of local abrasives along with the process parameters are shown in Figure 2. It can be observed that lower traverse rates produce decreased taper of cut. While abrasive samples 1 and 2 (containing a large proportion of single mesh size abrasive) produce better taper of cut; sample 3 produced inferior taper of cut where two mesh sizes dominate. Pressure at level 2 has produced minimum taper of cut. Surface finish produced is better at medium pressure and low traverse rates. The sample containing single mesh size (sample 1) produced improved finish. The surface profiles obtained in the tests are shown in Figure 3. Further studies are contemplated.

2.2.3 Procedure for Studies on Recycling

Black granite of 105 mm thick with a trapezoidal cross section had been cut to study the influence of AWJM process parameters. Cutting efficiency and surface finish of the cut surface have been analyzed. The fineness number of fresh garnet abrasives has been 55.18. Studies include the influence of three parameters; waterjet pressure, transverse rate and abrasive mass flow rate. The ranges for parameters are selected so as to avoid through cut of material of 105 mm.

The debris obtained is collected from the catcher tank using a special net that can withstand the residual energy of the used waterjet. This net also restricts further damage of abrasives. The closeness of properties of abrasives and black granite makes it difficult to separate effectively. Washing, settling and drying has been employed. The percentage of retrieved material from debris is determined. The recycled abrasives have been used to cut the granite at the same levels of parameters to determine their cutting efficiency. The finish obtainable on cut surface with fresh and recycled abrasives is then compared. Scanning electron microscope analysis has carried out to qualitatively study the angularities and size of the abrasives.

2.2.3.1 Observations/Discussions

About two thirds of material from the debris is recycled. The fineness number of used abrasive is determined as 53.66. Table 5 shows the cutting efficiency (calculated as the percentage of depth of cut compared to fresh abrasives) of recycled abrasives. This is in the range of 48 to 79 %. The typical surface finish obtained on granite using fresh abrasives and recycled abrasives are shown in Figure 4. Surface finish is found improved with recycled abrasives. Finer and improved roundness of recycled abrasives as compared to fresh abrasives is probably responsible for the improved finish. Cutting process resulted in the rounding of sharp edges of original local garnet abrasives can be seen from Figure 5.

3. CONCLUSIONS

Economical production must focus on cost reduction. Effective use of abrasives is essential in this context. Locally available garnet abrasives have been experimented to determine the depth of cut of black granite and are found to be satisfactory in performance. A multi-regression empirical model has been validated with this data. This data can be used in the selection of AWJM process parameters. Based on Orthogonal experimentation, it is found that abrasive sample containing one predominant mesh size will yield minimum taper of cut as well as improved finish. Medium pressure and low traverse rate produce improved taper of cut and surface finish. Use of recycled local abrasives will result in decreased cutting efficiency but they are found to produce improved finish of cut surface. Further detailed investigations with partial recharging of abrasives and their suitability for economic production are planned. Economic analysis of the AWJM in cutting granite using local abrasives, with and without recycling, is under way.

4. ACKNOWLEDGMENTS

The authors express sincere thanks to the Department of Science and Technology, Government of India, for the financial support under Science and Engineering Research Council, to undertake this research work.

5. REFERENCES

Chakravarthy, P.S., Babu, N.R., Ramakumar, M.S., Robert, H. and Chetty, O.V.K., "Investigations on abrasive waterjet cutting granites", *Proceedings of 5th Pacific Rim International Conference on Water Jet Technology*, pp.433-440, International Society of Water Jet Technology, Delhi, India, 1998.

Gowrishankar, S., "Studies on abrasive waterjet machining on black granite", B.Tech project report, pp.16-30, IIT Madras, India, May 1998.

Guo. N.S., Louis, H., Meier, G., and Ohlsen, J., "Modeling of abrasive particles disintegration in the abrasive Water-jet cutting in relation to the recycling capacity", Proceedings of 12th International conference on Jet Cutting Technology, pp.567-585, Rouen, France, 1994.

Guo. N.S., Louis, H., Meier, G., and Ohlsen, J., "Recycling of abrasives in abrasive water jet cutting", *Proceedings of 11th International conference on Jet Cutting Technology,* St. Andrews, Scotland, 1992.

Knapp, M., and Ohlsen, J., "Recycling of abrasive material in abrasive waterjet cutting", *Proceedings of 12th International conference on Jet Cutting Technology*, pp.511-519, Rouen, France, 1994.

Martine, P., "Changes of garnet during abrasive waterjet generation and cutting materials", *Proceedings of 12th International conference on Jet Cutting Technology*, pp.543-551, Rouen, France, 1994.

Momber A.W. and Radavan Kovacevic, Principles of abrasive waterjet machining, p230, Springer, 1998.

Momber, Andreas.W., Pfeiffer, Dirk, Kovacevic, Radavon, and Schuenemann, Rene, "Influence of abrasive grain size distribution parameters on the abrasive waterjet machining process", *proceedings of the 1996 24th NAMRC conference*, pp.6, Society of Manufacturing Engineers, MR 1996.

Ohman, J.L., "Abrasives: Their characteristics and effect on waterjet cutting", *Proceedings of 7th American waterjet conference*, pp.363-374, Waterjet Technology Association, Seattle, Washington, 1993.

Vasek, J., Martinee, P., Foldyna, J., and Hlavac, L., "Influence of properties of Garnet on cutting process", *Proceedings of 7th American waterjet conference*, pp.375-387, Waterjet Technology Association, Seattle, Washington, 1993.

Table 1. Sieve analysis of three sample types.

Weight of each sample: 500 gms.

Sample Type	Retained (gms.) on Mesh Number					Fineness No.
	48	52	72	85	100	
1			500			52
2		75	350		75	54.40
3		210	210	40	40	54.56

Table 2. (a) Experimental factors and levels

Factor level → **Variables ↓**	**1**	**2**	**3**
Waterjet Pressure, MPa	200	300	350
Transverse Rate, mm/min	50	125	200
Sample of abrasive, Type	1	2	3

(b) L_9 Orthogonal Array Experimentation

Experiment No → **Factor level↓**	**1**	**2**	**3**	**4**	**5**	**6**	**7**	**8**	**9**
1	1	2	3	3	1	2	2	3	1
2	1	2	3	1	2	3	1	2	3
3	1	2	3	2	3	1	3	1	2

Table 3. Results of experimentation with sample types.

Experiment No.	**1**	**2**	**3**	**4**	**5**	**6**	**7**	**8**	**9**
Kerf width, mm at Jet entry on work	0.76	0.68	0.85	0.73	0.67	0.67	0.73	0.75	0.85
Kerf width, mm at Jet exit on work	0.57	0.68	0.57	0.51	0.54	0.57	0.44	0.75	0.63
Kerf width ratio	1.32	1.00	1.49	1.41	1.23	1.16	1.68	1.00	1.35
Surface finish, R_a,μ m	10	17	24	14	19	21	31	9	5

Table 4. Cutting efficiency of recycled abrasives

Pressure (MPa)	**Mass flow rate (gm/min)**	**Traverse speed rate (mm/min)**	**Depth of cut (mm) for fresh abrasives**	**Depth of cut (mm) for recycled abrasives**	**Cutting efficiency %**
120	5	50	15	10	66.7
330	5	50	27	13	48.1
200	6	50	19	15	78.9
250	6.5	50	22	17	77.3

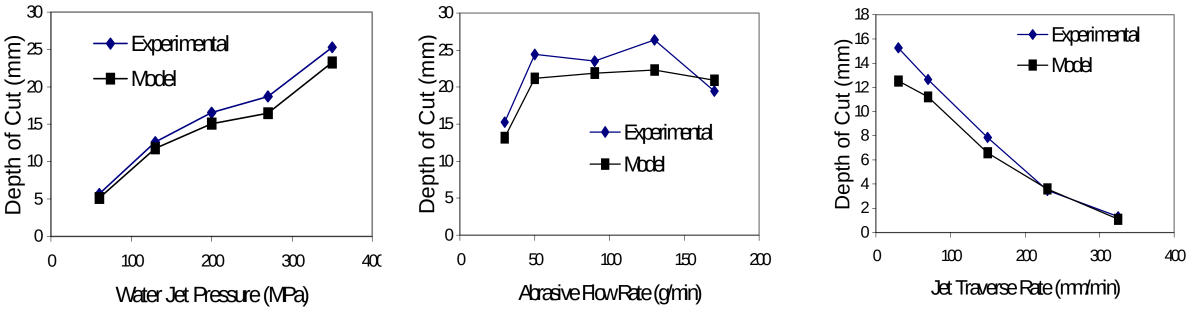

Figure 1. Influence of AWJM process parameters with local abrasives and empirical model verification.

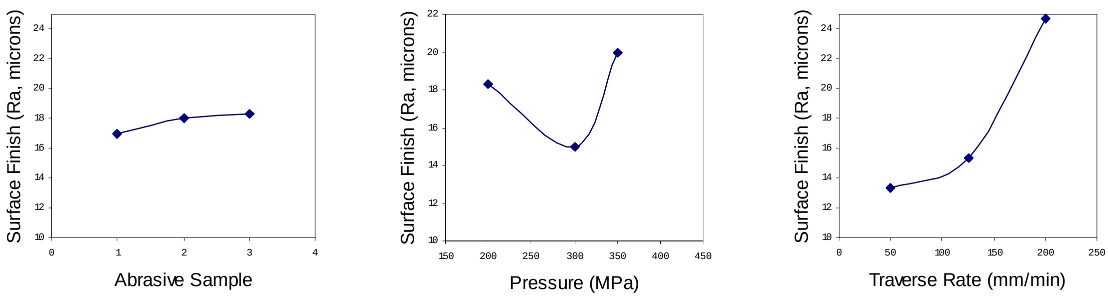

(a) Effect on taper of cut

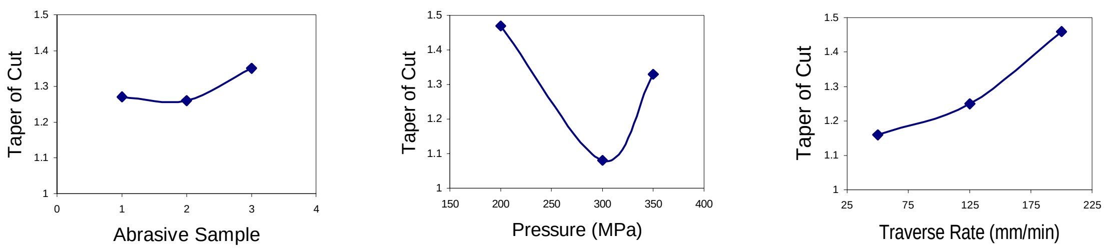

(b) Effect on finish of cut surface

Figure 2. Responses of L_9 Experimentation with local abrasives.

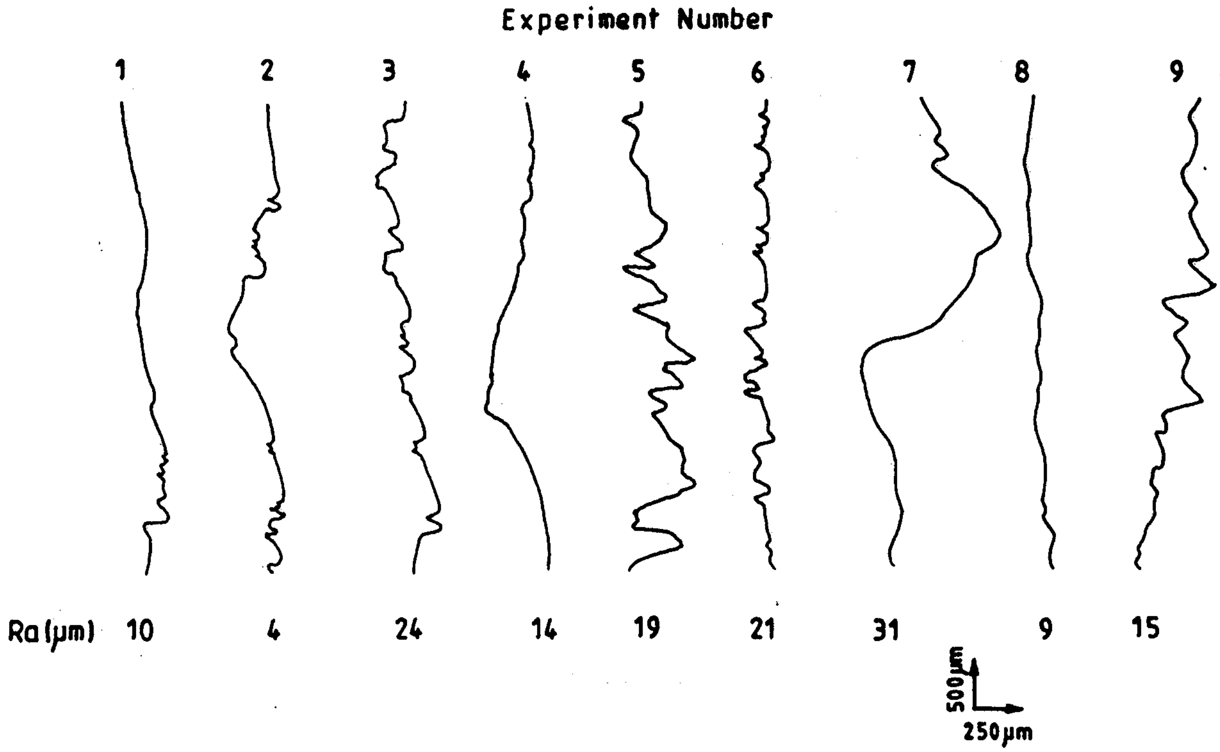

Figure 3. Surface profiles of cut surfaces- L_9 experimentation

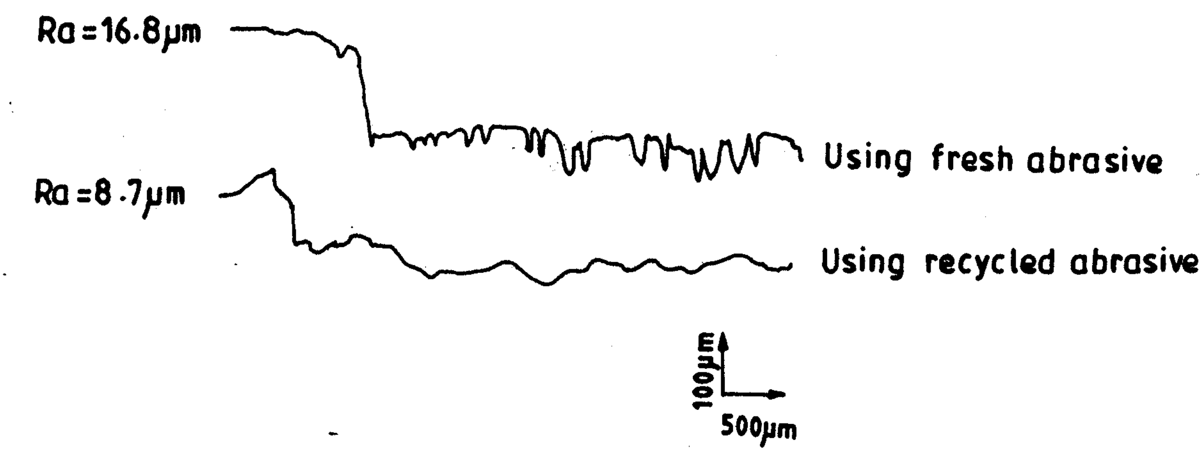

Figure 4. A typical set of surface profiles obtained using fresh and recycled abrasive

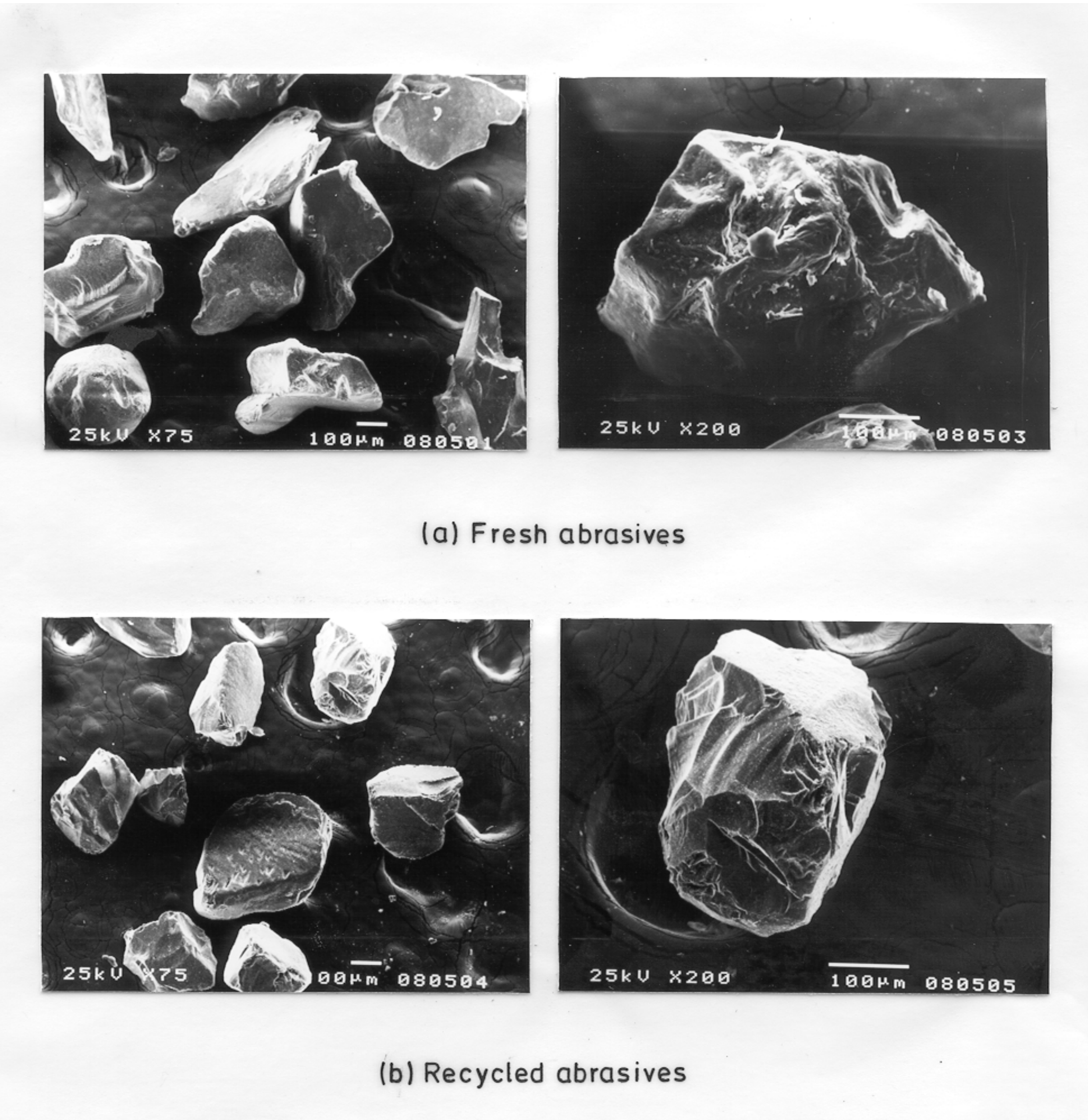

Figure 5. Scanning Electron Micrographs of fresh and recycled abrasives

10th American Waterjet Conference
August 14-17, 1999: Houston, Texas

Paper **31**

A NEW TYPE OF HIGH PRESSURE WATER JET MILL

Fang Mei, Gong Weili, Chen Yufan
School of Resources Engineering
University of Science & Technology Beijing
Beijing, P.R. China

ABSTRACT

The bright prospects for material disintegration with high-pressure water jet have been proved in a great deal of investigations undertaken by many scholars. The existing water jet mills are far from being satisfactory for extensive application in industries. A new type of water jet mill, based on the principle of self-resonating and the abrasive entrained water jet, is proposed in the paper. The self-resonating water jet mill is expected to be of high grinding efficiency and less energy consumption with low primary costs, continuous operation and long service life. A series of experiments were conducted for optimization of the structural parameters of this new water jet mill, as well as testing its performance. The obtained experimental results show that the new water jet mill is advantageous over the existing ones. The study indicates very good potentials for the practical application of the self-resonating water jet mill in material ultra-fine comminution.

1 INTRODUCTION

The high-pressure water-jet (hpwj) as a tool for cutting, cleaning and excavating operations is well known and well accepted by many industries. The hpwj application for materials comminution, however, is an ultrafine comminution technology newly developed in the past dozen years.

Mazurkiewicz et al. (1992) introduced their study on hpwj application for materials disintegration, involving in wood pulping, waste paper pulping, municipal solid waste recycling, as well as their outstanding invention of dual-disc water jet mill for coal and minerals comminution, starting new chapter of hpwj technology. The dual-disc hpwj mill, in combination with the existing mechanical mill, can be regarded as the first set of water jet mill based on straight water jet.

Another type of water jet mill is based on the principle of DIAjet, conventionally referred to as a high-pressure homogenizer. A number of companies and institutions develop and produce high-pressure homogenizer such as AKW (Germany), APVRASNNIEA/S (Denmark), and CUMT (P. R. China). The third type of water jet mill is based on the principle of abrasive entrained water jet (AWJ). Its typical model is the target-type water jet mill developed at USTB (Fang Mei et al., 1997, P. R. China), having been put into industrial application for ultra-fine mica comminution.

In comparison with conventional ultra-fine grinding equipments, the water jet mills has the advantages of high grinding efficiency, less energy consumption, simple structure and substantial savings with regard to the manufacture costs, as well as low maintenance and space requirements. However, they still have some drawbacks in techniques. For instance, the dual-disc hpwj mill has mechanical moving parts and not made full use of the jet energy. DIA jet based mill is most energy efficient, but its application is severely limited for its complicated structure, high manufacture costs and inaccessibility to continuous operation. The target-type water jet mill is very simple in structure, easy to operate, but is inefficient in use of the jet energy due to its abrasive entraining mechanism, which makes the abrasive particles unable to be well mixed with jet stream and fully accelerated.

In principle, both straight water jet and abrasive water jet on which the existing water jet mills are based all belong to continuous water jets. Among various kinds of water jets, cavitating jets and pulsating jets are new types, which are of high efficiency. As far as the means to create cavitating jets and pulsating jets were concerned, the self-resonating is an advanced one, which features with simple structure and high reliability. Combining abrasive entrained water jet with self-excited oscillator forms a new type of water jet that can be noted as “Self-Resonating Abrasive Water Jet (SRAWJ)”. The SRAWJ is a kind of abrasive water jet pulsed and cavitated by the built-in Helmholtz resonator, thus the jet performance was greatly enhanced.

A new type of water jet mill based on the principle of SRAWJ is proposed, referred to as self-resonating water jet mill (SR water jet mill). In the presence of SRAWJ, the structure of SR water jet mill is as simple as that of the target-type water jet mill, meanwhile, the energy efficiency is nearly the same as the DIAjet mill. The study introduced in this paper involves in the experimentation and design of the new mill. The performance of SR water jet mill is tested and optimum range of the structural parameters has been obtained.

2 SELF-RESONATING WATER JET MILL

Self-resonating, in simple words, is the occurrence of pressure disturbance when a steady jet stream passing though the exit convergent section of an Organ-Pipe Resonator or a Helmholtz Resonator. The pressure disturbance feeding bake to the resonating chamber would induce pressure oscillation. According to the theory of marine acoustics, the pressure oscillating amplitude will be amplified when the pressure oscillation frequency is consistent with the inherent frequency of the resonating chamber. Thus the fluid within the chamber is induced to self-resonate and the continuous jet was transformed into a discontinuous one.

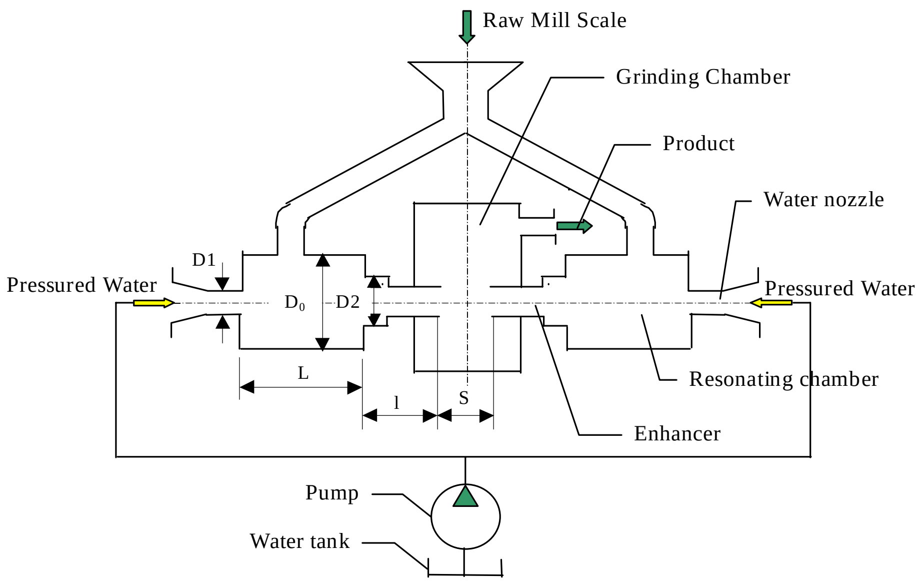

Figure 1 Schematic drawing of SR water jet mill

The self-resonating water jet mill is shown in Figure1. Pressured water through water nozzle forms a steady high-speed spray penetrating into Helmholtz resonating chamber. The boundary shear layer is formed within Helmholtz resonating chamber. Owing to the viscosity of the fluid, a series of vortex are produced by the shearing action. Since the axial symmetry of the chamber, vortices exist in the structure of vortex ring and move down stream. As the vortices collide with the exit wall of the resonating chamber, the pressure disturbance wave with certain frequency is induced and transmitted upstream. If the frequency of the pressure disturbance wave is in agreement with the inherent frequency of the resonating chamber, the disturbance wave will be amplified in the shear layer. The enhanced disturbance wave moves downstream and collides with the exit wall of the chamber again. The above process forms a closed loop, hence results in shear layer oscillating with great amplitude, then generates a pressure fluctuating field within the resonating chamber. The continuous abrasive jet is thus converted into discontinuous one.

Large vortex structure will promote cavitating effect as discussed by Li Gensheng et al. (1992). If the SR water jet mill were properly designed, the low-pressure zones in the center of the vortices would be low enough to generate gas bubbles in the fluid within the chamber. In addition, while materials are drawn into the resonating chamber, air along with material particles is entrained into the chamber altogether. The spreading of the entrained air to the cavitation zones of the fluid will produce large number of gas core. This is the relationship between the fluid pressure in the resonating chamber (p_d) and the water jet stream pressure (p_u) that can be simplified to the ratio of chamber pressure to jet pressure. The equation should also include the fluid vapor pressure (p_v) in a form that generates a term known as the cavitation index (σ) given by the relationship (David A. Summers, 1995),

$$\sigma = \frac{p_d - p_v}{p_u - p_v} \quad (1)$$

The vapor pressure p_v increases and the chamber pressure p_d decreases when the entrained air enter into the chamber. Consequently, the cavitation number decreases and the cavitation action is enhanced. Hence, the abrasive water jet modulated by the self-resonating oscillation is a pulsating abrasive jet with plenty of bubbles inside.

The vacuum is produced by the self-resonating oscillation of the fluid within the resonating chamber, causing the existence of the pressure difference between the feed bin located directly above the jet mill and the resonating chamber. The feed materials are transported pneumatically from the feed bin into the chamber by the joint action of its gravitation and the pressure difference.

The material particles entrained are whirled into the center of jet stream by the huge vortices produced within the chamber, which enables these particles to be well mixed with the stream. The enhancer fully accelerates the entrained particles. Finally form is a pulsed and cavitated jet column consisting of three phases, liquid, gas, and solid particles. Since transient velocity of pulsating jet is much higher than that of the continuous jets, being accelerated by the pulsating, the particles in SRAWJ gain greater speed than in AWJ. Furthermore, the vortex-whirled entraining mechanism of SRAWJ enhances the entraining ability and increases the entraining rate of the feed material. Based on these features mentioned, SR water jet mill is much efficient in utilizing jet energy and in comminuting material.

Inside the grinding chamber, the material particles counter-spraying from the two enhancers collide with each other and comminuted into very fine particles by the joint action of cavitating pressure and water hammer pressure. The product is discharged though the outlet of the grinding chamber.

Theoretical analyses for grinding force is derived as follow,

The cavitating jet impact pressure (Shen Zhonghou, 1998) p_i can be expressed by the Lord Rayleigh equation:

$$p_i = \frac{p_s}{635}\left[\exp(2/3a)\right] \tag{2}$$

where, p_s is the continuous jet impact pressure (stagnation pressure), $p_s = \rho u^2/2$, and a is the gas constant of the fluid expressed as the ratio of the partial pressure of the gas to the stagnation pressure at the beginning of the collapse. While $a = 1/6 \sim 1/12$, substituting a into equation (2), the relation between p_i and p_s can be obtain,

$$p_i = (8.6 \sim 124)p_s \tag{3}$$

The equation (3) reveals the fact that the cavitating jet impact pressure is 8.6~124 times as high as the continuous jet impact pressure under the same pump pressure and flow rate.

The solid particles being accelerated by pulsed jets generated from self-resonating action might be in the form of discrete particle groups. The calculation of the colliding force between the particles can be simplified to single particles impinging upon one another. The model of single particles counter-impinging is shown in Figure 2. The impinging pressure of the solid particle can be calculated by water hammer equation:

$$p_H = \rho c u_P \tag{4}$$

Where, c is the sound velocity in solid material; ρ is the density of the solid material; u_P is the impinging velocity of the particle. As the material particles entrain rate up to 20%, the particle velocity is about seventy percent of water jet velocity (Jiang Shan 1996). u, water velocity at the enhancer exit, hence u_P is 1.4 times of u, considering of two particles travel in the opposite direction. According to equation (4), the particle impinging pressure p_H can be further expressed as:

$$p_H = 1.4\rho c u \tag{5}$$

For instance, comparing p_H to the continuous jet impact pressure p_s, while $\rho = 7000\,kg/m^2$, $c = 4000\,m/s$, $u = 300\,m/s$, from equation (5) and $p_s = \rho u_P^2/2$, The obtained results are,

$p_H = 11760 MPa$, and $p_s = 617.4 MPa$. That is, the water hammer pressure p_H is 19 times as high as the continuous jet impact pressure p_s.

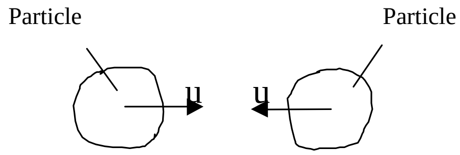

Figure 2 Model of single particle counter-impinging

The theoretical analysis results indicate that the self-resonating water jet mill has higher comminuting efficiency than the water jet mill based on AWJ under the comparable conditions.

3 EXPERIMENTAL STUDY

The experiments conducted were designed for understanding the relationship between the structural parameters and the output rate of the SR water jet mill. Initial conditions are, the raw material (permanent-magnet ferrite products) is mill scale with particle size range from 0.1~3 mm, pump pressure 45 MPa, flow rate 75 $l/\min$, pump power 75 KW. The jet mill output rate is defined as the ratio of particle grade under 75 μm to the coarse of above 75 μm.

The obtained experimental results are shown in Figure3 ~ Figure7. The output rate of the SR water jet mill versus chamber diameters shown in Figure 3. The optimum chamber diameter is in the range of 40~50 mm, within which higher output rate may be achieved.

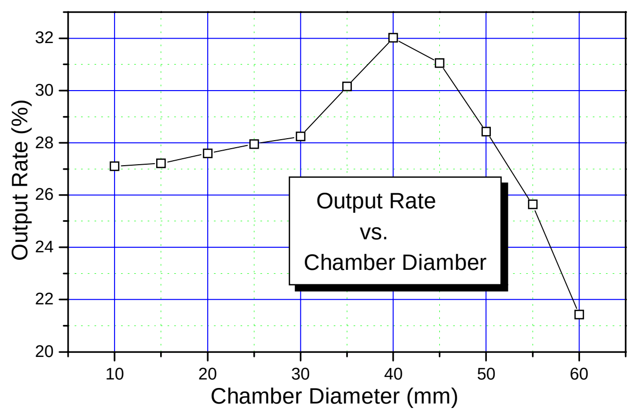

Figure 3 Output Rate vs. Chamber Diameter

The correlation between the output rate and chamber length is shown in Figure 4. When the chamber length is under 10 mm, the output rate of the water jet mill nearly remains stable. When the chamber length is above 10 mm, the output rate increases rapidly, and the maximum output rate is achieved at the chamber length equal to 14 mm. The output rate decreases while the chamber length from 14 mm to 16 mm, beyond 16 mm drops steeply. The output rate trends indicates an optimum chamber length exit, that the jet pressure oscillating amplitude generated in self-resonating will reach its highest point, and the output rate reaches its maximum value. This optimum length depicted in Figure 4, ranges from 13 mm to 16 mm.

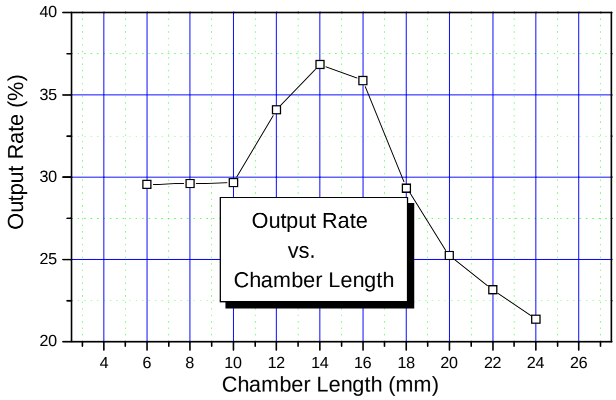

Figure 4 Output Rate vs. Chamber Length

Variation of the output rate vs. the variation of the enhancer diameter has shown in. Figure5. The water jet mill output rate is lower, when the enhancer diameter is under 6 mm, for the material particles (feed size, 0.1~3.0 mm) tend to be blocked. When the enhancer diameter is above 8 mm, the output rate declines rapidly, for the radial diffusion of the jets occurs while the enhancer diameter increasing. The appropriate enhancer diameter range from 6 to 8 mm as the material particles could be fully accelerated without clogging and jet diffusing.

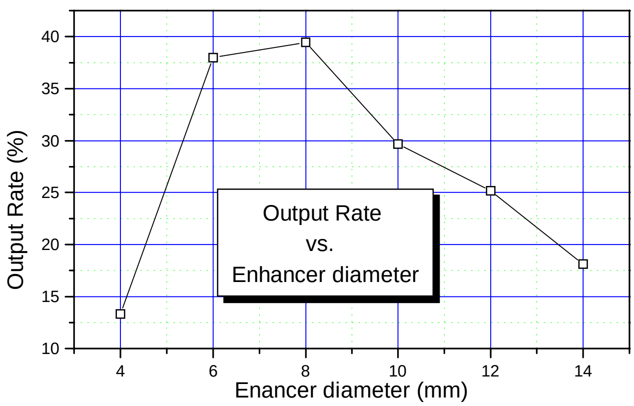

Figure 5 Output Rate vs. Enhancer Diameter

The relationship between the output rate and the length of the enhancer is presented in Figure 6. The output rate varies little before the enhancer length reach 60 mm. The output rate increases when the length increases, at 70mm, that the output rate climbs up to the highest point. Within the range of 60~80 mm of the enhancer length, higher output rate is achievable, for a suitable distance in the enhancer is indispensable so that the particles could be fully accelerated. The output rate declines sharply at an enhancer length over 80 mm for the energy loss.

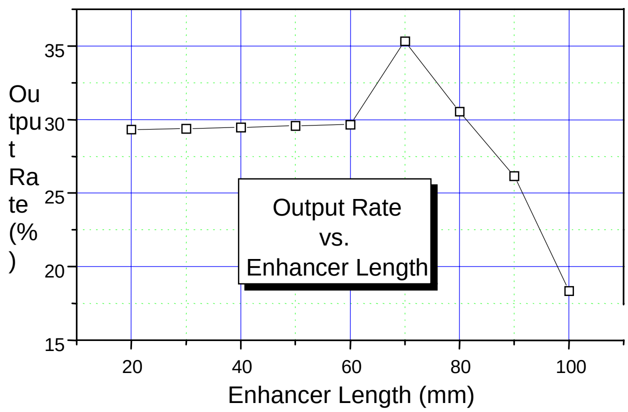

Figure 6 Output Rate vs. Enhancer Length

The variation of the output rate verses the standoff distances is shown in Figure 7. The output rate increases slightly at the standoff distance under 30 *mm*, at which the output rate attains to the maximum value, then decreases steeply. In case of smaller standoff distance the air bubbles produced by self-resonating collapse and vanished at the target (refers to material particles) before the bubbles grew up. The overlong standoff distance leads to the descending of the output rate, as the axial jet velocity decaying while the standoff distance increasing. The appropriate standoff distance falls in the range of 25~35 *mm*, within which the cavitation effect is stronger, thus the highest output rate achieved.

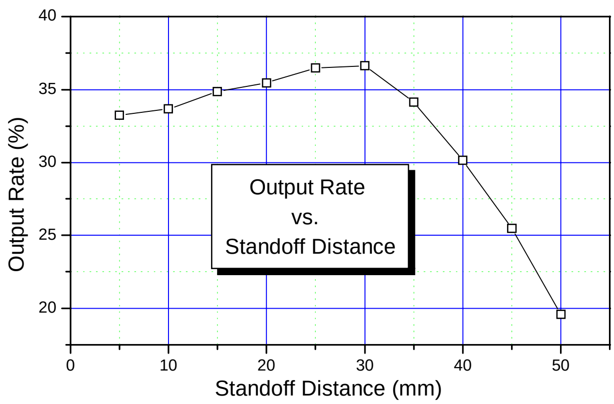

Figure 7 Output Rate vs. Standoff Distance

A test for comparison of the performance between the self-resonating water jet mill and the AWJ based water jet mill was made with three kinds of feed material size distribution, 0.1~1.0 *mm*, 1.0~3.0 *mm*, and 3.0~10.0 *mm*. The obtained experimental results are depicted in Figure8. When the feed material grades are 0.1~1.0 *mm*, 1.0~3.0 *mm*, and 3.0~10.0 *mm*, the output rate of AWJ based water jet mill are 27.10%, 9.70% and 6.19%; the output rate of the SR water jet mill are 44.34%, 24.39% and 8.11%. The later are 1.64, 2.51 and 1.31 times as high as the former respectively. The grade of feed material within 3.0~10.0 *mm* is in the shape of thin slice, results in larger resistance than the small-sized material which is nearly in the shape of sphericity.

Therefore, higher output rate can be achieved when the feed grade is relatively smaller. The experimental results elucidate that the self-resonating water jet mill is of high efficiency in material grinding than that of the AWJ based water jet mill.

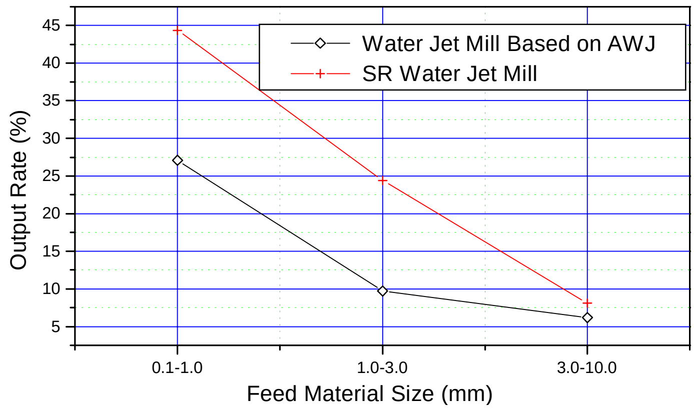

Figure 8 Output Rate vs. Feed Material Size

4 CONCLUSION

With the improvements of the abrasive mixing mechanism, the performance of SRAWJ is greatly enhanced. Therefore, the energy efficiency of SRAWJ is much higher than AWJ and close to DIAjet. Compared to the water jet mill based on AWJ the SR water jet mill is more efficient in grinding material. Comparing to DIA jet based water jet mill, the outstanding advantages of SR water jet mill lie in simple structure, easy operation, and continuous production, which allows substantial savings with regard to manufacturing costs, as well as less wear problems due to its counter-impinging for material fragmentation. Brittle materials of different hardness can be ground with SR water jet mill.

The optimum structural parameters for higher output rate were obtained:

- Chamber diameter: 40~50 mm.
- Chamber length: 13~16 mm.
- Enhancer diameter: 6~8 mm.
- Enhancer length: 60~80 mm.
- Standoff distance: 25~35 mm.

The study carried out at USTB indicates great potential for material comminution with SR water jet mill. The most important area of application for this type of water jet mill can be found in the disintegration of brittle high hardness materials. Further study is necessary to make the SR water jet mill, from an engineer’s point of view, satisfactory, so that the SR water jet mill can find its role in many industries.

5 REFERENCES

David, A., Summers, “Waterjetting Technology,” pp. 711, E & FN Spon, an imprint of Chapman & Hall, 2-6 Boundary Row, London, 1995.

Fang Mei, Jiang Shan, and Gong Weili, “Mechanism of Particle comminution with high pressure water jet,” *Proceedings of the first China Particle Science Conference*, pp.178-181, China Particle Science Association, Beijing, 1997.

Jiang Shan, “The Study of Mechanism and Technology of Comminuting Particles by High Pressure Water Jet,” Report of Post Doctoral Programe, pp.52-57, USTB, Beijing, 1996

Li Gensheng, Zhou Changshan, Xu Yiji, Zhou Guangchen, and Ma Jiaji, “Experimental Study of Impact Pressure Fluctuations for Self-Resonating Cavitating Water Jets,” *Proceedings of the Third Pacific Rim International Conference on Water Jet Technology*, pp. 91-107, Taiwan, Taiwan, 1992.

Mazurkiewicz, M., Galecki, G., “Materials Disintegration by High Pressure Water Jet-State of the Technology Development,” *Proceedings of the Third Pacific Rim International Conference on Water Jet Technology*, pp. 149-162, Taiwan, Taiwan, 1992.

Shen Zhonghou, “Application and Prospects of Water Jet Technology in Petroleum Engineering,” *Proceedings of the Third Pacific Rim International Conference on Water Jet Technology*, pp. 1-28, Taiwan, Taiwan, 1992.

6 NOMENCLATURE

Abbreviations

AWJ	Abrasive Water Jet (Here exclusively for abrasive entrained water jet)
CUMT	China University of Ming and Technology
DIAjet	Direct Injection Abrasive Water Jet
hpwj	high pressure water jet
SRAWJ	Self-Resonating AWJ
USTB	University of Science & Technology Beijing

Symbols

D_0	diameter of resonating chamber
D_1	diameter of water nozzle
D_2	diameter of enhancer
l	length of enhancer
L	length of resonating chamber
S	standoff distance

10th American Waterjet Conference
August 14-17, 1999: Houston, Texas

Paper 32

MICA PARTICLE SIZE DIMENSION DISTRIBUTION

AFTER WATER JET COMMINUTING

Fang Mei, Xu Xiaodong, Chen Yufan
School of Resources Engineering
University of Science & Technology Beijing
Beijing, P.R. China

Xu Shuhong
Beijing Information Technology Institute
Beijing, P.R. China

ABSTRACT

Evaluating the quality of various kind of comminuting results needs to study the comminuted product distribution, and also has to find an accurate way to describe the distribution mathematically. In this article, according to the fractal geometry theory, the author regarded the comminuting process as a kind of fractal formation, and set up the model of mica comminuting particle size, and deduced the distribution function from the fractal model accorded with *G-S* distribution function. The author also deduced the relation between the index of particle size distribution α and the fractal distribution dimension number D is $\alpha = E-D$. (E means the topology dimension). The comminuted particle size distribution can be described and predicted by the distribution dimension. The experiments of mica comminuting with high-pressure water-jet proved that the expected fractal distribution of the mica particle product. Additionally, the relation between comminuting pressure, nozzle diameter and fractal distribution dimension is regard as, D is directly proportional to the water pressure, while inversely proportional to the nozzle diameter, and the value of D is between *2.005-2.445*.

Organized and Sponsored by the WaterJet Technology Association

1 INTRODUCTION

The earlier study was concerned with the calculation of specific surface area and the average particle size by using the particle size characteristic function, and concerned with the formula deduction on how to calculate the partial sieving efficiency. Recently, both the calculation and the deduction were related to particle size distribution and energy consumption of comminuting process. As to the particle size distribution of the comminuted product (Xu Xiaohe, et al. 1994), they may be divided into two categories, i.e. *G-S* and *R-R* distribution.

2 MATHEMATICAL DESCRIPTION OF PARTICLE SIZE CHARACTERISTIC

G-S Particle Size Distribution Function (PSDF) is regarded as:

$$y_n = (x_n/R)^{\alpha} \tag{1}$$

where, y_n Accumulated percentage product of screen under-flow,
x_n Particle size,
R Particle size mode (i.e. the particle size in contrast with y_n=100%),
α Distribution mode , a constant concerned with the material features.

P. Rosin and E. Rammler deduced the *R-R* PSDF based on the coal particle comminuting.

$$y_n = 1 - \exp\left[-(x_n/k)^m\right] \tag{2}$$

where, x_n Particle size,
y_n Weighted percentage of screen underflow (mesh size equals to x_n),
m a constant relevant with the material features,
k a constant concerned with the breakage pattern.

According to the statistic theory, Benett acquired the PSDF of single breakage, and it is similar to the *R-R* distribution function.

$$B = 1 - \exp\left[-(y/a)^b\right] \tag{3}$$

where, B --- weight percentage of screen underflow (mesh size equals to y), however, Bennett did not endow parameters a and b with any definite physical meaning, consequently, a and b have to be fixed by experiments.

Broadbent and Collcott have discussed the particle size distribution under the condition of step by step (progressive) breakage with the method of Matrix algebra, they found that

$$B = \left[1 - \exp\left(y/x\right)\right] \cdot \left[1 - \exp\left(-1\right)\right] \qquad (4)$$

A.M. Gaudin and T. P. Meloy studied the Mineral Particle Size Distribution Function of single breakage with the theory of probability, and they deduced the following formula

$$M\left(x\right)/M_0 = 1 - \left(1 - x/x_0\right)^{\gamma} \qquad (5)$$

where ,

M_0	total weight of the crushed mineral,
M(x)	weight of screen underflow (particle diameter equals to x),
x_0	input mineral particle diameter,
γ	the breakage ratio in engineering.

R. R. Klimped and L. G. Austin got the result as follow,

$$B\left(y/x\right) = 1 - \left[1 - \left(y/x\right)\right]^{\gamma_l} \cdot \left[1 - \left(y/x\right)^2\right]^{\gamma_s} \cdot \left[1 - \left(y/x\right)^3\right]^{\gamma_v} \qquad (6)$$

where,

y	characteristic dimension of the crushed particle,
x	characteristic dimension of the particle before crush,
$\gamma_l, \gamma_s, \gamma_v$	parameters related to linear defect, surface defect, and volume defect.

Tanaka and Zhu Yi et al deduced the following equation with damage theory and probability analysis,

$$y_n = 1 - \exp\left[-\left(x_n/k\right) - \left(x_n/j\right)^2 - \left(x_n/i\right)^3\right] \qquad (7)$$

where, *k, i, j* are all constants,

Kolmogrov logarithm normal distribution function is:

$$y_n = \Phi\left[\ln\left(x_n/k\right)^m\right] \qquad (8)$$

where, y_n, x_n, *m, k* the same meaning with that of R-R Distribution Function,

Φ Gauss function .

Generally speaking, logarithm normal distribution is suitable for fine grinding, especially for super-fine grinding mineral product, most other kinds subtle powder material, such as crystal structure, sediment material and so on are fit for Logarithm Normal Distribution Function.

Since *G-S* and *R-R* PSDF and other revised distribution function are all the results of experiments, they are not able to explain the internal meaning of the particle size distribution.

In former research, most of the mathematical models that were put forward are based on two basic concept of selection and breakage. In the following parts, the mica comminuting process is simplified as fractal formation. The Characteristics Equation of the particle size distribution is based on fractal theory.

3 THE FRACTAL MODEL OF MICA COMMINUTING PROCESS

Fractal geometry, created and developed by B. B. Mandelbrot, is mainly concerned about the study of the similar objects. Simply speaking, Similarity means the total can be obtained by enlarging its limited parts. The part and the total have some statistical similarity on form, function and communication, etc. Actuarially, the large and the small fragments of the crushed mica are shown to be similar in several ways. When the geometry structure of small mica fragments are enlarged appropriately, they showed great similarity with the large ones.

In fractal geometry, fractal parameters are measured by dimension number *D* (Zhang Jizhong, 1995), based on the self-similarity theory, the dimension number *D* can be described as follow,

$$D = \ln N(r) / \ln(1/r) \tag{9}$$

where, r linear similarity ratio,
$N(r)$ numbers measured by the linear similarity ratio r.

Mica is made up of laminated structure. Large pieces are piled up from small ones, hence, forming a great deal of stratification. When mica crushed by high- pressure water-jet, water wedges were created and developed, they were lacerated continually until they were torn into tiny self-similar powder. Theoretically, the powder considered to be made up of mica fragments, which have infinite surface area and their thickness as little as possible. Therefore, mica fragments can be described as two dimensional triangle (triangle is the unit of all plane figures, any polygon can be broken into several triangles). Consequently, the breaking down process of triangles may be regarded as the model of mica comminuting. One triangle can be easily broken down into 4 small triangles, the 4 small triangles can be broken down into 4^2 smaller ones, and the program can be going on infinitely, it was shown in Figure1.

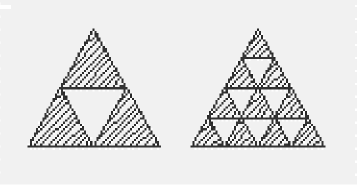

Figure 1 Fractal Model of Crushed Mica

During the comminuting process, the form of those broken pieces are the reduced pattern of the former total one, This process just satisfied the condition of self-similarity in fractal geometry.

For this fractal geometry model, each side of the triangle can be divided equally by 2, 4, 8 etc. After each crushing, each side of the triangle is 1/2, 1/4, 1/8 ... of those of the former ones.

According to the definition of partial dimension, r = 1/2, 1/4, ... N=4.
So that, $D = \ln N(r) / \ln(1/r) = 2, 1, 0.67, \ldots 0.$

Assuming the largest length of the source mica is k, x_n means the length of the particle size after n times crushing, then, based on fractal formation theory, the particle size is reduced continuously according to the linear similarity ratio r,

$$x_n = r^n \cdot k \tag{10}$$

Hence,
$$n = \ln(x_n / k) / \ln r \tag{11}$$

For
$$N^n = N^{\ln(x_n/k)/\ln r} = (x_n/k)^{-\ln n/\ln(1/r)}$$

from equation (10), we can get: $N^n = (x_n/k)^{-D}$

so that
$$y_n = (x_n/k)^{E-D} \tag{12}$$

where, E means the topology dimension.

From above, we may get the result that, mica particle size complied with a certain fractal distribution law during its comminuting process. In contrast with the equation (2) and (12), It shows that the fractal model of mica comminuting process satisfied the *G-S* partial size distribution rule, and to a deeper degree, we got the geometry meaning of the particle distribution index α in the comminuted product. The relation of α and the partial dimension number D is as follow,

$$\alpha = E - D \tag{13}$$

From the equation (12), It is safe to say, if k and D are known, the particle size distribution rule of mica are successfully determined. While k can be calculated statistically by the large particles, the largest length of the particles, and the distribution dimension number D can be calculated numerically.

Triangle is only a specific pattern of mica powder, other general geometry structure such as circle and irregular polygon. and their continually breaking down process may also be regarded as the fractal model of mica comminuting.

Table1 Influence of Water Pressure to Distribution Dimension

Water pressure (MPa)	Grade (μm) size distribution	0–43	43–75	75–150	150–250	250–500	500–1000
10	Weight (g)	3.80	2.90	6.60	10.20	25.70	31.40
	product percentage (%)	4.71	3.60	8.19	12.66	31.89	38.96
	Accumulated percentage (%)	4.71	8.31	16.50	22.16	61.50	100
20	Weight (g)	3.90	2.30	4.70	5.90	13.60	11.40
	product percentage (%)	9.33	5.50	11.24	14.11	32.54	27.27
	Accumulated percentage (%)	9.33	14.83	26.07	40.18	72.72	100
30	Weight (g)	5.30	3.60	6.90	7.40	13.70	5.60
	product percentage (%)	12.47	8.47	16.24	17.41	32.24	13.18
	Accumulation percentage (%)	12.47	20.94	37.18	54.59	86.83	100
42	Weight (g)	16.20	7.47	17.25	14.30	19.60	8.20
	product percentage (%)	19.53	8.92	20.80	17.24	23.63	9.89
	Accumulated percentage (%)	19.53	28.45	49.25	66.49	90.12	100
50	Weight (g)	9.80	5.30	8.70	7.50	8.70	2.40
	product percentage (%)	23.10	12.50	20.50	17.69	20.52	5.66
	Accumulated percentage (%)	23.10	35.60	56.10	73.79	94.31	100

Table 2 Influence of nozzle diameter to Distribution dimension

Nozzle diameter (mm)	grade (μm) size distribution	0 | 43	43 | 75	75 | 150	150 | 250	250 | 500	500 | 1000
2.4	Weight (g)	27.50	18.70	22.00	27.80	56.00	30.50
	product percentage (%)	15.11	10.00	12.09	15.27	30.77	16.76
	accumulated percentage (%)	15.11	25.11	37.20	52.47	83.24	100
1.7	Weight (g)	16.20	7.40	17.25	14.30	19.60	8.20
	product percentage (%)	19.53	8.92	20.80	17.24	23.63	9.89
	Accumulated percentage (%)	19.53	28.45	49.25	66.49	90.12	100
1.0	Weight (g)	9.50	4.75	6.60	7.30	8.00	2.35
	product percentage (%)	24.68	12.34	17.14	18.96	20.78	6.10
	Accumulated percentage (%)	24.68	37.02	54.16	73.12	93.90	100

4 EXPERIMENTAL STUDY

Here, the mica was comminuted by pre-mixed abrasive water-jet (Jiang Shan, et al, 1995), mica works as abrasive. The ordinary wet screening method has been used. Let the weight of each grade particle divided by the total amount of the sample, we got the production ratio of each particle grade, added up all the production ratio under a certain particle grade, we got the accumulated percentage. The experimental data and results are shown as Table 1 and Table 2.

5 RELATION BETWEEN COMMINUTING PARAMETERS AND DISTRIBUTION DIMENTION

5.1 Influence of Water Pressure to Distribution Dimension

Marking out the particle size distribution data in Table 1 into a figure coordinated with double logarithm axes, and they approximately forms a line shown in Figure 2. From the slope of the lines, while water pressure increasing, the fine particles in the comminuted product are increased.

So with the number of the distribution dimension, the drafted equations of all the lines in the figure are as follows,

$$y = -0.975 + 0.995x \quad (P=10MPa);$$
$$y = -0.386 + 0.83x \quad (P=20MPa);$$
$$y = -0.168 + 0.789x \quad (P=30MPa);$$
$$y = 0.268 + 0.638x \quad (P=42MPa);$$
$$y = 0.458 + 0.577x \quad (P=50MPa).$$

The slope of the line drafted is α,

Therefore, D_{10}=2.005, D_{20}=2.17, D_{30}=2.211, D_{42}=2.362, D_{50}=2.423.

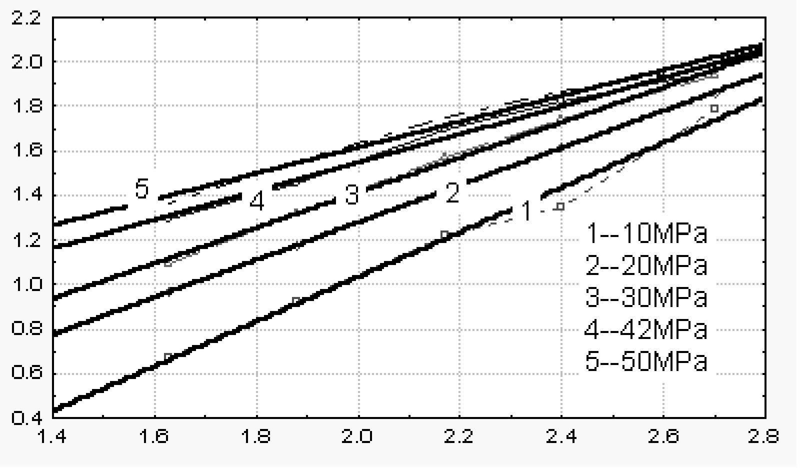

Figure 2 Particle Size Distribution of Comminuted Mica with Different Water Pressure

5.2 Influence of Nozzle Diameter to the Distribution Dimension

Marking out particle size distribution data in Table 2 into a figure coordinated with double logarithm axes, and they approximately forms a line shown in Figure 3. From the slope of the lines, the result is that, the smaller the nozzle diameter, the more fine particles in the comminuted product, and the greater the number of the distribution dimension.

The drafted equations of lines in the Figure 3 are as follows,

$$y = 0.101 + 0.675x \quad (d_1=2.4mm);$$
$$y = 0.268 + 0.637x \quad (d_2=1.7mm);$$
$$y = 0.529 + 0.546x \quad (d_3=1.0mm);$$

The slope of the line drafted is α,

Therefore, D_1=2.324,D_2=2.362,D_3=2.454.

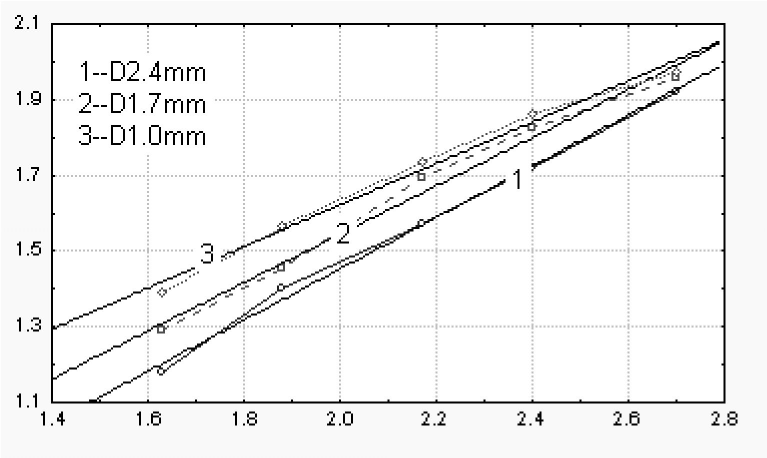

Figure 3 Particle Size Distribution of Comminuted Mica with Different Nozzle Diameter

6 CONCLUSION

(1) Fractal geometry is a modern tool for comminuting study. The primary investigation of the fractal model in the mica comminuting process showed that, the process might be regarded as the formation of a fractal structure. With such a model, that the particle size distribution is accorded with *G-S* distribution rule. The particle size distribution index α of the accumulated product is related to the distribution dimension number *D* of fractal model, that is $\alpha = E - D$. The comminuted products may be correlated to the fractal model. It is a new method for mica comminuting study.

(2) Provided that the distribution dimension number *D* is known, from Equation $y_n = \left(x_n / k\right)^{E-D}$, the particle size distribution of the comminuted product may be predicted.

(3) Experimental study shows that the distribution dimension number *D* is directly proportional to water pressure, while inversely proportional to nozzle diameter, and the value of *D* is between 2.005-2.445

7 REFERENCE

1 Jiang Shan, Bai Junying, Fang Mei, Yin Qiusheng, Particle Size Characteristic Equations of Mica Comminuted with High Pressure Water Jet, The Journal of China Safety Science, China Safety Science Journal Publishing House, Oct. 1995.

2 Xu Xiaohe, Song ShouZhi, Li Gongbo, Fractal Geometry and Comminuting Characteristic, China Mining No 1. 1994, China Mining Publishing House.

3 Zhang Jizhong, Fractal, ISBN 7-302-01868-5/Z.87, Tsing hua university publishing house, Aug. 1995.

8 NOMENCLATURE

B	weight percentage of screen underflow (mesh size equals to y),
D	the partial dimension number,
E	the topology dimension,
i, j	constants,
k	a constant concerned with the breakage pattern,
m	a constant relevant with the material features,
M_0	total weight of the crushed mineral,
M(x)	weight of screen underflow (particle diameter equals to x),
$N(r)$	numbers measured by the linear similarity ratio r,
R	particle size mode (i.e. the particle size in contrast with y_n =100%),
r	linear similarity ratio,
x	characteristic dimension of the particle before crush,
x_0	input mineral particle diameter,
x_n	particle size,
y	characteristic dimension of the crushed particle,
y_n	weight percentage of screen underflow (mesh size equals to x_n),
y_n	accumulated percentage product of screen under-flow,
α	distribution mode ,(a constant concerned with the material features),
γ	breakage ratio in engineering.
γ_l	parameter related to linear defect,
γ_s	parameter related to surface defect,
γ_v	parameter related to volume defect,
Φ	Gauss function.

10th American Waterjet Conference
August 14-17, 1999: Houston, Texas

Paper **33**

THE CARVING OF THE MILLENNIUM ARCH

E. Sandys
ARBS
New York, NY, U.S.A

S. Porter
OPHIR RF
Los Angeles, CA, U.S.A

D. Summers, G. Galecki, R. Fossey, J. Blaine, J. Tyler
University of Missouri-Rolla
Rolla, Missouri, U.S.A.

ABSTRACT

The University of Missouri-Rolla has received the gift of a major sculpture by the international artist, Edwina Sandys. The work comprises five pieces of rock carved from an initial set of three granite blocks weighing 100 tons. As completed the sculpture will be in two parts, an initial three part assembly forming an arch and two figures, standing separately. The two figures are carved from the vertical members of the three-part arch and are polished, while the outer surfaces of the original rock are left unfinished.

The blocks for the assembly are trimmed using a high-pressure waterjet lance operated on a cutting table measuring 6m by 2.4m and able to cut to a depth of 2.4m. The figures themselves are then cut from the trimmed blocks, using the same table.

The development of the technology for cutting the figures is described, as are the development and final cutting of the figures. An initial 1/12th scale model was first cut using an abrasive waterjet system on a smaller cutting table. This was followed by the cutting of a half-scale model before the final shapes were cut. Options for the different stages of the cutting are reviewed with an explanation as to the choices that were made for the different cutting operations. Problems, and their solutions, are described.

1. INTRODUCTION

The sculptor, Edwina Sandys, conceived the design of a stone circle, similar in dimension to the larger stone circle of the British megalith Stonehenge, to mark the turn of the millennium. One circle of such stones is to be located on each continent, but with the selection of the material for the circles being a choice for that continent. To distinguish the sculptures further, figures will be carved from the vertical legs of the stone uprights, and these figures will then be disposed around the circle bringing additional meaning and impact to the work.

In the discussion of this work with Scott Porter, an alumnus of the University of Missouri-Rolla, he decided that the creation of one segment of such a circle, would be an appropriate sculpture to be housed on the UMR campus, as a memorial to his parents and his late wife. The choice of the campus was motivated in part by the experience at UMR in carving the UMR-Stonehenge using high-pressure waterjets. An individual sculpture, based on the concept of the Millennium Circle was therefore developed by the artist. This has been titled the Millennium Arch.

Artist's impression of Millennium Arch on proposed site at Castleman Hall
The height and color of the sculpture are somewhat exaggerated.

Figure 1. Artist's Concept of the Millennium Arch.

In concept, the Arch will consist initially of a trilithon of two vertical stones, capped by a horizontal lintel. The legs of the arch will each measure some 15 feet tall by roughly 5 feet wide and 30 inches deep. The legs will be recessed some eighteen inches into the ground and some six inches into the capstone, which measures some 15 feet long, 3 feet high and 42 inches wide. There will be an overhang around the capstone of roughly six inches on each side of the vertical legs. The monument is to be made from Missouri Red Granite, a rock quarried in the South-Eastern part of the state. One figure will be carved from each of the vertical legs - one being a male figure and the other female. These shapes (which for identification will be called positives) are to be cut from the rock so that an inverse shape (the negative) is left in the vertical stone. The interior surface of this cut, and the surfaces of the positives are to be polished while the rest of the rock is to be left in a natural form. Because of the experience at the High Pressure Waterjet Laboratory in carving granite, and the need for the thin precise cut that such a technique would generate in separating the positive and negatives.

2. INITIAL EXPERIMENTS

In early discussion of the size of the sculpture the size had centered around a rock thickness of some eighteen inches. As the design evolved, however, this was changed to reflect a more appropriate measurement for the size of the piece, and ultimately a thickness of thirty inches was fixed by the artist. This dimension had several immediate impacts on the manner in which the rock was to be prepared. In the very earliest discussions it had been anticipated that the positive could be carved from the rock using a single, slow moving 10,000 psi abrasive slurry jet system. Earlier work at UMR had shown that it was possible to cut rock to a depth of eighteen inches with such a system, although the cutting speed would be quite slow. However, the additional depth of cut made this approach more difficult. In addition, another concern became evident. In order to establish the parameters for the method of cutting the rock, and to get some idea of the relative benefits of the different approaches, a test block of granite was prepared. For simplicity this was a single block of the Red Granite measuring 4 feet to a side, which was mounted on a turntable. Different cutting heads could then be mounted above the rock which would turn below the jet cutting a slot into the upper surface of the rock.

At the 14th International Conference on Waterjet Technology in Brugge, the research team at Cagliari (ref. Bortolussi, et at.) had found that by speeding up the speed at which an abrasive jet cuts over a steel plate, that the surface of the cut could be kept smooth. This is a critical issue in the carving of the sculpture. With the rock being thirty inches thick, any roughness in the cut edges will make it impossible to separate the positive after it has been cut out. A test was therefore carried out with a DlAjet system, with the relative traverse speed of the rock under the nozzle being set at 400 inches/min the speed recommended by the Italian team. For the first few inches the slot walls were relatively straight although it was difficult to remove all the garnet from the slot. In these tests a 5,000 psi system was used, at a feed rate of 10 gpm, with 1 lb/gallon of 40 mesh garnet sand as the abrasive. After six inches of cutting depth, however, it was clear that the walls of the slot were becoming irregular and it could be anticipated that this roughness would get progressively worse as the cut deepened. This would make it impossible to separate the two components, and this alternative was therefore not practical.

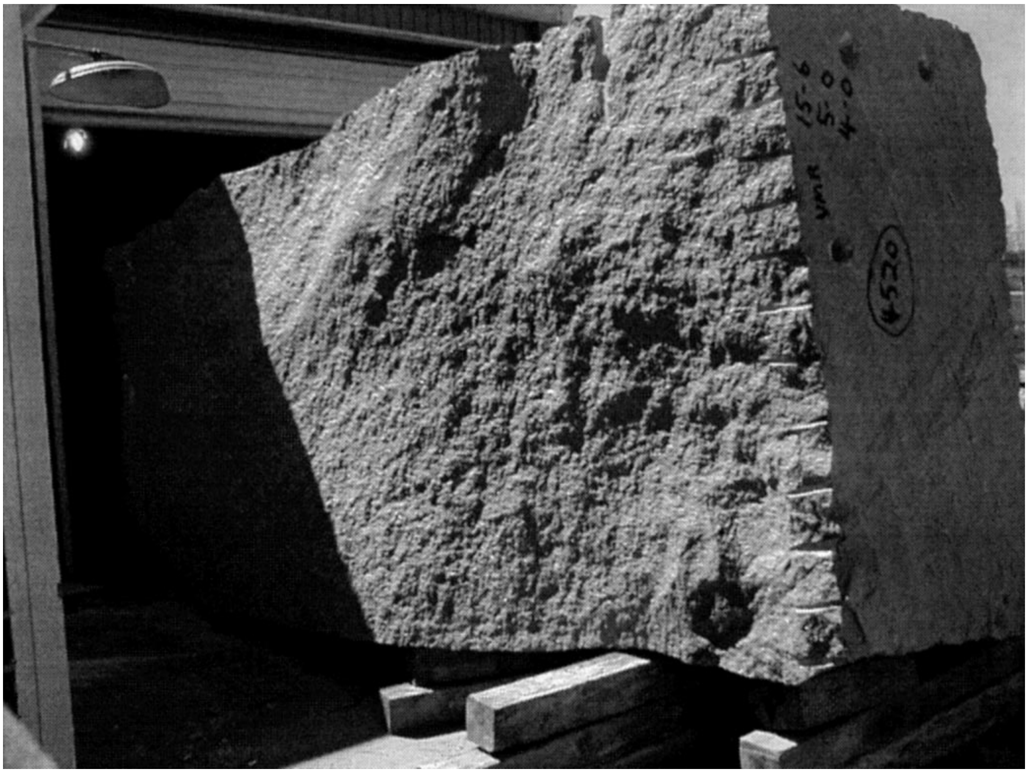

Figure 2. Shape of one of the rocks as received.

Figure 3. Cutting results from the small test block (The DIAjet cut cannot be seen as it was made on the underside of the block to stop the sand filling the slot).

Further consideration of the use of conventional abrasive jet techniques also raised similar concerns. In a normal abrasive cut the nozzle does not advance into the cut, which is made at roughly three times the width of the cutting nozzle orifice. Thus, a jet coming from a nozzle 0.06 inches in diameter would have a minimum width of around 0. 1 8 inches. Any process which would cut a very thin slot would also incur the risk that the positive could not be easily separated after the cut. (This apart from the normal logistic problems of raising one 15 ton stone from the center of another.)

A wider cut was, therefore, judged to be necessary, and this would allow the nozzle to enter the cut. This would improve cutting efficiency, since the energy loss between the nozzle and the cutting point would be minimized. Two alternative processes could be considered, the same plain high-pressure waterjet technique used for carving the original UMR Stonehenge and an alternative system developed by George Savanick at the US Bureau of Mines which used an abrasive injection technique. It was decided, for simplicity and utility to use the plain waterjet system for the initial part of the work. This is partly described herein and relates to the initial shaping of the rough blocks to the overall dimensions required for the sculpture. As an initial starting point the same concepts used for the carving of the earlier monument were to be used, although the driving system would need to be changed.

3. SELECTION OF THE CUTTING TABLE

When the first granite sculpture was carved at Rolla, the cuts were made as simple straight cuts down the sides of the blocks. The mechanism to move the lance could, therefore, be made in a very simple manner. It consisted of a lightweight support beam (made from a section of radio antenna mast) on which the lance platform was moved backwards and forwards using a fractional hydraulic motor to drive a bicycle chain attached to the platform. The lance platform was made up of a vertical plate with the lance mounted on a second plate which also held a hydraulic motor which rotated the lance assembly. The lance then could be lowered (typically 1/4 to 1/3 inch) after each pass using a third hydraulic motor attached to a lead screw between the two platforms. A similar vertical drive was, therefore, built for this work.

In contrast with the earlier model, the cutting was to be carried out inside a building. This was to allow cutting to proceed during the winter months, but it imposed a limitation on the cutting system. This is because the first rock to be cut was roughly 7 feet high and the cutting lance assembly would need to begin the cut with the lance extended above the rock surface. With the building being less than 15 feet high this was not enough space to fit the lance and the cuts were, therefore, made with three separate lance lengths each of which took a cut of some 30 inches.

The complex geometry of the positive shapes also meant that the lance platform would need to be driven with an X-Y table, rather than with simple linear motion. Some time was spent in examining the options for making such a table, which had to be able to cut in a space measuring 20 feet by 8 feet with an 8 foot depth of cut. The initial thought was to use precision lead screws and build a very stable, but heavy table. However, the reaction forces from the lance would be small, and a much lighter table, using drive belts rather than the screw feed was chosen. In addition, the initial decision to use bellows to protect the guide rails proved to be expensive and would have taken some time to acquire the parts needed. The table purchased has a sliding metal cover that was, at the time thought adequate.

It is pertinent to comment that the amount of spray and fine granite chips thrown out by the cutting jet rapidly covered the table once it has been assembled. The table was mounted on an 8 foot high frame, and during the trimming process most of the paint was stripped from this by the particle impact. The grit also got into the drive mechanism of the table. However, the particles were confined, once cutting had started, by the walls of the slot. A plywood plate, covered with artificial turf, was mounted under the lance assembly and this controlled the majority of the particles. Extending wooden boards along the sides of the Y platform so that they covered the longer and more exposed mechanism of the X drive protected those surfaces. These two protective measures kept the larger particles of granite from the drives, and the fine particles, carried by the mist and spray were not large enough to pose a problem for the drive. Thus, the cutting could be achieved with a significantly less expensive drive than had originally been anticipated.

Figure 4. Rock inside the cutting table (view from above).

Motion for the cutting lance was controlled through a software program supplied with the table, running from a PC. The operations were controlled in LabView which monitored the position of the lance platform during the cut. The program and table were able to reproducibly cut down through the 7 foot block leaving a relatively flat surface prior to the second cutting operation to remove the positive figures. On only one occasion did the program appear to malfunction, suddenly moving the lance perpendicular to the slot at an inappropriate point. Although the motors stalled without damage, the table was much lighter than the rock, and as a safety relief had not been positively locked down. This glitch, therefore, moved the table, which had to be relocated before cutting could continue. As a precaution the cutting lance stabilized at a home position after each pass and this point proved very useful for making corrections to the relative positioning of the lance, and checking on movement as the work continued.

4. CUTTING THE HALF-SCALE MODEL

In order to develop experience in running the table and to better understand the parameters and problems of operation, a half-scale model of the work was first cut using Georgia granite. A block of granite was, therefore, located within the cutting table, oriented initially so that as the lance was moved in a rectangular path it would cut the face, top, back and base of the slab. The edges were to be left in a natural condition. The intent was to cut a block measuring 7.5 feet by 42 inches by 30 inches and then cut this in half to get the two pieces required for the smaller legs. The outer perimeter of the block was cut by programming a rectangular path into the computer.

Because of the peculiarities of the system, the head could not turn an exact 90 degree angle, and a small radius had to be input to the program. Since the comers affected would be buried when the sculpture was erected, this was not seen as a problem.

Several nozzle orientations were tested during the cutting of the first block, and the parameters for optimal cutting were redefined. Speed control over the rotation of the lance was found to be a critical issue. The lance moves at a speed of up to 10 feet per minute or 2 inches per second. Two opposing jets of equal angle and diameter (for balance) issue from the end of the lance and cut forward. They are oriented to cut sufficient clearance on the sides of the lance as the nozzle moves into the slot. However, the rotation speed of the nozzle is a major factor in cutting effectiveness. If the lance is rotating at 120 rpm, then a jet passes across the center of the slot every 0.25 seconds. In this time the lance has moved forward 0.5 inches, and thus, the jet passage will leave ridges in the center of the floor of the slot. If these ridges are small enough then they will break under the action of the jet. If, however, they are too wide, then they will not be removed and will pronto the path of the nozzle and lance and block the advance.

During the cutting operation on the two rocks, a higher rotation speed was found to be more effective than a slower one and during the cutting of the half-scale model the drive system for rotation was changed. First it was changed from an electric motor to an air motor. This was because the electric motor did not have sufficient power to give the higher speed ranges sought. The drive was then changed to hydraulic from air, since it was found that the air motor did not have sufficient accuracy in speed control to maintain the levels of speed in the required range during a cutting operation.

The range control of speed is important since the other dimension that must be maintained is the width of the slot. If the lance is rotating too rapidly then the depth of cut achieved on each pass is reduced and this reduces not only the advance depth but also the width. The problem that this generates is not immediately obvious but becomes apparent some four to six passes later when the nozzle reaches the plane in which the jet was cutting. At that point the slot is either too narrow for the nozzle to pass, in which case the lance sticks, or particularly with the geology of the second block, the lance is slightly deflected from the vertical by the protruding crystals. In subsequent passes below that point, the lance continues to be deflected from the vertical by the protruding rock and the deflection becomes worse as the lance cuts deeper. Eventually, the point is reached where the deflection carries the lance to the point where it contacts the other side of the slot and the movement jams.

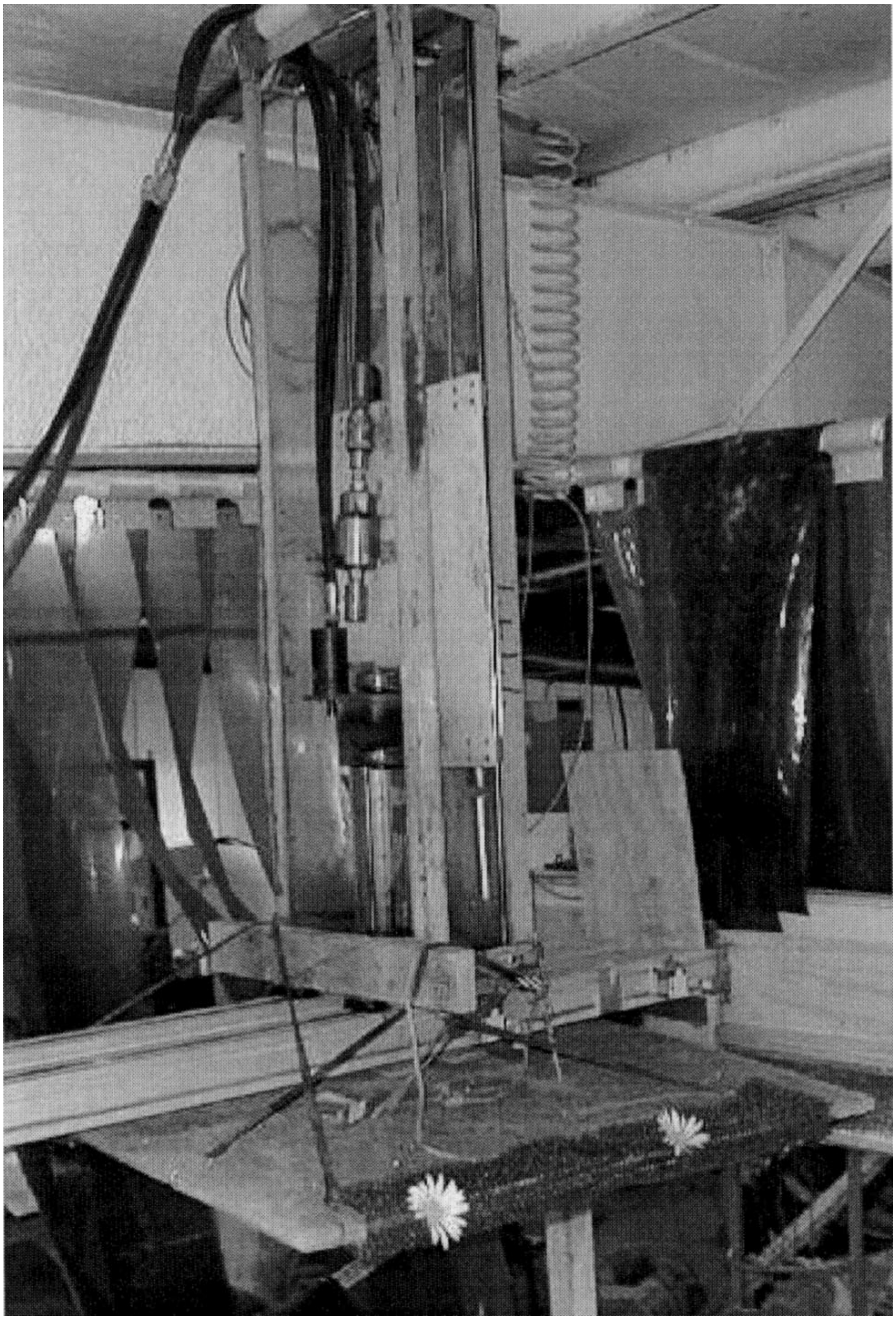

Figure 5. Detail of the lance drive mechanism and debris restraint board.

It is critical cognize that the problem does not lie in the plane in which the jet is currently cutting, but higher up the slot at that point where the protrusion from the side wall of the slot started to form. With experience, the operator learned to note the position that the lance was starting to stick as it moved around the profile. On the subsequent pass the lance would be halted at that point and, with pressure and rotation sustained, the lance was raised and lowered about an inch. This generally removed the protruding crystals and eased the passage of the lance.

5. HANDLING THE ROCK

The three rocks which make up the basic arch shape were brought to UMR "as quarried" using a drill and split technique to remove rock to roughly the desired shape. While, particularly with the capstone, the resulting rock had significant artistic appeal, the shapes were not easily oriented for placing within the table. The rock tends to split along existing boundaries to different phases within the block. Within the first of the big blocks cut three separate phases were found, with a significant and different layer of rock at the interfaces. These phases were more difficult to split and thus, the rock block shape bulged at the locations of the harder rock. These bulges took the rock beyond the dimension of the cutting table.

The rock was rolled into position on rollers, but had first to be trimmed to remove the highest point of the excess rock. Given the location of the rock within the laboratory, a non-explosive method was needed. An expansive cement known as Bristar ™ was used. This material was mixed and loaded in plastic tubes and inserted into small drilled holes over the length of fragment to be removed. Overnight the swelling of the material was sufficient to break the rock along the line of the holes, the fragment was removed and the rock was now small enough (at six feet thick) to slide into the table on the supporting rollers.

Once the rock had been positioned, the table was moved into the required position around the rock and aligned to cut to the desired shape. As discussed earlier the path of the lance was set up so that, for the half-scale the block was initially cut to 7.5 feet long by 30 inches wide, and then the block was cut in half. For the full-scale blocks the rock was cut 15 feet long and 30 inches wide. One unanticipated problem that arose was that the size of the off cuts had not been fully appreciated. The main blocks were quite stable after they had been cut, but the fragments on the side of the block were very narrow and not very stable. Thus, once the blocks were close to being finally cut the off-cut was stabilized using chains and blocks and held in position until the main block had been removed from the table. At that point, the table was moved over to provide enough room and the rock rolled over into a stable configuration.

6. TRIMMING THE FIRST BLOCK TO SIZE

When the pattern was laid out to cut the first block to shape, the table was programmed so that the slot cut would lie along the two ends of the block and one of the sides. This meant that the fourth slot would cut inside the block and roughly one foot in from the block side. On each end, any residual rock on the outside of the slot was removed as the slot cut down, reducing binding problems. It also helped to see what particular features were causing the lance to stick.

The Millennium Arch is made from Missouri Red Granite a rock which is made up of larger crystals than the Georgia granite with which the Lab has most cutting experience. The rock, in addition, was found to contain a number of different geological layers within the blocks being carved. While this variation had some artistic advantages, it proved to create some challenges in the cutting operation. This is particularly the case since the outline cut for the vertical legs meant that the lance must trim the face and back of the block, a cutting depth of 6 feet. The cut slot width was on average 1.5 inches and the lance width was 1.0 inches. There was thus, very little tolerance between the edge of the lance and the rock. Individual crystals of quartz exceeded this 0.25 inch size range on occasion. It was not possible to visually detect the changes to the rock geology along the major slot in the rock as the lance moved downwards. It was possible to monitor the position and correlate this with surface features.

Figure 6. View of the West side of the rock, showing partially removed rib, and an area ground down.

From this it became clear that there were several different zones within the rock. The block had been selected because of its predominantly darker pink (or mahogany) shade. At one end of the block a pinker zone of rock was found, and the interface between the two was made up of a zone, roughly one inch thick, of very fine crystals, which appeared to be all quartz. A zone of larger and darker crystals swept through the lower part of the pinker zone. Within the mahogany zone there was a surface expression of a stronger feature which could not be visibly detected as a change in rock structure. However, when the cutting lance was moving through these zones, clear differences in performance could be seen.

The operational parameters of the system were such that the simplest effective was to control the cutting performance of the lance was to adjust the traverse velocity. The softer rocks proved to be the pinker material and this could be cut at full speed. Interestingly the darker crystalline band within that zone could be cut at the same speed. The crystals themselves appeared to be a smoky quartz and would be left as protrusions in the rock after a pass. However, the subsequent pass would cut the rock out from under them and they did not present much change in the cutting parameters. It is probable that the softer rock could have been cut faster than it was since the slot depth in that region was typically one inch deeper than in the zone where the mahogany layer was being cut. For the majority of the mahogany layer a cutting speed of 75% of maximum kept the slot width at the size required and moved the floor of the slot down consistent with the lance movement (0.25 inches/pass or 2.5 inches/hour). The nozzle orifices were typically one inch above the floor of the cut in this rock. The jet angles were 15 degrees outward inclined. Within that zone the higher surface expression also affected the rock, since within that zone the cutting lance had to be slowed to 50% speed in order to maintain the slot dimensions (on each side of the block). Finally, in order to maintain the width of the cut around the corners as the lance moved around, the speed in the corner zone was reduced to 25% of maximum.

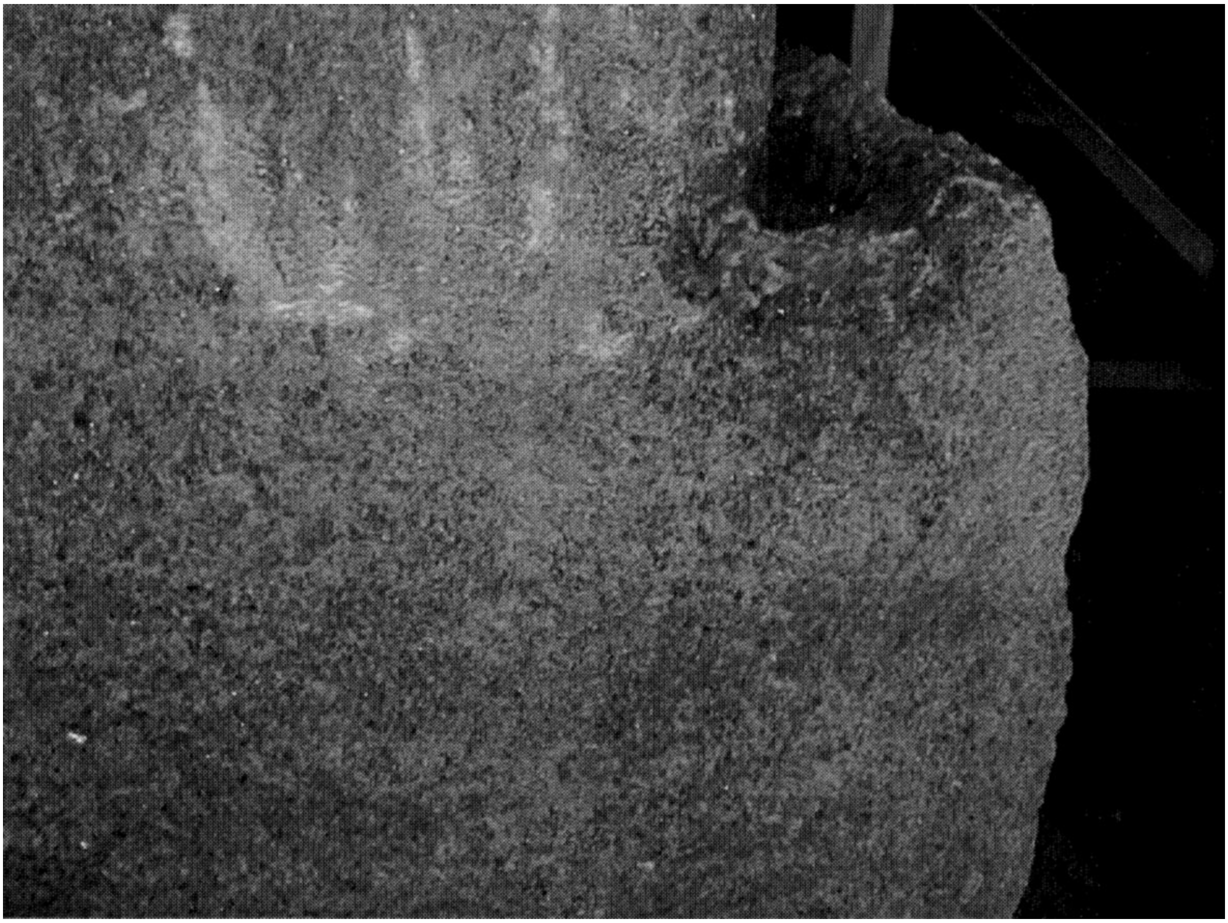

Figure 7. Showing the different textures of the rock surface.

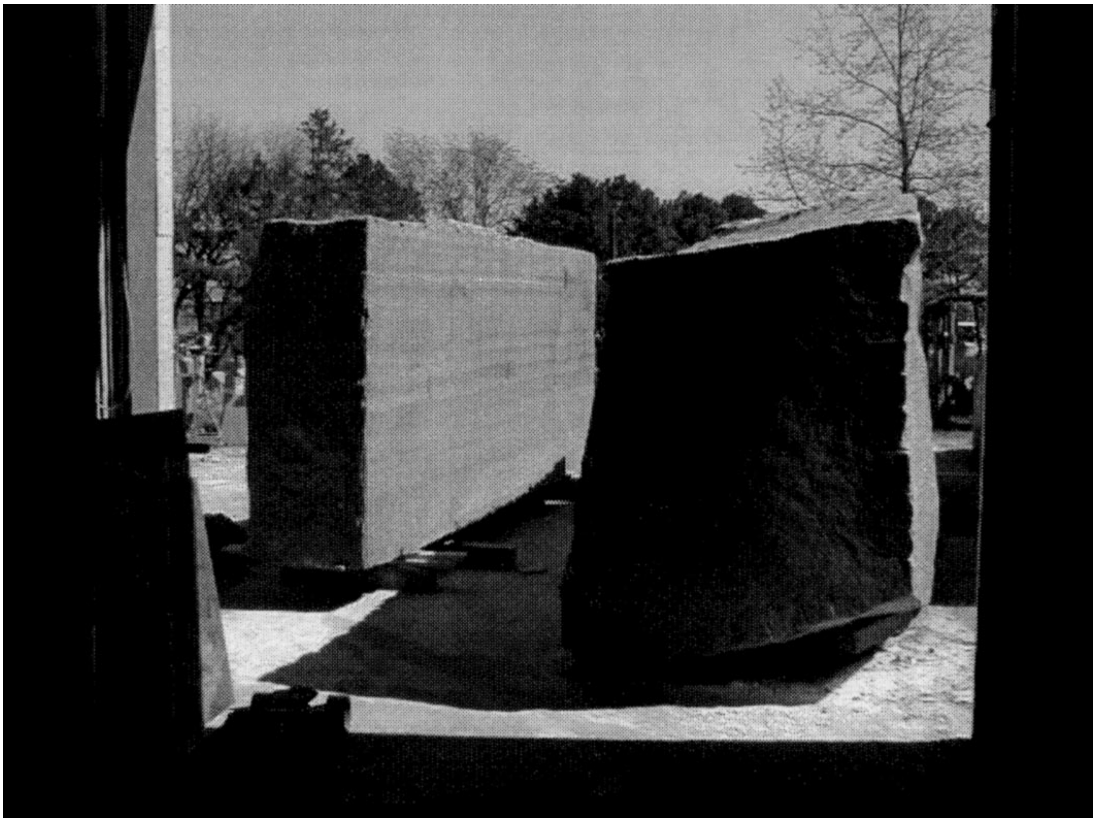

Figure 8. Before and after cutting.

Where these speeds were maintained, and this required adjustment at intervals as the zone widths moved along the cut, then the rock could be cut for intervals of several hours without problems. The process of stopping the lance and carrying out a vertical ream at the sticking points also helped to speed the cutting process. It took in all some 30 hours to cut the first of the vertical legs to shape, and as this paper is being prepared the second rock is being moved into the table for trimming to shape. We anticipate that, following this it will take two weeks to cut the half- scale models and then an additional two weeks each to cut the positives from the 30 inch thick legs. The sculpture will then be polished and the vertical legs mounted on the site. A template will then be cut to the shape and position of the legs. Based on that template two six inch recesses will be cut into the capstone, which can then be mounted in place.

7. CONCLUSIONS

There has been considerable development of waterjet use in the granite industry over the past five years, with ultra-high pressure pumps now being broadly used in quarries for extracting the primary blocks. In addition, conventional abrasive waterjets are broadly used for shaping granite inlays and tiles to provide very attractive surfaces.

In this paper we have shown that it is possible to carve rock to complex shapes with waterjets at much lower pressures, 13,000 psi, than is broadly used. These shapes can be carved in rock blocks which are up to 6 feet thick. The potential that this brings to the ability to carve even more intricate works in the future is one which is exciting and eagerly anticipated.

8. ACKNOWLEDGEMENTS

This work could not have been carried out without the gracious financial contribution and continuing involved interest of Scott Porter. Equally, without the artistic talents of Edwina Sandys we would have been nowhere. It is a considerable pleasure to recognize their efforts for the university and in working to inspire us to carry out this project.

9. REFERENCES

Bortolussi, A., and Ciccu, R., "Contour Cutting of Thick Steel Plates," 14'h International Conference on Jetting Technology, Brugge, Belgium, 1998, pp. 273-284.

10th American Waterjet Conference
August 14-17, 1999: Houston, Texas

Paper **34**

ROCK DISINTEGRATION USING WATERJET-ASSISTED DIAMOND TOOLS

R. Ciccu, B. Grosso, G. Ortu
Department of Geoengineering and Environmental Technologies
University of Cagliari, Italy

M. Agus, A. Bortolussi
Mineral Science Study Centre of C.N.R., Cagliari, Italy

J. Vašek, P. Jekl
Institute of Geonics, Ostrava, Academy of Sciences of the Czech Republic

ABSTRACT

Mechanical excavation of hard rocks using conventional tools is not yet viable from both the technical and economic point of view due to the poor performance of the equipment in terms of excavation rate and specific energy as well as to the high wear rate of the mechanical instrument if the rock is also abrasive. A new opportunity is opened by the development of tools with special design coated with a layer of polycrystalline diamond. However they are very delicate to handle because of the fragility to impact of the active tip which is also sensitive to the high-temperature heat generated by the contact with the rock. The assistance of a water jet in front of the tool is the only way for efficient cooling as well as for supporting the mechanical action in the initiation and propagation of fractures.

Linear grooving experiments have been carried out at the Waterjet Laboratory of the University of Cagliari in the frame of a bilateral programme involving the National Research Council of Italy and the Academy of Science of Czech Republic. Data of forces and displacement as a function of time have been recorded and processed by means of a computer in order to monitor the tool performance in real time. Tests have been carried out on two rock samples with different toughness by varying the vertical load (pushing force) and the features of the water jet (pressure and flowrate). Performance has been evaluated in terms of specific energy (mechanical and hydraulic) and wear has been assessed with high-resolution optical fibre microscopy.

The paper describes the laboratory set-up used for the tests and illustrates the results obtained outlining the prospects of the technology.

1. INTRODUCTION

In underground mining and civil engineering works, going below surface begins with the process of rock disintegration. Hard rocks present a special problem if mining machines with mechanical tools are to be used (Vašek 1996).

Intensive wear of the edge of wedge-type mechanical tools or their total destruction is the result of the interaction with rocks difficult to disintegrate. Wear process has been intensively studied for decades (Deketh, 1995; Verhoef, 1997) and many findings of interaction process were obtained. Steel wedges were replaced with tungsten carbide bits when harder rocks were to be cut (EU Commission, 1978; Krapivin, Rakov and Sysoev, 1990). Synthetic and polycrystalline diamond seem to be the material for the tool of the future (Field, 1992).

Parallel with the development of materials for tool bits, the possibility of water jet assistance has been studied (Fowell and Tecen, 1983; Barham and Tomlin, 1987; Kovscek and Taylor, 1988; Hood, Nordlund and Thimons, 1990; Vašek, 1992; Vašek and Mazurkiewicz, 1997; Bortolussi, Ciccu, Grosso, Ortu and Vašek, 1997).

A new experimental program on water jet assisted mechanical breakage of rocks and coal within a co-operation agreement involving the CNR Centre at the University of Cagliari in Italy and the Institute of Geonics of the Academy of Sciences of the Czech Republic in Ostrava has recently been undertaken. The first results of this co-operation are the subject of the present paper.

2. EXPERIMENTS

Linear grooving tests have been carried out on two different lithotypes (a granite and a volcanic rock, both from Sardinian quarries) under well defined experimental conditions, aiming at obtaining some preliminary indications, to be confirmed later on with further long-run experiments, concerning the possibility of cutting hard materials with polycrystalline diamond tools availing of the assistance of a water jet.

2.1 Materials

The “Rosa Beta” granite is isotropic in texture and has a holocrystal, hypidiomorphic, uneven grain structure. Its approximate mineral composition is 30.0 % quartz, 35.0 % K-feldspar, 25.9 plagioclase, 9.5 % biotite and accessory minerals. Mean crystal size is about 4 mm for quartz, 4.5 mm for K-feldspar, 2 mm for plagioclase and 0.6 mm for mica and other mafic minerals.

Other properties of interest are:

- Point-load strength: 47.3 MPa
- Porosity: 0.63 %
- Specific surface of pores: 0.04 cm^2/g

The dacitic pyroclastite, locally known as “Serrenti stone”, has a composition characterised by the presence of plagioclase, amphiboles (horneblendite), biotite, quartz and secondary constituents, in order of decreasing importance.

Its fabric is porphyritic with abundant microcrystalline matrix and frequent large phenocrysts (less than 10 % by volume). The rock is rather porous as shown by its relatively low density and by the 30% decrease in compressive strength after freezing cycles.

Some significant characteristics are reported in table 1.

Table 1. Mineral composition, physical and mechanical properties of the rock samples used for the grooving tests.

CHARACTERISTICS	Rosa Beta	Serrenti stone
- Bulk specific gravity [kg/m^3]	2,622	2,277
- Absorption coefficient [%]	0.33	
- Knoop hardness [MPa] (*)	6,442	
- Compressive strength [MPa]	165	78.4
- The same after 20 freezing cycles [MPa]		64.6
- Flexural strength [MPa]	15.6	
- Impact test (minimum fall height) [cm]	58	
- Abrasion resistance [mm/km]	2.32	
- P-wave velocity [m/s]	4,760	

(*) *Weighted average of the hardness of the various components*

2.2 Equipment

The test bench consists of a carrier platform which can be traversed horizontally along a couple of parallel cylindrical bars by means of a hydraulic piston capable of imparting a force of some thousands of N. Friction is kept low with the help of a twin pair of lubricated axial bearings. A rolling ball is placed between the piston head and a vertical plate in the platform in order to allow the vertical displacement of the pick holder which is free to move along two parallel rods, guided by two sets of bearings rigidly applied to the same platform. The pick is forced down against the work piece under a vertical load which can be varied by applying a known static weight.

The test bench is shown in the photograph of Figure 1.

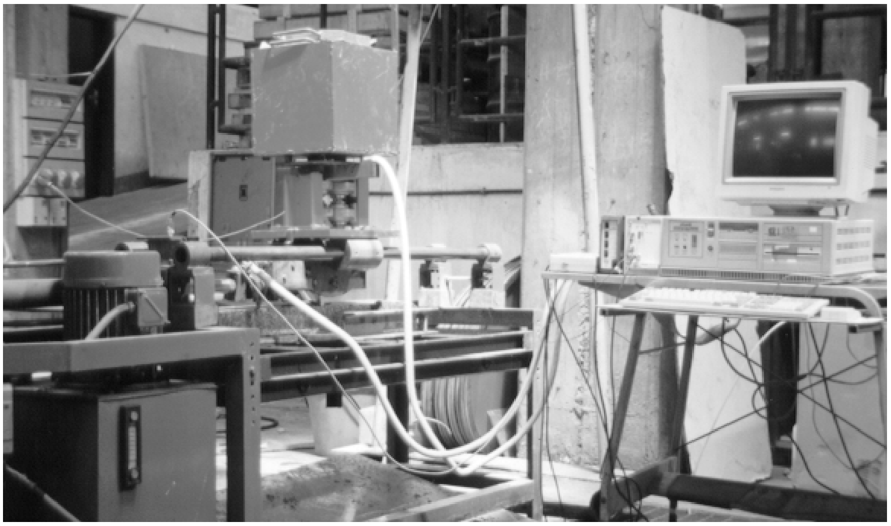

Figure 1. View of the experimental apparatus

Experimental conditions allowed by the test bench are the following:

- Traverse velocity: 0.5 m/s
- Length of the grooves: up to 0.6 m
- Depth of cut: up to 15 mm
- Horizontal force: up to 5,000 N
- Vertical force: up to 3,000 N
- Power of the hydraulic pump: 4.2 kW

The pick is mounted into a cylindrical sleeve inside the holder body. Rotation is hindered by means of a tooth-notch coupling and axial movement is controlled by a multiple-disk spring located at the bottom of the sleeve in order to absorb the dynamic impacts transmitted by the rock.

The position of the pick holder can be adjusted in order to modify the angle of attack.

The pick has the shape of conventional conical tools but the tip is cut flat so that its frontal face is a semicircle with a diameter of 12 mm, entirely covered with a 0.8 mm thick layer of polycrystalline diamond.

Consequently the area of contact with the rock a circular segment delimited by a chord and an arc with a variable length depending on the depth of cut.

A water jet can be applied in front of the pick by means of a nozzle fitted into a nozzle holder, the position of which can be adjusted in order to modify the direction of the jet with respect to the pick as well as the stand-off distance.

Water is supplied via a flexible high-pressure hose connected to a plunger pump capable of delivering a maximum flow rate of 10 l/min under a pressure of 50 MPa.

A detail of the pick assisted by a water jet is shown by the photograph of Figure 2.

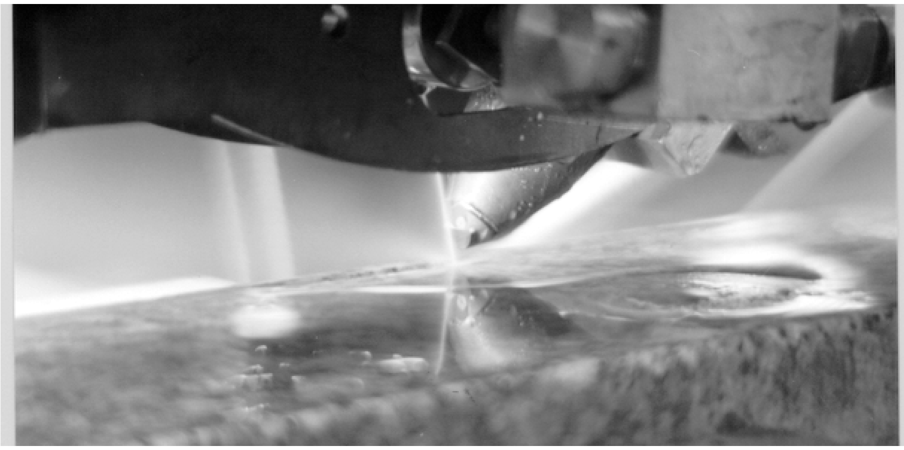

Figure 2. The waterjet-assisted diamond tool used for the experiments

2.3 Tests

Cutting tests have been carried out on each lithotype using two new picks
The vertical loads applied were the following:

- For the dacite: 1.6 kN
- For the granite: 2.0 kN

In the tests with waterjet assistance the working pressure was kept around 30 MPa at the 0.3 mm nozzle, while in the tests without waterjet the tool was cooled by a spray of tap water.

The tests with the first pick enabled to put into light the wear behaviour of the tool without waterjet assistance.

A first series of 32 grooves were made on the dacite stone reaching a total length of about 20 m without observing any major damage except for some occasional chipping near the bottom of the contact arc of the pick.

A second series of 16 grooves with the same pick was made on granite but after 8 tests (corresponding to a total length of less than 5 m) a considerable damage occurred, so that the subsequent 8 grooves were produced with a much lower depth of cut and a considerable loss of efficiency since the pick tended to slide over the rock with reduced penetration.

The tests with the second pick were aimed at putting into evidence the advantage of using a water jet placed in front of the tool.

Four series of grooves have been made as described below:

- First: 31 grooves on dacite with waterjet (total length: 18.6 m)
- Second: 15 grooves on dacite without waterjet (total length: 9.0 m)
- Third: 16 grooves on granite with waterjet (total length: 9.6 m)
- Fourth: 10 grooves on granite without waterjet (total length: 6.0 m)

During the first two series only occasional chipping in the lower tip of the tool was observed but with no loss of efficiency, as witnessed by the constant average value of the depth of cut.

No damage was also observed in the third series in spite of the much higher hardness of the rock whereas during the fourth series a major damage showed up consisting in the detachment of a large scale from the diamond layer after 9 grooves. Therefore the event of rupture and the kind of damage occurred in a very similar way for the two picks.

The features of the test rocks and the grooves obtained are shown in figures 3 and 4.

Figure 3. Typical grooves on dacite with waterjet assistance

In the case of the dacite the grooves were several mm deep and their side contour quite irregular due to the detachment of large scales. In the case of granite the grooves were much smaller and more regular due to the absence of large scales since the cut was essentially the result of a crushing action only.

No difference in the geometric features of the grooves could be observed in both rocks with or without the assistance of a water jet. However after rupture the depth of grooves in granite was reduced almost by half.

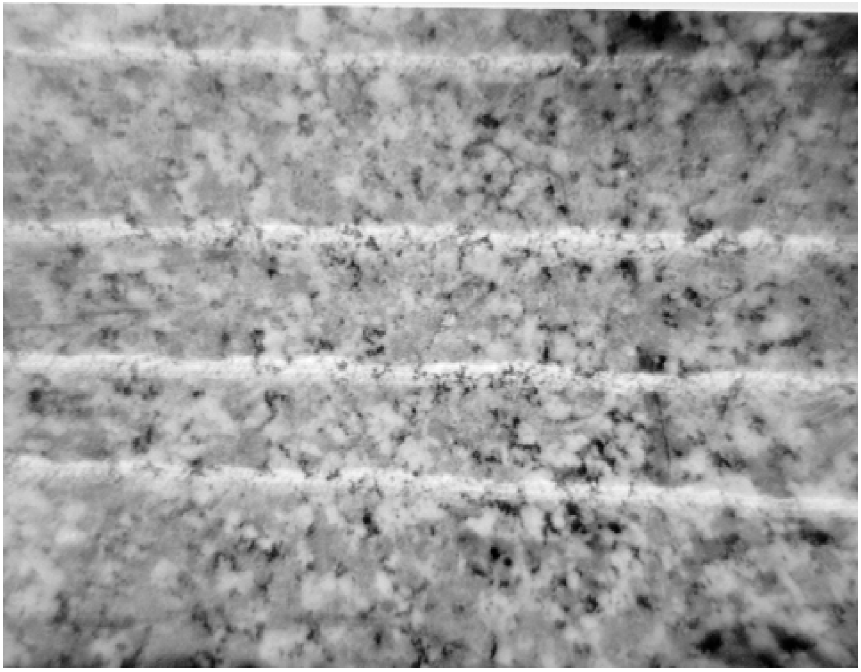

Figure 4. Typical grooves on granite with waterjet assistance

2.4 Measurements

Both horizontal and vertical forces have been measured in real time by means of piezoelectric probes connected to a high-frequency data acquisition system.

Horizontal displacement has also been measured as a function of time using a wire transducer.

The depth of cut for each test has been determined every 4 cm of groove length using a high accuracy mechanical comparator.

The state of wear of the tool has been observed visually after each test and computer photographs with an optical-fibre microscope have been taken after every group of four tests using a 20 times magnification lens.

The pick was also weighed using a balance with an accuracy of 0.05 g.

3. EXPERIMENTAL OUTCOME

3.1 Cutting results

The diagrams of horizontal and vertical forces for a typical grooving test in the dacite rock is shown in figures 5 and 6, with and without the application of waterjet, respectively. The average value of the depth of cut of the groove is also shown.

Although the difference is not particularly evident it appears that forces with waterjet are slightly lower while oscillation is less frequent and more ample especially for the vertical force.

Similar diagrams are shown in figures 7 and 8 in the case of granite.

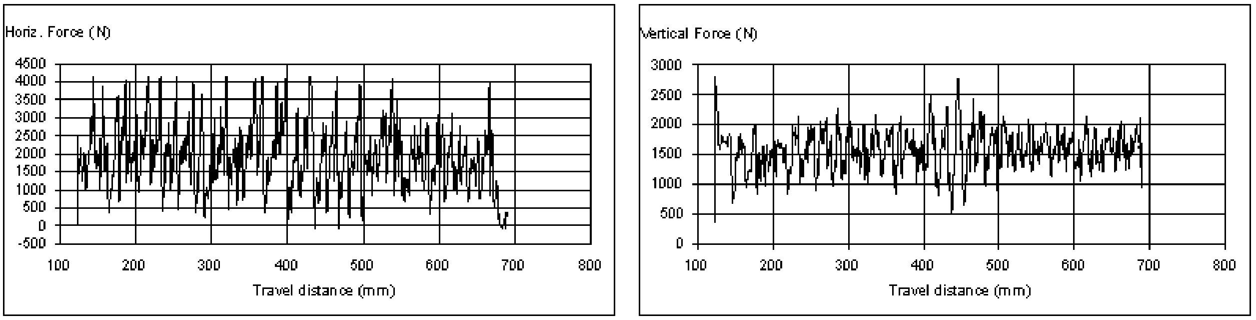

AVERAGE DEPTH OF CUT: 4.55 mm

Figure 5. Horizontal force (left) and vertical force (right) in a grooving test in dacite with the assistance of a water jet in front of the pick.

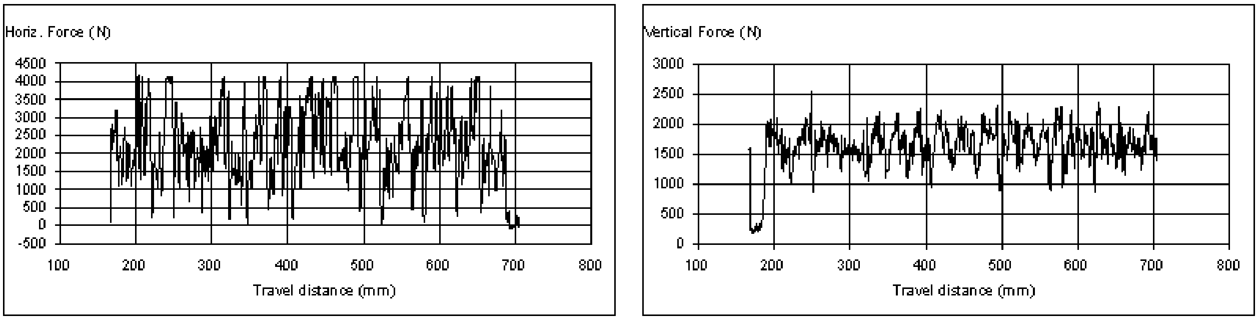

AVERAGE DEPTH OF CUT: 4.71 mm

Figure 6. Horizontal force (left) and vertical force (right) in a grooving test in dacite without waterjet

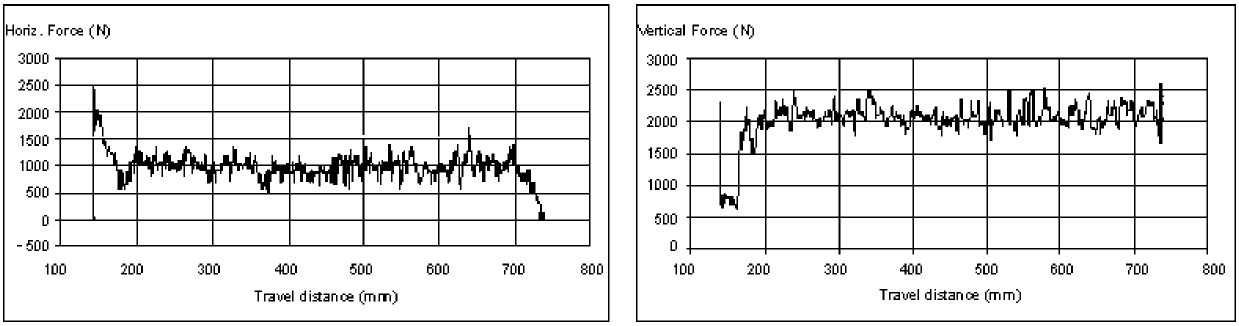

AVERAGE DEPTH OF CUT: 0.61 mm

Figure 7. Horizontal force (left) and vertical force (right) for a grooving test in granite without waterjet

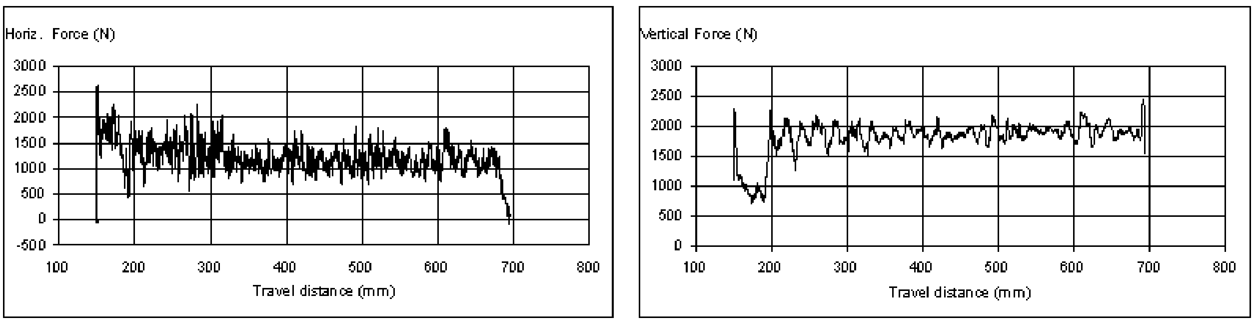

AVERAGE DEPTH OF CUT: 0.66 mm

Figure 8. Horizontal force (left) and vertical force (right) for a grooving test in granite with the assistance of a water jet in front of the pick.

Again the vertical force is a bit lower when using a water jet but in this case the frequency of oscillation appears somewhat higher.

The diagram of horizontal and vertical forces for a grooving test in granite without waterjet immediately after the rupture of the pick is shown in figure 9.

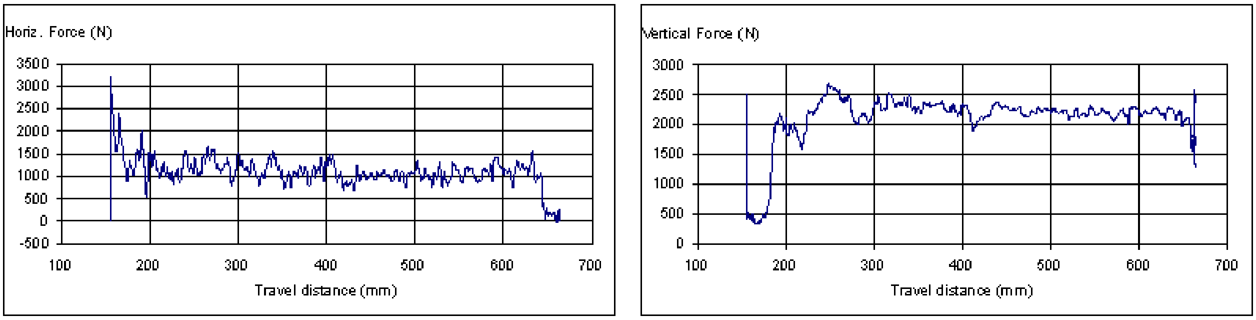

AVERAGE DEPTH OF CUT: 0.45 mm

Figure 9. Horizontal force (left) and vertical force (right) for a grooving test in granite without waterjet immediately after the rupture of the pick.

The vertical force resulted to be even higher than that before rupture while the depth of cut is much lower. At the same time the horizontal force appears steadier showing that the pick tended to slide on the rock.

3.2 Wear process

Wear undergone by the picks during the grooving tests is documented by the photographs of figures 10 and 11, a and b.

The results of the parallel series of tests with the two rocks enable to draw the following conclusions regarding the wear of the picks, although further investigation with new picks is needed in order to establish their full technical life in different rocks with or without waterjet assistance:

- In medium-tough materials like a dacite diamond-hardened tools show good strength properties and their duration can be expected to be long enough for a industrial application even without the assistance of a water jet, although no figures of duration can be provided being the research still at its early stage.

a) *b)*

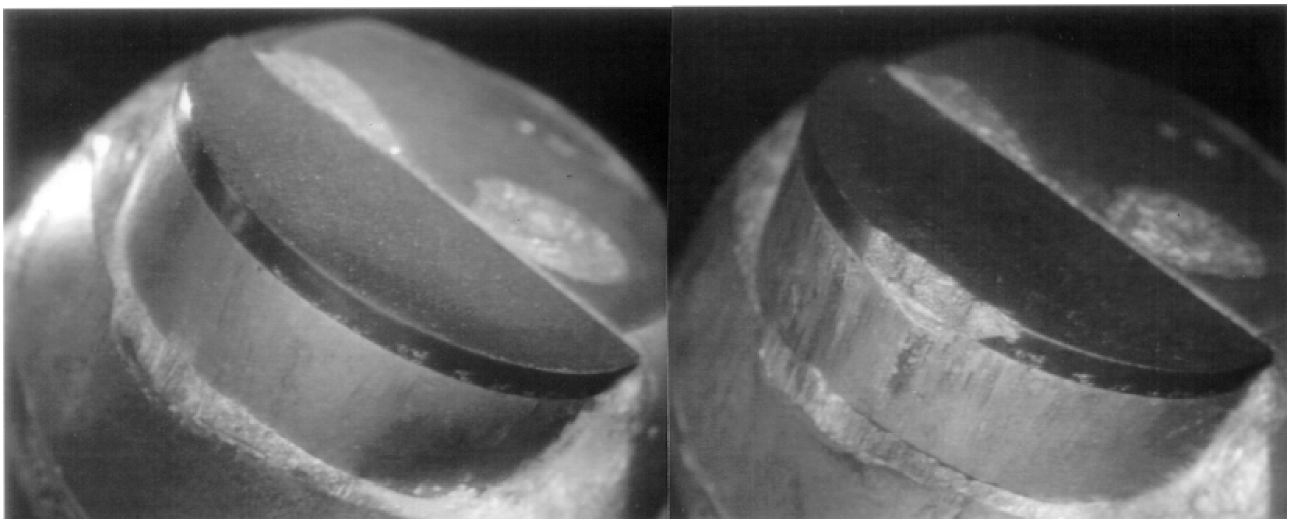

Figure 10. Aspect of the tool tip at 20X magnification in cutting experiments without waterjet assistance

a) before cutting experiments
b) after 20 m of groove in dacite

c) *d)*

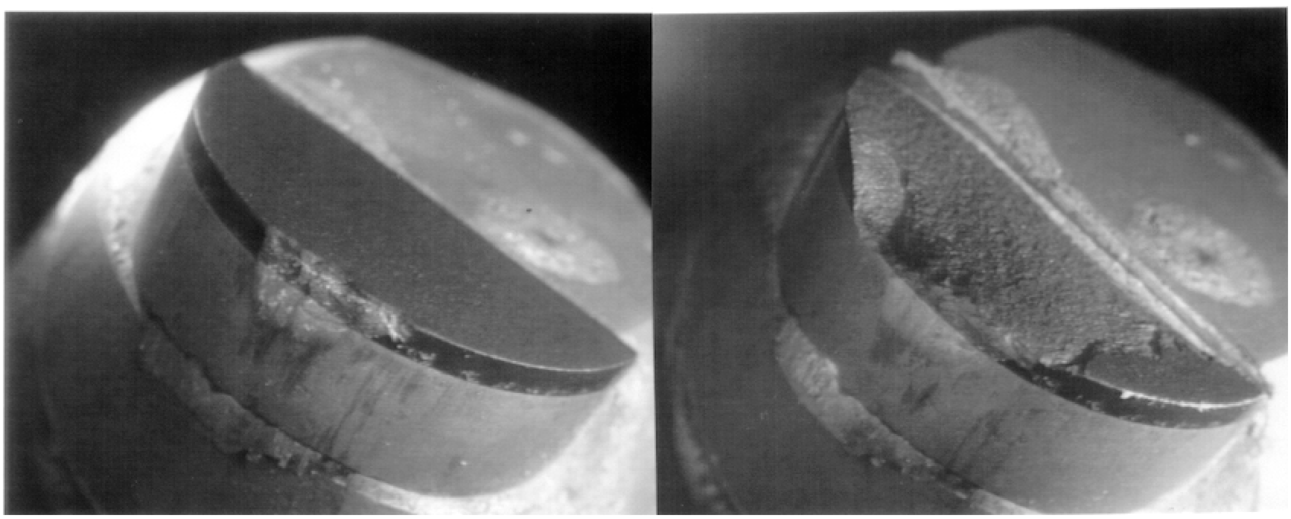

Figure 11. Aspect of the tool tip at 20X magnification in cutting experiments without waterjet assistance in granite

c) before rupture of the tip
d) after rupture of the tip

- In very tough materials like sound, not weathered granite, tool duration is much lower but it can be substantially increased with the assistance of a water jet. In fact the diamond tip broke-off into large scales after less than 5 m of groove with both picks, whereas in the case of waterjet assistance no chipping was observed after an overall travel distance of 10 m.

- It should be very interesting to investigate the behaviour of the tool in granite by applying larger forces in order to increase the depth of cut and thence the excavation rate to a level of industrial significance. Under these conditions wear rate can be higher but maybe not proportional to the applied load since stress will be distributed over a longer contact arc which is a critical factor for picks working with a sharp edge like those used for the experiments.

4. CONCLUSIONS

The first range of cutting tests with polycrystalline diamond tool with and without assistance of water jet at 30 MPa pressure were performed on softer dacite and hard granite (compressive strength: 78,4 MPa for dacite and 165 MPa for granite).

After 31 grooves (with total length of 18.6 m) without assistance of water jet and after the next 15 grooves (with total length of 9.0 m) cut on dacite, only minor wear of cutting wedge was observed. Moreover, no notable influence of assistance of water jet was detected, too.

After the next 16 grooves (with total length of 9.6 m) on granite with assistance of water jet no more wear on cutting blade was observed. On the other side, without water jet assistance, after the next 10 grooves (with the length of 6.0 m) total rupture of polycrystalline diamond layer happened and tests with this pick were finished.

The new range of tests under broader scale of water pressure and of water flow rate is scheduled in order to find out the conditions enabling to prolong the life time of this tools.

5. ACKNOWLEDGEMENTS

Work carried out in the frame of a joint research program between CNR of Italy and the Academy of Sciences of Czech Republic with the financial support of MURST (Special Projects with 60% contribution) and the support of the project No: A2086801 of the Grant Agency of the Academy of Sciences of the Czech Republic.

6. REFERENCES

Vašek, J., "Problems of cutting picks hard rock disintegration," *Proceedings of the 5th Int. Symp. On Mine Planning and Equipment Selection, Balkema, Rotterdam 1996, pp. 445-449.*

Deketh, H.J.R., "Wear of Rock Cutting Tools – Laboratory of rock cutting tools," *Balkema, Rotterdam, 1995, pp. 1-144.*

Verhoef, P.N.W., “Wear of Rock Cutting Tools – Implications for the site investigation of rock dredging projects,” *Balkema, Rotterdam, 1997, pp. 1-327.*

Krapivin, M.G., Rakov, I. J., Sysoev, N.I., Gornyje instrumenty, “ *Nedra , Moskva, 1990, pp.1 - 256.*

EU Commission, “Continuous Mining System: Stone and Stone/Coal Headings,” *Final Report on ECSC Research Project 6220-AB/8/804, 1975, pp. 1 – 64.*

Field, E.J., “The Properties of Natural and Synthetic Diamond,” *Academic Press, London, 1992, pp. 1 – 710.*

Fowell, J.R., Tecen, O. “Studies in Water Jet Assisted Drag Tool Excavation,” *Proc. of the 5th Int. Congress on Rock Mechanics, Melbourne, Australia, 1983.*

Barham, K.D., Tomlin, G.M. , “High Pressure Water Assisted Rock and Coal Cutting with Boom –Type Roadheaders and Shearers,” *Proc. of the 8th Int. Symp. On Jet Cutting Technology, Durham, 1986, pp. 57-70.*

Kovscek, C.D., Taylor, D.C., Thimons, D.E. “Techniques to Increase Water Pressure for Improved Water-Jet-Assisted Cutting,” *Bureau of Mines, RI 9201, 1988.*

Hood, M., Nordlund, R., Thimons, D.E. “A Study of Rock Erosion Using High-Pressure Water Jets,” *Int. J. of Rock Mech. Min. Sci. and Geomech. Abstr. ,1990, pp. 77-86.*

Vašek, J., Mazurkiewicz, M. “Tool/Rock Interface Assisted By High Pressure Waterjets,” *Proc. of the 9th American Waterjet Conf. , 1997, Vol. I, pp. 473-482.*

Bortolussi, A., Ciccu, R., Grosso, B., Ortu, G., Vašek, J. “Waterjet-Assisted Rock Breakage with Cutting Tools,” *Proc. of 4th Int. Symp. On Mine Mechanisation and Automatisation, 1997, Vol. 1, pp. A4-21- A4-27.*

10th American Waterjet Conference
August 14-17, 1999: Houston, Texas

Paper **35**

THE INFLUENCE OF ROCKS PARAMETERS DURING THE CUTTING PROCESS USING HIGH PRESSURE WATER JETS

A. Magyari, N. Ilias, S. Radu, A.A. Magyari
University of Petroşani, Petroşani, Romania

ABSTRACT

Nowadays in almost all of the ornamental rock open pits in Romania, for rock cutting are used conventional technologies. These technologies produce fissures in marble, granite or sandstone blocks and also some dangers in the buidings around the open pits. At the University of Petrosani was developed the technology of high pressure water jets cutting. The paper present the laboratory and in situ tests made on a waste range of materials as granite, sandstone, marble, a.s.o. and the results are compared with a theory developed, in order to improve their accuracy.

Organized and Sponsored by the WaterJet Technology Association

1. INTRODUCTION

In order to establish the influence of each abrasive water jet and rock parameter on the cutting process was developed a model which tries to explain the interaction between the jet and the rock be cut.

This model propose a means of analysing the efficiency of the abrasive water jet in the process of material (rock) cutting. The method of evalution of rock cutting starts from the premise that the jet power is used to cut a Δv volume of rock. The rock is characterized by unique parameter A, that is the resistance of the rock against the jet attach.

Regarding this model, the final simplified relation of h is obtained:

$$h = k_1 \frac{d_1 \cdot (\rho_p + \rho_0) \cdot p_0^{\frac{3}{2}}}{A \cdot u^{0,33}} - \frac{\pi}{2} \cdot d_1 \tag{1}$$

where: d_1-the diameter of the water jet nozzle or abrasive water jet nozzle; P_0-initial pressure of the jet; u-the jet moving speed on the rock; ρ_a-abrasive density; ρ_0-water density.

In relation (1) it can be noticed that the cutting process starts from a pressure P_s, called threshold pressure, as a starting point for the cutting process and, implicitly, for slit-making. The resistance of the rock against the jet action A can be identified from equation (1):

$$A = \frac{k_1 d_1 (\rho_p + \rho_0) p^{\frac{3}{2}}}{(h - \frac{\pi}{2} d_1) u^{0,33}} \tag{2}$$

This characteristic of the rock takes into account the nature of the rock and its porosity, the size of the sample, its fissures and permeability, etc.

2. EXPERIMENTS WITH CONTINUOUS AND ABRASIVE WATER JETS.

In order to perform experiments for the determination of the efficiency of hydraulic jets in rock and materials cutting and to establish the laws of the cutting process, a special stand equipped with a high-pressure pump Woma, type 1502P was achieved (maximum pressure 157 MPa, flow rate 33l/min). The stand allows the variation of the jet speed during its movement over rock or material samples, as well as of the distance between the nozzle and the samples.

Various devices for forming water jets and different types of nozzles were tested on this stand. After the tests we concluded that, for the used pressures, the best results have been given by the nozzles made of industrial sapphire, cylinder-shaped and with diameters ranging from 0.6 mm to 1.2 mm.

Both the devices with one, two or three jets and the portable cutting devices, realized according to an original conception gave unexpected results at the low and high pressures used. With these devices, slits of a certain depth were made in coal, grit stone and marble. We observed that, the deepest slits in homogeneous and abrasive rock were made. The nozzle diameter between 0.8 to 0.9 mm was found to be optimum during our tests.

In order to analyze the valability of the proposed theory we compared the model with the test results made in our laboratory.

A series of slits were realised in marble with water jets and abrasive water jets, the abrasive being carborundum.

As can be seen in figures 1 to 5 it is a good similitude between the model and the experiments. The differences, especially for water flow rate (fig. 5) and nozzle diameter (fig. 4) are caused of imperfected measurements and the few number of tests.

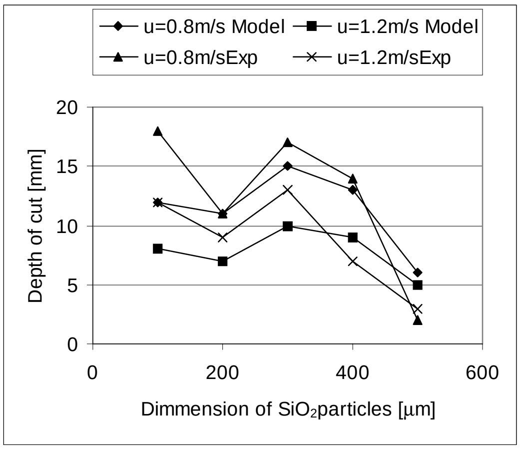

Figure 1

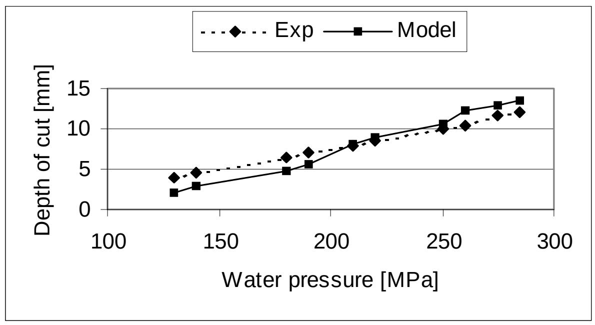

Figure 2

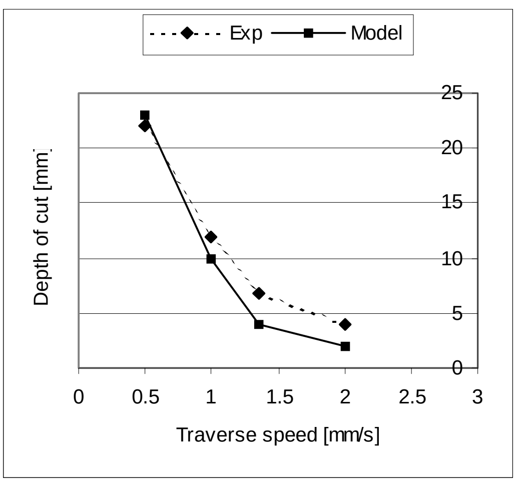

Figure 3

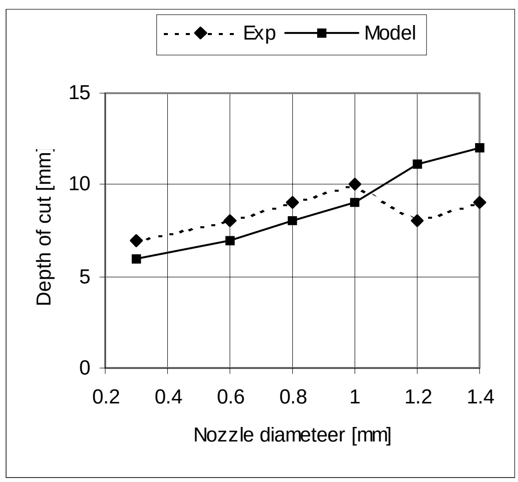

Figure 4

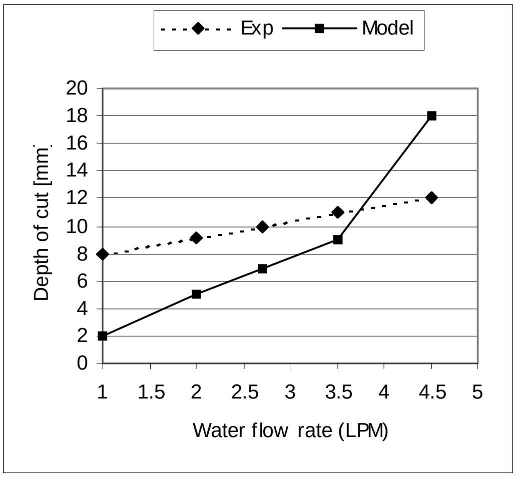

Figure 5

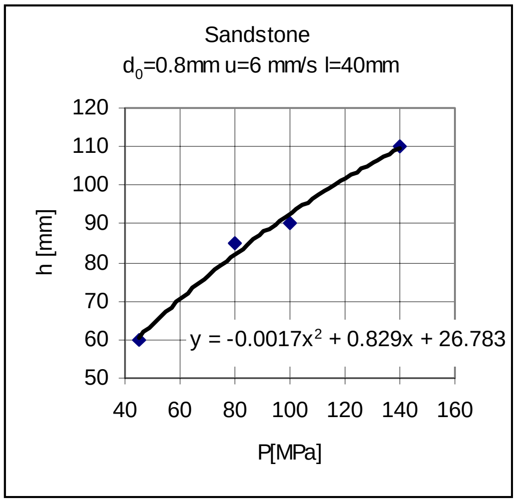

Figure 6

Another aim of the tests was to determine the dependence of the depth of the slot and the jet parameters.

a. The influence of the attack angle.

Was observed that the best results were obtained when the water jet was directed perpendicularly to the rock.

b. The influence of the water pressure.
A lot of tests were made in order to observe the influence of the water pressure. We observed that the depth of the slit is increasing with the growth of the pressure. The dependence is nonlinear (fig. 6), deepest slope were obtained in homogenous and abrasive rocks.

c. The influence of the nozzle diameter.
The slit dimensions (depth and breadth) are influenced by the jet nozzle. Though, we expect that the depth of the slit will grow with the nozzle diameter, our tests show that (fig. 7) for each range of pressure is un optimum of nozzle diameter.

d. The influence of the traverse speed.
For all the tested rocks was found a dependence $u^{-\alpha}$, where α is a constant coefficient for each type of rock. We observed that if the traverse speed is growing, the deep of the slit is reducing. All that, I recommend more passages with higher speed than less passages with lower speed.

e. The abrasive concentration effect in the cutting process.
For the all types of tested abrasives we observed some optimum values of the abrasive concentration to obtain the deepest slits. For example, in the case of cutting granite with water jet and the abrasive is carborundum (fig. 8), the best results were obtained for 0.2 and 1.2 kg/min.

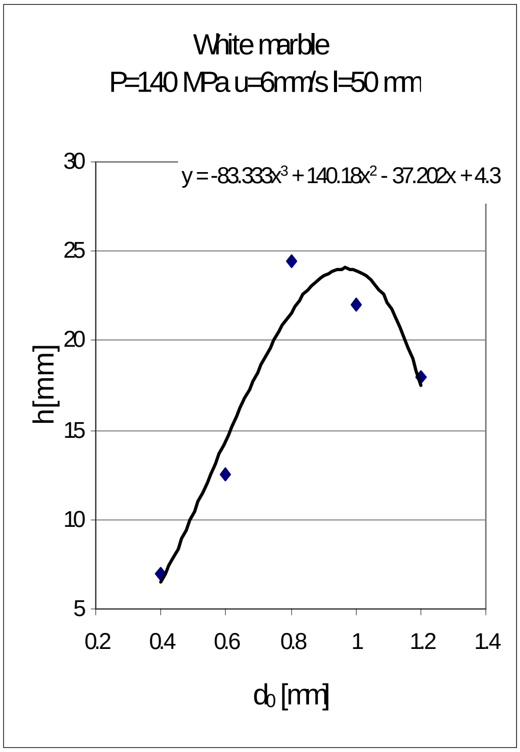

Figure 7

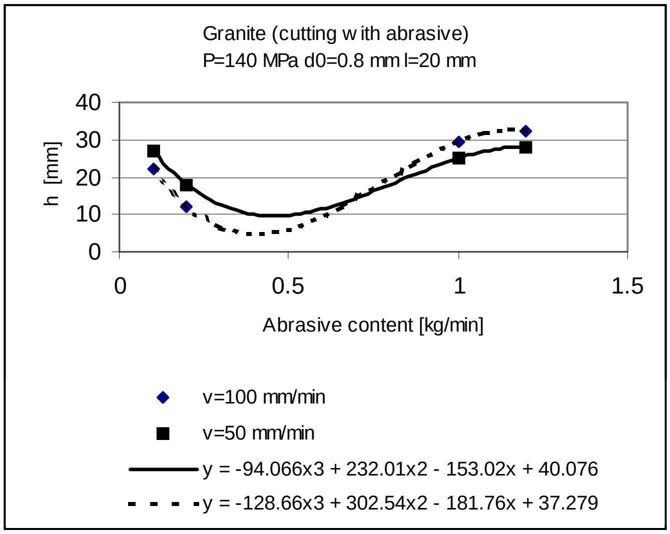

Figure 8

f. The influence of abrasive granulation.

During our tests we used abrasives with 10 to 600 µm granulation. The best results were obtained with abrasives with 100-150 µm granulation (fig. 9). The with and the surface quality of the slit is also influenced by the abrasive granulation.

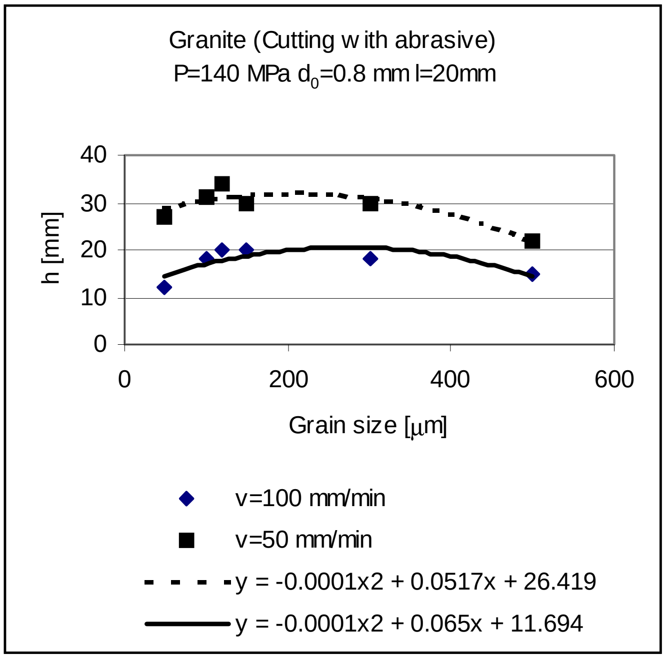

Figure 9

4. CONCLUSIONS

After some years of laboratory tests we proved that the water jet technology is the nonconventional clean technology which has given promising results. High pressure water jets and especially abrasive water jets, due to their high power transmission, are a "revolutionary" instrument and technology used for hard rock cutting and finishing, and the mentioned advantages seems to foresee it a certain future.

Considering our results and the experiments made by foreign specialists we decided to continue our research and to extend the use of high pressure water jets, to all kind of materials and rocks.

5. REFERENCES

Deliac, E., F.Decrocq, M.Diallo, D.Huck & Y.Lefin 1985. Etude de la decoupe des roches par des jets d'eau a haute pression avec ou sans additif chimique. Industrie Minerale-Les Tehnique, p.281-291.

Hood, M., R.Nordlund & E.Thimons 1990. a Study of rock erosion using high- pressure water jets. Int. J. Rock. Mech. Min. Sci. and Geomech. Abstr., vol 27, N°. 2 p. 77-86.

Iliaş, N., Magyari,A. Radu,S. Achim,M., 1993. The results of high pressure jets used in rock cutting and in assisted rock cutting. Proceedings of International Symposium on Mine Mechanisation and Automation, june 7-10, Lulea, Sweden.

Ilias, N., Magyari A., Radu S., Achim M., Magyari A.A., Water Jet and Abrasive Water Jet Performances in Materials Cutting. Proceedings of 5th Pacific Rim International Conference on Water Jet Technology, New Delhi, India, 3-5 february 1998.

Nikonov, G.P., I.A.Kuzmici & N.A.Goldin 1988. Razrunjenie gornîh parod ctruiami vodî vîsokogo davlenia. Moscova: Nedra.

Radu, S. 1991. Une nouvelle approche pour l'evaluation du decoupaged'une roche par un jet d'eau, Travail de stage, ENSM Paris, CGES Fontainebleau, august, p.40.

Summers D.A. 1990. The applications of waterjets to hard rock cutting, MINTECH-90 The annual review of international mining technology and developpement, U.S.A.

10th American Waterjet Conference
August 14-17, 1999: Houston, Texas

Paper 36

A STUDY OF NEAR WELL-BORE FORMATION PROCESSING WITH HIGH PRESSURE ROTATING WATER JETS

G. Li, J. Ma, Z. Huang, D. Zhang, Z.Shen
University of Petroleum
Dongying, Shandong, P.R.China

ABSTRACT

High pressure water jet removing impurities in formations is a new way developed recently to increase oil production and water-injection rates. This paper describes the basic principles of high pressure rotating water jets removing impurities and the laws of the tool's rotating speeds, impact pressure and variations of impact pressure with stand-off distance. The field-test results were obtained from over 200 oil and water-injection wells in Liaohe, Shengli, Zhongyuan, Huabei etc., and indicate that this technology has such advantages as: simplicity of use, low prices, high success rate, wide application, and significant effectiveness. From this, it is profitable and promising to increase production in highly watercut oilfields.

Organized and Sponsored by the WaterJet Technology Association

1. INTRODUCTION

In order to keep production stable and decrease the production-reducing amplitude, the marginal, heavy oil, and low permeability reservoirs have been more developed recently; on the other hand, various enhancing measures are being studied and applied in China and other countries. Generally speaking, there are two philosophies to enhance recovery: one, taking the whole reservoir into consideration (improving the sweeping area of injection water, the displacement efficiency, and increasing the percentage of residual oil); or consideration on a single well (taking physical, chemical and other methods to improve production). As far as a single well is considered, due to liquid pollution and impurities from plugging during drilling, completion, workover and water injecting, it is unavoidable that the near wellbore permeability become reduced, even leading to non-production. In recent years, many physical and chemical measures to deal with near wellbore formations have been developed (ГГвахитов et al, 1985; Guo,1995; Hu,1996), notably hydraulic resonation, ultrasonic wave, electric-hydraulic pulse, and artificial earthquakes etc. Although they have made some contributions, there are still problems such as complicated procedures, higher costs, limitations of bottomhole conditions, and reduction of bottomhole energy, negating effectiveness.

In this technology, high pressure water jets (lower frequency) generated through controllable rotary head impacts the formations directly; at the same time, the nozzles can also generate higher frequency oscillation waves, cavitating noise (ultrasonic wave) to remove impurities. Self-resonating cavitating jet is a new kind of technology developed in recent years(Johnson, et al, 1982), and much work has been done on its principles and functions(Li, et al,1991;1997). This shows that it has a more intense pressure oscillation and better rock erosion effectiveness. Its oscillation amplitude can reach 24%--37%; at the same pump pressure, its rock erosion rate is two to four times higher than that of common jets (Shen, et al, 1991). Also, the cavitating action can generate transient pressure 8.6 to 124 times higher than jet impact pressure (Conn, et al, 1976) accompanied with high frequency cavitating noise.

2. BASIC THEORY

The tool consists of filters, one-way valve, centralizer, rotary controller and self-oscillation nozzles (Fig 1). While working, the tool is connected to the tubings and down hole to the perforation intervals. Then, clean water (or water added to paraffin inhibitor, or expansion inhibitor or clay stabilizer) is pumped through the tubings, filters, one-way valve, rotary-jet-producing facilities to generate four jets, two of which are inclined to drive the head rotation. Its rotary speed can be adjusted by the dampener. At the same time, the tubings are moved up and down by the drawwork. There are four powerful jets at every circle impacting perforations directly. Through calculation (Yuan, 1986), the jet impact force can reach over 250N and jet power being over 130Kw. Fig 2 and Fig 3 are hydraulically pulsed curves and high frequency jet oscillating curves respectively.

The impurities in the perforations become loose and will be removed with the back flow. On the other hand, there will appear micro-fracture nets in the near wellbore formations under the repeated jet impacts. With the wave and micro-fracture spreading, the permeability increases greatly. Furthermore, the oil molecular structure can be changed with the action of high frequency oscillations and cavitating noise; as a result, the oil viscosity decreases while its flow ability and recovery efficiency increases.

Jet impacting depths can reach over 600mm due to its directed and concentrated power; the rotary speed can be adjusted from 0.5 to 400 rpm through changing pump pressure, jet deflecting angle and dampener. The whole sections of perforations can be dealt with by drawing the tool up and down, and the perforations and the surrounding formation receives three kinds of forces: direct hydraulic pulse impact, the cavitating thermal force and the ultrasonic waves. As a result, its processing effectiveness will be superior to that of single physical methods. So, the technology not only has the significant characteristics of addition simplicity, low costs, centralized energy, and deep processing depth, but jet pressure, rotary speed, processing interval and processing time can be selected according to impurity type and degree of pollution. So, with the advantages of good selection, wide applications, and easy connection with other processing methods, this technology proves both feasible and beneficial.

3. EXPERIMENTAL FACILITIES AND MEASUREMENTS

The whole tool was experimented on the multi-function experiment rack for jets in the High Pressure Water Jet Research Center. The experimental system is shown in Fig 4.

The experiment rack mainly consists of the central pipe and the 7□casing simulated wellbore. The central pipe can be driven by a motor up and down. The rotating head is installed at the bottom of the central pipe, and it will rotate while jacking in the wellbore. The height of the simulated wellbore is 500 mm. There are two holes opposite one another in the middle of the wellbore wall. One is connected to pressure sensor; the other is to pressure gauge or core container. The sensor and core container can be extended and extrapolated to simulate the different perforation depths. When the rotary head is rotating, the jets from the nozzle aim at the holes. Then the core in the container is impacted, and the impacting signal also is detected simultaneously. The signal is analyzed by HP Dynamic Signal Analyzer and printed by printer and graph plotter.

The experiment medium is clean tap water, which is pressured by two triplex plunger pumps. The single pump rated pressure is 50 MPa. The rated displacement is 90 l/min, and the jet pressure is adjusted through regulation valve. The characteristics of rotating head and impacting pressure can be achieved by changing pump pressure.

4. RESULTS AND ANALYSIS OF LABORATORY EXPERIMENTS

4.1 Rotating Characteristics of Rotary Head

The rotation of the head is one of the critical points for impacting all of perforations. At the beginning, the rotating head sealed with non-damping liquid-film was tested. However, the rotary speed was too quick to be controlled and the hydraulic energy impacted into the perforations was negated. Later, the damping liquid was used to control rotary speed through the equilibrium between rotary dynamic momentum and rotary resistance (including the seal friction, the damping-liquid resistance and so on). Under the condition of constant nozzle diameter with changing the pump pressure and damping-liquid, the rotary speed can be detected through measuring the pulse number. In this paper, the rotary speed was tested under 8 pump pressures and 3 kinds of damping-liquids (their viscosity orders from low to high are liquid 1,liquid 2 and liquid 3). The results are shown in Fig 5, from which such results can be obtained that for the same damping-liquid, rotary speed increases as the pump pressure increases apparently; at constant pump pressure, the higher damping-liquid viscosity result in the lower the rotary speed; For the damping-liquid 3 with the highest viscosity, its speed is only 0.5 rpm (pump pressure being 5.0 MPa), while for the damping-liquid 1, the highest rotary speed can reach 348 rpm (pump pressure being 20.0 MPa).

4.2 Relationship between Pump Pressure and Impact Pressure at Casing Surface

Fig 6 indicates the testing results of impact pressure at casing surface under different pump pressures. With the increase of pump pressure, the impact pressure at the casing surface will increase linearly. When the pump pressure is 4.0MPa, the impact pressure is 3.2MPa; while the pump pressure is 20.0MPa, the value reaches 17.8 MPa. So, the impact pressure is about 80- 90 per cent of pump pressure.

4.3 Relationship between Impact Pressure and Radial Distance

In order to test the processing depth to formations, the impact pressure at different radial distance was measured under determined pump pressures of 10.0, 13.0 and 20.0 MPa respectively. Taking the casing surface as the first point to be recorded, the measure point was extended to 50, 100, 200, 300, 400, 500 and 600mm one by one; the results of which are shown in Fig 7. Under the constant pump pressure, the impact pressure reduces gradually with the increase of radial distance. Under pump pressure of 13.0 and 20.0 MPa, even the radial distance increases up to 600mm; the impact pressures still reach 2.2 and 3.0 MPa respectively, which means, simulating the conditions at bottomhole, the jet impacting distance can get to over 600 mm.

5. FIELD EXPERIMENTS AND APPLICATION

5.1 Application Range and Well-Selecting Instructions

(1) Wells with high permeability and certain production capacity, but suffering from production reduction or non-production due to formation pollution near wellbore.
(2) Wells with characteristics of acid sensitivity and water sensitivity, not easy to implement acidification and other methods.
(3) Well with thin pay zones and intervals, not easy to implement other remolding methods at respective zones.
(4) Wells with low formation energy and impossible to drain after acidification.
(5) Wells that are needed to adjust output sections; water-injection wells needed to adjust injecting sections.

(6) As the pre-process before implementation of acidification, steam injection, polymer injection, sand control, etc.

5.2 Operation Facilities and Requirements

(1) One drawwork, two 400-type cementing trucks, two water tank trucks both with 15m ^{3} capacity.
(2) The implemented wells should be installed with wellhead self-seal assembly, and the return water pipe line should be connected with a water storage pool.
(3) The high pressure standing elbow, hose and tee connecting to the 400-type cementing trucks, should be cleaned and well sealed.
(4) According to the depth of perforations and pollution degree, the working pressure can be controlled from 15 to 30 MPa and the flow rate at about 400 l/min.
(5) The working medium is clean water. To ensure match between the working fluids and the rocks and fluids bottommhole, such additives as expansion presenter, block-remover, clay stabilizer, etc. should be added to the clean water according to the formation characteristics.

5.3 Operation Process and Procedure

(1) Flush well with clean water or additive water. Kill wells with expansion prevention fluid. Pullout the tubings and detect the surface for sand.
(2) Tubings should be cleaned and selected carefully according to perforation depth and its interval. The tool should be connected in this sequence: the first-filter+one-way valve + the second-filter + stabilizer + dampener +rotary head; then, the assembly is connected to the tubings and sent to the well bottom 1 m above the top perforation section.
(3) Positively wash the well with clean water to displace the impurities in the tubings.
(4) After above procedures, open up the well head to throw the ball into the tubing's to switch off the one-way valve. Then connect the cementing trucks, adjust the pressure at to 15 to 30 MPa, and pump liquid in positive circulation. At the same time, the tubings are drawn by the drawwork up and down (the slower the better) to impact all of perforations until 1 m below the last perforation; then pull up and repeat. Such procedure should be repeated four to five times.
(5) When the work is over, the tool is put down to the wellbottom, and the surface flow line should be reversed to clean the perforation sections and carry the impurities out of the well at large displacement in negative circulation for two to three cycles.
(6) Pull out all the tubings and clean the tool, lower oil well pump or water-injection tools as routine to start production.

5.4 Field Applications

From early 1995 to May.1997, this technology had been tested and applied in over 200 wells in Liaohe, Shengli and Zhongyuan etc. oilfields.

Only in the year 1995, when the Jinzhou Oil Company of Liaohe Oilfield implemented the technology in 23 oil-producing wells and effectively in 21 wells, did the rate reach 91%. The average increase amplitude per oil-well was 20 to 50% and the valid period was over 90 days. In that year, the net increase reached 8892t, and the economic benefit was 4.11million RMB. For instance, Jin2-14-02well was a producing well in Jin99 Block. In November 1993, its normal production was 6 t/d; in December this year, after checking pump due to pump leakage, nothing was produced. Data analysis indicated that the liquid supply capacity of pay section was poor. Because of the workover pollution and wax deposition during the process of oil production, the perforations were blocked. After non-production, some other block removing measures were taken, but nothing was effective. In Jan. 1995, the technology was implemented, and this well was processed by one 400-type cementing truck for about two hours. Then, the well's production capacity was recovered. During the early stage after usage of this technology, the oil production was 10 t/d. The highest production ever reached 18 t/d. In the year 1995, the accumulated increase production reached 3642t. The stimulation effectiveness of several typical wells in this Company is shown in Table 1.

From February 1996 to December 1996, the technology was implemented in 43 water-injection wells of 7 units in Shengli Oil Company of Shengli Oil Field, and 38 wells were valid, so, the efficiency rate reached 88%. The average increase of injected-water for single wells was 30 to 90 percent; the accumulated water volume was more than 300,000m^3. In 1993, the measure of chemically removing impurities was implemented in the well of 3-6-172 in Tuo-7 Block, while its water intake capacity became poorer than before. In 1995, another measure of chemical stimulating and hydraulic oscillations was tested in this well; its effectiveness was still poor and was short either. In February 1996, the technology was used in this well and significant effectiveness was made; the water-injection volume per day rose from 17 m^3 to 300 m^3. The window of effectiveness had exceeded 200 days and the accumulated increase reached 56415 m^3, greatly changed the injectivity index. The other typical wells are indicated in Table 2.

From May 1996 to April 1997, 42 wells in Zhongyuan Oilfield were implemented with the technology; 34 wells valid, the effective rate reached 94%. Among them, all of the 24 oil wells were successful; the accumulated increase of oil was 2377.7 t. 18 water-injection wells were implemented, with 16 wells valid, and the effective rate reached 88.9%. The accumulated increase of injection-water was 62564 m^3, and the average window of effectiveness was 157 days.

6. CONCLUSIONS

6.1 The technology can generate powerful hydraulic pulses impacting against perforations at bottomhole. Simultaneously, it can produce high frequency oscillating jet, cavitating thermal, and ultrasonic forces impacting the formation, effectively removing impurities near wellbore.

6.2 Laboratory experiments indicate that, with the increase of pump pressure, the rotary speed and jet impacting pressure to the surface increase correspondingly. Under constant pump pressure, jet impacting pressure decreases gradually with the increase of distance. At 20.MPa, the jets acting depth can reach over 600 mm.

6.3 Field tests indicate that with the average window of effectiveness of over 90 days, the effective rate of this technology can reach over 90%, increasing production 20%-- 50 % per oil-well on average; while in water-injection wells, they are 88% and 30%--90% respectively.

6.4 Compared with other formation processing measures, this technology has such advantages as simplicity, low costs, centralized energy, high processing depths, and wide application etc.

7. ACKNOWLEDGEMENTS

The work described in this paper was supported by the Natural Science Foundation of Shandong Province and by the China National Petroleum Corporation.

8. REFERENCE

Conn, A.F., Rudy,S.L., "Cutting Coal with the CAVIJET Cavitating Water Jet Method, " *Proceedings of the 3rd International Symposium on Jet Cutting Technology,* BHRA Fluid Engineering, Cranfield, UK, 1976

Guo, L.," Physically Processing Oil-Reservoir Achieving Good Effectiveness," *Oil Drilling and Production Technology,* Vol. 17(2), 1995

Hu, B., "Wave Fields Enhancing Production," *Petroleum Industry Press*, Beijing, 1996

Johnson, V.E., Conn, A.F., Lindenmuth,W.T., Chahine,G.L., Frederick,G.S.,"Self-Resonating Cavitating Jets," *Proceedings of the 6th International Symposium on Jet Cutting Technology,* pp.1-25, BHRA, Fluid Engineering, Cranfield, UK, 1982

Liu, B., "Comprehensive Description of Elastic Wave to Improve Oil Recovery," *World Petroleum Industry*, 1995

Li, G., Shen, Z., "Characteristics of Impacting Pressure of Self-Oscillating Cavitating Jet and Effectiveness of Rock Erosion," *High Pressure Jet*, 1991

Li, G., Shen, Z., "The Application and Prospect of High Pressure Water Jet Technology Used in Oil Production," *The 14th Young Scientists Forum Reports Collection,* pp.83-91, Coal Industry Press, Beijing, 1996

Li, G., Shen, X., "The Principle of Cavitating and Cavitating Erosion and Its Effecting Factor," *Journal of Petroleum University,* pp. 97-102, Vol. 21(1), 1997

Shen, Z., Li, G., Wang, Z., Xu, Y., "New Jet Theory and Prospects of Its Application in Drilling Engineering," *Proceedings of the 13th World Petroleum Congress,* pp.397-405, Buenos Aires, Argentina, 1991

Yuan, E.," Engineering Fluid Mechanics," *Petroleum Industry Press*, Beijing, 1986

ГГвахитов, эмсимкин, translated by Cai, T., "Using Physical Field to Produce Oil From Formation," *ИЗДательство, «Недра»,* МОСКВА, 1985

Table 1 Effectiveness in Jinzhou Oil Company

well	before usage of the technology (oil/liquid,m^3)	after usage of the technology (oil/liquid,m^3)	average production (m^3/d)	total increment (t)	valid days
2-14-02	stop	0/10	10	3642	364
2-14-04	3/6	5/32	2	201	100
2-14-11	3/60	8/78	5	422	84
12-503	3/31	11/62	8	382	C
7-25-30	1/11	8/18	7	312	C
7-34-37	2/67	15/61	13	574	C

Statistics time: the end of December 1995
"C " indicates that the well was continually valid.

Table 2 Effectiveness in Shengli Oil Company

well	before usage of the technology		after usage of the technology		increment per day (m^3)	valid days	total increment (m^3)
	injection pressure (MPa)	injection rate (m^3/d)	injection pressure (MPa)	injection rate (m^3/d)			
36172	15.0	17	12.7	317	300	170	48882
36166	14.0	67	14.6	140	73	112	5995
312176	13.0	150	11.0	300	150	105	15324
37346	12.0	0	15.0	83	83	49	2114
35G110	14.1	82	14.2	131	49	88	3967
2323	14.6	105	15.2	215	110	C	5610

Statistics time: the end of November 1996
"C " indicates that the well was continually valid.

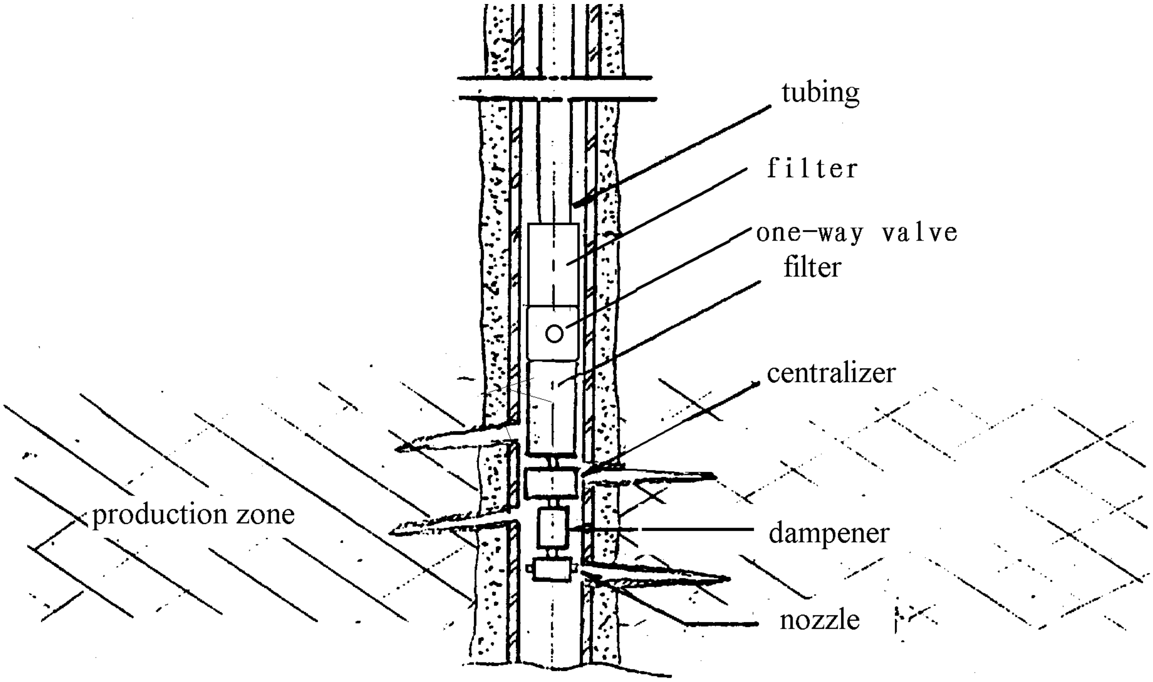

Fig. 1 **Schematic of Bottomhole Assembly**

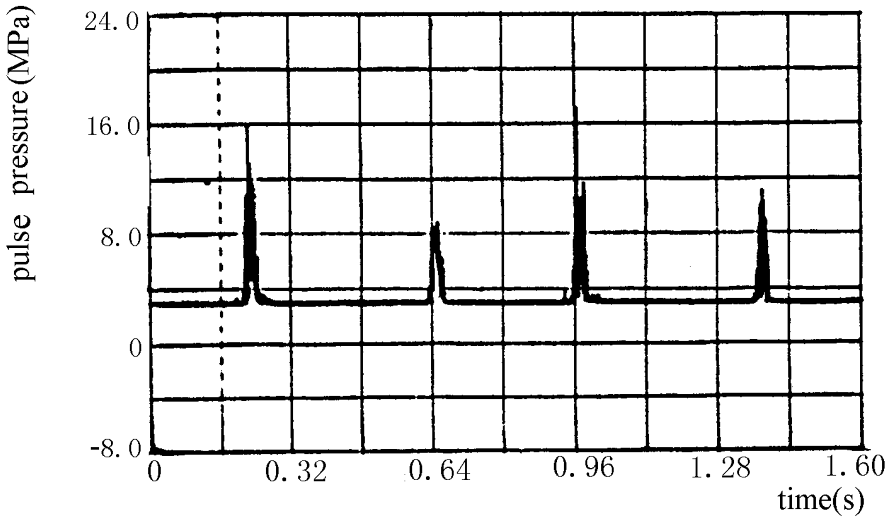

Fig. 2 Wave Curve of Hydraulic Pulse

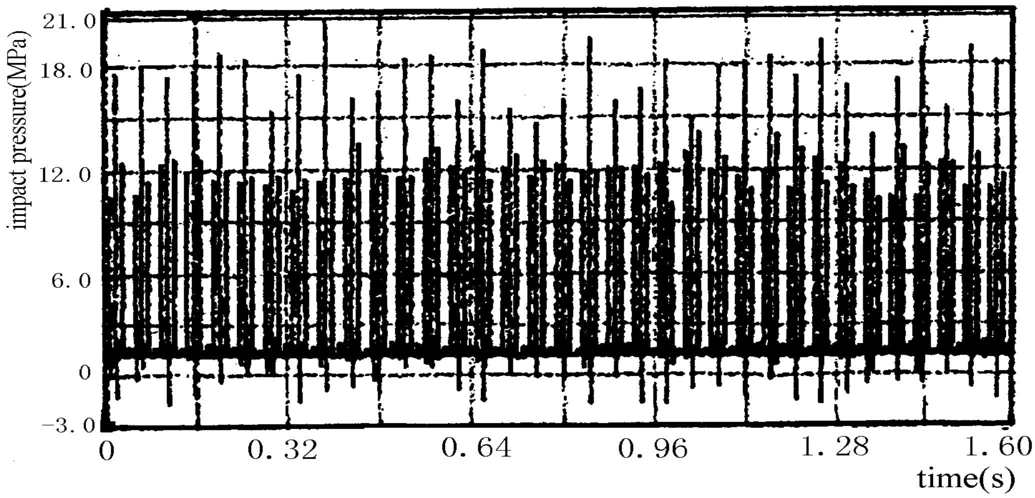

Fig. 3 Oscillating Pressure of Water Jet

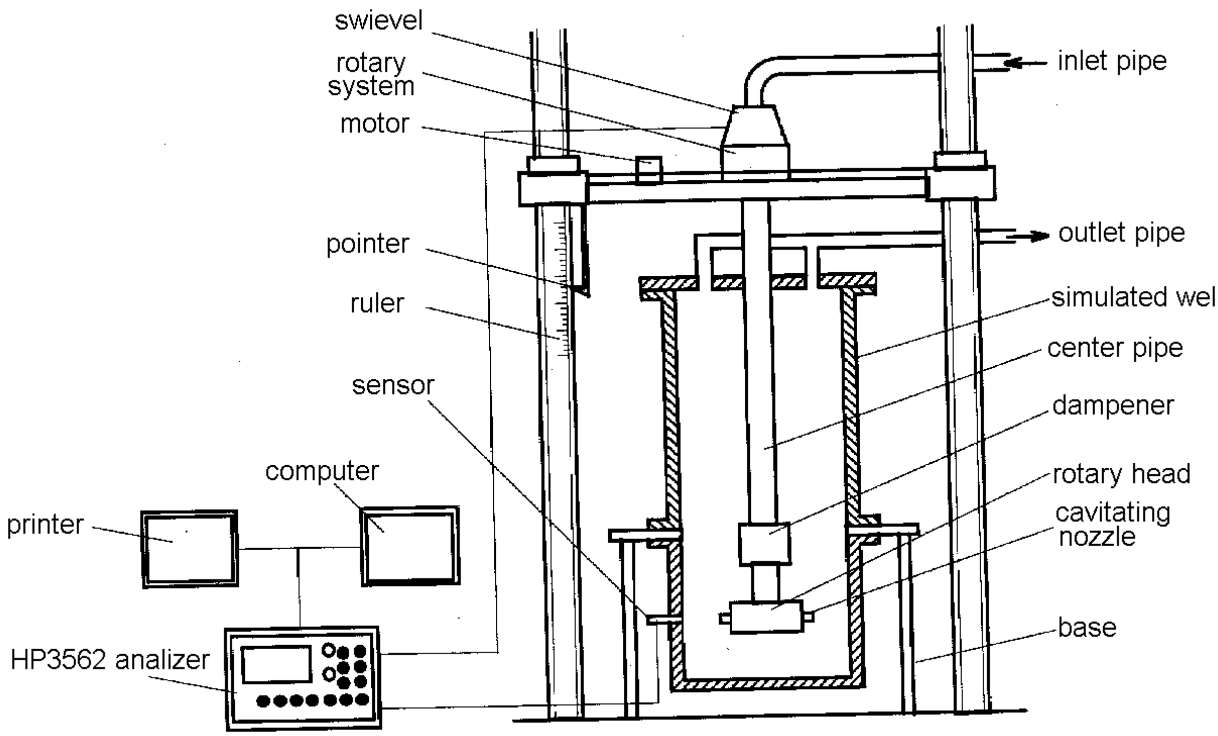

Fig.4 Schematic of Experiment System

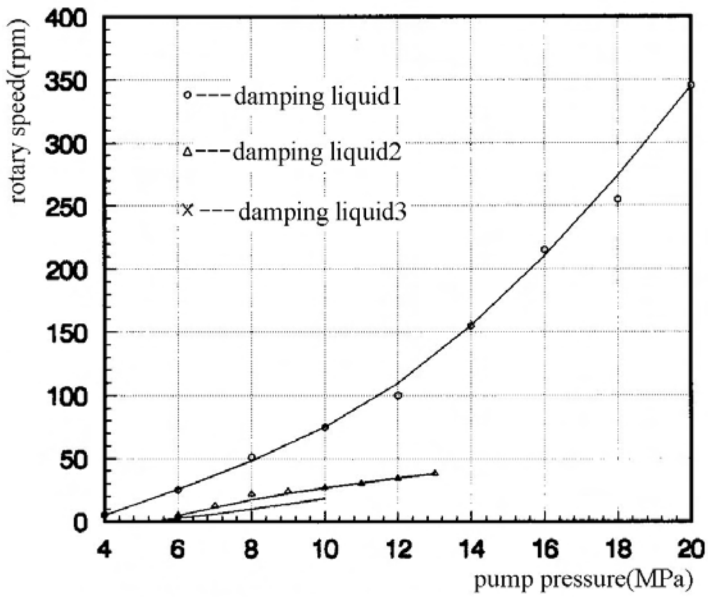

Fig. 5 Relationship between Rotary Speed and Pump Pressure

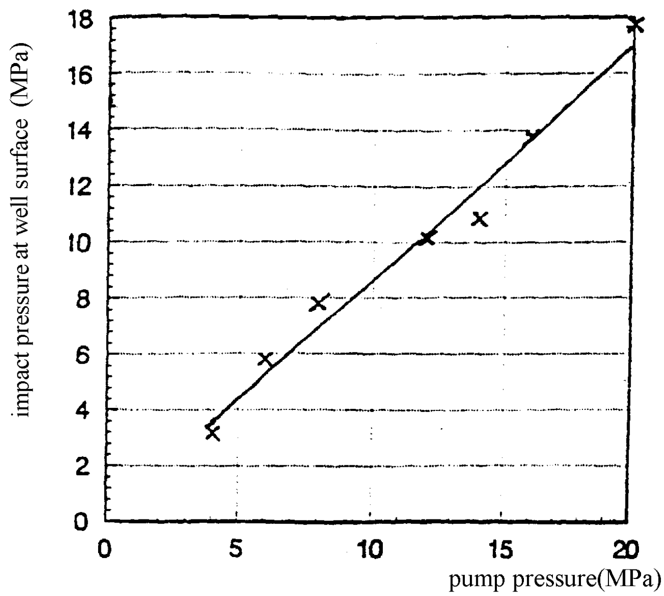

Fig. 6 Relationship between Impact Pressure at Well Surface and Pump Pressure

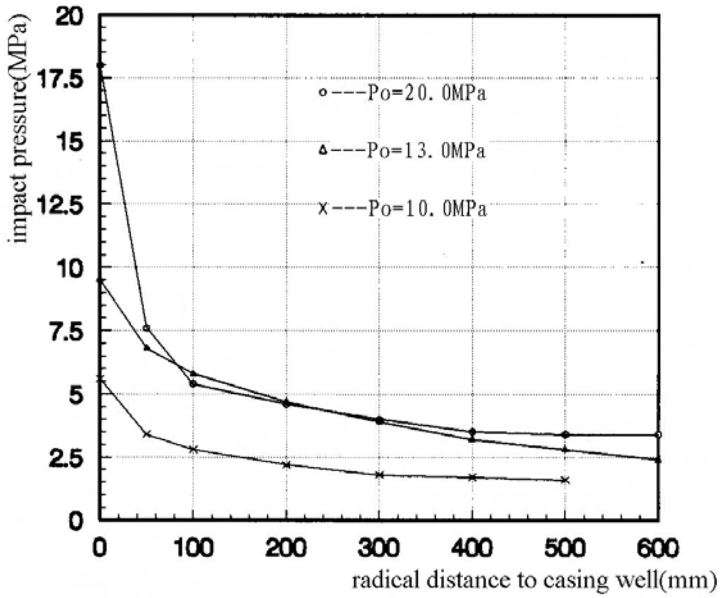

Fig7. Relationship between Impact Pressure and Radical Distance

10th American Waterjet Conference
August 14-17, 1999: Houston, Texas

Paper **37**

THEORETICAL AND EXPERIMENTAL INVESTIGATION OF A HIGH ENERGY WATERJET EFFICIENCY ON THERMALLY TREATED ROCKS

L. M. Hlaváč
VŠB - Technical University
Ostrava, Czech Republic

ABSTRACT

Thermally treated rocks constitute a special group of materials with unusual not very common properties. Nevertheless, these materials grow to be of great interest in several industrial sectors as well as in basic research. To be able to predict effects of water jet impact on such materials the appropriate properties of few representative rocks have been studied after thermal treatment. The water jet disintegration processes have been studied on heated rock samples (up to 900 ^{0}C), on rock samples in usual air conditions after thermal treatment (normal air pressure, temperature during cutting process about 20 ^{0}C, former preheating of rock samples up to 1100 ^{0}C) and on frozen rock samples (temperatures -10 ^{0}C and -100 ^{0}C). The most interesting results of both theoretical and experimental investigation of the problem are the topics of the paper. The preliminary experimental results are largely discussed and correlated with presented theory.

Organized and Sponsored by the WaterJet Technology Association

1. INTRODUCTION

The intention to study the behaviour of the thermally treated rocks being hit by waterjet arose several years ago during some experiments aimed at rock disturbing by laser jet. The decisive impulse for initiation of presented research on rocks came from the practice, however. One tip in the Czech Republic, containing coal as a waste material, started to burn few years ago. It overruns the surrounding countryside and therefore it needed to be transferred to another place being simultaneously snuffed out and cleared from coal. Nevertheless, due to very high temperatures inside the tip, much more than 1000 ^{0}C, the rock materials inside the tip were heated and many of them changed their phases. Subsequent physical and chemical processes determined the new material structure that became similar to glass made from various rock forming materials. Materials in the tip are still very hot with temperatures near to the 1000 ^{0}C. The investor started to think about using waterjet to be able to disjoin these materials in the tip. It was the signal inspiring the priority of the basic physical research of rocks' behaviour. The contemporary aim is to study waterjet disintegration processes on the rock type matter in states similar to the ones constituting the lava alluvion, meteorites, surface of other planets in our Solar system and on heated rocks below their melting points. To obtain the relationship between rock temperature and waterjet efficiency for the largest possible temperature scale the frozen rocks were also studied. The first set of experiments was realised on acidic igneous rock (granite), alkaline igneous rock (basalt) and typical sedimentary rock (sandstone).

2. THEORETICAL BASIS

The basic physical phenomenon influencing the penetration of the liquid jet through the solid state material is the tightness of the bonds. The lower the temperature of material the tighter the bonds among atoms and the higher the energy being to supply for breaking them. Therefore, the basic relationship between rising temperature of the solid state matter and its responsive disintegration ability by liquid jet needs to follow an upward trend. The character of the relationship should be influenced primarily by material dilatability and changes in cohesion on the contact planes (between two grains - mostly of various rock forming materials - or between grains and binding matter among them). Regarding the mentioned influencing factors the relationship between temperature and disintegration ability of material does not need to be continuous. The discontinuities should occur induced by exceedingly high energy content of material overcoming the limit temperature for breaching of the weakest bonds in material. Below this temperature the material disintegration ability should follow very similar dependence on temperature as dilatability. Above this temperature the disintegration ability should be determined by density of extremely week material and limited by jet reach according to the jet energy content.

To be able to determine the appropriate relationship between depth of disintegration and sample temperature the respective coefficients of dilatability for rock materials must be known. Therefore, the experimental work was aimed also at determination of these coefficients. The coefficients can be determined both for increasing and for decreasing temperatures. The first results of these experiments are very interesting but not verified by repeated tests yet.

According to the previous theory published in the most complete form at the 8th American Water Jet Conference (Hlaváč, 1995) the depth of disintegration induced by liquid jet is determined by equations

$$h_{n+1} = \frac{\pi\, d_o \sqrt{2\, \rho_o\, \mu^3\, p^3\, \gamma_R^3\, e^{-5(\xi L + \xi^* h_n^*)}}\,(1 - \alpha_n^2)\cos\theta}{4\,\chi\,\rho_M\, v^{\frac{\rho_o}{\rho_M}} \left[\alpha_n^2\, e^{-2(\xi L + \xi^* h_n^*)}\,\mu\, p\, \gamma_R + \frac{\rho_o}{\rho_M}\,\sigma\right]} \qquad \textbf{(1)}$$

$$\alpha_n = 1 - \frac{C_x^2 \sqrt{2\,\mu^3\, p^3\, \gamma_R^3}\,\rho_M^*\, k^*}{8\sqrt{\rho_o}\,\eta\,\sigma_s\, a\, e^{3(\xi L + \xi^* h_n^*)}} \qquad \textbf{(2)}$$

$$h_n^* = h_1 + h_2 + h_3 + \ldots + h_{n-1} + h_n \qquad \textbf{(3)}$$

The equation (1) is the same as the equation (10) in the quoted paper (unfortunately a small misprint slip into it then because the term $(1 - \alpha_n)$ was printed in proceedings instead the correct term $(1 - \alpha_n^{\ 2})$ in the nominator of the fraction). The system of equations was prepared for both single and multiple passes. The depth of disintegration made by single pass can be determined for n = 0. Variation of temperature influences the parameter σ in the denominator of the fraction in the equation (1). Simultaneously the variable α also varies due to change over the rock material parameters in the fraction in equation (2). Therefore, the resulting relationship between rock temperature and depth of disintegration is not very clear. Nevertheless, it can be generally presumed that for lower temperatures the depth of disintegration will be lower and for higher temperatures it will be higher than for normal one. Another experience shows that the rocks become much less consistent being warmed-over a certain temperature point, start to be brashy and even for normal temperature after cooling off the depth of disintegration is several times greater than for untreated rock. If the fact that the rock internal structure breaks down above certain temperature is taken into account, the depth of jet penetration into rock material is to be nearly constant above that temperature. The amount of disintegration made by jet (depth of kerf) has been described by mathematical functions both for increasing and decreasing temperatures.

$$h = h_{max}\, e^{\ln\left(\frac{h_{eo}}{h_{max}}\right)\frac{(t_{cr} - t)}{t_{cr}}} \qquad \textbf{(4)}$$

$$h = h_{max}\, e^{\ln\left(\frac{h_{eo}}{h_{max}}\right)\frac{(t_{cr}-t)}{2t_{cr}}} \qquad \textbf{(5)}$$

Equations (4) and (5) are supposed to be valid for increasing and decreasing temperatures of rock type material respectively. They were derived assuming very simple relationship between the amount of disintegration and rock temperature. These relationships should be further precised according to the results of research aimed at studies of rock material dilatability.

3. EXPERIMENTAL RESULTS

Unfortunately, the first set of experiments was much more initiatory than it was supposed to be. The experimental results, obtained for temperatures lower than 0 ^{0}C, are corresponding with theoretical relationship determined by equation (4) that is supposed to be valid for material without stage transformation. The heated rocks, however, were disintegrated by water jet only during the cooling off process after preheating up to 1100 ^{0}C not during the process of heating. It was the reason causing that the material structure breaking down induced by overcoming the critical temperature influenced the results obtained both for high temperatures, i.e. 400, 600 and 900 ^{0}C and for 20 ^{0}C after preheating up to 1100 ^{0}C. The depths of kerfs determined experimentally for mentioned temperatures were correlated with theoretical values obtained using equation (5). The results are correlated with theoretical relationships in Figures 1 and 2 for water pressure 350 MPa, stand-off distance 13 mm (determined by properties of commercial equipment used for experiments), traverse rate 25 mm.s^{-1} and nozzle diameters 0.1 and 0.25 mm respectively.

The most important information resulting from up to date experiments are summarized in Table 1. It is evident that only a small part of experiments necessary for correlation with theory was realized yet. Nevertheless, the set of experiments aimed at detailed study of estimated relationships is just being in progress and much more representative results are to be got within few months.

4. DISCUSSION

Theory submitted in the paper seems to describe the amount of disintegration caused by high energy water (liquid) jet on thermally treated rocks satisfactorily. Concordant with theoretical assumptions the frozen rocks are more consistent and worse fracturable as it is shown in Fig. 1 through 5. There do not seem to be any anomalous behaviour in the range of temperatures below 0 ^{0}C. Nevertheless, the light increase of the depth of disintegration for temperature -100 ^{0}C can be caused by jet energy losses due to the fact that some portion of water in contact with frozen rock starts to freeze.

The experimental results obtained on sandstone (sedimentary rock) correlate directly with theoretical prediction in spite of the fact that relation between temperature of the rock sample and the depth of disintegration is expressed by very simple physical relationship. The correlation between experimentally determined depth of disintegration caused by water jet in heated samples of sandstone and theoretical relationship is also very good (Fig. 1 and 2). The high correlation is evident even though the experimental results were obtained under conditions that are not in accordance with typical experimental procedure. The theoretical relationship can be precised taking into account greater amount of the rock material properties and water (or other liquid) parameters. Nevertheless, the divergence between experiment and theory in the case of sandstone seems to be below error in measurement caused primarily by rock properties variation.

The situation is quite different in the case of basalt. The experimental results of the depth of disintegration determined for decreasing temperature using the small nozzle diameter (0.1 mm) very closely follow the curve calculated from theory for increasing temperature (Fig. 3). In spite of the fact that the quantity of results does not provide the chance to do definite conclusions, it can be presupposed that this phenomenon can be caused by the fact that basalt is very compact rock material with elastic behaviour in wider range of parameters than other rocks (specially sandstone or granite). Nevertheless, the results obtained with the greater nozzle diameter (0.25 mm) show (Fig. 4) that overcoming the critical (or characteristic) temperature the heated rock material may become less consistent than it is supposed in theory.

Behaviour of the granite is rather surprising. Overcoming the critical (characteristic) temperature granite becomes much weaker and this phenomenon has to be introduced into the theoretical relationship using temperature depending coefficient of weakening. The experimental results were obtained only for the small nozzle diameter (0.1 mm) because dimensions of the rock samples were limited by dimensions of the kiln and impact of water jet from the nozzle with the greater diameter (0.25 mm) caused breaking down of the granite samples by all temperatures except 20 ^{0}C. Acquired experimental results are correlated with theory in Fig. 5.

The drop of disintegration depth observed for all studied rock materials by 900 ^{0}C considering both respective theoretical values and experimental data obtained for 600 ^{0}C is another phenomenon to be mentioned. It is supposed that the drop of the water jet efficiency is caused by the fact that the gradient of temperature inside the kerf (produced in a rock sample by water jet) overcomes a specific value limiting the heat transfer from rock to water during water jet penetration process. Overcoming this value the heat transfer becomes enough for water evaporation before penetration into the depth corresponding to maximum initial energy of the jet. The energy of a vaporized amount of water is lost and therefore the total efficiency is lower than for lower temperatures.

5. CONCLUSIONS

The up-to-date conclusions of the presented theoretical and experimental investigation to the problem of disintegration of heated rocks by water jet are as follows:

- the depth of disintegration in sandstone is satisfactorily described by presented theory for the whole range of tested temperatures;
- the theoretical description of the jet impact onto heated rock must be based on more parameters for better correlation with experimental results on rocks like basalt;

- the implementation of the temperature depending coefficient of weakening seems to modify the theory sufficiently for materials similar to granite;
- the depths of disintegration made by water jet in frozen rocks without preheating are satisfactorily described by presented theory;
- the theoretical description of the energy losses caused by jet evaporation for highly heated rocks has to be added;
- the set of experiments including tests on rocks for both increasing and decreasing temperature is to be completed.

6. ACKNOWLEDGEMENTS

The author is grateful to the Grant Agency of the Czech Republic supporting the work by project No. 106/98/1354.

7. REFERENCES

Hlaváč, L.M.: "Physical Analysis of the Energy Balance of the High Energy Liquid Jet Collision with Brittle Non-Homogeneous Material," *Proceedings of the 8th American Water Jet Conference*, pp. 681-697, Water Jet Technology Association, St. Louis, Missouri, 1995.

8. NOMENCLATURE

α_n coefficient of losses in liquid jet velocity during interaction with material
γ_R compressibility factor
C_x coefficient of resistance of material structure to the jet
d_o water nozzle diameter [m]
η dynamic liquid viscosity [N.s.m^{-2}]
h depth of disintegration in material [m]
h_{eo} experimental depth of kerf for 0 ^{0}C (it may be considered equal to the depth of kerf made by 20 ^{0}C without any temperature treatment of the rock) [m]
h_{max} maximum theoretical depth of kerf calculated from equation (1) for σ = 0 MPa [m]
h_n depth of disintegration made in n-th pass of liquid jet, h_o = 0 [m]
h_n^* total depth of disintegration after n passes [m]
θ angle of an incidence of the jet measured between a normal line at the point of jet's axis projection through material surface and jet axis [rad]
k^* dynamic material permeability [m^2]
L standoff distance [m]
μ nozzle discharge coefficient
ξ coefficient of attenuation of jet caused by resistance of the medium between nozzle and material [m^{-1}]
ξ^* coefficient of attenuation of jet caused by resistance of the medium in kerf made in material during previous passes [m^{-1}]

p	pressure difference p_o-p_m [Pa]
p_o	liquid pressure before the nozzle inlet [Pa]
p_m	pressure of the medium between nozzle and material [Pa]
ρ_o	liquid density in noncompressed state [kg.m^{-3}]
ρ_M	specific volume weight of material (including pores) [kg.m^{-3}]
$\rho_M{}^*$	specific weight of material (without pores) [kg.m^{-3}]
σ	material strength [Pa]
σ_s	material shear strength [Pa]
t	temperature [^{0}C]
t_{cr}	critical temperature for phase transformation phenomena [^{0}C]
v	modified traverse rate [m.s^{-1}]
χ	coefficient of reflected jet expansion due to mixing with disintegrated material

9. TABLES

Table 1. Experimental results on thermally treated rocks.

rock type	**nozzle diameter [mm]**	**ρ [kg.m^{-3}]**	**ρ* [kg.m^{-3}]**	**temperature [^{0}C]**						
				-100	**-10**	**20**	**20↓**	**400**	**600**	**900**
S	0.1	2518	2453	3.2	3.1	3.8	6.0	9.2	11.0	10.7
S	0.25	2537	2477	9.1	10.3	11.0	19.0	32.0	32.3	34.0
B	0.1	2904	2882	1.0	1.1	1.5	1.4	1.7	4.0	4.9
B	0.25	2911	2887	2.8	2.3	2.7	6.9	14.1	17.9	15.7
GD	0.1	2624	2523	1.4	1.8	2.5	8.6	20.0	34.9	32.8
GD	0.25	2628	2481	4.3	4.9	6.5	45.9	⊗	⊗	⊗

Legend: **S -** sandstone
B - basalt
GD - granodiorite
ρ - average specific volume weight on rock before thermal treatment
ρ* - average specific volume weight on rock after thermal treatment
20↓ - the kerf made by 20 ^{0}C after cooling from the temperature 1100 ^{0}C
⊗ - the jet cut through the sample (limit thickness for kiln was 50 mm)

10. FIGURES

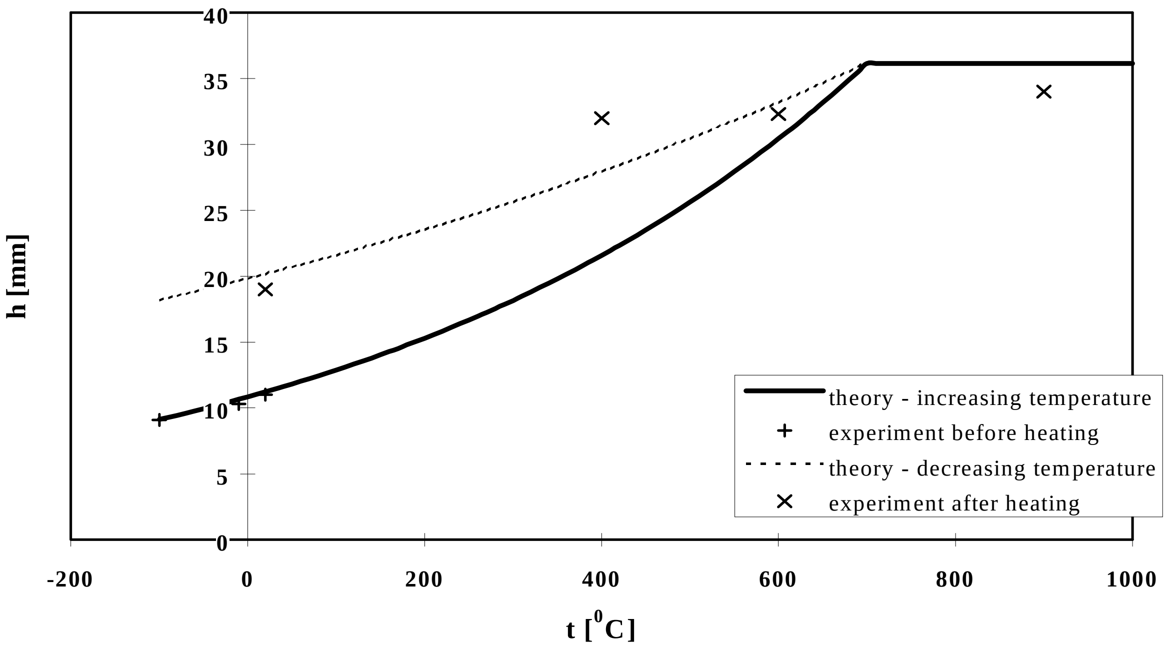

Figure 1. Relationship between temperature of sandstone sample and the depth of kerf made by water jet with nozzle diameter 0.25 mm.

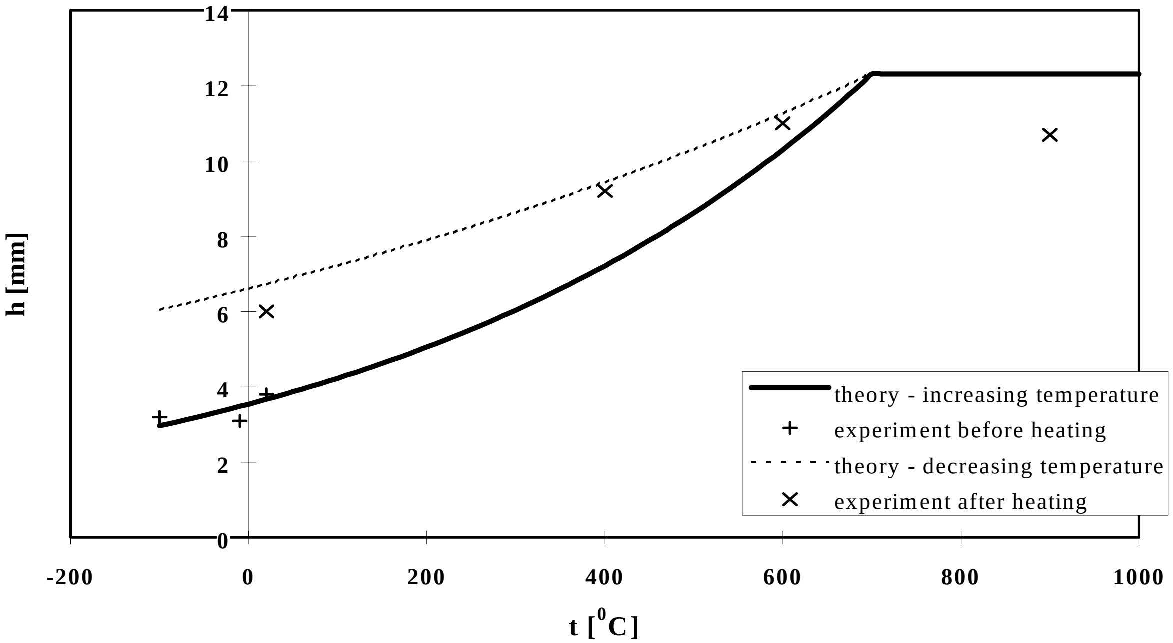

Figure 2. Relationship between temperature of sandstone sample and the depth of kerf made by water jet with nozzle diameter 0.1 mm.

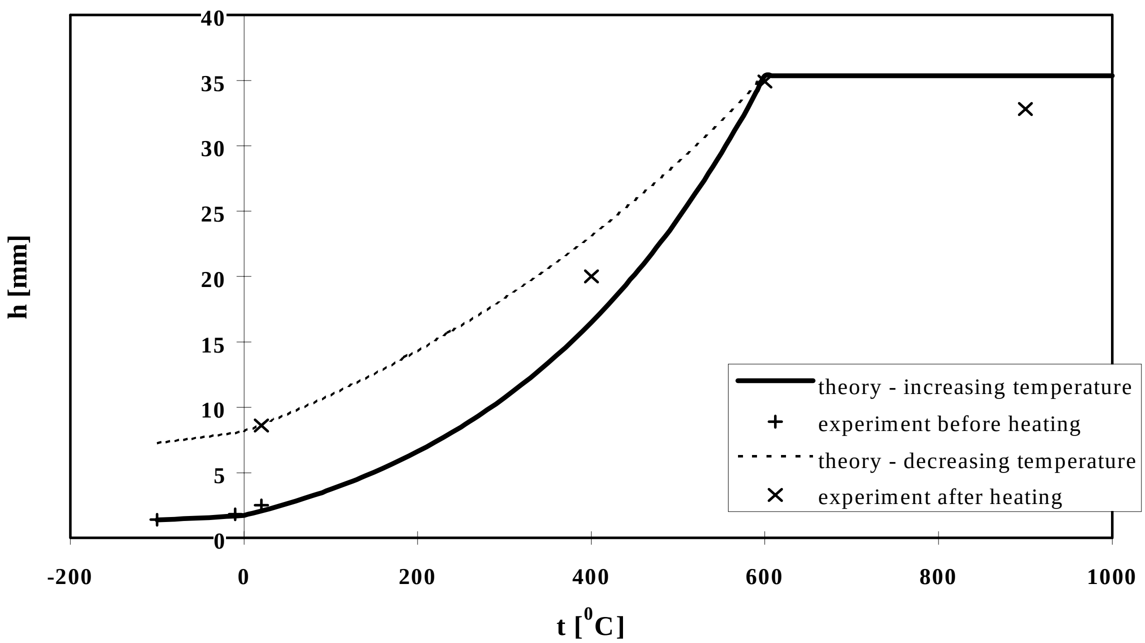

Figure 3. Relationship between temperature of granodiorite sample and the depth of kerf made by water jet with nozzle diameter 0.1 mm.

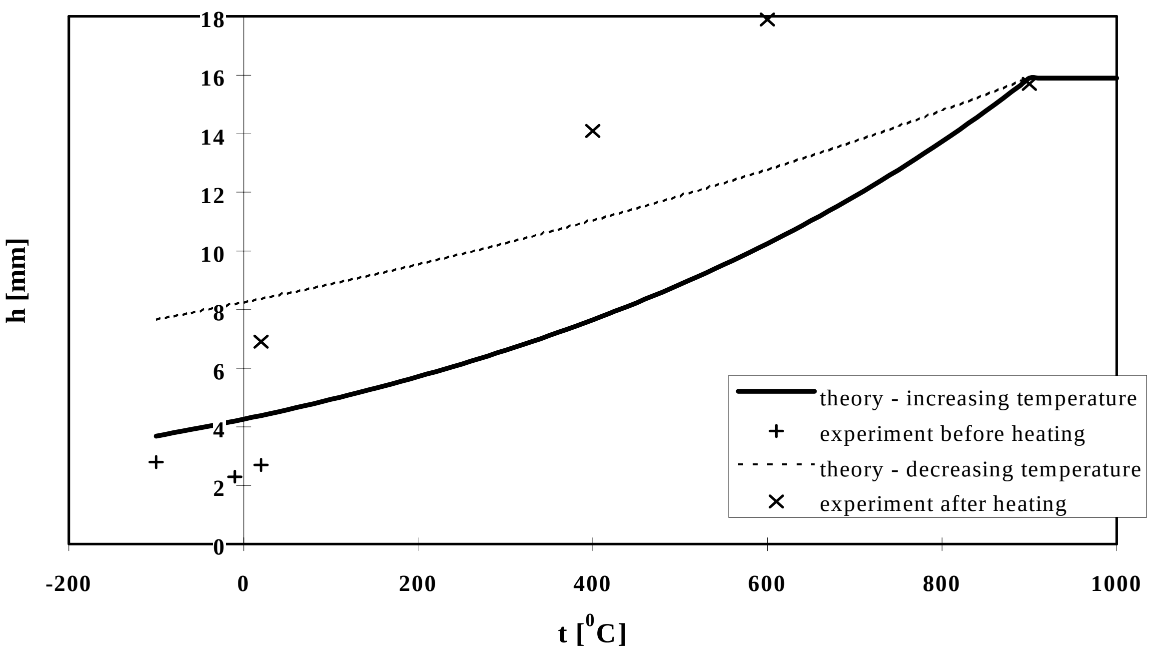

Figure 4. Relationship between temperature of basalt sample and the depth of kerf made by water jet with nozzle diameter 0.25 mm.

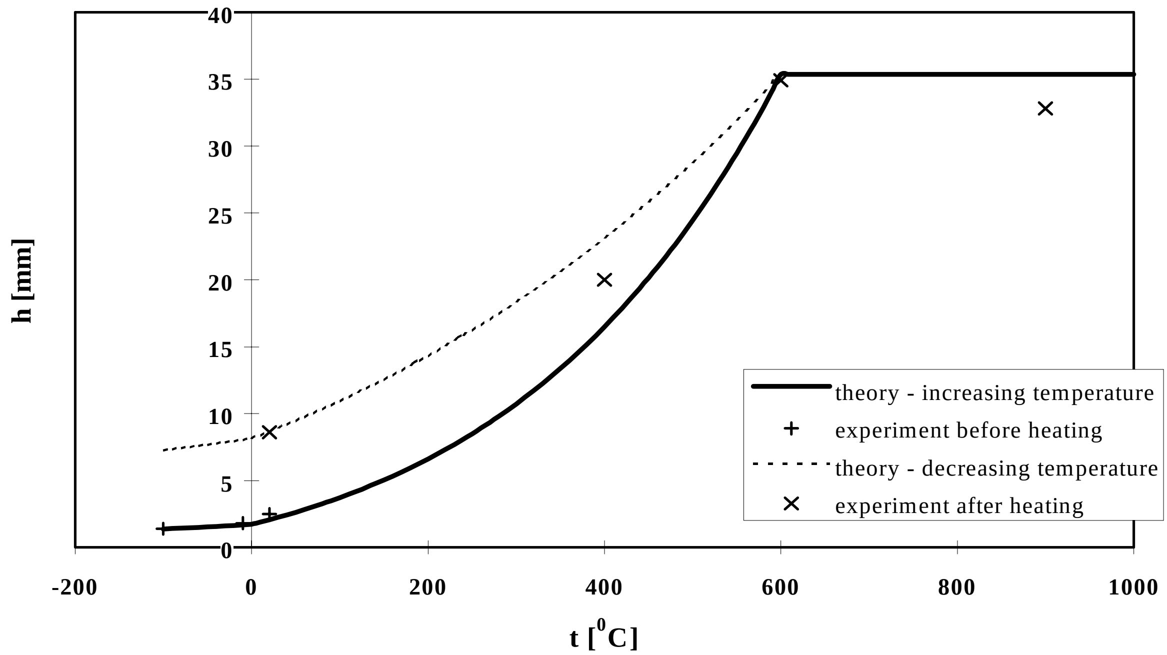

Figure 5. Relationship between temperature of granodiorite sample and the depth of kerf made by water jet with nozzle diameter 0.1 mm.

10th American Waterjet Conference
August 14-17, 1999: Houston, Texas

Paper 38

CALCULATION OF THE EFFICIENCY RATE OF HIGH PRESSURE PUMPS

N. Herbig
Schnifis, Austria

F. Trieb
BÖHLER Hochdrucktechnik GmbH
Kapfenberg, Austria

ABSTRACT

A theoretical method is described to calculate the efficiency rate of high pressure pumps. The calculated values are compared with experimental data. The data were measured with the aid of an experimental set-up that was designed for the optimisation of high pressure pumps.

Due to the amount of simplifications required to keep the theoretical calculation simple, the deviations of theoretical and experimental data are small under rated load conditions. A further comparison with other data from relevant literature showed that this new design/development of a high pressure pump has led to improved efficiency levels.

Organized and Sponsored by the WaterJet Technology Association

1 THEORETICAL CALCULATION OF EFFICIENCY RATE

1.1 Components and operation of a high pressure pump

High pressure pumps that are used for industrial applications at the moment mainly consists of two parts: a hydraulic system (radial or axial piston pump) and a high pressure system with the intensifier and the accumulator. An electrical motor is used for the drive of the hydraulic system. In order to estimate the efficiency rate of the high pressure pump it is necessary to determine the efficiency rate of all main components. The calculation of the efficiency rate is based on the efficiency rates of the individual components.

The efficiency rates of the main individual components are shown in Figure 1. The width of the arrows symbolises the amount of use and lost power. The input to the electrical motor is 100 % electrical power. This electrical power is transformed by the electrical motor into mechanical power of the pump shaft. This transformation also causes losses due to heat and idle. The hydraulic pump feeds hydraulic oil to the consumer, the intensifier. This process causes losses in the form of heat and leakage. Loss of flow is caused by the whole piping system. It is very difficult to determine this kind of loss by means of measurement. The intensifier develops work on translation and work on adiabatic compression. Also, this process causes losses in the form of heat and leakage. The high pressure piping causes further loss of flow.

1.2 Efficiency rate

Normally, the term ”efficiency rate” describes the relation between optimal process and process with loss. The efficiency rate is one of the most important parameters of power transmitting machines. The efficiency rate of a high pressure pump is determined by the efficiency rates of the individual components such as the electrical motor, hydraulic pump, hoses, intensifier etc. Due to the above-mentioned relations it is necessary to determine efficiency rates of individual components in order to calculate the efficiency rate of the high pressure pump.

1.2.1 Efficiency of electrical motor

The electrical motor works as a drive and transforms electrical power into mechanical power of the pump shaft. This transformation process involves a certain loss. Part of the input power is transformed into heat, idle, etc. Electrical motors have an efficiency rate η_{el} of approximately 0.9 /1/.

1.2.2 Efficiency rate of hydraulic system

The mechanical power of the hydraulic pump is used to increase stored power of the hydraulic fluid between entrance and outlet of the hydraulic pump and for all losses (leakage and loss of flow) that occur inside the pump. To increase the power of the fluid it is necessary to develop work on translation and work on adiabatic compression. The occurring losses of the pump are transformed into heat and the temperature of the fluid at the outlet of the pump.

The balance of energy can be described as follows if micro-dynamic processes, the energy of the electrical and magnetic field, the chemical energy and the sound energy, the kinetic energy and the potential energy in comparison to the pressure energy are not considered and if there is no increase and decrease of heat of the system (2):

$$Q_{m1}\left(u_1 + \frac{p_1}{\rho_1}\right) + M\omega = Q_{m2}\left(u_2 + \frac{p_2}{\rho_2}\right) + Q_{mLe}\left(u_{le} + \frac{p_{Le}}{\rho_{Le}}\right) \tag{1}$$

The equation compares the input energy (inner energy, pressure energy and power of drive) with the energy after the transformation process (inner energy, pressure energy and loss of leakage). The values of the entrance of the pump are indicated by index ”*1*” and values of the outlet of the pump are indicated by index ”*2*”. The index ”*Le*” represents the values of the external leakage. The value ”$M\omega$” describes the striking power of the electrical drive (electrical motor) and can be calculated as follows:

$$M\omega = Q_{m2}p_2 + Q_{mLe}p_{Le} - Q_{m1}p_1 \tag{2}$$

Going on the assumption that the inner energy of the fluid is constant and that the fluid is not compressible (ρ = const.) the efficiency rate of the pump can be described as follows:

$$\eta_{t,ax} = \frac{Q_{m2}p_2 + Q_{mLe}p_{Le} - Q_{m1}p_1}{\rho M\omega} \quad . \tag{3}$$

The above-mentioned simplifications cause a deviation of approximately 1 % due to a pressure difference of 35 MPa (the maximum pressure difference of an axial piston pump used for a high pressure system is approximately 20 MPa).
If there is no leakage ($Q_{m1}=Q_{m2}$) the equation (3) can be simplified:

$$\eta_{t,ax} = \frac{Q_m(p_2 - p_1)}{\rho M\omega} \tag{4}$$

or

$$\eta_{t,ax} = \frac{V(p_2 - p_1)}{M\omega} \quad . \tag{5}$$

According to DIN ISO 4391 (3), the efficiency rate is defined as the ratio of the difference of hydraulic power of the outlet and the entrance of the pump and the mechanical power:

$$\eta_{t,ax,DINISO} = \frac{V_2p_2 - V_1p_1}{M\omega} \quad . \tag{6}$$

On condition that external leakage is 0 ($V_1=V_2$), the definition (6) is equal to equation (5).

If the leakage is $V_1=V_2+V_{Le}$, the efficiency rate can defined as follows:

$$\eta_{t,ax,DINISO} = \frac{V_2\left(p_2 - p_1\right) - V_{Le}p_1}{M\omega} \quad . \tag{7}$$

In contrast to equation (4) and (5) the numerator of equation (7) is reduced by the power of external leakage. It is not considered that this power is already included in the real power of drive for the hydraulic pump. Due to the experimental measurement of the power of drive including the total input power of the pump (mechanical power) the calculated value of the efficiency rate according to DIN ISO 4391 (3) is always lower than the real rate.

Due to the division of losses it is necessary to distinguish corresponding efficiency rates. Normally there is a volumetric and a hydraulic-mechanical efficiency rate. The total efficiency rate is defined as follows:

$$\eta_{t,ax} = \eta_{v,ax}\eta_{hm,ax} \quad . \tag{8}$$

The volumetric efficiency rate η_v represents the ratio of the real flow of volume V_r at the outlet of the pump and the theoretical volume flow V_{theo}:

$$\eta_{v,ax} = \frac{V_r}{V_{theo.}} = \frac{V_r}{nV'_{theo.}} \quad . \tag{9}$$

The real mass flow can be described as follows:

$$V_r = V_{theo.}\eta_{v,ax} = nV'_{theo.}\eta_{v,ax} \quad . \tag{10}$$

The real mass flow V_r at the outlet of the hydraulic pump is defined by the equation (11).

$$V_r = V_{theo.} - V_L = nV'_{theo.} - V_L \quad . \tag{11}$$

The volumetric efficiency rate can be calculated with the aid of equation (12):

$$\eta_{v,ax} = 1 - \frac{V_L}{nV'_{theo.}} \quad . \tag{12}$$

The hydraulic-mechanical efficiency rate $\eta_{nm,ax}$ of a hydraulic pump is the ratio of the theoretical drive torque M_{theo} and the real drive torque M_r at the inlet of the hydraulic pump:

$$\eta_{hm,ax} = \frac{M_{theo.}}{M_r} \quad . \tag{13}$$

Using the equation for the theoretical drive torque, equation (13) changes to

$$\eta_{hm,ax} = \frac{\Delta p V_{theo.}}{2\pi M_r} \quad . \tag{14}$$

The real drive torque of the hydraulic pump can be calculated by means of

$$M_r = M_{theo.} + M_L \tag{15}$$

and it results that

$$\eta_{hm,ax} = 1 - \frac{M_L}{M_r} \quad . \tag{16}$$

Finally, the total efficiency rate $\eta_{t,ax}$ can be calculated as follows:

$$\eta_{t,ax} = \eta_{v,ax}\eta_{hm,ax} = \frac{V_r}{nV'_{theo.}} \frac{\Delta p V_{theo.}}{2\pi M_r} = \frac{\Delta p V_r}{M_r \omega} \quad . \tag{17}$$

Using the following data (4), the total efficiency rate $\eta_{t,ax}$ can be calculated:

$$\begin{aligned} &\Delta p = 100 \text{ bar} = 10 \text{ MPa} = 1{,}450 \text{ psi} \\ &V_r = 100 \ \frac{1}{\min} = 100 \frac{1}{60000} \ \frac{\text{m}^3}{\text{s}} \\ &M_r = 113 \text{ Nm} \\ &\omega = 2\pi n = 2\pi \ \frac{1450}{60\text{s}} \end{aligned} \quad . \tag{18}$$

$$\eta_{t,ax} = 0.97$$

The total efficiency rate of the axial piston pump $\eta_{t,ax}$ shows only small variations concerning the whole pressure range.

1.2.3 Efficiency rate of the double acting intensifier

Calculation of the efficiency rate of the intensifier is similar to the calculation of the hydraulic system that conforms to the literature except for some minor simplifications. Concerning the efficiency rate of the intensifier it was not possible to find any calculations in the literature and therefore the only possibility is to carry out experiments to verify the results.

The hydraulic piston of the double acting intensifier is forced by oil fed by the axial piston pump. The real drive power for the intensifier can be calculated by the efficiency rate of the hydraulic pump and the real mechanical power:

$$M_{r,dai} = \eta_{t,ax}\omega M = Q_{Oil1} p_{Oil2} \quad . \tag{19}$$

The forced surface of the hydraulic piston (Figure 2) can be calculated as follows:

$$A_{Hy.P,a} = A_{Hy.P} - A_{Pl} = \frac{\pi}{4}\left(d_{Hy,P}^2 - d_{Pl}^2\right) \tag{20}$$

A balance of power gives the following result taking into consideration the above-mentioned simplifications for the intensifier shown in Figure 2:

$$\begin{aligned} Q_{m,w2}\frac{p_{w2}}{\rho_{w2}} + Q_{m,Oil2}\frac{p_{Oil2}}{\rho_{Oil2}} &= -Q_{m,w1}\frac{p_{w1}}{\rho_{w1}} + Q_{m,Oil1}\frac{p_{Oil1}}{\rho_{Oil1}} \\ Q_{m,w2}\frac{p_{w2}}{\rho_{w2}} + Q_{m,Oil2}\frac{p_{Oil2}}{\rho_{Oil2}} &= -Q_{m,w1}\frac{p_{w1}}{\rho_{w1}} + \eta_{t,ax}\omega M \end{aligned} \quad . \tag{21}$$

Thus it is possible to calculate the efficiency rate of the intensifier $\eta_{t,dai}$ as follows:

$$\eta_{t,dai} = \frac{Q_{m,w2}\frac{p_{w2}}{\rho_{w2}} + Q_{m,Oil2}\frac{p_{Oil2}}{\rho_{Oil2}} + Q_{m,w1}\frac{p_{w1}}{\rho_{w1}}}{\eta_{t,ax}\omega M} \quad . \tag{22}$$

The unknown values for the calculation can be specified:

1. $$\rho_{Oil} = \rho_{Oil1} = \rho_{Oil2} \tag{23}$$
2. $$\rho_{w2} = \rho_{w1} e^{p_{w2}/E} \tag{24}$$
3. $$Q_{m,w2} = \rho_{w2} A_{Pl} v \tag{25}$$
4. $$Q_{m,w1} = \rho_{w1} A_{Pl} v \tag{26}$$
5. $$Q_{m,Oil2} = \rho_{Oil2} A_{Hy.P,a} v \tag{27}$$
6. The velocity of the piston v depends on the flow rate of the oil that is delivered by the axial piston pump:

$$v = \frac{Q_{Oil}}{\frac{\pi}{4}\left(d_{Hy,P}^2 - d_{Pl}^2\right)} \quad . \tag{28}$$

Equation (22) can be transformed using equations (23) to (28). The efficiency rate of the intensifier can be calculated as follows:

$$\eta_{t,dai} = \frac{\frac{Q_{Oil}}{\frac{\pi}{4}\left(d_{Hy,P}^2 - d_{Pl}^2\right)}\left[A_{Pl}p_{w2} + A_{Hy.P,a}p_{Oil2} + A_{Pl}p_{w1}\right]}{\eta_{t,ax}\omega M}$$

$$= \frac{\frac{Q_{Oil}}{\left(d_{Hy,P}^2 - d_{Pl}^2\right)}\left[d_{Pl}^2\left(p_{w2} + p_{w1}\right) + \left(d_{Hy,P}^2 - d_{Pl}^2\right)p_{Oil2}\right]}{\eta_{t,ax}\omega M} \quad . \tag{29}$$

$$= \frac{d_{Pl}^2\left(p_{w2} + p_{w1}\right) + \left(d_{Hy,P}^2 - d_{Pl}^2\right)p_{Oil2}}{\left(d_{Hy,P}^2 - d_{Pl}^2\right)p_{Oil1}}$$

Using the following diameter $d_{Hy,P}$ = 105 mm (4.13 in) and d_{Pl} = 22 mm (0.89 in) (ratio of cross section 1:20) and a working pressure of 350 MPa (50,767 psi) an efficiency rate of 87.6 % can be achieved. If there is an additional volumetric efficiency rate (3 % loss) the efficiency rate is reduced to 85.6 %.

As shown above a volumetric efficiency rate $\eta_{v,dai}$ and a hydraulic-mechanical efficiency rate $\eta_{hm,dai}$ can be defined.

1.2.4 Efficiency rate of the high pressure system

The total efficiency rate of the high pressure pump η_t can be calculated as the product of the three efficiency rates of the main individual components, the electrical motor η_{el}, the hydraulic system $\eta_{t,ax}$ and the intensifier $\eta_{t,dai}$:

$$\eta_t = \eta_{el}\eta_{t,ax}\eta_{t,dai} \quad . \tag{30}$$

2 EXPERIMENTAL STUDY ON THE EFFICIENCY RATE OF A REAL HIGH PRESSURE SYSTEM

For experimental determination of the efficiency rate, the current, voltage, flow rate of water and number of strokes of the intensifier were measured for different nozzle diameters (0.25 and 0.35 mm (0.01 and 0.0138 in)). The experimental set-up is shown in Figure 3.

A conventional voltmeter was used to measure the present voltage at the electrical motor. Using a current meter the current consumption of the electric motor was determined. A pressure transducer of Hydrotechnik type PR15 and a high pressure transducer of Gefran Sensori type

HPE 30 5M were used to measure the hydraulic pressure during the stroke. The electrical signal of the pressure transducer was recorder by a measuring computer of Dewetron and analysed with the software DasyLap V2.0.

2.1 Electrical Power

The power consumed by the three phase electrical motor can by calculated using the measured values voltage U and current I and with the aid of the following equation:

$$P_{In} = U \cdot I \cdot \sqrt{3} \cdot \cos\varphi \tag{31}$$

Reactive independence of a circuit with alternating current causes a phase difference between current and voltage. The angle φ occurs between the pointer of voltage U and current I in the diagram. In order to calculate the power, the real voltage and the active current (current component equal to polarity) are necessary. The factor $\cos\ \varphi$ is called the power factor.

2.2 Flow rate power of the high pressure system

The flow rate of the high pressure systems depends on the working pressure and the nozzle diameter.
The amount of water fed at a special working pressure can be determined by using a measuring glass as shown in Figure 3. The power P_{out} can be calculated using flow rate Q and generated pressure p:

$$P_{Out} = V_r \cdot (p_2 - p_1) = V_r \cdot p \tag{32}$$

$$P[kW] = \frac{p[bar] \cdot V_r\left[\frac{l}{\min}\right]}{600} = \frac{p[MPa] \cdot V_r\left[\frac{l}{\min}\right]}{60} \ . \tag{33}$$

2.3 Efficiency rate

The total efficiency rate of the high pressure pump can be calculated using the measured data of input and output power:

$$\eta_{total} = \frac{P_{Out}}{P_{In}} \ . \tag{34}$$

Figure 4 shows the dependence of electrical power and efficiency rate on hydraulic power. The pressure range between 200 (29,010 psi) and 350 MPa (50,767 psi) (preferred pressure range for different applications) shows efficiency rates between 25 and 70 %. The low efficiency rates at low working pressures are mainly caused by the variation of the efficiency rate of the electrical motor. Increasing hydraulic power by using increased nozzle diameters or higher working pressures causes the ratio of input and output energy to change to higher values.

The fundamental result is equal to the results of Chalmers (5). His paper presents the results of investigations concerning a high pressure pump with a drive power of 30 kW. The electrical power required was determined for a special hydraulic power. The calculated efficiency rate increases distinctly up to a hydraulic power of 10 kW and reaches a maximum value of 58 % at a maximum hydraulic power of 20 kW.

The calculated efficiency rates reach a maximum value of 70 % with increasing hydraulic power. The high electrical power required at low hydraulic power is caused by wasted power of the motor. The wasted power increases more severely when the further the motor is not operated under rated load conditions (1).

Due to the variation of the load the power factor also changes. For all calculations (equation 31) a constant power factor was used that was given for rated load conditions for the electrical motor.

Considering the real power factor the graph of the electrical power in dependence on the hydraulic power would decrease between 10 and 20 % in the range of low loads. This is shown in Figure 5 by a broken line. This results in higher values for the efficiency rates (shown by dotted line in Figure 5).

3 COMPARISON OF THE EFFICIENCY RATES FROM THE EXPERIMENTAL STUDIES AND THE THEORETICAL EFFICIENCY RATES

The theoretical efficiency rate of the high pressure system can by calculated by equations 17, 22 and 30. Figure 6 shows the theoretical and the efficiency rates from the experiments in dependence on the working pressure for nozzle diameters 0.25 and 0.35 mm (0.01 and 0.0138 in). The plotted graphs show that there is only a correspondence between theory and practice in the range of high powers, that means for high working pressures and large nozzle diameters.

The theoretical efficiency rate is always above the experimental one. This is due to the simplification that only the main components of the high pressure pump were considered. In this case transformation of power into heat by friction, losses due to flow conditions and leakage is not considered by the given calculation. Furthermore, the data used for the components are only valid for the rated load condition, but are used for all calculations. As discussed above the efficiency rate of the electrical motor differs extremely in dependence on the actual load. This is the main reason for the deviation between theory and practice.

The transformation of pressure energy of the water to kinetic energy of the waterjet is not free of losses. These losses were also not considered during calculation. Furthermore, the compressibility of water is also neglected. This effect is important in the range of high pressures (> 200 MPa / 29,010 psi). This is a further reason for the fact that theoretical efficiency rates are higher than experimental ones.

4 CONCLUSION

This paper presents a simple calculation of the efficiency rate of a high pressure pump. Only the main components of a high pressure pump were considered in this calculation. Furthermore, several kinds of energy have to be neglected. Also, the compressibility of water and the transformation of pressure energy of water to kinetic energy of the waterjet were not considered during calculation. The theoretical values were compared with experimental ones.

By measuring the input power and the output power of the high pressure pump it was possible to calculate a maximum efficiency rate of 70 % under rated load conditions. A comparison with other data from relevant literature showed that this new high pressure system from BÖHLER Hochdrucktechnik has improved efficiency levels.

The calculation of the efficiency rate of a high pressure pump, as shown in this paper, can be improved by employing better data of all relevant components. The deviation between the theoretical efficiency rate and experimental efficiency rate for a nozzle diameter of 0.35 mm (0.0138 in) and a working pressure between 350 and 400 MPa (50,767 and 58,020 psi) can be ascribed to the simplifications (see framed data in Figure 6).

5 REFERENCES

(1) Nürnberg, W.: "Die Prüfung elektrischer Maschinen", 4. Auflage, Berlin / Göttingen / Heidelberg: Springer Verlag, 1959.

(2) Matthies, H. J.: "Einführung in die Ölhydraulik", 2. Auflage, Stuttgart: Teubner Verlag, 1991.

(3) DIN ISO 4391 - Pumpen, Motoren und Kompaktgetriebe

(4) Technical documentation, Mannesmann-Rexroth: Axial piston pump A10V

(5) Chalmers, E. J.: "Pressure fluctuation and operating efficiency of intensifier pumps", Proceedings of the 7th American Water Jet Conference, pp. 327 – 336, Water Jet Technology Association, Seattle, Washington, Paper 22, 1993.

NOMENCLATURE

$d_{Hy,K}$	[mm]	Diameter of hydraulic piston
d_{Pl}	[mm]	Diameter of plunger
n		Number of strokes / Revolutions (rpm)
p	[MPa]	Pressure
p_w	[MPa]	Pressure of water
p_{Oil}	[MPa]	Pressure of hydraulic oil
u	[W]	Inner energy
$A_{Hy.P}$	[mm^2]	Cross section of hydraulic piston
$A_{Hy.P,a}$	[mm^2]	Active cross section of hydraulic piston

A_{Pl}	[mm^2]	Cross section of plunger
I	[A]	Current
M	[Nm]	Torque
M_r	[Nm]	Real drive torque
$M_{r,dai}$	[Nm]	Real drive torque of double acting intensifier
M_L	[Nm]	
M_{theo}	[Nm]	Theoretical drive torque
P_{out}	[W]	Output power
P_{In}	[W]	Input power
Q_m	[kg/s]	Mass flow rate
V_r	[kg/s]	Real mass flow rate
V_L	[kg/s]	
V_{theo}	[kg/s]	Theoretical volume
V'_{theo}	[kg/s]	Theoretical volume per revolution
U	[V]	Voltage
ρ	[kg/m³]	Density
η_{el}	[%]	Efficiency rate of electrical motor
$\eta_{t,ax}$	[%]	Efficiency rate of axial piston pump
$\eta_{v,ax}$	[%]	Volumetric efficiency rate of axial piston pump
$\eta_{hm,ax}$	[%]	Hydraulic-mechanical efficiency rate of axial piston pump
$\eta_{v,dai}$	[%]	Volumetric efficiency rate of the intensifier
$\eta_{hm,dai}$	[%]	Hydraulic-mechanical efficiency rate of the intensifier
$\eta_{t,dai}$	[%]	Total efficiency rate of the intensifier
η_{total}	[%]	Total efficiency rate
ω	[1/s]	Angular frequency
$cos\ \rho$		Power factor

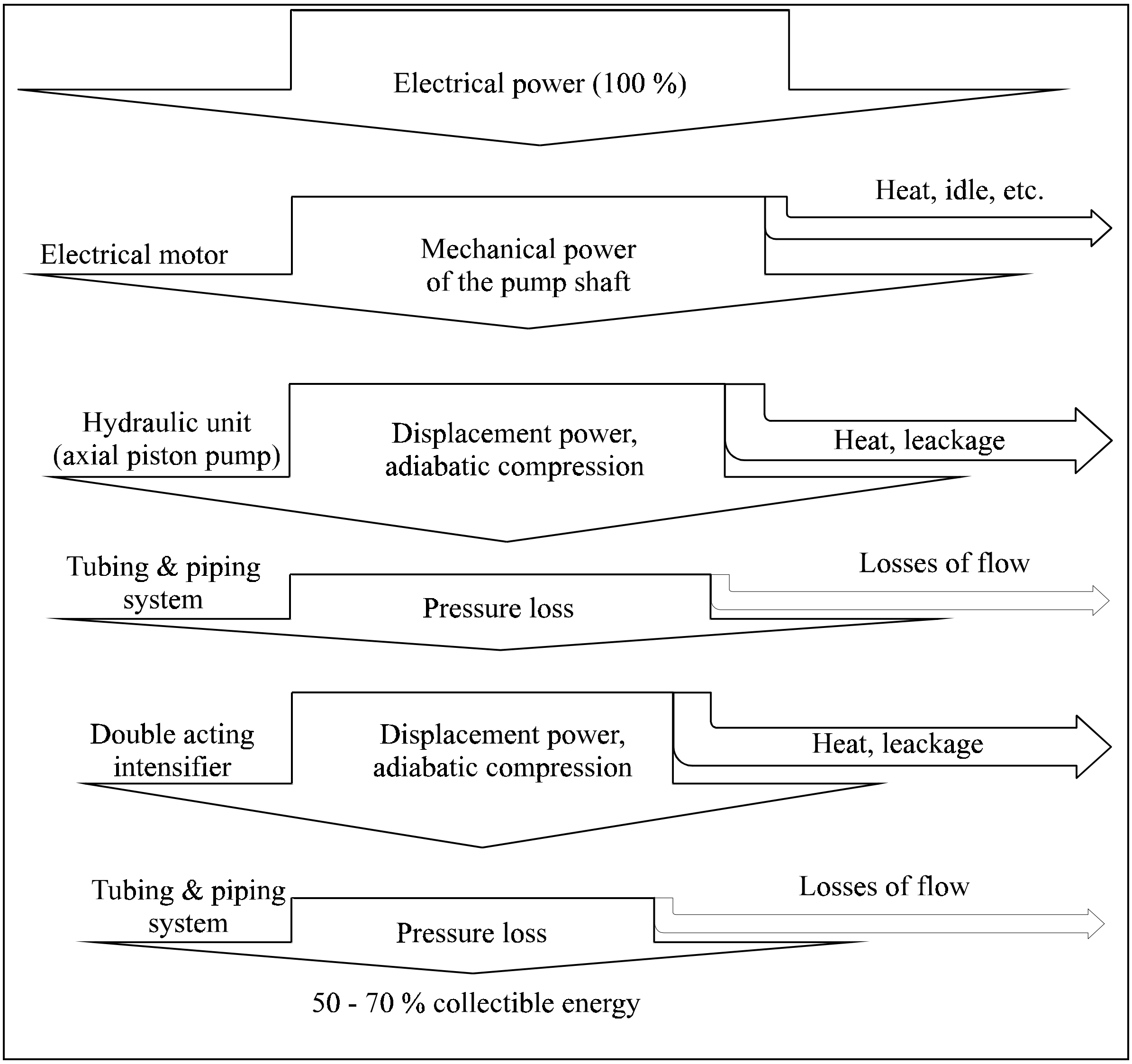

Figure 1. Collectible energy and losses of a high pressure pump.

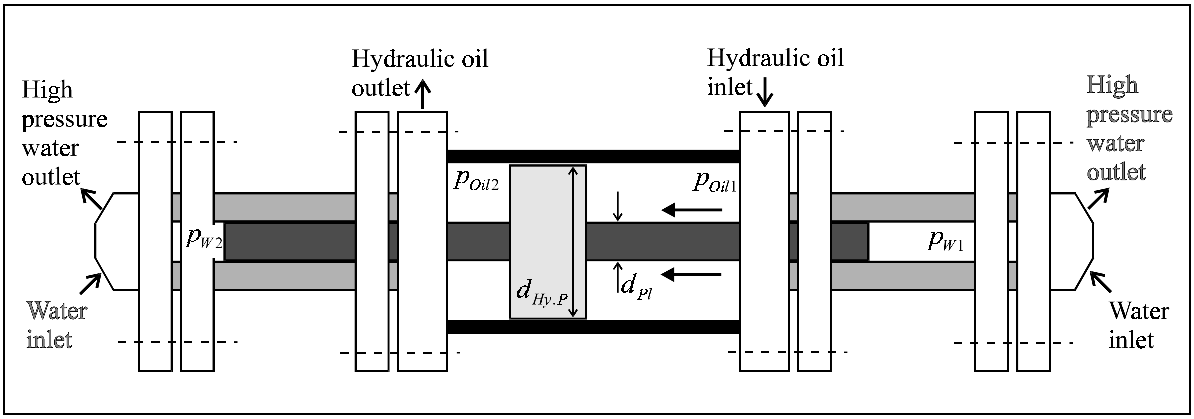

Figure 2: Determination of the active cross section of the hydraulic piston and acting pressures

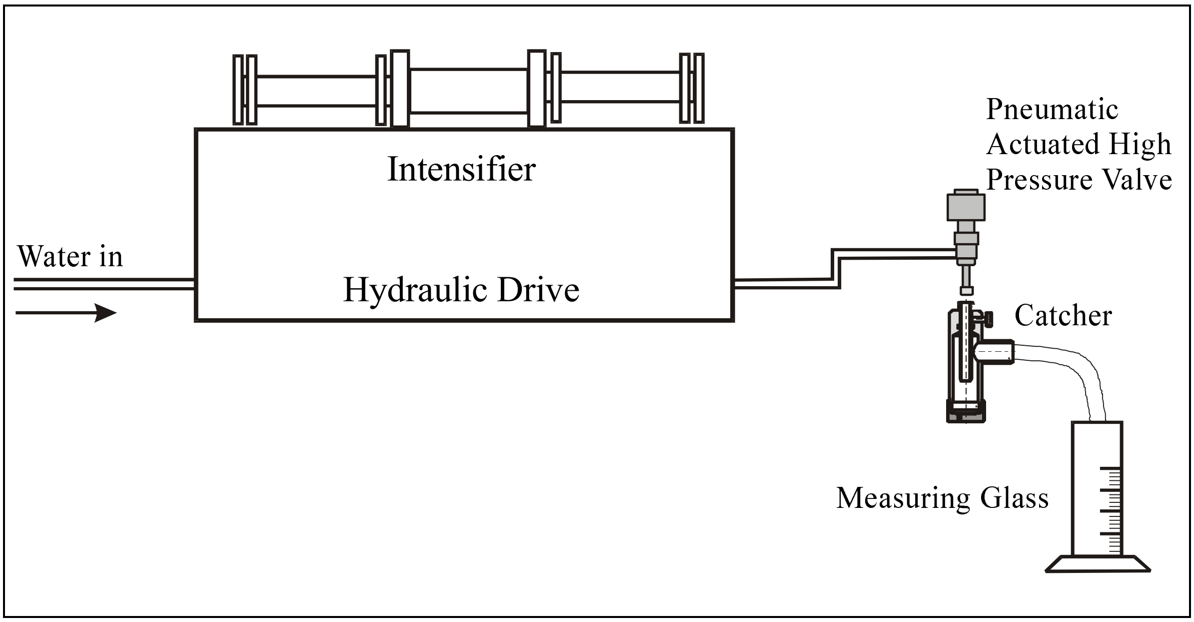

Figure 3: Experimental set-up.

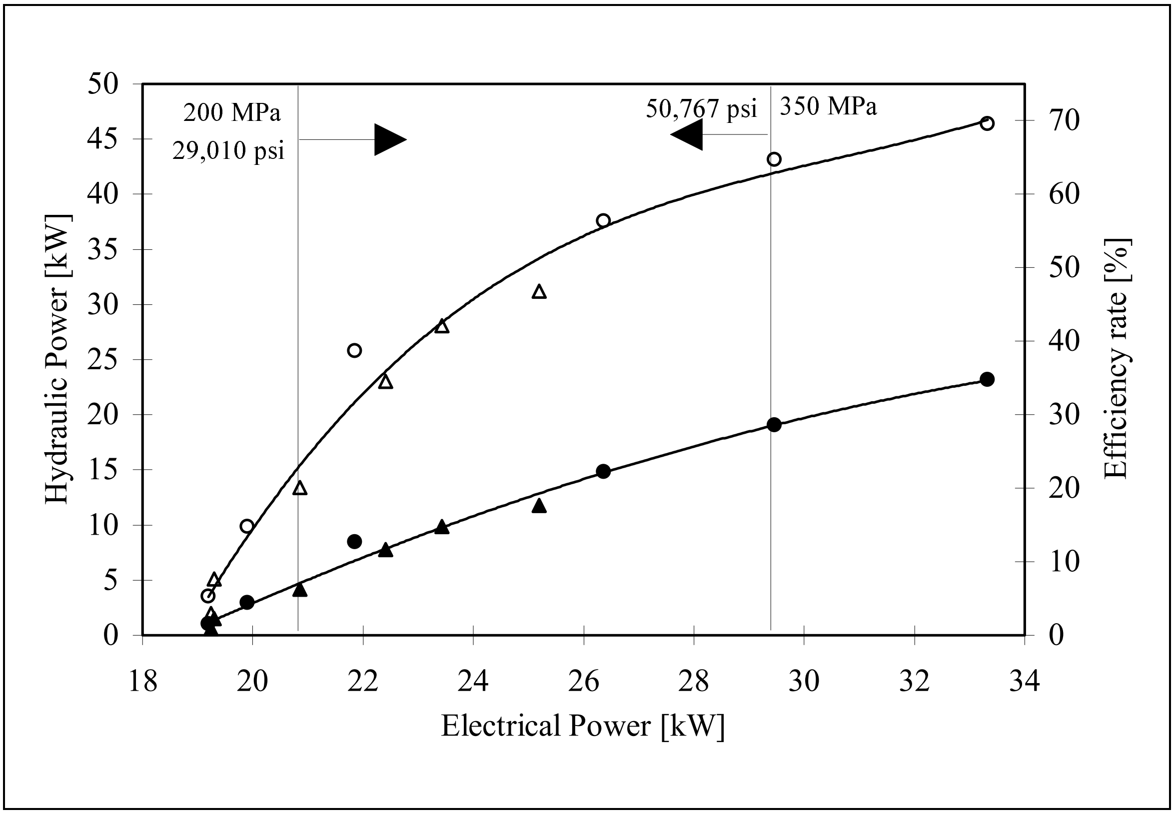

Figure 4: Hydraulic power and efficiency rate in dependence on electrical power for nozzle diameter 0.25 mm (triangles) and 0.35 mm (circles).

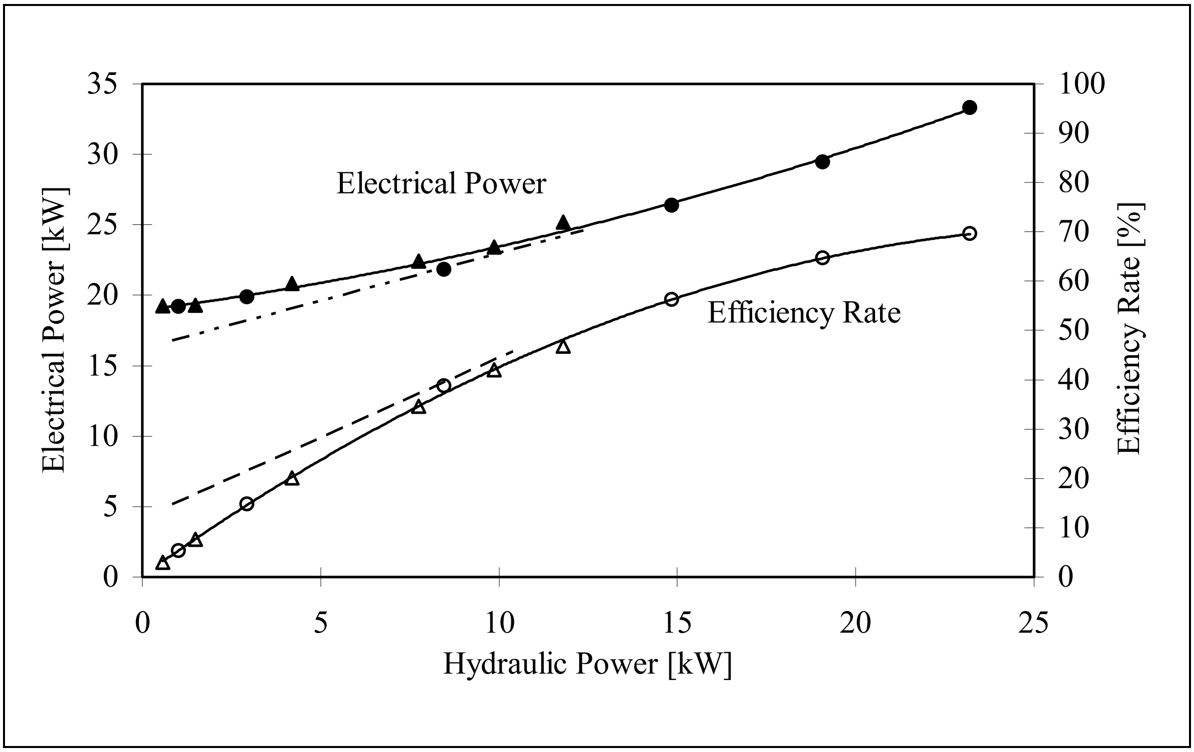

Figure 5: Electrical power and efficiency rate in dependence on hydraulic power for nozzle diameter 0.25 mm (triangles) and 0.35 mm (circles).

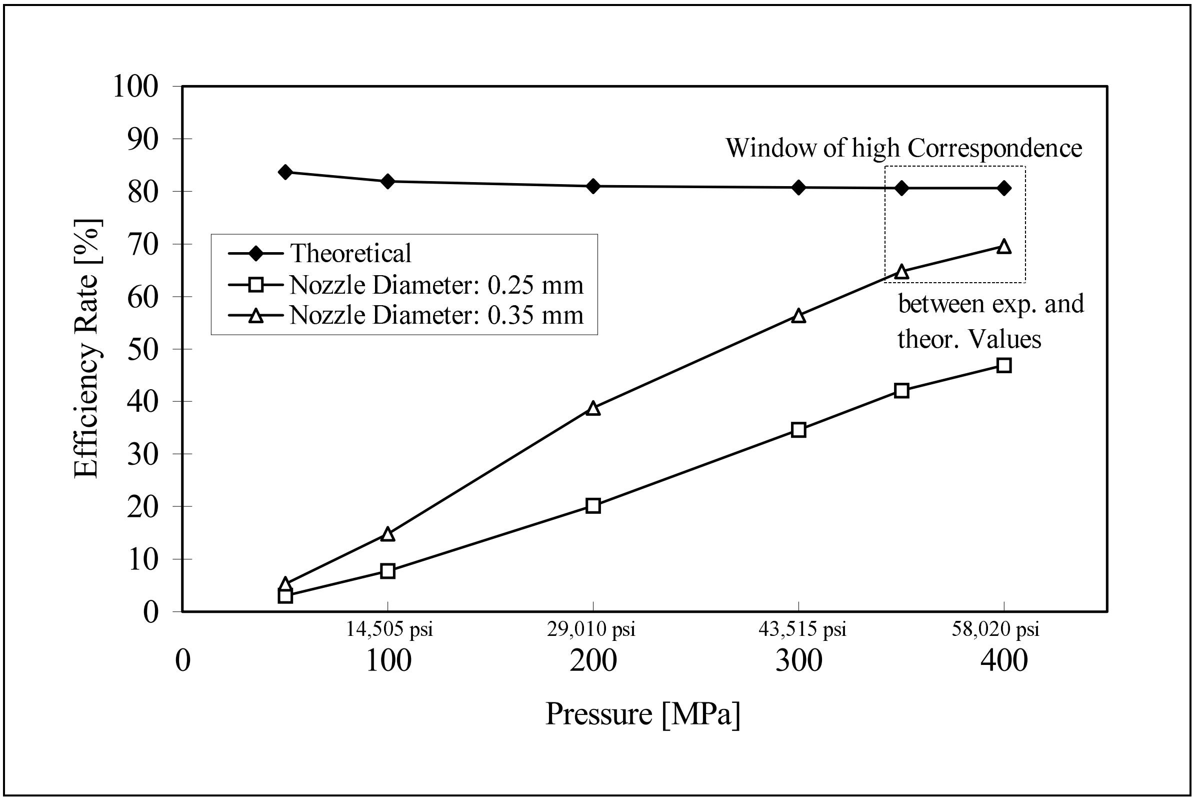

Figure 6: Comparison between theoretical and experimental efficiency rate.

10th American Waterjet Conference
August 14-17, 1999: Houston, Texas

Paper 39

THE DEVELOPMENT OF NEW WATERJET PUMPS

Gene G. Yie
Jetec Company
Auburn, Washington, U.S.A.

ABSTRACT

A pump is the heart of any fluid power systems. Waterjet processes in particular depend on the availability of suitable pumps because of their uncommonly high pressures and flow rates involved. As the waterjet industry grows, the demands on pumps have also grown. Many new waterjetting applications require that pump system be more powerful and yet more economical, more compact and yet more productive, more reliable and yet more versatile. These requirements are not being met satisfactorily by the currently available pumps and fluid pressure intensifiers. Jetec Company recognized this situation and initiated the development of modern pumps and intensifiers. By exploring new design concepts, Jetec has successfully conceived several new direct-drive pumps and pressure intensifiers that exhibit interesting capabilities. This paper discusses the many features of the direct-drive pumps that are under development at Jetec.

Organized and Sponsored by the WaterJet Technology Association

1. INTRODUCTION

The term “direct-drive” pump implies a pump that is driven directly by a motor or engine in contrast to a fluid pressure intensifier that is operated with a pressurized fluid such as compressed air or hydraulic oil. This distinction was necessary because intensifiers were commonly used in very high pressure applications while direct-drive pumps were not. However, this distinction is disappearing as many direct-drive pumps have been upgraded in their pressure capabilities and are invading the territories traditionally occupied by intensifiers, such as in waterjetting applications.

A common direct-drive pump is the crankshaft pump, which is named after the crankshaft assembly shared by all pumps of this type, much like that of automotive engines. It is called a triplex pump when it has three pistons and three cylinders. It is called a quintuplex pump when it has five pistons and five cylinders. They typically have a so-called “power end,” which is the crankcase that houses the crankshaft assembly and the piston rods, and a “fluid end,” which houses the plungers and check valves for the system fluid. The power end is typically made of cast iron and contains lubricating oil for the crankshaft, bearings, and piston rods. The fluid end generally consists of stainless-steel cylinders and a rectangular manifold assembly in which inlet and outlet fluid passages are bored. This type of pump has been extremely popular in agricultural and industrial operations for many years. The similarities between the crankshaft pumps and the automotive engines may have contributed to the pump’s popularity. On the plus side, crankshaft pumps are plentiful, ruggedly built, relatively simple in construction, and reliable in their intended applications. On the minus side, crankshaft pumps are heavy, bulky, inflexible, and have relatively low pressure capability.

In industrial waterjetting applications, crankshaft pumps have been the main equipment to date. Fluid-operated intensifiers now occupy only a small high-pressure niche of the applications due partly to their relatively high cost as they require the presence of a hydraulic power pack. As the waterjetting applications become more popular, the operating pressure is raised steadily. As a result, the operating pressure of crankshaft pumps is pushed higher and higher although some of them are not meant for such high pressures resulting in frequent breakdown. And yet there have not been many new pumps developed specially for high-pressure water applications. Jetec Company believed that waterjet applications deserve new and improved pumps and proceeded to develop such pumps. This effort resulted in a new rotary pressure intensifier that possesses some unique capabilities (Yie, 1997), and now a family of new direct-drive pumps.

2. AXIAL-PISTON PUMPS

Jetec’s new pump is the type commonly referred to as “axial-piston” pump that has been very popular in hydraulic applications. Inside these pumps, there are multiple plungers that are parallel to each other and to the center axis of a drive shaft. In most hydraulic pumps, the drive shaft is connected to a drum that has cavities to accommodate the multiple plungers. On one end, these plungers are in contact with a disk, commonly referred to as a swash plate that can be set at an angle with the center axis. On the other end, the drum is in contact with a check valve disk having the inlet and outlet ports. As the drum rotates, the plungers will rotate with the drum and will oscillate inside the drum cavities by means of a retainer disk or bias springs. By virtue of the stationary check valve disk positioned against the drum cavities, the oscillating motion of the plungers is synchronized with the port operation such that fluid inside the cavities is pressurized and then pushed out. Most hydraulic pumps have seven plungers and have a typical pressure capability of 2,000 to 5,000 psi; some special ones can go up to more than 10,000 psi.

This axial-piston pump design has many advantages. Those in hydraulic applications are noticeably more compact and smooth in operation when compared to crankshaft pumps. The power transfer from a prime mover to the pump pistons is direct and well balanced. However, their pressure capability is relatively low due to the check valves involved and to some other design aspects. Jetec adopted this parallel-piston approach and added other features to expand its pressure capability and to improve its versatility to suit the waterjetting operations. In Jetec's pump design, the drum that houses the plungers does not rotate; it is stationary. The drive shaft is connected to a slanted cam disk that abuts a set of plungers. The other end of these plungers is exposed to a bias force that could be from a spring or a pressurized fluid. When the cam disk rotates, each plunger will oscillate (and rotate as well in some pumps) in respect to their cage. This motion is then utilized to pressurize a system fluid in conjunction with suitable check valves. Several types of check valves were incorporated and resulted in several types of pump, each having its own unique capabilities.

3. LOW-PRESSURE PUMPS

One family of direct-drive pumps under development at Jetec has multiple plungers that oscillate and rotate against a slanted cam disk by virtue of the fact that plungers have one end matching that of the cam disk, as shown in Figure 1. The oscillating and rotating motion is utilized to provide inlet and outlet check valves that are built into each plunger. As the plungers rise and fall and rotate inside their cavity, the inlet and outlet check valve slots carved around the plungers are in a predetermined relationship with the inlet and outlet ports drilled in the pump body. The system fluid will flow in and out of each cavity in accordance with the plunger's motion, thus needing no separate check valves. There is a fluid inlet and a fluid outlet and a sealed chamber that houses the bearings and the cam disk. The end result is a very simple and compact piston pump that is also a fluid motor if the direction of fluid flow is reversed.

This pump/motor is built to have either clockwise or counterclockwise rotation. Its flow capability is a function of plunger displacement and operating speed. It can have very high flow capability if there are many plungers and the pump is operating at a very high rpm. Its pressure capability is a function of the fit of the plungers inside their cavities. It is estimated that a water pressure of 5,000 psi (350 bar) may be attainable with this type of pump without any modification of the check valves or the presence of any additional seals. A small 6-piston pump of this type is shown in a photograph presented in Figure 2; its internal piston chamber is shown in a photograph presented in Figure 3. This pump has six 0.312-inch-diameter axially-parallel pistons set to have 0.35-inch stroke, and can be operated up to 3,000 rpm for a maximum flow rate of about 2.0 gpm. It is 1.75 inches in diameter and 6 inches in length, weighing 3 lbs.

This family of pumps is ideal for hydraulic applications where compactness and reversibility are of value. They can be made to operate with water and other fluids if seals are incorporated to isolate the bearings. The self-priming capability of this pump allows it to be used in fluid transfer applications as well. As a fluid-powered motor, it can generate considerable torque if the pressure of the working fluid is substantial. It is estimated that pump and motor of this type can attain a maximum pressure capability of about 5,000 psi. The motor's speed, however, will be relatively low due to its small rpm/displacement ratio. Because of its dual capabilities, two units tied together can function as a fluid pressure intensifier in which one functions as a motor and the other as a pump; the motor accepts the working fluid while the pump accepts the system fluid. However, the basic design approach can be employed to construct a dedicated fluid pressure intensifier having only one set of pistons. It can also be used to construct unique fluid distribution valves, such as the one used in Jetec's rotary intensifiers.

4. MEDIUM-PRESSURE PUMPS

When a pump of the type described earlier is modified by adding an outlet check valve, its pressure capability can be significantly increased. The pump plungers can still have their built-in inlet check valve but will have separate outlet poppet-, disk-, or ball-type check valve. As a result, the pump's pressure capability can be readily increased to 20,000 psi (1,400 bar) or higher. Once separate outlet check valves are introduced, the pump is no longer reversible as a motor. A 8-piston pump of this type in shown in a photograph presented in Figure 4 and its interior is shown in a photograph presented in Figure 5. This pump has 0.375-inch-diameter plungers, 0.4-inch stroke, and can be operated at 2,500 rpm, indicating a peak flow rate of 3.8 gpm. It is only 2.5 inches square and 8 inches long, weighing 12 lbs.

This family of axial-piston pumps is intended in the future for light- and medium-duty waterjet applications at pressures up to perhaps 25,000 psi (1,700 bar). It is still quite simple in construction but does not have any convenience features such as pressure adjustment or flow shutoff. Its main attraction will be compactness and relatively low cost. Jetec believes that it will be useful in constructing fluid-jet thrusters or pulse-jet nozzle assemblies by connecting it directly to a hydraulic or electric motor.

5. HIGH-PRESSURE PUMPS

This type of pumps is currently receiving the bulk of attention at Jetec; it is intended to provide the features desired by many current and future waterjetting processes. It is still the axial-piston type having multiple pistons that are positioned around a center axis and abut a slanted rotating cam disk. The pistons may rotate and oscillate in their cavities or may only oscillate. The check valves for the system fluid are no longer built into the pistons; they are conventional types. In Jetec's setup, each pump piston assembly is treated as a module. There can be as many as fourteen piston modules in a single pump. These modules are divided to two groups and positioned in two concentric circles; each group is driven by a separate cam disk having its slanted face facing each other across the center axis, as shown in Figure 6. The purpose is to improve the force balance on the radial bearings of the cam disks.

Further, the pump piston modules are independent to each other; they share only the cam disks and fluid cavities. A working fluid, which could be a lubricating oil, the system fluid, or a third fluid, is introduced into each piston module to serve multiple purposes. Ideally, a lubricating oil having its own power pack and a heat exchanger should be used as the working fluid. This fluid is then circulated through the pump at a modest pressure of about 200 psi and is used to lubricate the pump parts and to control the pump's operation. When the working fluid is at its full pressure and flow, the pump is operating at its peak capacity. When the working fluid is reduced in pressure and flow, the pump's output is reduced accordingly. When the working fluid is dumped, the pump's output is stopped. Thus, this pump behaves much like a pressure-compensated hydraulic pump that its output can be manipulated by an operator. Otherwise, it is truly a high-pressure, high-flow pump that can be powered directly by an electric or hydraulic motor, or an engine.

Figure 7 presents a side view of a direct-drive axial-piston pump of this type. It is 6 inches in diameter, 13 inches in overall length, 46 lbs. in weight, and is sized to accept a maximum power input of about 50 hp. This particular pump has10 piston modules positioned in two concentric circles, each having five modules spaced 72 degrees apart. Each piston module is complete with its own high-pressure cylinders, as shown in a photograph presented in Figure 8. Ultimately, one pump housing will be able to accept several sets of piston modules, each having plungers of selected diameters and representing different power levels. For example, a set of ten piston modules having 0.188-inch-diameter plungers will have a peak power capability of about 30 hp when the pump is operated at 40,000 psi and is rotating at 1,800 rpm for a maximum flow output of about 1.3 gpm. If a set of ten piston modules having 0.250-inch-diameter plungers is installed, this pump will have a maximum power capability of 50 hp and a maximum flow rate of 2.3 gpm at 40,000 psi.   It is apparent that this pump is very compact for its flow and power capabilities. It is estimated that a 500-hp pump of this type will not be larger than 10 inches in diameter and could have 14 piston modules.

6. DISCUSSION

A pump is simply a device in which energy is transferred from a rotating shaft to a fluid. It is a good pump if the energy is transferred safely and efficiently. There are no other major issues involved in the pump's design. It is the same in waterjetting applications. There is no reason that waterjetting pumps need to be big and bulky since the flow rates involved are really very low when compared to many other fluid processes. To provide a compact, high-flow waterjetting pump, there must be multiple pistons operating at a reasonably high speed. Thus, packing the pistons in an axially-parallel geometry appears to be logical and desirable. Since water is not a good lubricant, forced oil lubrication must be applied to prolong the life of seals and plungers. Once a lubricating oil is involved, it is wise to use this oil for other purposes as well. Jetec followed these rules in the development of its high-flow, direct-drive pumps.

7. CONCLUSIONS

The direct-drive pumps presented here are intended primarily for high-speed operations, such as 1,800 rpm or higher. Such speed is possible because of the small components and short strokes involved. Jetec believes that it is advantageous to use small pump parts for several reasons - their inertia is much lower; they can be made better at less cost; and they are easier to assemble and service. By grouping the multiple pistons, check valves and cylinders into modules, the disadvantage of having so many parts is lessened. Jetec is currently fine tuning the performance of these new pumps. The data available to date indicate that they are worthy of the efforts involved. The design concept appears to be correct, practical, and functioning. However, the long-term reliability of these pumps remains to be evaluated. Further information pertained to these pumps will be presented in future papers.

8. REFERENCES

Yie, G. G., "A Pulsation-Free Fluid Pressure Intensifier, "*Proceedings of the 9th American Waterjet Conference,* pp. 365-372, Water Jet Technology Association, St. Louis, Missouri, 1997.

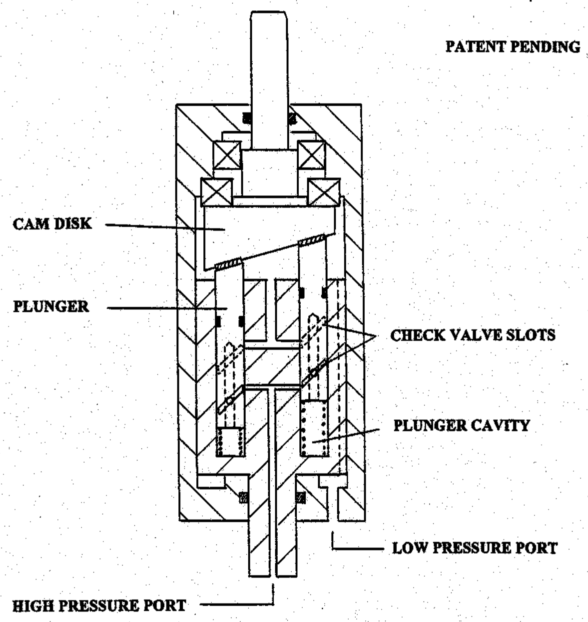

Figure 1. Schematic Drawing of Jetec's 6-Piston Rotary Pump

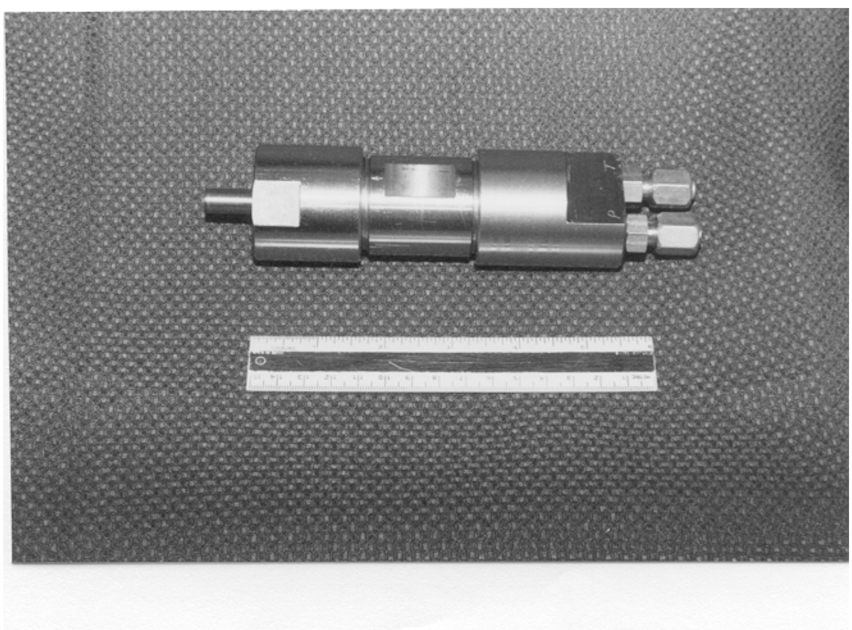

Figure 2. Side View of Jetec's 6-Piston Rotary Pump

Figure 3. Interior of Jetec's Small 6-Piston Rotary Pump

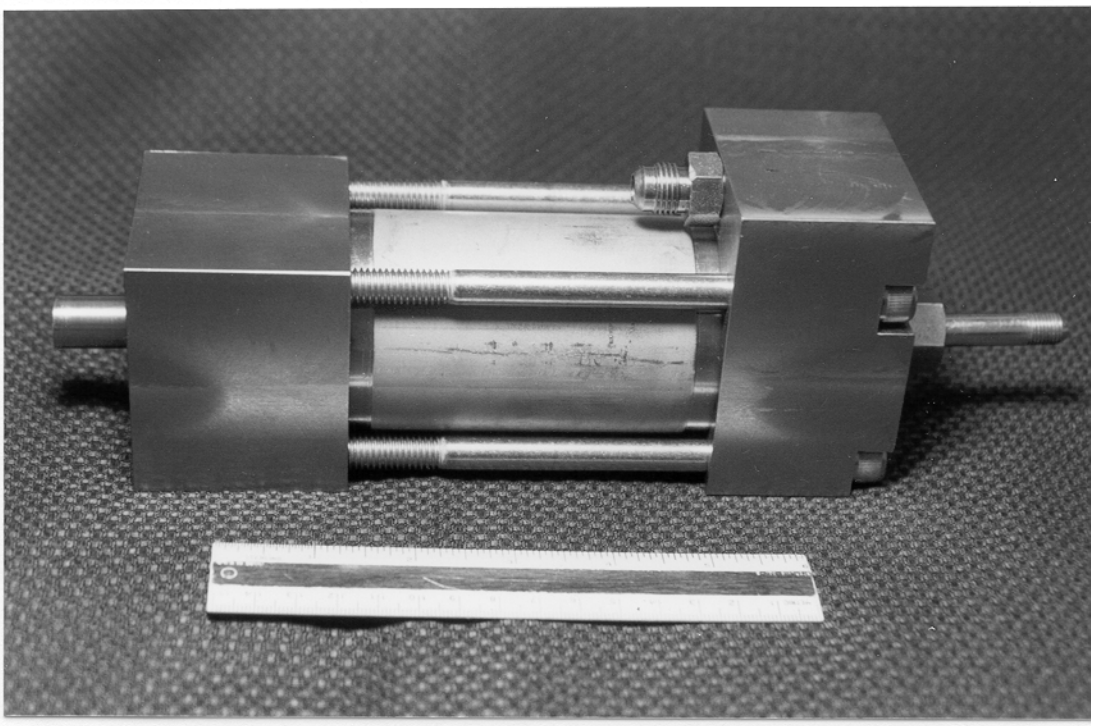

Figure 4. Side View of Jetec's 8-Piston Medium-Pressure Rotary Pump

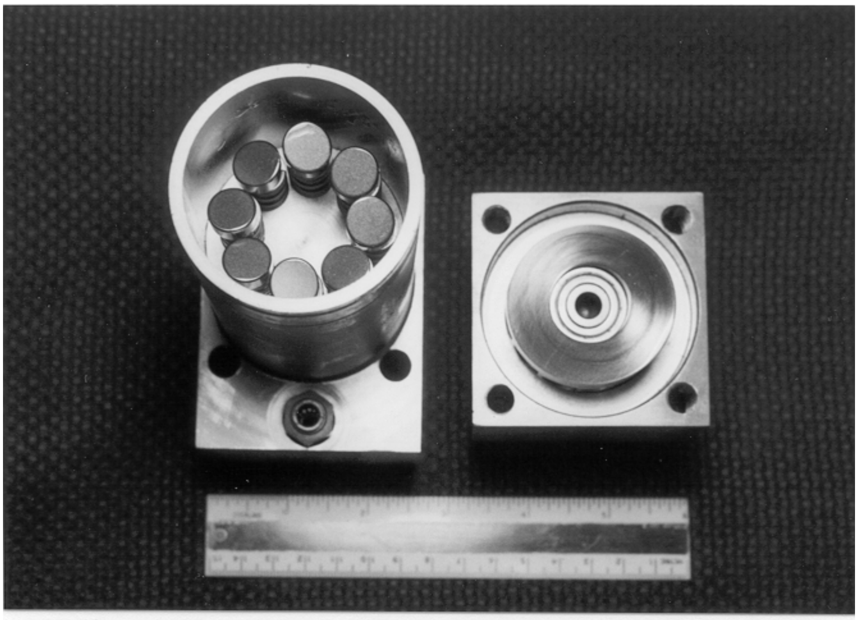

Figure 5. Interior of Jetec's 8-Piston Rotary Pump

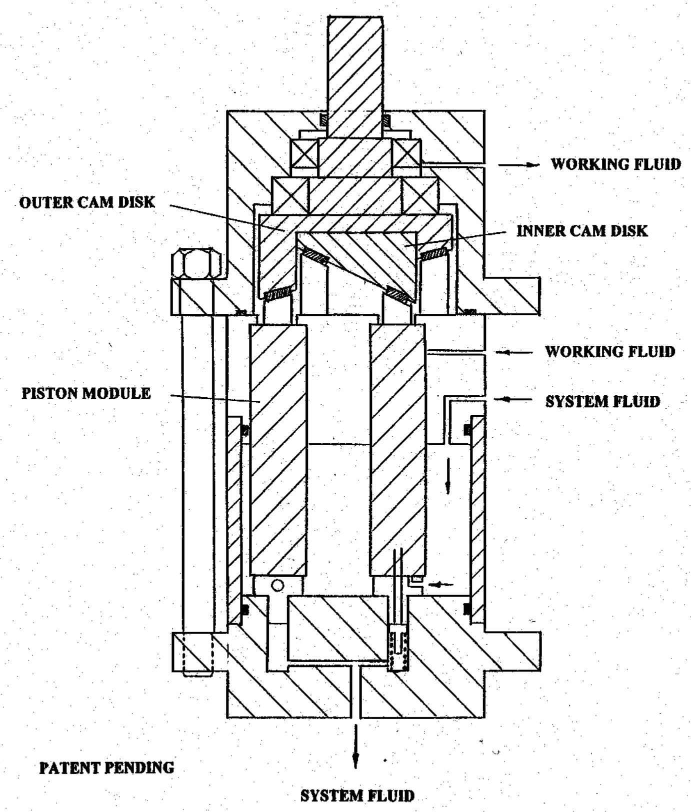

Figure 6. Schematic Drawing of Jetec's High-Pressure Rotary Pump

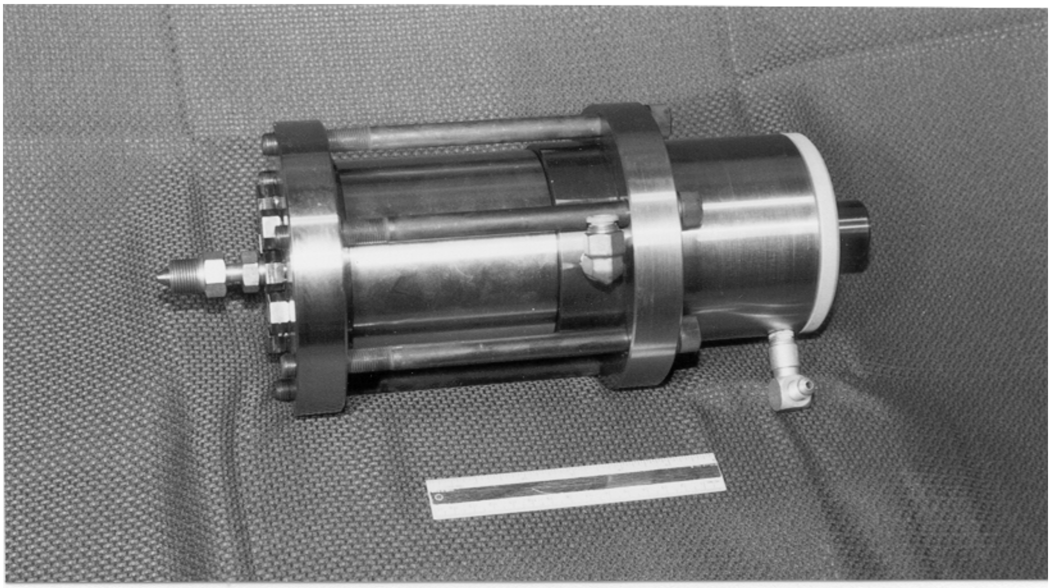

Figure 7. Side View of a Prototype 10-Piston Rotary Pump

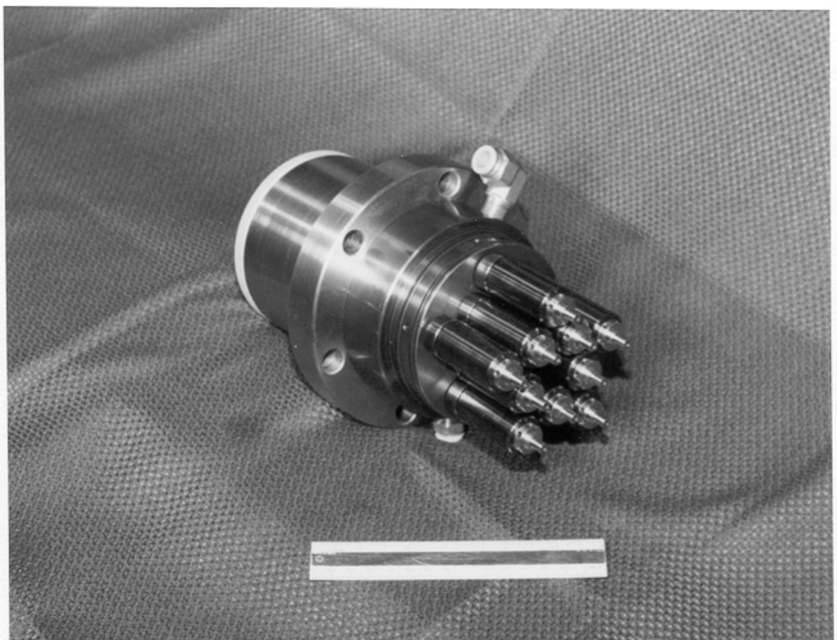

Figure 8. Modular Piston Assemblies of Jetec's 10-Piston Rotary Pump

10th American Waterjet Conference
August 14-17, 1999: Houston, Texas

EXTENDED TECHNOLOGIES FOR

ULTRA HIGH PRESSURE WATERJET CUTTING SYSTEM

Huang W. P., Xue S. X., Chen Z. W., Fan Y. B., Peng H. J.
General Machinery Research Institute, Bureau of National Machinery Industry
Hefei, Anhui Province, P. R. China

Yang Y. H., Shi D. J.
Jet Cleaning Equipment Factory
Yangma, Jianyang, Sichuan Province, P. R. China

ABSTRACT

After we have successfully developed the 300 MPa ultra high pressure abrasive waterjet cutting system, our latest commercial researches are focused on the extended technologies, which are ultra high pressure moving seal, even and continuous supply of abrasive, safety alarm and break points guarantee, pressurized water supply and its fine filtering, water return in cutting head and numeric control (NC or CNC) system, etc. These seemed not to be major problems could influence directly the functions and reliability of the cutting system. In this lecture, we put up the detail methods to solve these problems and describe the structures of combined seal, screw type abrasive supplier and pneumatically driven relief valve. The fine settlements of these problems guarantee the spread out of Chinese waterjet cutting systems and their usage in metal and nonmetal materials plates cold cutting.

1. INTRODUCTION

The abrasive waterjet cutting is a highly new technology concerned mainly with fluid mechanics combined with other technologies like pump, valve, seal, material and automatic control. Each set of ultra high pressure abrasive waterjet cutting system is consisted of the main pump or intensifier, flow control valve, pipeline and its connection, pressure regulating vessel, abrasive supplier, cutting head, catcher, cutting table and control system, etc. (Shown in Figure 1). Keys to ensure the steady work of ultra high pressure waterjet cutting system are listed as below:

- The ability to form a complete set of machine;
- The service life of seal, valve, hydraulic head and piston;
- The cutting ability of cutting head and service life of nozzles;
- Even and continuous supply and control of abrasive;
- Control of cutting head movement and total system working.

Because of ultra high pressure pump having the characteristic of its positive displacement, there are many problems caused by the direct overflow in ultra high pressure and ramping raise of pressure after overflowing in cutting system that uses ultra high pressure pump as pressurized water source, such as the block up of abrasive transportation pipe caused by abrasive wetted by water return in cutting head, the transition period for pressure rising from low pressure to rated pressure during start of cutting again after overflowing and setting of pausing time at initial cutting point.

2. STRUCTURE OF ULTRA HIGH PRESSURE RECIPROCATING SEAL

The reciprocating pump used for waterjet cutting has a small flow rate of 2~3L/min. and works under ultra high pressure, so high reliability, long service life ultra high pressure reciprocating seal becomes one of the keys to make cutting system work steadily. Under pressure up to 300 MPa, single soft stuffing seal can not meet our needs. So we adopt the combined seal made of both soft stuffing and metal sleeve gasket instead of single soft seal. Its basic structure is shown in Figure 2.

Shape of sealing muff is the crux to form micro clearance needed. Outside of sleeve gasket bears high pressure and is elastically deformed, so the hard to machine micro clearance between piston and gasket is formed. This clearance lets high pressure drop down gradually and achieves sealing purpose. At the meaning, seal between gasket and cylinder can be solved by installing static seal using a triangular washer. But in actual uses, serious leakage is often found. Answer to this question lies on the floating characteristic of sleeve gasket. Micro swinging of gasket can result in failure of triangular washer seal. This micro swinging is caused usually by the bad alignment among the axes of gasket, piston and cylinder. In serious condition, it may lead to holding together of piston and gasket. So it needs to raise the precision of machining and assembling these three parts, let their axes be in good alignment to achieve better sealing effect. Since the contact between sleeve gasket and piston belongs to metal to metal contact, we machine several annular grooves on inner side wall of gasket to store the leakage water and use as cooling and lubricating medium to prevent pump from overheating. This leakage can be blocked up by soft stuffing seal after the metal sleeve gasket. This soft seal ensures that the clearance after metal gasket has a positive pressure to compensate the inadequacy of clearance seal and prevent the air from inhaling into sealing cavity in pump's suction stroke.

Because that the clearance seal must have a small leakage to work normally and leakage quantity can influence working pressure of system greatly, we use the frequency converter as power supplier for electric motor to ensure that the system can work under steady pressure over a long period of time. When leakage quantity gets large and system pressure becomes falling down, the automatic control system can increase pump's rotation speed through converter so as to increase working flow rate and compensate for leakage. The converter can be operated manually or automatically by feedback of pressure signal.

3. ABRASIVE SUPPLIER SYSTEM

Normal abrasive supplier system often uses vacuum sucker and small hole throttle to control the abrasive flow rate. There must be installed with abrasive valve to control abrasive pipeline opening or shutting off. This simple control pattern has the disadvantages of blocking of little hole, uneven supply of abrasive and hard-to-controlled abrasive flow rate. The usual settlements to these problems often make the abrasive supplier become much more complicate so that cost of system becomes enlarged and total system becomes hard to spread out.

In our development, we solve these problems thoroughly in a different way by using the screw type abrasive supplier. Its basic concept is shown in Figure 3.

In this supplier, the feed screw rod driven by micro electric motor makes abrasive fall from barrel into transportation pipeline in a even and continuous flow. Abrasive enters cutting head through the sucking function of vacuum generated in mixing chamber of cutting head. If the micro motor is stopped, system stops supplying abrasive to cutting head at once so the abrasive valve can be omitted.

The flow rate of abrasive is determined by shape and size of screw thread and rotation speed of motor. Their relationships are governed by the following equation:

$$Q = \pi D S n \rho N X 10^{-3} / \cos\gamma \qquad \text{g/min}$$

where, D is the diameter of screw thread in mm;

γ is the spiral angle, $\gamma = \mathrm{arctg}(P/\pi D)$, P is the thread pitch in mm;
S is the area of screw thread in mm^2;
n is the rotation speed of micro motor;
ρ is the heap density of abrasive in g/cm^3;
N is the number of spiral threads.

In our actual use, the rotation speed of motor is 77r/min., abrasive used is $80^{\#}$ garnet and its measured heap density is 1.85g/cm^3. Based on these data, the calculated abrasive flow rate of 40.6 g/min. is well coincided with the actual tested flow rate of 40g/min. Because flow rate is in direct proportion to rotation speed of motor, we can easily adjust abrasive flow rate by adjusting the rotation speed. To the feed screw rod in our system, flow rate can be increased up to 180g/min. if rotation speed is raised to 300r/min. and can fulfill normal needs of cutting well enough.

The air valve shown is used to control the flow rate of sucked air. During transportation period of abrasive in pipeline to cutting head, it needs to supply a determined quantity of air into transportation pipeline in order to maintain the fluidity of abrasive and prevent it from piling in pipe. The longer and more curves of the pipeline, the larger quantity of air is needed. But if the airflow is too large, it is easy to cause the jet diffusing and reduce its cutting ability. So it needs to be carefully adjusted.

4. PNEUMATICALLY DRIVEN RELIEF VALVE

In intensifier system, if cutting head is not working temporarily, we can just shut off the pneumatically driven stop valve before head, let system keep in the state of high pressure and piston of intensifier keep in motionless state. If we want the head to work again, we can simply open the stop valve; jet can be generated immediately. But for waterjet cutting system using ultra high pressure pump, it needs to relieve under ultra high pressure, that is to say, the ultra high pressure relief valve must be installed in such system. To guarantee the safety of ultra high pressure pump, the relief valve must be placed in position just near the outlet of pump, not near and before the cutting head.

Reliability and its service life of seal are keys to develop if direct pressure relief is wanted under pressure of 300 MPa. Structure of relief valve that we have developed is shown in Figure 4.

In this valve, when the air cylinder is not connected to compressed air source, the valve core is fitted tightly on the valve seat by compressed spring and system is kept in state of ultra high pressure. If the cutting head is wanted not to work, we can simply energize coil of the 2-positions 3-ports electric valve to let the valve core be lifted by piston of air cylinder driven by connected compressed air. By doing like this, the main system relieves and returns to atmospheric pressure. The spring compressed force is adjusted according to the diameter of valve core and working pressure of system. Normally, the start-up pressure is set to 1.03~1.10 times of maximum working pressure, so the relief valve will start to relieve and act as the protective guard for exceeded pressure if the system pressure exceeds the start-up pressure caused by block-up of nozzles and other reasons.

The pneumatically driven relief valve can also be controlled by pressure monitor. The monitor checks system working pressure through sensors and can be set the alarm pressure. When system pressure is raised approaching alarm pressure, pressure monitor will start to alarm by sound and flashing light. If system pressure keeps raising and exceeds the preset start-up pressure, relay in pressure monitor will be closed, coil of the 2-positions 3-ports valve is energized, valve is opened to let the compressed be inlet into cylinder and system starts to relieve. Besides these control patterns for relief valve, we can also control this valve through the control signal sent from cutting head control system. When cutting head is moved to the initial cutting point or preset breaking points in cutting paths, the computer port will send the signal to relieve system just by energizing coil of the 2 positions 3 ports air valve like above.

5. SETTLEMENT OF WATER RETURN IN CUTTING HEAD

In waterjet cutting system using ultra high pressure positive displacement pump as high pressure water source, when relief valve opens, system pressure will fall directly from ultra high pressure to atmospheric pressure; on the contrary, when system starts to work and relief valve is closed, system pressure is raised from normal pressure to ultra high pressure. Because of the influence of system pipeline and installed pressure regulation vessel, the process of pressure rising becomes very slowly. The cutting head sucks abrasive out of abrasive transportation pipe with help of vacuum in pipe generated by suction of high speed waterjet. When system pressure is very low, effective waterjet is not formed out of the water nozzle, the low pressure water will flow into the abrasive pipeline, this usually is called water return. If water nozzle is not well coaxial with abrasive nozzle or relief valve opens while cutting head encounters breakpoint and abrasive pipe is in vacuum pressure, this phenomenon is very serious. If not well controlled, the returned water will wet abrasive in pipe or even flush into abrasive barrel, stop the transportation process.

According to our tests, water return usually occurs during period of relief valve relieving or pressure rising. To overcome this, we put up two ways. First, we install check valve just before cutting head and think that there will have no water left and water return is prevented because it will close if system pressure falls low due to pressure relieving through relief valve. But actual tests show that this way does not work during process of system pressure rising. The reason is that the water nozzle is still in low pressure though there has some pressure before head after check valve is opened. Though period time of water return is shortened, the effect is still serious enough to cause the system malfunction. Besides this, this check valve has water resistance and interfere with the fluid field before cutting head. These are not favorable to head working well. Second, we draw the returned water directly from cutting head. But tests show that it is very difficult to fulfill because of the very rapid process of water return. On the other hand, when cutting head is in normal working, water drawing device must be closed tightly. But because of the abrasive particles contained in returned water, it is impossible to shut off thoroughly.

These two ways can not work, we have to think this question systematically and put up the following way. First, we must ensure that there is no abrasive left in transportation pipe before we want to stop cutting. We can stop supplying abrasive first when cutting head encounters a breakpoint and open the relief valve after abrasive in transportation pipe is sucked thoroughly clearly. This process only lasts few seconds and is achieved very conveniently. Second, in order to keep system maintaining a certain pressure after pressure relieving, let the waterjet be formed by cutting head but have no cutting ability, we set a throttle hole in relief port of relief valve. By doing like this, we can keep the relief pressure stabilized at several mega-pascal.

This way not only solves the problem of abrasive blocked up caused by water return thoroughly, but also raises the speed of pressure rising and ensures that the system has a higher cutting efficiency.

6. CONCLUSION

Normally, the intensifier is used as the pressure source in most waterjet cutting systems around world. Based on Chinese situation, we have successfully developed the total set of waterjet cutting system adopting the ultra high pressure pump as the pressure source, solved the problems such as reliability and life of ultra high pressure pump, even supply of abrasive, water return prevention and pneumatically controlled pressure relief, etc. and commercialized it.

Compared with intensifier system, our ultra high pressure pump system has the advantages of simpler structure, lower cost, lower pressure pulsation and higher efficiency and a vast vista.

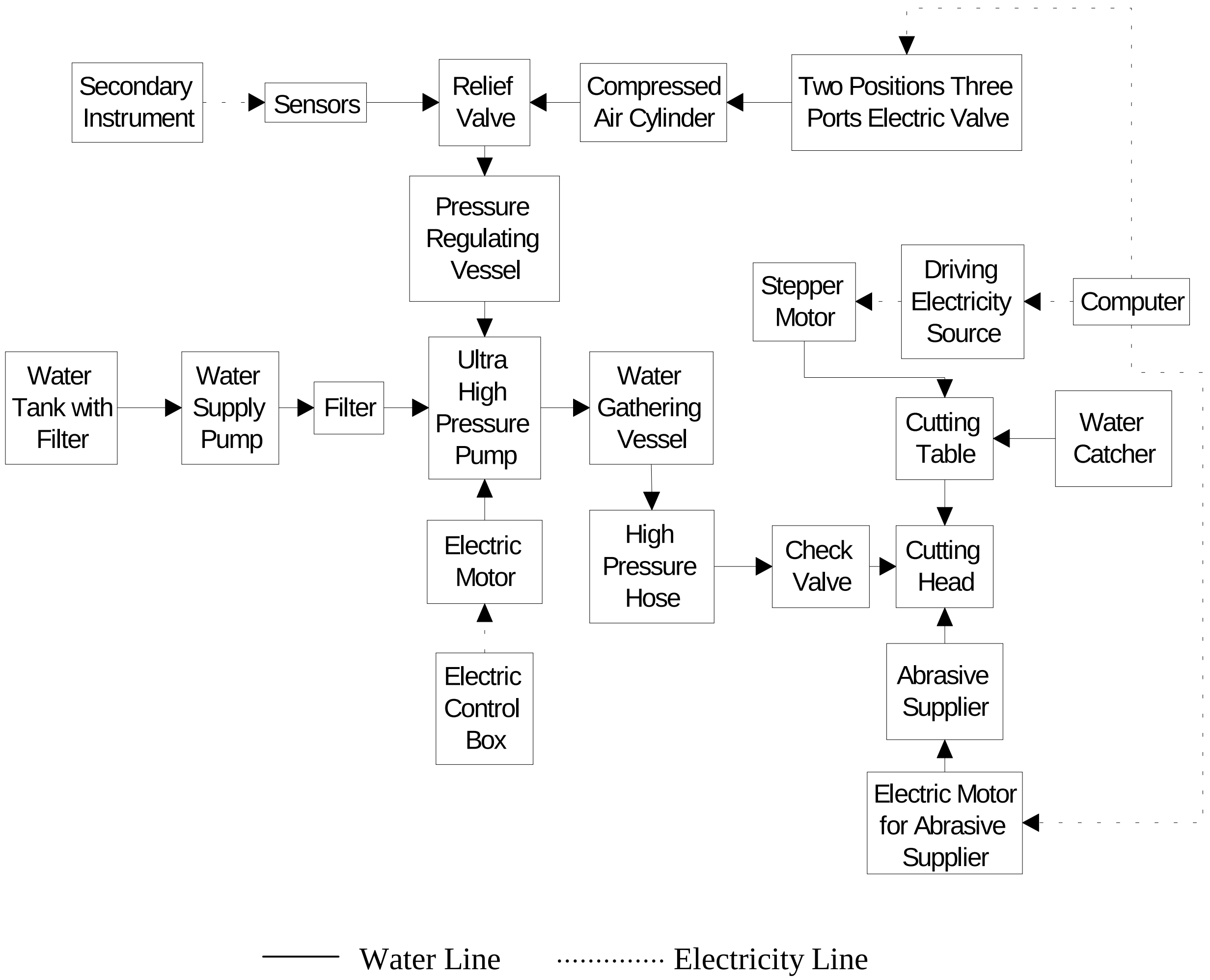

Figure 1. Sketch Diagram of Waterjet Cutting System Using Ultra High Pressure Pump as the High Pressure Water Source

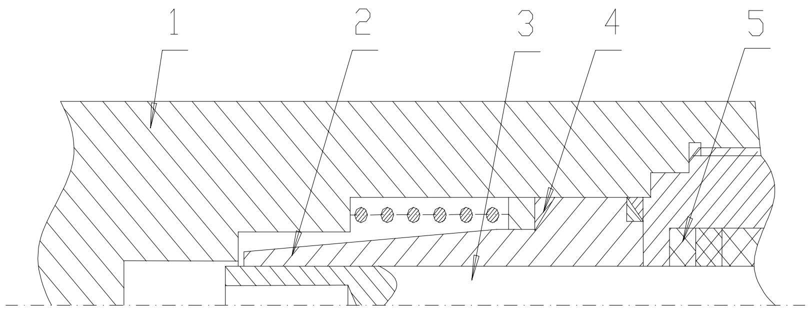

Figure 2. Structure of Ultra High Pressure Reciprocating Seal

1. Cylinder Body 2. Sealing Sleeve Gasket 3. Piston

4. Triangular Washer 5. Sealing Stuffing

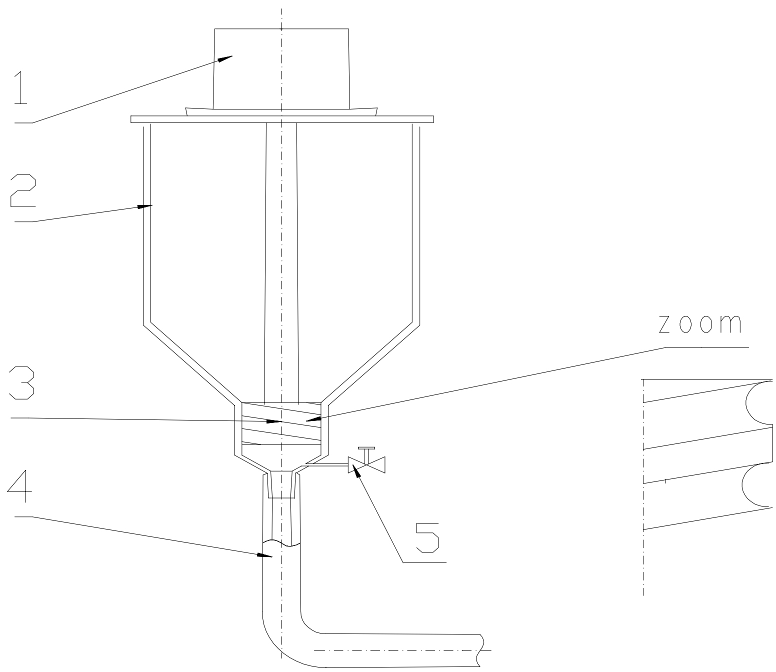

Figure 3. Principle of Screw Type Abrasive Supplier

1. Driven Electric Motor 2. Abrasive Barrel 3. Feed Screw Rod
4. Abrasive Transportation Pipe 5. Air Inlet Valve

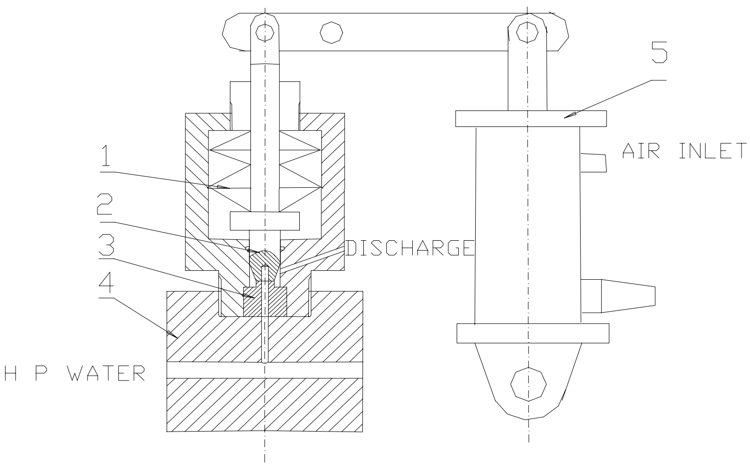

Figure 4. Pneumatically Driven Ultra High Pressure Relief Valve

1. Compressed Spring 2. Valve Rod 3. Valve Core 4. Three ports part 5. Air cylinder

10th American Waterjet Conference
August 14-17, 1999: Houston, Texas

Paper **41**

CORROSION PREVENTION STUDY ON MATERIALS USED IN HIGH–PRESSURE WATER JET CLEANING MACHINES

Yang Jiao (Vice-Director), Leyao Zhang (Director)
High-Pressure Water Jet Cleaning Technology Center of Beijing Yanshan Petrochemical (Group) Co., Ltd.

Fanhua Li (General Manager)
Beijing Duoke New Technology Development Co.
Beijing, China

ABSTRACT

The main components of high-pressure water jet cleaning machines and equipment are often corroded because of their constant contact with water and air. This is a relatively common, simple but difficult problem, which not only reduces service lifetime and increases maintenance and operation costs but also reduces application efficiency of machines and equipment. In this paper, combined with working practice, corrosion-proof materials and technology commonly used are analyzed. And through comparison with nickel-phosphorus plating, and by tests and industrial application, it is pointed out that the nickel-phosphorus plating of the main components can improve their chemical and physical properties and is, at present, a good methods to solve the corrosion prevention problem for high-pressure water jet cleaning machines and equipment.

Most components of high-pressure water jet cleaning machines are metallic materials, and they are often in contact with water and air during operation and sometimes in contact with corrosion media, therefore the high-pressure water jet cleaning field has long been puzzled by the corrosion problem. To solve this problem, commonly used methods include the application of corrosion-proof materials such as stainless steel and copper etc., the adopting of surface treatment technology such as chromium plating and galvanization etc., which are all found some shortages with application results unsatisfactory.

1. ANALYSIS ON COMMONLY USED MATERIALS

1.1 Stainless steel

Stainless steel features excellent corrosion-resistant properties while also meets requirements for mechanical strength, but has the following problems:

1.1.1 Lacking material source, especially for some components with special requirements, such as large forging for pump casing head, spring steel, abnormal shaped proximate matter, etc.

1.1.2 Sticking is likely to occur between two stainless steel parts connected with screw during assembling and operation, leading to damage of such parts.

1.1.3 Difficult to fabricate. The fabrications of stainless steel parts, whether lathe, milling, tapping or heat treatment, are all more difficult than those of carbon steels.

1.1.4 Expensive. The costs of stainless steel materials are generally 4 to 5 times those of carbon steels, and even higher for special shapes.

1.2 Copper

Copper possesses certain corrosion resistant properties and is easy to be fabricated, while its source of supply and price are all feasible, but its strength can hardly meet the requirements of high-pressure water jet cleaning components, especially of parts requiring certain hardness.

1.3 Other materials

Titanium products possess corrosion-proof properties, but their source of supply and prices become a significant drawback. Engineering plastics such as polytetrafluoroethylene etc. exhibit less strength, hardly capable of fulfilling the requirements of the parts of high-pressure water jet cleaning machines.

2. ANALYSIS ON SURFACE TREATMENT

2.1 Chromium plating

Chromium plating can prevents corrosion, but the parts with chromium plating are added some uneven extra thickness which must be machined again to meet the fit tolerance. Whereas some locations such as screws and dowel holes are unable to be machined, and hence the chromium plating can not provide the solution for the corrosion prevention of these locations.

2.2 Galvanization

Galvanization is a basic corrosion-prevention technique by which extra thickness is not added. But its corrosion-prevention capacity is rather small, which would quickly lose function under the condition of friction and long time contact with water, air and corrosive media.

The above brief analyses on materials and surface treatments show that these are all failed to meet the requirements of corrosion prevention for high-pressure water jet cleaning machines and equipment. Through these analyses, we realized that it is a good fortune for the high-pressure water jet cleaning field if there is a surface treatment technology by which the parts do not add thickness, while possess enough hardness, abrasion resistance and corrosion resistance.

3. SELECTION OF NEW TECHNOLOGY

By years of efforts, we have found a new method, the chemical plating of nickel-phosphorus alloy, which can basically meet these requirements. The chemical plating of nickel-phosphorus, developed by American scientist A. Brenner and G·Riddel, is conducted through chemical reaction between plating liquid and part's surface, which results in a plating layer of non-crystalline nickel-phosphorus alloy. This technology is in the form of chemical penetrating, and hence does not add thickness to the parts treated, while the treated surface possesses very high hardness and abrasion resistance. On the basis of step tests, industrial application was conducted for many parts and components, yielding good results. In practice, it is proved that this technology features the following characteristics:

3.1 Even plating layer.

The plating layer is formed by catalytic redox reaction between the plating liquid and the surface of the parts treated, without edge and corner influence, and no limitation of geological shapes of the parts treated. Screws, narrow slots, small holes, and slits can all be plated satisfactorily with no burrs and without missing-plating.

3.2 The plating layer possesses high hardness and superior abrasion resistance.

The hardness of the plating layer is HRC 50~55, and after heat treatment, it reaches HRC 63~69. The non-crystalline state of the plating layer begins to change into micro-crystalline structure at a temperature of 300°C, increasing the hardness and abrasion resistance of the plating layer.

3.3 The plating layer has high bond.

It is formed by the penetration of plating liquid into the surface of the parts treated, and the plating liquid has a thermal expansion coefficient similar to steel, therefore the plating layer possesses good adhesion, 300~400 MPa, higher than that of electroplated chromium layer, and hence is unlikely to peel.

3.4 The plating layer possesses superior corrosion resistance.

Since the plating layer is in amorphous state (non-crystalline state), being no such crystal defects as crystal boundary and grain boundary sliding etc., and its structure is monotonous and uniform, therefor galvanic corrosion is unlikely to occur, and corrosion resistance is superior. The porosity of the plating layer is low, and this provides ideal shielding layer to protect the base metal from corrosion. The corrosion resistance of such parts is superior to stainless steel when used in many media (see Table 1.)

Table 1. Comparison of Corrosion Conditions between the Plating Layer and 1Cr18Ni9Ti

No	Medium	Concentration %	Temperature °C	Corrosion Rate, mm/a	
				Plating Layer	1Cr18Ni9Ti
1	NaOH	20	Boiling	0.001	0.06
2	NaOH	40	Boiling	0.021	0.45
3	HCL	10	20	0.017	1.01
4	H_2SO_4	10	20	0.048	0.45
5	HF	40	30	0.012	
6	H_3PO_4	85	50	0.102	0.0125
7	H_3PO_4	50	20	0.002	0.0125
8	HNO_3	40	20	0	0.0125
9	HCOOH	85	Boiling	0.12	1.3

3.5 Wide application.

This technology can be used to plate such materials as steel, iron, copper, aluminum and alloys. The friction factors between this plating layer and other friction pairs are relatively small. In addition, both new and used parts can all be plated, and for corroded parts, this plating provides restoration.

3.6 The chemical plating does not require high temperature, hence does not cause deformation.

3.7 Low cost. In consideration of material cost, fabrication difficulty, and assembling cost, the chemical plating technology has a great advantage in price.

Because of these characteristics, this technology is capable of satisfying the requirements of the high-pressure water jet cleaning field for corrosion prevention of some parts.

4. INDUSTRIAL APPLICATION

For years, we conducted industrial applications for different parts successively, and the results are satisfactory.

4.1 Pump casing is the most important component for high-pressure pump. Corrosion prevention of carbon steel pump casing is a difficult task. In order to prevent corrosion, the carbon steel pump casings after pump operation were blue-treated and painted each half-year, but failed to prevent corrosion damages. Some pumps are used less than 3 years (operating time is less than 2 years) when they are discarded because of corrosion. After chemical plating of nickel-phosphorous for the pump-casing head (Fig.1), the pump casing obtains the results of a stainless steel pump. It has no corrosion in 3 years, with all fitting surface as smooth as the original fineness (A, B, C…), and with screw holes (D, E…) convenient for assembling with bolts. And what is even worth mention is that three used pump casings, after chemical nickel-phosphorous plating, were operated again for more than 3 years instead of discarded.

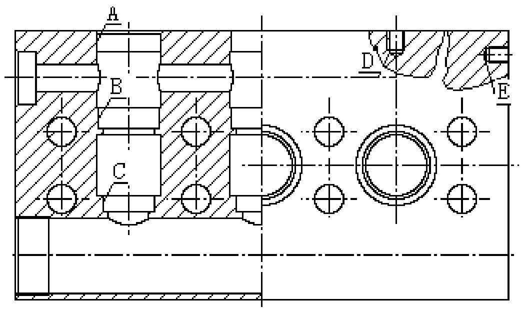

Figure 1. High-Pressure Pump Casing

4.2 The cross head connection bar (Fig.2) of the high-pressure pump is the critical component of the dynamic sealing between the driving side and the outside. The lubrication oil inside and the dust and water outside should be separated here appropriately, otherwise oil leaks from here, resulting in lacking lubrication and hence in burning of bush, or dirt and water enter crankcase, resulting in emulsification of the lube and hence in burning of bush too. It is because of this, the fineness and the corrosion prevention of the cross head connection bar is of great significance. This component is often generally considered to be in contact with oil constantly and hence is unlikely to be corroded, and therefore carbon steel is selected. The actual condition is that this component is often in contact with water during operation because of the leakage of the plunger filler, and exposes to air after operation, and therefor, rusty spots appear not a long time after putting into service. In many pumps we used, the following phenomena occurred in the past: the lube in the crankcase of the pumps is emulsified under the condition of no other water leakage. After analysis, it is realized that this phenomenon is caused by the rusty sports. Because of the existence of rusty spots, the tiny amount of water stayed in the pits of the rusty spots is brought into the crankcase in each stroke, and retained inside the crankcase when passing through the oil scriber of the oil sealing. Thus four-to-five hundreds' "brought-in" per second quickly makes the lube emulsified. After the cross head connection bar is plated with nickel-phosphorous layer, increasing its corrosion resistance, this phenomena never occurred again, solved the tough task of corrosion prevention for this component. What is even worth mention is that the hardness of this component increased drastically after plating, and its abrasion resistance is increased, thus its service life is increased greatly.

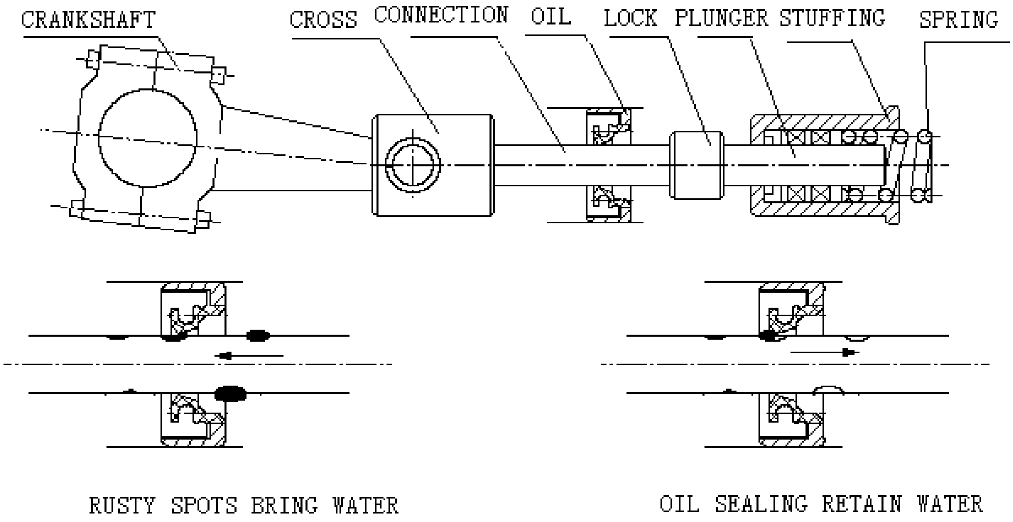

Figure 2. Cross-Head Connection

4.3 The body of the pedal valve is also an important component of the water cleaning equipment (Fig.3). There are screw holes on the valve body (A, B, C, and D), that serve as the flow channel for the high-pressure water flowing in and out. Therefor it is required that the fitting gap of the screw is small, and its precision and fineness is high. And the equipment is often dismounted during routine maintenance. In the past, different type of stainless steels are chosen to be used as the valve body and connections but screw sticking often occurs in the process of disassembling and assembling, resulted in discarding of both the valve body and connection. After the valve body is manufactured by using carbon steel and chemically penetrated with nickel-phosphorous, this sticking phenomena never occurred again, thus the problem of valve body sticking, discarding and the corrosion has solved.

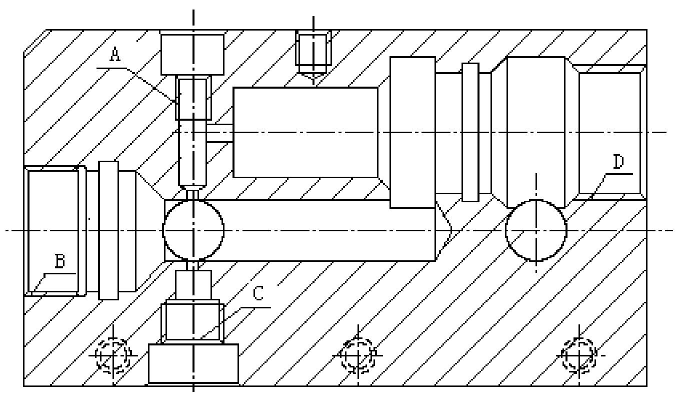

Figure 3. The Body of Pedal Pressure-Regulating Valve

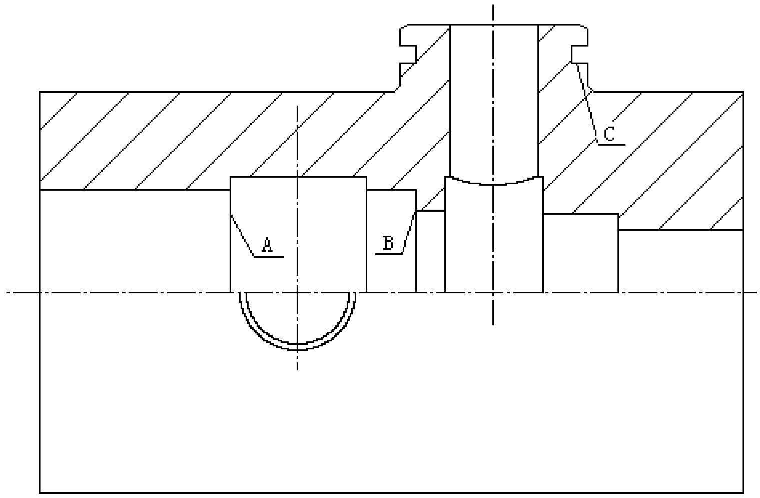

Figure 4. The Body of Pressure-Regulating Valve

4.4 The body of the pressure-regulating valve is a component of the high-pressure pump set (Fig.4). This component is a product already produced with carbon steel, thus corrosion-proof treatment is need. Other surface treatment methods lead to non-uniform plating layer and burrs, hampering assembling and usage. Whereas the chemical penetration of nickel-phosphorous basically does not change component dimension and tolerance, and does not form plating burrs at corners and circular slots (A, B, C etc.). This provides convenience for assembling and usage, and thus the corrosion-proof treatment of a ready-produced product is accomplished to ensure its excellent corrosion resistance.

4.5 The three-dimensional rotary water cleaning head is also a critical accessory for the high-pressure water jet cleaning equipment. Its casing body (Fig.5) is in direct contact with the materials blasted, which mostly are corrosive. This component often produced by using stainless steel. The properties of this material lead to difficulties in the process of fabrication, no matter forging, milling and boring. After substitution with carbon steel plated with nickel-phosphorous, the fabrication difficulties are reduced dramatically, and fabrication cost is reduced by 50%. After several years on trial, its corrosion resistance is no lower than that of stainless steel, endured the corrosion of such media as acids and alkalis etc, satisfying application requirements.

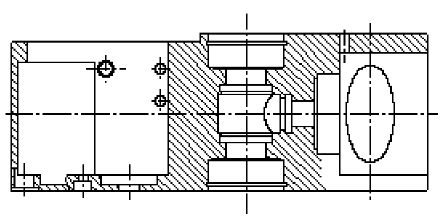

Figure 5. The Casing Body of Plasting Head

4.6 The butterfly spring is an important component in the pressure-regulating valve of the high-pressure pump set (Fig.6). Determined by its working characteristics, this component can only be manufactured with spring steel, since other materials are unable to attain such high mechanical properties (strength, hardness and elastic force). But the corrosion resistance of the spring steel is very low, and after long time in contact with water, corrosion is inevitable. When such component is plated with chemical penetration of nickel-phosphorous, not only the corrosion problem is solved but also the mechanical properties are preserved, thus the service life is increased.

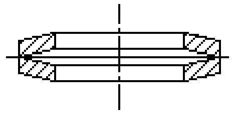

Figure 6. Butterfly Spring

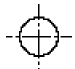

Figure 7. Steel Ball

4.7 The steel balls (Fig.7) are important components of the high-pressure water jet cleaning pump set, and also serves as fittings of multiple-size and small quantity. These steel balls are installed in the safety valve, pressure-regulating valve and pedal valve to serve as high-pressure sealing parts, and they are in constant contact with water. A tiny corrosion of these steel balls will cause leakage. The steel balls on the market are mostly made of bearing steel, and their corrosion resistance is very low. Whereas stainless steel balls are difficult to place orders since when the ordered quantity for one size ball is less than several hundreds, they are not enough for starting production. And the hardness of the stainless steel balls are low, thus when used as sealing ball in a valve, the ball is often damaged to have notches under press, losing sealing capability. When using balls of bearing steel and plated with nickel-phosphorous penetrating technology, good results are obtained: not only preserved the hardness, roundness and fineness of the balls, but also satisfying the requirements for corrosion resistance.

5. CONCLUSION

The above industrial application of the high-pressure water jet cleaning components after nickel-phosphorous plating obtained good technical economical benefits. The fabrication and maintenance costs are greatly reduced, the operation reliability of the high-pressure water jet cleaning equipment is increased, the service life is extended, and the requirement for long period high-pressure water jet cleaning operation is met. This technology, with its easy way of application, low cost and good results, is a satisfactory method for corrosion prevention of high-pressure water jet cleaning components.

6. REFERENCES

1. Weide Wang, Yanrong Hu "Investigations of Technology of Chemical Plating of Nickel-Phosphorous Alloy" Chemical Equipment Technology, Vol.18, No.4, 1997. (In Chinese.)

2. Cheng Zhang, "Analysis of Ni-P-Si_3N_4 Composite Chemical Plating Structure" Surface Technology, Vol. 27, No.1, 1998. (In Chinese.)

3. Wenqi Zhang, etc., "Corrosion Data" Metal Corrosion Handbook, Part IV, Chapter 35,1987. (In Chinese.)

10th American Waterjet Conference
August 14-17, 1999: Houston, Texas

WATER-JETTING PRODUCTIVITY STUDY

FOR THE MARINE INDUSTRY

Gordon G. Kuljian, Senior Engineer
Darren C. Melhuish, Staff Engineer
Corrpro Companies, Inc.
West Chester, PA

ABSTRACT

The National Shipbuilding Research Program commissioned a two year study to investigate the productivity of water jetting in the ship building and ship repair industry. Data will be presented on production rates of coating removal from various freeboard, underwater hull, ballast tank, and non-skid decking areas. Contamination removal efficiency, water-jetting's impact on the adhesion of coatings, and worker productivity issues will also be presented.

Organized and Sponsored by the WaterJet Technology Association

1. INTRODUCTION

Recent developments in water-jetting equipment technology as well as coating technology have brought water-jetting to the forefront of the coating industry as a means of surface preparation. Aside from the advancements of related water-jetting technologies, one inherent benefit of water-jetting is the clean surface left behind. Since the surface is thoroughly washed with high or ultra-high pressures of potable water, surface contamination levels are generally below the acceptable levels set by industry specifications.

In 1996, the National Shipbuilding Research Program's (NSRP) Surface Preparation and Coatings Panel (panel SP-3) commissioned Corrpro to assess productivity of water-jetting when used for coating removal in representative areas of a ship, such as the outer hull, inside tanks, non-skid weather decks. Over the course of the study, ten separate visits were made to various ships undergoing repair pier-side, in dry-dock, or in new construction and one visit was made to an offshore pumping station. During each visit the coated surfaces were evaluated prior to water-jetting to determine coating type, thickness, contamination, adhesion, and overall condition. During the actual water-jetting, productivity data was gathered which included downtime for the production run. Information on equipment type, as well as operating pressures and flow rates were collected. After the blasting was complete the blasted surface was again evaluated for adherence of remaining coatings (dependent on removal specification), resultant surface contamination levels and overall effectiveness of the blast.

This report will serve to summarize the type and results of data collected for the NSRP. A presentation of all data collected during the two year study would be too voluminous for the Proceedings paper, however all data will be included in the Final NSRP report, due to be issued in Fall 1998.

A summary of the visits (to both private ships and US Navy ships) is presented in Table 1. An "(O)" designates the process used "open-cycle" equipment, and a "(C)" designates the process used closed-cycle equipment. (Closed-cycle equipment is defined as where the process jetting water is recovered, treated, and disposed of on-site and/or re-used as blasting media for the project.)

2. PRODUCTION RATES

Over the course of various water-jetting visits, three types of coating removal specifications were observed; selective stripping, "spot and sweep" blasting, and complete blasting to bare metal. Selective stripping was the most common and highlights one of the unique advantages that water-jetting has over traditional abrasive blasting. Selective striping was often specified to remove top-layers of a coating system down to well-adhered primer or an intermediate coat, without damaging the undercoats. (In abrasive blasting situations, damage to underlying layers typically results in untimely rework of areas effected by the sweep blast.) Another method frequently observed was sweep and spot blasting to bare metal. The intent of this removal was to stress the coating system by applying a sweep blast, which would allow only tightly adherent paint to remain. With spot and sweep blasting, all corroded areas were spot blasted to bare metal. For the selective stripping and the spot and sweep blast to bare metal specifications open cycle, hand-held lances were observed. The third observed removal specification was the total removal of coatings down to bare metal. Open and closed cycle robotic and open cycle hand-held units were observed for this type of removal.

2.1 Production Rates for Selective Stripping

Graph 1 represents production rates for structures that received a partial coating system removal down to a specified "tightly" adhered coating. All coating removal was performed using open cycle, hand-held lances. Production runs [where m^2/hour/gun (ft^2/hour/gun) is computed] ranged from one hour to eight hours, depending on the dynamics of the situation. *Down time (nozzle off) is reflected in the production data presented, in order to portray more useful numbers to the reader. For example, if a certain crew can remove coatings at a rate of 27.9 m^2/hour (300 ft^2/hour), for only thirty minutes at a time before the equipment needs thirty minutes of maintenance, then their true production rate should be expressed as 13.95 m^2/hour/gun (150 ft^2/hour/gun).*

The first grouping of data (Graph 1), labeled "LPD-6", contains seven production runs that were observed during jetting on a U.S. Navy amphibious transport ship. The first six are for freeboard coating removal of ~ 305 μm (12 mils) of gray silicone alkyd down to an intact anti-corrosive epoxy (Navy F-151). The last production run in this group represents the removal of a 3-coat anti-fouling layer down to the topcoat of anti-corrosive epoxy on the underwater hull. Production rates ranged from 4.5 m^2/hour/gun (48 ft^2/hour/gun) to 11.9 m^2/hour/gun (128 ft^2/hour/gun) with an average of 7.9 m^2/hour/gun (85 ft^2/hour/gun). The pump equipment operated at 277.6 MPa (40,000psi) at a flowrate of 22.7 lpm (6 gpm). The nozzle on the lance contained 5 jewels and was air spun at 3500 rpm.

The second group, "Hull 648" contained three production runs observed during the dry docking of a double hull cargo ship. The coating removal specified was to remove all three coats of anti-fouling [~ 432 μm (17 mils) total] down to sound gray anti-corrosive epoxy on the underwater hull. The data was taken during new construction; the anti-fouling had started to delaminate from the anti-corrosive layer prior to immersion. Production rates ranged from 2.6 m^2/hour/gun (28 ft^2/hour/gun) to 4.2 m^2/hour/gun (45 ft^2/hour/gun) with and average of 3.6 m^2/hour/gun (39 ft^2/hour/gun). The pump equipment operated between 159.6 MPa (23,000 psi) and 173.5 MPa (25,000 psi) at a flowrate of 22.7 lpm (6 gpm). The nozzle on the lance contained 5 jewels and was air spun at 3500 rpm.

The third group of data represents production rates observed on LST-1194, an U.S. Navy tank landing ship. The removal specified was to remove all alkyd [approximately 6 layers at 76-102 μm (3-4 mils) each] and epoxy coatings [2 coats at 152-203 μm (6-8 mils) each] down to the inorganic zinc primer on the freeboard areas. Production rates ranged from 1.1 m^2/hour/gun (12 ft^2/hour/gun) to 7.0 m^2/hour/gun (75 ft^2/hour/gun) with an average of 4.0 m^2/hour/gun (43 ft^2/hour/gun). The pump equipment operated at 263.7 MPa (38,000 psi) with a flowrate of 22.7 lpm (6 gpm). The nozzle on the lance contained 5 jewels.

The final group of data on Graph 1 were the production rates observed from the exterior shell of the offshore pumping station. The removal specified was to selectively strip the painted surface down to intact primer, and remove all corrosion products down to bare metal. The coating system for the exterior shell consisted of four coats totaling 355.6 μm (14 mils). For this outer shell area, about 304.8 μm (12 mils) of coating was selectively stripped. The production rates for the exterior shell ranged from 5.9 m^2/hour/gun (63 ft^2/hour/gun) to 10.7 m^2/hour/gun (115 ft^2/hour/gun) with an average of 8.3 m^2/hour/gun (89 ft^2/hour/gun). The pump equipment operated between 124.9 MPa (18,000 psi) and 138.8 MPa (20,000 psi) at a flowrate of 30.3 lpm (8 gpm). The nozzle on the lance contained 2 jewels and was hydraulically spun at 4800 rpm.

Note that the production rates for selective stripping are somewhat similar for the removal of the freeboard system on the LPD-6 and LST-1194 as well as that exterior shell of the pumping station. The lower observed productivity levels on the Cargo Hull 648 were chiefly due to worker orientation. In all other outer hull trials, workers were standing up, usually working from a high-lift, and blasting perpendicular to a vertical hull. On the Hull 648, the blasters were removing coating on the cramped underbelly where they were sitting down, holding the guns vertically or at an angle toward the horizontal surface overhead. The low docking blocks created a cramped situation for the workers, thereby lowering productivity.

2.2 Production Rates for Spot and Sweep Blasting to Bare Metal

Graph 2 represents rates for blasting, which called for a spot and sweep blast. The sweep blast was intended to stress the coating system leaving only tightly adherent paint remaining, as well as create a clean profile in the existing coating. Corroded areas were spot blasted to bare metal. All coating removal was performed using open cycle, hand-held lances.

The first group of data (Graph 2), labeled “LPD-6 (ballast tank)” were production rates from the water-jetting of ballast tank 8-84-4W. The scope of work was to spot blast to bare metal all corroded areas and sweep blast all other areas in order to remove staining, and provide a clean, profiled surface for subsequent coating adhesion. This ballast tank had a two coat MIL-P-23236 epoxy system, averaging 248.9 μm (9.8 mils) DFT. Production rates ranged from 8.4 m^2/hour/gun (90 ft^2/hour/gun) to 21.9 m^2/hour/gun (236 ft^2/hour/gun) with an average of 15.9 m^2/hour/gun (171 ft^2/hour/gun). The pump equipment operated between 124.9 MPa (18,000 psi) and 138.8 MPa (20,000 psi) at a flowrate of 30.3 lpm (8 gpm). The nozzle on the lance contained 2 jewels and was hydraulically spun at 4800 rpm.

The second group of data represents the production rates observed for the removal of damaged shop primer on the outer hull of the chemical tanker during new construction. The blasters were to sweep blast the entire painted surfaces and remove any damaged areas down to bare metal (i.e. charred areas from internal welding, areas damaged by scraping and handling, erection joints). The shop primer ranged from 12.7 to 50.8 μm (0.5 to 2.0 mils). Production rates ranged from 13.6 m^2/hour/gun (146 ft^2/hour/gun) to 33.9 m^2/hour/gun (365 ft^2/hour/gun) with an overall average of 18.4 m^2/hour/gun (198 ft^2/hour/gun). The pump equipment operated at 277.6 MPa (40,000 psi) with a flowrate of 20.8 lpm (5.5 gpm). The nozzle on the lance contained 5 jewels.

The final group of data on Graph 2 was the production rates observed from the internal tanks of the offshore platform. The coating system for the tanks consisted of only two coats: epoxy primer [~ 25 μm (1 mil)], epoxy top-coat [~ 254 μm (10 mils)]. The average production rate for the spot and sweep blast inside of the tanks was 14.6 m^2/hour/gun (157 ft^2/hour/gun). The pump equipment operated between 124.9 MPa (18,000 psi) and 138.8 MPa (20,000 psi) at a flowrate of 30.3 lpm (8 gpm). The nozzle on the lance contained 2 jewels and was hydraulically spun at 4800 rpm.

Note the higher (compared to selective stripping, Graph 1) production rates when a specification called for a "spot and sweep," as in the case of the LPD-6 (ballast tank), chemical tanker, and pumping station (internal tank) data. Also note that the production rates for these (three) spot and sweep observations achieved values around the 14.0 m^2/hour/gun (150 ft^2/hour/gun) mark; fairly consistent for three separate scenarios.

Interestingly, on the ballast tank observation, we noted that water-jetting inside ballast tanks created added stressors on the worker, all which aid in jeopardizing productivity. For example, the water from a high pressure lance may exit the nozzle in excess of 150 deg. F, creating a hot misty fog within a matter of seconds after pulling the trigger. Depending on the situation, lighting and ventilation were less than ideal for the task. Typical water jetting equipment involves wet suits, in addition to other standard safety gear. The combination of wet suits, a hot/humid environment, and less than ideal ventilation (to ventilate and dissipate mist) can create a very demanding work environment. We observed that workers doing ballast tank water-jetting were blasting only approximately (45%) of the time, whereas in blasting easier configurations, such as along the outer hull, workers could attain a 95% blasting efficiency (calculated as trigger time ÷ total time from start of blasting).

2.3 Production Rates of Coating Removal to Bare Metal

Graph 3 represents production rates for areas on the ship where total coating system removal down to bare metal was either specified, or required due to prior corrosion and coating failure.

The first group of data (Graph 3), labeled "LPD-6 (outer hull)" contains only one production run (an area of anchor chain damage) where coating was removed to bare metal. This system included three coats of anti-fouling [~ 76 μm (3 mils) remaining], and two coats of anti-corrosive epoxy [~ 356 μm (14 mils) DFT] to be removed with open cycle hand-held lances. The production rate for this area was 14.1 m^2/hour/gun (152 ft^2/hour/gun). The pump equipment operated at 277.6 MPa (40,000 psi) with a flowrate of 22.7 lpm (6 gpm). The nozzle on the lance contained 5 jewels and was air spun at 3500 rpm.

The next data grouping, "CVN-70" contains three production runs, all of flight deck non-skid removal from the nuclear aircraft carrier USS CARL VINSON, using a robotic closed-loop system. (The robotic system, developed for use by the Navy, has been described in prior articles, and consists of a rotating nozzle which operates in a pre-programmed pattern along a manipulator frame, attached at the end of a standard high-reach. The effluent is fully recovered, filtered, and re-introduced as blasting water.) The specification required an SSPC SP-10 Near-White metal blast. The decking material consisted of a 76-102 μm (3-4 mil) epoxy primer under a thick [up to 3810 μm (150 mils)] non-skid matrix of epoxy and aluminum oxide grit. Production rates ranged from 11.3 m^2/hour (121 ft^2/hour) to 13.6 m^2/hour (146 ft^2/hour) with and average of 12.5 m^2/hour (134 ft^2/hour). The pump equipment operated at between 208.2 MPa (30,000 psi) and 222.1 MPa (32,000 psi) with a flow rate of 37.9 lpm (10 gpm). The six inch wide nozzle on the robotic arm contained 22 jewels.

The final group, "Oil Tanker" contains eleven production runs for coating removal using a robotic semi-closed cycle system, with partial effluent recovery. The entire freeboard coating system {one coat modified chlorinated rubber [~127 μm (5 mils)] and two coats of anti-corrosive epoxy [~279 μm (11 mils) total)]} was to be removed completely to bare metal. About the first twelve feet of the underwater hull area directly under the freeboard area was also to be removed down to bare metal. This system consisted of two coats of ablative anti-fouling [totaling ~356 μm (14 mils)], and two coats of anti-corrosive epoxy [totaling ~279 μm (11 mils)]. In both the freeboard and underwater hull areas, 100% removal of the red anti-corrosive epoxy was not achieved, however. Approximately 5% to 20% of epoxy primer residue still remained after blasting. Production rates ranged from 15.1 m^2/hour (162 ft^2/hour) to 73.7 m^2/hour (792 ft^2/hour) with an average of 43.8 m^2/hour (471 ft^2/hour). Two pumps operated at 250 MPa (36,260 psi) with a total flow rate of 100 lpm (26.417 gpm). The robotic arm housed two hydraulically spun nozzles. Each nozzle contained two jewels and covered and area of 30 cm (11 $^{13}/_{16}$ inches). The wide distribution in production rates was due to changes in hull configuration, as well as operator experience.

2.4 Distribution of Production Rates

Graph 4 shows the production rates of all water-jetting observations. Graph 5 is similar to Graph 4, but represents the overall average production rates observed at each vessel. As seen from both Graphs 4 and 5, the production rates from the Oil Tanker exceeded all other production rates. A correlation between the CVN-70 and the Oil Tanker would not be meaningful since the two represent the removal of two totally different coating systems. However, both systems represent a semi-automated method of coating removal, waste handling, and treatment, which demonstrates the grouping of all technologies, associated with shipyard water-jetting. All other methods utilized hand-held lances and open-cycle jetting, which is simpler, less involved way of removing coating.

3. CONTAMINATION REMOVAL USING WATER-JETTING

One of the more recognized advantages of pressurized water as a means of surface preparation is its ability to remove contamination on either a coated or bare substrate to levels well below those that are believed to be detrimental to coating performance (Conference Seminar, 1995; Kuljian, 1998). A portion of this study involves the documentation of surface contaminates (as measured as chlorides and conductivity) on a surface prior to and after coating removal via water-jetting in order to confirm contamination removal. In some cases, surface contamination was measured both before and after blasting, however initial surface readings were not obtained in all cases for various reasons (e.g. hull accessibility, or in ability of retrieval cell to adhere to anti-fouling paint).

Note: In all cases, final surface contamination and chloride levels were measured within a few hours after water-jetting, and do not necessarily represent the surface condition just prior to coating. It is important to ensure the levels are low directly prior to painting, as well. The period from when a surface is initially blasted to the time it is coated can be several days, during which time increased quantities of contaminants can settle on the cleaned surface, usually resulting in varying levels of flash rusting. Most contractors incorporate a "secondary cleaning" to remove residual contaminants and flash rusting, to restore the surface to acceptable specifications.

3.1 Chlorides

Chloride contamination has been identified as a major contributor to premature coating defects caused by ionic contamination. Therefore, surface chloride levels were measured prior to and after water-jetting for comparison.

Graphs 6 and 7 depict all chloride data captured to-date. Graph 6 includes all visits in which potable water was used for jetting. In Graph 6, initial chloride contamination levels were quite low (under 10 $\mu g/cm^2$). All final readings were under 3 $\mu g/cm^2$, with the majority of readings under 1 $\mu g/cm^2$. Although initial readings were low in most cases, LPD-6 tank readings show that water-jetting does reduce surface chlorides to below acceptable levels. The U.S. Navy has identified 3 $\mu g/cm^2$ as the upper limit for acceptability for coating an immersed surface and 5 $\mu g/cm^2$ as the upper limit for coating an above-waterline surface (Kuljian, 1996). Realizing this, one can see that water-jetting is very effective in removing contaminants and producing a clean surface for coating.

Graph 7 contains the chloride data from the offshore visit, where filtered seawater was used for blasting. The surfaces were next washed down with ~70 MPa (10,000 psi) potable water. The initial chloride levels on the pumping station were high (up to 40 $\mu g/cm^2$), but these levels were significantly (78% to 97%) reduced after the secondary (fresh water) blast. As a test, chloride measurements were taken after the filtered seawater blast and prior to the fresh water rinse on the exterior shell only. For the exterior shell as noted in Graph 7, levels were quite high (70 $\mu g/cm^2$) confirming the necessity of the secondary fresh water blast.

The effectiveness of contamination removal for the offshore pumping station platform should only be compared with itself. Comparisons of other "before" and of other "before and after" surface contamination numbers would not be meaningful since filtered seawater was used for jetting. All other water-jetting observations used a potable water source for blasting.

3.2 Conductivity

If contaminants other than (or in addition to) chloride are present, conductivity measurements may provide information if such substances can be detrimental to coating longevity. Conductivity samples were captured using 3 milliliter distilled, deionized water (typically 0-1 $\mu S/cm$) injected into a blister patch. Results were normalized for a 5ml solution conductivity. Graphs 8 and 9 depict the conductivity data gathered to-date. Graph 8 includes all visits in which potable water was used for blasting. Graph 9 contains the data gathered on the offshore visit which was blasted with filtered seawater, followed by a secondary fresh water blast [~70 MPa (10,000 psi)].

In most cases, conductivity levels dropped significantly after water-jetting. On Graph 8, fifteen of twenty-two final conductivity readings were under 20 μS/cm and twenty-one of twenty-two were under 40 μS/cm. (For reference, our experience has shown typical city tap water to range in conductivity from 80 μS/cm to 130 μS/cm.) Although no standard currently exists for acceptable criteria for conductivity, these readings further confirm waterjetting's ability to provide a suitably clean surface for coating.

The data on Graph 9 shows that blasting with seawater with a secondary fresh water blast did significantly (77% to 92%) reduce the surface conductivity. However, the residual surface conductivity was still high compared with the final values achieved with potable water. As a test, conductivity measurements were taken after the filtered seawater blast and prior to the fresh waster rinse on the exterior shell only. For the exterior shell, as noted in Graph 9, conductivity levels were quite high (960 μS/cm) confirming the necessity of the secondary fresh water blast.

4. OTHER FACTORS OF INTEREST

4.1 Surface Profile

As stated earlier, the high speed spinning action of the high and ultra-high pressure jetting water impacting on coatings can create a measurable surface profile in the existing coating. The resulting profile aids in subsequent coating adhesion. Throughout the study, we measured resultant "coating profile" and discovered that the waterjetting process, when using a spinning nozzle, can produce profiles in paint ranging from 43.2 to 111.8 μm (1.7 to 4.4 mils), as measured using ASTM D-4417, Method C.

4.2 Coating Adhesion

Where possible, tensile adhesion of the coating system, both prior to and after water-jetting, was determined to assess any detrimental effects that waterjetting may have on remaining coating. The notion that during a "spot and sweep" blasting operation the high and ultra-high pressure water impacting on aged coatings would, in some way, compromise existing adhesion was tested. Interestingly, similar tensile adhesion values (as measured by ASTM D-4940) to initial adhesion resulted after sweep water-jetting. Basically, if the coating's adhesion was questionable, the high, or ultra-high pressure water would remove the weak coating. If the remaining coating was still intact and well adhered the jetting would merely profile the coating and the coating would remain well adhered.

4.3 Factors Affecting Production Rates

Numerous factors can affect production rates in a water-jetting operation. The single most important factor is a combination of existing coating type and condition, coupled with the experience and organization of the crew. We noticed that experienced crews can work up to twice as productive as inexperienced crews, performing identical work. Similarly, removal of well-adhered high-build deck coating will not proceed with the speed of a thirteen-year old, degraded epoxy in a tank. The working configuration also plays an important role in affecting productivity. Jetting the cramped flat under-bottom of a ship is at least twice as slow as removing the same coating system on the flat vertical side of an underwater hull. Similarly, maneuvering inside a heavily stiffened internal tank can certainly slow down an operation.

4.4 Flash Rusting

Flash rusting is a factor which must be dealt with on practically all jobs encountered. When a coating is removed to bare metal, the resultant moisture in the air, coupled with any other contaminants that may settle on the surface, will create some degree of flash rusting. Depending on a number of factors, this “rust bloom” may grow in intensity with time. In such cases, if the coating specification requires it, the bloom will have to be removed with a secondary blast, followed immediately (after the surface dries) by coating. Inside tanks, the rusting problem can be significantly reduced by properly sized and placed ventilation, and by the use of dehumidification. A related problem exists with the use of common desiccant dehumidification, where the dry air is of significantly higher temperature of ambient, thereby adding to the heat stress of the workers. The use of refrigerant dehumidification should be explored in such situations.

With the closed loop machinery, the blast residue and water is vacuumed away immediately. Adding to this is an evaporative effect caused by the increased temperature of the substrate due to the kinetic energy of the pressurized water impacting the substrate. Flash rusting is not an issue in such situations. In such scenarios, we have witnessed the substrate remaining rust-free for several days, provided no rain or other contaminants foul the blasted surface.

Some coating systems will not tolerate rust blooming, whereas many are designed for be applied over flash rusting. In all ballast tank scenarios, the entire surface was “sealed” with a penetrating sealer type coating (either a moisture-cured urethane or an epoxy-ester) followed by two coats of barrier coating. Well written specifications with clear guidance on acceptable limits of flash rusting, and, how to correct such occurrences if they occur, are key for water-jetting jobs to progress smoothly. Education by all inspection parties, in interpreting flash rusting is also imperative.

5. CONCLUDING REMARKS

In recent years, water-jetting has been used more and more by ship builders and ship repairers as a means of preparing surfaces for repainting. As learned from this study, a wide variety of situations are ideal for water jetting, such as:

- touch-up and maintenance of underwater-hull coating systems
- touch-up of internal tank systems
- full removal of decking materials
- full removal of coating systems

- selective (partial) removal of coating layers (such as anti-fouling, or freeboard coatings), leaving full intact coating layers
- preparation of pre-construction primer for re-coating (in new-construction)

As learned in the study, some localities even prohibit the use of open air abrasive blasting in their shipyard activities, leaving water-jetting as the sole productive medium for coating removal.

The study also revealed that different means of coating removal (open cycle/closed cycle), different objectives of coating removal (selective stripping/full removal/spot and sweep), and different types of coating being removed all play a determining role in the observed production rate. Just as important, is the experience of the operator, and the configuration of the blaster (interior tank vs. flat hull), in determining production rate. All of the above factors are integral in determining production rates of any large-scale general coating removal process, such as abrasive grit blasting.

Differences in overall job productivity [as opposed to m^2/hour (ft^2/hour)] between water-jetting and other methods arise when considering other factors, such as equipment size and maneuverability, the waste stream created, and impact on other trades. In this study, a welcome advantage of shipyard water-jetting versus traditional means was that water-jetting does allow the work of other trades to proceed directly adjacent to water-jetting, a situation uncommon during abrasive blasting.

It is the opinion of the authors that for large-scale, quick turn-around coating removal on a ship underwater hull or free-board, the automated, or semi-automated robotic type machinery that contains all blasting water and effluent, represent the most promise for impacting the ship-repair industry. These machines can efficiently remove coatings down to the original substrate without the fear of flash rusting, and provide excellent surfaces for immediate re-coating.

6. REFERENCES

Conference Seminar – Water Jetting / Water Blasting; The Lydia Frenzel Conference Series, June 6, 1995, Virginia Beach, VA.

Kuljian, G., Parks, A.R., Kaznoff, A. “State-Of-The-Art Procedures for Ensuring Optimum Coating Longevity in Navy Tank Coatings Operations,” Presented at SSPC-96, Charlotte, NC, November 1996.

Kuljian, G., Holmes, B. “U.S. Navy Experiences with Water-Jetting,” *Protective Coatings Europe,* February 1998.

7. TABLES

Table 1. Summary of Visits

SHIP	DESCRIPTION	DATE	TYPE of WORK
USS DULUTH (LPD-6)	(O) FREEBOARD	FEBRUARY 1997	MAINTENANCE
USS DULUTH (LPD-6)	(O) UNDERWATER HULL	FEBRUARY 1997	MAINTENANCE
USS DULUTH (LPD-6)	(O) BALLAST TANKS	MARCH 1997	MAINTENANCE
CARGO SHIP HULL 648	(O) UNDERWATER HULL	MARCH 1997	NEW CONSTRUCTION
USS LAMOURE COUNTY (LST-1194)	(O) OUTER HULL	MAY 1997	MAINTENANCE
USS CARL VINSON (CVN-70)	(C) NON-SKID DECK	JULY 1997	MAINTENANCE
OIL TANKER	(C) FREEBOARD	JULY 1997	MAINTENANCE
USS CLEVELAND (LPD-7)	(O) BALLAST TANKS	AUGUST 1997	MAINTENANCE
USS TORTUGA (LSD-46)	(C) FREEBOARD	OCTOBER 1997	PIERSIDE DEMONSTRATION
CHEMICAL TANKER	(O) UNDERWATER HULL	JANUARY 1998	NEW CONSTRUCTION
OFFSHORE PUMPING STATION	(O) TANKS AND OUTER HULL	MARCH 1998	MAINTENANCE

Key: "(O)" Open-cycle water-jetting.
"(C)" Closed-cycle water-jetting.

8. GRAPHICS

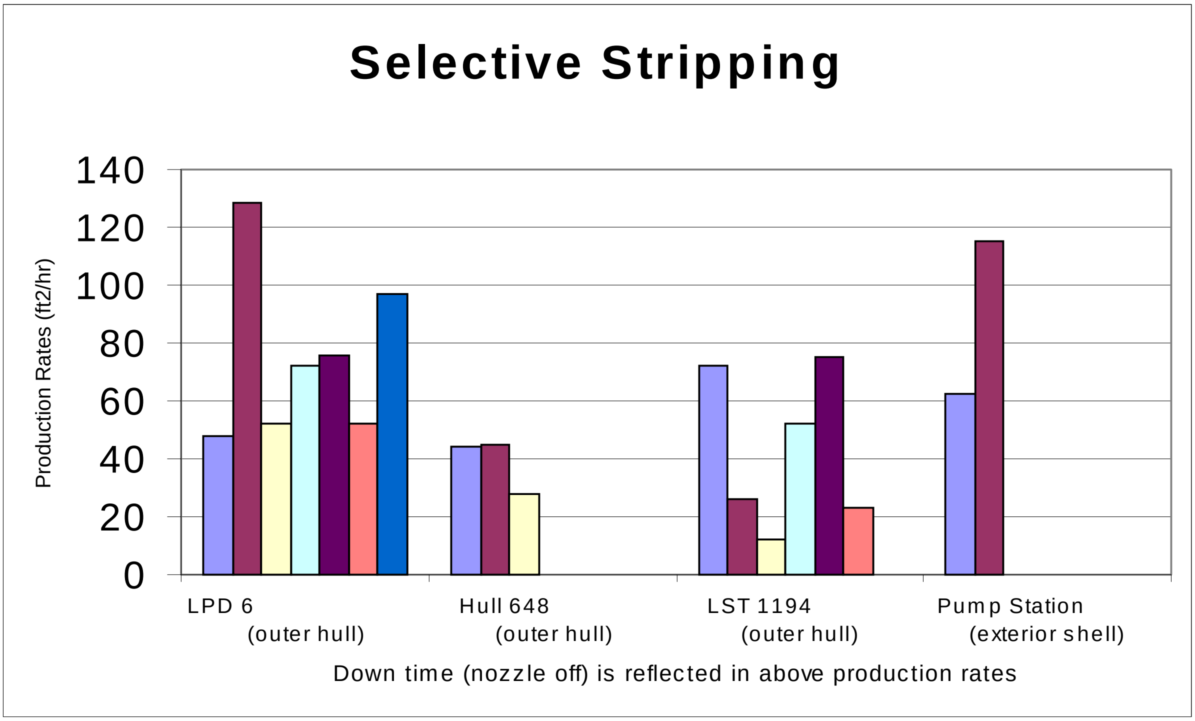

Graph 1. Production Rates for Selective Stripping.

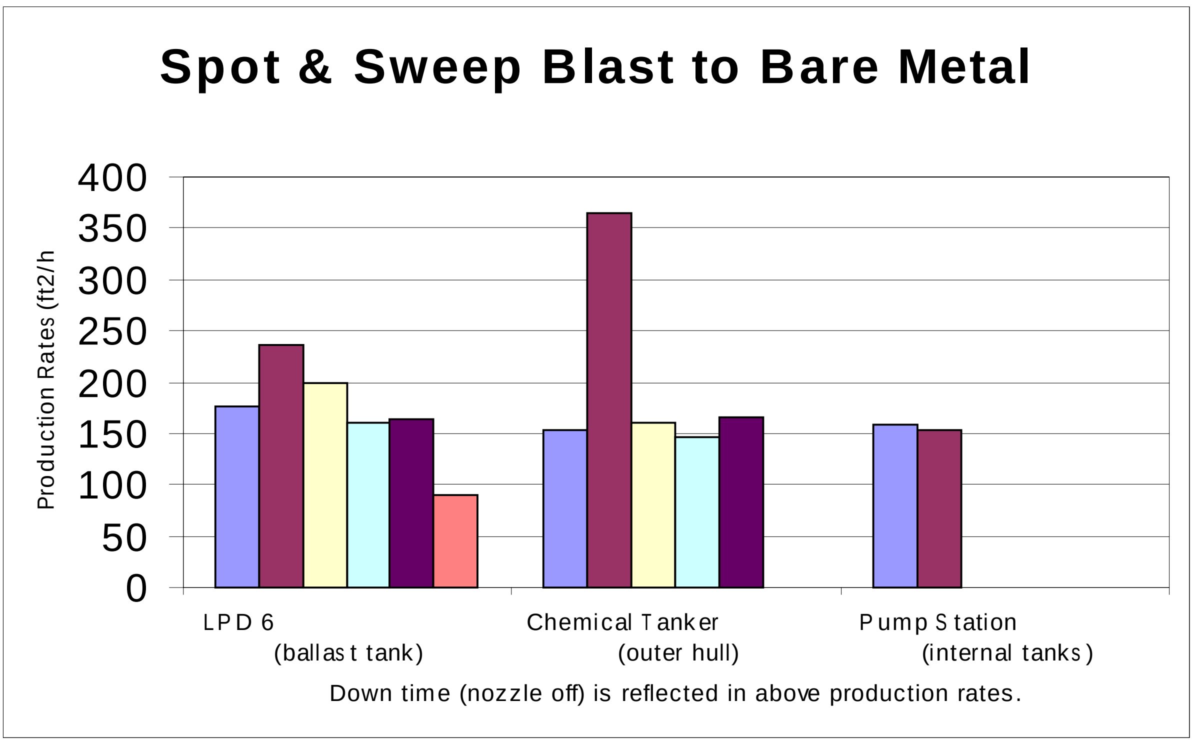

Graph 2. Production Rates for Spot and Sweep Blasting to Bare Metal.

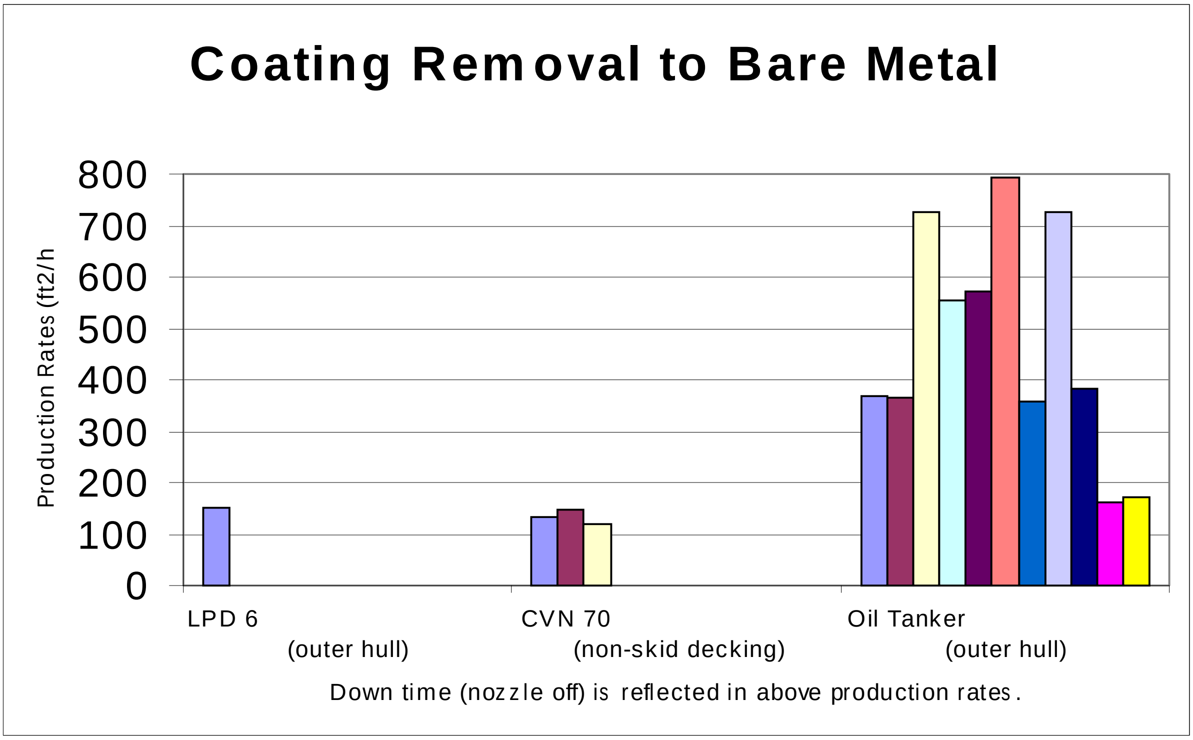

Graph 3. Production Rates for Coating Removal to Bare Metal.

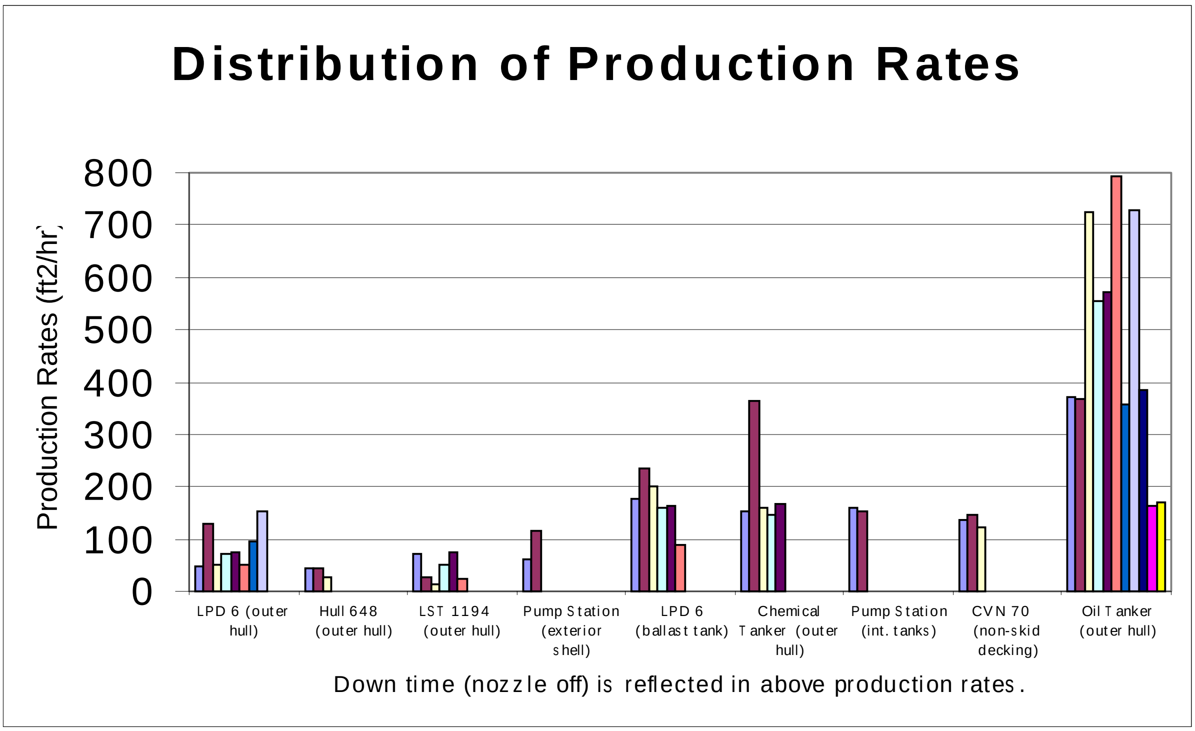

Graph 4. Distribution of Observed Production Rates.

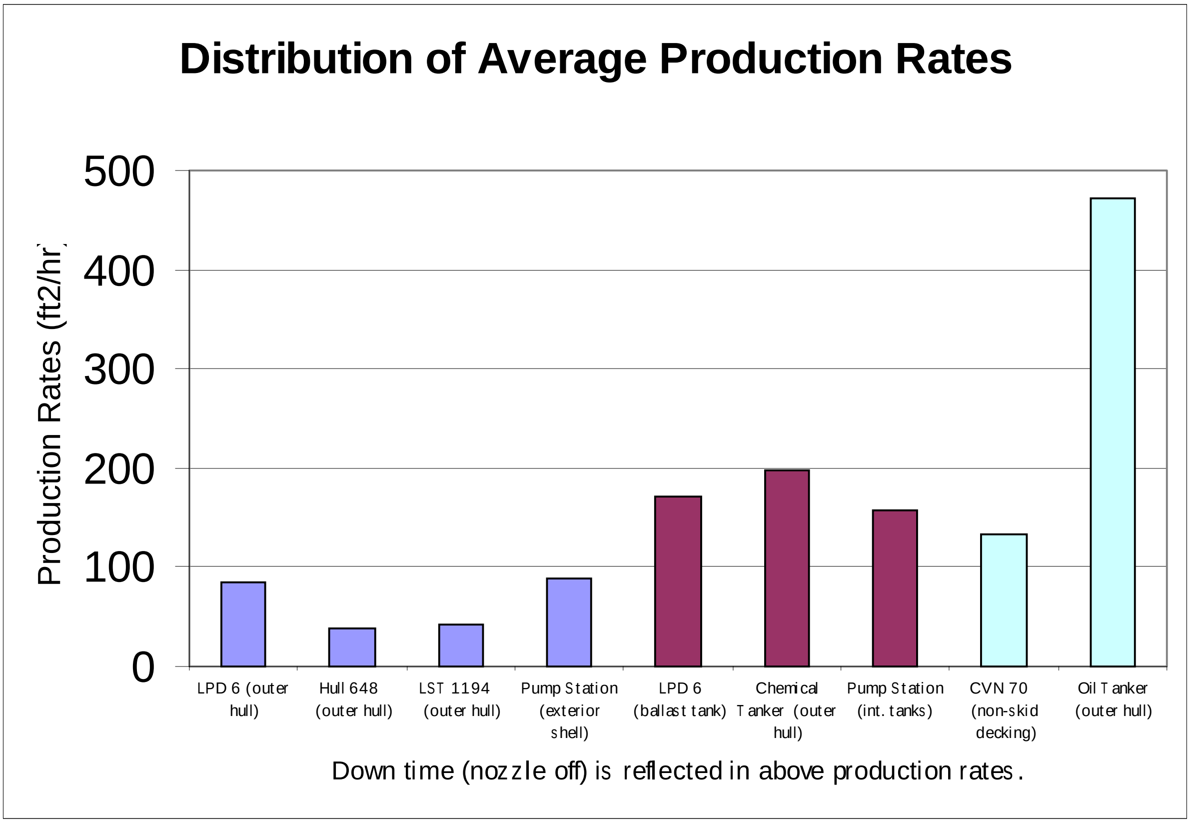

Graph 5. Distribution of Averaged Observed Production Rates.

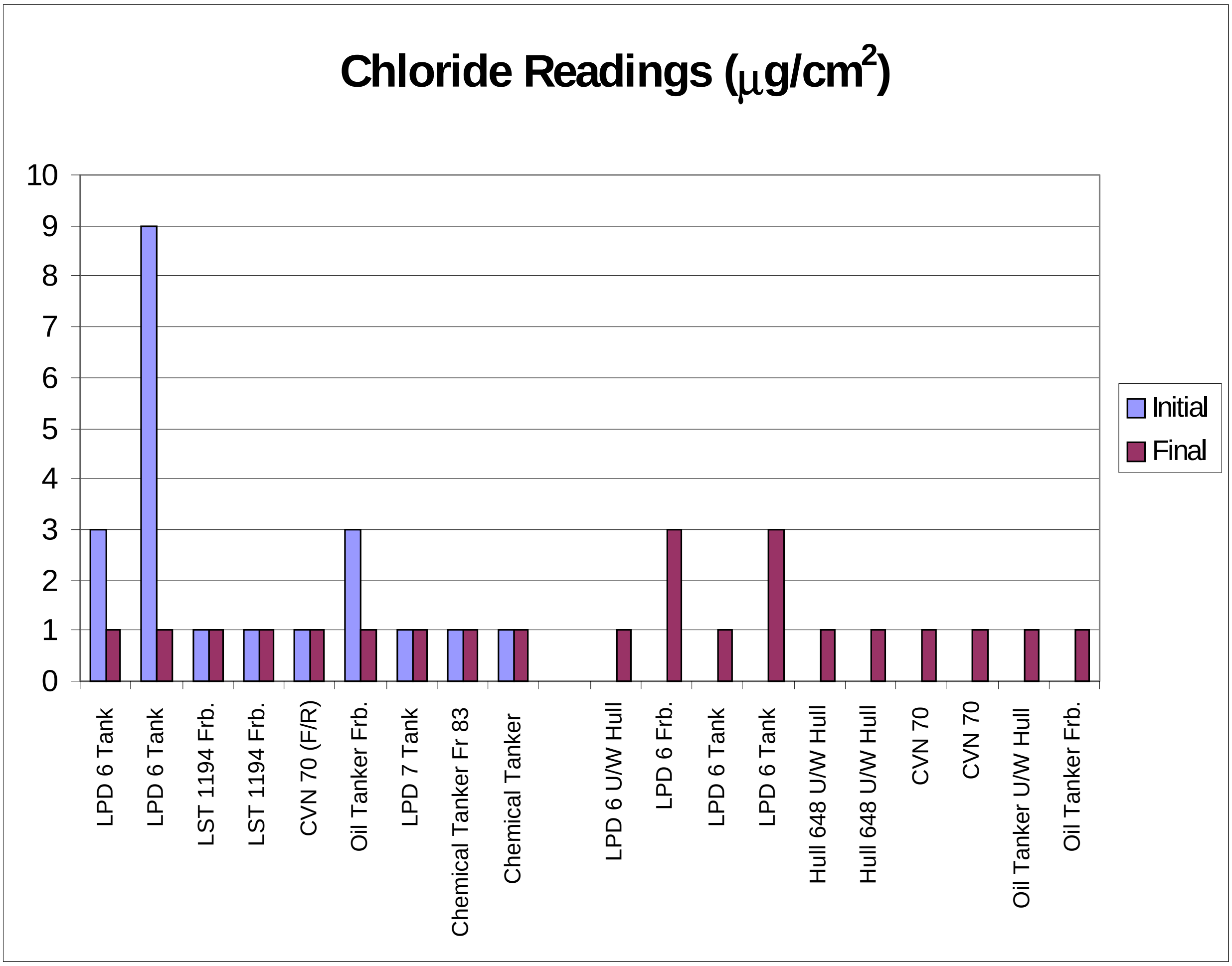

Graph 6. Chloride measurements using potable water for hydroblasting.

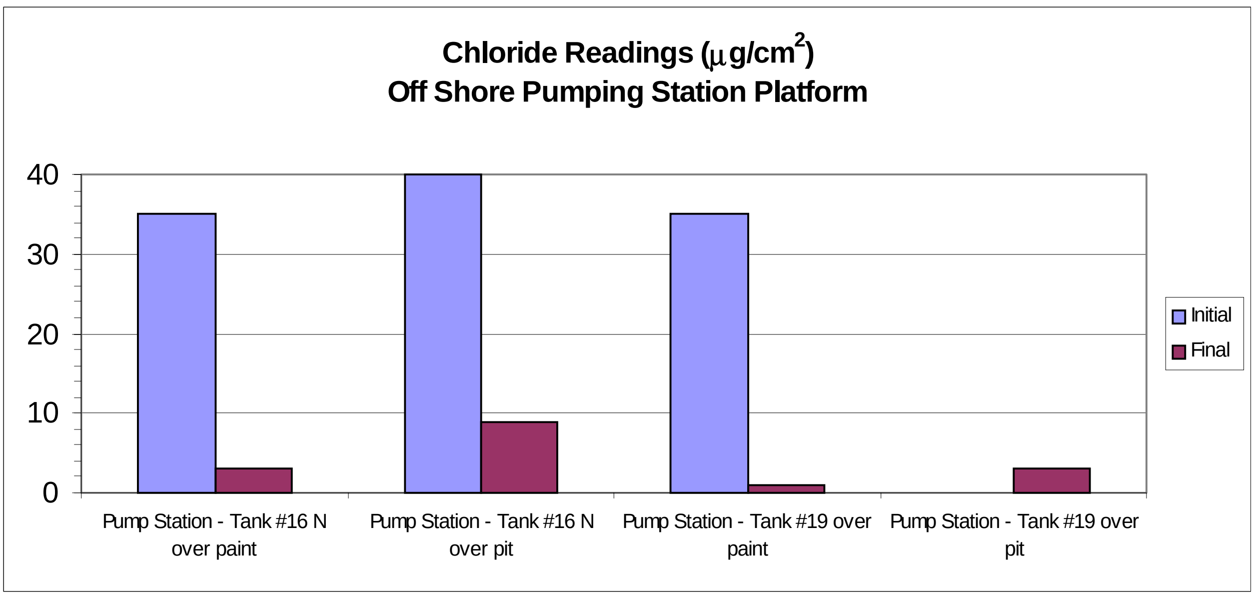

Graph 7. Chloride measurements using filtered seawater for hydroblasting followed by a potable water rinse.

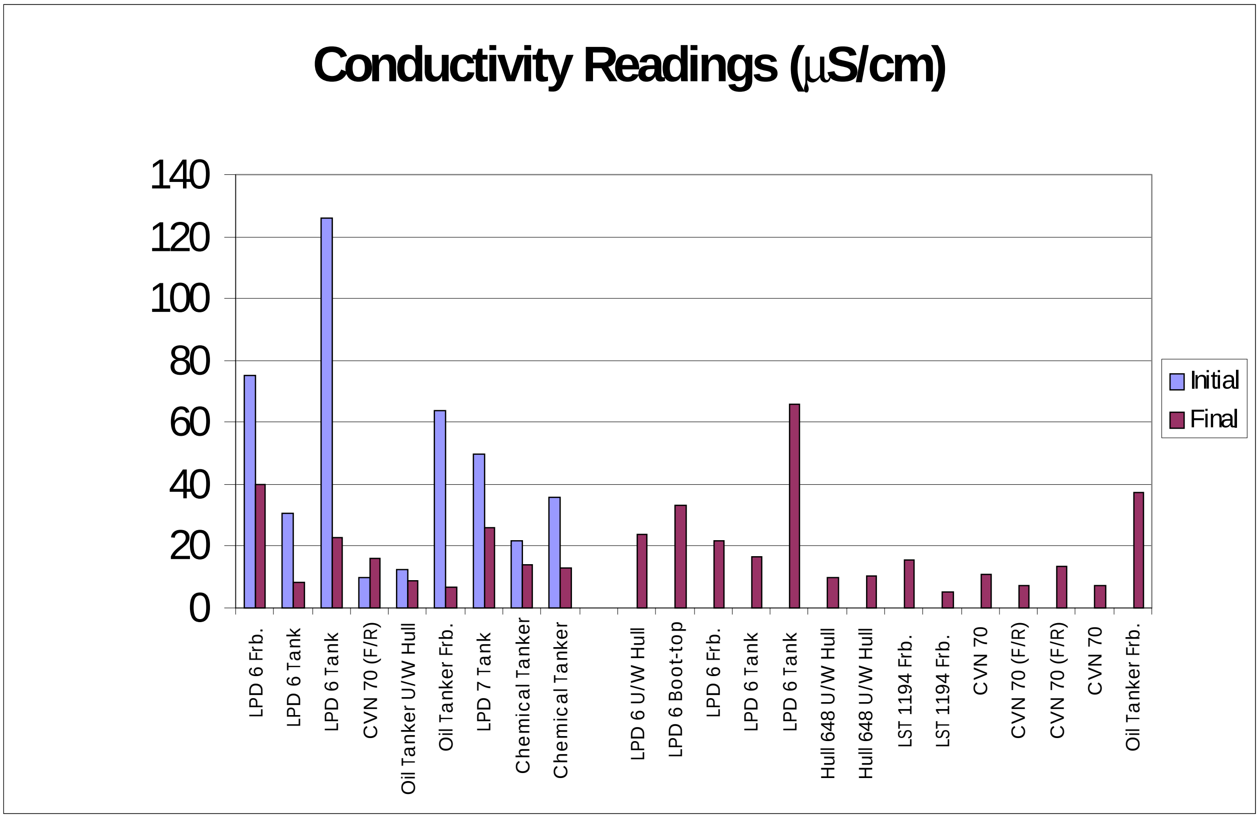

Graph 8. Conductivity measurements using potable water for hydroblasting.

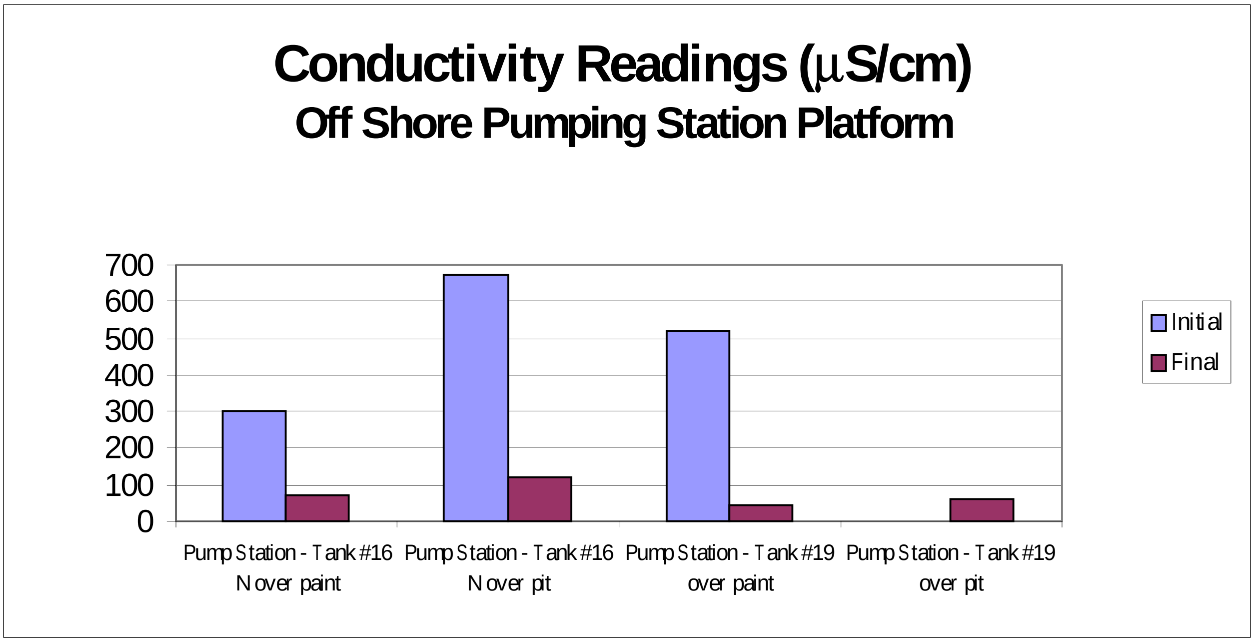

Graph 9. Conductivity measurements using filtered seawater for hydroblasting followed by a potable water rinse.

10th American Waterjet Conference
August 14-17, 1999: Houston, Texas

Paper **43**

HYDROKINETIC USAGE IN THE CLEANING OF EXCHANGER TUBES AND PIPES

Patricia McGrew Garcia
AIMM Marketing
Houston, Texas, U.S.A.

Brooks Bradford, Sr.
AIMM Technologies, Inc.
LaMarque, Texas, U.S.A.

ABSTRACT

Hydrokinetics™ is a methodology for cleaning the interior diameter of pipes and tubes, such as those found in heat exchangers, chillers and reboilers. The process induces resonant frequency vibrations into a liquid stream at pressures far lower than normal hydroblasting pressures. Several engineering principles are involved, including hydraulic pressure, induced cavitation, off-frequency pulsation, resonant frequency and water jetting. The vibration transfers to the metal of the tube or pipe and also to the material that is fouling the interior of the tube or pipe. Due to the difference in the densities, the vibrations take place at different frequencies and the bond between the metal and the fouling material is broken. Once the bond is broken, the fouling material flushes out in the same liquid stream. Tube or pipe configurations that are problematic for hydroblasting, such as coils or tight-radius 180º turns, generally can be cleaned with Hydrokinetics™. Fouling materials that respond poorly to erosion technologies often respond well to Hydrokinetics™. This includes thin laminars of fouling material that may be bonded tightly to the interior wall and lengthy solid plugs. Hard scales or rubbery layers, which can be problematic for hydroblasting, are also excellent applications for the use of Hydrokinetics™.

1. INTRODUCTION

This paper discusses Hydrokinetics™, a method of cleaning inside a pipe or tube which has fouling material layered inside or solidly plugged within it. The bond with the fouling material is broken by first filling the pipe or tube with liquid, applying pressure pulsations to the liquid to the extent that a standing wave is formed within the incompressible liquid therein. The pipe or tube is cleaned via the formation of induced shock waves occurring upon collapse of microscopic bubbles resulting from cavitation.

The cleaning of the interior of tubes and pipes has historically been via erosion, by water blasting, pigging, chemical circulation, wire brushing, or drilling, intended to remove the inner surface of the fouling material until it is entirely or almost entirely removed. Hydrokinetics™ is an introduction to a non-erosion technique, which breaks the bond between the tube or pipe interior wall and the adhering fouling material and washing out entire masses of foulant.

2. EMBODIMENT

2.1 Applicable Environment

In virtually every conceivable industry involved in manufacturing, production or processing, fluids or gases are transported through piping, tubing, lines or other open-ended columns. The columns are of an infinite range of lengths and diameters and made from a variety of materials. They are frequently straight, but more often than not, they have bends, U-turns, coils, spirals, and such. Often piping or tubing is in sets or bundles. Frequently fluids or gases contact the exterior of the piping or tubing as well as the interior to cool or heat the fluids or gases. Sometimes piping is exposed to the elements and, if not insulated, the fluids or gases that might be flowing within can be heated or cooled. Transportation of fluid and gases within the pipes or tubes is generally at a specified flow rate. Adversity such as faulty operations or changes in the flow rates results in deposits collecting on the interior walls of the pipes or tubes. These deposits may be referred to as fouling material.

The cleaning of the interior of tube and pipes poses problems not applicable to exterior surface cleaning, such as walkways, tank walls, and tube exteriors. Tube and pipes often have small orifices and long lengths. Obviously, it is difficult or infeasible to see the location of the heaviest deposits of material to be cleaned away, making it impossible to know where efforts should be concentrated. Also, for mechanical methods such as hydroblasting, wire brushing and drill, fouling material deposits are difficult to reach. For hydroblasting, this requires long lances, special tips, and mechanisms for moving the lances into the tubes and pipes. If there are bends or turns, the problem is compounded. An alternative to hydroblasting is to circulate acids or caustics. To protect the pipe or tube metal, chemical circulation is and should be treated as a science, using only qualified specialty companies. Disposal of used contaminated chemicals is a consideration. In the event a tube or pipe is solidly plugged, chemicals obviously cannot be circulated. Larger lines are sometimes cleaned via pigging, whereby a scapping and wiping device, referred to as a pig, is pushed through the pipe or tube by fluid or gas. Probably the most commonly used cleaning method is hydroblasting.

The removal of such fouling material generally takes place during a planned shutdown, a costly loss of production added to the actual cost of maintenance. Additionally, cleaning of the interior of the pipes or tubes may frequently be required when a shutdown is not scheduled but when there are signs of a need, such as when flow is impeded. In cases where piping or tubing is intended to cool or heat the interior or exterior fluids or gases, the buildup of fouling material can act as unwanted insulation and degrade the heat transfer. Pipes or tubes also logically need to be cleaned if a different medium is processed. Where a unit is permanently dismantled, the pipes and tubes must be cleaned when the debris within them poses any environmental concern.

Typically at maintenance time, piping and tubing is dismantled and removed from the structure, entailing expensive pipefitting, crane work, etc. When piping or tubing with bends, flanges, valves, etc. is involved, additional work is needed to remove them, leaving only straight sections of piping or tubing, in order to ease conventional cleaning. Pipes and tubes that are bundled together are commonly left bundled together, but most bends and such are generally removed.

Hydrokinetics™ was originally conceived to provide an atmosphere in which workers were not exposed to chemicals or high pressure water, whereby all affluence would exit away from the workers. In addition to the safety impact, it was learned during development that dismantling was not required, other than to provide an entrance and an exit to the pipes or tubes to be cleaned. Bundles can be Hydrokinetically™ cleaned without removal from their structure.

2.2 The Science of Hydrokinetics™

Hydrokinetics™ is a multi-velocity based sonic system; whereby an induced sonic shock is used to break the cohesion between the fouling material and the pipe or tube wall so the fouling material is washed away in the liquid in the pipe or tube. Hydrokinetics™ generally removes a very high percentage of the fouling material even where it has several layers of buildup. It is effective on any type of fouling material that will respond to the induced sonics. For instance, in a dairy, Hydrokinetics™ can remove butterfat buildup in lines, or in a plant using seawater, Hydrokinetics™ can remove muscles or clams clinging to the interior of the lines. Tests have shown Hydrokinetics™ to be particularly effective for removing petrochemical-based deposits. Organic compounds are highly degraded in this environment, and inorganic compounds can be oxidized or reduced. In petrochemical plants, the system can remove monomers, co-polymers, water scale, etc., including soft, sticky fouling materials, hard, brittle fouling materials, and consistencies in between. Further, Hydrokinetics™ can remove extremely thin films of fouling materials, solid plugs of fouling material, and all the degrees of buildup in between.

It is an important, but not necessarily essential, that the flow of the fluid stream from the Hydrokinetics™ system be as streamlined or laminar as possible. This is opposed to a “boundary layer flow” in which the outer portion of the radius of the stream is slowed by frictional drag and flows at a slower velocity than the inner portion of the stream, or turbulent flow. The fluid stream changes from laminar flow to boundary layer flow at the outlet of the Hydrokinetic system. In the pipe or tube to be cleaned, which has been filled with static fluid, a pulsating fluid stream, pumped into the center of the pipe, sets up a reflected shock wave and resultant standing wave in the column of fluid. The standing wave frequency will pass through the resonant frequencies of the fouling material. The fluid collapses bubbles during the low-pressure pulse resulting, in cavitation. In addition to the breaking of the cohesion between the pipe or tube wall and the fouling material, loose or easily removed fouling material simply washes out in the fluid stream along with the larger mass of fouling material broken from the pipe or tube wall.

2.3 Blockage Devices

Hydrokinetics™ induces a sonic, subsonic or supersonic resonance (hereinafter called sonics) in a tube or pipe for cleaning purposes. Hydrokinetics™ is not, but may first appear to be, pigging. No scrapping or wiping devices is used with Hydrokinetics™, but in instances where the pipe is not completely blocked with fouling material, a blockage may be inserted in the pipe. This blockage is helpful for the induction of sonics. This blockage can be anything of sufficient size and texture to close off the interior diameter of the pipe or tube and may be compressible or incompressible, depending on the particular situation. In the event of a solidly fouled pipe or tube, no manually inserted blockage is necessary since the fouling material serves as the blockage. The blockage often is blown from the pipe or tube before or with the fouling material, rather than behind the fouling material as in a pigging process. The blockage device is proportioned to the size of the pump used. With a smaller pump, tighter clearance around the blockage is used. Due to the fluid flowing around it, the sonics affect is on the downstream edge of the blockage. The blockage device does not violently contact the fouling material. However, the blockage device is often distorted when it exits the pipe or tube, due to the sonics and high velocity to which it has been exposed. Grooves are often formed along the exterior of the blockage devices, and are cut from the back of the device to the front from the cavitation around the blockage, as discussed herein.

2.4 Equipment

Hydrokinetics™ is based on slow filling of the pipe or tube via a multi-cylindered positive displacement pump, and then the releasing of high velocity fluid into the relatively static fluid in the pipe or tube. The pump should have an odd number of cylinders or should feed a pulsating device, and the pump should be equipped with an unloader valve. Hydrokinetics™ requires at least two valves in addition to the unloader valve to induce resonance into the liquid in the pipe or tube. Via the proprietary Hydrokinetic™ equipment, sonics is induced in the liquid of the system upstream of the blockage, at the pump or pulse-generating device, and enhanced by velocity accelerators.

This system cleans when the necessary frequency range does not exceed an augmented frequency range, such as the frequency range arrived at from the 120º pulsation of a triplex pump with the pump rotating at approximately 450 rpms and modulated through the unloader system at a pressure low enough to avoid structural damage to the fouled pipe or tube.

To induce a sonic wave into a pipe or tube via this system, a pump or other high-pressure fluid source, an unloader valve, fluid accelerators(s), two or more valves, and a ram and nozzle assembly are needed. A lance is not a required part of Hydrokinetics™. The fluid source may be smooth or pulsating, for example an odd-numbered, multi-cylinder positive displacement pump. The fluid source can connect to a pulsation source downstream to add pulsations to the fluid flow. Hydrokinetics™ entails the delivery of a fluid stream from the pump or other fluid source into pipes or tubes via apparatus that creates sound waves in the fluid system. Being of different materials, the resonance transfers to the pipe or tube and to the fouling material at different rates, breaking the bond between the two. Once the bond is broken, the fouling material washes out in the fluid stream. The system is not dependent upon erosion or scrapping as in conventional hydroblasting or pigging. There are instances when the time allowed for erosion technologies is limited as production is ceased for cleaning, a costly situation. In such cases, Hydrokinetics™ can be used as the breaking of the bond and extrusion of the fouling material is logically faster than the eroding away of such material.

When a pipe or tube is to be cleaned with Hydrokinetics™, it is first opened on both ends. A nozzle is mounted onto the pipe to close off the entry end, and a volume of fluid flows into the pipe or tube. When the tube or pipe is full, the obstruction caused by the fouling material or the manually inserted blockage will cause the pressure to suddenly increase. This increase initiates the cavitation and cleaning process. It is important that this pressure be compatible with the pipe or tube to assure its integrity. During pressure tests, the circumferential stress is not to exceed 90% of the yield strength of the pipe or tube. Hydrokinetics™ uses pressure far less than this and for shorter durations of time generally used in pressure testing. The Hydrokinetic™ pressure is calculated and pre-set on the aforementioned unloader valve.

2.5 Pressures

For tubing, such as in heat exchangers, coolers, chillers, etc., the pressure can be calculated via Barlow's Formula, a generally accepted engineering formula. As the tubes to be cleaned are not new, the pressure arrived by the formula is reduced, often by 25%. Thus the formula for cleaning tubes would be calculated as:

$$P = (2t \text{ x } S \div OD) - 25\%$$

where P is the pressure, t is the tube wall thickness, S is the strength of the metal, and OD is the outer diameter of the tube.

When dealing with pipe, generally there are flanges, bolts and gaskets to be considered. These items may be less strong than the pipe itself. Therefore, a separate formula, derived by Don E. Bray, Ph. D., P.E., is used for pipe, as follows:

$$P = (1.5t \text{ x } Y) \div ID$$

where P is the pressure, t is the pipe wall thickness, Y is the standard minimum yield stress, and ID is the inner diameter of the pipe. Depending on the age of the pipe, this calculation may be reduced by some percentage.

2.6 Hydrokinetic™ Cavitation

Referred to herein as cavitation, large bubbles or cavities, imploded by fluid pressure, are a source of vibrations. Intense ultrasound waves generate large alternating stresses within a liquid by creating regions of positive and negative pressure. A cavity can form and grow during the episodes of negative pressure but when the cavity attains a critical size, it implodes, generating intense localized heat and tremendous pressure. Vibrations are due to the tremendous turbulence, heat and pressure of the imploding cavities, providing a unique environment for high-energy reactions.

Hydrokinetic™ cavitation can be generated by inducing intense sound waves in a liquid. Such waves create, alternately, compression and expansion, which in turn can form the bubbles subject to implosive. Of course, compression cycles exert a pressure on the liquid molecules forcing them together. Conversely, expansion cycles exert a negative pressure that pulls the molecules away from one another. During the expansion cycle, a sound wave of sufficient intensity can generate cavities. Bubbles in liquids are inherently unstable, as large ones tend to float to the surface and small ones tend to re-dissolve into the liquid. Bubbles absorb energy with the compression and expansion cycles of sonic waves. The growing cavity can eventually reach a critical size where it will most efficiently absorb energy from the sound wave. The critical size depends on the frequency of the sound wave. Once a cavity can no longer absorb energy efficiently, it can no longer sustain itself and the liquid rushed in and the cavity implodes. A liquid is held together by attracting forces, which determine surface tension of a liquid. For a cavity to form, a large negative pressure associated with the expansion cycle of the sound wave overcomes the liquid tensile strength. Less pure liquids have weaker tensile strengths. Therefore bastardizing fluid mediums, such as extremely pure water, with soda or a metalliferous liquid can enhance the cavitation. With such bastardized mediums, the pressure waves drive small particles into one another at high speeds with collisions so intense that the metal powders are melted at the point of impact. Further, the adhesive nature of a liquid is reduced when the liquid is cut with air or other gases, or when gas is dissolved in the liquid. When a gas-filled crevice is exposed to a negative pressure cycle from a sound wave, the reduced pressure makes the gas in the crevice expand until a bubble is released into solution. Most liquids, such as plant water, are sufficiently contaminated by small particles to enhance cavitation.

During implosion, the gases and vapors inside the cavity are compressed, generating intense heat that raises the temperature of the surrounding liquid, creating a very small local hot spot that dissipates quickly. However, at any given time, the temperature of the bulk of the liquid remains unaffected. If the cavity forms near solid surface, such as the surface of the fouling material or pipe or tube interior wall, the implosion will be asymmetric, expelling a jet of liquid at roughly 400 kph. The jet develops opposite from and moves toward the solid surface. The jet, as well as the waves from the cavity implosion, erode solid surfaces, remove non-reactive coatings and fragment brittle powders. Reactions are further facilitated by high temperatures and pressures associated with cavity implosion near the surface. The Hydrokinetics™ system of resonating the fouling material and the pipe or tube wall at different frequencies, degradation of the fouling material, and deep cleaning of the pipe or tube wall surface, is further impacted by the bombardment of high-speed jets of heat and energy for the imploding cavities. Hydrokinetics™ is effective at clearing fouling material from pits in the pipe or tube walls. The intensity of cavity implosion can be altered by changing frequency, acoustic intensity, temperature, static pressure, choice of fluid, and choice of gas. Implosion proceeds more slowly as ambient temperature increases so the fluid stream can be cooled or heated to enhance cleaning.

2.7 Extrusion of Fouling Material

There is of course a frequency at which the pipe, depending upon its composition, will begin to vibrate, and a frequency of which the fouling material, depending upon its composition, will begin to vibrate. Composition is the size, thickness, density, support structure and other criteria that mandate this frequency. Because the pipe or tube and the fouling material are of different compositions, they will vibrate at different frequencies, except in the rare instances where both the pipe or tube and the fouling material vibrate at the same frequencies because of the combination of the components which create their compositions. When the frequency at which each will vibrate is met in the fluid stream by the build up of pressure in the pulsations, this frequency will result in the vibration of the pipe and separately in the vibration of the fouling material. This separate vibration results in a breaking of the bond between the pipe or tube wall and the fouling material. Once this cohesion is broken, the blockage which inhibited the flow of the fluid stream will wash forward under the pressure inherent to the system and the blockage and fouling material will wash out of the pipe or tube.

As Hydrokinetics™ acts on the bond between the fouling material and the interior pipe or tube wall, after removal the fouling material is relatively unchanged, not being eroded into a granular or particulate form. The fouling material is generally expelled in large sections and has the same form is it had inside the pipe or tube, often appearing to be a mold of the tube interior. Due to the large sections of fouling material, collection of the foulant is ecologically compliant. When fouling material is eroded and therefore granulated or particulated, collection can be problematic.

Further, as erosion is dependent upon large quantities of fluid, in instances whereby water is monitored or conserved, Hydrokinetics™ can offer a lower water-usage alternative. Hydrokinetics™ does not require the addition of chemicals. Thus areas which are environmentally sensitive are provided with a measurable difference in water consumption, water treatment and affluence with the Hydrokinetic™ cleaning methodology.

3. CONCLUSION

Via proprietary Hydrokinetic™ equipment, sonics can be induced in a standing fluid column within a pipe or tube for the purpose of breaking the bond between the fouling material and the interior tube wall and removal of the fouling material. This waterjetting methodology provides an alternate cleaning process to conventional hydroblasting, ultrahigh waterblasting, chemical circulation, oven baking, wire brushing, drilling, etc. particularly in situations where downtime is critical, ecology is a factor, safety issues prevail, or conventional methods have been strained.

4. ACKNOWLEDGEMENTS

Our Thanks To: Ralph Garcia, AIMM Technologies, Inc.; Dr. Alex Haubold, Independent Consultant; Don E. Bray, Ph.D., P.E., Texas A&M University; Peter Smit, Smet Kinetics Corporation; and Miguel Morrett, AIMM de Venezuela, S.A.Miguel.

5. REFERENCES

"The Chemical Effects of Ultrasound", *Scientific American* (February 1989)

"Hydrokinetics™ Pipe Cleaning", Don E. Bray, Ph. D., P.E., (December 1998)

"Fluid Power & Electrical Control Designer's Manual, 40th Edition", Womack (1996)

"Flow of Fluids through Valves, Fittings, and Pipe, Technical Paper No. 410", the Engineering Department of Crane Co. (1988)

ASME Code for Pressure Piping, B31, Process Piping, The American Society of Mechanical Engineers, 1996 Edition (1996)

U.S. Patent No. 5,423,917 "Method for Cleaning Heat Exchanger Tubes by Creating Shock Wave and Mixing the Liquid with Injected Air", (February 1993)

U.S. Patent No. 5,674,323 "Method and Apparatus for Cleaning Columns by Inducing Vibrations in Fouling Material and the Column", (June 1995)

6. NOMENCLATURE

Hydrokinetic™ and Hydrokinetics™ - The trademarked names used by AIMM Technologies, to refer to the patented process whereby resonant frequency vibration induced in a fluid is used to clean the interior diameter of pipes or tubes.

P - In formulas herein, the maximum pressure used for the Hydrokinetics™ process
ID - Interior diameter of a pipe or tube
OD - Outer or exterior diameter of a pipe or tube
t - The thickness of the wall of a pipe or tube
S - The maximum strength of the pipe or tube material
Y - The standard minimum yield stress of the pipe or tube material

7. TABLES

Loss Of Polymer Production During Shutdown

	Time required	*Product per hr*	*Production lost*	*Product value*
Conventional	27 hours	11,000 lbs	297,000 lbs	$118,800
Hydrokinetics™	3 hours	11,000 lbs	33,000 lbs	$ 13,200

Water Usage During Shutdown

	Time required	*Water required*	*Water consumed*	*Liquid affluent*
Conventional	27 hours	1200 gallons/hr	32,400 gal	32,400 gal
Hydrokinetics™	3 hours	256 gallons/hr	768 gal	768 gal

Examples of Possible Hydrokinetic™ Applications

CATEGORY	APPLICATION	COMMENTS
PRODUCTS	Rubber, latex, similar sticky products	Product tends to cling to walls during production. Cleaner walls will stay cleaner longer.
	Polycarbonates or hard plastics	Breaking of the bond removes rods of material. Erosion is time prohibitive.
	Polymers, soft plastics, and gels	Hydrokinetics removes large "rubber snakes" for reduced downtime.
	Calcium carbonate and hard scales	Breaking of the bond removes rods of material. Erosion may be time prohibitive.
	Solid plugs of any consistency of product	Solid plugs are as easily Hydrokinetically removed as any other degree of fouling.
TUBE BUNDLES	U-bundles	U's, even tight radius, resonant just as the straight runs of pipe, providing clean turns.
	Odd configurations	Coil, loops, serpentines respond to Hydrokinetics just as straight runs do.
	Small tubes	Tubes that are difficult to lance due to size. Also small tubes tend to solidly plug.
	Verticals	Hydrokinetics™ does not require removal or crane work.
	Bundles in tight spaces	Hydrokinetics™ does not require removal to cleaning area
	Bundles which tend to solidly plug	Plugged tubes are as easy for Hydrokinetics as any other degree of fouling.
PIPING	Reactors and units made of piping	Hydrokinetics cleans large diameter loop reactors and similar configurations without dismantling.
	Long runs	Hydrokinetics cleans long without removal from pipe rack (over one mile should be discussed).
	Solid plugs	Hydrokinetics™ does not require exact location of plug.
	Odd configurations	Hydrokinetics cleans multiple 45ºs, 90ºs, 180ºs, etc., under roads, overhead, in place.

9. GRAPHICS

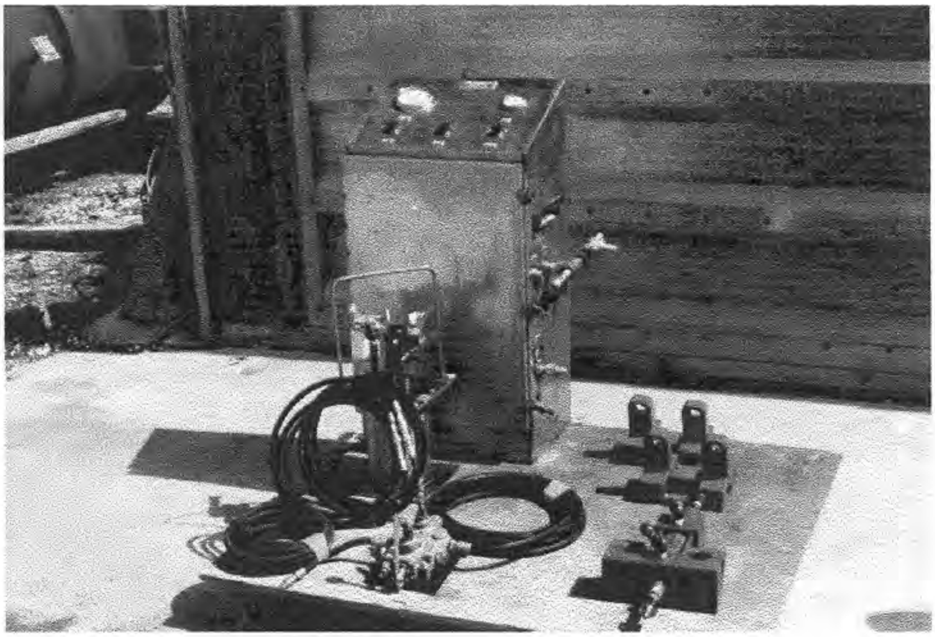

PROPRIETARY HYDROKINETIC™ EQUIPMENT

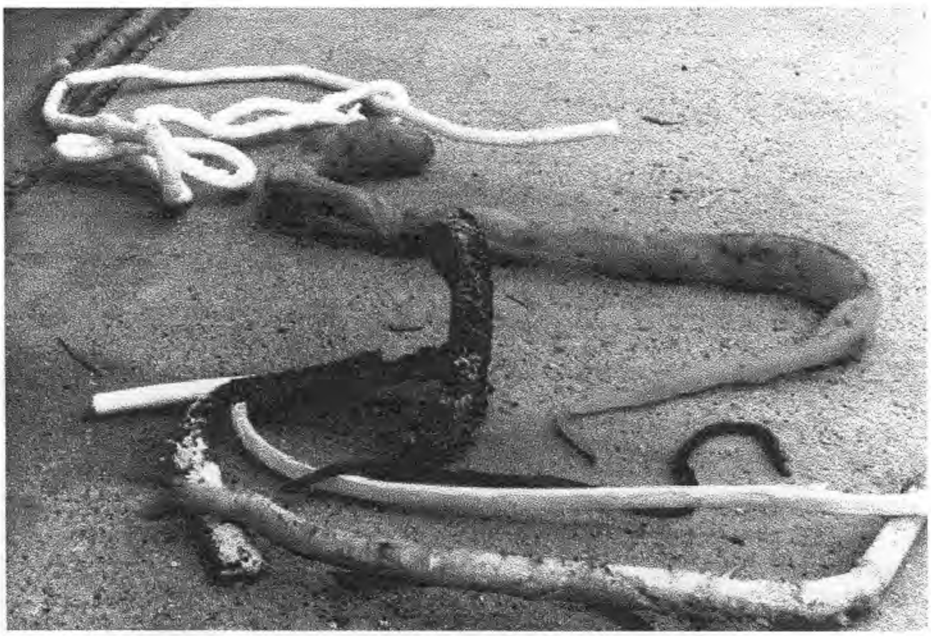

SAMPLES OF FOULING MATERIAL REMOVED VIA HYDROKINETICS™

10th American Waterjet Conference
August 14-17, 1999: Houston, Texas

Paper 44

THE STUDY ON THE CLEANING PROCESSING FOR UNDER GROUND LAID PIPELINE WITH LARGE DIAMETER USING HIGH PRESSURE WATERJET

Zeng Yanli, Ouyang Xianwu, Lu Wenzhu, Liu Guangheng
Shenyang Institute of Instrumentation Technology
Shengyang, P. R. China

Ning Guoqiang
Shenyang Huitian Thermoelectricity Co. Ltd.
Shengyang, P. R. China

ABSTRACT

It is presented in this paper the novel cleaning processing for defocusing on the interne wall of the pipeline (diameter Φ 720mm) and blowing off the separated fouling matter to the mouth of the well (mouth distance 200m) using the high pressure water jet and elevating it ground upward. Field experiment results show, the above mentioned novel cleaning processing is possessed of certain significance for cleaning other pipelines like this.

Organized and Sponsored by the WaterJet Technology Association

1. INTRODUCTION

On the pipe wall of the long distance transmission pipeline with large diameter (ϕ350mm) some fouling and corroded matters can be deposited because of the foreign matters in the transmitted medium and some reasons of the processing technology. The formation of the fouling matters will make significant effects on the operation potency of the equipment and increase the energy loss and material loss. However this situation can be improved in certain degree through various measures such as treating the water, adding the chemical agent, adopting rationally processing parameters etc., but it is still impossible, fully to avoid the fouling formation. Therefore the correctly choosing a method to clean the pipeline is an indispensable link.

The wax and naphthalene on the interne wall of the oil transmission pipeline and gas transmission pipeline can be removed with electronic pig and the result is good. But it is up to now still lacking in the ideal cleaning processing for the long distance transmission water pipeline with large diameter, the cleaning with chemical agent has although a certain effect, but the cleaning processing is very complicated. It can contaminate the environment and corrode the pipeline. General speaking, it is not adopted. However the high pressure water jet cleaning can overcome the same problems caused by chemical cleaning, but the conventional water jet cleaning can not solve following problems: (1) well distance is long (200m) (2) pipeline is under ground laid (Operator can not enter into) (3) separated fouling matter can not be quick and safe removed out of the well after cleaning. These problems must be solved with special water jet cleaning processing and equipment.

2. NATURAL SITUATION OF THE EXPERIMENT PIPELINE

The experiment pipeline was laid in 1980. It is field heat supplying main pipeline laid under ground in the channel. The transmitted medium is water at low temperature (<95 °C). The diameter of the pipeline is ϕ720mm, pipe wall thickness is 8mm. The designed flow rate is 5500t/h. (due to the increase of the load the practical flow rate is 6300t/h). The designed lifetime of the pipeline is 15 years. Now, it is still in extended service. Because the water medium was not strictly deoxygenated and softened, the separated oxygen ion and calcium ion as well as magnesium ion after heating made serious oxygen corrosion and fouling on the interne surface of steel pipe. Therefore there are much corroded pitting and hard deposited water scales (ca. 10mm) on the pipe wall and specific local remains only 3.1 mm thick. The interne surface roughness of the pipeline is reduced, the water flow area decreased, the water flow resistance increased, the water operation of the heat supplying system deteriorated and the energy loss of the heat supplying system increased, as well as the effect of the normal heat supplying influenced. If replacing the old pipe with new pipe for one meter must be paid 10000 Yuan RMB comprehensive cost. Because out of the investment capital, it is impossible to replace this many thousand meters pipeline. The service life of the pipeline can be extended only by the way to coat anticorrosion layer after cleaning.

3. STUDY ON THE CLEANING PROCESSING

According to the basic theory of the fluid flowing when the fluid flows along the pipe, the energy loss happens at same time due to the friction between the fluid molecules and the pipe wall. The relationship of the loss along the way pro meter pipe length (specific differential pressure) R, pipe diameter d and the water flow rate is as follows:

$$R=6.38\times10^{-3} \quad \frac{\lambda G_1^{\,2}}{\gamma\, d^5} \quad (\mathrm{kg/m^2\,.m})$$

Where R = Loss along the way pro meter pipe length, $\mathrm{kg/m^2.m}$

G = Water flow rate, t/h

d = Inside diameter of the pipe, m

λ = Friction coefficient of pipe interne wall

γ = Volume weight, $\mathrm{kg/m^3}$

From the above mentioned relationship: If the pipe is critically corroded and fouled, then the d value will decrease, λ value increase, R value increase, the pressure of circulating water pump of the pipeline and the electrical loss also will become greater. The cleaning purpose is to decrease λ value, increase d value, that means the deposited fouling matters on the pipe wall must be removed away in order to return the normal operator of the pipeline.

For cleaning the pipeline with little diameter the cleaning operation can adopt backward jet nozzle assembled on the front top of the high-pressure rubber hose. The high-speed backward jets drive the nozzle forward and fulfil the cleaning operation. But it is not suitable for cleaning operation of the pipeline with large diameter, because the high-pressure rubber hose and jet nozzle are very small referred to the pipe diameter. Its knock forces for separating the fouling and the cleaning covering area are not ideal. Therefore a special cleaning processing equipment must be adopted.

3.1 Determination of the Effective Cleaning Parameters

The major parameters influencing the water jet cleaning processing equipment are: jet flow rate, jet flow speed, distance between the jet nozzle and operating surface (target distance) as well as the relative moving velocity between the jet nozzle and operating surface.

We have made many experiments to clean the fouled pipe wall with the cleaning machines GS52/50 and GS70/63 manufactured by our institute with the hand-controlling spraying gun connecting the cylindrical spraying head which operating pressure is matched with the flow rate. At pressure 45MPa the fouling matters began to fall down, especially at 55-60MPa faster and more. In consideration many factors in practical cleaning, such as target distance, the relative moving velocity between the jet nozzle and the pipe wall can not reach to the ideal value and the power distribution of many nozzles cleaning is not concentrated, the cleaning pressure is determined to 70MPa and the flow rate to 63l/min.

3.2 Cleaning Processing and Equipment

Because the pipeline to be cleaned is laid underground, it is allowed to open a well mouth in each 200m. That the operator can not work in the pipeline means we must control the cleaning operation (cleaning the interne wall of the pipeline laid under ground) on the ground. The difficulties are: (1) the optimal target distance can not be guaranteed, because the fouling is not homogeneous (2) the match relation between the feed speed of the cleaning equipment in the pipeline and the cleaning covering area is not easy to determine due to the influence by many factors (3) the separated fouling matters are very fast removed out. Through many experiments and design improvement we have developed a novel rotating feed cleaning processing equipment, precession sledge. The above mentioned problems are solved with this precession sledge.

The cleaning processing equipment consists of two parts, the adjustable speed reducing self-rotating spraying head and the sledge support. The schema of the cleaning operation with sledge rotating feed equipment shows as follows in Fig. 1.

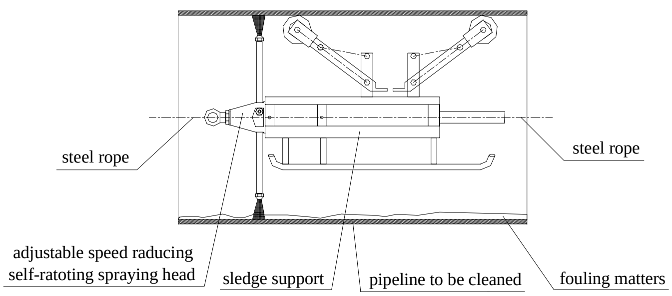

Fig. 1 Scheme of the cleaning operation with sledge rotating feed equipment

The spraying head is equipped with two bias jet nozzles used for forming the torque to the spraying head and two cleaning jet nozzles. These four jet nozzles are well distributed in direction of the circle. They bring the cleaning operation to success together. The target distance between spraying head and fouling on the pipe wall is designed as adjustable. The rotating speed is controlled in the range 350~450 rpm. In order to fulfil the forward and backward operation, the both ends of the equipment are connected with two winding machines set up on the ground by the well mouths. The winding machine is controlled manual. Every two revolutions mean the equipment displaces one meter.

The cleaning goes on as following processes: The two winding machines work actively or passively. The equipment is 1m forward fed first, then backward 0.5m, following in order and advances step by step, every pipe section is cleaned for three times. Cleaning 1m pipe length needs 5 min. This is one of the means to solve the problems of the covering area to be cleaned. We use this processing to clean 700m pipeline. Before cleaning the pipeline is seriously fouled and corroded. Its corrosion class is C (GB8923). After cleaning the fouling matters on the wall surface are fully removed, but the special hard rust spots on the local surface remain partially. However it can reach the rust cleaning class Csa2 (GB8923-88). The surface can conform to the general demands for inside prevention of the corrosion.

3.3 Blowing off the Separated Fouling Matters

Using a special designed blowing remover the separated fouling matters can be removed away. This fouling matter remover is special designed for the cleaning machine with 10MPa pressure and 160l/min flow rate. The blowing off operation of the fouling remover in the pipeline shows in following scheme Fig.2.

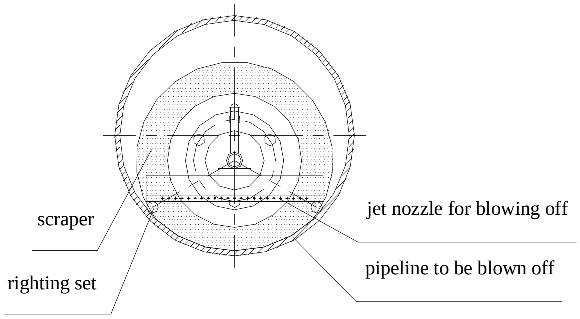

Fig.2 the blowing off operation of fouling remover in the pipeline

Both ends of the fouling remover are connected with two winding machines based on the ground and drawn forward or backward. The separated fouling matters can be blown off from a well mouth to the other well mouth through the many forward high speed jet fluid sprayed from the jet head with large volume of flow before the fouling remover. The scraper behind the fouling remover sweeps off the residual separated fouling matters to the end well mouth. A bag filter is hung in the end well mouth .The water also is filtered and the fouling matters remain in the bag. After the operator has the bag elevated upward and the fouling matters treated on the ground, the cleaning operation is end.

4. ANALYSIS OF THE ECONOMICAL BENEFIT

Using this technology to clean 1 m pipeline like this and prevent it from corrosion, the user has to pay ca. 200 Yuan RMB only, but to lay 1 m pipeline like this the user must pay 10000 Yuan RMB comprehension cost. So this technological processing is possessed of a great economical value to restoration of old pipelines.

5. CONCLUSION

The cleaning processing equipment and the flexible outside diameter of the fouling remover can be adjusted through regulating the size of the hack lever, therefore they can carry out the similar cleaning operation of the pipeline with diameter ϕ350mm ~ 1400mm. This technological processing also is possessed of widespread use perspective for like this pipeline in thermoelectricity, aluminum and heat supplying industry.

6. REFERENCES

1. Xue Shengxiong etc., The Technique and Application of the High Pressure Water Jet, Publishing house for machine-building industry, Beijing, Aug. 1998.

2. He Ping etc., Heat Supplying Engineering, Publishing house for architecture industry, Beijing, Sept. 1980.

10th American Waterjet Conference
August 14-17, 1999: Houston, Texas

Paper 45

CLEANING THE OIL-GAS LINES ON CATALYTIC CRACKER UNIT IN OIL REFINERY USING HIGH-PRESSURE WATER JET TECHNIQUE

Leyao Zhang (Director), Yang Jiao (Vice-Director), Qizhuang Zhang (Deputy Director)
High-Pressure Water Jet Cleaning Technology Center of
Beijing Yanshan Petrochemical (Group) Co., Ltd.

ABSTRACT

In recent years, the use of high-pressure water jet cleaning techniques to clean equipment of many types and in different media and work conditions becomes an increasingly wide accepted practice in petrochemical enterprises in order to meet the requirements of production and maintenance. In this paper, the high-pressure water jet cleaning of the oil-gas line on the catalytic facilities in oil refinery enterprises is introduced briefly in combination with the cleaning practice in this field. Our purpose is to further the study and discussion among domestic and foreign friends of the same trade and to improve equipment step by step, optimize cleaning techniques so as to raise the efficiency and quality of the oil-gas pipeline cleaning to a new height.

1. INTRODUCTION

During overhauling petrochemical equipment the pressurizing water jet flow technique has been recognized as one of the new techniques for equipment management and application by Chinese Petrochemical General Corporation. Recently this technique has been well popularized, developed and advanced for its popularization and application because of trying to work hard on it. There are ordinarily few simple appliances and few workers doing the job as their second post in almost all the oil works and there are few full-time workers in few works do the cleaning by themselves. These are suitable only for the individual equipment and common work condition. Its advantage is that the cleaning organization is simple and the operation is very fast, but there are some disadvantages having worse cleaning quality and lower worker and equipment utilization ratio. It cannot suit the needs of the cleaning very much when the complex work condition, some difficulty and large working surface are occurred. Cleaning with specialization and socialization team and on a large scale is the best. The cleaning teams in society understand a few production technology, a few equipment construction and a few safety knowledge operated in the condition of high temperature, high pressure, combustible and explosive. Their consciousness to safety and adaptability are not enough. However, if the workers of refinery do the cleaning by themselves, all the disadvantages above can be overcome. They not only do the work very safe but also control and decrease the cost for overhaul. Pressurizing water jet flow technique has many advantages described above: It changes all the defects of other techniques. It makes improvement to the cleaning quality, efficiency, safety and environmental protection better. It creates good factors for shortening the production set/equipment downtime and prolonging the operating time and for optimizing running. Certainly it occupies a dominant position in the cleaning area. So this technique is very available to increase the economic and social effect.

2. BACKGROUND

When the catalytic sets in Yanhua Refinery was overhauled in March, 1990, the serious coke in the oil-gas pipeline with diameter of 1120mm. (Fig.1) and between the settler and fractionating column was found and the coke thickness reached to 150-200 mm. (Fig.2). It should be thoroughly removed at once, otherwise it will not only affect the sets running on time, but also their running for a long period.

Millions of dollars come when the catalytic cracker unit once operates. If the catalytic sets run earlier and/or for a more time, more than millions of dollars will be got, so it is very beneficial to the enterprise and society to do so. Coke is always happened on the inner wall of the oil-gas pipelines due to the heavy oil produced, it should be removed at regular intervals for normal production, once the production is in unsteady running, coke will occur more easily, it is necessary to clear away the coke in time. So, that is just the point which kind of technique for cleaning coke we shall adapt.

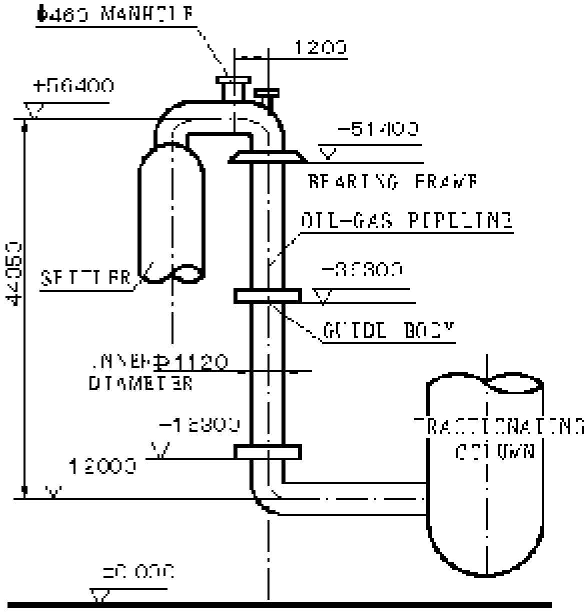

Figure 1. Oil-gas line

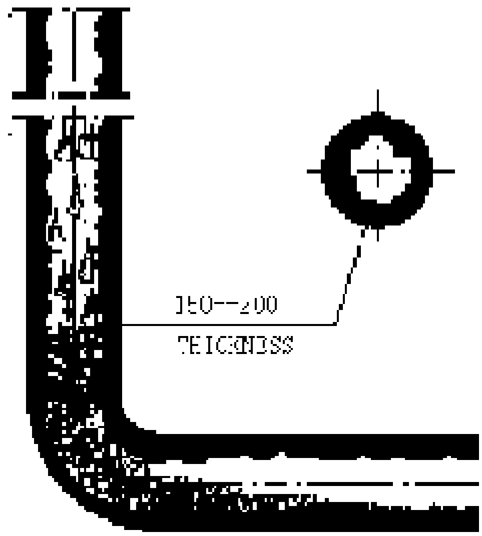

Figure 2. Coke aspect

3. COMPARISON AND CHOICE OF SCHEME

There were several schemes for choice at that time. One of them was to drill a hole on the top of the pipeline for taking soft elevator or cableway basket to go down into the pipe (Fig. 3) and removing the coke by hand. With this scheme the operating is not safe for the worker who goes down into the pipe, the much powder dust is harmful to the man, the work efficiency is low, the rate of progress slowly, the working-hours long and the cleaning quality is worse. The second scheme was to take the pipeline apart one part by one and each part was lifted up to the ground and cleaning by hand (Fig. 4).

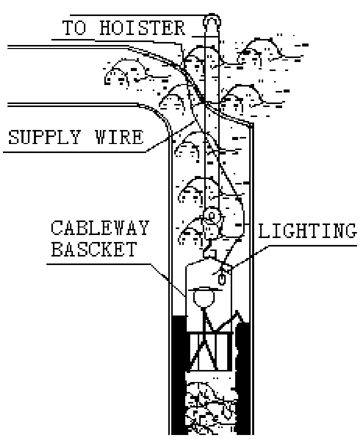

Figure 3. Coke removing by hand

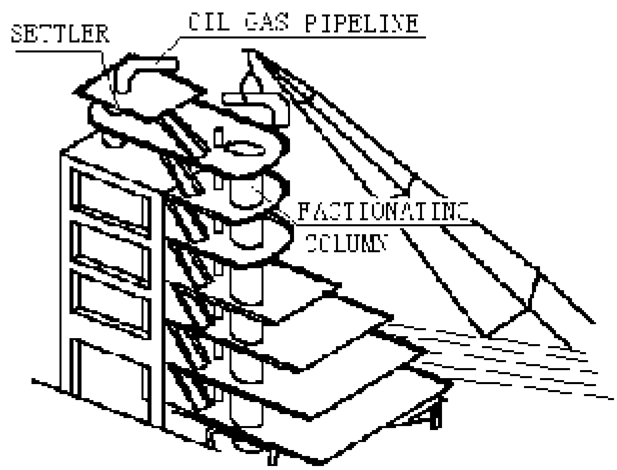

Figure 4. Take the pipeline apart, one part by one

But the hanging operation was quietly difficult because there were many equipment sets in the direction of south-north, platforms and ladder in the east and 15 meters of pipeline existed (Fig.6.) in the west in situ. Also, it was very difficult to weld the pipes making from Cr-Mo steel together.

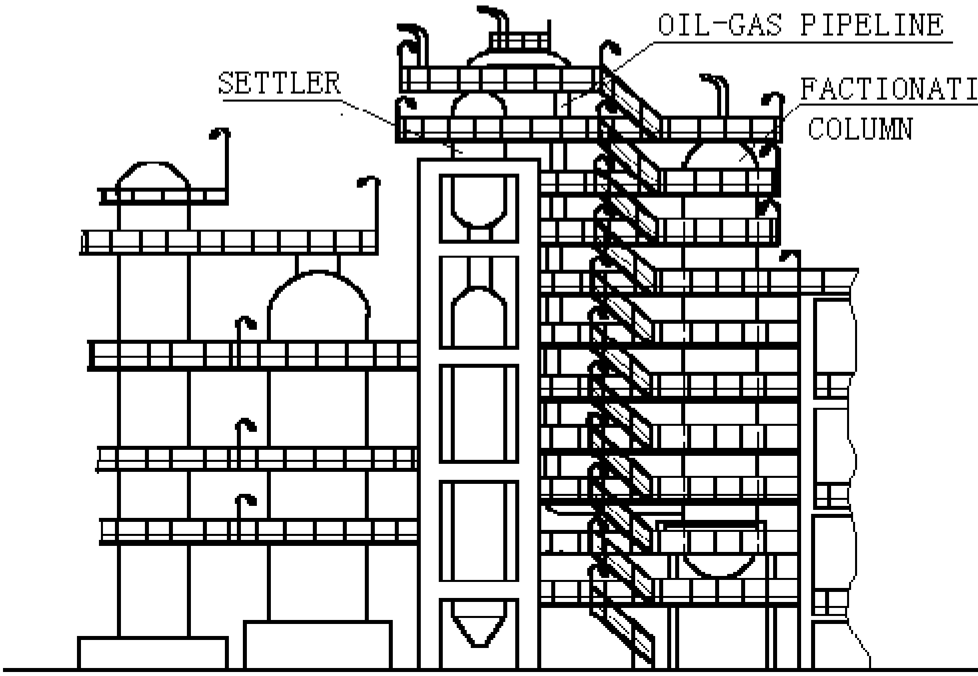

Figure 5. Schematic diagram of the pipeline position

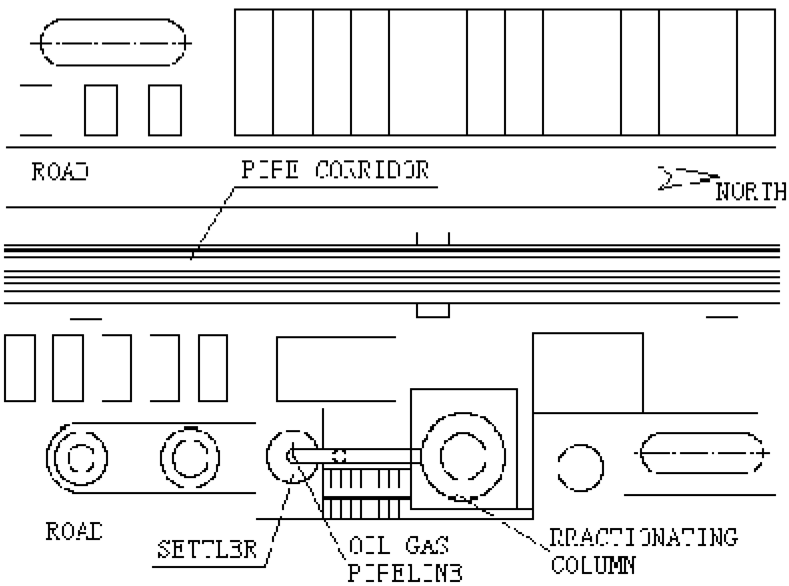

Figure 6. Schematic diagram of the pipeline position

There were still many defects such as long working hours, very cost and worse coke cleaning quality for the second scheme. Scheme 3 uses the pressurizing water jet flow technique to clear away the coke automatically. Because it has high cleaning speed, good quality, no powder dust, no pollution, short working time and lower cost, and no necessity the worker entering into the pipe, it overcomes the defects of scheme 1 and 2. Therefore, scheme 3 is confirmed and selected.

4. PUT THE SCHEME INTO PRACTICE

After the Pressurizing Water Jet Flow Technique Center , YANHUA Corp. received the cleaning task in March,1990, laying out a practice scheme, designing working appliances, study and manufacture of equipment, preparing utensils and materials and testing in a large scale had been done. At last the operation of cleaning coke in situ had been put into practice (Fig. 7.) .

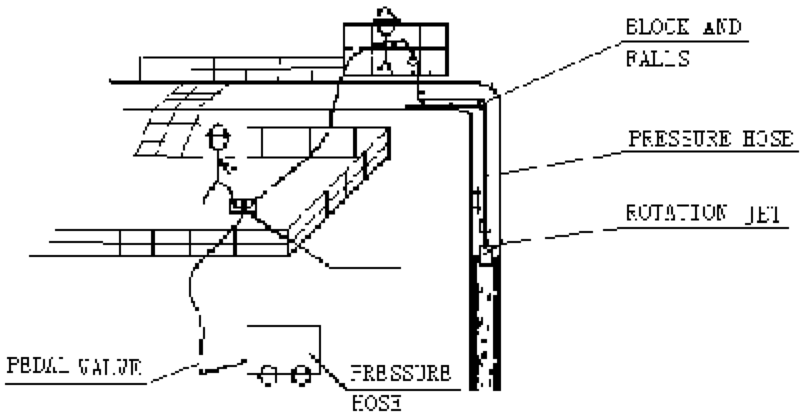

Figure 7. Schematic diagram of the cleaning system

At first a set of block and falls was set on the top between the former manhole on the overlaying horizontal section and the inner center line of the oil-gas pipeline. Connected a pressure hose to the exit of the pedal valve and positioned the pressure hose on the center line of the vertical tube through the block and falls. In front of the hose there was an automatic twin-rotation jet nozzle to connect to. Through the pressure hose the pressurized water with 50 MPa was pressed by the pressure pump to a platform which datum mark is 56 m The turning on or off of the water is controlled by the pedal valve. The cleaning nozzle head can rotate automatically to complete the coke removing process. It spent 18 days and more than 20 cubic meters of coke had been cleared away for the first cleaning due to solving the various problems constantly on every site points. The cleaning with safety, good quality and low cost had been achieved and the running of this cracker set had been ensured on time except that the longer working hours needed due to using not too perfect technology and working appliances. It was the first time for cleaning the oil-gas pipeline on catalytic cracker unit of refinery enterprise in this country to use the pressurizing water jet flow technique. It opened a new cleaning way and a new application area for cleaning to use this new technique. The design, study and application of this new technique fills a blank in this area in this country.

5. PERFECTING THE SCHEME

Hereafter, Pressurizing Water Jet Flow Technique Center, Yanhua Corp. improves the cleaning technology and perfects the cleaning working appliances for several years to make the cleaning efficiency obvious raised. Going on safety and quality premise the working hours for cleaning one oil-gas pipeline decreased from 18 days to 11 days, 7 days and even 5 days. At present it is enough for 3 days. The working hours can be still shorten if there are good organization and coordination in situ. Up to date many oil-gas line of many enterprises of Chinese Petrochemical General Corp. have been cleaned, see the following table for details:

Table 1. Comparison Table of Different Refineries

No	Unit	Set of Catalytic Cracker	Pipeline Diameter mm.	Lining	Working Time/ Times Hours/ times
1.	Beijing Yanhua Refinery	First	1120	Partial	1996.6 1998.4
2.	Beijing Yanhua Refinery	Second	1120	No	1990.3 1991.4 1992.3 1992.11 1993.4 1994.1 1994.4 1995.4 1996.8 1997.5 1998.4 1998.9
3.	Beijing Yanhua Refinery	Third	1120	No	1998.3
4.	Shahghai Gaohua Refinery	First	1220	No	1998.1 1998.10
5.	Shanghai Gaohua Refinery	Second	1220	No	1993.6 1993.12 1994.5 1994.12 1997.5 1998.7
6.	Shijiazhuang Refinery	First, Combined	1120	No	1994.4 1995.3 1996.5 1997.4 1998.8
7.	Shijiangzhuang Refinery	Second	1220	Yes	1995.10
8.	Jinzhou Shihua Refinery	First	820	No	1994.3 1995.3 1995 1997.4
9.	Jinzhou Shihua Refinery	Second	920	No	1994.3 1995.3 1996 1997.4 1998.9 1998.12
10.	Jiujiang Refinery	First	1020	No	1997.4
11.	Anqing Shihua Refinery	Second	1120	Yes	1997.6
12.	Dalian Shihua Refinery	First	1020	No	1997.7

The main contents of the practical scheme are:

5.1 According to the different pressure pump the pressure and the quantity of flow data are established as following:

pressure P1 = 50 MPa quantity of flow Q1 = 100 L/Min.
pressure P2 = 70 MPa quantity of flow Q2 = 54 L/Min (two pumps in parallel)
pressure P3 = 100 MPa quantity of flow Q3 = 84 L/Min

5.2 The pressure numerical digit of the cleaning head must be conformable to that of the pressure pump.

5.3 The pressure numerical digit of the pedal valve must be variable with that of the pressure pump and controllable.

5.4 The pressure numerical digit of the pressure hose both in front and behind the pedal valve must be conformable to that of the pressure pump and the inner diameter of the hose is 10 mm. In order to decrease the pressure loss, facilitate the cleaning work and shorten the working hours, use a steel pipe of thick wall with 12 mm.in thickness and mount it on the bearing frame as water-supply line. Connect the pipe to the pedal valve by a short pressure hose to conduct pressure water to a platform which datum mark is 56 meters. This kind of steel pipe has been mounted respectively on the set of second catalytic cracker unit of Yanhua Refinery and that of the first and second cracker of Jinzhou Shihua Refinery.

5.5 The twin-jet nozzle which diameter is 1.2, 1.5 or 1.75 mm. and angle is 13 degree is made of hard alloy.

5.6 During cleaning the coke on the vertical pipe wall having 56 meters long, in order to simplify the technology and working appliances and to shorten the working hours, it is necessary to perforate a hole on the elbow of the top part to place the cleaning head in the line (Fig. 8) and to perforate the another hole on that of bottom part to drain the residue (Fig. 9).

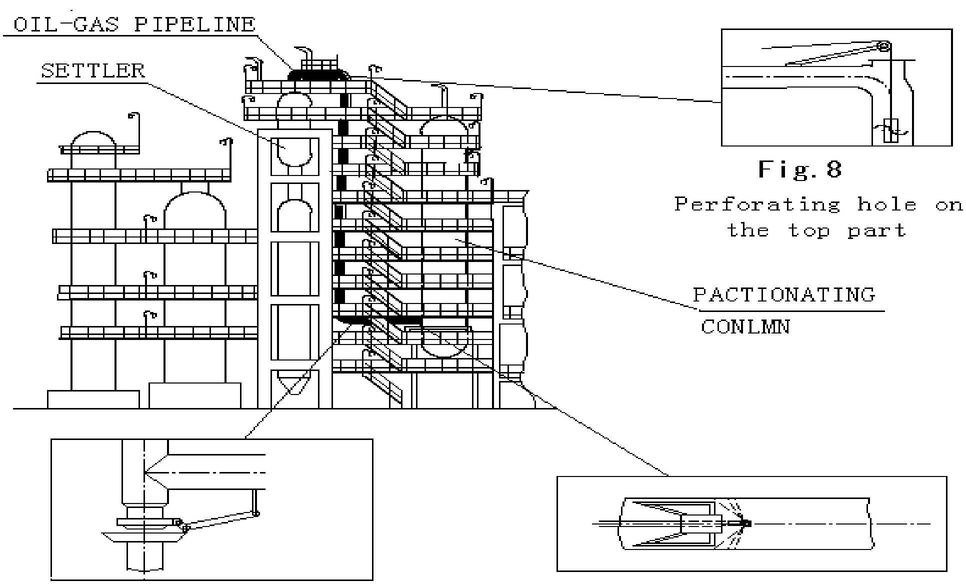

Figure 9. Perforating hole on the bottom part **Figure 10.** Cleaning coke in horizontal pipeline

5.7 Whether by hand or automatically by the special designing working appliances, it depends on the length of the pipe during cleaning all the horizontal pipes of the oil-gas pipeline (Fig. 10).

5.8 Hours in situ and the buck and boost (advancing and retreating) speed and distance of the cleaning head depends on the degree of difficulty for cleaning and the coke thickness and hardness.

6. SAFETY STEPS

Because the pressurizing water jet flow has a higher pressure (50-100 MPa) and a faster flow speed (several times as long as the velocity of sound) and there is the special requirement for the safe production and overhaul in petrochemical enterprise, it is quiet necessary to pay attention to the safety when the oil-gas pipeline is cleaned by pressurizing water jet flow. The safety steps should be available and performed very seriously. The main points of the safety steps are:

6.1 The pressure pump should be in good condition and its pressure gage should be calibrated within the standardizing measuring range; The control system should be sensitive for operation; The safety valve and the overflow valve should be effective and reliable.

6.2 The automatic cleaning head runs very flexibly; the control of pedal valve should be reliable; The pressure numerical digit of the pressure hose should be conform to standard and the hose should not be broken at all.

6.3 The cleaning operation must be performed according to cleaning technology seriously.

6.4 The enclosure or obvious mark should be built for the cleaning point including the hole for draining residue, anybody who does not do the cleaning thing should not be permitted to enter into the operation area and to move and use any cleaning equipment and appliance.

6.5 In general the pressure pump is not the anti-explosion machine, its starting in situ should be after going through the procedure according to the regulation.

6.6 The materials in the oil-gas pipeline cleaned should be cleared away and replaced up to standard, and isolated from the system. If necessary, treat it with blind plate.

6.7 Anybody who enters the pipeline for working appliance designing, quality inspecting or cleaning by hand should have the certificate for passing in and out.

6.8. Anybody who enters the pipeline must wear safety belt and be served by special guardian.

6.9 The coke scrap coming from the cleaning should be removed from the pipeline in time. If necessary, pay attention to ventilation.

6.10 The contact between the operator who operates the pump and the pedal valve and the cleaning worker must be unblocked, fast, accurate and reliable.

6.11 There must be reliable safety measure during working in high altitude, in much wind, in rain, in very hot and cold day, in the night and continuously.

6.12 The other safety rules published by the Chinese Petrochemical General Corp. and the petrochemical enterprises or by this branch of trade (this enterprise) and the related requirement of "The Safety Rules for the Pressurizing Water Jet Flow Cleaning" should still be conformed.

7. CONCLUSION

It cannot be avoided to coke in the oil-gas pipeline in production process. The pressurizing water jet flow technique is, to date, the best effective method for coke cleaning. The pressurizing water jet flow technique for coke cleaning has been more and more confirmed and welcome due to a series of its advantages to the others. The inescapable responsibility and obligation of the engineering workers studying the pressurizing water jet flow technique is to do their best to serve the petrochemical enterprises and the other trades. Cleaning the oil-gas pipeline is a cleaning subject under special condition. We wish the joint efforts must be made together with the domestic and external colleagues, the leaders, engineers and workers in refinery enterprises to study this task more deeply, to solve the problem better and to contribute much more for the society.

8. REFERENCE

Leyao Zhang, Yang Jiao and Qizhuang Zhang, "Pressurizing Water Jet Flow under Special Condition in Petrochemical Enterprise", *Theses Collection of the Forth Rim Pacific International Conference on Water Jet Flow Technique*, April, 1995.

10th American Waterjet Conference
August 14-17, 1999: Houston, Texas

Paper 46

LABORATORY EXPERIMENTS FOR CLEANING AND POLISHING THE SURFACE WITH HYDRAULIC JETS

S. Radu, N. Ilias, A. Magyari, A. A. Magyari
University of Petrosani, Romania

ABSTRACT

The recent experiments performed in the hydraulic cutting laboratory from the University of Petrosani were based on cleaning the surfaces with continuous hydraulic jets of medium and high pressure. Using this procedure the sedimented slag from the furnace doors and the paint on the metallic objects have been cleaned. The paper also presents a cleaning equipment adaptable to an industrial ievel. Another preoccupation is represented by polishing the roof glass with abrasive hydraulic jets, the abrasive being a special abrasive clay, the caolin, used not only by specialised industrial processes but also in manual polishing.

1. INTRODUCTION

This paper is among the first of this kind and presents the use of medium and high pressure water jets for the cleaning of material surfaces.

The aim of this research is to establish the efficiency of water jets in cleaning the ash deposited during the process of coal choking on the doors and the frames of the ovens at the Coal Processing Plant in Calan.

2. THE DESIGNING OF A WATER JET CLEANING MECHANISM

At present, the doors and the frames of ovens are cleaned manually, which involves the use of a large number of unskilled workers, a poor cleaning quality, heat losses caused by the opening of the doors over large periods of time, as well as the emission of noxious gases into the atmosphere. Another cleaning methods the use of the charging machine, a complex mechanism which also performs other operations. The shortcomings of this method are the non-uniform cleaning and the rapid wear of the brushes.

Starting from the existing mechanical cleaning installation and slightly changing it, we designed a new mechanism whose cutting tools are the water jets provided by the hydromonitors. Thus, we took over the existing automatic mechanism in which we replaced the brushes with a nozzle support system mounted on six lateral trolleys (fig. 1).

Fig. 1. Water jet cleaning mechanism

1.mounted door
2.support
3.handle
4.guide roll
5..nozzle support frame with tangent jet
6.nozzle support frame with direct jet
7.hose
8.quick joint with staples
9.fixing board
10.bolt
11.body

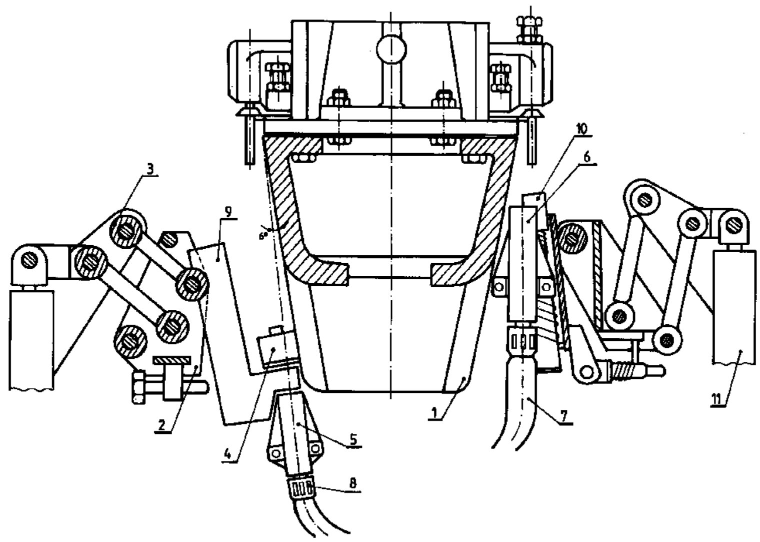

The cleaning of the door is achieved in two complete trolley movements on the door perimeter, one of them clockwise and the other counter clockwise. The nozzle support frames with direct jets (6) alternate with those with tangent jets (5).

In order to avoid the sprinkling of the brick wall, the whole assembly is provided with a metallictightening frame fixed on the lateral surface of the door before the beginning of the cleaning operations. The frame also collects and guides the hydraulic agent towards the basin situated under the door cleaning mechanism.

3. LABORATORY EXPERIMENTS FOR THE DETERMINATION OF CLEANING PERFORMANCES

By using the stand in the Hydromechanization laboratory at the University of Petrosani and slightly changing it for the fixing of the pieces of frame covered by ash, we conducted the first experiments.

The pieces of frame were cut out of the door of an oven which is no longer in operation and they were fixed on the stand. The ash deposits were of 4-8 mm. To get as close as possible to the real situation, the pieces of frame were heated at a temperature of 400-500◦C, which is the usual temperature of oven operation.

During the experiment, the pressure of the jet, the distance between the sample and the hydromonitor, as well as the diameter of the nozzle were changed. We notice that the ash was completely removed at a pressure of 50 MPa and a single move of the jet or at 30 MPa and two successive moves (fig. 2)

The optimal distance for cleaning was found to be of 100 mm (fig. 3). From among the tested nozzles, the optimal one proved to be the sapphire nozzle with a diameter of 0,8 mm. In the future, new types of elliptical nozzles will be also achieved.

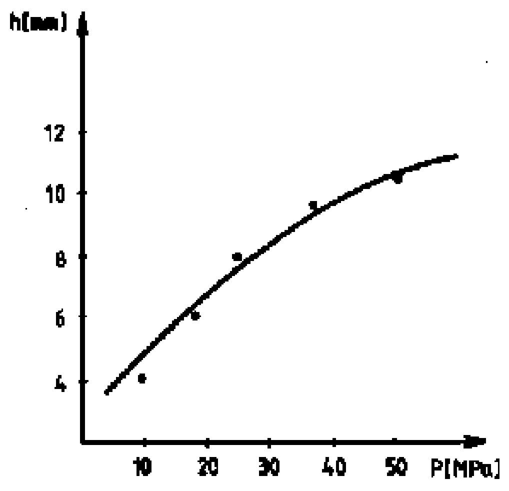

Fig. 2. Cleaning depth according to jet pressure.

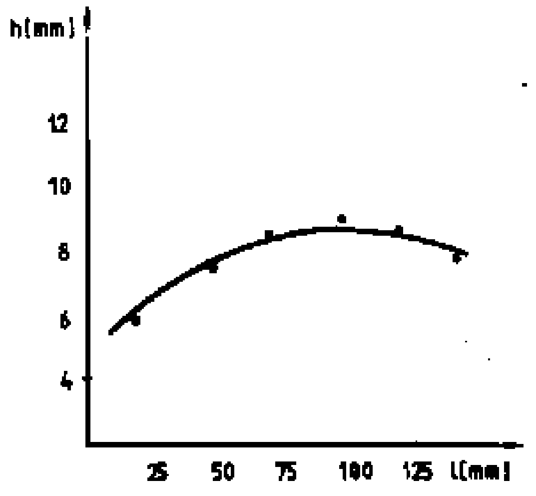

Fig .3 Cleaning depth according to distance.

4. CONCLUSION

Knowing the problems which the specialists at the Coal Processing Plant in Calan have to face and using the high pressure water jets cleaning technology, we can draw the following conclusion:

- the designed mechanisms is simple and robust, easy to achieve, it does not required skilled personnel and its costs are low;
- the quality of the cleaned surfaces is high;
- its operation is safe;
- the number of workers necessary for operation is reduced;
- the contact between the hydraulic agent and the heated metal does not bring about distortions;
- irrespective of the degree of frame loading with ash, two successive movements ensure a perfect frame cleaning.

The results obtained so far require the carrying on of our research, which involves the change of the jet speed and the use of water jets contains chemical additives.

5. REFERENCES

Ilias N., Magyary A., Radu S., Achim M., Magyari A .A., " Water Jet and Abrasive Water Jet Performances in Material Cutting.", *Proceedings of 5th Pacific Rim International Conference on Water Jet Technology*, New Delhi, India, 3-5.02.1998.

Radu S. "Contribution to the use of high pressure water jets for rock cutting." Ph.D. Thesis, University of Petrosani. Romania, 28.02.1998.

10th American Waterjet Conference
August 14-17, 1999: Houston, Texas

Paper 47

WATERJET USE DEALING WITH THE PROBLEM OF ANTI-PERSONNEL LANDMINES

D.A. Summers, O.R. Mitchell, S.J. Thompson, R. Denier, E. Bames
University of Missouri-Rolla
Rolla, Missouri, U.S.A.

ABSTRACT

The problems of locating and dealing with landmines have been an ongoing issue since before the time of the Second World War. While some mines can be effectively found using metal detecting equipment, the move toward the use of plastic, particularly for anti-personnel landmines (APL) has made their detection more difficult.

At the same time the high rate of false alarms that are generated, particularly in areas that have seen conflict, require an ability to examine the potential landmine so that its nature can be identified. Given that most such targets lie within 20 cm of the surface, this requires an ability to search to this depth and to then uncover the item for visual inspection. As a third corollary to this approach the ability to then neutralize the item remotely would significantly increase the speed of operations, and the safety of the operators.

A method is described in which high-pressure waterjets can be used to locate the presence of a plastic APL using the acoustic response to waterjet impact. The mine is then uncovered using a rotating high-pressure waterjet system, which includes a jet pump for soil removal. The mine is then cut into parts by an abrasive waterjet stream, using the same flow rate and pressure as for the first two parts of the process.

Refinements in the technology to improve performance, particularly in the detection phase of the operation are described.

1. INTRODUCTION

The problems of locating and dealing with landmines have been an ongoing issue since the First World War because it is reported they continue to kill, maim, or cripple one hundred people per day every day of the year. The people that reside in the countries of former or current conflicts that suffer the most are those that depend on agriculture for their livelihood. They have suffered loss of both livestock and human life, which has resulted in them not being able to work their land.

The search for mines has become increasingly more difficult with the advancement of technology and development of non-metallic materials. The use of wood, plastic and other non-metallic materials in both the case and firing mechanism components has made landmine detection increasingly difficult or impossible. Mines containing more than two grams of metal are easily detectable with state of the art metal detecting equipment depending on depth of burial, orientation and technique of using a particular detector. Compliance with the most recent international treaties pertaining to delectability requires that all mines currently in production must contain eight grams of metal.

Most anti-personnel (AP) landmines are deployed on top of the ground or buried at various depths up to 20 cm. The current standard operating procedure (SOP) for non-mechanical demining requires a person to be exposed to life threatening circumstances during the entire process of unearthing and visually examining the mine/target for identification. The most commonly practiced procedure after identification is to Blow In Place (BIP) which prevents the deminer from physically having to handle the mine however, they have to place the explosive charges on the mine. This procedure is extremely time-consuming and yet must be applied for each target because there is no way to differentiate a false positive from Unexploded Ordnance (UXO) until it is visually examined.

2. APPROACH

The problem of false positives is exacerbated in areas of previous conflict due to presence of metal fragments and unexploded sub-munitions, which requires the same systematic interrogation of each target to determine the appropriate next actions.

The demining system being developed by the University of Missouri - Rolla (UMR) team features High Pressure Waterjet (HPW) technology as a prime sub-system on a platform that is;

- Remotely controlled
- Operator friendly
- Capable of detecting landmines to depths of 20 cm. minimum
- Capable of exposing the mine for remote visual examination
- Capable of remote hazard mitigation if required

The original proof of concept platform was built and tested using a Pointman robotic vehicle, built by REMOTEC, Inc. for the US Army, and a commercial Toro Hydroject 4000 Aerator to deliver the high pressure water source (Fig. 1). The Toro unit develops

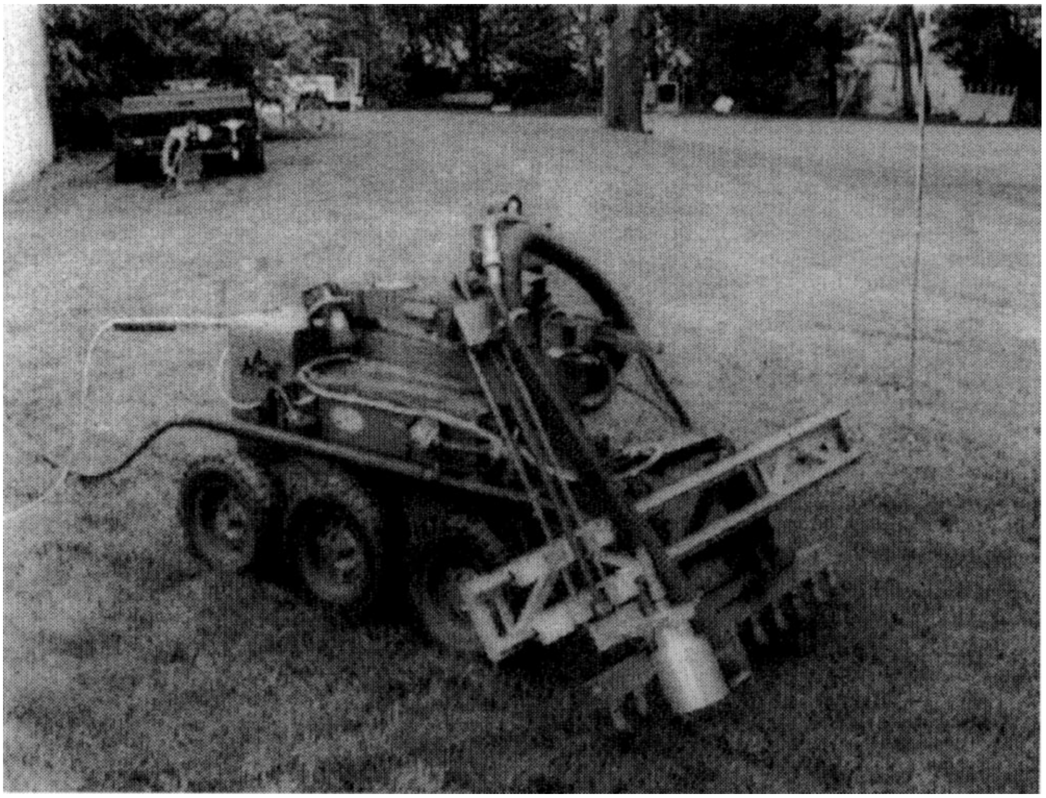

Figure 1. Original Proof of Concept Platform

5,000 psi pulsed water to eleven jets aimed downward to penetrate six inches (I 5 cm) into the ground. (Fig 2) The purpose of this penetration can be varied, and will be discussed later. The second-generation system replaces the Pointman with another REMOTEC supplied vehicle called Wolverine and is being modified to provide mounting for the HPW system. Both vehicles have on-board video cameras that allow the operator to not only see where he/she is going but also have real time visual observation and control during the soil removal and dissection of the mine. The Wolverine is in service with several law enforcement and anti-terrorist agencies and provides a much more robust, powerful and stable platform for the HPW system. Particular attention has been given to incorporating commercially available off the shelf hardware wherever possible to eliminate the additional cost and long lead time of specially fabricated items required for spares. Commercially available off the shelf hardware will provide an abundant inexpensive source for parts that may be damaged or destroyed during operation.

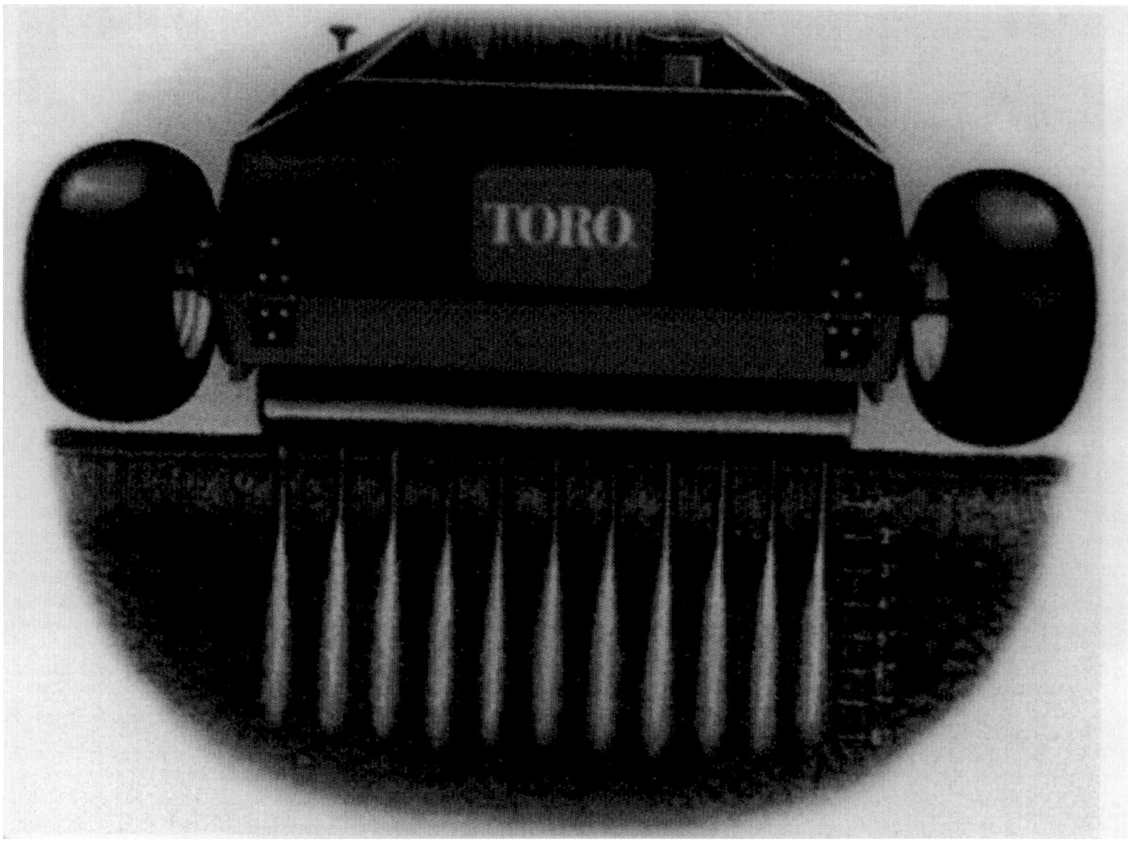

Figure 2. Toro 4000 Acroject Penetrating Soil

The primary modifications to these vehicles was to remove the waterjet manifold from the aft end of the TORO unit and mount it on the forward end of the Pointman/Wolverine and design/install the rotatin2 HPW system so that the search and remediation is always conducted forward of the vehicle. (Fig 3)

Figure 3. Pointman with Manifold and Soil Sucker

The integration of HPW with the other technologies on a single remote controlled platform will significantly reduce the time and increase the safety required for the demining operation. The system uses the acoustic response of the HPW impact to locate targets on top of the ground and buried up to 20 cm. deep including those fabricated from plastic, wood and other non-metallic materials. When a buried target is located it is exposed using a rotating HPW system which includes a jet pump for soil/water removal (Fig. 4). If the exposed target is an UXO device, it will then be destroyed by cutting it

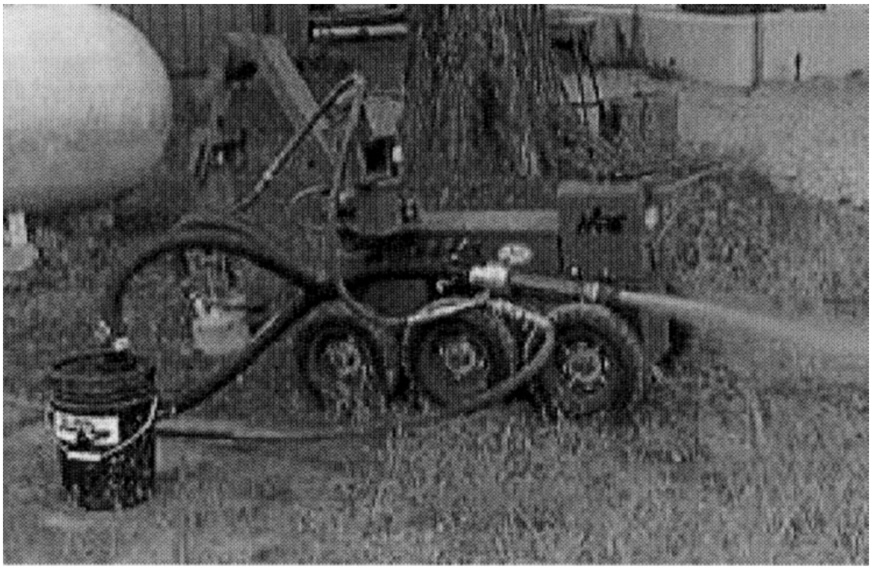

Figure 4. Exposing Potential Landmine

with an abrasive waterjet stream using the same flow rate and pressure as the first two parts of the process (see Fig. 5). UMR has successfully demonstrated the ability of the

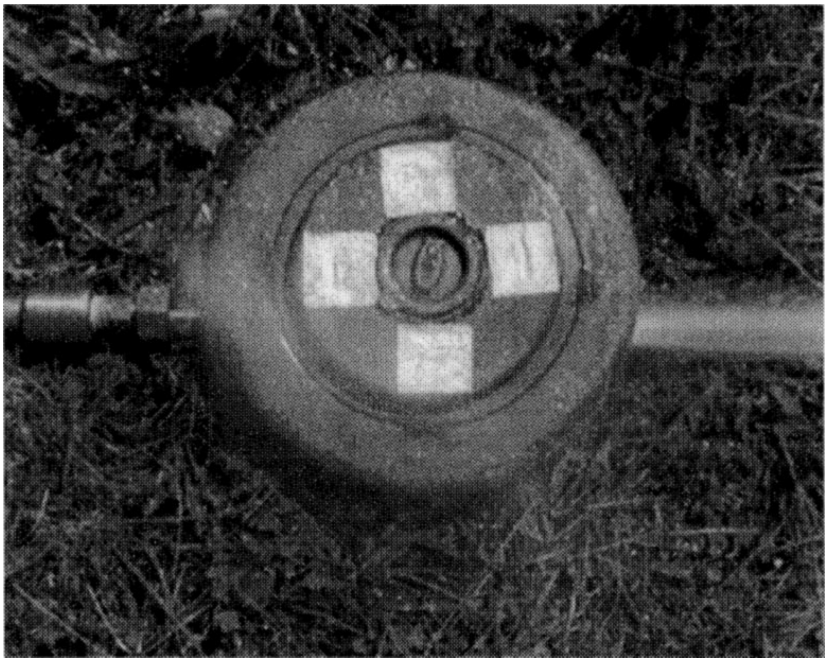

Figure 5. Abrasive Waterjet Bisecting Landmine

HPW system to not only uncover targets under long established root systems (Fig. 6) but

Figure 6. Hole Removing Soil and Roots

also cut through an armed mine fuse without causing initiation (see Fig 7 and 8). The HPW system is also being adapted to provide the ability to defeat thick underbrush such

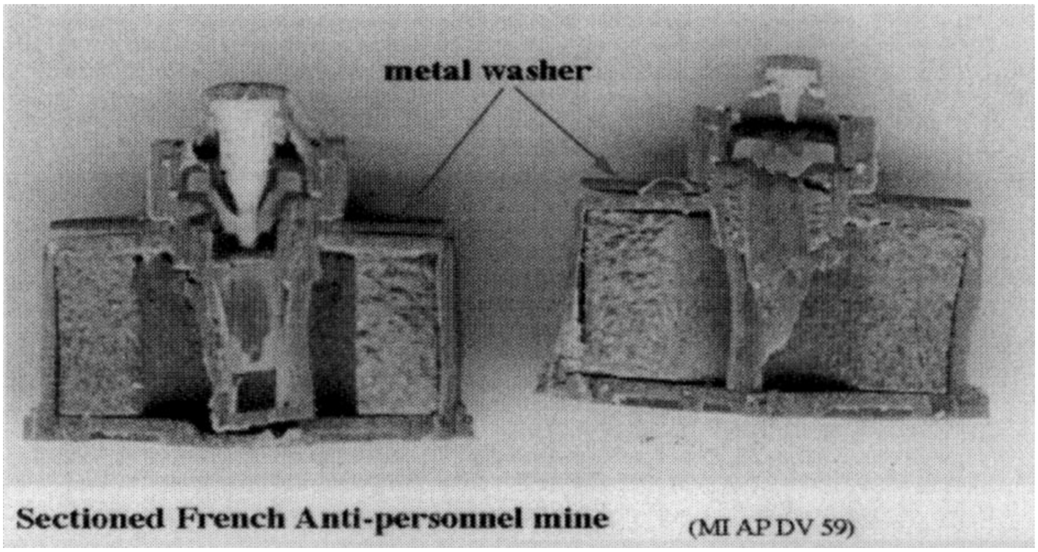

Figure 7. Landmine and Fuse Bisected with Waterjet

Figure 8. Bisected M606 Mine Fuse

as found in post conflict areas that have proven to be too dangerous to enter. The significance of these facts is there are no other demining systems in the field in or in development that possess all of these capabilities. Some systems currently in development report they can deal with underbrush and detect mines however, they do not provide for remote hazard mitigation.

A major portion of the landmines deployed throughout the world contains cast TNT as the base explosive charge, which is fragile and easily destroyed by impingement of the HPW after entry through the external case of the mine. The primary fuse systems can also be destroyed without causing an explosive event in most cases however, if an explosive event occurs it will be less hazardous because it will be a low order rather than high order event. A low order explosive event can range from a slow bum to propagation of the flame front through the energetic material at a rate less than thirty-three hundred meters per second (3300 m/s). High order detonation is defined as propagation of the flame front through an energetic material at a rate of thirty-three hundred meters per second (3300 m/s) or greater.

The following technologies are currently being investigated and considered for integration into the system to improve performance in the detection phase of the operation.

* **Doppler Radar**
Doppler radar has been successfully utilized in lab tests by aiming it at the point of entry of the HPW into the ground and measuring the movement of the soil when the water strikes a buried object.

* **Thermal Imaging**
Thermal imaging using elevated water temperature in the HPW system enhances detection because the water is dispersed over the buried object thereby causing a prominent thermal image as opposed to the instances when the water is simply injected into the ground. In Figure 9, upper left hand picture, it is obvious that the

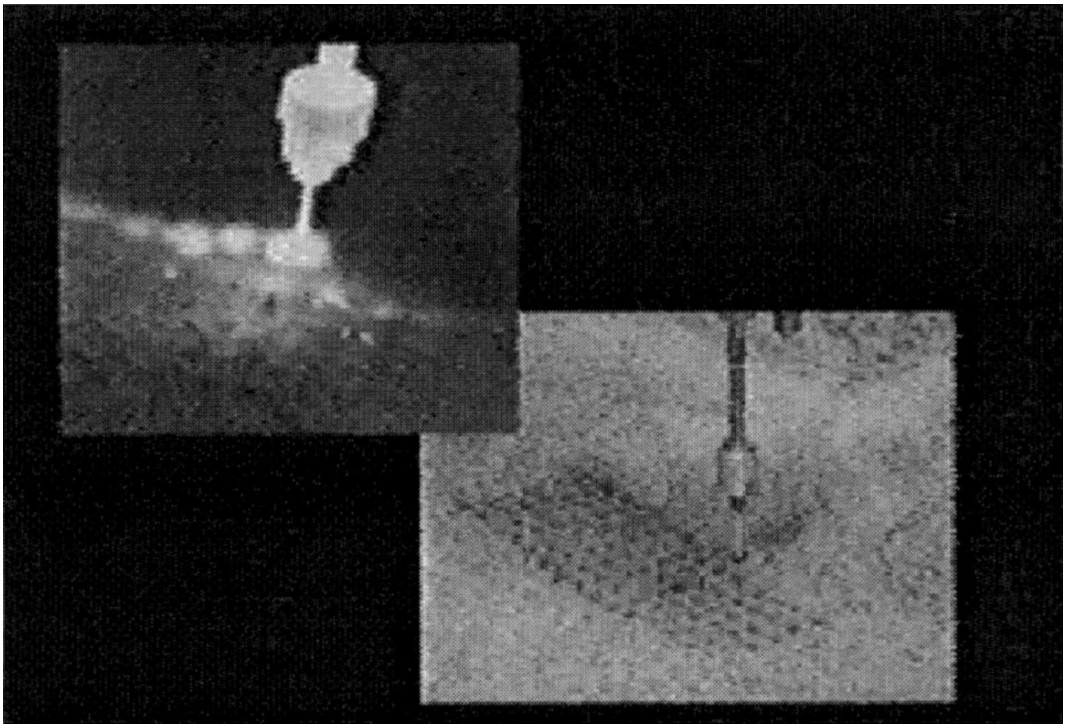

Figure 9. Thermal Image of Elevated Temperature Waterjet

first three hits of the HPW simply enter the ground while last two are impinging on an object beneath the surface causing the thermal image at that point to be larger than all of the others. The lower, right picture is the same event without thermal imaging and it can be seen that the sand immediately under the nozzle is reacting to the water hitting a buried object.

* **Audio**

Audio changes caused by the HPW impinging on buried objects has been successfully demonstrated in the laboratory by positioning microphones near the waterjet nozzle during the search operation. (Fig. 10) The acoustic reflection of different materials has enough discretion that sophisticated analysis systems can point out the difference between a buried rock, pipe, or landmine. This technique requires advanced signal processing and is influenced by noises commonly encountered in the field. Additional testing is planned to define microphone configurations and positioning to overcome system susceptibility to background noise.

* **Olfactory**

An olfactory system used in conjunction with the HPW to detect presence of nitrogen concentrations has been successfully demonstrated. This combination allows the olfactory system to "sniff" immediately after the HPW has punched a hole in the ground to provide a path for latent Nitrogen, associated with UXO'S, to be detected. Lab testing has been successful for isolated concentrations of latent nitrogen. The system must now

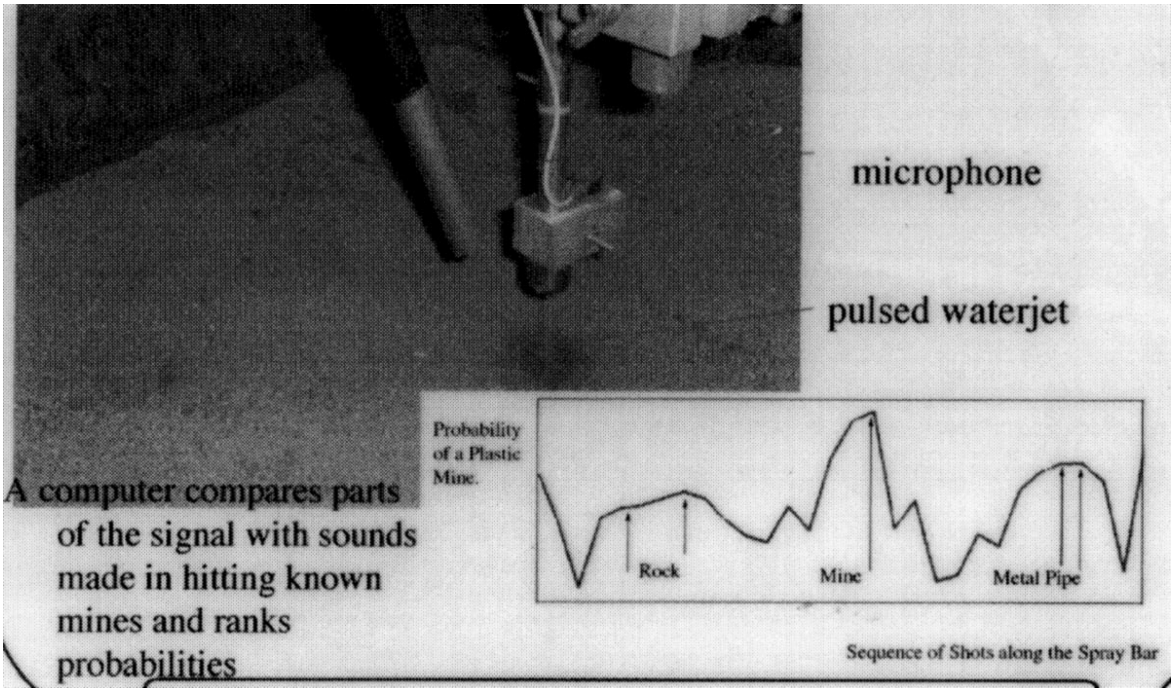

Figure 10. Auditory Mine Detection

be tested in areas that simulate post conflict conditions where residue from exploding devices covers the area where landmines/IJXOs are buried.

* **Ground Penetrating Radar**
Ground penetrating radar will serve as the detection system for locating buried targets and the HPW will provide the ability to uncover and mitigate the hazard. Preliminary GPR testing utilizing techniques developed by UMR have proven successful and will be the focal point of additional testing planned for the near future.

3. CONCLUSION

The use of high-pressure water systems for demining is operational in Angola and although it is a very basic application the users are happy with the system because it eliminates the necessity of an individual to be in harms way prodding for mines. The technique employed there simply washes the mines out of the ground, which then must be manually dealt with for disposal.

We believe the use of HPW in conjunction with one or more complimentary sub-systems is both feasible and practical in most areas around the world. The system defined herein provides a safer environment, from detection to hazard mitigation, and keeps personnel out of harms way.

We believe there is a very solid foundation to base future studies and testing upon and as with all research and development programs we anticipate experience will help perfect our techniques and enhance our design.

10^{th} **American Waterjet Conference**
August 14-17, 1999: Houston, Texas

Paper **48**

DEMILITARIZATION OF CHEMICAL WEAPONS

USING HIGH PRESSURE AMMONIA FLUID JETS

Paul L. Miller
Teledyne Brown Engineering
Huntsville, Alabama

Mohamed Hashish
Flow International Corporation
Kent, Washington

ABSTRACT

Teledyne-Commodore has researched the use of high pressure 320 MPa (45,000 psi) liquid anhydrous ammonia as an alternative fluid for both abrasive fluid jet cutting of live chemical warfare munitions and fluid jet washout of chemical agents, explosives, and propellants. The use of anhydrous ammonia has numerous advantages over conventional water for chemical weapon demilitarization applications as was demonstrated in live testing at the U.S. Army's Redstone Arsenal during 1998.

Organized and Sponsored by the WaterJet Technology Association

1. INTRODUCTION

As part of the chemical weapons reduction treaties signed by the United States, large stockpiles of chemical weapons are slated for disposal. Historical methods of chemical weapons disposal, such as ocean dumping, open burning, or open detonation (OB/OD), are no longer acceptable practices. Chemical neutralization by either chlorination or hydrolysis was developed to allow for the destruction of toxic chemical agents. These processes provided reasonable destruction efficiencies, but created larger quantities of toxic waste that had the potential for recombination back to the original toxins. The government switched to chemical weapon incineration in an effort to overcome the problems associated with caustic hydrolysis.

Incineration, however, is not considered an environmentally friendly destruction process by many environmental groups. Local citizens' concern for the proximity of these thermal processors to population centers energized many citizen action committees to vociferously challenge any construction of chemical weapon incinerators. Currently, chemical weapon incineration has been banned by four states where chemical weapons are being stored.

Another major problem with current technologies for the destruction of chemical weapons is the process of mechanical disassembly in order to access the explosive materials and the chemical agents. This reverse assembly process is complex and complicated by system deterioration and items that were sealed during assembly. Corrosion of the chemical weapons further complicates the destruction technologies, as many of the explosive components are saturated with chemical agent and may not be readily treated with a standard neutralization process.

In an effort to destroy the chemical weapons in an environmentally safe manner that would be acceptable to local communities, the U.S. Army Chemical and Biological Defense Command (CBDCOM) has pursued the development of alternative, non-thermal technologies. Teledyne-Commodore has developed and integrated both a non-thermal destruction technology and high pressure ammonia fluid jets to safely access these dangerous munitions and destroy their contents in an environmentally safe manner.

2. FLUID JET OPERATIONS WITH A SUPERHEATED LIQUID

The use of anhydrous ammonia was chosen as the most appropriate fluid for the demilitarization of the chemical weapons because of the ease with which fluid can be integrated into the subsequent chemical process. The chemical process for the actual destruction of the chemical agents uses alkali metals dissolved in anhydrous ammonia to form the aggressive Solvated Electron Technology (SET™) solution. Chemical agents and explosives treated by the SET solution are completely destroyed within seconds. Melvin (1994) has also advocated the use of anhydrous ammonia on high explosives, and his extensive research has shown the safety of using this liquid in such an application.

Melvin developed an ammonia washout process for the removal of rocket propellants through a combination of kinetic energy breakup of the propellant surface and utilization of the aggressive solvent nature of the ammonia. Testing of Melvin's operation began in 1993 at Hercules Aerospace, which later became Alliant Techsystems' Global Environmental Solutions (GES). Several tests were run on Melvin's washout system at pressures up to 241 MPa (35 ksi) for very short durations. This system was later removed from GES and transferred to Redstone Arsenal Test Area 10 for final integration and testing. As part of their independent research, Teledyne-Commodore installed and tested their ammonia fluid jet system with Melvin's assistance in the building adjacent to Melvin's at Redstone Arsenal.

The application of superheated liquid or liquefied gases in high pressure fluid jets is not a new topic of research. Lienhard and Day (1970) as well as Dunsky and Hashish (1995) have explored the use of high pressure, superheated liquid or liquefied gases for specific applications. The use of high pressure, cryogenically liquefied nitrogen gas was developed and tested for the removal of military propellants at Tyndall Air Force Base, according to Savanick (1994).

Although much of the published fluid jet work is focused on cryogenically liquefied gases, the properties of superheated liquids for the space and missile programs have also been well studied. For example, Lienhard and Day (1970) modeled the breakup of the superheated liquid jet stream into an incoherent spray from either flashing of the liquid or aerodynamic instability in the late 1960s. Other work by Huzel and Huang (1971) focused on both pumping of such liquids and jet formation during discharge. These aerospace pumps developed for large rocket motors produced almost 14 MPa at 900 $kg \cdot sec^{-1}$. Teledyne-Commodore Brown combined several established concepts to develop the ammonia fluid jet's system based on the existing body of work and the simplicity of system integration with the remainder of the chemical process.

2.1 Material Properties

Ammonia as a Process Fluid - Anhydrous ammonia is a pungent, colorless gas at room temperature. Although the aqueous solution of ammonia has been known since antiquity, ammonia has only been produced commercially in the anhydrous form for slightly over a 125 years, according to Motz (1929). Ammonia is one of the largest volume commodity chemicals produced in the world today, with some 90 million metric tons produced and consumed each year according to Lauriente (1995). The principal uses for ammonia are in the production of or use as a fertilizer and as a refrigerant gas. Fertilizer anhydrous ammonia is directly injected into the ground and supplies the necessary nitrogen macronutrient. Ammonia is known to ASHRAE (1994) as Refrigerant 717 and has received renewed attention in recent years in the heating, ventilation, and air conditioning (HVAC) field due to the scheduled phaseout and increasing cost of ozone-depleting chlorofluorcarbons (CFC) and halocarbons (HCFC).

The use of ammonia as a solvent for chemical processes is also extensively known in the chemical engineering field. Some typical properties of anhydrous ammonia as a process fluid are:

Vapor Pressure – Ammonia exists as a liquid along the vapor-pressure curve from the triple-point temperature, T_t = 195.48 K, to the critical temperature, T_{crit} = 405.41 K. At ambient temperature, ammonia is liquefied at 0.78 MPa. Thus, to form an ammonia liquid jet at room temperature, the ambient pressure must be maintained above 0.78 MPa to maintain the superheated liquid. If the ammonia jet temperature is maintained at lower than 239.8 K, then a cryogenic liquid ammonia jet can be formed without the need for increasing the back-pressure above the atmospheric level. Table 1 shows the required jet temperatures at different back-pressures to obtain a liquid ammonia jet, along with other properties.

Ammonia is a gas at room temperature with a vapor pressure that can be approximated by equation 1, adapted from Dean (1985).

$$\log p = 9.485 - 926.132/(t - 32.93) \quad (1)$$

where p = pressure in pascals
t = degrees kelvin.

The ability for the ammonia to flash to vapor is used extensively by Teledyne-Commodore as a method of recovering the ammonia after the secondary chemical processing of the dissolved materials. This flash to vapor characteristic also allows for minimizing the process exothermic reactions since substantial heat is absorbed (5.581 kcal·mol^{-1}) in the vaporization of the liquid.

Table 1. Ammonia-saturated liquid data - NIST (1998)

Temp. (K)	Pressure (MPa)	Density (kg/m^3)	Volume (m^3/kg)	Internal Energy (kJ/kg)	Enthalpy (kJ/kg)	Entropy (J/g·K)	C_v (J/g·K)	C_p (J/g·K)	Sound Spd. (m/s)
239.56	0.10000	682.29	0.0014656	47.45	47.599	0.40684	2.8553	4.4465	1770.0
254.30	0.20000	663.65	0.0015068	113.46	113.76	0.67424	2.8306	4.5195	1665.0
263.93	0.30000	651.03	0.0015360	157.10	157.56	0.84269	2.8149	4.5675	1596.6
271.27	0.40000	641.14	0.0015597	190.68	191.31	0.96824	2.8032	4.6062	1544.0
277.29	0.50000	632.86	0.0015801	218.41	219.20	1.0694	2.7939	4.6401	1500.7
282.43	0.60000	625.65	0.0015983	242.26	243.21	1.1546	2.7862	4.6712	1463.3
286.95	0.70000	619.21	0.0016150	263.31	264.44	1.2286	2.7797	4.7006	1430.3
291.00	0.80000	613.35	0.0016304	282.26	283.56	1.2942	2.7740	4.7289	1400.4
294.67	0.90000	607.95	0.0016449	299.55	301.03	1.3533	2.7691	4.7564	1373.1
298.05	1.00000	602.92	0.0016586	315.50	317.16	1.4072	2.7648	4.7835	1347.9

Viscosity – The viscosity of anhydrous ammonia is approximately one-quarter that of water at room temperature. Published data from Pinevich (1948) gives the viscosity at 303 kelvin as 1.38·10^{-4} pa·sec^{-1} as compared to water at 7.973·10^{-4} pa·sec^{-1}. The lower viscosity of the ammonia liquid allows for substantially lower pressure drop in the fluid jet system. The surface tension of ammonia as reported by Stairs and Sienko (1956) is also only 1.805·10^{-2} N·m^{-1}, about one-quarter that of water at $7.066 \cdot 10^{-2}$ $N \cdot m^{-1}$. Ammonia fluid jets provide enhanced cutting ability over waterjets since a lower surface tension has a pronounced effect on the efficiency with which abrasive particles enter and are entrained into the fluid jet stream.

Density – The density of anhydrous ammonia liquid is reported by Cragoe and Harper (1921) as only 595.2 $kg \cdot m^{-3}$, as compared to water at 995.7 $kg \cdot m^{-3}$ at 303 kelvin. The lower density of ammonia is an important factor in the increased cutting efficiency identified during the testing of the abrasive ammonia fluid jet cutting tests. The approximate velocity of a fluid jet is given by Hashish (1989) in equation 2 as:

$$V = (2 \cdot p \cdot \rho^{-1})^{0.5} \tag{2}$$

where V = velocity in $m \cdot sec^{-1}$
p = pressure in pascals
ρ = density in $kg \cdot m^{-3}$.

Consequently, the 29% increase in fluid jet velocity is translated almost directly into improved cutting speed.

Solvent Action - Ammonia is the most important non-aqueous protonic solvent in the chemical field. As described in Jolly and Hallada (1965) anhydrous ammonia is an excellent solvent for non-electrolytes that are insoluble in polar media, as well as being a significant solvent for items soluble in water. Most hydrocarbons, for instance, are soluble in ammonia. Although the dielectric constant of ammonia is only about 30% that of water, most ionic salts are soluble in ammonia as well as water. Notable exceptions are sulfates, carbonates, and phosphates with high lattice energies. Like water, ammonia readily forms hydrogen bonds that allow materials that likewise form hydrogen bonds to be soluble in ammonia. These materials include sugars, esters, amines, and phenols which are all very soluble in ammonia.

Ammonia also forms solutions with many metals. Most of these reactions are reversible, although some form irreversible amalgams. All metals that dissolve in ammonia eventually form a metal amide with the release of hydrogen gas. Classic dissolved metals are the solvated electron chemistries of alkali metals in ammonia first studied by Weyl (1864), as well as the alkaline earth metals. The downstream process operation Teledyne-Commodore uses for the efficient destruction of hazardous chemicals is the ammonia-alkali metal reaction with the dissolved agent.

Ammonia is ideal as a solvent for the demilitarization of chemical weapons as it dissolves and desensitizes the common military explosives, according to Hendrickson et al (1993). Ammonia has also been shown in testing by Teledyne-Commodore at U.S. Army surety laboratories to dissolve the major chemical warfare agents used by the various nations since the First World War. The agents that ammonia was tested on include:

- GA (Soman)
- GB (Sarin)
- GD (Tabun)
- GF
- HD (Distilled Mustard)
- HT (Mustard)
- L (Lewisite)
- VX.

In a similar manner, high explosive materials are quite soluble in anhydrous ammonia. According to Melvin (1994) the common military explosives are all soluble with ammonia and reasonably stable. The exceptions are glycerol trinitrate (NG) and 2-methyl 1,3,5 trinitrobenzene (TNT) which decompose through ammonolysis.

Other energetic materials cited by Melvin (1994) that dissolve quite readily and are stable in ammonia are hexahydro- 1,3,5-trinitro-, 1,3,5-triazine (RDX), octohydro- 1,3,5,7-tetranitro-, 1,3,5,7-tetrazocine (HMX), ammonium picrate (Exp D), 1,3,5-trinitrophenol (PA), and ammonium perchlorate (AP).

Melvin (1994) also showed that the dissolved energetic materials could be recovered from the ammonia solution and reutilized for resource recovery and recycling.

2.2 Equipment Integration

Teledyne-Commodore contracted with Flow International to integrate ammonia into a fluid jet system utilizing refrigeration grade anhydrous ammonia fluid. The anhydrous ammonia was pumped in standard waterjet equipment that had minor modifications to the seals and to some internal parts for higher reliability. The initial tests using a pair of 18.75 kWe *Cougar* pumps were less than satisfactory and a larger 150 kWe *25XQ-A* quad intensifier was substituted with excellent results.

All testing was performed within a certified pressure vessel rated to 1.7 MPa and certified to ASME pressure vessel standards. The fluid jet penetrations were all o-ring or graphite packing sealed to prevent the release of ammonia vapor to the work area. The pressure vessel was also fitted with temperature, pressure, and process location instrumentation, which allowed the entire operation to be performed from a remote control room located approximately 200 meters away. The use of ammonia did not require any special precautions and many inert operations were attended by research personnel in close proximity to the equipment during test runs. During live explosive operations, all personnel were sequestered in the control room as required by military safety regulations.

Multiple high explosive filled training rockets were sectioned using the ammonia fluid jet as an abrasive fluid jet cutter operating at pressures to 320 MPa with 180 micron (80 mesh) abrasive. No abrasives were used for the washout of explosives and propellants as the combination of the erosive action of the high velocity ammonia liquid and the high solvent action was sufficient.

After the target materials were washed out and dissolved using the high pressure ammonia fluid jet, the solution was pumped to a secondary process chamber and the hazardous materials destroyed. At the conclusion of the process, the ammonia was recovered and recycled by evaporating the gas to a commercial refrigeration compressor and recompressing the gas to a liquid. The ammonia stream was then reusable and returned to the intensifier for further work.

3. CONCLUSION

The ammonia fluid jet process is a proven system based on conventional waterjet technology with only minor modifications. The ammonia system has some unique capabilities of being able to dissolve various materials that are insoluble with water or form emulsions. The use of ammonia in the fluid jet cutting process also allows for substantially higher process rates and provides a rapid method of removing the process liquid through evaporation and recovery.

4. REFERENCES

ASHRAE Handbook, "System Practices for Ammonia Refrigeration", *Refrigeration*, American Society of Heating, Refrigerating and Air Conditioning Engineers, 1994.

Cragoe, C., and Harper, D. *Bur. Stds. Sc.Pp.*, Vol. 420, page 313, 1921, *as cited in* Jolly, W. L., and Hallada, C. J., "Liquid Ammonia," *Non-Aqueous Solvent Systems*, Waddington, T. C., ed., Academic Press, pages 1 – 45, 1965.

Dean, J. A., ed., *Lange's Handbook of Chemistry*, 13th ed., pages 10-29, 1985.

Dunsky C. M. and Hashish, M., "Feasibility Study of the Use of Ultrahigh-Pressure Liquefied Gas Jets for Machining of Nuclear Fuel Pins," Paper 35, *8th American Water Jet Conference*, August 1995.

Hashish, M., "Pressure Effects in Abrasive-Waterjet Machining," *Trans. ASME J. Eng. Mat'l and Technology*. Vol. III, page 221, July 1989.

Hendrickson, K. A., Losee, L. A., Stevens, P. M., and Mitchell, D. H.; "Materials Hazards Testing in Support of the Army Large Rocket Motor Demilitarization Pilot Plant Materials," Hercules Aerospace Company, Magna, UT, *Joint 1993 JANAF Propulsion Meeting and 30th JANAF Combustion Subcommittee Meeting*, Monterey, CA, November 15-18, 1993. [*Unclassified – Approved for Public Release; Unlimited Distribution.*]

Huzel, D. K. and Huang, D. H., *Design of Liquid Propellant Rocket Engines, 2nd ed.*, National Aeronautics and Space Administration, NASA SP-125, 1971.

Jolly, W. L., and Hallada, C. J., “Liquid Ammonia,” *Non-Aqueous Solvent Systems*, Waddington, T. C., ed., Academic Press, pages 1 – 45, 1965.

Lauriente, D. H., *Chemical Economics Handbook*, as cited in http.//www-cmrc.sri.com/CIN, 1995.

Lienhard, J. H. and Day, J. B., “The Breakup of Superheated Liquid Jets” *Trans ASME Journal of Basic Engineering*, pages 515-522, September 1970.

Melvin, W. S., Method to Extract and Recover Nitramine Oxidizers from Solid Propellants Using Liquid Ammonia, U.S. Patent #5,285,995, February 8, 1994.

Motz, W. H., *Principles of Refrigeration*, Nickerson and Collins, 1929.

National Institute of Standards and Technology (NIST), “Saturation Properties for Ammonia–Pressure Increments,” from NIST Standard Reference Database, *NIST Chemistry WebBook*, http://webbook.nist.gov/cgi, 1998.

Pinevich, G., *Kholod. Tekh.* Vol. 20, No. 3, page 30, 1948, *as cited in* Jolly, W. L., and Hallada, C. J., “Liquid Ammonia,” *Non-Aqueous Solvent Systems*, Waddington, T. C., ed., Academic Press, pages 1 – 45, 1965.

Stairs, R. A., and Sienko, M. J., *J. Amer. Chem. Soc.*, Vol. 78, page 920, 1956, *as cited in* Jolly, W. L., and Hallada, C. J., “Liquid Ammonia,” *Non-Aqueous Solvent Systems*, Waddington, T. C., ed., Academic Press, pages 1 – 45, 1965.

Weyl, W., *Annln Phys*, Vol. 121, page 601, 1864, *as cited in* Jolly, W. L., and Hallada, C. J., “Liquid Ammonia,” *Non-Aqueous Solvent Systems*, Waddington, T. C., ed., Academic Press, pages 1 – 45, 1965.

10th American Waterjet Conference
August 14-17, 1999: Houston, Texas

Paper 49

HIGH VOLUME-LOW PRESSURE NUCLEAR WASTE REMOVAL — THE SLUICING CONCEPT

R. Fossey, D.A. Summers and G. Galecki
High Pressure Waterjet Laboratory
University of Missouri-Rolla
Rolla, Missouri

ABSTRACT

Many concepts are under review for the cleaning of underground nuclear waste storage tanks. These tanks, which threaten populations throughout the U.S. and the world, are filled with varying materials that have radically different characteristics. Many of these tanks have been cleaned using the confined sluicing end effector developed jointly by PNNL, UMR, and Waterjet Technology Inc. While this proved to be effective, it was viewed as somewhat slower than might be possible with a more "brute force" attack. Toward this end, PNNL and UMR have run trials on high flow, low-pressure jets for removing this material. The paper will address some of the issues and problems discovered and comparative results of both submerged and non-submerged sluicing.

Organized and Sponsored by the WaterJet Technology Association

1. INTRODUCTION

Many concepts are under review for the cleaning of underground nuclear waste storage tanks. These tanks, which threaten populations throughout the U.S. and the world, are filled with varying materials that have radically different characteristics. Many of these tanks have been cleaned using the confined sluicing end effector developed jointly by PNNL, UMR, and Waterjet Technology Inc. While this proved to be effective, it was viewed as somewhat slower than might be possible with a more "brute force" attack. Toward this end, PNNL and UMR have run trials on high flow, low-pressure jets for removing this material.

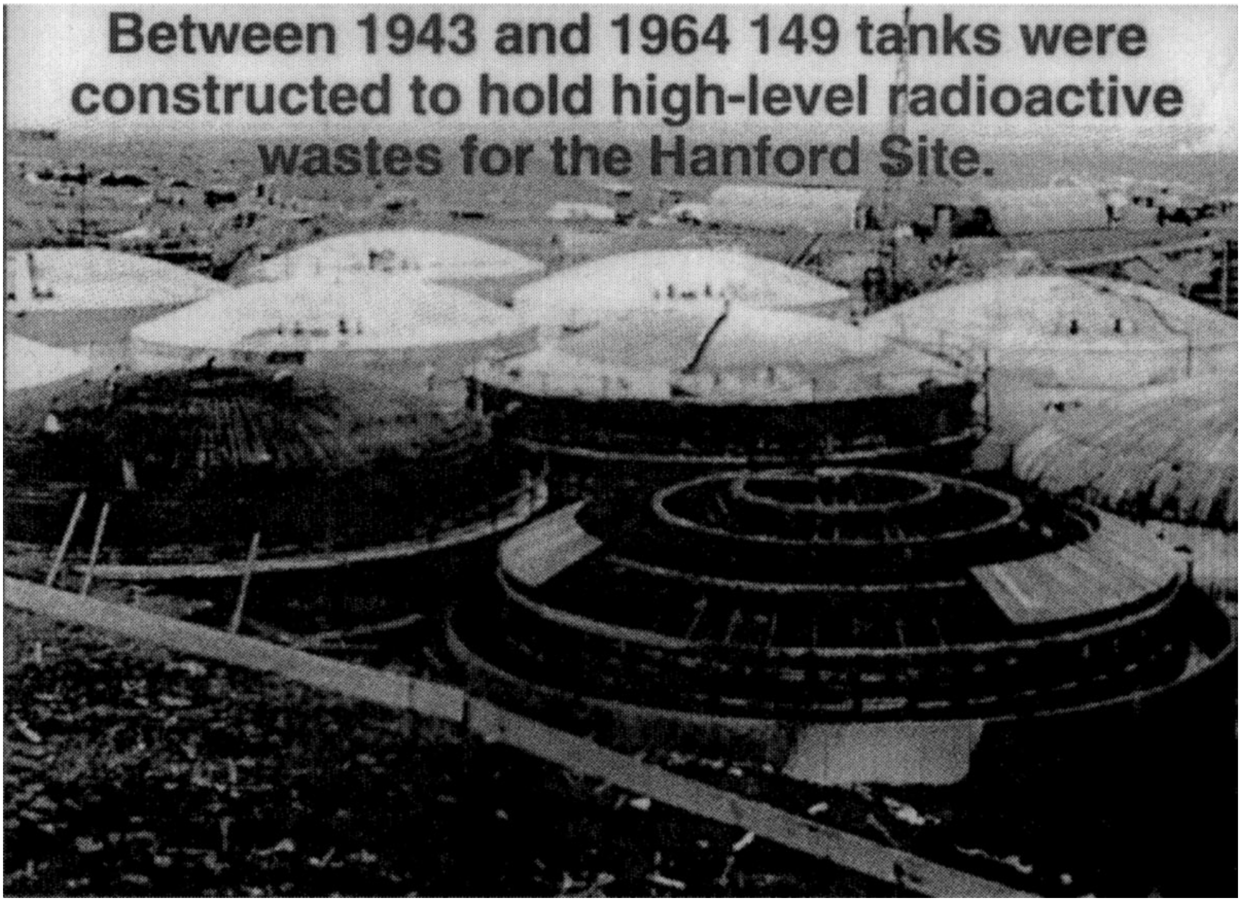

Figure 1. Construction of Concrete and Stainless Steel Nuclear Waste Storage Tanks

Waste tanks at several nuclear research, development, and production locations around the United States contain extremely hazardous materials, both toxic and radioactive. These tanks, which are fabricated of concrete and stainless steel, have aged and are showing signs of potential leakage. The contents that have been in the tanks in isolation have the potential to do irreparable harm to the environment if they are released, and a method of removal was needed that would be effective against the tank contents but non- damaging to the tank walls. A number of excavation techniques were proposed for this task, among them waterjet mining and high pressure scarifying, but all showed some drawbacks.

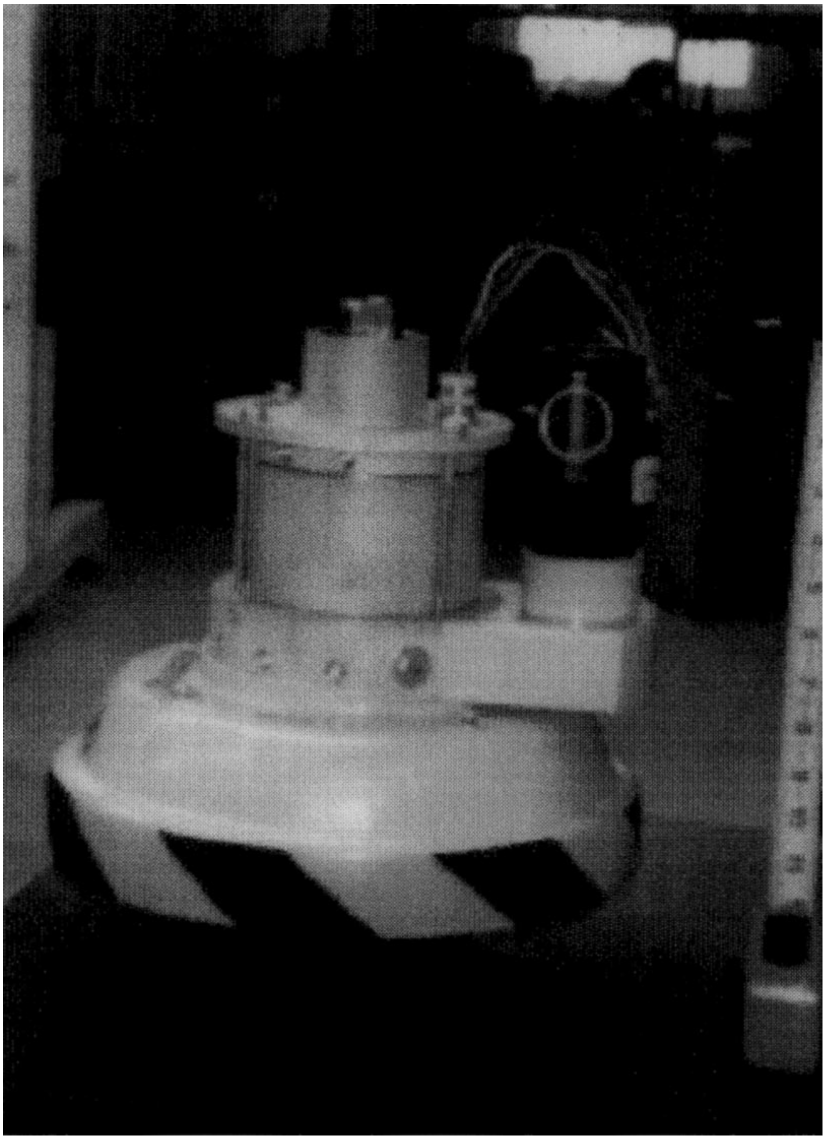

Figure 2. Waterjet Nuclear Waste Mining Tool,
The CSEE (Confined Sluicing End Effector)

2.BACKGROUND

During the early days of nuclear energy through the cold war years, the U.S. Department of Energy mandated the storage of nuclear waste in underground storage tanks that were considered to be a safe method of dealing with the problem. Large tank farms, some

Figure 3. One Section of a Tank Farm.

containing hundreds of tanks with volumes of 1,000,000 gallons each, were sited close to the nuclear production facilities in Hanford, Washington, and Oak Ridge, Tennessee among others. For the ensuing years, this method of dealing with nuclear waste was deemed acceptable and it was continued. Continued monitoring of these storage areas began disclosing alarming signs of leakage and the potential of drastic environmental degradation, and these areas were added to the EPA's list of super fund sites for immediate cleanup. A tri-party agreement was worked out between the Department of Energy, the Environmental Protection Agency, and the state of

Washington to remediate the Hanford site and the Pacific Northwest National Laboratory (PNNL) was tasked to determine methods that could be used to facilitate cleanup.

Tank contents are anything but homogeneous, with much of the materials within being unknown due to lack of records. Early measurements of volume in the tanks were made by the technicians

Figure 4. Photograph of Waste Tank Contents

dropping rocks from above and timing the fall time to impact. Later measurements were made by lowering a tape measure into the tank and recording distance to the content level. The tapes were then dropped into the tanks to be stored with whatever other contents were present. Visual documentation of tank contents was impossible for years due to the lethal level of radioactivity, which also fogged camera tenses and disrupted electronics. Hardened cameras were developed that could record the visible portions of the tank interiors and contents, and these records confirmed the mixture of ingredients present.

The tanks that are targeted for cleanup are up to 65 feet in diameter and have minimal access, creating the need to excavate material up to 65 feet away through an opening about two feet in diameter. Obviously, logistics and physical constraints are an important consideration in any attempt at site remediation, as is the high level of radioactivity present.

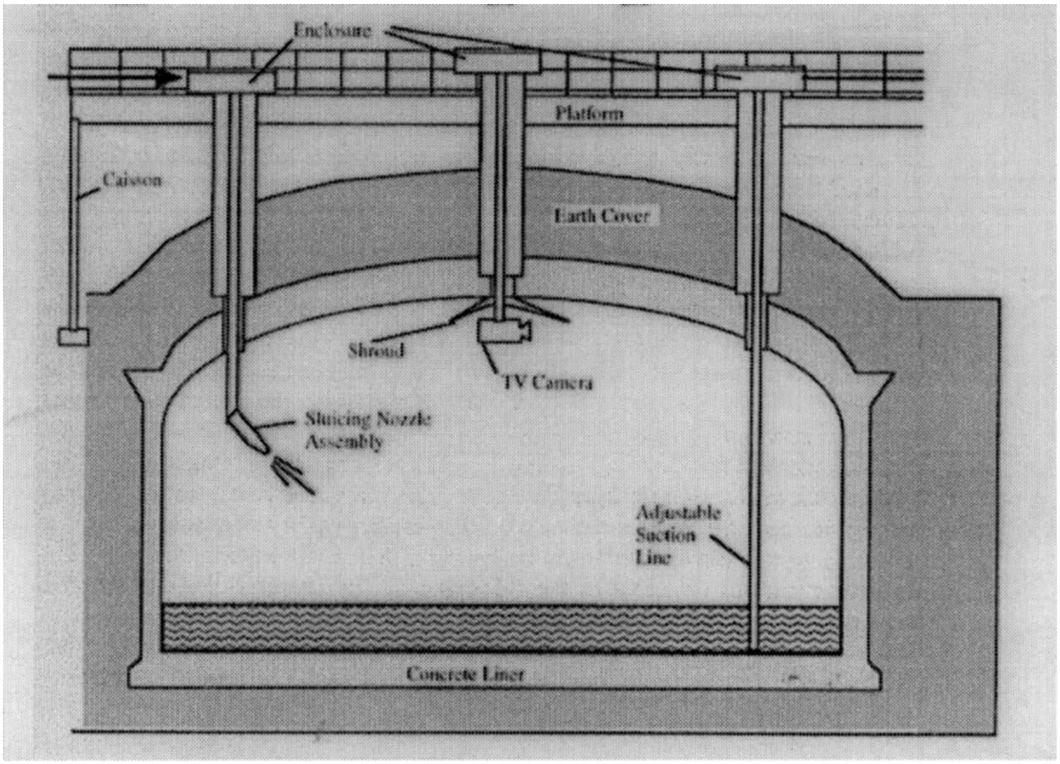

Figure 5. Representation of Underground Storage Tank Showing Limited Access

During the California gold rush of the 1850s, hydromining with monitors successfully moved large quantities of material to expose gold bearing ore. This practice continued to

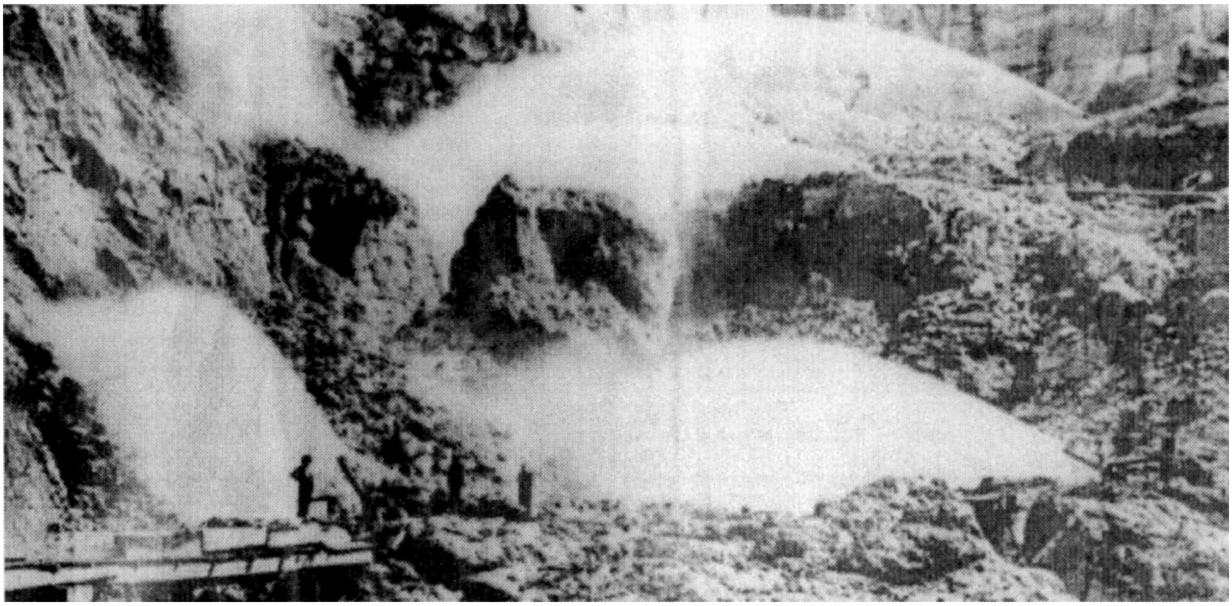

Figure 6. Hydraulic Mining in California ca 1852

be fairly widespread until the late 1800s and is still in use in some select applications. The concept was to be investigated for use in the previously mentioned tanks as a rapid method of mobilizing the contained waste for removal. Earlier tests in the UMR facility

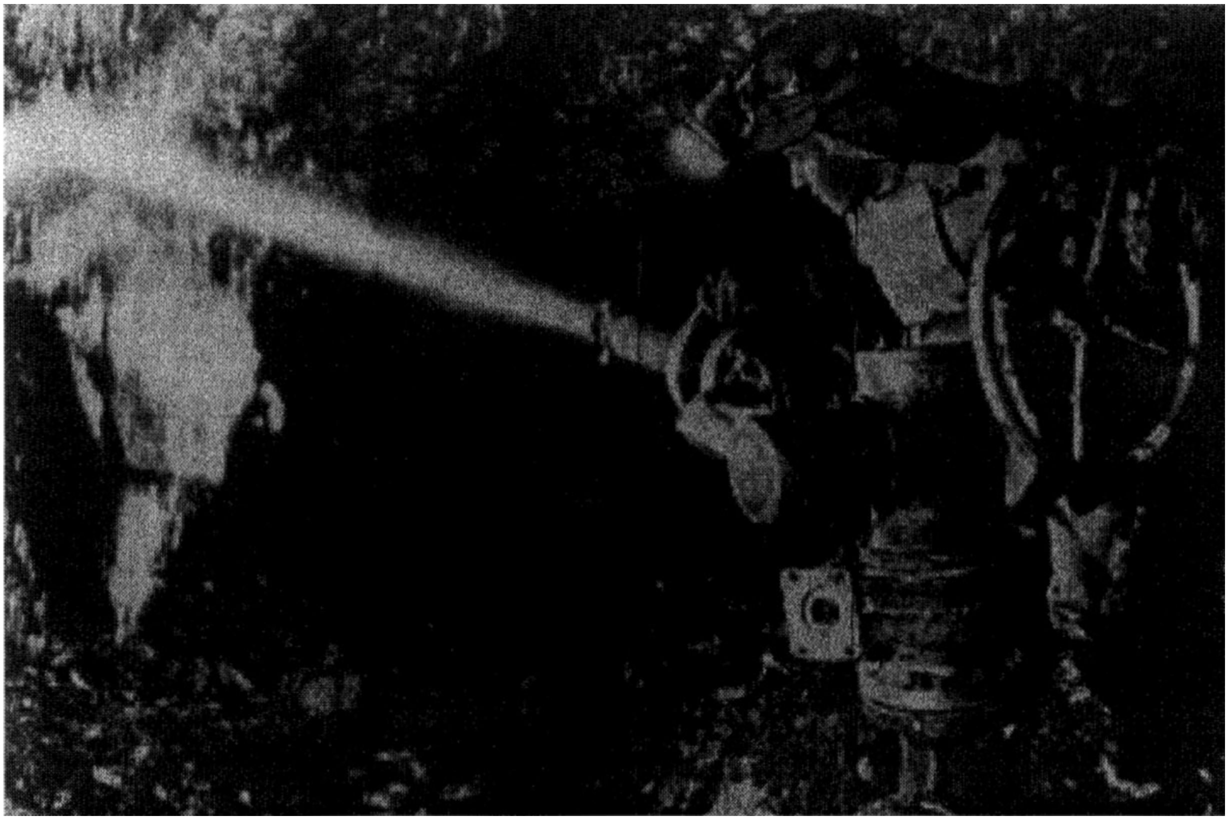

Figure 7. Russian Miner Hydromining Coal

were extremely disappointing due to the loss of cohesion of the jet over the 65-foot throw distance. In those tests a considerably less efficient nozzle was used.

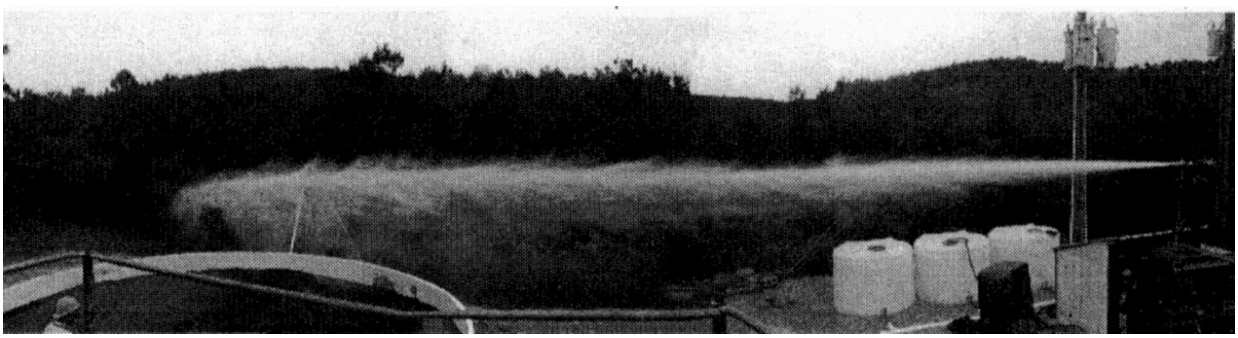

Figure 8. Original Nozzle Test

3. APPROACH

As mentioned previously, the concept of sluicing was used extensively in early gold mining and was very successful in moving large volumes of material. The approach to be used in this test series was to build a better nozzle and to carefully control the traverse speed, pressure, and flow of a similar jet and determine how efficiently it could move material in comparison with trials on other methods. The jet was to be aimed at a point some four feet from the far edge of the tank and oscillated between an intersect point with the left wall and the intersect point on the right wall until all the material falling within the conical section was removed. The jet would then be lowered until the jet arc was eight feet from the far

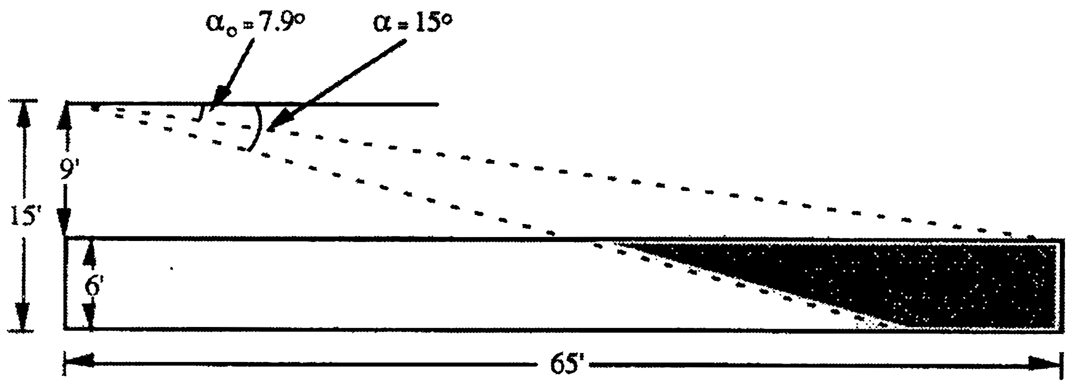

Figure 9. Material Removal Concept

wall and the oscillation distance increased from left wall to right wall until the material within that cone was removed. The nozzle was then to be lowered to twelve feet, then sixteen with the oscillation distance likewise increased to reach from wall to wall. Periodic measurements of material removal rates were to be taken.

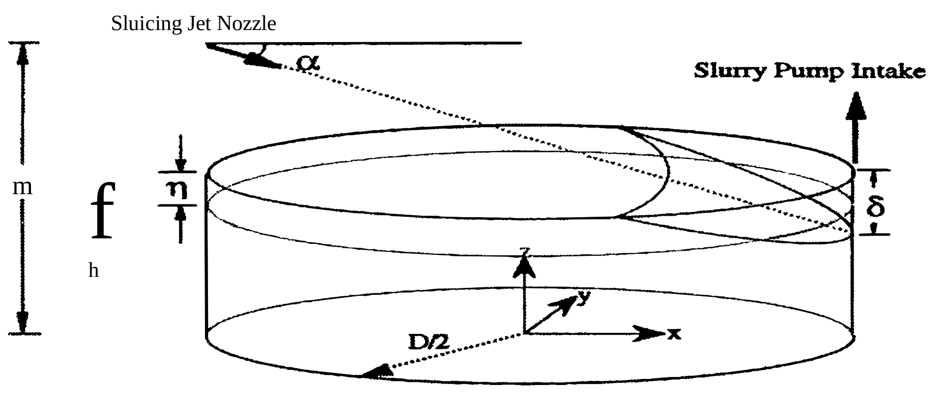

Figure 10. Sluicing Pattern

4. SET UP

UMR's experimental mine was chosen for the tests, as there is minimal traffic and large areas that can absorb simulant overspray. There is also easy access to the site for equipment construction and installation as well as handling of simulant and water.

Figure 11. Test Site at UMR Experimental Mine

A simulant tank was fabricated, due to limited level space, which was 30 feet in diameter and located 35 feet from a nozzle position. This tank is five feet deep and contained four feet of simulated waste. The new nozzle, which was designed and built at the PNNL facilities in Hanford, was attached to a deck gun which is a commercially available and used by fire departments for precisely training large volumes of water on specific areas. This deck gun has controllable pitch and yaw settings for repeatability of sweep angle. By angling the nozzle to a precise downward angle and controlling the sweep, the entire energy of the resulting waterjet could be played over the surface of the simulant. To closely simulate the conditions available in-tank at the sites, the gun position was elevated to nine feet above the surface of the simulant and positioned 65 feet from the far wall of the tank.

The simulant chosen consisted of clay based soil that was screened due to the removal pump that was located in the tank to remove the mobilized simulant. This material is relatively insoluble in water but is of fine enough structure that suspension is fairly easy and settling is not too rapid.

Figure 12. Wet Simulant in Tank Showing Sump Pump

A series of four 1500-gallon clean water supply tanks was situated above a specially modified centrifugal main pump such that gravity could assist the water supply. The pump was capable of 400 gpm at 350 psi, but a combination of considerations led

Figure 13. Pump feeding the Deck Gun

researchers to opt for 150 psi at 350 gpm, which is an acceptable pressure/flow combination for actual fieldwork. The pump supplied pressurized water through a four- inch line with 13 feet of rise to the nozzle.

A slurry pump was set in the back edge of the simulant tank with the capability of removing the mobilized slurry nearly as fast as it is produced by the jet action. This slurry was pumped through a four-inch line that was valved to send the flow to a 200 gallon scaling tank or four 1500-gallon receiving tanks. During each test the slurry was captured for ten seconds in the scaling tank where weight was compared to volume for a percentage of solids mobilized during that test. The slurry that was captured in the 1500- gallon tanks was allowed to separate by settling for six hours minimum and the level of solids measured in comparison to the total level for percentage confirmation as well as total solid volume removed.

The nozzle that was designed for this series of tests includes a one-inch diameter orifice, a two and one half-inch entry section, a seven-inch acceleration section, and a three-inch

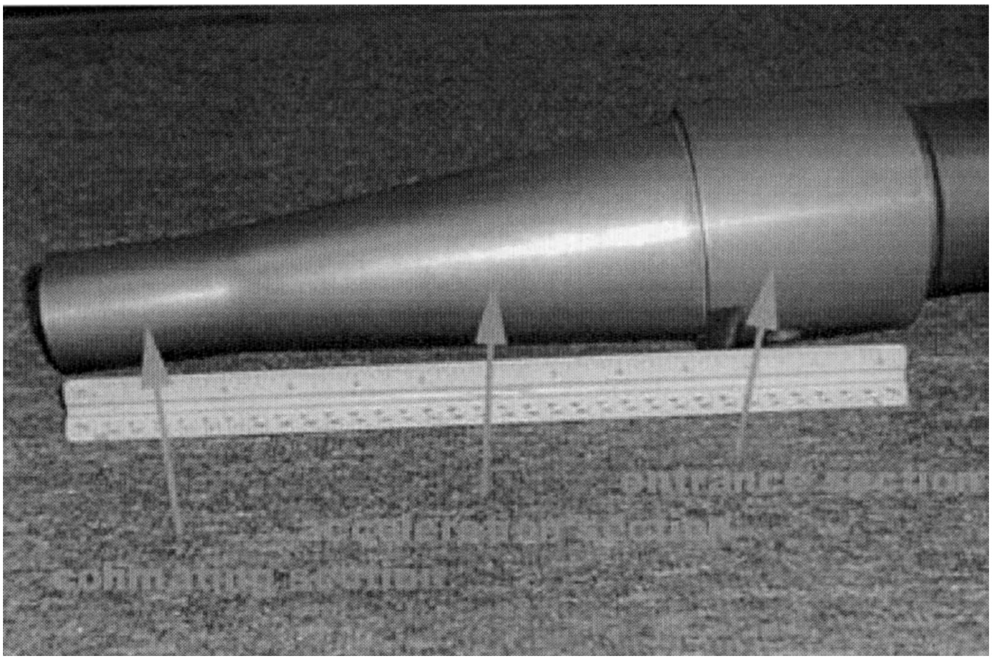

Figure 14. PNNL Sluicing Nozzle

collimating section. A flow straightener preceded the nozzle. This setup provided a much more cohesive jet over the 65-foot throw than did the previously used nozzle from the earlier tests.

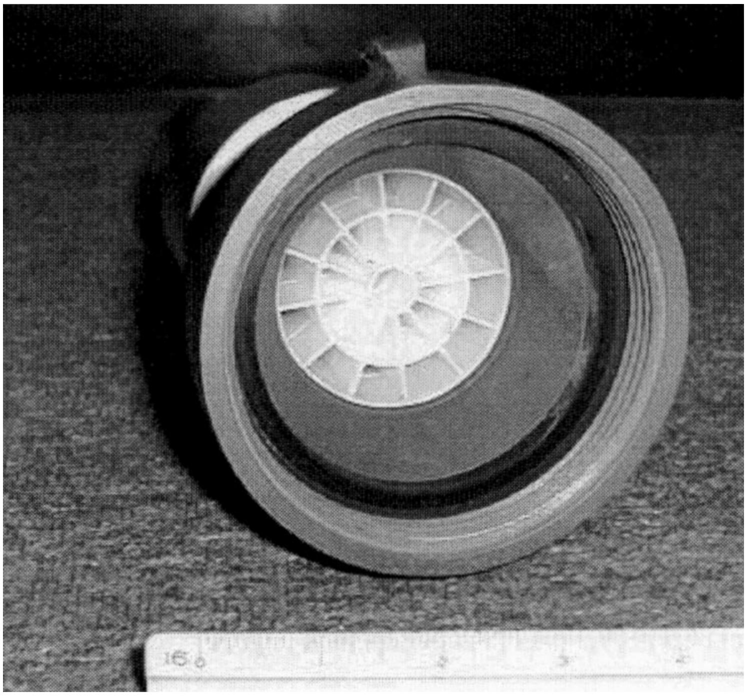

Figure 15. Flow Straightener

5. OPERATION

Each test distance (4 ft., 8 ft., 12 ft, etc) was segmented into two-minute periods of oscillation, followed by preliminary analysis of the results. This produced roughly 700 gallons of slurry, of which approximately 35 gallons were diverted into the scaling tank.

Figure 16. Scaling tank

By accurately measuring the volume of material in the tank, and precisely weighing it, a ratio of solids to water could be obtained and a volume of solids ascertained. Confirmation of the removal rates was obtained by physically measuring the remaining simulant in the tank both along a repeated chord parallel to the jet path, and along the rear wall of the tank and comparing those measurements to that of the starting level. The two- minute runs were repeated until all material from the back wall to the four-foot cutting

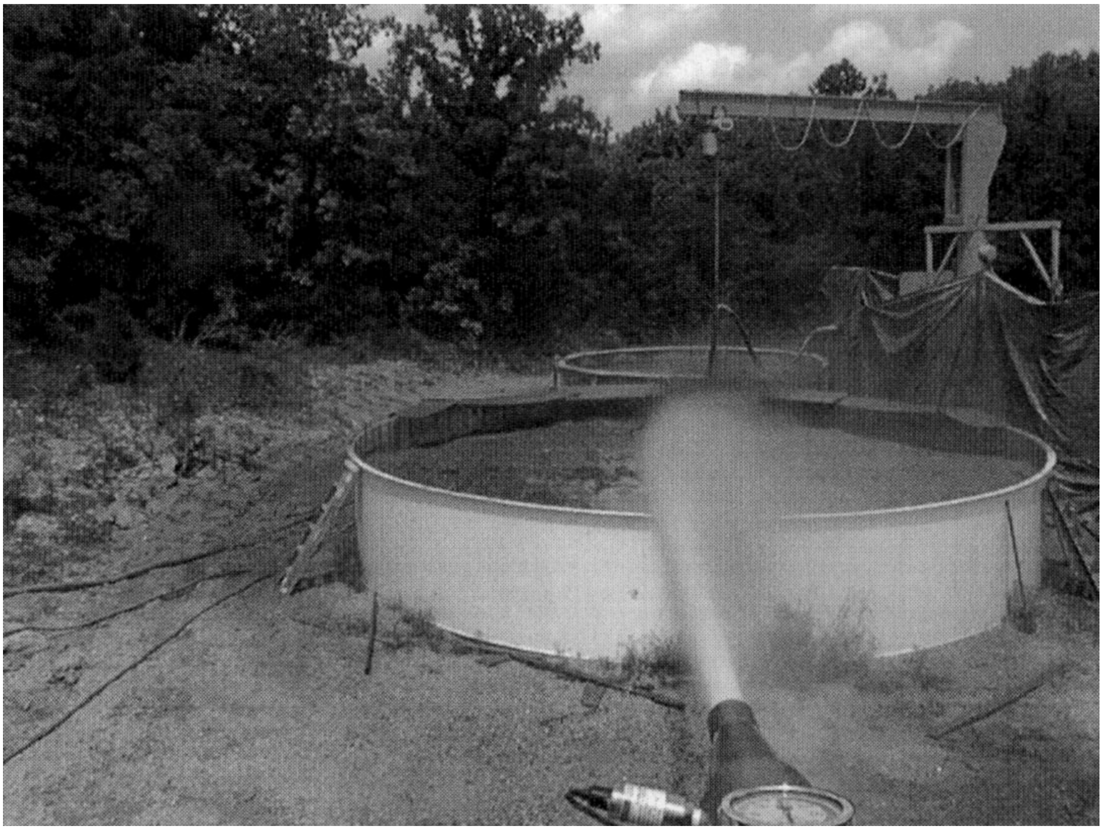

Figure 17. Test in Progress

arc was removed. The nozzle was then lowered incrementally so the jet impact point was eight feet from the back wall and the two-minute operations repeated until all the material was removed from the back of the tank to the eight-foot arc. This was followed by the 12-foot are and the 16-foot arc. It might be noted that some operational parameters were modified as needed to try to overcome some unexpected conditions that will be reported later.

The completion of these tests was followed by a repeat, for comparison, of the same tests but with the simulant covered by one foot of water.

6. OBSERVATIONS AND RESULTS

The tests were performed over the summer months, and the "dry" tests, those which were conducted without cover of water, began with acceptable results, although little comparative data could be found. As the nozzle angle was declined, however, from the 8-foot arc to the 12 foot, an observable drop in solids removal began to emerge. This was in opposition to the theoretical considerations that held that the lower nozzle angle provided a less oblique the angle of impact and better material removal results. Observations of the remaining simulant pointed to three reasons for the reduction. The first, and arguably most obvious, was that the clay had started as a semi-dry material which had become saturated, which had continued to be eroded

Figure 18. Erosion Pattern

fairly well. Over a long July fourth weekend, the top layer of about a foot had dried and baked in the hot Missouri sun and had turned to a substance more akin to brick than dirt. This led to less penetration of the jet and more deflection as evidenced by the "ski slope" pattern of the surface.

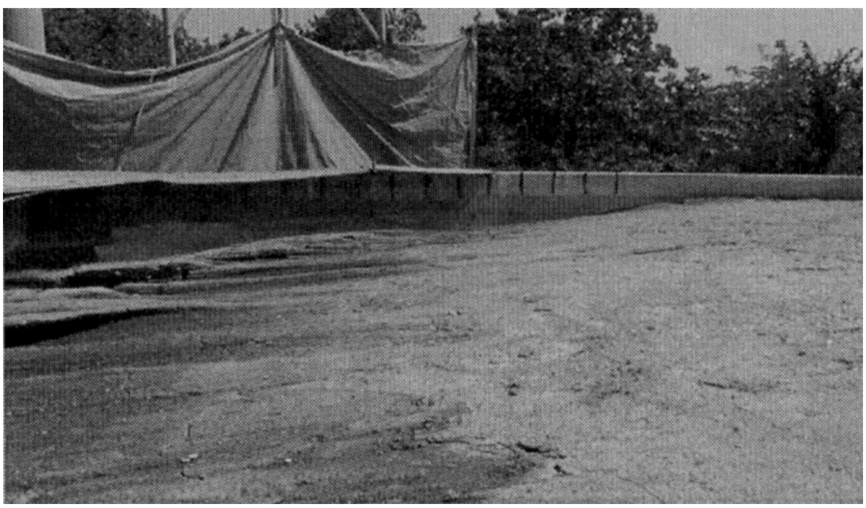

Figure 19. “Ski Slope” effect

This pattern was caused in part by the jet pushing material in front of it as it deflected and in part because the material had a higher resistance to penetration so the jet cut in very little before deflecting. It was also noted that the simulant hadn't baked evenly creating the gully and ridge configuration familiar to natural erosion pattern observers. The declination angle of the nozzle was modified at times to reduce the angle variation from previous runs. Thus, when moving from the eight-foot distance to the twelve, the step-down was tried incrementally to reduce the berm formation that resulted in higher jet deflection rates.

A secondary phenomenon which was noted early on in the testing process was the erosion along the back wall due to turbulence as the jet moved back and forth over stimulant

Figure 20. Turbulence Created Trough

surface. This zone increased rapidly during the early runs, but, as testing progressed, the zone of turbulence expanded much more slowly until it virtually stopped increasing. The amount of simulant mobilized by the turbulence therefore was reduced as time went on.

Testing at the 16-foot are level was continued, with the hope that the more obtuse angle would provide greater penetration and a return to the earlier success. Unfortunately, the removal rate stayed low and the berm in front of the jet became even more pronounced. It was then determined to add more simulant, smooth it down and cover the whole thing with a foot of water.

The second series of tests, the submerged tests, were carried out with the same protocol as the dry test had been. The material removal rate looked degraded, or considerably

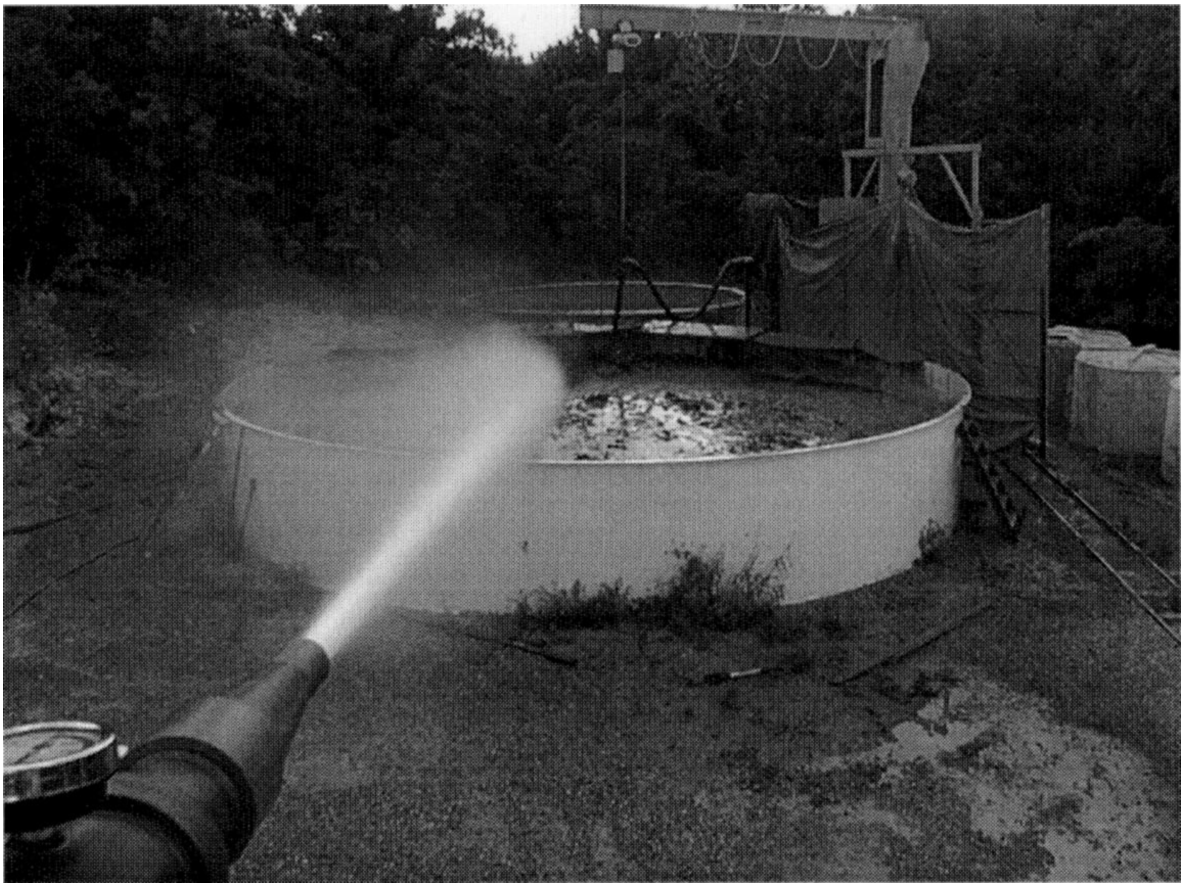

Figure 21. Submerged Test

worsened in comparison with that of the early dry tests. Confirmation was duly made by measurement and the removal pattern had changed. Repeated testing at the four-foot arc showed that after the first run, even with more runs than before at that distance, the removal rate dropped off dramatically and confirmation measurements along the chord

Figure 22. Taking a Chord Measurement

and/or rear wall were meaningless. The nozzle declination angle was increased to begin at the eight-foot arc level, and the same results occurred. The material removed under the water cover appeared to be totally from turbulence and the turbulence was redistributing the mobilized material to other sections of the tank. It was also observed that a greater amount of slurry was being forced over the sides of the tank than was being pumped into the slurry collection tanks. The turbulence created by the jet sweeping over the surface of the water covered simulant began setting up waves which would be further shaped by the edges of the tank and become focused at points along either side where they would far surpass the height of the tank wall and break over the side. It was deduced that as far as sluicing is concerned, the water cover virtually stopped material mobilization.

7. CONCUSIONS AND RECOMMENDATIONS

The sluicing concept appears to have a place in material movement, although there are some concerns. Among those concerns is the volume of water needed to mobilize the material, which in radioactive conditions creates a huge volume of additional waste to treat. Of additional concern is the amount of slurry that is splashed into areas that are not targeted, such as onto the walls and even out of the tank.

It appears that target material consistency plays an important part in efficiency with the sluicing concept, just as it does in more conventional applications of waterjetting. As mentioned in the paper "The Carving of the Millennium Arch" elsewhere in these proceedings, variations in target material create challenging conditions for the waterjet operator. As increased resistance to waterjet impact is met, parameters must be changed to maintain consistency of resolution.

8. REFERENCES

"The Carving of the Millennium Arch", Summers et al Proceedings of the 10th US Waterjet Conference, Houston, TX, August 1999.

"Development of a Waste Excavation End Effector", Galecki et al Proceedings of the 12th International Conference on Jet Cutting Technology, Rouen, France, October 1994.

"Monitoring Gas Retention and Slurry Transport During the Transfer of Waste from Tank 241-C-106 to Tank 241-AY-102", Stewart et al PNNL Report to D.O.E., July 1997.

10th American Waterjet Conference
August 14-17, 1999: Houston, Texas

Paper **50**

HIGH PRESSURE WATER DYNAMIC FRACTURE OF ROCK

Gongbo Li*
Department of Mechanical Engineering & Applied Mechanics
University of Rhode Island
Rhode Island

Qingshou Chen & Hengqian Ran
China University of Geosciences
Beijing, P.R. China

ABSTRACT

A method and system for safe fracture of rock, concrete and other brittle solid materials using high pressure water is provided. Experiments in laboratory and field have demonstrated that the system is capable of breaking rock and concrete with efficiency and safety and its size is in small a scale.

----

*Current address of the first author: 4212 Fuller Hollow Rd, Vestal, NY13850, U.S.A

1. INTRODUCTION

The traditional way of breaking of rocks, and other brittle solid materials by explosive blasting, while being able to fracturing the hardest of rocks at acceptable efficiencies, is environmentally unfriendly---the violent nature of explosive means people and machines are withdraw from the vicinity of the rock mass when blasting operation takes place; tremendous shock wave, vibration and noise, overbreak, flying debris are obviously dangerous.

A number of attempts have been made in the past to develop alternatives to conventional rock breaking techniques, including hydraulic fracturing 1-3. Although 30 MPa which is more than the tensile strength of most rock is easily obtained with conventional hydraulic equipment, the large sizes of a hydraulic pump and power supply limit application of this method. Actually, a continuously static pressure provided by a pump is not necessary. If a pressure pulse of a certain magnitude with sufficiently short rise time could be produced in a hydraulic system by denoting a little explosive or propellant, a high pressure water system of quite small a scale for inducing rock fracturing would be feasible. Our work has led to the development of the hydraulic system capable of generating rock fractures with ease, efficiency and safety.

The basic fuel and oxidizer ingredients of an explosive, upon detonation, are immediately converted to high pressure, high temperature gases. The all hazards mentioned above result from too quickly expanding gas. The use of water in blasting hole has been well documented by Denisart et al 4, in 1976. Who introduced the firing of steel pistons into shallow water-filled holes, that energy in a blast could be fast redistributed with water filled in a hole for its less compressibility than that of air. A preliminary laboratory and field research of us revealed that high pressure water in rock could give very efficient and safe breakage with explosive. The object of our study was to minimize that part of explosive energy consumed in crushing and pulverizing the area immediately adjacent to the borehole wall, to low initial peak pressures but average distributed pressure. The air in hole was considered a form of energy absorber, which first stored and later released energy that produced noise, flying debris etc. When rock was broken. In contrast to air boreholes, a fluid of column water will efficiently transmit explosive pulse to the medium. It was this unique ability of water to change that hazards part of explosive energy into rock fragmentation.

In this paper, a method and apparatus for safe fracture of rock, concrete and other brittle solid materials using high pressure water is provided. The apparatus comprises a firing chamber with a propellant cartridge and a reusable water seal assembly including a nut, a weal gum, wedges etc.. In the desired separation plane of rock mass, a moderately high pre-tensile stress zone is firstly established by sealing high pressure water in a row of holes. A little explosive or other firearm ammunition in the firing chamber is ignited, the impact pulses create a high water pressure in the boreholes sufficient to fracture rock without overbreak, which just causing the rock splitting. This method and apparatus may be applied in construction, tunnel excavation, quarry mining, demolition of reinforced concrete foundations and so on.

2. EXPERIMENTAL PROCEDURES

The research program to develop and evaluate potential applications of high pressure water dynamic fracture technique was primarily an experimental program, with testing conducted on two steps. Experiments first were designed to provide the data of stress distribution along borehole. Experimental were conducted in homogeneous blacks of rock or concrete in an explosive testing laboratory. Secondly, experiments on a field scale, comparable to the that which might be utilized in a commercial trending machine, were conducted in a quarry.

2.1 Laboratory Tests

To generate this water pressure pulse a small shock tube driven by explosive was built. Fig. 1 shows the overall design. The output of the setup is water pressure pulse that can be measured in amplitude and duration by using strain gages bonded on the surface of steel tube. The amount of explosive driver is 10 g. Some material properties for granite used in the tests are as follows: density 2.7G/cm^3, compressive strength 300 MPa, modulus 6.9 GPa. The rock models were about 450*450*450mm. The concrete models was cylinder with 600mm in diameter and 450mm high. A 40mm diameter borehole was drilled in the center of block, normally to a depth of 50mm. The water was full of the tube. When the charge is detonated from one end of tube it will drive a water pulse. Table 1 gives a summary of the results obtained in this series of tests and figure 2 shown some fracture patterns. A time history of a strain in typical point of steel tube was depicted in Fig.3. The noise present in the recording is due to sensitive to the accelerations set up by water pressure pulse in the steel tube generated by the explosive. Based on the data measured from strain gages, the pulse wave velocity can be calculated as

V =distance between two strain gages / difference of arrival time for pulse

So v is 1126 m/s in average. The velocity decreases slightly along the steel tube from 1176 m/s to 1052m/s (see table 1). Fig.4 shows the water pressure perpendicular to the direction of pulse propagation. For measurement locations (1) and (2), the pressure is almost same during the initial compressive pulse. The pressure then begins to drop at the location (3) for absorption energy of water. There is somewhat increase after location (3), due mostly to release of water expanding energy.

2.2 Experimental quarrying tests

All of the field-scale tests were carried out in the quarry located in suburb of Beijing. With the excellent improvement in rock breakage realized in the laboratory tests, a patent apparatus for safe fracture of rock was designed and manufactured (as shown in Fig. 5,6). A small drilling machine was employed to drill boreholes. Some apparatus with a loaded cartridge containing 8 g explosive were housed in the holes. And then locked in place by turning the nut with a wrench until the apparatus were secure. Water was filled into holes. Finally, ignition of explosive within the sealed hole created great water pressure resulting in the fracture of rock (see Fig.6).

This initial feasibility research revealed four significant features of high pressure water dynamic fracture:

1. able to control the fracturing direction;
2. non tremendous shock waves and noise;
3. good fracturing capability with safety;
4. size of system is of small a scale and economic, commercial.

3. CONCLUSION

Laboratory experiments have confirmed that more than 30 MPa water pressure can be induced in a borehole with 10 g explosive, which is high enough to fragment rock models. Field applications of the hydraulic system have shown that the efficiency and safety of rock fragmentation. In both testing, sealing water is important to obtain optimum results. The system is established to meet commercial requirements for good performance in a broad variety of rock type and condition.

4. REFERENCES

1. Noma T., Murayama H., Kadota S., Ueda S., (1991):Development of Static-fracturing Method of Rock Mass and Concrete Using Hydraulic Pressure, *Proc. Japan Soc. Civ. Engrs*, No.427, pp.203-211

2. Kolle J. J. & Fort J. A., (1988): Application of Dynamic Rock Fracture Mechanics to Non-explosive Excavation, *Proceedings of the 29th U.S. Symposium on Rock Mechanics*. pp.571-578

3. Gongbo L., Guodong J. & Xiaohe X., (1991): Theoretical Analysis on New Abrasive-water jet system, *Proceedings of the Second International Conference on Measurement and Control of Granular Materials*, Chengde, China, pp.283-287

4. Denisart at al, (1967): U.S. Patent, No. US3988037

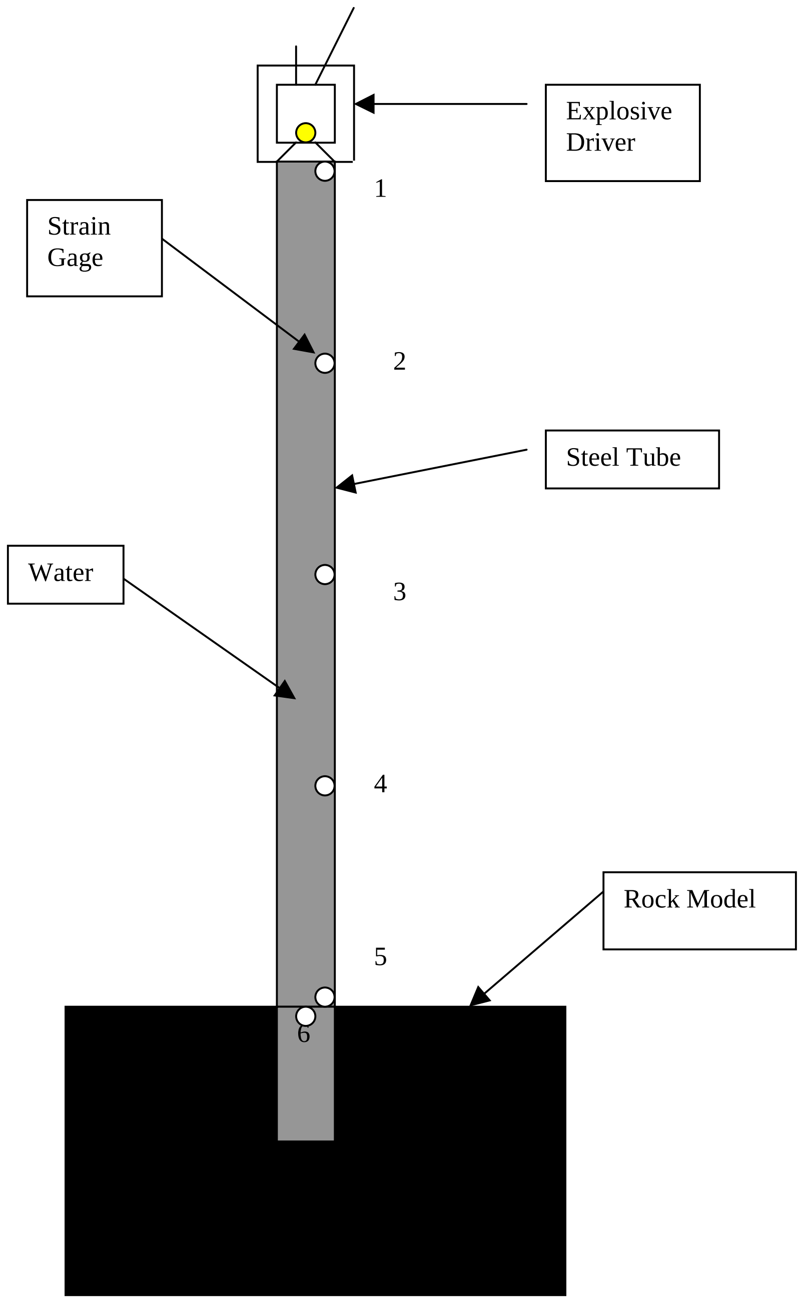

Fig. 1, Schematic diagram of experimental setup for laboratory tests

Table 1 Average test results

Measure location No.	Distance to explosive (m)	Pressure (MPa)	Arrival time (micros.)	Calculated pulse velocity (m/s)
1	0	50.6	0	
2	0.05	49.1	2	
3	0.25	30.9	172	1176
4	0.45	45.1	344	1150
5	0.65	43.1	536	1052
6	0.70	86.6	546	

Fig.2 Some rock and concrete fracture patterns

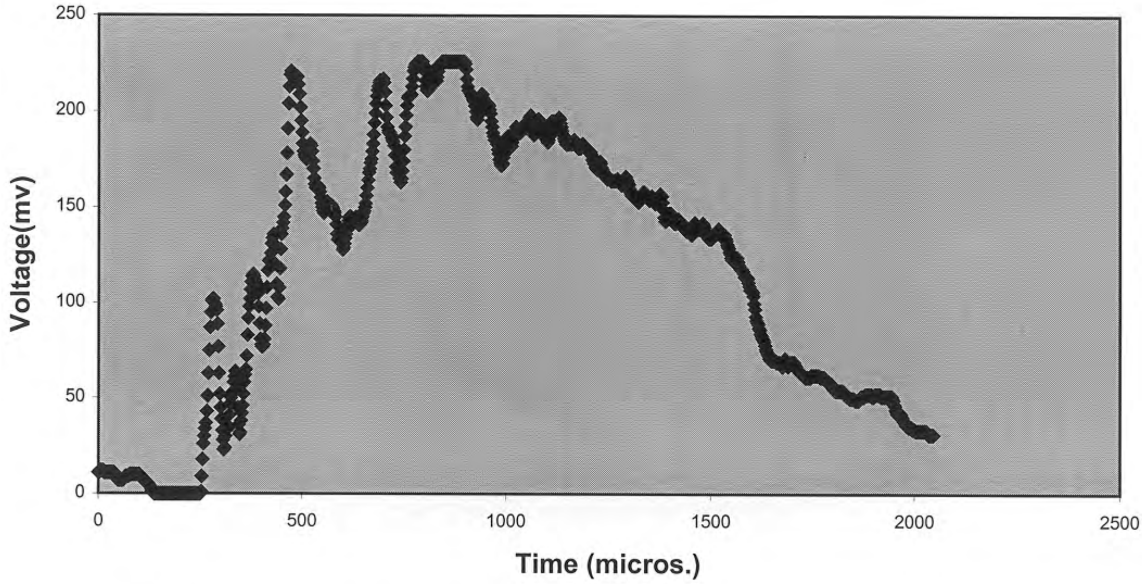

Fig.3, Strain signal from high pressure water produced by explosive

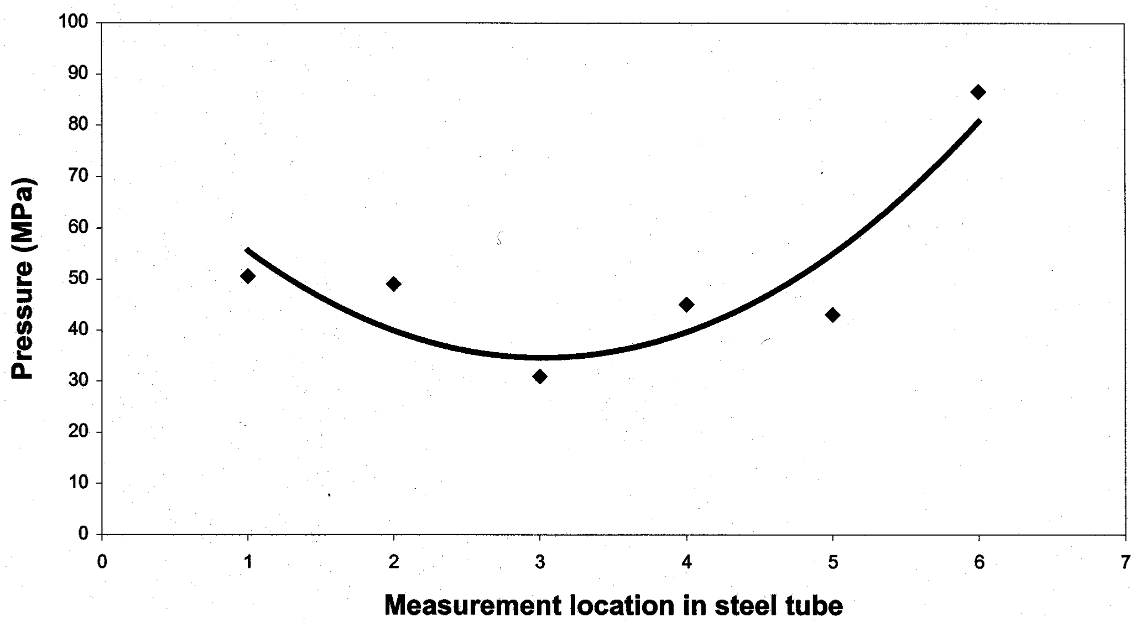

Fig. 4, Pressure in guage hole along steel tube

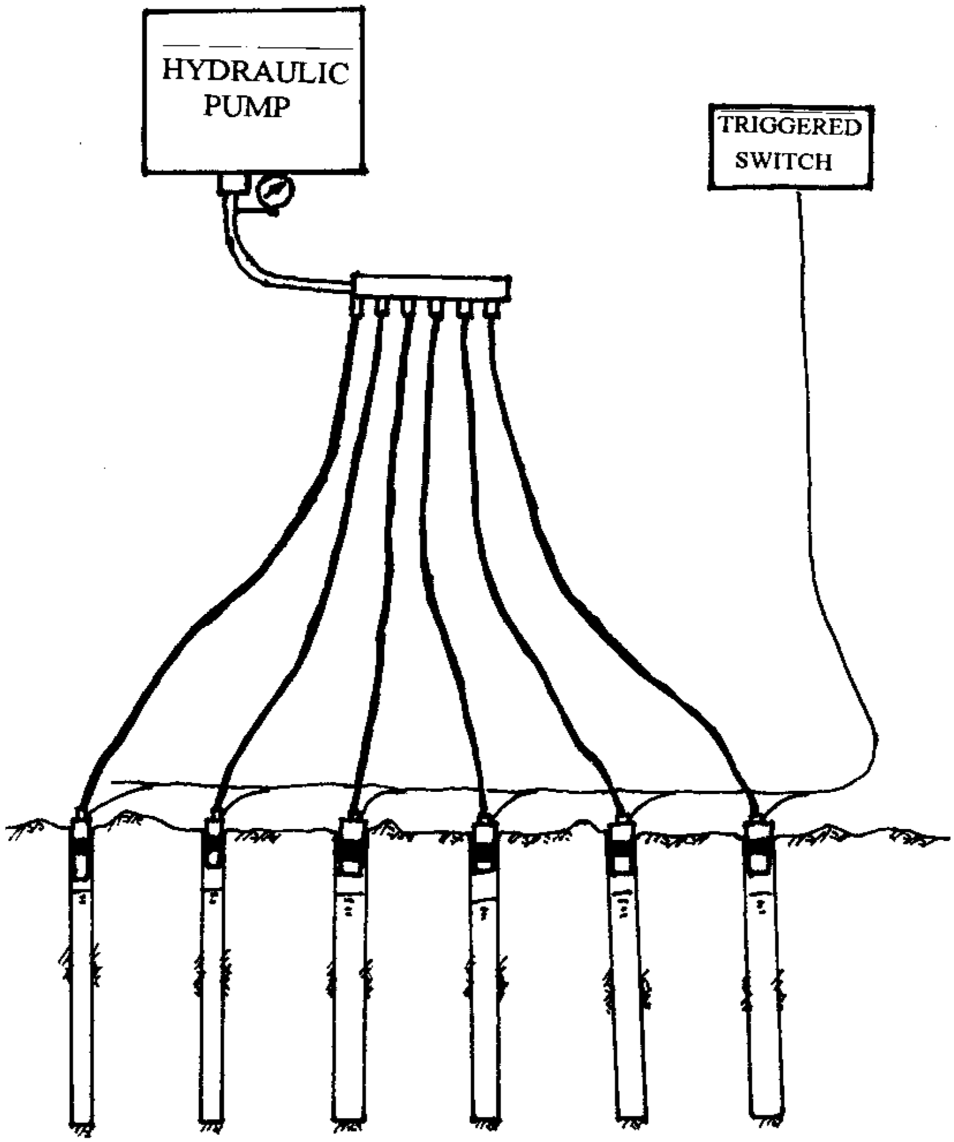

Fig. 5 Schematic of the rock breaking operation

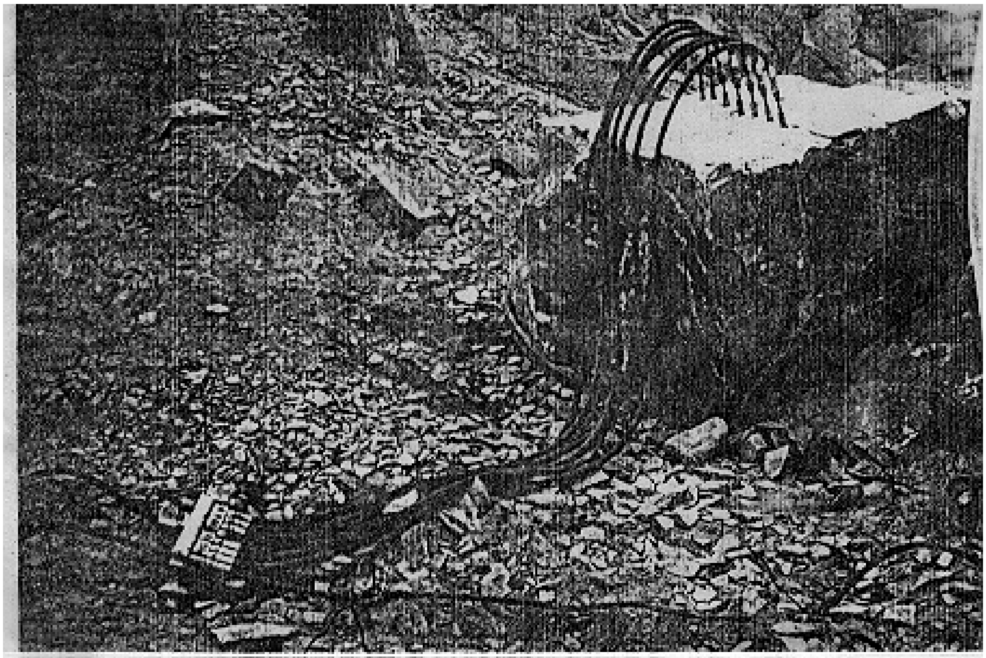
(a)

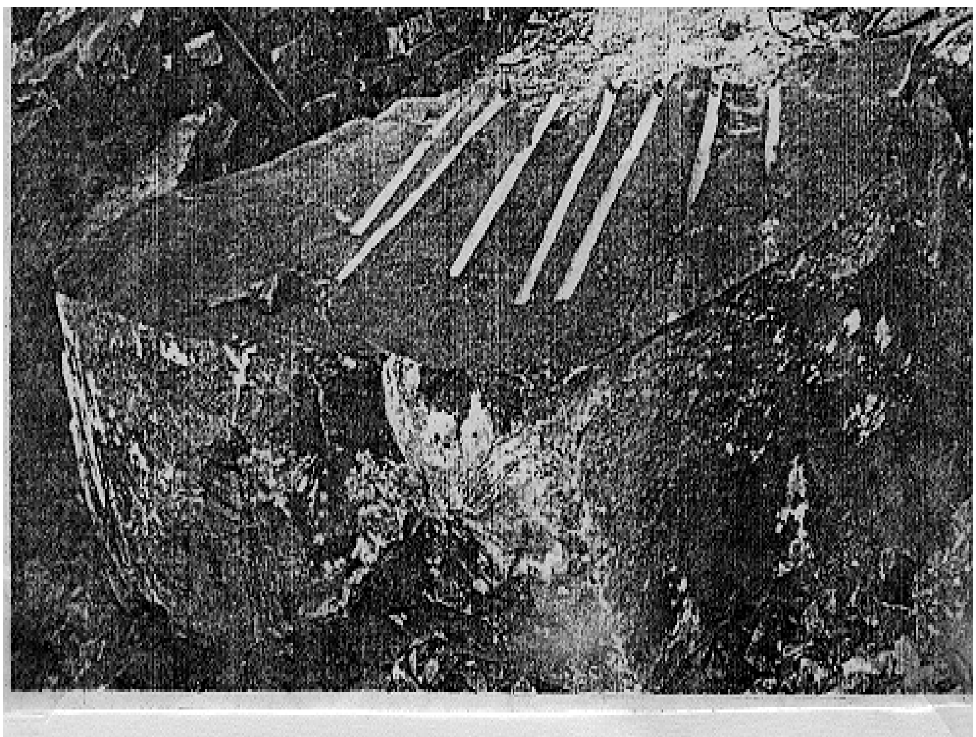
(b)

Fig. 6 Field-scale testing system

10th American Waterjet Conference
August 14-17, 1999: Houston, Texas

Paper **51**

A COMPARISON OF SURFACE PREPARATION FOR COATINGS BY WATER JETTING AND ABRASIVE BLASTING

Lydia M. Frenzel, Ph.D.
Advisory Council
San Marcos, Texas, U.S.A.

ABSTRACT

Water Jetting, with and without abrasive addition, continues to impact the maintenance industry and displace some of the traditional areas of dry abrasive blasting. This presentation focuses on the similarities and differences in the visual reference photographs which are used in the global industry.

Keywords: waterjetting, surface preparation, hydroblasting, standards, water blasting, standards, metal, standards, specification, NACE, SSPC, ISO, paint.

Organized and Sponsored by the WaterJet Technology Association

1. INTRODUCTION AND BACKGROUND

Since 1985, the continued improvement in nozzles, seals, and pumps make it possible for reliable removal of coatings and rust. Water jetting and wet abrasive blasting methods have gone from a rare oddity to acceptance by the marine industry and becoming the preferred process for removal of lead based paint or asbestos. The Technology Publishing Company's (TPC) annual survey of painting contractors indicates that fifty percent (50%) of the identified painting contractors use some type of high pressure or ultra-high pressure waterjetting or wet abrasive process. One individual contracting firm says they have cleaned over 20 million square feet of surface. Coatings manufacturers, notably International Paint Co. (Akzo Nobel), Hempel's Paints, and Jotun have produced videos, technical product literature, and visual reference photographs to train their technical representatives and clients. Ameron, Bridge-Cote of Canada, Devoe, Euro-Navy, Sigma, W&J Leigh & Co., Watson Coatings, and Wasser Hi-Tech Coatings are additional coating manufacturing companies who actively embrace the use of water in surface preparation.

Organizations such as SSPC (Society for Protective Coatings), NACE Int. (National Association of Corrosion Engineers), and ISO (International Standards Organization) provide the grounds for consensus documents, that is, documents which are defined as a “general agreement” or a “majority of opinion.” Consensus recommended practices and technology updates provide a Common Language to describe problems. Every industry tends to define the same problems in different terms. Adopting consensus language saves time and money. Environmental concerns are driving movement to include water. Water Jetting and Wet Abrasive Blast Cleaning are displacing traditional abrasive blasting in certain areas. Adversarial points of views exist within the coatings industry. It took ten years to build a consensus and issue the first standard on the use of high pressure waterjetting jointly by NACE and SSPC in 1995.[3] NACE and SSPC have issued two other documents since that time.[2,11] In 1998, ISO also started work on a separate water jetting standard as they did not know the extent of the American activities.

Over the years, European and American philosophies drifted apart in the adoption of consensus language for abrasive blasted cleaned steel. In simplistic terms, the Americans use standards language allowing a percentage coverage of stains, while the Europeans use a criteria of tightly adherent material. The visual reference photographs for abrasive blast cleaning showed examples of rusted steel, but not removal of coatings. Projects involving removal of coatings for repainting often call for leaving sound, adherent coatings on the substrate, not removing all of it to leave slight stains. These pictures don't exist as consensus photographs. The development of photos for high pressure water jetting is bringing the European and American working philosophies together as we consider the maintenance practices on a global basis.

In the fall of 1998, Dr. Frenzel drafted a letter which was sent to ISO over Ken Tator's, as the designated U.S. country expert to ISO TC 35 SC 12, signature with full support of SSPC and NACE organizations.

" Dr. Lydia Frenzel, chair of the NACE and SSPC Joint Task Groups on water jetting and wet abrasive blast cleaning (TG D and TG I), and I would like to establish communication on a regular basis between the ISO working groups on surface preparation concerning water jetting and the Joint Task Groups in a mutually beneficial manner. Dr. Frenzel and I meet on a regular basis. We are concerned that the ISO groups may not fully aware of standards activities in the North America and wish to avoid conflict between working groups. We hope there will be commonality in standards development between the North American and the European communities. ....

We recognize that an independent set of photographs should be prepared so that coatings manufacturers do not have to refer customers to material originally prepared by a competitor. The U.S. National Shipbuilding Research Program funded the preparation of a set of photographs of surfaces prepared by water jetting specifically for standards preparation. These new photographs have been released to SSPC and NACE for preparation of visual reference photographs. ....

.....[we] hope that we can work together and provide a commonality to the water jetting and wet abrasive efforts."

Following this letter, ISO had a representative to the SSPC/NACE Task Group meeting in November, 1998, and members of the NACE/SSPC Task Group and the SSPC Executive Director, Dr. Bernard Appleman, met informally with ISO Working Group 2 on Water Jetting in March, 1999. Documents and working photos were exchanged. We opened communications and are currently working on development of new visual reference photographs for the Water Jetting of substrates, in particular steel, with the Europeans. This is vitally necessary as coatings suppliers and contractors work globally.

The majority of the slides used in this presentation are proprietary to individual companies or are actual slides of the draft photos under consideration by the standards groups. As such, they are not reproduced in this paper.

2. DEFINITIONS USED BY COATINGS INDUSTRY

The paper will be using definitions from SSPC and NACE technical reports and standards which are closely aligned with the WJTA Recommended Practices for the Use of Manually Operated High Pressure Water Jetting Equipment.[1,2,3] The SSPC and NACE documents are used by the coatings professionals. In these documents, the distinction is made that blast cleaning or blasting involves the use of solid abrasives whereas water cleaning or water jetting is the use of water alone without abrasives. "Water Blasting" is such a generic and wide-spread term that it hasn't been defined in the consensus process.

Wet Abrasive Blast Cleaning (WAB) covers procedures, equipment, and materials involved in a variety of air/water/abrasive, water/abrasive, and water-pressurized abrasive blast cleaning systems. Air/water/abrasive blasting is the specific cleaning method in which water is injected into the air/abrasive stream generated by conventional air-pressurized abrasive blasting equipment. Water/abrasive blasting is a cleaning method in which abrasive is injected into the water stream generated by conventional fluid pumps.

Other generic terms to describe specific air/water/abrasive blast cleaning methods are: Water Shroud or Wet-Head blasting, wet blasting, low volume water abrasive blasting, and slurry blasting. Other generic terms to describe specific water/abrasive blast cleaning methods are: slurry blasting, abrasive water jet (AWJ), or abrasive injected water jetting/blasting (AIWJ).

High Pressure Water Jetting (HP WJ) is cleaning performed at pressures from 70 to 216 MPa (10,000 to 30,000 psi). Ultrahigh Pressure Water Jetting (UHP WJ): cleaning performed at pressures above 216 MPa (,000 psi). Low Pressure Water Cleaning (LP WC) is cleaning performed at pressures less than 34 MPa (5,000 psi) High Pressure Water Cleaning (HP WC) is cleaning performed at pressures from 34 to 70 MPa (5,000 to 10,000 psi).

The terms hydroblasting, hydrojetting, water blasting, and water jetting describe the process in which pressurized water is directed through a nozzle to impact a surface. However, it is noted that the terms hydroblasting or water blasting is used generically to describe cleaning methods that range from low pressure water cleaning to ultrahigh pressure water jetting.

In the coatings industry, water jetting does not provide the primary anchor pattern. The use of water alone is primarily for recoating or relining projects for which there is an adequate, preexisting profile. Abrasive and water combinations can be used on older substrates or new projects to establish a new profile or anchor pattern.

3. COATINGS FAILURES AND SURFACE PREPARATION

In the world of corrosion control and painting, it should be obvious to everyone that the job is to get the surface clean enough to accept the paint system. This process is called surface preparation. Surface Preparation is- **creating the situation so that the coatings will perform as expected.** Remarks in this paper will be limited to processing metal substrates rather than wood, concrete, or plastic and will not include chemical processes such as etching or phosphating.

If you don't produce a clean surface so that the paint will adhere, the world will move elsewhere. DO a GOOD JOB, the world will beat a path to your door. Expectations for the quality of surface preparation in coatings have escalated in the past few years. Change increases exponentially. This is the trend of the future. Preparing for change is preparing for the future. Using water in surface preparation, with and without abrasive, is part of the future. Think of the future of your business. If you adapt what you see and hear to your particular needs, you will be part of the future.

It is frequently said that ninety percent (90%) of all coatings failures are the fault of the surface preparation. It is also said that "seventy-five percent (75%) of all coating failures are the fault of the contractor." There are many factors that influence the performance or lifetime of a coating system in addition to the surface preparation, such as formulation, application, and service conditions. Lou Vincent examined failure modes of protective coatings in a presentation to SSPC in November, 1998 and identified twenty-two types.[4] Three of those twenty-two failure modes are directly related to surface preparation- adhesion loss, blisters, and delamination.

Those three failure modes accounted for 58% of the failures in 55 field case occurrences and 46% of the failures in 101 literature articles occurrences. While this is not the 75-90% generally cited, adhesion loss, blisters, and delamination are clearly the primary failure modes. The other 40-50% of the failures are spread between nineteen different types of failures.

The use of water in maintenance applications, not new steel construction, can have a very positive increase of the adhesion of the coatings and can reduce the chance for blisters and delamination. This positive benefit is why the use of water is the future evolution of surface preparation.

4. THREE ELEMENTS FOR A SUCCESSFUL PROJECT

People are driven to include water by environmental, safety, and economic considerations. They are not embracing water for the benefit of enhanced performance. To make water work in a project, you have to understand that THREE viewpoints must converge in bid specifications and they must all be represented in the negotiations and planning of a project.

The viewpoints of the
- **owner/operator**
- **contractor**
- **and coatings manufacturer**

must all come together.

This may seem obvious but it is an often neglected principle. The guarantee for a good job is forced on the coatings manufacturer and contractor. The contractor may be prevented from using wet abrasive blasting (WAB)[2] or water jetting (WJ)[3] even though the coatings manufacturer and contractor both agree that WAB or WJ may be preferable to clean a surface if the client or owner only has knowledge or training in dry abrasive blast cleaning. Why?- because "the customer (in this case, the owner) is always right." If the customer only has experience in dry abrasive blasting, then the contractor and coating manufacturers working together must overcome steep opposition and provide education.

People in the coatings and maintenance industry are afraid of change. There is a lot of resistance towards change. It is easy to understand. Mistakes come back to haunt us. As an industry, we are to be blamed for slow acceptance-because we don’t talk to each other. Everybody is jealously guarding their secrets. If an engineer learns something that will give him lower maintenance costs or an edge on the competition, he doesn't like to share that secret. The goal of zero defects on every job is a slow, ongoing process. This presentation is part of education. Education is the key to understanding.

5. THREE COMPONENTS OF SURFACE PREPARATION

Surface Preparation- **creating the situation so that the coatings will perform as expected.**

There are three components to Surface Preparation - All are necessary even though the emphasis in the past has been only on visible cleanliness and anchor profile.

- **Visible Cleanliness**
- **Anchor Profile**
- **Invisible Contaminants**

Everyone in the coating industry is trained on the visible requirements from day one. The coatings manufacturers control the anchor profile requirements. The third component, **Invisible Contaminants,** is one component that people are still unaware of even after at least fifteen years of education. All three components are all equally important. While all three are necessary for good coatings performance, it is the last component, the invisible contaminants, that demands water and which requires reform.

The addition of water in surface preparation evolution is occurring because coatings manufacturers have recognized the secret and success of water in dealing with invisible salts. The coatings manufacturers have really understood that water is the "True Grit of the 21st Century." The coatings manufacturers have come forward with videos, pictures, and have rewritten their specifications so that surfaces can be cleaned with dry abrasive blasting and/or various water/abrasive methods.

One major obstacle of the acceptance of water in surface preparation is the appearance. Another major obstacle is the formation of flash rust. Part of the maintenance industry will never accept the appearance of the surface when water is used in surface.

5.1 Anchor Profile

5.1.1 New Metal

First how does one create the profile on a new piece of metal? The profile or anchor pattern is specified by the coating manufacturer. In simplistic terms, the profile of the substrate is generally considered to be the dominant factor in coating adhesion.

Water Jetting by itself is generally not used to create the initial profile even though creating a surface profile can be accomplished with water jetting alone on small objects with careful controls. [5,6] Automated equipment must be used to control the depth, transverse rate, and stand-off distance. The process is too slow for large pieces. However, when the profile is produced by water alone, the adhesion is greatly enhanced.[5]

The major surface profile on a metal substrate is defined by the abrasive and is typically formed by a dry, abrasive blast technique. Because of environmental restraints on visible dust, Wet Abrasive Blasting (WAB) is finding a market in new steel construction. WAB covers techniques which range from mostly abrasive, mixed with a little water to suppress the dust, to mostly water with a little abrasive. The pressure range of the water flow can be anywhere from 50 psi to 40,000 psi.

The anchor profile, or pattern, on the substrate is specified by the coatings manufacturer to a depth, such as 0.002-0.003 inches (50-75 microns). Rounded particles such as steel shot give a rounded, crater-like appearance where the width of the depression is greater than the depth. It is thought that hardened sharp angular abrasives tend to cut into the metal, leaving sharp edges, creating hackles (small slivers of steel standing perpendicular to the surface). Particles moving faster will make a deeper indentation compared to the same particle moving slower.

An analogy is throwing a baseball at a mud flat. Throw a large softball relatively slow and you will make a rounded impression with a lip. Throw a small hard ball relatively fast and you will make a deeper rounded impression. Throw a sharpened pyramid at an angle, and you will create a ridge. Some of the mud will splatter off, but most of the mud gets shifted to the new profile.

Abrasives do not necessarily remove the metal because metal is malleable, but you are creating a macroscopic pattern. This pattern may or may not remove existing corrosion cells.[7] This initial profile provides the cleaned nib to which the paint adheres.

5.1.2 Old Metal

There are many situations where abrasives are needed when older surfaces are being blasted. Abrasives are used in tight corners and for the back side of plates where the particles can be rebound or ricochet. In marine areas, there is frequently a very tightly adherent black layer of rust which is resistant to removal by water jetting alone. Addition of a little abrasive into the water stream will speed the production rate and help break this brittle layer. Abrasives can be used to ricochet on all sides of a small compartment whereas it may be difficult to direct a jet stream of water towards all the surfaces.

Abrasives change the existing profile. Abrasives erodes or abrades the surface from the top. A US Standard 100 mesh screen has openings for 125 micron particles. When the contractor is cleaning with 125 micron particles, contaminants which are in cracks or crevices or pits simply cannot be reached or removed. Crevices become filled with spent abrasive when a contractor is trying to remove pack rust between plates. Subsequently the paint gets applied over "clean" abrasive and fails prematurely. If there are invisible contaminants on the surface, abrasive blasting can drive the contaminants into the surface or form a pocket of metal in which the contaminant is buried.

Waterjetting can be described as a series of small droplets in the 5-10 micron range hitting the surface at supersonic speeds. The droplets implode (cavitate) and drill through coatings or rust; then spread laterally and shear at the interface, much like ultrasonic cleaning, to lift materials. A series of microscopic “pock marks” form on the macro surface. The craters and pits get "deep cleaning."

The measured profile in gross terms, for example 0.002inch (50 microns), is still the same for a surface cleaned by abrasive and by water jetting, but the microscopic details are different. The amount of surface area per square unit area is increased for the WJ cleaned surface. Figure 1 and 2.

Abrasive blasting changes the surface from the top down; water cleans the surface from the bottom of the pits up. These two different types of actions lead to two distinct visual appearances. Waterjetting cleans the existing profile and opens it. Abrasive blasting ignores the pits and cracks. There is a synergistic effect in using abrasives and water because you can get the advantage of both processes.

In a direct comparison of UHP WJ with abrasive blasting, Materials Evaluation Laboratories concluded "The pressurized water method was considered the best preparatory cleaning for non-destructive inspection. It offered a more authentic representation of the surface than the other methods evaluated….Pressured water had minimal disturbance of micro-structural features. "[8]

In a direct comparison of water blasting at 10,000 psi versus abrasive blasting for penstock relining,[9] Tom Aldinger reported that water blasting would give as good or better adhesion than abrasive blast to SSPC SP10 (near-white) on 60 year-old pen stock. Water blasting produced a clean surface without rust and loose paint residues. Atlas Cell testing in deionized water at 140 Deg. F was then used to compare immersion service performance for coatings on the water blast and abrasive blast surfaces. At the end of the Atlas Cell test, the investigators found a thin film of water and black rust under both the urethane and epoxy coatings on the abrasive blast surface with complete adhesion failure in the immersion zone. The water blast surface had coating adhesion 3 times greater compared to the coating on the abrasive blast surface. Any substrate corrosion on the water blast surface was local without any underfilm spreading. Underfilm corrosion has also been noted in cases where salt was deliberately added to the surface even though the paint was applied before any rust was present.[10]

"Adhesion begins at the bottom of the pits" said James Denny, Vice-President of International Coatings at Corrosion96. Water Jetting cleans the bottom of the pits. It is the experience of International Coatings and the marine industry that coatings adhere better and last longer on surfaces which have been cleaned by Water Jetting. Coatings manufacturers understand that when you use water for cleaning a profile you get better adhesion sometimes as much as two fold. Van Kuiken's patent illustrates this point. The micro profile is fractal for waterjetting. Loss of adhesion as a failure mode disappears.

5.2 Invisible Contaminants

Invisible contaminants such as oil and grease generally lead to delamination as a coating failure. Delamination also can be caused by a minimal substrate profile. Invisible contaminants such as salts, chemicals, or water soluble substances lead to osmotic blistering as a coating failure mode. The removal of the invisible contaminants leads to longer performance by the coating system. The ability to remove chemical contaminants (salts), particularly from badly pitted and corroded steel, is a major advantage of the water jetting process.[11,12]

WJ and WAB do such a good job of removing invisible contaminants from the surface, even if intact coatings are left on, that blisters from chemical contaminants and delamination from oil and grease disappear.

5.3 Visible Appearance

If WJ and WAB are so good at surface preparation, why is there a resistance for its adoption? Surfaces cleaned by water alone do not look like surfaces modeled by abrasives. Flash rusting on a steel surface can occur very quickly as a result of the very fine, sharp edges. Most of the resistance is based on the visible appearance.

Contractors, inspectors, and coatings personnel use the SSPC/NACE and ISO written standards and visual reference photographs for training and acceptance on jobs.

The written standards include:
NACE NO. 5- SSPC SP-12 for water jetting
SSPC SP-5 for abrasive blasting
SSPC SP-10 for abrasive blasting
SSPC SP-6 for abrasive blasting
SSPC SP-7 for abrasive blasting

Visual reference Photographs include:
Dry Methods
ISO 8501-1 for dry abrasive, hand-tool or power-tool cleaning, flame cleaning
SSPC VIS-1 for dry abrasive blast cleaning
SSPC VIS-3 for hand and power tool cleaning- This shows removal of coatings.
Wet Methods
International Paint For Water Jetting issued in 1994
International Paint for Slurry Blasting (Wet Abrasive Blast cleaning)
Hempel's Photo Reference for Steel Surfaces cleaned by Water Jetting
Jotun Photo Reference for examples of flash rusting
Schiffbautechnisch Gesellschaft No. 2222 Guide for water jetting
SSPC- VIS 4 (I) NACE No. 7 Interim Guide and Visual Reference Photographs for Steel Cleaned by Water Jetting- issued in 1998

Even though the visible references are for supplemental purposes in the US, in practicality, people use them as a primary standard. SSPC VIS-1 and ISO 8501-1 are the two visual reference photographs series used in training. They depict dry abrasive cleaned steel which have not been painted. Emphasis is on uniformity. Inspectors and owners are just beginning to use the VIS-4 (I) Reference Photographs for Water Jetting (which is the same set of photos as International Paint Water Jetting Standards. These also only depict unpainted steel.

As we go through the standards, keep in mind that visual reference photographs are designed to be illustrative of the situation. Direct correlation to existing dry media blasting standards is inaccurate or inappropriate when describing the capabilities of waterjetting and the result achieved with waterjetting as a process.

Abrasives hit from the top, erode the surface, provide plastic flow to the metals, tend to make the surface look uniform and “erase” different areas. There is a tendency to drive existing contaminants into the surface. Observers with an experienced eye tend to neglect the pits. They tend to look at the top surface.

WJ stresses the adhesion between two materials. WJ retains the metallic surface profile, tends to clean the pits first and leave material at the top peaks, and accentuate the non-uniformity of a surface. The experienced observer sees black stains on the top where heavy rust was present, or coatings on the top of the surface- rather than stains in the bottom of the pits so the observer see something which is a new experience even though the pits are cleaned.

The visual photographs SSPC VIS-1 and ISO 8501 only depict the situations of rusted steel. Water jetting is used primarily in removal of coatings, where frequently the objective is to retain as much tightly adherent coating as possible. There was a need to address the question of maintenance in visual reference photographs.

The following phrase exists in all the written standards. “Acceptable variations in appearance that do not affect surface cleanliness include variations caused by type of steel, original surface condition, thickness of the steel, weld metal, mill or fabrication marks, heat treating, heat affected zones, blasting abrasive, and difference in the blast pattern.” Figures 3 and 4 illustrate WJ-1 cleaning and the variation in appearance. That variation does not appear in the abrasive photographs.

5.3.1 Clean to Bare Substrate- "White Metal"

NACE No. 5- SSPC - SP 12 WJ-1
WJ-1 surface shall be free of all previously existing visible rust, coatings, mill scale, and foreign matter and have a matte metal finish.

ISO 8501-1 Sa 3
When viewed without magnification, the surface shall be free from visible oil, grease and dirt, and shall be free from mill scale, rust, paint coatings and foreign matter. It shall have a uniform metallic color.

SSPC-SP 5 NACE 1
When viewed without magnification, the surface shall be free of all visible oil, grease, dust, dirt, mill scale, rust, paint, oxides, corrosion products, and other foreign matter.

5.3.2 Very Thorough Cleaning, "Clean Almost to Bare Substrate"

NACE No. 5- SSPC SP-12 WJ-2
WJ-2 surface shall be cleaned to a matte finish with at least 95 percent of the surface area free of all previously existing visible residues and the remaining 5 percent containing only randomly dispersed stains of rust, coatings, and foreign matter.

SSPC SP 10 NACE No. 2 “Near White Blast Cleaned Surface”

RANDOM staining shall be limited to no more than 5 percent of each unit area of surface ... , and may consist of light shadows, slight streaks, or minor discoloration caused by stains of rust, stains of mill scale, or stains of previously applied paint.

ISO 8501-1 Sa 2 1/2 Very Thorough Blast Cleaning:
When viewed without magnification, the surface shall be free from visible oil, grease and dirt, and from mill scale, rust, paint coatings and foreign matter. Any remaining traces of contamination shall show only as slight stains in the form of spots or stripes.

HB 2.5 Very Thorough Hydroblast Cleaning (International Paint)
When viewed without magnification, the surface shall be free from visible oil, grease, dirt, loose rust, paint coatings and foreign matter. A brown-black discoloration of ferric oxide may remain as a lightly adherent thin film on corroded and pitted steel.

In conversations with major coatings manufacturers, Dr. Frenzel has come to understand that the coating manufacturers' technical staff are not including the brown-black discoloration of ferric oxide as part of the staining criteria. They are looking for stains of material other than black ferric oxide. Thus a WJ-1 or WJ-2 may be extremely mottled if the steel surface has been heavily corroded.

5.3.3 Thorough Cleaning, “Commercial Blast”

NACE No. 5- SSPC SP-12 WJ-3
WJ-3 surface shall be cleaned to a matte finish with at least two-thirds of the surface free of all visible residues (except mill scale), and the remaining one-third containing only randomly dispersed staining of previously existing rust, coatings, and foreign matter.

Notice that we are now including the idea that mill scale might remain on the surface. This is recognition of the types of projects in which WJ is used. The language is for staining, not for the coating itself. However, the marine industry is interpreting this to mean the coatings and foreign matter can remain on if it is dispersed.

SSPC SP- 6, NACE No. 3 Commercial Blast
Random staining shall be limited to no more than 33 percent_of each unit area of surface as defined, and may consist of light shadows, slight streaks, or minor discoloration caused by stains of rust, stains of mill scale, or stains of previously applied paint.

ISO 8501 Sa 2 Thorough Blast- Cleaning
When viewed without magnification, the surface shall be free from visible oil, grease and dirt, and from most of the mill scale, rust, paint coatings and foreign matter. Any residual contamination shall be firmly adhering.

HB 2 Thorough Hydroblast Cleaning (International Paint)
When viewed without magnification, the surface shall be free from visible oil, grease, dirt and from most of the rust, paint coatings and foreign matter. Any remaining contamination and staining shall be firmly adherent.

Tightly adherent coatings, mill scale and rust can remain in the ISO definition, but not in the SSPC/NACE definitions.

5.3.4 Brush off Blast, Removal of Loose Material

NACE No. 5/ SSPC SP-12 WJ - 4
WJ-4 surface shall have all loose rust, loose mill scale, and loose coatings uniformly removed.

SSPC SP- 7 Brush Off Blast
Tightly adherent mill scale, rust, and paint may remain on the surface. Mill scale, rust, and paint are considered tightly adherent if they cannot be removed by lifting with a dull putty knife.

ISO 8501 Sa 1 Light Blast Cleaning
When viewed without magnification, the surface shall be free from visible oil, grease, and dirt, and from poorly adhering mill scale, rust, paint coatings and foreign matter.

GLOBAL PERSPECTIVE

For WJ-1 "Clean to bare substrate" and WJ-2 "very thorough cleaning" specifications, the WAB and WJ appearance is dark compared to dry blasting. It may also be streaked from the drying of the water. This appearance is very normal and accepted by the coatings manufacturers. On older steel, heat marks, tooling, and dark stains in corrosion areas remain very visible with WJ. WJ accentuates those differences; abrasive blasting tends to make the surface "appear" uniform.

When VIS-4(I) was issued, the NACE/SSPC task group modified the language to accommodate both the adherent (ISO) and the percentage (NACE-SSPC) concepts and started to bring the European and United States philosophies closer together. Because of obstacles arising in the field in refurbishment projects, there was an immediate need for photographs depicting coatings removal. In January, 1997, after a review and selection of new photographs, the National Shipbuilding Research Program SP-3 Technical Advisory Chairman for Water Jetting Photographs requested an early revision of NACE No.5- SSPC SP-12 so that the language might reflect the retention of coatings. It was obvious from the selection of the photographs and the issuance of the Hempel's reference set that there was a wide gap between the language and the practice. In all of these cases, technical representatives of coatings manufacturers, owners, and experienced WJ contractors were involved.

The perception of percentage coverage is an unrecognized problem. Every experienced inspector thinks that he can tell what 5% and 33% coverage is. That simply is not true. This was very evident as the new photos were being screened.

Coverage is a topic to itself and is depicted in illustrations of 5% and 30% coverage from "The Book of Spots."[13] Each person views a surface differently. Whether the spots are sharp or diffuse, nearly the same color or contrasting colors, on a uniform, lightly profiled or a non-uniform, heavy pitted surface, will make a difference. Since 1996, Dr. Frenzel has been educating the experienced personnel first on the NSRP Technical Advisory Committee and subsequently the NACE/SSPC task group on percentage coverage. Figures 5, 6, and 7 illustrate three different representations of five percentage coverage.

In practice, the marine coatings industry embraced NACE No. 5/ SSPS SP-12 and immediately interpreted it to allow islands of tightly adherent paint to remain as compared to stains of paint because it is used in maintenance and repainting. The original "staining" language arose because solid particles don't get into the crevices. The paint remains as stains in the pits and crevices. In WJ without abrasive, intact coating remains on the top of the surface. The new photos under consideration where coatings are being removed all depict the retention of coatings. Coatings manufacturers have positively endorsed this position.

With the advent of computer digitization, new photos are also being considered for SSPC- VIS 2/ASTM D 610 "Standard Method of Evaluating Degree of Rusting On painted Steel Surfaces." The concept of percentages with large, medium, and small, pinpoint spots is a challenge because the appearance in pin point corrosion at 30% is that the entire surface is covered.

6. SUMMARY

The written definitions are similar in that they describe four visual cleanliness conditions. They differ with respect to the presence of mill scale and tightly adherent coating as compared to percentage staining. Based on the discussion of the task group members, it is the author's opinion that the current ISO photographs and the SSPC/NACE written definitions are inadequate to address the problems of retention of sound coatings in maintenance. The appearance of old metal surfaces cleaned by WJ without any abrasive is very different from those cleaned with abrasives.

There is no discrepancy when all coatings and rust layers are removed by WJ or WAB. However, WJ finds its forte in partial removal of coatings. It is the partial removal and spot blasting with WJ and WAB with soft abrasives that is forcing the adoption of new visual photographs and a revision of the written standards language. The WJ task groups of NACE, SSPC, and ISO are addressing this question. Water jet cleaning is bringing the European and United States standards organizations together into a coalition effort.

7. ACKNOWLEDGEMENTS

Thanks to International Paint, Jotun, Hempel's, Cavi-Tech Inc. for permission to use their photographs in non-commercial presentations. The members of the SSPC and NACE task groups have volunteered thousands of hours. Special thanks to Aqua-Dyne, Butterworth Jetting, Carolina Equipment & Supply, Flow Int., and NLB Corporation, Doug & June Koppang, Aulson Co., Cavi-Tech, Fluidyne, Freemyer Co., Hartman-Walsh Painting, UHP Projects, Valley Systems,, Leo Kosowan, Roland Hernandez, and Dan Bernard for support and discussion.

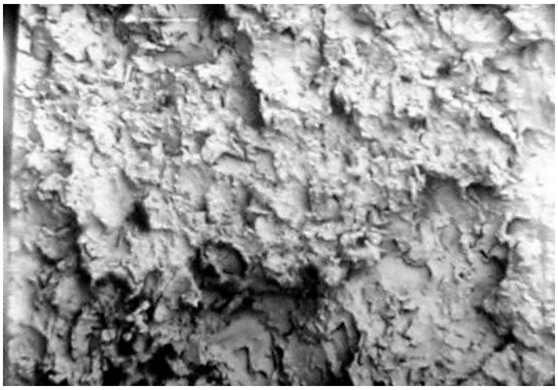

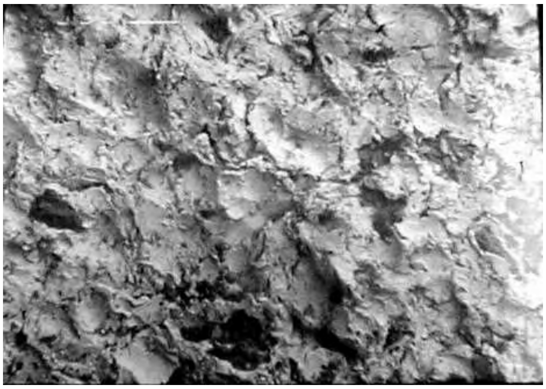

Figure 1. Steel Cleaned with HP WJ
130x magnification. Upper right white bar is 10 microns. originally blasted, then rusted, then cleaned with HP WJ to "white metal" WJ-1. You can see the original impacts of the abrasive. All crevices are cleaned; the dark areas are shadows.

Figure 2 Steel Cleaned with Abrasive
130x magnification. Upper right white bar is 10 microns. Originally blasted, then rusted, then blasted to white metal. You can see the impacts, the flattened surface. The dark areas are materials caught in the lower layer under the top surface.

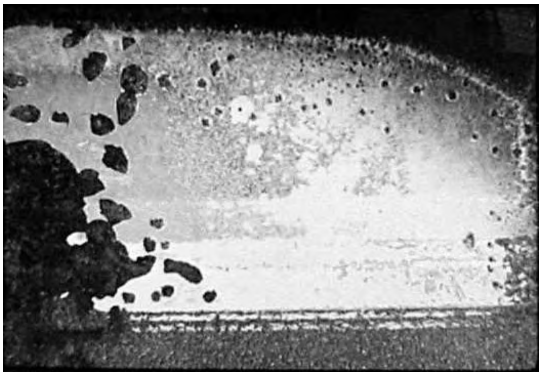

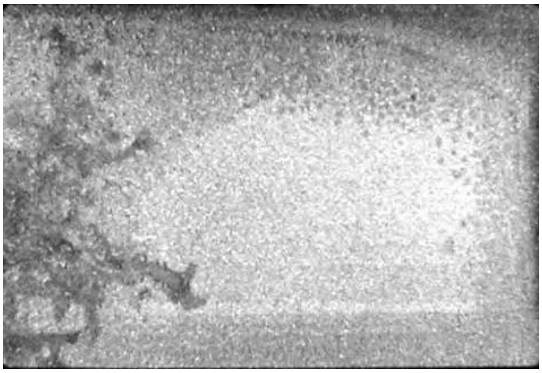

Figure 3 Multilayer Paint cleaned with WJ
Original size 6 x 10 inches
partial removal of paint. Complete removal on lower edge.

Figure 4 WJ-1 "Clean to bare substrate"
Upper right and left show typical examples of carbon stain and the appearance of corroded steel which is cleaned to WJ-1. The steel under the paint is uniform and appears "white" in this black and white printing.

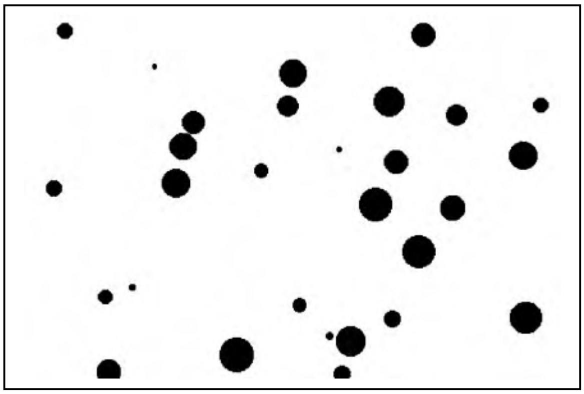

Figure 5 Five Percentage coverage-
Larger Spots in a Distribution of 1:10

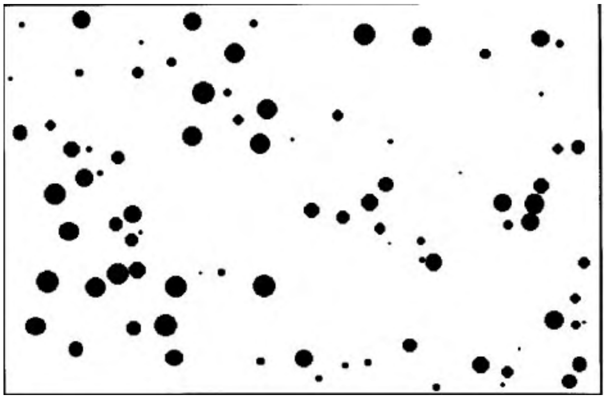

Figure 6 Five percentage coverage-
Smaller spots in a distribution of 1:10

Figure 7   Five percent coverage-
Uniform distribution of Very Small Dots.

---

[1] "Recommended Practices for the Use of Manually Operated High Pressure Water Jetting Equipment," WJTA, St. Louis MO

[2] SSPC-TR2/ NACE 6G198, SSPC/NACE Joint Technical Report, "Wet Abrasive Blast Cleaning," issued May, 1998. SSPC Tel: 412-281-2331

[3] Joint Surface Preparation Standard NACE No. 5/SSPC-SP 12; "Surface Preparation and Cleaning of Steel and Other Hard Materials by High- and Ultrahigh-Pressure Water Jetting Prior to Recoating,", issued 1995. NACE Tel: 281-228-6200 Separate document "Surface Preparation of Concrete" includes WJ cleaning of concrete.

[4] Vincent, L.D. , "Increasing the Value of Coatings", Proceedings of the SSPC 1998 Seminars, November, 1998, SSPC 98-11 "Failure Modes of Protective Coatings and Their Effect on Management," p. 125-128.

[5] VanKuiken, Jr., L.L., Byrnes, L.E., & Kramer, M.S., High Pressure Water Jet Method of Blasting Low Density Metallic Surfaces, U.S. Patent 5,380,564, Issued Jan. 10, 1995

[6] Taylor, Thomas A., "Surface Roughening of Metallic Substrates by High Pressure Waterjet," Surface & Coatings Technology, Vol. 76-77 (1995), 95-100

[7] Frenzel, Lydia M.; Nixon Jonell, "Surface Preparation using High Pressure Water Blasting," NACE Corrosion89, paper No. 397, April, 1989

[8] Materials Evaluation Laboratories, Claude Mount, January 1991, work performed for Shell Oil Company, Report number 9501

[9] Aldinger, Tom (Bechtel), Viswanath, Bala (Pacific Gas and Electric), Dick Vass (Vass Industries), SSPC 1994 Conference, Industrial Maintenance Coatings- Current Trends and Practices, "Water Blasting versus Abrasive Blasting for In situ Penstock Relining"

[10] Morcillo, M. & Simancas, J., JPCL, Sept. 1997, p. 40 "effects of Soluble Salts on Coating Life in Atmospheric Service" and G.C. Soltz., "The Effect of Substrate Contaminants on the Life of Epoxy Coatings Submerged in Sea Water," National Shipbuilding Research Program, March, 1991, task 3-89-2

[11] SSPC-VIS 4(I) NACE No. 7 "Interim Guide and Visual Reference Photographs for Steel Cleaned by Water Jetting, SSPC Pub. 98-07; NACE Item NO. 22016

[12] Howlett, Jr., J.J. and Dupuy, R., Ultrahigh-Pressure Water Jetting for Deposit Removal and Surface Preparation, Materials Performance (MP), No.1, Jan, 1993, p. 38

[13] Advisory Council, "The Book of Spots", depicting 1-30% coverage and 20% with different relative spot sizes. Computer generated to be exact.

10th American Waterjet Conference
August 14-17, 1999: Houston, Texas

EROSION OF STEEL SUBSTRATES WHEN EXPOSED TO ULTRA-PRESSURE WATERJET CLEANING SYSTEMS

R. K. Miller, G. J. Swenson
Thiokol Propulsion Division
Brigham City, Utah, U.S.A.

ABSTRACT

From 1985 to 1995, waterjet cleaning of reusable rocket motor hardware was accomplished using high flow (10 to 20 gpm), lower pressure (10,000 to 15,000 psi), fixed nozzle systems. Preliminary testing of ultra-pressure (40,000 psi), multi-orifice, rotary nozzle, waterjet systems showed significant improvement in removal rates for thin adhesives and paint systems. Prior to implementation of this new technology, testing was conducted to quantify erosion rates on steel substrates. This paper details erosion data from three different test plans and quantifies erosion rates of steel substrates when exposed to ultra-pressure waterjet cleaning systems. Data includes erosion rates from exposure to various possible failure modes of an automated cleaning system.

Organized and Sponsored by the WaterJet Technology Association

1. INTRODUCTION

Since the early 1980's waterjet cleaning of reusable solid rocket motor hardware was accomplished using high flow (10 to 20 gpm), lower pressure (10,000 to 15,000 psi), fixed nozzle systems. Preliminary testing of ultra-pressure (40,000 psi), multi-orifice, rotary nozzle waterjet equipment showed significant improvement in removal rates for thin adhesives and paint systems. However, the cleaning methods had to be relatively non-erosive in order to retain the required component design safety factors. Testing was conducted to quantify erosion rates on steel substrates. Erosion data from three different studies are included. Data includes erosion rates from exposure to various possible failure modes of an automated cleaning system.

1.1 Background

The three tests followed the same basic format. Initial testing determined the optimum cleaning parameters for the particular waterjet equipment being used. After optimum paint/adhesive removal parameters were established and verified, erosion testing was conducted using those established parameters. Erosion testing was conducted using 2.0" x 2.0" x 0.25" D6AC steel coupons, (D6AC is roughly equivalent to 4340, Hardness R_C 43 – 48). The coupons were weighed, using a calibrated 160-gram electronic balance, before and after waterjet exposure. Erosion rates were calculated based on weight loss, material specific weight, test coupon surface area and the number of exposure passes. These calculated erosion values assume even erosion over the entire surface of the coupon. Maximum erosion at any one location is dependent on the nozzle overlap pattern. Calculating erosion based on weight loss proved to be the only method sensitive enough to detect the slight erosion of D6AC steel by the established waterjet cleaning process. All erosion testing was conducted on bare metal coupons to simulate a 'worst case condition'. In addition, machine failure mode testing was conducted using 8" x 12" x 0.5" steel panels. Failure mode testing included zero nozzle rpm, zero sweep rate and combinations.

1.2 1992 Test Setup

The first test was conducted in 1992 using leased equipment, manufactured by Jet Edge, Inc., Minneapolis Minnesota. The system used for this test consisted of a Jet Edge Model 536® Intensifier pump, a Gyro-jet® nozzle rotator and a ten-jet modified 'S' pattern nozzle, using 0.012 in. diameter sapphire orifices. Maximum adhesive removal rates were obtained, and subsequent erosion testing was conducted, using the following parameters:

- Water Pressure: 36,000 psi (at the pump)
- Nozzle Speed: 1,000 rpm
- Nozzle Standoff: 1.0"
- Nozzle Angle: Normal to the surface being cleaned
- Sweep Rate: 70 inches per minute

1.3 1995 and 1998 Test Setup

The remaining tests were conducted using waterjet equipment manufactured by Flow International, Kent, Washington. The system used for these tests consisted of a FLOW EQ® Intensifier pump, a FLOW Model 2410® offset drive and a FLOW five-jet multi-radius housing, using 0.017 in. diameter sapphire orifices. Maximum adhesive removal rates were obtained, and subsequent erosion testing was conducted, using the following parameters:

- Water Pressure: 40,000 psi (at the pump)
- Nozzle Speed: 500 to 1,500 rpm (1,300 rpm nominal)
- Nozzle Standoff: 1.0" to 2.5" (2.5" nominal)
- Nozzle Angle: Normal to the surface being cleaned
- Sweep Rate: 30 to 60 inches per minute (60 ipm nominal)

2. OBJECTIVES

2.1 1992 Testing

The initial testing completed in 1992 was conducted to determine the feasibility of using ultra-pressure, rotary nozzle waterjet technology in the refurbishment of rocket motor components. Contaminant removal rates, substrate erosion, surface finish effect and effect on downstream bonding processes were compared to the established cleaning processes at the time. These processes included lower pressure (10 – 15K) waterblast and zirconium silicate gritblast.

2.2 1995 Testing

The 1995 testing was conducted to qualify a new automated ultra-pressure, rotary nozzle, waterjet system for use on space shuttle flight hardware. Data from the testing verified that the new system would safely and efficiently remove contaminants without damaging the hardware. This hardware was designed to be reused up to 20 times. Component wall thickness was designed with the assumption that each refurbishment would remove up to 0.001 in. of material from the steel substrate wall thickness.

2.3 1998 Testing

The 1998 testing qualified the same automated system for use on Minuteman III Stage 1 hardware. The task of the Minuteman Propulsion Replacement Program (PRP) is to remove old propellant, insulation and adhesives from the steel hardware and then to reline and reload the hardware. The Minuteman hardware was not designed for reuse and therefore has minimal allowances for erosion of the steel substrate. This testing verified that the minimum allowable erosion of 0.0001 in. would not be exceeded during the cleaning process.

3. DISCUSSION

3.1 Normal Operating Parameters Erosion

The established normal operating parameters for D6AC steel waterblast cleaning are as follows:

- Water Pressure: 40,000 psi (at the pump)
- Nozzle Speed: 500 to 1,500 rpm (1,300 rpm nominal)
- Nozzle Standoff: 1.0 to 2.5 inch (2.5 inch nominal)
- Nozzle Angle: Normal to the surface being cleaned
- Sweep Rate: 30 to 60 ipm (60 ipm nominal)

The aforementioned test studies implemented testing from which data was collected to evaluate material (D6AC steel) erosion during typical waterjet refurbishment operations. Figure 1 displays the average erosion calculated from the test data at varying number of exposure passes and also compares the erosion of waterjet cleaning methods to that of a previously used zirconium silicate media gritblast paint removal method.

All normal operating parameter erosion testing was conducted using 2.0” x 2.0” x 0.25” D6AC steel coupons. Each test coupon was weighed before and after exposure to the waterjet cleaning process. The erosion values obtained from the test data were determined by calculating the weight difference of each test sample (before and after waterjet exposure) and then dividing by the material (D6AC steel) specific weight and coupon exposed surface area. Appropriate conversion factors were also implemented to determine the erosion (mils) of D6AC steel. The following equation was implemented:

$$\frac{\Delta W}{Area} \times \frac{1}{0.283} \times \frac{1}{453.59} \times 1000 = Erosion\,(mils)$$

Where: ΔW = Test sample weight difference (grams)
Area = Surface area exposed to waterjet (in.^{2})
0.283 = Specific weight of D6AC steel (lb./in.^{3})
453.59 = Conversion factor (grams/lb.)

Erosion testing conducted at the established normal operating parameters shows that the level of erosion of D6AC steel is minimal (< 0.02 mils). Also, in comparing the single pass waterjet erosion of 0.009 mils, which is typical of the current paint removal operation, to that of the zirconium silicate paint removal erosion of 0.7 mils, the level of material erosion is decreased by approximately 98%.

Another interesting condition that was observed during the testing is presented in Figure 2. The rate of D6AC steel erosion (inches/pass) when exposed to the ultra-pressure waterjet cleaning process is not linear. The erosion rate is only slightly different between the first and second exposures (~ 11%) while the third and subsequent exposures display a much larger variation in the erosion rate. In fact, the data show that the initial exposure removed up to 88% more material than the subsequent exposures.

3.2 Failure Simulation Erosion

Ultra-pressure waterjet process failure simulation testing was conducted to evaluate the typical erosion of D6AC steel during a specific process parameter failure and assess the need for critical parameter control limits. Critical parameters are defined as those parameters that have the greatest effect on material erosion. The critical parameters are identified as Water Pressure, Nozzle Rotation, Nozzle Standoff, and Sweep rate (Rate of material past the nozzle).

All failure simulation testing was conducted using 8” x 12” x 0.5” steel (D6AC) panels. Erosion values were determined by direct measurement of the depth of the eroded pit or groove (see Figures 3, 4, and 5).

Dwell time testing was conducted to simulate complete failure of D6AC steel hardware movement during exposure to the ultra-pressure waterjet spray (0 rpm nozzle rotation, 0 ipm sweep rate). This simulated stall causes pits to be eroded in the surface of the steel hardware. Dwell testing was conducted during both the 1992 and 1998 tests. Figures 6 and 7 present dwell testing erosion rates (inches/exposure time) for D6AC steel. Nozzle standoff was maintained at one inch for the testing conducted in 1992. During the 1998 testing the nozzle standoff was varied between 1 inch and 2.5 inches. The maximum erosion rate experienced was 0.0017 in./sec.

Additional failure simulation was conducted to evaluate D6AC steel erosion when a single process parameter failure is realized. Two such simulation tests were performed. The first was a simulation of sweep rate failure only by holding the sweep rate to 0 ipm and varying nozzle standoff (1 to 2.5 inches) and nozzle rotation speed (500 to 1,500 rpm). Second, a simulation of nozzle rotation failure only was performed by holding the nozzle rotation speed to 0 rpm and varying the nozzle standoff (1 to 2.5 inches) and sweep rate (30 to 60 ipm). The erosion rates resulting from the sweep rate failure simulation testing and the nozzle rotation failure simulation testing are presented in Figures 8 and 9 respectively.

Based on the failure simulation testing erosion rates, any prolonged exposure of D6AC steel to the ultra-pressure waterjet system will cause significant material erosion. Thus, it is imperative that automated waterjet systems be designed with devices to control and monitor critical process parameters.

4. CONCLUSIONS

Erosion testing conducted at the established normal operating parameters shows that the level of erosion of D6AC steel is minimal (< 0.00002 inch). This level of erosion is 98% less than that caused by the zirconium silicate, dry abrasive, blast system previously used for paint and adhesive removal.

Multiple exposure testing showed that the erosion caused by the waterjet process is not linear. The data show that the initial exposure removed up to 88% more material than subsequent exposures.

Failure simulation testing shows that any prolonged exposure, at zero nozzle rpm and / or zero sweep rate, will cause significant material removal, (0.0017 in./sec.).

To prevent unacceptable erosion of steel substrates it is essential that automated systems be designed with devices to control and monitor the critical processing parameters. These systems must also be equipped with the means to automatically and immediately shut off the flow of high pressure water when established critical parameter limits are violated.

5. REFERENCES

Miller, R.K., "Evaluation of Erosion of D6AC Steel Using The High Pressure, Rotary Nozzle Waterblast System At H-7 For Minuteman III Stage 1 Propulsion Replacement Program", Thiokol Propulsion Division, Brigham, Utah, Document No. TR11407, December 14, 1998.

Schiffman, R.L., "Final Report For CTP-0352, High Pressure Waterjet Cleaning Qualification", Thiokol Propulsion Division, Brigham, Utah, Document No. TWR-66639, September 15, 1995.

Swenson, G.J., "RSRM Paint and Chemlok Removal Using An Ultra-Pressure, Rotary Nozzle Waterblast System; The Effect On Surface Finish, Erosion, And Bonding", Thiokol Propulsion Division, Brigham, Utah, Document No. TWR-61757, March 1992.

6. NOMENCLATURE

gpm	gallons per minute
in.	inch
ipm	inches per minute
K	1,000
lb.	pound
mil	$1x10^{-3}$ inches
psi	pounds per square inch
rpm	revolutions per minute

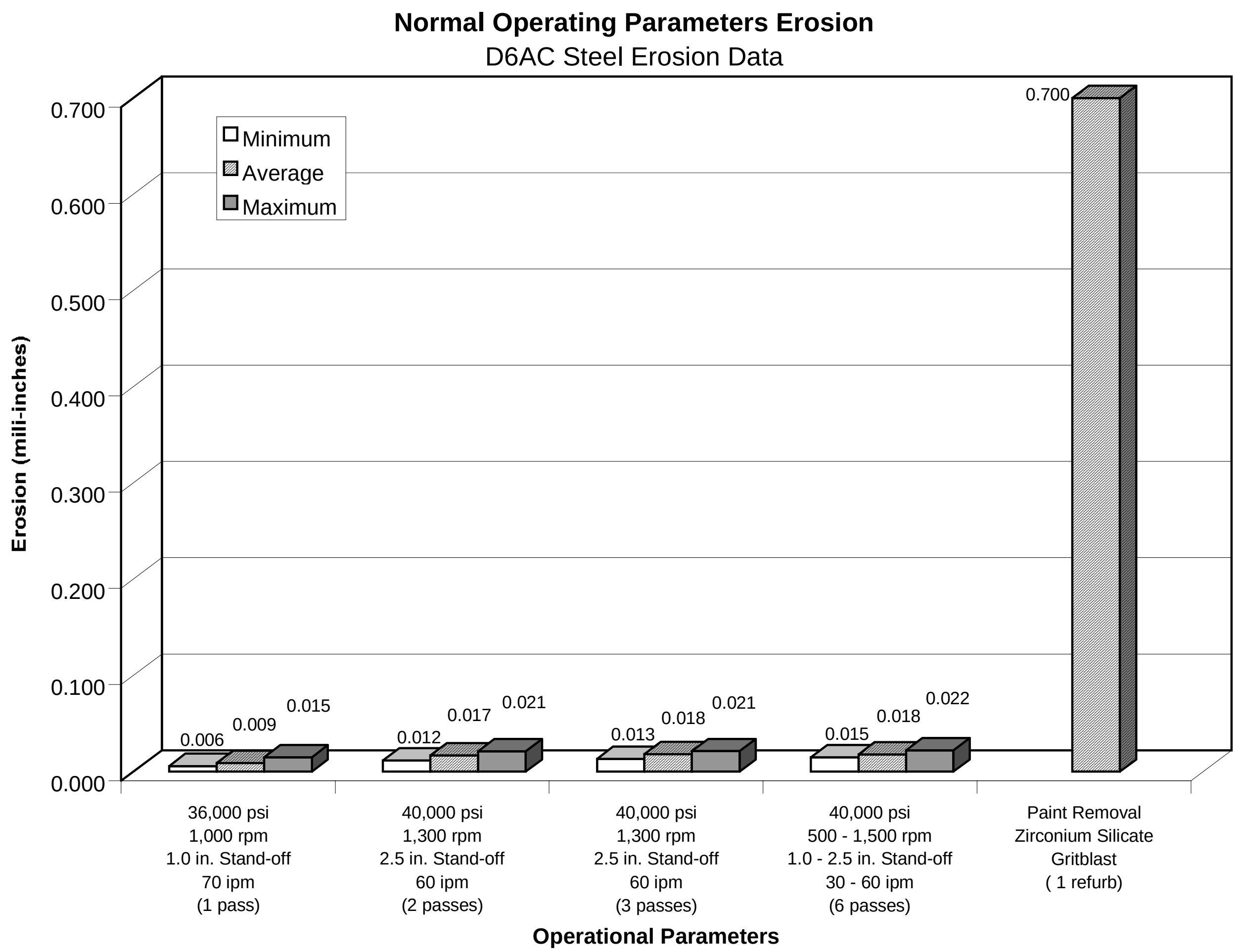

Figure 1. Waterjet Erosion versus Gritblast Erosion

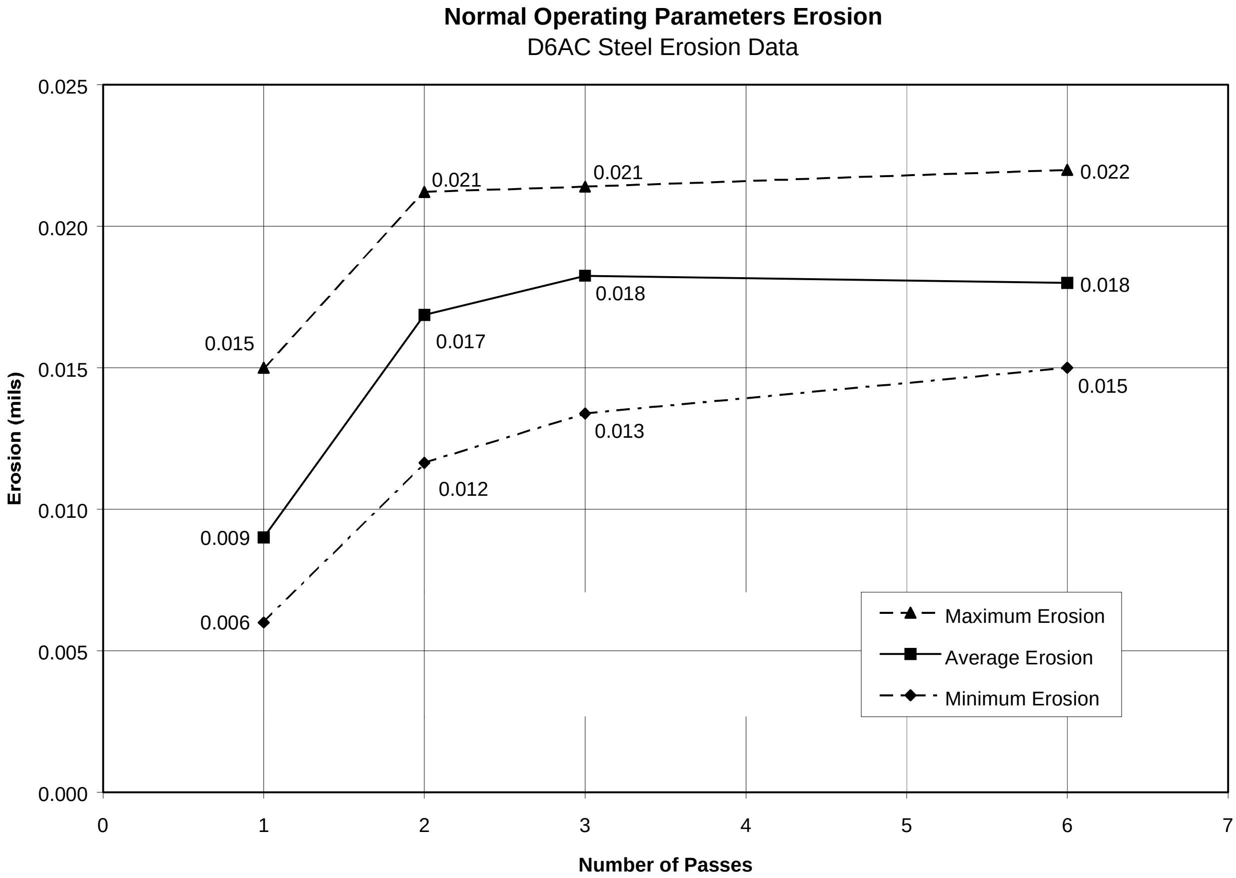

Figure 2. D6AC Steel Erosion Variation per Waterjet Exposure

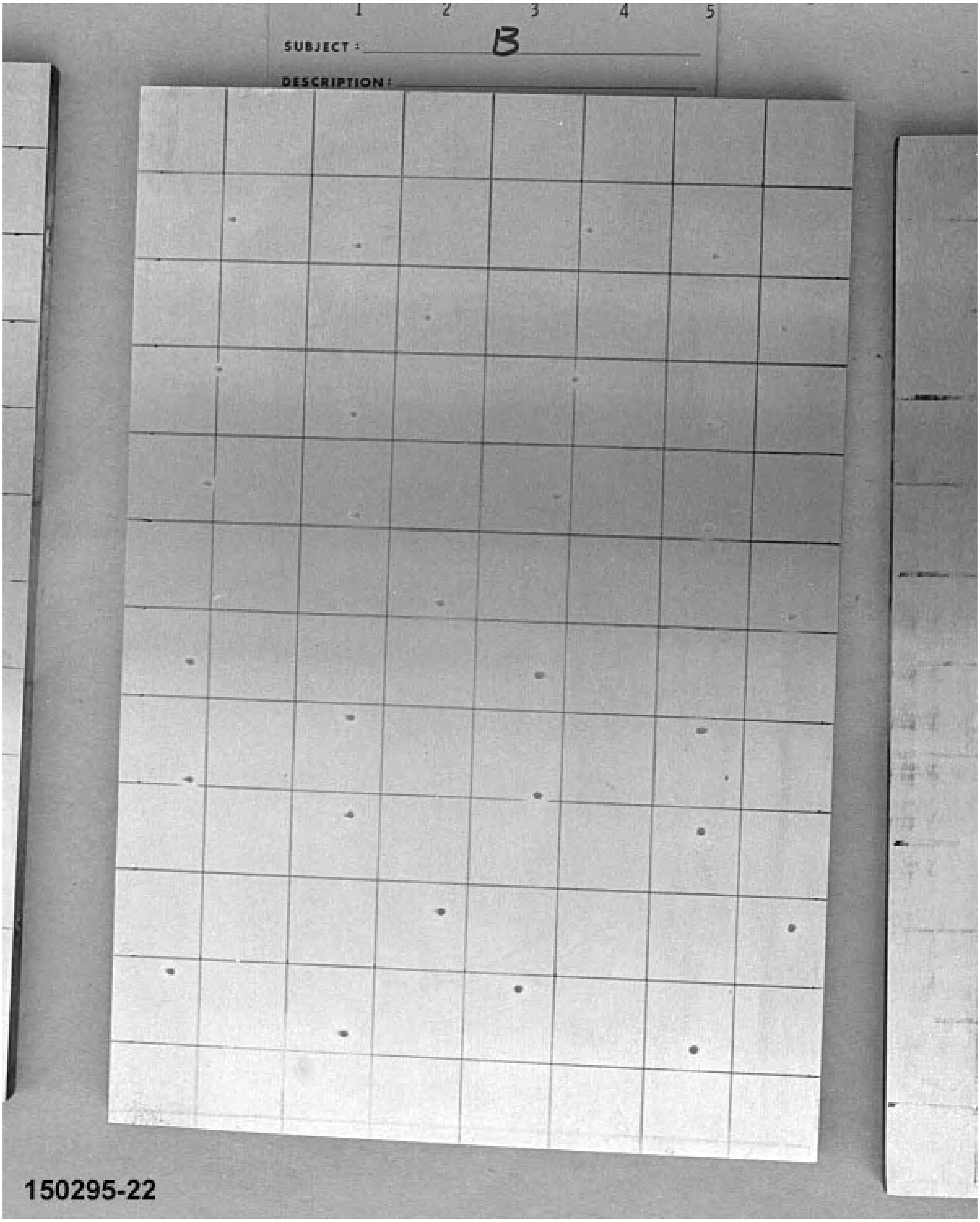

1998 Testing: 0 rpm nozzle rotation, 0 ipm sweep rate

Figure 3. Dwell Time Failure Simulation Test Panel

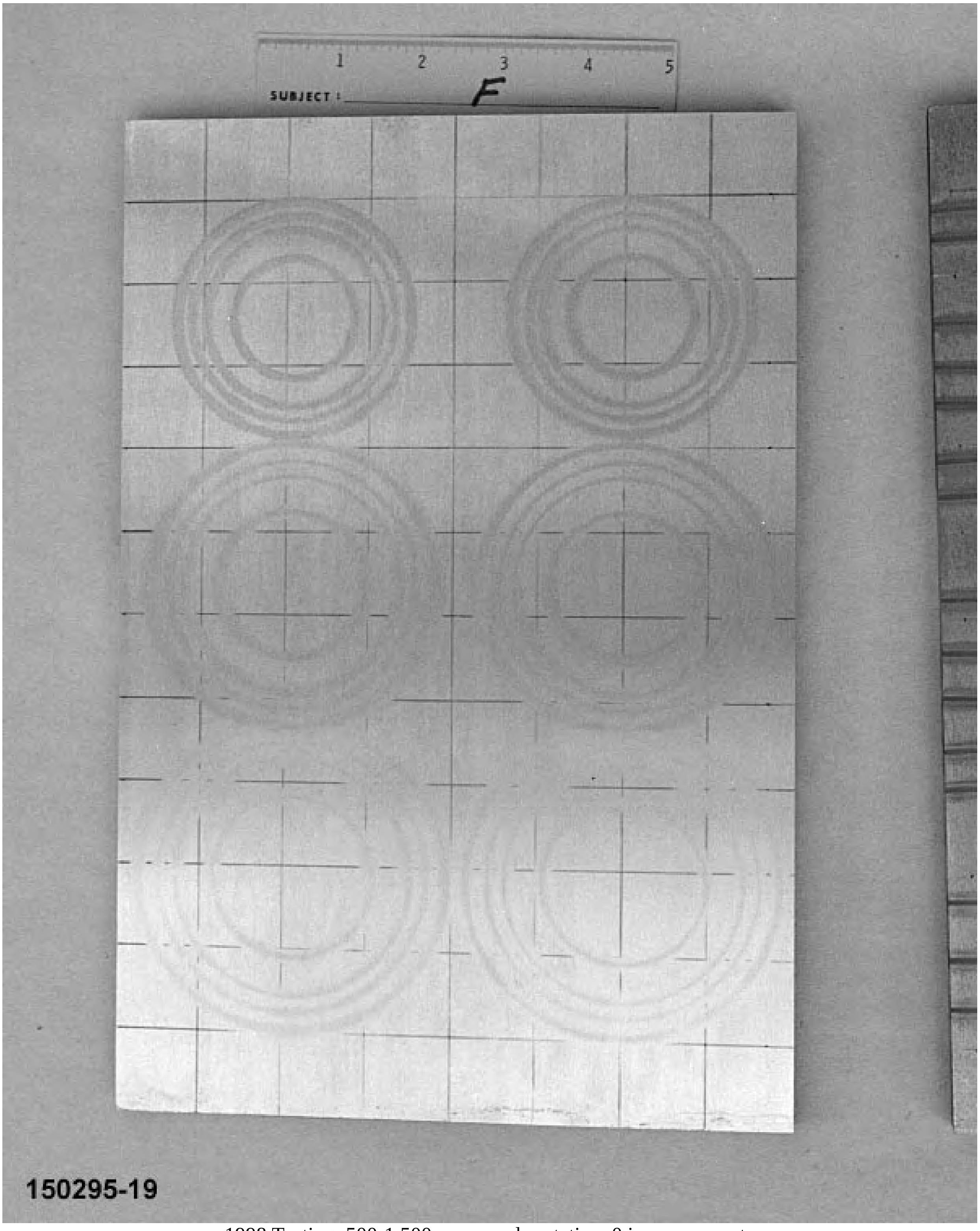

1998 Testing: 500-1,500 rpm nozzle rotation, 0 ipm sweep rate

Figure 4. Sweep Rate Failure Simulation Test Panel

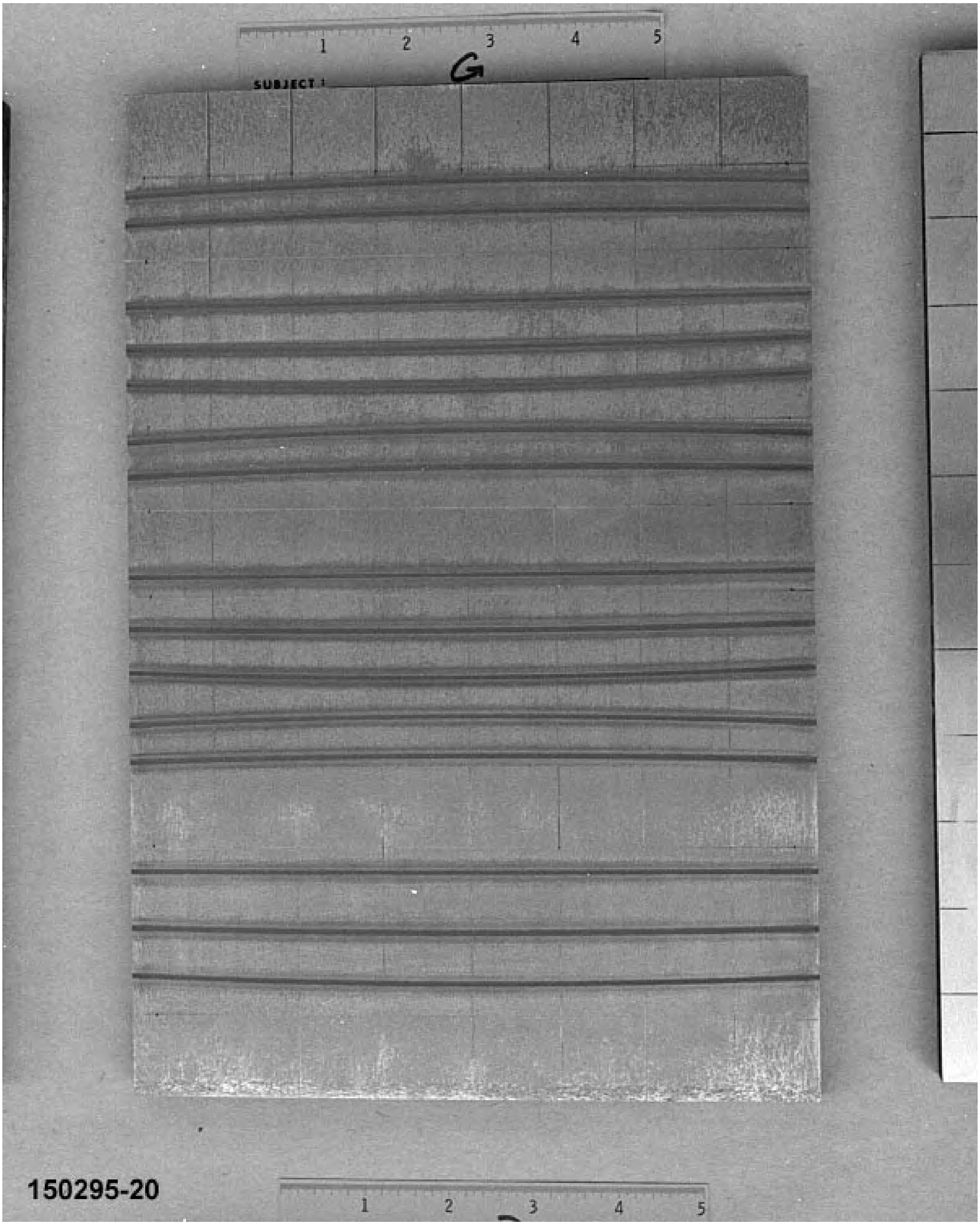

0 rpm nozzle rotation, 30 – 60 ipm sweep rate

Figure 5. Nozzle Rotation Failure Simulation Test Panel

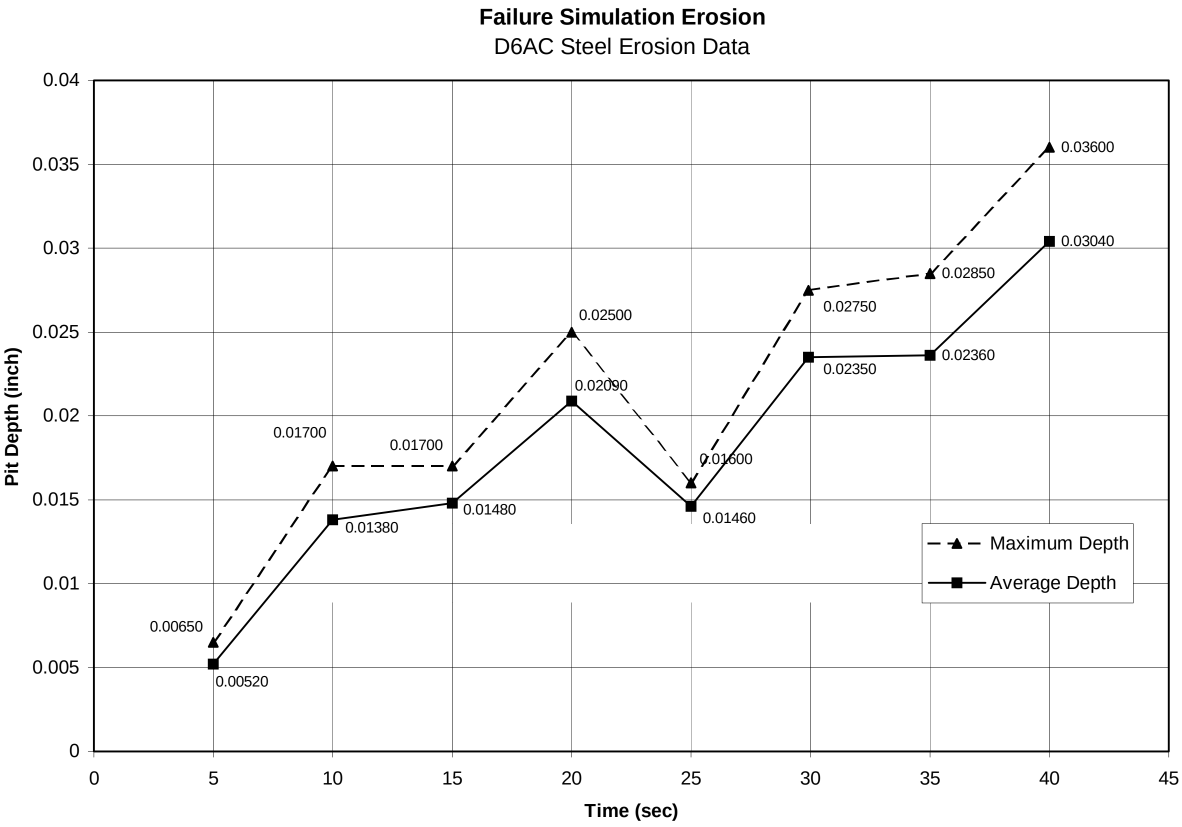

Figure 6. 1992 Failure Simulation Erosion Data (Dwell Time vs. Erosion)

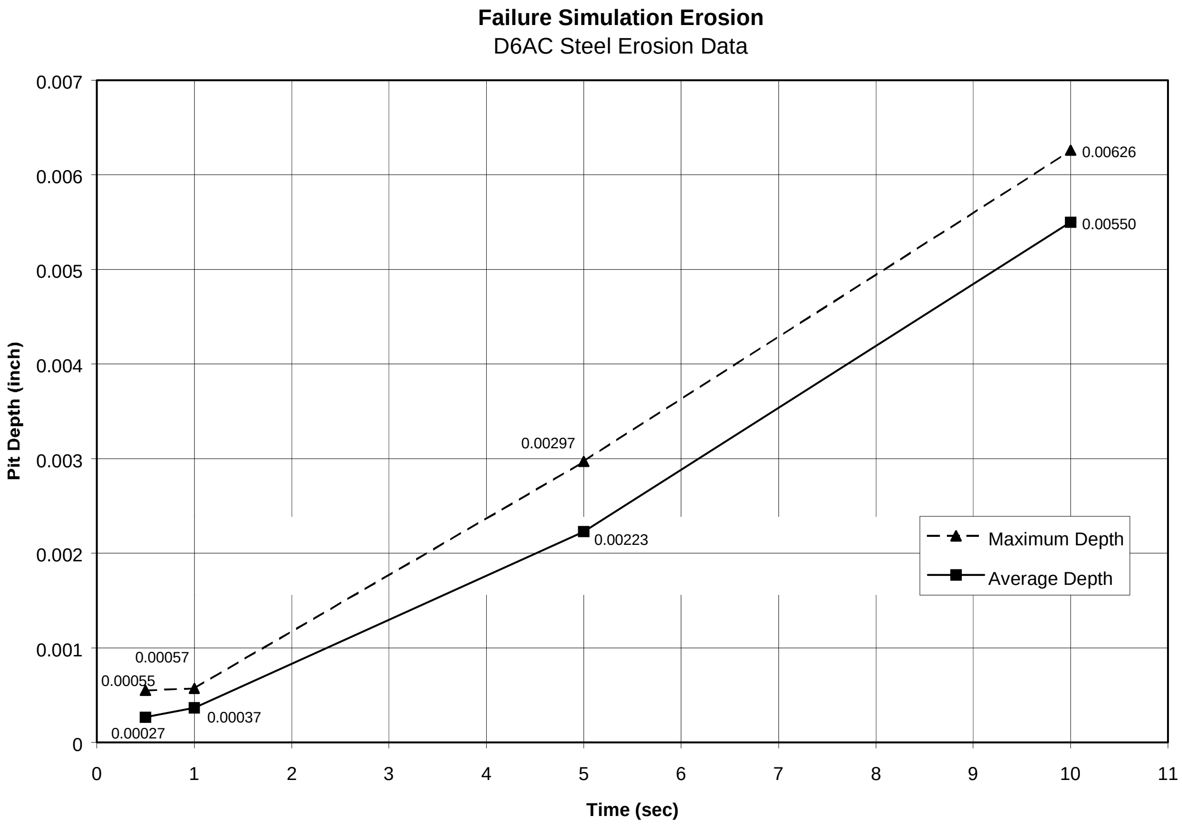

Figure 7. 1998 Failure Simulation erosion Data (Erosion vs. Dwell Time)

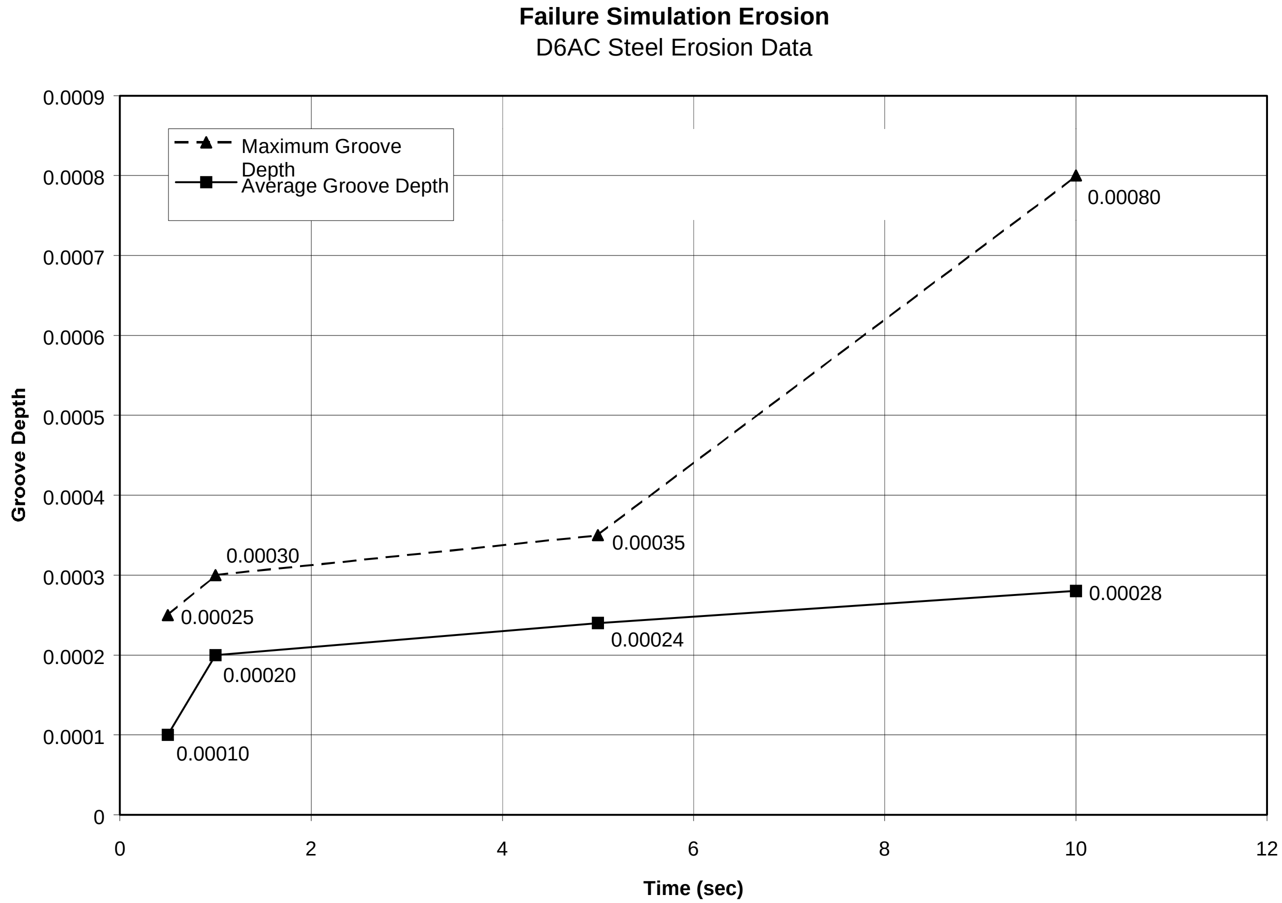

Figure 8. Sweep Rate Failure Simulation Erosion Rates

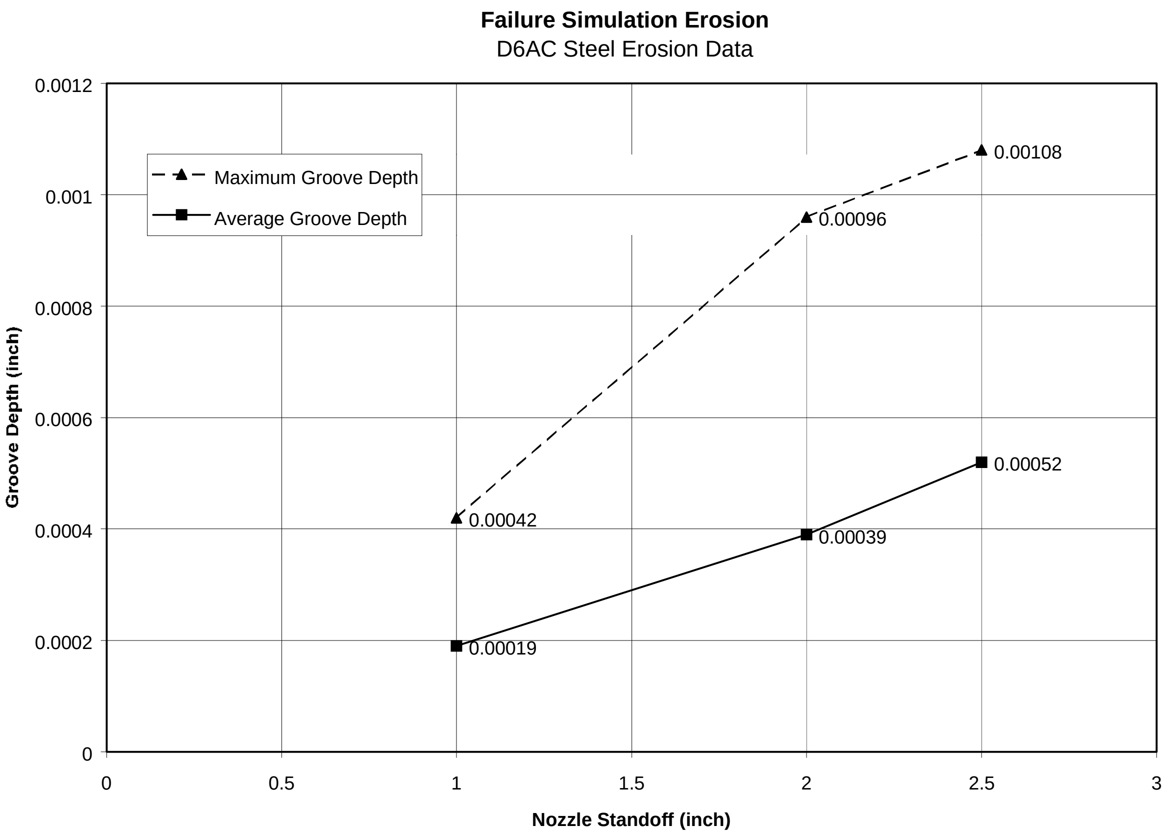

Figure 9. Nozzle Rotation Failure Simulation (Erosion vs. Nozzle Standoff)

10th American Waterjet Conference
August 14-17, 1999: Houston, Texas

Paper **53**

REMOVAL OF HARD COATINGS FROM THE INTERIOR OF SHIPS USING PULSED WATERJETS: RESULTS OF FIELD TRIALS

M. M. Vijay, W. Yan, A. Tieu and C.Bai
$^{V}L_{N}$ Advanced Technologies, Inc.
Gloucester, ON., Canada

S. Pecman
Department of National Defence
Hull, Quebec, Canada

ABSTRACT

A pre-commercial pulsed waterjet machine (FluidPulse™) was designed, manufactured and field tested for the Department of National Defense (DND) of Canada. The purpose of the machine was to remove several types of hard coatings (Alkyd Marine Enamel, Amercoat 68HS, International Intertuf KTE, etc) from the interior of HMC (Her Majesty's Canadian) naval ships. Prior to manufacturing the machine, extensive work was conducted in the laboratory using ultrasonically modulated high-frequency (20 kHz) pulsed waterjets. In this paper, a brief summary of the design, laboratory work and, highlights of the field trials are presented. Field trials were conducted on the HMC ship "Halifax", in dry dock at Halifax, Canada. Its potential was also demonstrated in a private dockyard on the St-Lawrence Seaway at Les Mechins, Quebec, Canada. It is shown that the machine met all the contractual requirements (portability, mobility, etc) and, achieved a removal rate of 3.2 to 4.5 m^2/hr (≈ 34 - 48 ft^2/hr), in excess of the specified value. These results were achieved at a pressure and hydraulic power in the range respectively of 31 - 41 MPa (≈ 4,500 - 6,000 psi) and 12 - 16 kW (≈ 16 - 21 hp). Problems encountered during the field trials are also reported.

Organized and Sponsored by the WaterJet Technology Association

1. INTRODUCTION

The front and rear views of the forced pulsed waterjet machine are shown in Figs. 1 and 2 respectively. $^{V}L_{N}$ Advanced Technologies obtained the contract to design, manufacture and field test the machine for the removal of hard coatings from the Department of National Defense (DND) in September 1998. The contract was awarded based on the extensive previous work done in the Waterjet Laboratory of the National Research Council of Canada {Puchala & Vijay (1984), Vijay (1992), Vijay, et. al. (1993), Vijay & Foldyna (1994), Vijay, et.al. (1995), Vijay, et.al. (1997), Vijay (1998a, 1998b)}. This work had consistently shown that low pressure (≈34.5 MPa), high-frequency (≈15- 20 kHz) forced pulsed waterjets can be used to cut metals {Vijay & Foldyna (1994)}, rocks (Vijay, 1998a) and to remove several types of coatings {Vijay, et.al. (1997, 1998b)}. The DND issued a statement of work (SOW) based on "Requirements Definition" which is summarized in **Appendix A**. Prior to manufacturing the machine, arrangements were made to visit the HMC ship, "Iroqois" which was being refurbished at Lauzon, Quebec. During this visit, the operations that were in progress for removing the coatings from top deck to several areas in the bilge were observed and photographed. Measurements of the doors in bulkheads and hatches were taken. "Requirements Definition" was developed based on the discussions held with several operators who were using various techniques (needle guns, grinding wheels, etc.) to remove the deteriorated coatings and other technical staff.

In this paper the following topics are discussed: (i) description of the machine, (ii) laboratory test results obtained with the ultrasonic gun, (iii) field trials and (iv) conclusions and recommendations. It should be pointed out that no discussion on: (a) the basics of the pulsed jet technique, (b) characteristics of the coatings, (c) mechanism of material removal, etc., are given in this paper as these have already been reported by Vijay (1992), Vijay & Foldyna (1994), Vijay, et.al. (1993, 1995, 1997) and Vijay (1998a, 1998b). However, for the sake of completeness, the basic configuration of the nozzle body used in the hand-held gun is shown in Fig. 3. As the water flows through the nozzle, the vibrating tip modulates the flow and generates high-frequency forced pulsed waterjets {Vijay, et.al. (1995)}. All the variables indicated in Fig. 3 influence the performance of the machine {Vijay & Foldyna (1994)}.

2. DESIGN AND DESCRIPTION OF THE MACHINE

The manufacture of the forced pulsed waterjet machine was completed in the 1st week of March 1999. It was manufactured according to the contractual specifications summarized in **Appendix A**.

2.1 General Description

The machine, general views of which are illustrated in Figs. 1 and 2, basically consists of a pump, an ultrasonic power generator with a converter {piezoelectric transducer; a magnetostrictive transducer can also be used (see Vijay, 1998b)}, a high-pressure dump gun, a high-pressure hose and accessories which ensure safety of the operator. The pump is rated to deliver a water flow rate of 22.7 litre/min (6 usgpm) at a maximum pressure of 41.4 MPa (6000 psi). The ultrasonic power generator has a capacity of 1.5 kW of output at a resonant frequency of 20 kHz. All components, except the gun, are enclosed in an aluminum cabinet. In order to comply with the “requirements definition” (**Appendix A)**, the components were selected carefully and tested before incorporation into the machine

The water, air and electrical requirements are grouped into three major systems as input, output and control. In order to ensure safety (that is, to avoid confusion), all inputs are located at the rear panel (Fig. 2) and the outputs at the front panel (Fig. 1) of the machine. The description of each, including the gun, is given in the following **Sub-sections**.

2.2 Inputs

The system requires a water source to provide a flow of 22.7 litre/min (6 usgpm). A city water system is adequate for this purpose. However, a source capable of supplying 30 litre/min (≈8 usgpm) of water is recommended in order to prevent damage due to cavitation in the inlet ports of the pump. The system also requires a compressed air source to provide air to cool the piezoelectric converter. Excessive temperature rise of the converter will deteriorate its operation or, damage it permanently.

As specified in the SOW, the machine requires a 3-ph, 440 V and 30 amp electrical power source to run the pump at its full capacity. All the three inputs are located in a recess at the bottom right of the rear panel of the machine (Fig. 2) and are provided with quick connects for ease of connection and disconnection of the electrical cable, air and water supply hoses.

2.3 Outputs

The outputs consist of (a) high-pressure water up to 41.4 MPa and (b) a shielded coaxial cable, enclosed in an air hose. The fittings and adapters for these outputs are located in a recess at the bottom left corner of the front panel (Fig. 1) and, once again, are provided with quick connects as required by the SOW. The high-pressure water is transported through a high-pressure hose to the gun where the modulation of the stream to generate high-frequency pulses of water takes place (Fig. 3). Air, purified and dried through a filter system installed in the machine, flows in the annulus around the coaxial cable in the hose. This cable-hose assembly is connected to the gun to provide air to cool the converter. The shielded cable carries high-voltage, high-frequency electric pulses to the converter which in turn sets up mechanical oscillations in the nozzle.

2.4 Control Panel

The control panel is at the front of the machine and contains all the switches and the pilot lights to indicate whether a particular component is on or off (Fig. 1). The main switch supplies the electric power to all the components. The pressure gauges for measuring the air pressure, water inlet pressure and the pump outlet pressure are also located on the front panel.

2.5 The Gun

As specified in the SOW, a hand-held gun was designed and manufactured for the removal of the coatings by an experienced operator. It consists of a 1.22 m (≈ 4 ft) long barrel on which the ultrasonic converter and the nozzle are mounted (see Fig. 11). It is in the nozzle that the modulation of the water stream takes place to produce the high-frequency pulsed waterjets (Fig. 3).

3. DESIGN CONSIDERATIONS

Right from the outset, in designing the machine all the requirements stated in the SOW, were taken into account. The most significant feature of the machine is the safety considerations, of both the operator and the machine itself. Other design features of the machine include ease of operation, transportation, mobility on the ship, etc.

3.1 Safety

One of the most important considerations in the design of any high-pressure waterjet equipment is the safety of the operator. In designing the pulsed waterjet machine, the guidelines published by the US Water Jet Technology Association (WJTA, 1994) were strictly followed. All high-pressure and electrical components in the machine, if operated properly, were designed to fail safely. The location of the clearly visible instrumentation cluster with the pilot lights at the front panel is an indication of the concern for safety. As a further example, the ultrasonic system in the machine will not be powered unless air supply is turned on and, the gun is pressurized with water. For this reason pressure switches were incorporated to detect the air and water pressures. If the conditions for safe operation are not met, the ultrasonic power generator would be turned off automatically.

3.2 Operating Considerations

Normally in high-pressure waterjet applications, generally presence of two individuals is recommended (WJTA, 1994). However, the machine was designed so that it could be operated by a single, well-trained and well-experienced individual. The operator can rely on the instruments and pilot lights on the front panel to make any decision regarding the operation. Other hazard is the splashing water. This can be prevented by the provision of an appropriate shield at the nozzle.

3.3 Transportation Considerations

Since the machine was specially designed for use in the interior of HMC ships, its size and weight fully met the specifications stated in the SOW. The dimensions and weight were such that it could be moved around the ship quite easily. The input and output fittings were all designed to be quick connect so that when the machine is transported from one place to another, the hoses and cables could be detached and transported separately. This facilitates its movement on board the ship from deck to deck or, from one location to another on the same deck.

3.4 Laboratory Investigation

The purpose of the laboratory investigation was to find the optimum combination of parameters for each type of coating using the hand-held gun designed in parallel with the machine. The contract stipulated a removal rate of 2.32 m^2/hr (25 ft^2/hr) for all the coatings stated in the SOW (**Appendix**

A). The coatings were on steel panels (30.5 X 30.5 X 0.32 cm) abrasive blasted to SSPC-SP10. The average blast profile was 0.064 mm (2.5 mil).

The tests were conducted using a nozzle-piezoelectric converter assembly powered by an ultrasonic generator capable of delivering 3.0 kW. However, it was set to operate only up to 1.5 kW, the rated power of the unit in the machine. The diameter of the nozzle used in the gun was 1.37 mm.

Two kinds of tests were conducted in the laboratory: (a) using the X-Y gantry where standoff distance and traverse speed could be set precisely (useful for robotic controlled operations) and, (b) hand-held tests. In each test, the area removal rate was calculated. As the rated pressure of the machine was 41.4 MPa (6,000 psi), most of the tests were conducted at this pressure {**note:** in the field, the pressure was only 31 MPa (4,500 psi)}.

Results obtained on all types of coated samples were almost similar {see also, Vijay (1998b)}. For the sake of illustration, the area removal rates achieved for AMERCOAT 68HS are depicted in Fig. 4. These results clearly show that: (i) the area removal rate depends strongly on the traverse speed, (ii) it is somewhat insensitive to variation in standoff distance in the range from 18 mm (≈ 0.7 in) to 32 mm (≈ 1.25 in). This is encouraging because in hand-held operations the operator may not be able to maintain a steady standoff distance and, (iii) the rates of removal achieved under controlled conditions (that is, using the X-Y gantry) exceeded the rates specified in the contract.

For all the samples tested, the quality of the substrate was also examined. The quality was considered to be good when all layers of the paint, including the primer, were completely removed by the jet. It was deemed to be poor when some paint (or primer) was left or, the base metal was damaged. Fig. 5 shows typical appearance of substrate of a panel from which all the three layers of coatings (1-GP-48, 1-GP-61 & 1-GP-61) were removed. Tests were conducted consecutively side-by-side at P = 30.6 MPa (≈ 4,400 psi), V_{tr} = 10 m/min and S = 38.1 mm (1.50 in). As can be seen clearly, a smooth substrate was achieved with the pulsed waterjet. Also, an area removal rate of 3.2 m^2/hr (≈ 34 ft^2/hr) was achieved.

In preparation for the field trials, several tests were conducted by one of the staff members (not experienced) using the hand-held gun. For the sake of illustration, a single photograph is shown in Fig. 6 (non-skid AMERCOAT 68 HS). Although close to bare metal finish was achieved, some streaks of top thick layer remained. The mean area removal rate was about 1.2 m^2/hr (≈ 13 ft^2/hr). It is believed, however, that once appropriate operating conditions are set, an experienced and skillful operator would achieve the specified rates of removal and the required surface finish without any difficulty.

In summary, the laboratory investigations indicated: (i) All coatings including the primer could be removed with the pulsed waterjet at a pressure in the neighborhood of 34.5 MPa, (ii) The optimum standoff distance was in the range of 18 to 32 mm which provides some flexibility to the operator in hand-held operations, (iii) The maximum area removal rate including the primer was of the order of 4.5 m^2/hr (48 ft^2/hr) and could be increased further by increasing the traverse speed, (iv) A favorable surface profile (0.064 mm; 2.5 mil) for strengthening the adhesion between the substrate and fresh coating could be achieved by employing appropriate operating parameters, (v) The pulsed waterjet machine could remove several types of coatings with only minor variations in the operating parameters, (vi) Operation at low pressures (≈ 34.5 MPa; 5,000 psi) would make it safe and economical compared to the ultra-high pressure continuous waterjet (NLB, 1997) and, (vii) Since only pure (tap) water is used with no need of any agents to soften the coatings, toxic chemicals, abrasives, etc., it would be ecologically congenial.

4. FIELD TRIALS

4.1 General Remarks

The objectives of the field trials are stated in the SOW (**Appendix A**). Field trials were conducted at CFB Halifax, Nova Scotia, on the ship HMC Halifax Patrol Frigate. On the return trip to Ottawa, the potential of the machine was also demonstrated at a private dockyard at Les Mechins (Verreault Industries), Quebec. It should be pointed out that, due to bulkiness of the waste water collection and treatment system (see Fig. 15), it was not transported along with the machine to Halifax. Instead, it was deemed adequate to rent a wet vacuum system to collect the waste water for analysis later in Ottawa.

4.2 Highlights of the Field Trials

4.2.1 Transportation

As the field trials were scheduled to take place on March 10 at Halifax, the machine was loaded onto a F-250 Ford Pickup Truck (see Fig. 7) on the 8th. The outside temperature was -17^{o}C with strong winds. Adverse weather conditions prevailed throughout the trip, varying from snow to freezing rain, sleet and torrential rain with strong winds. Nonetheless, it was possible to arrive at the docks in Halifax at 13.30 hrs on the 9th as required by the navy.

4.2.2 Loading the Machine on to the Ship

The weather at Halifax was also quite hostile with freezing rain on the 1st day and, downpour on the day of the trials with strong winds. While waiting for the fork lift, a tour of the Halifax Patrol Frigate was made so that a work plan could be prepared. This was particularly important in view of the fact that the field operations were required to be conducted to the strict time schedules of the staff at the dock (crane operators worked till 15.00 hrs and the DND staff and contractors till 16.00 hrs). As the crane operators were not available on the 9th, the machine was prepared to be loaded on to the deck on the 10th. At 8.00 hrs on the 10th, it was moved by a fork lift to a loading bay. After some delays, the machine was lifted relatively easily by a crane and placed on the main deck (Fig. 8). It was then pushed through the door of the main hangar to the deck on the bow of the ship where the tests were planned to take place. Icy conditions remained on some parts of the deck.

4.2.3 Mobility

Figure 9 shows that the machine could be easily moved through the main hangar by only one person.

Figure 10 shows that it could be easily maneuvered through the doors in the bulkheads, with a little assistance by a second person to push over the ramps (about 15 cm high). Figure 11 shows the final location of the machine ready to be connected to air, water and electric power supplies.

4.2.4 Electric Power Source

The electric motor required a source of 460V, 3ph, 30 amps for satisfactory operation. Initially, however, this was not available close to the machine. A 25 amp source was available, but it was not satisfactory. As the electricians required more time to connect the machine to the right source of power, testing was delayed until 13.30 hrs. During this time, since the machine was on the open deck, it was exposed to severe rain storm. When the machine was finally wired for running, it was about 13.45 hrs.

4.2.5 Trials

While waiting for the electrical power supply, a wet vacuum cleaner and a bale sorbent boom (tube socks) were obtained from the local suppliers. The purpose of the tube socks was to prevent the water from flowing over the edges of the deck on to the ground (see Figs. 12 and 13). Although an experienced water blasting operator was standing by, most of the tests were conducted by a staff member of VLN. The deck, which was in the process of being refurbished, had many areas covered with rust (Fig. 12). When the machine was started, rusty and loose paint skins were easily blasted off in large chunks with the continuous jet at 31.0 MPa (4,500 psi). When the ultrasonic power was turned on, for a few moments the pulsed jet removed the primer exposing the bare white metal (Fig. 12). However, continued testing to remove larger areas showed that the jet was no longer pulsed, that is, ultrasonic power was not reaching the tip in the nozzle. While attempts were in progress to troubleshoot the ultrasonic system, the Naval Officer in charge announced that the time allotted for testing was over and, issued the instruction to pack up the machine. Therefore, the tests were terminated. Although the removal rates could not be confirmed, the machine met all the other requirements specified in the SOW.

It should be remarked in passing that once off the ship, the machine was taken to a local electrical workshop for troubleshooting. It was left there overnight for drying. On the next day, an electronic technician conducted a few diagnostic tests and found, after drying the electrical plug which connected the ultrasonic generator to the main control panel, that it was functional. Short circuiting due to the heavy and freezing rains was suspected to be the main cause of faulty function of the ultrasonic unit.

4.2.6 Tests at Les Mechins

The machine was taken to this site hoping to accomplish the tasks which were not possible at Halifax. Even here the weather conditions were not favorable for conducting systematic tests. The tests commenced at about 15.00 hrs after arriving at the site (see Fig. 7) at about 11.30 hrs on the 12th. Here the tests were conducted outdoors, keeping the machine indoors in a shed. The curious staff of Verreault Industries placed a variety of coated components for testing (see Figs. 13 and 14). In this field demonstration, the main objective was simply to show the capability of pulsed waterjet, not the removal rates. The demonstration was successful as the machine removed most of the coatings as shown in Fig. 14.

4.2.7 Analysis of Waste Water

Due to incessant rain at Halifax, no waste water was collected during the trials. However, tests were repeated at Ottawa using the waste water treatment system shown in Fig. 15. The system consists of an electrically driven suction unit and two drums which could be easily disconnected to dispose of the waste. The first drum (to the right side of the electrical unit) collects the suspended particles (paint, etc). The second drum removes dissolved metallic components, oil, etc. Tap water and waste water were given to a chemical laboratory for analysis. The results are summarized in Table. 1. A comparison of these values to the values listed in the SOW (**Appendix A**) shows that the system met the requirements and, the treated water was considered to be safe for disposal into city sewers.

4.2.8 Discussion

The following observations are made from the field trials conducted at the two locations: (i) The machine's overall compact size, 0.787 X 0.838 X 1.40 m (31" X 33" X 55"), made it ideal for use on the ship, (ii) As the weight was well balanced, it could be maneuvered about the ship with relative ease; The tow bar was found to be very useful and, necessary not only for short distance hauling but also, for long distance towing, (iii) Rubber casters, with swivels and locking features, were found to be durable enough to withstand the weight and vibration of the machine; The wheel size was found to be satisfactory to roll over most lips and bumps with ease and control, (iv) Control panel buttons were robust to withstand rough handling in industrial setting; Pilot lights were large and bright to be seen clearly from a reasonable distance, (v) Placing the inlet and outlet receptacles respectively on the rear and front of the machine and, having non-interchangeable fittings, eliminated confusion and thus enhanced safety and, (vi) If only the moisture in the electrical plug was the problem for the faulty operation of the ultrasonic unit, wide variation in the temperature, did not appear to affect its performance.

The following lessons were learnt from the limited field trials: (i) The machine needs to be designed for prolonged operations in the field under wet weather conditions including, high humidity, (ii) To ensure a long service life of the control panel, it should be shielded and sealed (using a gasket) with plexiglass to prevent problems that could be caused by moisture and, (iii) Wherever possible, the machine should be placed in a dry place, especially in view of the fact that almost 30.5 m ($\approx$100 ft) long high-pressure hoses can be used to reach the working areas.

5. CONCLUSIONS FROM THE FIELD TRIALS

The main conclusion from the field trials was to recognize the shortcomings of the pre-commercial machine and, to rectify them before putting it for regular use on the market. The field experience was in fact a lesson for debugging the machine. Since then many modifications have been incorporated to make it robust, reliable and user friendly for continual use.

6. REFERENCES

NLB Corp., "Surface Preparation with High-pressure and Ultra-high Pressure Water Jetting," NLB Corp. Wixom, Michigan, USA, 1997.

Puchala, R. J. and Vijay, M.M., "Study of an Ultrasonically Generated Cavitating or Interrupted Jet: Aspects of Design," *Proceedings of the 7th International Symposium on Jet Cutting Technology*, Paper B2: 69-82, BHR Group, Cranfield, Bedford, UK., 1984.

Vijay, M. M., "Ultrasonically Generated Cavitating or Interrupted Jet," *U. S. Patent No. 5,154,347*, 1992.

Vijay, M. M., Foldyna, J., and Remisz, J., "Ultrasonic Modulation of High-speed Waterjets," *Proceedings of the International Conference Geomechanics 93*, pp. 327-332, A.A. Balkema, Rotterdam, Netherlands, 1994.

Vijay, M. M., Foldyna, J., "Ultrasonically Modulated Pulsed Jets: Basic Study," *Proceedings of the 12th International Symposium on Jet Cutting Technology*, pp. 15-35, BHR Group, Cranfield, Bedford, UK., 1994.

Vijay, M.M., Lai, M.K.Y., and Jiang, M., "Computational Fluid Dynamic Analysis and Visualization of High Frequency Pulsed Waterjets," *Proceedings of the 8th American Water Jet Conference*, pp. 557-572, Water Jet Technology Association, St. Louis, Missouri, USA, 1995.

Vijay, M.M., Debs, E., Paquette, N., Puchala, R.J., and Bielawski, M., "Removal of Coatings with Low Pressure Pulsed Waterjets," *Proceedings of the 9th American Water Jet Conference*, pp. 563 - 580, Water Jet Technology Association, St. Louis, Missouri, USA, 1997.

Vijay, M.M., "Pulsed Jets: Fundamentals and Applications," *Proceedings of the 5th Pacific Rim International Conference on Water Jet Technology*, pp. 610-627, International Society of Water Jet Technology, Ottawa, Canada, 1998a.

Vijay, M.M., "Design and Development of a Prototype Pulsed Waterjet Machine for the Removal Hard Coatings," *Proceedings of the 14th International Conference on Jetting Technology*, pp. 39-57, BHR Group, Cranfield, Bedford, UK., 1998b.

WJTA, "Recommended Practices for the Use of Manually Operated High-pressure Water Jetting Equipment," Water Jet Technology Association, 1100, St. Louis, Missouri, USA, 1994.

7. ACKNOWLEDGMENTS

The authors are grateful to the Department of National Defense for the contract. Assistance rendered in the field trials by Mr. D. Larkin of the National Research Council of Canada is greatly appreciated.

Sincere thanks to Mr. R. Chisholm and his crew members at Halifax and Mr. J. Mooney and his crew at Les Mechins for going “beyond the call of duty” for assisting VLN at the field trials.

Table 1. Analysis of tap and waste water (done by Accutest Laboratories, Ltd., Nepean, ON., Canada).

Parameter	Units	MDL (Method detection unit)	Tap Water	Waste Water
BOD 5	mg/L	1	11	23
Total suspended solids	mg/L	2	ND (not detected)	2
Faecal Coliforms	cts/100 mls	1	0	0
Chlorine residual	mg/L	0.02	0.10	0.19
pH			7.54	7.52
Oil & grease	mg/L	1	ND	ND
Cd	mg/L	0.005	ND	ND
Cr	mg/L	0.01	ND	ND
Co	mg/L	0.01	ND	ND
Pb	mg/L	0.05	ND	ND
Zn	mg/L	0.01	0.02	0.06
Ni	mg/L	0.01	ND	ND
CN - (Oxidizable)	mg/L	0.02	ND	ND
CN - (Total)	mg/L	0.02	ND	ND
Phenols	mg/L	0.001	ND	0.004
Tributyltin	mg/L	0.020	ND	ND

APPENDIX 1: STATEMENT OF WORK (SOW)

A.1. BACKGROUND

The removal of coatings from military ships is required for maintenance and other purposes. Paint removal from ships generally involves open grit blasting. Current regulations require that any grit blasting carried out on a ship afloat must be contained and no grit allowed to drop over the ship’s side. In dry dock there are no such restrictions. Open grit blasting is carried out and the grit is collected and analyzed for metal leachates and sent to landfill. Grit blasting has been used for many years and is inexpensive. The volume of waste generated by the process is of concern but until environmental legislation make disposal of paint waste cost- prohibitive, grit blasting remains the most effective and economical way to remove paint. Future areas of environmental concern are the possible requirement to capture air borne debris during grit blasting. Scaffolds would be built around the ship or area to be blasted and the entire area covered with plastic sheets. This is currently a requirement in many US shipyards. In Canada this type of air quality control regulations rests with local authorities or regions and the requirements could differ in each jurisdiction.

The Department of National Defence and Canadian Forces policy on the Environment PS/92 requires the Department to reduce the amount of hazardous waste generated by Defence activities. Alternative means for coatings removal is an area where waste generation could potentially be reduced. Pulsed waterjet, a relatively low pressure waterjet, can be used for coatings removal. Since it uses only water, environmental problems are restricted to the disposal of the paint only. The reduction in dust/air contaminant generation has additional benefits. During work in spaces such as machinery rooms, tanks and bilges, the requirement to seal openings against dust ingress is greatly reduced, as are the worker health and safety precautions required.

A.2. SCOPE

This document outlines the requirements for the construction and trial of an ultrasonically enhanced waterjet coatings removal system for use on the interior of HMC Ships.

A.3. TECHNICAL REQUIREMENTS

A.3.1. System Description

The system shall be a manually operated portable ultrasonically enhanced water jet system for the **removal of coatings from the interior surfaces of HMC Ships.** The waterjet removal system shall include a wet vacuum system to collect the coatings contaminated water and a separation system to filter out the coatings and upgrade the water quality to allow for discharge to municipal waste. The prototype shall include either a magnetostrictive or a piezoelectric transducer to generate the pulsed waterjets.

A.3.2. Application

The system shall be designed to remove coatings normally used on and in HMC Ships. The identified coatings are:

1. Red oxide primer to Canadian General Standards Board (CGSB) Standard 1-GP-48 over coated with marine alkyd to CGSB standard CAN/CGSB-1.61-95;
2. Zinc rich epoxy primer CGSB CAN/CGSB- l. l83-92 over coated with epoxy non slip deck coating CGSB standard l-GP-l92;
3. Low temperature curing epoxy coating CGSB CAN/CGSB-1.207-M91

A.3.3. Application Areas may include:

Internal and external decks, tanks (fresh water, bilge, fuel, waste water), void spaces and machinery rooms.

A.3.4. Performance

(a) **Removal Rate:** The performance of the water jet coating removal system shall be comparable to needle gun, hand held grinder or other manual methods for coatings removal in terms of rate of removal and quality of the resulting surface profile. The rate of removal is related to the age, condition and type of coating system, the material of the substrate and its preparation in addition to the skill of the operator. A removal rate of not less than 25 ft^2/hour for removing the red oxide primer/marine alkyd coating system on a steel substrate that has been abrasively blasted to SSPC-SP 10 (average blast profile 2.5 mil) shall be deemed satisfactory. The resultant steel surface should retain the profile at 2.5 mil and comply with NACE/SSPC WJ-l/SC-l. In order to achieve the specified removal rate, the nozzle body for the prototype may be either multiple orifices or rotating nozzles.

(b) **Vacuum Collection and Effluent Treatment:** The wet vacuum/separation system shall be capable of collecting all used water and removed coatings from all surfaces including flats, corners, crevices at a rate that will minimize the formation of rust haze. Effluent shall then be filtered to separate coating residue from water. Waste water is intended to be discharged to sewer at a purification level acceptable for municipal waste water.

(c) **Mobility:** The water jet coatings removal system and the vacuum collection component shall be wheel or track mounted for ease of manual movement within the ship. Maximum dimensions must permit movement through doors. Door dimensions are typically 60" high and 32" wide. Means must be provided to man handle, without undue strain on the operator, the system over the 6" lip at each hatch. Hatch dimensions are typically 36" square. The system must include built in lifting rings to facilitate movement from one deck to another with tackle ordinarily available on board.

(d) **Weight:** Maximum: 318 kg (700 lbs). The nozzle assembly (nozzle, ultrasonic generator, wand, handle and trigger unit) shall be as compact as possible, to permit its use in confined spaces. The pressure hose with power lines from the main unit to the nozzle assembly shall be not less than 15 m (50 ft).

(e) **Utilities:** The power is to be obtained from universal 440V, 3 phase, 60 Hz outlets located throughout the ship. The power cable is to be not less than 7.5 m (25 ft). Water: municipal potable water; The water connection is to be quick connect.

(f) **Design:** The equipment shall be designed for effectiveness, ease of use and safety. System shall be capable of being transported by light truck prudently driven at normal speeds over paved surfaces or equivalent without damage. Tie down rings shall be provided. Lifting rings capable of supporting a weight of 2.5 times the wet weight of the equipment (coatings removal and collection system, and filtration system) shall be provided.

The system shall perform to specification at ambient temperatures between 2 and 40°C, with a relative humidity level of up to 100%. When not in use, the equipment shall be capable of being stored in unheated covered storage at temperatures from -40 to +40°C, provided that all water and water-containing additives have been drained prior to storage. The system must contain adequate drain cocks to make this possible.

Motors shall be totally enclosed fan cooled (TEFC). Motors, wiring, controls and supply connections shall comply with National Electrical Manufacturers Association (NEMA) and other relevant codes. Total system, from nozzle assembly through the power unit to point of electrical supply shall be grounded. Complete system shall be splash proof. Interlocks shall be provided to ensure instant shut down (e.g. deadman switch). Design shall prevent any access to high pressure water or electricity without breach of the interlock.

(g) **Operator Controls:** On the power unit: Pump power on/off; Pressure setting in 3.45 MPa (500 psi) increments from 1000 psi 6.9 MPa (1,000 psi) through 41.4 MPa (6,000 psi); Ultrasonic generator on/off; Interlock to ensure no ultrasonic generation is possible without a minimum 6.9 MPa (1,000 psi) water pressure; On the nozzle assembly: On/Off trigger unit.

(h) **Materials of Construction:** Materials of construction shall be appropriate for a marine environment (non-corrosive, moisture, fungus and mildew resistant)

(i) **Safety:** Equipment shall be designed in accordance with recommended good practice, as provided by the U.S. Water Jet Technology Association.

(j) **Environment:** The equipment, method of operation, collection and disposal of debris and used water shall comply with applicable standards. The Guidelines for Effluent Quality and Waste water from Federal Facilities and the Nova Scotia metal finishing effluent guidelines for discharge into municipal sewers are used as the standards for the quality of used process water prior to discharge to municipal water treatment facilities. In general the effluent shall be:

- Free from materials and heat in quantities, concentrations or combinations which are toxic or harmful to human, animal, waterfowl or aquatic life;
- Free from anything that will settle in receiving waters forming putrescent or otherwise objectionable sludge deposits, or will adversely affect aquatic life or waterfowl;
- Free from floating debris, oil, scum and other material in amounts sufficient to be noticeable in receiving waters;
- Free from materials and heat that alone, or in combination with other materials will produce colour, turbidity, taste or odour in sufficient concentrations to create a nuisance or adversely affect aquatic life or waterfowl in receiving waters;
- Free from nutrients in concentrations that create nuisance growths of aquatic weeds or algae in the receiving waters.

Specific limits: 5 day BOD: 20 mg/l; Suspended solids: 25 mg/l; Fecal coliforrns (MF method): 400 CFUs per 100 ml (after disinfection); Chlorine residual: 0.5 mg/l min., after 30 minutes contact time 1.0 mg/l max; pH: 6-9; Phenolic compounds: 20 µg/l; Oil/grease: 15 mg/l. Chlorine residual only applicable where chlorination is used for disinfection. Temperature of the effluent shall not alter the ambient water temperature by more than 3°C.

Heavy metal acceptable quality of discharge as detailed in the metal refinishing effluent guidelines:

Cadmium: 1.5 mg/l; Chromium: 1.0 mg/l; Copper: 1.0 mg/l; Lead: 1.5 mg/l; Zinc: 2.0 mg/l; Nickel: 2.0 mg/l; Cyanide (oxidizable): 0.1 mg/l; Cyanide (total): 3.0 mg/l; Tributyltin: 0.001 µg/l;
(Note: As the prototype coatings removal system is being designed for internal use, the fecal Coliforms, chlorination and Tributyltin limits may not be applicable).

(j) Accessory equipment: Accessory equipment shall include a storage tank with metering equipment to add to the water stream anti corrosion, cleaning, de-greasing and anti-chlorine chemicals. It is recognized that the use of such chemicals may require their removal prior to re-coating the substrate. Also the use of such additives and/or their removal may complicate the environmental considerations in disposal.

(k) Operating Manual: The UEW system, wet vacuum collection system and filtration system shall be provided with the following information:

Starting, operating and shut down procedures; Safe operation guidelines; Maintenance instructions; Storage instructions; Transportation instructions; Specifications; List of and source of spare parts; Mechanical and electrical drawings. It is highly desirable that the equipment be designed so that maintenance can be performed by non specialist personnel.

A.4. FIELD TRIALS

Upon construction of the prototype, field trials will commence as soon as practicable. The location of the trial will be determined through consultation with the Technical Authority. The trials report will consist of an:

1.01 Evaluation of the transportation of equipment;
1.02 Confirmation of removal system and profile as specified;
1.03 Evaluation of collection system as specified;
d. Evaluation of the equipment performance (coatings removal rate, vacuum collection efficiency, separation efficiency) under field conditions;
e. Evaluation of system operating and maintenance instructions;
f. Evaluation of the mobility of the equipment within a ship (through hatches, etc.).

Any deficiencies in the equipment or instructions identified during the trials shall be corrected to the satisfaction of the technical authority before final delivery of the prototype to the Department of National Defence. The Design Authority may coordinate an evaluation of the system by non-contractor personnel. The maintenance of the prototype after acceptance by the Department will be through external contract.

Fig. 1. Photograph showing the front view of FluidPulse™ - pulsed waterjet machine.

Fig. 2. Photograph showing the rear view of FluidPulse™ - pulsed waterjet machine.

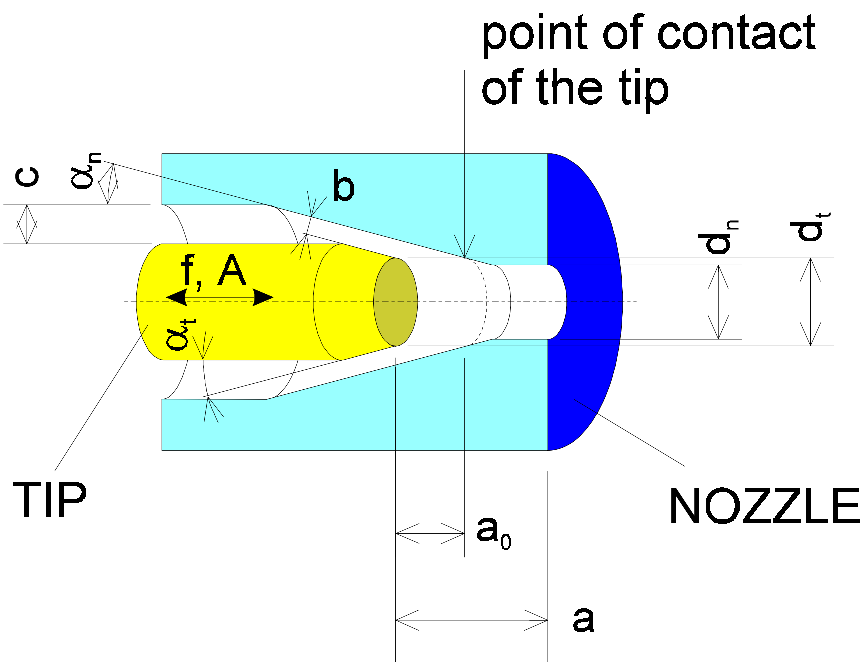

Fig. 3. Geometric configuration of the ultrasonic nozzle.

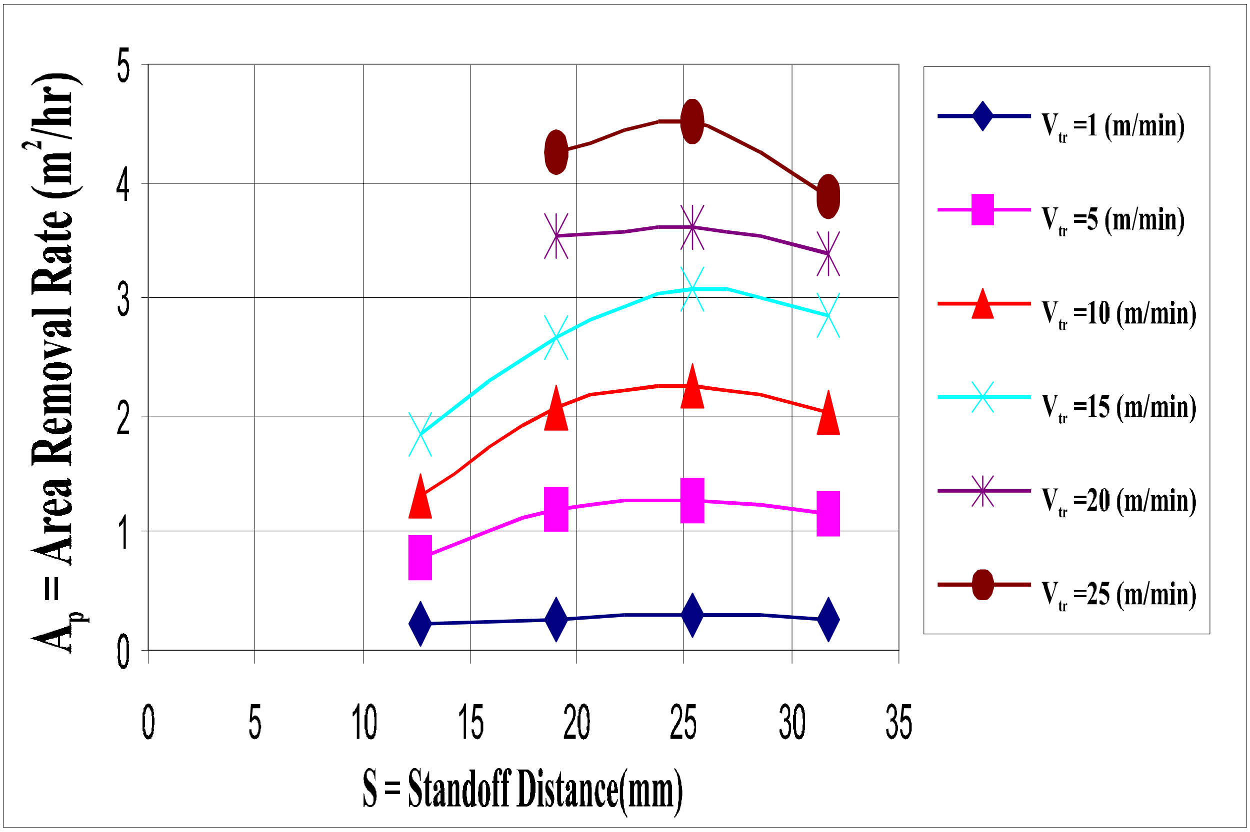

Fig. 4. Area removal rate versus standoff distance (P = 41.4 MPa, d_n = 1.37 mm and f = 20 kHz). Sample: AMERCOAT 68 HS, Non-skid.

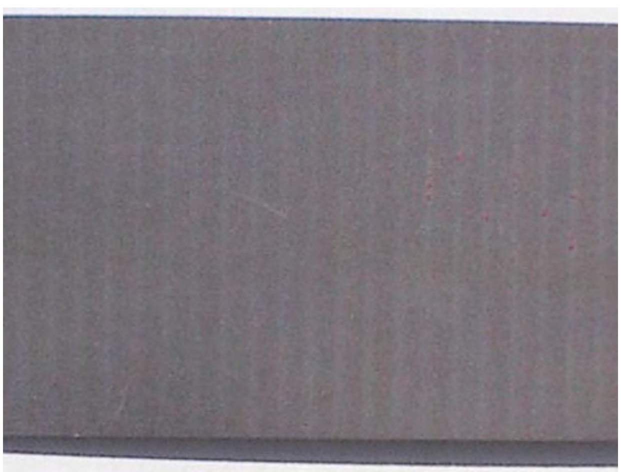

Fig. 5. General appearance of the de-coated panel consisting of three layers of coatings (1-GP-48, 1-GP-61, 1-GP-61). Tests conducted on a gantry at controlled conditions (P = 30.6 MPa, d_n = 1.37 mm, V_{tr} = 10 m/min, S = 38.1 mm. Removal rate = 3.2 m^2/hr).

Fig. 6. General appearance of the AMERCOAT 68HS panel de-coated using hand-held gun (P = 41.4 MPa, d_n = 1.7 mm) Removal rate = 1.2.m^2/hr.

Fig. 7. A general view of the dock at Les Machins, St-Lawrence Seaway, Quebec showing the pulsed jet machine in the pick-up truck. The machine was transported from Ottawa to Halifax (Nova Scotia) in adverse weather conditions satisfying the requirement of "portability".


Fig. 8. The machine being hoisted on to the deck of the ship (HMC Halifax) with access to the door of the hangar satisfying the requirement of "maneuverability".


Fig. 9. The machine being moved, by a single individual, into the main hangar through the door. This shows that the machine is light enough satisfying the requirement of "mobility".


Fig. 10. Moving the machine through an access door in the bulkhead, another requirement. Ramps were placed over the 15 cm lips to facilitate moving the machine through the door.

Fig. 11. A general view of the machine on the bow deck..

Fig. 12. A close-up view of the work area showing the deteriorated surface of the deck (extensive rust spots). Visibility of white spots indicates that the pulsed water jet has removed both the top rough layer and the fine primer. Bale sorbent boom (appears like a white rope) was used to contain the spread of water.

Fig. 13. A general view of the setup at Les Machins (a private dock) for demonstration of the machine.

Fig. 14. A close-up view of the metallic components from which the coatings were removed with the pulsed waterjet machine.

Fig. 15. Water treatment system used in conjunction with the pulsed waterjet machine to collect and filter water for disposal into the municipal sewer systems. (Photograph: Courtesy of Always Clean, Aurora, Ohio, USA).

10^{th} American Waterjet Conference
August 14-17, 1999: Houston, Texas

Paper **54**

EXPERIMENTAL AND THEORETICAL INVESTIGATION OF THE DECOATING PROCESS BY PURE WATERJET

H. Louis, W. Milchers, F. Pude
Institute of Material Science
University of Hannover
Germany

ABSTRACT

In this paper experimental results and a modelling approach of the decoating process of an epoxy resin coated steel plate are presented. The model describes the fatigue of the work piece by a linear accumulation of the damages done by single droplets. The subsequent erosion is approximated by a simple function of the masses and velocities of the impacting droplets. To fit these functions to the measured erosion rate numerical optimisation is successfully applied.

Organized and Sponsored by the WaterJet Technology Association

1. INTRODUCTION

Despite the numerous experimental studies concerning cleaning applications (for example Wu et al. (1995), Schikorr et al. (1982) and Conn (1993)) the theory of the cleaning process and coating removal has not been researched intensively. Studies of the modelling of the cleaning have been published by Meng et al. (1997) and Liu et al. (1998). They have derived an equation for the cleaning width as a function of the stand-off distance for stationary cleaning and extended this model to moving nozzles (Meng et al. (1998)) with the erosion model of Springer (1976).
In general cleaning will be performed with a jet that is broken up in separated droplets, so it is necessary to describe the impact of droplets on solid surfaces. The research concerning this topic was primarily performed in the field of rain erosion (see Adler (1979), Rochester et al. (1979) and Lesser (1995) for an overview). The impact produces a zone of compression inside of the droplet, which leads to maximal pressures near the border of the contact zone between the droplet and the solid. This compression exists until the movement of the contact zone border is slower than the sound velocity in liquid; afterwards an outflow jet is generated with speeds much higher than the impact velocity.

To estimate the effect of the droplet impact on the material a description of the possible damage processes is necessary. The following processes have to be considered:

1. plastic deformation like extrusion of material,
2. mechanical waves (Rayleigh surface waves, pressure waves and tensile release waves),
3. outflow jetting,
4. hydraulic penetration.

The processes can generate and enlarge cracks and pores, which lead to erosion by the separation of material from the surface.

On coated materials some more effects can occur. Near the interface between the coating and the substratum the intensity of the stress waves is doubled, and if there are pores near the interface the dominating pressure wave will be reflected as a tensile wave. A tensile wave can also be generated by the reflection of the pressure at the surface of the coating. Schikorr (1986) reported that the substratum could have a kerfing effect on the coating if pressure waves cross the interface. But the most dominating effect of the layered structure is the inhibition of crack growth through the material interface, which reduces the erosion rate.

2. EXPERIMENTS

The cleaning process is examined by decoating of samples, which consist of an epoxy resin layer with approximate thicknesses of 0.1-0.3 mm on mild steel plates. The used nozzle has a diameter of 1 mm; the standoff distances are set to 335 mm, 250 mm, 150 mm and 100 mm. The applied pressures lie in a range between 25 MPa and 45 MPa. The time the jet acts on the coating is varied by changing the traverse rate, and the resulting kerf geometry is obtained with an OMECA MicroCAD Gray code measuring system.

As examples two images of work pieces after the removal are shown in figure 1. The first picture shows a part of the kerf at the beginning of the cleaning process. The machined surface is rough and shows wavy structures, which are oriented normal to the traverse direction. In contrast to this the structures directly above the steel interface that appear after long loading times are bubble-like and very regular (figure 2), so they seem to be a result of the sample production and not of the erosion process. The borders of the kerf show large remaining of brittle fracture that becomes even larger at the end of the process. At the surrounding material no damage is visible. A frequent phenomenon is a small lift of the surface directly beneath the kerf (see figure 3).

An example for the evolution of the kerf geometry is shown in figure 4. At short loading times the kerf is deepened rapidly but in the vicinity of the material interface the vertical erosion speed decelerates. The kerf width is asymptotically reaching a maximum value. The profiles of the kerbs show steep kerf walls and the whole geometry becomes more and more box-shaped with increasing loading time.

We have observed that a minimum pressure and a minimum loading time have to be applied to erode the surface. If this threshold is exceeded, the kerf almost immediately reaches depths above 60% of the coating thickness. In contrast to this the complete removal of the coating can only be achieved with the slowest traverse rates of 125 mm/min and a pressure of 45 MPa in a working distance above 150 mm.

The dependence of the kerf width of the loading time can easily be fitted by the function

$$b_E = b_{max} \cdot \left(1 - \exp\left(-l(t - t_0)\right)\right).$$

The kerf width is also strongly influenced by the thickness of the layer. Figure 5 shows the results of four measurements with exactly the same working parameters but different coating thicknesses. The kerf width reaches much higher values for thicker coatings.

The results summed here indicate the following properties of the removal process:

- after a short period of damage accumulation the erosion starts,
- near the jet axis most of the layer is removed rapidly,
- near the material interface to the substratum the erosion rate decreases and depends strongly on the distance to the substratum,
- the kerf width reaches a maximum value at a loading time of infinity an the kerf will almost have the shape of a flat rectangular then.

There are at least two different possibilities to explain the kerf width and shape:

1. The erosion of the coating starts after a period of damage accumulation. This accumulation until failure takes longer in greater distances to the jet axis due to a lower velocity and mass flow rate which explains the successive growth of the kerf. The maximal kerf width is determined by the spreading of the jet. The subsequent erosion is comparably fast until the neighbourhood of the substratum is reached. This leads to a kerf that is shaped more rectangular. The interaction of kerf width and the coating thickness is difficult to interpret.

To explain this a mechanism for the decrease of the erosion ability for thinner coatings has to be found.

2. An alternative mechanism for the kerf broadening that might explain the greater kerf depths for thicker coatings is the erosion due to the outflowing water or due to the jets that are generated when the compression zone of the droplet is released. This water hits the steep kerf walls and generates cracks that lead to an enlargement of the kerf. The material that is not covered anymore by the undamaged surface is eroded by the impinging droplets.

Indications for the importance of the jetting are the periodic structures at the kerf ground and the uplifted peaks at the vicinity of the kerf (figure 2), but to validate the role of jetting further investigations will be done.

3. MODEL DESCRIPTION

The model represents three processes:

1. the accumulation of damage before the erosion begins,
2. the erosion of the coating without the influence of the material interface,
3. the erosion of the coating near the material interface.

The first process is usually described by the fatigue of the material, where each stress cycle like a droplet impact increases the damage by a certain amount, which depends on the stress magnitude. If the Palmgren-Miner-formulation of linear damage accumulation is valid, one can sum the contributions of the single droplets to the damage:

$$s = \sum_i \frac{n_i}{N(\sigma_i)} \Rightarrow \dot{s}(x,y) = \int_{x'}\int_{y'}\int_{r_d}\int_{v_d} \frac{\dot{n}_d(x',y',v_d,r_d,t)}{N(\sigma(x-x',y-y',v_d,r_d))} dv_d dr_d dy' dx'.$$

This formulation includes knowledge about the droplet spectrum and the damage distribution near the surface due to the droplet impact. To simplify this equation we replace the number of droplet impacts with the mass flow and the droplet spectrum with a representative diameter and velocity. The number of impacts until failure is expressed with the simple identity:

$$N(\sigma) = \left(\frac{\sigma_u}{\sigma}\right)^b.$$

which is in good agreement with measurements of the fatigue behaviour (Anonymous (1995)). The equivalent dynamic stress of the droplet impacts is assumed to be one half of the water hammer pressure:

$$\sigma = 0.5 \cdot \rho_l c_l v_d .$$

The resulting formulation is:

$$\dot{s} \approx k \cdot \dot{m} \cdot \left(\frac{\rho_l c v_d}{2\sigma_u} \right)^b .$$

If the damage parameter s reaches the value 1, the erosion of material starts. Values for the parameter b can be found in the literature. Springer (1976) proposes to use 20.9 for the most materials, whereas from the figures in Anonymous (1995) a value of 13 can be derived. Because the application of one value for almost all materials was criticised by Adler (1979) and others, the last reference is used.

The erosion rate without considering the influence of the material interface can be estimated with the energy, which is transferred from the droplet to the coating. We use some simple assumptions concerning the duration, pressure and contact area of the droplet impact, which frequently are used for the description of the droplet impact (Rochester et al. (1979)):

$$t_I = \frac{r_d v_d}{2c_l^2},$$
$$A_c = \pi r_d v_d t,$$
$$\sigma = \rho_l c_l v_d .$$

With these formulations the energy can roughly be estimated by the following equation:

$$E_d = \int_{t=0}^{t_e} \sigma_I v_I A(t) dt \approx \left(\rho_l c_l v_d \frac{Z_s}{Z_l + Z_s} \right) \cdot \left(v_d \frac{Z_l}{Z_l + Z_s} \right) \cdot \int_{t=0}^{rv/2c^2} 4\pi r_d v_d t \cdot dt = \frac{3m_d v_d^5}{8c_l^3} \frac{Z_l Z_s}{(Z_l + Z_s)^2},$$
$$\dot{e} = \frac{\partial^2 E_d}{\partial A \partial t} \approx \dot{n}_d \frac{3\overline{m}_d \overline{v_d^5}}{8c_l^3} \frac{Z_l Z_s}{(Z_l + Z_s)^2} = \frac{3\dot{m}\overline{v_d^5}}{8c_l^3} \frac{Z_l Z_s}{(Z_l + Z_s)^2} = k \cdot \dot{m} \cdot v_d^5 .$$

This energy calculation is very rough, because the response of the target material is just described as 1-dimensional elastic behaviour without considering the Poisson ratio, and the correlation between the droplet mass and velocity is neglected.

This dependence of the erosion rate on the droplet velocity can be found in some of the experimental studies (Rochester et al (1979), Heymann (1979)), although the exact value of the exponent varies with the testing method and the materials. The independence of the erosion rate from the diameter of the droplet can also be found in the compilation study of Heymann (1979). We assume that the erosion rate of homogenous material is proportional to this energy, because the coating shows short ductile cracks that can be considered to be controlled by the energy:

$$\dot{z}_{hom\,og} \propto \dot{e} .$$

The proportionality is valid only after the erosion has started and before any influence of the material interface has to be taken into account. The lower erosion speed near the steel surface can be explained by the shorter crack length and the smaller particles that are removed, further the value of the effective Young's modulus changes in this region. We take this into account by reducing the erosion rate by a factor:

$$\dot{z}_{.} = \dot{z}_{homog} \cdot \left((z_C - z)/z_C\right)^{k_2}.$$

So the system of equations we want to fit to the measurements is:

$$\dot{s} = k_1 \dot{m} v_d^b,$$
$$\dot{z} = \begin{cases} k_3 \dot{m} v_d^5 \left((z_c - z)/z_c\right)^{k_2} & s > 1 \\ 0 & s \le 1. \end{cases}$$

To calculate these values a description of the mass flow rate and the velocity of the jet are necessary. For this purpose the equations of Yanaida et al. (1980), (1978) is used:

$$\dot{m} = 5.6 \cdot \rho_l \cdot v_0 \cdot \left(\frac{r_0}{k_4 h}\right)^2 \left(1 - \left(\frac{r}{k_4 h}\right)^{3/2}\right)^3$$

for the mass flow rate and:

$$v = v_0 \left(1 - \left(\frac{r}{k_4 h}\right)^{3/2}\right)^2$$

for the velocity. The values of $k_1.k_4$ are fitted to the data by numerical optimisation. The minimised property is the sum of the squared differences between the model predictions and the real measurements, which is called the cost function:

$$I = \sum_i (z_{i,e} - z_i)^2.$$

Because the dependence of the erosion rate on the damage level is not continuous, the use of more elaborate algorithms like the optimal control is circumvented. The simplex algorithm of Nelder and Mead (Press et al. (1992)) is applied instead.

4. RESULTS

For the optimisation 5-7 measured profiles which represent different loading times are used. Compared to the measurements the model predictions are calculated on a finer time grid of 50 steps but on a coarser spatial grid of 50 nodes. The simulated kerfs, which represent loading times where measurements are available, are used to calculate the cost function.

One result of the fitting procedure of a data set obtained with a pressure of 45 MPa at a distance of 250 mm is shown in figure 6. It is visible that the general features of the kerfs can be obtained with this procedure, although deviations remain. The rectangular shape of the measured profiles at higher loading time can not be fully reproduced by the simulations.

The jet width parameter k_4 which has been calculated from the experiments shows values between 0.029-0.038 which corresponds to the results of Yanaida et al. (1978), (1980). The exponent k_2 of the erosion deceleration due to the material interface lies in a range between 2.3-2.9.

The results do not prove that the mechanism, which is implicitly contained, is correct. The approach calculates the erosion volume as a consequence of impacts from above without taking into account jetting phenomena. To ensure that this description is appropriate more experimental work has to be done.

5. CONCLUSIONS

In this study first results of removal experiments and simulation tests with epoxy resin coated steel are introduced. The experiments indicate that the process can be divided into different stages:

- damage accumulation,
- rapid erosion of the upper part of the layer,
- slow erosion of the coating near the steel surface.

To describe these processes simple equations for the damage and erosion rate are derived and successfully fitted to the experimental data by an optimisation technique. Further work will be done to assure that the removal mechanism is fully understood and to include a more exact description of the jet and the work piece into the model.

6. ACKNOWLEDGEMENTS

The authors are members of the Working Group on Water Jet Technology (AWT), Germany.

7. REFERENCES

Anonymous, "Fatigue and Tribological Properties of Plastics and Elastomers", Plastics Design Library, 1995.

Adler, W. F., "The Mechanics of Liquid Impact" *Treatise on Materials Science and Technology Vol. 16:Erosion*, pp. 127-183, 1979.

Brunton, J. H., Rochester, M. C., "Erosion of Solid Surfaces by the Impact of Liquid Droplets", *Treatise on Materials Science and Technology Vol. 16:Erosion*, pp. 185-248, 1979.

Conn, A. F., "Waterjet Cleaning for In-Factory Applications", *Proceeding of the 11th International Conference on Jet Cutting Technology*, pp. 443-449, Dordrecht, 1992.

Heymann, F. I., "Conclusions from the ASTM Interlaboratory Test Program with Liquid Impact Erosion Facilities", *Proceedings of the 5th International Conference on Erosion of Liquid and Solid Impact*, pp. 20.1-20.10, Cambridge, 1979.

Lesser, M. B., "Thirty Years of liquid Impact Research: a tutorial Review", *Wear* 186-187, pp. 28-34, 1995.

Leu, M., Meng, P., Geskin, E. S., Tismeneskiy, L., "Mathematical Modelling and Experimental Verification of Stationary Waterjet Cleaning Process", *Journal of Manufacturing Science and Engineering* Vol. 120, pp. 571-579, 1998.

Meng P., Decaro L. S. M., Geskin, E. S. Leu, M. Huang, Z., "Mathematical Modelling of Waterjet Cleaning", *Proceedings of the 9th American Waterjet Conference*, pp. 509-524, Dearborn, 1997.

Meng, P., Geskin, E. S., Leu, M, Li, F., Tismeneskiy, L., "An Analytical and Experimental Study of Cleaning with Moving Waterjets", *Journal of Manufacturing Science and Engineering*, Vol. 120, pp. 580-589, 1998.

Press, W. H., Teutolsky, S. A., Vetterling, W. T., Flannery, B. P., "Numerical Recipes in C", Cambridge University Press, 1992.

Schikorr, W., "Beitrag zum Werkstoffabtrag durch Flüssigkeitsstrahlen hoher Relativgeschwindigkeit", Dissertation, University of Hannover, 1986.

Schikorr, W., Louis, H., "Fundamental Aspects in Cleaning with high speed Waterjets", *Proceedings of the 6th International Conference on Jet Cutting Technology*, pp. 217-228, Guildford, 1982.

Springer, G. S., "Erosion by Liquid Impact", Scripta Publishing Co., Washington, 1976.

Wu, S. S., Kim, T. J., "An Application Study of plain Waterjet Process for Coating Removal", *Proceedings of the 8th American Water Jet Conference*, pp. 779-792, Houston, 1995.

Yanaida, K., Ohashi, S. A., "Flow Characteristics of Water Jets" *Proceedings of the 5th International Conference on Jet Cutting Technology*, pp. 33-44, Hannover, 1980.

Yanaida, K., Ohashi, S. A., "Flow Characteristics of Water Jets in Air", *Proceedings of the 4th International Conference on Jet Cutting Technology*, pp. 39-53, Canterbury, 1978.

8. NOMENCLATURE

A:	area
b:	parameter of fatigue behaviour
b_E:	kerf width
b_{max}:	maximal kerf width
c_l:	speed of sound in liquid
E_d:	energy of droplet impact
e:	energy per area
h:	stand-off distance
I:	cost function
k_x, l:	empirically fitted parameters
m:	mass per area
m_d:	droplet mass
n_d:	number of droplet impacts per area
$N(\sigma)$:	number of impacts until failure
P:	pressure
r_d:	droplet radius
r:	distance from the jet axis
r_0:	nozzle radius
s:	damage
t:	time
v_d:	droplet velocity
v_0:	jet velocity at nozzle exit
v:	traverse rate
x,y:	co-ordinates
z:	kerf depth
z_c:	coating thickness
z_e:	experimental kerf depth
Z_l,Z_s:	acoustic Impedance of liquid, solid
ρ_l:	density of liquid
σ:	stress
σ_u:	ultimate tensile strength

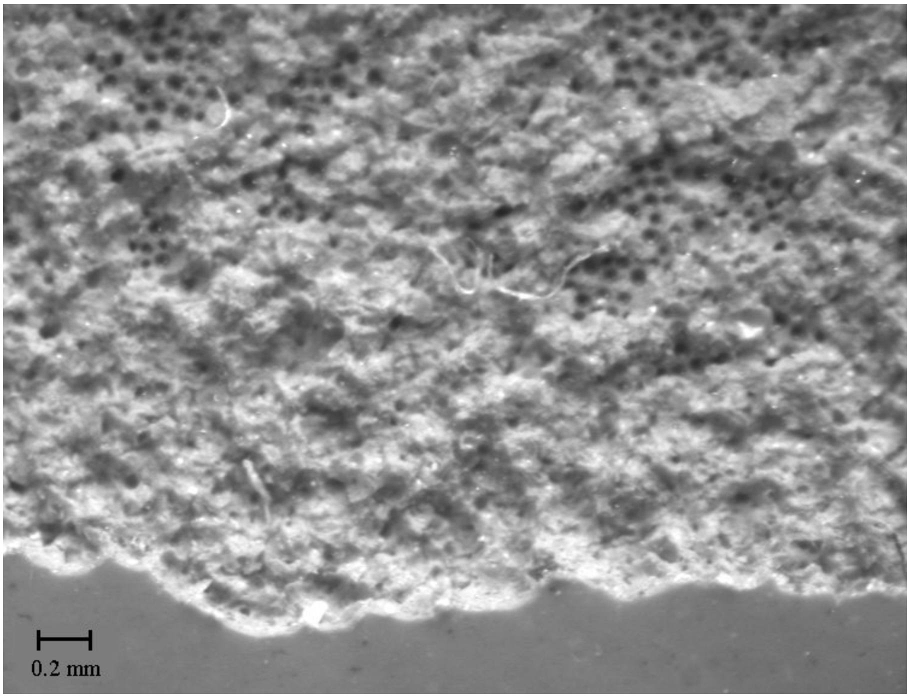

Figure 1: Photo of kerf (v=125 mm/min, P=45 MPa, h=250 mm).

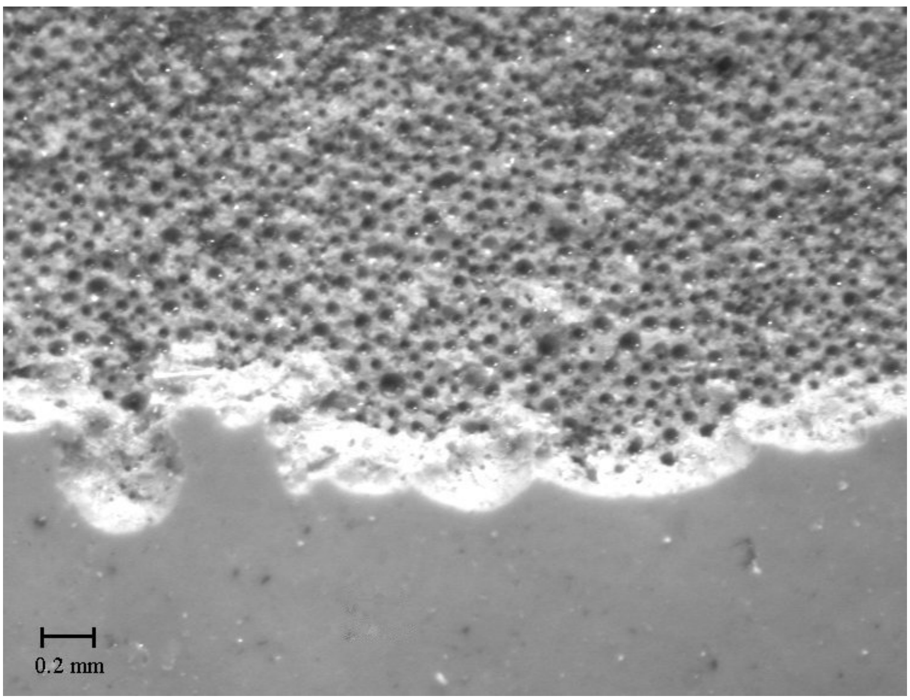

Figure 2: Photo of kerf (v=2000 mm/min, P=45 MPa, h=250 mm).

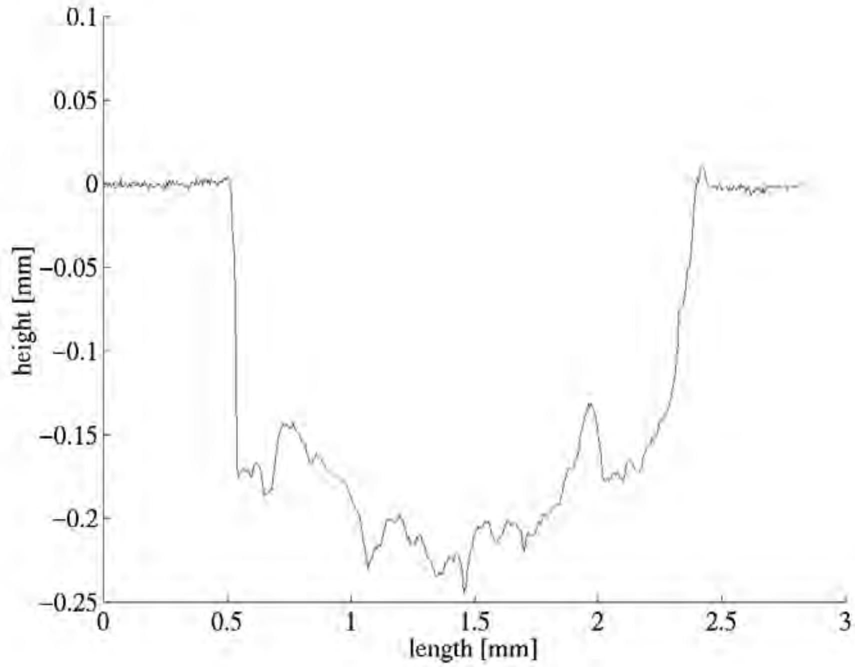

Figure 3: Typical kerf with peaks at the border of the kerf.

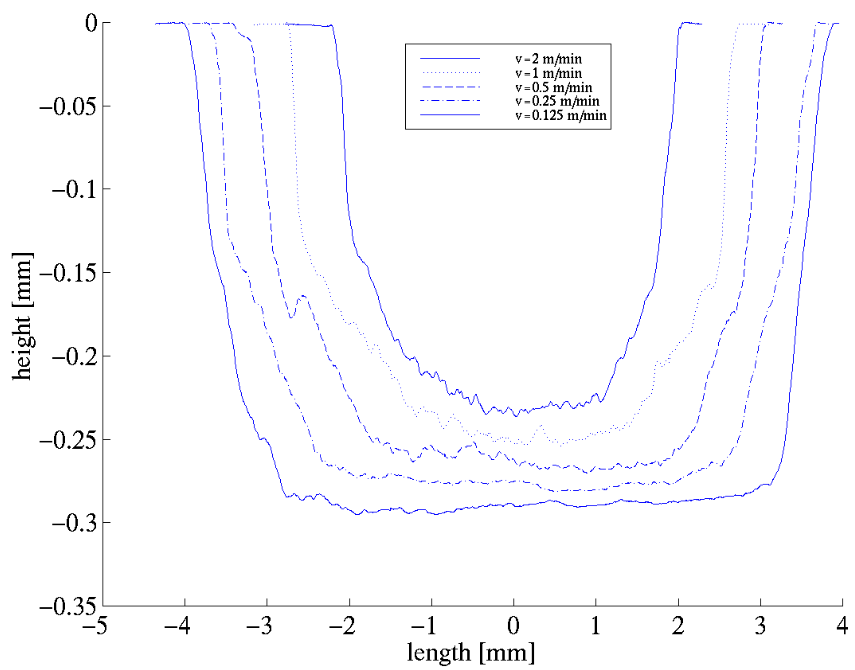

Figure 4: Evolution of averaged kerfs (P=45 MPa, h=250 mm).

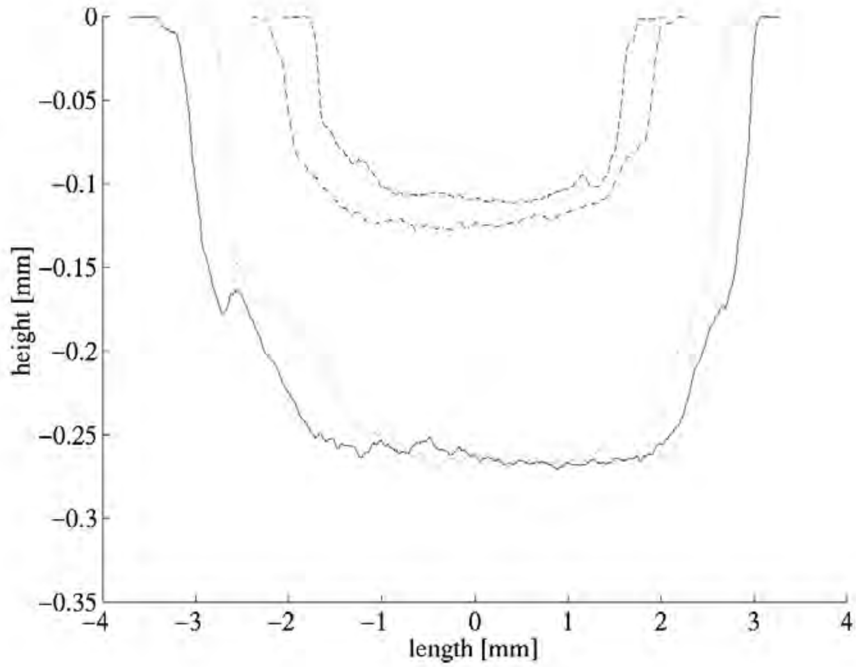

Figure 5: Four kerfs generated with v=500 mm/min, P=45 MPa, h=250 mm. The coating thickness is equal to the maximum kerf depths.

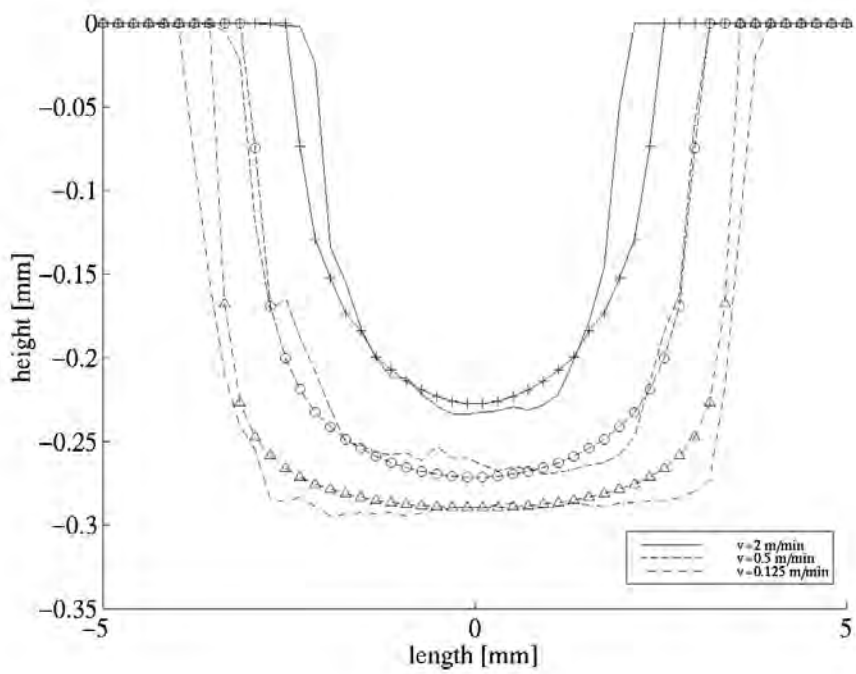

Figure 6: Comparison between measured and simulated kerf geometries with P=45 MPa, h=250 mm. Lines with symbols represent simulated geometries.

10th American Waterjet Conference
August 14-17, 1999: Houston, Texas

Paper **55**

PURCHASING AND RUNNING A

PROFITABLE ABRASIVE WATERJET

Michael Ruppenthal
Flow International Corporation
Kent, WA, U.S.A.

ABSTRACT

What are the major issues to consider when evaluating an abrasive waterjet cutting system? And once you've purchased a system, how do you run it profitably? It is important that you do the appropriate research before purchasing a system. The capabilities of the waterjet system must meet the requirements of your specific application. What is your application? What material do you plan on cutting and to what thickness? How large is your facility? Are you doing precision cutting or rough cutting? Answering these kinds of questions will help you decide what type of system is best for you. Abrasive waterjet technology continues to advance and users are finding that waterjets can be a profitable solution. The information covered in this paper applies to two dimensional, flat-stock cutting systems. This paper focuses on the major product features you should be aware of and how to use these powerful features to run a profitable shop.

Organized and Sponsored by the WaterJet Technology Association

1. INTRODUCTION

There are several items that should be considered before purchasing an abrasive waterjet system. The first section of this paper, Keys to Purchasing an Abrasive Waterjet, will touch on how to evaluate the different product features offered by manufacturers, including the high pressure pump, table and catcher tank, cutting head, software and the service and support you should expect from the manufacturer. Once you've made the decision to purchase and the system is installed on your floor, how do you run the machine to ensure that it is operating efficiently and creating a profit for you? The second section of this paper, Running a Profitable Abrasive Waterjet, will provide you with some insight on how to optimize the features of your waterjet system to create a profit for your shop.

2. KEYS TO PURCHASING AN ABRASIVE WATERJET

This section covers the major equipment features to research when evaluating an abrasive waterjet system for purchase. These are some of the issues you should consider when researching different brands of equipment. Take a close look at your application to decide what features and options will work best for you.

2.1 Choosing the High Pressure Pump

The pump that is best for you is the one that optimizes cutting for your particular application(s). If you are cutting various metals of different thicknesses, a higher horsepower pump would be recommended. If you're cutting thinner material, a lower horsepower pump is sufficient, however it may limit your cutting speed. Be sure to ask your sales representative about component life and maintenance of the pump.

There are two main types of pumps: crankshafts and intensifiers. Crankshaft pumps use a crank case and pistons while intensifiers use hydraulics. Crankshaft pumps generate a higher percentage of horsepower to the nozzle. Intensifier pumps can generate pressures of up to 3793 bar [55,000 psi]. Pressures can also be controlled and changed easily with both types of pumps. When cutting brittle materials such as marble or glass, the ability to decrease the pressure is advantageous for preventing any unnecessary cracking or surface frosting. Both styles are easy to maintain, with some having integrated sensors and common sense troubleshooting. Intensifier pumps are usually stand-alone pumps and must be controlled at the pump. They can be positioned further away, with most users placing them within 6.1 meters [20 feet] of the cutting table. If you're concerned about noise level in your shop, you may choose to put the pump in a separate room.

Pump horsepower ranges from 25 to 200 or more. Which horsepower is best for your application? You want to make sure that you maximize the horsepower of the pump. For example, if you're running a 100 horsepower pump, your maximum flow rate is 7.57 liters per minute [2 gallons per minute]. This means that you can run up to a 0.51 mm [0.020 in] orifice. If you're only using one cutting head and a 0.25 mm [0.010 in] orifice, you are not maximizing the horsepower of the pump. By running dual cutting heads with a 0.25 mm [0.010 in] orifice in each head, you would be maximizing the output of the pump. Make sure that the pump horsepower you choose will flow enough water to support your application.

2.2 Table and Catcher Tank Features

2.2.1 Table Size

Again, your specific application will help determine the table size that is best for you. Will the table hold standard material sizes? How much space is available in your facility? How far will the nozzle travel? These are a few of the questions you should consider. If you don't have enough space in your facility, you obviously are not going to choose a larger table. Manufacturers usually offer a wide range of sizes to fit your specific needs. If you're cutting sheet metal, the table should be able to hold standard sheet sizes. For example, if your material is 1.21 m x 2.43 m [48 in x 96 in], make sure that the work envelope is at least that large.

2.2.2 Rigidity

The rigidity of the table effects the accuracy of the finished part. Make sure that the system you are considering is rigid enough to support your application, especially if you plan on using multiple cutting heads. This extra weight may cause inaccuracies in your finished parts. Most systems which have been designed using finite element analysis (FEA) are engineered to handle waterjet applications and have been properly tested for rigidity.

2.2.3 Accuracy and Repeatability

More often then not, you will want your parts to be highly accurate. But how accurate? Some industries, such as stone and tile, do not require highly accurate parts. Most industries, however, do require high tolerance parts. Some machines can produce parts to ± 0.076 mm [± 0.003 in]. A number of waterjet machine tool companies manufacture different machine lines with different accuracy, one being slightly more accurate than the other. Higher accuracy machines will usually require a larger capital investment.

Most manufacturers will claim that a high precision machine has a positioning accuracy of ± 0.076 mm [± 0.003 in]. Some machines are capable of cutting at even higher positioning accuracy, but manufacturers are cautious when quoting finished part tolerances. Find out the dynamic accuracy measurements, making sure that these measurements were taken at a variety of speeds. Ask the manufacturer for documentation on accuracy and reliability. Many perform ball-bar tests on their machines, but just because they perform a ball-bar test does not guarantee that the machine is accurate. Be sure to learn what the ball-bar test actually means, and ask them to perform a bar-bar test at your facility once the machine is installed.

Repeatability is another important item to consider. Make sure that your parts can be cut with the same tolerance time after time. If you cannot reproduce the parts to the same specifications, the machine does not have reliable repeatability and this could cost you money in the end. Have the sales representative cut sample parts in different areas of the machine to ensure that the parts come out to specification each time.

2.2.4 Catcher Tank

The catcher tank is a critical aspect of the cutting system. You’ll want to look for individual material support slats that can be quickly and easily removed for certain applications and for replacement. Slats should be deep (i.e. 10 cm [4 in]) to provide long life as the jet will nick the top of the slat during abrasive waterjet cutting. Often times you can even cut replacement slats on your abrasive waterjet system. If you plan on cutting underwater, make sure that the catcher is equipped with water level control. Cutting underwater reduces noise and surface frosting. Make sure that the water level can be raised to at least 5 cm [2 in] above the work surface.

2.3 Cutting Head Alignment and Life

The most important thing to look for in the cutting head is precision tool alignment. Most cutting heads are pre aligned. You should avoid manually aligned tooling as the potential for operator error is introduced. If the orifice is not aligned properly, the mixing tube may wear out faster and will not wear cocentrically, as water will be hitting the side of the mixing tube instead of straight down. The accuracy of your finished part may be compromised. You should be able to change out the orifice and mixing tube quickly and easily (in just minutes). Also look for the ability to change the abrasive nozzle out with a waterjet nozzle. This will give you the option to cut foam, rubber and other waterjet-only applications.

What is the average life of the orifice and mixing tube? You’ll probably find that most manufacturers will quote about the same mixing tube life. Wearing of the mixing tube will effect you differently depending on your application. If you’re cutting precision parts, a worn mixing tube will effect your part more than if you’re doing rough work, in which case you will find that a worn mixing tube is not a concern.

Orifices are made from rubies, sapphires or diamonds. Diamonds are heavily used in pure waterjet cutting applications such as paper slitting, where the system is running 24 hours a day, 365 days a year. In abrasive waterjet cutting, the cost per hour of when running with a diamond may be higher than ruby or sapphire. It is recommended that you change out the orifice at the same time that the mixing tube is replaced. For this reason, rubies and sapphires are recommended since they generally have the same life as the mixing tube. Diamonds are more expensive, but also last longer. Manufacturers may offer some or all three orifice materials.

2.4 Powerful Software Capabilities

Two main types of control systems are available: CNC and PC controls. CNC controls are more traditional and requires more training and experience than PC controls. PC controls are easy to learn and are becoming more and more accepted in the industry. Many waterjets sold today are equipped with PC controls, with the exception of CNC controls used in 5-axis machining. The easier it is to program your parts, the better. If possible, have your part programmed and cut while you watch. Companies can perform demonstrations which will help you get a feeling of how quick and easy it will be for you to reproduce that part on your floor.

There are many items to look for when evaluating software. Here are some questions you should ask yourself. Can you control the sequence of entities that are to be cut first? What software is available to scan and convert artwork? Is there a nesting program available? Does the software automatically tell the machine to speed up at straight lines and slow down at curves and corners? Is the controller capable of stationary and dynamic piercing? Can you stop cutting at anytime and resume from the point where you stopped? Does the controller compensate for tool wear? Can you purchase additional seats of software for programming in your office?

Each of the above questions can be critical to your decision to purchase a waterjet. You should not be limited by your software. Make sure that the software has all the capabilities that you will need for your specific application. You could lose valuable production time and sacrifice the quality of your finished parts if the software you are using has limited capabilities.

2.5 Company Service and Support

How do you decide on which waterjet manufacturer to purchase from? Take a look at the company or companies that you are seriously considering purchasing from. You will probably schedule a company visit at which time you will meet employees and possibly see the manufacturing facility. Learn all you can about the company and what aftermarket services and support are available. Are there service representatives close to your facility? What are hours of operation and how will they support you? What kind of support does the firm offer you once you have purchased the machine? Is there training available and if so, what kinds of courses are offered?

Another way to find out more about the company is to talk to a customer who owns the brand of equipment you are considering. Ask them what their experience has been working with the company and especially with technical service and customer service. Do they enjoy working with the company? Is the response timely and friendly? Did they run into any difficulties? One of the best ways to find out more about a company is to talk to its customers first hand.

3. RUNNING A PROFITABLE ABRASIVE WATERJET

Now that you know what to look for before purchasing an abrasive waterjet system, let’s take a look at how to run that waterjet profitably. As abrasive waterjet technology continues to advance, increasing numbers of users are discovering how abrasive waterjets can run efficiently and profitably. Abrasive waterjet technology continues to reach new levels of productivity and is moving into applications previously not perceived to be within its capability through improvements in configuration options, cutting techniques, automation and accuracy.

3.1 Simple Setup and Fixturing

The goal of any job shop or production environment is to maximize the amount of time the waterjet machine is cutting and minimize the time associated with loading and unloading material. Waterjets cut with little force and therefore save valuable time that is normally spent on fixturing. Cutting 6.35 mm [0.25 in] thick steel, for example, requires little to no fixturing. For those times when fixturing may be necessary, for instance, when cutting parts from a small piece of material, fixturing must be fast and easy in order to maximize profitability. Fixturing can be as simple as using clamps and weights, using a positioning square, or an “L” shaped piece of metal to orient the work piece. In a production or in-house environment, waterjets lend flexibility. Since in-house production involves cutting the same parts, it may make sense to cut one dedicated fixturing piece to use for all materials.

3.2 Stacking Material

Stacking sheets of material is another method for increasing the profitability of your manufacturing environment. An abrasive waterjet has the ability to cut stacks of materials up to 2.5 cm [1 in] in total thickness while maintaining part tolerance. Although stacking may not improve effective cutting speed in all applications, it will reduce material loading and related set-up time. This resulting time-savings can have a positive impact on part yield per hour. And by minimizing material unloading, the machine runs more continuously meaning more parts are coming off your table.

3.3 Shuttle Tables Reduce Material Handling

Utilizing shuttle tables is another method to increase profitability and save valuable setup time. Shuttle tables are recommended for a production environment. Automatic shuttle tables and swivel columns allow an operator to load material on one table as the waterjet cuts material on the second table. The table with the finished parts then rotates or “shuttles” out of the work envelope, being replaced by the table just loaded with uncut material. This can also be accomplished manually, by simply having an operator load the second table and slide the material into the work envelope. This sophisticated method of material handling and delivery minimizes non-cut time and optimizes material throughput since the waterjet machine is always cutting. Minimizing the time spent handling material contributes to greater part yield per hour and thus more profit for your shop.

3.4 Operating at Peak Performance

Running your abrasive waterjet system at peak performance can contribute to significant cost savings. The key to achieving peak performance from an abrasive waterjet machine is using an appropriate sized orifice with the appropriate pump horsepower while flowing an appropriate amount of abrasive consistently. For example, if you’re cutting 6.35 mm [0.25 in] aluminum at 3793 bar [55,000 psi], with a 50 horsepower pump, you would use an abrasive flow rate of 0.59 kg/minute [1.3 lb./minute], water rate of 3.63 liters/minute [.96 gallons/minute], and an orifice/mixing tube combination of 0.36 mm x 1.02 mm [0.014 in/0.040 in]. Any variance in these parameters, such as higher horsepower with a smaller orifice and you're not maximizing your horsepower and therefore wasting money. On the other hand, if you do not have enough horsepower and are trying to cut with a larger orifice, the system will not operate at all. You want to make sure that you are optimizing the output of your pump.

3.5 Monitoring the Waterjet's Performance

Historically, abrasive waterjet cutting systems have been somewhat operator intensive. That is, an operator needed to be at the machine continually to monitor tool wear, consistency of abrasive flow, pump conditions, loading and unloading work material and refilling the abrasive hopper. The operator also had to periodically clean out the catcher tank, which can be a tedious, messy, and time-consuming task.

While there are some shops who still operate their machines this way, times have changed. Performance monitoring is a powerful feature that is now available. This feature takes the guesswork out of monitoring your machine's performance by automatically ensuring that all parameters are in sync. While waterjets cannot be considered "lights out machines," performance monitors can allow operators to leave the machine unattended for periods of time, usually about one to two hours, to perform other tasks. Operators can use this extra time to program other parts, operate another machine, or prepare the next batch of material for setup. Some performance monitoring systems feature electronic monitoring devices that detect unacceptable cutting conditions and shut down the machine automatically when one or more of the operating parameters is out of sync. These monitors constantly check tooling conditions during cutting operations and shut the machine down if any fluctuations or variations are detected. Performance monitoring reduces the chance for scrapping material and optimizes tool life.

3.6 When To Use Multiple Cutting Heads

Multiple cutting heads can have a tremendous impact on the profitability of your shop. Abrasive waterjets are typically equipped with a single cutting head. While appropriate for low-volume and some high-volume work, a single cutting head may limit production capabilities. By adding one, two, three or even four cutting heads to an abrasive waterjet system, an operator can substantially increase output and sacrifice little in cut speed. Taking the two to four additional parts per cutting cycle gained from the additional cutting heads, an operator can increase effective cutting speed per cycle and consequently part yield per hour.

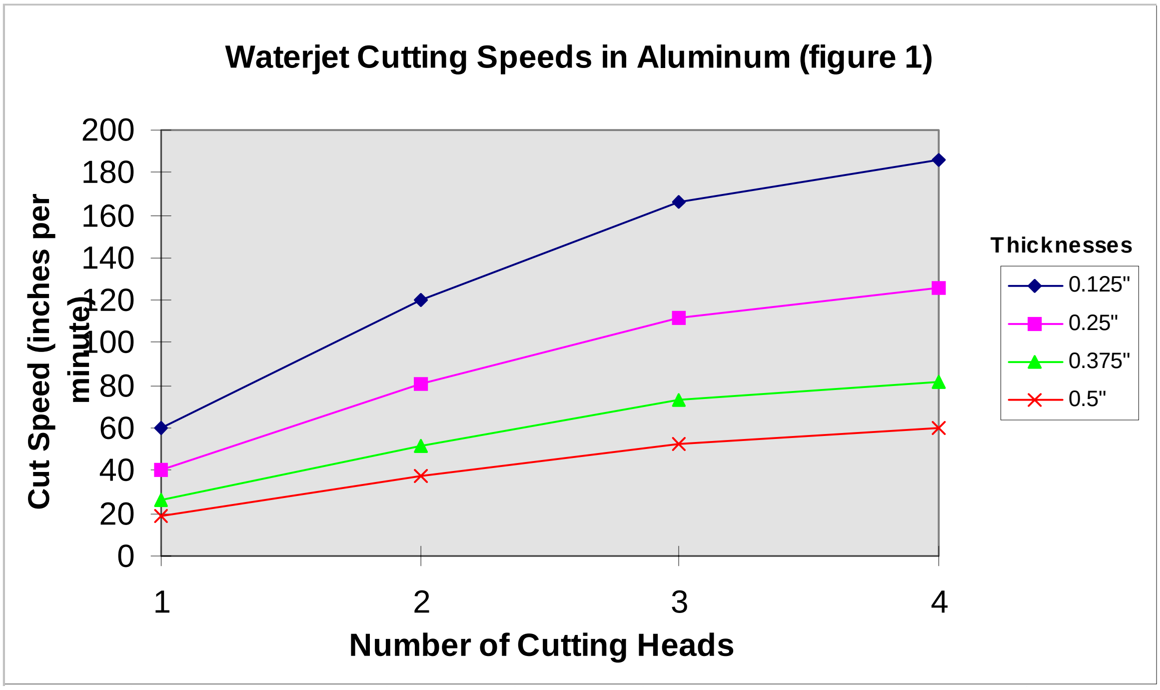

Figure 1. Abrasive waterjet cutting speeds in aluminum.

Figure 1 illustrates the cut speed when cutting aluminum with an increasing number of cutting heads. You can see that as you increase the number of cutting heads, you can increase the total inches per minute that you are able to cut. You'll also notice that having multiple cutting heads will be more beneficial when cutting thinner materials since cutting speeds are much higher for thin materials. The rates are based on cutting a 5.08 cm [2 in] diameter circle in various thicknesses as listed to the right of the graph. The finished part has a smooth, clean edge from top to bottom. Cut speeds can be higher depending on edge finish requirements.

While logic would dictate that multiple cutting heads on a machine equals the ability to cut more parts faster, this isn't necessarily the case. Multiple cutting heads are most efficient when cutting large quantities of the same part and when cutting smaller parts when it is difficult to obtain efficient nesting. Multiple cutting heads also typically make the most sense when a job shop or manufacturing environment has a backlog of work. With peak performance, the benefit of multiple cutting heads is the ability to cut more parts per hour. Remember that the cost per inch and the time to run the job are most important. If a shop's work is not backlogged, cost per inch is key. The decision to invest in multiple cutting heads depends on the nature of projects a job shop or production facility has.

If the nature of backlog varies, it may be a good idea to invest in multiple cutting heads, and use them only as needed. Some shops run a single head for most jobs and employ a second or third cutting head as needed, depending on the project. Many job shops run multiple cutting heads approximately 50 percent of the time or less, while in-house production shops may have the capabilities to run them 100 percent of the time.

3.7 Using Software to Increase Profitability

There are a variety of waterjet software packages and PC-based control systems available to maximize productivity. Many waterjet software packages seamlessly convert “G” code to PC code with a simple point and click. PC-based software programs are easy to learn, easy to use, and easy to program, which reduces time spent training new employees on how to use the waterjet system. Shops can also save money since there is no need to pay a special machinist or programmer to do the work. PC packages can scan a variety of intricate designs and artwork provided by customers and can easily convert files from the CAD programs used by so many. A few software packages available contain a cutting library of materials so operators can select the type of material and thickness to quickly cut a single part or to cut the same shape out of different materials. Another key feature of software programs is the job calculator function, in which operators can quickly calculate the cost of a particular project, which saves you time trying to figure out how much a job is going to cost you. The job calculator function is beneficial for shops when quoting jobs.

Nesting packages are another valuable tool in which to further maximize productivity. There are numerous nesting packages available. Some are compatible with any machine tool while others are waterjet specific. A waterjet-specific nesting package is highly recommended. In evaluating the different waterjet-specific nesting packages available, remember that performance is key. Some software nesting packages can contain many features, which can make them difficult to use. The best application is a powerful yet simple nesting package that allows the operator to multitask – programming the next part to cut while one job is still on the cutting table. PC-based waterjet software packages contain unique features that allow the waterjet to cut according to the particular job. Waterjet specific software is very intelligent, recognizing when to cut faster (on straight sections) and when to cut slower (on corners).

3.8 Selecting the Right Abrasive

When utilizing an abrasive waterjet system, selecting the right abrasive plays a key role in maximizing cost per inch. There are many different types of abrasive, the two most common types being waterjet and sandblasting abrasive. You should always use waterjet abrasive, as it has the characteristics that optimize cutting for an abrasive waterjet. Waterjet abrasive, or garnet, has been shown to cut up to 30 percent faster than sandblast abrasive due to the hardness, consistency, angularity, and friability of the garnet. Sandblast abrasive does not cut as well as garnet since it tends to be softer and rounder.

When selecting abrasive, you want to choose an abrasive that has consistent shape, weight, hardness, and angularity. Consistency of abrasive particles provide a consistent flow rate, which is an important factor in cutting high quality parts. Minimal dust is another advantage to using waterjet garnet, since excessive dust can have an adverse affect on both the machine and the work environment.

4. CONCLUSION

Thoroughly researching both the product and the company is critical to the purchase of an abrasive waterjet system. You want to make sure that the equipment will support your application(s) and that you will receive the service and support that you need after the sale. If you've made an investment in an abrasive waterjet system, you want to get the most out of that investment. By utilizing the above techniques and technology, you can be on your way to maximizing the profitability of your waterjet—and increasing your bottom line.

USING 40,000 PSI WATER JETTING FOR FIELD WORK

Michael T. Gracey, P.E.
Industrial Pressure, Inc.
Houston, Texas U.S.A.

ABSTRACT

40,000 PSI high-pressure water is being used on a project in a Mexican shipyard to remove existing coating for re-application. This paper will discuss the hardware used such as positive displacement pumps, flow splitters, tumble boxes and rotating handguns. Pump flows, discharge pressures and the results of jobs in the field will also be discussed. Illustrations are included showing the surfaces being prepared with Ultra-High pressure water and the hardware being used up to 40,000 PSI.

1. INTRODUCTION

In an article (Reference 1) written in 1996 entitled IS 40K KING? the question was proposed “What happened to 30,000 psi”? There were also statements about how the present equipment has developed into dependable 30,000-psi and 40,000 psi versions. In a recent field application for 40,000 psi, there was good reason to re-think using 30,000 psi instead of 40,000 psi as well as doubting whether the dependable stage has been reached for Ultra-High pressure equipment. A paper (Reference 2) given at the Society for Protective Coatings 1998 Seminars discusses several actual case studies in the use of Ultra high pressure water jetting. This paper discussed the advantages of eliminating the cost of grit and its disposal while allowing other work to continue adjacent to water jetting operations. Standards for surface preparation using high-pressure water are being developed as described in a paper (Reference 3) given at the Waterjet Conference in 1997. Since that time, there has been progress in promoting the use of Ultra high-pressure water and in developing standards, cost comparisons and the exchange of information.
Also at the Waterjet 1997, a paper (Reference 4) was given tracing the acceptance of UHP water jetting for surface preparation. Personally, I am all for water jetting and feel it has a great future. The following is a case study from a slightly different perspective.

2. DESCRIPTION OF THE FIELD JOB

The customer called around April of 1998 with a request for a quotation on 40,000-psi equipment to remove coatings from an offshore rig. Of course the pump unit, accessories & spare parts had to be delivered within 3 weeks after receipt of order (this always compounds the problems). A 40,000-psi pump was purchased, because the time was so short and the process of getting the hose, guns, nozzles, flow splitters and tumble boxes ready and tested before shipment to Mexico. All went surprisingly well and the system was assembled and tested for a few days before the truck arrived. Figure 1 shows the Semi-Submersible drilling rig at dockside in Mexico. The coating was to be removed for repainting using two rotating hand held guns with multiple sapphire nozzles. The equipment arrived safely and a start-up man was dispatched for on-site training. Figure 2 shows the scaffolding and coating removal work progressing.

3. DESCRIPTION OF THE EQUIPMENT

The customer ordered a pump unit for operation at 40,000 psi and 8-gpm as shown in Figure 3. The pump was driven by a 200 H.P. diesel engine and skid mounted for the dock side work. Water quality was a concern, so a primary filtration package was built with a sand filter and two bag filters sized to 10 Microns as show in Figure 4. The pump had additional filtration to 1 micron and a charge pump was added that maintained 40-psi suction pressure and adequate flow for the pump. Because the customer wanted a dual gun operation, there were two flow splitters, two tumble boxes, four air hoses, interconnecting hose, eighteen sections of 40,000 psi hose (with heavy black hose cover) and two rotating guns. This equipment and accessories would probably work fine for short duration jobs, but this was a continuous production situation and the customer did not expect to have any trouble with the new system.

4. PROBLEMS ENCOUNTERED

After three days of start-up & training, the technician, returned to the USA, leaving the equipment running very well at 40,000 psi. A week later the breakdowns began with stuffing box cracks, hose leaking and gun swivels failing. The technician returned to the job site and repaired the pump and gun swivels while preparing to replace the heavy black covered hose with lighter whip hoses. The rotating guns begin to break shafts and use seals at an unsatisfactory rate while sapphire nozzles were being supplied by the dozens. Eventually all the Ultra-High pressure hose was replaced with another brand and the spare parts ordered with the unit were being depleted.

The hose that was obtained on the rush basis was rated at 45, 310 psi working pressure and 90,625 psi burst by placing a heavy black hose over the wire re-enforced high-pressure hose material. It was too heavy, but time did not allow replacement before shipping. The weight of the hose made working with the rotating guns very difficult and tended to break the delicate HP swivel shafts. Whip hoses were added as soon as possible and then the entire 18 sections of hose were replaced with another brand that had a clear plastic cover over a hose rated for 48,000 psi working pressure and 120,000 psi burst.

The high-pressure pump cracked it first stuffing box (cylinder) after the first week of operation. Then it continued to crack cylinders about every 40 hours until the job could not continue. Another unit was sent to the job site that could produce 30,000 psi and the 40,000-psi unit was returned to the US for further testing & repair. Cylinder material was changed, the manufacturing process was changed and the pump was run around the clock. An antenuator was added and a final set of cylinders was installed of the type that had been run in a test program being conducted by the pump manufacturer. The pump also cracked valve seats during this whole process of trying to get the pump to run at a continuous 40,000 psi. After this testing program, the unit was returned to the job site in Mexico. The unit was on the job for another two weeks before an engine problem occurred that was due to improper packaging and the new hose begin to fail under the strain. When a valve seat broke, the customer demanded pump replacement, so our top people were sent to the job site to try to resolve the conflict. It was found that the 30,000-psi unit was doing a good job and so the customer was agreeable to reducing the pressure on the 40,000-psi unit to around 30,000-psi.

The customer required that the pump unit operate 2 guns, so a flow splitter was used. The wear items in the flow splitter were being replaced on a regular basis and the water stream from the internal nozzles caused more problems.

The water jet inside the splitter hits a stainless steel plug before the water turns 90 degrees; this is done to protect the hose from internal damage. The stainless steel plugs wear rapidly, allowing particles of stainless steel to flow to the tumble box, the rotating gun and eventually to the nozzles. Hence, premature wear and over pressuring of the system. Figure 5 shows the flow splitter device used in the system (two required).

Then there are the tumble boxes (remotely actuated valves) which were another source of maintenance concerns. The pneumatic operators jam after a while and the valve body wears fairly rapidly at 40,000 psi. Without functioning tumble boxes, the work can not progress. Repair of these boxes along with the repair of the flow splitter has been a considerable part of the maintenance. Figure 6 shows the air actuated tumble boxes used in the dual gun system.

5. MAINTENANCE & SAFETY

The training in maintenance and water jetting safety given to the operators in Mexico has helped throughout the process of keeping the equipment running. Even though the operators and maintenance people in the field have learned the system fairly well, things happen that are not fully understood. A conference call indicated that the big picture was not understood: a knock in the power frame of the pump was reported and the job was stopped. After full discussion of what to do and overnighting parts, the next day the pump well cover was removed and a broken plunger was discovered. A maintenance man and operator not understanding what was knocking caused the shutdown and the days of delay. Safety has been good at the job site and credit should go to the trainer sent to the job site before the work could begin.

6. CONCLUSIONS

Each pressure range has its place in the industry and probably always will, but this project has indicated these things:

- Don’t use any more pressure than necessary to do the work
- It cost more to run 40,000 psi than it does 30,000 psi
- Use a single gun when you can
- 40,000 psi systems are still in development for production work

The water jetting industry has a bright future and we will all be trying to invent better pumps, better accessories and improve personnel safety.

7. REFERENCES

1. Michael T. Gracey, June 1996, IS 40K KING?, Cleaner Times, Little Rock, Arkansas USA.

2. Richard F. Schmid, November 15-19, 1998, ULTRA HIGH PRESSURE WATER JETTING FOR COATING REMOVAL, SSPC 1998 Seminars, Orlando, Florida USA.

3. Lydia M. Frenzel, Ph.D, August 23-26, 1997, CONTINUING IMPROVEMENT INITIATIVES OF SURFACE PREPARATION WITH WATERJETTING, 9th American Waterjet Conference, Dearborn, Michigan USA.

4. Richard Schmid, August 23-26, 1997, UHP WATERJETTING GAINS ACCEPTANCE FOR SURFACE PREPARATION, 9th American Waterjet Conference, Dearborn Michigan USA.

Figure 1 – Job in Mexico

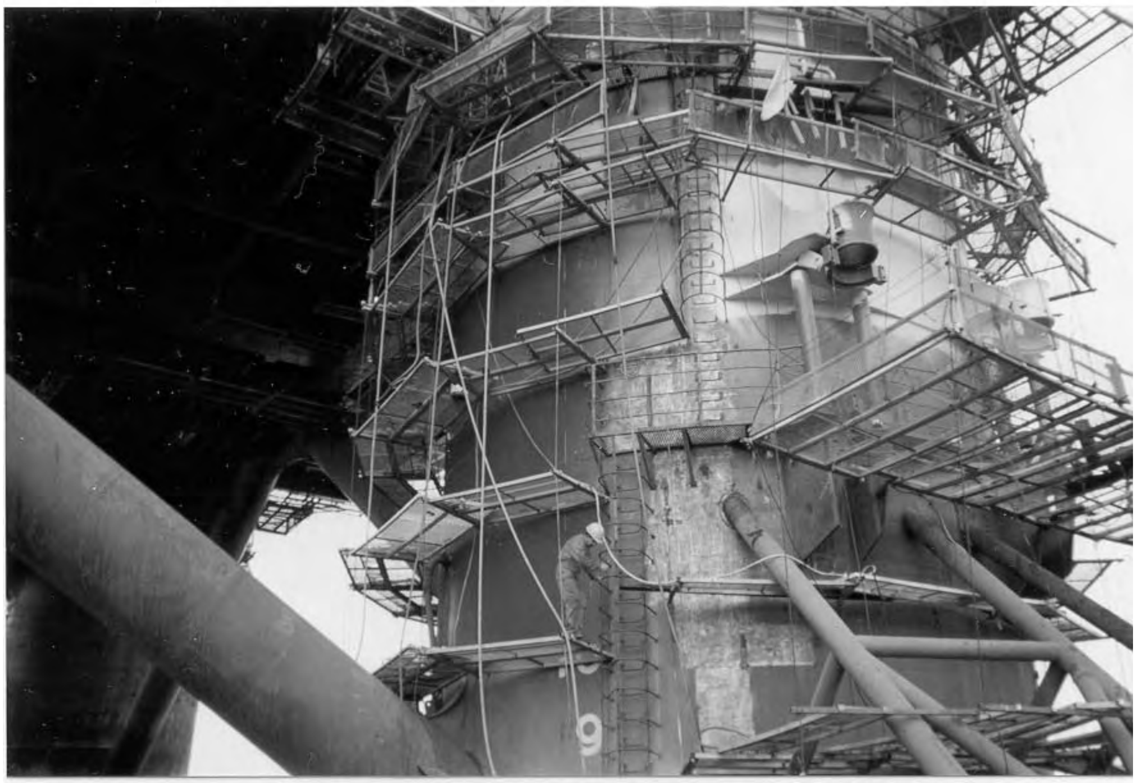

Figure 2 – Removal of Coating with UHP

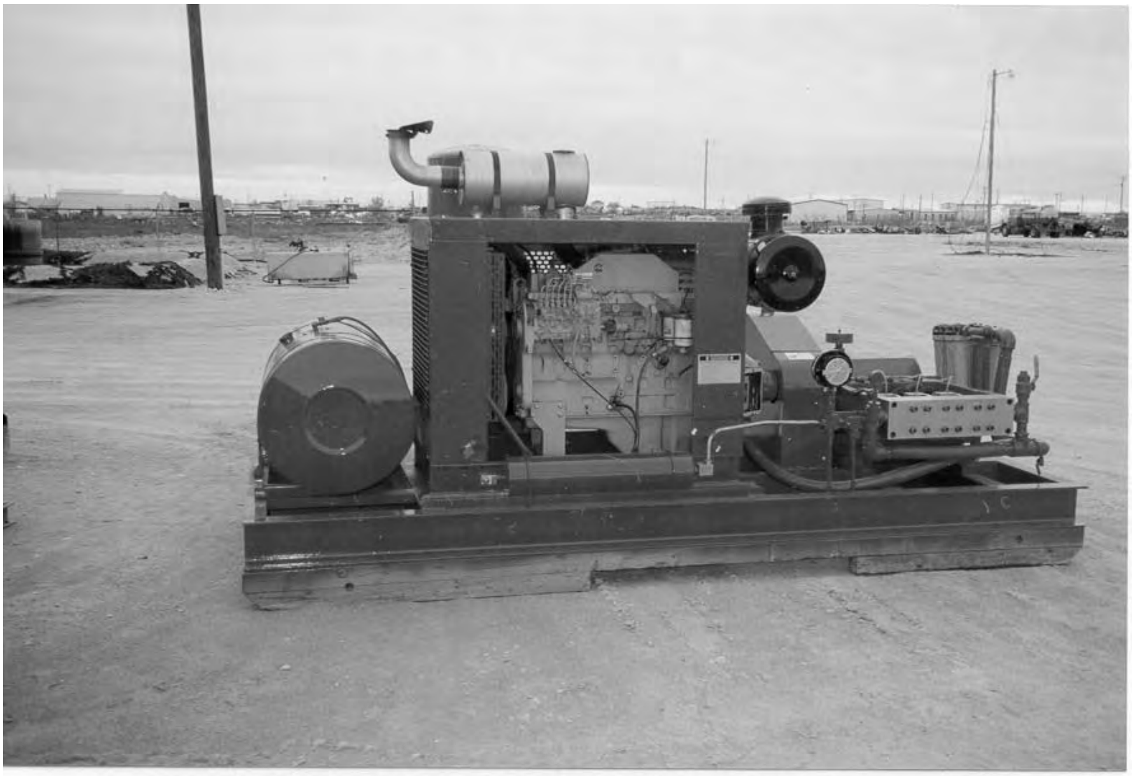

Figure 3 – 40,000 psi Pump Unit

Figure 4 – Primary Filtration Package

Figure 5 – Flow Splitter Device

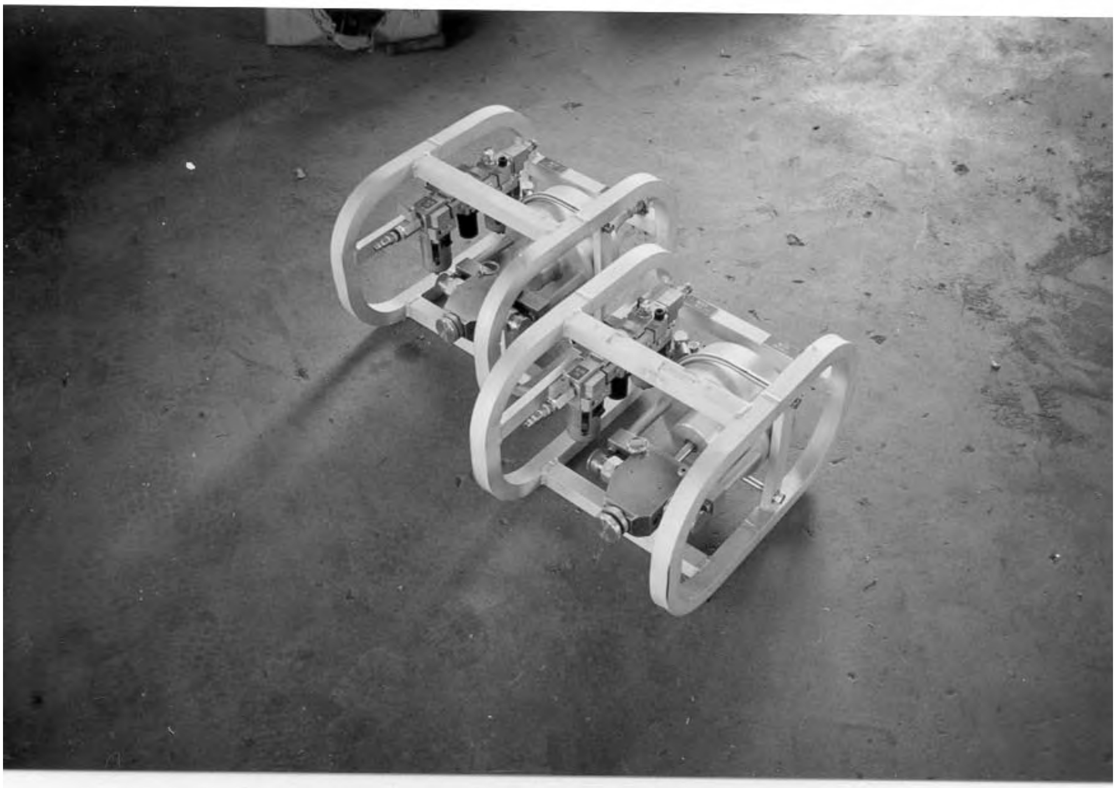

Figure 6 – Tumble Boxes

10th American Waterjet Conference
August 14-17, 1999: Houston, Texas

Paper **57**

DESIGNING AND BUILDING

A WATERBLAST TRAINING COMPLEX

R. Bruce Wood
MPW Industrial Services, Inc.
Hebron, Ohio

ABSTRACT

This paper will describe a Training Complex designed and built at MPW Industrial Services, Inc.'s Hebron, Ohio, headquarters. The Complex consists of a 40-foot high training tower incorporating several areas for hands-on waterblast training, including a 16-foot vertical condenser with confined space access; a stack-tool tower; an area for overhead waterblasting; and the means to string waterblast hose 40 feet up and back down.

A 35-foot tank truck shell incorporates confined space access to a horizontal heat exchanger, while a separate stand-alone horizontal tube bundle is also available for hands-on lancing experience.

A 6-inch underground polyethylene pipe with elbows is also available for line moleing experience.

The paper will include photos of the Training Complex in use, as well as the philosophy behind the development of the Complex.

Organized and Sponsored by the WaterJet Technology Association

1. INTRODUCTION

"Each employer…shall furnish to each of his employees employment and a place of employment which are free from recognized hazards that are causing or are likely to cause death or serious physical harm to his employees;…"

With this broad statement the Occupational Safety and Health Administration (OSHA) officially put employers on notice that they are to be held responsible for ensuring that employees who are, or can reasonably be expected to be, exposed to "recognized hazards" are properly prepared to handle those tasks safely. In the absence of more specific legislation, the general duty clause is OSHA's first line mechanism to encourage workplace safety.

Since OSHA has no specific guidelines for safety involving high pressure waterjets, the mandate, vague at best, leaves interpretation to the investigating officer, which in turn leads to subjective enforcement standards that can vary with the individual inspector and the particular circumstance. In an industry such as ours, the training an individual receives can be a key factor in preventing accidents, as well as in the subsequent accident investigation.

Training employees to safely and effectively operate high pressure waterjet equipment is no longer a happenstance event that may or may not take place in the field under the guise of "on-the-job training." Not only is effective training mandated by the federal government, it is a primary step in a contractor's competitive edge, a necessary self-defense against rising medical and insurance costs, and a true sign of professionalism and leadership in an industry that is still in its infancy.

As any competent trainer will tell you, the retention time in learning from a video is low – 30% or less. In short, an effective training program consists of telling the training what is to be done, showing the trainee, and then having the trainee demonstrate back to the trainer that he has acquired the skill in which he is being trained. Let's make sure we understand this – even demonstrating back to the trainer that he can properly perform a task does not mean that we have a competent, seasoned employee; this comes only with experience and time on the job. Training does, however, reduce the potential for a serious accident as the new employee enters the work force to get that hands-on experience.

As customers demand that a contractor supply competent, trained employees, putting an employee with "Joe," who has been doing the work for many years, and hoping it will rub off, is no longer a valid means of training an employee. Not only may "Joe" be ineffective in training another person, his main interest is in getting the job done – not in teaching someone else to do it.

Therefore, in order to provide an environment in which a person can be safely and effectively trained, the concept of a "training complex" is born. The effectiveness of this training area is improved as we go beyond just a place to "try a gun and a lance," and begin to duplicate, as much as possible, the environment in which the trainee will be expected to work.

Ideally, this "complex" will provide the trainer and the trainee a place to work together to properly set up a job site, inspect and prepare the equipment, and then permit the trainee to get hands-on experience in as many facets of what he may face in the field as possible. Examples of this experience are in starting up and shutting down a pump, running hose (including up and down stairs), "shot-gunning", moleing and lancing, waterblasting overhead, confined space entry, etc.

Let's explore some ideas for a "training complex," as instituted at MPW Industrial Services, Inc.'s corporate headquarters in Hebron, Ohio.

2. THE FIRST STEP

The waterjetting trainee's first exposure at MPW, following classroom instruction in the basics, is in setting up a waterblast area, including barriers and signs, pump, hose runs, etc. The training complex has a waterblast pump dedicated to the purpose of training. (Figure 1.)

Figure 1. MPW's training area, showing trainees setting up area for blasting

In this exercise, the trainee learns how to recognize the equipment, assemble it and inspect it for safe operation, and then how to actually use it. All of the equipment – hose, guns, lances, stanchions, signs and barrier tape, foot pedals, etc. – are kept in the training complex as dedicated equipment.

The destructive force of a waterjet stream is demonstrated by cutting a wood 2" x 4" clamped to a stand. (Figure 2.)

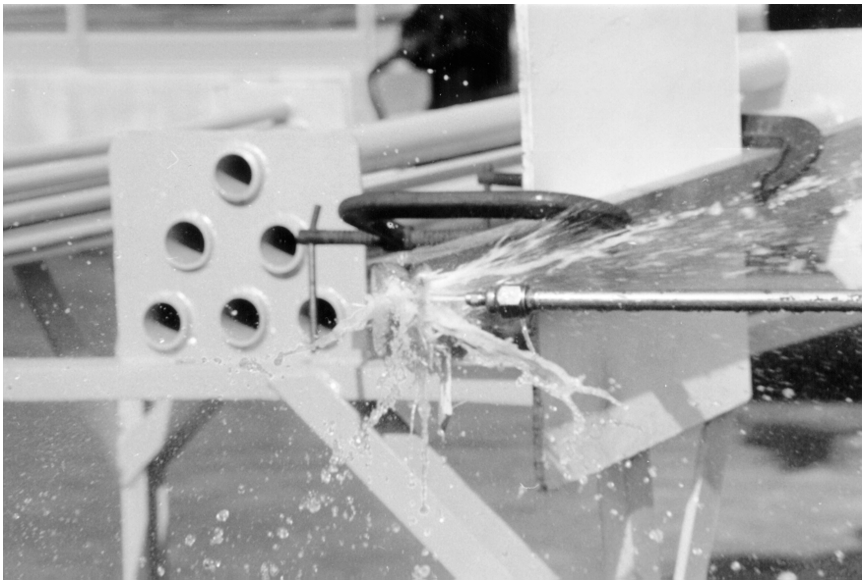

Figure 2. Trainer demonstrating the destructive power – and therefore the danger – of waterblasting

To get the feel of having a waterblast gun at his or her shoulder, the trainee blasts paint off of a target plate, slowing moving toward the plate as the instructor has his hand on the trainee's shoulder. One good idea here is to have a foot-pedal in series with the waterblast gun, so that if the trainee suddenly finds himself off balance, another person can quickly kill the pressure to prevent a possible accident. In this case, a sudden lurch forward and a fall are better than a potential waterblast injury. (Figure 3.)

Figure 3. Trainee blasting at target plate, with trainer back-up

By the same token, the trainee's initial exposure to lancing is through a series of pipes welded horizontally to a stand to simulate a heater exchanger. The use of a double foot pedal also makes this a safer training exercise. (This stand may be seen behind target plate in Figure 3.)

3. THE TOWER

The heart of the training complex at MPW is a forty-foot tall training tower. (Figure 4.) This tower is approximately twelve feet square at the base, built with 8-inch wide-flange columns. The top of the main tower structure is at a height of 30 feet, with a platform at the 40-foot level accessible by a ladder. With this design, the trainee is exposed to an industrial setting, including climbing the final ten feet to the top. (This has an additional benefit of determining a trainee's comfort level at heights.)

Figure 4. Training tower.

As can be seen in Figure 4, the tower has several intermediate levels; the first has access by a short ladder to a level where a trainee can get a feel of waterblasting overhead. In this exercise, as he is blasting a thick paint coating, he experiences the feeling of becoming drenched with water and debris. (Figure 5.)

Figure 5. A trainee blasts overhead to get the feel of getting drenched with water

On the next level, entry into a confined space, which encompasses one quadrant of the floor area on that deck, permits the trainee to lance a 16-foot vertical heat exchanger which has been plugged off with a weak sand-mortar mixture. (Obscured in lower left of Figure 4, right center of Figure 5.) A removable panel on the outside of this section gives access to a clear polycarbonate panel, thus permitting the training exercise to be viewed from outside the tower. The access door to the confined space has a rail above it both inside and outside, similar to a boiler entrance door through which a trainee may someday be expected to enter a boiler. (Figure 6.)

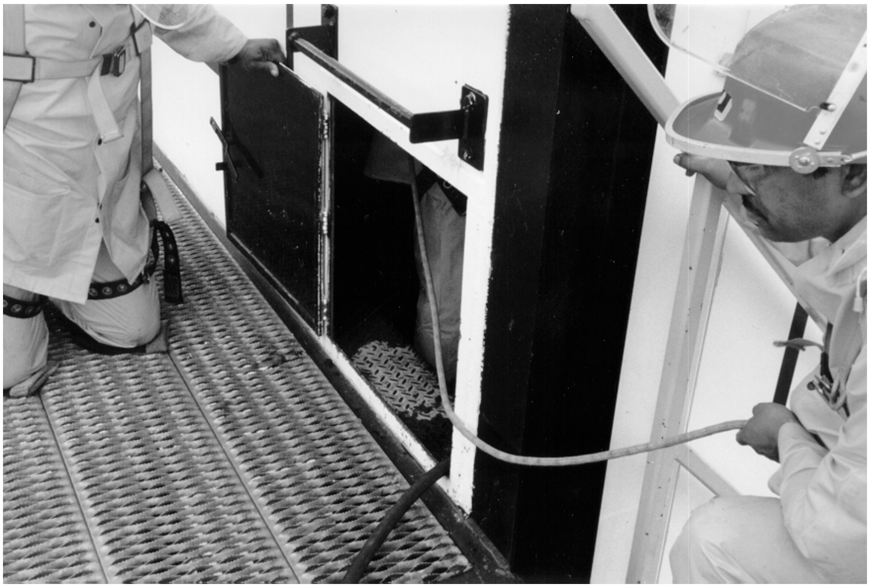

Figure 6. Entry into the confined space area

As shown in Figure 7, the bottom of the tube bundle is guarded with clear polycarbonate panels, not only to prevent injury to a bystander, but also to see the force of the lance jets as they emerge from the tubes.

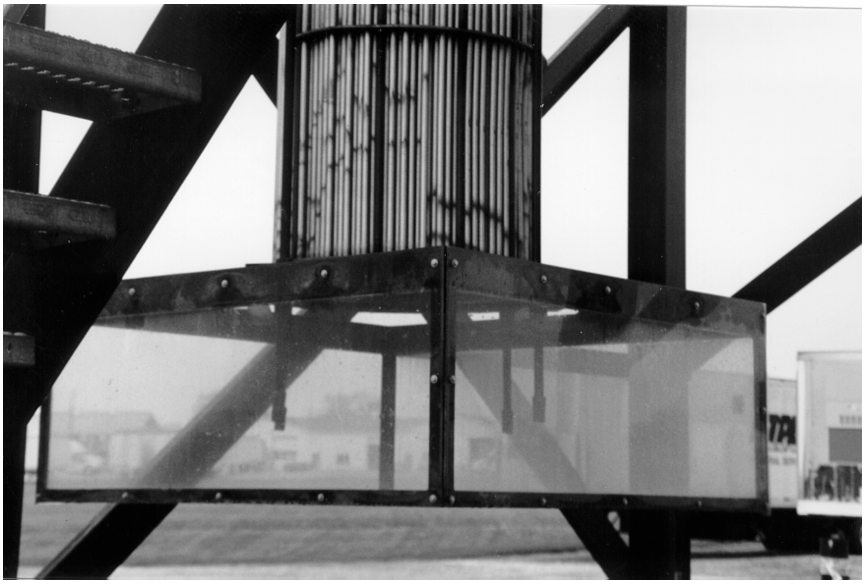

Figure 7. Exit end of the bottom end of the tube bundle, showing guard

On the top level of the main tower, a trap door permits a person to be lowered from a tripod to get experience in a boson's chair or work harness. (Figure 8.)

Figure 8. Trap door through which a trainee can be lowered with harness and tripod

By climbing to the very top, the trainee has access to the top of a 36-inch diameter, 10-foot long vertical stack, and can be trained in the use of stack tools.

By running waterblast hose to the top of the tower and back, the trainee can learn how to tie off hose at rails, as well as run hose safely up stairways, across walkways, etc. (Figures 9 and 10.)

Figure 9. A waterblast hose tied off properly at a rail

Figure 10. Waterblast hose tied off properly along a stair rail

4. HORIZONTAL TANK AND TUBE BUNDLE

By using a discarded tanker shell, MPW created a horizontal confined space area which permits a trainee to be lowered into a tank, then lance a horizontal tube bundle while inside the confined area. (Figures 11 and 12.)

Figure 11. Tanker shell with internally mounted horizontal tube bundle. Note horizontal tube bundle in foreground

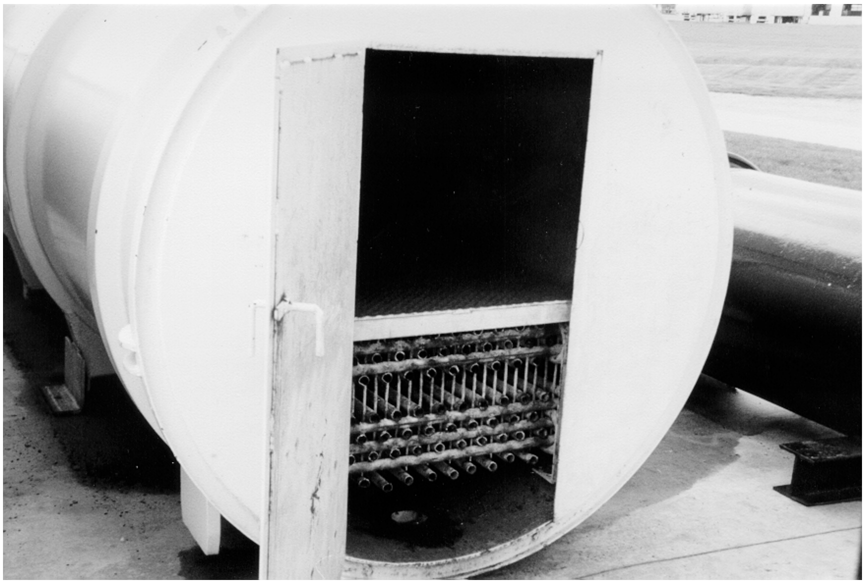

Figure 12. Exit end of tube bundle installed in tanker shell

In addition to the lancing exercise, the other end of the tank has a clear polycarbonate viewing port in a confined space section that can be sealed off. This area can be used for advance confined space entry training, with smoke introduced and the trainee, already on an external supply, expected to use his 5-minute escape bottle to get out of the tank.

A horizontal tube bundle offers the opportunity for more realistic lancing of this type of process equipment (Figure 13.)

Figure 13. Trainee lancing tube bundle. Note instructor using a second foot pedal

5. UNDERGROUND PIPE

A 6-inch pipe buried underground with both ends exposed, having two elbows, provides a moleing experience for trainees. This teaches them the difference between moleing and lancing, with the use of a turn-prevention nipple next to the nozzle to prevent the nozzle from turning around in the pipe and coming back out at them – a frequent cause of injuries that has resulted in fatalities. (Figure 14.)

Figure 14. Trainee moleing 6-inch buried polyethylene pipe

6. CONCLUSION

When asked when the Training Complex will be completed, our answer is probably – perhaps hopefully – never. There will always be new ideas and improvements to enhance the training environment, and changes will be made as time and money permits. For example, 3-inch or 4-inch pipe drains could be run from upper levels, to permit an exercise in lancing this type of drain.

In any case, this is one way a training complex might look. With the creative use of discarded and scrap materials, one can come up with numerous ideas on how to provide an environment which simulates the typical workplace. Scrap tube bundles sit in the boneyards of many customers and can frequently be bought for scrap prices or obtained free; roll-off boxes and tanks of various sizes may be used. 21,000- gallon oil-field frac tanks can be cut welded and tubes added, and confined spaces of various sizes can be built in.

The most important thing is to give a trainee a place to get a hands-on education in the often difficult, and always potentially dangerous, work field that he is about to enter.

10th American Waterjet Conference
August 14-17, 1999: Houston, Texas

Paper **58**

APPLICATION EXAMPLES OF WATERJET CUTTING PROCESSING

Xue Sheng Xiong, Huang Wang Ping, Peng Hao Jun
General Machinery Research Institute, Bureau of National Machinery Industry
Hefei, Anhui Province, P. R. China 230031

Li Yue Feng, Song Jing Wei
Hua Zhen Machinery Equipment Co., Ltd.
Guangzhou, Guangdong Province, P. R. China

ABSTRACT

The 300 MPa waterjet cutting system used for metal or nonmetal plates cutting has been commercialized in China. In this paper, we introduce several waterjet cutting application based on the waterjet cutting system developed by ourselves, which are: 1) cutting, putting together and adhering of polyhedron; 2) cutting through or semi-cutting through effect of entire pattern achieved by using different cutting speed; 3) compensation for width of cutting seam; 4) high power multi-heads waterjet cutting manufacturing line; 5) cutting effect of artificial multi-layer composite plates and 6) robot waterjet cutting.

Organized and Sponsored by the WaterJet Technology Association

1. INTRODUCTION

In August 1998, the technical appraisal of 300 MPa waterjet cutting system managed and mainly developed by the Hefei General Machinery Research Institute was passed by the National Machinery Industry Bureau of China. This marks that the ultra high pressure waterjet cutting technology has entered its commercialized stage.

This set of ultra high pressure waterjet cutting system developed by writers adopts the three pistons ultra high pressure pump as source of high pressure water. Its power is 15~30 kW. It consists of ultra high pressure pump, pressure regulation vessel, pneumatically driven relief valve, safety valve, X-Y two dimensional cutting table, abrasive supply system, cutting head, numeric control system and its software, etc. Sale price of total system is less than 100 thousands dollars (Shown in Figure 1). In this paper, we mainly discuss the summarization of our experiences during period of product development and service after sale. To technologies used in total set of system, please refer to our another paper titled "Extended Technologies for Ultra High Pressure Waterjet Cutting System".

2. CUTTING OF POLYHEDRON

The local cutting of stereoscopic polyhedron can be accomplished by the two dimensional plain cutting system assisted with special designed jigs or clamps. After that, these cut pieces are put together using adhesive and the designed stereoscopic pattern is formed. This process is often used for cutting of symmetrical patterns such as pentagram or hollow hexahedral column and is very fit for usage in architectural decoration.

To be an example, the cutting process of a stereoscopic pentagram is explained as following. First, we divide the pentagram into ten same triangular elements. Each element is tilted an α angle employing the side a coinciding with bottom plane as datum and a triangular wedge is formed. Second, we clamp raw cutting material on the triangular wedge, cut surface and a surface c tilted an α angle to horizontal plane in sequence. Side b is always in vertical position to horizontal plane and is not needed cutting. By adhering these cut elements together, the stereoscopic pentagram is formed. Its outline is always perpendicular to horizontal plane. Inlaying it into plane with a hollowed-cut pentagram and making upside of surface a be on an equal footing to up surface of plate, the effect of towering planes has much lingering charm as shown in Figure 2.

3. COMBINATION EFFECT OF CUTTING THROUGH AND SEMI-CUTTING THROUGH

As we also know, one of the advantages for waterjet cutting is that we can set breakpoint at any time at our wish to machine complicated plane designed pattern. In waterjet cutting tests, it is easy to regulate working conditions such as type of abrasive and its grain size and working parameters of waterjet to achieve maximum cutting speed for a given thickness material. Under that speed, the given material can be cut through. Meanwhile, it is obvious to find that if cutting speed exceeds that critical speed, the given material becomes unable to cut through, that is to say, it only can be semi-cut through. If we apply these two methods skillfully to cutting a complicated plane pattern, make the cut through paths become outlines and semi-cut through paths become lines, their combination forms a live drawing combined lines to surfaces. Figure 3 shows a copper plate drawing. The semi-cut through lines are made by applying two times cut through speed cutting. The added lines increase the vitality of entire drawing obviously.

4. COMPENSATION FOR WIDTH OF CUTTING SEAM

Usually, width of abrasive waterjet cutting seam is about 1 mm. Though this precision can fully meet normal cutting demands, the 1 mm wide adhesive line is not able to show its fine art in hyper -critical male and female models piecing together. Especially to the piecing together formed by plates, it is hoped to have no such colored adhesive line left. That is to say, it is demanded the width of cutting seam reaches near zero. This kind of seemed not be able to realize demand is very easy to fulfill by software. We cut the different color male and female models separately, expand their outlines half width of normal cutting seam respectively or keep one's outline maintain the same as usual, just expand another's outline width of normal cutting seam in control software. The compensation effect of zero cutting width is achieved by fitting the male and female parts together. Of course, if you want to use the cut material for exchanged colors piecing together, this compensation method wastes the material because the expanded material is small to have no use. If gaps are allowed to be left between cut colored blocks, it is needless to use this compensation method. But if zero seam width is wanted, this kind of compensation method is must be used (Figure 4).

5. MULTI-HEAD WATERJET CUTTING MANUFACTURING LINE

During our participation in the 9th American Waterjet Technology Conference, our Chinese delegation visited the multi-head waterjet cutting system in a U.S.A. company. In China, our research on it is brought up by the needs of floor bricks manufacturers and their production lines.

As we have investigated, the last process in floor bricks manufacturing is trimming and grinding the edge of bricks. This process first cuts the opposite two edges of brick at the same time using diamond grinder, then turns the brick round at an angle of 90° and cuts the other two edges. The manufacturing quality standards require that diagonal error is less than 1 mm and defect is not allowed to exist in four edges. Before our research succeeds, the adopted process whose substance is milling used 4 or 5 pairs of grinding wheels whose diameters were 250 to 300 mm. driven by electric motors to trim and grind step by step. The rigid collision between grinding wheels and brick often make the rims collapse. Most bricks with lightly collapsed rim are repaired by using another grinding head to mill and chamfer at the angle of 45°, some with badly collapsed rim have to be cut smaller and become defectives or rejects. Reject rate of this process is around 5% and defective rate usually is 20%. These make it urgent for manufacturers to find new substitute producing process for mechanical trimming and grinding and increase high-class product rate.

Our first generation waterjet cutting system works under the parameters of p=300 MPa, Q = 2.5 L/min., P = 15 kW, d = 0.25 mm and d_a = 0.8~1 mm. Purpose to choose these parameters is to minimize investment risks and achieve waterjet cutting process. In tests using the single cutting head installed, the maximum line cutting speed for floor brick is 1.3 m/min., while the being used production line's moving speed is 2.5 m/min.. So it needs two cutting heads working at the same time. The reason to choose waterjet-cutting process is that waterjet cutting is a non-contact cold machining process. When using this process, edge of brick is not easy to collapse and milling or chamfering process is no longer needed. There is no obvious wide gap left when piecing together the bricks. So the waterjet cutting process can essentially improve the quality and increase the high-class product rate of floor bricks.

Improvement to our former measure is achieved by increasing power of the system up to 55 kW and flowrate up to 9 L/min. The two cutting heads working together make the cutting speed increase to 2.5~3 m/min. Based on used system and experiences gathered from tests, the new design is being carried out. It is believed that a revolution will be brought out to trimming process for Chinese floor bricks production industry if this method succeeds and is spread out. We also welcome foreign friends to cooperate with us to invest and exploit the huge market in China.

6. CUTTING OF ARTIFICIAL COMPOSITE PLATES

It is worth paying much attention to cutting of artificial composite plates used in luxurious construction fitting up and decoration. Usually, the artificial composite plate is made by two different kinds of plate adhered together. Purpose to use this material is first, to lower cost, upper or surface plate uses high class material while bottom plate uses normal material; second, to increase feeling of thickness for entire pattern and third, to utilize the change of colors, lights and shades made by two different materials in different places for a better decoration effect. Example discussed in this paper is a large pattern cut with a 2 mm thick stainless steel plate compounded with a 12 mm thick glass plate. Since it is much easier to cut glass plate compared with stainless steel plate, to cutting conditions discussed here, cutting the mentioned composite plate is equal to cutting the pure stainless steel plate.

Cutting of artificial composite material has a wide range of use. Normally, the lower material is easy to cut compared with the upper material. It has no special demand for waterjet cutting, even the cutting speed also has no great change. The only notice while waterjet cutting is to adhere the two different kinds of material together tightly and make them to be an entire one before cutting.

7. ROBOT WATERJET CUTTING

In fact, the two-dimensional plane waterjet cutting system that we have successfully developed belongs to one kind of robot waterjet cutting system. But in practice, the robot waterjet cutting is usually specified to three-dimensional waterjet cutting. Based on experiences gathered from our development of two-dimensional cutting system, we elementarily develop the three-dimensional robotic waterjet cutting system.

The newly developed system is changed from the existed and commercialized robot system. It has six freedoms, which are line movement of axis X, Y, Z and rotation of axis X, Y, Z. Because of the characteristic of non-contact cutting of waterjet cutting and small reacting force that is only less than one hundred Newtons, waterjet cutting system has little influence on the structure of robot and its control system. The total robot system is driven and controlled fully electrically, its maximum load is 100N, and repeating orientation precision is ±0.25mm. Maximum synthesized speed is 1m/min. Maximum moving range for each axis is: line movement of axis X is 1m, axis Y is 0.8m and axis Z is 0.3m; rotation of axis X is ±120°, axis Y is ±120°, axis Z is 300°. The total system is controlled through computer CNC and has standard computer interface and ports. Cutting parts and their dimensions can be input through CAD software or scanner. During cutting, the shape and dimension of being cutting parts, track of head movement and current position of head can be displayed on monitor. Set or pause at initial point and breakpoint and repeated cutting of none cutting through path can be fulfilled automatically or manually. Total system can achieve the cutting of two-dimensional plane, three-dimensional camber and ripple surface.

8. CONCLUSION

The examples discussed above show the state and application level of Chinese ultra high-pressure waterjet cutting technology. Though some of the applications still need to be improved, it has found the basis of success. It is believed that the rapid developing Chinese waterjet cutting technology and its large market will go to mature through the international exchange of technology and economy information during years though start of Chinese waterjet technology research was late.

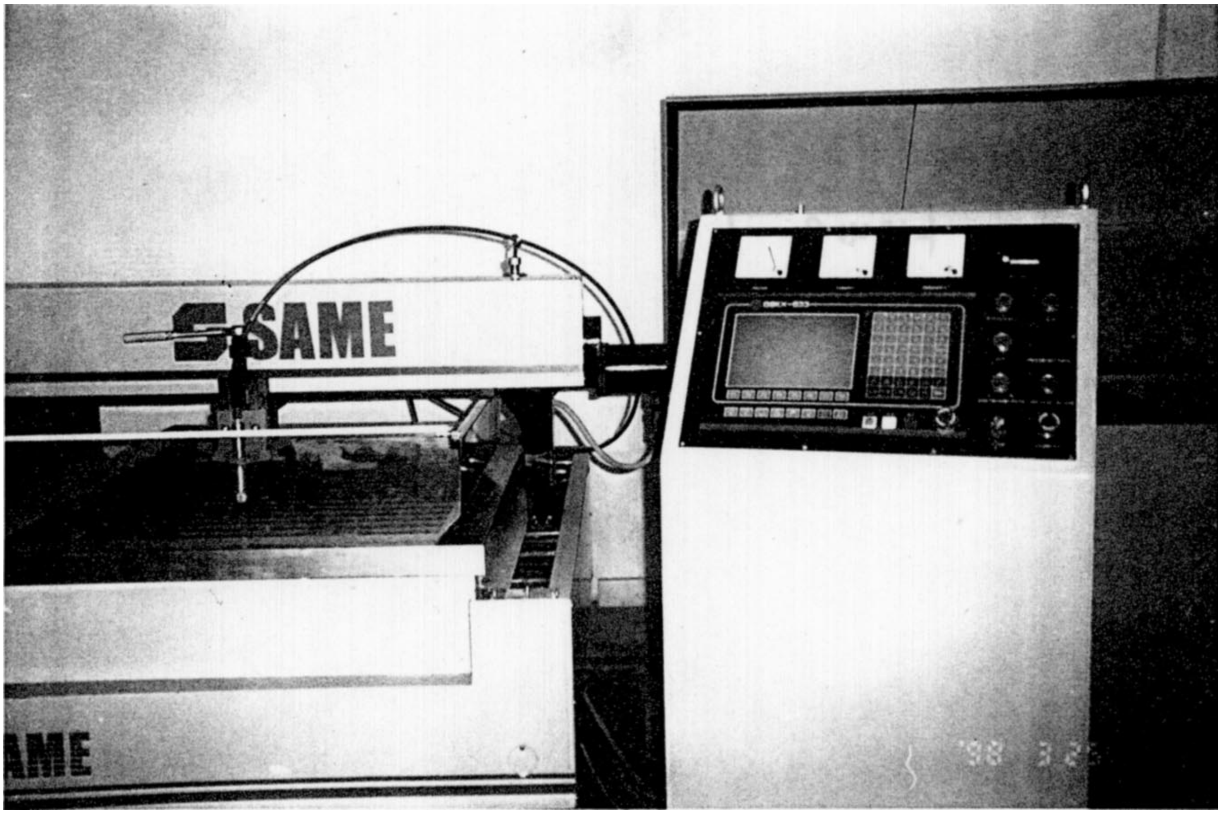

Figure 1. Waterjet Cutting System

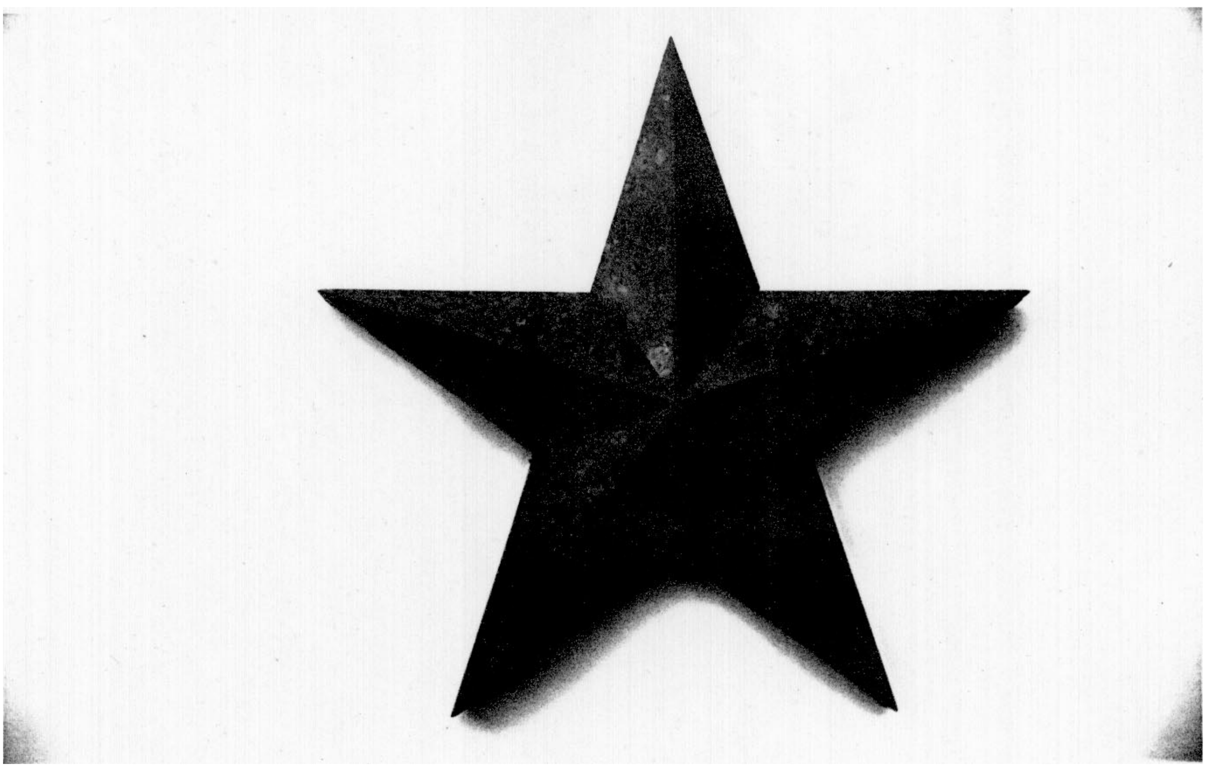

Figure 2. Stereoscopic Pentagram and Its Triangular Elements

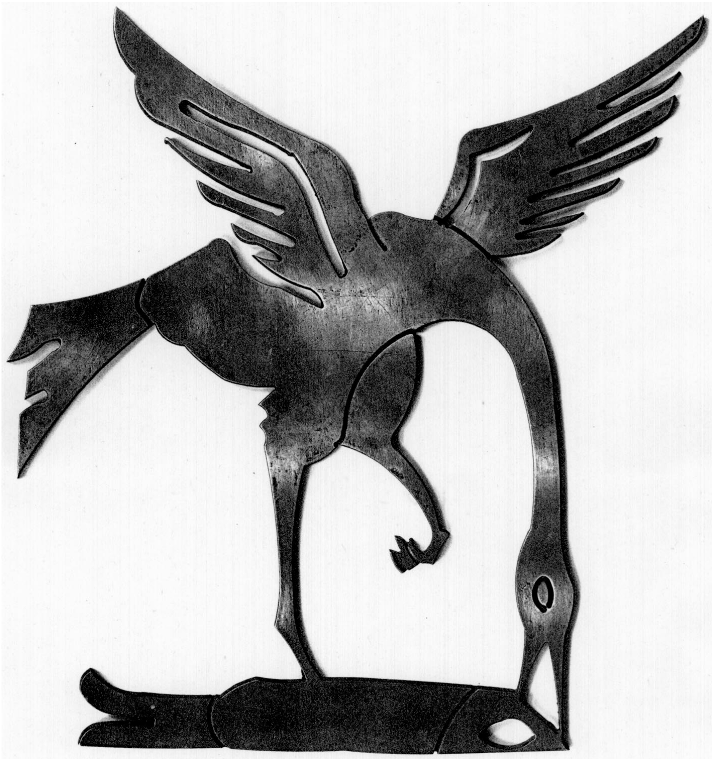

Figure 3. Combined Effects of Cutting Through and Semi-cutting Through

Figure 4. Piecing Together Pattern with Zero Cutting Seam Width

10th American Waterjet Conference
August 14-17, 1999: Houston, Texas

Paper **59**

THE DEVELOPMENT OF HIGH-POWER PULSED WATERJET PROCESSES

Gene G. Yie
Jetec Company
Auburn, Washington, U.S.A.

ABSTRACT

Pulsed waterjets have been known to have significant advantages over continuous waterjets in many applications. High-power pulsed waterjets in particular have intrigued many investigators due largely to their potential in some tough jobs in mining and construction operations. The word “water cannon” has been synonymous to such pulsed waterjet equipment. Unfortunately, these early efforts have not been very successful due mainly to the difficulties in generating and controlling the required force on water in these processes. This situation will be changed. Jetec Company has recently developed two processes for generating high-power pulsed waterjet that circumvented the previous difficulties. These processes involve sending pressurized water from a pump, any pump, into an energy storage device equipped with a unique on-off valve that allows unimpeded, fully-powered, high-speed water pulses to be generated at a downstream nozzle. By separating the pressurization of water from the pulsing mechanism, a practical, versatile, and reliable pulsed waterjet process is realized. By varying the water pressure, water flow rate, gas charge pressure, piston power ratio, valve timing, and nozzle diameter and geometry, pulsed waterjet of different characteristics can be generated. This paper discusses the processes in more detail and presents a list of their many potential applications.

Organized and Sponsored by the WaterJet Technology Association

1. INTRODUCTION

The word “waterjet” is now a common term; it is used to describe a high-speed, high-energy stream of water generated with special pumps and nozzles to perform a wide variety of work. Waterjets are generated today at a static pressure up to35,000 psi to clean industrial equipment, and at pressures up to 60,000 psi to cut many different materials. With the addition of abrasive particles, waterjets are used today to cut many hard materials such as glass, concrete, and metals in conjunction with tracking and robotic motion systems. These processes share the feature of having waterjets in the form of a continuous stream although on-off valves are used occasionally to interrupt the flow. These waterjet processes continue to grow and expand; new applications can be expected when new and improved tools are made available.

Pulsed waterjet, or pulsejet, is a different form of waterjet in which the flow of water is deliberately interrupted and the water stream is in the form of discontinuous pulses or slugs. The size of these pulses and their spacing in terms of time or distance may vary widely. The pulses could be small slugs that appear to human eyes as a continuous stream but are discreet slugs in reality. They could also be individual powerful slugs, as in the case of water cannons that resemble cannon shells in action. The objective for generating such waterjet pulses may also vary among various processes. In general, the main purpose is to enhance waterjet’s cutting capabilities as pulsejets are known to pack more impact energy and to have much less jet interference, among other benefits, when impacting a target.

A pulsejet could also be considered as a high-energy form of waterjet that is somewhat analogous to the capacitor discharge in electrical systems in which energy is stored to a high voltage and then discharged abruptly. When water is pressurized, stored, and then released rapidly through a suitable nozzle, it can do work that continuous waterjet cannot do or doesn’t do very well. Pulsed waterjets can also be a way of performing big jobs with a small-capacity pump when large pumps are not available or not suitable. An example of such situation is in the application of waterjet inside oil or gas well casings that are too small for accommodating large pumps. A similar situation exists in remote drilling of rock with waterjet where the pump is preferably located near the cutting tools to avoid the use of long sections of high-pressure hose. There are also waterjet applications in which only a massive dose of high-speed waterjet can achieve the desired results; examples include fracturing concrete, ice, rock, and minerals with waterjets. Even in common waterjet cleaning and blasting operations, it has been well known that waterjet in discreet pulses can cut materials much better than continuous waterjet. Thus, the desirability of pulsed waterjet technology of several different forms has been well known and accepted. Unfortunately, interrupting water flow at a very high pressure is not an easy task and the development of viable pulse jet technologies has been slow and is very much at its infancy to date. Jetec Company has been pursuing the development of improved pulsejet processes for many years; it has finally developed two processes that appear to be practical and useful.

2. BACKGROUND

2.1 High-Frequency Pulsejets

One form of pulsed waterjet is the high-frequency type in which the jet stream is obviously in slug or interrupted form; lawn sprinklers are example of this type. Another one is the very-high-frequency type in which the jet stream appears to be continuous to bare eyes but in reality consists of many closely-spaced slugs such that the number of slugs per unit of time could be up to several thousands per second. In between, there are other pulsejets in various forms mostly operating at relatively low pressures.

There are many methods for generating pulsejets. Using a single-plunger pump will instantly generate pulsating waterjet. Even a triplex pump having three pistons will generate pulsejet if the hose or tube between the pump and the nozzle is not too long. In most waterjet operations, hoses cannot be avoided and pressure and flow pulsations from a pump are mostly damped out. As a result, special nozzles are used to modulate the water flow in order to generate pulsejets. The basic method involved in modulating the water flow may vary among different processes; it could be mechnical, fluidynamic, mechanical-fluidynamic, electro-mechanical, magnetic, or other combinations. For example, rotating vans have been used in a nozzle to produce pulsejets. Piezoelectric tranducers have been used to modulate a fluid flow. Internal fluid resonance has been applied to construct pulsejet nozzles. And someday magneto-hydrodynamic principle may be applicable to constructing nozzles or pumps for pulsejet applications. Until then, high-frequency pulsejet is mostly a nozzle affair and is limited to relatively low pressures and low power output as large pulsejet nozzles may have technical difficulties

2.2 Low-Frequency Pulsejets

There are processes that can produce pulsed waterjets only at very low frequencies. The equipment involved is commonly referred to as "water cannon," which implies high power capability. There are two basic processes; they differ on how the energy is applied to the water.

2.2.1 Impact-Piston Processes

The most intriguing method for generating high-power pulsejets is the impact-piston approach in which a column of water inside a cylinder is impacted with a high-speed piston of substantial mass. The kinetic energy of the piston is rapidly transferred to the water column. Being incompressible, a portion of the water will be ejected out of the cylinder through a nozzle, which must be of a special design to facilitate the energy transmission and the generation of a high-speed pulsejet. The important process design factors include the driving and cocking mechanism of the piston, the shaping and containment of the water column, and the nozzle geometry. In general, compressed gas is used for driving the piston and hydraulic oil is used for cocking the piston. There are many variations in driving and cocking the impact piston; some processes involved a self-oscillatory piston capable of high-frequency operations.

It has been reported that impact-piston process can produce pulsejet of extremely high velocity and therefore very high impact pressure. In all cases, the impact of the piston on the water column is of very short time duration. Therefore, the water slugs generated by such water cannons are also of short duration and the efficiency of energy transfer during the piston-water impact is very important to the effectiveness of the process. It can be very difficult to generate such pulsejets if the power involved is very high, as the piston must be cocked against a compressed gas. The amount of compressed gas involved can be substantial such that valving and controlling the gas flow can be troublesome. Since the water is introduced at a very low pressure, it must be contained properly prior to the impact. Thus, the timing of water fill, the cocking of the impact piston, and the triggering must all be precisely controlled in order for the process to function properly. These difficulties prevented the realization of commercially viable processes of the impact-piston type despite that numerous promising results in breaking rock and concrete have been observed in laboratory and field tests.

2.2.2 Pressure-Extrusion Processes

Another type of water cannons that has been investigated in the past is the so-called “pressure-extrusion” type, which implies that a column of water is pushed out of a cylinder under pressure by a moving piston. The term seems to imply that speed of the piston in this case is slower than that of impact-piston processes. In actuality, the speed of the piston in both processes is determined by the magnitude of the driving force involved, and the cocking and triggering method. In both cases, the piston must first be pushed with a fluid to store the driving energy in a gas, and then cocked in a ready position while the cocking fluid is being withdrawn. Then the piston is quickly released to move toward the water column. If there is air between the piston and water, the piston will accelerate in speed before impacting the water column and the process is referred to as an impact-piston process. If the piston is in contact with the water at all times and there is no air or gas in between, the piston serves only as the intermediate between the compressed gas and the water and the process is referred to as pressure-extrusion type. Since the compressed gas is doing the pushing and the piston travel is generally quite short, the speed of the piston is mainly a function of the gas expansion and therefore does not vary very much in the two processes. The contact time between the piston and water, however, varies a great deal in these two processes.

The pressure-extrusion processes allow a much greater amount of water to be ejected through a nozzle. Therefore, the total amount of energy that can be packed in each jet pulse is also much greater than that of impact processes. This aspect is of significant importance in some pulsejet applications. The frequency of pulse generation in extrusion processes is determined mostly by the size of the water cylinder and the method of operating the cannon. The speed of the jet pulses is a function of the cannon└F operating pressure, mode of piston drive, and the design of the nozzle. In most cannons, there will be a gas piston and a connected water plunger; their cross-sectional area ratio determines the force relationship inside the cannon. If hydraulic oil is employed for cocking the gas piston, it must be introduced at a pressure greater than that of the stored gas on the other side of the piston. While the power piston is being cocked, water enters into the water cylinder under a precharge pressure. The power piston is then cocked by various means to allow the cocking oil to be evacuated completely from the cocking chamber. The power piston is then released from its cocked position to push against the water. The water inside the cylinder is pressurized rapidly by the moving plunger from the precharge pressure to that determined by the gas pressure and the intensification ratio. The piston-plunger set will then be decelerated and stopped when the water inside the chamber is emptied. The result of this process is a bell-shaped pressure pulse when the water pressure inside the chamber is plotted against the plunger travel.

The requirement for dumping the cocking oil rapidly in the process described above is difficult to satisfy with ordinary hydraulic dump valves and the cocking of the power piston under high gas pressures proved to be very difficult as well. Thus, few practical processes based on the gas-drive-oil-cock approach have been developed. A variation of the pressure-extrusion process was successfully constructed and tested back in the 1970's (Yie 1976, Yie et al., 1977). This process involved the use of pressurized oil as the driving fluid, which is introduced into the cannon between a floating gas piston and a power piston, and a low-pressure gas as the power piston└╤ cocking fluid. The pressurized oil first cocks the gas piston and then flows through a valved port to reach the power piston. This port is opened by the power piston when it is cocked fully, thus allowing the cannon to be fired under control. This operable pulsejet cannon was successfully tested on fracturing concrete. A schematic diagram of this previous cannon is presented in Figure 1. The testing showed that a slug of high-speed water of sufficient mass could break concrete effectively because of the creation and propagation of secondary fractures. The effect of the jet pulses on concrete or other porous/brittle materials was shown to be a complex process that cannot be adequately explained by the simple drop impact models employed in some past analyses.

Although the pressure-extrusion process of pulsejet generation described above showed promise, there were some nasty technical difficulties. For example, the presence of hydraulic oil between the driving gas and the power piston and the need for flowing through a port slow down the energy transfer. The loss in efficiency is particularly significant if the oil viscosity is affected by the ambient temperature. Further, the containment of water inside the water chamber continues to be a problem; the incorporation of a check valve at the nozzle proves to be difficult but necessary in vertical cannon operations. That previous water cannon is also very expensive to construct and inflexible in operation. As a result, commercially viable water cannon of that pressure-extrusion type is also not available today.

3. JETEC'S PULSEJET PROCESSES

Jetec Company has been involved in the development of pulsed waterjet technology for many years. It developed two pressure-extrusion types of water cannons of large capacity in the past but neither went beyond the experimental stage due to operational shortcomings. Jetec recently explored a new approach for generating pulsed waterjet of high pressure and high power capabilities. It consists of separating the pressurization of water from the mechanism of forming the jet pulses. In this approach, pressurized water from a pump, any pump is transported into a pulsejet generator that may resemble a single-acting pressure intensifier having a compressed gas of a prescribed pressure against the power piston. The pressurized water is accumulated inside a high-pressure chamber against the plunger, which pushes the power piston to compress the gas further. The pulsejet generator is equipped with a fast acting on off valve that can be opened on commend to release the accumulated water through a nozzle. Once the valve is open, the water inside the chamber will be pushed out by the plunger until the plunger is stopped at the end of its travel and the valve is closed. Because of the presence of the compressed gas, the jet pulse issued by the generator will have power instantly and at the end as well albeit at a reduced level. If the gas reservoir is large and the water chamber volume is small, a near step-shaped jet pulse can be produced. This pulsejet is therefore more powerful than that produced by water cannons having bell-shaped power profile. There are two different approaches, depending on the on-off valve involved.

3.1 Internal-Valve Approach

Jetec developed a unique on-off valve for the pulsejet generator to control its operation internally and automatically. This valve is situated inside the water chamber in the form of a valve seat, a valve poppet, and an elongated valve stem that is situated inside a hollow plunger, as shown in a schematic drawing presented in Figure 2. The valve port is normally closed by the valve poppet when not in operation and during the introduction of pressurized water into the chamber. As the plunger is pushed up by the water, the valve poppet stays down on the valve seat until the valve stem└╒ upper shoulder is engaged by the plunger. Continued upward motion of the plunger will dislodge the valve poppet and expose the poppet end to the water pressure, thus sending the valve poppet assembly upward rapidly into the hollow plunger and opening the valve port. The pressurized water inside the chamber flows out of the port and the plunger moves down until it is stopped by a cushion device. The valve will then automatically close the port to start the next cycle. Because of the fact that valve poppet moves away from the valve port area, there is no obstacles to impede the water flow to the nozzle. The generator is thus capable of producing very clean pulsejets. A photograph showing a PJG-4.5-60K pulsejet generator is presented in Figure 3. This generator has a 4.5-inch-diameter power piston and is capable of operating at 60,000 psi (4,100 bar) water pressure.

Jetec's pulsejet generator does not add any energy to the water; it merely serves as an energy storage device and as a self-actuating on-off valve. The valve opens when the chamber is full and closes when the chamber is empty. The maximum static pressure of the water is that produced by the pump. The pump pressure determines the precharge pressure of the driving gas, which is also a function of the intensification ratio of the generator. If the generator has a piston-plunger ratio of 20:1 and the pump└╒ output is 60,000 psi, the gas pressure inside the generator cannot exceed 3,000 psi during its operation. Thus, by knowing the total volume of the gas chamber, the desired initial precharge gas pressure can be estimated by treating the gas as an ideal gas going through adiabatic expansion. If this gas pressure is set too low, the water will lose some of it pressure in the process. If the gas pressure is set too high, the generator will not function, as the water is incapable of moving the plunger to its full stroke.

The stroke length of this pulsejet generator is a function of the valve design; it can be changed by changing the length of the valve stem. The total volume of each jet pulse is the amount of water displaced by the plunger during each stroke and therefore can be sized over a wide range. The frequency of pulse generation is basically a function of the pump└╒ output. Thus, this pulsejet generator can be operated within a wide frequency range by fitting it with different pumps. Its pressure capability is essentially limited by the pump└╒ pressure capability. Therefore, it is ideally suited for use with small fluid pressure intensifiers to perform some big jobs that operate intermittently.

Jetec's pulsejet generator can be fitted with various nozzles to perform the desired pulsejet work. The generator can also be fitted with devices for using the water pulses to perform work other than waterjetting. For example, the pulsejet can be used to propel capsules or other objects, to deliver selected additives, or to drive tools.

3.2 External-Valve Approach

Jetec's pulsejet technology also includes a process involving a pulsejet generator having an on-off valve that is situated outside the generator as shown in a photograph presented in Figure 4. The generator is simply a gas-powered high-pressure water accumulator having a gas piston and a connected water plunger of selected diameter ratio. There is no on-off valve inside the water chamber. Instead, there is a unique on-off valve situated between the pulsejet generator and the nozzle. This valve is capable of opening a large port quickly on commend and providing a near-obstacle-free passage for the pressurized water to flow from the water chamber of the pulsejet generator to the nozzle. The valve's on-off operation does not require a large external force and does not involve powerful impact to cause damage to internal parts. It has very high pressure and flow capabilities. For example, a 2-inch-diameter air actuator operating at 60 psi can operate one of Jetec's on-off valve having a port opening of 0.2 inches in diameter at 40,000 psi. This valve is well suited for repeated operations and is therefore ideal for use in this pulsejet process. Since this valve can be commended by the operator, the pulsejet's characteristics can be varied at will or programmed in advance. This valve can also be operated by hand or foot, thus allowing pulsejets to be produced with portable devices. By virtue of this unique valve, various pulsejet systems can be configured to perform different tasks. The pulsejet generator can be a simple accumulator or a more elaborated device; it could even be a section of flexible hose. A simplified schematic drawing of this valve is presented in Figure 5.

4. DISCUSSION

The pulsejet processes developed by Jetec are truly the pressure-extrusion types in the purest sense. They are quite simple and have many advantages over all previous processes. They can be the first practical high-power pulsejet process and can open up many new waterjet applications as well as some other fluid system applications. Jetec is conducting tests at present to evaluate the performance and reliability of the experimental equipment as well as to investigate the potential applications of these processes. Data available to date indicate that both the internal and external valves are of practical design capable of extended service under demanding conditions. The potential problem areas include the high-speed seal for the piston and plunger, and the valve poppet. The accumulator portion of the process equipment is a well-proven system widely employed in the industry. Jetec's findings will be reported in future papers.

5. POTENTIAL APPLICATIONS

Jetec believes that its pulsejet processes can have many applications including the following:

5.1 Pure Waterjet Applications

These applications involve the use of pulsed waterjet to perform a task in which both the water and its energy are of value.

- Industrial cleaning and blasting applications for improved effectiveness and conservation of water and power.
- Excavation and hydrodemolition applications.
- Remote geotechnical cutting, drilling, and blasting applications.
- Fire-fighting applications.
- Agricultural irrigation applications.
- Underwater applications.
- Pest-control applications.
- Crowd-control applications.
- Water-fountain display applications.
- Manufacturing applications such as metal forming and hole punching.

5.2 Material-Delivery Applications

These applications involve the use of pulsejet energy to deliver a selected material and to perform a task in which both the water and the delivered material are of value.

- Abrasive-jet material cutting, drilling, punching, and demolishing applications.
- Fire-fighting applications, in which selected fire-extinguishing materials are delivered with the pulsed waterjet for greater power, distance, accuracy, and effectiveness.
- Launching pellets, capsules, projectiles, or other objects for various purposes.
- Injection of selected substances into soil, trees, wood, rock, foundations, and other substrates for a wide variety of purposes.

- Delivery of fertilizer, insecticide, herbicide, and other substances in agricultural processes for improved aim and distance of travel.

- Seeding in agricultural applications.

- Decommissioning ordnance, sweeping for buried mines, and other demilitarization applications.

5.3 Synergistic Processes

These applications involve pulsejet being utilized as a medium for powering special tools or as a tool for use with other conventional tools.

- Oil-, gas-, and geothermal-well drilling and servicing applications in which pulsed waterjets or slurry jets are used alone or with cutters, drills, and other conventional rock crushing tools.

- Mining and construction processes in which slots or holes must be made in rock or concrete rapidly.

- Pulsejet-operated borers, jackhammers, post/pile drivers, and rock breakers for increased power and productivity.

- Underwater tools.

5.4 Non-Water Applications

These pulsejet applications involve fluids other than water.

- Industrial pulverization, homogenization, emulsification, and particle grinding applications in which mixtures or slurries are placed under powerful shearing conditions in the form of pulsed jets.

- Injection of vaccine, medicine, preservatives, and other selected substances in biological and industrial applications.

- Fuel injection in engines, burners, and combusters.

- Injection of glues in lamination processes.

- Injection of chemicals into high-pressure reactors.

- Applications in fluid systems as a flow chopper or dump valve.

- Flame thrower in military applications.

6. REFERENCES

Yie, G. G., “A Pulsed Water-Jet Method for Breaking Concrete Pavement.” *Institute of Gas Technology Report - Project 9508*, Chicago, 1977.

Yie, G. G., Burns, D. J., and Mohaupt, U. H., “Performance of a High-Pressure Pulsed Water-Jet Device for Fracturing Concrete.” *Proceedings of the 4th International Symposium on Jet Cutting Technology*, pp.H6 67-86, BHRA Fluid Engineering, Cranfield, U.K., 1978.

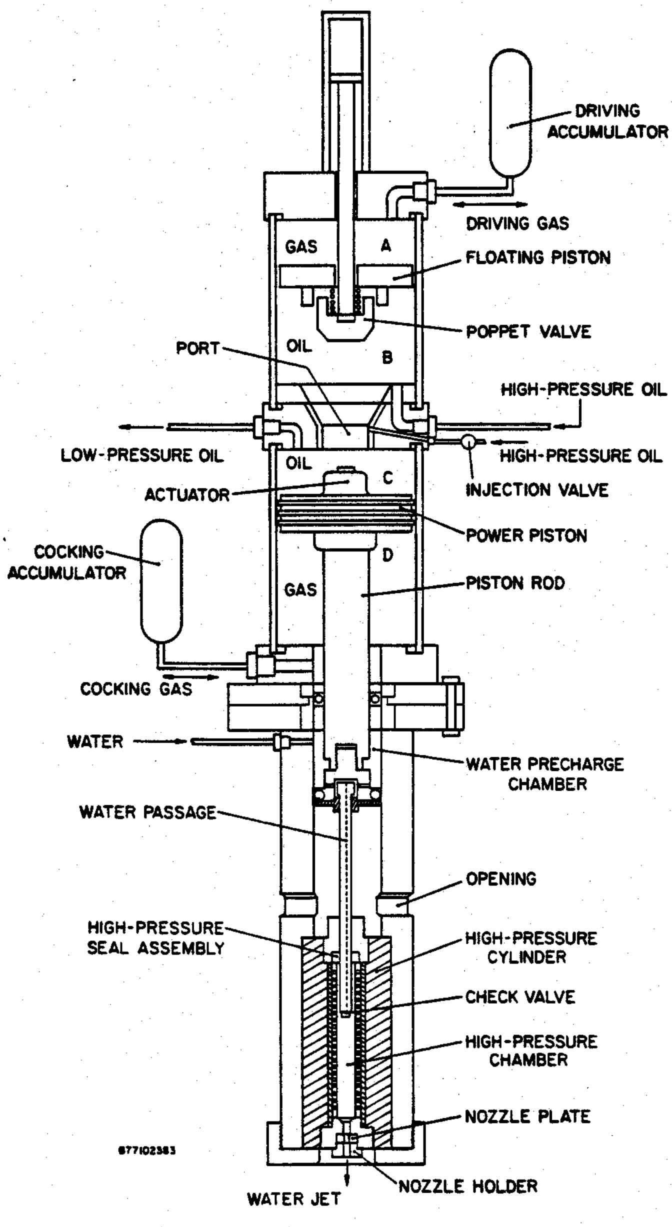

Figure 1. A Pressure-Extrustion Type of Water Cannon Developed in 1970's

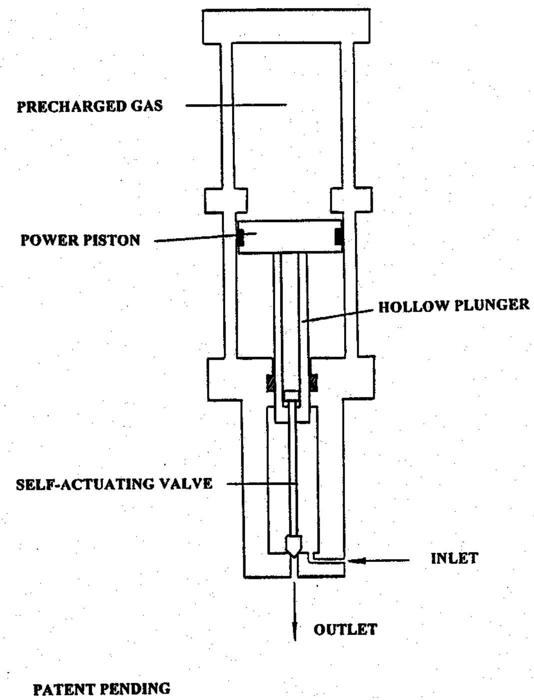

Figure 2. Schematic Drawing of Jetec's Internal-Valve Pulsejet Generator

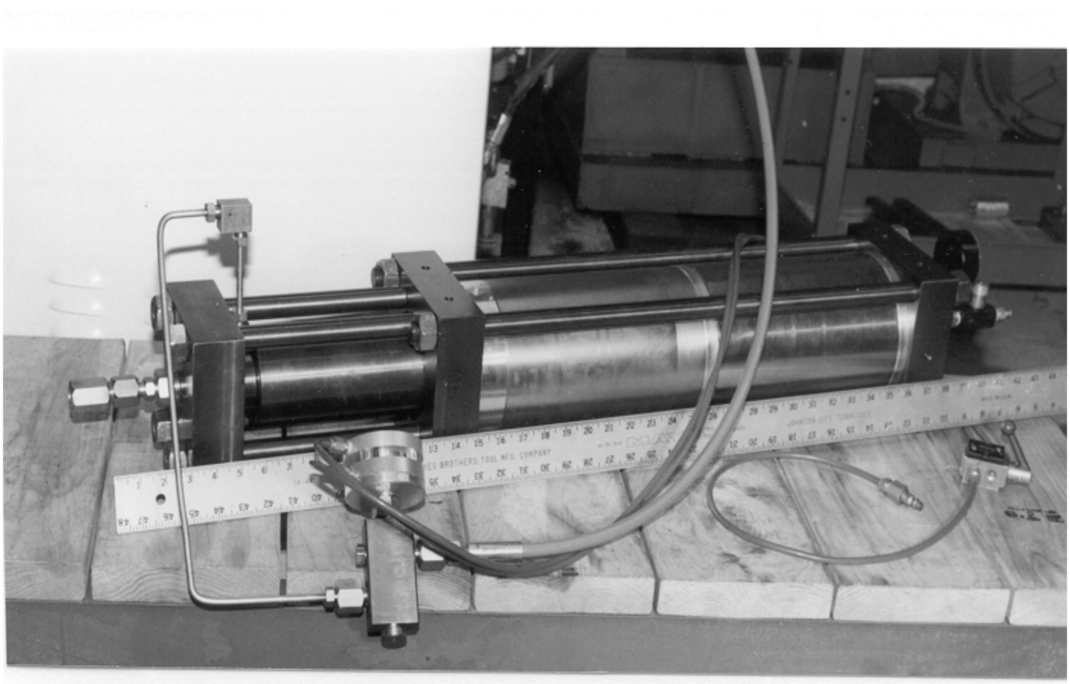

Figure 3. Jetec's 60,000-psi Internal-Valve Pulsejet Generator

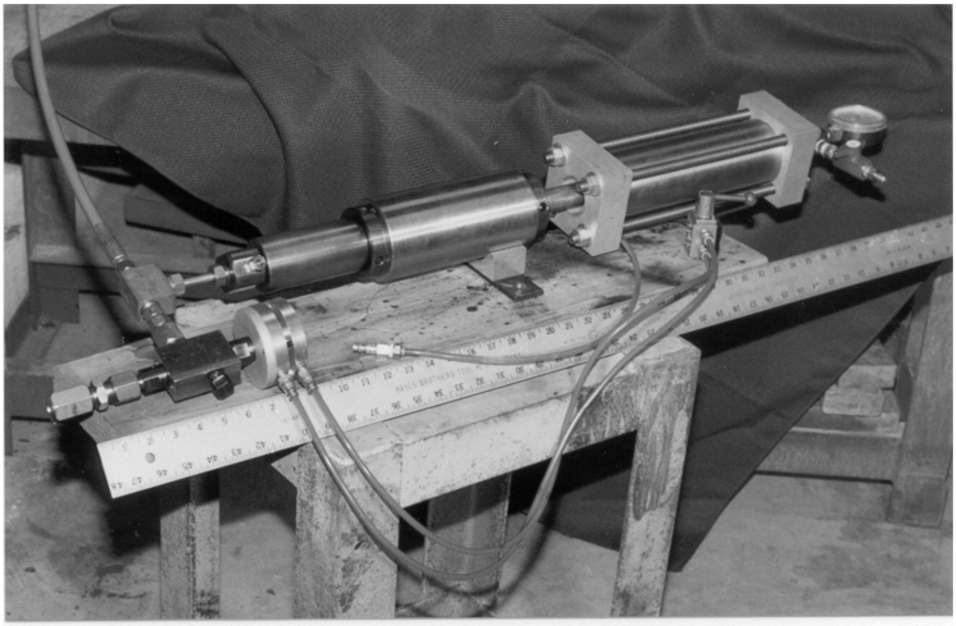

Figure 4. Jetec's Experimental External-Valve Pulsejet Generator

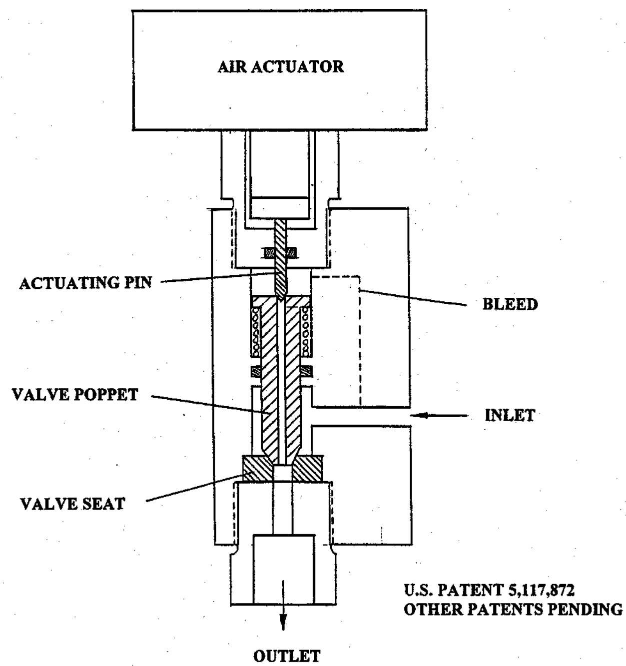

Figure 5. Schematic Drawing of Jetec's Instant High-Flow On-Off Valve

10th American Waterjet Conference
August 14-17, 1999: Houston, Texas

Paper 60

A NEW HIGH EFFICIENT PULSATING NOZZLE

USED FOR JET DRILLING

B. J. Sun
Petroleum University, China
Dongying, Shandong, P. R. C.

C. E. Zhao
Dagang Petroleum and Natural Gas Corp.
Tianjin, P. R. C.

ABSTRACT

Except for cooling bit, a high- pressure water jet is applied to fracture rocks and clean out cuttings in the bottom of the oil well in jet drilling engineering. The paper gives a simple description on the design of the new organ-pipe type self-resonating pulsating jet with the purpose of enhancing the jet erosion efficiency and prolonging the nozzle life span. Hydrodynamic impact pressure measurement experiment, rock erosion test and preliminary probation in drilling engineering were carried out using the new designed nozzles. The results show that the new self-resonating pulsating nozzle jet has stronger erosion capability than the cone-type or conventional organ-pipe self-resonating nozzle jet. The field test results in drilling engineering on several oilfields also show that the outlets of the newly designed nozzles have stronger anti-scouring ability than conventional organ-pipe self-resonating nozzle.

Organized and sponsored by the WaterJet Technology Association

1. INTRODUCTION

Except for cooling bit, a high- pressure water jet is applied to fracture rocks and clean out cuttings in the bottom of the oil well in jet drilling engineering. This practice can reduce the probability of re-fracturing of the rock debris by the drill bit, as well as to increase the drilling speed. Mini-extended and extended nozzles are developed in order to reduce velocity attenuation and enhance the energy of the jet at the bottom of the well. They convert hydraulic pressure to kinetic fluid-flow energy with a minimum of flow disturbance, thereby focussing the stream of fluid against the floor of the formation and across the cutting face of the bit (Smith, et al, 1987). Another new kind of highly efficient jet for erosion and cleaning is the organ-pipe self-resonating pulsating jet whose high velocity stream fluctuates as it flows through the nozzle (Shen, et al, 1987, 1891, 1992; Johnson, et al, 1982, 1984; Sun, et al, 1993, 1998). It has a higher pulsating velocity and transient impact force in comparison with the common jet. It was found that a pulsating nozzle installed on drilling bits could generate a more highly efficient jet flow often needed to fracture rocks and clean cuttings. The organ-pipe self-resonating pulsating nozzle has a simpler configuration and easier operation in drilling engineering. Experimental results (Johnson, et al, 1982) show that the organ pipe pulsating nozzle mounted on Smith F2-CE bits can enhance drilling speed by about 10~30 percent over a conventional nozzle. However, the walls of the outlets of the nozzles are more easily eroded by high-speed fluid flow. One can increase the anti-scouring ability of the outlet of organ pipe nozzles by thickening their outlet parts; this will reduce the pulsating velocity and decrease the erosion characteristic of the jet (Sun, et al, 1994, 1998; Shen, et al, 1987). Preliminary results indicate that the average life span of organ-pipe self-resonating nozzles will not usually exceed 80 hours (Shen et al, 1991) due to scouring problem in the nozzle exits. Moreover, organ pipe pulsating nozzles have a section with sudden diameter reduction, which may create vortices at the exit and increase energy loss (Gerhart & Gross, 1985). The mean purpose of this study is to develop a high efficient and long life span jet nozzle.

The new type organ-pipe self-resonating pulsating nozzle as described in the paper has less energy loss and stronger erosion ability for rocks. Moreover, the field test results in drilling engineering on several oilfields show that the outlets of the newly designed nozzles have strong anti-scouring ability compared with the conventional ogan-pipe pulsating nozzle.

2. THE DESIGN OF THE NEW NOZZLE AND TEST RESULTS

2.1 The design of the new self-resonating pulsating nozzle

Our purpose on the new nozzle design is to reduce the jet head loss and prolong the nozzle life span, which would be demonstrated by the jet erosion efficiency for rocks and increased real drilling time of the new nozzle in engineering uses. The erosion effect for rocks of jet depends on mean impact pressure, and the peak and amplitude value of the pressure fluctuation. The mean nozzle life span depends on the thickness b of the exit. However, the conventional organ-pipe pulsating nozzle is composed of an upstream reduction section with a ratio of $(D_{s}/D_1)^2$, and a downstream section with $(D_1/d_1)^2$ (Sun, et al 1993, 1998; Shen, et al, 1991). Such a ration change would lead to large energy losses and would not make the outlet of these nozzles strong enough, which can be known from the following analysis. On the principle of fluid mechanics, the energy loss can be represented by head loss

$$h_l = kv^2 / 2g \tag{1}$$

Where k is the head loss coefficient, and v is the jet velocity of the nozzle exit. An empirical equation for the loss coefficient for a sudden diameter reduction is (Gerhart, et al, 1985)

$$k \approx 0.42[1-(d_1 / D)^2] \tag{2}$$

Based on our practical case, let d_1=10mm, D=15mm, then k=0.23. If flow rate Q=7.2l/s, then the head loss h_l =98.7m, which is nearly 10 percent of the total pump head.

For a smooth contoured reduction, we can obtain the loss coefficient based on the data given by Gerhart, et al (1985, pp489), so when d_1/D = 0.6, the value of k for an abrupt reduction is 7 times more than that for smooth contoured reduction. From this datum, if we use smooth contoured reduction design, the nozzle energy loss maybe deduced.

A large number of experiments have been conducted in order to study the influence of the outlet thickness on the erosion of organ-pipe nozzles (Sun, et al, 1994, Shen, et al, 1987). The results indicate that the erosion capability of the jet spray from an organ-pipe nozzle becomes greater with decreasing exit thickness. This decrease, of course, will also decrease the strength of the nozzle exit. In order to increase the anti-scouring capability of the nozzle outlet and decrease the energy loss of the jet flow, the up stream reduction is designed as an exponent surface that can generate fluctuating pressure efficiently. The down stream reduction is designed as a streamlined surface which can feed back turbulent pressure and make the jet self-resonate efficiently as demonstrated by experiment (Sun, et al, 1993, 1998), as show in fig.1.

Due to the complexity of turbulent flow we cannot design the new nozzle by a purely theoretical equation alone. Acoustic analyses and experimental study together give the following equation to estimate the length of the organ-pipe (Sun, et al, 1993, 1998):

$$L_p = Hnd_1 / MS_{d1}, \tag{3}$$

where H=0.5□0.55 is a constant, n is the mode number of the organ pipe, $S_{d1} = fd_1 / v$ is the Strouhal number and M is the Mach number. This new configuration design makes the jet core become longer, and can generate a preferable pulsating jet (Sun, et al, 1993). The gradual reduction configuration makes the nozzle exit stronger and more able to withstand the scouring of high velocity jet flow.

Suppose there is a large number of axi-symmetrical vortices in the jet flow, whose axial positions may be distributed at random, and whose vorticities concentrated in the central region around the axis, neglecting the interferences among vortices. Let *b* represents the radius of a vortex ring. The following result had been obtained (Shen, et al, 1992)

$$b \propto t^{0.5} \tag{4}$$

The results show that the radius of the vortex ring becomes larger with $t^{0.5}$ law. If the radius of the vortex ring increases, a large pulsed velocity can be produced. For a thick outlet of a nozzle, some big vortices will be destroyed due to the "absorption" of the nozzle outlet wall (Sun, et al, 1998). Experimental results indicate that the jet pulsation becomes larger and the jet erosion capability becomes stronger if the thickness of the nozzle outlet is less. But the thinner nozzle outlet can not bear strong scouring of high velocity jet. In order to prevent the vortex from breaking down at the nozzle outlet due to "absorption", we design the profile of the nozzle outlet as a quarter circular arc, as show in fig.1. Another benefit of this design is to overcome the head loss due to sudden enlargement of the organ-pipe exit (Gerhart , et al, 1985). When the high velocity jet spray leaves the exit, there is a large velocity difference between the jet and ambient fluid, it must cause acute fluid momentum exchange and vortex movement, all of which must consume the energy of the jet. So, the profile of the external expanding part of the nozzle plays a very important role in creating the self-resonating pulsation feature of the jet.

2.2 Experimental results in laboratory

The test equipment we used is shown in the paper of Shen, et al (1991) and Sun, et al (1993). The liquid used in the test is tap water. All tests are conducted to simulate well bore just under atmospheric pressure and normal temperature. A rock specimen box can be mounted on the chassis in the erosion experiments. Mini-extended conventional cone and organ-pipe self-resonating nozzles are tested simultaneously with the newly designed mini-extended and the new self-resonating nozzle. The diameters of all tested nozzles are *10 mm*.

The impact pressure measurement test along jet axes has been conducted (Sun, et al, 1993, 1998). The same tests were conducted with cone and organ-pipe nozzle. The results showed that the new nozzle has the least energy loss among three kinds of tested nozzles. Therefore, more energy of the jet flow can concentrate on rock surface for its erosion. Moreover, it provides a larger pulsating pressure, which is beneficial for rock erosion. It is verified by the erosion experiment results as described in the reference paper (Sun, et al, 1998). For the purpose of comparison, all tests were conducted under the same pump pressure conditions. Two parameters are adopted to compare jet erosion capability. The first is the volume erosion rate V, which is the erosion volume per second. The second is the depth erosion rate H that comes from the average erosion depth per second. The rock specimen used was isotropic natural Zibo sandstone. Its physical characteristics measured before the experiments are shown in table 1. The results show that the volume erosion rate of the new nozzle jet is 3.2 times greater than that of the organ-pipe nozzle jet and 5.5 times greater than that of the cone nozzle jet. Similarly, it was demonstrated that the average depth erosion rate of the new nozzle is almost 100% greater than that of the organ-pipe nozzle jet and 1.8 times greater than that of the cone nozzle jet at their optimizing dimensionless stand-off distances. The results mentioned above show that the new self-resonating pulsating nozzle jet has the strongest erosion ability among the three tested nozzles.

3. PRELIMINARY PROBATION RESULTS IN DRILL ENGINEERING

Table 2 shows some preliminary probation results of the newly designed nozzle jets equipped on J22 drilling bits at Dagang oil field in 1996~1997. All listed results are compared with the conventional nozzle jet under very similar conditions. Every bit is mounted with three new designed nozzles. Table 3 represents some probation results of 98 newly designed nozzles equipped with H517 and H126 bits at Dagang oilfield in 1998. The results show that the new nozzles can enhance the drilling speed by 5.13~52 percent in general. Table 4 shows some preliminary probation results of the newly designed nozzle jets equipped on H517 drilling bits at Jilin oil field in 1998. It shows the new nozzles can increase in penetration rates by 8.9~13.6 percent. Moreover, their life test results show all tested nozzles can work exceeding 120 hours accumulatively. All of them can work the same time as cone nozzle, which is very important for its application in engineering. Under very similar conditions, the average life span of the organ type self-resonating nozzles is 78.82 hours (shen, et al, 1991). These Preliminary field test results demonstrate that the gradual reduction configuration makes the newly designed nozzle exit stronger and more able to withstand the scouring of jet flow. Further field tests are still in progress at other fields.

Other authors (Johnson, 1982, 1984; shen, et al, 1991; sun, et al, 1994) have discussed the mechanism that caused the erosion rate of pulsating jet improvement under atmospheric condition. Self-resonating pulsating jet afford at least three preferable advantages over the cone nozzle jet: more cavitation erosion; improved chip cleaning effect and greater transient impact pressure for breaking up. That may be true in the case of the beginning of an oil well drilling. At a large depth well, the ambient pressure becomes high, and the probability of cavitation due to jet impact pressure fluctuation and vortices movement maybe reduce (Hammitt, 1980). For our study, first, the newly designed nozzle jet has less head loss, which is benefit to rock breaking up and chip cleaning out. Second, the new nozzle pulsating jet form a series of ring vortices that across the hole bottom generates a substantial pressure fluctuation at this surface. These pulsation of negative pressure should overcome most normal hold-down pressure, and thus lift the chips previously created by the mechanical bit, even at depths where cavitation is suppressed (shen, et al, 1991). Finally, the big peak pressure of the jet pressure fluctuation affords greater erosion capability in some incompact stratum. So, the new nozzle jets have a very bright future in oil well drilling.

4. CONCLUSIONS

From the above discuss we can get the following conclusions:

1. The experimental data and field test results in drilling engineering indicate that the new self-resonating pulsating nozzle can generate less energy loss and has a stronger erosion capability

in comparison with the cone nozzle and conventional organ-pipe self-resonating nozzle. Bits with these new nozzles can increase in penetration rates by 5.13~52% over those with conventional nozzles.

2. The new design of the nozzles has successfully overcome the short life-span shortcoming of the conventional organ-pipe self-resonating nozzles. They all have a life of 120 hours at least.

ACKNOWLEDGMENT

The authors wish to thank Professor G. S. Li, Professor R. Y. Wang, Y. J. Xu, H. B. Chen, and Engineers in Dagang and Jilin oil field for their help in the study. This work was supported by Dagang Petroleum and Natural Gas Corp, China.

REFERENCE

Frederick G. Hammitt, Cavitation and Multiphase Flow Phenomena. McGraw-Hill Inc., 1980.

Johnson V. E, “The Development of Structured Cavitating Jets for Deep-Hole Bits,”SPE 11060, 1982.

Johnson V. E., “Enhance Liquid Jet Erosion”U.S. Patent 4,474,251, 1984.

Philip M. Gerhart & Richard J. Gross, Fundamental of Fluid Mechanics, Addison-Wesley publishing company, inc., 1985.

Shen, Zhonghou, Wang, Ruyuan, Sun, Baojiang, “Theory of Vortex and Design of Self-resonating Jet Nozzles,”The Third Pacific Rim International Conference on Water Jet Technology, pp255□264, 1992.

Shen, Zhonghou, Li, Gensheng & Zhou, Changshan, “Experimental Study on Self-excited Resonant Pulse Jet Nozzle for Roller Bit,” J. of the University of Petroleum, China, vol.15, No.3, pp36~43, 1991.

Shen, Z. H., Li, G. S. And Zeng, C. Y. “Experimental Study on Rock Erosion by Self-resonating Cavitating Jets,” International Water Jet Symposium, Beijing, China, pp2-35~2-43, 1987.

Smith, R.D., et al , “Crossflow Rotary Cone Rock Bit with Extended Nozzle,”U.S. Patent 4,687,067, 1997 , 1987.

Sun, Baojiang, Wang, Ruyuan, Sheng, Zhonghou "Discussion on High Efficient Pulse Jet Nozzle Used for Jet Drilling,"Oil Drilling and Production Technology, vol. 15, pp13～19, 1993.

Sun, Baojiang, Wang, Ruyuan & Shen, Zhonghou, "Design of a New Type of Self-resonating Pulsating Nozzle," J. of the University of Petroleum, China, vol.18, No.3, pp31~34, 1994.

Sun, Baojiang, Yan, Dachun. "A Study on Energy Concentration and Self-resonating Jet Nozzle and Its Application in Drilling Engineering", The Third international conference on fluid mechanics, Beijing, pp565~570, July 7-10, 1998.

NOMENCLATURE

h_l: head loss;

v: jet velocity;

D_1: the diameter of organ-pipe;

Q: flow rate;

n: the mode number of the organ pipe ;

M: Mach number;

b: the radius of a vortex ring;

f: resonating frequency of the jet.

k: head loss coefficient;

d_1: the diameter of nozzle exit;

D_s: the diameter of inlet of the nozzle;

L_p: the length of the organ-pipe;

H: constant

S_d: Struhal number;

t: time;

Table 1 The physical characteristics of the isotropic natural Zibo sandstone

density	porosity	elasticity modulus	hardness	tensile strength	compressive strength	Poisson's ratio	grain size
2g/cm^3	15%	5×10^7N/m^2	5.1N/m^2	0.025N/m^2	0.545N/m^2	0.34	0.05~0.3mm

Table 2 . Some Probation results of new designed nozzles at Dagang oilfield in 1996~1997

Bits No.	layers	Drill peed (m/hr)	Improve rate of Drill Speed	Pump Pressure (Mpa)	Drilling Depth (m)	Bits model
1	S2	2.94	40%	19	3062~3249	J22
2	S3	8.17	52%	20	2085~2317	
3	Ed	7.06	14%	19	2430~2570	
4	S2	6.34	23%	17	2609~2966	
5	S2	3.63	11.8%	17	2816~3014	

Table 3 Some Probation results of new designed nozzles at Dagang oilfield in 1998

layers	bit number	bits model	drill peed (m/hr)	increase in Drilling speed	pump Press -ure(Mpa)	footage m/per bit
Kongdian group	36	H517	4.76	14.7%	18	265.61
ES	23	H517	4.34	36.91%	20	270.56
Ed	12	H517	6.16	8.64.1%	19	302.22
Ng	10	H517	7.99	5.13%	17	474.03
Nm	17	H126	15.36	9.64%	18	135.72

Table 4 . Some Probation results of new designed nozzles at Jilin oilfield in 1998

Bits No.	layers	Drill peed (m/hr)	Improve rate of Drill Speed	Pump Pres-sure(Mpa)	Drilling Depth(m)	Bits model
1	Yuantou group	5.2	10.5%	14	1300~1520	H517
2	Denglouku group	3.13	13.6%	15	1520~1790	
3	Denglouku group	3.06	8.9%	15	1562~1696	

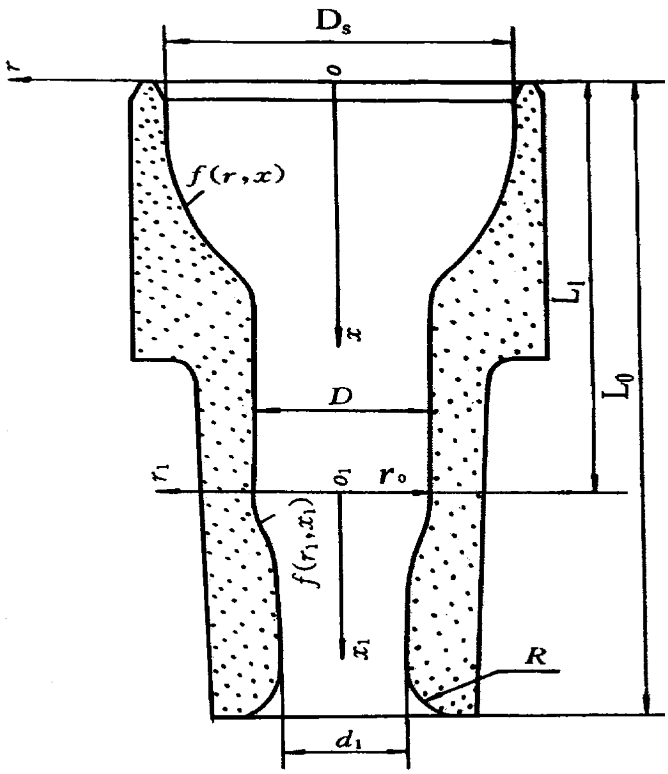

Figure 1 Diagram of the new nozzle

10th American Waterjet Conference
August 14-17, 1999: Houston, Texas

Paper **61**

DEVELOPMENT OF HIGH EROSIVITY CAVITATING AND ACOUSTICALLY ENHANCED WATER JETS FOR WELL SCALE REMOVAL

K. M. Kalumuck, G. L. Chahine, G. S. Frederick, and P. D. Aley
DYNAFLOW, INC.
Fulton, MD

ABSTRACT

The walls of geothermal wells often experience rapid build up of scale deposits due to the high dissolved solids content of geothermal fluids. As the liquid is brought up from deep wells, its pressure drops, and the water flashes to steam resulting in precipitation of dissolved minerals. Existing means of addressing this problem such as chemical inhibitors, removal with conventional water jet blasting, drilling with a workover bit, or acids are costly and not always effective, particularly with the harder scales such as silica. Our ongoing effort seeks to develop cavitating and acoustically enhanced water jets for geothermal well scale removal. These technologies have been proven to enhance the erosive power of liquid jets by several fold in various cutting, cleaning, and drilling applications particularly for hard materials and thus promise to substantially enhance the performance of down-hole cleaning tools, particularly for the removal of hard scale.

Initial results from laboratory experiments on cutting of both actual and simulated are presented. Experiments are reported under simulated down hole conditions over a range of ambient pressures and standoffs. Scale removal and cleaning rates are compared with those obtained from conventional water jet nozzles, and the improvements presented.

Organized and Sponsored by the WaterJet Technology Association

1. INTRODUCTION

Build up of scale deposits on the walls of geothermal wells can occur rapidly due to the high dissolved solids content of geothermal fluids, e.g., up to 250,000 ppm in the Salton Sea geothermal field (Glowka, 1997). Scale formation is a significant problem for both the well and for surface heat transfer equipment. Geothermal brines contain a variety of dissolved salts including carbonates, silicates, sulfates, and metal sulfides. Currently this is dealt with either by the use of chemical additives to inhibit scale formation or the periodic removal of scale through the use of a workover rig drill bit, high pressure water jets, or acids. However, such procedures are costly. Chemical inhibitors do not currently exist for silica scales (Glowka, 1997), and their use raises environmental concerns.

Scale in geothermal wells forms due to a decrease in solubility of dissolved minerals. This can be due to temperature decrease or flashing of some of the water to steam. The latter often occurs due to depressurization of the geothermal fluid as it rises in the well. The depth range over which scale forms varies with the geothermal site and the specific well at the site. As reported by Benoit (1987), scale formation investigated at seven Dixie Valley well bores was found at depths between approximately 240 and 1300 m (800 and 4,300 ft). The local ambient pressures, P_a, corresponding to these depths varies between approximately 2.4 and 13 MPa (350 and 1,900 psi).

One technology recently proposed for scale removal is the use of an ultrasonic device. The recent Advanced Geothermal Drilling Systems Workshop recommended further exploration of this concept. Cleaning occurs due to the excitation of the growth and collapse of cavitation bubbles by the high frequency acoustic waves. Physically, cleaning is achieved through cavitation. In the present effort we apply cavitation in a more direct manner by the use of acoustically enhanced cavitating water jets which can be made to be much more efficient and aggressive than ultrasonic devices.

Cavitating and self-resonating jet technologies have been proven to enhance the erosive power of liquid jets in a number of cutting, cleaning, and drilling applications. Removal of harder scales, such as calcium carbonate, barium sulfate, strontium sulfate, and silicates is a particularly good area of potential application for this technology as the relative improvement in erosivity of cavitating and interrupted jets has been found to increase with target hardness. (See, for example, Chahine et al., 1995). In this study we investigated two related technologies – one that employs cavitation and one that breaks the jet up into a series of slugs that produce water hammer type pressures upon impact. These technologies enable operation in both submerged and non-submerged conditions (such as when the well is blown down with compressed air).

2. DYNAJETS WATERJET TECHNOLOGIES

Cavitation is mainly known for its harmful effects, namely, loss of performance, erosion, and noise. The usual procedure to prevent these deleterious effects is to avoid the phenomenon by proper design and by limiting the operating conditions. However, attempts to induce and harness cavitation for useful purposes have been increasingly successful. Ultrasonic cavitation methods take advantage of the erosive power of cavitation for cleaning, emulsification, and mixing. In water jets, cavitation has for some time now been purposely induced in order to increase jet erosive power.

Experimental observations of submerged jets show the tendency of the turbulent eddies in their shear layer to organize in large structures. Excitation of a submerged jet with periodic acoustic signals produced upstream of the nozzle by transducers or loud speakers shows a remarkable change of the jet structure into discrete ring vortices when the excitation frequency, *f,* matches the predominant natural frequencies of the non-excited jet. This corresponds to a Strouhal number, $S_{d,}$, close to 0.3 or one of its integer multiples. The Strouhal number is defined as

$$S_d = \frac{fd}{V}, \tag{1}$$

where *V* and *d* are the velocity and the diameter of the jet. This natural tendency of a submerged jet to organize into large structures is of great interest in aerodynamics for air jet studies. Crow and Champagne (1971), and many others since, studied this phenomenon extensively and showed experimentally that forced excitation of the jet at the preferred frequency enhances the structuring. The voracity is then mainly concentrated in ring-shaped large structures.

The potential of this phenomenon for submerged water jets was recognized and utilized to develop useful submerged jets having very high amplitude, periodic, oscillatory discharge without the use of moving parts in the supply system. (See, for example, Johnson et al., 1984 and Chahine et al., 1984a and b.) The passive excitation is obtained hydroacoustically and structures the shear layer of the jet into discrete, well-defined ring vortices when the excitation frequency, *f*, matches the jet's preferred value. This can be obtained by feeding the final jet-forming nozzle with various types of acoustic chambers (for example, Helmholtz chambers or organ-pipe tubes) tuned to resonate at the desired frequency; and by shaping the nozzle so as to feed back the pressure oscillations which occur at the exit. Such devices are forms of “whistles" which self-excite and thus are totally passive. These jets are termed STRATOJET®s[1] and have shown enhanced erosivity from increased cavitation activity. The large pressure oscillations associated with the intensification of cavitation, with resonance in the nozzle assembly, and with the production and disappearance of large vortical structures greatly improve the erosion and cleaning capabilities.

2.1 Principles of Operation of Self-Resonating Cavitating Jets

One possible type of STRATOJET® configuration is shown in Figure 1. It uses an organ-pipe acoustic chamber whose resonant frequency is selected to match the desired structuring frequency defined by the critical Strouhal number of the jet. This concept offers the simplest system design and has been used successfully for erosion studies and noise generation (Chahine and Johnson, 1985; Chahine et al., 1984b; Chahine et al., 1986; Chahine et al., 1987).

[1] U.S. Patents: 4,262,757 4,389,071 4,474,251 4,508,577 4,681,264 4,716,849

The principles of operation of an organ-pipe STRATOJET® are schematically represented in Figure 1. Two predominant sources of pressure fluctuations can be distinguished in addition to the classical unexcited turbulent shear layer between the jet and the surrounding liquid. One of these sources corresponds to the volume fluctuations of the moving vortex bubble rings formed in the center of the large structures of the self-excited jet. The other source of pressure fluctuations is more complex and relates to the exit area of the jet where high amplitude oscillations of the main flow characteristics are interrelated with the shear layer-nozzle lip interaction. The acoustic signals from both areas are forcing functions to the resonating chamber in the nozzle assembly. These signals strongly interact; they are both fed back and amplified by the organ-pipe.

Acoustic resonance is achieved in the nozzle feed-tube assembly when a standing wave forms in the “organ-pipe" section (length: L, diameter: D). Peak resonance will occur when the fundamental frequency of the organ-pipe is near the preferred jet structuring frequency. The exact resonance frequency is dependent on the contractions at each end of the organ-pipe, and the first mode resonance in the pipe will occur when the sound wavelength in the fluid is either two or four times L.

2.2 Effects of Jet Structuring on Cavitation Inception

The dimensionless parameter characterizing cavitation is the cavitation number, σ,

$$\sigma = \frac{P_a - P_v}{1/2\rho V^2}, \tag{2}$$

where P_a is the ambient or far field pressure, P_v is the vapor pressure of the liquid, ρ is the liquid density, and V is the characteristic velocity - the jet mean velocity. In deep wells, the ambient pressure is hydrostatic and directly related to hole depth. In the case of high-pressure submerged jets, $P_a >> P_v$, and for well-designed nozzles $1/2\rho V^2$ may be approximated by the pressure drop, ΔP, across the nozzle. Thus

$$\sigma \approx \frac{P_a}{\Delta P}. \tag{3}$$

The particular value at which cavitation is incipient is defined as

$$\sigma_i = \left(\frac{P_a}{\Delta P}\right) \text{ at inception.} \tag{4}$$

Thus if the operating conditions for a submerged jet are such that $\sigma/\sigma_i < 1$, cavitation will occur, and as σ/σ_i continues to decrease below unity the amount of cavitation will increase. When a cavitating jet impinges against a surface, the cavities formed in the jet collapse on that surface and produce very high local pressures and very high speed microjets. The resulting pressures are much greater than the jet stagnation pressure ($1/2\rho V^2$), and the resulting cleaning or cutting action is substantially greater than when the jet is not cavitating. A great advantage of the

STRATOJET® class of jets is an increase in σ_i over conventional jets by a factor of 3 with current designs. The ability to achieve cavitation at high ambient pressures is of particular importance to deep well operations. *Self resonating jets produce cavitation for much higher ambient pressures than conventional jets thus enabling operation at deeper depths* and producing better performance at lower nozzle pressures than conventional jets.

The increase in σ_i is due to the decreased pressures at the core of the structured vortices generated. For the scale depth conditions at Dixie Valley noted above, the cavitation number ranges between 0.07 and 0.38 for a jet operating pressure of ΔP = 34.5 MPa (5,000 psi).

2.3 Self-Resonating Pulsed Jet Technology

The SERVOJET® jet system is also an acoustically self-resonating jet originally developed to generate water "slugs" or drops at known frequencies and to operate in non-submerged conditions - i.e., in air. Interrupted liquid jets have been proven to be advantageous over steady jets due to their large water hammer type impact pressures. Details of our development of self-resonating interrupted water jets can be found in Chahine et al. (1983). In a submerged condition, it operates similar to the STRATOJET® and structured cavitation is generated in the shear layer created between the high speed water jet slugs and the surrounding liquid. However, the STRATOJET® configuration is usually preferred since it involves fewer flow contractions and expansions and thus less pressure losses and little interaction with the working fluid. In air jet erosivity is improved by jet interruption leading to slug and drop production.

3. EXPERIMENTAL SETUP AND PROCEDURES

3.1 Test Facility

Experiments were conducted in DYNAFLOW's High Pressure Cell (HPC) capable of ambient pressures up to approximately 19.3 MPa (2800 psi). A photograph of the HPC is presented in Figure 2. The HPC is a cylindrical pressure vessel with inside dimensions of approximately 24 cm (9.5 inch) diameter and 71 cm (28 inch) length with three quartz view ports circumferentially spaced and located near its mid length. Constructed for studies of deep hole drilling with cavitating jets, it includes a fixture in which rocks are placed and rotated at various speeds for cutting beneath the jet. Another fixture enables the rock to advance at a controlled rate towards the nozzle thus enabling actual drilling. The rock surface being cut is visible in the view ports. Ambient pressure is adjusted and maintained by a choke plate which acts as a back pressure valve in the outflow line. The jet flow is driven by a Weatherford five piston positive displacement pump capable of up to 76 liters/min at 69 MPa (20 gpm at 10,000 psi) or 42 liters/min at 138 MPa (11 gpm at 20,000 psi).

Nozzle acoustic resonance was checked with a Piezotronics 101-A04 pressure transducers (5 mv/psi sensitivity) located in the HPC wall and used to measure the fluctuating component of the pressure, P'. The output of the transducer was monitored with both a digital rms meter to obtain the rms value of the fluctuating pressure component and with a spectral analyzer to ascertain the fluctuation frequency content and determine the peak (resonant) frequencies of the nozzles. These measurements were used to determine whether or not a particular self-resonating nozzle has achieved good acoustic resonance - an important factor in achieving good performance. The organ-pipe length for the self-resonating nozzle was "tuned" to the jet exit velocity (i.e., to ΔP).

3.2 Target Materials and Characteristics

In order to carry out meaningful laboratory tests of scale removal, an appropriate target material needs to be employed. Ideally, actual scale should be used as the target material. This, however, has several problems associated with its use. It requires removal and transportation of the scale from its source – a geothermal well site – and storage under conditions that do not affect its mechanical properties. This includes maintenance of a wet environment. In addition, actual field generated scale involves inherent sample to sample variability due to both potential local inhomogeneities and differences between samples taken from different locations and acquired at different times. A similar problem arises in tests of rock cutting by water jets. Depending on the rock type, substantial sample to sample variation can be found due to local composition variation and flaws as well as bedding plane orientation. For this reason, such samples are always tested in the same orientation in which they were cut from the formation. We have found for rock that use of a more repeatable and uniform property material as a target material for initial development and screening of designs is desirable. We have utilized man-made simulated rock and aluminum plate (6061-T6) for this purpose with great success (Chahine et al., 1995).

In the current project, initial development and screening was conducted with simulants. A set of samples made of cement (sand, but no aggregate) was investigated. In order to assess the effect of cure time on the hardness of these simulants, a series of tests were conducted on 5.1 cm (2 in.) thick samples of both fiber-reinforced and quick-set cements. Repeated cuts of each sample were performed for a series of increasing cure times between 3 and 7 days. For these tests, the samples were submerged, and a 1.3 mm (0.053 in.) diameter conventional jet (Spraying Systems Washjet ¼ MEG 0005) operating at 34.5 MPa and 21 liters/min (5,000 psi and 5.4 gpm) was translated across the surface at 2.5 cm/s (1 in/s) and at a 2.5 cm (1 in.) standoff. As can be seen in Figure 3, the results show a continuing decrease in measured cut depth with time indicating a continued increase in hardness that is significant. For the top of the fiber reinforced cement the cut depth varied from 8 mm (0.31 in.) at 3 days cure to 2 mm (0.085 in.) for 7 days cure time. Similar variations with cure time were found on the other sample surfaces tested. The top surface of the fiber-reinforced cement was found to be consistently the hardest. The cut depth in the fast set sample was approximately 40% greater than that in the bottom of the fiber reinforced indicating an approximately 40% greater cutting resistance for the fiber reinforced cement. Based on these results, we determined that to achieve sample uniformity we needed to control and/or adjust for the cure time. We thus endeavored to test samples with cure times of approximately 3 days and to conduct comparison tests head-to-head on the same samples.

Samples of silica and calcium carbonate geothermal scale were obtained from CalEnergy Company, Inc. (Ridgecrest CA). We have performed cutting tests on these samples to compare them under the same conditions with the various simulants. The comparison tests were conducted with a 0.86 mm (0.034 in) diameter SERVOJET® operating at 34.5 MPa and 5.7

liters/min (5,000 psi, 1.5 gpm) and translating across the sample at various speeds between 1.3 and 5.1 cm/s (0.5 and 2 in/s) at a standoff of 5.7 cm (2.25 in. or 66 diameters). The tests were conducted submerged at atmospheric ambient pressure. The calcium carbonate experienced the onset of damage – a surface pecking - at 5.1 cm/s (2 in/s) while sustaining a cut 3.2 mm (0.125 in) deep and 13 mm (0.5 in) wide at 1.3 cm/s (0.5 in/s). The harder silica exhibited no damage at 5.1 and 2.5 cm/s (2 and 1 in/s) while sustaining the onset of damage at 1.3 cm/s (0.5 in/s). Similar results were produced in the top surfaces of a fast set and a fiber reinforced cement, respectively. At 1.3 cm/s (0.5 in./s), the fast set exhibited a cut 2.8 mm (0.11 in) deep cut 20 mm (0.78 in) wide while the fiber reinforced experienced the onset of erosion with a depth of about 0.6 mm (0.025 in). Based on these data, the fiber reinforced cement (top surface) was selected to simulate silica and the fast set cement selected to simulate calcium carbonate. The silica, being the harder scale, and its fiber reinforced cement simulant, were the primary focus of testing.

4. SIMULATED SCALE EROSION TEST RESULTS

In order to assess jet performance under downhole conditions, cutting tests were conducted in our High Pressure Cell on samples of fiber reinforced cement. Three jet types designed to operate at comparable flows and pressures were employed: a conventional jet, a self-resonating organ pipe STRATOJET®, and a self-resonating SERVOJET®.

In order to assess the best pressure at which to test the cavitating resonating STRATOJET®, the rms pressure fluctuations were measured as the pressure drop was varied for a constant value of the cavitation number (σ = 0.3). The pressure fluctuations normalized by pressure drop across the nozzle showed a local maximum at a pressure drop of 41.4 MPa (6,000 psi).

Both cut depths, h, and diameters, w, were measured. Nominal volumes, $\mathcal{V}$, were calculated by assuming a cylindrical cut hole whose volume is given by

$$\mathcal{V} = \pi w^2 h/4. \qquad (5)$$

At a 2.5 cm standoff (X_{so}/d_o = 19) and P_a = 3.5 MPa (500 psi), ΔP was increased until the onset of erosion of the sample. For the conventional jet, this occurred for 180 sec exposure at ΔP = 34.5 MPa (5,000 psi) and 50 sec exposure at ΔP = 41 MPa (6,000 psi). A series of tests varying the ambient pressure, standoff, and exposure time was then conducted for the three jet types at ΔP = 41.4 MPa. A similar evaluation was performed under non-submerged conditions – “in air”.

4.1 Influence of Ambient Pressure

Figures 4-6 present the measured cut depths, h, as functions of time for up to 120 sec exposure for the three jet types at a 2.5 cm standoff (X_{so}/d_o = 19) and ambient pressures of 1, 2.1 and 3.5 MPa (150, 300 and 500 psi; σ = 0.025, 0.05, 0.083). The strong influence of cavitation number or ambient pressure is apparent with an order of magnitude variation in the cut depths between ambient pressures of 1 and 3.5 MPa. The STRATOJET® run at P_a = 1 MPa was stopped after only 10 sec due to it cutting through nearly the entire 5.1 cm thickness of the sample. These data show that the STRATOJET® significantly outperforms the other two nozzle types at all three ambient pressures. The SERVOJET® employed is better than the conventional jet at P_a = 1 MPa, about the same at P_a = 2.1 MPa, and poorer at P_a = 3.5 MPa.

The corresponding average hole diameters, w, and nominal volumes, $\mathcal{V}$, (as calculated from relation (5)) are presented in Figures 7 and 8. As can be seen, the variations in diameter and volume are much less than the variations in depth. The diameters are also seen to change very slowly with time after an initial period. The relative rankings of the three jet types are the same for width and volume as for depth. The STRATOJET® is clearly the best performer over the entire range investigated. It should be noted that at P_a = 1 MPa, the SERVOJET® produces a cut volume approximately twice that of the conventional nozzle.

4.2 Influence of Standoff

Figures 9 and 10 present the influence of standoff at a P_a = 1 MPa (150 psi, σ=0.025). Again, the STRATOJET® has the largest cut depths at all three standoffs. This is followed by the SERVOJET® at 2.5 and 5.1 cm standoffs At a 7.6 cm. Standoff, neither the conventional nor the SERVOJET® produced a measurable cut depth after 120 sec. The STRATOJET® was also found to produce the largest diameters and volumes (Figure 10) at all three standoffs. It is clearly the preferred jet for operation at these conditions.

4.3 In-Air Tests

Figures 11 and 12 present, respectively, the cut depths and diameters, for operation of the three jet types in air (not submerged) at atmospheric pressure at standoffs of 2.5, 5.1, and 7.6 inches. In terms of depth, the STRATOJET® at a 2.5 cm standoff is the best performer. There are three cases with cut depths comparable to each other – the STRATOJET® and SERVOJET®at a 5.1 cm standoff and the conventional jet at a 7.6 cm standoff. The best standoff for the conventional jet for cut depth is 7.6 cm. It should also be noted that the SERVOJET® exhibits a cut depth at a 5.1 cm standoff approximately twice as large as that cut at 1 or 3 in standoffs indicating an optimal standoff of approximately 38 nozzle diameters. However, the SERVOJET® produces a cut diameter significantly larger than either of the other two jets. At standoffs of 5.1 and 7.6 cm, its cut diameter is 3.5 times that of the conventional jet, while it is twice that of the conventional jet at a 2.5 cm standoff. The STRATOJET® cut diameters fall in between those of the SERVOJET® and the conventional jet. This results in the largest volumes being created by the SERVOJET® at 5.1 and 7.6 cm standoffs followed by the STRATOJET® at 2.5 cm standoff.

5. CONCLUSIONS

The current effort seeks to develop improved methods of removal of hard scale from geothermal wells. Experiments were conducted utilizing both actual and simulated scale with three classes of water jets: cavitating self-resonating STRATOJET® and SERVOJET®, and a conventional jet operating at the same conditions under both submerged and "in-air" conditions for a range of standoffs and ambient pressures. Under submerged conditions, the STRATOJET® was found to produce the largest cut depths and volumes. Volume increases of as much as a factor of 25 over the conventional jet were measured. Under "in-air" conditions, the STRATOJET® produces the deepest cut and largest volume at a standoff of 19 diameters (2.5 cm). However, at larger standoffs, the larger SERVOJET® "footprint", due to the generation of discrete water slugs, results in a volume removal three to five times that of the other jets with a maximum removal rate at a 39 diameter standoff (5cm). These results strongly indicate the potential for application of the cavitating self-resonating STRATOJET® to well mineral scale removal under submerged conditions and either this jet or the self-resonating . SERVOJET® under "in-air" conditions.

6. ACKNOWLEDGMENTS

This work was funded by the U. S. DOE under Contract No. DE-FG07-981D13684.

7. REFERENCES

Benoit, W. R., "Early Stage Carbonate Scaling Characteristics in Dixie Valley Wellbores," *Transactions, Geothermal Resources Council*, vol. 11, October 1987.

Chahine, G., Conn, A., Johnson, V., and Frederick, G., "Passively Interrupted Impulsive Water Jets," *6th Intl. Conf. on Erosion by Liquid & Solid Impact*, Cambridge, U.K., Sept. 1983.

Chahine, G .L., Genoux, Ph. F., and Liu H.L., "Flow Visualization and Numerical Simulation of Cavitating Self-Oscillating Jets," *7th International Symposium on Jet Cutting Technology*, Ottawa, Canada, June 1984.

Chahine, G. L., Genoux Ph. F., Johnson, V.E. Jr., and Frederick, G. S., "Analytical and Experimental Study of the Acoustics and the Flow Field Characteristics of Cavitating Self-Resonating Water Jets," *Sandia National Laboratories, Albuquerque, NM, Contractor Report SAND84-7142*, September 1984.

Chahine, G. L. and Johnson, V.E. Jr., "Mechanics and Applications of Self-Resonating Cavitating Jets," *Proceedings of the International Symposium on Jets and Cavities, ASME, WAM*, Miami, FL, November 1985.

Chahine G.L., Genoux Ph. F., Liu, H. L., and Johnson V.E. Jr., “Analytical and Experimental Study of Self-Resonating Jets: Nozzle-Jet and Wall-Jet Interactions," *Sandia National Laboratories, Albuquerque, NM, Contractor Report SAND86-7124*, September 1986.

Chahine G.L., Johnson V.E. Jr., Kalumuck K.M., Perdue T.O., Waxman D.N., Frederick G.S., and Watson R.E., “Internal and External Acoustics and Large Structures Dynamics of Cavitating Self-Resonating Water Jets," *Sandia National Laboratories, Albuquerque, NM, Contractor Report SAND86-7176*, July 1987.

Chahine, G. L., Kalumuck, K. M., and Frederick, G. S., “Cavitating Water Jets for Deep Hole Drilling in Hard Rock,” *Proc., 8th American Water Jet Conf.*, Houston, TX, August 1995.

Crow, S. and Champagne, T., “Orderly Structure in Jet Turbulence,” *Journal of Fluid Mechanics*, vol. 48, August 1971.

Glowka, D., ``Recommendations of the Workshop on Advanced Thermal Drilling," Sandia National Laboratories Technical Report SAND97-2903, December 1997.

Johnson, V. E., Jr., Chahine, G. L., Lindenmuth, W. T., Conn, A. F., Frederick, G. S., and Giacchino, G. J., “Cavitating and Structured Jets for Mechanical Bits to Increase Drilling Rate, Part 1: Theory and Concepts; Part 2: Experimental Results,” *Journal of Energy Resources Technology*, vol.106, June 1984.

8. GRAPHICS

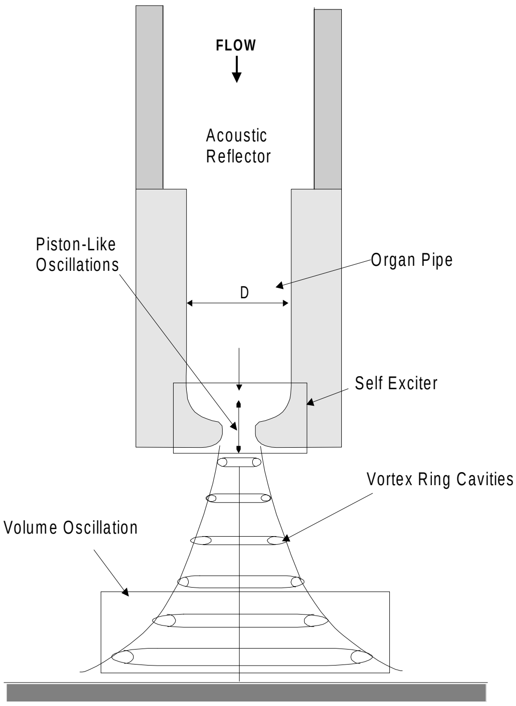

Figure 1. Schematic of Principles of Operation of an Organ-Pipe STRATOJET®

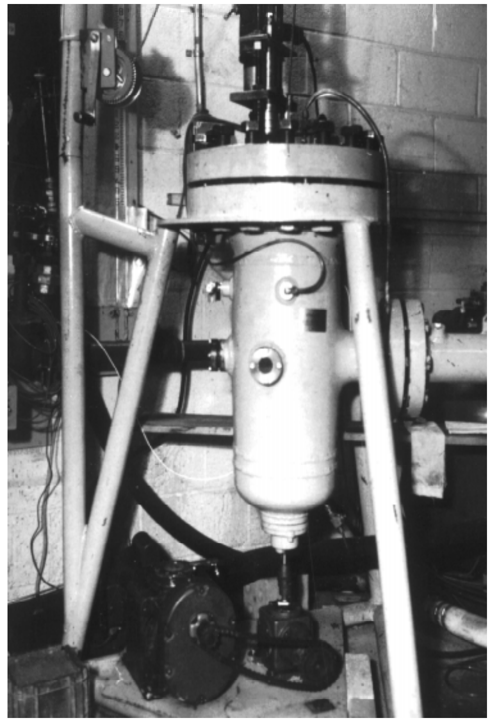

Figure 2. DYNAFLOW's High Pressure Cell (HPC) Capable of Ambient Pressures Up to 19.3 MPa (2800 psi).

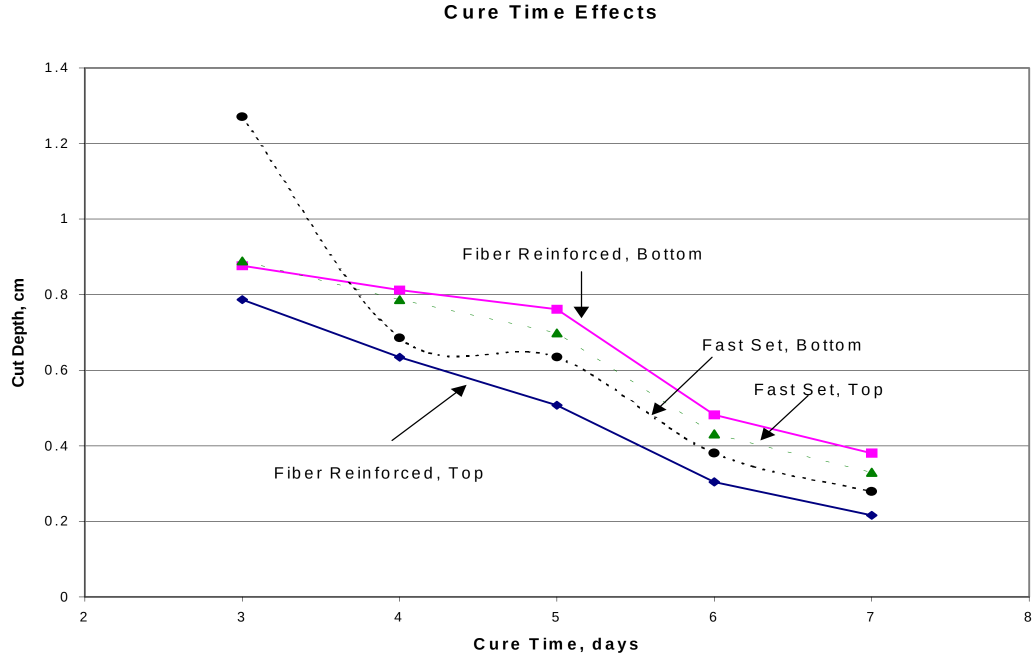

Figure 3. Influence of Cure Time of Laboratory Cement Samples on Cut Depth.

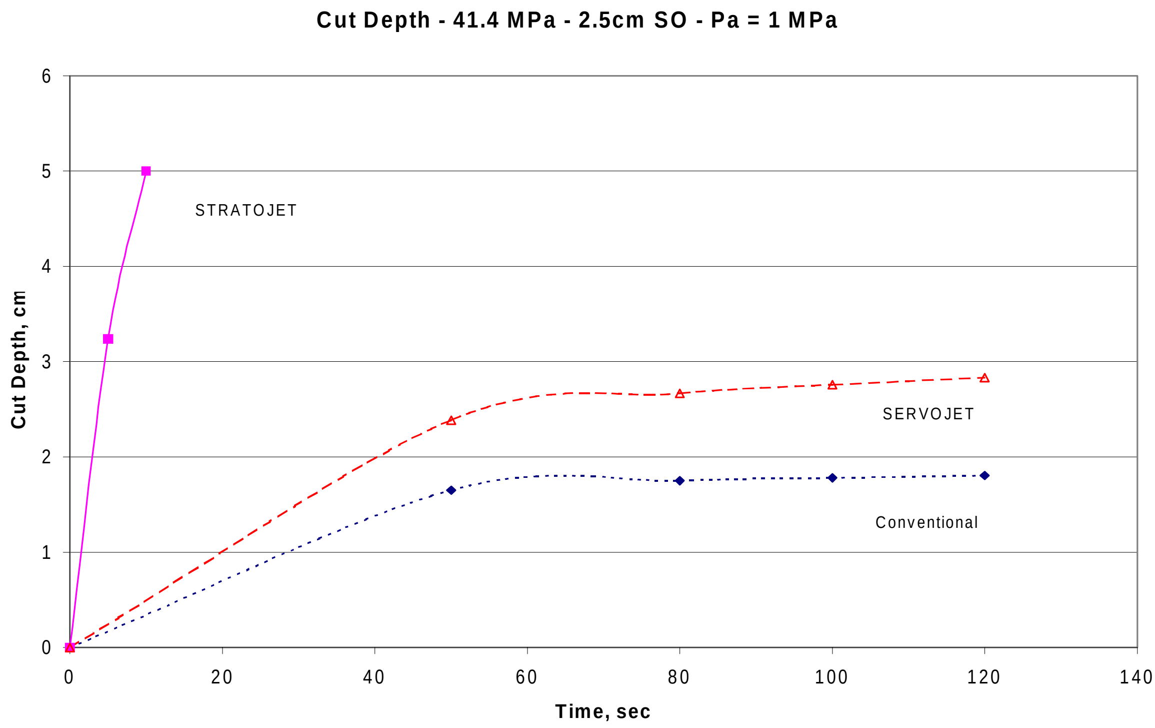

Figure 4. Progression of Depth of Erosion with Time for Three Nozzle Types at an Ambient Pressure of 1 MPa (150 psi). Standoff = 2.5 cm (1.0 in.). ΔP = 41.4 MPa (6,000 psi) Flow Rate = 0.37 l/s (5.9 gpm).

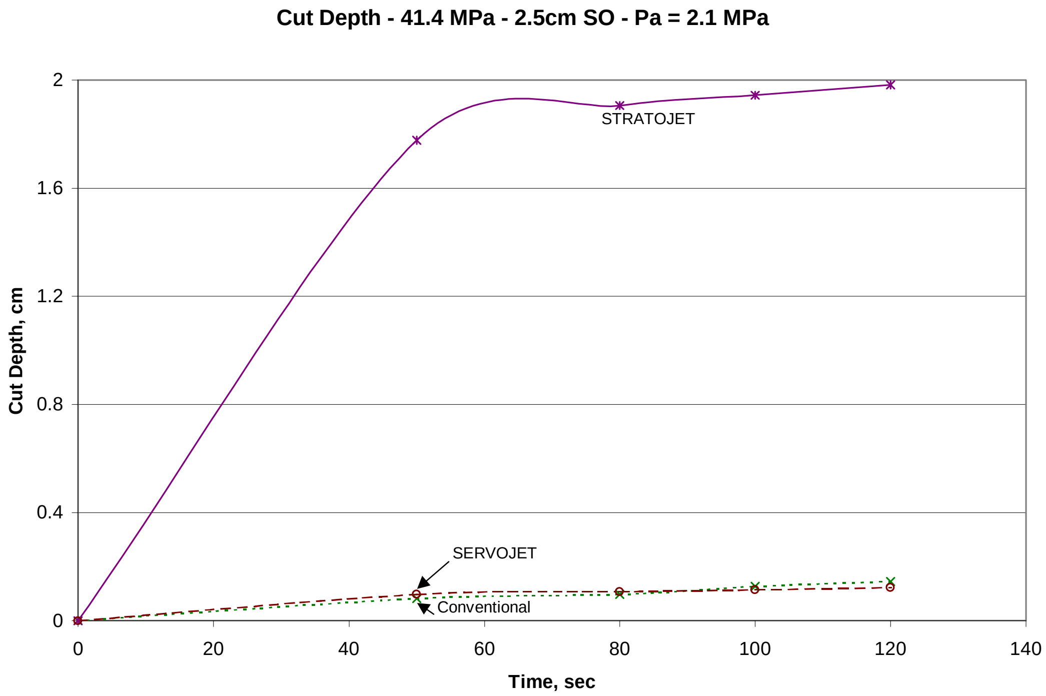

Figure 5. Progression of Depth of Erosion with Time for Three Nozzle Types at an Ambient Pressure of 2.1 MPa (300 psi). Standoff = 2.5 cm (1.0 in.). ΔP = 41.4 MPa (6,000 psi).

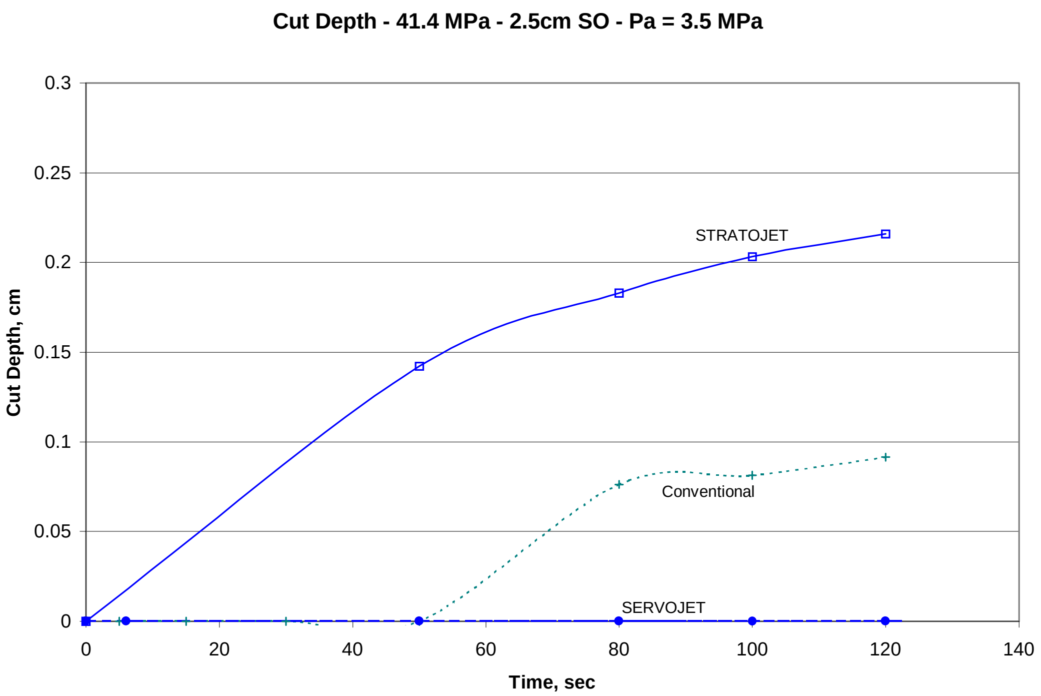

Figure 6. Progression of Depth of Erosion with Time for Three Nozzle Types at an Ambient Pressure of 3.5 MPa (500 psi). Standoff = 2.5 cm (1.0 in.). ΔP = 41.4 MPa (6,000 psi).

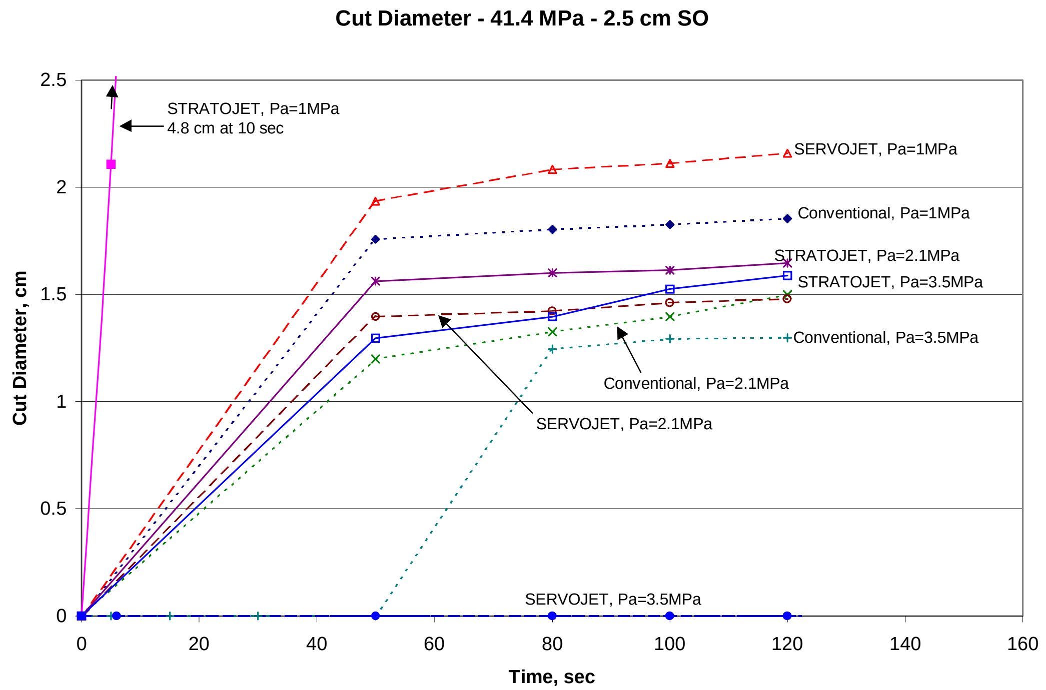

Figure 7. Progression of Diameter of Erosion with Time for Three Nozzle Types and Three Ambient Pressures. Standoff = 2.5 cm (1.0 in.). ΔP = 41.4 MPa (6,000 psi).

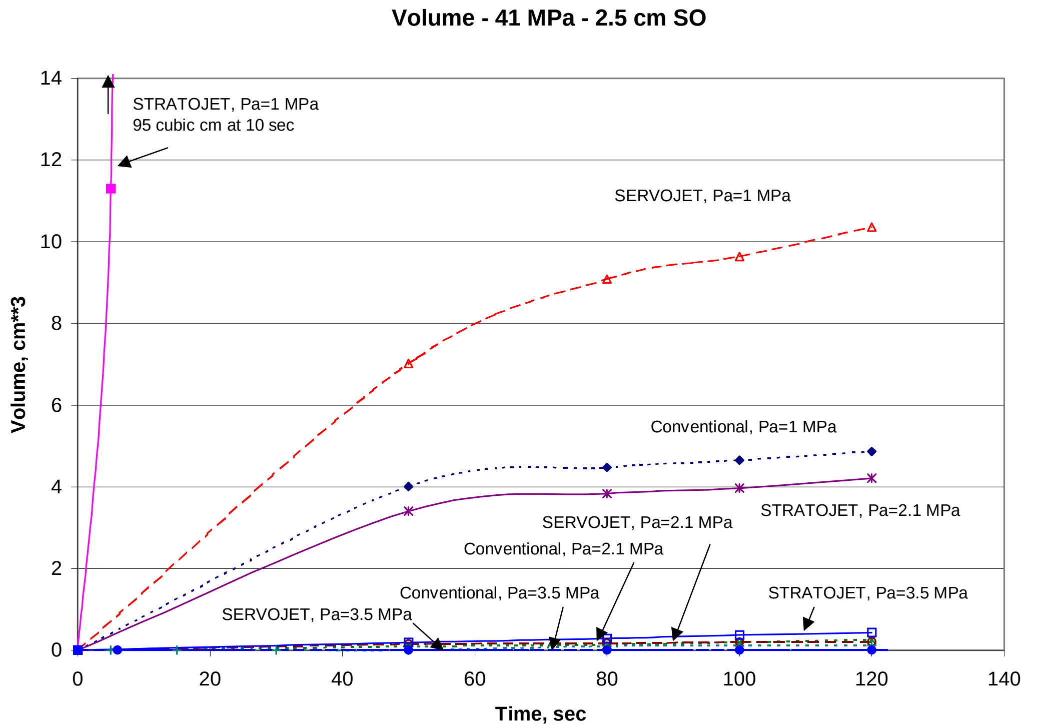

Figure 8. Progression of Volume of Erosion with Time for Three Nozzle Types and Three Ambient Pressures. Standoff = 2.5 cm (1.0 in.). ΔP = 41.4 MPa (6,000 psi).

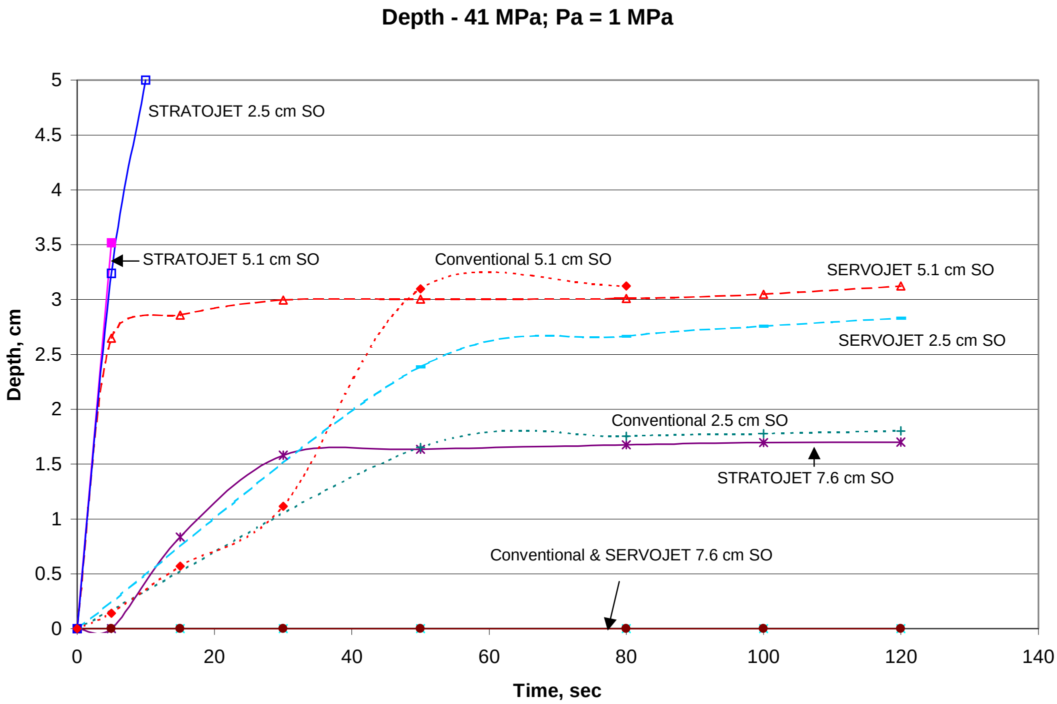

Figure 9. Influence of Standoff on Progression of Depth of Erosion with Time for Three Nozzle Types. ΔP = 41.4 MPa (6,000 psi), P_a = 1 MPa (150 psi).

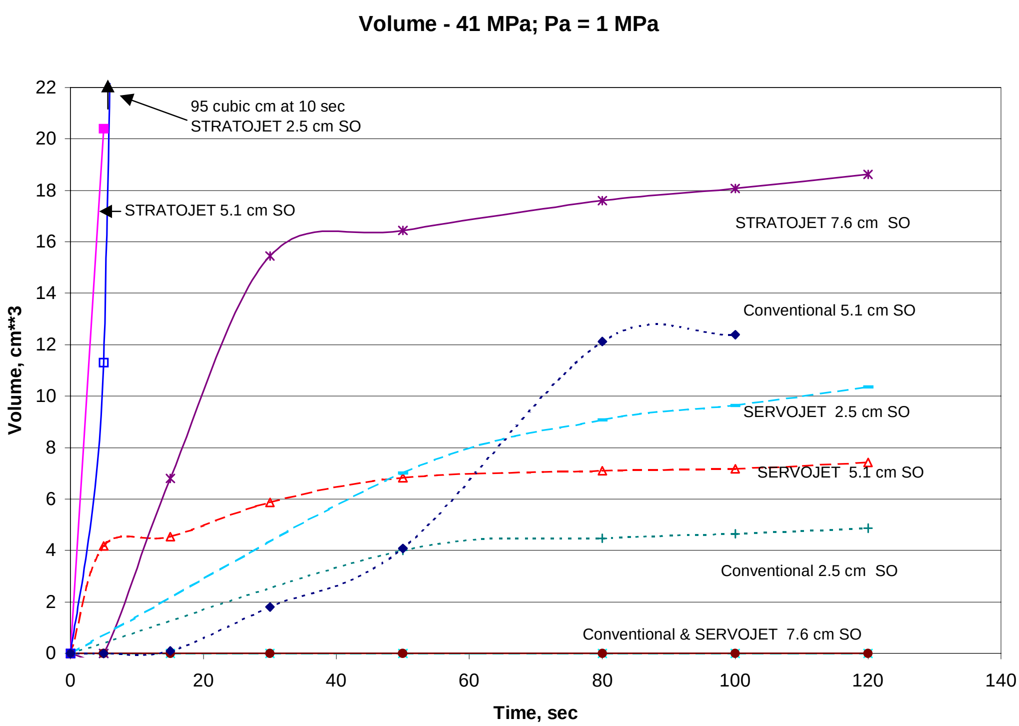

Figure 10. Influence of Standoff on Progression of Volume of Erosion with Time for Three Nozzle Types. ΔP = 41.4 MPa (6,000 psi), P_a = 1 MPa (150 psi).

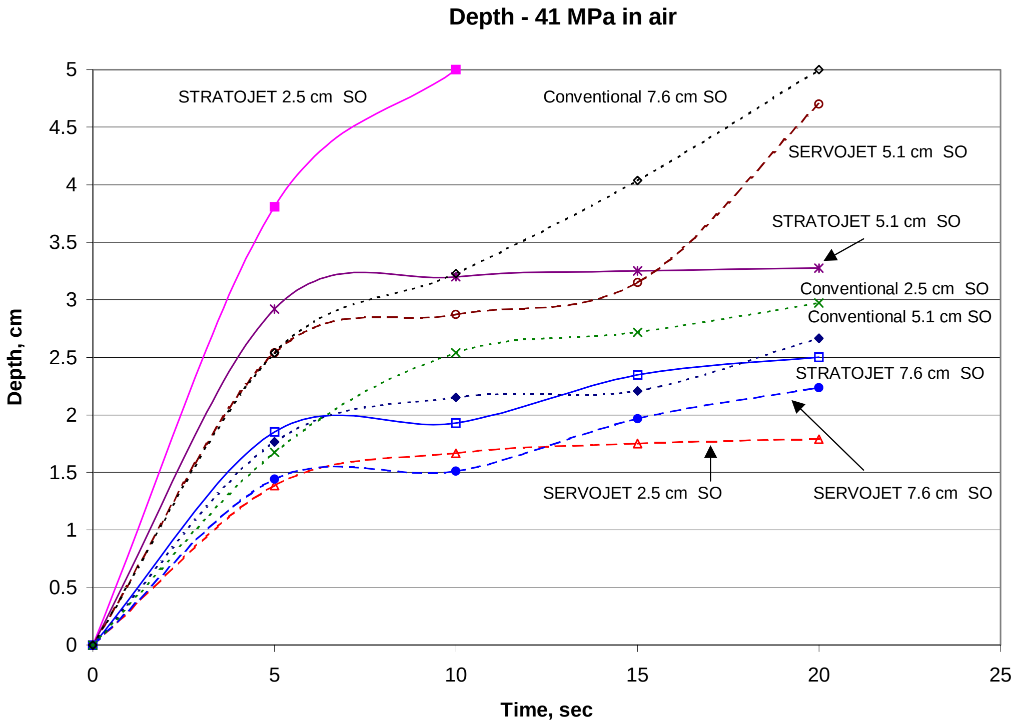

Figure 11. Influence of Standoff on Progression of Depth of Erosion with Time for In-Air Operation of Three Nozzle Types. ΔP = 41.4 MPa (6,000 psi).

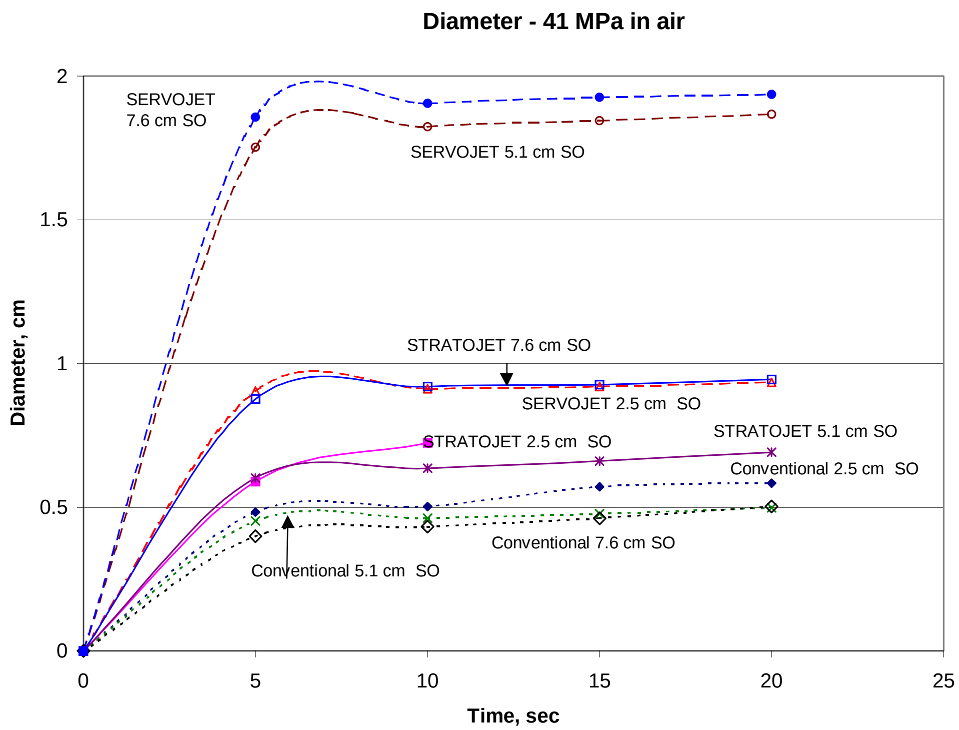

Figure 12. Influence of Standoff on Progression of Diameter of Erosion with Time for In-Air Operation of Three Nozzle Types. ΔP = 41.4 MPa (6,000 psi).

10th American Waterjet Conference
August 14-17, 1999: Houston, Texas

Paper 62

AN EXPERIMENTAL RESEARCH ON A NEW TYPE OF HIGH PRESSURE CAVITATING WATERJET DEVICE

Jingzhi Liu, Jinmu Zhu, Hongqi Lu
Wuhan University of Hydraulic and Electrical Engineering
Wuhan, Hubei, P. R. China

ABSTRACT

A high-pressure cavitating waterjet-cutting device, which is similar to a jet pump and can better induce cavitation, is presented. This new device is experimentally compared with conventional single-nozzle cutting device in the case of non-submerged condition. Test results indicate that on the same operating conditions the energy consumption of jet-pump type device is lower and cutting depth is deeper than that of conventional single-nozzle device. The optimum operating parameters of this new device are put forward on the basis of test results.

Organized and Sponsored by the WaterJet Technology Association

1. INTRODUCTION

High-pressure waterjet technology has come into wide use in many fields, such as milling, cleaning and cutting of various metal and non-metal materials. Though high pressure waterjet cutting has many advantages, at present the operating pressure of conventional high pressure waterjet cutting devices is very high for effective working, operating pressure for common cleaning is about 30 MPa, and for cutting rock or metal materials above 300 MPa. So much high operating pressure bring about many difficulties for materials, sealing and processing technology of high pressure generators and increase of device cost. In addition, due to higher energy consumption real application of this technique is greatly limited. So the principal problems need to be solved in high pressure waterjet cutting field are how to enhance cutting efficiency of high pressure water jet and how to reduce operating pressure in the same cutting effects.

At present study on high pressure waterjet is mainly concentrated on pulsed, abrasive and cavitating waterjet. Cavitating waterjet cutting is that when cavitating waterjet flows to the target surface a very high pressure concentrated on very small area of the target surface will occur due to collapse of cavities contained in waterjet. It is combination of this collapse pressure and impact pressure of speedy waterjet that causes a damage of material. So, in comparison to non-cavitating waterjet cavitating waterjet has higher cutting or cleaning efficiency in the same operating pressure.

In this paper a new type of high-pressure waterjet device i.e. jet-pump type waterjet cutting device is presented. This device can induce formation of cavities in waterjet and enhance cutting efficiency greatly.

2. EXPERIMENT

2.1 Working Principle of Jet-Pump Type Waterjet Cutting Device

It is well known that nuclei (gas or steam cavities) existed in liquid can change the tensile strength of liquid. The quantity and size of nuclei in liquid has a great effect on formation, growing and collapse of cavities. Jet-pump waterjet device can draw proper amount of air into waterjet and induce formation of cavitating waterjet.

Jet-pump type waterjet cutting device consists of first-stage nozzle, suction chamber, throat pipe and second-stage nozzle, as shown in Fig. 1. High-pressure water ejected from the first-stage nozzle form a speedy jet flow, in this process the pressure energy of main water becomes kinetic energy of jet flow. Because of adsorption of jet flow surface, air surrounding jet flow in suction chamber is carried into suction chamber so as to make the pressure of suction chamber be lower than atmospheric pressure, thus air outside suction chamber will be drawn into suction chamber.

If the quantity of air drawn into suction chamber is artificially controlled, the pressure in suction chamber will be very low, even equal to the vapor pressure of main water. As proper air is drawn into jet flow, the quantity and size of nuclei in jet flow increase and cavitation is induced. In this process cavitation bubbles and jet water are mixed uniformly inside throat pipe to form cavitating flow, and cavitation bubbles are compressed and are in the critical state of collapse at the front of throat outlet. Once the cavitating jet flow ejected from the second-stage nozzle impacts on the target surface cavitation erosion of material will occur.

2.2 Experimental Installation

Experimental installation of high-pressure cavitating waterjet cutting is as shown in Fig. 2. Tap water flows into water tank 1 through valve 15, high-pressure pump 3 sucks in water from the tank. High pressure water supplied from the pump is delivered to unloading valve 5, a part of high pressure water out of the unloading valve is delivered to waterjet cutting device 9, the other flows back to the water tank through turbine flowmeter 7. A circular specimen of alloy aluminum 11 is fixed on the top of screw located at carrier 12 which can be moved left or right by a servo motor 13. The standoff distance (i.e. separation between the first-stage nozzle outlet and specimen surface) can be set to any desired value by adjusting the screw.

In the experiments, rated pressure of high pressure pump is 35 MPa, rated flow rate is $1\times10^{-3} m^3/s$, operating pressure of the first- stage nozzle is measured by pressure gauge / transducer 8, and its flow rate is equal to the difference between discharge of high pressure pump at a certain pressure and by-pass flow rate, the by-pass flow rate is measured by turbine flowmeter 7; the flow rate of suction air is measured by glass rotary flowmeter 10; erosion amount of specimen due to impact of waterjet is determined by weighing the specimen before and after test with a precision balance with minimal reading of 0.1 milligram.

3. ANALYSIS OF EXPERIMENTAL RESULTS

3.1 Main Parameters

3.1.1 Specific Energy E_s

Assuming the specimen mass before and after test is m_1 and m_2 respectively, the eroded amount Δm of specimen due to impact of high-pressure waterjet is:

$$\Delta m = m_1 - m_2 \tag{1}$$

The mean kinetic energy unit time E_k at the outlet of the first-stage nozzle may be calculated out by following equation:

$$E_k = \frac{1}{2}\rho_0 Q_0 u_1^{\ 2} = \frac{1}{2}\rho_0 \frac{\pi d_1^{\ 2}}{4} u_1^{\ 3} \tag{2}$$

The consumed mean kinetic energy for eroding unit mass of specimen is defined as specific energy, that is:

$$E_s = E_k / \Delta m \tag{3}$$

Specific energy is an important index for judging cutting effect. Due to introduction of this index it is possible to compare the cutting performance of different cutting devices in different operating pressure. Obviously the cutting device with lower specific energy has higher cutting efficiency.

3.1.2 Dimensionless Standoff Distance $\bar{x}$

The ratio of standoff distance x, which is the separation between outlet section of the first-stage nozzle and target surface, to the radius r_1 of the first-stage nozzle outlet is called as dimensionless standoff distance, that is:

$$\bar{x} = x / r_1 \tag{4}$$

3.1.3 Area Ratio m

$$m = f_3 / f_1 \tag{5}$$

Where f_1 and f_2 are the sectional area of the first-stage nozzle outlet and throat pipe respectively.

3.2 Analysis of Experimental Results

An investigation of different area ratio, different length of throat pipe, different standoff distance, different nozzle type and different suction air amount for effect on eroded rate was made by experiments.

(1) It can be seen by waterjet cutting tests at air that material erosion caused by waterjet impact is mainly the result of cavitation damage. Fig. 3 shows the configuration of jet flow field, where Y_i

and Y_e are inner and outer boundary of jet boundary layer respectively, X_c is the length of jet initial zone. As a specimen of alloy aluminum is set at jet initial zone, the erosion area of the specimen is annular, the center of annular area is a non-eroded circular smooth zone, the diameter of which corresponds to the diameter of jet flow nucleus at the location of specimen surface. The smaller standoff distance, the bigger circular smooth zones. The outer boundary of annular eroded area corresponds to the diameter of cavitating waterjet at the location of specimen surface. With increase of standoff distance the annular eroded area also becomes big, and the central smooth area becomes small. As the standoff distance is equal to or greater than X_c, the eroded area of specimen becomes circular and central smooth area disappears. It was believed that the smaller standoff distance, the bigger erosion amount. But it is not true. In jet flow nucleus the time-average velocity of jet is maximum and equal to a constant, that means maximal dynamic pressure impacting on the specimen surface may be got, but in this zone there are not formation and collapse of cavitation cavities, so no erosion of material. In jet transitional zone, because of viscosity, turbulent diffusion and vortex effects of jet flow cavitation will occur in the jet boundary layer. It is impact effects of the cavitation cavities that result in bigger erosion amount of material.

(2) As shown in Fig. 4., the last specific energy of jet pump type device is less than that of conventional single-nozzle type device. It can be seen from this that. Under the conditions of the same operating pressure and erosion amount, energy consumption of the former is lower than the latter. In general, 36% of energy may be saved.

(3) According to Fig. 4., near by the least value of specific energy, change of dimensionless standoff distance $\bar{x}$ with specific energy for jet pump type device is bigger than that for the conventional single nozzle type device. So the effective cutting zone of the former is wider than the latter, that means the cutting depth of the former is greater than the latter. Range of dimensionless standoff distance of jet pump type cutting device for effective cutting is:

$$20 \le \bar{x} \le 120 \tag{6}$$

But for conventional single-nozzle device the range of $\bar{x}$ is:

$$100 \le \bar{x} \le 128 \tag{7}$$

In addition, due to left moving of the effective cutting zone for jet pump type device the smaller standoff distance can be adopted, in order to get a narrow cutting seam.

(4) For jet pump type of cutting device, the throat length L_t and area ratio m has a greater effect on cutting efficiency. If the throat is too short, air cannot be mixed into the center of waterjet, so that cavitation can not grow up efficiently and cutting effect is not good; if the throat is too long,

the cavitation bubbles may collapse previously in the throat. According to the test results, the dimensionless throat length $\overline{L_t} = L_t / r_1$ should be:

$$\overline{L_t} = 12.5\sqrt{m} \tag{8}$$

and the relation of dimensionless standoff distance $\bar{x}$ to area ratio m should be:

$$\bar{x} = 0.808m + 67.6 \tag{9}$$

4. CONCLUSIONS

A jet pump type high-pressure waterjet cutting device has the advantages of bigger cutting depth, lower energy consumption, and narrower cutting seam over conventional single-nozzle waterjet devices, because manufacture precision has a great effect on device performance the self-simulation characteristic of jet flow can not be satisfied again. The further study is necessary.

5. ACKNOWLEDGEMENTS

The authors are very grateful to the National Natural Science Foundation of China for providing funds for this research. The authors also wish to acknowledge the effort of staff of pumps and pumping station laboratory during the experimental work.

6. REFERENCES

Knapp, R. T., Daily, J. W. and Hammitt, F. G., "Cavitation," McGraw-Hill, New York, 1970.

Liu, J. Z., "The Effective Measures for Enhancing Cutting Capacity of High Pressure Waterjet," *Proceedings of the 3rd National Jet Technology Conference (in Chinese)*, pp. C4, 1-20, Fluid Engineering Association of China, Guongzhou, China, 1989.

Vijay, M. M. and Brienely, W. H., "Feasibility Study of Cutting Some Materials of Industrial Interest with High Pressure Water Jets," *Proceedings of the 2nd U. S. Water Jet Conference*, pp. 289-298, University of Missouri-Rolla, 1983.

7. NOMENCLATURE

E_k – mean kinetic energy unit time at the nozzle outlet;
E_s – specific energy;
L_t – length of throat;
$\overline{L_t}$ – dimensionless length of throat;
p_0 – operating pressure of main water at the nozzle inlet;
p_s – suction pressure of air;
Q_0 – flow rate of high pressure water;
Q_s – flow rate of suction air;
X_c – length of jet initial zone;
Y_e – outer boundary of jet boundary layer;
Y_i – inner boundary of jet boundary layer;
d_1 – diameter of first-stage nozzle outlet;
f_1 – sectional area of first-stage nozzle outlet;
f_3 – sectional area of throat pipe;
m – area ratio of jet pump type waterjet device;
m_1 – specimen mass before test;
m_2 – specimen mass after test;
Δm – erosion amount of material;
r_1 – radius of first-stage nozzle outlet;
u_1 – velocity at first-stage nozzle outlet;
x – standoff distance;
$\bar{x}$ – dimensionless standoff distance;
ρ_0 – density of main water at nozzle outlet.

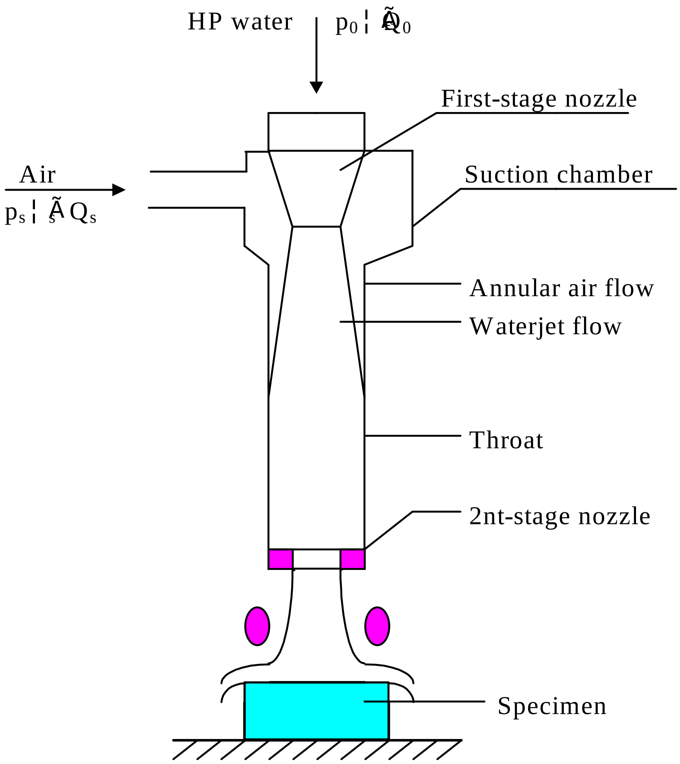

Figure 1. Schematic Drawing of Jet Pump Type Waterjet Cutting Device

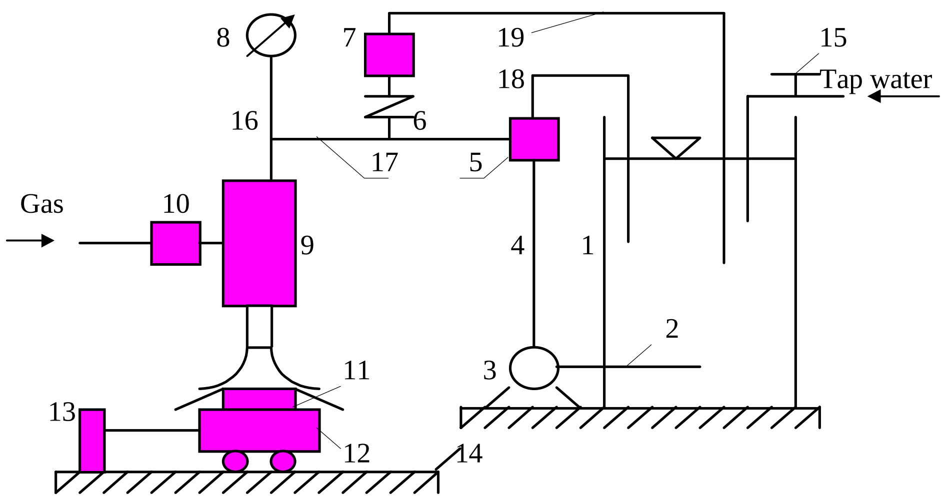

Figure 2. Schematic of Experimental Installation for High Pressure Waterjet Cutting

1. water tank; 2. suction hose; 3. high-pressure pump; 4. high-pressure discharge hose; 5, 6. unloading valve; 7. turbine flowmeter; 8. pressure gauge; 9. cutting device; 10. glass rotary flowmeter; 11. specimen; 12. carrier; 13. servo motor; 14. test bed; 15. valve; 16, 17, 18, 19. pipe

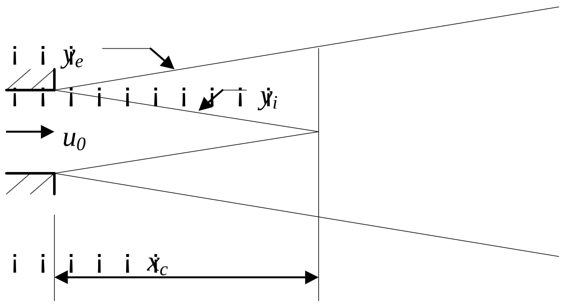

Figure 3. Configuration of Jet Flow Field

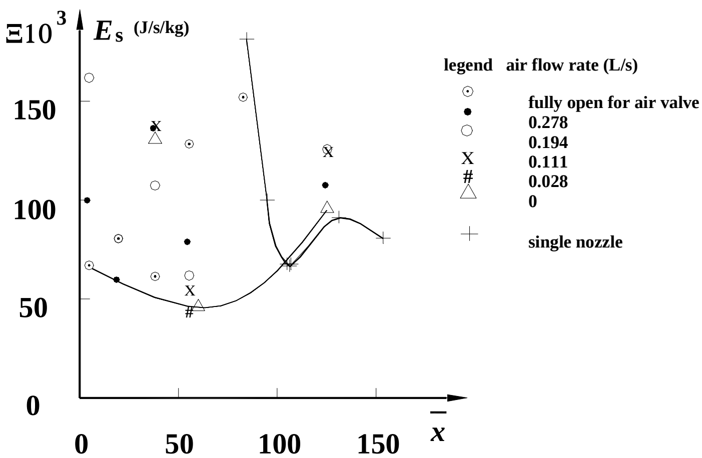

Figure 4. Comparison of Cutting Performance between Jet Pump Type and Conventional Single-Nozzle Type Cutting Device

10th American Waterjet Conference
August 14-17, 1999: Houston, Texas

Paper 63

MODELLING OF TURNING OPERATION

FOR ABRASIVE WATERJETS

A. Henning
Institute for Production Engineering and Automation
Fraunhofer Society
Stuttgart, Germany

ABSTRACT

New developments of innovative materials and higher requirements in industrial production create needs for both flexible and universal machining methods. Especially when machining very hard materials or compounds the abrasive waterjet qualifies as the tool of choice in many applications. So far industrial use of abrasive waterjet was focused on sheet cutting operations. With higher complexity of industrial product also geometrical requirements increase. Here the abrasive waterjet offers a wide range of possibilities for complete machining. Besides 5-axis machining also turning operations can be used for near net shaping with the same tool even for different materials. So far adaptive control strategies for machining optimization were not available, though.

In this paper new empirical approaches to process modelling of the abrasive waterjet process are developed. The turning operation is used here to obtain empirical information about the effect of the very particle impact. So better understanding of the abrasive waterjet process can be expected resulting in control and optimization algorithms to improve quality and performance of the process.

Organized and Sponsored by the WaterJet Technology Association

1. INTRODUCTION

Waterjet techniques have been extensively explored and used for cutting processes. Here many models have been developed that describe the influence of jet parameters on the cutting outcome in different ways. These models yet cannot be directly transferred to milling or turning operation since operating conditions are very different. Milling and turning processes however are of great interest for machining hard materials and for finishing operation (see Figure 1). Also in combination with cutting operation it can be used for complete machining and near net shaping of complex geometry's [HAS98].

Turning operation with the abrasive waterjet have not found many applications yet because of difficulties with the control of the process. Other than in planar operation the process takes place at an already machined surface with large variation of impact conditions. This makes prediction of the machining outcome very difficult.

In this paper a modelling approach for turning operation is presented. Taking the geometric conditions (i.e. the original profile) into account the outcome can be predicted calculation the very effect of the particles. With this experimental setup also further information about the effect of very particles on the material can be obtained [HEN95].

2. ROTARY PROCESSES

In the literature so far several approaches for turning operation with abrasive water jets can be found (e.g. Ansari [ANS92], Hashish [HAS87], and Zeng [ZEN94]). The main focus of these investigations was put on empirical and modelling studies for rotary cutting operation, though. As in planar operation also in rotary operation cutting and ablation processes can be found. The processes can be distinguished by the characteristics of the machining parameters (e.g. high velocity) and of the machining outcome (e.g. no striation structures).

2.1 Rotary Cutting Process

The rotary cutting process is characterized by cyclic step propagation with major wear at the front surface of the turned part. The jet and the abrasive particles are reflected at this process in axial direction (Figure 2a) [ANS93].

At rotary cutting the machining typically starts at the face of the shaft and propagates along the shaft-axis at a high feed rate. While moving along the axis with the workpiece turning cyclic step formation is initiated. In accordance with planar cutting steps develop and propagate on the workpiece surface at consequent revolutions through accumulation of the effects of multiple particle impacts. Plateaus can not develop, though, because of the high velocity of the workpiece in the process zone. Due to jet lag effects the shape of the machined workpiece is characterized by a curved shoulder (see Figure 2a) [ANS92]. The surface shows significant striation structures making this a limiting factor for industrial usage of the process [HAS87]. With rotary cutting the abrasive jet is reflected in both radial and axial direction. Damages due to secondary wear of axially reflecting particles also limit possibilities for machining complex three-dimensional geometry with a rotary cutting process.

2.2 Rotary Ablation Process

The rotary ablation process corresponds to a large extent with the stable planar milling process without striation formation. At every revolution of the workpiece a kerf is generated through the impact of abrasive particles. Due to the high velocity of the workpiece in the process zone the generated kerf-depth very shallow. So the machining conditions and the impact situation of the particles (especially the impact angle) is well defined by the process of the previous revolution. Different from cutting processes no discontinuous i.e. cyclic step formation processes can occur at rotary ablation. The process advances by accumulation of many well-defined particle impacts at the circumference of the workpiece.

When machining three-dimensional shapes the jet is moved in axial direction at a high feed rate in scanning mode. So machining conditions (i.e. impact angle) can be controlled closely and can be adapted to the individual situation. Also axial reflection of the particles resulting in secondary wear at the workpiece are avoided (Figure 2b). This makes the rotary ablation process suitable for generation of complex geometrical structures in turning operation.

For modeling of the particle impact this process suits very well. Other than in planar operation the velocity in the process zone can be chosen freely reducing the effect of multiple impacts. Also machining conditions (esp. impact angle) can be varied in a wide range. With close control of the current profile geometry very good conditions for empirical modeling can be found.

2.3 Nomenclature

For the exact description of the turning process it is necessary to define the geometrical parameters at the workpiece. Other than in planar operation where the process conditions are constant i.e. the process propagates through an undamaged workpiece in turning operation the workpiece geometry changes with progress of the process. With this progress the machining conditions vary significantly. In Figure 3 relevant parameters are defined. The origin of the coordinate system is situated in the axis of the workpiece.

The position x defines the fixed machining position of the abrasive jet over the workpiece. The medium impact angle α, though, does vary within the process through reduction of the machining radius:

$$\cos\alpha = \frac{x}{r(t)} \tag{1}$$

This medium impact angle, though, only gives a first approximation to the real impact angles that vary over the kerf profile within the abrasive jet (Figure 4). For evaluation of the angle dependent ablation potential this has to be taken into account.

The velocity f of the workpiece in the process zone also depends on the actual machining situation i.e. the current radius r(t) and the number of revolutions per minute n.

$$f = 2 \cdot r(t) \cdot \pi \cdot n \tag{2}$$

The result parameters as well correspond with the current machining situation and thus vary within the process with changing machining geometry (Figure 3).

The depth of the kerf k represents a result parameter, which can be determined easily.

Kerf depth $$k = r_1 - r_2 \tag{3}$$

The depth of the kerf alone cannot describe the quantitative outcome of the process because the kerfing area A_K and the ablated volume depend on the current radius r(t) as well.

$$A_K = \pi \cdot (r_1^2 - r_2^2) \tag{4}$$

with r(t) = r_1 $$A_{KR} = \pi \cdot k \cdot (2 \cdot r(t) - k) \tag{5}$$

Therefore the kerf-area depends on the current radius r(t) and the depth of the kerf k. With this the kerfing performance P_K and the ablationrate Q_K can be defined as follows:

Kerfing performance $$P_K = A_K / t_k \tag{6}$$

Ablation rate $$Q_K = dV_K / dt \tag{7}$$

with the ablated Volume V_K

$$V_K = \int_0^{2\pi} \int_{y1}^{y2} (r - r(t, y)) \cdot dy \cdot d\varphi \tag{8}$$

3. RESULTS AND DISCUSSION

Very good control of machining parameters qualifies the rotary ablation process as a tool for empirical studies and modelling approaches. In this paper the effects of different machining parameters on the turning outcome were to be evaluated. For the empirical study kerfs were generated at constant machining conditions and fixed position of the abrasive waterjet over the workpiece using the rotary ablation process. The duration of the process was varied generating discrete time-series of profiles.

In Figure 6 the time dependent development of the kerf profile can bee seen. The depth of the kerf increases with duration of the process while the width remains about constant. As expected the kerfing performance P_K and the ablation rate Q_K increase with higher water pressure and thus higher hydraulic power. The width remains the same.

As shown in Figure 7 the rotary speed of the workpiece is no important factor for the process- neither quantitative nor qualitative. With the rotary speeds the number of revolutions per time unit increases. The operational time per area unit on the workpiece per revolution decreases at the same amount. So the load per area on the workpiece remains the same independent from the rotary speed. Also the direction of rotation did not show significant influence. At very low rotary speed and thus high kerf depth per revolution, though, it can come to effects through changing front formation.

In Figure 8 the influence of the jet position on the development of the kerf profile is illustrated. The medium impact angle changes not only with the position of the jet but also within the process (bottom graph). Also the position of the jet shows great influence on both the qualitative and quantitative outcome of the kerf profile. The kerf depth shows a maximum at a position between x=15mm and x=17.5mm, which corresponds with a starting medium impact angle of about 40 to 45°. For higher impact angles the width of the profile increases.

As stated before the medium impact angle only gives an average for a first description. For a closer look at the angle dependent performance of the jet the gradient of the profile and the distribution of the abrasive jet has to be taken into account (see Figure 4).

For three different materials experiments were carried out and the profiles were evaluated: steel (Figure 10), Aluminum alloy (Figure 12), and glass (Figure 13) For steel a maximum kerfing performance can be found at an impact angle of approximately 45° (Figure 10). For glass the maximum can be found at 90° (Figure 13) and for Aluminum alloy at 0° (Figure 12). The results show very close qualitative correspondence with equivalent theoretical wear characteristics for brittle and ductile material as well as for different wear mechanisms (deformation/chipping wear) found in literature (e.g. [FIN78]).

4. CONCLUSION

Turning is a very promising extension of the multiple possibilities of machining with abrasive waterjets qualifying it as a universal tool for complete machining of innovative materials. Besides industrial use for machining hard-to-machine materials the turning process was introduced in this paper as a powerful tool for fundamental modelling of the interaction between abrasive particle and material. This modelling can not only give more and more detailed information about microscopic processes but can also lay the foundation for adaptive control and thus better performance of abrasive waterjet machining.

5. ACKNOWLEDGEMENT

I gratefully acknowledge Prof. H. Louis, Dr. A. Laurinat and Dr. J. Ohlsen of the University of Hanover for their technical support and contribution in this work.

6. REFERENCES

[ANS92]	Ansari, A.I; Hashish, M.; Ohadi, M.M.	Flow Visualization Study of the Macromechaniscs of Abrasive-waterjet Turning. *Experimental Mechanics*, 1992.
[ANS93]	Ansari, A.I.; Hashish,M.	Volume removal trends in abrasive waterjet turning effect of abrasive waterjet parameters. *PED*-Vol.64, Manufacturing Science and Engineering, ASME 1993.
[FIN78]	Finnie, I; McFadden, D.H.	On the velocity dependence of the erosion of ductile metals by solid particles at low angels of incidence. *Wear* 48, 1978.
[HAS87]	Hashish, M.	Turning With Abrasive-Waterjets - A First investigation. *Journal of Engineering for Industry*, Vol. 109, 1987.
[HAS98]	Hashish, M.	The waterjet as a tool; *14th International Conference on Jetting Technology in 1998,* Brugge Belgium.
[HEN95]	Henning, A.	Drehen mit Abraisivstrahlen, Diploma Thesis, 1995, Institute of material Science, University of Hanover, Prof. H. Louis
[ZEN94]	Zeng, J.; Munoz, J.	Intelligent automation of AWJ Cutting for efficient production. *Proc. 12th International Symposium on Jet Cutting Technology*, Ruen, France, 1994

Editor's Note: Please observe that figure numbers are not consecutive.

7. FIGURES

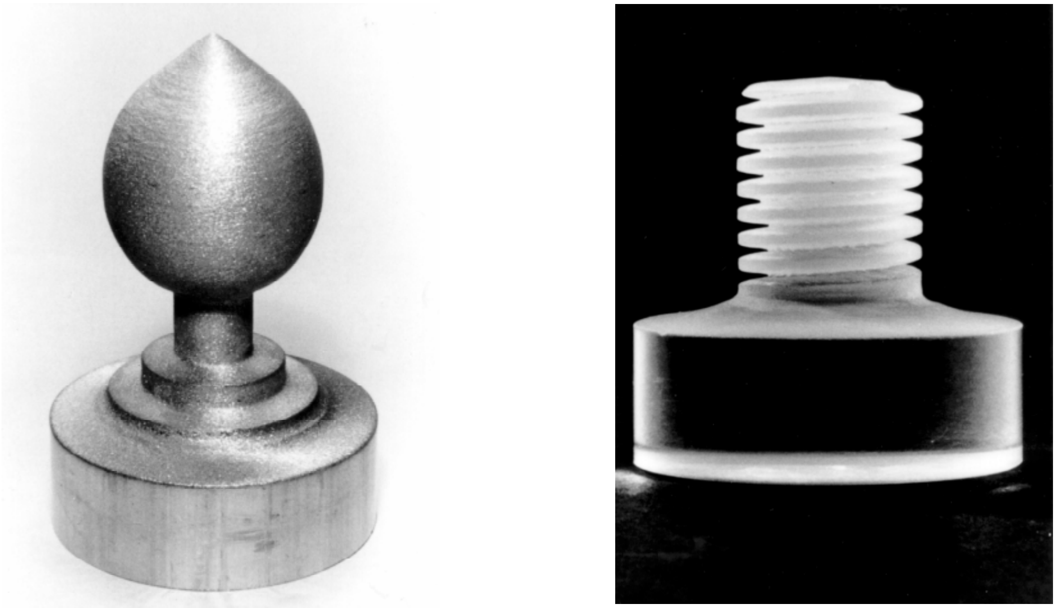

Figure 1: Machining Examples of Rotary Ablation [HEN95]

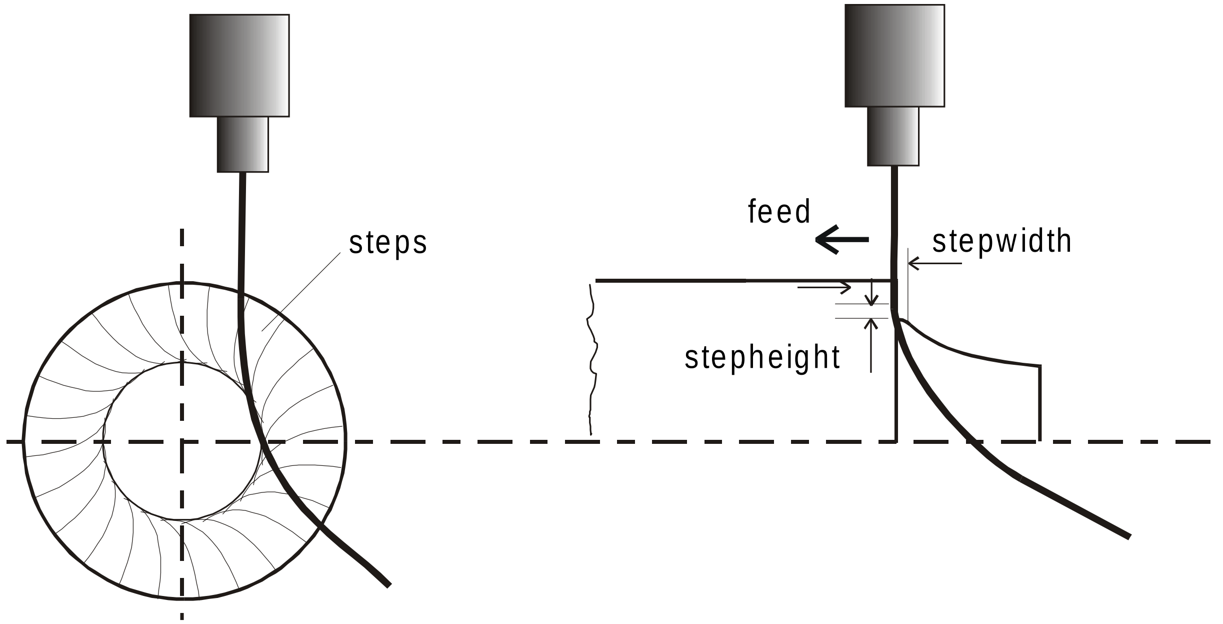

a) Step formation at rotary cutting

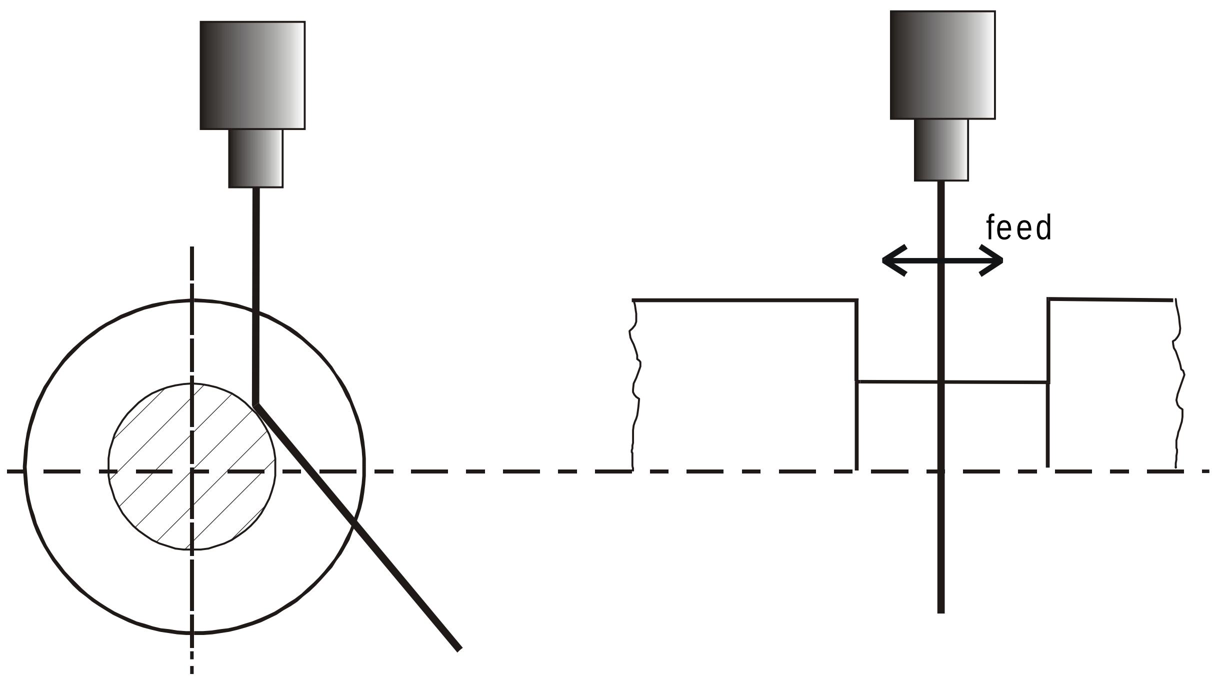

b) Radial reflection at rotary ablation /HEN95/

Figure 2: Comparison between Rotary Cutting (a) and Rotary Ablation (b)

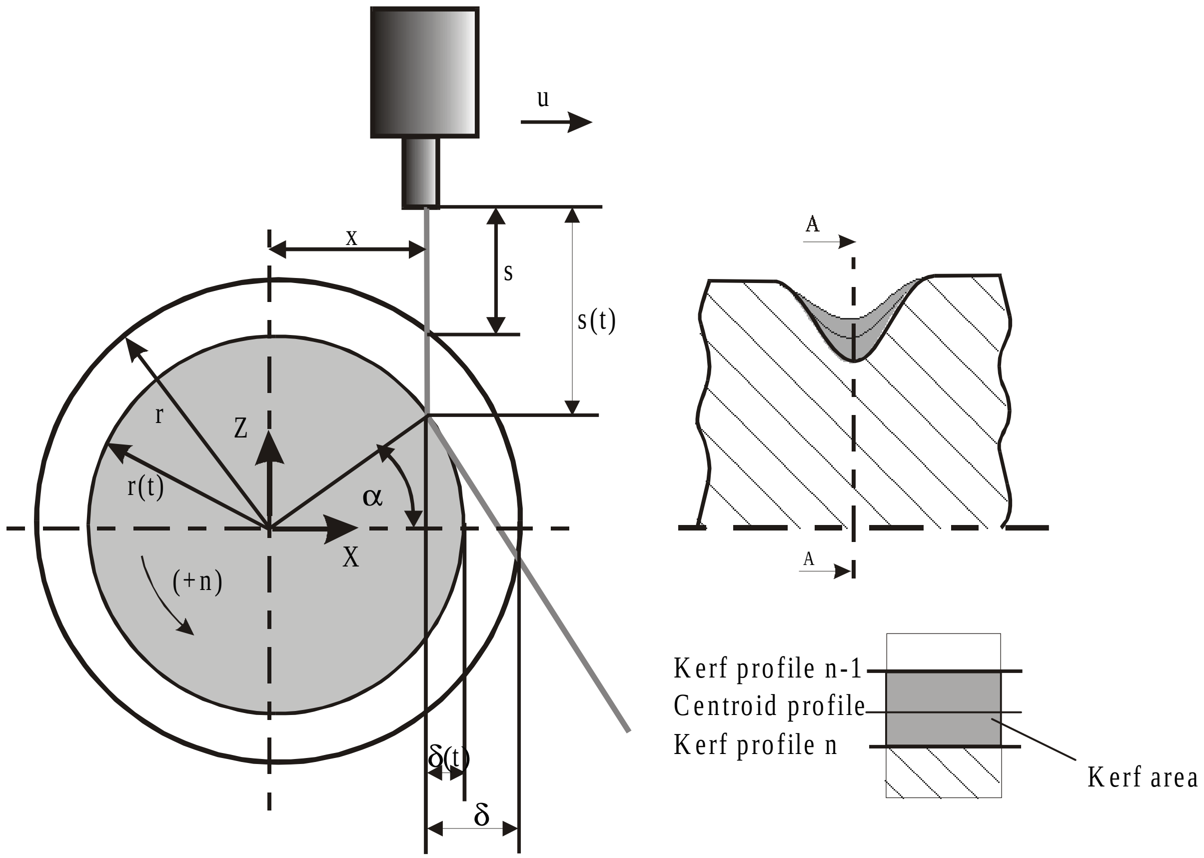

Figure 3: Nomenclature of Geometrical Parameters at Turning processes

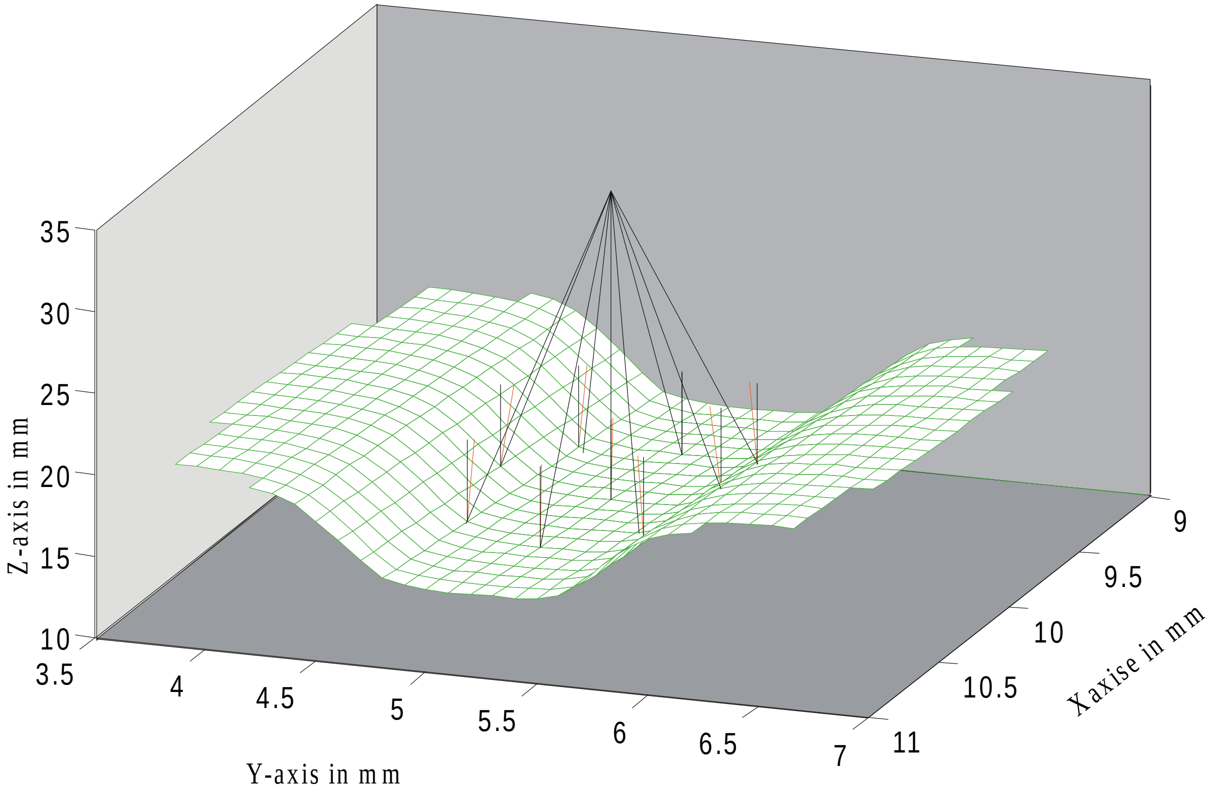

Figure 4: Variation of particle impact angle within the kerf profile

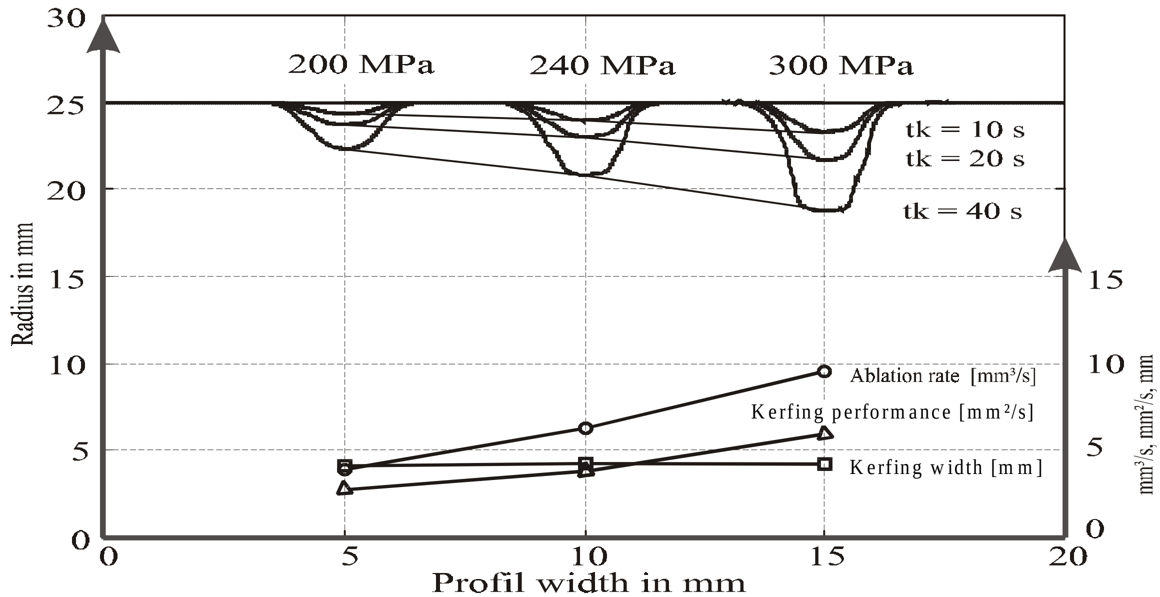

p = var.	dF = 0,9 mm	x = 17,5 mm	n = 76 min-1	m_A = 300 g/min
d_D = 0,17 mm	lF = 40 mm	s = 15 mm	dW = 50 mm	HP80

Figure 6: Time series and effect of the water pressure

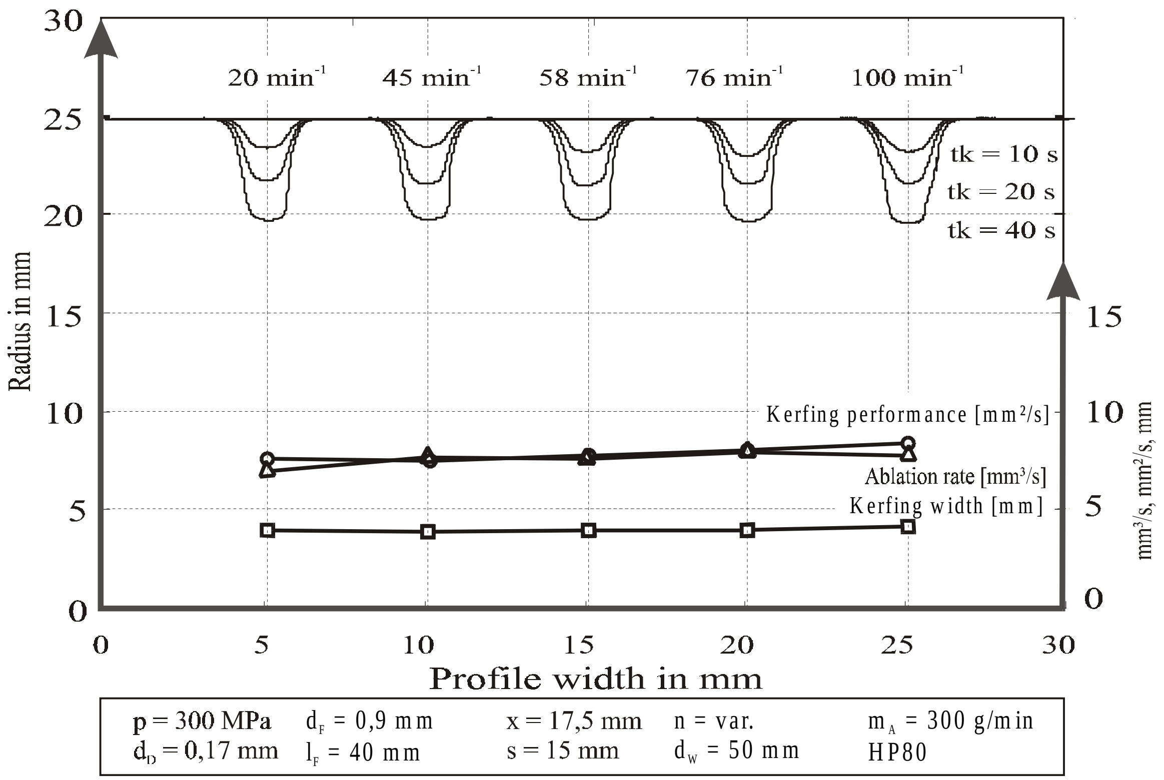

Figure 7: Effect of Rotational Speed

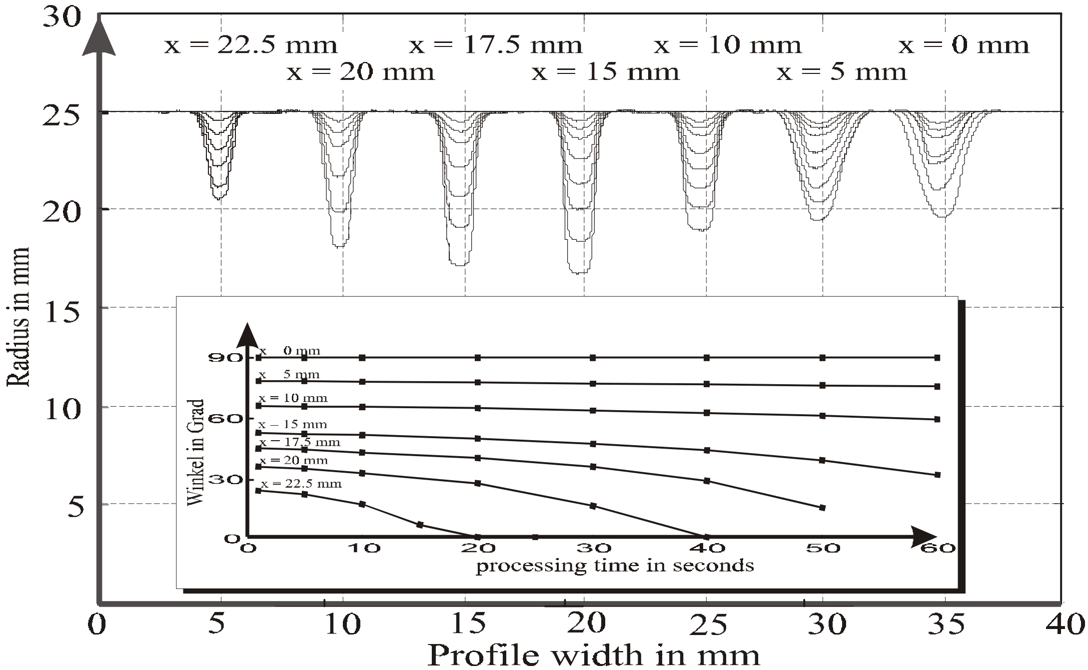

p = 300 MPa	d_F = 0,9 mm	x = var.	n = 76 min^{-1}	m_A = 300 g/min
d_D = 0,17 mm	l_F = 40 mm	s = 15 mm	d_W = 50 mm	HP80

Figure 8: Effect of Jet Position

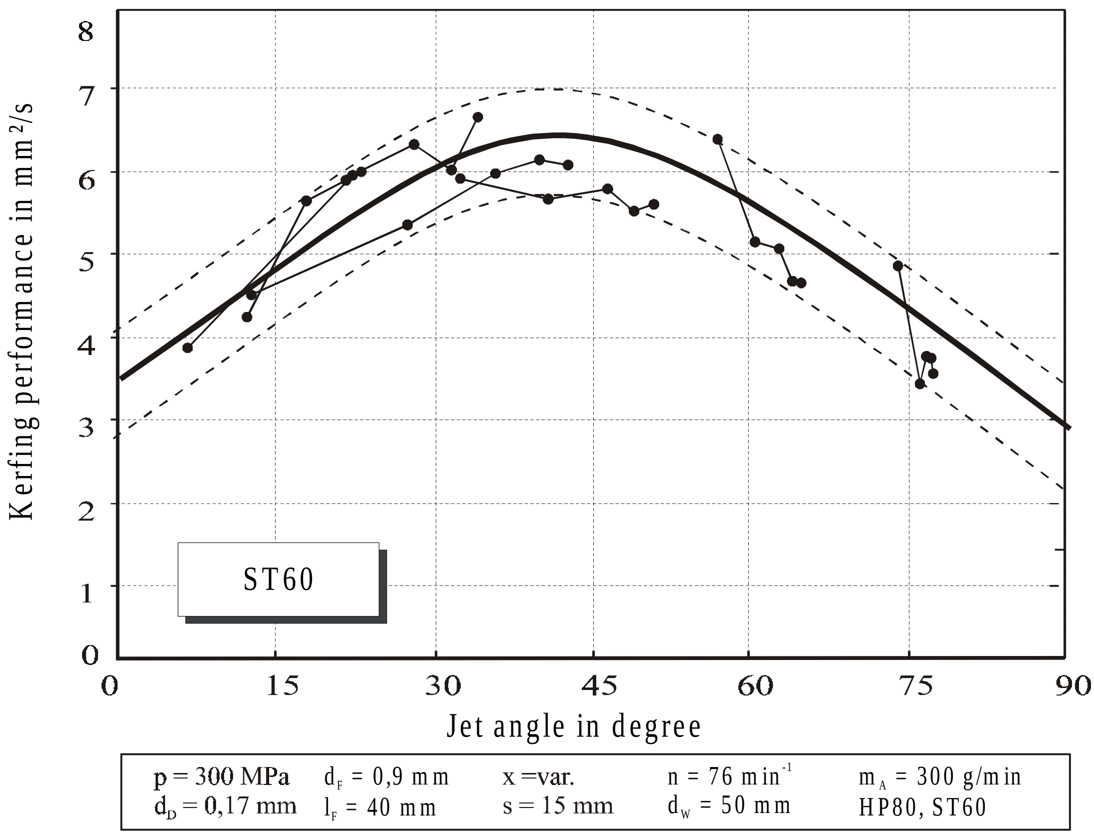

Figure 10: Effect of impact angle on kerfing performance at Steel

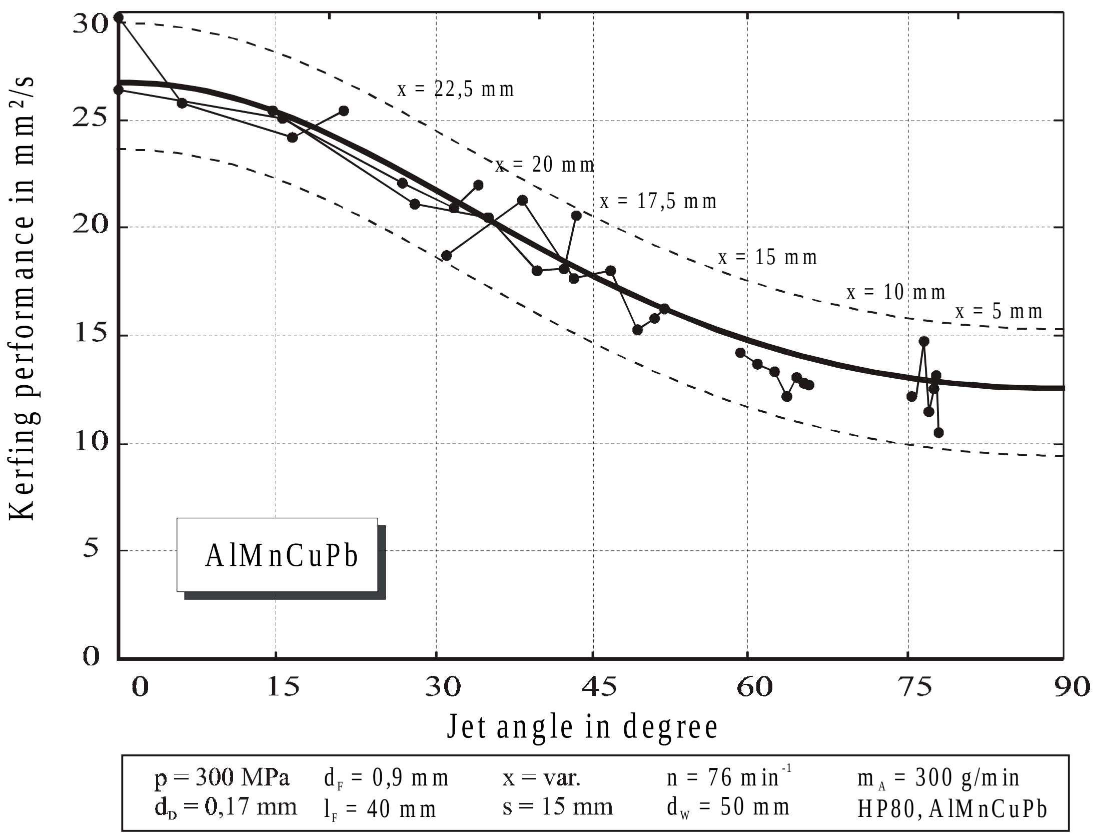

Figure12: Effect of impact angle on kerfing performance at Aluminum alloy

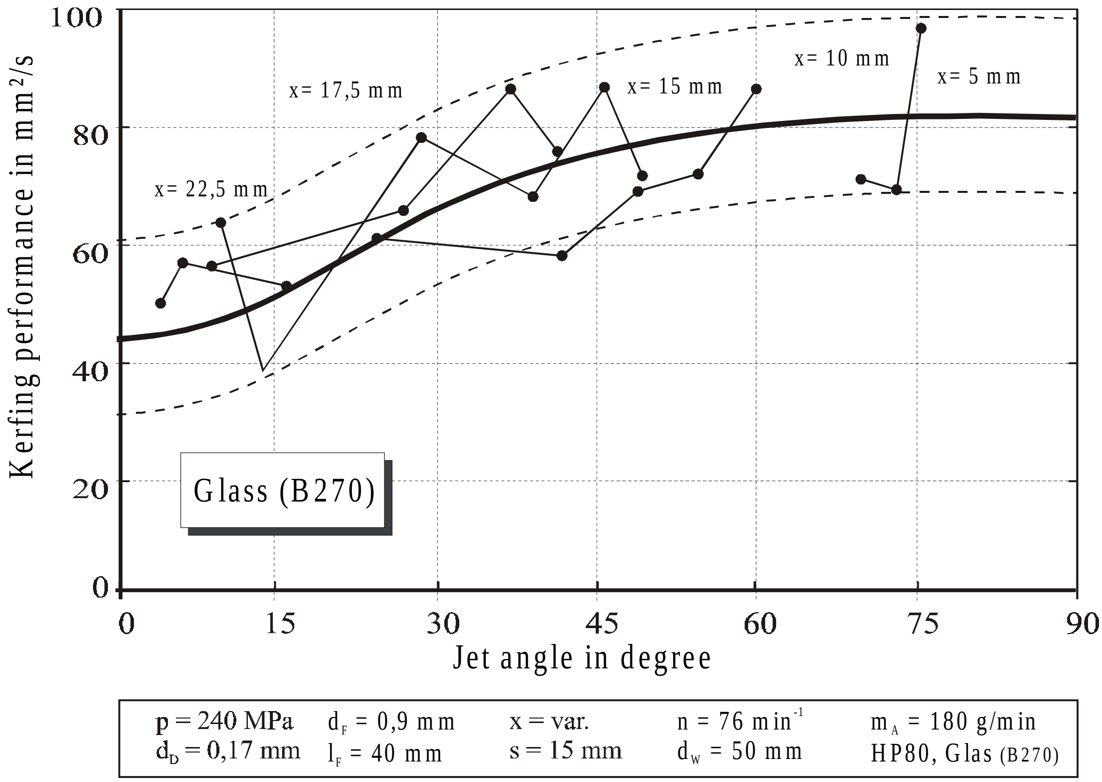

Figure 13: Effect of impact angle on kerfing performance at glass

10th American Waterjet Conference
August 14-17, 1999: Houston, Texas

Paper **64**

STATUS AND POTENTIAL OF WATERJET

MACHINING OF COMPOSITES

Mohamed Hashish
Flow International Corporation
Kent, Washington

ABSTRACT

Waterjets (WJs) and abrasive-waterjets (AWJs) have been accepted in the industry for many composite trimming applications. For example, the composite tail wing on the Boeing 777 airplane is trimmed with an AWJ. The AWJ produces high-quality surfaces free from chipping and delamination. Generally, the morphology and geometrical features of cuts in composites, such as kerf taper or waviness, are similar to those observed in other monolithic materials. However, depending on the composite structure, micro and macro effects may be significantly different. This paper presents data and observations on linear cutting, turning, drilling, milling, and repair of composites. In general, waterjet technology is an ideal fit for the machining of composites. Precision machining can be accomplished using accurate manipulators and advanced processing techniques, such as pressure ramping and lead angle implementation. Machining accuracies of 0.025 mm have been demonstrated. Waterjet technology can potentially be used for near-complete component fabrication.

Organized and Sponsored by the WaterJet Technology Association

1. INTRODUCTION

The use of advanced materials such as composites has been escalating rapidly over the past two decades, coincident with the introduction of AWJ technology to the marketplace. This paper discusses WJ/AWJ machining processes for composites. These processes include cutting, turning, drilling, and milling for part manufacturing or repair using waterjets, AWJs, abrasive suspension jets, or cryogenic jets. Typical problems that have been encountered when machining composite systems with these types of jets include:

- Delamination – Delamination may occur during piercing with a WJ or an AWJ or during cutting if abrasives are interrupted. Although the piercing problem has been resolved in the lab, starting holes are still being drilled with mechanical drills in the field.
- Reliability – Significant advances have been made on AWJ reliability. A need still exists, however, for improved robustness via enabling hardware. For example, a quick-acting on/off valve is needed to quickly stop the jet if the abrasive flow is interrupted.
- Edge quality – The AWJ produces high-quality edges for most composites, but the bottom edge accuracy and the quality of cuts in relatively thick honeycomb structures need to be improved.
- Cost effectiveness – Waterjets have proven to be cost effective for a wide range of composites. However, the cutting of hard CMCs and other hard composites is relatively slow and not cost effective. These materials can be cut using hard abrasives such as SiC, but nozzles wear out rapidly.

In the following, Section 2 discusses current composite systems and applications, and Section 3 reviews the work that has been done using WJ/AWJ technology for the machining of composites. Most industrial uses to date have applied the technology for trimming. Section 4 discusses the application of waterjet technology for various machining processes and provides some performance data. Section 5 summarizes the conclusions of our discussion.

2. COMPOSITE SYSTEMS

Most of today's composite materials are used in the aircraft, aerospace, marine, and automotive industries. Ongoing government and industry R&D programs are accelerating the use of advanced engineered materials such as organic, metal, and ceramic matrix composites (OMCs, MMCs, and CMCs) in jet aircraft engines. For example, the Integrated High Performance Turbine Engine Technology (IHPTET) program has as its goals the doubling of turbofan and turbojet thrust-to-weight ratios and the reduction of specific fuel consumption by 40% by the year 2003. Much of this performance improvement is expected to be accomplished through the use of these new materials. In general, the engine cold section will incorporate OMCs, MMCs, and intermetallics, while the hot section (combustors, turbines, exhaust) will require the high-temperature capabilities of some intermetallics, single-crystal superalloys, CMCs, or carbon/ carbon composites. More specifically, lightweight cold-section OMC components may include fan frames, fan blades, inlet and outlet guide vanes, stator vanes, cases, and control housings. For example, the PMR polyimides developed at NASA Lewis in the 1970s were a major advance in high-temperature resins. Continuous service temperatures up to 288°C can be withstood by these materials (Serafini, 1987). Graphite-PMR-15 structural parts are used on General Electric

Aircraft Engines such as the F110 and F404 military engines and in the Pratt and Whitney PW-1120 and 1130 turbojet and turbofan engines.

Metal matrix composites provide high specific strength and stiffness. MMC incorporation into such structures as fan blades, compressor rotors, impellers, shafts, cases, and frames is projected. Recently, the Air Force and ARPA launched the Titanium Matrix Composite Turbine Engine Component Consortium (TMCTECC) in cooperation with several major engine manufacturers (Kandebo, 1994). The goal of this program is to establish an affordable MMC industrial base for the 21st century, utilizing conventional Ti6-4 alloys for the matrix material and continuous silicon carbide fibers as reinforcements. The first components selected for commercialization under the TMCTECC project are fan frames and hollow core fan blades to replace the state-of-the-art hollow titanium wide-chord fan blades currently in use. In addition, Ti6-4/SiC MMC compressor blings fabricated by Pratt & Whitney have already been tested in the Joint Technology Demonstrator Engine.

Intermetallics may find use in moderate- to high-temperature engine components. Titanium aluminides, specifically gamma TiAl, may be used for the last stages of the compressor, while high-temperature intermetallics such as NiAl are candidates for turbine blades or vanes.

Ceramic matrix composites, using creep-resistant ceramic fibers, are anticipated for use in the highest-temperature components, such as combustors, turbines, augmentors, and nozzles. Carbon/silicon carbide combustor liners and high-pressure turbine rotors have been fabricated and rig tested. Other designs have incorporated SiC/SiC CMCs for these components and exhaust system components as well.

Jahanmir et al. (1998) have provided a comprehensive look at the state of the art of different composite systems and methods used to machine them. In aircraft manufacturing, AWJs are now used to cut a variety of composite structures to final dimensions. Boeing uses AWJs for final machining of the I-beam stiffeners used in the tail of the 777 and also for drilling of some composite parts. Honeycomb and other sandwich composite structures are the highest strength-to-weight and stiffness-to-weight materials systems available today. These highly efficient composites or laminates consist of a core (or core structure) bonded to an outer skin. AWJs are used to cut these materials for satellite applications in addition to a wide range of aircraft parts.

3. BRIEF REVIEW OF WJ/AWJ COMPOSITE MACHINING

Significant work has been done on the use of waterjets and abrasive-waterjets for the trimming of composites. A study by Schwartz (1983) showed that waterjet trimming of molded and cured composites can increase productivity by 80%. The results of this study also indicated that the cutting of internal shapes with a waterjet required predrilled holes.

High-pressure plain waterjets operating at 414 MPa have been used for cutting a number of epoxy composites (Hurlburt and Cheung, 1977). The cut edges are generally acceptable; however, poor-quality cuts were observed in materials that contained hard fibers, such as boron.

A study on AWJ cutting of MMCs (Neusen et al., 1987) suggested that the aluminum matrices of Al/SiC composites are smeared during the cutting process. Cut and broken silicon carbide particles were found near the AWJ-cut surface. These observations have been contradicted by others (Korican, 1987).

AWJ and diamond cutting of composites have been compared in a study using Al/SiC and Al_2O_3/SiC composite workpieces (Ramulu and Taya, 1988). It was shown that AWJ cutting is about 20 times faster than diamond cutting, but surfaces are generally about 10 times rougher.

The AWJ was also used in experiments involving the cutting and piercing of TiB_2/SiC and Al/SiC composites (Hamatani and Ramulu, 1988). The kerf and hole geometry and morphology were then quantitatively studied. It was observed that surface softening occurred in the MMC, but no explanation was given. During the piercing of the CMC, high temperatures were observed, indicating that the penetration process may not be totally free from thermal effects. It was observed, however, that no thermal degradation occurred to composite surfaces. The jet thermal effect is then highly questionable, and more work is needed on cutting mechanics.

The authors also addressed surface and subsurface damage, which was found to be greater in the MMC than in the CMC. Ramulu and Arola (1997) observed that the material removal when machining graphite/epoxy occurs by a brittle shearing mechanism that fractures and micro machines the constituents of the composite material. Jenkins et al. (1997) indicated that AWJs do not in any way degrade CFCC under elevated temperature conditions. AWJ-turning experiments on Mg/B_4C MMC have indicated that machining the MMC is only slightly more difficult than machining the matrix material alone (Hashish, 1987). It was found that the reinforcement particles may contribute to the surface roughness of an MMC surface cut by an AWJ. The testing of turned specimens (Lavander and Smith, 1985) indicated that AWJ machining does not affect the mechanical properties of the material but generally produces a rough surface.

Not much literature exists on developing special predictive models for waterjet cutting of composite materials. Hoogstrate et al. (1998a) presented an approach to identify waterjet parameters using several experimental data, predictive models, and logical rules. Hoogstrate et al. (1998b) also addressed the cutting of hybrid laminated metal materials consisting of very distinct basic materials such as aluminum and glass fibers. These materials are combined into one material in such a way that a layered structure is formed in which each layer consists of one of the basic materials. Machining such laminated materials introduces a new challenge, which was addressed by Hoogstrate et al. (1998b).

4. MACHINING OPERATIONS

Table 1 shows several different machining operations (linear cutting, drilling, milling, and turning) and lists the relevant machining parameters. In the following sections, these operations are discussed with respect to their application for the machining of composites.

4.1 Linear Cutting

Plain waterjet cutting of composites is limited to thin sheets and relatively soft materials. Plain waterjets tend to delaminate composites if they are thick, if they contain hard elements, or if

Table 1. AWJ Operations and Machining Parameters

AWJ Parameters	Machining Parameters			
	Linear Cutting	Drilling	Milling	Turning
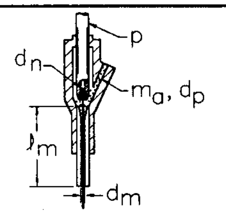	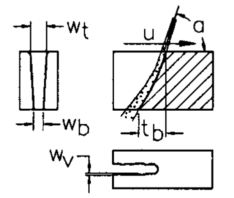	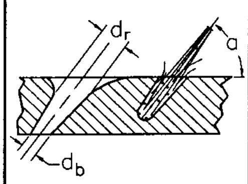	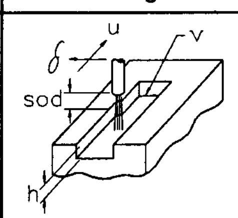	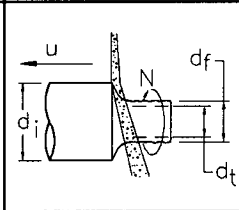
Pressure Waterjet Diameter Mixing Tube Length Mixing Tube Diameter Abrasive Material Abrasive Size Abrasive Flow Rate Abrasive Condition	Angle Standoff Distance Traverse Rate Number of Passes Material Thickness	Angle Standoff Distance Dwell Time Pressure Profile Material Thickness	Traverse Rate Lateral Increment Number of Passes Number of Sweeps	Rotational Speed Direction of Rotation Angle Traverse Rate Initial Diameter Final Diameter Depth of Cut
	Machining Requirements (Dependent Variables)			
	Traverse Rate Surface Finish Width of Cut	Diameter Drilling Time Hole Shape	Volume Removal Rate Depth Control	Turned Diameter Surface Finish Machining Time

cutting occurs at high traverse rates. Generally, increasing the pressure tends to reduce delamination during cutting but not during piercing. This has been confirmed by cutting fiberglass at pressures up to 690 MPa (Hashish, 1998a).

The features of linear AWJ cutting are shown in Table 1. Typical kerf shape characteristics include rounding at the top surface, tapering, burrs (in some materials), roughness, and waviness. Rounding occurs due to the jet's spreading before it engages with the material. Taper occurs due to loss of energy by the jet or further expansion while cutting. Thus, tapered cuts may be either convergent or divergent. Burrs occur when cutting metallic composite materials or structures such as honeycomb. Thin sheets of metal may tend to bend. The action of abrasive impact causes deformation that results in burrs at the exit. No burrs have ever been observed at the entry (top surface) of WJ/AWJ cuts. Roughness is attributed to the micro mechanics of the cutting process. With abrasives, the abrasive particle size will be the most critical parameter. Waviness is related to the macro mechanics of the cutting process. The cyclic nature of the kerf penetration process and the reduction in effective jet diameter as kerf depth increases contribute the most to waviness. Other effects include jet instability and side deflection. These features are generic. However, the micro/macro mechanisms will affect the surface characteristics of a machined composite material, and they are strongly dependent on the structure and properties of the material. The degree to which these micro/macro features affect the machining results depends on their relative values. For example, if the reinforcing particles in a composite are much smaller than the effect of an abrasive particle impacting the matrix material, then the reinforcing particles will have little or no effect on the machined surface finish compared to the effect of the abrasive particles on the matrix material. Of course, if the jet is cutting along a continuous fiber in a composite material, then the structure of the composite will significantly affect the micro/macro characteristics of the penetration process.

Figure 1 shows the effect of SiC volumetric concentration in an Al/SiC MMC. Kerf widths are shown for the top and bottom sides of cuts made in 13-mm-thick samples with varying SiC concentrations. When the SiC particle content is increased, the cuts become more tapered, indicating greater resistance to jet penetration. Kerf taper correlates with surface waviness, i.e., more tapered cuts are also more wavy or striated. The produced surfaces are relatively smooth at the top but become wavy as the depth increases.

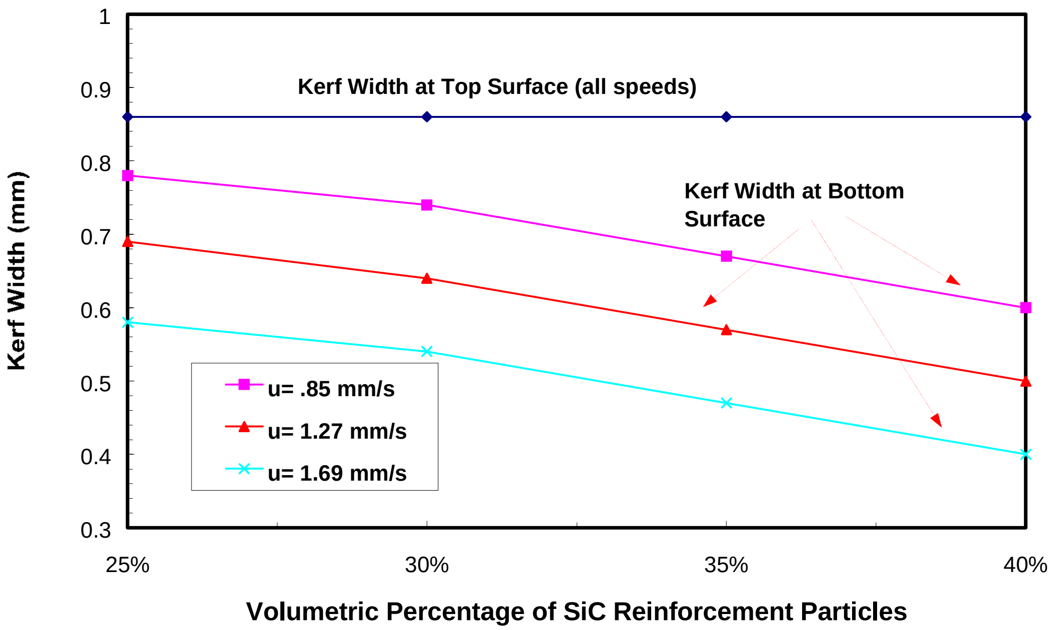

Figure 1. Effect of SiC Content on Cutting of Al/SiC MMC

The cutting of graphite epoxy composites has been highly successful with AWJs. High-quality finished surfaces are produced. Taper control can easily be accomplished by traverse rate adjustment. A wide plateau of parameters has been found acceptable for cutting relatively thin (10-mm) sections of graphite epoxy. This is because AWJs are mostly being used now for relatively loose tolerance trimming. More precise cutting of thick sections can be accomplished, however, with AWJs using accurate manipulator systems with 5-axis capability. For example, a taper of 0.025 to 0.050 mm is achievable in 25-mm-thick composites. Figure 2 shows a high-quality cut in an 18-mm-thick graphite epoxy sample.

Figure 3 shows examples of honeycomb structures. Cutting this class of materials introduces additional macro mechanics of jet-material interaction. Typically, when cutting a honeycomb sheet, the jet encounters voids and then thin ribs of material. Both of these elements affect the jet differently. The voids allow the jet to expand before striking the bottom plate of the honeycomb sandwich. This expansion will produce a wider kerf width than at the top plate and will result in erosion of some of the adjacent walls. The relatively large standoff distance when cutting the bottom plate results in rounding and burrs. A cut at the bottom of a honeycomb structure appears as a series of punched holes. When the jet encounters a wall, it deflects. This causes additional erosion to adjacent walls. The jet then tends to erode, rather than cut, the rest of the wall as it passes over it. Cutting at a lead angle (a few degrees) has been found most effective for

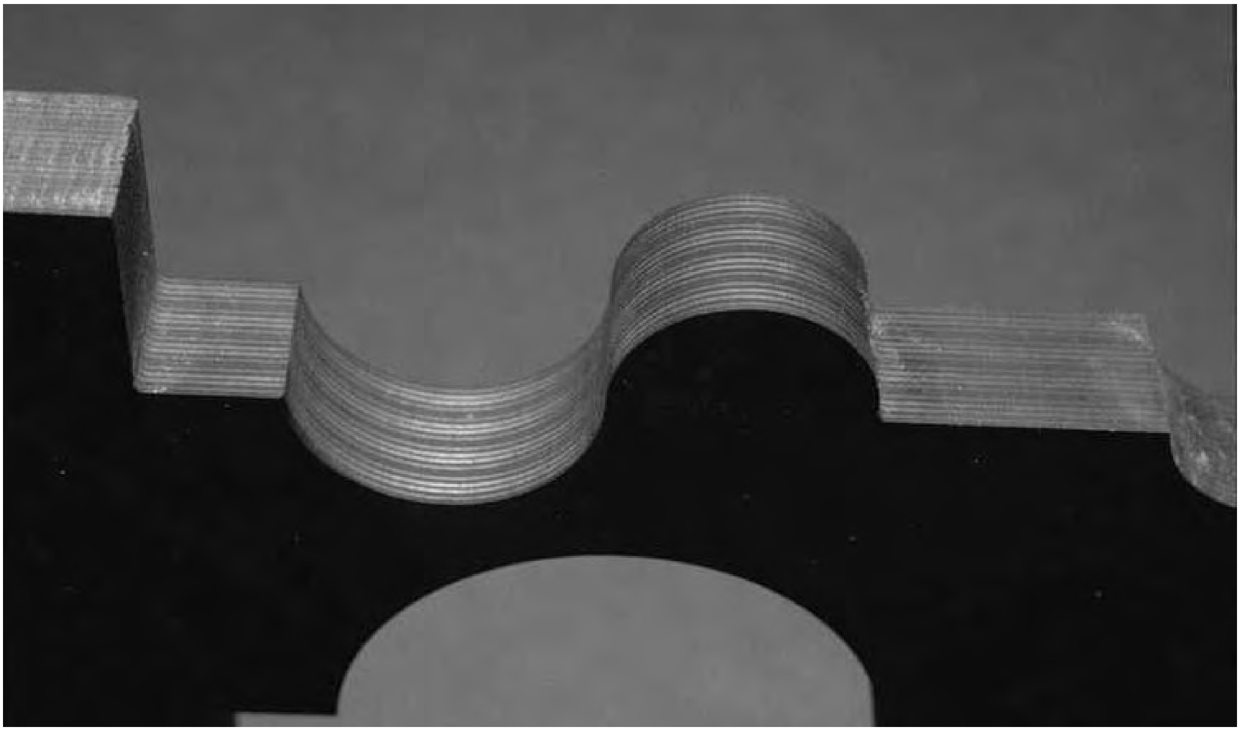

Figure 2. AWJ Through Cuts in 18-mm-thick Graphite Epoxy Composite

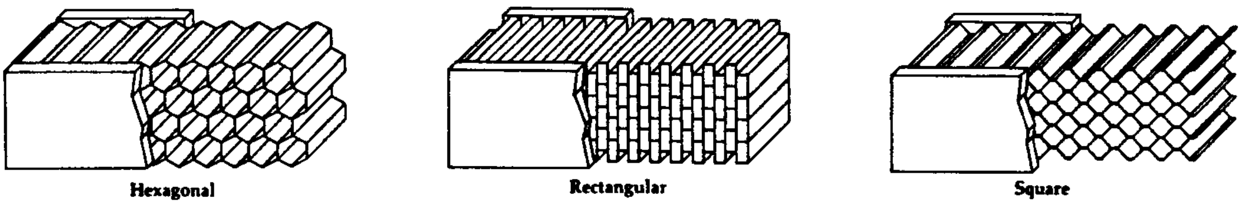

Figure 3. Examples of Honeycomb Structures

honeycomb. This allows the jet to engage more with the material, rather than voids, and thus reduces its “free air” spreading. The use of tilt angles (a fraction of a degree) has also been found effective in improving edge quality at the bottom of the cut. Figure 4 shows example cuts.

Abrasive suspension jets (ASJs) offer new capabilities over AWJs. These include higher cutting speeds, smaller features, and the ability to cut hard composite materials such as carbides and CMCs. Figure 5 shows some data on depth and width of cut in various types of ceramics and CMCs.

Laboratory tests have proven the feasibility of cutting with liquefied gas jets such as liquid nitrogen (LN_2). This will be useful for hollow composite cutting or in environments that must either be kept very clean or in which the composite contains water-sensitive elements. The use of subliming or soluble materials, such as solid CO_2 or sodium bicarbonate, may provide sufficient hardness at cryogenic temperatures to be efficient in removing workpiece material. This area needs further work for application to composite machining in the field.

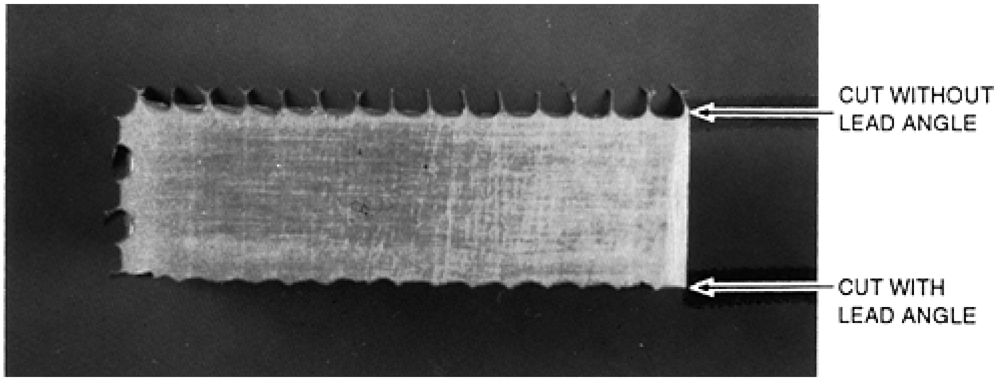

Figure 4. Bottom Surface of 25-mm-thick Honeycomb Cut with an AWJ with and Without a Lead Angle (9°)

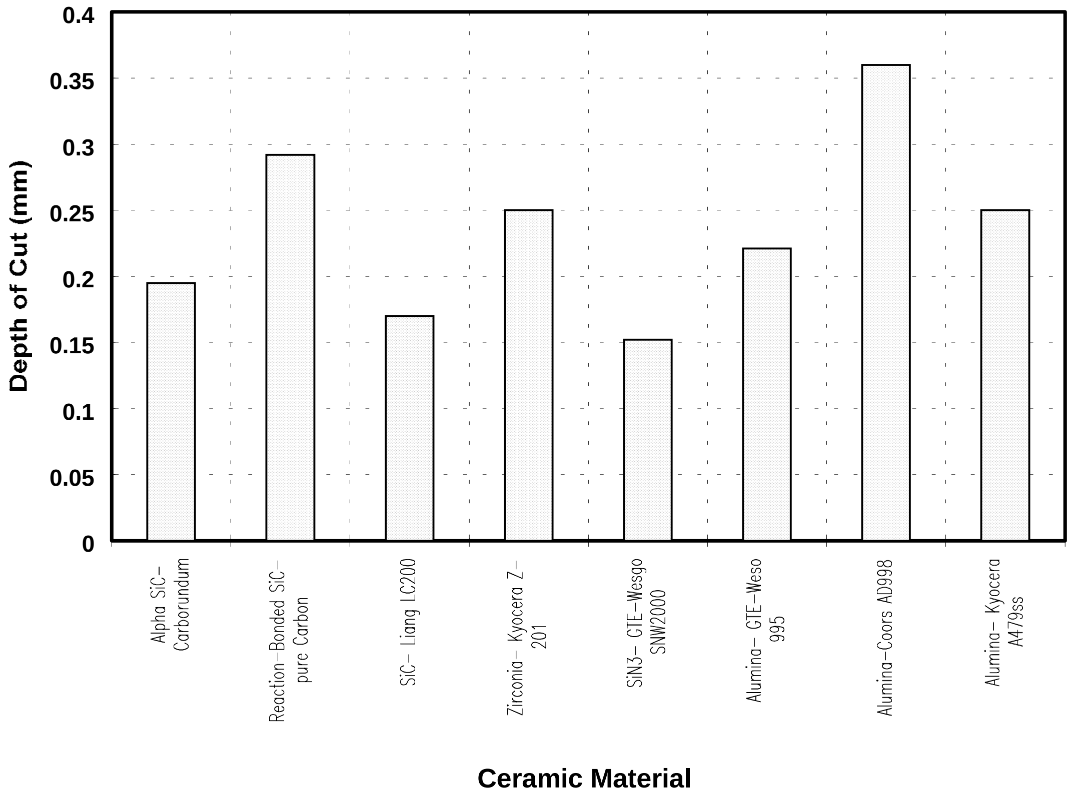

Figure 5. ASJ Depth of Cut in Various Types of Ceramics

4.2 Turning

The turning of composite materials such as MMCs and CMCs results in significant problems when using traditional turning and grinding techniques. These could be related to technical or economical results. OMCs are typically not turned to produce parts. However, with the ability of the AWJ to turn these materials, new concepts may arise in the fabrication of these materials. Table 1 shows the process and parameters of AWJ turning.

The trends observed in AWJ turning are qualitatively similar to those seen in linear cutting. Figure 6 shows the effect of traverse rate on the machined diameter of an Mg/B_4C MMC rod (initially 17 mm in diameter) for a fixed depth of cut of 2.53 mm. Increasing the traverse rate will result in less volume removal and, consequently, a larger final diameter. Figure 6 also shows the target diameter, as set by the radial position of the jet. It was noted that the difference between the target and the machined diameters is reduced by increasing the pressure and reducing the traverse rate.

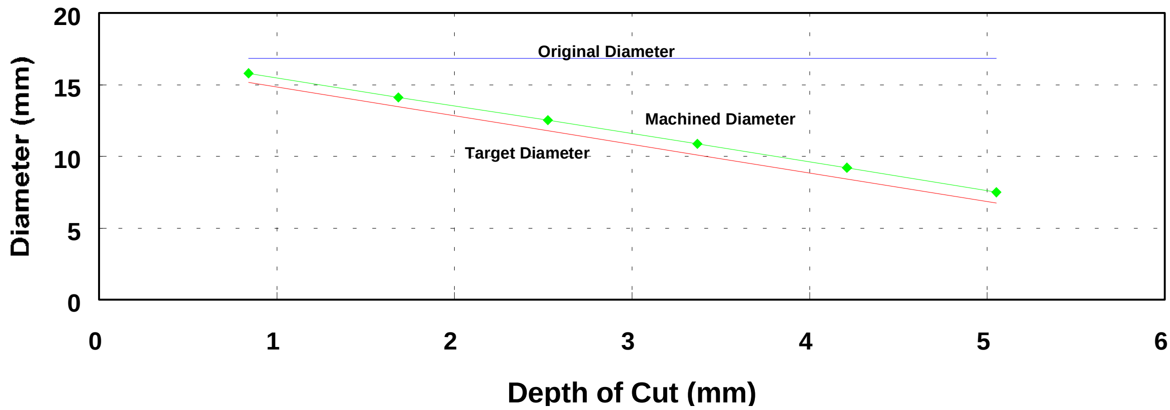

Figure 6. Effect of Traverse Rate on the Machined Diameter of an Mg/B_4C MMC Rod (Initially 17 mm in Diameter) for a Fixed Depth of Cut of 2.53 mm (207-MPa pressure; 60-mesh garnet abrasive at 12.6 g/s; 0.21 mm/s traverse rate; 360 rpm)

Figure 7 shows a titanium aluminide sample turned with an AWJ from an initial diameter of 9.5 mm to precise dimensions for mechanical testing. The turning process, though experimentally deterministic, is still not well developed. Many trials need to be performed in order to meet a tight tolerance and finish specification, especially when curved features are also included. A strategy needs to be developed to address generic turning features such as curves and cones. This is similar to linear cutting, where cutting around corners and curves requires a special strategy to maintain uniformity of surface quality.

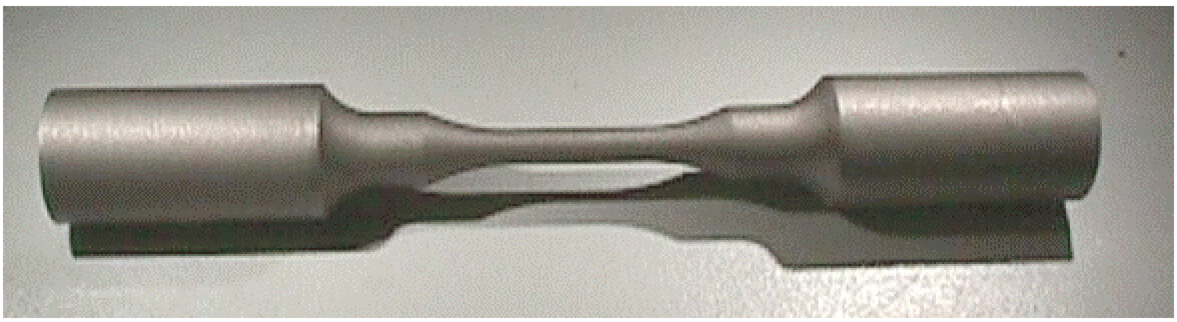

Figure 7. AWJ-Turned Gamma Titanium Aluminide Sample

Figure 8 shows a turned part of graphite epoxy composite. Inspection of the turned surface did not show signs of adverse effects. AWJ-turned threads in a similar composite material showed no mechanical distortions.

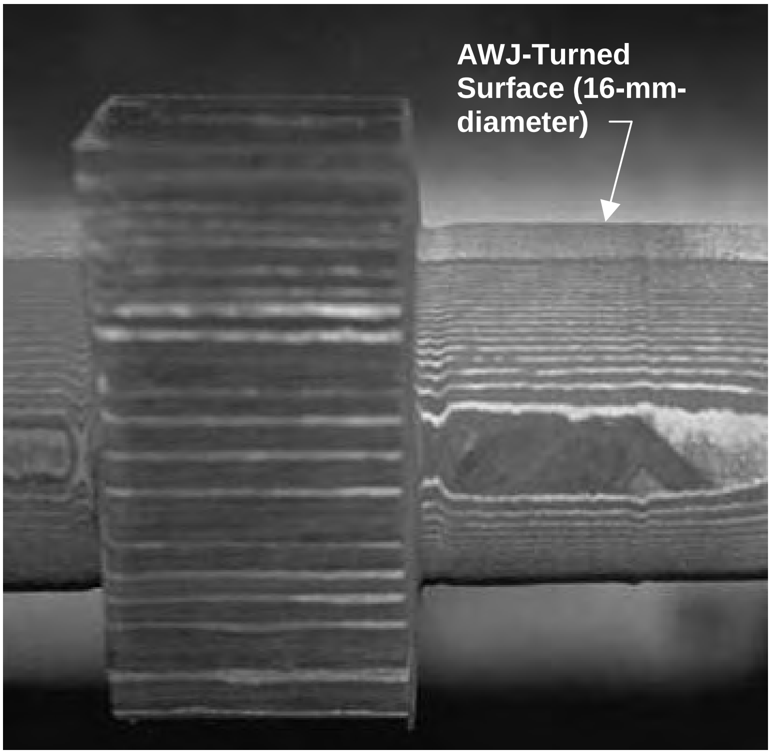

Figure 8. AWJ-Turned Graphite Epoxy

The processes of turning and cutting can be combined to improve the volume removal rate. With this method, prior to turning a part, a number of linear cuts can be made to reduce the initial diameter. A number of experiments were conducted using a 51-mm-diameter Mg/SiC (20%) rod by first cutting out a minimum of three segments and then turning the produced polygonal shape to its final diameter. Using this approach, the machining time was reduced by over 50%. The AWJ turning process is insensitive to the original shape of the part, as was demonstrated by turning wedge-shaped graphite epoxy segments for an aircraft application.

Jet-assisted turning and WJ/mechanical hybrid turning are areas for future work. Work on a hybrid lathe has been reported (Hashish, 1989). In that study, the AWJ was used to produce a diameter 0.25 mm greater than the required diameter. The machined surface was simultaneously finished using a solid single-point tool immediately behind the AWJ. The AWJ on the hybrid lathe was also used to turn threads in Mg/B_4C.

4.3 Drilling

Needs have been emerging in many aerospace and automotive applications for high-quality, precise small-diameter holes drilled at different angles. In many hole-drilling applications, however, solid tools or lasers have not been able to provide satisfactory results. A process for composite and brittle material drilling with AWJs has been developed where the jet pressure is gradually increased during drilling using a computer-controlled pump. Starting with a relatively low pressure does not cause fracture or surface delamination, and a continuous increase in pressure maintains a sufficient jet drilling strength at the material face to eliminate fracture or delamination.

Delamination is the main mode of failure when drilling layered materials such as graphite epoxy. This is primarily due to excessive hydrodynamic jet pressure, which causes layer separation. A similar mechanism was proposed by Ho-Cheng and Dharan (1988) for solid tool machining, where excessive thrust results in delamination. Hole pressurization will result in water flowing between the separated layers, resulting in an increase in the amount of delamination. Figure 9 shows holes drilled in 19-mm-thick graphite epoxy composite without any delamination.

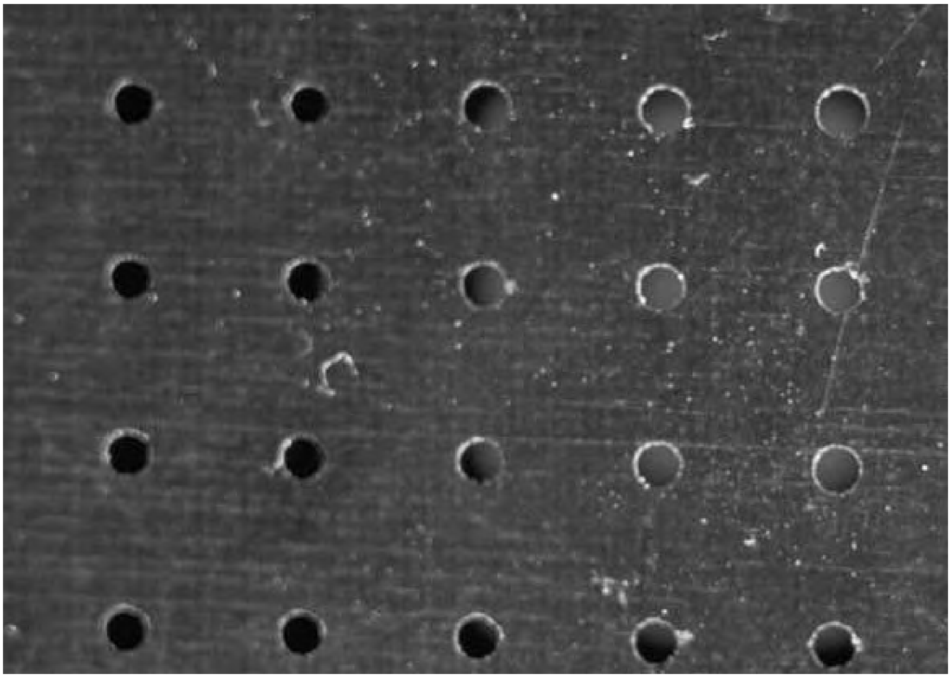

Figure 9. AWJ-Drilled Holes in Graphite Epoxy

Hole drilling at shallow angles results in additional jet/material effects. Figure 10 illustrates potential problems that may occur when drilling coated materials. Chipping at the surface may occur at the first instant of jet impact. Cracking may also occur while the jet is piercing through the material due to excessive pressures generated by the jet inside the hole. The jet may also bounce at the interface of the coating and the base material and cause a shadow hole or a teardrop-shaped hole if the shadow hole combines with the hole being drilled.

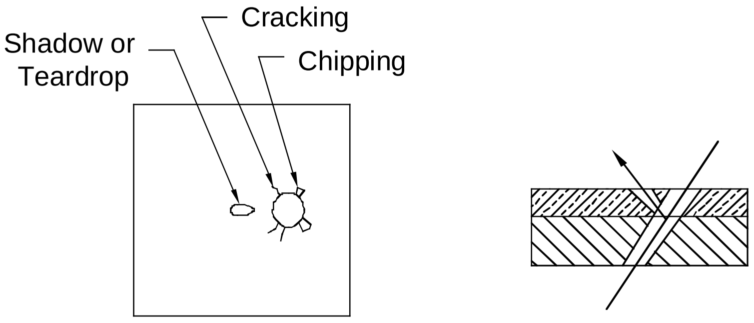

Figure 10. Possible Problems of Drilling Through Coated or Layered Materials

Holes drilled using pressure ramping are shown in Figure 11 for a TBC-coated jet engine shroud. Cross-sectional views of 0.5-mm holes drilled in a ceramic matrix composite showed that undercutting can be eliminated with proper ramp rates (Hashish and Whalen, 1993).

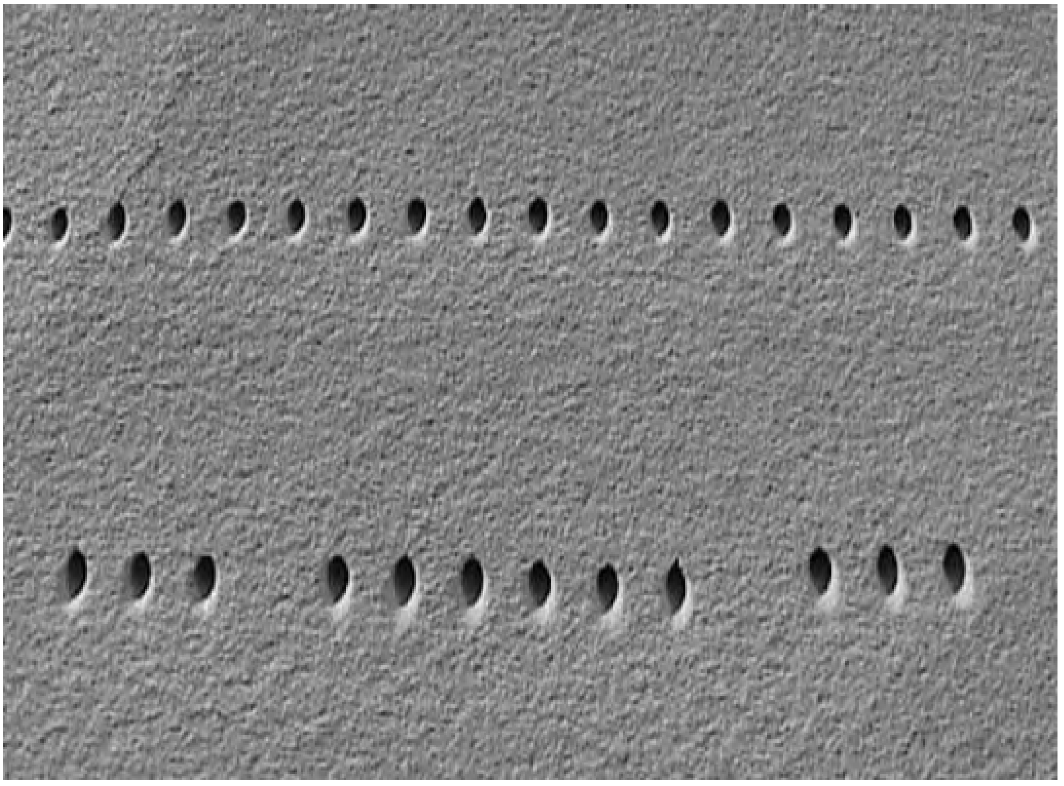

Figure 11. AWJ-Drilled Holes (0.5 mm in diameter) in TBC Material Using Pressure Ramping and a 25° Lead Angle

The hole size can be controlled by selecting the process parameters and the dwell time. The larger the dwell time, the larger the final hole size. Accurate control over the dwell time is needed to control the hole size within certain tolerance limits. Another interesting observation is that the drilling time is improved by reducing the water flow rate and increasing the abrasive flow rate into the hole. A reason for this is related to the hydrodynamic drag of the backflow, which reduces the jet's effectiveness.

4.4 Milling

The AWJ milling process is conducted by performing many cuts (spaced more closely than the AWJ nozzle diameter) across the workpiece surface. Multiple passes of the overlapping kerfs are used to achieve controlled depth. In principle, the machining of controlled geometries can be accomplished by either of the two following approaches.

1. Varying the material removal rate (by varying the traverse rate or the jet pressure, for example) over different regions of the workpiece with a fixed jet motion. Regions with high material removal rates are machined to greater depths.

2. Maintaining a fixed material removal rate over all areas and controlling the exposure time of the jet over the workpiece. Regions experiencing longer exposure times are machined to greater depths.

The latter approach is generally easier to implement for AWJs. The nozzle traversing index, λ, is the distance that the AWJ is moved between adjacent passes and is usually expressed as a percentage of the jet diameter (e.g., if the jet diameter is 1.0 mm, then an index of 80% would indicate a jet overlap of 0.2 mm from pass to pass). Previous research has indicated that the AWJ milling process is generally insensitive to variations in nozzle standoff distance if the standoff is less than about 35 mm (Hashish, 1998b).

AWJ milling today is an empirically deterministic process, which means that the results of the process can be predicted only when enough data have been collected so that the material removal characteristics are known. These characteristics vary with the type of material of the workpiece and, of course, the AWJ process parameters. Typical milling parameters for composites are to use a waterjet diameter of 0.127 mm and a mixing tube diameter of 0.3 mm at pressures up to 345 MPa.

The milling of isogrid shapes in graphite epoxy (Figure 12) was conducted to demonstrate the degree to which the depth of milling can be controlled. This approach involved the use of steel masks. It was found that depth control can be accomplished to 0.05-mm accuracy. The material can be milled ply by ply if needed.

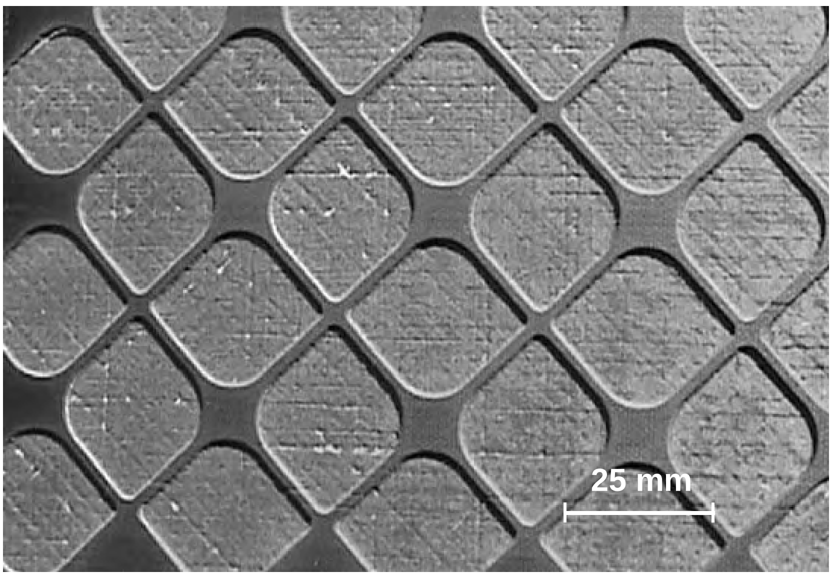

Figure 12. Milled Isogrid Shape in Graphite Epoxy

The milling of titanium aluminide material was also conducted to produce the geometry shown in Figure 13. The surface finish of the milled part can be improved by using finer and finer abrasives as the milling process proceeds. During the final passes, the abrasives should be switched off to remove all abrasives that may have been embedded into the surface.

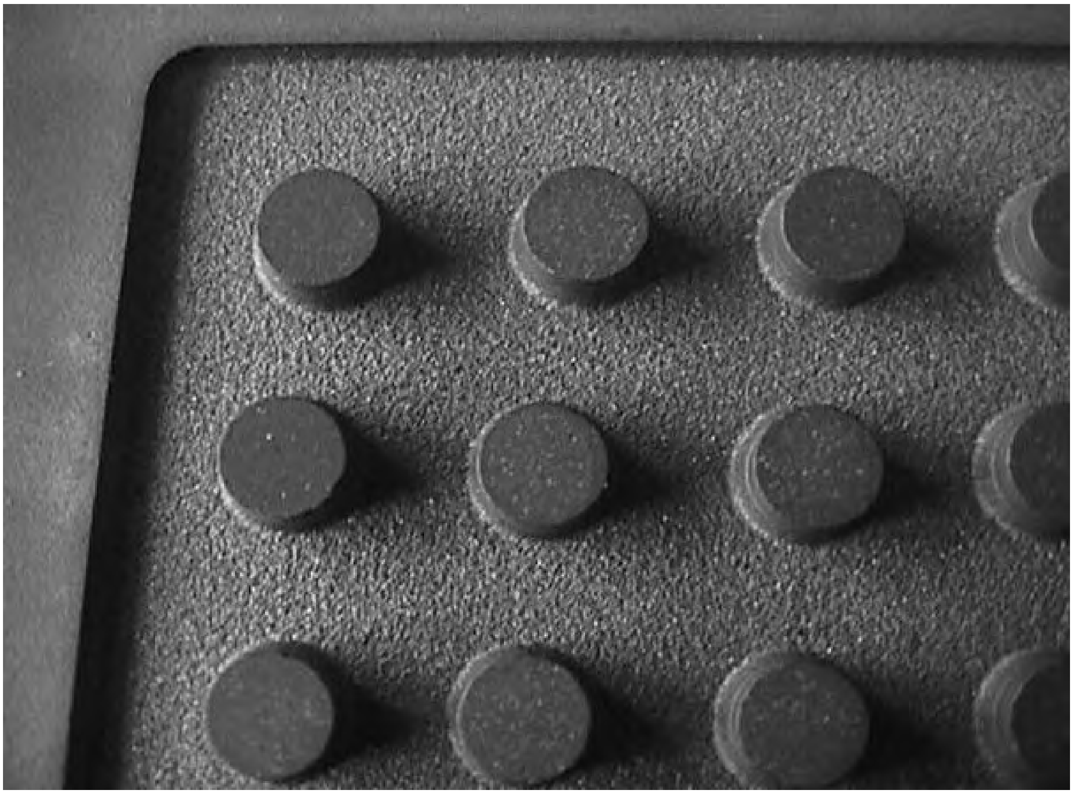

Figure 13. AWJ-Milled Bosses (5 mm in diameter) in Gamma Titanium Aluminide

4.5 Repair of Composite Structures

The repair of composite structures involves removing the damaged material and rebuilding the damaged area. The flexibility of AWJ cutting in a wide range of materials and shapes makes it suitable for the repair of composite structures. Figure 14 shows typical joint designs used in adhesive-bonded composite repairs. For repairs of large composite structures, scarf angles corresponding to 1:30 to 1:40 rise/run ratios are desired ($1.43^{\circ} < \theta < 1.91^{\circ}$). Currently, these types of low-angle surfaces are created by hand with small abrasive drum or disc tools. The process is time consuming and imprecise.

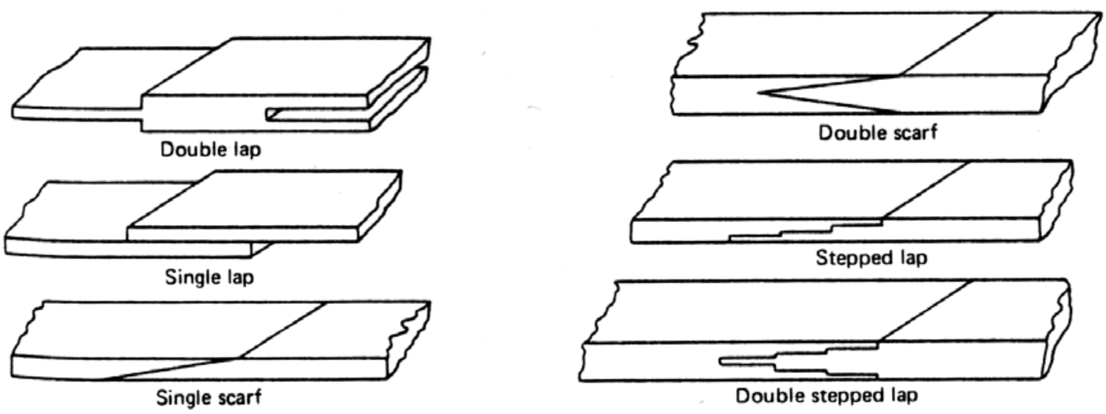

Figure 14. Typical Composite Joint Designs

An AWJ can be robotically scanned over the surface along a single axis, producing an angled or stepped geometry in only one direction. The results of one-dimensional tests have been very promising. All straight-scarf angles were between 5.0° and 6.0°. The material removal rate and surface roughness obtained with 220-mesh abrasives in graphite epoxy were 60 μm/pass and 38-50 μm Ra, respectively. Figure 15 shows a milled scarf joint in graphite epoxy.

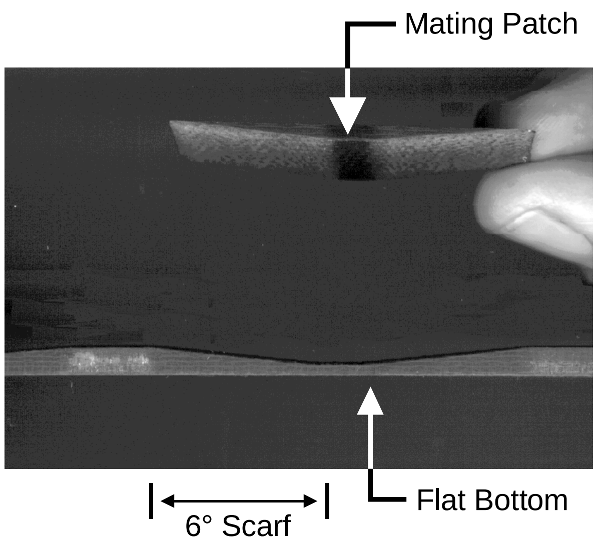

Figure 15. AWJ-Milled Scarf Joint in Graphite Epoxy

5. CONCLUSIONS

Waterjets and abrasive-waterjets are powerful tools for machining a wide range of composite materials. They have already been accepted in the industry for trimming operations. The state-of-the-art machining capabilities are summarized below:

- A wide range of composites can be trimmed with WJs and AWJs to acceptable tolerances.
- Linear cutting can be accomplished to 0.025-mm precision in a wide range of composite materials. The use of a 5-axis manipulator is particularly important when cutting honeycomb composites to control the quality of the cut at the bottom.
- The AWJ has been demonstrated for precision turning of composite materials. Software similar to that used for cutting needs to be developed before this process is suitable for commercial use.
- AWJ milling can be accomplished to 0.025-mm accuracy. Complex geometries can be milled using masks without affecting the integrity of the material.
- Pressure ramping has significantly improved the composite drilling process. Holes in the 0.5-mm range, with less than 0.05-mm standard deviation, can be AWJ-drilled.
- The cutting and milling processes can be used for composite repair. Accurate scarf joints can be AWJ-milled.
- Efforts are needed to implement WJ and AWJ advances in actual manufacturing applications. These efforts include modeling, software development, controls, and special hardware.

ACKNOWLEDGMENTS

Some of the work presented in this paper was performed at Waterjet Technology, Inc. (previously Flow Research, then QUEST Integrated) under several Small Business Innovation Research (SBIR) programs. The AWJ cutting tests were conducted at Flow International. The author is grateful for this support. Thanks also to Hammond Publications for editing this paper.

REFERENCES

Hamatani, G., and Ramulu, M., "Machinability of High Temperature Composites by Abrasive-Waterjet," *Symposium on Machining Composites*, ASME, PED Vol. 35, p. 49, 1988.

Hashish, M., "Turning with Abrasive-Waterjets - A First Investigation," *ASME Journal of Engineering for Industry*, Vol. 109, p. 281, 1987.

Hashish, M., "Machining of Advanced Composites with Abrasive-Waterjets," *Manufacturing Review*, Vol. 2, No. 2, pp. 142-150, 1989.

Hashish, M., "Waterjet Machining of Composites and Ceramics," Chapter 13 in *Machining of Ceramics and Composites*, edited by S. Jahanmir, M. Ramulu, and P. Koshy, Marcel Dekker, Inc., NY, 1998a.

Hashish, M., "Controlled Depth Milling of Isogrid Structures with AWJs," *ASME Transactions, Journal of Manufacturing Science and Engineering*, Vol. 120, pp. 21-27, 1998b.

Hashish, M., and Whalen, J., "Precision Drilling of Ceramic Coated Components with Abrasive-Waterjets," *ASME Transactions, Journal of Engineering for Gas Turbine and Power*, Vol. 115, No. 1, pp. 148-154, 1993.

Ho-Cheng, H., and Dharan, C., "Delamination During Drilling in Composite Laminates," *Machining Composites*, edited by M. Taya and M. Ramulu, ASME, PED-Vol. 35, December, pp. 39-47, 1988.

Hoogstrate, A. M., van Luttervelt, C. A., and Kals, H. J. J., "A Strategy for Process Optimization in Precision Abrasive-Waterjet Cutting of Monolithic and Laminated Materials," *Proceedings of the 5th Pacific Rim International Conference on Water Jet Technology*, New Delhi, India, February 3-5, pp. 75-85, 1998a.

Hoogstrate, A. M., van Luttervelt, C. A., and Kals, H. J. J., "Abrasive Waterjet Cutting of Hybrid Laminated Metal Materials," *Proceedings of the 5th Pacific Rim International Conference on Water Jet Technology*, New Delhi, India, February 3-5, pp. 86-101, 1998b.

Hurlburt, G. H., and Cheung, J. B., "Waterjet Cutting of Advanced Composite Materials," SME Paper Number MR77-225, 1977.

Jahanmir, S., Ramulu, M., and Koshy, P., editors, *Machining of Ceramics and Composites*, Marcel Dekker, Inc., NY, 1998.

Jenkins, M., Ramulu, M., and Fehlmann, K., "Abrasive Waterjet Machining Effects on the High Temperature Degradation and Mechanical Properties of a Ceramic Matrix Composite," *Proceedings of the 9th American Water Jet Conference*, WJTA, August, pp. 157-171, 1997.

Kandebo, S. W., "U.S., Europe Race for MMC Payoff," *Aviation Week & Space Technology*, Aug. 22, pp. 20-22, 1994.

Korican, J., "Waterjet and Abrasive Waterjet Cutting," *Engineering Materials Handbook*, Vol. 1 - Composites, ASM, Metals Park, Ohio, p. 673, 1987.

Lavander, C. A., and Smith, M. T., “Evaluation of Waterjet-Machined Metal Matrix Composite Tensile Specimens,” Report Number PNL-5858, Pacific Northwest Laboratory, Richland, WA, p.175, 1985.

Neusen, K. F., Rohatgi, P. K., Vaidyanathan, C., Alberts, D., “Abrasive Waterjet Cutting of Metal Matrix Composites,” *Proceedings of the 4th American Water Jet Conference*, ASME, NY, pp. 175-181, 1987.

Ramulu, M., and Arola, D., “Abrasive-Waterjet Process Dependent Performance of Polymer Composites Under Static and Dynamic Loading,” *Proceedings of the 9th American Water Jet Conference*, WJTA, August, pp. 29-46, 1997.

Ramulu, M., and Taya, M., “An Investigation of the Machinability of High-Temperature Composites,” *Proceedings of the 12th Conference on Composite Materials and Structures*, 1988.

Schwartz, M. M., “Water Cuts Composite Aircraft Parts,” *American Machines*, Vol. 127, p. 103, 1983.

Serafini, T., “High Temperature Applications,” in *Engineered Materials Handbook*, Vol. 1 - Composites, ASM International Handbook Committee, pp. 810-815, 1987.

10th American Waterjet Conference
August 14-17, 1999: Houston, Texas

Paper **65**

THE ABRASIVE WATERJET AS A PRECISION METAL CUTTING TOOL

J. Zeng, J. Olsen, and C. Olsen
OMAX Corporation
Auburn, Washington, U.S.A.

ABSTRACT

This article will provide a general description of the abrasive waterjet technology and an illustration of the concept of using it as a precision metal cutting tool. It will address the operating principles, equipment and control, physical parameters of the process, metal removal rate, dimensional control, corner radii, taper, surface finish, possible surface damage, as well as health, safety, and environmental issues. Some examples of applications will be given. Its advantages and limitations, compared to other traditional and non-traditional machining methods, will be discussed.

Organized and Sponsored by the WaterJet Technology Association

1. INTRODUCTION

The idea of cutting with water could be as old as the Chinese phrase "dripping water penetrates rock". In the modern waterjet technology, the "dripping water" is replaced by a high velocity water stream, which penetrates rock in seconds. The modern waterjet technology was initiated by Dr. Norman C. Franz in 1968, with the first patent for high-pressure waterjet cutting. The first commercial waterjet cutting system was built to cut laminated paper tubes in 1971. Since then, waterjet technology has experienced a steady growth. Advances in the automobile industry, material science, and space technology in 70's and 80's demanded and stimulated the outgrowth of new ideas and novel technologies in manufacturing. In the early 80's, the idea of entraining abrasive into waterjet was promoted by Hashish (1982) and commercial abrasive waterjet ("AWJ") systems became available.

Due to the crudeness and unreliability of the early stage nozzle, abrasive waterjet was thought to be a very imprecise process. It was tried only when other technologies could not handle the job. Early abrasive waterjet machines were made by simply hanging an abrasive waterjet nozzle on a crude X-Y table such as used for oxy-acetylene torch cutting. The controls were either optical tracers which followed a line drawn on paper or crude versions of the CNC controllers used to control machine tools. As nozzle technology improved it became apparent that greater precision could be obtained by moving the nozzle more precisely. More precise tables were introduced that were controlled by the same CNC controllers used in precision machine tools. Thanks to the pioneering materials development work of Boride Products Inc., we now have nozzles that keep their cutting properties constant over many hours of operation. In 1992 Zeng et al. published a comprehensive semi-empirical model of the abrasive waterjet cutting process. Olsen (1996) described how to incorporate this model into a PC based machine tool controller. With this type of control, the user simply enters the material type, thickness and desired cutting quality. The computer takes care of the rest. The precision and user-friendliness achieved through better nozzle and control technology has changed people's perspectives about this technology. Modern machine shops now use abrasive waterjet machines side by side with other traditional or non-traditional machine tools to cut 2D parts out of all kinds of materials and profit from the use because of their productivity, quick turn-around time, and relative low cost.

The purpose of this article is to provide a technology overview to the existing waterjet community as well as potential users within the entire manufacturing community. The authors believe that better understanding and better communication will promote awareness and further growth of this technology.

2. OPERATING PRINCIPLES

An abrasive waterjet is formed by entraining abrasive particles into a high velocity water stream. The essence of abrasive waterjet machining is rapid erosion combined with rapid cooling. In most cases, water does not participate in material removal. It serves as an energy carrier as well as a flushing medium. Bulk material removal is the result of accumulated micro-cutting effects of individual abrasive particles as in conventional grinding. The individual abrasive particle simply digs into the material and scoops out a small piece of it (Figure 1) (Zeng, 1992). Some of the abrasive particles may even strike a second or a third time on the material.

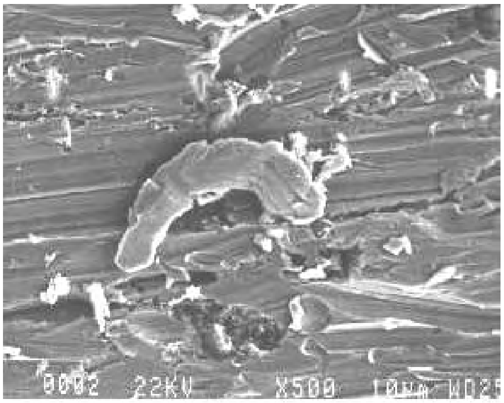

Figure 1 A ship formed on a 304 SS part during the AWJ cutting process

3. EQUIPMENT AND CONTROL

A typical AWJ machine is composed of a high-pressure pump, motion equipment and control, nozzle and abrasive system, a working table and waste collecting unit. A typical layout is shown in Figure 2.

3.1 High Pressure Pumps

There are two types of high pressure pump currently available in the industry: intensifier and crank drive pumps. Intensifier and crank drive pumps share the same pumping principle. In both cases a plunger is pushed into a closed chamber raising the pressure and expelling the pumped fluid through an outlet check valve. Then, the direction of the plunger motion is reversed and low-pressure fluid fills the chamber through an inlet check valve. The continuously reciprocating plunger provides the pumping action. See Figure 3. The difference in the two technologies is simply the means by which the plunger is moved. The crank pump uses a crank similar to the one in an automobile engine. The intensifier drives the plunger with a hydraulic cylinder usually with oil. Ultrahigh pressure was once the exclusive domain of the intensifier pump. Today several crank drive pumps are manufactured for service above 240 MPa (35,000 psi), cranks are moving into high pressure service because they are simpler, much more efficient, and costs less.

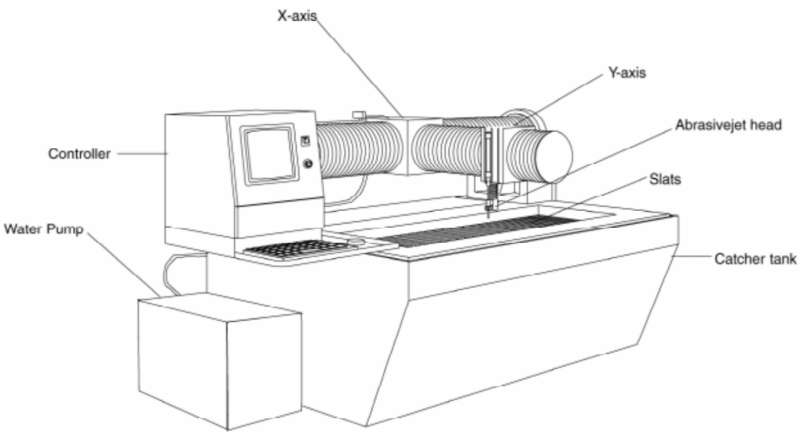

Figure 2 A typical layout of an abrasive waterjet machine tool.

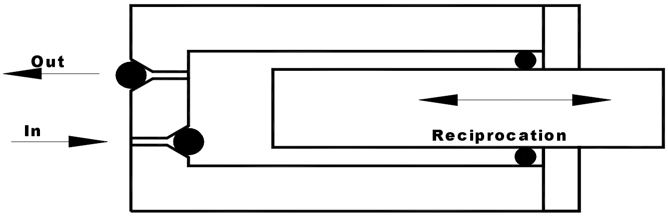

Figure 3 A diagram of a high pressure plunger pump.

3.2. Motion Equipment and Control

The motion equipment for AWJs is similar to those used for laser and wire EDM. A typical AWJ machine tool includes a precision X-Y axis rigidly mounted to the cutting table, pre-loaded linear bearings, and precision ball screws. The motion track has complete protection against water, dirt, and grit. Special damping mechanisms are also used to achieve smoother motion. The X and Y axis are driven by brushless servo motors, which are controlled with a CNC controller.

Older CNC controllers describe the path in a series of lines and arcs where the speed can be set on each line or arc and an acceleration can be chosen with which to change speeds. These controllers were essentially proprietary computers where the user had very little or no access to the fundamental software that performed the various functions. Today, the controller is evolving toward a piece of software that runs on a PC. The open PC architecture provides the same advantages for machine tools that it has for offices. Today's PC controls for abrasive jetting, incorporate a model of the cutting process and drive the machine at the exact speeds at every point of the path to achieve the requested cut quality. The machine automatically speeds and slows for corners and other features of the geometry so as to achieve maximum precision. Moreover, this type of control performs the calculations with such rapidity and accuracy that it is possible to make single parts to high precision with about the same effort required to plot a drawing on paper.

Figure 4 An abrasive waterjet nozzle

3.3. Nozzle and Abrasive System

A schematic of an abrasive waterjet nozzle is shown in Figure 4. An orifice, typically made out of sapphire or diamond, is used to convert potential energy of high pressure water into kinetic energy of a high velocity water stream. The downstream section is constructed to be like an air ejector. It includes a suction chamber and a converging nozzle. The water stream entrains air in the suction chamber and the mixture discharges from the converging nozzle. Vacuum pressure is thus built up in the suction chamber, which allows entraining abrasive particles. The suction chamber and the converging nozzle are therefore often called "mixing chamber" and "mixing tube", respectively. The abrasive waterjet discharging from the mixing tube is actually a mixture of abrasive, water, and air. While air helps entraining abrasive, it has no contribution in material removal and it brings in a negative effect by dispersing the jet. A well designed nozzle minimizes air flow. The mixing tube is another important part. The most critical aspect of the mixing tube is the wear resistance of its material. Currently, most mixing tubes in use are made of ROCTEC™(a trademark of Boride Products Inc.), which allows continuous operation of up to

100 hours.   A long tube with a small bore diameter gives a small kerf and more precise cuts, but the extreme will restrict the flow. The optimum design is one with smallest bore diameter and longest tube without sacrificing the cutting efficiency.

Abrasive is sucked into the nozzle from a nearby container. The container has a metering device that sets the flow rate and a gate to start/stop the flow. The metering device is either a vibratory feeder with frequency or magnitude control or simply an opening that can be mechanically adjusted. Some abrasive systems have two containers. A small one with metering and gate functions is placed close to the nozzle to minimize response time. A large container is placed on the floor for easy loading. Abrasive is then pneumatically conveyed to the small container with either dense phase or dilute phase conveying mechanism. In dense phase conveying, abrasive is stored in a pressure vessel and then pushed through the convey line in “slugs”. It uses a small amount of air at a relatively high pressure. Its low conveying velocity minimizes wear on the convey line. The dilute phase system uses a large amount of air to suspend and blow abrasive through the convey line at a relatively high velocity. It operates at low pressure and usually costs less.

3.4. A Working Table and Waste Collecting Unit

The working table is where workpiece is placed and fixed. A steel grid is often used to support the workpiece. Since the machining force is minimal, simple clamping device or even a weight is sufficient to hold the workpiece in place. Underneath the working table is a waste collecting tank. To reduce noise level, the tank is filled with water so that cutting can take place while submerged. In some cases, used abrasive is processed through a recycling unit and part of it is re-used.

4. PROCESS PARAMETERS AND OPTIMIZATION

AWJ cutting has more variables than a traditional machining process. The main process parameters that affect cutting speed and quality, and typical parameter values are listed as follows:

Process Parameters	**Scopes**
Workpiece material and thickness	any material up to about 250 mm or 10 inch thick
Water pressure	242 – 380 MPa (35 to 55 ksi)
Orifice diameter	0.18 – 0.56 mm (0.007 – 0.022 inch)
Mixing tube diameter, length	ID is about 2 – 3 times of Orifice ID, Length is about 45 – 133 times of the ID.
Abrasive material, size, and flow rate	Typical materials are garnet, olivine, and copper slag. Mesh #50 – 220. Flow rates 0.227 – 0.9 kg/min (0.5 – 2.0 lb/min)
Stand-off distance	0 – 3 mm (0 – 0.12 inch)

Cutting speed is predicted with the following semi-empirical equation based on the model published by Zeng et al. in 1992:

$$u = \left(\frac{f_a N_m P_w^{\ 1.594} d_o^{\ 1.374} M_a^{\ 0.343}}{C q h d_m^{\ 0.618}} \right)^{1.15} \tag{1}$$

where u: the cutting speed (mm/min or inch/min), f_a : abrasive factor, N_m : machinability number, P_w : water pressure (MPa or kpsi), d_o : orifice diameter (mm or inch), M_a : abrasive flow rate (g/min or lb/min), q: quality level index (1 to 5 from roughest to smoothest, see section 5); h: workpiece thickness (mm or inch), d_m : mixing tube diameter (mm or inch), C : system constant (788 for Metric units or 163 for English units).

The effect of workpiece material is represented by the material characteristic constant, "Machinability Number". Figure 5 is a list of machinability numbers for various engineering materials. For metals not shown in this list, its machinability number can be estimated by analogy to other metals with similar hardness.

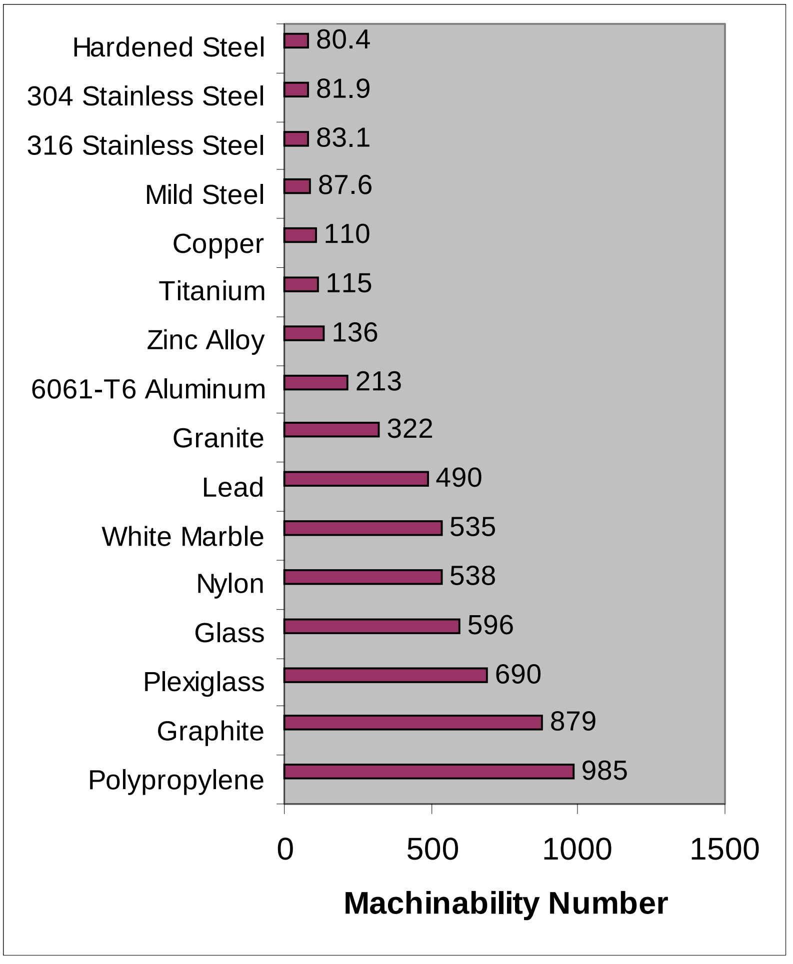

Figure 5 Machinability numbers of selected engineering materials.

The abrasive factor is used to account for the differences in cutting speeds resulted from the use of different abrasive materials. Its value should be calibrated for each different abrasive material in a way such as that described by Zeng & Kim (1995). Its values for a few abrasives are provided here as a reference:

Abrasive Factor	Abrasive Material
$f_a = 1$	Garnet
$f_a = 0.86$	Olivine
$f_a = 0.84$	Crushed Glass

The effect of abrasive flow rate represented by this model is valid only up to a certain point, where cutting speed will not further increase with higher abrasive flow rates. The optimum abrasive flow rate is a function of the mixing tube diameter, orifice diameter, and water pressure. Variation of abrasive size within the ordinary range (mesh 50 – 150) has little effect on the cutting speed, but finer abrasive is usually used to achieve smoother surface finish (Zeng & Munoz, 1994).

This model does not include the effect of stand-off distance. As a general rule, the stand-off distance should be set small enough to just avoid jamming the nozzle or plugging the nozzle during piercing. A typical value is 2 mm (or 0.050 inch). The value of the system constant reflects orifice and nozzle efficiency as well as other systematic variables and should be calibrated accordingly.

5. QUALITY OF CUT

The sources of errors that will affect the quality of cut by an AWJ includes the random side-to-side deflection of the jet (striation marks), backward deflection of the jet (jet lag), energy dissipation along the thickness coordinate, dispersing of the jet, particle size and particle embedding, etc.

On a typical AWJ cut surface at its maximum speed, regardless of the material and thickness, the surface shows a similar pattern, starting out to be smooth, sand-blasted-like at the top, then gradually showing

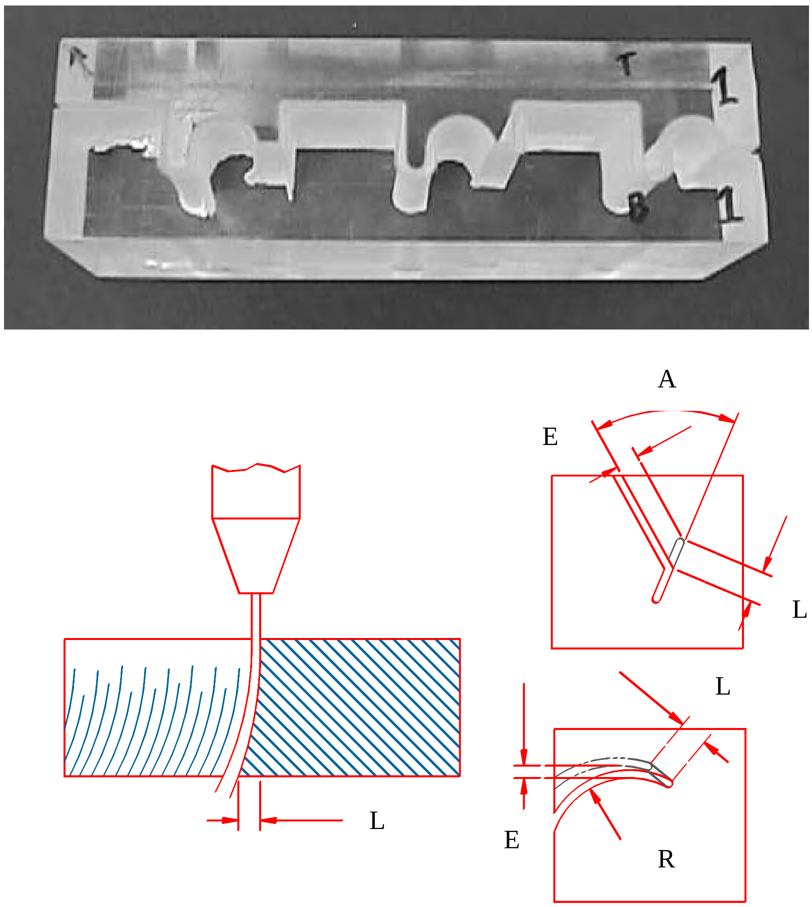

Figure 6 Geometric errors of abrasive waterjet cutting.

some feather-like striation marks and growing worse and worse towards the bottom. These striation marks are the results of random deflection of the jet by the top portion of the workpiece (Zeng & Munoz, 1997). The magnitude of these striation marks is much larger than that of surface roughness caused by abrasion of individual particles. A quality level index (q) stands for the quality of the upper 1/q section of a separation cut surface. For convenience, descriptions are given for the following five quality levels:

Quality Levels	Descriptions
q = 1	criteria for separation cuts. usually, q < 1.5 should be avoided.
q = 2	rough surface finish with striation marks at the lower half surface.
q = 3	smooth/rough transition criteria. slight striation marks may exist.
q = 4	striation free for most cases.
q = 5	Best surface finish.

This quality index is derived for linear cuts. When cutting an arc section or a sharp corner, geometric errors are created due to the fact that the jet is bent backward (see Figure 6). When moving at the speed given by equation (1), the jet lag distance is calculated with the following equation:

$$L = 0.182 \frac{h}{q} \tag{2}$$

For a sharp corner, where the direction changes by angle A, the maximum permissible lag is related to the error limit E by L = E/sinA (see Figure 6). The quality index (q) for corner cutting is therefore calculated by:

$$q = \frac{0.182hE}{\sin A} \tag{3}$$

Similarly, for an arc of radius R, the quality index (q) is calculated by:

$$q = \frac{0.182h}{(R + E)^2 - R^2} \tag{4}$$

By introducing Equation (3) or (4) into Equation (1), the cutting speed for a given error limit E at a sharp corner or an arc is calculated. It has been observed that the side-to-side flopping of the jet in a straight line cut is about 10% of the lag amount. To be consistent with this observation, the value of E is thus set to 0.1L.

Even when speed limits based on desired quality are not exceeded, a large acceleration towards this speed limit will cause undesirable marks on the part. The spacial acceleration is related to variation of the lag by:

$$\frac{du}{ds} = \frac{6.32uq}{h}\frac{dL}{ds} \tag{5}$$

By setting a limit to the rate of change of lag length with distance along the curve, dL/ds, the maximum spacial acceleration is determined. A typical value of dL/ds limit is 0.1.

By adjusting the cutting speed constantly, e.g., slowing down when approaching a sharp corner or a small arc, these geometry errors can be minimized. Implementation of this scheme is done with the latest sophisticated controller and software.

Taper of the kerf is controlled by two opposite trends. The jet loses energy as it cuts deeper into the workpiece and thus tends to form a “V”-shaped kerf. On the other hand, the natural shape of the jet is diverging, which tends to form a kerf of opposite shape. The actual kerf shape depends on the jet coherency and material hardness as well as thickness. The taper of the kerf is minimized by controlling (usually reducing) the cutting speed to balance these two trends. Sometimes, stand-off distance and mixing tube diameter are also used as controlling factors. In die cutting application, taper becomes desirable and is achieved with the same methods.

Cutting of ductile materials tends to leave some small burrs at the bottom of kerf (Groppetti et al. 1998). They are either caused by the shearing action of the jet when the remaining material is thin enough or by the chip forming action of individual abrasive particles. Burr is more significant on soft materials and less significant when low cutting speeds and fine abrasive particles are used.

Dispersing of the jet forms a radius and a frosting band on top of kerf (Groppetti et al. 1998). This radius tends to increase as the cutting speed decreases. It is controlled by any methods that reduces the dispersing of the jet, including reducing stand-off distance, reducing air in-take, and improving jet coherency with better orifice design and better alignment.

According to the study by Groppetti et al. (1998), the kerf surface is hardened by the AWJ cutting process by up to 60% of the base material hardness. In AWJ cutting of soft materials such as aluminum, particle embedding is occasionally found on the cut. A cleaning pass of the jet without abrasive is recommended if particle embedding becomes a concern.

6. HEALTH, SAFETY, AND ENVIRONMENTAL ISSUES

An exposed abrasive waterjet can generate a hazardous noise level (80-95 decibels) (Mason, 1996). Hearing protection is required. Latest AWJ machine tools do most machining under water, which reduces the noise to a pleasant level (under 75 decibels). Today's machines are placed right out on the shop floor rather than in the sound proof rooms of yesterday.

Silicosis of the lungs is another concern. Cutting with abrasives containing a large amount of free silica is discouraged. According to Martinec & Skoda (1998), the use of garnet is a safer choice compared to quartz and other silicates. Machining under water also reduces airborne dust and splash, providing a safer and more comfortable working environment.

Water under pressure is only marginally compressible. In the case of breaking high-pressure tubing and other components, the pressure would quickly drop to a safe level. However, mechanical danger of high-pressure components does exist. The danger usually comes from bad work habits and designs. Maintenance under pressure should always be avoided. Eye protection should always be used when working around high-pressure equipment. High-pressure components are designed with "weep holes" so that they will fail in a manner that causes them to leak in a safe manner. Special attention for safety is given to those systems equipped with high-pressure accumulators, which are used to even out pressure fluctuations. Although modern designs are quite safe, some accidents have occurred in the past. Pressure relief prior to catastrophic failure should be a standard feature for such accumulators.

Of course, the jet being a cutting tool, can cut virtually anything including human parts. Due to the high pressures used in abrasive waterjet machining, there is often a misconception that it is dangerous. An understanding of the process, however, reveals that this is not the case. It is no more dangerous than any other machining process. Since the jet exposure is minimized to nearly zero, it is even safer than a band saw.

The primary concern with environmental issues is what to do with the wastewater and solids. Secondary to that, but also of critical importance, is the water that goes into the system for both cutting and cooling.

Modern pumps recycle cooling water. This provides for lower consumption, and less wastewater generated. The wastewater from cutting is usually around or less than 3.8 lpm (1 gpm), typically treated as gray water sewage, and dumped directly into the sewer. Alternately, it can be filtered and recycled in areas where water is scarce, or regulations are particularly strict. The quality of water entering the system is critical because it effects the life of high-pressure components. Dissolved solids in the water can accumulate on parts, such as the jewel, and reduce effectiveness, and increase wear. Either fresh water or recycled water should be processed to remove dissolved or undissolved solids to an allowable level. Cost of doing so is currently the main factor that prevents standardization of recycling wastewater from cutting.

The solids generated (spent garnet and metal) can be used as landfill, unless there are high levels of toxic metals left over from machining hazardous materials such as lead. Used abrasive can be recycled to save operating costs without sacrificing cutting efficiency and quality (Knaupp & Ohlsen, 1994). Abrasive recycling is getting more and more attention from the industry.

7. ADVANTAGES, LIMITATIONS AND APPLICATIONS

Abrasive jets are now being accepted as machine shop tools and are being integrated into the overall production of parts in both job shops and production shops. Users have found strong financial incentives for their use.

Writing shop routes that include the use of AWJs requires a basic understanding of the characteristics of AWJ machining. The easiest way to understand what can be done with abrasive jets is to imagine what could be done with a very stiff strong 0.76 mm (.030”) diameter end mill 50 mm (2”) long that can drill its own hole. The jet can be used for any type of profiling both external and internal. Some traditional operations that are often replaced with abrasive jet machining include: drilling, broaching, gear cutting, profile milling, blanking, punching, slotting, slitting, sawing, extrusion (for short pieces), and wire EDM (but lower precision).

Finished part tolerances to +/- 0.13 mm (0.005”) can be held in materials up to 50 mm (2”) thick with tighter tolerances in thinner parts. A slight taper or even barrel shape may occur on the machined surface and this is the main error that causes the +/- 0.013 mm (0.005”) limit. Surface finish has a sandblasted appearance and second operations are required to produce a polished surface.

Material properties do not have a large effect on the process other than influencing the speed nor are they degraded by the machining process. Insulating and highly reflective materials, which raise problems for EDM and laser, machine well. No problems are encountered if the material has a layer of mill scale. Sandwiches of various materials and stacks of the same material machine well. There is no heat-affected zone or hard layer on the cut surface. Difficult to machine materials such as Titanium, Inconel, hardened steel and even glass are easily machined by the jet. Heat-treated parts with thin sections often distort during heat treat causing scrap. The AWJ machining rates are not affected by the heat treatment, so the raw material can be hardened, the parts machined and then followed by a final grind if necessary. Precision hardened spur gears, blanking dies and a variety of other hardened parts can be produced in this manner.

Very thin (0.25 mm and less) parts may have a rolled edge, but in general very little burr is produced. At the other extreme roughing thick parts to save conventional machining time or material is often done even in up to 150 mm (6”) thickness.

The jet deflects if a grazing cut is attempted producing a very high taper. For high precision at least 1.5 mm (.060”) should be removed from the surface. Machining the entire part from a plate is the most common operation and multiple parts can be nested to fully use the stock. The scrap that is produced is in valuable chunks rather than oily chips. Odd shaped holes, slots and profiling can be done as a second operation on parts started on a lathe or mill.

One of the very most important features is both obvious and overlooked. All machining is done with a single tool. Any flat part from a spur gear to a plate with square holes to a complex artistic shape can be made without tool changing or qualifying a second tool. Setup requires only placing the stock and setting the tool tip at the top surface. Very short runs or even a single piece are economical. In fact, abrasive jet machining is probably the lowest cost method for making any single flat part.

Modern automatic programming systems take the geometry from a CAD file and directly generate a tool path with all speeds set. In case no CAD file is available, very rapid drawing programs usually come with the machine. In general it takes far less time to input a tool path than to layout a part manually with layout dye, scribers and center punches and accuracy is far better. The computer controlled jet machining eliminates the non-value-added work of laying out the part, changing tools and making setups.

Cutting forces are at most a few pounds so that only minimum clamping is required. These low forces permit making very thin sections without distortion from the cutting process. Thin wall honeycomb has been cut from solid plate.

The process is capable of locating holes very accurately, but the slight taper may cause a problem or perhaps the hole must be threaded. AWJ machining followed by tapping, reaming or counterboring is a very common process. These secondary operations can be performed on a very simple machine like a drill press that is included as part of the work cell. The tap or reamer centers itself precisely in the slightly tapered hole and produces a precision hole at the exact location specified.

Odd shaped holes particularly those with sharp internal corners are difficult to make in low volume without a broach or shaped punch. AWJ machining can make such holes either as part of the primary process of machining the part from plate or as a secondary process after the part has been formed by another process.

Custom panels for electrical switches, pilot lights etc. can be painted or powder coated and stocked as plain panels. Then, the custom hole pattern can be formed by AWJ machining with less than 5 minutes setup and without the need for refinishing. Just in time production can be achieved.

Prototype blanked parts can be easily made to any desired shape and when the part is accepted, much of the die making work can be done with an AWJ. Blanks for hydroforming and bending can be made economically at low volume and then finished with those respective processes.

Round parts such as rings and flanges are often blanked with an AWJ and then finish bored or threaded on a lathe. No flame hardened edges break the lathe tools and often one or more of the surfaces needs no further machining.

Families of parts for a single machine or assembly can be nested together to be made from plate of a thickness common to all the parts. A variety of parts for a single assembly are then made in a single setup. Inventory is lowered with all the attendant benefits.

Because of the ease of making square and rectangular holes, many of the assembly techniques used in woodworking can be used for metals to make self jigging parts for precision weldments or other press together assemblies.

As an example, Figure 7 shows some of the parts used in an OMAX JetMachining® Center. They were made with an abrasive waterjet either completely or with secondary operations such as tapping and black anodizing.

Figure 7 Some the parts used on an abrasive waterjet machine were cut with an abrasive waterjet.

Compared to laser, AWJs cut slower for sheet metals. However AWJs can machine thicker and many materials that lasers cannot or do not do well such as aluminum and copper. By stacking up, AWJs can cut as fast or even faster on sheet metals. AWJs do not create thermal distortion or heat-related microcracking. No toxic fumes and fires to worry about, AWJs are more environmentally friendly. Capital equipment costs for AWJs are generally much lower than that for a laser. Modern AWJs machine tools are typically much easier to operate and maintain than laser.

Compared to wire EDM, AWJs are not as precise, but much faster and more versatile in machining a wider variety of materials with no heat-affected zone. Many EDM shops purchase AWJs to complement their EDM machining capability.

Compared to conventional milling, AWJ setup and fixturing are much faster and when you are done, the clean-up is faster, too. There is no tool changing needed. One single tool compensation offset allows machining unlimited number of holes of different sizes. Wear on tool is often less, especially in harder and gummier materials. Its smaller kerf means getting more parts out of the same material.

In summary, the advantages to abrasive waterjet machining are the following:

- Fast setup and programming
- Very little fixturing for most parts
- Machine virtually any 2D shape (and some 3D)
- One tool offset for all geometry and sizes
- Very low machining force
- No heat generated on the parts
- No start hole required

- Machine any materials including very hard and very tough ones in a wide thickness range
- Environmentally friendly
- Scrap is in the form of chunk, not chips and still valuable

Its limitations includes:

- Jet lag causing geometric inaccuracy in small arcs and sharp corners
- In some cases, taper may be inevitable, particularly for thick pieces
- Cut slower than laser for sheet metals and less precise than EDM
- Initial investment and operating cost is higher than conventional machine tools

A quote from Frost & Sullivan's market research report "World Special Machine Tools Markets" (1998) is used as the concluding remark:

> "The waterjet machine tool market has emerged as the fastest growing market segment, with a growth rate forecast at 9.1 percent for the forecast period, says Frost & Sullivan analyst Vinay Kaul. Both the waterjet machining process and the laser machining process cut metals and several other materials. However, the waterjet machines are less expensive than laser machines, and are functionally superior to conventional metal cutting machines. Waterjet technology has become a viable solution for end users, due to the availability of sophisticated software."

8. ACKNOWLEDGEMENTS

The authors are thankful to Ms. Rockie Ward for reviewing this article.

9. REFERENCES

Groppetti, R., Gutema T., and Lucchio, A. Di., "A Contribution to the Analysis of Some Kerf Quality Attributes for Precision Abrasive Waterjet Cutting," *Proceedings of the 14th International Conference on Jetting Technology*, pp. 253-269, BHR Group, Brugge, Belgium, 1998.

Hashish, M., "Steel Cutting with Abrasive Waterjets," *Proceedings of the 6th International Conference on Jetting Technology*, pp. 447-487, BHRA, University of Surry, U.K., 1982.

Knaupp, M., and Ohlsen, J., "Recycling of Abrasive Material in Abrasive Water Jet Cutting," *Proceedings of the 12th International Conference on Jet Cutting Technology*, pp. 511-519, BHR Group, Rouen, France, 1994.

Martinec, P. and Skoda, V., "Garnet Minerals – Fibrogenicity of Respirable Dust Particles," *Proceedings of the 14th International Conference on Jetting Technology*, pp. 347-353, BHR Group, Brugge, Belgium, 1998.

Mason, F., “Water with Attitude: Waterjet Cutting Basics,” *Forming & Fabricating*, pp. 43-49, June, 1996.

Olsen, C., “Waterjet Web Reference,” HTTP://WWW.WATERJETS.ORG, June 1999.

Olsen, J. H., “Motion Control with Precomputation,” *US Patent* No.5,508,596, 1996.

“World Special Machine Tools Markets”, *Frost & Sullivan Research Publication*, Code: 5447-10, June 24, 1998.

Zeng, J., “Mechanisms of Brittle Material Erosion Associated with High Pressure Abrasive Waterjet Processing,” *Doctoral Dissertation*, University of Rhode Island, Kingston, Rhode Island, 1992.

Zeng, J. and Kim, T.J., “Machinability of Engineering Materials in Abrasive Water Jet Machining,” *International Journal of Water Jet Technology*, Vol. 2, No. 2, pp. 103-110, 1995.

Zeng, J., Kim, T.J., and Wallace, R.J., “Quantitative Evaluation of Machinability in Abrasive Waterjet Machining,” *Proceedings of the 1992 Winter Annual Meeting of ASME, “Precision Machining: Technology and Machine Development and Improvement,”* PED-Vol.58, pp. 169-179, Anaheim, 1992.

Zeng, J. and Munoz, J., “Optimization of Abrasive Waterjet Cutting --- The Abrasive Issues,” *Proceedings of the Waterjet Machining Technology Conference*, Paper No. MR94-247, SME, Chicago, Illinois, 1994.

Zeng, J. and Munoz, J., “Surface Finish Evaluation for Abrasive Waterjet Cutting,” *Proceedings of the 9th American Waterjet Conference*, pp. 1-14, WJTA, Dearborn, Michigan, 1997.

10th American Waterjet Conference
August 14-17, 1999: Houston, Texas

Paper **66**

ON THE DEVELOPMENT OF AN INTELLIGENT ABRASIVE WATERJET CUTTING SYSTEM SOFTWARE

Pawan Singh
Quantum Technologies International
Bethlehem, PA

Greg Mort and Ihab Kain
AAB-IR Waterjet Systems
Wixom, MI

ABSTRACT

The paper will outline the process used in developing a commercial intelligent software for operating abrasive waterjet cutting systems that has the potential of revolutionizing abrasive waterjet cutting. The software's salient feature is its embedded knowledge, manifested through various algorithms and schema included in the software. As a result, a user can go from a CAD drawing to actually cutting the part in less than a minute, irrespective of the complexity of the part. Further, by continuously monitoring the shape of the profile and intelligently adjusting the cutting speed, the software helps produce parts with a cut quality that has rarely been achieved before.

The software development began with a market research study that identified key metrics the users value most in a cutting system software. From this study, a blueprint for best-in-class software was developed, with a goal to establish a new benchmark in software usability, capabilities and power. The power of the software comes from an embedded knowledge base that automatically defines optimum cutting parameters, optimum piercing characteristics, and optimum cutting speed that varies along the profile. The software automatically defines cutting path, applies offset and lead-in/lead-outs, and creates rectangular nesting.

Simplicity, versatility and openness add immeasurably to the power of the software. The software, arranged in the form of software Wizard, leads the user from the drawing to cutting with only a few clicks. Further, the user can modify, adjust, or override the automatic attributes. The software uses a commercial software engine to create CNC code that is displayed in text editor window. The software uses a commercial software engine to create CNC code that is displayed in text editor window. The software includes file management features, cost computations, job report and cutting simulation.

The paper will focus on the methodology used in developing the software from the concept evolution to its commercialization, and compare the software results in cut quality and time savings with the results from the standard industry practices before the development of the software. Results show that the new software has more than met its promise of overarching goals set before the beginning of the development.

10th American Waterjet Conference
August 14-17, 1999: Houston, Texas

Paper **67**

ABRASIVE WATERJET CUTTING — LOWERING YOUR OPERATING COST WHILE INCREASING YOUR TOTAL PROFIT

Dennis Chisum
International Waterjet Parts
Ephrata, WA

- Down time leading to higher operating cost.
  - Changing abrasive
  - Changing material
  - Cleaning tank
  - Maintenance

- How cleanliness and routine maintenance reduces operating cost.

- Multiple heads versus just one.
  - 13/40 versus dual 10/30 or 11/40 combinations.
  - Percentage of single head cutting versus two heads.
  - Utilizing your pump while getting the best bang for the buck.
  - Percentage of increased production.

- Different abrasives and there specific needs.
  - Different abrasives for different jobs.
  - Percentage of what grit for most jobs.
  - Benefits in buying in truck load qtys.

- Reduce programming time.
  - Controller which allows the operator to change offsets on the fly.
  - Controller which is user friendly. Allows minor changes to be done without totally reprogramming the job.
  - Having a programmer who understands the operation of the machine.

- Inexpensive tooling materials.
  - Using the waterjet to make your tooling.

- Cutting head wear parts, their condition and how it effects the efficiency.

- Water quality and how it effects the life of components.

- Understanding the tolerance capabilities of the abrasivejet and how best to use them to increase your profits.

- Different materials for your cutting table surface.

- Different sources for your spare parts.

Organized and Sponsored by the WaterJet Technology Association

10th American Waterjet Conference
August 14-17, 1999: Houston, Texas

Paper **68**

A COMPREHENSIVE WATERBLAST

HEALTH & SAFETY PROCESS

Michael A. Zustra, CIH
MPW Industrial Services, Inc.
Hebron, Ohio, U.S.A.

ABSTRACT

MPW Industrial Services, Inc. is establishing a comprehensive waterblast health & safety program that strives for continuous improvement. The program relies on integrated systems that have been devised to ensure that all waterblast and related hazards are recognized, assessed and controlled.

The program is based on five elements:

- management leadership
- employee involvement
- job site analysis
- hazard prevention/control
- training

Tools, or systems, have been developed to facilitate the recognition, evaluation and control of hazards. They include:

- safety improvement committees
- safety observer program
- job safety analysis (JSAs)
- health & safety assessments
- safety performance recognition
- incident investigation

1. INTRODUCTION

MPW Industrial Services has established a comprehensive health & safety process. The process is proactive and based in integrated management systems that have been devised to ensure that waterjetting and other workplace hazards are recognized, assessed and controlled.

The application of quality management systems to occupational health and safety has increased in recent years. Health and safety management is experiencing a movement away from strict compliance with established standards toward management systems. Several governmental and consensus organizations have drafted guidance documents on the use of occupational health and safety management systems (OHSMS). The U.S. Occupational Safety and Health Administration (OSHA) has promulgated voluntary guidelines for safety and health program management. OSHA has also instituted the Voluntary Protection Program, a formalized program for organizations that agree to comply with tight requirements for using occupational safety and health management systems. Australia, New Zealand, Korea and many European nations are developing formalized OHSMS standards. The American Industrial Hygiene Association has drafted an ISO-compatible OHSMS guidance document and the American National Standards institute is investigating OHSMS standards. Adoption of a global OHSMS standard by the International Organization for Standardization (ISO) is an eventuality.

The systems approach seeks to minimize or eliminate workplace hazards whether or not required by regulation. MPW's health & safety process is proactive, prevention-oriented. The systems that have been implemented prevent injuries and illnesses by ensuring that internal policy, procedures, specifications and systems themselves are being followed, and important activities are done, standardized and documented. Like other quality processes, the systems are quantifiable and a mechanism for continuous improvement.

2. GUIDELINES

All aspects of MPW's health & safety process fall into a framework that guides the process. The process seeks to recognize and understand all hazards and potential hazards in the work area, control the hazards, and train personnel to ensure that they are aware of and understand the hazards to which they may be exposed and know how to perform tasks safely. The guidelines are management leadership, employee involvement, job site analysis, hazard prevention and control and training.

2.1 Management Leadership

Senior managers must be the leaders of the health & safety process. Management must make a clear statement that safety is valued by the organization. A written policy must clearly communicate these values to all employees so that they take appropriate actions when conflicts arise. Management should also set organizational safety performance goals, and objectives for meeting the goals, so that employees may clearly understand expectations, and can view their effort as a contribution toward achievement of the goals and objectives.

Much as production and quality are line functions, so should be safety. Managers must take control of the process and be accountable for the health and safety of workers under their supervision. Responsibilities for maintaining a safe work site, as well as the provision of authority and adequate resources, should also be assigned to subordinates.

It is important that managers be visible in demonstrating their commitment to safety. They must "walk the talk" to confirm that health & safety is important to them. Managers must set the example by knowing and following all the rules. They should point out unsafe acts or conditions as they inspect operations, and begin each meeting with a comment or question about pertinent safety issues. If employees see their managers stressing workplace safety, they will also become interested.

2.2 Employee Involvement

Employees with their hands on the waterjet gun everyday are most likely to be injured, and probably know best how to safely perform a task. It makes sense then that these employees must be active in the health & safety process to maximize the effectiveness of the process.

A goal of the health & safety process, with regard to employee involvement, is to develop an awareness among employees whereby safety is considered before each job is performed, every time, no matter how small the job. An evolution of sorts must occur before this positive safety culture can exist. Employees must go from mere participation in the process, to being empowered to act within the guidelines of the process, to ultimately taking ownership of the process. Employee participation begins with an understanding of management's commitment to health and safety, company safety policy and process objectives, work rules and procedure, and the discipline/award system. Involvement develops so employees can be independent of supervisory control. They have personal knowledge, have made a personal commitment to health and safety, care about their personal safety and seek individual recognition for their contribution to the health & safety process. In the last phase of employee involvement, workers begin to take a proprietary interest in the process. They help co-workers conform, care about the safety of others, rely on one another, and take pride in the overall process.

2.3 Job Site Analysis

An effective health & safety process must be able to anticipate harmful occurrences. To do that, systematic actions must be taken to ensure workplace hazards and potential hazards are fully characterized.

Initially, a comprehensive hazard inventory must be compiled. The inventory should include a listing of tasks performed and hazardous materials encountered. Each task should be broken down into sub-tasks so that specific hazards encountered in performing the work are identified, and preventive methods or controls are devised. As new tasks are added, or when there is a change of facilities, equipment, processes or materials to existing tasks, the inventory must be updated. Supervisors must perform routine health and safety inspections to verify compliance with the job analyses. Workers who perform and are familiar with the task can also be utilized to observe work being performed to help in finding unsafe acts and conditions.

Incident investigation should be viewed as another opportunity to identify hazards, develop control methods and detect flaws in the health & safety process. Root and contributing causes of accidents should be uncovered and measures should be taken to prevent recurrence. Accordingly, a periodic statistical review of accident types and resulting injuries and illnesses should be conducted to reveal patterns that may be indicative of common deficiencies.

2.4 Hazard Prevention and Control

Once identified, hazards should be removed or controlled. Ideally, engineering controls, such as substitution of less harmful materials, ventilation, or alteration to a process, are implemented to completely eliminate exposure to a hazard. If engineering controls are not possible, as is often the case when working in a customer's facility, personal protective equipment (PPE) or administrative controls, or a combination of the two may be applied to prevent unsafe and unhealthful exposure. PPE must be checked frequently to ensure it is in use and continues to function effectively. Administrative controls, which should be considered a last resort, include rotation of work crews to minimize the relative duration of exposures and transfer of personnel who have reached the upper limits of allowable exposure.

Other measures that may be taken to prevent accidents are the provision of a preventive maintenance program, preparation for emergencies and implementation of a medical surveillance program.

2.5 Training

The role of an effective health and safety training program is to ensure that all personnel understand and can ably fulfill their role in the health & safety process. Managers must be taught to set the example. Supervisors must be able to recognize, evaluate and control workplace hazards, sometimes with the support of health & safety professionals. Employees must understand the hazards of the tasks they perform, safe work practices that will minimize exposure, and emergency response procedures.

3. SYSTEMS

MPW has implemented several systems, or control programs, to ensure that important health and safety functions are done in accordance with internal requirements every time. These systems have been formalized and are woven into the fabric of the organization.   Because they have become part of MPW's operating methodologies, they are self-sustaining, requiring minimal oversight. Since all are hard copy programs, verification of use of the systems can be tracked.

3.1 "Commitments" to Health & Safety

MPW has developed two formal "commitment to health & safety" documents. The management "Commitment to Health and Safety" details corporate goals and objectives for the health & safety process. The company's goal is simple: Zero accidents in performing all aspects of our work. The objectives were borne out of the corporate Safety Improvement Committee (discussed below) and largely detail basic tenets of the process. Corporate leaders and members of the Safety Improvement Committee signed the document. Framed copies of the "Commitment to Health and Safety" hang in every MPW office. Laminated versions are required to be posted at every job site.

The "Personal Commitment to Health and Safety" is an extension of the top management commitment. It reiterates company goals and communicates five basic personal health and safety responsibilities: know job hazards, comply with specifications, wear PPE, report all workplace hazards and immediately report incidents. Administration of the program is tiered through supervisors to employees. Every employee from the Chairman to the newest hire signs the "personal commitment." Completed documents have been posted in office spaces. A hard hat sticker is issued to personnel as they enroll.

Many benefits have been derived from the "commitments to health and safety." Employees now clearly understand that management has made safety a priority, and have full knowledge of their role in the process. Since the "commitments" were done at the start of the process, it was also a highly visible means of kicking the process off.

3.2 Hazard Inventory

The corporate hazard communication standard has been modified to require semi-annual reporting of complete hazard inventories by each MPW location. Included in the inventory are tasks performed and chemicals to which employees are potentially exposed. Location managers are asked to update the inventory as new tasks are added, or facilities, equipment, processes or materials change.

In addition to acting as the starting point for a thorough job site analysis, maintenance of the hazard inventories has enabled location managers to become more aware of workplace hazards and potential hazards, and therefore, better able to prevent accidents from occurring.

3.3 Job Safety Analysis (JSA)

JSAs are job-specific planning tools that help identify engineering controls, safe work practices, PPE and administrative controls that may be required to perform a job safely. Typically, JSAs are co-written by a member of the operations staff (technicians, foremen or supervisors) and a health & safety professional. JSAs are developed by breaking down the job into basic steps, specifying hazards that could arise during each step, and then devising control methods for each hazard. JSAs have been developed for all major tasks and most smaller, less complex tasks.

In addition to further developing job site characterization, JSAs are also a valuable training tool. The work crew that will perform the task is trained on the content of the JSA prior to beginning work. Not only does JSA training develop worker safety skills, but overall safety awareness also improves. Additionally, employee ownership of the health & safety process is enhanced by worker participation in the development of JSAs.

3.4 Health & Safety Assessments

Job sites must be audited frequently to gauge how well the organization, health & safety systems and people within the organization are performing toward providing a safe workplace. MPW performs audits, or assessments, at three levels. Onsite supervisors conduct weekly hazard control inspection using a checklist-type form with yes/no responses. The assessment is broad-based in its coverage of the health and safety aspects of an operation, including a review of job setup, PPE use, fire protection, material handling, hazard communication, walking/working surfaces, power tools, environmental factors, vehicles/equipment, containers, warning/signaling devices and electrical equipment. The inspection is a self-assessment, conducted mainly to help the supervisor detect potential hazards so they can be corrected before an incident occurs. A record of all assessments, however, is maintained by the supervisor and reviewed periodically by offsite managers and health and safety personnel.

Offsite managers conduct assessments of their own once a month. Unlike onsite supervisors, managers assessments are objective, and focus on job site compliance with health & safety process systems. The form used to conduct the assessment, the Health & Safety Management Systems Review, contains evaluation criteria that measure progress toward achieving company objectives. The evaluation criteria are pointed questions that are weighted according to their relative importance in the process. The reviewer's responses to each evaluation criterion are also weighted: 0=does not meet, 1=partially meets, 2=meets the criteria. The result is a quantitative value that scores the audited job sites compliance with health & safety process systems. A Safety Improvement Committee reviews the management assessments, where scores can be compared with other job sites, other geographic regions and other work-types to define specific areas of the health & safety process most in need of attention.

Staff health & safety professionals conduct assessments that are both hazard control inspections and health & safety systems reviews. Health & safety auditors log "areas of improvement" identified during the audit on the assessment form. Due dates for abatement of hazards are mutually agreed upon by the auditor and the job site supervisor. Each "area of improvement" is coded to a particular hazard category (PPE use, material handling, hazard communication) and tracked.

3.5 Safety Observer Program

The purpose of the Safety Observer program is to get systematic feedback from employees who observe work in progress to determine if the work is being performed according to plan. Since workers with their hands on the tools can be a valuable health and safety resource, it is critical that a positive line of communication between worker and supervisor be established and maintained.

Safety observers are randomly selected at a job site by the site supervisor. The number of observers and frequency of observations will vary depending on the complexity and redundancy of the task being observed. The assigned observer will typically make two 15-minute dedicated observations during the workday to watch a task being performed by co-workers. The observer should be familiar with the task being observed, but on occasion, the observer should come from outside the job classification or work group performing the task. The observer's role is to determine if the task observed is being done according to MPW standards. Unsafe acts and unsafe conditions are identified, with the focus of the observation on the work task being done, not on the individual performing the task. Positive aspects of safety performance are also noted. The observer completes the Safety Observer form documenting his or her findings, and submits the form to the job site supervisor at the end of the shift. The observer may also recommend actions to be taken to improve job site safety. At the next day's toolbox safety meeting, the observer presents an oral report. The job site supervisor is required to respond, in writing on the Safety Observer form, to deficiencies identified.

The Safety Observer program has paid dividends. Not only do supervisors get useful input from employees that will improve safety performance, but workers feel empowered by their participation in the program and the resulting improvements. In a larger sense, the safety observer program has helped create a more positive safety culture; an active team-oriented climate where the safety of co-workers is important.

3.6 Accident Investigation

Accidents and "near miss" incidents must be investigated so that their causes and means for preventing their repetitions are identified, rather than being a search for "whom to blame." To make the investigation process most effective, first line investigation is conducted by the injured employee and the direct supervisor. Initial investigation and reporting must be timely and thorough. Local managers and health & safety professionals review the accident report for completeness and to ensure that initial corrective actions have been taken. The report is then forwarded to the regional Safety Improvement Committee (SIC) for formal review. The SIC analyzes accidents in depth to uncover direct and contributing causes and to identify any shortcomings in policies, standard operating procedures, training, safe work practices or systems that might allow similar incidents to occur again. If flaws are uncovered, Safety Bulletins containing lessons learned are distributed immediately. Disciplinary action may be taken if poor performance is identified as a cause.

3.7 Toolbox Safety Meetings

Safety meetings are held at the start of each shift to set the tone for the day. Job site supervisors typically lead the meetings. Each supervisor has receiving formal instruction on the conduct of toolbox meetings, training techniques and meeting content. The meetings usually focus on the work at hand: job safety analyses for upcoming work are reviewed and the safety observer's oral report is delivered. Previously identified deficiencies that have been remedied or other job site safety improvements might also be discussed. When Safety Bulletins are issued or safety-related internal correspondence is distributed, these are presented to the crew. User-friendly lesson plans that will be used for “refresher” training on topics such as heat stress, confined space entry, lockout/tagout will soon be developed.

3.8 Health & Safety Plans

A site-specific health and safety plan (HASP) or a Safety/Environmental Worksheet is developed for every job. These documents, which address hazards unique to each job and hazard control measures that are to be implemented, are written by health & safety practitioners and are used on-site as a tool to communicate site-specific health and safety requirements. HASPs, which are more comprehensive than Safety/Environmental Worksheets, are written for longer, more complex projects. HASPs contain a detailed description of the facility and the work processes involved, and information on key personnel, job hazard analysis, regulated work areas, protective equipment, decontamination, air monitoring, emergency response, training requirements and medical surveillance. Safety/Environmental Worksheets are developed for short duration or single-task work. Worksheets are in a checklist form and address the scope of work, physical and chemical hazards present, PPE required and emergency information.

3.9 Safety Improvement Committee

SICs act as steering groups for the health & safety process. They are multi-level and multi-disciplinary: multi-level in that they are organized at the corporate, zone and local levels within MPW’s organization chart; multi-disciplinary in that many functions (operations, engineering, maintenance, sales, human resources) are represented on the committee. At the zone and local levels, field personnel, including crew leaders and laborers, are committee members. SICs meet monthly and are chaired by the most senior business manager at each level.

During meetings, SICs reevaluate all elements of the health & safety process. Meeting agendas include a review of safety performance indicators, goals and objectives, health & safety procedures and the adequacy of training programs. An in-depth review of recent incidents takes place where injured employees and their supervisors are interviewed to determine root and basic causes of the accident. SICs devise corrective actions for systemic problems uncovered and are the source of disciplinary action for poor safety performance. It is through the corporate SIC that criteria for high pressure hose inspection were devised, and development of a network of physicians that would treat waterjet injuries was initiated. Periodically, injury/illness statistics are compiled for SIC analysis of trends in incident causes or injury types.

3.10 Other Systems

As the health & safety process progresses, other systems will be implemented. They include:

- Mechanism to formally and quantitatively integrate supervisors' and managers' participation in the health & safety process into their overall performance evaluation
- Safety award system whereby teams and individuals that demonstrate outstanding safety performance are rewarded
- Written progressive disciplinary system that will assist supervisors in controlling the work environment
- System to document the tracking of hazard correction at the local level

4. CONCLUSIONS

Adoption of health & safety management systems does not come easily. OHSMS redefines thinking on how things are done in an organization. It involves a paradigm shift away from the traditional methods of managing health and safety. The traditional health and safety management method is *reactive*, where health and safety professionals investigate accidents, identify and correct unsafe acts and conditions, monitor the use of PPE, and generally act as safety "cops." OHSMS requires a culture change where safety is a core value, part of the business fabric, rather than just an add-on. In the *proactive* OHSMS culture, workers and line management take ownership of workplace health and safety.

Benefits associated with the use of OHSMS, however, are many. The use of health and safety management systems has proven to be effective in reducing workplace accidents. OSHA estimates that "Star" level VPP participants ("outstanding work sites") avoid 2097 lost workday injuries annually, while "Merit" level participants ("stepping stone to Star") have a lost workday case rate that is 35% below the national average. In the first eleven months of the health & safety process, MPW has seen its total OSHA-recordable accident rate (TOR) drop by 33% and the lost workday incident rate reduced by 60%. MPW has reduced its costs for worker's compensation insurance and other costs of injuries and illnesses, and now uses the health & safety process as a selling tool. For workers, the health & safety process has contributed to the quality of work life, enhanced participatory skills and improved employee morale.

5. REFERENCES

U.S. Department of Labor, Occupational Safety and Health Administration, "Safety and Health Program Management Guidelines; Issuance of Voluntary Guidelines," *Federal Register*, January 26, 1989.

Pierce, F.D., "Total Quality for Safety and Health Professionals", Government Institutes, 1995.

"Occupational Health and Safety Management Systems: An AIHA Guidance Document," American Industrial Hygiene Association, Fairfax, Virginia, 1996.

American Industrial Hygiene Association Board of Directors, "Boldly Going Where No Association Has Gone Before- Release of OHSMS Guidance Document Places AIHA in Leadership Position for International Management Systems," *The Synergist*, pp. 31-32, 1996.

10th American Waterjet Conference
August 14-17, 1999: Houston, Texas

Paper **69**

FACTORS INFLUENCING THE LEAKAGE CHARACTERISTICS OF NPT AND NPTF THREADED CONNECTORS

William A Lees
Maxbar, Inc.
Houston, Texas

P. Shaun Crofton
Mechanical Engineering Department
Imperial College
London, U.K.

ABSTRACT

At inception, the water jet cleaning industry was largely confined to the use of operating pressures of up to 5,000 psi. Working pressures have steadily increased, and NTP fittings are now commonly used at pressures of up to 20,000 psi. Concern has frequently been expressed about the use of NPT fittings at higher and higher pressures, but little factual and objective information is available on their performance. Industry standards for high pressure fittings have generally originated from the high pressure chemical industry, but the needs of the water jet industry are creating a growing demand for fittings larger and more robust than the traditional instrumentation style fitting, but smaller and lighter than the heavy flanged fittings designed for permanent, in-plant installations.

Since any fitting is prone to leakage and potential failure when over-pressurized, it is of interest from a safety and reliability point of view to establish the factors which determine the leakage characteristics of NPT and NPTF threaded connectors.

This work describes the results of a preliminary experimental program designed to assess the safe working pressure of two of the more popular sizes of NPT and NPTF threaded connectors, ¼" and ½". Since it is not uncommon to find apparently indiscriminate mixtures of NPT and NPTF male and female parts being used in a single connection, the leakage pressure of various permutations of mating thread forms has also been determined. Finally the method of joint preparation in terms of joint sealant using a conventional PTFE sealing tape or a proprietary sealing compound has also been investigated.

Organized and Sponsored by the WaterJet Technology Association

1. INTRODUCTION

Despite the widespread use of NPT fittings, most research orientated organizations have been reluctant to conduct any quantitative research into their behavior because the joint is not amenable to finite element or other computer analysis, the fittings are entirely generic, and there seem to be so many variables that can affect performance. Indeed, many are sweepingly critical of the use of NTP fittings, and recommend that they should not be used at all. However, there appears to be no objective justification for this broad condemnation, and the fact remains that they are used daily with success. Two major questions are: at what pressure will the connection leak, and at what pressure will it fail catastrophically and blow out? A preliminary, objective and quantitative study was conducted to begin to examine the major factors governing the behavior of NPT fittings at high pressure.

Two variations of NPT threads were tested because they can be interchanged, and they also allow the effect of thread manufacturing tolerances to be investigated. The threads, namely NPT (National Pipe thread, Tapered, and NPTF, also known as “Dryseal” are defined by the American National Standard Institute. The NPTF thread has been designed specifically for sealing, (originally without sealing compound, hence the name “Dryseal”), whilst the NPT thread has been designed for general purposes, including mechanical (non-pressurized) connections, and pressurized connections using pipe dope. The two threads are identical except that in the NPTF thread no clearance is allowed between the rest and root of the thread, to reduce leakage.

Two of the more popular sizes were covered, ¼”, and ½”. The fittings were made from 316 stainless steel.

Tests were conducted dry, with no lubricant, with PTFE tape, and with a proprietary thread sealant/lubricant, at a variety of tightening torques. The variables included in these tests were:

Size
Thread
Torque
Lubricant/sealant

2. MATERIALS

2.1 Fittings

The male fittings were made from cold drawn 316 stainless steel bar, 25mm (1”) hexagon for both the ¼” and ½” male fittings (plugs) with a yield strength of 62,400 psi. The female fittings were made from 40mm (1-9/16”) hexagon for the ¼” female fittings, and 50mm (2”) hexagon for the ½” female fittings (couplings) with a yield strength of 58,900 psi. Hexagon sizes are across flats (A/F). The A/F dimension of the sockets was chosen to give a ratio of inside to outside diameter of at least 3. With such a heavy wall thickness, the effect of the wall thickness of the fitting is effectively eliminated as a variable in these experiments. Threads were cut using new, ground, taps and dies (non-adjustable type) and were checked for dimensional accuracy using plug and ring gauges.

2.2 Thread Sealant

The fittings were tested with no lubricant (dry) as a baseline, and also with the usual PTFE tape, and with “Threadmate”, (a Parker Hannifin, Inc. product) a commercial thread sealant/lubricant. The version of Threadmate used for these tests was a mixture of PTFE particles, an extreme duty anti-galling lubricant, and heavy oil, the whole forming a yellow grease or paste.

3. TEST METHOD

The fittings were tested using simple pressure test equipment. The plugs were tightened into the coupling using a standard commercial torque wrench, then the pressure was increased slowly using an air operated high-pressure pump. The test fluid was a very low viscosity hydraulic oil. Pressure was monitored using a transducer and computer. During testing, the fittings were immersed in water in an open-topped steel tank. Leakage was determined to have occurred when a drop or drops of oil were seen on the surface of the water. In some tests bubbles of air were seen to come from the connection at pressures lower than the liquid leakage pressure. Pressures were not increased above 80,000 for any test, even if no leakage had occurred, as it was felt that there was very little probability of anyone using NPT fittings above 80,000 psi in the waterblast industry.

Two methods of tightening were used:

a. Progressively increasing the tightening torque after each leak.

b. Tightening directly to the maximum torque (“reference” test).

The maximum torque was limited to 100 ftlb for the ¼” fittings, and 150 ftlb for the ½” fittings, to avoid torsional yielding of the plugs during tightening.

The combinations tested are summarized in the tables below:

¼” Size		**Male (plug)**	
		NPT	**Dryseal**
Female	**NPT**	Dry, Sealant	
(coupling)	**Dryseal**	Dry, Sealant, PTFE	

½" Size		Male (plug)	
		NPT	Dryseal
Female	**NPT**	Dry, Sealant, PTFE	Dry, Sealant, PTFE
(coupling)	**Dryseal**	Dry, Sealant, PTFE	Dry, Sealant, PTFE

4. NPT AND DRYSEAL THREADS

The only difference between NPT and NPTF threads is the specification for the truncation of the threads. NPT threads are designed to be easily machined, and to be able to seal pressure with the aid of some form of thread dope or sealant. The root and crest tolerances of NPTF (Dryseal) threads are specified so that there is no clearance between the mated threads when they are made up. Clearly this requires higher tolerance machining, but, with suitable materials such as brass, and with low pressures, in theory no sealant is required for a leak-proof connection. In practice this is not easy to accomplish, and NPTF threads have acquired a reputation for unreliable sealing, particularly in applications involving frequent temperature changes (such as engines). It is also possible to machine the threads so that there is interference between the root and crest, but not between the thread flanks. It is conceivable, therefore, that an NPT thread with a good sealant could be as reliable, or more reliable, than an out-of-tolerance NPTF thread.

5. CURRENT PRACTICE

Current practice in the waterblast industry is to use either 316 or 17-4 PH stainless steels, limiting the working pressure to 15,000 psi (occasionally 20,000 psi for ¼") for fittings up to and including ½", and 10,000psi for ¾" and 1". Fittings larger when 1" are very seldom used. The different working pressures for the different sizes are based on the change of the ratio of the area exposed to pressure to the shear area of the threads. As the fittings become larger, the stress on the threads increases. Whilst this is somewhat simplistic, and assumes amongst other things that the load on the threads is evenly distributed along the length of the thread, these guides-lines have evolved from a great deal of successful experience. The connections are usually made up using PFTE tape as a lubricant and sealer.

6. TEST RESULTS

6.1 ¼" Size

6.1.1 ¼", Dry

The results of the ¼" fittings tested with neither sealant nor PTFE tape (just bare metal) are shown in Fig. 1. The fittings were tightened to 10ftlb, pressure tested until they leaked, de-pressurized, tightened further, re-tested and so on, up to 100 ftlb. In addition, “reference” tests were done by tightening directly to 100 ftlb and pressure testing.

The “re-tighten” tests show an approximately linear increase in leakage pressure with torque, with a wide variation in final leakage pressure, approx. 5,000 psi. By contrast, the “reference” test is more consistent, and much higher at 35,000 psi.

6.1.2 ¼”, with Sealant

The results of the ¼” fittings tested with sealant are shown in Fig. 2. The fittings were tightened to 10ftlb, pressure tested until they leaked, de-pressurized, tightened further, re-tested and so on, up to 100 ftlb. In addition, “reference” tests were done by tightening directly to 100 ftlb and pressure testing.

Leakage pressure increases rapidly with increasing tightening torque up to 68,000 psi at 50ftlb. Continuing to tighten to 100 ftlb reduced the leakage pressure. The effect of over-tightening is confirmed by the reference test. Tightening directly to 100 ftlb results in an even lower leakage pressure (41,000 psi) than the tighten-leak-tighten tests.

6.1.3 ¼” with PTFE Tape

The results of the ¼” fittings tested with PTFE tape are shown in Fig. 3. The fittings were tightened to 10ftlb, pressure tested, de-pressurized, tightened further, re-tested and so on, up to 100 ftlb. In addition, “reference” tests were done by tightening directly to 100 ftlb and pressure testing.

As with the sealant, leakage pressure increased rapidly with increasing torque, up to 80,000 psi (test stopped with no leakage) at 30 ftlb. Continuing to tighten to 100ftlb caused the joint to leak at 44,000 psi, the same as the directly tightened reference test.

6.2 ½” Size

6.2.1 ½” Dry

The results of the ½” fittings tested with neither sealant nor PTFE tape (just bare metal) are shown in Fig. 4. The fittings were tightened to 10ftlb, pressure tested until they leaked, de-pressurized, tightened further, re-tested and so on, up to 150 ftlb. In addition, “reference” tests were done by tightening directly to 150 ftlb and pressure testing.

The general trend was for the leakage pressure to decrease until a tightening torque of 40 ftlb, and then to increase up to 150 ftlb. Maximum leakage pressure of approximately 5,000 psi corresponded to the maximum tightening torque of 150 ftlb.

Considerably more scatter was noted for the reference tests, with the leakage pressure ranging from 12,000 psi to 40,000 psi for the Male & Female NPT combination, and the Male NPTF &

Female NPT combination respectively. The Male and Female NPTF combination, which might reasonably have been expected to be the best performer, fell in the middle at just under 20,000 psi.

6.2.2 ½”, with Sealant

The results of the ½” fittings tested with sealant are shown in Fig. 5. The fittings were tightened to 10 ftlb, pressure tested until they leaked, de-pressurized, tightened further, re-tested and so on, up to 150 ftlb. In addition, “reference” tests were done by tightening directly to 150 ftlb and pressure testing.

The considerable scatter is immediately apparent, with no clear trend, except that, with one exception, leakage pressure increased with tightening torque to the maximum tested. Leakage pressure varied from 2,000 psi to 80,000 psi (test stopped, no leakage).

The reference tests are much less scattered, and are grouped in the 40,000 psi area.

6.2.3 ½”, with PTFE Tape

The results of the ½” fittings tested with PTFE tape are shown in Fig. 6. The fittings were tightened to 10 ftlb, pressure tested until they leaked, de-pressurized, tightened further, re-tested and so on, up to 150 ftlb. In addition, “reference” tests were done by tightening directly to 150 ftlb and pressure testing.

There is much less scatter in the PTFE tape tests than in the sealant tests, with the final leakage pressure lying between 40,000 and 52,000 psi, in the same area as the sealant reference tests. However, none of the PTFE tests came close to the maximum pressure of 80,000 psi achieved with the sealant.

7. CONCLUSIONS

7.1 Effect of Threadform

When the tests program was initially considered, it was assumed that the NPTF/NPTF combination would perform best, followed by an NPTF/NPT combination, and finally the NPT/NPT, based on the fact that the NPTF thread is designed to ensure that there is no clearance between the root and crest, eliminating the spiral leakage path.

However, it is clear from the tests that there is no combination that consistently out-performed the others. This could be attributed to the high tightening torques tending to flow the thread plastically. Given the similarities of the dry tests, the lack of a clear “best combination” cannot be attributed to any effect of sealants. Just how far the threads can be truncated without significantly affecting performance is a important issue, especially for female threads, as even a modest truncation can greatly reduce the torque required to cut the thread, an important consideration when machining tough, high strength materials.

7.2 Tightening Torque

From the results of the 1/4” tests with both PTFE tape and Threadmate, it appears as though there is a definite reduction in leakage pressure when the tightening torque exceeds approximately 50 ftlb. This suggests that the plastic deformation of the threads has reached a point where the threads are deforming, allowing leakage. The tests on the 1/2” threads show that leakage pressure continues to rise up to the maximum torque tested, 150 ftlb.

7.3 Blow-out Pressure

An interesting and unexpected result was the ability of both the 1/4” and 1/2” fittings to withstand 80,000 psi not only without blowing out, but without leakage. This indicates that correctly tightened NPT fittings in good condition and made from the materials used for these tests (typical of materials used in the waterblast industry) do in fact have a good margin of safety against blow-out, even at 20,000 psi.

7.4 Leakage Pressure

Tests were conducted on dry fittings to form a baseline for establishing the effectiveness of sealants and lubricants.

For the 1/4” fittings tightened directly to 100ftlb the leakage pressure is approximately doubled from 35,000 psi (dry) to 68,000 psi (sealant) and 80,000+ psi for the PTFE tape. The effect is very noticeable in the tests that were re-tightened after each leakage. Re-tightened dry joints achieved a maximum leakage pressure of less than 10,000 psi, compared to 80,000+ psi with PTFE tape. “Used” fittings can be successfully re-used if they are re-coated with PTFE tape or sealant.

Again, for the 1/2” fittings tightened directly to 150 ftlb the leakage pressure is approximately doubled from around 20,000 psi to around 40,000 psi for both PTFE tape and sealant. As for the 1/4” fittings, re-tightened dry fittings performed poorly compared to the re-tightened fittings with tape or sealant.

There appears to be no consistent difference between the PTFE tape and the sealant as far as leakage pressures determined by these tests.

The leakage pressure of the 1/4” fittings made from these materials, installed with sealant/tape and tightened to a maximum of 50 ftlb is *approximately* 70,000 to 80,000 psi.

The leakage pressure of the 1/2” fittings made from these materials, installed with sealant/tape and tightened 150 ftlb is *approximately* 40,000 psi. It is possible that the leakage pressure may be higher with higher tightening torques.

8. FURTHER WORK

Very clearly this is only a preliminary study, and much remains to be done. Obviously an important variable that was not addressed in this study was the strength of the material. No discussion or rating of fittings can omit this fundamental variable. It is quite meaningless to debate the performance of NPT fittings without a clear reference to the strength of the material that the fittings are made from. Future studies will study this in more detail, especially with a view to determining if there is an optimum combination of material properties.

9. DISCLAIMER

These are the results of a brief, preliminary study. These results and comments are not intended to be recommendations or approvals for the use of any type of fitting at any pressure.

10. ACKNOWLEDGMENTS

The assistance of the staff and technicians of Imperial College are gratefully acknowledged.

Fig. 1   1/4", Dry

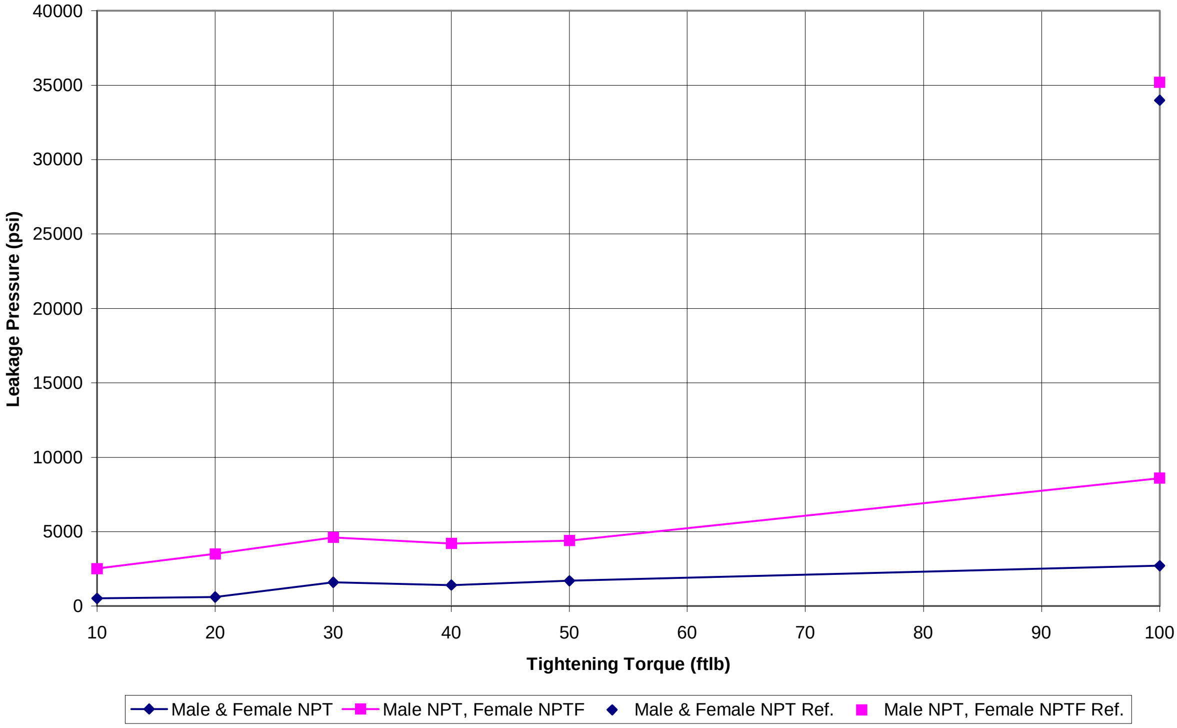

40000
35000
30000
25000
20000
15000
10000
5000
0
Leakage Pressure (psi)
10
20
30
40
50
60
70
80
90
100
Tightening Torque (ftlb)
Male & Female NPT
Male NPT, Female NPTF
Male & Female NPT Ref.
Male NPT, Female NPTF Ref.

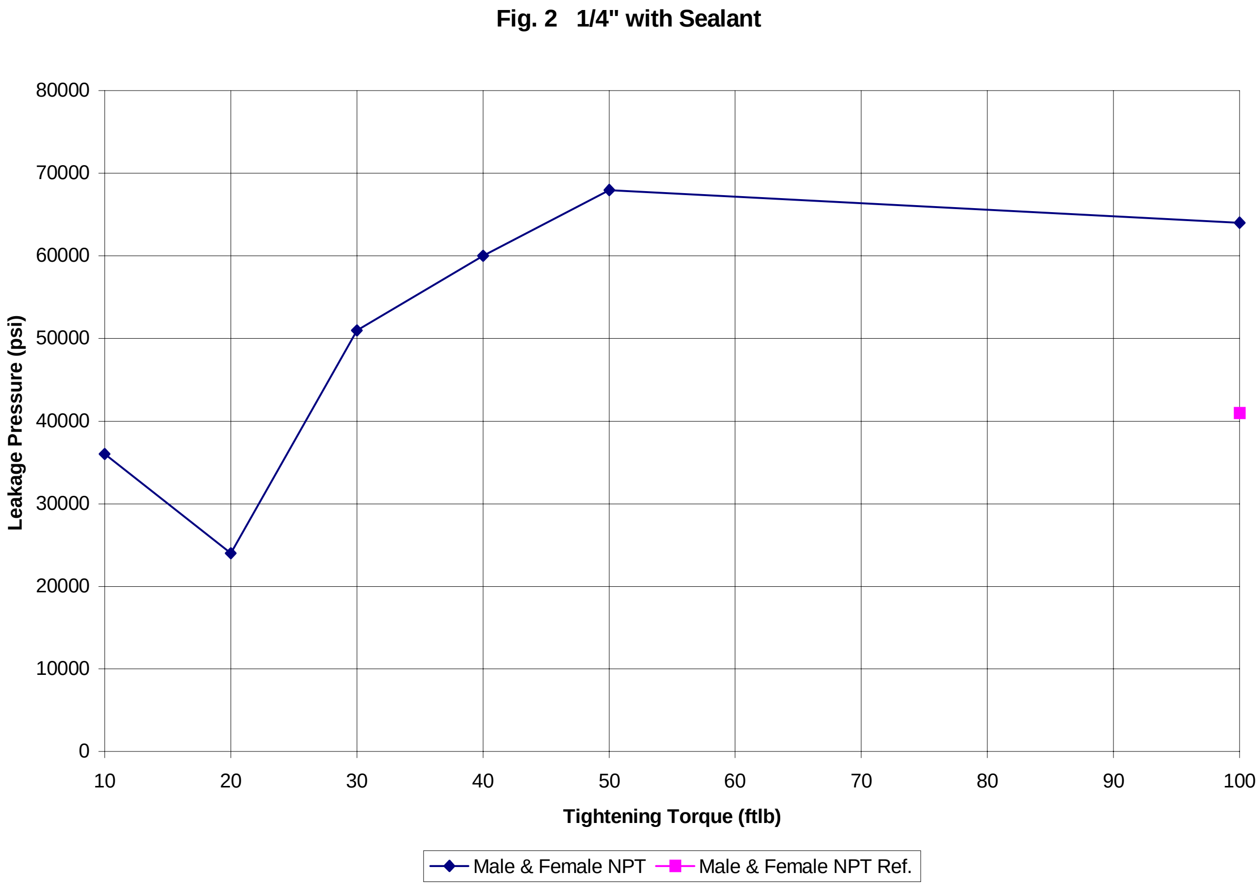
Fig. 2 1/4" with Sealant
80000
70000
60000
50000
40000
30000
20000
10000
0
Leakage Pressure (psi)
10
20
30
40
50
60
70
80
90
100
Tightening Torque (ftlb)
Male & Female NPT
Male & Female NPT Ref.

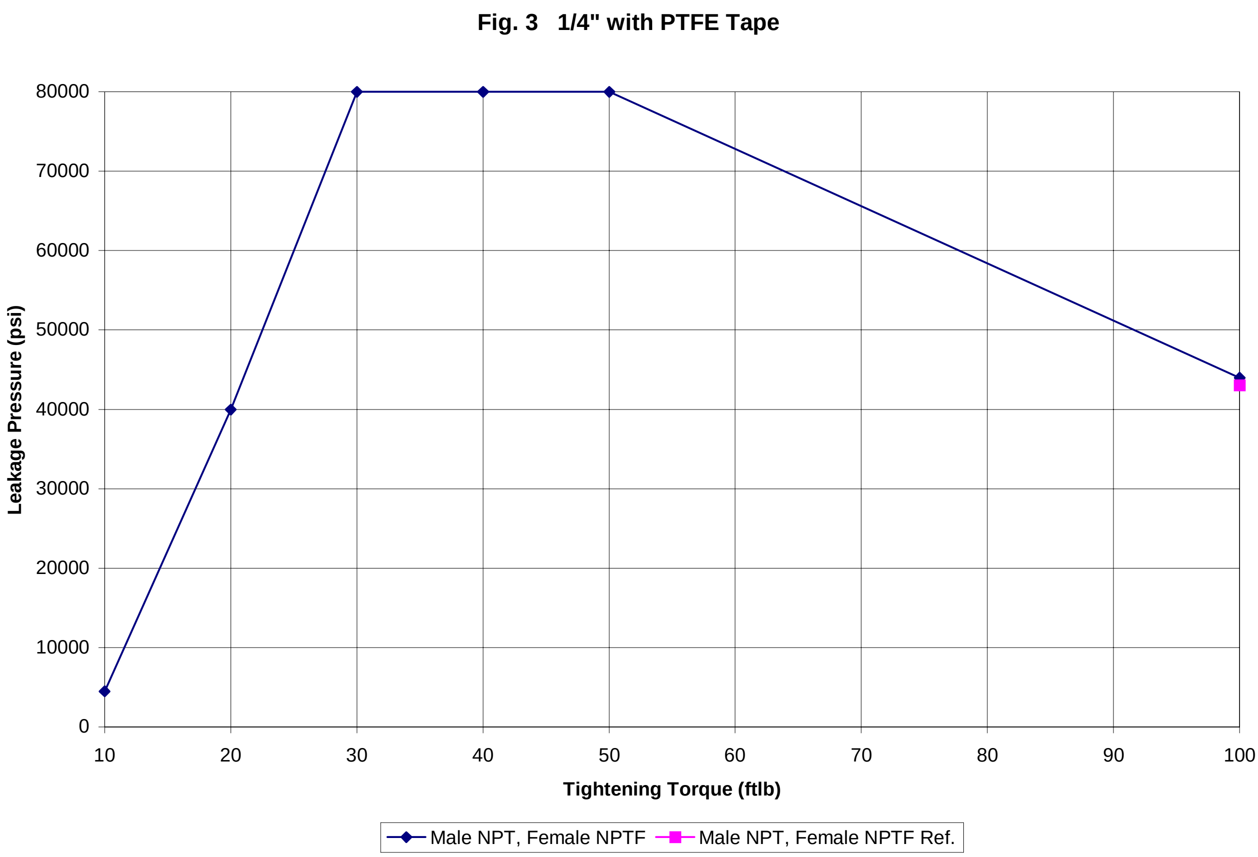
Fig. 3 1/4" with PTFE Tape
Leakage Pressure (psi)
80000
70000
60000
50000
40000
30000
20000
10000
0
10
20
30
40
50
60
70
80
90
100
Tightening Torque (ftlb)
Male NPT, Female NPTF
Male NPT, Female NPTF Ref.

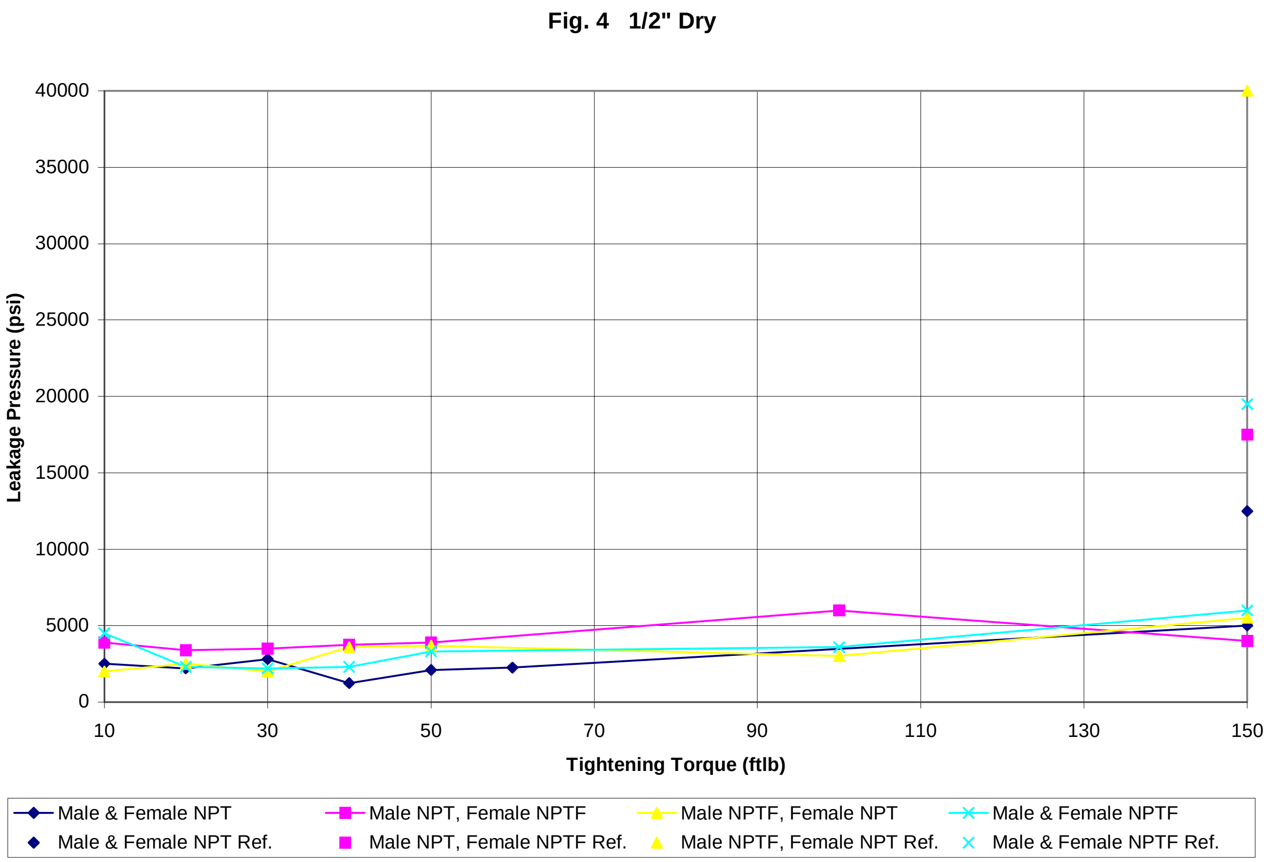
Fig. 4 1/2" Dry
Leakage Pressure (psi)
40000
35000
30000
25000
20000
15000
10000
5000
0
10
30
50
70
90
110
130
150
Tightening Torque (ftlb)
Male & Female NPT
Male NPT, Female NPTF
Male NPTF, Female NPT
Male & Female NPTF
Male & Female NPT Ref.
Male NPT, Female NPTF Ref.
Male NPTF, Female NPT Ref.
Male & Female NPTF Ref.

Fig. 5   1/2" with Sealant

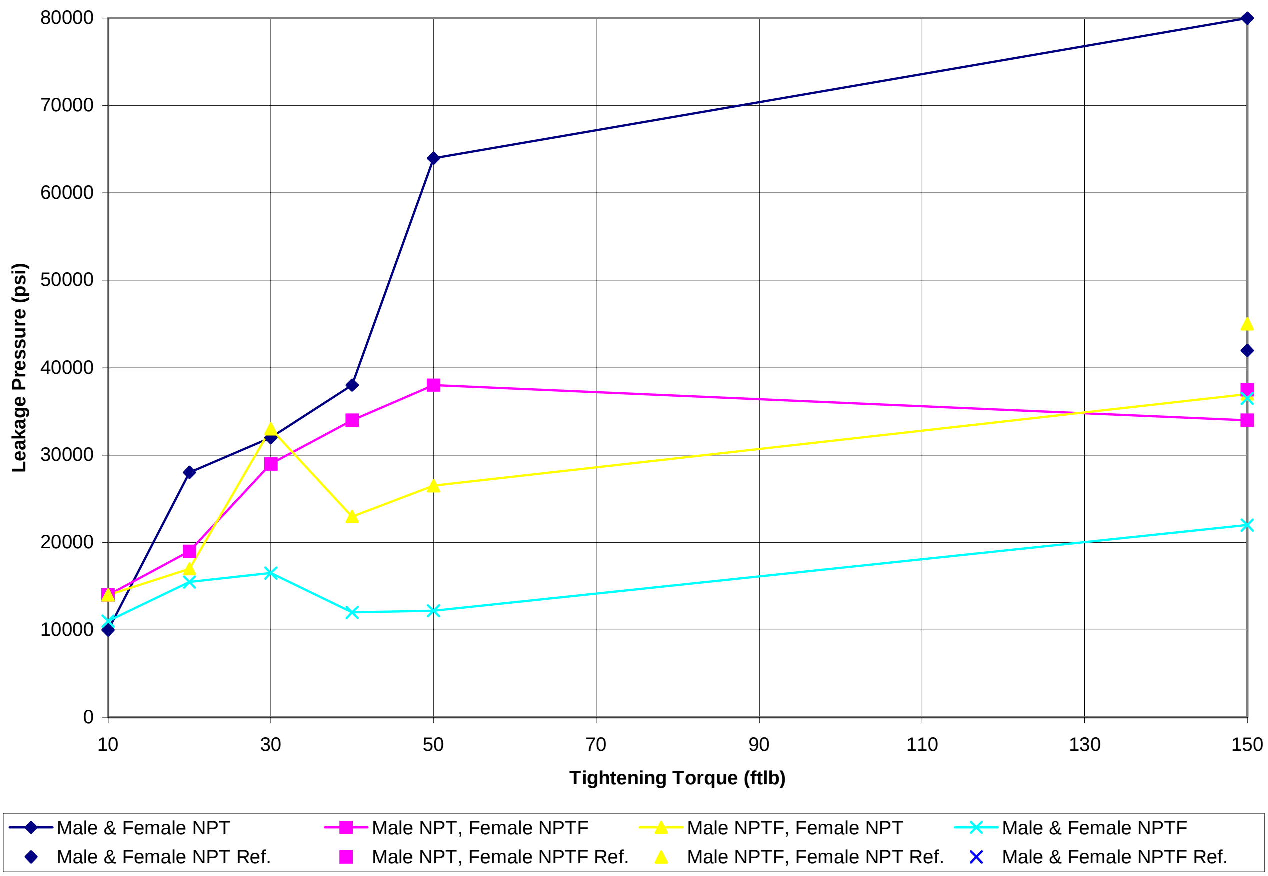

Fig. 6   1/2" with PTFE Tape

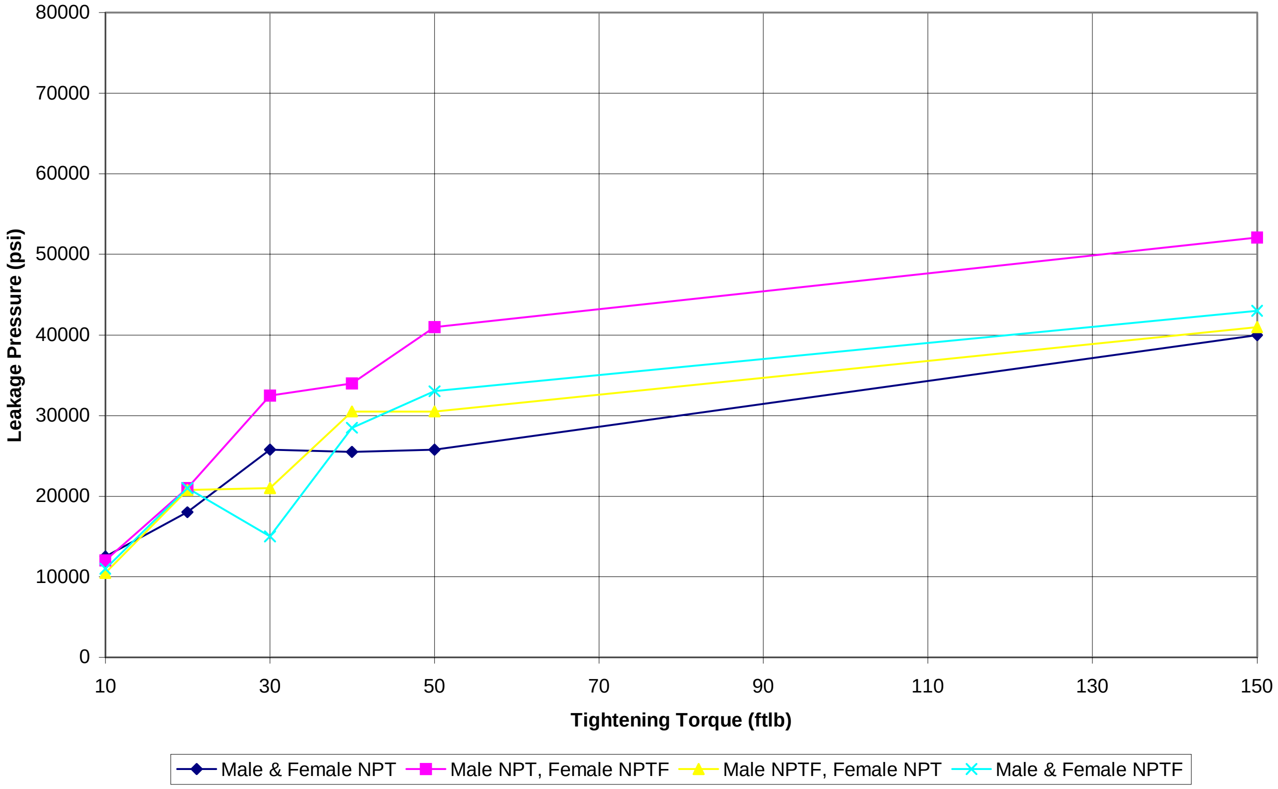

10th American Waterjet Conference
August 14-17, 1999: Houston, Texas

Paper **70**

FLUID JET IGNITION HAZARDS SAFETY ANALYSIS

Paul L. Miller
Teledyne Brown Engineering
Huntsville, AL, USA

ABSTRACT

The use of high-pressure abrasive fluid jets has caused concern among safety professionals due to the presence of sparks during the cutting operations on certain metals. These sparks were analyzed as to their size, velocity, and temperature, and compared against unclassified military formulas for ignition probabilities. As a further test of the probabilistic model, abrasive waterjet tests were conducted against steel, titanium, and zirconium targets in flammable gas environments.

Organized and Sponsored by the WaterJet Technology Association

1. INTRODUCTION

The need to cut or process materials can often occur in areas where flammable gases, liquids, and solids are present. NFPA 70 (1996) classifies these environments as hazardous. Cutting metals using a heat-producing torch or saw in these hazardous locations is contraindicated because the flammable materials could ignite from either the process heat or from the incandescent swarf thrown from the process materials.

In recent years, non-traditional technologies for cutting materials have evolved and been perfected. Radically different from those used only twenty years ago, these non-traditional processes include ultrasonic machining, electrochemical machining, and fluid jet machining. As in any machining process, each of these processes contains certain advantages and disadvantages that must be understood before evaluating the risks and benefits. The purpose of this paper is to specifically address the hazards of using fluid jets for the abrasive cutting of metals in flammable environments.

2. STATEMENT OF PROBLEM

The use of abrasive fluid jet systems in flammable environments presents certain operational parameters that are of concern to the safety professional. The two major areas of concern are the mechanisms associated with abrasive fluid jets and the conditions that are required in order to initiate a flammable reaction within a hazardous environment. In order to properly evaluate the hazards associated with abrasive fluid jet cutting of materials within a flammable environment, an analysis of the processes and parameters for ignition was first performed which incorporated the military pyrophoric ignition model. Once these mechanisms were understood, a series of verification tests were performed in order to validate the model when used with abrasive fluid jets.

2.1 Mechanisms of Fluid Jet Operation

The abrasive fluid jet system works by pressurizing water (the most common fluid used) to high levels and converting the pressure to velocity by means of a small diameter orifice. Downstream of the orifice an abrasive stream is fed either by aspiration or by a compressed gas stream. The mixing of the fluid jet stream accelerates the abrasives to nearly one quarter the speed of the jet stream, which can be as high as 1000 $m \bullet s^{-1}$ (3300 fps). The high-velocity abrasive particles act as single-point cutting tools to remove small amounts of target material with each particle impact. The major components of an abrasive fluid jet machine are the hydraulic intensifier, the orifice assembly, and the abrasive mixing assembly. The intensifier increases the pressure of the water by means of hydraulic pistons from approximately 0.7 MPa inlet pressure to as high as 1000 MPa (150,000 psi). The upper limit of 1000 MPa is functionally set by the freezing point of water at room temperature. Currently, few systems are designed to operate at these pressures. Instead, most of the systems operate in the 200 to 400 MPa (30 to 60 Ksi) range to maximize the reliability of the equipment. The lower pressure is limited by the need for the kinetic energy of the cutting medium to exceed the yield strength of the target material.

Once the fluid jet is formed downstream of the orifice, the abrasive is entrained into the fluid stream in a mixing chamber. The three major fluid jet companies differ slightly in their approaches to entraining the abrasives with the same net results. The abrasive is fed from a hopper to the mixing chamber either by the suction formed by the passage of the fluid jet through a venturi, or by positive pressure. In either case, the abrasive is then fed into the water stream. In using positive pressure, excess gas is introduced. Since this excess gas is then entrained into the fluid jet stream, this process effectively lowers the density and performance of the mixture.

The final component of the fluid jet system is the focusing tube, typically fabricated from tungsten carbide or boron nitride. The function of the tube is to re-collimate the water stream that has been disrupted by the introduction of the large mass of abrasive that the fluid stream had to accelerate. The typical diameter of the focusing tube is about three times that of the orifice. A nominal abrasive fluid jet cutting combination would use a 3.6×10^{-4} m (0.014 inch) orifice in conjunction with a 1.1×10^{-3} m (0.043 inch) focusing tube.

2.1.1 Abrasive Fluid Jet Cutting Process

Abrasive fluid jet cutting is essentially forming a kerf by numerous individual abrasive grains These grains are accelerated by the fluid stream and act by gouging out minute particles (swarf) from the target material. To evaluate using fluid jets in hazardous locations, three considerations must be reviewed: the abrasive effects, the fluid stream spray, and spark formation from the swarf.

2.1.2 Abrasive Effects

The type, size, and quantity of abrasive used are all critical parameters for efficient cutting with the abrasive fluid jet system. A *de facto* industry standard is a variety of garnet abrasive mined by Barton Abrasives in upstate New York. Other materials that can be used as abrasives in fluid jet systems include copper slag, steel shot, silica sand, and olivine sand. Materials containing free silica, such as certain quartz sands, should be avoided due to their formation of both toxic silica fines and the potential generation of electric discharge from the piezoelectric action of quartz crystal deformation.

For typical fluid jet steel cutting operations, the abrasive size is usually specified as 180 microns (80 mesh). Abrasive materials finer than 100 microns can be used, but the cutting rate diminishes rapidly. Typical mass ratios of abrasive to fluid are 10% to 15%. According to Swanson (1987), the abrasive is accelerated under nominal conditions to well over 50 $m \cdot \bullet s^{-1}$ and may reach velocities in excess of 200 $m \bullet s^{-1}$ in the short distance through the focusing tube.

2.1.3 Spray Formation

The liquid fraction of the abrasive fluid jet remains coherent for less than a few thousand diameters from the orifice. The flow rate from the orifice, at 300 MPa, is about $7.5x10^{-5}$ $m^3 \bullet s^{-1}$ or about 4.5 liters per minute. During the cutting action, the temperature of the fluid jet rises from ambient to between 338 K and 353 K (65º and 80º C) because of the mechanical work added to the fluid from mechanical compression. (Although water is commonly thought of as incompressible, at the higher pressures used in fluid jet systems the water has about 11% compressibility.) After the jet stream has broken up due to dissipation or impact, the fluid is atomized and appears as a dense fog that is generally directed by momentum away from the cutting nozzle.

2.1.4 Spark Formation from the Swarf

The eroded pieces from the target material, known as swarf, are ejected under force from the cutting region and are collected along with the residual abrasive components for disposal. The swarf forms the most likely candidate for igniting hazardous material as the ejecta is potentially very hot from the energy imparted to it from the kinetic energy of the abrasive particles. The size of the swarf is governed to a large degree by the initial size of the abrasive particles forming it. The abrasive used in abrasive fluid jet cutting is substantially reduced in the process of fluid jet entrainment and may average only 50% of its original size. The impact of the abrasive grains in the mixing and focusing tubes of the fluid jet apparatus tends to attrit the grains into much smaller sizes. In a hazard analysis performed in 1992, swarf collected from cutting ASI 4130 steel with 180 micron (80 mesh) Barton garnet at 320 MPa (45 Ksi) water pressure yielded a mixture of garnet and steel distributed as shown in Table 1. The largest swarf particle found by scanning electron microscopy (SEM) was approximately 100 microns. The surfaces of the materials, both garnet and metal, showed distinctively sharp edges, precluding that neither material was subjected to sufficient heat to cause edge rounding or melting. This useful marker provided an upper limit for the localized heating effects at the point of swarf formation. The melting point of steel is about 1700 K (1400° C) and that of garnet-like materials is about 2300 K (2000º C). Since the materials were not melted, nor appeared from the SEM data to be oxidized, the actual temperature the swarf reached was much lower.

2.2 Flammable Material Ignition Parameters

In order for flammable materials to ignite, conditions that take the low-rate chemical decomposition kinetics to a rate high enough to propagate into a combustion wave must occur. These parameters are typically compatible concentrations of fuel and oxidizer, along with a suitable ignition source. Other parameters present can either encourage the reaction rate or inhibit the reaction growth.

2.2.1 Flammability Limits

Most materials require a separate oxidizer, such as oxygen from the air, to burn. The reactive combination of fuel and oxidizer is typically called the flammability range. Not all mixtures of flammable gases and air are reactive enough to generate sufficient heat to propagate or sustain a burning event. The lowest concentration limit for flammable vapor to propagate in a given atmosphere is the lower flammability limit (LFL) or the lean mixture limit, and the upper concentration limit is the upper flammability limit (UFL) or the rich mixture limit.

The flammability limits for hydrogen/air mixtures, according to Coward and Jones (1952), are between 4% and 74%. These flammability limits change radically with different combinations in the gas mixtures. Standard air contains about 21% oxygen and 78% nitrogen. The rest of the materials are gases such as argon and carbon dioxide. If the nitrogen content is replaced with a different diluent gas, for instance argon, the flammability limits may be substantially different and the ignition energies reduced.

The ultimate flammable mixture is the undiluted combination of a fuel and an oxidizer. Such mixtures are commonly found in liquid-fueled rocket engines which deliver the incredible energy releases necessary for space travel (Huzel and Huang, 1971). Many other operations may find an oxygen-enriched atmosphere (OEA) containing in excess of 21% oxygen. In OEAs the upper flammability limits are substantially increased while the lower limits are approximately the same as in air. The ignition energies are thus reduced by several orders of magnitude. According to NFPA 53 (1994), OEAs are so dangerous that even stainless steels will burn in them. The loss of three astronauts during a launch rehearsal in *Apollo-1* using an OEA may have been the most public loss, but numerous individuals are killed or injured each year in industrial accidents or during medical procedures in which OEAs are used.

Different chemicals require significantly different ignition energy levels in order to initiate a burning reaction. The energy levels for a wide range of materials are published in NFPA 53 (1994). A few representative materials have been selected for Table 2.

2.3 Ignition Sources

A flammable concentration alone is not sufficient for combustion to occur. An ignition source must supply the necessary energy of activation in order for the chemical reaction to proceed at a rate faster than the dissipation of energy into the environment. Typical ignition sources can be generalized as:

- Electric discharge sparks
- Thermal sources in excess of the autoignition temperature (AIT)
- Adiabatic compression
- Catalytic ignition
- Kinetic energy sparks
- Pyrophoric sparks.

2.3.1 Electric Discharge Sparks

The formation of electric discharge sparks from fluid spray is particularly important as the flow of liquid can easily contain several thousand volts due to triboelectric generation. This problem received worldwide attention in the late 1960s when three very large petroleum tankers ignited during water washdown operations. Safety hazard analyses by ESCIS (1988) identify that static electric charges occur in the following four circumstances: 1) liquids flowing through piping at rates greater than 1 $m \bullet s^{-1}$; 2) liquids passing through fine filters or orifices; 3) liquids being sprayed; and 4) liquids impacting fixed parts. These conditions essentially describe the entire fluid jet cutting process. In testing in which low conductivity water was used, a distinct pink corona discharge was present at the tip of the ungrounded waterjet focusing tube indicating ionization of the local air, not water vapor, according to Rosebury (1993). Based on ESCIS (1988), a large corona would have a static potential in excess of 3000 $kV \bullet m^{-1}$.

Vos (1971) further concludes that the charge generation is proportional to the square of the jet velocity and inversely proportional to the square of the fluid's conductivity. Additives to the fluid that improve the surface activity and fluid impact increase the charge generation.

The control of static generation can be achieved by proper grounding and bonding of the system components. Proper grounding and bonding procedures to eliminate spray charge accumulation are available from numerous sources such as NFPA 30, NFPA 77, chemical process handbooks such as Perry (1984), and military handbook MIL-HDBK-419 (1982). In addition, waterjet manufacturing companies, according to Reynolds (1998), can suggest proprietary fluid additives to minimize electrostatic generation.

2.3.2 Thermal Sources in Excess of Autoignition Temperatures

In order for flammable combinations of hydrocarbons in air to ignite from a thermal source, the thermal source must be of sufficient size and surface temperature must be in excess of 813 K (540º C), according to API Pub 2216 (1991). These thermal sources are commonly an exothermic flame source or a large heated piece of material, such as an exhaust manifold. This method of ignition is not likely with an abrasive fluid jet since the presence of massive quantities of liquid typically prevents component temperatures from exceeding 373 K (100º C).

2.3.3 Adiabatic Compression Ignition

Adiabatic compression is a process in which a gas is compressed mechanically, thereby raising the temperature of the compressed gas through mechanical work. This ignition through compression is the basic operating principal behind the diesel engine. Although the impact of the fluid jet stream can create localized pressures far exceeding the compression ratios of a modern diesel engine, the compressed area under the fluid stream is minuscule. Liquid flooding the area also limits any heat generation.

2.3.4 Catalytic Ignition

Certain chemicals substantially lower their energy of activation in the presence of specific catalytic materials. A classic reaction is the room temperature reaction of hydrogen in air in the presence of Raney nickel. The use of abrasive fluid jets on these certain materials may release finely divided catalytic reactants into the hazardous atmosphere and initiate a reaction. Metals that would release reactant catalysts for specific chemical mixtures would contain nickel, palladium, platinum, and, possibly, gold. Although cutting a precious metal with an abrasive fluid jet is unlikely because of the metal's intrinsic value, the potential for cutting high nickel alloys is possible. The presence of strong catalytic sources, however, would likely cause a surface reaction that would lead to an ignition long before the components were cut by the fluid jet. For this reason, the catalytic reaction process is also unlikely to be a major ignition source, but should be researched prior to any operations with hazardous materials.

2.3.5 Kinetic Energy Sparks

Bernstein and Young (1957) identify that three distinctively different types of sparks may form an ignition source in a flammable gas environment: friction sparks, impact sparks, or electrical sparks. Friction and impact sparks are similar in nature and are the result of two hard materials' respectively abrading or impacting each other. Electrical sparks are the result of a discharge between two items having different electrical potential. Although these three types of sparks may look identical, they perform very differently. Electrical spark ignition has a well-developed methodology, as detailed by Roux et al. (1993). Repeatable results can be achieved when electrode size, shape, and material are described along with the spark duration and gap. For these reasons most of the sensitivity tests on energetic materials are based on electrical spark initiation tests.

The energy levels required for electrical and impact sparks to ignite materials, however, may be significantly different and have different initiation mechanisms. The thermal ignition of materials is a physically complex task. In a study performed by Dixon-Lewis (1978), the minimum thermal ignition kernel, defined as the initial spheroid of ignited material, for non-pyrophoric metal in a hydrogen/air mixture, is approximately $2x10^{-3}$ m. Studies by Cutler (1974), Cutler (1978), Silver (1937), and Paterson (1940) investigate hot particle ignition of flammable gases. These studies show that for a given ignitable material, the temperature necessary for a given probability of ignition is inversely proportional to the heated particle's surface area. These studies also found that the temperature required for thermally hot particles to ignite hydrogen/air goes up significantly for particles less than $4x10^{-3}$ m in diameter. For $2x10^{-3}$ m diameter metal particles, the temperature required for Silver (1937) to give the 50% ignition probability in hydrogen/air was 1203 K (930º C), as compared with NFPA 325's (1994) hot plate ignition temperature of 773 K (500º C).

In Silver's (1937) work, hot particles fashioned from quartz spheres of various sizes were propelled through various gas samples, and the temperature of the particle varied. These particles were projected at about 4 $m{\bullet}s^{-1}$ (13 $ft{\bullet}s^{-1}$) through the gas mixture and the reaction, if any, was recorded. Paterson (1940) repeated Silver's work at slower speeds, 1.2 $m{\bullet}s^{-1}$ (4 $ft{\bullet}s^{-1}$), and duplicated the pronounced effect that particle size has on the thermal requirements to ignite a hydrogen gas sample. In addition, Paterson commented that the effect of particle speed had an even greater effect of shifting the ignition curves to hotter particles to achieve ignition, as shown in Figure 1. Since the swarf from an abrasive fluid jet is most likely traveling at some fraction of the initial abrasive particle velocity, it is likely that the thermal sparks are traveling at least a full order of magnitude faster than either Paterson's or Silver's test spheres.

Scull (1952) supports the suggestion that common metal sparks are incapable of igniting hydrocarbon vapors in air:

> "…Explosive mixtures of gasoline vapors and air at atmospheric pressure and temperatures of 70° to 120° F would not ignite when exposed to sparks produced by the impact breaking of piano wire, contact of two pieces of hardened steel, steel in contact with a rotating emery wheel, or the sparks from red-hot steel. Such sparks ordinarily lack the thermal energy required to ignite inflammable mixtures. Ordinary white friction sparks produced by grinding steel in air are actually small metal particles, which oxidize or burn in air after being initially heated by being torn off in the grinding process. These sparks ***will not ignite*** petroleum vapors unless the metal is held to the wheel for a long time to preheat the metal and thereby increase the thermal energy of the spark.…" (emphasis added)

Another form of kinetic energy heating is in the impact cratering of the surface as the energy is transferred from the striking abrasive particle to the target surface. Research performed by Titman and Wynn (1954) showed a 15% ignition probability in a hydrogen/air gas mixture when mild steel pieces impacted against each other with a force of about 500 joules. In the same series of tests, steel and brass spheres were projected at sandstone targets. The steel and brass spheres were 6.3×10^{-3} m (0.25 inch) in diameter and weighed 1.04×10^{-3} kg and 1.13×10^{-3} kg respectively. The 50% probability of ignition in a hydrogen/air atmosphere was about 17 joules. The kinetic energy transfer mechanism is also an unlikely ignition mechanism as the kinetic energy in a fluid jet abrasive particle is substantially less than one joule. Given that garnet has a density of about 3.8×10^2 kg•m^{-3}, the energy released from a 500 m•s^{-1} cubic particle of garnet of 180 µ on a side would be less than 280 mJ.

Finally, in a series of tests by Sanders, Griffiths, and Moodie (1980) with abrasive slurry jets on mild steel and sandstone, the cutting process did not ignite hydrogen/air or methane/air mixtures in their test chambers. Unfortunately, these tests used a cutting process that is different from the abrasive fluid jet systems more commonly used today. According to Sanders (1982) the pressures in these early tests were limited to about 35 MPa to 85 MPa, compared to the 300 MPa systems currently used, and the abrasives used were either copper slag or sand rather than today's garnet. None of these tests, however, attempted to cut pyrophoric metals.

2.3.6 Pyrophoric Metals

Certain metals are classified as pyrophoric and require very little energy to cause an extensive release of thermal energy. These metals are not just releasing the thermal energy that was kinetically imparted to them by an abrasive particle, but are actually exothermicly reacting (burning) in the atmosphere, either spontaneously, or when the surface is abraded. A study performed on incendiary metals for military applications by Hillstrom (1973) identified fourteen pyrophoric metals; an additional five metals have since been suggested as being pyrophoric (see boxed area in Figure 2). Metals tend to be pyrophoric, according to the military's formula, if the oxide volume is larger than the parent metal volume *and* the free energy of oxide formation per oxygen atom exceeds approximately -105 kg-cal/mole, as shown in Figure 2. According to the formula, iron (steel) would not be pyrophoric, whereas titanium would be marginally pyrophoric, and zirconium would be markedly pyrophoric.

2.3.7 Ignition Inhibition

The opposite of an ignition source is an ignition inhibitor. Certain materials can radically modify the LFL and UFL of flammable vapors by either thermal or thermal chemical effects. The most pronounced effects are those of halogenated compounds that actively interfere with the ignition process. Less effective than the halogen compounds are the "inert" gases, principally carbon dioxide, water vapor, nitrogen, helium, and argon. Segeler (1965) states that the effectiveness of the inerting gases is in the order stated, namely CO_2, H_2O, N_2, He, and Ar. These materials act by displacing the oxidizer from the reaction zone of the ignition kernel and by directly removing heat from the reaction zone. As stated earlier, the substitution of certain noble gases, such as argon, for atmospheric nitrogen may actually increase the ignition potential, while the introduction of large quantities of water vapor may inhibit the chance of ignition through energy absorption.

This concept of ignition inhibition by removing energy from the reaction is supported by Mitani (1983) in his work on the use of liquid sprays to prevent ignition. In the normal course of the operation of an abrasive waterjet, over 7.5×10^{-5} $m^3 \bullet s^{-1}$ (1.1 gpm) of water is directly injected into the zone of cutting and is atomized into a dense fog. It is highly possible that in some cases the ratio of water mist to the existing flammable atmosphere creates its own inert gas blanket around the cutting operation that extends for some distance in all directions. As shown in Table 3, water vapor has been proven to be a significant ignition inhibitor in the case of hydrogen gas and hydrocarbon ignition.

2.3.8 Summary of Ignition Process

The process of abrasive fluid jet cutting of metals in hazardous environments contains many of the potential mechanisms for ignition of common flammable materials. For these reasons, the entire process for fluid jet cutting was tested in a series of controlled test cuts using four different metals using an abrasive water jet at 300 MPa (45 ksi) in a series of flammable hydrogen gas environments of differing minimum ignition energy levels. Hydrogen was chosen as being both the most sensitive flammable material and a common reference test material. The use of hydrogen also provides additional statistical margin for operations using abrasive waterjets in the hydrocarbon/air mixtures. The minimum ignition energy for aliphatic or aromatic hydrocarbon/air mixtures are a full order of magnitude greater than that required to ignite hydrogen/air. Likewise, hydrocarbon/air MIE are almost two hundred times greater than the MIE for the hydrogen/oxygen mixture.

3. TEST METHODOLOGY

3.1 Test Overview

In order to test the limits of abrasive fluid jet hazards, a series of tests was arranged to pierce cut various metals with an abrasive waterjet inside of a controlled atmosphere of flammable gases. The test materials included ASI 1020 low carbon steel, ASI 4130 chrome-molybdenum steel, titanium, and zirconium metals. Atmospheres ranged from hydrogen/air to hydrogen/oxygen. The metals were cut using a 300 MPa (45 ksi) waterjet using 180 micron (80-mesh) Barton 80 HP garnet. A series of forty-five plunge cuts established statistical accuracy. The plunge cut was chosen to maximize the potential for spark formation.

3.2 Test Chamber

Due to the potential hazards of performing a series of tests in OEAs, the cubic test chamber was limited to about 2.8×10^{-2} m^3 (1 ft^3) and constructed of 9×10^{-3} m (3/8 inch) steel plate in accordance with TM5-1300 (1992). Construction of the chamber utilized full penetration welds followed by interior surface polishing to minimize surface effects on the testing. The chamber was proof-tested at 150% maximum expected pressure prior to being placed into service. The volume of the box was adjusted with internal void-filling objects to achieve 2.53×10^{-2} m^3 (0.89 ft^3), which equates to one mole of gas at a room temperature of 293 K (20º C).

To achieve visibility for photographic purposes the front closure plate was constructed of two redundant sheets of 3×10^{-3} m (1/8 inch) Lexan™ polycarbonate and restrained using 3×10^{-3} m (1/8 inch) cross wires. The pressure relief vent consisted of the rear side's being left open and covered with 4×10^{-5} m (0.002 inch) aluminum foil. The foil was secured using 1.2×10^{-2} m wide strip magnets to form a gas-tight seal. In order to discharge the atmosphere in the event of a "failure to ignite" from the cutting action, a hole was drilled and threaded into one of the side plates and a sparkplug was inserted. Electrical energy for the sparkplug was provided by a 5 kV ignition transformer.

3.3 Test Setup

The testing was performed at Ingersoll-Rand's McCartney Works facility in Baxter Springs, KS, during the last week of 1998. An Ingersoll-Rand *Streamline II™* waterjet intensifier, using high-purity water from their reverse osmosis water polishing system, was used to deliver 7×10^{-5} $m^3 \bullet sec^{-1}$ (1.1 gpm) at 300 MPa (45 ksi) with 0.5 $kg \bullet min^{-1}$ (1.1 $lb \bullet min^{-1}$) Barton 80 HP garnet aspirated into the cutting head assembly. The test chamber cutting head was set up with a

$3.6x10^{-4}$ m (0.014 inch) diameter diamond orifice and a $1.02x10^{-3}$ m (0.040 inch) Borazon™ focusing tube. The fixture was arranged so that the nozzle maintained a $3x10^{-3}$ m (0.13 inch) standoff from the target plates. Specific attention was paid to assure that the equipment was properly grounded and bonded per military safety regulations.

The metal plates were positioned in the test chamber and the test chamber sealed using the aluminum foil blowout panel and the magnetic strips. A purge line to the chamber was left open and the chamber was flooded with either compressed shop air or CGA specification Type I, Grade A-E oxygen, depending on the oxidizer fill required for the test sequence. To maximize the ignition sensitivity of the flammable gas mixture, the chamber was filled with a measured amount of CGA specification Type I, Grade A-D hydrogen gas. The fuel/oxidizer mixture was determined from Lewis and von Elbe (1961) as 20% H_2 in air and 30% H_2 in oxygen.

The mixtures provided a range of minimum ignition energies over an order of magnitude, thereby allowing the ignition potential to be bracketed. This procedure allowed for certain metals to ignite gas mixtures at different levels of sensitivity. The sensitivity of hydrogen in an OEA is too dangerous for the mixture to be safely handled except in extremely rare and controlled conditions. According to Berkey et al. (1988), the human body can store many times the energy necessary to achieve the minimum ignition energies needed for hydrocarbon ignition. The static discharge from touching a metal object in such atmospheres can result in serious injuries. The oxygen-enriched mixtures used were quite capable of developing a high-order detonation in excess of 2500 $m \bullet sec^{-2}$, or approximately that of a primary high explosive, as shown in (Lewis and von Elbe, 1961).

During testing, the operators retreated approximately 5 meters (15 feet) from the test chamber and remotely operated the waterjet equipment. The pneumatic actuating valve for the cutting head was attached to an automatic sequencing timer set to cut for approximately 8 seconds, sufficient time to cut through the metal targets. “Successful” ignitions were determined by the rupture or blow-off of the safety relief vent covered with aluminum foil. In the event of an ignition “failure,” the chamber was intentionally ignited by the sparkplug igniter to purge the hazardous mixture. The test chamber and target were then cleaned prior to the next test.

3.4 Test Samples

Test coupons used in these tests were $6.25x10^{-3}$ m (0.246 inch) ASI 1020 steel, $6.8x10^{-3}$ m (0.268 inch) ASI 4130 steel, $6.4x10^{-3}$ m (0.252 inch) chemically pure (CP) titanium, Gr. 2, and $7.53x10^{-3}$ (0.296 inch) zirconium 730. These materials contained certifications that indicated compliance with either ASI or military specifications.

3.5 Data Collection and Reduction

The data collecting and reduction for the testing was managed by M&R Services using 35 mm still photography, high resolution videography, acoustic recording, and computerized data management.

4. RESULTS

The testing of the different metals with the abrasive fluid jet at the different sensitivities yielded the results shown in Table 4.

The ignition event was very fast as shown in the sequence of pictures taken from the video of cutting zirconium metal in an oxygen atmosphere. Note that the time sequence is only one frame apart in Figures 3-a through c. Figure 3-d shows the sparks from cutting zirconium metal. Few, if any sparks were visible from cutting steel. Titanium provided an intermediary level of sparking.

Most tests were terminated when five ignitions occurred within the test sequence. Exceptions to this pattern were 4130 steel and zirconium. Additional tests were included with 4130 steel in oxygen-enriched hydrogen due to the randomness of the ignitions. Only two tests were conducted on zirconium in oxygen-enriched hydrogen because the gas mixtures detonated both times. None of the other 250 ignitions (the “failures” were also intentionally ignited by the electric sparkplug) created the shock wave that the zirconium ignitions produced with oxygen-enriched hydrogen.

The metals all sparked to different degrees. The two steels produced different types of sparks based on their alloying elements. The titanium and zirconium produced a profusion of bright white sparks, typical of these metals. The zirconium was so sensitive to spark formation that sparks were produced when shop air was used during the cleaning process to blow off the residual abrasives.

5. DISCUSSION

The results of the testing indicate that abrasive fluid jets using water and 180 micron garnet abrasives can cut certain metals in the most dangerous flammable hydrogen environments, and almost any metal in flammable gas/air mixtures. The tests also indicate that some risk remains when pyrophoric metals are cut using abrasive waterjets in those environments. The number of tests were statistically significant and delivered a usable statistic. The statistical analysis of the testing as shown in Table 4, demonstrated that in a binomial probability for single-sided events, the majority of tests of hydrogen in air achieved a 95% safety margin at a 90% confidence interval. The reader is cautioned that even with the large numbers of tests performed, some level of uncertainty always remains.

Certain systematic errors may affect the statistics either positively or negatively in field operations. The published data on minimum ignition energies may be accurate for certain laboratory test setups, but actual field conditions may be safer as flammable gas mixtures outside of controlled conditions may require substantially higher energy levels to ignite. Changes in the equipment setup, such as abrasive, orifice, or focusing tube sizes, may, however, adversely affect the results.

6. CONCLUSIONS

The presence of sparks from abrasive fluid jets has been a concern of safety professionals. An analysis of the spark mechanisms from fluid jets was compared with military studies on ignition of flammable materials. From this comparison it was concluded that the abrasive fluid jet cutting of metals does follow the prediction obtained from the military studies on incendiary materials. These predictions state that steels would be safe to cut, titanium would be marginally safe, and zirconium would pose a substantially higher risk than either steel or titanium.

In an effort to validate these conclusions, a series of live tests were performed. The series of tests performed on cutting ASI 1020 steel, ASI 4130 steel, titanium, and zirconium metals with an abrasive waterjet in a flammable gas environment showed that there is a very low probability of ignition while cutting these metals in a typical flammable gas environment using abrasive waterjets. This conclusion should not be construed as a minimization of the very real risks in operating any equipment in such an environment. Although the action of the abrasive fluid jet may not ignite the hazardous materials, all other ignition sources must be adequately addressed as even the impact when the cut-off object drops may be sufficient to ignite certain atmospheres.

A review of the ignition sources has reduced the probable ignition mechanisms associated with abrasive fluid jet cutting operations to electrostatic ignition and pyrophoric metal reactions. With proper grounding and bonding, the electrostatic mechanism can be reasonably controlled. The cutting of pyrophoric metals in a flammable atmosphere may be more difficult to completely control. Whenever possible, the area where pyrophoric metal cutting is to be performed should be inerted with an inert gas blanket. If possible, the use of a water blanket to submerge the items to be cut may provide additional safety.

The results showed that the risks of cutting of ASI 1020 steel in oxygen-enriched hydrogen is acceptably low enough to be considered safe, while the risks of cutting ASI 4130 is not. When the hazard for cutting either steel with an abrasive waterjet in a hydrocarbon/air mixture is calculated, the almost 200 times higher sensitivity of the hydrogen/oxygen combination provides sufficient justification for the safety of the abrasive fluid jet. For cutting steels in flammable hydrocarbon environments, the fluid jet method may be the safest cutting method available. The data from the cutting of the two pyrophoric metals provides a safety margin of almost an order of magnitude over that required to ignite hydrocarbon/air mixtures. For most operations, this safety margin will be quite adequate as field conditions will rarely achieve the optimum fuel mixtures and quiet air conditions that are seen in the testing laboratories.

The use of abrasive fluid jet cutting systems for cutting metals in hazardous environments appears to be an acceptable risk under most circumstances. In special cases in which the sensitivities of the hazardous mixtures or reactivity of the metal being cut are extreme, additional verification tests should be performed. The safety professional must always evaluate both the probabilities and the consequences when passing judgment where personnel or property is at risk.

7. REFERENCES

API Pub. 2216, 2nd ed., Ignition Risk of Hydrocarbon Vapors by Hot Surfaces in the Open Air, American Petroleum Institute, January 1991.

Berkey, B. D., Pratt, T. H., Williams, G. M., "Review of Literature Related to Human Spark Scenarios," *Plant / Operations Progress*, Vol. 7, No. 1, p. 32, Jan 1988.

Bernstein, H. and Young, G., *Sparking Characteristics and Safety Hazards of Metallic Materials, NAVORD RPT 5205, (AD 127 905) [Unclassified - Distribution Unlimited]*, p. 1, 8 Apr. 1957.

Coordinating Research Council, *Handbook of Aviation Fuel Properties (ADA 132 106) [Unclassified - Distribution Unlimited]*, Table 8, Society of Automotive Engineers, 1983.

Coward, H. F., and Jones, G. W., *Limits of Flammability of Gases and Vapors, U.S. BuMines Bull 503*, p. 17, 1952.

Cutler, D. P., "The Ignition of Gases by Rapidly Heated Surfaces," *Combustion and Flame*, Vol. 22, pp. 105-109, 1974.

Cutler, D.P., "Further Studies of the Ignition of Gases by Transiently Heated Surfaces," *Combustion and Flame*, Vol. 33, pp. 85-91, 1978.

Dixon-Lewis, G., "Effect of Core Size on Ignition Energy by Localized Sources," *Combustion and Flame*, Vol. 33, p. 320, 1978.

Expert Commission for Safety in the Swiss Chemical Industry (ESCIS), "Static Electricity: Rules for Plant Safety," *Plant/Operations Progress*, Vol. 7, pp. 4 and 17, January 1988.

Hillstrom, W. W., *Formation of Pyrophoric Fragments, BRL MR 2306 (AD 765 447) [Unclassified - Distribution Unlimited]*, p. 11, Ballistic Research Laboratories, Aberdeen Proving Ground, MD, June 1973.

Huzel, D. K., and Huang, D. H., *Design of Liquid Propellant Rocket Engines, NASA SP-125, 2nd ed. [Unclassified - Distribution Unlimited]*, p. 27, National Aeronautics and Space Administration, 1971.

Lewis, B., and von Elbe, G., *Combustion, Flames and Explosions of Gases, 2nd ed.*, p. 333, Academic Press, Inc., 1961.

Lyman, Taylor, ed., *Metals Handbook*, p. 20, American Society for Metals (ASM), 1948.

M&R Services, 113 Wandering Lane, Suite 301, Harvest, AL 35749-8266.

MIL-HDBK-419 Grounding, Bonding, and Shielding [Unclassified - Distribution Unlimited], Department of Defense USGPO.

Mitani, Tohru, "A Flame Inhibition Theory by Inert Dust and Spray," *Combustion and Flame*, Vol. 43. p. 243, 1983.

NFPA 30, Flammable and Combustible Liquid Code, National Fire Protection Association, Batterymarch, MA, 1996.

NFPA 325 Fire Protection Guide on Hazardous Materials, 8th ed., Table 325M-59, National Fire Protection Association, Batterymarch, MA, 1984.

NFPA 53, Fire Hazards in Oxygen Enriched Atmospheres, National Fire Protection Association, Batterymarch, MA, 1994.

NFPA 70, National Electric Code, Article 500 (Defined as Class I or Class II hazardous locations), National Fire Protection Association, Batterymarch, MA, 1996.

NFPA 77, Static Electricity, National Fire Protection Association, Batterymarch, MA, 1996
O'Donoghue, Michael, *A Guide to Man-Made Gemstones*, p. 23, Van Nostrand Reinhold, 1983.

Paterson, Stewart, "The Ignition of Inflammable Gasses by Hot Moving Particles", *Phil. Mag. S. Series 7*, Vol. 30, p. 443, December 1940.

Perry, R. H., ed., *Perry's Chemical Engineers' Handbook, 6th ed.*, McGraw-Hill Book Company, New York, NY, 1984.

Reynolds, R.E. (Skip), Ingersoll-Rand Waterjet Division, *Personal Communication*, December 1998.

Rosebury, F., *Handbook of Electron Tube and Vacuum Techniques*, p. 213, American Institute of Physics, New York, NY, 1993.

Roux, Michel, Auzanneau, Max, and Brassy, Claude, "Electric Spark and ESD Sensitivity of Reactive Solids (Primary or Secondary Explosive, Propellant, Pyrotechnics), Part One: Experimental Results and Reflection Factors for Sensitivity Test Optimization," *Propellants, Explosives, Pyrotechnics*, Vol. 18, p. 317, 1993.

Saunders, D. H., "A Safe Method of Cutting Steel and Rock," Paper K5, *6th Int. Symposium on Jet Cutting Technology*, p. 505, BHRA Fluid Engineering, 1982.

Saunders, D. H., Griffiths, N., Moodie, K., *Water Abrasive Jet Cutting in Flammable Atmospheres, RR1608*, British Hydrodynamic Research Association Fluid Engineering, June 1980.

Scull, W. E., *Relationship Between Inflammables and Ignition Sources in Aircraft Environments, NACA TR 1019 [Unclassified - Distribution Unlimited]*, p. 315, National Advisory Committee for Aeronautics, USGPO, 1952.

Segeler, C. George, ed., *Gas Engineers Handbook*, p. 2-75, American Gas Association, 1965.

Silver, Robert, "The Ignition of Gaseous Mixtures by Hot Particles," *Phil. Mag. S.*, Vol. 23, No. 156. Suppl., p. 647, April 1937.

Swanson, R. K., Kilman, M., Rarver, W., and Wellman, R., "The Study of Particle Velocities in Water Driven Abrasive Jet Cutting," *Proc. 4th U.S. Waterjet Conference*, p. 103, ASME, 1987.

Titman, H., and Wynn, A. H. A., *The Ignition of Explosive Gas Mixtures by Friction, Research Report No. 95*, p. 12, Ministry of Fuel and Power (UK) Safety in Mines Research Establishment, July 1954.

TM5-1300 Structures to Resist the Effects of Accidental Explosions (AD M000 097) [Unclassified - Distribution Unlimited], Department of Defense Explosive Safety Board, 1992.

Vos, B., "Electrostatic Charge Generation during the Washing of Tanks with Water Sprays -IV: Mechanism Studies", *Static Electrification*, Institute of Physics, London and Bristol, May 1971.

Wynn, A. H. A., *The Ignition of Firedamp by Friction Research Report No. 42*, p. 14, Ministry of Fuel and Power (UK) Safety in Mines Research Establishment, July 1952.

8. NOMENCLATURE

AIT	Autoignition Temperature
BHRA	British Hydrodynamic Research Association
CGA	Compressed Gas Association
CP	Chemically pure
ESCIS	Expert Commission for Safety in the Swiss Chemical Industry
LFL	Lower Flammability Limit
MIE	Minimum Ignition Energy
NFPA	National Fire Protection Association
OEA	Oxygen-Enriched Atmosphere
SEM	Scanning Electron Microscopy
UFL	Upper Flammability Limit

Table 1. Distribution of Particle Size in Swarf Created from Cutting ASI 4130 Steel with 180 Micron Garnet

Micron Size	< 10	10-20	20-30	30-40	>40
Percent	55.7%	26%	12.3%	3.7%	2.3%

Table 2. Energy Levels and LFLs and UFLs of Hydrogen and Common Hydrocarbons
[From Coordinating Research Council (1983), Lewis and von Elbe (1961), and NFPA 53 (1994)]

	Minimum Ignition Energy (MIE) (mJ)		LFL/UFL (mol%)	
Material	**Air**	**Oxygen**	**Air**	**Oxygen**
Hydrogen	0.02	0.001	4.0-75	4.0-95
Av Gasoline (87 Octane)	0.20		1.2-7.0	
Jet-A	0.20		0.6-4.7	
Jet-B (JP-4)	0.20		1.3-8.0	
Benzene	0.22		1.3-7.9	1.3-30
Butane	0.25	0.009	1.8-8.4	1.8-49
Ethane	0.25	0.002	3.0-12.4	3.0-66
Propane	0.25	0.002	2.2-9.5	2.4-57
Hexane	0.29	0.006	1.2-7.4	1.2-52
Methane	0.30	0.003	5.0-15	5.1-61
Toluene	2.50		1.2-7.1	
Ammonia	>1000.0		15.0-28	15-79

Table 3. Water Vapor's Inhibiting Effects on Hydrogen and Methane
[Adapted from Segeler (1965)]

Percent Water Vapor in Air	Flammability Limit (LFL/UFL) for Hydrogen	Flammability Limit (LFL/UFL) for Methane
0%	4-74%	5-15%
50%	8-72%	9-18%
67%	13-71%	14-28%
75%	18-71%	19-33%
80%	25-71%	26-35%
83%	31-71%	34-36%
86%	38-70%	INERT
88%	47-68%	INERT
89%	INERT	INERT

Table 4. Test Results

Target Mat'l	**Mixture**	**MIE (mJ)**	**Total Tests**	**Ignitions**	**Percent Ignitions**	**Safety Interval @ 90% CI***
1020	H2/O2	0.0012	45	0	0%	95%
4130	H2/O2	0.0012	58	7	12%	80%
4130	H2/Air	0.0170	45	0	0%	95%
Ti	H2/O2	0.0012	7	5	71%	0%
Ti	H2/Air	0.0170	45	0	0%	95%
Zr	H2/O2	0.0012	2	2	100%	0%
Zr	H2/Air	0.0170	50	2	4%	90%

* Calculated on Honeywell Defense Systems Division's *Reliability Computer* for one-shot devices.

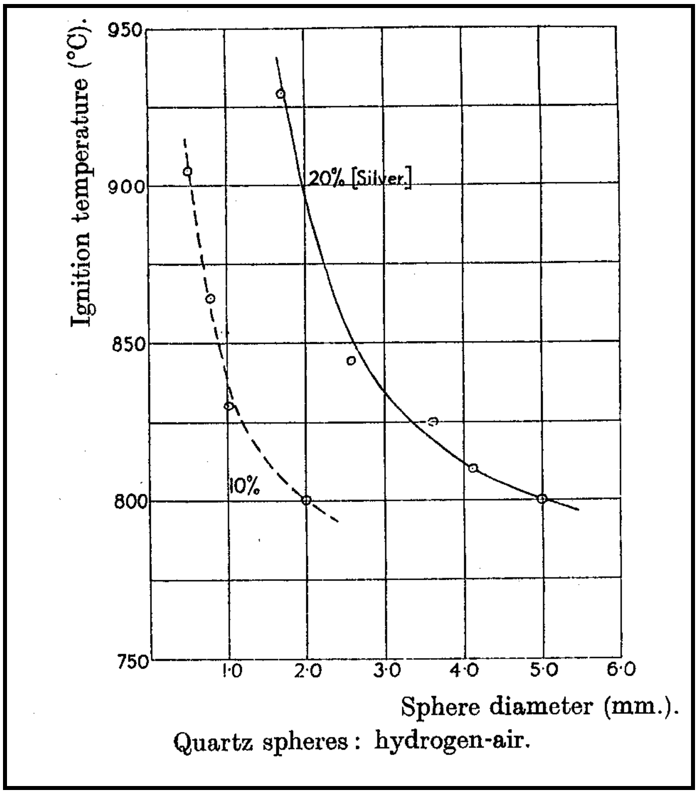

Figure 1. Paterson's (10% H_2 at 1.2 m•s^{-1}) and Silver's (20% H_2 at 4 m•s^{-1}) Test Data

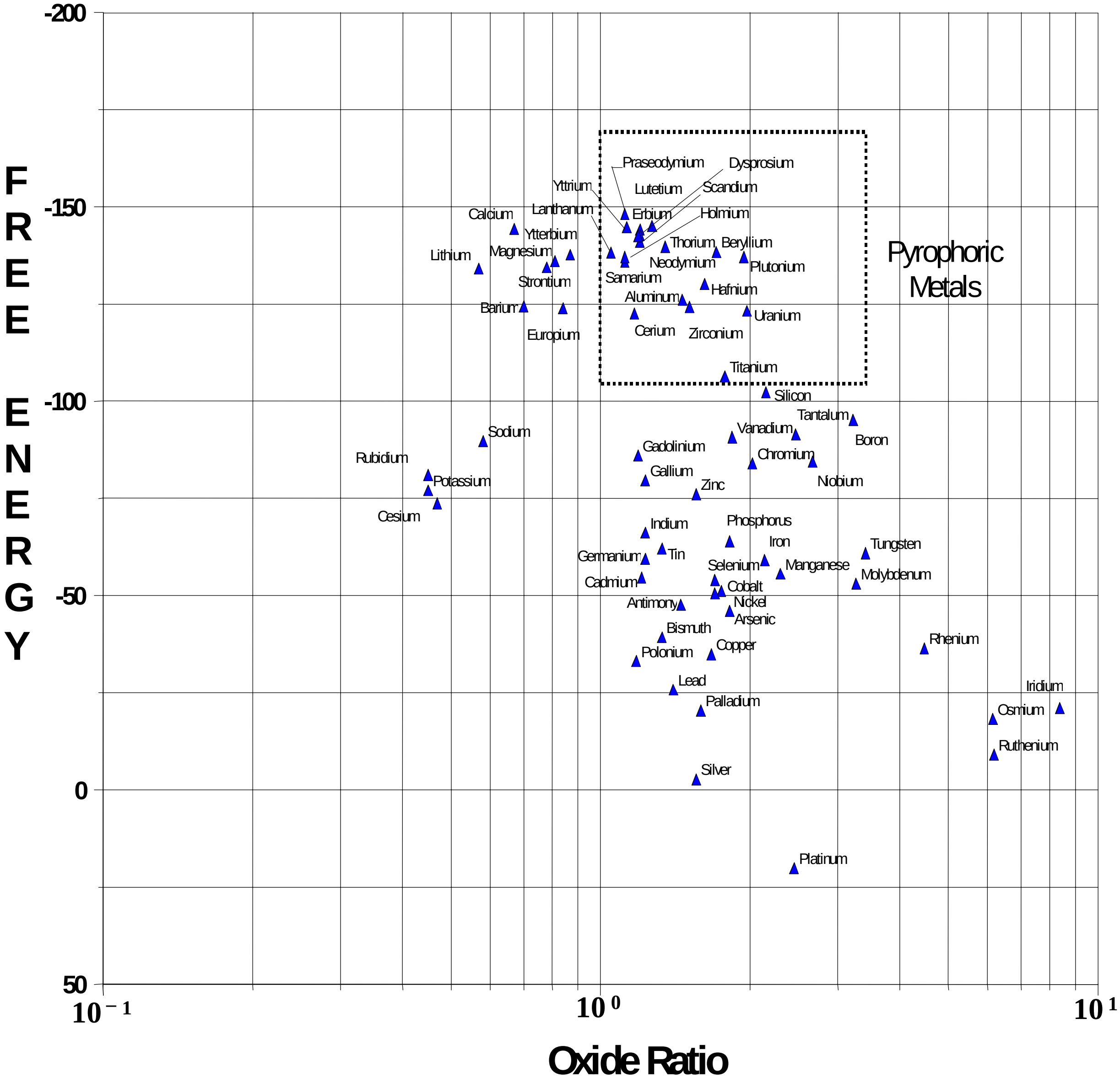

Figure 2. Pyrophoric Metals
[From Paterson (1940)]

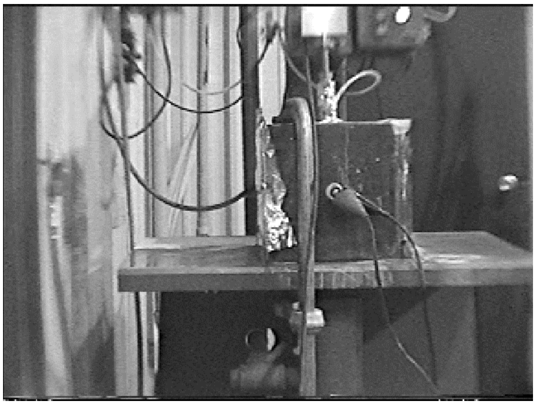

Figure 3-a. T= –0.03 seconds

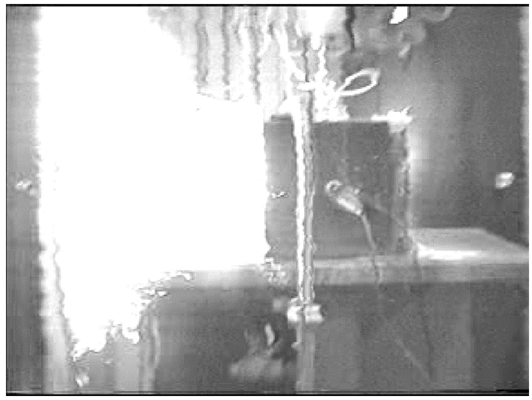

Figure 3-b. T= 0.00 seconds

Figure 3-c. T= +0.03 seconds

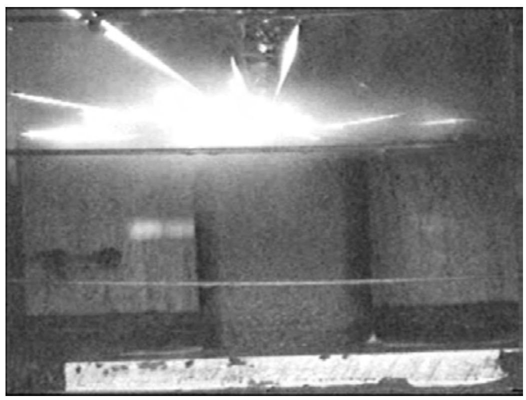

Figure 3-d. Zirconium spark

10th American Waterjet Conference
August 14-17, 1999: Houston, Texas

Paper 71

ULTRA HIGH PRESSURE WATERJETTING

FOR COATING REMOVAL

Richard F. Schmid
Flow International Corporation
Kent, Washington, USA

ABSTRACT

Ultra high pressure (UHP) waterjetting is gaining acceptance as an alternate and many times preferred method of surface preparation. However, knowledge of its applications and advantages is somewhat unknown in the industry. This paper will focus on several actual case studies of projects where waterjetting has been used.

Organized and Sponsored by the WaterJet Technology Association

1. LEAD BASED PAINT REMOVAL - HAND HELD WANDS

The first case study involves removal of lead based paint with hand held UHP waterjetting lances from a large Navy vessel.

The vessel name was the Cape Inscription; it is a roll on, roll off transport shipowned by the United States of America acting through the Maritime Administration Department of Transportation, (MARAD); it is part of the ready reserve fleet. American Presidents Line (APL) is the contracted manager of the vessel. Specifications for the project and management of the project was the responsibility of APL.

The original plan for this project was to strip and recoat the entire outside surface of the ship. The first phase of the project of work was done on the freeboard and underwater hull of the ship; this segment was specified and conducted with conventional gritblasting and recoating and was completed as planned. When tests were conducted on the above deck surfaces and structures, lead based paint was discovered and the project was halted. The specifications were then rewritten and the project was sent out for rebidding.

The change in the specifications revolved around changing the standard of surface preparation from conventional gritblasting to ultra high pressure waterjetting. Waterjetting was recognized as having both ecological and cost savings benefits for this project.

This second stage totaled a removal of 99,458 square feet using UHP waterjetting.

Lead based paint removed from all areas above deck line

The areas to be stripped and recoated were virtually all surfaces including all exterior bulkheads and structures above the deck.

The project was awarded to a local San Pedro, California boat yard; they were awarded the contract as the general contractor. Their scope included all phases of project management, surface preparation, water control and filtration, staging, and re-application of the coating. This case study will focus on the unique aspect of this project which was the use of UHP waterjetting as the means of surface preparation.

Worker removing lead based paint with hand held waterjet lance

The surface preparation was one of the most critical phases of this project. The general contractor was very careful in their selection of the UHP waterjetting subcontractor. They selected a large waterjetting contractor out of Newport News, Virginia to do the UHP waterjetting. This was based on their broad background in the use of waterjetting for coating removal on vessels combined with their experience in removing lead based coatings and their past experience of working on other MARAD vessels.

The specifications required a minimum of 35,000 psi waterjetting . However, the waterjetting contractor selected three 40,000 psi pumps to maximize productivity.

Water treatment system

Because the coating contained lead, care had to be taken to contain, collect, filter, and dispose of the water. The ships deck drains were modified to contain and collect the water as well as paint chips and then discharge to the filtration system. The outside deck drains were closed off to eliminate the water from draining into the bay. The remaining deck drains were carefully tied together to discharge all the water and paint chips to the filtration system.

The water was collected on the dock in large Baker tanks where the water was then filtered and discharged to the Los Angeles city sewer system. Prior to initial discharge, run off water was tested at an independent lab and results were presented to the Los Angeles Water Authority and permits were issued for the water to be discharged as a standard industrial waste water.

2. TANK FLOOR REMOVAL - ROBOTIC WATERJETTING TOOL

The second case study involves using a 40,000 psi waterjet robotic surface preparation system. This project was conducted by a specialty surface preparation and coating contractor from Sulfur, Louisiana. The robotic system used was a vacuum attached robot that both stripped all coating and transported all water and coating to a filter system where coating was filtered out in 1 cubic yard bags.

The project entailed removing all fiberglass bonded epoxy coating from the bottom and 2 feet up the sides of a fuel storage tank for inspection of the tank floor. Coating thickness was up to100 mils in many places. The project was to determine if the floor should be replaced or repaired. The tank was constructed in 1954 for a Lake Charles, LA based oil refinery. The tank was 150 feet in diameter, and the total area removed on the floor was 20,000 sq. ft. The tank had been out of service for approximately 6 years.

Prior to work startup, the top was cut off the tank because it needed replacement. An access door (approximately 10'x12') was cut in the side of the tank to allow for easy access in and out of the tank. The tank was degassed and monitored daily to allow for safe operations inside of the tank.

The reason the coating was removed was to allow the bottom of the tank to be inspected for corrosion by visual inspection, magnetic imaging reading and sonogramming.

Filtration bag full of paint solids being disposed of

Hand held tools were used to strip the coatings around the detailed features where the robot could not reach. All detail work was cut back 8 to 12 inches from the features to allow for the robot to easily maneuver into these areas. Edge work took approximately 9 hours to complete. Detail work with hand tools was done prior to robotic work to prevent waterjetting from contacting area already cleaned by robot and causing light flash rusting.

Hand held waterjet lance used to remove coating in edges and around areas non accessible by robot

Robot in full operation - Note paint ready surface immediately behind robot

The waterjetting robot was used to remove coatings 2 feet up around the entire inside circumference of the tank. Next, the robot was used to remove the coating from the entire 20,000 sq. ft of tank bottom. All removed coating was filtered out into one cubic yard filter bags; ten bags were filled during the project. All coating was captured in these bags and water was filtered out.

The entire project was conducted in only 6 days; there were a total of ten bags of spent coatings collected. Average production rate was 465 sq. ft./hr. Previously, gritblasting had been used, and it was very costly to collect and dispose of the grit. All grit had to be transported back out of the opening in tank and loaded in trucks; 20 roll off tanks were required to hold the spent abrasive. Disposal costs were $850/per roll off container, plus transportation costs. Future costs are expected to rise due to tighter restrictions.

Close up of lap welds - Robot had to seal over welds up to 3/4 inch high

Sonogram machine

Beyond reducing overall project costs by eliminating grit disposal costs, waterjetting offered the following advantages on this project. Sonogramming was conducted during waterjetting. With gritblasting, sonogramming could not be conducted until all work was completed and grit was removed. The prepared surface was cleaner; 40,000 psi water pressure was able to clean the smallest pits and not pack them with sand. Workers were not exposed to abrasive blast dust or to the fiberglass epoxy coating in dust form and worker fatigue was also reduced.

3. SHIP COATING REMOVAL - ROBOTIC WATERJETTING SYSTEM

The third case study involves using a 40,000 psi waterjetting robotic surface preparation system to remove the coating from a small cargo ship.

The project entailed removing the failed coating from a 220 ft. bulk cargo ship. The ship was in drydock for a major conversion which included a 30 ft. mid-section extension. While in dock, all coating was to be removed. The coating system on the freeboard was a standard marine epoxy system that had failed in many places. This coating was very easy to remove with the waterjetting robot; removal rates were in excess of 650 sq. ft./hr.

Robotic system in full operation on vertical surface of ship

The surface of this ship was in extremely poor condition; there were many dents that measured over 12 inches deep. The robot was able to crawl over most dents and irregularities. Most areas were accessed by moving the robot from top to bottom. However, some of the larger areas were accessed by operating the robot horizontally.

Robot in full operation - upside down - removing coatings from bottom of hull

The bottom of the hull was also prepared using the robot operated in the overhead position. The areas accessible with the robot were very small due to the complexity of the dolly that the ship was mounted on. Areas not accessible with the robot were cleaned using hand held lances.

The water was filtered from the collected paint and corrosion product. Paint and corrosion was left in the 1 cubic yard haul away filter bags and water filtered through the bag. The filtered water was tested and determined clean enough to be disposed of into the central waste water system.

Waterjetting offered many advantages on this project. First and most important, it reduced project cost by eliminating the need to purchase, collect and dispose of grit. Second, it allowed for welding and steel work to be conducted right adjacent to the stripping operation which would not have been possible with gritblasting which reduced overall project cost. Also, due to the vacuum system, the robot prepares a paint ready surface that can immediately be coated. Coating just after the removal eliminates the risk of weather induced flash rust.

4. PETROCHEMICAL TANK COATING - ROBOTIC WATERJETTING

The project entailed removing the lead based paint from the sides and top of a floating roof petroleum storage tank in Lake Charles, LA. The tank measured 200 ft. diameter and was approximately 35 ft. high. Because of high level of lead in the coating, extreme precautions were required for the project.

The specifications called for a two step process to be used; the first step to be the removal of the coating with a special sandblast nozzle surrounded with a water ring to wet the grit and dust. The second step was a light sweep blast just prior to coating to remove any flash rust caused by weather, or from the water ring on the sandblast nozzle.

Robot removing coating from side of petrochemical tank - note paint ready surface right behind robot

A specialty coating contractor of Sulfur, LA. worked with the tank owner to replace the first part of the specification with waterjetting. The secondary sweep was still specified to assure a new anchor pattern was established and that any flash rusting was removed. However, after the project started, the local paint representative for PPG approved their coating system to go directly over the waterjetted surface. However, due to original specification, a light sweep was still used prior to coating.

The contractor used a 40,000 psi waterjetting robot surface prep system to remove the coatings to eliminate all airborne dust. Hand held waterjetting lances were used to prepare areas inaccessible to the robot.

Health hygienists from the oil company that owns the tank placed lead detection monitors on the equipment to test for airborne lead particles. One monitor was placed right on the robot, one was placed near the air exhaust of the vacuum unit, and one was placed on the operator. All lead monitors read a non-detectable lead level.

All water and paint was vacuumed at the robot and transported to the filter system where the effluent was filtered through one cubic yard fabric bags. After testing for lead, the water was deemed suitable to be drained to the central waste water treatment center.

The coating was 10-30 mils thick and, although hard to remove, it was easily removed in a single pass with the robotic system. The project lasted 10 working days.

All lead based paint removed without any tarping, tenting or shrouding

The waterjetting offered many advantages. It allowed for a very safe operation for nearby workers (no airborne lead as would be seen with gritblasting); all monitors showed non-detectable levels. Also, overall project costs were reduced; no expensive shrouding or tarping was required to contain lead laden grit and disposal of tons of lead laden grit was eliminated.

5. CONCLUSION

As the advantages of waterjetting become better understood, we see more projects turning to waterjetting. One of the fastest growing applications is lead based paint removal where the environmental benefits of waterjetting make it the cost effective method. In addition, the introduction of robotic surface preparation systems are making larger size projects cost effective with waterjetting.

10th American Waterjet Conference
August 14-17, 1999: Houston, Texas

Paper 72

SURFACE PREPARATION OF CONCRETE AND METAL WITH HIGH PRESSURE AND ULTRA HIGH PRESSURE WATER

Ted Kupscznk
NLB Corporation
Wixom, MI

ABSTRACT

Presentation will focus on the proper procedures for cleaning and preparing concrete and metal surfaces – both horizontal and vertical – so that new coatings can be applied. Removing contaminants is essential for new coatings to adhere properly, but good adhesion also depends on a suitably rough surface or profile.

The advantage of water jetting will be discussed relative to coating and contaminant removal without damage to the original profile. Also new developments and accessories which enable semi automated and fully automated vacuum recovery and containment of water and removed debris will also be discussed.

Organized and Sponsored by the WaterJet Technology Association

10th American Waterjet Conference
August 14-17, 1999: Houston, Texas

Paper 73

NOZZLE PERFORMANCE IN ROTARY APPLICATIONS

D. Wright, J. Wolgamott, G. Zink
StoneAge, Inc.
Durango, Colorado, U.S.A.

ABSTRACT

Waterblast cleaning is widely used due to improved productivity, effectiveness and environmental friendliness. The development of new waterjet tools and more capable pumping equipment has contributed to this acceptance. A critical aspect of all these tools is the jet quality produced. The flow path through these tools is often very disruptive, which results in turbulent upstream conditions and poor jet quality. The type of nozzle used can mean using an expensive pump to its fullest advantage, or throwing away up to 50% of its power.

This paper studies the performance of common, commercially available nozzle types under both poor and good upstream conditions. Variations in flow, pressure, standoff distance, traverse velocity and jet angle were compared. Flow conditioning methods such as vanes, screens and feeder tubes were evaluated for relative performance. The range of study included flow rates of 7.5 to 150 lpm (2 to 40 gpm), pressures from 35 to 105 MPa (5000 to 15000 psi) and standoff distances from 3.8 to 185 cm (1.5 to 73 in.), corresponding to 50 to 1000 nozzle diameters.

A mixture of cement and sand was used as a target material. The volume removed was measured to determine jet effectiveness. Resulting jet performance was quantified and compared to real life cleaning tasks.

1. INTRODUCTION

The performance of a waterjet cleaning tool is dependent on applying the necessary power to the surface for proper cleaning. Once the jet exits the nozzle, it begins to lose power as it travels through the surrounding air. The better the jet quality (the tighter the jet) the more power it will deliver to the target surface. Jet quality is influenced primarily by the upstream flow path conditions and the particular nozzle design.

Jet power deteriorates over distance after it leaves the nozzle. When this distance is expressed in terms of nozzle diameters, the deterioration is uniform for all sizes of a nozzle style. For this reason, standoff distances are best expressed in terms of nozzle diameters. This method of expressing performance was first suggested by Leach and Walker (1966). For example, if the standoff distance to the surface to be cleaned is 750 mm (30 in.), the distance in terms of nozzle diameters for a .75 mm (.030 in.) diameter nozzle would be 1000 nozzle diameters; while for a 1.8 mm (.073 in.) diameter nozzle this distance would be 410 nozzle diameters. If both jets had the same pressure at the nozzle, the jet from the larger nozzle would reach the surface with more remaining power than the smaller nozzle jet.

Material to be removed from a surface has a minimum threshold pressure, below which it will not be affected. Therefore, it must be attacked with a certain minimum amount of power for effective cleaning. If this pressure is known, along with the standoff distance and the rate of deterioration of the jet through the air, minimum operating conditions of pressure and flow can be estimated. This paper addresses the rate of deterioration of various nozzle types and the effect on this rate with different upstream conditions. Standoff distance, nozzle size, pressure, surface speed, and jet angle were tested over a typical range of operating values.

2. TEST PROCEDURE

Test samples measuring 30 cm square by 14 cm thick (12 in. square by 5.5 in thick) of a cement/sand aggregate were prepared from a single mixed batch. An apparatus consisting of an air powered gearbox, high pressure water swivel, and nozzle head was used to rotate the jet resulting in specific surface speeds across the sample. The carriage with the nozzle head attached advanced 5 mm (.2 in.) with each revolution of the head. This was accomplished with a tooth belt drive from the rotating shaft to a threaded shaft. This equipment is shown in Figure 1. The sample was masked with a steel plate to expose a fixed surface area of the sample measuring 7.6 by 10 cm (3 by 4 in.) A typical test sample is shown in Figure 2. After the tests had been run, the volume removed was measured using the struck sand method. This entailed pouring sand into the blasted out void, scraping off level with the top, and then collecting and measuring the resultant volume of sand. A total of 260 tests were conducted over a period of 3 months.

3. STUDIES

3.1 Nozzle Type Performance

Nine types of nozzles were tested with both poor and good upstream conditions at various flow rates and pressures. The cross sections and nozzle types are described in Figure 3. These nozzles are commonly used in waterblasting operations. Each nozzle was tested at standoff distances of 50, 200 and 500 times the nozzle diameter. Surface speed across the samples for all tests was .6 m/sec (2 ft/sec). Section 3.3 provides a description of the upstream conditions used.

The results of nozzle performance with good upstream conditions are shown in Figure 4. With good upstream conditions, nozzle I and nozzle B had the best performance. Nozzle I uses the carbide insert as nozzle B, combined with a transition section to blend the nozzle entrance. The internal geometry of these nozzles, in terms of inlet taper and length, is the closest to the optimum found by Shavlovsky (1972) and Savanick and Frank (1976). Their studies showed an optimum inlet angle between 10 and 14 degrees, and a straight section of nozzle 3 to 4 times the orifice diameter.

The results of nozzle performance with poor upstream conditions are shown in Figure 5. Under poor upstream conditions, nozzle A had the best performance. This is due to the vane type flow conditioner, described in Section 3.4. The use of this type flow conditioner would improve the performance of any nozzle type when operating under poor upstream conditions.

The type of nozzle used can mean using an expensive pump to its fullest advantage, or throwing away up to 50% of its power. This study measured performance in terms of volume of material removed; some nozzles are optimized for other purposes, such as fan jets, which are optimized for surface cleaning. It was observed during these tests that different nozzle types had different impact patterns, which would result in different cleaning paths. For example, nozzle F cut a very narrow path, and left ribs of material between passes. Nozzle C cut a wider path than the other nozzles, which would be useful in surface cleaning where complete coverage is required.

3.2 Effect of Flow and Pressure

A single nozzle type was tested at a variety of conditions to measure performance over a range of standoff distances. Nozzle type A was tested with both poor and good upstream conditions, at standoff distances of 50, 200, 500 and 1000 times the nozzle diameter, at pressures of 35, 70 and 105 MPa (5000, 10000 and 15000 psi), and at flow rates of 19, 57 and 150 lpm (5, 15 and 40 gpm) at each of the pressures. Surface speeds across the samples for all tests were .6 m/sec (2 ft/sec).

Figure 6 shows the relationship of performance to standoff distance for the three different flow rates. A nozzle with good upstream conditions will decay by 35 percent between 50 and 500 nozzle diameter standoffs, while a nozzle with poor upstream conditions will decay by 60 percent over the same range. Figure 7 shows the relationship of performance to standoff in nozzle diameters for the three different pressures. A similar rate of decay occurs with pressure as did with flow. From this analysis, expressing performance versus standoff distance in terms of nozzle diameters appears reasonable within this range of flows and pressures.

3.3 Effect of Upstream Conditions

Two types of nozzle heads were used; one typical of poor upstream conditions found in common waterjet tools, the other to represent good upstream conditions. These two heads are shown in Figure 8. A feeder tube was used to produce good upstream conditions. Ideal feeder tubes are straight and axially symmetric with a smooth bore leading to the nozzle. The good upstream condition used for these tests was based on findings by Shavlovsky (1972), where the length of the feeder tube should not be less than 40 to 50 times the inside diameter. For this study, the length of feeder tube used was 61 cm (24 in.) with an inside diameter of 1.2 cm (.46 in.), resulting in a ratio of length to inside diameter of 52 times.

Figure 9 shows the results obtained with poor upstream conditions using nozzle type B, relative to the results obtained by Leach and Walker (1966) when testing the Shavlovsky nozzle design. Leach and Walker measured the performance of a nozzle by measuring the stagnation pressure of the jet on a surface relative to the pressure at the nozzle, whereas this study measured nozzle performance in terms of volume of material removed. The results appear very similar.

Figure 10 compares nozzle type B, poor upstream conditions, with the same nozzle, good upstream conditions tested at a flow rate of 19 lpm (5 gpm). This shows that good upstream conditions can double the performance found with poor upstream conditions. Overall, all nozzle types showed an average improvement of 45% over poor upstream conditions.

The importance of good upstream conditions increases as flow rates increase. This can be seen in Figure 11, comparing poor and good upstream conditions at flow rates of 19, 57 and 151 lpm (5, 15 and 40 gpm). At 19 lpm (5 gpm), the ratio of poor upstream performance divided by the good upstream performance was .76, while at 151 lpm (40 gpm), this ratio dropped to .46. At the highest flow rate, the inside diameter of the feeder tube used for good upstream conditions was only 3.5 times the nozzle diameter used for this condition. Shavlovsky (1972) found that increasing the inside diameter of the feeder tube up to ten times the nozzle diameter gave the optimum performance.

3.4 Effect of Flow Conditioning

Limitations of access to pipes, ducts or vessels often require that nozzle head designs with poor upstream conditions be used. In these cases, more compact methods of flow conditioning become important. Four different methods of flow conditioning were evaluated at 70 MPa (10000 psi), 57 lpm (15 gpm) at standoff distances of 200, 500 and 1000 nozzle diameters. Figure 12 shows the four types evaluated. The cone and screen type flow conditioners showed no performance improvement at the conditions tested. However, other field results at flow rates above 300 lpm (80 gpm) have shown screens to be beneficial.

The effect of the vane type flow conditioner to improve poor upstream conditions is shown in Figure 13, relative to results obtained with no flow conditioning, and results with good upstream conditions. The vane flow conditioner provided an improvement of 40 percent over a nozzle without one, but was still 25 percent less effective than the nozzle with good upstream conditions.

Further study was conducted on the effect of length feeder tubes when used for flow conditioning. The use of feeder tubes has limitations; the length of feeder tube is often limited by the size of the access to the vessel or pipe to be cleaned. Using feeder tubes, or nozzle arms, as they are commonly called, serves the purpose of reducing the standoff distance to the surface, as well as conditioning the flow.

Figure 14 shows the performance of feeder tubes with increasing ratio of length to inside diameter. Lengths of 5, 10, 25 and 60 cm (2, 4, 10 and 24 in.) with an inside diameter of 1.2 cm (.46 in.) were compared in these tests. Nozzle A, with the vane type flow conditioner, was used in these tests, conducted at 70 MPa (10000 psi), 57 lpm (15 gpm). The ratio of the inside diameter of the feeder tube to the nozzle diameter was 6.5. The shortest section improved jet performance by 22 percent overall. Improvement was seen out to the maximum lengths tested, with increasing effect as standoff distance was increased.

3.5 Effect of Surface Speed

Tests were conducted to study the effect of jet surface speed. Surface speeds of 1.5, 3, 6 and 12 m/sec (5, 10, 20 and 40 ft/sec) at standoff distances of 200, 500 and 750 nozzle diameters were tried. Multiple passes were made at the faster speeds to achieve a constant energy application. A single pass was made at 1.5 m/sec (5 ft/sec), two passes at 3 m/sec (10 ft/sec), four passes at 6 m/sec (20 ft/sec), and eight passes at 12 m/sec (40 ft/sec).

The testing of surface speed effect was done using poor upstream conditions, at 70 MPa (10000 psi), 57 lpm (15 gpm) with nozzle A. The results are shown in Figure 15. The maximum performance was achieved with eight passes at 12 m/sec (40 ft/sec) at a 200 nozzle diameter standoff. At a standoff of 500 nozzle diameters the optimum effect occurred with four passes at 6 m/sec (20 ft/sec). At a standoff of 750 nozzle diameters, the optimum effect occurred with a single pass at 1.5 m/sec (5 ft/sec).

In a single pass, slower speed results in a deeper cut. There are cases where a single slow pass can result in penetration to a boundary layer, such as a hard, brittle material in a steel vessel, which results in larger pieces being spalled off at the boundary layer. This method of material removal might be more efficient than slowly eroding the material in shallow fast passes.

3.6 Effect of Nozzle Angle

Tests were conducted to determine jet performance relative to exit angles from the head. The sample surface remained parallel to the axis of rotation, so the angle of impingement was the same as the exit angle. Figure 16 illustrates the angles tested.

Performance of the angled jets relative to 90° was affected by the direction of progression of successive passes of the angled jets. Plowing describes the progression in the same direction as the jet; dragging is progression opposite to the jet angle, as shown in Figure 16. When the jet was plowing, the performance with the 45° and 135° angle was 12 percent better than that achieved with the 90° jet. However, if the angled jet traveled in the dragging direction, the performance of the 45° and 135° angle was 27 percent less than that of the 90° jet. Figure 17 shows the effect of jet angle and direction of travel on jet performance. Overall, with nozzle A, the jet exiting at 45° exhibited 10 percent better quality than the jet exiting at 135°.

The improved performance resulting from the plowing direction of travel was dependent on the cumulative effect of successive passes; the path spacing used for these tests was close to matching the jet path width. Single, independent passes at 45° were not as effective as the 90° angle of attack.

4. CONCLUSIONS

4.1 Nozzle Selection

The results of the tests performed on various nozzles showed a difference in performance of up to 50 percent between nozzle types. The optimum performance with good upstream conditions was obtained by the nozzle type with a geometry that has been proven in tests by others to be the best. When poor upstream conditions exist, nozzles with vane type flow conditioners should be used when possible.

4.2 Upstream Conditions

Poor upstream conditions reduce jet performance by 25 to 55 percent compared to performance with good upstream conditions. The deterioration increases with increasing flow rate. Poor upstream conditions can be improved through the use of flow conditioning. The vane type flow conditioner is inserted behind a nozzle, and will improve performance by up to 40 percent.

Feeder tubes or nozzle arms are useful for reducing standoff distance; they also act as flow conditioners. A length of 4 times the inside diameter of the feeder tube improved performance by 22 percent. Feeder tubes with lengths up to 50 times their inside diameter have greater effect at large standoff distances.

4.3 Surface Speed

The effect of surface speed was dependent on standoff distance. At a 200 nozzle diameter standoff, the optimum was found to occur at or above 12m/sec (40 ft/sec) when multiple passes were made. At a standoff distance of 750 nozzle diameters, the optimum occurred with a single pass at 1.5 m/sec (5 ft/sec).

4.4 Jet Angle

The jet angle exiting the head between 45° and 135° affected jet quality by up to 10 percent. However, performance differences of between 12 and 25 percent were seen depending on direction of travel over the surface relative to the jet angle.

5. REFERENCES

Leach, S.J., and Walker, G.L., "Some Aspects of Rock Cutting by High Speed Water Jets," *Phil. Trans. Royal Society*, Vol. 260A, pp. 295-308, London, UK, 1966.

Savanick, G.A., and Frank, J.N., "Force Exerted by Water Jet Impact at Long Standoff Distances," *Third International Symposium on Jet Cutting Technology*, pp. B5-59-B5-68, BHRA Fluid Engineering, Cranfield, UK, 1976.

Shavlovsky, D.S., "Hydrodynamics of High Pressure Fine Continuous Jets," *First International Symposium on Jet Cutting Technology*, pp. A6-81-A6-92, BHRA Fluid Engineering, Cranfield, UK, 1972.

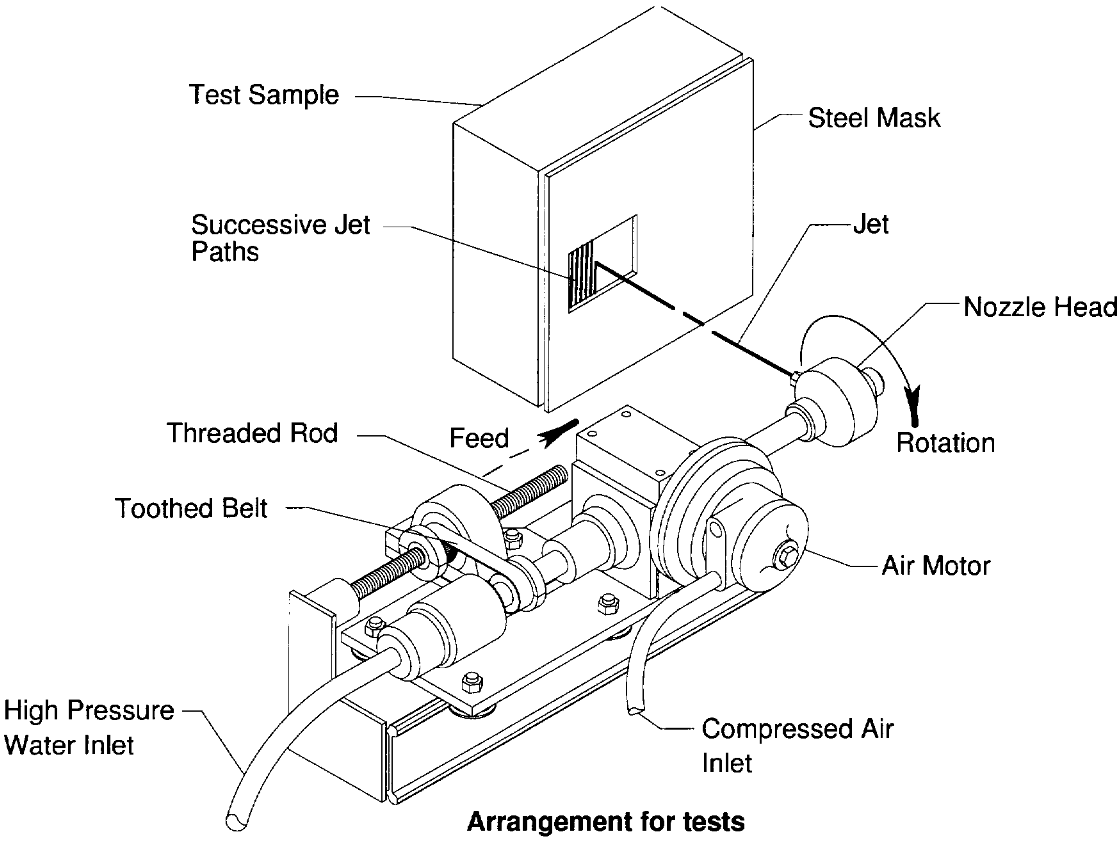

Arrangement for tests

Figure 1

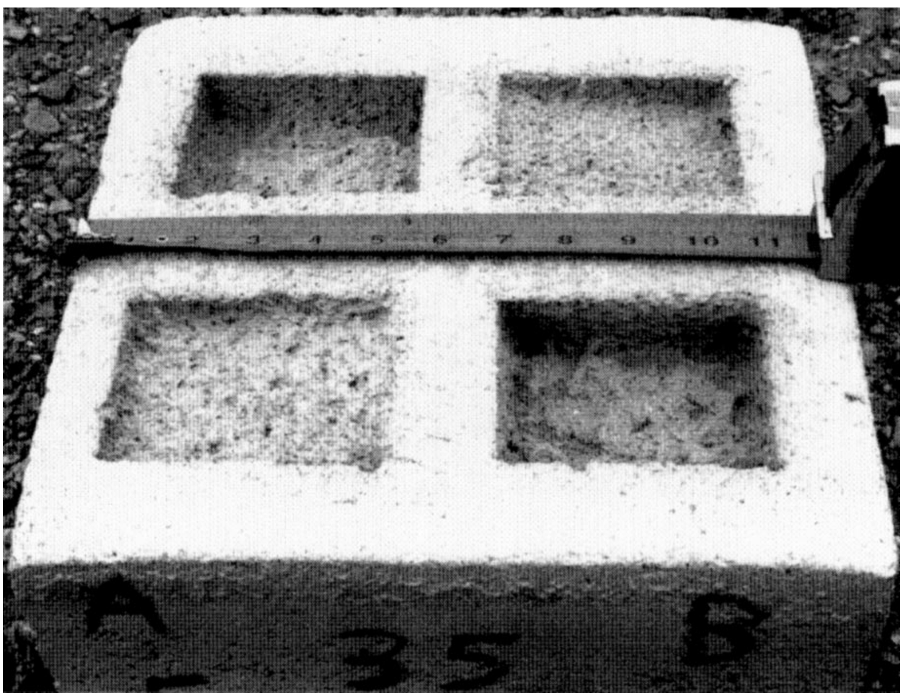

Test sample

Figure 2

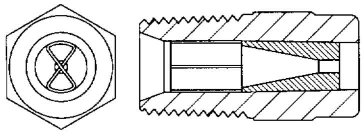

Carbide, round orifice with vane flow conditioner
Nozzle A

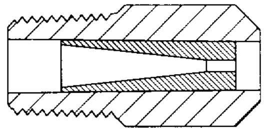

Carbide, round orifice
Nozzle B

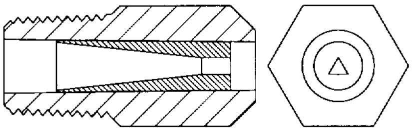

Carbide, triangle orifice
Nozzle C

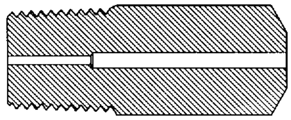

Steel, round orifice
Nozzle D

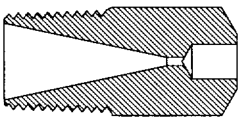

Steel, round orifice
Nozzle E

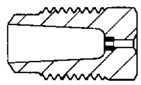

Sapphire, round orifice
Nozzle F

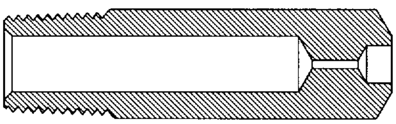

Steel, round orifice
Nozzle G

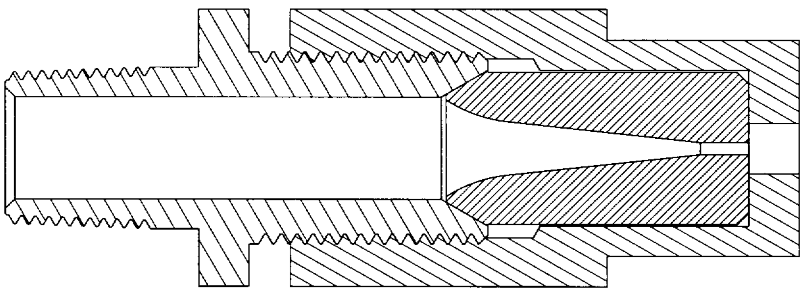

Carbide, round orifice
Nozzle H

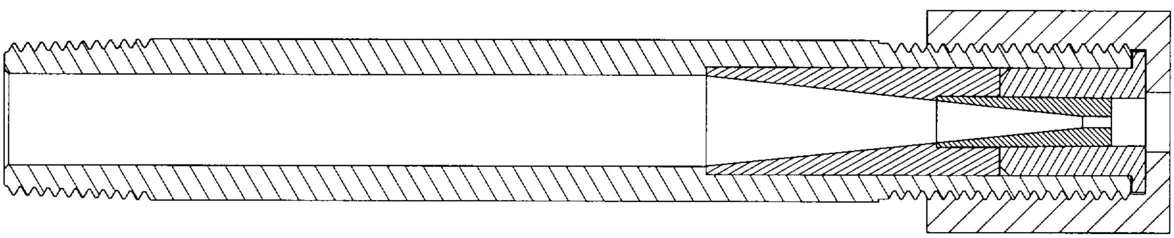

Carbide, round orifice
Nozzle I

Nozzle types used for testing, shown full scale

Figure 3

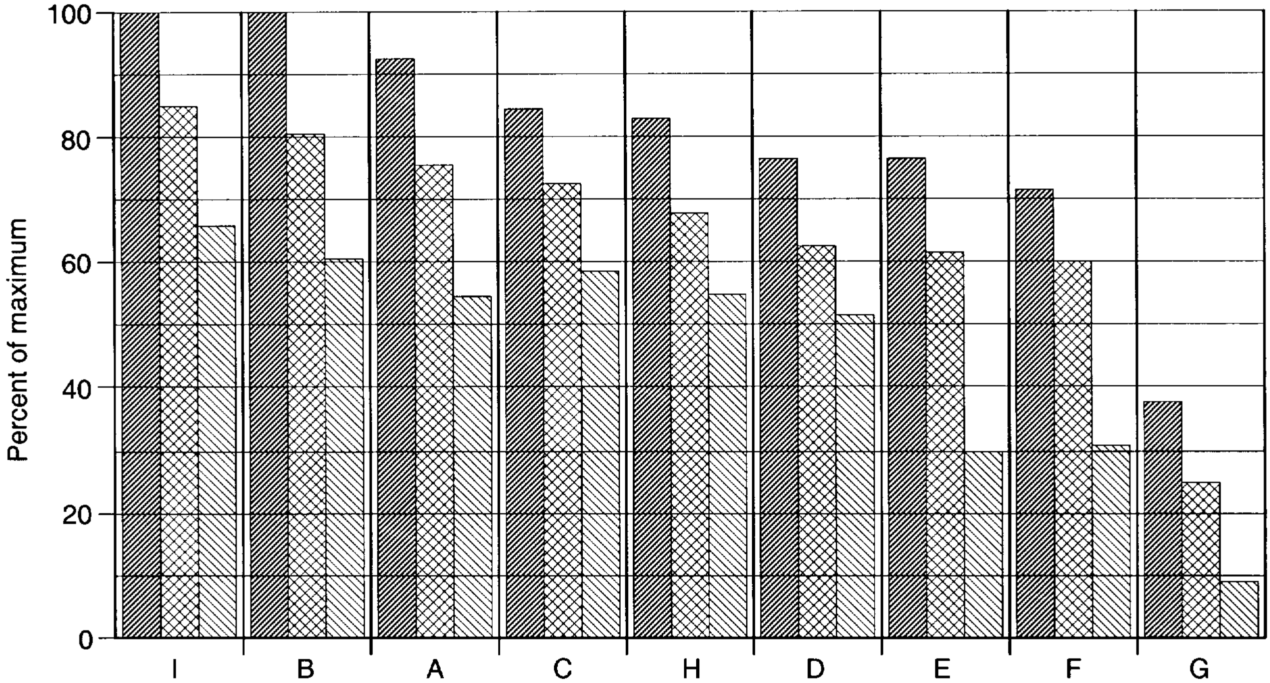

Performance of nozzle types with good upstream conditions at standoffs of 50, 200 and 500 nozzle diameters

Figure 4

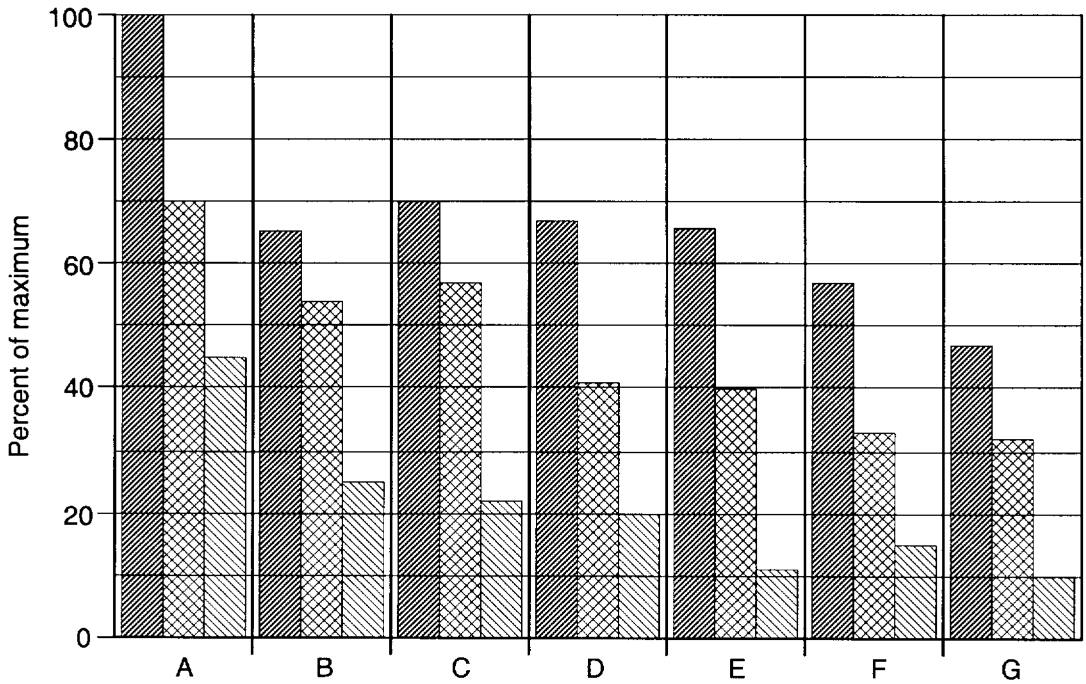

Performance of nozzle types with poor upstream conditions at standoffs of 50, 200 and 500 nozzle diameters

Figure 5

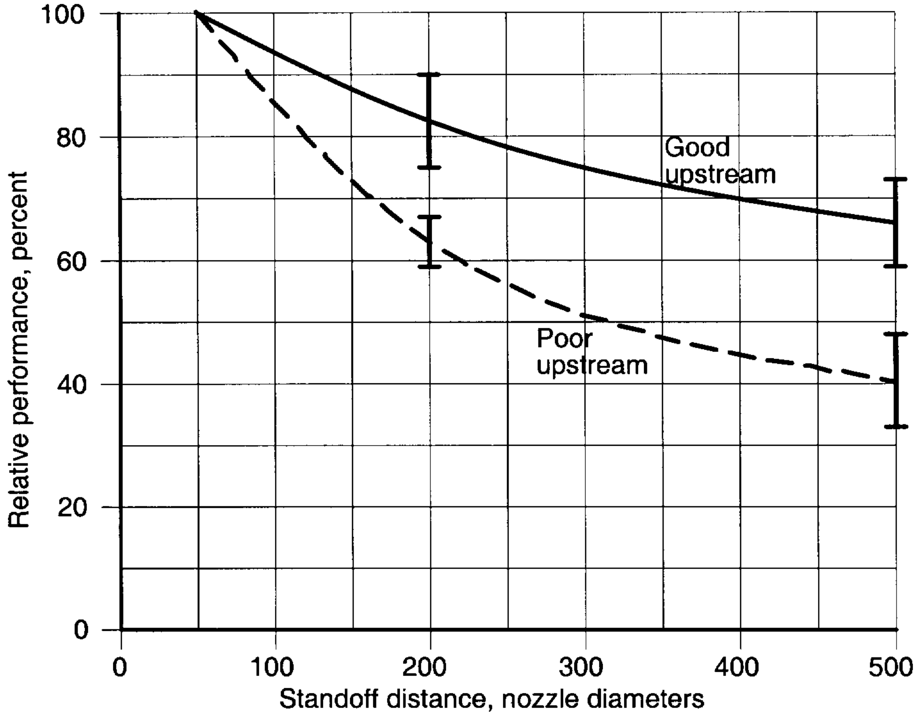

Performance with good and poor upstream conditions, tested with flow rates of 19, 57 and 151 lpm (5, 15 and 40 gpm)

Figure 6

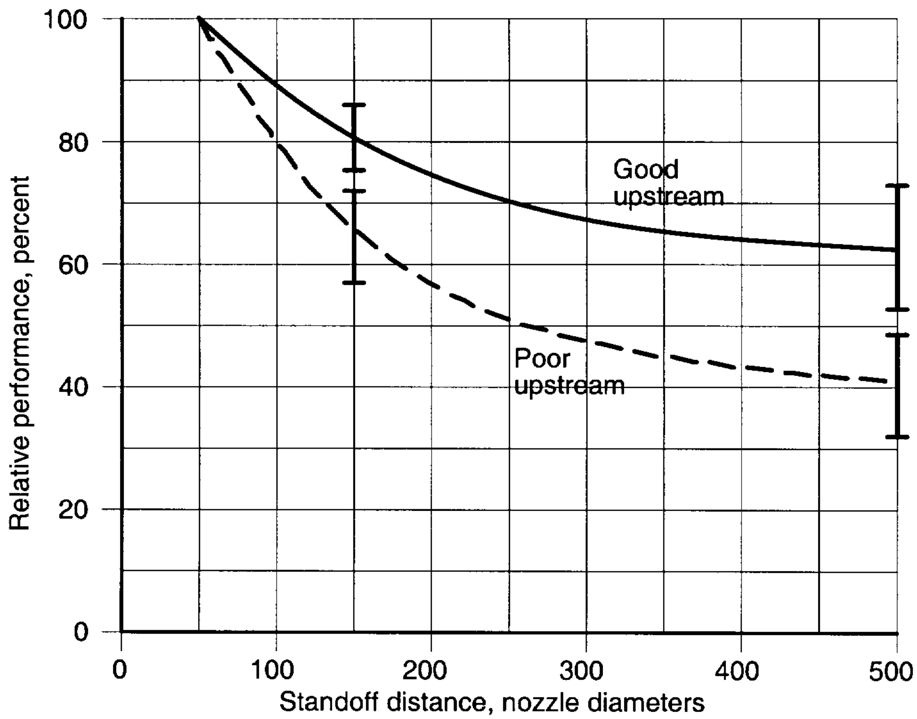

Performance with good and poor upstream conditions, tested with pressures of 35, 70 and 105 MPa (5, 10 and 15 ksi)

Figure 7

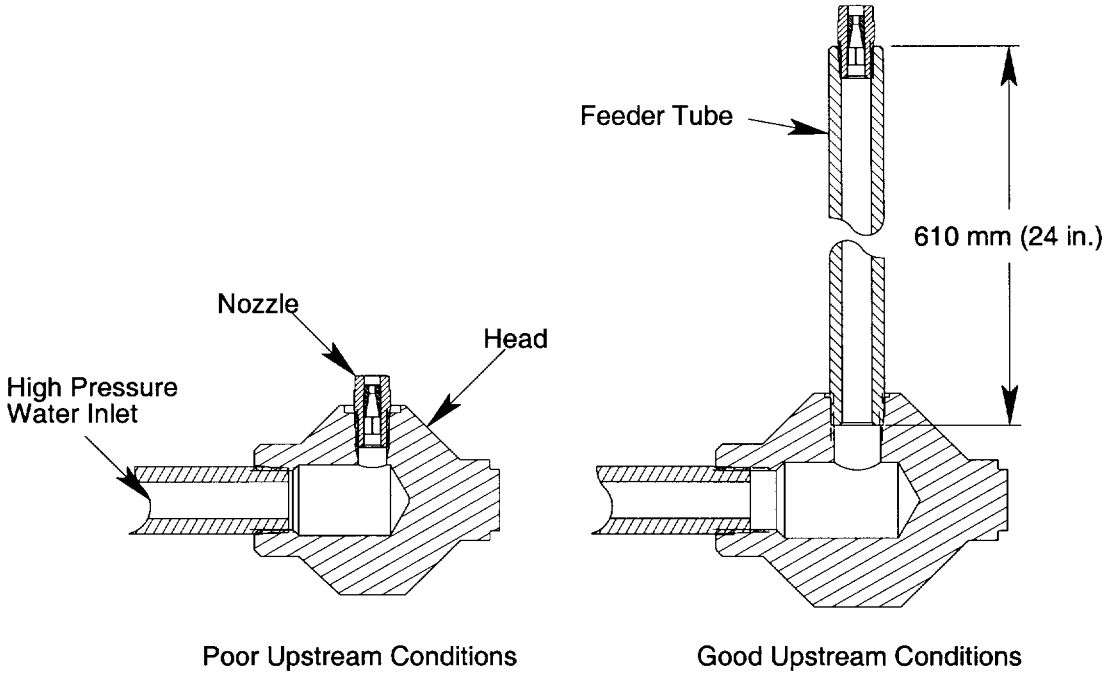

Nozzle heads used for tests

Figure 8

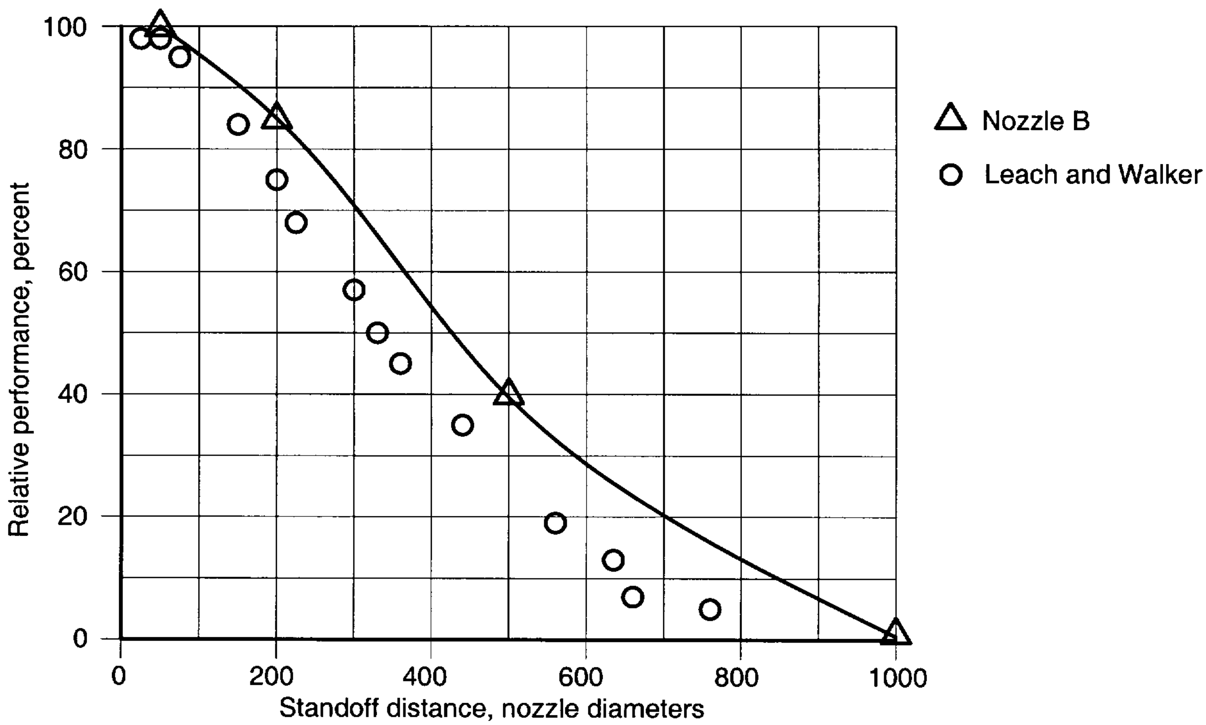

Performance of Nozzle B with poor upstream conditions compared to results obtained by Leach and Walker (1966)

Figure 9

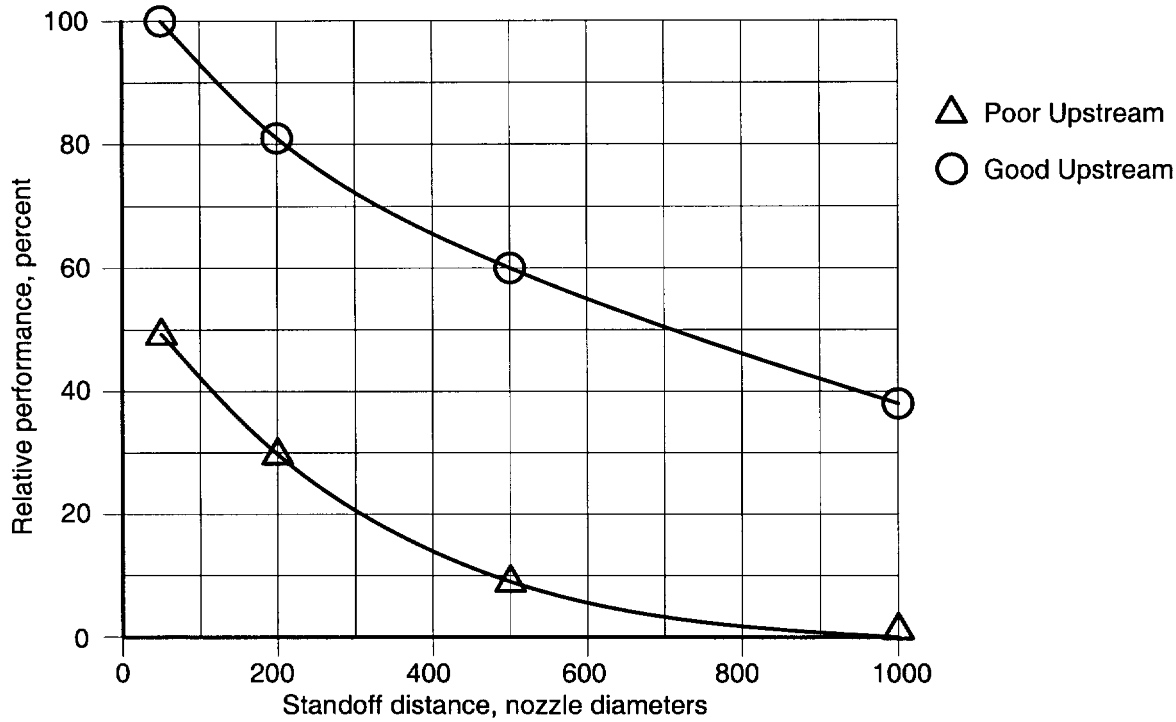

Performance of Nozzle B with poor upstream conditions compared to results with good upstream conditions

Figure 10

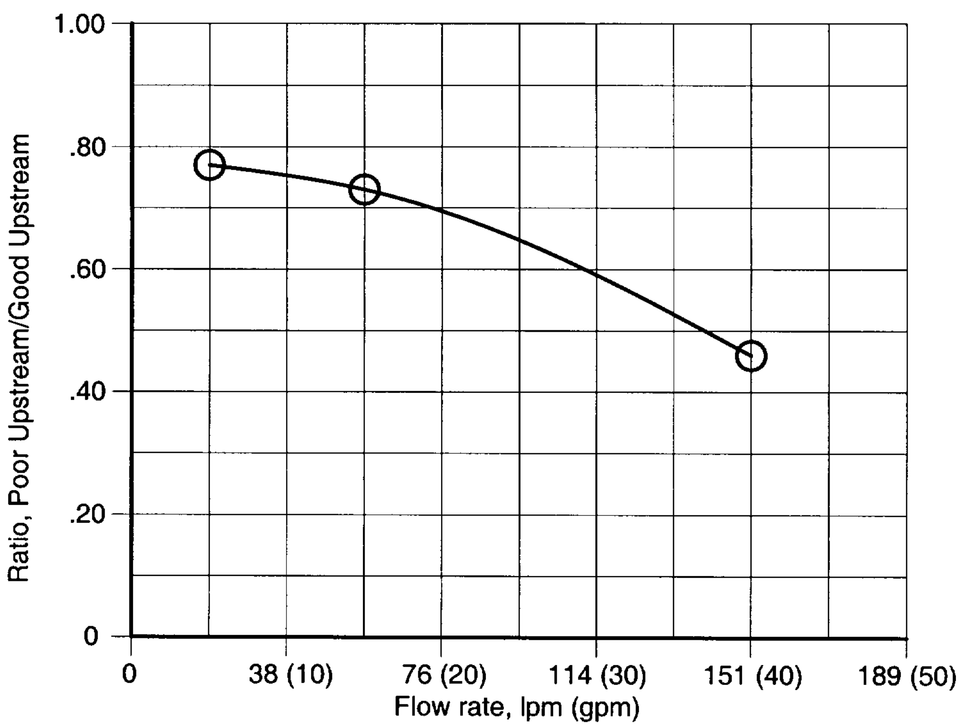

Performance of Nozzle A with increasing flow rate as a ratio of poor versus good upstream

Figure 11

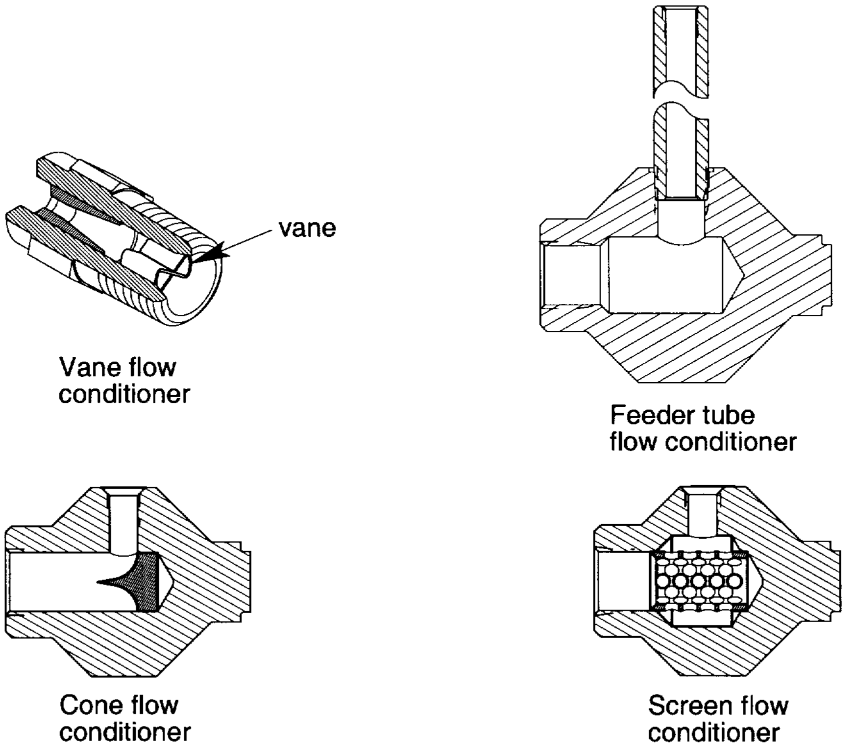

Four types of flow conditioning methods tested

Figure 12

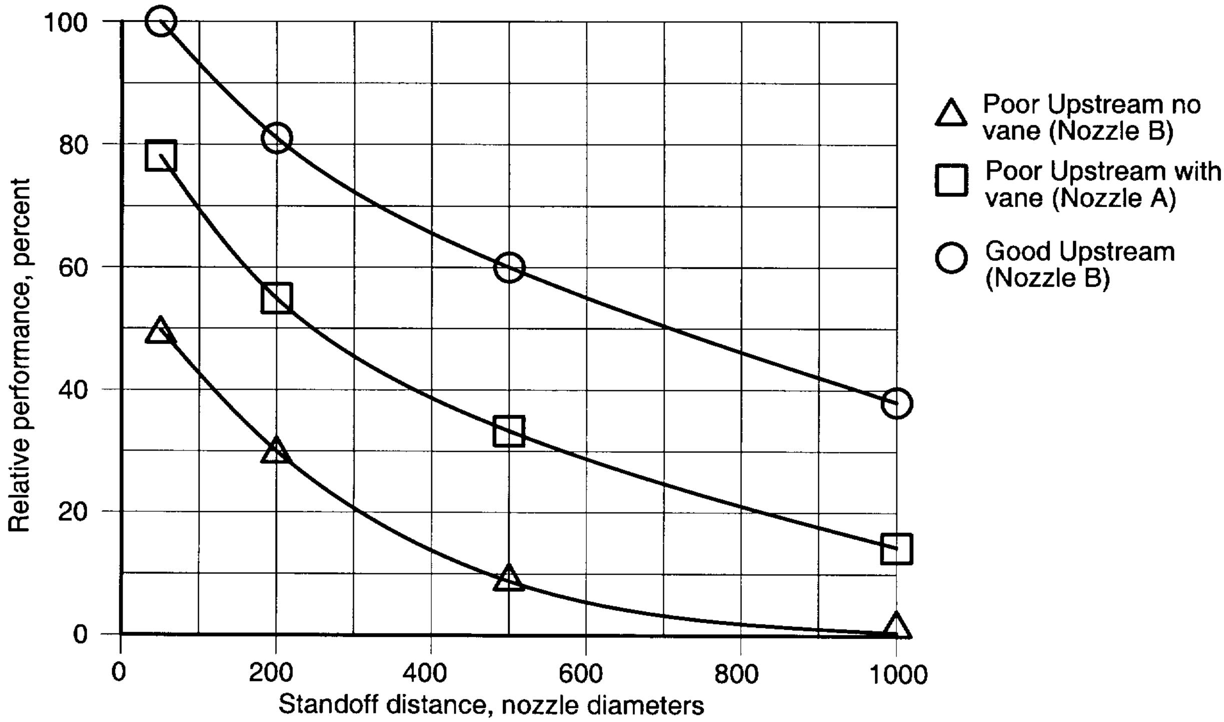

Relative performance of vane flow conditioner

Figure 13

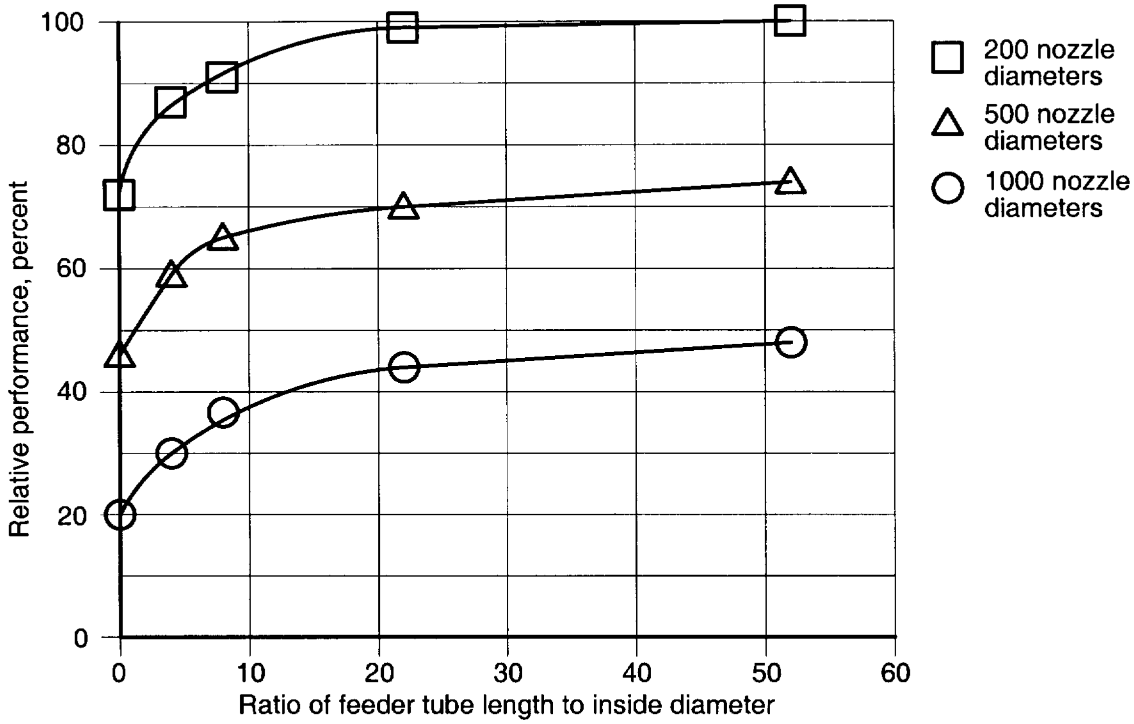

Performance of Nozzle A with increasing length of feeder tube at three standoff distances

Figure 14

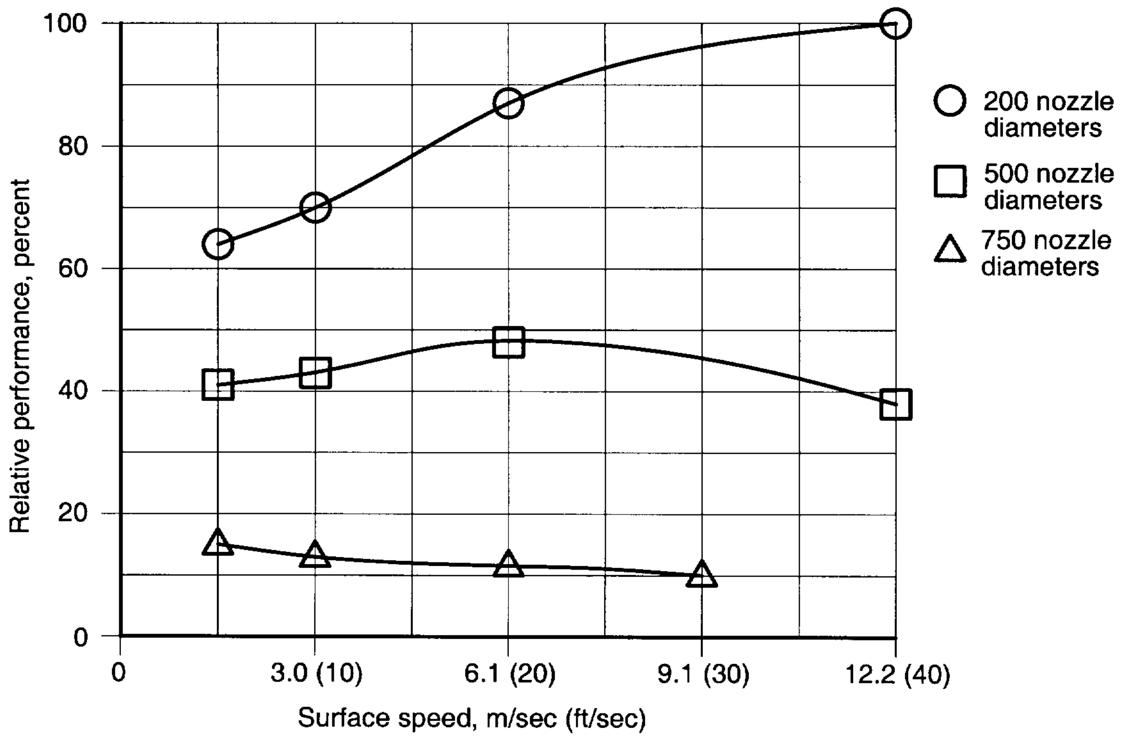

Performance versus surface speed at three standoffs

Figure 15

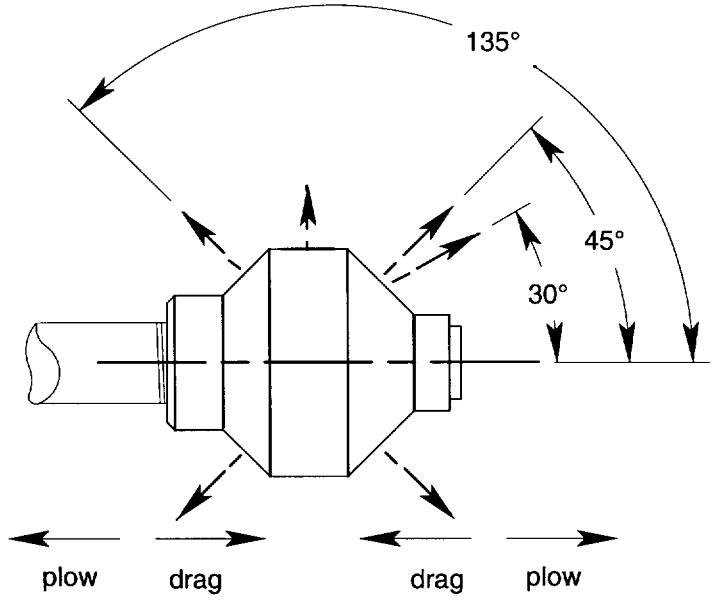

Nozzle exit angles tested
Figure 16

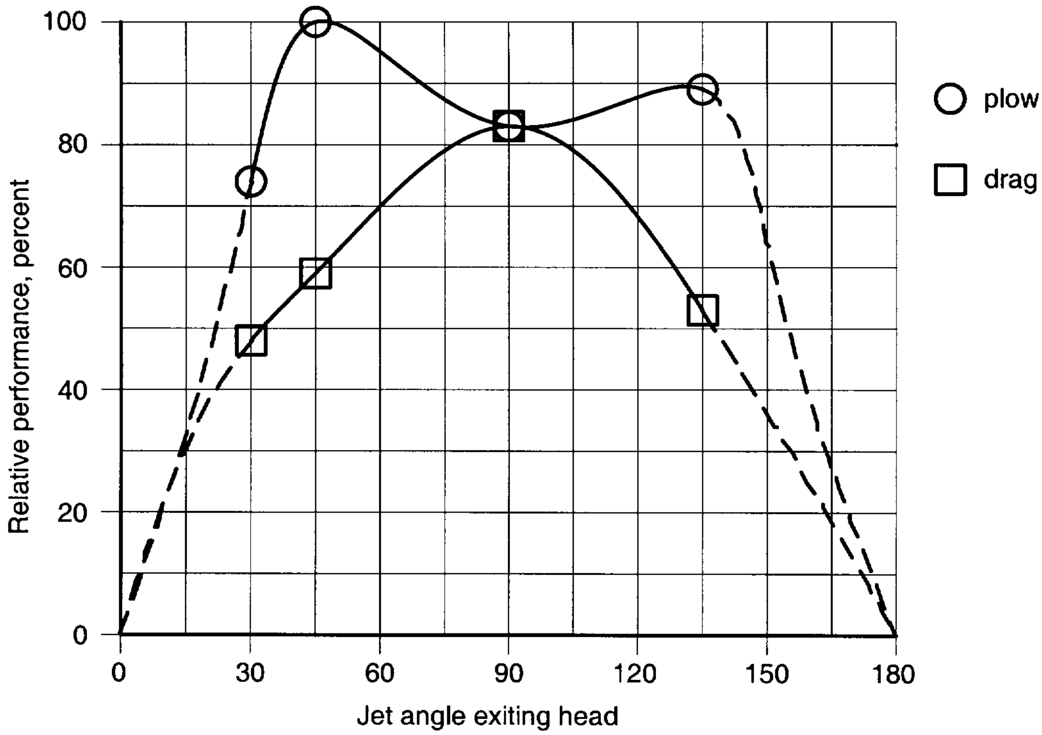

Performance versus jet angle and direction of traverse
Figure 17

10th American Waterjet Conference
August 14-17, 1999: Houston, Texas

Paper **74**

MATHEMATICAL MODELING OF THICK WALL TUBING

Thomas Thrash
Charles Britton
HydroChem Industrial Services
Houston, Texas, USA

ABSTRACT

Very few manufacturers of thick wall tubing publish ratings of their tubing. The water blasting market is unique and demanding. It requires tubing not readily available, which often means special mill runs to user specifications of length, size and material. To help determine the maximum allowable working pressure of the tubing used by HydroChem, we developed a computer model that would estimate the yield and burst pressure of a thick wall tube. This model was verified by testing samples. Burst tests were performed on commercial pipe as well as custom tubing to verify the computer model and determine safe operating limits of standard pipe and tubing.

1. INTRODUCTION

Tubing used for water jet lances must be evaluated for safe operating parameters. When custom or other non-rated tubing is used, there should be a method of rating the tubing for allowable operating pressure. Since industrial water jets operate at relatively high pressures, such as 69 to138 MPa (10,000 to 20,000 psi), the burst pressure of the lance tubing can become a limiting factor.

While it would be easy to use a very high safety factor to avoid any bursting risk, this could unnecessarily compromise the water jet design for small diameter tube cleaning. By using well-established design criteria for calculating stresses in thick-walled tubing, a reliable and safe method can be used for rating lance tubing. Widely available spreadsheet software can be programmed for calculating the critical yield and burst pressures base on material properties and tubing dimensions. HydroChem Industrial Services has developed an Excel spreadsheet to perform these calculations.

To verify the accuracy of these results, HydroChem tested the actual burst pressures and compared the results for various tubing samples. The burst pressure is much easier to determine than the tubing yield pressure without sophisticated laboratory facilities.

2. BURST PRESSURE MODELING

A thick-walled cylinder is defined as one having the ratio of wall thickness to inner radius greater than 0.1. In this case, the stresses in the tubing are recognized as varying as a function of the radius. This compares to a thin-walled cylinder where the wall stresses are assumed to be constant.

There are four stresses to consider when modeling a thick-walled cylinder: longitudinal, tangential, radial, and shear. For the purposes of this investigation, only constant internal pressure is taken into account. The following variables are used in the equations for modeling thick-walled cylinders:

a = outer radius (OD/2)
b = inner radius (ID/2)
r = internal wall radius where $b<r<a$
p = uniform internal pressure

Figure 1 provides a graphic illustration of the variables and stresses present in a thick-walled cylinder.

The longitudinal stress (σ_1) is uniform through the wall thickness except for end effects that can be neglected for this analysis. The equation for this stress is (Boresi et al.):

$$\sigma_1 = \frac{p\,b^2}{(a^2-b^2)} \tag{1}$$

The tangential or hoop stress (σ_2) at any radius is described by the equation (Young):

$$\sigma_2 = \frac{p\,b^2\,(a^2+r^2)}{r^2\,(a^2-b^2)} \tag{2}$$

This stress is greatest at the inner radius where r = b:

$$\sigma_{2,max} = \frac{p\,(a^2+b^2)}{(a^2-b^2)}$$

The maximum radial stress (σ_3) is also at the inner diameter and is the negative, compressive reaction to the internal pressure (Linghaiah):

$$\sigma_{3,max} = -p \tag{3}$$

The maximum shear stress (τ) is a function of both the tangential and radial stresses as seen in the following equation (Young):

$$\tau_{max} = \frac{\sigma_{2,max} - \sigma_{3\ ,max}}{2} = \frac{p\,(a^2+b^2)}{2(a^2-b^2)} + \frac{p}{2} = \frac{p\,a^2}{(a^2-b^2)} \tag{4}$$

The equivalent stress generated by the longitudinal, tangential, and radial stresses is (Dawson):

$$\sigma_e = \sqrt{}[((\sigma_2 - \sigma_3)^2+(\sigma_1 - \sigma_3)^2+(\sigma_2 - \sigma_1{}^2))/2] \tag{5}$$

If the pressure term is left out of the component stresses, an equivalent stress factor (σ'_e) based solely on geometry can be determined. The yield pressure can then be calculated by dividing the material yield strength by the equivalent stress factor:

$$p_y = \frac{\sigma_y}{\sigma'_e} \tag{6}$$

Another method of determining yield stress is by determining the isotropic (or fully plastic) yield stress (Dawson):

$$p_{iy} = 2\,\tau_y\,\ln(b/a) = \frac{2\,\sigma_y\,\ln(b/a)}{\sqrt{3}} \tag{7}$$

Since the yield and isotropic yield pressures are difficult to measure, calculating and then checking the burst pressure (p_b) is a useful method of determining the modeling accuracy. This equation is given by the expression (Faupel & Fisher):

$$p_b = (2 - (\sigma_y/\sigma_u))\, p_{iy} \tag{8}$$

where σ_u is the ultimate tensile strength of the material. For a brittle material where σ_y/σ_u approaches 1, the burst pressure becomes the isotropic yield stress.

3. EXAMPLE CALCULATION

An example of this analysis is seen in the following case. Please note that for the program, no pressures are used in calculating the longitudinal, hoop, and radial stresses. These are really geometric factors used later in the program to calculate the yield and burst pressures.

MATERIAL
2” OD x 1” ID 304 Stainless Steel
a = 25.4 mm (1”)
b = 12.7 mm (0.5”)
σ_y = 275.8 MPa (40,000 psi)
σ_u = 620.6 MPa (90,000 psi)

LONGITUDINAL STRESS FACTOR

$$\sigma'_1 = \frac{b^2}{(a^2-b^2)} = \frac{(12.7)^2}{((25.4)^2 - (12.7)^2)} = 0.333$$

HOOP STRESS FACTOR

$$\sigma'_{2,max} = \frac{(a^2+b^2)}{(a^2-b^2)} = \frac{((25.4)^2 + (12.7)^2)}{((25.4)^2 - (12.7)^2)} = 1.667$$

RADIAL STRESS FACTOR

$$\sigma'_{3,max} = -1$$

EQUIVALENT STRESS FACTOR

$$\begin{aligned}\sigma'_e &= \sqrt{\,[((\sigma'_2 - \sigma'_3)^2+(\sigma'_1 - \sigma'_3)^2 + (\sigma'_2 - \sigma'_1)^2)/2]} \\ &= \sqrt{\,[((1.667- (-1))^2 + (0.333-(-1))^2 + (1.667- 0.333)^2)/2]} \\ &= 2.309\end{aligned}$$

YIELD PRESSURE

$$p_y = \frac{\sigma_y}{\sigma'_e} = \frac{275.8 \text{ MPa}}{2.309} = 119.4 \text{ MPa } (17{,}100 \text{ psi})$$

ISOTROPIC YIELD PRESSURE

$$p_{iy} = \frac{2\,\sigma_y \ln(b/a)}{\sqrt{3}} = \frac{2\,(275.8)\ln(25.4/12.7)}{\sqrt{3}} = 220.7 \text{ MPa } (32{,}000 \text{ psi})$$

BURST PRESSURE

$$p_b = (2 - (\sigma_y/\sigma_u))\, p_{iy} = (2 - (275.8/620.6))\ 220.7 = 343.3 \text{ MPa } (49{,}800 \text{ psi})$$

4. TUBING BURST TESTING

HydroChem Industrial Services performed burst tests on tubing samples to check the accuracy of the tubing modeling program. The apparatus used for these tests is shown in Figure 2. The pump for this system is a pneumatically powered three-stage pump capable of compressing the working fluid, which is water, to 690 MPa (100,000 psi). Water is a safer medium to use than air, because the water possesses less stored energy and thus reduces the likelihood of a violent rupture. The test part was placed in a containment vessel filled with water when it was pressurized, and the pressure slowly increased until bursting occurred.

A few of the burst samples and the corresponding burst pressures are shown in Figure 3. The more ductile samples, particularly the stainless steel pipe, showed a considerable amount of plastic deformation before rupturing. The least ductile samples, the 4130 pipe, showed the least amount of deformation before bursting. The size of the burst opening was almost twice as long in the 4130 as the stainless steel samples. Only one sample, the 1/4" schedule 40 galvanized pipe, failed laterally at the NPT pipe threads. All the other samples failed longitudinally.

5. COMPARISON OF ACTUAL AND PREDICTED RESULTS

The calculated and actual results are summarized in Table 1. For five of the samples, the actual burst pressures are greater than the calculated by an average of 17%. These are the five most ductile specimens that were pressurized. These samples failed at approximately twice the isotropic yield pressures, so there was a great deal of plastic deformation.

The results for the more brittle 4130 samples provide a striking contrast. These specimens failed at less than the calculated burst pressure—as much as 9% less for the 1/8" schedule 40, 4130 pipe. The burst pressures for the 4130 samples are much closer to the isotropic yield pressures.

6. CONCLUSIONS

The formulae used in calculating the tubing burst pressures provide a useful guide for determining allowable system working pressures. The results were low for less ductile materials, so perhaps the ductility factor in equation 8 needs improvement. A working pressure based on 33% of the burst pressure seems a reasonable balance of safety and economics for lance tubing.

Industry standards do not exist for high pressure tubing used for lancing. Special attention is needed to ensure you acquire quality tubing that safely meets your pressure demands. It is customary for pipe to be purchased using nominal specifications. This permits wall thickness to vary ±15% and can reduce the maximum allowable working pressure by more than 25%. Acquiring lances from unqualified suppliers could place water blasting personnel at risk.

7. OBSERVATIONS

Some of the pipe-threaded connections leaked before the sample burst. However, none of the pipe-threaded connections experienced catastrophic failure due to thread shear in the axial direction. Low strength materials such as 304 stainless steel required the threaded connections to be retightened repeatedly before the pipe burst. High strength materials such as 4130 pipe did not require retightening and held pressure up to eight times the normal operating pressure. Standard cone and high pressure connections were more difficult to keep sealed than pipe-threaded connections.

8. REFERENCES

Boresi, A., Schmidt, R., and Sidebottom, O. "Advanced Mechanics of Materials," Fifth Edition, John Wiley & Sons, 1993.

Dawson, V.C.D. "High Pressure Containment in Cylindrical Vessels." High Pressure Technology, Vol. 1, pp. 229-234, 1977.

Faupel, J. and Fisher, F. "Engineering Design." Second Edition, John Wiley & Sons, 1981.

Lingaiah, L. "Machine Design Data Handbook," McGraw-Hill, 1994.

Young, W. "Roark's Formulas for Stress & Strain," Sixth Edition, McGraw-Hill, 1989.

Table 1. Excel Program Calculations and Actual Results of Samples in Figure 3

SI Units

												0.33
	O.D.	I.D.	YIELD	TENSILE				P YIELD	P YIE ISO	P BURST CALC	P BURST ACTUAL	P WORK
DESC.	(mm)	(mm)	(MPa)	(MPa)	HOOP	LONG	EQUIV	(MPa)	(MPa)	(MPa)	(MPa)	(MPa)
1/4" Sch.40 BLACK	13.72	9.25	241	414	2.6667	0.8333	3.1754	76	110	156	183	51
1/4" Sch.40 GALV.	13.72	9.25	241	414	2.6667	0.8333	3.1754	76	110	156	200	51
1/8" Sch. 80 4130	10.29	5.46	758	838	1.7838	0.3919	2.4108	315	555	608	552	200
1/4" Sch. 80 4130	13.72	7.67	758	838	1.9092	0.4546	2.5194	301	509	557	552	184
1/4" Sch. 80 SS	13.72	7.67	241	586	1.9092	0.4546	2.5194	96	162	257	303	85
1/2" Sch. 160 SS	21.34	11.84	241	586	1.8895	0.4447	2.5024	96	164	261	283	86
9/16" Tube SS	14.27	7.92	241	586	1.8903	0.4452	2.5031	96	164	261	303	86

English Units

												0.33
	O.D.	I.D.	YIELD	TENSILE				P YIELD	P YIE ISO	P BURST CALC	P BURST ACTUAL	P WORK
DESC.	(in)	(in)	(psi)	(psi)	HOOP	LONG	EQUIV	(psi)	(psi)	(psi)	(psi)	(psi)
1/4" Sch.40 BLACK	0.540	0.088	35,000	60,000	2.6667	0.8333	3.1754	11,026	15,940	22,582	26,500	7452
1/4" Sch.40 GALV.	0.540	0.088	35,000	60,000	2.6667	0.8333	3.1754	11,026	15,940	22,582	29,000	7452
1/8" Sch. 80 4130	0.405	0.095	110,000	121,500	1.7838	0.3919	2.4108	45,611	80,433	88,046	80,000	29,055
1/4" Sch. 80 4130	0.540	0.119	110,000	121,500	1.9092	0.4546	2.5194	43,645	73,815	80,802	80,000	26,665
1/4" Sch. 80 SS	0.540	0.119	35,000	85,000	1.9092	0.4546	2.5194	13,887	23,487	37,302	44,000	12,310
1/2" Sch. 160 SS	0.840	0.187	35,000	85,000	1.8895	0.4447	2.5024	13,988	23,813	37,820	41,000	12,481
9/16" Tube SS	0.562	0.125	35,000	85,000	1.8903	0.4452	2.5031	13,979	23,784	37,774	44,000	12,466

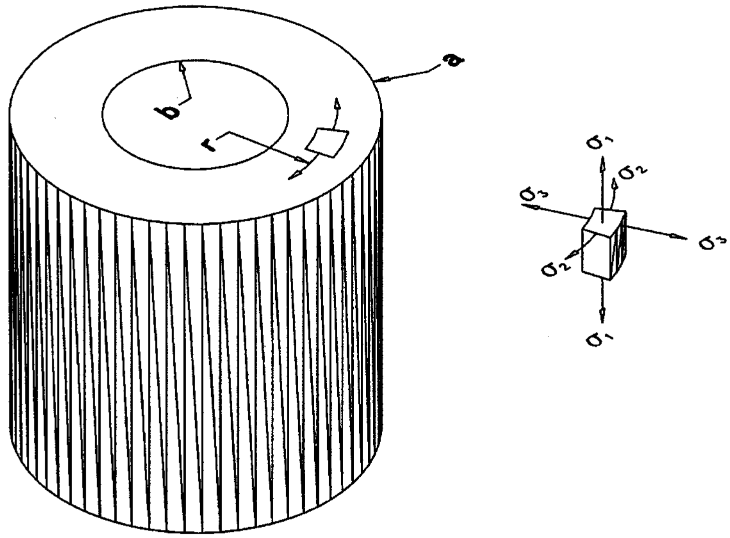

Figure 1. Thick-walled Cylinder Variables and Stresses

Figure 2. Test Pump and Containment Vessel

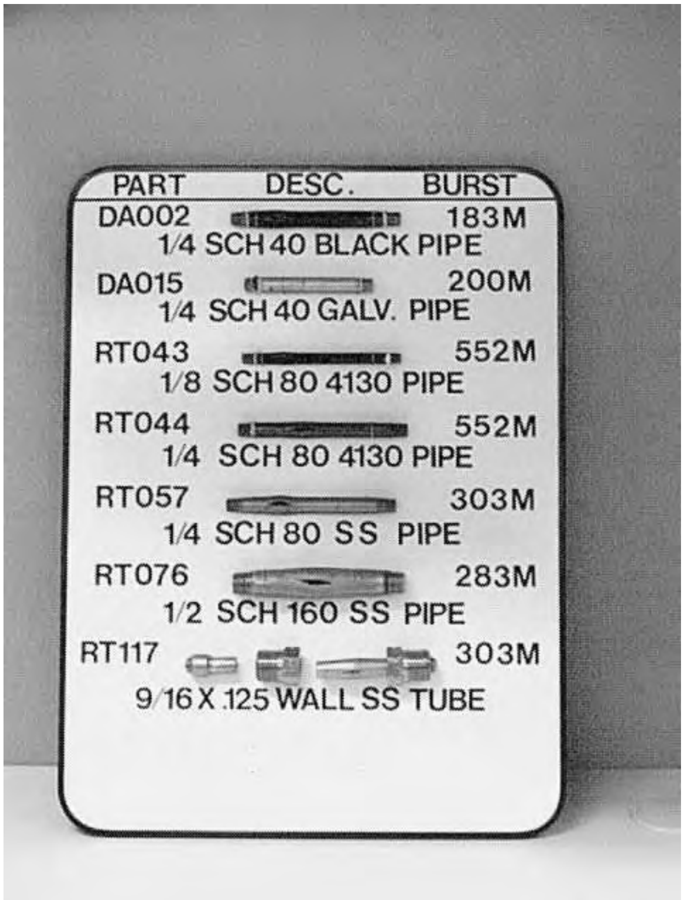

Figure 3. Burst Tubing Samples